NASA TECHNICAL MEMORANDUM

NASA TM X-73306

ASTRONAUTIC STRUCTURES MANUAL VOLUME II

Structures and Propulsion Laboratory

August 1975

NASA

George C. Marshall Space Flight Center
Marshall Space Flight Center, Alabama

MSFC - Form 3190 (Rev June 1971)

TECHNICAL REPORT STANDARD TITLE PAGE

1. REPORT NO.	2. GOVERNMENT ACCESSION NO.	3. RECIPIENT'S CATALOG NO.
NASA TM X-73306		

4. TITLE AND SUBTITLE	5. REPORT DATE
ASTRONAUTIC STRUCTURES MANUAL VOLUME II	August 1975 6. PERFORMING ORGANIZATION CODE
7. AUTHOR(S)	8. PERFORMING ORGANIZATION REPORT #
9. PERFORMING ORGANIZATION NAME AND ADDRESS George C. Marshall Space Flight Center Marshall Space Flight Center, Alabama 35812	10. WORK UNIT NO. 11. CONTRACT OR GRANT NO.
12. SPONSORING AGENCY NAME AND ADDRESS National Aeronautics and Space Administration Washington, D. C. 20546	13. TYPE OF REPORT & PERIOD COVERED Technical Memorandum 14. SPONSORING AGENCY CODE

15. SUPPLEMENTARY NOTES

Prepared by Structures and Propulsion Laboratory, Science and Engineering

16. ABSTRACT

This document (Volumes I, II, and III) presents a compilation of industry-wide methods in aerospace strength analysis that can be carried out by hand, that are general enough in scope to cover most structures encountered, and that are sophisticated enough to give accurate estimates of the actual strength expected. It provides analysis techniques for the elastic and inelastic stress ranges. It serves not only as a catalog of methods not usually available, but also as a reference source for the background of the methods themselves.

An overview of the manual is as follows: Section A is a general introduction of methods used and includes sections on loads, combined stresses, and interaction curves; Section B is devoted to methods of strength analysis; Section C is devoted to the topic of structural stability; Section D is on thermal stresses; Section E is on fatigue and fracture mechanics; Section F is on composites; Section G is on rotating machinery; and Section H is on statistics.

These three volumes supersede NASA TM X-60041 and NASA TM X-60042.

17. KEY WORDS	18. DISTRIBUTION STATEMENT
	Unclassified — Unlimited

19. SECURITY CLASSIF. (of this report)	20. SECURITY CLASSIF. (of this page)	21. NO. OF PAGES	22. PRICE
Unclassified	Unclassified	974	NTIS

APPROVAL

ASTRONAUTIC STRUCTURES MANUAL
VOLUME II

The information in this report has been reviewed for security classification. Review of any information concerning Department of Defense or Atomic Energy Commission programs has been made by the MSFC Security Classification Officer. This report, in its entirety, has been determined to be unclassified.

This document has also been reviewed and approved for technical accuracy.

A. A. McCOOL
Director, Structures and Propulsion Laboratory

☆U.S. GOVERNMENT PRINTING OFFICE 1976-641-255/447 REGION NO. 4

TABLE OF CONTENTS

TABLE OF CONTENTS (Concluded)

LIST OF ILLUSTRATIONS

LIST OF ILLUSTRATIONS (Continued)

LIST OF ILLUSTRATIONS (Continued)

LIST OF ILLUSTRATIONS (Concluded)

DEFINITION OF SYMBOLS

Symbol	Definition
A	Cross-sectional area of plate without hole - $in.^2$
a	Diameter of hole; one-half length of side of rounded rectangular hole; minor diameter of elliptical hole - in.
A_b	Diameter of bead reinforcement - in.
B	Bead factor (Fig. B10-25)
b	Major diameter of elliptical hole; one-half length of side of rounded rectangular hole; one-half length of side of square plate - in.
c	Distance from center of hole to edge of plate; distance between holes; distance between rows in a double row of holes - in.
D	Plate flexural rigidity - psi
e	Displacement of hole from center line of plate - in.
F	Ratio of bead cross-sectional area to hole cross-sectional area
h	Thickness of plate - in.
h_b	Height of bead reinforcement - in.
K	Stress concentration factor
K_t	Theoretical stress concentration factor
K_e	Effective or significant stress concentration factor
K_{tB}	Stress concentration factor (Fig. B10-27)

DEFINITION OF SYMBOLS (Continued)

Symbol	Definition
K_{tB}^{*}	Stress concentration factor for plate with reinforced hole
L	One-half span of a beam - in.
M	Bending moment - in.-lb
M_θ, M_n	Bending moments in plates - in.-lb/in.
P	Axial tensile load - lb
p	One-half distance between holes - multiple hole patterns - in.
q	Uniform normal load intensity on plate or beam - psi or lb/in.
R	Radius of large hole in plate - in.
R_1, R_2	Radius of holes (Fig. B10-15) - in.
r	Radius of hole - in.
s_1	Distance from edge of large hole to center of small circular notch - in.
w	Width of plate - in.
w_{max}	Maximum deflection in plate - in.
β	Angle of obliquity of hole - deg
γ	R_1/R_2 (Fig. B10-16)
η	s_1/R_1 (Fig. B10-15)
θ	Angle of stagger between holes in double row of holes - deg
σ	Stress applied to semi-infinite plate - psi

DEFINITION OF SYMBOLS (Concluded)

Symbol	Definition
λ	2a/w (Fig. B10-8)
μ	b/a (Fig. B10-8)
ρ	Radius of rounded corner; radius of hole - in.
σ_{max}	Maximum localized stress at edge of hole - psi
σ_{net}	Stress based on net section - psi
σ_o, σ_{nom}	Nominal stress in plate without hole - psi
σ_1	Largest value of stress in a biaxial stress field - psi
σ_2	Smallest value of stress in a biaxial stress field - psi

TABLE OF CONTENTS

SECTION B7

THIN SHELLS

B7.0 Thin Shells

Basic relationships governing the behavior of shells whose thicknesses are small relative to their surface dimensions and to their principal radii of curvature are summarized in this section. This thinness admits various approximations to the three-dimensional stress state. The degree of approximation best suited for a particular analysis depends on the shell shape, the type of loading, and the material of which the shell is made. Consequently, there exists a variety of approximate thin-shell theories.

The various thin shell theories to be used in subsequent analyses are discussed below. The purpose is to familiarize the analyst with the foundations upon which commonly employed shell equations are based.

B7.0.1 Thin Shell Theories

Theories of thin shells may be broadly classified according to the fundamental theories which they approximate:

I The Theory of Linear (classical) Elasticity

II Nonlinear Elasticity

III Inelasticity

The most common shell theories are those based on linear elasticity concepts. These theories adequately predict stresses and deformations for shells exhibiting small elastic deflections; they are also adaptable to some buckling problems.

The Nonlinear Theory of Elasticity forms the basis for finite and large deflection theories of shells. These theories are often required when dealing with shallow shells, buckling problems, and highly elastic membranes. The nonlinear shell equations are considerably more difficult to solve and therefore are more limited in use.

Shells in the inelastic range will not be discussed in this section.

B7.0.2 Thin Shell Theories Based on Linear Elasticity

The classical three-dimensional equations of Linear Elasticity are based upon the following assumptions:

1. Displacement gradients are small; i.e.,

$$\frac{u_i}{x_j} \ll 1$$

where u_i = generalized displacement, i = 1, 2, 3

x_j = generalized coordinate, j = 1, 2, 3

2. Products of displacement gradients are therefore negligible compared to the gradients themselves. By this assumption, strains and rotations are necessarily small and they become linear functions of the displacement gradients, i.e.,

$$\epsilon_1 = \frac{\partial u_1}{\partial x_1}; \quad \epsilon_2 = \frac{\partial u_2}{\partial x_2}; \quad \gamma_{12} = \frac{\partial u_1}{\partial x_2} + \frac{\partial u_2}{\partial x_1};$$

etc.

3. It is further assumed that the Generalized Hooke's Law holds, an assumption which is naturally compatible with the small strain condition. Hooke's Law, in its general form, states that the six components of stress at any point are linear functions of the six components of strain at that point.

When dealing with thin plates or shells, the stresses in planes parallel to the surface are of prime importance, the normal stresses being of little practical significance. Hence, a complete three-dimensional solution is generally not warranted. Sufficiently accurate analyses of thin plates and shells can be performed using simplified versions of the general Linear Elasticity equations.

The selection of the proper form of these approximations has been the subject of considerable controversy among the many investigators in the field. As a result, there is in existence a large number of general and specialized thin shell theories, developed within the framework of linear elasticity. The most commonly encounter-

ed theories will be discussed in the subsequent sections and classified according to the assumptions upon which they are based.

The various linear shell theories will be classified into five basic categories:

1. First-Order Approximation Shell Theory

2. Second-Order Approximation Shell Theory

3. Shear Deformation Shell Theory

4. Specialized Theories for Shells of Revolution

5. Membrane Shell Theory

In the case of thin shells, the simplified bending theories of shells are (in general) based on Love's first-approximation and second-approximation shell theories. Although some theories do not adhere strictly to Love's two original approximations, they can be considered as modifications thereof and will be categorized as either a first or second approximation.

Although the Shear Deformation and Specialized Shell theories presented are based on Love's first-approximation, they are classified separately because of their particular physical significance.

Linear membrane theory is the limiting case corresponding to a zero-order approximation, or momentless state.

B7.0.2.1 First-Order Approximation Shell Theory

Love was the first investigator to present a successful approximate shell theory based on linear elasticity. To simplify the strain-displacement relationships and, consequently, the stress-strain relations, Love introduced the following assumptions, known as first approximations and commonly termed the Kirchhoff-Love hypothesis:

1. The shell thickness, t, is negligibly small in comparison with the least radius of curvature, R_{min}, of the middle surface; i. e., $\frac{t}{R_{min}} << 1$ (therefore, terms $\frac{z}{R} << 1$).

2. Linear elements normal to the unstrained middle surface remain straight during deformation, and their extensions are negligible.

3. Normals to the undeformed middle surface remain normal to the deformed middle surface.

4. The component of stress normal to the middle surface is small compared with other components of stress, and may be neglected in the stress-strain relationships.

5. Strains and displacements are small so that quantities containing second-and higher-order terms are neglected in comparison with first-order terms in the strain equations.

The last assumption is consistent with the formulation of the classical theory of linear elasticity. The other assumptions are used to simplify the elasticity relations.

By the thickness condition, assumption (1) above, the ratios $\frac{z}{r_1}$ and $\frac{z}{r_2}$ are negligible relative to unity. From this condition, the ten stress resultants that act on an infinitesimal element (N_ϕ, N_θ, Q_ϕ, Q_θ, $Q_{\theta\phi}$, $Q_{\phi\theta}$, M_ϕ, M_θ, $M_{\phi\theta}$, and $M_{\theta\phi}$) reduces to eight, since $Q_{\phi\theta} = Q_{\theta\phi}$ and $M_{\phi\theta} = M_{\theta\phi}$.

Assumption (2) of Love's first approximation is analogous to Navier's hypothesis in elementary beam theory, i. e., plane sections remain plane during bending.

The strain equations are further simplified through assumption (3), by which transverse shear deformations are neglected. As a consequence, normals to the middle plane not only remain straight but remain normal and have the same rotation as the middle surface. The degree of error introduced by this assumption naturally depends on the magnitude of transverse shearing forces; in local areas around a shell edge such shear deformations may be comparable to bending and axial deformations, and cannot be ignored. In general, however, shells loaded by continuously distributed surface forces, and having flexibly supported edges, can be assumed to have negligible transverse shear deformations.

By the fourth assumption, forces applied to the surface of the shell are stated to be so distributed that directly imposed stresses are small. Furthermore, direct normal stresses through the thickness, f_z, are taken to be insignificant due to the large radius-to-thickness ratios of the shell.

Practically speaking, the solution of the simultaneous differential equations of Love's first order approximation theory is possible only in rare cases, or with additional approximations. In the case of a loaded structure, the general solution of the nonhomogeneous differential equations consists of a particular solution of the nonhomogeneous differential equations and the general solution of the homogeneous differential equations. In the case of an unloaded structure the solution consists of only the general solution of the homogeneous differential equations.

The nonhomogeneous solution of Love's equations, to a first approximation, equals the solution of the corresponding extensional (pure membrane) problem. The homogeneous solution is a self-equilibrating system of stress resultants which satisfy compatibility conditions at the edges of the shell (edge effect) and in other regions of discontinuity.

Thus, there are two extreme cases possible within the first approximation: (1) the inextensional or pure bending case in which middle plane strains are neglected compared with flexural strains, and (2) the extensional or membrane case in which only middle plane strains are considered. The general or mixed case lies between these two extremes.

B7.0.2.2 Second-Order Approximation Shell Theory

In Love's second approximation, restrictions on the t/r ratios are relaxed to such an extent that normal stresses induced by flexure and corresponding normal displacements are no longer negligible. By considering the second-order effects of such normal displacements, the strain components parallel to the middle surface become nonlinear functions of middle-plane curvature changes.

Assumptions (2) and (3) of the first-order theory are retained in the second approximation. Thus, displacements are said to vary linearly across the thickness of the shell, whereas, strains are nonlinearly distributed.

It is characteristic of second approximation theories that strains and constitutive relations contain second-order terms in the thickness coordinate, z.

The theory is applicable for small deflections of highly curved shells subjected to predominantly flexural strains.

B7.0.2.3 Shear Deformation Shell Theories

In the development of the first-and second-order shell theories the effects of transverse shear deformation were neglected. This neglect resulted because of the geometrical assumptions that normals remain normal. It is possible that for some loads or shell configurations, the transverse shear strains can no longer be neglected and, therefore, these effects must be included in the theory.

When the effects of shear deformation are included, the shear strains no longer vanish and, as a result, the rotation expressions are no longer determinate.

Since the shear forces are now related to deformations, they can be eliminated from equilibrium equations. Thus, five boundary conditions are necessary at each boundary (Reference 1).

B7.0.2.4 Specialized Theories for Shells of Revolution

The bending shell theories previously discussed can be simplified considerably for specialized conditions of geometry and loading. Some of the simplified shell theories resulting from consideration of shells of revolution of specific geometry will be presented in this section. These theories are based on first-order approximation; however, for purposes of illustration they are classified separately. In this section, the simplified shell theories are presented for shells of particular interest. Included are the Reissner-Meissner theories, Geckeler's approximations, shallow-shell theory, Donnell's theory, and others.

I. General Shells of Revolution Axisymmetrically Loaded

For the case of axisymmetrical deformation, the displacement in the θ direction ($\bar{v}$) is zero, and all derivatives of displacement components with respect to θ are also zero. From symmetry, the resultant forces $Q_{\phi\theta}$, Q_{θ}, and $M_{\phi\theta}$ vanish. Two second-order ordinary differential equations in the two unknown displacement components $\bar{u}$ and $\bar{w}$ can be obtained. Rather than obtain equations in this manner, however, a transformation of dependent variables can be performed leading to a more manageable pair of equations which, for shells of constant meridional curvature and constant thickness, combine into a single fourth-order equation solvable in terms of a hypergeometric series. Historically, such a transformation of variables was first introduced by H. Reissner (1913) for spherical shells and then generalized to all shells of constant thickness and constant meridional curvature by E. Meissner (1914). Meissner next showed (1915) that the equations for a general shell of revolution are also transformable to Reissner-Meissner type equations provided the thickness t and the radius r_1 both vary so as to satisfy a certain relationship for all values of ϕ, (the "Meissner condition").

Reissner-Meissner type equations are the most convenient and widely employed forms of the first-approximation theory for axisymmetrically loaded shells of revolution. It is seen that they follow exactly from the relations of Love's first approximation when the meridional curvature and thickness are constant, as they are for cylindrical, conical, spherical, and toroidal shells of uniform thickness. Furthermore, they follow directly from Love's equations in the more general case provided special restraints on the variation of thickness and geometry are satisfied.

Using a more recent version of the Reissner-Meissner equations (Reference 2), toroidal shells of constant thickness were investigated by Clark (Reference 3) and ellipsoidal shells of constant thickness by Naghdi and DeSilva (Reference 4). In the latter case, the Meissner type condition, which would require the radius r_1 to be constant, is obviously not satisfied. It is shown, however, that assuming the Meissner condition to be satisfied yields a justifiable approximation for ellipsoidal shells.

II. Spherical Shells

For axisymmetrically loaded spherical shells of constant thickness, two simplified versions of the Reissner-Meissner equations are of engineering interest, namely Geckeler's approximation for nonshallow spherical shells and the Esslinger approximation for shallow shells.

For axisymmetrically loaded spherical shells of constant thickness, the fourth-order differential equation is:

$$\frac{d^4Q_\phi}{d_\phi{}^4} + A_3 \frac{d^3Q_\phi}{d_\phi{}^4} + A_2 \frac{d^2Q_\phi}{d_\phi{}^2} + A_1 \frac{dQ_\phi}{d_\phi} + A_oQ_\phi + 4\lambda^4 Q_o = 0$$

where

$$A_o = 1-3\csc^4\phi - \mu^2$$

$$A_1 = \cot\phi(2+3\csc^2\phi)$$

$$A_2 = 1-3\csc^2\phi$$

$$A_3 = 2\cot\phi$$

and

$$\lambda^4 = 3(1-\mu^2)\frac{R^2}{t^2}$$

SECTION B7.1

MEMBRANE ANALYSIS OF

TABLE OF CONTENTS

B7.1.0.0 MEMBRANE ANALYSIS OF THIN SHELLS OF REVOLUTION

In engineering applications, shells that have the form of surfaces of revolution find extensive application in various kinds of containers, tanks, and domes. Furthermore, this type of shell offers a convenient selection of coordinates.

Thin shells, in general, display large stresses and deflections when subjected to relatively small bending moments. Therefore, in the design of thin shells, the condition of bending stresses is avoided or minimized. If, in the equilibrium equations of such shells, all moment expressions are neglected, the resulting shell theory is called "membrane theory," and the state of stress is referred to as a "momentless" state of stress. There are two types of shells that comply with this membrane theory: (1) shells sufficiently flexible so that they are physically incapable of resisting bending, and (2) shells that are flexurally stiff but loaded and supported in a manner that avoids the introduction of bending strains.

The momentless state of stress in practical shell problems is difficult to achieve. However, with the comparison of the complete bending analysis and membrane analysis for a thin shell of revolution built in along its edges and having noncritical axisymmetric loading, the following conclusions can be made:

1. The stresses and deformations are almost identical for all locations on the shell except for a narrow strip of the shell surface adjacent to the boundary. This narrow strip is usually no wider than $\sqrt{Rt}$.
2. Except for the strip along the boundary, all bending moments, twisting moments, and vertical shears are negligible; this causes the entire bending solution to be practically identical to the membrane solution.

3. Boundary conditions along the supporting edge are very significant; however, local bending and shear decrease rapidly away from the boundary and may become negligible outside the narrow strip.

For cases where bending stresses cannot be neglected or when a more complete analysis is desired, see Section B7.3 for bending analysis.

Shells of revolution are frequently loaded internally or externally by forces having the same symmetry as the shell itself. This loading condition is referred to as axisymmetric loading and contributes significantly to the simplification of the analysis methods presented in this section.

B7.1.1.0 GENERAL

Before investigating the stresses and deflections of a shell of revolution, we must examine the geometry of such a surface. A surface of revolution is generated by the rotation of a plane curve about an axis in its plane. This generating curve is called a meridian. The intersections of the generated surface with planes perpendicular to the axis of rotation are parallel circles and are called parallels. For such surfaces, the lines of curvature are its meridians and parallels.

A convenient selection of surface coordinates is the curvilinear coordinate system ϕ and θ, where ϕ is the angle between the normal to the surface and the axis of rotation and θ is the angle determining the position of a point on the corresponding parallel, with reference to some datum meridian. (See Figure B7.1.1 - 1.) If the surface of revolution is a sphere, these coordinates are spherical coordinates used in geography; θ is the longitude and ϕ is the complement to the latitude; hence, we have the nomenclature of meridians and parallels.

Figure B7.1.1 - 1 shows a meridian of a surface of revolution. Let R be the distance of one of its points normal to the axis of rotation and R_1 its radius of curvature. In future equations, we will also need the length R_2, measured on a normal to the meridian between its intersection with the axis of rotation and the shell surface. Noting that $R \quad R_2 \sin\phi$, the surface of the shell of revolution is completely described by R_1 and R_2 which are functions of only one of the curvilinear coordinates, ϕ. R_0 will be the radius of curvature when $\phi \cdot 0$.

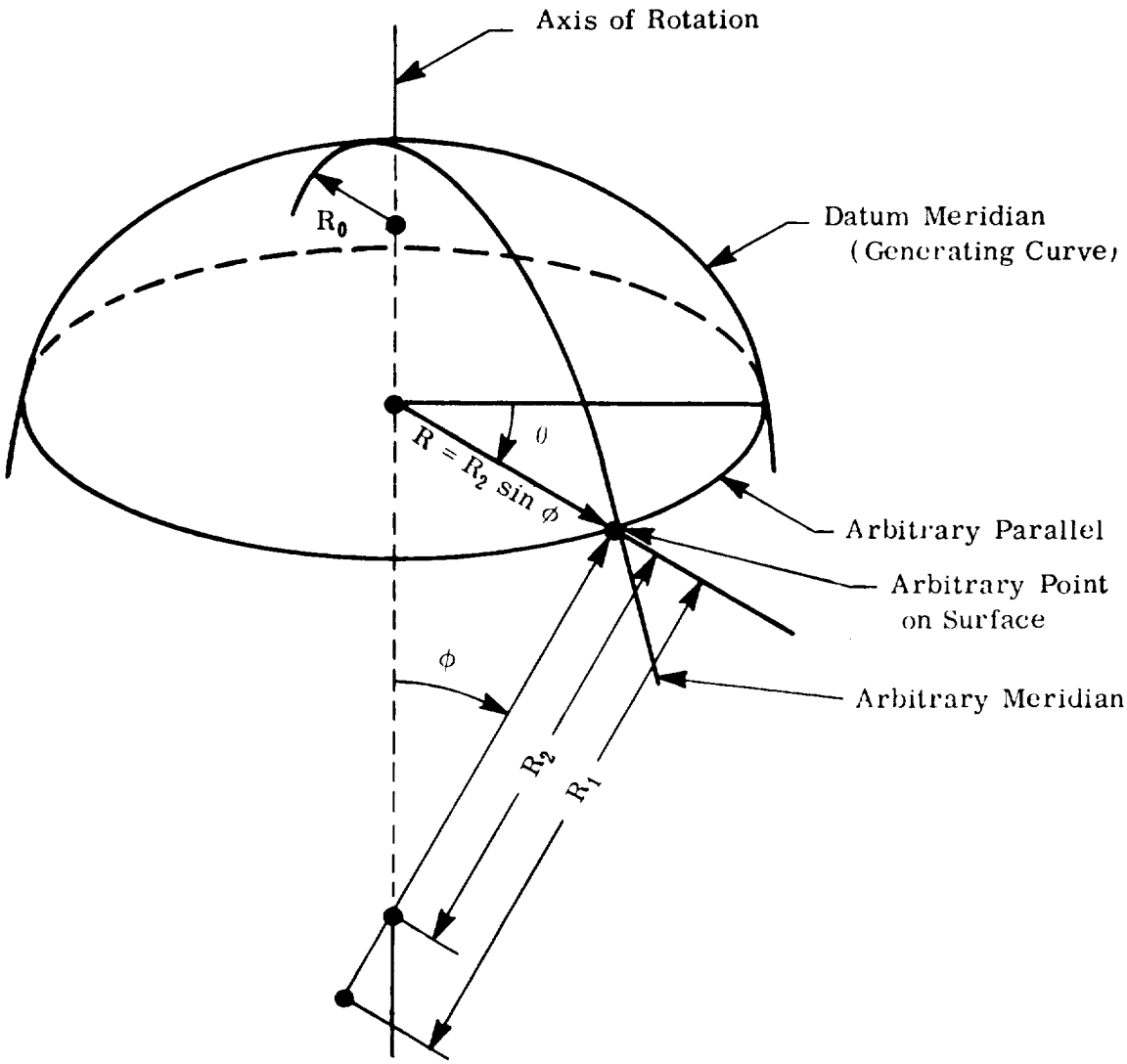

Fig. B7.1.1 - 1. Geometry of Surfaces of Revolution

The surface of revolution thus described will be that surface which bisects the thickness of the shell and will henceforth be referred to as the "middle surface" or "reference surface." By specifying the form of the middle surface and the thickness "t" of the shell at any point, the shell is entirely defined geometrically. Figure B7.1.1 - 2 shows an element of the middle surface of the shell.

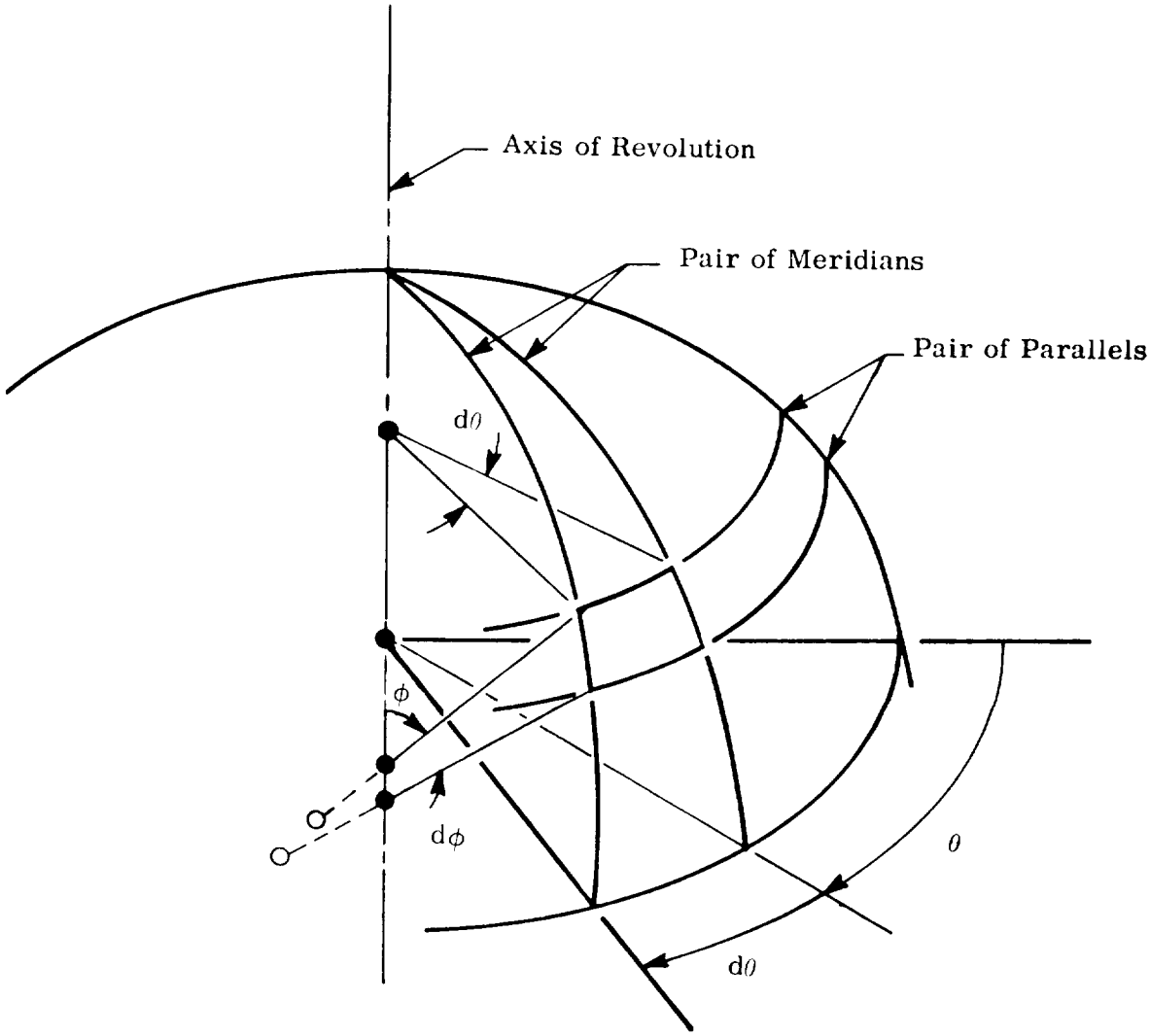

Fig. B7.1.1 - 2. Shell Element, Middle Surface

When the thickness of the shell is considered for analyzing the internal stresses, it becomes apparent that the radius of curvature "R" cannot be a principal radius of curvature; e.g., it is not normal to the shell surface (except when $R = R_2$ in the special case of circular cylinders). Henceforth, R_2 will be used as the principal radius of curvature of an element in the parallel direction. (See Figure B7.1.1 - 3.) The error introduced by this assumption will be negligible in all calculations. Note that R_1 is a principal radius of curvature in the meridional direction.

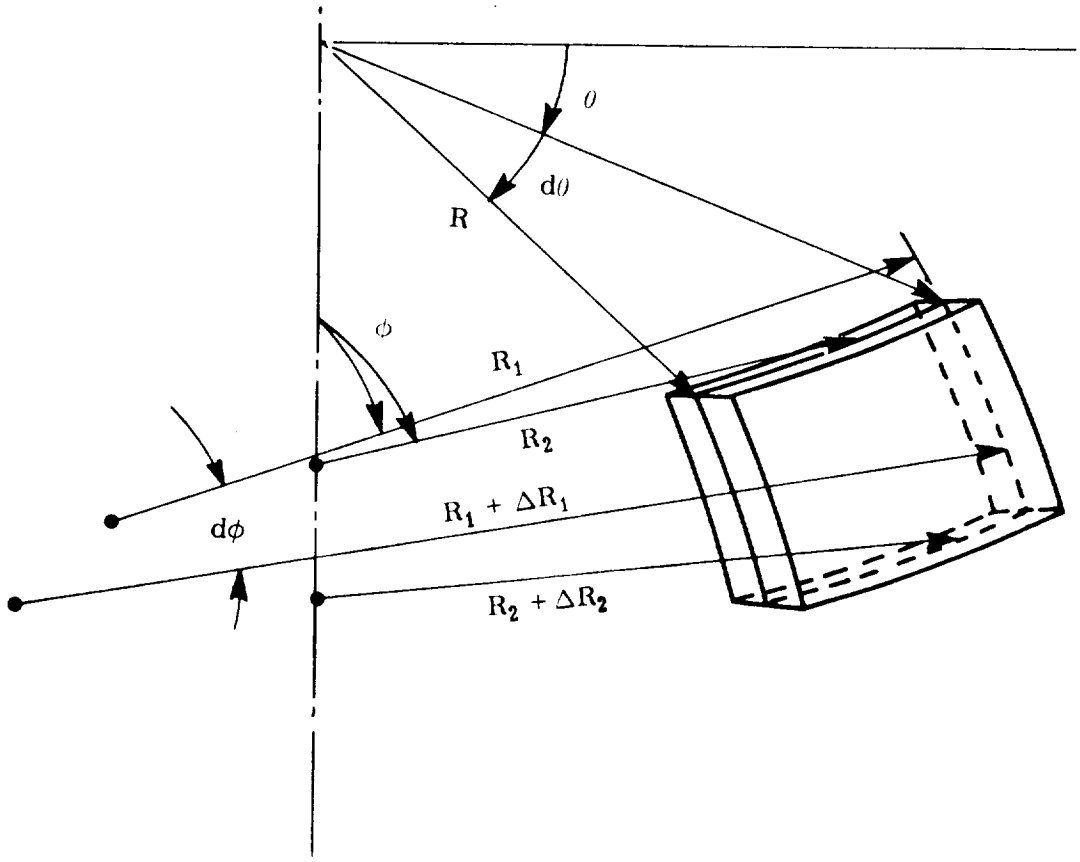

Fig. B7.1.1 - 3. Principal Radii of Curvature

Any element of a shell may have the usual internal stresses acting on the faces of the element. These stresses are indicated in Figure B7.1.1 - 4. For the analytical work that will follow, it is convenient to convert these stresses into the resulting forces and moments acting on the middle surface. In the section θ constant (Figure B7.1.1 - 4), the total force normal to this section is by definition $N_\theta \, ds_\phi$. It is the resultant of σ_θ stresses acting on this area.

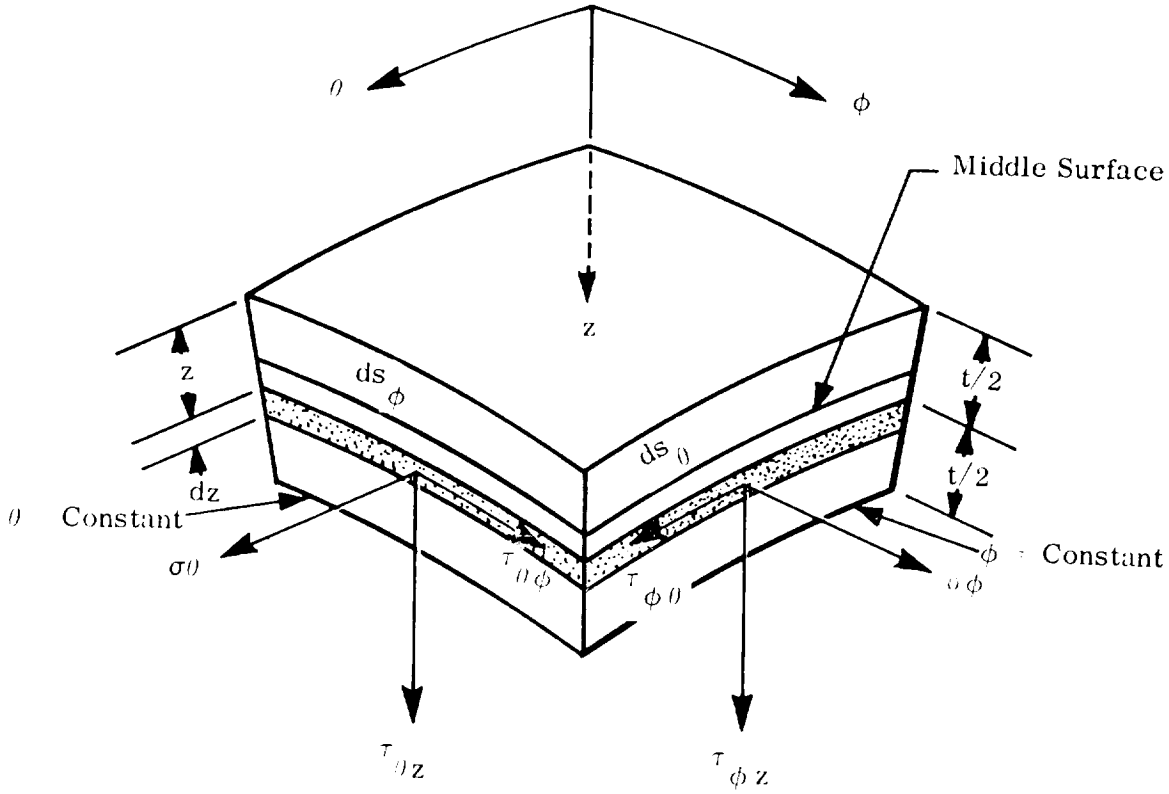

Fig. B7.1.1 - 4. Shell Stresses

Because of the curvature of the shell, its width is not simply ds_ϕ, but $ds_\phi \frac{(R_1 - z)}{R_1}$, and the force transmitted through it is $\sigma_\theta \, ds_\phi \left(1 - \frac{z}{R_1}\right) dz$.

The total normal force for the element ds_ϕ t is found by integrating from $-\frac{t}{2}$ to $\frac{t}{2}$.

$$N_\theta ds_\phi = \int_{-\frac{t}{2}}^{+\frac{t}{2}} \sigma_\theta ds_\phi \left(1 - \frac{z}{R_1}\right) dz \quad .$$

When ds_ϕ is dropped from both sides, we have the resulting normal force related to the normal stress. In a like manner, $\tau_{\theta\phi}$ and $\tau_{\theta z}$ must be integrated to obtain $N_{\theta\phi}$ and Q_θ. Altogether, we have

$$N_\theta = \int_{-\frac{t}{2}}^{+\frac{t}{2}} \sigma_\theta \left(1 - \frac{z}{R_1}\right) dz$$

$$N_{\theta\phi} = \int_{-\frac{t}{2}}^{+\frac{t}{2}} \tau_{\theta\phi} \left(1 - \frac{z}{R_1}\right) dz$$

$$Q_\theta = \int_{-\frac{t}{2}}^{+\frac{t}{2}} \tau_{\theta z} \left(1 - \frac{z}{R_1}\right) dz \quad .$$

Applying the same reasoning to the section ϕ - constant, we have

$$N_\phi = \int_{-\frac{t}{2}}^{+\frac{t}{2}} \sigma_\phi \left(1 - \frac{z}{R_2}\right) dz$$

$$N_{\phi\theta} \qquad \int_{-\frac{t}{2}}^{+\frac{t}{2}} \tau_{\phi\theta} \left(1 - \frac{z}{R_2}\right) dz$$

and

$$Q_{\phi} \qquad \int_{-\frac{t}{2}}^{+\frac{t}{2}} \tau_{\phi z} \left(1 - \frac{z}{R_2}\right) dz \quad .$$

Note the different radii of curvature for sections θ constant and ϕ constant. (Refer to Figure B7.1.1 - 2.)

If the stresses are not distributed uniformly across the thickness, bending and twisting moments may result. From θ constant (Figure B7.1.1 - 3), the bending moment is

$$M_{\theta} \qquad \int_{-\frac{t}{2}}^{+\frac{t}{2}} \sigma_{\theta} \left(1 - \frac{z}{R_1}\right) z dz$$

and the twisting moment is

$$M_{\theta\phi} \qquad \int_{-\frac{t}{2}}^{+\frac{t}{2}} \tau_{\theta\phi} \left(1 - \frac{z}{R_1}\right) z dz \quad .$$

In like manner, when ϕ = constant,

$$M_{\phi} = \int_{-\frac{t}{2}}^{+\frac{t}{2}} \sigma_{\phi} \left(1 - \frac{z}{R_2}\right) z\,dz \quad \text{and} \quad M_{\phi\theta} = \int_{-\frac{t}{2}}^{+\frac{t}{2}} \tau_{\phi\theta} \left(1 - \frac{z}{R_2}\right) z\,dz .$$

N_{θ}, N_{ϕ}, $N_{\theta\phi}$, $N_{\phi\theta}$, Q_{θ}, Q_{ϕ}, M_{θ}, M_{ϕ}, $M_{\theta\phi}$, and $M_{\phi\theta}$ describe the forces and moments acting on the sides of a rectangular shell element. The fact that the shell element is not necessarily rectangular will be considered when writing the equations of equilibrium in Section B7.1.1.4. Since these ten quantities are all results of stresses, a common name for the group as a whole is "stress resultants." Figure B7.1.1 - 5 shows these stress resultants acting on the middle surface of the shell element. According to membrane theory being considered in the chapter, resultant moments and resultant transverse shearing forces cannot exist. Also, in the assumption of thin shell theory, the quantities $\frac{z}{R_1}$ and $\frac{z}{R_2}$ are very small compared to unity; thus, the only unknowns are the three quantities N_{θ}, N_{ϕ}, and $N_{\theta\phi} = N_{\phi\theta}$. Three equilibrium equations can be written for these three unknowns; hence, the problem becomes statically determinate if the forces acting on the shell are known.

In the Geckeler approximation all terms except the first and last in the equation above are neglected, leaving:

$$\frac{d^4 Q_\phi}{d\phi^4} + 4 \lambda^4 Q_o = 0$$

Geckeler's equation is seen to be of the same form as the equation for the beam on an elastic foundation.

This approximation is valid for large values of λ and high angles ϕ; that is, for thin, non-shallow spherical shells. The approximation is particularly good in the vicinity of $\phi = 90^o$, however, it is considered to be sufficiently accurate for angles as small as $\phi = 20^o$.

For small angles ϕ, the Reissner-Meissner equations can be approximated by making the usual low angle assumption that sin $\phi \approx \phi$ and cos $\phi \approx 1$, a simplification considered in detail by Esslinger. The solution of these equations is in terms of derivatives of Schleicher functions.

Another approximation for non-shallow shells is based on the transformation:

$$\bar{Q}_\phi = Q_\phi \sqrt{\sin \phi}$$

This involves a slightly more accurate approximation than Geckeler's, and was introduced by O. Blumenthal. Complete solutions were given by Hetényi (Reference 5).

III. Circular Cylindrical Shells

For the case of circular cylindrical shells arbitrarily loaded, two first approximate theories are of prime importance: Love's first-approximation theory, and its simplified version due to Donnell.

Donnell simplified the strain displacement relations by ignoring the influence of the original shell curvature on the deformations due to bending and twisting moment. By this approximation the relations between moments and change in curvature and twist become the same as for flat plates.

Donnell's equations are specially applicable to shell stability problems (Reference 6 and section on shell stability), however, in their homogeneous form they have been widely used for problems of circular cylinders under line loads, concentrated loads, and arbitrary edge loads. A review of such solutions is presented in Reference 7.

IV. Second-Order Approximation Theories for Shells of Revolution

The second-order approximation theory of Flügge (Reference 8) and Byrne (Reference 9) retain the z/r terms with respect to unity in the stress resultant equations and in the strain-displacement relations. Flügge - Byrne type equations for a general shell are discussed by Kempner (Reference 10) who obtains them as a special case of a unified thin-shell theory. Applications of this second approximation theory have generally been restricted to circular cylindrical shapes, for which case solutions are obtained in References 9 and 11. In the latter reference the Flügge - Byrne type equations are considered as standards with which simplified first-approximation theories are compared.

Second-approximation equations are derived by Vlasov directly from the general three-dimensional Linear Elasticity equations for a thick shell (Reference 12). An excellent discussion of the assumptions made by Vlasov is given by Novozhilov (Reference 13).

V. Membrane Theory of Shells

The shell theories studied in the previous sections are generally referred to as "bending" theories of shells because this development includes the consideration of the flexural behavior of shells. If, in the study of equilibrium of a shell all moment expressions are neglected, the resulting theory is the so-called "membrane" theory of shells. Membrane analysis of shells is presented in Section B7.1.

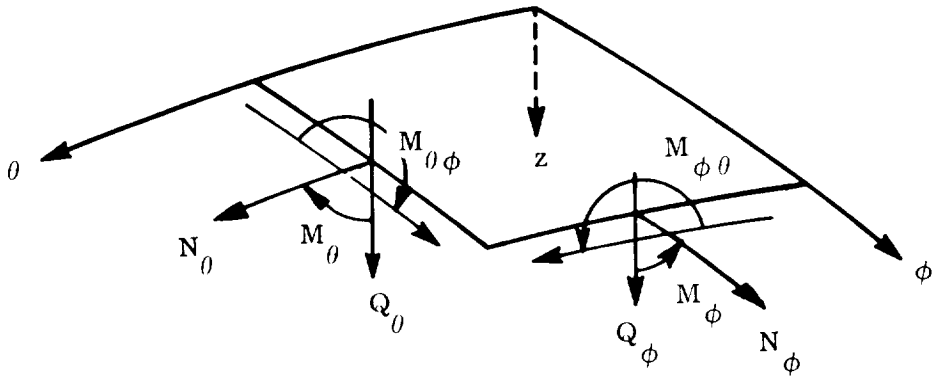

Fig. B7.1.1 - 5. Stress Resultants

B7.1.1.1 NOTATIONS

ϕ	Angle in vertical plane (measured from axis of rotation) defining the location of a point on the meridian
θ	Angle in horizontal plane that controls the location of a point on the shell
R	Radius of a point on the shell measured perpendicular to axis of rotation
R_1	Radius of curvature of meridian at any point
R_2	Radial distance between point on the shell and the axis of rotation
R_0	Radius of curvature when $\phi = 0$
t	Shell thickness
z	Coordinate in direction of surface normal
σ_ϕ, σ_θ	Internal normal stresses
$\tau_{\theta z}$, $\tau_{\theta\phi}$, $\tau_{\phi\theta}$	Inplane shear stresses
N_θ	Circumferential inplane force per unit length at θ constant.
$N_{\theta\phi}$	Shear per unit length acting at θ constant
Q_θ	Transverse shear at θ constant
N_ϕ	Meridional inplane force per unit length at ϕ constant
$N_{\phi\theta}$	Shear per unit length acting at ϕ constant
Q_ϕ	Transverse shear at ϕ constant

M_{θ}	Bending moment per unit length at section θ = constant
$M_{\theta\phi}$	Twisting moment per unit length at section θ = constant
M_{ϕ}	Bending moment per unit length at section ϕ = constant
$M_{\phi\theta}$	Twisting moment per unit length at section ϕ = constant
P_z, P_{θ}, P_{ϕ}	Loading components in radial, circumferential, and meridional directions, respectively
P	Vertical load
C	Constant of integration
ϕ_0	Angle defining opening in shell of revolution
u	Displacement in the direction of the tangent to the meridian
$\bar{u}$	Displacement in the vertical direction
v	Displacement in the direction tangent to parallel
w	Displacement in the direction normal to surface
$\bar{w}$	Displacement in the horizontal direction
E	Young's modulus
μ	Poisson's ratio
ϵ_{θ}	Strain component in circumferential direction
ϵ_{ϕ}	Strain component in meridional direction
a	Radius of sphere or major axis length of ellipsoid

ρ	Specific weight of liquid
h	Height of liquid head
b	Minor axis length of ellipsoid
n	Constant defining the shape of a Cassini dome
x	Coordinate along length of cylinder or along generatrix of cone surface
x_0	Distance from apex of cone to upper edge of cone measured along generatrix
α	Cone angle
s	Arc length

B7.0.3 Nonlinear Shell Theory

The small-deflection field theories discussed in the previous sections were formulated from the classical linear theory of elasticity. It is known that these operations, which are based on Hooke's Law and the omission of nonlinear terms both in the equations for strain components and the equilibrium equations, have a unique solution in every case. In other words, linear shell theory determines a unique position of equilibrium for every shell with prescribed load and constraints.

In reality, however, the solution of a physical shell problem is not always unique. A shell under identical conditions of loading and constraints may have several possible positions of equilibrium. The incorrect inference to which linear shell theory leads can be explained by the approximations introduced in the development of the shell equations. In this development, rotations were neglected in the expressions for strains and equilibrium in order that the equations could be linearized. It is essential in the investigation of the multiple-equilibrium states of a shell to include these rotation terms.

A theory of shells that is free of this hypothesis can be thought of as being "geometrically nonlinear" and requires formulation on the basis of the nonlinear elasticity theory. Additionally, the shell may be "physically nonlinear" with respect to the stress-strain relations. This latter type of nonlinearity forms the basis of inelastic shell theory and will not be discussed here.

The development of nonlinear shell theory is based on a general mathematical approach described by Novozhilov (Reference 14) for problems of nonlinear elasticity. Starting with the general strain-displacement relations, approximate nonlinear strain-displacement relations and equilibrium equations are derived by the introduction of appropriate simplifying assumptions. The equilibrium equations are obtained upon application of the principle of stationary potential energy.

Theories based on nonlinear elasticity are required in analyzing the so-called "large" deformation of shells. "Large" or finite deflection shell theories form the basis for the investigation of the stability of shells. In the case of stability, the effects of deformation on equilibrium cannot be ignored. The stability of shells will be considered in greater detail in Section C3.0.

REFERENCES

1. Baker, E. H., Cappelli, A. P., Kovalevsky, L., Rish, F. L., and Verette, R. M., "Shell Analysis Manual," North American Aviation, Inc., SID 66-398, June 1966.

2. Reissner, E., On the Theory of Thin Elastic Shells. H. Reissner Anniversary Volume (1949), pp. 231-247.

3. Clarke, R. A., "On the Theory of Thin Elastic Toroidal Shells," Journal of Mathematics and Physics, Vol. 29 (1950), pp. 146-178.

4. Naghdi, P. M., and C. N. DeSilva, "Deformation of Elastic Ellipsoidal Shells of Revolution," Proc. 2nd U. S. National Congress of Applied Mechanics (1954), pp. 333-343.

5. Hetényi, "Spherical Shells Subjected to Axial Symmetrical Bending," Intern. Assoc. of Bridge and Struct. Engr., Pub., Vol. 5, Zurich (1938), pp. 173-185.

6. Donnell, L. H., Stability of Thin-Walled Tubes Under Torsion. NACA, TR NO. 479 (1933).

7. Pohle, F. V., "Solutions for Simplified Circular Cylindrical Shell Equations," Symposium on the Mechanics of Plate and Shells for Industry Research Associates, Polytechnic Institute of Brooklyn, March 1960.

8. Flügge, W., "Statik und Dynamik der Schalen," Berlin, Germany: Springer-Verlog (1957).

9. Byrne, Ralph, Jr., "Theory of Small Deformations of a Thin Elastic Shell," Seminar Reports in Mathematics, University of California, at Los Angeles, published in Math, N. S. Vol. 2, No. 1 (1949), pp. 103-152.

10. Kempner, J., Unified Thin-Shells Theory, Symposium on the Mechanics of Plates and Shells for Industry Research Associates, Polytechnic Institute of Brooklyn, PIBAL No. 566 (March 9-11, 1960).

11. Kempner, J., "Remarks on Donell's Equations, "Journal of Applied Mechanics, Vol. 22, No. 1 (March 1955).

12. Vlasov, V. Z., General Theory of Shells and Its Applications in Engineering, NASA Technical Translations, NASA TTF - 99 (1949).

13. Novozhilov, V. V., The Theory of Thin Shells. Graningen, The Netherlands: P. Noordhoff Ltd., (1959)

14. Novozhilov, V. V., Foundations of the Nonlinear Theory of Elasticity, Rochester, New York; Graylock Press (1953).

B7.1.1.2 SIGN CONVENTIONS

In general, the sign conventions for stresses, displacements, loads, coordinates, etc., are given in the various figures in Section B7.1.1.0. The following is a list of appropriate figures.

Coordinates	Figure B7.1.1 - 1
Stress Resultants	Figure B7.1.1 - 5
Stresses	Figure B7.1.1 - 4
Loads	Figure B7.1.1.4 - 4
Displacements	Figure B7.1.1.4 - 4, Figure B7.1.1.4 - 5

B7.1.1.3 LIMITATIONS OF ANALYSIS

The limitations and assumptions of Section B7.1 are as follows:

1. The analysis is limited to thin shells. A thin shell is usually defined as a shell where the t/R relation can be neglected in comparison to unity. However, this definition is artificial and arbitrary unless those values which are negligible in comparison to unity are defined. For example, if it is assumed that the usual error of five percent is permissible, then the range of thin monocoque shells will generally be dictated by the relation $t/R < 1/20$. The great majority of shells commonly used are in the $1/1000 < t/R < 1/50$ range. This means that they belong to the thin-shell family. If an error of 20 to 30 percent is permissible, the theory of thin shells can be used with caution even when $t/R \leq 1/3$.
2. Flexural strains are zero or negligible compared to direct axial strain.
3. The deflections, rotations, and strains are small. (See Section B7.0 for detailed definition.)
4. The shell is homogeneous, isotropic, and monocoque and is a shell of revolution.
5. It is assumed that Hooke's Law holds (stress is a linear function of strain) and the stresses are within the elastic range.
6. The boundaries of the shell must be free to rotate and to deflect normal to the shell middle surface.

7. Abrupt discontinuities must not be present in shell shape, thickness, elastic constants, or load distribution.
8. Linear elements normal to the unstrained middle surface remain straight during deformation, and their extensions are negligible.
9. Transverse shear strains are zero throughout the thickness.
10. Surface stresses and body forces are negligible.
11. Only nonshallow shells are considered (See Section B7.0.)

B7.1.1.4 EQUATIONS

I GENERAL

The equations presented in this section are for the membrane or primary solution of the shell. The effects of boundary conditions (secondary solutions) not compatible with membrane theory will be treated in Section B7.3 on bending theory. Because the bending and membrane theories give practically the same results except for a strip adjacent to the boundary, the effects of moments and shears near boundaries can be calculated by using bending theory and can be superimposed over the membrane solution. The results thus obtained will be almost identical to those obtained by using the complete, exact bending theory.

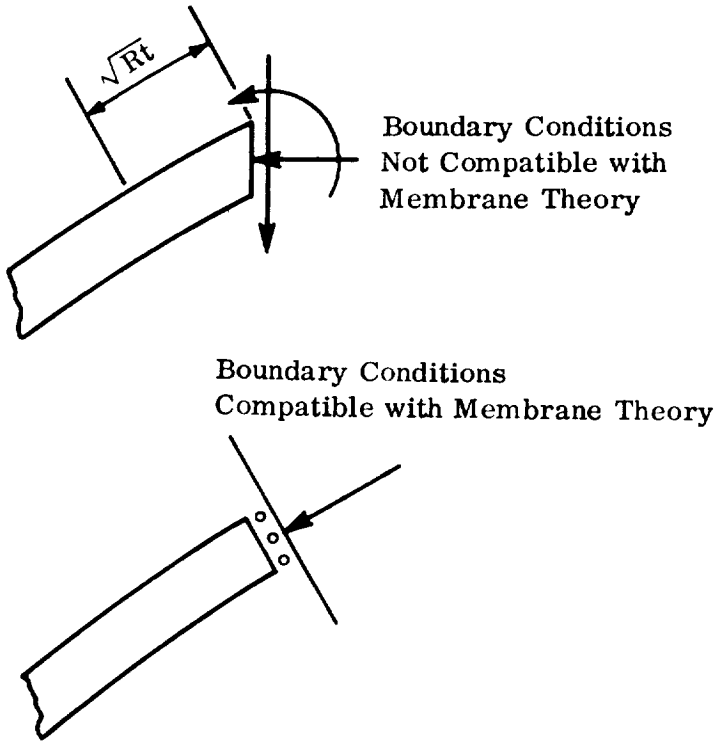

Fig. B7. 1. 1. 4 - 1. Boundary Conditions

B7.1.1.4 EQUATIONS

II EQUILIBRIUM EQUATIONS

The membrane solution is begun by considering the equilibrium of the middle surface of the shell element, cut by two meridians and two parallels (Figure B7.1.1.4 - 2a). The conditions of its equilibrium will furnish three equations in three unknowns, adequate to determine the three unknown stress resultants: the meridional force N_ϕ, the hoop force N_θ, and the shear $N_{\theta\phi} = N_{\phi\theta}$.

Beginning with the forces parallel to a tangent to the meridian, the shear transmitted by one edge of the element is $N_{\theta\phi} R_1 d\phi$, and on the opposite edge it is $\left(N_{\theta\phi} + \frac{\partial N_{\theta\phi}}{\partial \theta} d\theta \right) R_1 d\phi$. Only their difference, $\frac{\partial N_{\theta\phi}}{\partial \theta} R_1 d\theta d\phi$, enters the equilibrium condition. In the same way, we have the difference in the two meridional forces. Bearing in mind that both the force N_ϕ and the length $Rd\theta$ vary with ϕ, we have $\frac{\partial}{\partial \phi}(RN_\phi) d\phi d\theta$. The hoop forces also contribute. The two forces $N_\theta R_1 d\phi$ on either side of the element lie in the plane of a parallel circle where they include an angle $d\theta$. They, therefore, have resultant force $N_\theta R_1 d\phi d\theta$ situated in that plane and pointing towards the axis of the shell. Resolving this force into normal and tangential components shows that $N_\theta R_1 d\phi\, d\theta \cos\phi$ (Figure B7.1.1.4 - 2b) enters the condition of equilibrium. Finally, considering the component of some external force, $P_\phi RR_1 d\theta d\phi$, the equilibrium equation reads:

$$\frac{\partial N_{\theta\phi}}{\partial \theta} R_1 d\theta d\phi \quad \frac{\partial}{\partial \phi}(RN_\phi) d\phi d\theta - N_\theta R_1 d\phi\, d\theta \cos\phi + P_\phi RR_1 d\theta d\phi = 0 .$$

Noting that all terms contain $d\theta d\phi$ gives:

$$\frac{\partial}{\partial \phi}(RN_{\phi}) + R_1\frac{\partial N_{\theta\phi}}{\partial \theta} - R_1 N_{\theta}\cos\phi + P_{\phi}RR_1 = 0 \quad . \tag{1}$$

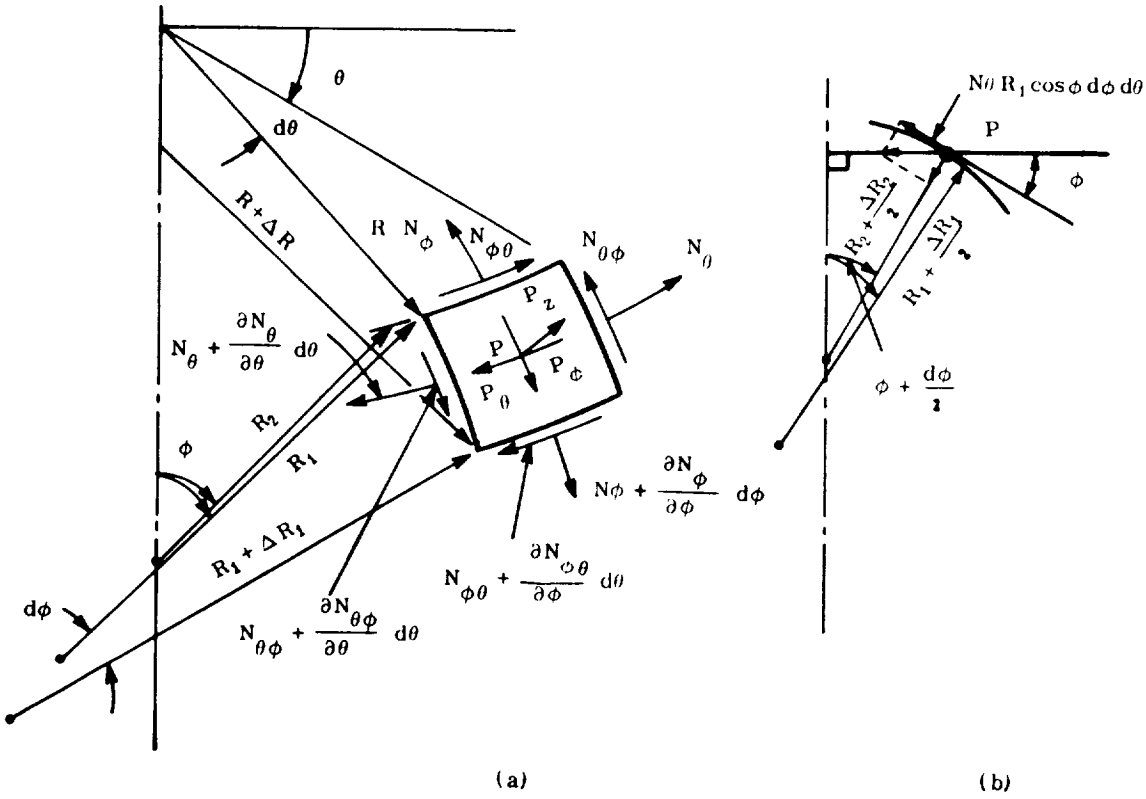

Fig. B7.1.1.4 - 2. Equilibrium of Shell Element

By similar reasoning, we obtain an equation for the forces in the direction of the tangent to a parallel circle.

$$\frac{\partial}{\partial \phi}(RN_{\phi\theta}) + R_1\frac{\partial N_\theta}{\partial \theta} + R_1N_{\theta\phi}\cos\phi + P_\theta RR_1 = 0 \quad . \tag{2}$$

The third equation is derived from forces perpendicular to the middle surface of the shell.

$$N_\theta R_1 \sin\phi + N_\phi R - P_z RR_1 = 0 \quad .$$

Dividing by RR_1 and using the geometric relation $R = R_2 \sin\phi$, we arrive at the third equation of equilibrium.

$$\frac{N_\phi}{R_1} + \frac{N_\theta}{R_2} = P_z \quad . \tag{3}$$

The problem of determining stresses under unsymmetrical loading reduces to the solution of equations (1), (2), and (3) for given values of the load P_ϕ, P_θ, and P_z.

However, it was stated previously that only axisymmetric loading would be considered in this section. For this type of loading, the stresses are independent of θ and $N_{\theta\phi} = N_{\phi\theta} = 0$. Therefore, the equations of equilibrium reduce to:

$$\frac{d}{d\phi}(RN_\phi) - R_1N_\theta\cos\phi = -P_\phi RR_1 \tag{4}$$

$$\frac{N_\phi}{R_1} + \frac{N_\theta}{R_2} = P_z \quad . \tag{3}$$

B7.1.1.4 EQUATIONS

III STRESS RESULTANTS

By solving equation (3) for N_θ and substituting the results into equation (4), we obtain a first order differential equation for N_ϕ that may be solved by integration. N_θ can then be obtained by equation (3).

$$N_\phi = \frac{1}{R_2 \sin^2\phi}\left[\int R_1 R_2 (P_z \cos\phi - P_\phi \sin\phi)\sin\phi\, d\phi + C\right]$$

$$N_\theta = R_2\left(P_z - \frac{N_\phi}{R_1}\right) .$$

The constant of integration "C" represents the effect of loads applied above a parallel circle $\phi = \phi_0$. $2\pi C$ is the resultant of these forces. If the shell is closed, the loading will degenerate to the concentrated radial force P_z at the vertex of the shell. (See Figure B7.1.1.4 - 3a.)

If the shell has an opening, the angle ϕ_0 defines the opening and the loading (lantern type loading, Figure B7.1.1.4 - 3b) results in the following:

$$N_\phi = -\frac{P}{2\pi R_2 \sin^2\phi} , \qquad N_\theta \quad \frac{P}{2\pi R_1 \sin^2\phi} .$$

These loads may be treated as additive loads because of the loaded opening at the vertex of the shell. Bending stresses will be introduced at ϕ_0 but will tend to dissipate rapidly with increasing ϕ .

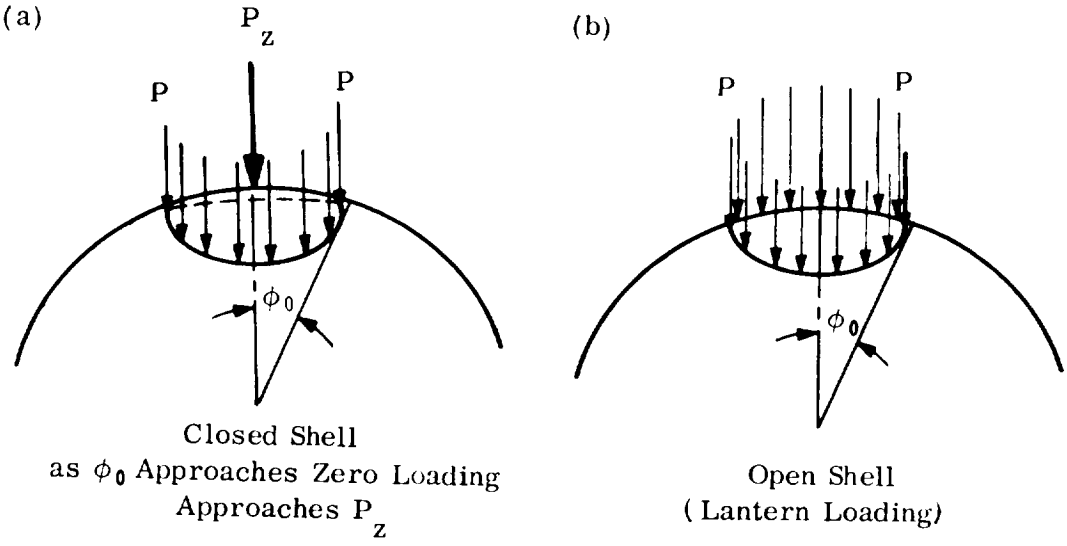

Fig. B7.1.1.4 - 3. Loading above $\phi = \phi_0$

B7.1.1.4 EQUATIONS

IV STRESS, STRAIN, AND DISPLACEMENT

Once the stress resultants, N_ϕ and N_θ, are obtained, stresses, strains, and displacements are readily obtained by the usual methods. For the symmetrically loaded membrane shell, the loading component and displacement in the circumferential direction are zero (Figure B7.1.1.4 - 4).

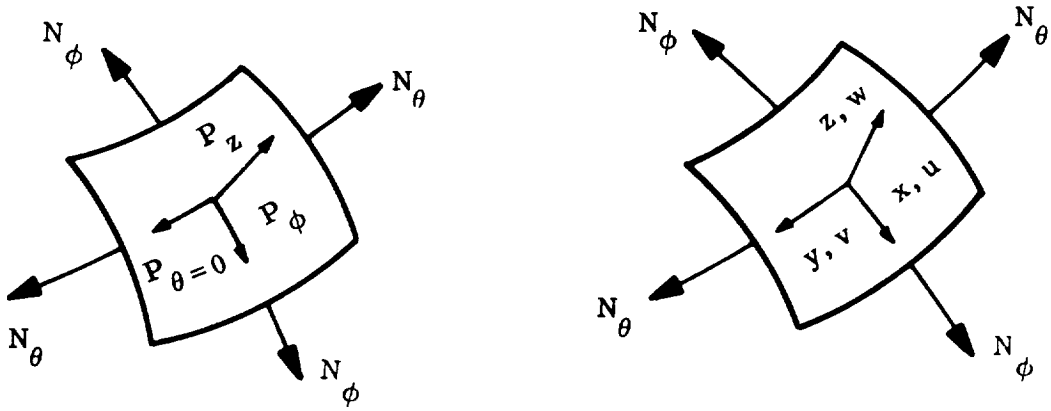

Fig. B7.1.1.4 - 4. Loads and Displacements

P_z = Radial component of loading acting on differential element

P_ϕ = Component of loading acting in X direction (tangential to meridian)

$P_\theta = 0$ = Component of loading acting in Y direction (tangential to parallel)

w = Small displacement of a point in the Z direction (normal to surface)

u = Small displacement in X direction (tangential to meridian)

v = 0 = Displacement in Y direction (tangential to parallel)

Because of assumptions of membrane theory and axisymmetric loading (e.g., $t/R \ll 1$, all moments $\cong 0$, and all shearing forces $\cong 0$) the normal stresses can be expressed simply as:

$$\sigma_\phi = \frac{N_\phi}{t} \quad , \quad \sigma_\theta = \frac{N_\theta}{t} \quad .$$

The strain components can be found either from σ_ϕ and σ_θ or N_ϕ and N_θ :

$$\epsilon_\phi = \frac{1}{Et}(N_\phi - \mu N_\theta) \quad , \quad \epsilon_\theta = \frac{1}{Et}(N_\theta - \mu N_\phi)$$

where E = Young's modulus

t = Thickness of shell

μ = Poisson's ratio .

The displacement components are computed next, thereby completing the solution of the shell problem. The general solution for u is

$$u = \sin\phi \left[\int \frac{f(\phi)}{\sin\phi}\, d\phi + C\right]$$

where C is a constant of integration to be determined from support conditions and

$$f(\phi) = R_1\epsilon_\phi - R_2\epsilon_\theta = \frac{1}{Et}\left[R_1(N_\phi - \mu N_\theta) - R_2(N_\theta - \mu N_\phi)\right]$$

$$= \frac{1}{Et}\left[N_\phi(R_1 + \mu R_2) - N_\theta(R_2 + \mu R_1)\right] \quad .$$

The displacement w can then be found from the equation

$$w = u\cot\phi - R_2\epsilon_\theta \quad .$$

Because the interaction process of two or more shells is often required, displacements are often calculated in terms of $\bar{u}$ and $\bar{w}$, the vertical and horizontal displacements. (See Figure B7.1.1.4 - 5.) Note that when $R_2 = R$, $u = \bar{u}$ and $w = \bar{w}$. The displacement $\bar{u}$ can be found in a manner similar to the solution for u. The general solution for $\bar{u}$ is

$$\bar{u} = R\epsilon_\theta \cot\phi - \int \frac{f(\phi)}{\sin\phi}\, d\phi + C$$

where $f(\phi) = R_1\epsilon_\phi - R_2\epsilon_\theta$ and C is again a constant of integration determined from support conditions. The horizontal displacement is simply

$$\bar{w} = R\epsilon_\theta \quad .$$

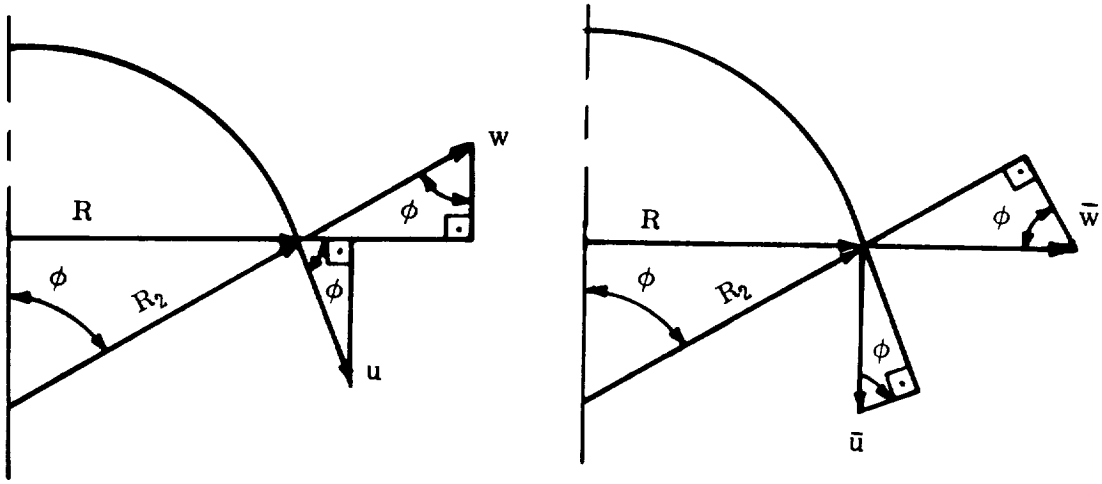

(u and w known)

$$\bar{w} = w\sin\phi + u\cos\phi$$
$$\bar{u} = -w\cos\phi + u\sin\phi$$

($\bar{u}$ and $\bar{w}$ known)

$$w = \bar{w}\sin\phi - \bar{u}\cos\phi$$
$$u = \bar{w}\cos\phi + \bar{u}\sin\phi$$

Fig. B7.1.1.4 - 5. Displacements

These formulas (Figure B7.1.1.4 - 5) can be used to convert from one form of displacement to the other, depending on the given solution and the requirements of the user.

B7.1.1.4 EQUATIONS

V SUMMARY

Application of the solutions presented in this section can be classified conveniently for the two following cases: general shell of revolution with general axisymmetric load distribution, and general shell of revolution subjected to uniform pressure. Table B7.1.1.4 - 1 presents a summary of solutions for these general cases.

The remainder of this section presents practical shell of revolution problems with various types of axisymmetric loading. Based on the various shell geometries, solutions for N_ϕ and N_θ are presented with the force-displacement relationships. The stresses can be calculated directly using the equations in Section B7.1.1.4 - IV.

Table B7.1.1.4 - 1. Summary of Equations, Axisymmetrically Loaded Shells of Revolution, Linear Membrane Theory

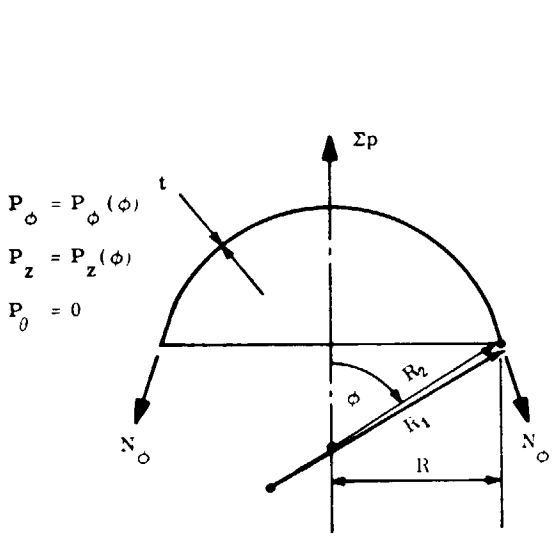

General Shell of Revolution
General Axisymmetric Loading

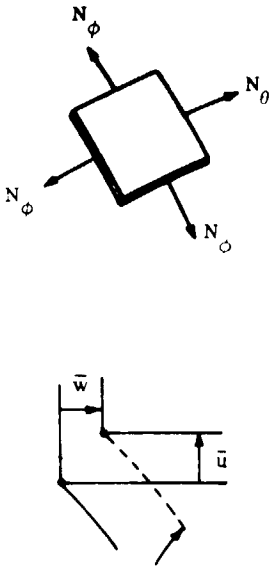

Deflected
Position

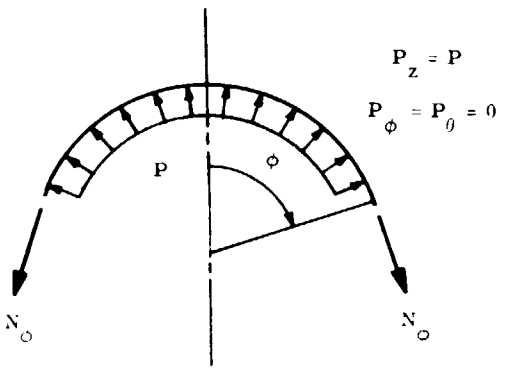

General Shell of Revolution
Uniform Pressure

$N_\phi = \frac{1}{R_2 \sin^2\phi}\left[\int R_1 R_2 (P_z \cos\phi - P_\phi \sin\phi)\sin\phi\, d\phi + C\right]$		N_ϕ	$\frac{R_2 P}{2}$
$N_\theta = R_2\left(P_z - \frac{N_\phi}{R_1}\right)$		N_θ	$\frac{R_2 P}{2}\left(2 - \frac{R_2}{R_1}\right)$
$\sigma_\phi, \sigma_\theta = \frac{N_\phi}{t}, \frac{N_\theta}{t}$		$\sigma_\phi, \sigma_\theta$	$\frac{N_\phi}{t}, \frac{N_\theta}{t}$
$\epsilon_\phi, \epsilon_\theta = \frac{1}{Et}(N\phi - \mu N_\theta), \frac{1}{Et}(N_\theta - \mu N\phi)$		$\epsilon_\phi, \epsilon_\theta$	$\frac{1}{Et}(N\phi - \mu N_\theta), \frac{1}{Et}(N_\theta - \mu N\phi)$
$\bar{w} = R\epsilon_\theta$		$\bar{w}$	$R\epsilon_\theta$
$\bar{u} = \bar{w}\cot\phi - \int \frac{R_1\epsilon_\phi - R_2\epsilon_\theta}{\sin\phi} d\phi + C$		$\bar{u}$	$\bar{w}\cot\phi - \int \frac{R_1\epsilon_\phi - R_2\epsilon_\theta}{\sin\phi} d\phi + C$

B7.1.2.0 DOME ANALYSIS

B7.1.2.1 SPHERICAL DOMES

This subsection presents the solutions for nonshallow spherical shells exposed to axisymmetric loading. Both closed and open shells will be considered. The boundaries of the shell must be free to rotate and deflect normal to the shell middle surface. No abrupt discontinuities in shell thickness shall be present.

Note that because of the geometry, $R_1 = R_2 = a$ (radius of spherical shell), and radial deflection $w = \Delta a$. Therefore, $\bar{w} \sin \phi$ and $\bar{u} = w \cos \phi$.

The following loading conditions will be considered: dead weight (Table B7.1.2.1 - 1); uniform load over base area (Table B7.1.2.1 - 2); hydrostatic pressure (Table B7.1.2.1 - 3); uniform pressure (Table B7.1.2.1 - 4); and lantern (Table B7.1.2.1 - 5). These tables begin on page 31.

Table B7.1.2.1 - 1. Dead Weight Loading
Membrane Stresses and Deformations, Closed Spherical Domes

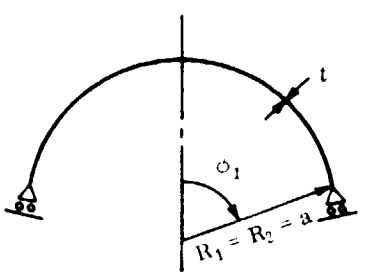

Regular

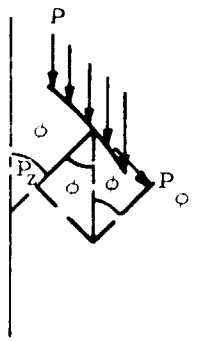

Dead Weight Loading

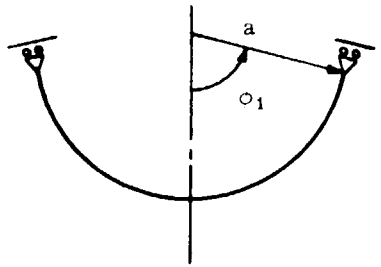

Inverted

$P_\theta = 0$

$P_\phi = P\sin\phi$

$P_z = P\cos\phi$

Regular	Inverted
$N_\phi = \frac{-ap}{1+\cos\phi}$	$N_\phi = \frac{ap}{1+\cos\phi}$
$N_\theta = -ap\left(\cos\phi - \frac{1}{1+\cos\phi}\right)$	$N_\theta = ap\left(\cos\phi - \frac{1}{1+\cos\phi}\right)$
$\sigma_\phi, \sigma_\theta = \frac{N_\phi}{t}, \frac{N_\theta}{t}$	$\sigma_\phi, \sigma_\theta = \frac{N_\phi}{t}, \frac{N_\theta}{t}$
$w = \frac{a^2p}{Et}\left[-\cos\phi + \frac{1+\mu}{\sin^2\phi}(1-\cos\phi)\right]$	$w = -\frac{a^2p}{Et}\left[-\cos\phi + \frac{1+\mu}{\sin^2\phi}(1-\cos\phi)\right]$
$\bar{w} = w\sin\phi$	$\bar{w} = w\sin\phi$
$\bar{u} = w\cos\phi$	$\bar{u} = w\cos\phi$

Table B7.1.2.1 - 1 (Concluded). Dead Weight Loading Membrane Stresses and Deformations, Open Spherical Domes

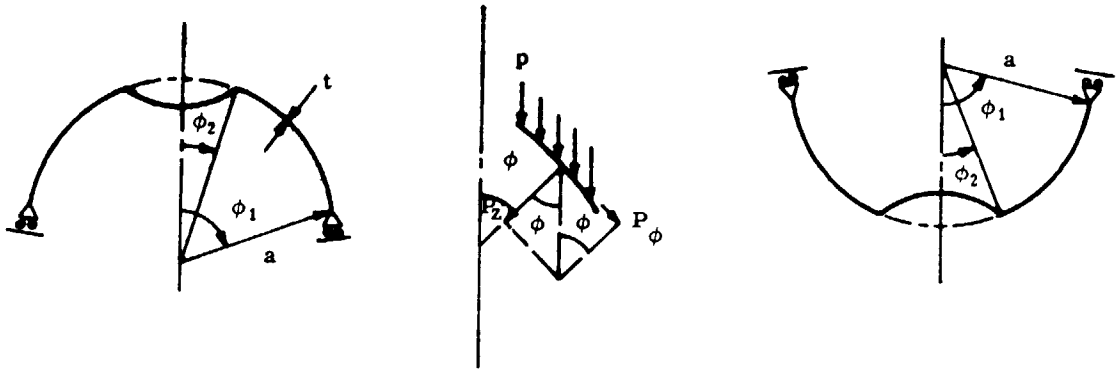

Regular | Dead Weight Loading | Inverted

$P_\theta = 0$

$P_\phi = P \sin \phi$

$P_z = P \cos \phi$

Regular	Inverted
$N_\phi = -\frac{ap}{\sin^2\phi}(\cos\phi_2 - \cos\phi)$	$N_\phi = \frac{ap}{\sin^2\phi}(\cos\phi_2 - \cos\phi)$
$N_\theta = -ap\left[\cos\phi - \frac{1}{\sin^2\phi}(\cos\phi_2 - \cos\phi)\right]$	$N_\theta = ap\left[\cos\phi - \frac{1}{\sin^2\phi}(\cos\phi_2 - \cos\phi)\right]$
$\sigma_\phi, \sigma_\theta = \frac{N_\phi}{t}, \frac{N_\theta}{t}$	$\sigma_\phi, \sigma_\theta = \frac{N_\phi}{t}, \frac{N_\theta}{t}$
$w = \frac{a^2p}{Et}\left[-\cos\phi + \frac{1+\mu}{\sin^2\phi}(\cos\phi_2 - \cos\phi)\right]$	$w = -\frac{a^2p}{Et}\left[-\cos\phi + \frac{1+\mu}{\sin^2\phi}(\cos\phi_2 - \cos\phi)\right]$
$\bar{w} = w \sin\phi$	$\bar{w} = w \sin\phi$
$\bar{u} = w \cos\phi$	$\bar{u} = w \cos\phi$

Table B7.1.2.1 - 2. Uniform Loading over Base Area
Membrane Stresses and Deformations, Closed Spherical Domes

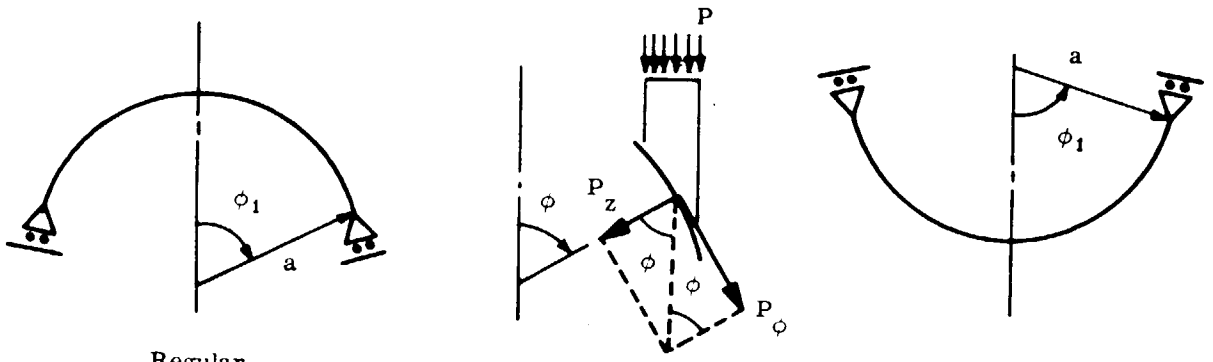

Regular

Inverted

Uniform Loading over Base Area

$P_\theta = 0$

$P_\phi = P \cos\phi \sin\phi$

$P_z = P \cos^2\phi$

Regular	Inverted
$N_\phi = -\frac{ap}{2}$	$N_\phi = \frac{ap}{2}$
$N_\theta = -\frac{ap}{2}\cos 2\phi$	$N_\theta = \frac{ap}{2}\cos 2\phi$
$\sigma_\phi, \sigma_\theta = \frac{N_\phi}{t}, \frac{N_\theta}{t}$	$\sigma_\phi, \sigma_\theta = \frac{N_\phi}{t}, \frac{N_\theta}{t}$
$w = \frac{a^2 p}{Et}\left[\frac{1+\mu}{2} - \cos^2\phi\right]$	$w = -\frac{a^2 p}{Et}\left[\frac{1+\mu}{2} - \cos^2\phi\right]$
$\bar{w} = w \sin\phi$	$\bar{w} = w \sin\phi$
$\bar{u} = w \cos\phi$	$\bar{u} = w \cos\phi$

Table B7.1.2.1 - 2 (Concluded). Uniform Loading over Base Area
Membrane Stresses and Deflections, Open Spherical Domes

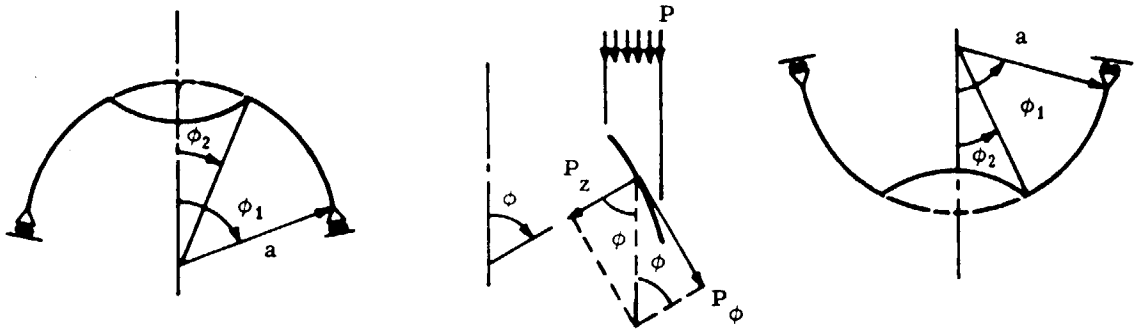

Regular | Uniform Loading over Base Area | Inverted

$$P_\theta = 0$$
$$P_\phi = P \cos\phi \sin\phi$$
$$P_z = P \cos^2\phi$$

Regular	Inverted
$N_\phi = -\frac{ap}{2}\left(1 - \frac{\sin^2\phi_2}{\sin^2\phi}\right)$	$N_\phi = \frac{ap}{2}\left(1 - \frac{\sin^2\phi_2}{\sin^2\phi}\right)$
$N_\theta = -\frac{ap}{2}\left(2\cos^2\phi - 1 + \frac{\sin^2\phi_2}{\sin^2\phi}\right)$	$N_\theta = \frac{ap}{2}\left(2\cos^2\phi - 1 + \frac{\sin^2\phi_2}{\sin^2\phi}\right)$
$\sigma_\phi, \sigma_\theta = \frac{N_\phi}{t}, \frac{N_\theta}{t}$	$\sigma_\phi, \sigma_\theta = \frac{N_\phi}{t}, \frac{N_\theta}{t}$
$w = \frac{a^2 p}{Et}\left[-\cos^2\phi + \frac{1+\mu}{2}\left(1 - \frac{\sin^2\phi_2}{\sin^2\phi}\right)\right]$	$w = -\frac{a^2 p}{Et}\left[-\cos^2\phi + \frac{1+\mu}{2}\left(1 - \frac{\sin^2\phi_2}{\sin^2\phi}\right)\right]$
$\bar{w} = w \sin\phi$	$\bar{w} = w \sin\phi$
$\bar{u} = w \cos\phi$	$\bar{u} = w \cos\phi$

Table B7.1.2.1 - 3. Hydrostatic Pressure Loading Membrane Stresses and Deformations, Closed Spherical Domes

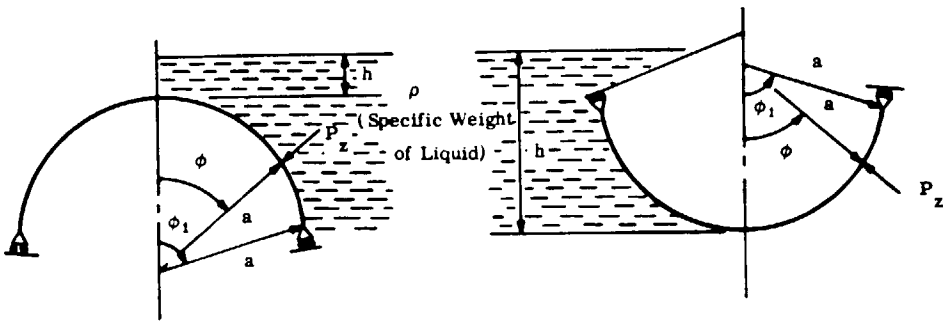

Regular

$P_\theta = P_\phi = 0$

$P_z = \rho[h + a(1 - \cos\phi)]$

$P_z = \rho[h - a(1 - \cos\phi)]$

Inverted

Regular	Inverted
$N_\phi = \frac{\rho a^2}{6}\left(1 + \frac{3h}{a} - \frac{2\cos^2\phi}{1+\cos\phi}\right)$	$N_\phi = \frac{\rho a^2}{6}\left(-1 + \frac{3h}{a} + \frac{2\cos^2\phi}{1+\cos\phi}\right)$
$N_\theta = -\frac{\rho a^2}{6}\left(-1 + \frac{3h}{a} - \frac{4\cos^2\phi - 6}{1+\cos\phi}\right)$	$N_\theta = \frac{\rho a^2}{6}\left(1 + \frac{3h}{a} - \frac{4\cos^2\phi - 6}{1+\cos\phi}\right)$
$\sigma_\phi, \sigma_\theta = \frac{N_\phi}{t}, \frac{N_\theta}{t}$	$\sigma_\phi, \sigma_\theta = \frac{N_\phi}{t}, \frac{N_\theta}{t}$
$w = -\frac{\rho a^3}{6Et}\left[3\left(1 + \frac{h}{a}\right)(1-\mu) - 6\cos\phi - \frac{2(1+\mu)}{\sin^2\phi}(\cos^3\phi - 1)\right]$	$w = \frac{\rho a^3}{6Et}\left[3\left(1 + \frac{h}{a}\right)(1-\mu) - 6\cos\phi - \frac{2(1+\mu)}{\sin^2\phi}(\cos^3\phi - 1)\right]$
$\bar{w} = w\sin\phi$	$\bar{w} = w\sin\phi$
$\bar{u} = w\cos\phi$	$\bar{u} = w\cos\phi$

Table B7.1.2.1 - 3 (Continued). Hydrostatic Pressure Loading (Partial) Membrane Stress Resultants, Closed Spherical Domes

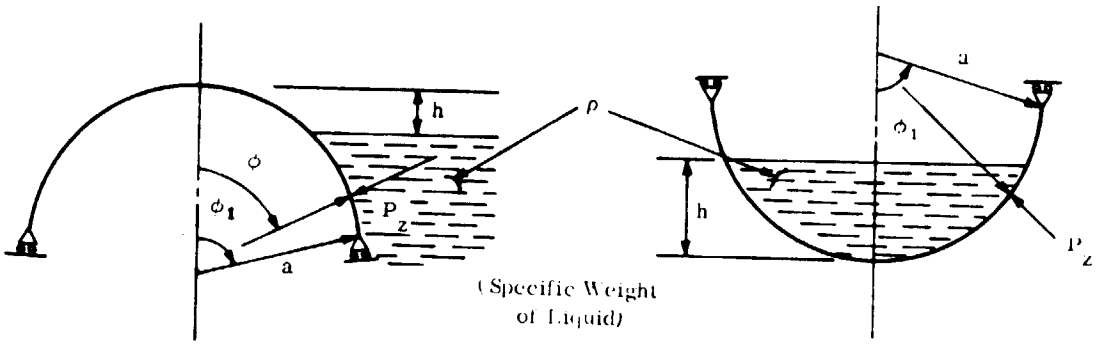

$P_z = \rho(a - a\cos\phi - h)$

$\phi' = 180 - \phi$

$P_z = -\rho(a - a\cos\phi' - h)$

Regular	Inverted
(Above Liquid Level)	(Above Liquid Level)
$N_\phi = N_\theta = 0$	$N_\phi = \frac{\rho h^2}{6}\left(3 - \frac{h}{a}\right)\frac{1}{\sin^2\phi'}$ $N_\theta = -\frac{\rho h^2}{6}\left(3 - \frac{h}{a}\right)\frac{1}{\sin^2\phi'}$
(Below Liquid Level)	(Below Liquid Level)
$N_\phi = -\frac{\rho a^2}{6}\left\{\frac{h}{a}\left[\frac{h}{a\sin^2\phi}\left(3 - \frac{h}{a}\right) - 3\right] - 1 - \frac{2\cos^2\phi}{1 + \cos\phi}\right\}$	$N_\phi = \frac{\rho a^2}{6}\left[\frac{3h}{a} - 1 - \frac{2\cos^2\phi'}{1 + \cos\phi'}\right]$
$N_\theta = -\frac{\rho a^2}{6}\left[1 - \cos\phi - \frac{h}{a}\right] - N_\phi$	$N_\theta = \rho a^2\left[\frac{h}{a} - 1 + \cos\phi'\right] - N_\phi$
$\sigma_\phi = \frac{N_\phi}{t}$, $\sigma_\theta = \frac{N_\theta}{t}$	$\sigma_\phi = \frac{N_\phi}{t}$, $\sigma_\theta = \frac{N_\theta}{t}$
For Deflections See Section B7.1.1.4 - IV	For Deflections See Section B7.1.1.4 - IV

Table B7.1.2.1 - 3 (Concluded). Hydrostatic Pressure Loading
Membrane Stresses and Deformations, Open Spherical Domes

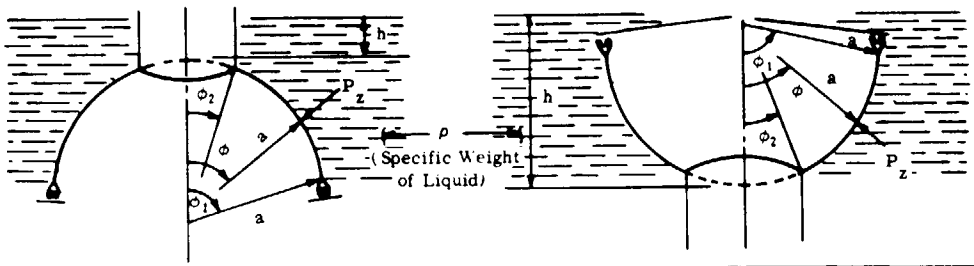

Regular	Inverted
$N_\phi = -\frac{\rho a^2}{6}\left[3\left(1+\frac{h}{a}\right)\left(1-\frac{\sin^2\phi_2}{\sin^2\phi}\right) - 2\left(\frac{\cos^3\phi_2 - \cos^3\phi}{\sin^2\phi}\right)\right]$	$N_\phi = \frac{\rho a^2}{6}\left[3\left(1-\frac{h}{a}\right)\left(1-\frac{\sin^2\phi_2}{\sin^2\phi}\right) - 2\left(\frac{\cos^3\phi_2 - \cos^3\phi}{\sin^2\phi}\right)\right]$
$N_\theta = -\frac{\rho a^2}{6}\left[3\left(1+\frac{h}{a}\right)\left(1+\frac{\sin^2\phi_2}{\sin^2\phi}\right) - \frac{2(2\cos^3\phi + \cos^3\phi_2) - 6\cos\phi}{\sin^2\phi}\right]$	$N_\theta = \frac{\rho a^2}{6}\left[3\left(1-\frac{h}{a}\right)\left(1+\frac{\sin^2\phi_2}{\sin^2\phi}\right) + \frac{2(2\cos^3\phi + \cos^3\phi_2) - 6\cos\phi}{\sin^2\phi}\right]$
$\sigma_\phi, \sigma_\theta = \frac{N_\phi}{t}, \frac{N_\theta}{t}$	$\sigma_\phi, \sigma_\theta = \frac{N_\phi}{t}, \frac{N_\theta}{t}$
$w = -\frac{\rho a^3}{6Et}\left\{3\left(1+\frac{h}{a}\right)\left[1-\mu+(1+\mu)\frac{\sin^2\phi_2}{\sin^2\phi}\right] - 6\cos\phi + 2(1+\mu)\frac{\cos^3\phi_2 - \cos^3\phi}{\sin^2\phi}\right\}$	$w = \frac{\rho a^3}{6Et}\left\{3\left(1+\frac{h}{a}\right)\left[1-\mu+(1+\mu)\frac{\sin^2\phi_2}{\sin^2\phi}\right] - 6\cos\phi + 2(1+\mu)\frac{\cos^3\phi_2 - \cos^3\phi}{\sin^2\phi}\right\}$
$\bar{w} = w\sin\phi$	$\bar{w} = w\sin\phi$
$\bar{u} = w\cos\phi$	$\bar{u} = w\cos\phi$

Table B7.1.2.1 - 4. Uniform Pressure Loading
Membrane Stresses and Deformations, Closed Spherical Domes

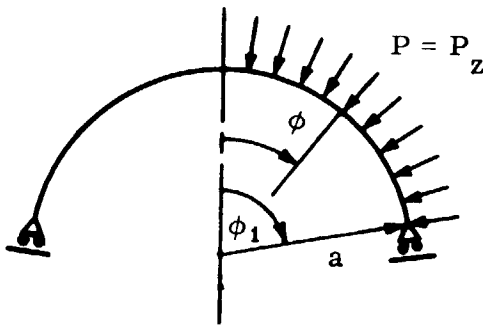

$P_\phi = P_\theta = 0$

Uniform Pressure Loading

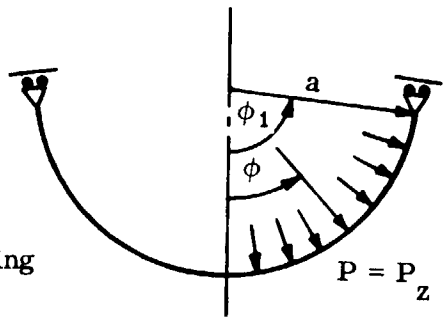

Regular	Inverted
$N_\phi = -\frac{ap}{2}$	$N_\phi = \frac{ap}{2}$
$N_\theta = -\frac{ap}{2}$	$N_\theta = \frac{ap}{2}$
$\sigma_\phi = \sigma_\theta = \frac{N_\phi}{t} = \frac{N_\theta}{t}$	$\sigma_\phi = \sigma_\theta = \frac{N_\phi}{t} = \frac{N_\theta}{t}$
$w = -\frac{a^2p}{2Et}(1-\mu)$	$w = \frac{a^2p}{2Et}(1-\mu)$
$\bar{w} = -\frac{a^2p}{2Et}\sin\phi\,(1-\mu)$	$\bar{w} = \frac{a^2p}{2Et}\sin\phi\,(1-\mu)$
$\bar{u} = -\frac{a^2p}{2Et}\cos\phi\,(1-\mu)$	$\bar{u} = \frac{a^2p}{2Et}\cos\phi\,(1-\mu)$

Table B7.1.2.1 - 4 (Concluded). Uniform Pressure Loading
Membrane Stresses and Deformations, Open Spherical Shells

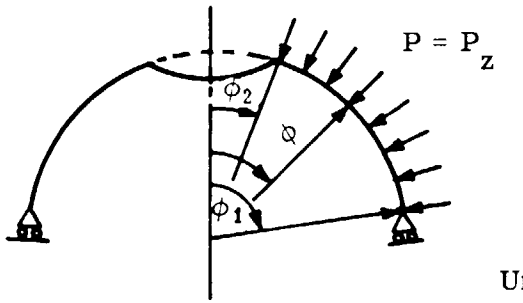

$P_\phi = P_\theta = 0$

Uniform Pressure Loading

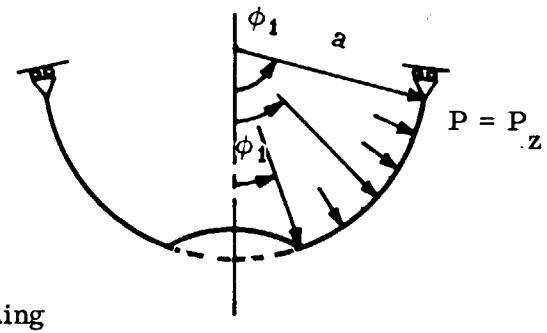

Regular	Inverted
$N_\phi = -\frac{ap}{2}\left(1 - \frac{\sin^2\phi_2}{\sin^2\phi}\right)$	$N_\phi = \frac{ap}{2}\,1\left(-\frac{\sin^2\phi_2}{\sin^2\phi}\right)$
$N_\theta = -\frac{ap}{2}\left(1 + \frac{\sin^2\phi_2}{\sin^2\phi}\right)$	$N_\theta = \frac{ap}{2}\left(1 + \frac{\sin^2\phi_2}{\sin^2\phi}\right)$
$\sigma_\phi, \sigma_\theta = \frac{N_\phi}{t}, \frac{N_\theta}{t}$	$\sigma_\phi, \sigma_\theta = \frac{N_\phi}{t}, \frac{N_\theta}{t}$
$w = -\frac{a^2p}{Et}\left[1 - \frac{1+\mu}{2}\left(1 - \frac{\sin^2\phi_2}{\sin^2\phi}\right)\right]$	$w = \frac{a^2p}{Et}\left[1 - \frac{1+\mu}{2}\left(1 - \frac{\sin^2\phi_2}{\sin^2\phi}\right)\right]$
$\bar{w} = w\sin\phi$	$\bar{w} = w\sin\phi$
$\bar{u} = w\cos\phi$	$\bar{u} = w\cos\phi$

Table B7.1.2.1 - 5. Lantern Loading
Membrane Stresses and Deflections, Open Spherical Domes

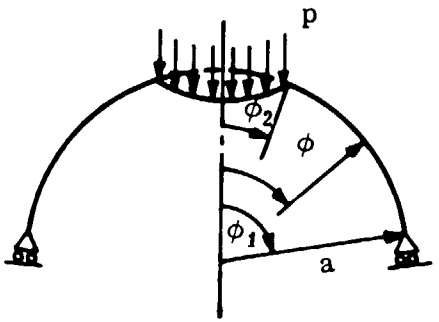

$$P_z = P_\phi = P_\theta = 0$$

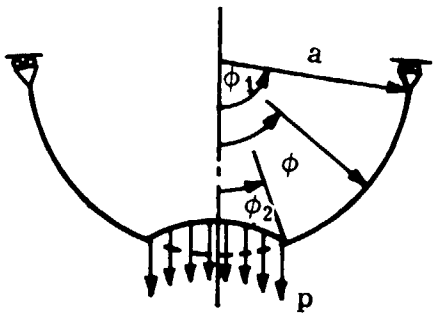

Lantern Loading

Regular	Inverted
$N_\phi = -\frac{p \sin\phi_2}{\sin^2\phi}$	$N_\phi = \frac{p \sin\phi_2}{\sin^2\phi}$
$N_\theta = \frac{p \sin\phi_2}{\sin^2\phi}$	$N_\theta = -\frac{p \sin\phi_2}{\sin^2\phi}$
$\sigma_\phi , \sigma_\theta = \frac{N_\phi}{t} , \frac{N_\theta}{t}$	$\sigma_\phi , \sigma_\theta = \frac{N_\phi}{t} , \frac{N_\theta}{t}$
$w = \frac{ap}{Et}\left(\frac{1+\mu}{\sin\phi}\right)$	$w = -\frac{ap(1+\mu)}{Et}\left(\frac{\sin\phi_2}{\sin^2\phi}\right)$
$\bar{w} = \frac{ap}{Et}(1+\mu)$	$\bar{w} = -\frac{ap}{Et}(1+\mu)\left(\frac{\sin\phi_2}{\sin\phi}\right)$
$\bar{u} = \frac{ap}{Et}(1+\mu)\cot\phi$	$\bar{u} = -\frac{ap}{Et}(1+\mu)\left(\frac{\sin\phi_2}{\sin\phi}\right)\cot\phi$

B7.1.2.2 ELLIPTICAL DOMES

This subsection presents the solutions for elliptical shells exposed to axisymmetric loadings. Only closed elliptical shells are considered. The boundaries of the elliptical shell must be free to rotate and deflect normal to the shell middle surface. Abrupt changes in the shell thickness must not be present. The following loading conditions will be considered: uniform pressure (Table B7.1.2.2 - 1); stress resultant and displacement parameters (Figs. B7.1.2.2 - 1 and -2); dead weight (Table B7.1.2.2 - 2); and uniform load over base area (Table B7.1.2.2 - 3). These tables begin on page 42.

Table B7.1.2.2 - 1. Uniform Pressure Loading
Membrane Stresses and Deflections, Closed Ellipsoidal Dome

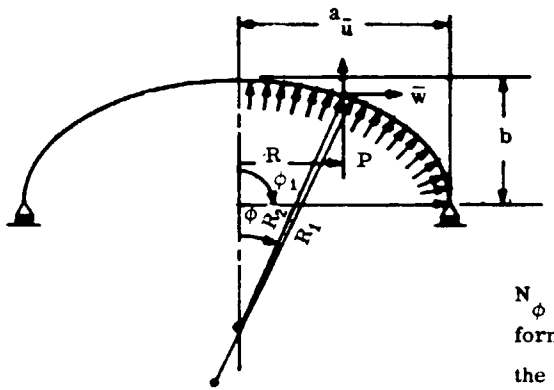

Uniform Pressure

$P_\phi = P_\theta = 0$

$P_z = P$

$$R_1 = \frac{a^2b^2}{(a^2\sin^2\phi + b^2\cos^2\phi)^{3/2}}$$

$$R_2 = \frac{a^2}{(a^2\sin^2\phi + b^2\cos^2\phi)^{1/2}}$$

N_ϕ and N_θ are plotted in nondimensional form in Figure B7.1.2.2 - 1 according to the following equations

$$N_\phi = \frac{R_2 p}{2}$$

$$N_\theta = \frac{R_2 p}{2}\left(2 - \frac{R_2}{R_1}\right)$$

$$\bar{w} = \frac{p R_2^2 \sin\phi}{2Et}\left[2 - \mu - \frac{R_1}{R_2}\right]$$

$$\bar{u} = \frac{a^2 p}{4Et}\left\{\left[3\left(\frac{a}{b}\right)^2 - 1 - 2\mu\right]\left[\frac{\cos\phi}{1 + K^2\sin^2\phi}\right] - 2\left(\frac{a}{b}\right)^2\cos\phi + \frac{bK}{a}\left[\left(\frac{a}{b}\right)^2 - \frac{1}{2} + \mu\right]\mathrm{Ln}\left[\frac{\frac{a}{b} + K\cos\phi}{\frac{a}{b} - K\cos\phi}\right]\right\}$$

Let $K = \sqrt{\left(\frac{a}{b}\right)^2 - 1}$

$$\frac{N_\phi}{ap} = \frac{a}{2b}\left\{1 - \left(\frac{R}{a}\right)^2\left[1 - \left(\frac{b}{a}\right)^2\right]\right\}^{-1/2}$$

$$\frac{N_\theta}{ap} = \frac{N_\phi}{a}\left\{2 - \frac{1}{1 - \left(\frac{R}{a}\right)^2\left[1 - \left(\frac{b}{a}\right)^2\right]}\right\}$$

$\bar{w}$ and $\bar{u}$ are plotted in nondimensional form in Figure B7.1.2.2 - 2, for t = constant and $\mu = 0.3$

$w = \bar{w}\sin\phi - \bar{u}\cos\phi$ $\qquad$ $u = \bar{w}\cos\phi + \bar{u}\sin\phi$

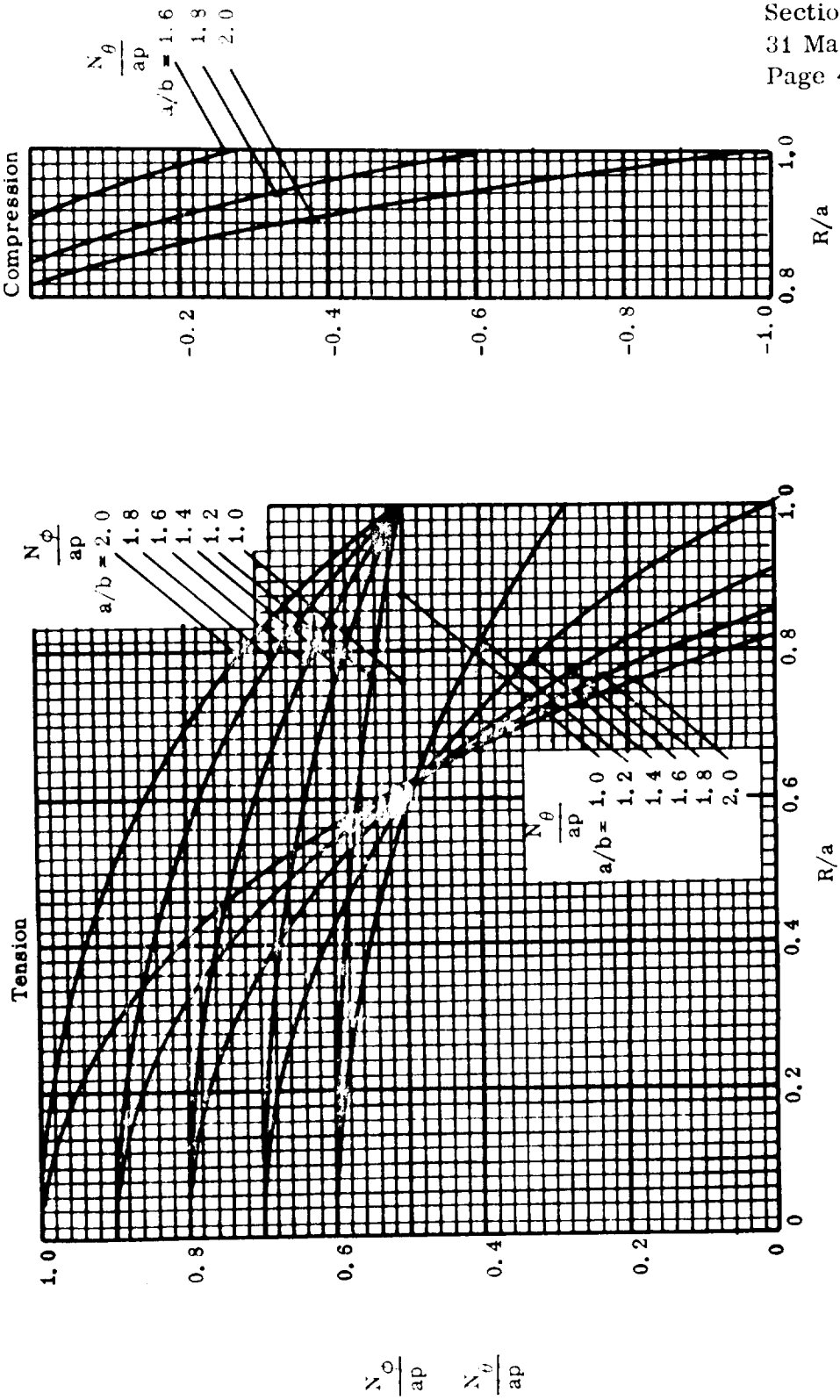

Fig. B7.1.2.2 - 1. Stress Resultant Parameters, Ellipsoidal Shell, Uniform Pressure

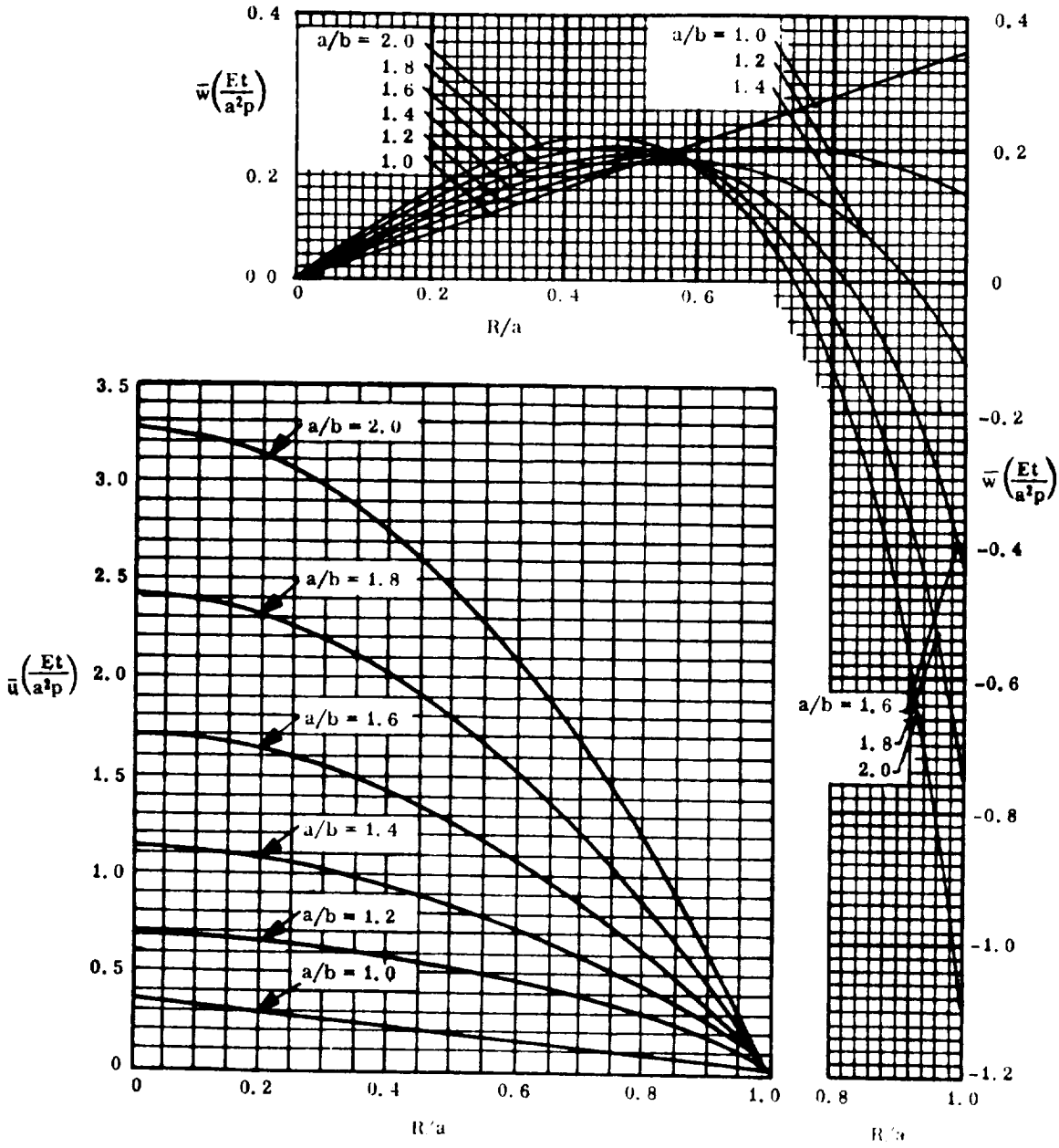

Figure B7.1.2.2 - 2. Displacement Parameters, Ellipsoidal Shells, Uniform Pressure

Table B7.1.2.2 - 2. Dead Weight Loading
Membrane Stress Resultants, Closed Ellipsoidal Dome

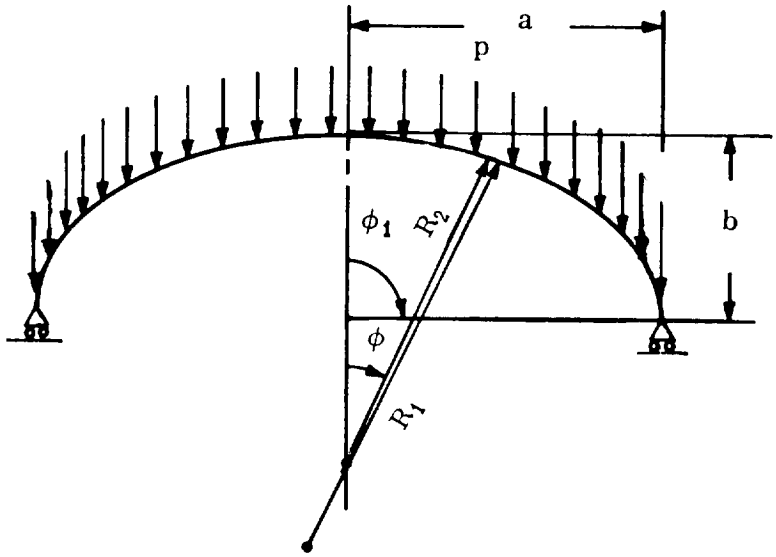

Dead Weight Loading

$P_\theta = 0$

$P_\phi = p\sin\phi$

$P_t = p\cos\phi$

Let $K = \sqrt{\dfrac{a^2 - b^2}{a}}$

$$N_\phi = -\frac{p}{2}\left[\frac{\sqrt{a^2\tan^2\phi + b^2}}{a^2\sin\phi\tan\phi}\right]\left[a^2 - \frac{a^2b^2\sqrt{1+\tan^2\phi}}{b^2 + a^2\tan^2\phi} + \frac{b^2}{K}\,\mathrm{Ln}\,\frac{(1+K)\sqrt{b^2 + a^2\tan^2\phi}}{b\,(K + \sqrt{1+\tan^2\phi})}\right]$$

$$N_\theta = p\left[\frac{(b^2 + a^2\tan^2\phi)^{3/2}}{2\tan^2\phi\sqrt{1+\tan^2\phi}}\left(\frac{1}{Ka^2}\,\mathrm{Ln}\,\frac{(1+K)\sqrt{b^2 + a^2\tan^2\phi}}{b\,(K + \sqrt{1+\tan^2\phi})} + \frac{1}{b^2} - \frac{\sqrt{1+\tan^2\phi}}{b^2 + a^2\tan^2\phi}\right) - \frac{a^2}{\sqrt{b^2 + a^2\tan^2\phi}}\right]$$

$$\sigma_\phi\,,\ \sigma_\theta = \frac{N_\phi}{t}\,,\ \frac{N_\theta}{t}$$

For deflections, refer to Section B7.1.1.4.

Table B7.1.2.2 - 3. Uniform Load over Base Area
Membrane Stress Resultants, Closed Ellipsoidal Dome

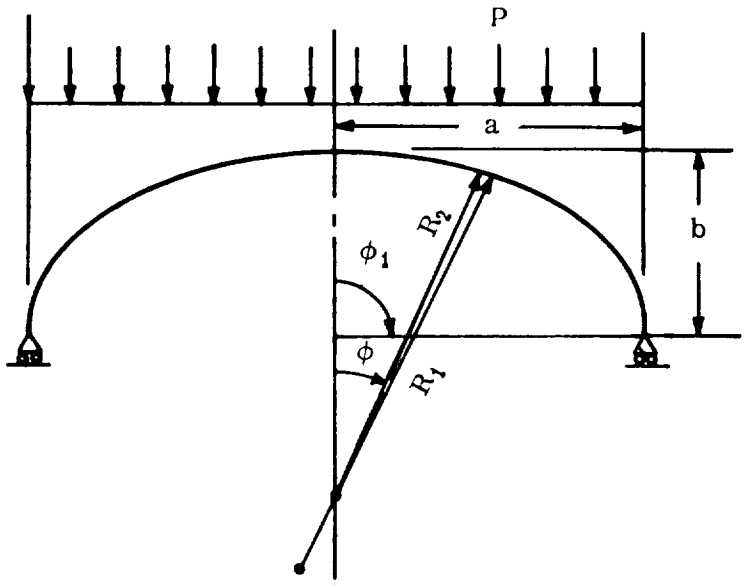

Uniform Loading over Base Area

$P_\theta = 0$

$P_\phi = p \sin\phi \cos\phi$

$P_z = p \cos^2\phi$

$$N_\phi = -\frac{P}{2} \frac{a^2\sqrt{1 + \tan^2\phi}}{\sqrt{b^2 + a^2\tan^2\phi}}$$

$$N = -\frac{a^2 p}{2b^2} \frac{b^2 - a^2\tan^2\phi}{\sqrt{b^2 + a^2\tan^2\phi}\sqrt{1 + \tan^2\phi}}$$

$$\sigma_\phi, \sigma_\theta = \frac{N_\phi}{t}, \frac{N_\theta}{t}$$

For deflections, refer to Section B7.1.1.4.

B7.1.2.3 CASSINI DOMES

This family of shells is useful as bulkheads. The equation of the Cassinian curve as a meridian (see Table B7.1.2.3 - 1) is

$$(r^2 + z^2)^2 + 2a^2(r^2 - z^2) = 3a^4 \quad .$$

The useful property of this shell (zero curvature at $z = 0$, $r = a$) is preserved by making the substitution nz for z, where $n > 1$ but not much greater than 2.

$$(r^2 + n^2z^2)^2 + 2a^2(r^2 - n^2z^2) = 3a^4$$

$$R_1 = \frac{2\left[\, r^2(a^2 + n^2z^2) + n^4z^2(a^2 - r^2)\,\right]^{3/2}}{3n^2a^3(a^2 - r^2 + n^2z^2)}$$

$$R_2 = \frac{2a\left[\, r^2(a^2 + n^2z^2) + n^4z^2(a^2 - r^2)\,\right]^{1/2}}{a^2 + r^2 + n^2z^2}$$

This subsection presents solutions for the Cassini dome subjected to uniform pressure loading. Only a closed dome will be considered. The boundaries of the shell must be free to rotate and to deflect normal to the shell middle surface. No abrupt discontinuities in the shell thickness shall be present. Because of the limited usefulness of this shell, a detailed solution is presented for $n = 2$. Nondimensional plots are presented for N_ϕ and N_θ according to the following equations:

$$\frac{N_\phi}{ap} = \frac{2}{5(4K + 3)}\left[5(16K^4 + 24K^3 - 7K^2 + 8K + 3)\right]^{1/2}$$

$$\frac{N_\theta}{ap} = \frac{4(64K^5 + 144K^4 + 44K^3 - 85K^2 - 36K + 23)}{(4K + 3)^2\left[5(16K^4 + 24K^3 - 7K^2 + 8K + 3)\right]^{1/2}}$$

where $K = \left[1 - \frac{15}{16}\left(\frac{R}{a}\right)^2\right]^{1/2}$

Nondimensional plots are also provided for $\bar{w}$ and $\bar{u}$ for t = constant and $\mu = 0.3$.

Table B7.1.2.3 - 1. Uniform Pressure Loading
Membrane Stresses and Deflections, Closed Cassini Dome

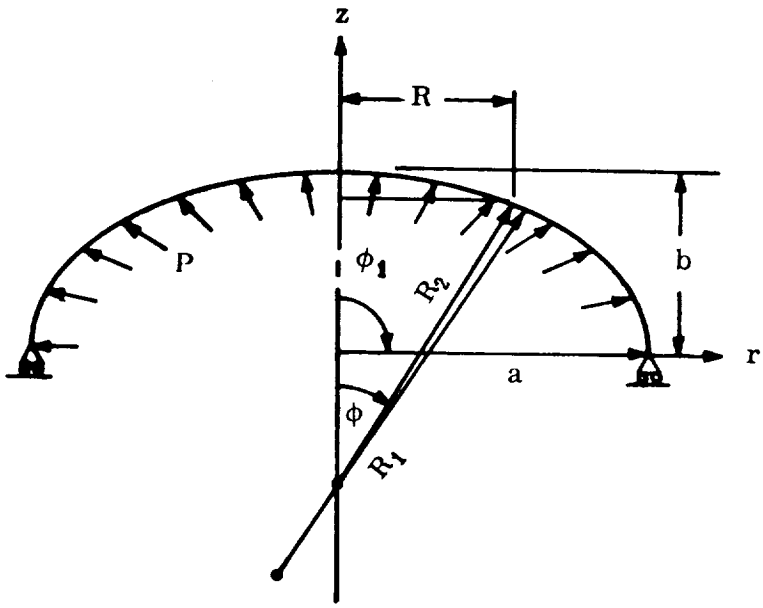

Special Case, n = 2

$$b = \frac{a}{2}\sqrt{\frac{11}{5}}$$

Uniform Pressure Loading

$$P_\phi = P_\theta = 0$$

$$P_z = p$$

$$N_\phi = \frac{R_2 p}{2}$$

$$N_\theta = \frac{R_2 p}{2}\left(2 - \frac{R_2}{R_1}\right)$$

$$\sigma_\phi , \sigma_\theta = \frac{N_\phi}{t} , \frac{N_\theta}{t}$$

$$\bar{w} = \frac{pR_2^2 \sin\phi}{2Et}\left(2 - \mu - \frac{R_2}{R_1}\right)$$

$$\bar{u} = \bar{w}\cot\phi - \int \frac{R_1(N_\phi - \mu N_\theta) - R_2(N_\theta - \mu N_\phi)}{Et\sin\phi} d\phi + C$$

$$w = \bar{w}\sin\phi - \bar{u}\cos\phi$$

$$u = \bar{w}\cos\phi + \bar{u}\sin\phi$$

Equations for R_1 and R_2 are given in Section B7.1.2.3 .
See Figure B7.1.2.3 - 1 for nondimensional plots of N_ϕ and N_θ .
See Figure B7.1.2.3 - 2 for nondimensional plots of $\bar{w}$ and $\bar{u}$.

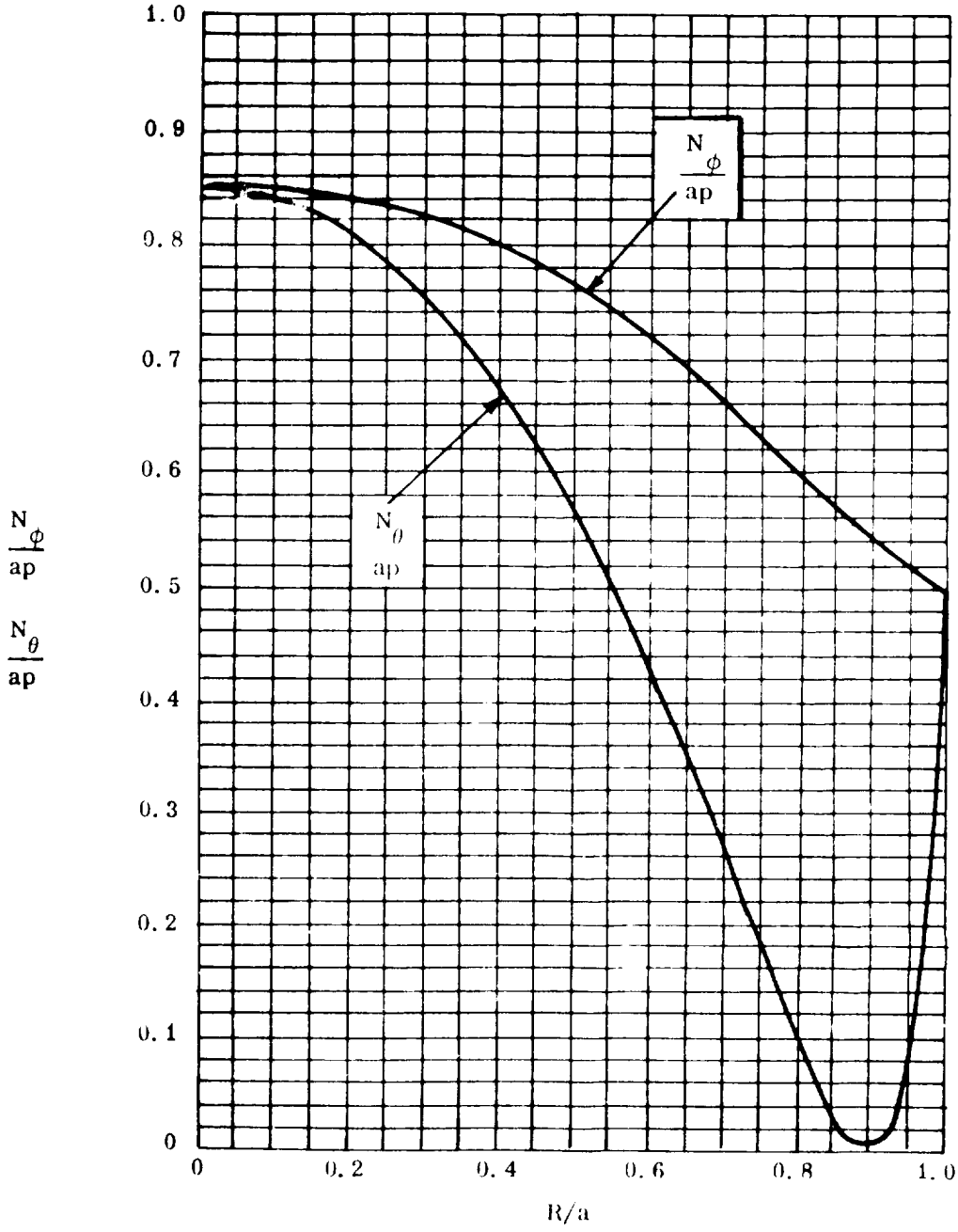

Fig. B7.1.2.3 - 1. Stress Resultant Parameters
Cassini Shells (n = 2), Uniform Pressure

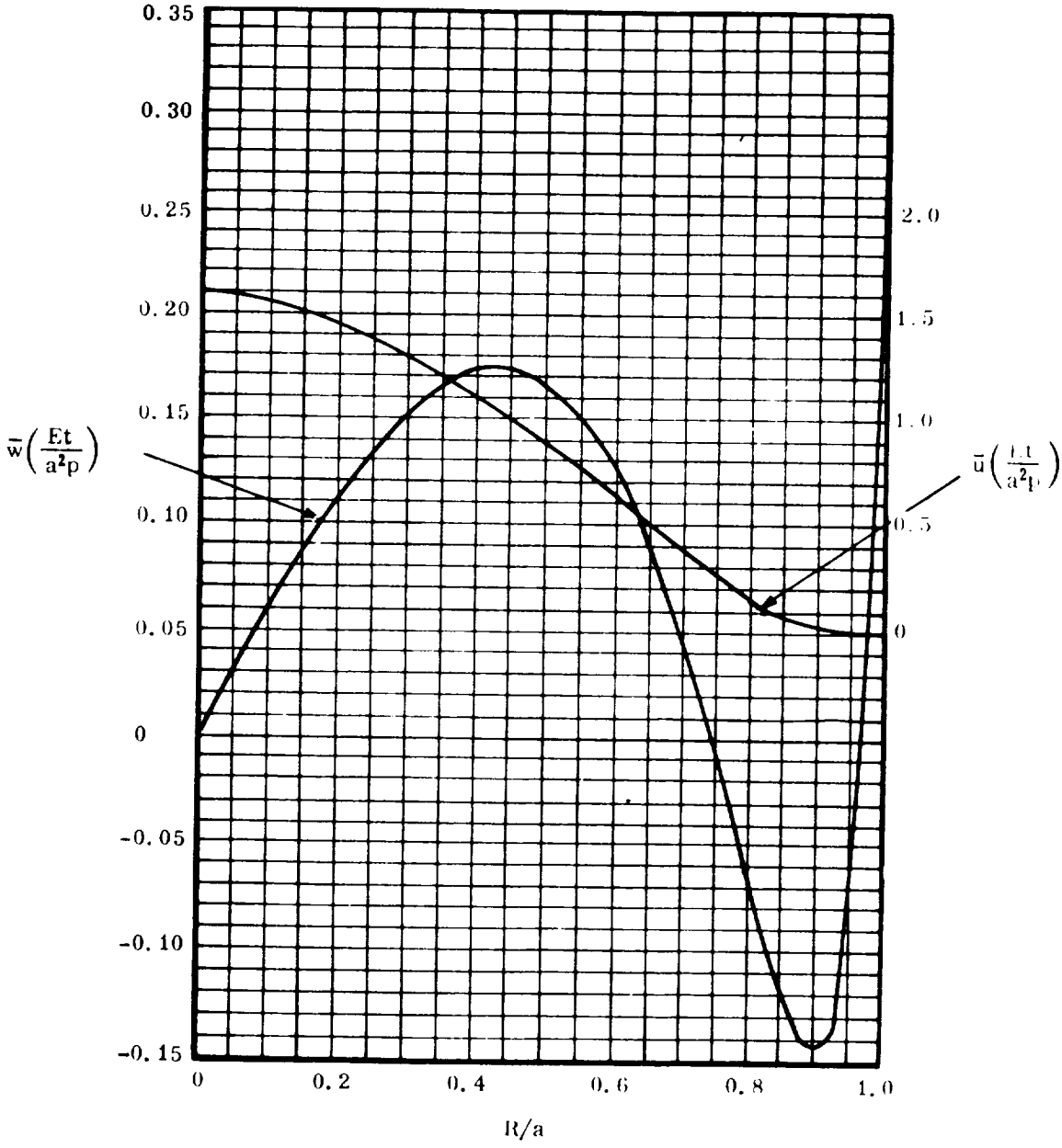

Fig. B7.1.2.3 - 2. Displacement Parameters
Cassini Shells (n = 2), Uniform Pressure

B7.1.2.4 CONICAL DOMES

This subsection presents the solutions for nonshallow conical shells exposed to axisymmetric loading. Both closed and open shells will be considered. The boundaries of the shell must be free to rotate and deflect normal to the shell middle surface. No abrupt discontinuities in the shell thickness shall be present.

Note the special geometry of the conical shell:

$\phi = \alpha =$ constant, $R_1 = \infty$

$R = x\cos\phi$ (Figure B7.1.2.4 - 1)

For convenience, solutions are presented in terms of x instead of R. All other notations are standard for shells of revolution as used in this chapter.

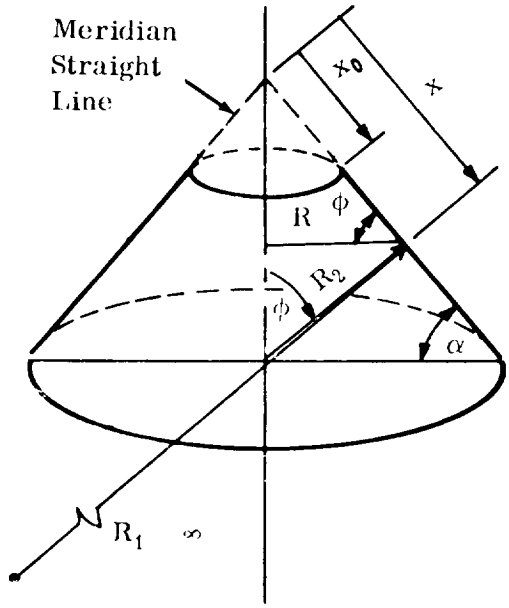

Fig. B7.1.2.4 - 1. Conical Shell Geometry

The following loading conditions will be considered: dead weight loading (Table B7.1.2.4 - 1); uniform loading over base area (Table B7.1.2.4 - 2); hydrostatic pressure loading (Table B7.1.2.4 - 3); uniform pressure loading (Table B7.1.2.4 - 4); and lantern loading (Table B7.1.2.4 - 5). These tables begin on page 53.

Table B7.1.2.4 - 1. Dead Weight Loading
Membrane Stresses and Deflections, Closed Conical Domes

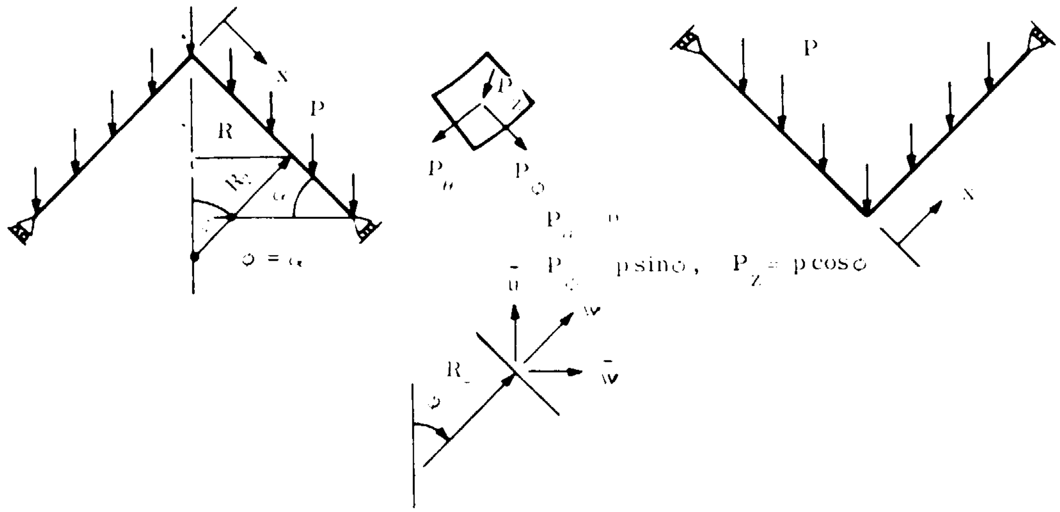

Regular		Inverted	
N_ϕ	$= -\dfrac{px}{2\sin\phi}$	N_ϕ	$= \dfrac{px}{2\sin\phi}$
N_θ	$= -\dfrac{px\cos^2\phi}{\sin\phi}$	N_θ	$= \dfrac{px\cos^2\phi}{\sin\phi}$
$\sigma_\phi, \sigma_\theta$	$= \dfrac{N_\phi}{t}, \dfrac{N_\theta}{t}$	$\sigma_\phi, \sigma_\theta$	$= \dfrac{N_\phi}{t}, \dfrac{N_\theta}{t}$
w	$= -\dfrac{px^2\cot\phi}{Et\sin\phi}\left(\cos^2\phi - \dfrac{\mu}{2}\right)$	w	$= \dfrac{px^2\cot\phi}{Et\sin\phi}\left(\cos^2\phi - \dfrac{\mu}{2}\right)$
$\bar{w}$	$= -\dfrac{px^2\cot\phi}{Et}\left(\cos^2\phi - \dfrac{\mu}{2}\right)$	$\bar{w}$	$= \dfrac{px^2\cot\phi}{Et}\left(\cos^2\phi - \dfrac{\mu}{2}\right)$
$\bar{u}$	$= -\dfrac{px^2\cos\phi\cot\phi}{Et}\left(\cos^2\phi - \dfrac{\mu}{2}\right)$	$\bar{u}$	$= \dfrac{px^2\cos\phi\cot\phi}{Et}\left(\cos^2\phi - \dfrac{\mu}{2}\right)$

Table B7.1.2.4 - 1 (Concluded). Dead Weight Loading
Membrane Stresses and Deflections, Open Conical Domes

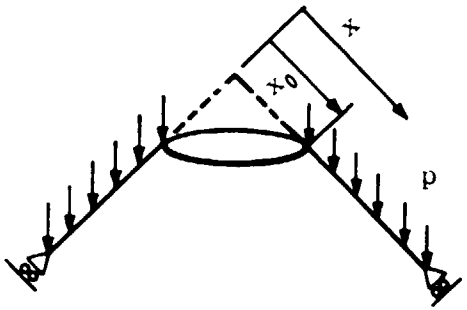

$$P_\theta = 0$$
$$P_\phi = p\sin\phi$$
$$P_z = p\cos\phi$$

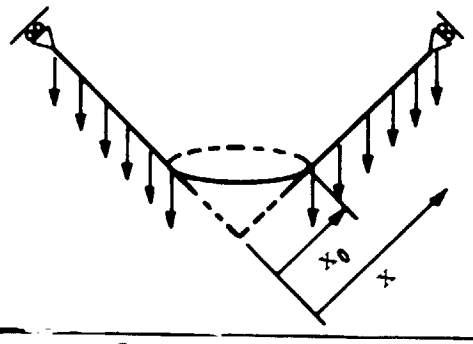

Regular	Inverted
$N_\phi = -\frac{p}{2\sin\phi}\left(\frac{x^2 - x_0^2}{x}\right)$	$N_\phi = \frac{p}{2\sin\phi}\left(\frac{x^2 - x_0^2}{x}\right)$
$N_\theta = -\frac{px\cos^2\phi}{\sin\phi}$	$N_\theta = \frac{px\cos^2\phi}{\sin\phi}$
$\sigma_\phi, \sigma_\theta = \frac{N_\phi}{t}, \frac{N_\theta}{t}$	$\sigma_\phi, \sigma_\theta = \frac{N_\phi}{t}, \frac{N_\theta}{t}$
$w = -\frac{px^2\cot\phi}{2Et\sin\phi}\left[2\cos^2\phi - \mu\left(\frac{x^2 - x_0^2}{x^2}\right)\right]$	$w = \frac{px\cot\phi}{2Et\sin\phi}\left[2\cos^2\phi - \mu\left(\frac{x^2 - x_0^2}{x^2}\right)\right]$
$\bar{w} = w\sin\phi$	$\bar{w} = w\sin\phi$
$\bar{u} = w\cos\phi$	$\bar{u} = w\cos\phi$

Table B7.1.2.4 - 2. Uniform Loading over Base Area
Membrane Stresses and Deflections, Closed Conical Domes

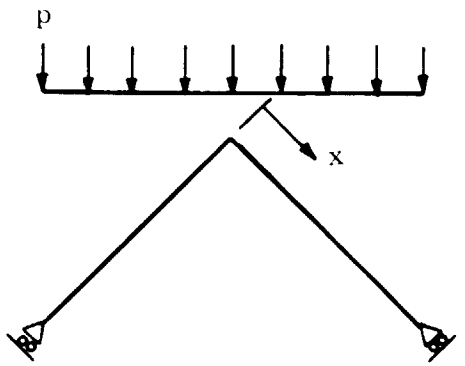

$P_\theta = 0$

$P_\phi = p \sin\phi \cos\phi$

$P_z = p \cos^2\phi$

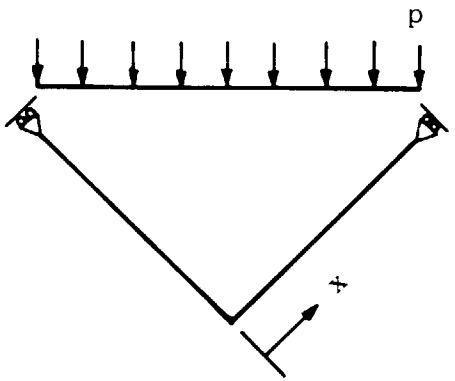

Regular	Inverted
$N_\phi = -\frac{px\cot\phi}{2}$	$N_\phi = \frac{px\cot\phi}{2}$
$N_\theta = -\frac{px\cos^3\phi}{\sin\phi}$	$N_\theta = \frac{px\cos^3\phi}{\sin\phi}$
$\sigma_\phi, \sigma_\theta = \frac{N_\phi}{t}, \frac{N_\theta}{t}$	$\sigma_\phi, \sigma_\theta = \frac{N_\phi}{t}, \frac{N_\theta}{t}$
$w = -\frac{px^2}{Et}\cot^2\phi\left(\cos^2\phi - \frac{\mu}{2}\right)$	$w = \frac{px^2}{Et}\cot^2\phi\left(\cos^2\phi - \frac{\mu}{2}\right)$
$\bar{w} = w\sin\phi$	$\bar{w} = w\sin\phi$
$\bar{u} = w\cos\phi$	$\bar{u} = w\cos\phi$

Table B7.1.2.4 - 2 (Concluded). Uniform Loading over Base Area
Membrane Stresses and Deflections, Open Conical Domes

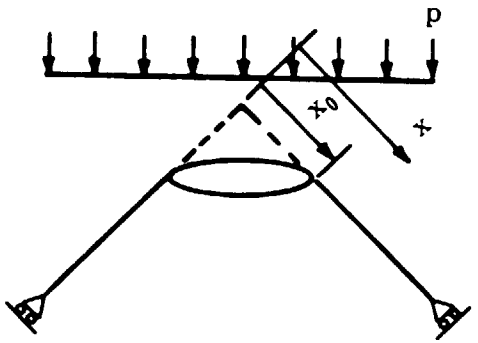

$P_\theta = 0$

$P_\phi = p \sin\phi \cos\phi$

$P_z = p \cos^2\phi$

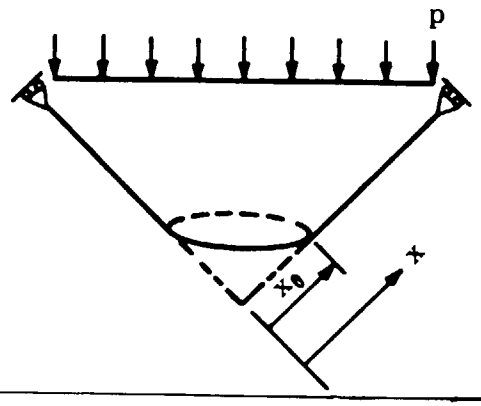

Regular	Inverted
$N_\phi = -\frac{p \cot\phi}{2} \frac{x^2 - x_0^2}{x}$	$N_\phi = \frac{p \cot\phi}{2} \left(\frac{x^2 - x_0^2}{x} \right)$
$N_\theta = -\frac{px \cos^3\phi}{\sin\phi}$	$N_\theta = \frac{px \cos^3\phi}{\sin\phi}$
$\sigma_\phi , \sigma_\theta = \frac{N_\phi}{t} , \frac{N_\theta}{t}$	$\sigma_\phi , \sigma_\theta = \frac{N_\phi}{t} , \frac{N_\theta}{t}$
$w = -\frac{px^2}{2Et} \cot^2\phi \left[2\cos^2\phi - \mu \left(\frac{x^2 - x_0^2}{x^2} \right) \right]$	$w = \frac{px^2}{2Et} \cot^2\phi \left[2\cos^2\phi - \mu \frac{x^2 - x_0^2}{x^2} \right]$
$\bar{w} = w \sin\phi$	$\bar{w} = w \sin\phi$
$\bar{u} = w \cos\phi$	$\bar{u} = w \cos\phi$

Table B7.1.2.4 - 3. Hydrostatic Pressure Loading
Membrane Stresses and Deflections, Closed Conical Domes

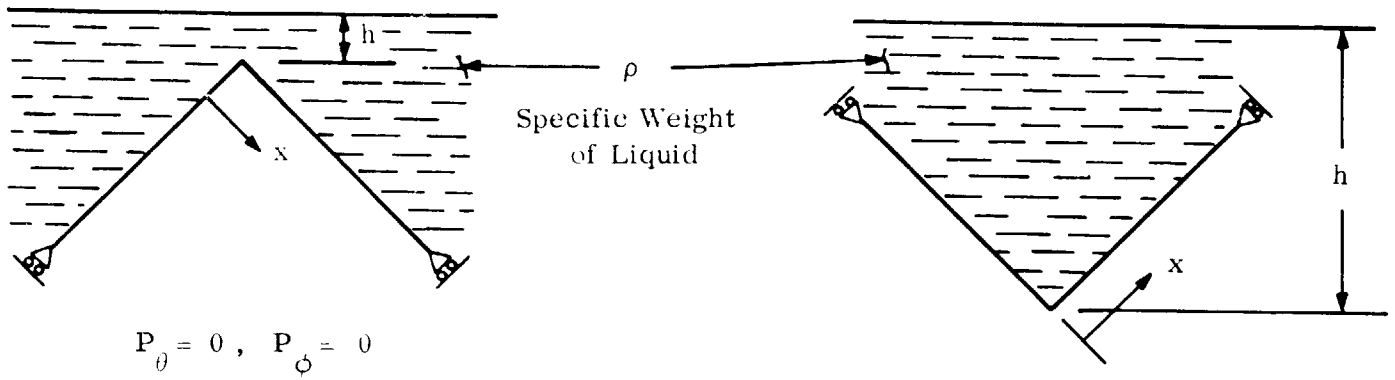

$P_\theta = 0\ ,\quad P_\phi = 0$

$P_z = \rho(h + x\sin\phi)$

$P_\theta = P_\phi = 0$

$P_z = \rho(h - x\sin\phi)$

Regular	Inverted
$N_\phi = -\rho x\cos\phi\left(\frac{h}{2\sin\phi} - \frac{x}{3}\right)$	$N_\phi = -\rho x\cos\phi\left(\frac{x}{3} - \frac{h}{2\sin\phi}\right)$
$N_\theta = -\rho x\cos\phi\left(\frac{h}{\sin\phi} - x\right)$	$N_\theta = -\rho x\cos\phi\left(x - \frac{h}{\sin\phi}\right)$
$\sigma_\phi = \frac{N_\phi}{t}\ ,\quad \sigma_\theta = \frac{N_\theta}{t}$	$\sigma_\phi = \frac{N_\phi}{t}\ ,\quad \sigma_\theta = \frac{N_\theta}{t}$
$w = \frac{\rho x^2}{Et}\cos\phi\cot\phi\left[\frac{h}{\sin\phi}\left(\frac{\mu}{2} - 1\right) - x\left(\frac{\mu}{3} - 1\right)\right]$	$w = \frac{\rho x^2}{Et}\cos\phi\cot\phi\left[x\left(\frac{\mu}{3} - 1\right) - \frac{h}{\sin\phi}\left(\frac{\mu}{2} - 1\right)\right]$
$u = w\sin\phi$	$u = w\sin\phi$
$v = w\cos\phi$	$v = w\cos\phi$

Table B7.1.2.4 - 3 (Continued). Hydrostatic Pressure Loading
Membrane Stresses and Deflections, Closed Conical Domes

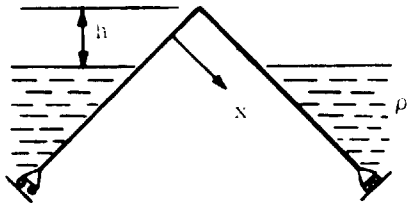

ρ = Specific Weight of Liquid

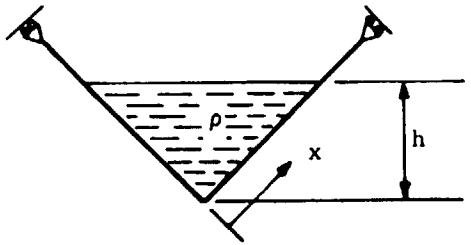

$P_\theta = P_\phi = 0$

$P_z = \rho(x \sin\phi - h)$

$P_\theta = P_\phi = 0$

$P_z = \rho(h - x \sin\phi)$

Regular	Inverted
(Above Liquid Level)	(Above Liquid Level)
$N_\phi = 0$	$N_\phi = \frac{\rho h^3 \cot\phi}{6x \sin^2\phi}$
(Below Liquid Level)	(Below Liquid Level)
$N_\phi = -\frac{\rho}{6x}\left[\frac{h^3 \cot\phi}{\sin^2\phi} + x^2(2x\cos\phi - 3h\cot\phi)\right]$	$N_\phi = \frac{\rho x}{2}(3h\cot\phi - 2x\cos\phi)$
(Above Liquid Level)	(Above Liquid Level)
$N_\theta = 0$	$N_\theta = 0$
(Below Liquid Level)	(Below Liquid Level)
$N_\theta = -\rho x(x\cos\phi - h\cot\phi)$	$N_\theta = \rho x(h\cot\phi - x\cos\phi)$
$\sigma_\phi, \sigma_\theta = \frac{N_\phi}{t}, \frac{N_\theta}{t}$	$\sigma_\phi, \sigma_\theta = \frac{N_\phi}{t}, \frac{N_\theta}{t}$
For Deflections, see Section B7.1.1.4 - IV.	For Deflections, see Section B7.1.1.4 - IV.

Table B7.1.2.4 - 3 (Concluded). Hydrostatic Pressure Loading
Membrane Stresses and Deflections, Open Conical Domes

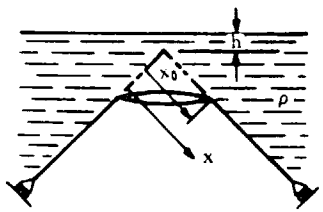

ρ = Specific Weight of Liquid

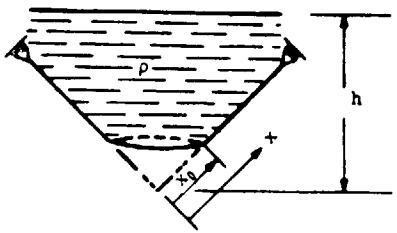

$P_\phi = P_\theta = 0$
$P_z = \rho(h - x\sin\phi)$

$P_\phi = P_\theta = 0$
$P_z = \rho(h - x\sin\phi)$

Regular	Inverted
$N_\phi = -\rho h\frac{x^2 - x_0^2}{2x}\cot\phi - \rho\frac{x^3 - x_0^3}{3x}\cos\phi$	$N_\theta = \rho h\frac{x^2 - x_0^2}{2x}\cot\phi - \rho\frac{x^3 - x_0^2}{3x}\cos\phi$
$N_\theta = -\rho x\left(h\cot\phi - x\cos\phi\right)$	$N_\theta = -\rho x\left(x\cos\phi - h\cot\phi\right)$
$\sigma_\phi, \sigma_\theta = \frac{N_\phi}{t}, \frac{N_\theta}{t}$	$\sigma_\phi, \sigma_\theta = \frac{N_\phi}{t}, \frac{N_\theta}{t}$
$w = \frac{\rho x^2}{Et}\cos\phi\cot\phi\left[\frac{\mu h}{2\sin\phi}\left(\frac{x^2 - x_0^2}{x^2}\right) + \frac{\mu}{3}\left(\frac{x^3 - x_0^3}{x^2}\right) - \frac{h}{\sin\phi} - x\right]$	$w = \frac{\rho x^2}{Et}\cos\phi\cot\phi\left[\frac{\mu}{3}\left(\frac{x^3 - x_0^3}{x^2}\right) - \frac{\mu h}{2\sin\phi}\left(\frac{x^2 - x_0^2}{x^2}\right) + \frac{h}{\sin\phi} - x\right]$
$\bar{w} = w\sin\phi$	$\bar{w} = w\sin\phi$
$\bar{u} = w\cos\phi$	$\bar{u} = w\cos\phi$

Table B7.1.2.4 - 4. Uniform Pressure Loading Membrane Stresses and Deflections, Closed Conical Domes

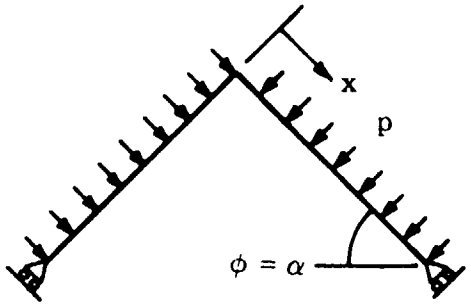

$P_\theta = P_\phi = 0$

$P_z = P$

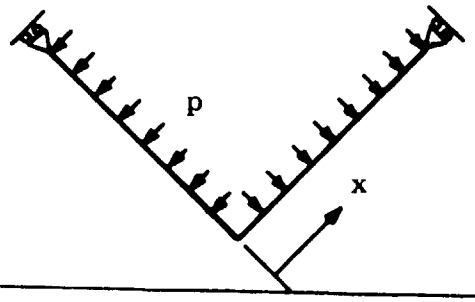

Regular	Inverted
$N_\phi = -\frac{px}{2}\cot\phi$	$N_\phi = \frac{px}{2}\cot\phi$
$N_\theta = -px\cot\phi$	$N_\theta = px\cot\phi$
$\sigma_\phi, \sigma_\theta = \frac{N_\phi}{t}, \frac{N_\theta}{t}$	$\sigma_\phi, \sigma_\theta = \frac{N_\phi}{t}, \frac{N_\theta}{t}$
$w = \frac{px^2}{Et}\cot^2\phi\left(1 - \frac{\mu}{2}\right)$	$w = \frac{px^2}{Et}\cot^2\phi\left(1 - \frac{\mu}{2}\right)$,
$\bar{w} = \frac{px^2}{Et}\cos\phi\ \cot\phi\left(1 - \frac{\mu}{2}\right)$	$\bar{w} = \frac{px^2}{Et}\cos\phi\ \cot\phi\left(1 - \frac{\mu}{2}\right)$
$\bar{u} = \frac{px^2}{Et}\cos\phi\ \cot^2\phi\left(1 - \frac{\mu}{2}\right)$	$\bar{u} = \frac{px^2}{Et}\cos\phi\ \cot^2\phi\left(1 - \frac{\mu}{2}\right)$

Table B7.1.2.4 - 4 (Concluded). Uniform Pressure Loading
Membrane Stresses and Deflections, Open Conical Domes

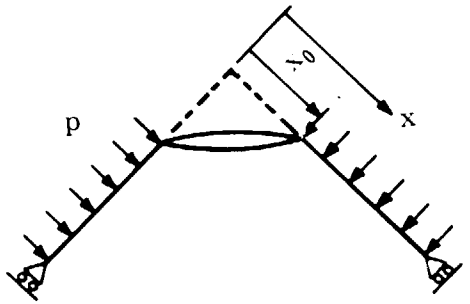

$P_\phi = P_\theta = 0$

$P_z = P$

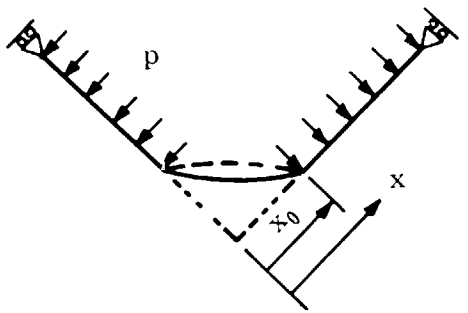

Regular	Inverted
$N_\phi = -\frac{p\cot\phi}{2}\left(\frac{x^2 - x_0^2}{x}\right)$	$N_\phi = \frac{p\cot\phi}{2}\left(\frac{x^2 - x_0^2}{x^2}\right)$
$N_\theta = -px\cot\phi$	$N_\theta = px\cot\phi$
$\sigma_\phi, \sigma_\theta = \frac{N_\phi}{t}, \frac{N_\theta}{t}$	$\sigma_\phi, \sigma_\theta = \frac{N_\phi}{t}, \frac{N_\theta}{t}$
$w = \frac{px^2}{Et}\cot^2\phi\left[1 - \frac{\mu}{2}\left(\frac{x^2 - x_0^2}{x^2}\right)\right]$	$w = \frac{px^2}{Et}\cot^2\phi\left[1 - \frac{\mu}{2}\left(\frac{x^2 - x_0^2}{x^2}\right)\right]$
$\bar{w} = \frac{px^2}{Et}\cot\phi\ \cot\phi\left[1 - \frac{\mu}{2}\left(\frac{x^2 - x_0^2}{x^2}\right)\right]$	$\bar{w} = \frac{px^2}{Et}\cot\phi\ \cot\phi\left[1 - \frac{\mu}{2}\left(\frac{x^2 - x_0^2}{x^2}\right)\right]$
$\bar{u} = \frac{px^2}{Et}\cos\phi\cot^2\phi\left[1 - \frac{\mu}{2}\left(\frac{x^2 - x_0^2}{x^2}\right)\right]$	$\bar{u} = \frac{px^2}{Et}\cos\phi\ \cot^2\phi\left[1 - \frac{\mu}{2}\left(\frac{x^2 - x_0^2}{x^2}\right)\right]$

Table B7.1.2.4 - 5. Lantern Loading
Membrane Stresses and Deflections of Conical Domes

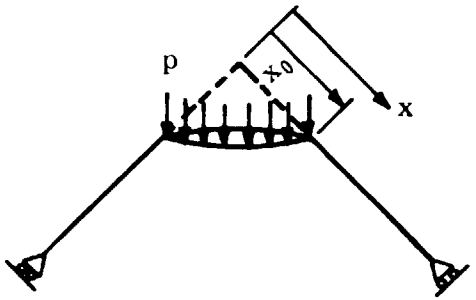

$$P_\phi = P_\theta = P_z = 0$$

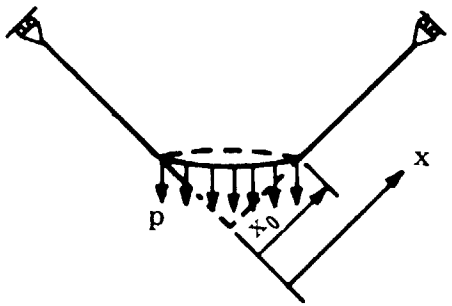

Regular	Inverted
$N_\phi = -\frac{px_0}{x\sin\phi}$	$N_\phi = \frac{px_0}{x\sin\phi}$
$N_\theta = 0$	$N_\theta = 0$
$\sigma_\phi, \sigma_\theta = \frac{N_\phi}{t}, \frac{N_\theta}{t}$	$\sigma_\phi, \sigma_\theta = \frac{N_\phi}{t}, \frac{N_\theta}{t}$
$w = \frac{\mu px_0}{Et}\left(\frac{\cot\phi}{\sin\phi}\right)$	$w = -\frac{\mu px_0}{Et}\left(\frac{\cot\phi}{\sin\phi}\right)$
$\bar{w} = \frac{\mu px_0}{Et}\cot\phi$	$\bar{w} = -\frac{\mu px_0}{Et}\cot\phi$
$\bar{u} = \frac{\mu px_0}{Et\sin\phi}$	$\bar{u} = -\frac{\mu px_0}{Et\sin\phi}$

B7.1.2.5 PARABOLIC DOMES

This subsection presents the solutions for nonshallow parabolic shells exposed to axisymmetric loading. Only closed shells will be considered. The boundaries of the shell must be free to rotate and deflect normal to the shell middle surface. No abrupt discontinuities in the shell thickness shall be present.

Note that because of the geometry of the parabolic meridian, the solutions simplify by use of the radius of curvature at the vertex R_0 where $\phi = 0$. For the parabolic shell at $\phi = 0$, $R_1 = R_2 = R_0$ twice the focal distance.

The following loading conditions will be considered: dead weight loading (Table B7.1.2.5 - 1); uniform loading over base area (Table B7.1.2.5 - 2); hydrostatic pressure loading (Table B7.1.2.5 - 3); and uniform pressure loading (Table B7.1.2.5 - 4). These tables begin on page 64.

Table B7.1.2.5 - 1. Dead Weight Loading
Membrane Stress Resultants for Closed Parabolic Domes

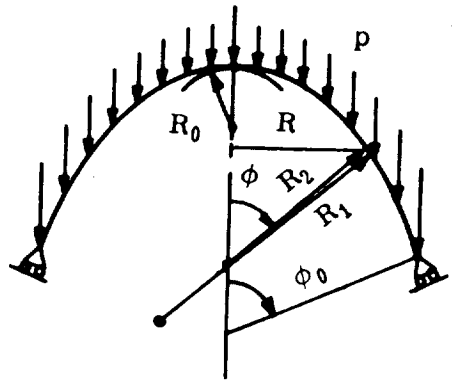

R_0 = z (Focal Distance)

$$P_\theta = 0\ ,\quad P_z = p\cos\phi\ ,\quad P_\phi = p\sin\phi$$

$$N_\phi = -\frac{pR_0}{3}\left(\frac{1-\cos^3\phi}{\sin^2\phi\,\cos^2\phi}\right)$$

$$N_\theta = -\frac{pR_0}{3}\left(\frac{2-3\cos^2\phi+\cos^3\phi}{\sin^2\phi}\right)$$

$$\sigma_\phi\ ,\ \sigma_\theta = \frac{N_\phi}{t}\ ,\ \frac{N_\theta}{t}$$

For Deflections, see Section B7.1.1.4 - IV .

Table B7.1.2.5 - 2. Uniform Loading over Base Area
Membrane Stress Resultants for Closed Parabolic Domes

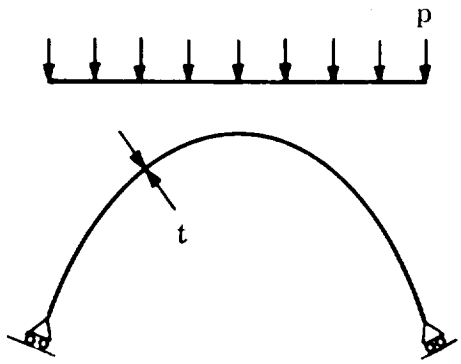

R_0 z (Focal Distance)

$$P_\theta = 0 \quad , \quad P_z = p\cos^2\phi \quad , \quad P_\phi = p\cos\phi\sin\phi$$

$$N_\phi = -\frac{pR_0}{2\cos\phi}$$

$$N_\theta = -\frac{pR_0\cos\phi}{2}$$

$$\sigma_\phi \, , \, \sigma_\theta = \frac{N_\phi}{t} \quad , \quad \frac{N_\theta}{t}$$

For Deflections, see Section B7.1.1.4 - IV.

Table B7.1.2.5 - 3. Hydrostatic Pressure Loading
Membrane Stress Resultants for Closed Parabolic Domes

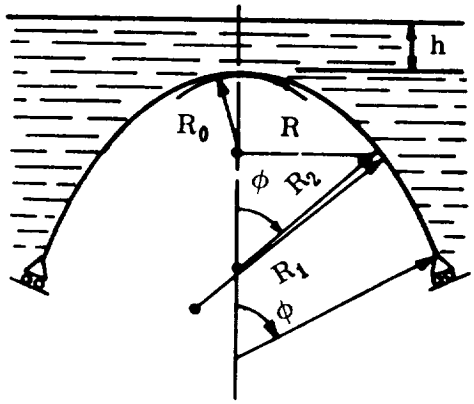

ρ = Specific Weight of Liquid

$$P_\theta = P_\phi = 0 \quad , \quad P_z = \rho\left(h + \frac{R_0}{2}\tan^2\phi\right)$$

$$N_\phi = -\frac{\rho R_0}{2\cos\phi}\left(h + \frac{R_0}{4}\tan^2\phi\right)$$

$$N_\theta = -\frac{\rho R_0 \cos\phi}{2}\left[h\left(2\tan^2\phi + 1\right) + R_0\tan^2\phi\left(\tan^2\phi + \frac{3}{4}\right)\right]$$

$$\sigma_\phi \, , \, \sigma_\theta = \frac{N_\phi}{t} \quad , \quad \frac{N_\theta}{t}$$

For Deflections, see Section B7.1.1.4 - IV .

Table B7.1.2.5 - 4. Uniform Pressure Loading
Membrane Stress Resultants for Closed Parabolic Domes

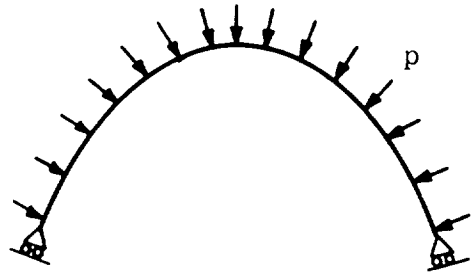

$$P_\theta = P_\phi = 0 \quad , \quad P_z = P$$

$$N_\phi = -\frac{pR_0}{2\cos\phi}$$

$$N_\theta = -\frac{pR_0}{2}\left(\frac{1+\sin^2\phi}{\cos\phi}\right)$$

$$\sigma_\phi \, , \, \sigma_\theta = \frac{N_\phi}{t} \quad , \quad \frac{N_\theta}{t}$$

For Deflections, see Section B7.1.1.4 - IV

B7.1.2.6 CYCLOIDAL DOMES

This subsection presents the solutions for nonshallow cycloidal shells exposed to axisymmetric loading. Only closed shells will be considered. The boundaries of the shell must be free to rotate and deflect normal to the shell middle surface. No abrupt discontinuities in the shell thickness shall be present.

The following loading conditions will be considered: dead weight loading (Table B7.1.2.6 - 1) and uniform loading over base area (Table B7.1.2.6 - 2). These tables begin on page 69.

Table B7.1.2.6 - 1. Dead Weight Loading
Membrane Stress Resultants for Cycloidal Domes

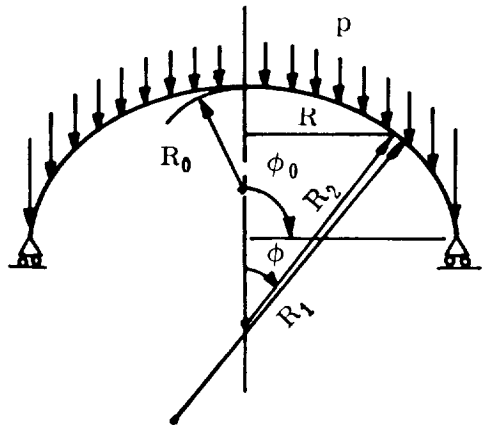

$$P_\theta = 0, \quad P_\phi = p\sin\phi, \quad P_z = p\cos\phi$$

$$N_\phi = -2pR_0\left(\frac{\phi\sin\phi + \cos\phi - \frac{1}{3}\cos^3\phi - \frac{2}{3}}{}\right)$$

$$N_\theta = -pR_0\left[\frac{1}{3}\left(\frac{1-\cos^3\phi}{\sin^2\phi\cos\phi}\right) - \frac{\phi}{2}\tan\phi - \frac{1}{2}\sin^2\phi\right]$$

$$\sigma_\phi, \sigma_\theta = \frac{N_\phi}{t}, \frac{N_\theta}{t}$$

For Deflections, see Section B7.1.1.4 - IV.

Table B7.1.2.6 - 2. Uniform Loading over Base Area
Membrane Stress Resultants for Cycloidal Domes

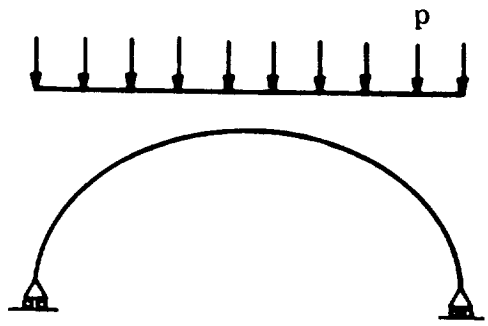

$$P_\theta = 0, \quad P_\phi = p\sin\phi\cos\phi, \quad P_z = p\cos^2\phi$$

$$N_\phi = -\frac{pR_0}{8}\left(\frac{2\phi + \sin 2\phi}{\sin\phi}\right)$$

$$N_\theta = -\frac{pR_0}{16}\left(\frac{2\phi + \sin 2\phi}{\sin\phi}\right)\left(4\cos^2\phi - \frac{2\phi}{\sin 2\phi} - 1\right)$$

$$\sigma_\phi, \sigma_\theta = \frac{N_\phi}{t}, \frac{N_\theta}{t}$$

For Deflections, see Section B7.1.1.4 - IV.

B7.1.2.7 TOROIDAL DOMES

This subsection presents the solutions for toroidal shells exposed to axisymmetric loading. Both closed and open shells will be considered. The boundaries of the shell must be free to rotate and deflect normal to the shell middle surface. No abrupt discontinuities in the shell thickness shall be present.

Note in Figure B7.1.2.7 - 1 that, because of the geometry of the toroidal shell, the definition of the angle ϕ is changed (for this subsection only) to increase the useful range of the solutions.

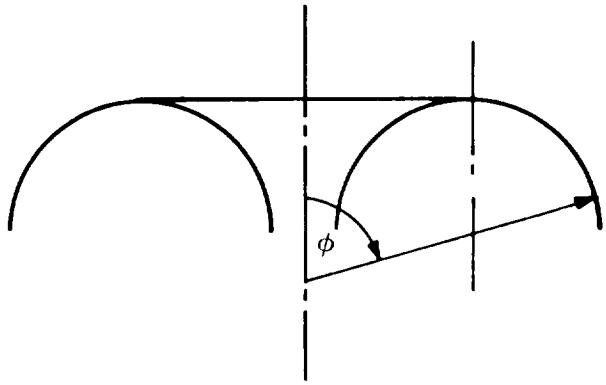

Useful Range $35^\circ \leq \phi \leq 90^\circ$

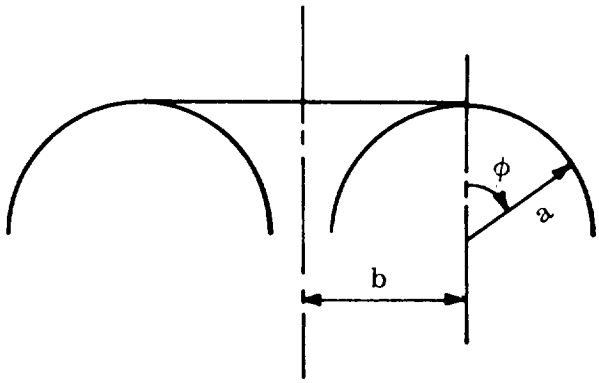

ϕ Definition (Section B7.7.1.2.7 - 1 only)

Fig. B7. 1. 2. 7. - 1. Toroidal Shell Geometry

There is also a special type of toroidal shell where the axis of revolution bisects the cross section. This type of shell is referred to as a pointed dome, and the angle ϕ is defined in Figure B7.1.2.7 - 2.

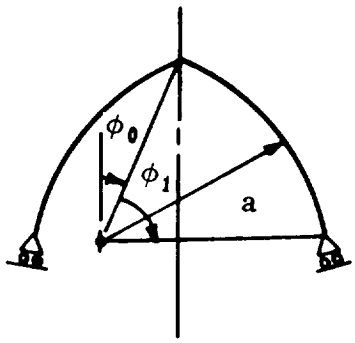

Fig. B7.1.2.7 - 2. Pointed Dome

The following loading conditions will be considered for regular toroidal shells and pointed domes.

Regular Toroidal Shells:

Dead Weight Loading (Table B7.1.2.7 - 1)

Hydrostatic Loading (Table B7.1.2.7 - 2)

Uniform Pressure Loading (Table B7.1.2.7 - 3)

Lantern Loading (Table B7.1.2.7 - 4)

Pointed Domes:

Dead Weight Loading (Table B7.1.2.7 - 5)

Uniform Loading Over Base Area (Table B7.1.2.7 - 6)

These tables begin on page 73.

Table B7.1.2.7 - 1. Dead Weight Loading
Membrane Stresses, Regular Toroidal Shells

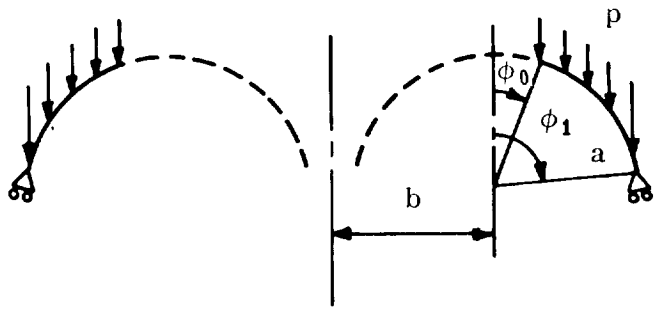

$P_\phi = P_\theta = 0$

$P_z = p$

$$N_\phi = -p\frac{ab(\phi - \phi_0) + a^2(\cos\phi_0 - \cos\phi)}{(b + a\sin\phi)\sin\phi}$$

$$N_\theta = -\frac{p}{\sin\phi}\left[(b + a\sin\phi)\cos\phi - b(\phi - \phi_0) - a(\cos\phi_0 - \cos\phi)\right]$$

$$\sigma_\phi, \sigma_\theta = \frac{N_\phi}{t}, \frac{N_\theta}{t}$$

Table B7.1.2.7 - 1 (Concluded). Dead Weight Loading
Membrane Stresses, Regular Toroidal Shells

For Symmetrical Cross Section ($\phi_0 = -\phi_1$)

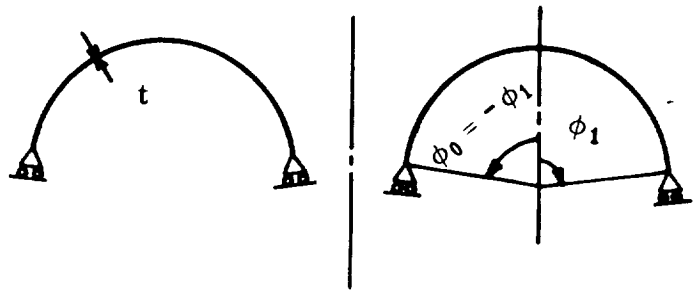

Loading Same as Above

$$N_\phi = -p\frac{ba\phi + a^2(1-\cos\phi)}{(b+a\sin\phi)\sin\phi}$$

$$N_\theta = -\frac{p}{\sin\phi}\left[(b+a\sin\phi)\cos\phi - b\phi - a(1-\cos\phi)\right]$$

$$\sigma_\phi, \sigma_\theta = \frac{N_\phi}{t}, \frac{N_\theta}{t}$$

Table B7.1.2.7 - 2. Hydrostatic Pressure Loading
Membrane Stresses, Regular Toroidal Shells

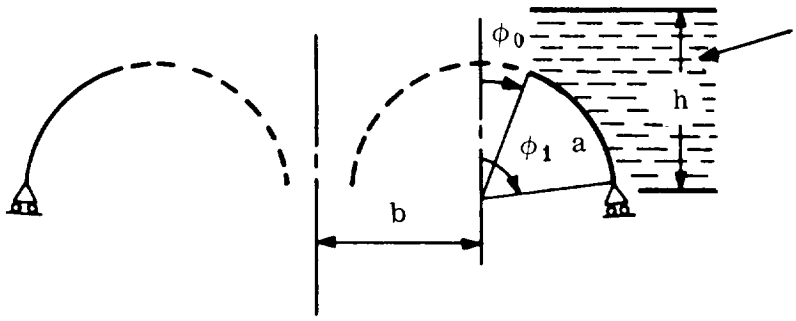

ρ = Specific Weight of Liquid

$P_\phi = P_\theta = 0$

$P_z = \rho(h - a\cos\phi)$

$$N_\phi = -\frac{\rho a}{(b + a\sin\phi)\sin\phi}\left[-bh(\sin\phi_0 - \sin\phi) + \frac{ah}{2}(\cos^2\phi_0 - \cos^2\phi) + \frac{ba}{2}(\sin\phi_0\cos\phi_0 - \sin\phi\cos\phi - \phi + \phi_0) - \frac{a^2}{3}(\cos^3\phi_0 - \cos^3\phi)\right]$$

$$N_\theta = -\frac{\rho}{\sin^2\phi}\left[(h - a\cos\phi)(b + a\sin\phi)\sin\phi + bh(\sin\phi_0 - \sin\phi) - \frac{ah}{2}(\cos^2\phi_0 - \cos^2\phi) - \frac{ba}{2}(\sin\phi_0\cos\phi_0 - \sin\varphi\cos\phi - \phi + \phi_0) + \frac{a^2}{3}(\cos^3\phi - \cos^3\phi)\right]$$

Table B7.1.2.7 - 2 (Concluded). Hydrostatic Pressure Loading
Membrane Stresses, Regular Toroidal Shells

For Symmetrical Cross Section ($\phi_0 = \phi_1$)

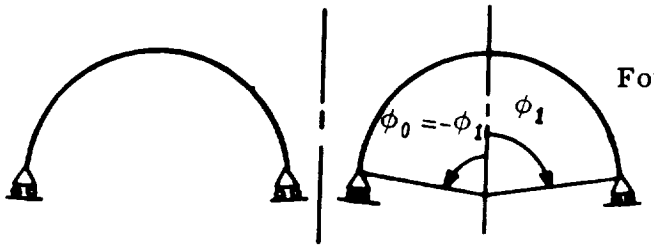

For Symmetrical Cross Section
$\phi_0 = -\phi_1$

Same Loading as Above

$$N_\phi = -\frac{\rho a}{(b + a\sin\phi)\sin\phi}\left[bh\sin\phi + \frac{ah}{2}\sin^2\phi - \frac{ba}{2}(\sin\phi\cos\phi + \phi) - \frac{a^2}{3}(1 - \cos^3\phi)\right]$$

$$N_\theta = -\frac{\rho}{\sin\phi}\left[\frac{ah}{2}\sin^2\phi - \frac{ba}{2}(\sin\phi\cos\phi - \phi) - a^2\left(\cos\phi\sin^2\phi - \frac{1 - \cos^3\phi}{3}\right)\right]$$

Table B7.1.2.7 - 3. Uniform Pressure Loading
Membrane Stresses, Regular Toroidal Shells

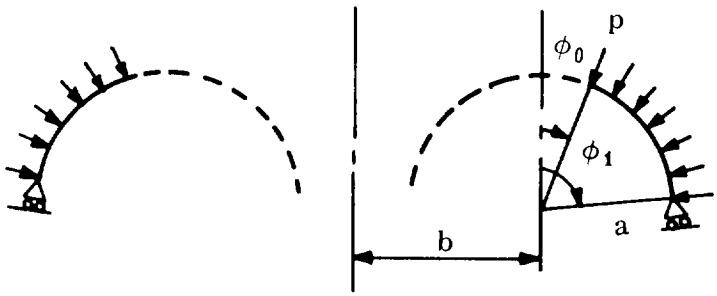

$P_\phi = P_\theta = 0$
or $P_z = P$

$$N_\phi = -\frac{p}{2(b + a\sin\phi)\sin\phi}\left[(b + a\sin\phi)^2 - (b + a\sin\phi_0)^2\right]$$

$$N_\theta = -\frac{p}{2\sin^2\phi}\left[2b\sin\phi_0 + a(\sin^2\phi_0 + \sin^2\phi)\right]$$

Table B7.1.2.7 - 3 (Concluded). Uniform Pressure Loading
Membrane Stresses, Regular Toroidal Shells

For Symmetrical Cross Section ($\phi_0 = -\phi_1$)

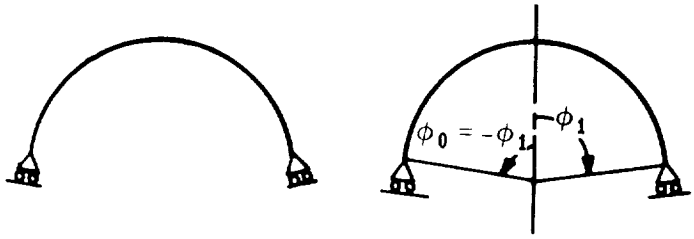

Same Loading as Above

$$N_\phi = -\frac{pa}{2}\,\frac{2b + a\sin\phi}{b + a\sin\phi}$$

$$N_\theta = -\frac{pa}{2}$$

Table B7.1.2.7 - 4. Lantern Loading
Membrane Stresses, Regular Toroidal Shells

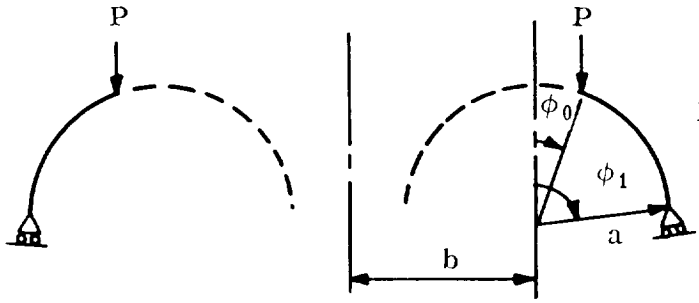

$$P_\theta = P_\phi = P_z = 0$$

$$N_\phi = -\frac{P(b + a\sin\phi)}{(b + a\sin\phi)\sin\phi}$$

$$N_\theta = -\frac{P}{a}\left(\frac{b + a\sin\phi_0}{\sin^2\phi}\right)$$

$$\sigma_\phi, \sigma_\theta = \frac{N_\phi}{t}, \frac{N_\theta}{t}$$

Table B7.1.2.7 - 5. Dead Weight Loading
Membrane Stresses, Pointed Toroidal Dome

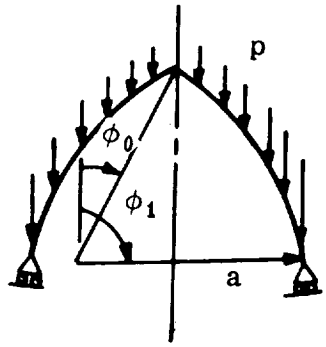

$$P_\theta = 0$$

$$P_\phi = p\sin\phi \ , \quad P_z = p\cos\phi$$

$$N_\phi = -pa\left[\frac{\cos\phi_0 - \cos\phi - (\phi - \phi_0)\sin\phi_0}{(\sin\phi - \sin\phi_0)\sin\phi}\right]$$

$$N_\theta = -\frac{pa}{\sin^2\phi}\left[(\phi - \phi_0)\sin\phi_0 - (\cos\phi_0 - \cos\phi) + (\sin\phi - \sin\phi_0)\sin\phi\cos\phi\right]$$

$$\sigma_\phi \ , \ \sigma_\theta = \frac{N_\phi}{t} \ , \ \frac{N_\theta}{t}$$

Table B7.1.2.7 - 6. Uniform Loading over Base Area
Membrane Stresses, Pointed Toroidal Dome

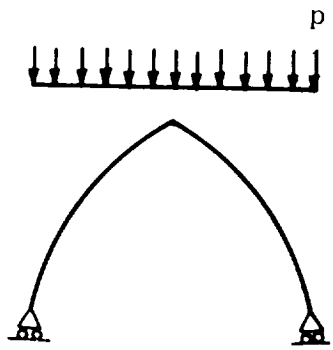

$$P_\theta = 0$$

$$P_\phi = p \sin\phi \cos\phi \ , \quad P_z = p \cos^2\phi$$

$$N_\phi = -\frac{pa}{2}\left(1 - \frac{\sin\phi_0}{\sin\phi}\right)$$

$$N_\theta = -\frac{pa}{2}\left(\cos 2\phi - 2\sin\phi \sin\phi_0 - \frac{\sin^2\phi_0}{\sin^2\phi}\right)$$

$$\sigma_\phi \ , \ \sigma_\theta = \frac{N_\phi}{t} \ , \ \frac{N_\theta}{t}$$

B7.1.3.0 CYLINDER ANALYSIS

Many types of cylinders can be analyzed using membrane theory. However, only the circular cylinder falls into the category of shells of revolution being discussed in this chapter.

B7.1.3.1 CIRCULAR CYLINDERS

The circular cylinder is a special type of surface of revolution. If the standard shell-of-revolution nomenclature is applied to the cylinder geometry, (Figure B7.1.3.1 - 1) analysis is straightforward.

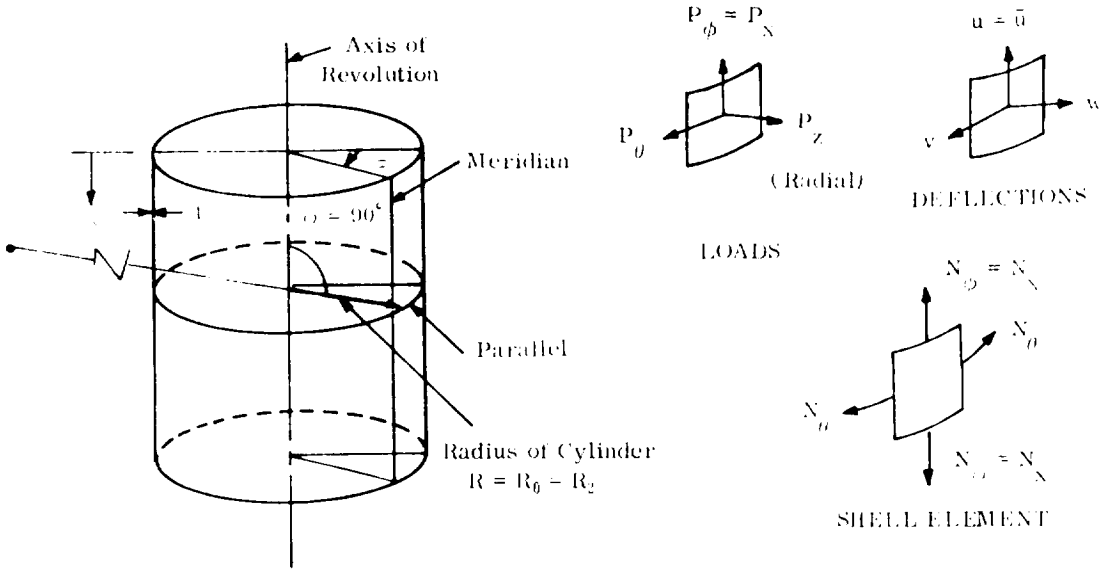

Fig. B7.1.3.1 - 1. Circular Cylinder Geometry

The following loading conditions will be considered for circular cylinders:

Linear Loading (Table B7.1.3 - 1)

Trigonometric Loading (Table B7.1.3 - 2)

Dead Weight Loading (Table B7.1.3 - 3)

Circumferential Loading (Table B7.1.3 - 4)

Axial Loading (Table B7.1.3 - 5) .

These tables begin on page 84.

Table B7.1.3 - 1. Linear Loading

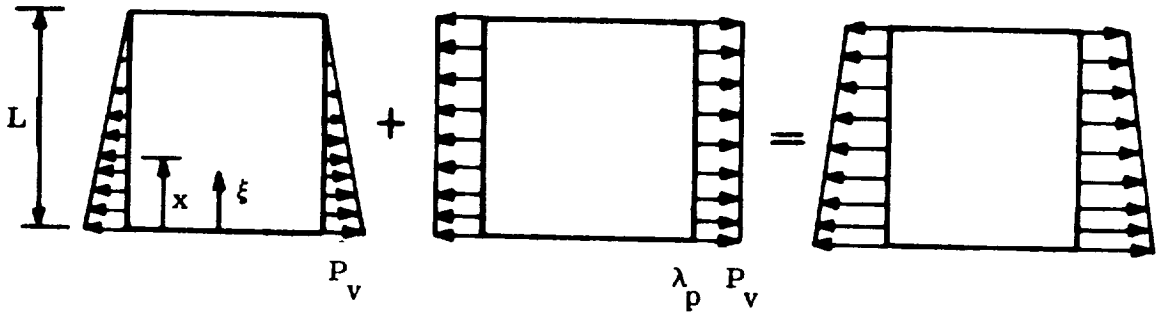

$$P_z = P_v(1 + \lambda_p - \xi)$$

where $\xi = \frac{x}{L}$

λ_p = coefficient defining ratio of uniform load to maximum value of linear load

$N_\theta = P_v R (1 + \lambda_p - \xi)$

$N_\phi = 0$

$N_{\phi\theta} = 0$

$\sigma_\theta = \frac{N_\theta}{t}$

$\bar{u} = \frac{1}{Et}\left[-\mu P_v R L \xi (1 + \lambda_p - \frac{1}{2}\xi)\right]$

$v = 0$

$\bar{w} = \frac{1}{Et}\left[P_v R^2 (1 + \lambda_p - \xi)\right]$

Table B7.1.3 - 2. Trigonometric Loading

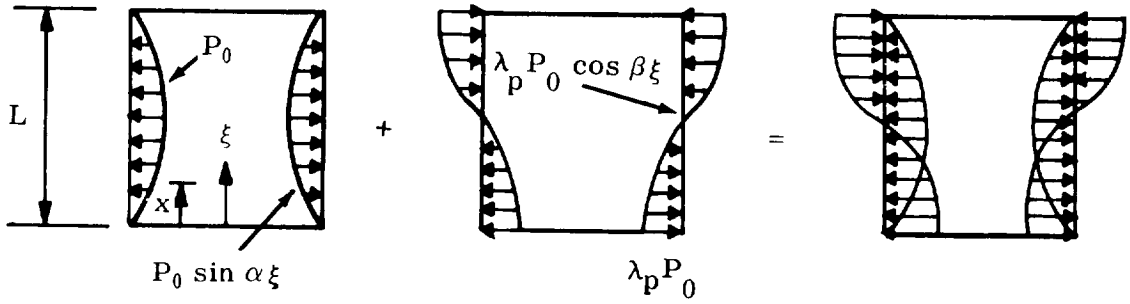

$$P_z = -p_0(\sin \alpha\xi + \lambda_p \cos \beta\xi)$$

where $\xi = \frac{x}{L}$

α, β = coefficients defining shape of sin and cos curves

λ_p = coefficients defining ratio of maximum amplitude of cos loading to maximum amplitude of sin loading

$N_\theta = P_0 R(\sin\alpha\xi + \lambda_p \cos\beta\xi)$

$N_\phi = 0$

$N_{\phi\theta} = 0$

$\bar{u} = \frac{\mu}{Et} P_0 R L\left(\frac{\cos\alpha\xi}{\alpha} - \lambda_p \frac{\sin\beta\xi}{\beta}\right)$

$v = 0$

$\bar{w} = \frac{1}{Et} P_0 R^2(\sin\alpha\xi + \lambda_p \cos\beta\xi)$

Table B7.1.3 - 3. Dead Weight Loading

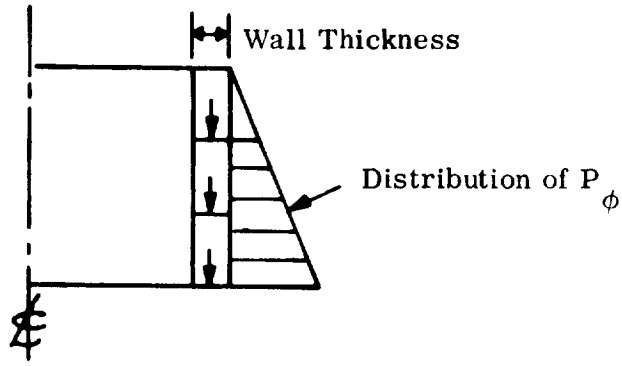

$$P_\phi = P_{\phi_0}(1 - \xi)$$

$$N_\theta = 0$$

$$N_\phi = P_{\phi_0} L\left(\frac{1}{2} - \xi + \frac{\xi^2}{2}\right)$$

$$N_{\phi\theta} = 0$$

$$\bar{u} = \frac{1}{Et}\left[P_{\phi_0} L^2 \xi\left(\frac{1}{2} - \frac{\xi}{2} + \frac{\xi^2}{6}\right)\right]$$

$$v = 0$$

$$\bar{w} = \frac{1}{Et}\mu P_{\phi_0} \alpha L \left(-\frac{1}{2} + \xi - \frac{\xi^2}{2}\right)$$

Table B7.1.3 - 4. Circumferential Loading

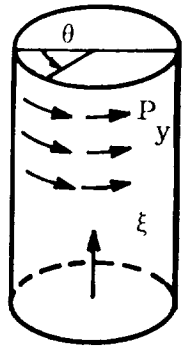

$$P_y = P_\theta$$

$$N_\theta = 0$$

$$N_\phi = 0$$

$$N_{\theta\phi} = P_\theta L (1 - \xi)$$

$$\bar{u} = 0$$

$$v = \frac{1}{Et}\left[2(1+\mu)\, P_\theta L^2 \left(\xi - \frac{\xi^2}{2}\right)\right]$$

$$\bar{w} = 0$$

Table B7.1.3 - 5. Axial Load

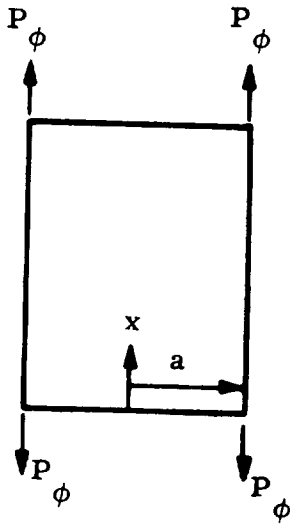

$$N_\phi = P_\phi$$

$$N_\theta = 0$$

$$N_{\phi\theta} = 0$$

$$\bar{u} = \frac{N_\phi x}{Et} + C$$

$$\bar{w} = -\frac{\mu a N_\phi}{Et}$$

$$v = 0$$

SECTION B7.2

LOCAL LOADS ON

TABLE OF CONTENTS

TABLE OF CONTENTS (Concluded)

B7.2.0.0 LOCAL LOADS ON THIN SHELLS

The method contained in this section for determining stresses and displacements in thin shells is based on analyses performed by P. P. Bijlaard. [1] These analyses represent the local loads and radial displacement in the form of a double Fourier series. The equations developed using these series and the necessary equilibrium considerations are readily solved by numerical techniques for stresses and displacements.

The stresses and displacements calculated by the methods of this section can be superimposed upon the stresses caused by other loadings if the specified limitations are observed.

The equations for determining stresses in spherical shells caused by local loads have been evaluated within the parametric ranges of space vehicle interest for radial load and overturning moment. The results of this evaluation have been plotted and are contained in this section for use in determining the stresses. A direct method is presented for determining the stresses in spherical shells caused by locally applied shear load or twisting moment. No method is provided to calculate displacements of spherical shells caused by local loads.

The equations for determining stresses and displacements in cylindrical shells caused by local loads have been programmed in Fortran IV for radial load and overturning moment. A direct method is presented for determining the stresses in cylindrical shells caused by a locally applied shear load or twisting moment. No method is provided to calculate displacements of cylindrical shells caused by locally applied shear loads or twisting moments.

B7.2.1.0 LOCAL LOADS ON SPHERICAL SHELLS*

This section presents a method of obtaining spherical shell membrane and bending stresses resulting from loads induced through rigid attachments at the attachment-to-shell juncture. Shell and attachment parameters are used to obtain nondimensional stress resultants from curves for the radial load and overturning moment load condition. The values of the stress resultants are then used to calculate stress components. Shear stresses caused by shearing loads and twisting moment can be calculated directly.

Local load stresses reduce rapidly at points removed from the attachment-to-shell juncture. The shaded areas in Figure B7.2.1.0-1 locate the region where stresses caused by local loads are considered.

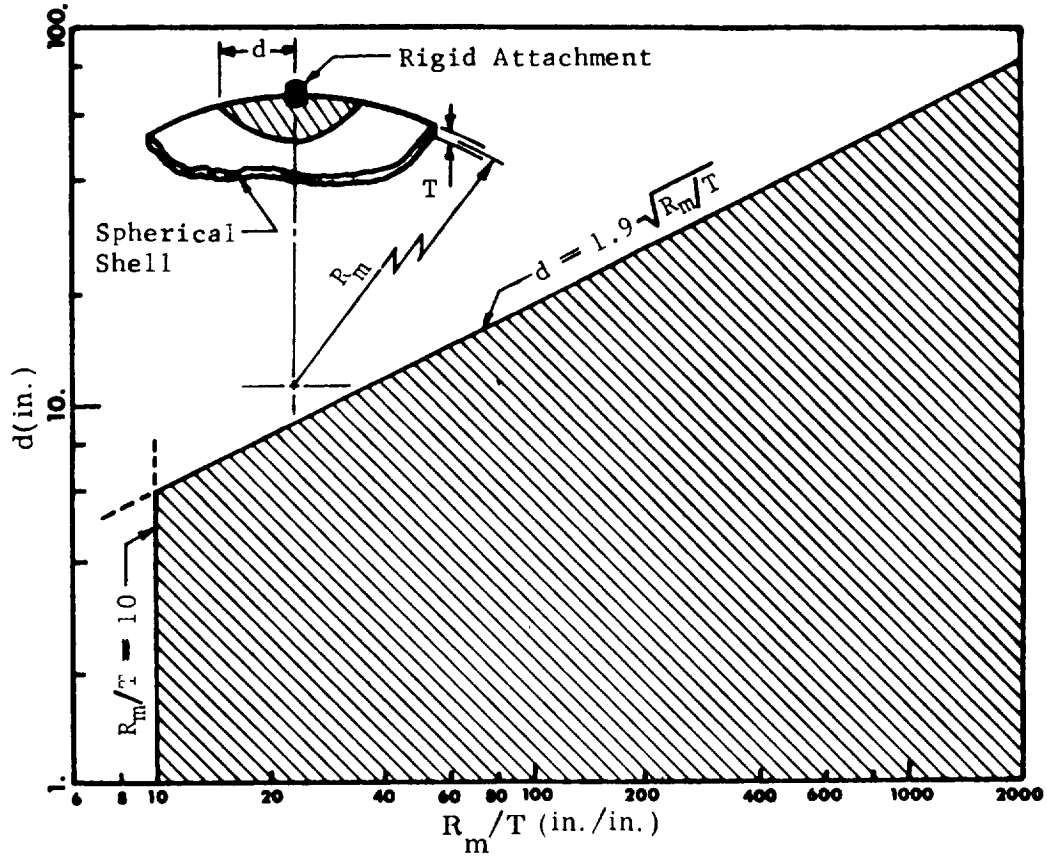

Fig. B7.2.1.0-1 Local Loads Area of Influence

* This section is adapted from the Welding Research Council Bulletin. No. 107, "Local Stresses in Spherical and Cylindrical Shells Due to External Loadings" [5].

B7.2.1.1 GENERAL

I NOTATION

- a - fillet radius at attachment-to-shell juncture, in.
- c - half width of square attachment, in.
- d - distance defined by Figure B7.2.1.0-1
- E - modulus of elasticity, psi
- f_x - normal meridional stress, psi
- f_y - normal circumferential stress, psi
- f_{xy} - shear stress, psi
- K_n, K_b - stress concentration parameters for normal stresses and bending stresses, respectively
- M_a - Applied overturning moment, in.-lb.
- M_T - applied twisting moment, in.-lb.
- M_j - internal bending moment stress resultant per unit length of shell, in.-lb/in.
- N_j - internal normal force stress resultant per unit length of shell, lb/in.
- P - applied concentrated radial load, lb.
- R - radius of the shell, in.
- r - radius of the attachment-to-shell, in.
- T - thickness of the shell, in.
- t - thickness of hollow attachment-to-shell, in.
- U - shell parameter, in./in.
- V_a - applied concentrated shear load, lb.
- ρ - hollow attachment-to-shell parameter, in./in.
- θ - circumferential angular coordinate, rad.
- Υ - hollow attachment-to-shell parameter, in./in.
- ϕ - meridional angular coordinate, rad.

B7.2.1.1 GENERAL (Cont'd)

I NOTATION (Cont'd)

Subscripts

a - applied (a = 1 or a = 2)
b - bending
i - inside
j - internal (j = x or j = y)
m - mean (average of outside and inside)
n - normal
o - outside
x - meridional coordinate
y - circumferential coordinate
z - radial coordinate

1 - applied load coordinate
2 - applied load coordinate

B7.2.1.1 GENERAL

II SIGN CONVENTION

Local loads applied at an attachment-to-shell induce a biaxial state of stress on the inside and outside surfaces of the shell. The meridional stress (f_x), circumferential stress (f_y), shear stress (f_{xy}), the positive directions of the applied loads (M_a, M_T, V_a, and P), and the stress resultants (M_j and N_j) are indicated in Figure B7.2.1.1-1.

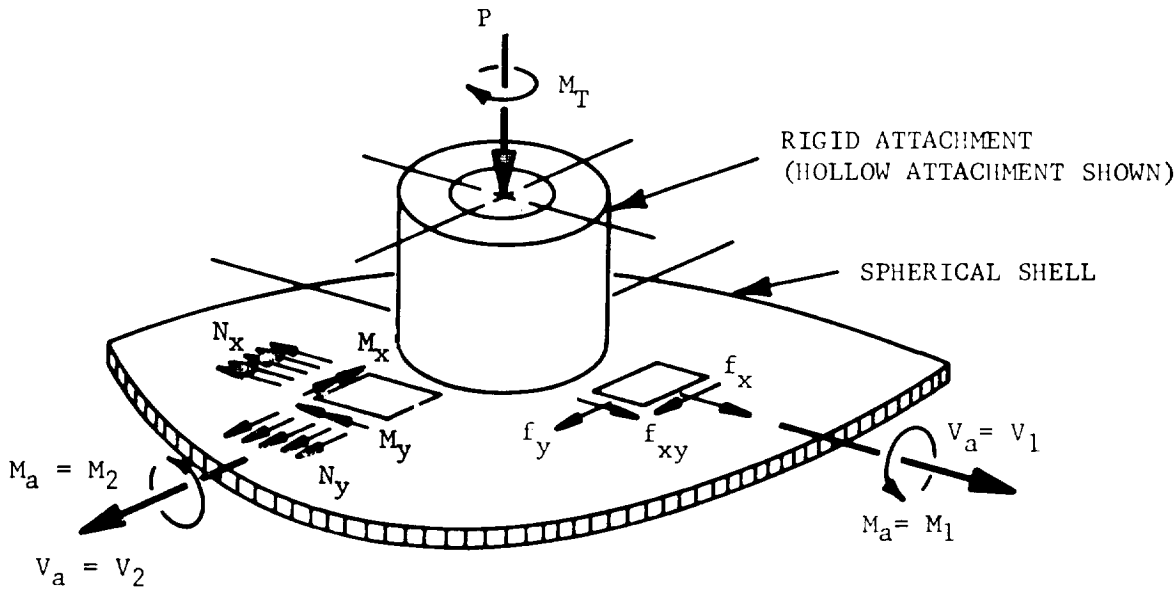

Fig. B7.2.1.1-1 Stresses, Stress Resultants, and Loads

The geometry of the shell and attachment, and the local coordinate system (1-2-3) are indicated in Figure B7.2.1.1-2. It is possible to predict the sign of the induced stresses, tensile (+) or compressive (-), by considering the deflection of the shell resulting from various modes of loading.

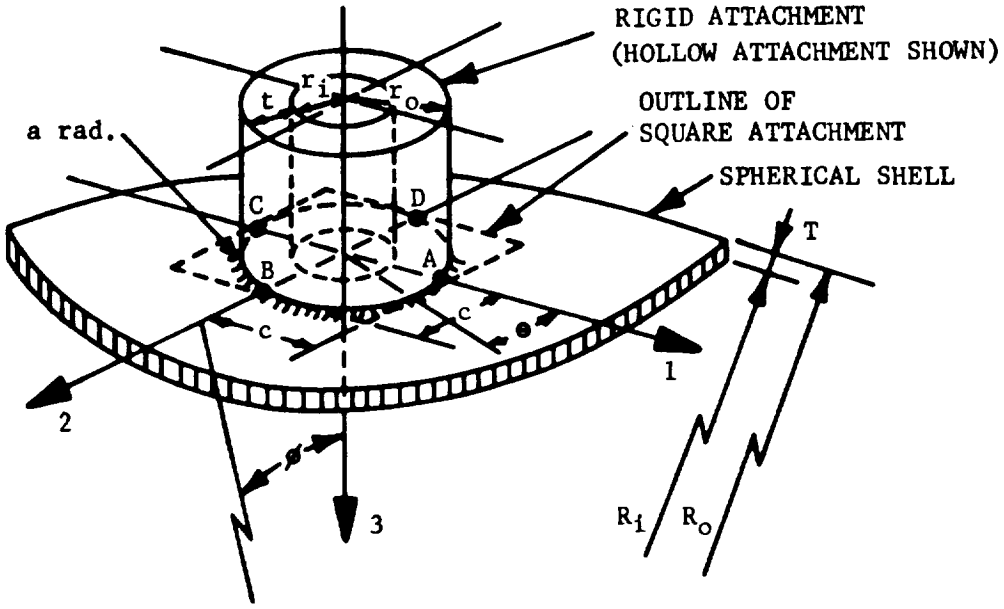

Fig. B7.2.1.1-2 Shell and Attachment Geometry

Mode I, Figure B7.2.1.1-3 shows a positive radial load (P) transmitted to the shell by a rigid attachment. The load (P) causes compressive membrane stresses and local bending stresses adjacent to the attachment. The compressive membrane stresses are similar to the stresses induced by an external pressure. The local bending stresses result in tensile bending stresses on the inside of the shell and compressive bending stresses on the outside of the shell at points C and A.

Mode II, Figure B7.2.1.1-3 shows a negative overturning moment (M_a) transmitted to the shell by a rigid attachment. The overturning moment (M_a) causes compressive and tensile membrane stresses and local bending stresses adjacent to the attachment. Tensile membrane stresses induced in the shell at C are similar to the stresses caused by an internal pressure. Compressive membrane stresses induced in the shell at A are similar to the stresses caused by an external pressure. The local bending stresses cause tensile bending stresses in the shell at C on the outside and A on the inside,and cause compressive bending stresses in the shell at A on the outside and at C on the inside.

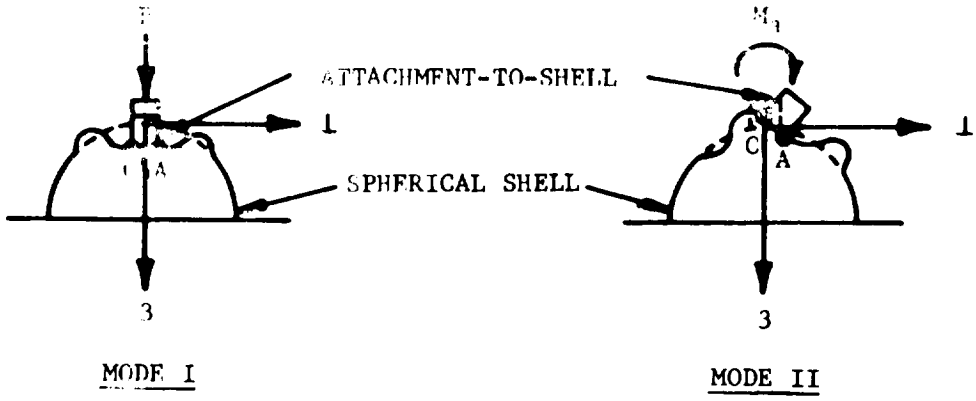

Fig. B7.2.1.1-3 Loading Modes

B7.2.1.1 GENERAL

III LIMITATIONS OF ANALYSIS

Four general areas must be considered for limitations: attachment size and shell thickness, attachment location, shift in maximum stress location, and stresses caused by shear loads.

A Size of Attachment with Respect to Shell Size

The analysis is applicable to small attachments relative to the shell size and to thin shells. The limitations on these conditions are shown by the shaded area of Figure B7.2.1.1-4.

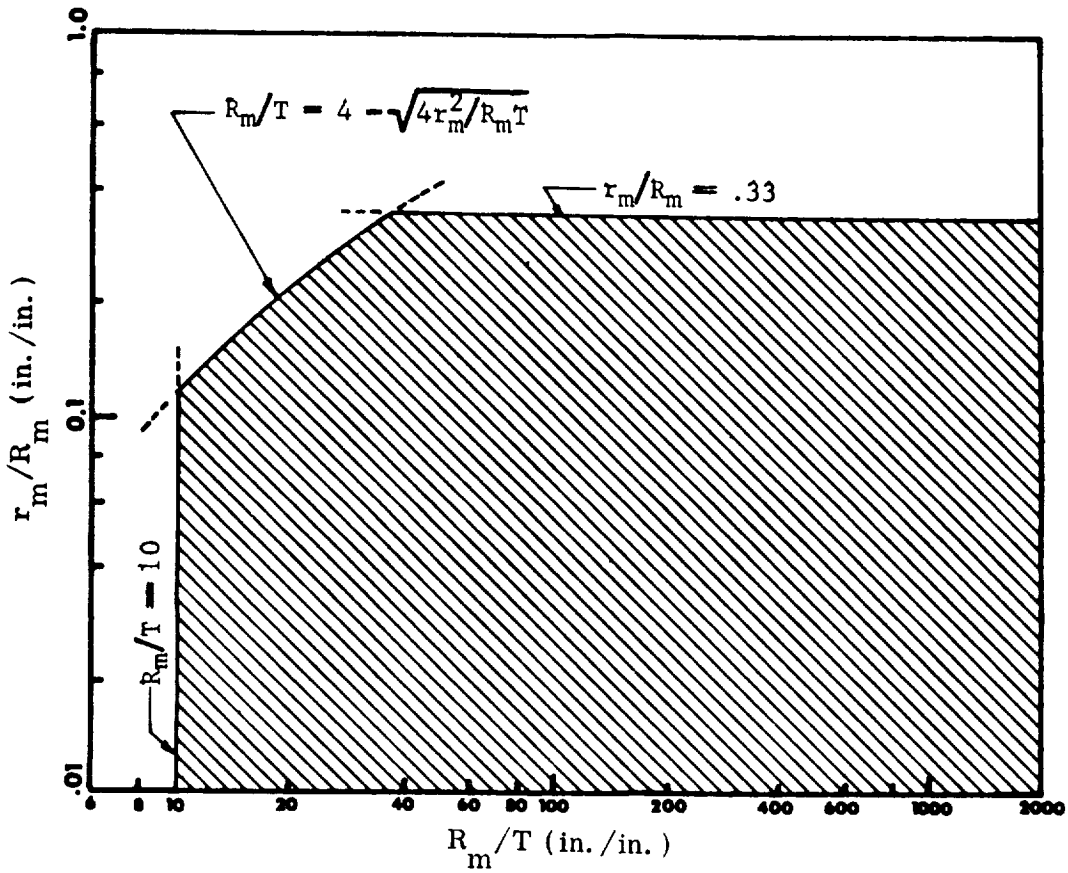

Fig. B7.2.1.1-4

B Location of Attachment with Respect to Boundary Conditions of Shell

The analysis is applicable when any part of the area of influence shown in Figure B7.2.1.0-1 does not contain any stress perturbations. These perturbations may be caused by discontinuity, thermal loading, liquid-level loading, change in section and material change.

C Shift in Maximum Stress Location

Under certain conditions the stresses in the shell may be higher at points removed from the attachment-to-shell juncture than at the juncture. The following conditions should be carefully considered:

1. In some instances, stresses will be higher in the hollow attachment wall than they are in the shell. This is most likely when the attachment opening is not reinforced, when reinforcement is placed on the shell and not on the attachment, and when very thin attachments are used.

2. For some load conditions certain stress resultants peak at points slightly removed from the attachment-to-shell juncture. The maximum value of these stress resultants is determined from the curves in Section B7.2.1.5 and is indicated by dashed lines.

When conditions are encountered that deviate from the limitations of the analysis, Appendix A of Reference 2 should be consulted.

D Stresses Caused by Shear Loads

An accurate stress distribution caused by a shear load (V_a) applied to a spherical shell is not available. The actual stress distribution consists of varying shear and membrane stresses around the rigid attachment. The method [2] presented here assumes that the shell resists the shear load by shear only. If this assumption appears unreasonable, it can be assumed that the shear load is resisted totally by membrane stresses or by some combination of membrane and shear stresses.

B7.2.1.2 STRESSES +

I GENERAL

Stress resultants at attachment-to-shell junctures are obtained from the nondimensional stress-resultant curves in section B7.2.1.5. These curves are plots of the shell parameter (U) versus a nondimensional form of the stress resultants (M_j and N_j). Figures B7.2.1.5-1 and B7.2.1.5-2 are used for solid attachments and Figures B7.2.1.5-3 through B7.2.1.5-22 are used for hollow attachments. Additional attachment parameters (Υ and ρ) are required to use Figures B7.2.1.5-3 through B7.2.1.5-22.

The general equation for stresses in a shell at a rigid attachment juncture in terms of the stress resultants is:

$$f_j = K_n (N_j / T) \pm K_b (6M_j / T^2) .$$

The stress concentration parameters (K_n and K_b) are functions of the ratio of fillet radius to shell thickness (a/T). The value of the stress concentration parameters for $R \gg r$ is equal to unity except in the following cases:

(a) Attachment-to-shell juncture is brittle material;

(b) Fatigue analysis is necessary at attachment-to-shell juncture.

When stress concentration parameters are used they can be determined from Figure B7.2.1.2-1.

The value of the stress resultant at the juncture is indicated by a solid line on the nondimensional stress resultant curves. When the maximum value for a stress-resultant does not occur at the attachment-to-shell juncture, it is indicated on the nondimensional stress-resultant curves by dashed lines. An incorrect but conservative analysis would assume this maximum stress to be at the juncture.

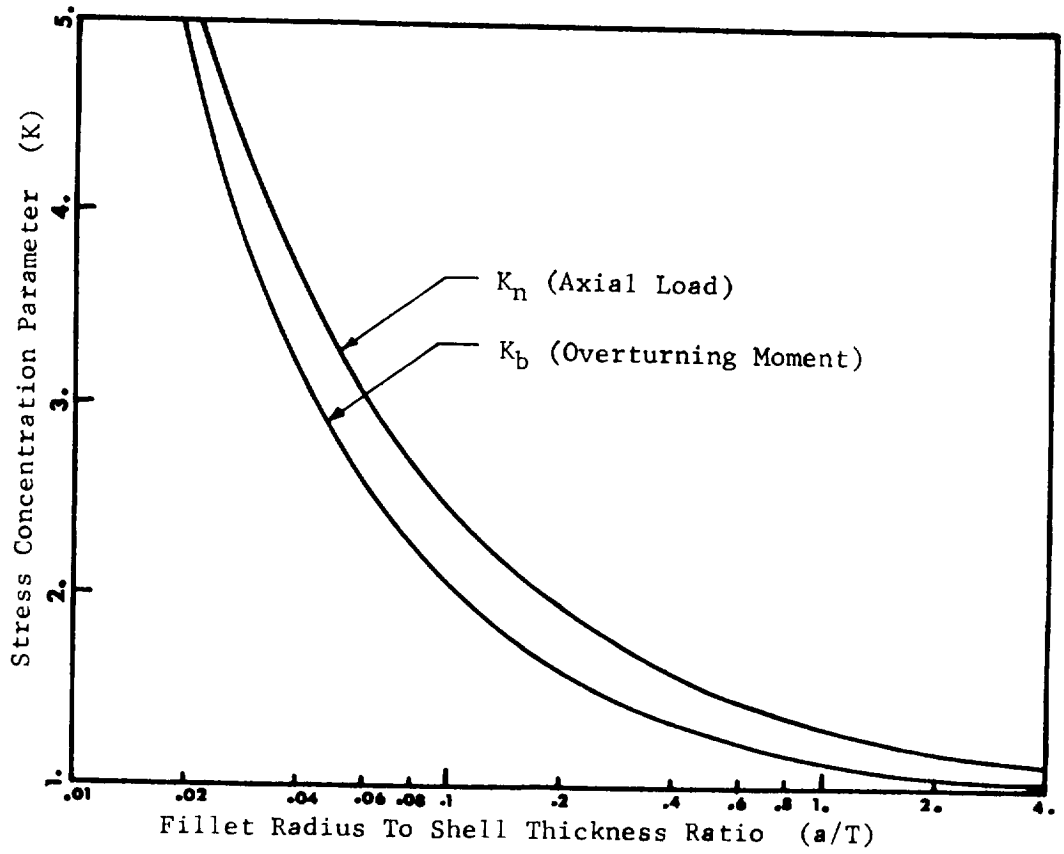

Fig. B7.2.1.2-1 Stress Concentration Parameters for R≫r

The stress calculation sheets (Figs. B7.2.1.2-2 and B7.2.1.2-3) can be used to calculate inside and outside stresses at four points (A, B, C, D on Figure B7.2.1.1-2)around the attachment. The stress calculation sheets also determine the proper sign of the stresses when the applied loads follow the sign convention used in Figure B7.2.1.1-1. The stress calculation sheets provide a place to record applied loads, geometry, parameters and all values calculated or obtained from the step-by-step procedures in paragraphs III-VI below.

STRESS CALCULATION SHEET FOR STRESSES IN SPHERICAL SHELLS CAUSED BY LOCAL LOADS (HOLLOW ATTACHMENT)

APPLIED LOADS

P = _____
V_1 = _____
V_2 = _____
M_T = _____
M_1 = _____
M_2 = _____

SHELL GEOMETRY

T = _____
t = _____
R_m = _____
r_m = _____
r_o = _____
a = _____

PARAMETERS

U = _____
T = _____
β = _____
K_n = _____
K_b = _____

STRESS	LOAD	NON-DIMENSIONAL STRESS RESULTANT	ADJUSTING FACTOR	STRESS COMPONENT	STRESSES* A_i	A_o	B_i	B_o	C_i	C_o	D_i	D_o
MERIDIONAL STRESS (f_x)	P	$\frac{N_x T}{P}$ =	$\frac{K_n P}{T^2}$ =	$\frac{K_n N_x}{T}$ =	–	–	–	–	–	–	–	–
		$\frac{M_x}{P}$ =	$\frac{6K_b P}{T^2}$ =	$\frac{6K_b M_x}{T^2}$ =	+	–	+	–	+	–	+	–
	M_1	$\frac{N_x T\sqrt{R_m T}}{M_1}$ =	$\frac{K_n M_1}{T^2\sqrt{R_m T}}$ =	$\frac{K_n N_x}{T}$ =			–	–			+	+
		$\frac{M_x \sqrt{R_m T}}{M_1}$ =	$\frac{6K_b M_1}{T^2\sqrt{R_m T}}$ =	$\frac{6K_b M_x}{T^2}$ =			+	–			–	+
	M_2	$\frac{N_x T\sqrt{R_m T}}{M_2}$ =	$\frac{K_n M_2}{T^2\sqrt{R_m T}}$ =	$\frac{K_n N_x}{T}$ =	+	+			–	–		
		$\frac{M_x\sqrt{R_m T}}{M_2}$ =	$\frac{6K_b M_2}{T^2\sqrt{R_m T}}$ =	$\frac{6K_b M_x}{T^2}$ =	–	+			+	–		
	TOTAL MERIDIONAL STRESSES (f_x)											
CIRCUMFERENTIAL STRESS (f_y)	P	$\frac{N_y T}{P}$ =	$\frac{K_n P}{T^2}$ =	$\frac{K_n N_y}{T}$ =	–	–	–	–	–	–	–	–
		$\frac{M_y}{P}$ =	$\frac{6K_b P}{T^2}$ =	$\frac{6K_b M_y}{T^2}$ =	+	–	+	–	+	–	+	–
	M_1	$\frac{N_y T\sqrt{R_m T}}{M_1}$ =	$\frac{K_n M_1}{T^2\sqrt{R_m T}}$ =	$\frac{K_n N_y}{T}$ =			–	–			+	+
		$\frac{M_y \sqrt{R_m T}}{M_1}$ =	$\frac{6K_b M_1}{T^2\sqrt{R_m T}}$ =	$\frac{6K_b M_y}{T^2}$ =			+	–			–	+
	M_2	$\frac{N_y T\sqrt{R_m T}}{M_2}$ =	$\frac{K_n M_2}{T^2\sqrt{R_m T}}$ =	$\frac{K_n N_y}{T}$ =	+	+			–	–		
		$\frac{M_y\sqrt{R_m T}}{M_2}$ =	$\frac{6K_b M_2}{T^2\sqrt{R_m T}}$ =	$\frac{6K_b M_y}{T^2}$ =	–	+			+	–		
	TOTAL CIRCUMFERENTIAL STRESS (f_y)											
SHEAR STRESS (f_{xy})	V_1		$\pi r_o T$ =	$\frac{V_1}{\pi r_o T}$ =			–	–			+	+
	V_2		$\pi r_o T$ =	$\frac{V_2}{\pi r_o T}$ =	–	–			+	+		
	M_T		$2\pi r_o^2 T$ =	$\frac{M_T}{2\pi r_o^2 T}$ =	–	–	+	+	–	–	+	+
	TOTAL SHEAR STRESS (f_{xy})											
PRINCIPAL STRESSES**	f_{max}	$\frac{f_x + f_y}{2} + \sqrt{\frac{(f_x - f_y)^2}{4} + f_{xy}^2}$ ***										
	f_{min}	$\frac{f_x + f_y}{2} - \sqrt{\frac{(f_x - f_y)^2}{4} + f_{xy}^2}$ ***										
	$f_{xy\,max}$	$\pm\sqrt{\frac{(f_x - f_y)^2}{4} + f_{xy}^2}$										

* IF LOAD IS OPPOSITE TO THAT SHOWN IN FIGURE B7.2 1 1-1 THEN REVERSE THE SIGN SHOWN.
** SEE SECTION A3.1.0.
*** CHANGE SIGN OF THE RADICAL IF $(f_x + f_y)$ IS NEGATIVE.

Fig. B7.2.1.2-2 Stress Calculation Sheet (Hollow Attachment)

STRESS CALCULATION SHEET FOR STRESSES IN SPHERICAL SHELLS CAUSED BY LOCAL LOADS (SOLID ATTACHMENT)

APPLIED LOADS

P = _____
V_1 = _____
V_2 = _____
M_T = _____
M_1 = _____
M_2 = _____

SHELL GEOMETRY

T = _____
R_m = _____
r_o = _____
a = _____

PARAMETERS

U = _____
K_n = _____
K_b = _____

STRESS	LOAD	NON-DIMENSIONAL STRESS RESULTANT	ADJUSTING FACTOR	STRESS COMPONENT	STRESSES* A_i	A_o	B_i	B_o	C_i	C_o	D_i	D_o
MERIDIONAL STRESS (f_x)	P	$\frac{N_x T}{P}$ =	$\frac{K_n P}{T^2}$ =	$\frac{K_n N_x}{T}$ =	–	–	–	–	–	–	–	–
		$\frac{M_x}{P}$ =	$\frac{6K_b P}{T^2}$ =	$\frac{6K_b M_x}{T^2}$ =	+	–	+	–	+	–	+	–
	M_1	$\frac{N_x T\sqrt{R_m T}}{M_1}$ =	$\frac{K_n M_1}{T^2\sqrt{R_m T}}$ =	$\frac{K_n N_x}{T}$ =			–	–			+	+
		$\frac{M_x \sqrt{R_m T}}{M_1}$ =	$\frac{6K_b M_1}{T^2\sqrt{R_m T}}$ =	$\frac{6K_b M_x}{T^2}$ =			+	–			–	+
	M_2	$\frac{N_x T\sqrt{R_m T}}{M_2}$ =	$\frac{K_n M_2}{T^2\sqrt{R_m T}}$ =	$\frac{K_n N_x}{T}$ =	+	+			–	–		
		$\frac{M_x \sqrt{R_m T}}{M_2}$ =	$\frac{6K_b M_2}{T^2\sqrt{R_m T}}$ =	$\frac{6K_b M_x}{T^2}$ =	–	+			+	–		
	TOTAL MERIDIONAL STRESSES (f_x)											
CIRCUMFERENTIAL STRESS (f_y)	P	$\frac{N_y T}{P}$	$\frac{K_n P}{T^2}$	$\frac{K_n N_y}{T}$ =	–	–	–	–	–	–	–	–
		$\frac{M_y}{P}$	$\frac{6K_b P}{T^2}$	$\frac{6K_b M_y}{T^2}$ =	+	–	+	–	+	–	+	–
	M_1	$\frac{N_y T\sqrt{R_m T}}{M_1}$ =	$\frac{K_n M_1}{T^2\sqrt{R_m T}}$	$\frac{K_n N_y}{T}$ =			–	–			+	+
		$\frac{M_y \sqrt{R_m T}}{M_1}$ =	$\frac{6K_b M_1}{T^2\sqrt{R_m T}}$ =	$\frac{6K_b M_y}{T^2}$ =			+	–			–	–
	M_2	$\frac{N_y T\sqrt{R_m T}}{M_2}$ =	$\frac{K_n M_2}{T^2\sqrt{R_m T}}$ =	$\frac{K_n N_y}{T}$ =	+	+			–	–		
		$\frac{M_y \sqrt{R_m T}}{M_2}$ =	$\frac{6K_b M_2}{T^2\sqrt{R_m T}}$ =	$\frac{6K_b M_y}{T^2}$ =	–	+			+	–		
	TOTAL CIRCUMFERENTIAL STRESS (f_y)											
SHEAR STRESS (f_{xy})	V_1		$\pi r_o T$	$\frac{V_1}{\pi r_o T}$ =							+	+
	V_2		$\pi r_o T$	$\frac{V_2}{\pi r_o T}$					+	+		
	M_T		$2\pi r_o^2 T$	$\frac{M_T}{2\pi r_o^2 T}$ =	–	–	+	+		–	+	+
	TOTAL SHEAR STRESS (f_{xy})											
PRINCIPAL STRESSES	f_{max}	$\frac{f_x + f_y}{2} + \sqrt{\frac{(f_x - f_y)^2}{4} + f_{xy}^2}$										
	f_{min}	$\frac{f_x + f_y}{2} - \sqrt{\frac{(f_x - f_y)^2}{4} + f_{xy}^2}$										
	$f_{xy\,max}$	$\sqrt{\frac{(f_x - f_y)^2}{4} + f_{xy}^2}$										

* IF LOAD IS OPPOSITE TO THAT SHOWN IN FIGURE B7.2.1.1-1 THEN REVERSE THE SIGN SHOWN.
** SEE SECTION A3.1.0.
*** CHANGE SIGN OF THE RADICAL IF $(f_x + f_y)$ IS NEGATIVE.

Fig. B7.2.1.2-3 Stress Calculation Sheet (Solid Attachment)

B7.2.1.2 STRESSES

II PARAMETERS

The following applicable parameters must be evaluated:

A Geometric Parameters

1. Shell Parameters (U)

a. round attachment

$$U = r_0/(R_m T)^{\frac{1}{2}}$$

b. square attachment

$$U = 1.413c/(R_m T)^{\frac{1}{2}}$$

2. Attachment Parameters (Υ and ρ)

a. hollow round attachment

$$\Upsilon = r_m/t$$

$$\rho = T/t$$

b. hollow square attachment

$$\Upsilon = 1.143c/t$$

$$\rho = T/t$$

B Stress Concentration Parameters

1. Membrane stress-stress concentration parameter (K_n)*

$$K_n = 1 + (T/5.6a)^{0.65}$$

2. Bending stress-stress concentration parameters (K_b)*

$$K_b = 1 + (T/9.4a)^{0.80}$$

* K_n and K_b values can be determined from Figure B7.2.1.2-1 with a/T values.

B7.2.1.2 STRESSES

III STRESSES RESULTING FROM RADIAL LOAD

A radial load will cause membrane and bending stress components in both the meridional and circumferential directions.

A Meridional Stresses (f_x)

Step 1. Calculate the applicable geometric parameters as defined in paragraph II above.

Step 2. Using the geometric parameters calculated in step 1, obtain the membrane nondimensional stress resultant ($N_x T/P$) for a solid attachment from Figure B7.2.1.5-1 or for a hollow attachment from Figures B7.2.1.1.5-3 through B7.2.1.5-12.

Step 3. Using P and T values and the membrane nondimensional stress resultant ($N_x T/P$), calculate the membrane stress component N_x/T from:

$$N_x/T = (N_x T/P) \cdot (P/T^2).$$

Step 4. Using the geometric parameters calculated in step 1 and the same figures as step 2, obtain the bending nondimensional stress resultant (M_x/P).

Step 5. Using P and T values and the bending nondimensional stress resultant (M_x/P), calculate the bending stress component $6M_x/T^2$ from :

$$6M_x/T^2 = (M_x/P) \cdot (6P/T^2).$$

Step 6. Using the criteria in paragraph I, obtain values for the stress concentration parameters (K_n and K_b).

Step 7. Using the stress components calculated in steps 3 and 5 and the the stress concentration parameters calculated in step 6, determine the meridional stress (f_x) from :

$$f_x = K_n (N_x/T) \pm K_b (6M_x/T^2).$$

Proper consideration of the sign will give values for the meridional stress on the inside and outside surfaces of the shell.

B Circumferential Stresses (f_y)

The circumferential stress can be determined by following the seven steps outlined above in paragraph A and by using the same curves to obtain the nondimensional stress resultants ($N_y T/P$ and M_y/P) and the following equations to calculate the stress components and circumferential stress:

$$N_y/T = (N_y T/P) \cdot (P/T^2)$$

$$6M_y/T^2 \quad (M_y/P) \cdot (6P/T^2)$$

$$f_y = K_n(N_y/T) \pm K_b(6 M_y/T^2).$$

B7.2.1.2 STRESSES

IV STRESSES RESULTING FROM OVERTURNING MOMENT

An overturning moment will cause membrane and bending stress components in both the meridional and circumferential directions.

A Meridional Stresses (f_x)

Step 1. Calculate the applicable geometric parameters as defined in paragraph II above.

Step 2. Using the geometric parameters calculated in step 1, obtain the membrane nondimensional stress resultant $[N_x T(R_m T)^{\frac{1}{2}}/M_a]$ for a solid attachment from Figure B7.2.1.5-2, or for a hollow attachment from Figures B7.2.1.5-13 through B7.2.1.5-22.

Step 3. Using M_a, R_m and T values and the membrane nondimensional stress resultant $[N_x T(R_m T)^{\frac{1}{2}}/M_a]$, calculate the membrane stress component N_x/T from:

$$N_x/T = [N_x T(R_m T)^{\frac{1}{2}}/M_a]\ [M_a/T^2(R_m T)^{\frac{1}{2}}].$$

Step 4. Using the geometric parameters calculated in step 1 and the same figures as step 2, obtain the bending nondimensional stress resultant $[M_x(R_m T)^{\frac{1}{2}}/M_a]$.

Step 5. Using M_a, R_m and T values and the bending nondimensional stress resultant $[M_x (R_m T)^{\frac{1}{2}}/M_a]$, calculate the bending stress component $6M_x/T^2$ from:

$$6M_x/T^2 = [M_x(R_m T)^{\frac{1}{2}}/M_a]\ [6M_a/T^2(R_m T)^{\frac{1}{2}}].$$

Step 6. Using the criteria in paragraph I, obtain values for the stress concentration parameters (K_n and K_b).

Step 7. Using the stress components calculated in steps 3 and 5 and the stress concentration parameters calculated in step 6, determine the meridional stress (f_x) from:

$$f_x = K_n(N_x/T) \pm K_b(6M_x/T^2)$$

Proper consideration of the sign will give values for the meridional stress on the inside and outside surfaces of the shell.

B Circumferential Stress (f_y)

The circumferential stress can be determined by following the seven steps outlined above in paragraph A and by using the same figures to obtain the nondimensional stress resultants $[N_y T(R_m T)^{\frac{1}{2}}/M_a]$ and the following equations to calculate the stress components and circumferential stress:

$$N_y/T = [N_y T(M_m T)^{\frac{1}{2}}/M_a][M_a/T^2(R_m T)^{\frac{1}{2}}]$$

$$6M_y/T^2 = [M_x(R_m T)^{\frac{1}{2}}/M_a]\,[6M_a/T^2(R_m T)^{\frac{1}{2}}]$$

$$f_y = K_n(N_x/T) \pm K_b(6M_x/T^2).$$

B7.2.1.2 STRESSES

V STRESSES RESULTING FROM SHEAR LOAD

A shear load (V_a) will cause a membrane shear stress (f_{xy}) in the shell at the attachment-to-shell juncture. The shear stress is determined as follows:

A Round Attachment

$$f_{xy} = \frac{V_a}{r_0 T} \sin \Theta \qquad \text{for } V_a = V_1$$

$$\text{or } f_{xy} = \frac{V_a}{r_0 T} \cos \Theta \qquad \text{for } V_a = V_2$$

B Square Attachment

$$\left.\begin{aligned} f_{xy} &= V_a / 4cT \quad (\text{at } \Theta = 90° \text{ and } 270°) \\ f_{xy} &= 0 \quad (\text{at } \Theta = 0° \text{ and } 180°) \end{aligned}\right\} \text{for } V_a = V_1$$

or

$$\left.\begin{aligned} f_{xy} &= V_a / 4cT \quad (\text{at } \Theta = 0° \text{ and } 180°) \\ f_{xy} &= 0 \quad (\text{at } \Theta = 90° \text{ and } 270°) \end{aligned}\right\} \text{for } V_a = V_2$$

B7.2.1.2 STRESSES

VI STRESSES RESULTING FROM TWISTING MOMENT

A Round Attachment

A twisting moment (M_T) applied to a round attachment will cause a shear stress (f_{xy}) in the shell at the attachment-to-shell juncture. The shear stress is pure shear and is constant around the juncture. The shear stress is determined as follows:

$$f_{xy} = M_T/2\pi \ r_0^2 \ T.$$

B Square Attachment

A twisting moment applied to a square attachment will cause a complex stress field in the shell. No acceptable methods for analyzing this loading are available.

B7.2.1.3 STRESSES RESULTING FROM ARBITRARY LOADING

I CALCULATION OF STRESSES

Most loadings that induce local loads on spherical shells are of an arbitrary nature. Stresses are determined by the following procedure:

Step 1. Resolve the applied arbitrary load (forces and/or moments into axial forces, shear forces, overturning moments and twisting moment components. (See paragraph B7.2.1.6, Example Problem.) The positive directions of the components and the point of application of the force components (intersection of centerline of attachment with attachment-shell interface) are indicated in Figure B7.2.1.1-1.

Step 2. Evaluate inside and outside stresses at points A, B, C and D for each component of the applied arbitrary load by the methods in paragraph B7.2.1.2.

Step 3. Obtain the stresses for the arbitrary loading by combining the meridional, circumferential and shear stresses evaluated by step 2 for each of the points A, B, C and D on the inside and outside of the shell. Proper consideration of signs is necessary.

B7.2.1.3 STRESSES RESULTING FROM ARBITRARY LOADING

II LOCATION AND MAGNITUDE OF MAXIMUM STRESSES

The location and magnitude of the maximum stresses caused by an arbitrary load require a consideration of the following:

A The determination of principal stresses (f_{max}, f_{min} and $f_{xy} = 0$ or $f_{xy} = max$) for the calculated stresses (f_x, f_y and f_{xy}) at a specific point.

B The orientation of the coordinate system (1, 2, 3) in Figures B7.2.1.1-1 and B7.2.1.1-2 with respect to an applied arbitrary load may give different values for principal stresses. These different values are caused by a different set of components.

C Whether or not the value for a stress resultant is obtained from the dashed lines or solid lines in Figures B7.2.1.5-3 through B7.2.1.5-22.

B7.2.1.4 ELLIPSOIDAL SHELLS

The analysis presented in this section (B7.2.1.0) can be applied to ellipsoidal shells with attachment at the apex because the radii of curvature are equal. For attachments not located at the apex (points of unequal radii), the analysis is incorrect, and the error increases for attachments at greater distances from the apex.

B7.2.1.5 NONDIMENSIONAL STRESS RESULTANT CURVES

I LIST OF CURVES

A Solid Attachments

1. Nondimensional Stress Resultants for Radial Load (P) B7.2.1.5-1
2. Nondimensional Stress Resultants for Overturning Moment (M_a) B7.2.1.5-2

B Hollow Attachments

1. Nondimensional Stress Resultants for Radial Load (P)

$\Upsilon = 5$	$\rho = 0.25$	B7.2.1.5-3
$\Upsilon = 5$	$\rho = 1.0$	B7.2.1.5-4
$\Upsilon = 5$	$\rho = 2.0$	B7.2.1.5-5
$\Upsilon = 5$	$\rho = 4.0$	B7.2.1.5-6
$\Upsilon = 15$	$\rho = 1.0$	B7.2.1.5-7
$\Upsilon = 15$	$\rho = 2.0$	B7.2.1.5-8
$\Upsilon = 15$	$\rho = 4.0$	B7.2.1.5-9
$\Upsilon = 15$	$\rho = 10.0$	B7.2.1.5-10
$\Upsilon = 50$	$\rho = 4.0$	B7.2.1.5-11
$\Upsilon = 50$	$\rho = 10.0$	B7.2.1.5-12

2. Nondimensional Stress Resultants for Overturning Moment (M_a)

$\Upsilon = 5$	$\rho = 0.25$	B7.2.1.5-13
$\Upsilon = 5$	$\rho = 1.0$	B7.2.1.5-14
$\Upsilon = 5$	$\rho = 2.0$	B7.2.1.5-15
$\Upsilon = 5$	$\rho = 4.0$	B7.2.1.5-16
$\Upsilon = 15$	$\rho = 1.0$	B7.2.1.5-17
$\Upsilon = 15$	$\rho = 2.0$	B7.2.1.5-18
$\Upsilon = 15$	$\rho = 4.0$	B7.2.1.5-19
$\Upsilon = 15$	$\rho = 10.0$	B7.2.1.5-20
$\Upsilon = 50$	$\rho = 4.0$	B7.2.1.5-21
$\Upsilon = 50$	$\rho = 10.0$	B7.2.1.5-22

B7.2.1.5 NONDIMENSIONAL STRESS RESULTANT CURVES

II CURVES

The following curves (Figs. B7.2.1.5-1 — B7.2.1.5-22) are plots of nondimensional stress resultants versus a shell parameter for the axial load and overturning moment loadings and for various attachment parameters.

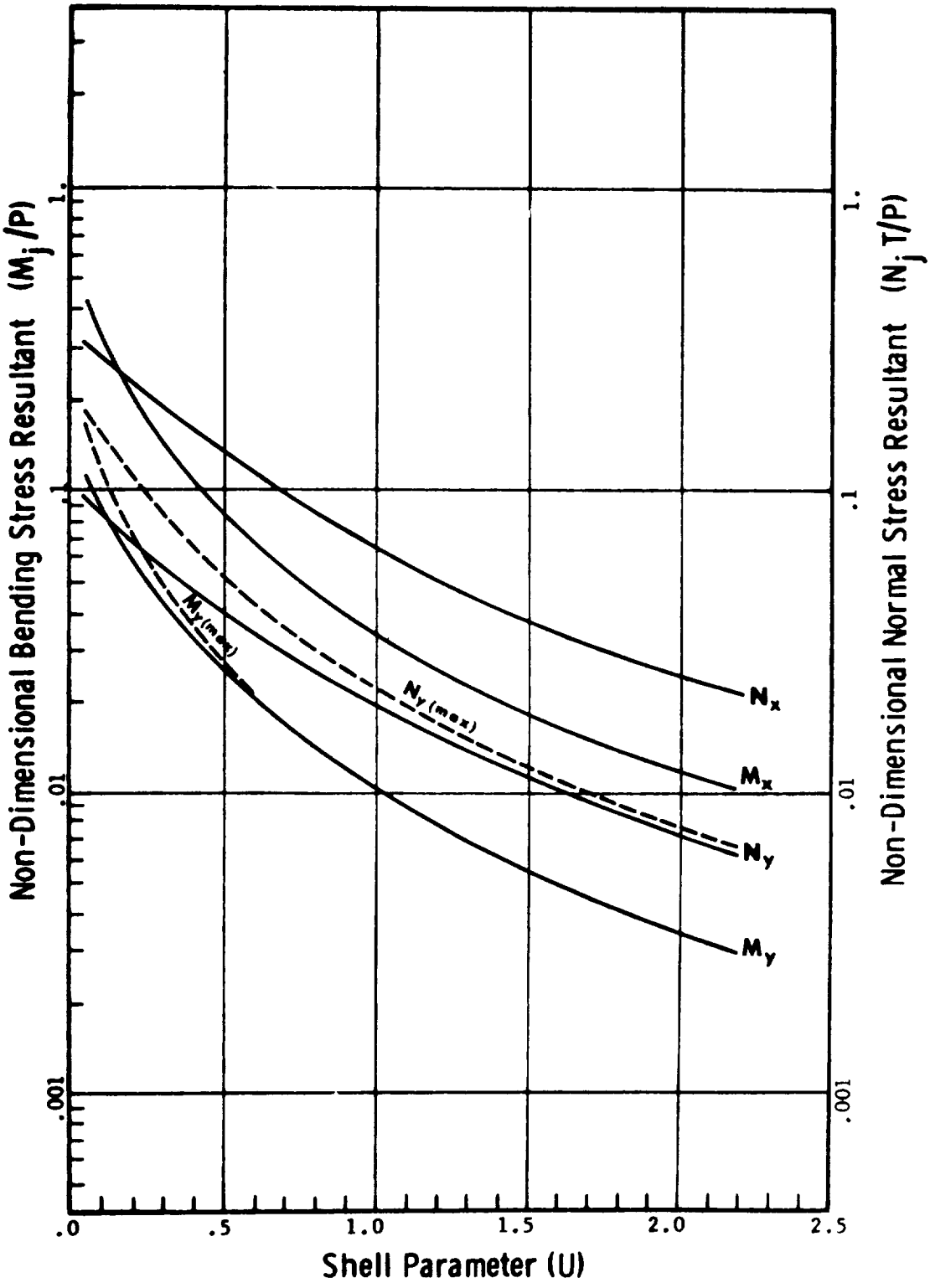

Figure B7.2.1.5-1 Non-Dimensional Stress Resultants for Radial Load (P) Solid Attachment

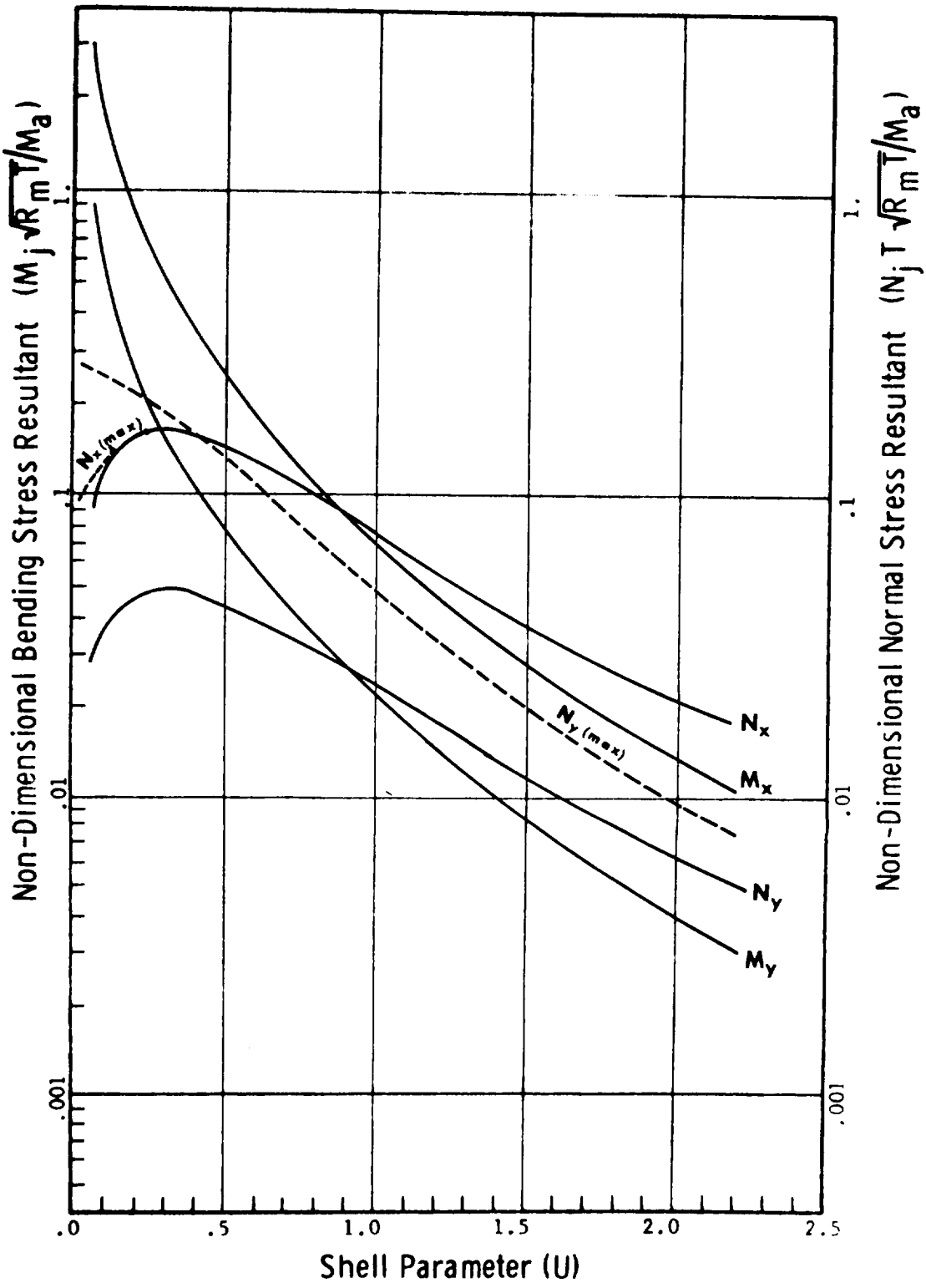

Figure B7.2.1.5-2 Non-Dimensional Stress Resultants for Overturning Moment (M_a) Solid Attachment

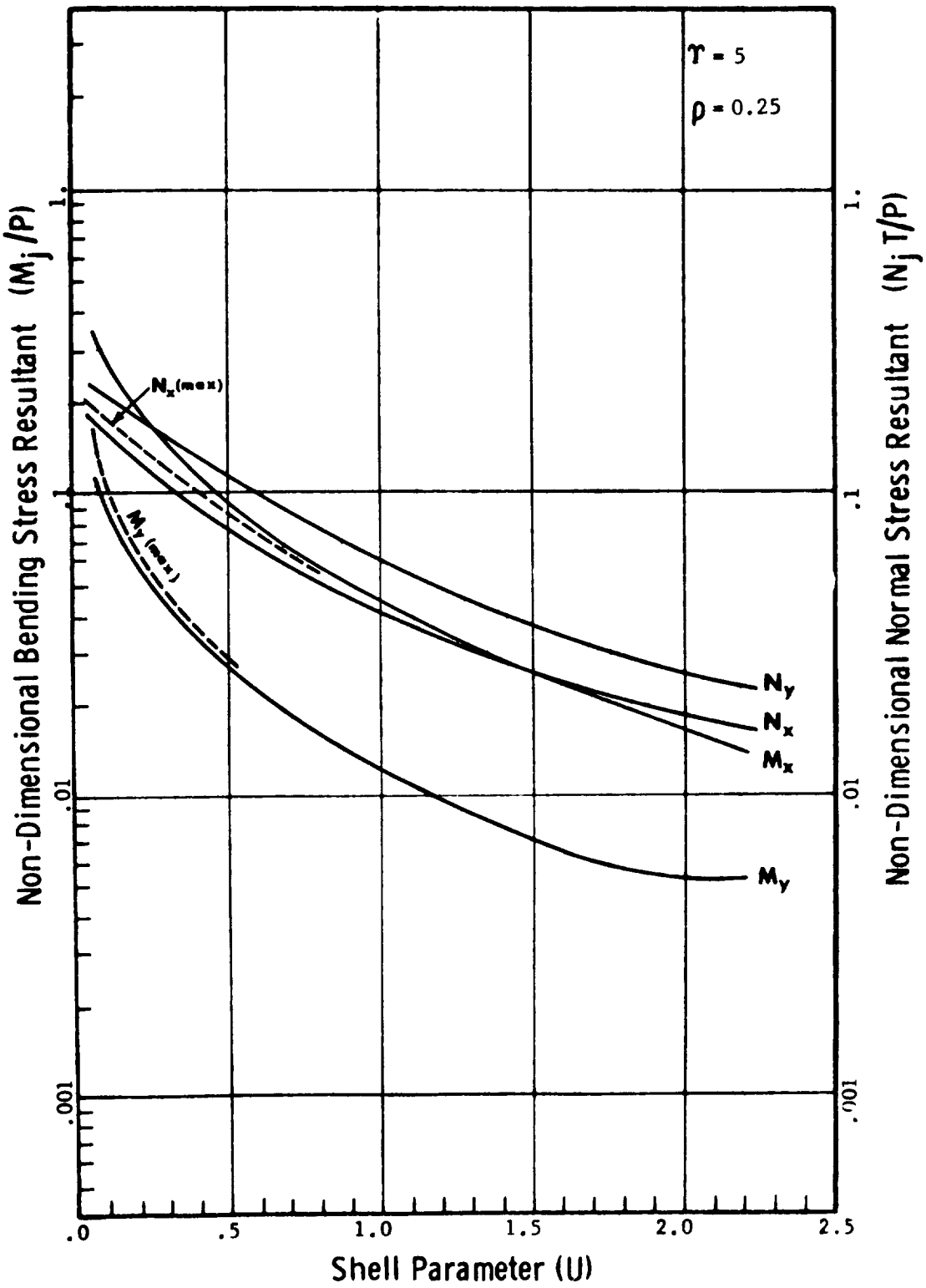

Figure B7.2.1.5-3 Non-Dimensional Stress Resultants for Radial Load (P)
Hollow Attachment $\Upsilon = 5$ and $\rho = 0.25$

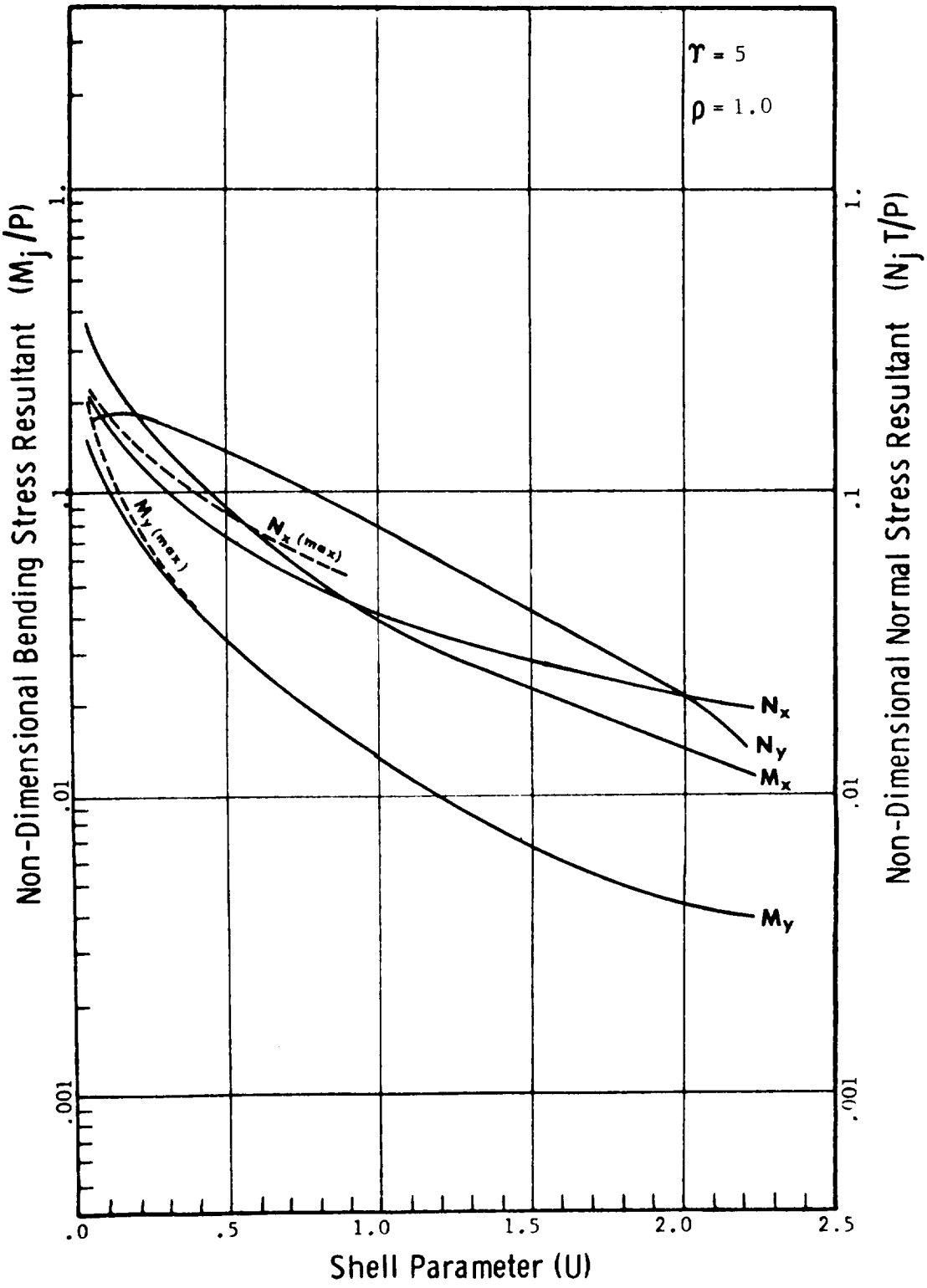

Figure B7.2.1.5-4 Non-Dimensional Stress Resultants for Radial Load (P) Hollow Attachment $\Upsilon = 5$ and $\rho = 1.0$

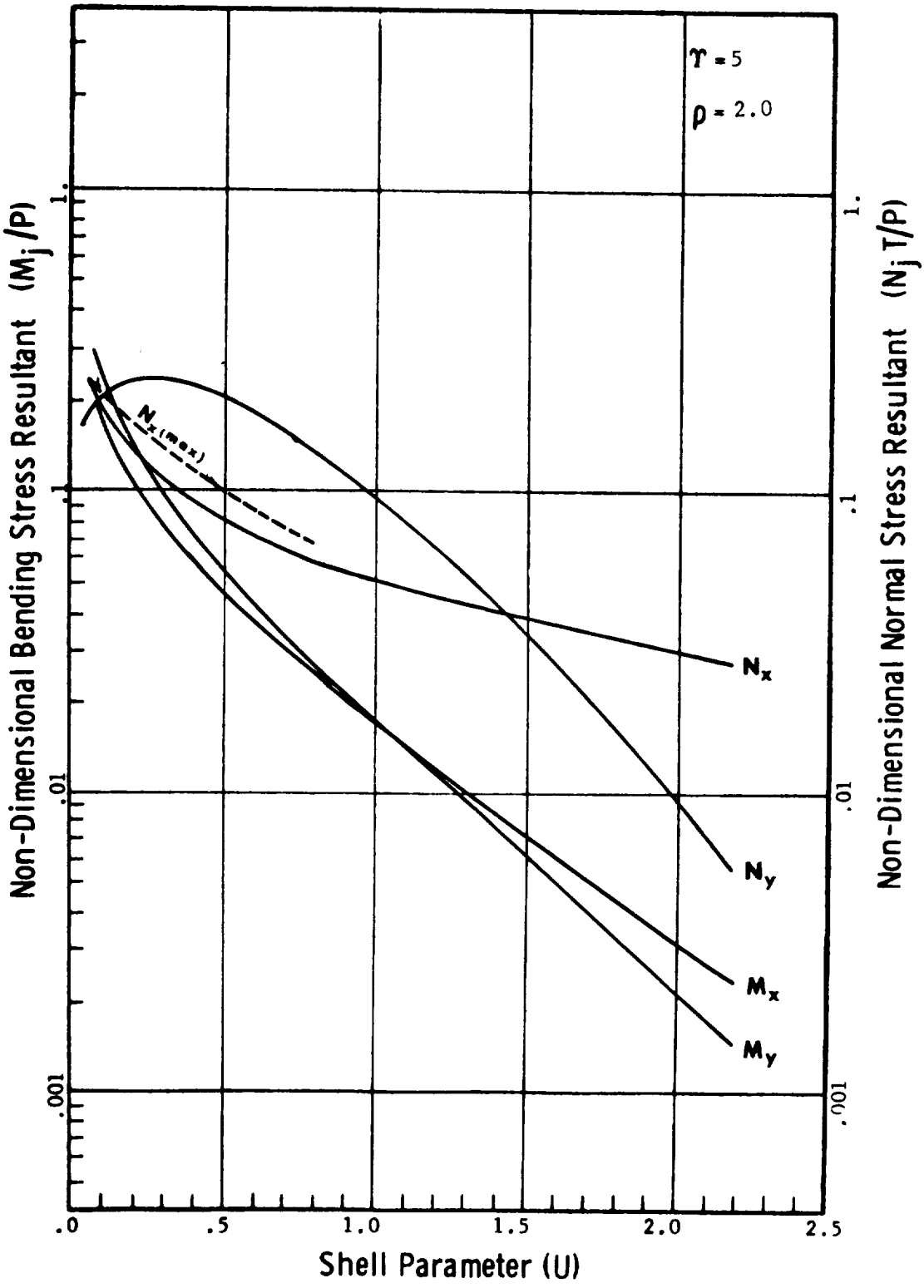

Figure B7.2.1.5-5 Non-Dimensional Stress Resultants for Radial Load (P)
Hollow Attachment $\Upsilon = 5$ and $\rho = 2.0$

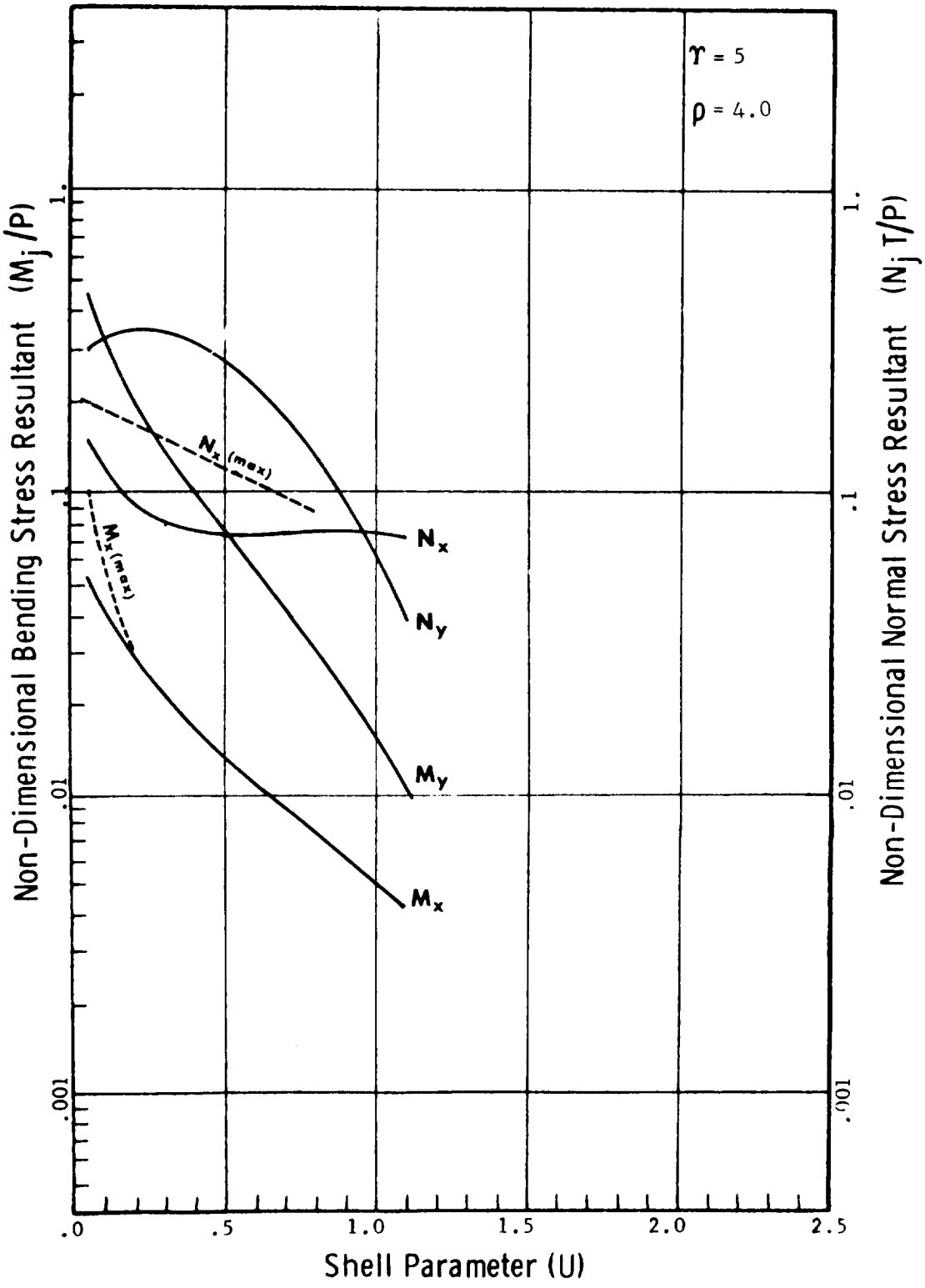

Figure B7.2.1.5-6 Non-Dimensional Stress Resultants for Radial Load (P) Hollow Attachment $\Upsilon = 5$ and $\rho = 4.0$

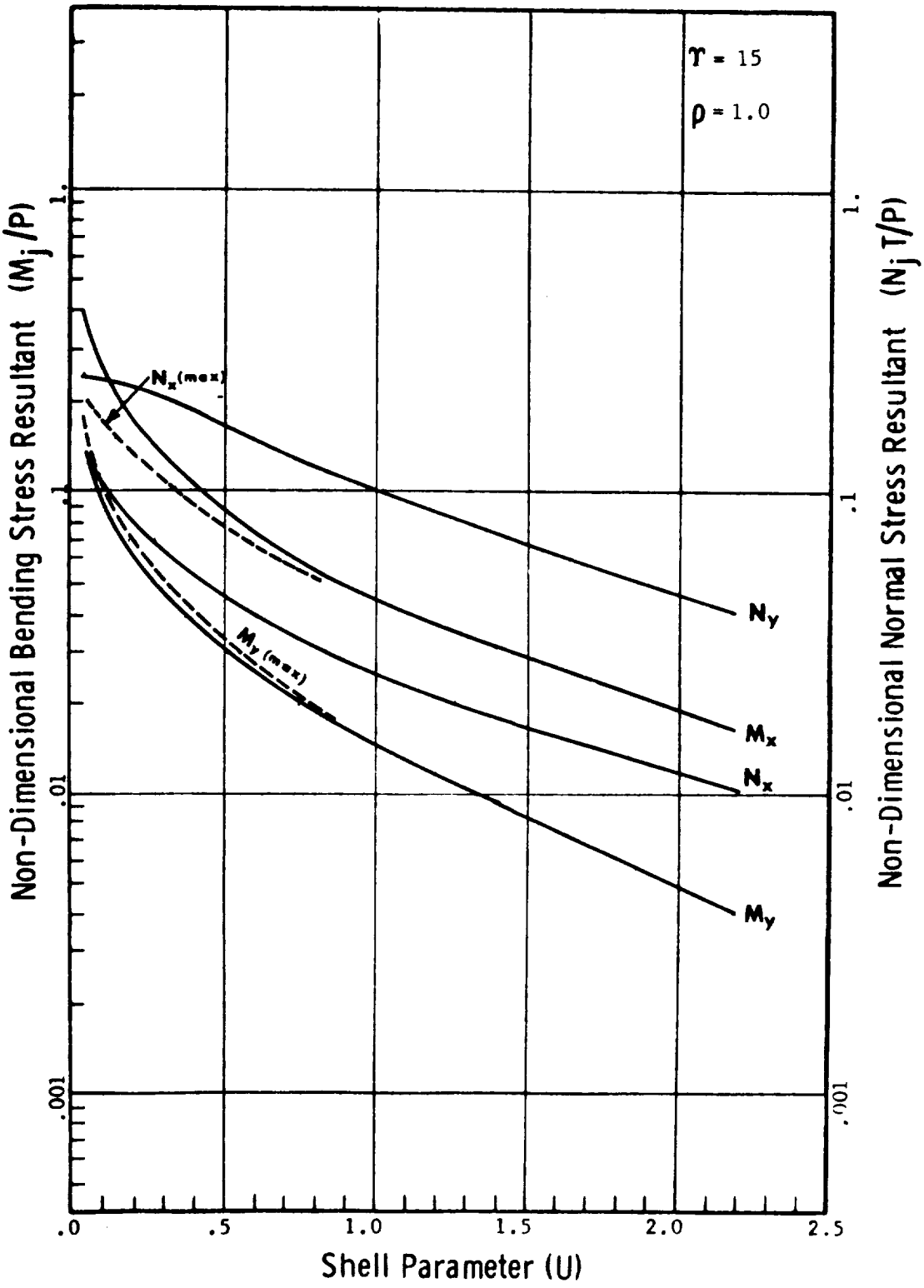

Figure B7.2.1.5-7 Non-Dimensional Stress Resultants for Radial Load (P)
Hollow Attachment $\Upsilon = 15$ and $\rho = 1.0$

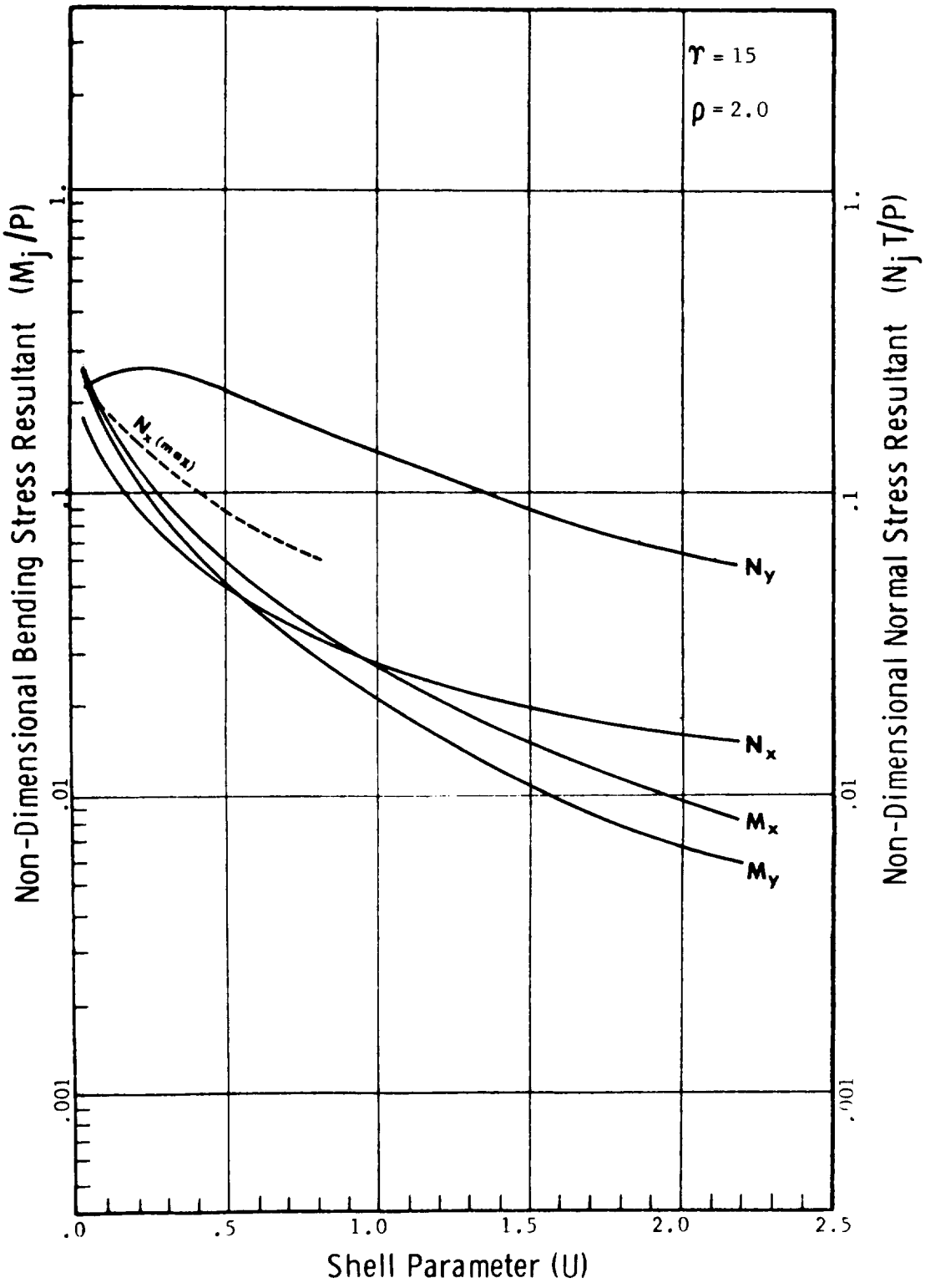

Figure B7.2.1.5-8 Non-Dimensional Stress Resultants for Radial Load (P)
Hollow Attachment $\Upsilon = 15$ and $\rho = 2.0$

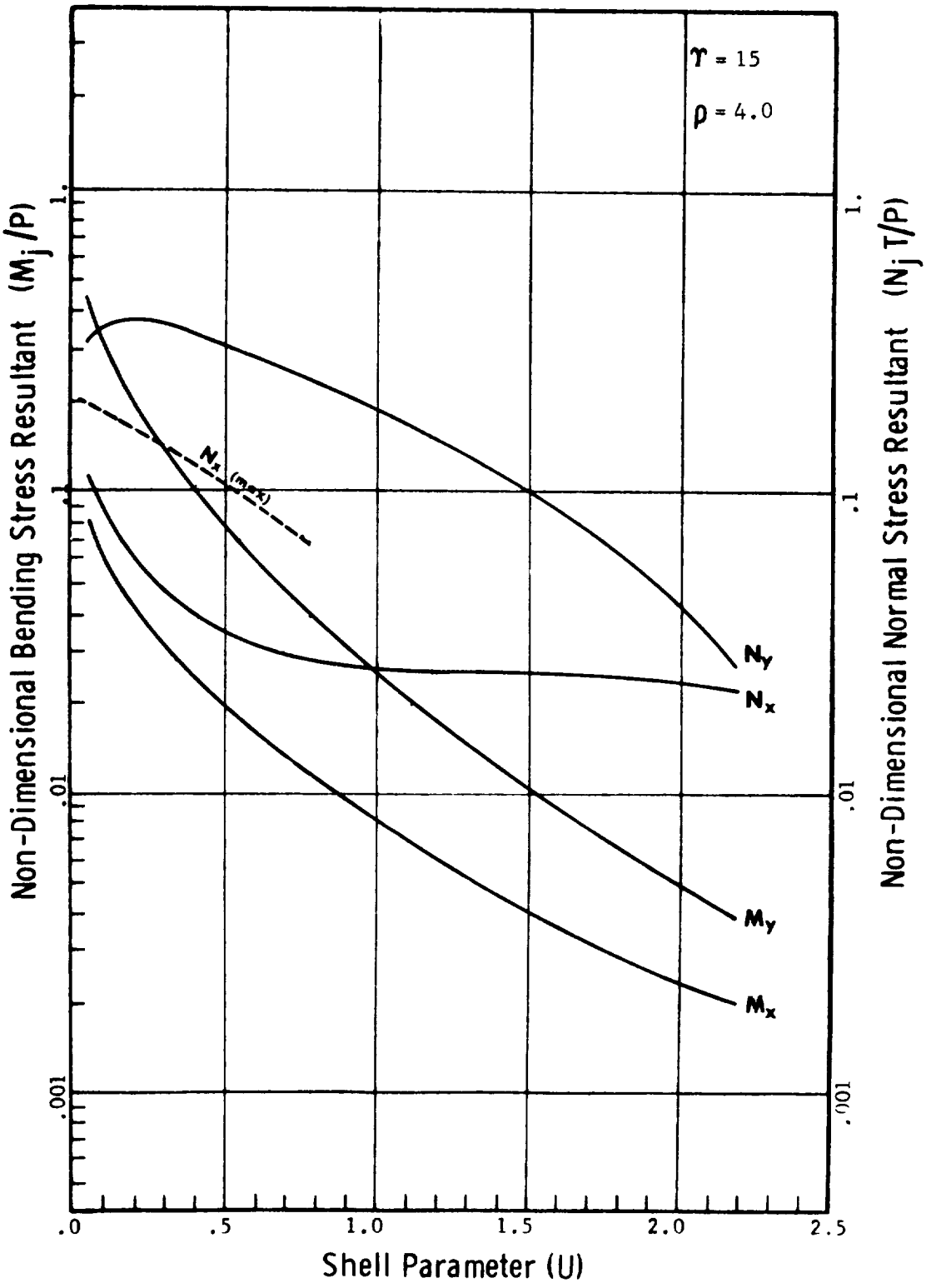

Figure B7.2.1.5-9 Non-Dimensional Stress Resultants for Radial Load (P) Hollow Attachment $\Upsilon = 15$ and $\rho = 4.0$

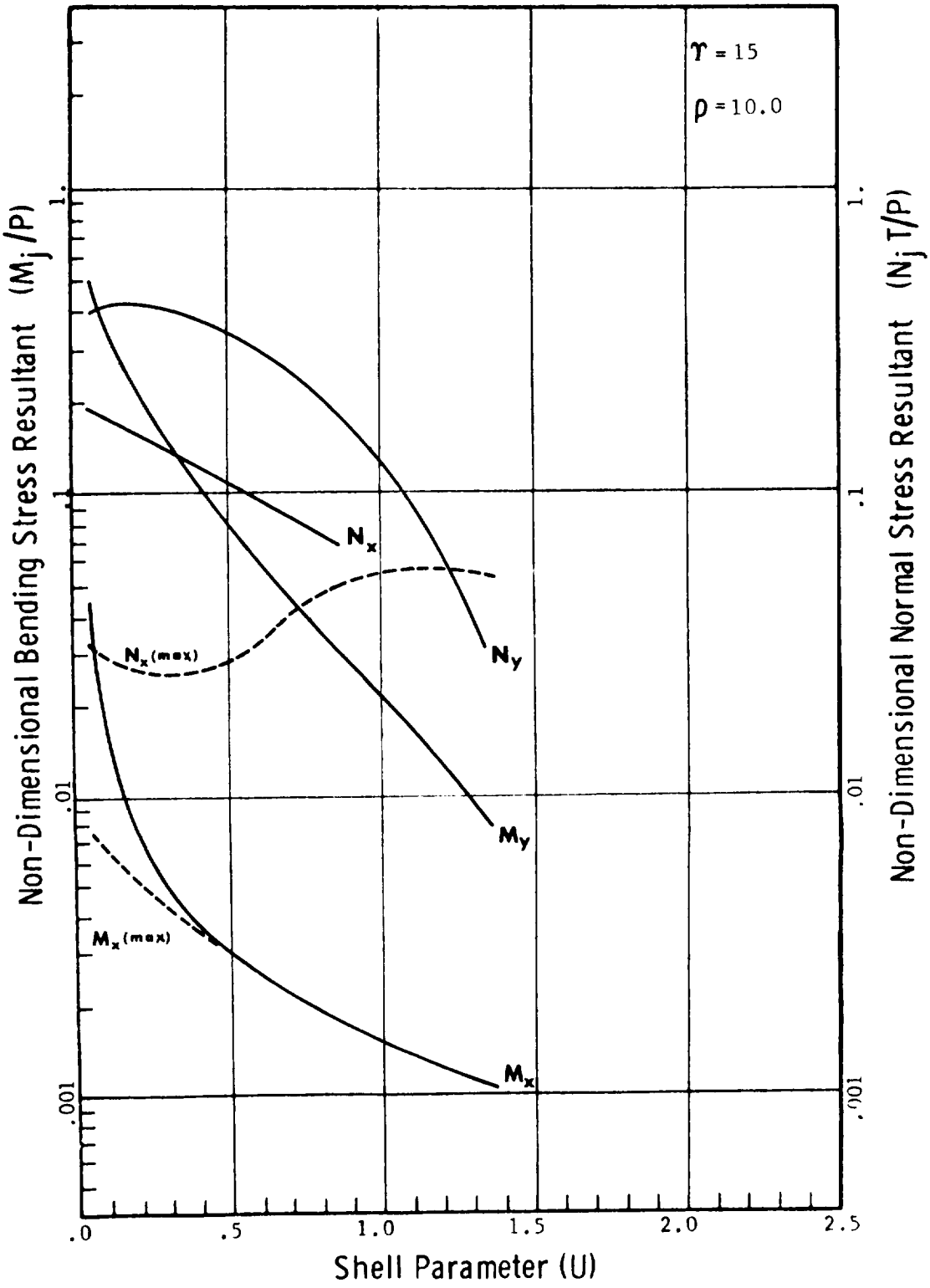

Figure B7.2.1.5-10 Non-Dimensional Stress Resultants for Radial Load (P) Hollow Attachment $\Upsilon = 15$ and $\rho = 10.0$

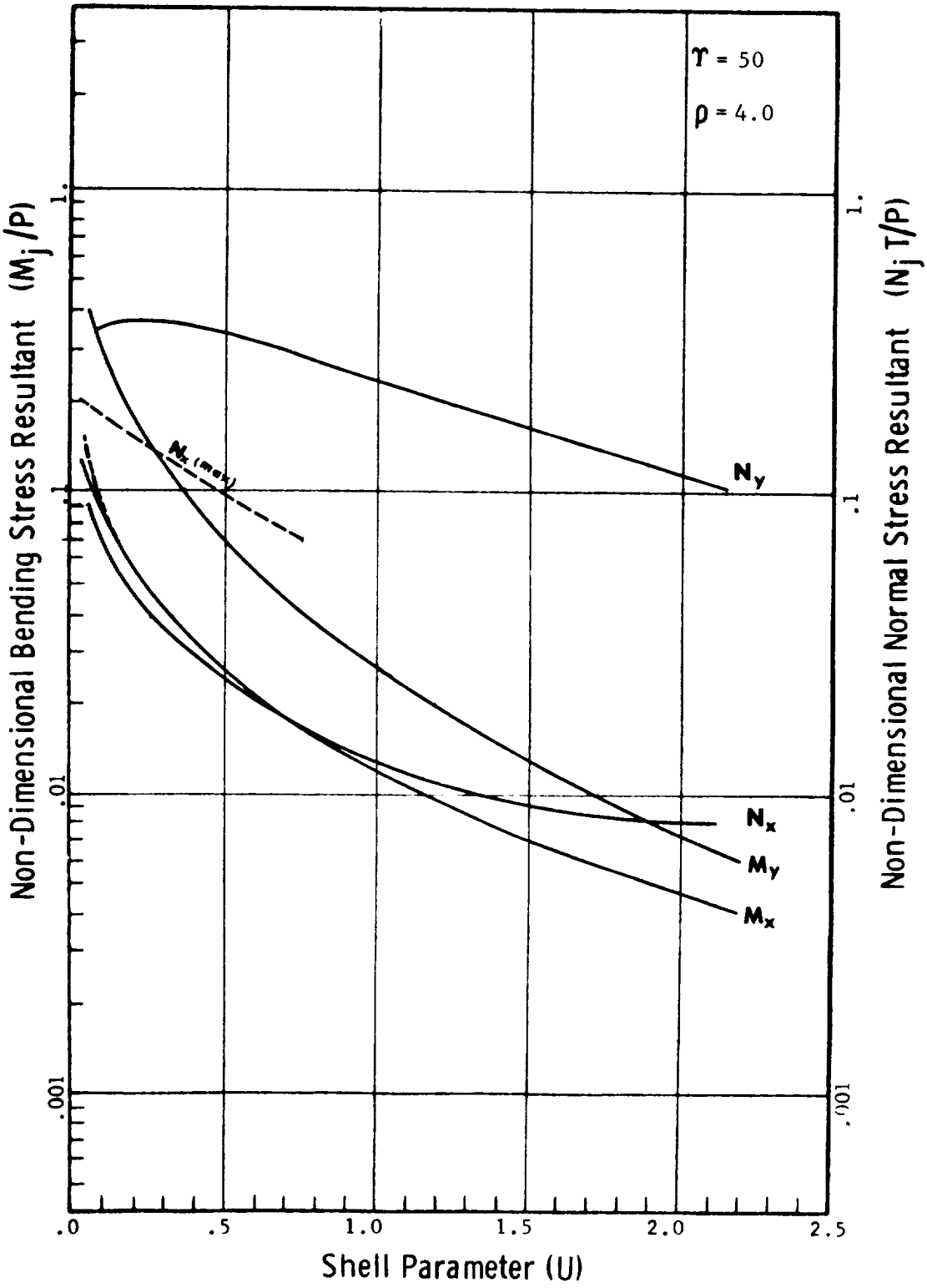

Figure B7.2.1.5-11 Non-Dimensional Stress Resultants for Radial Load (P)
Hollow Attachment $\Upsilon = 50$ and $\rho = 4.0$

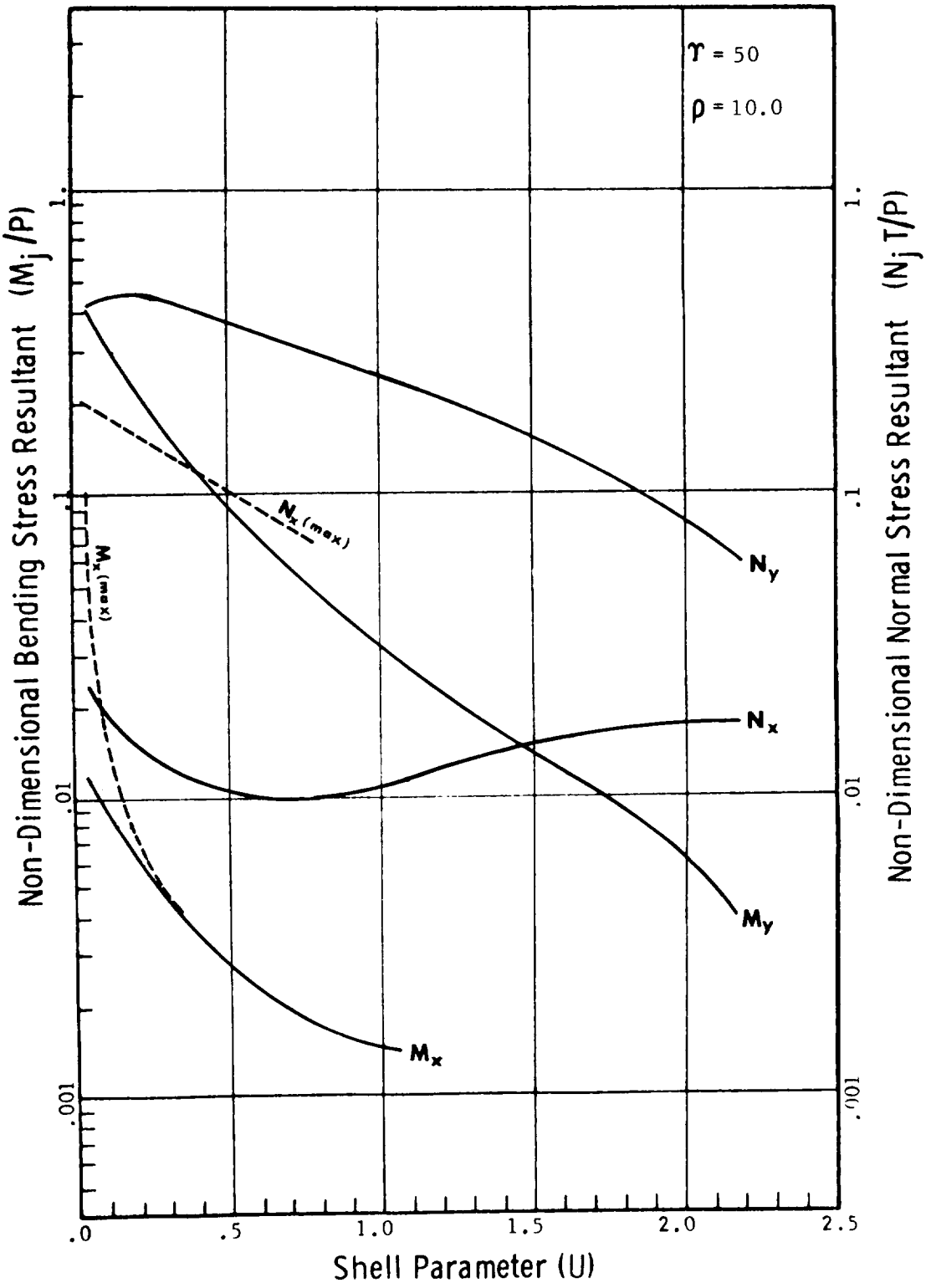

Figure B7.2.1.5-12 Non-Dimensional Stress Resultants for Radial Load (P) Hollow Attachment $\Upsilon = 50$ and $\rho = 10.0$

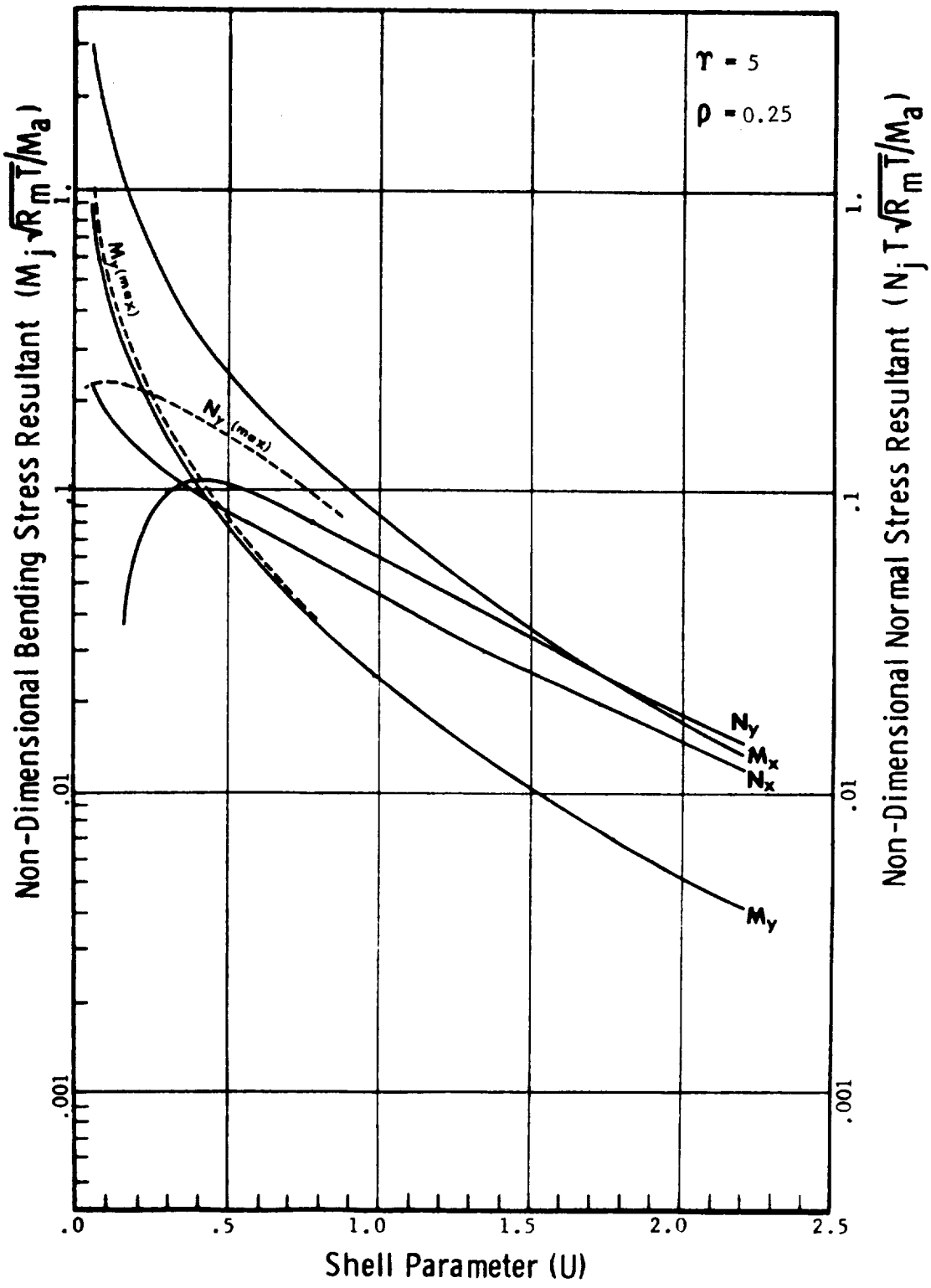

Figure B7.2.1.5-13 Non-Dimensional Stress Resultants for Overturning Moment (M_a) Hollow Attachment $\Upsilon = 5$ and $\rho = 0.25$

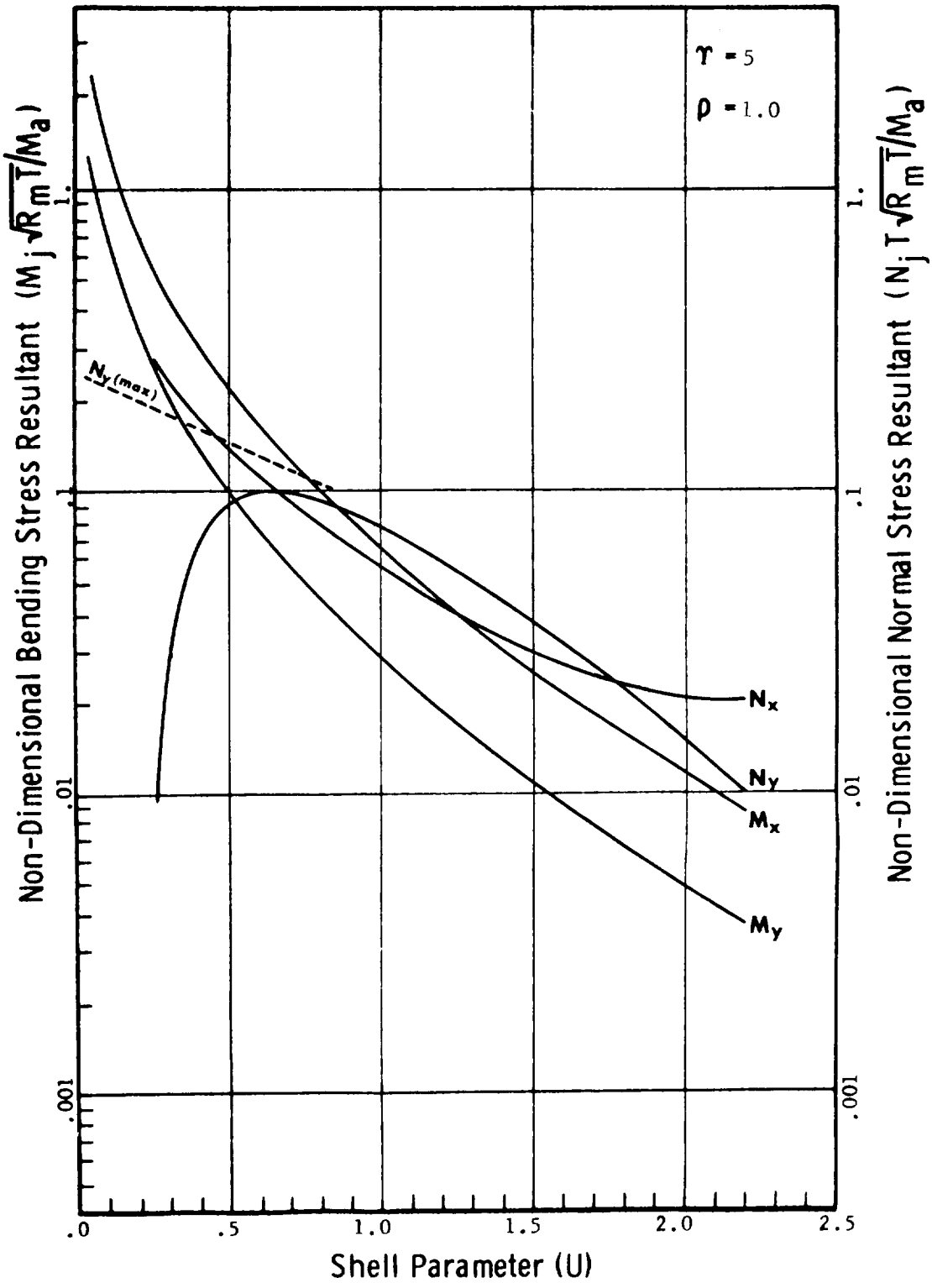

Figure B7.2.1.5-14 Non-Dimensional Stress Resultants for Overturning Moment (M_a) Hollow Attachment $\Upsilon = 5$ and $\rho = 1.0$

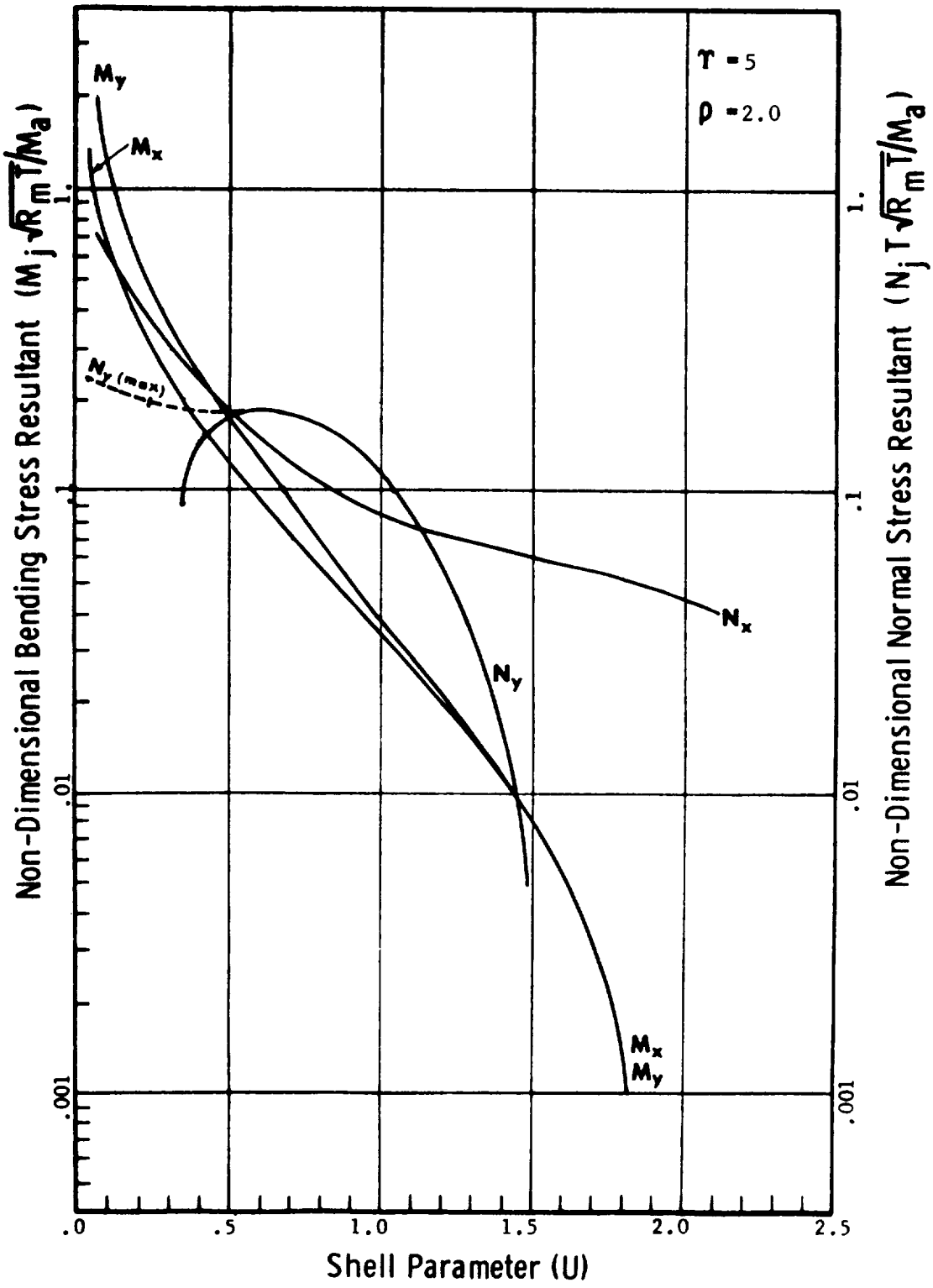

Figure B7.2.1.5-15 Non-Dimensional Stress Resultants for Overturning Moment (M_a) Hollow Attachment $\Upsilon = 5$ and $\rho = 2.0$

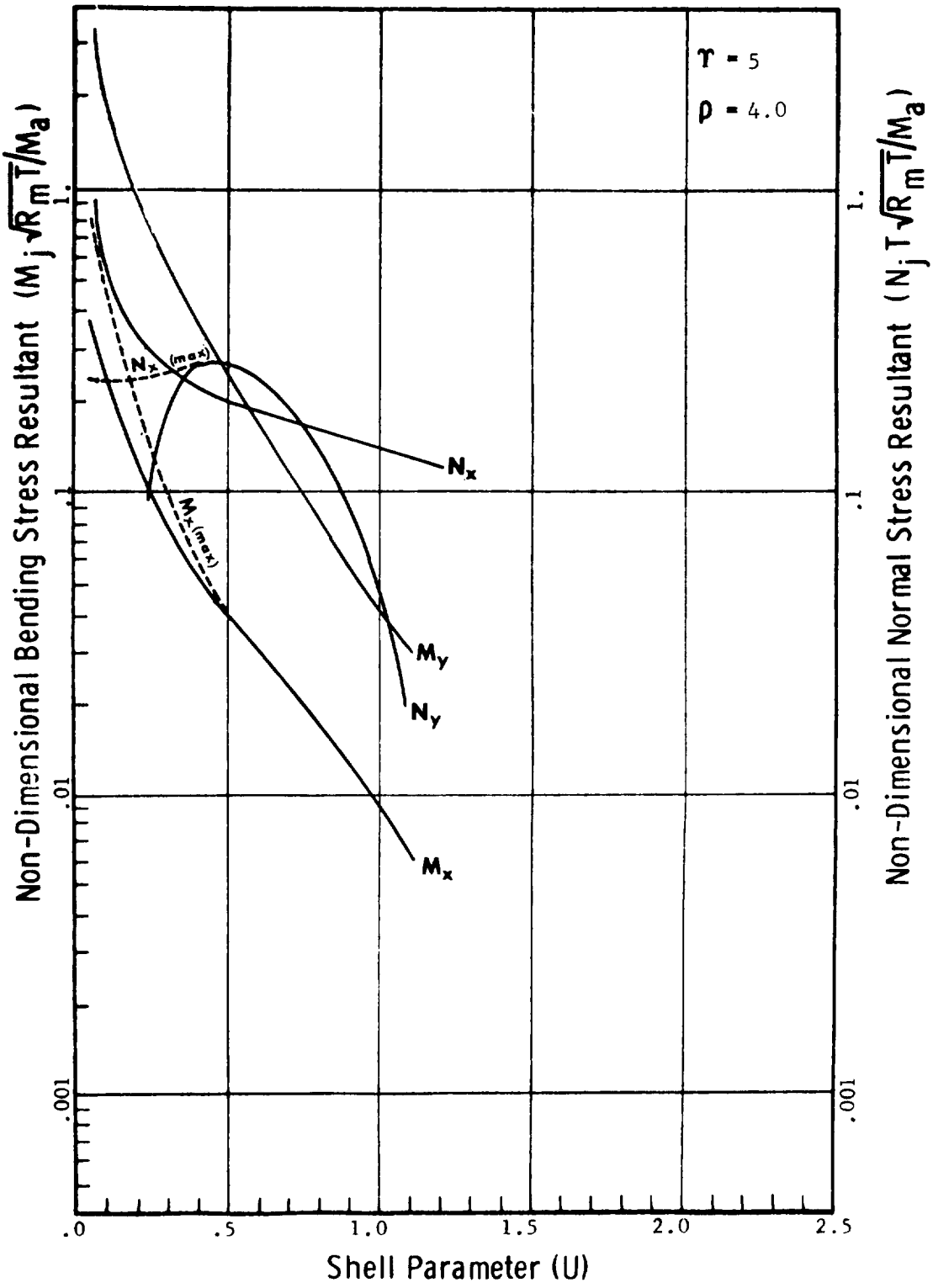

Figure B7.2.1.5-16 Non-Dimensional Stress Resultants for Overturning Moment (M_a) Hollow Attachment $\Upsilon = 5$ and $\rho = 4.0$

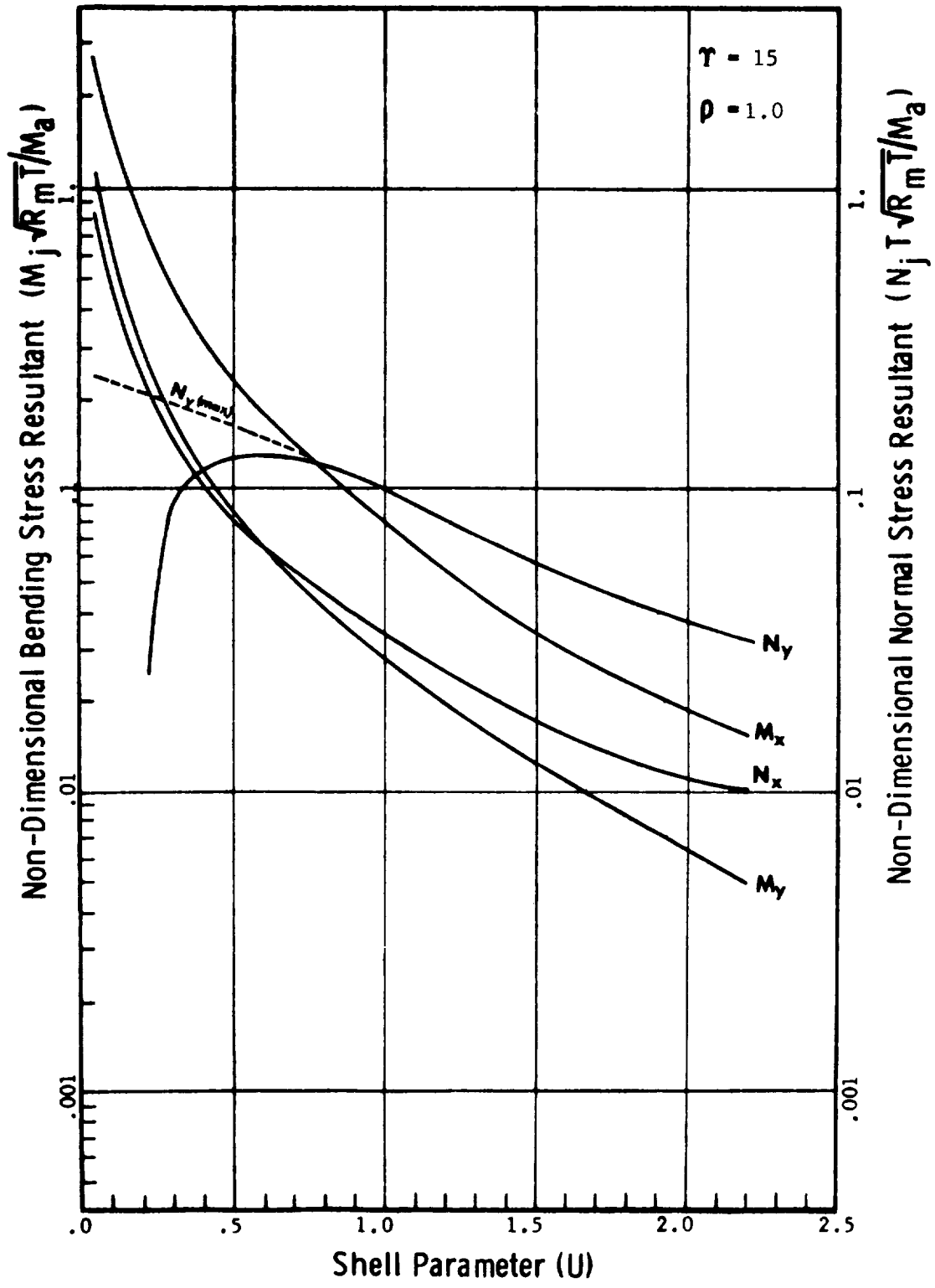

Figure B7.2.1.5-17 Non-Dimensional Stress Resultants for Overturning Moment (M_a) Hollow Attachment $\Upsilon = 15$ and $\rho = 1.0$

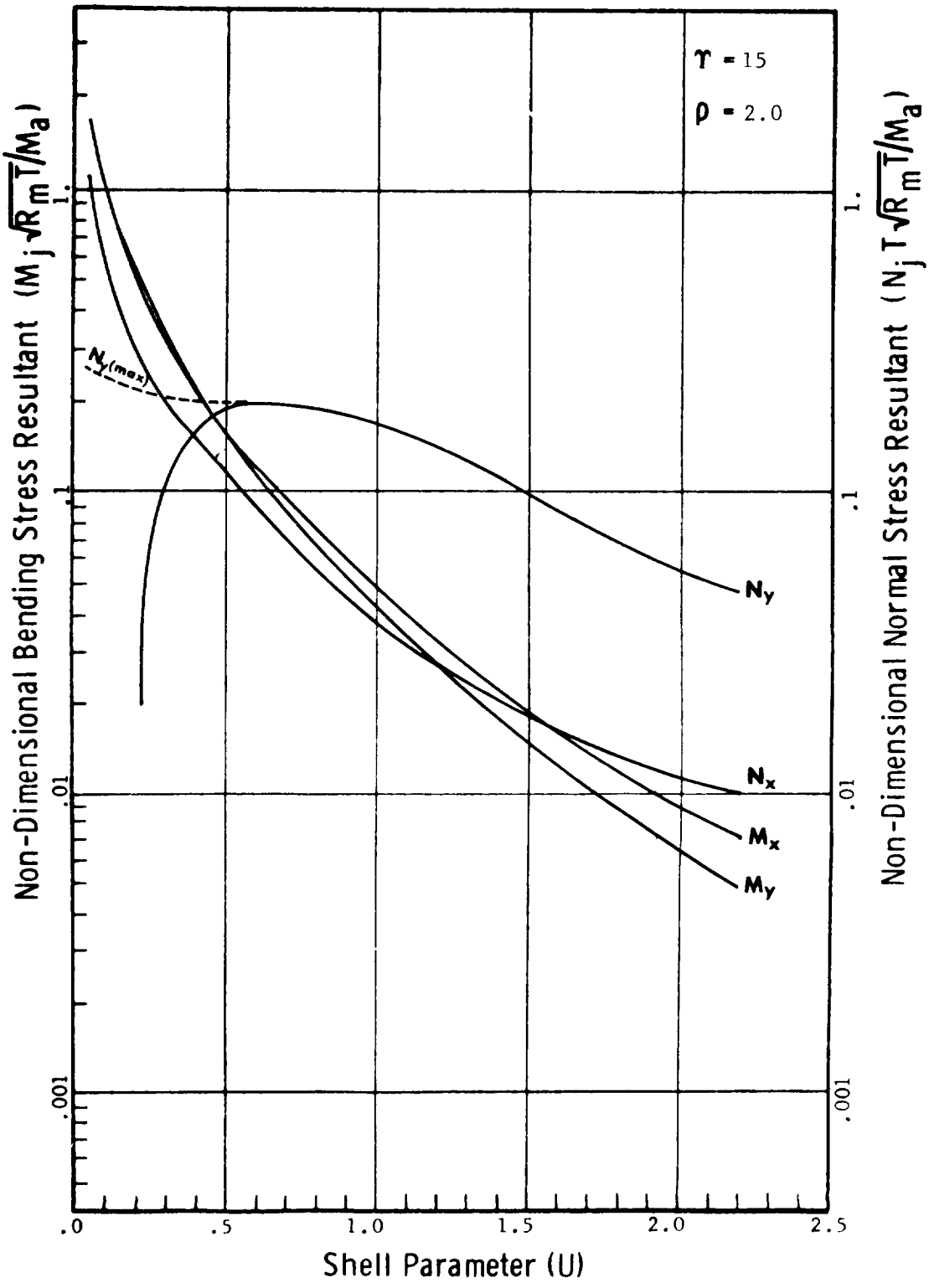

Figure B7.2.1.5-18 Non-Dimensional Stress Resultants for Overturning Moment (M_a) Hollow Attachment $\Upsilon = 15$ and $\rho = 2.0$

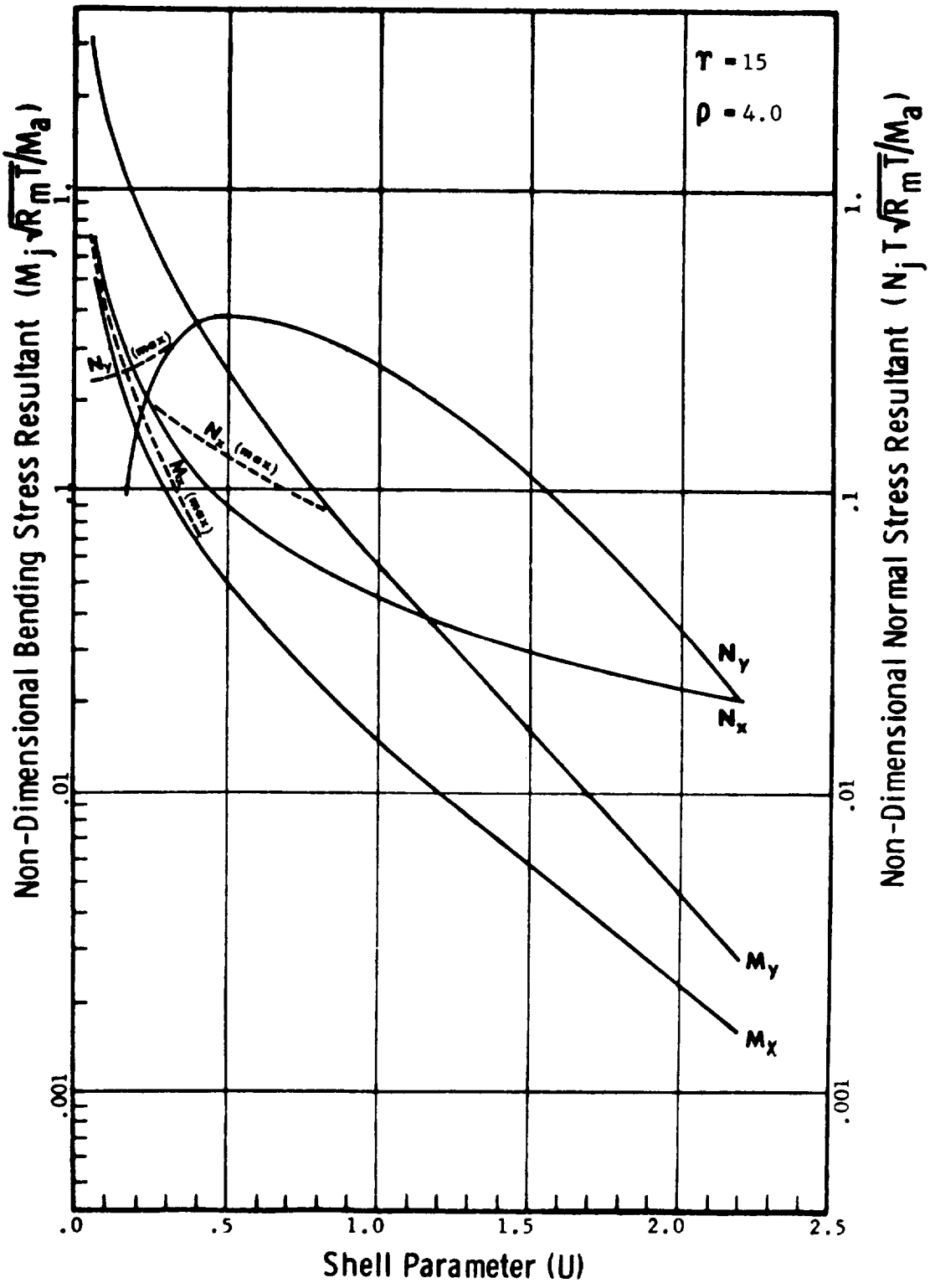

Figure B7.2.1.5-19 Non-Dimensional Stress Resultants for Overturning Moment (M_a) Hollow Attachment Υ = 15 and ρ = 4.0

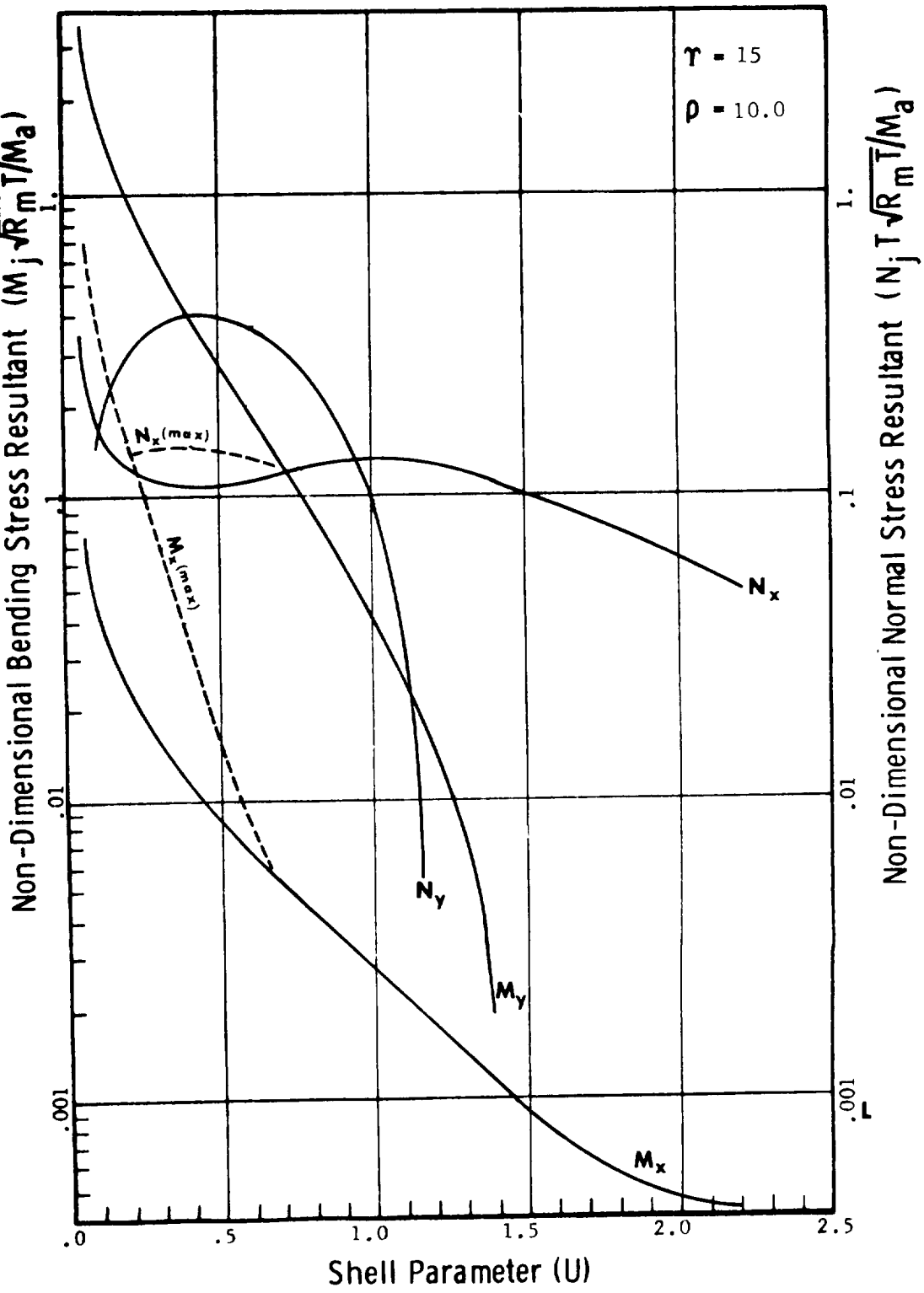

Figure B7.2.1.5-20 Non-Dimensional Stress Resultants for Overtirning Moment (M_a) Hollow Attachment Υ = 15 and ρ = 10.0

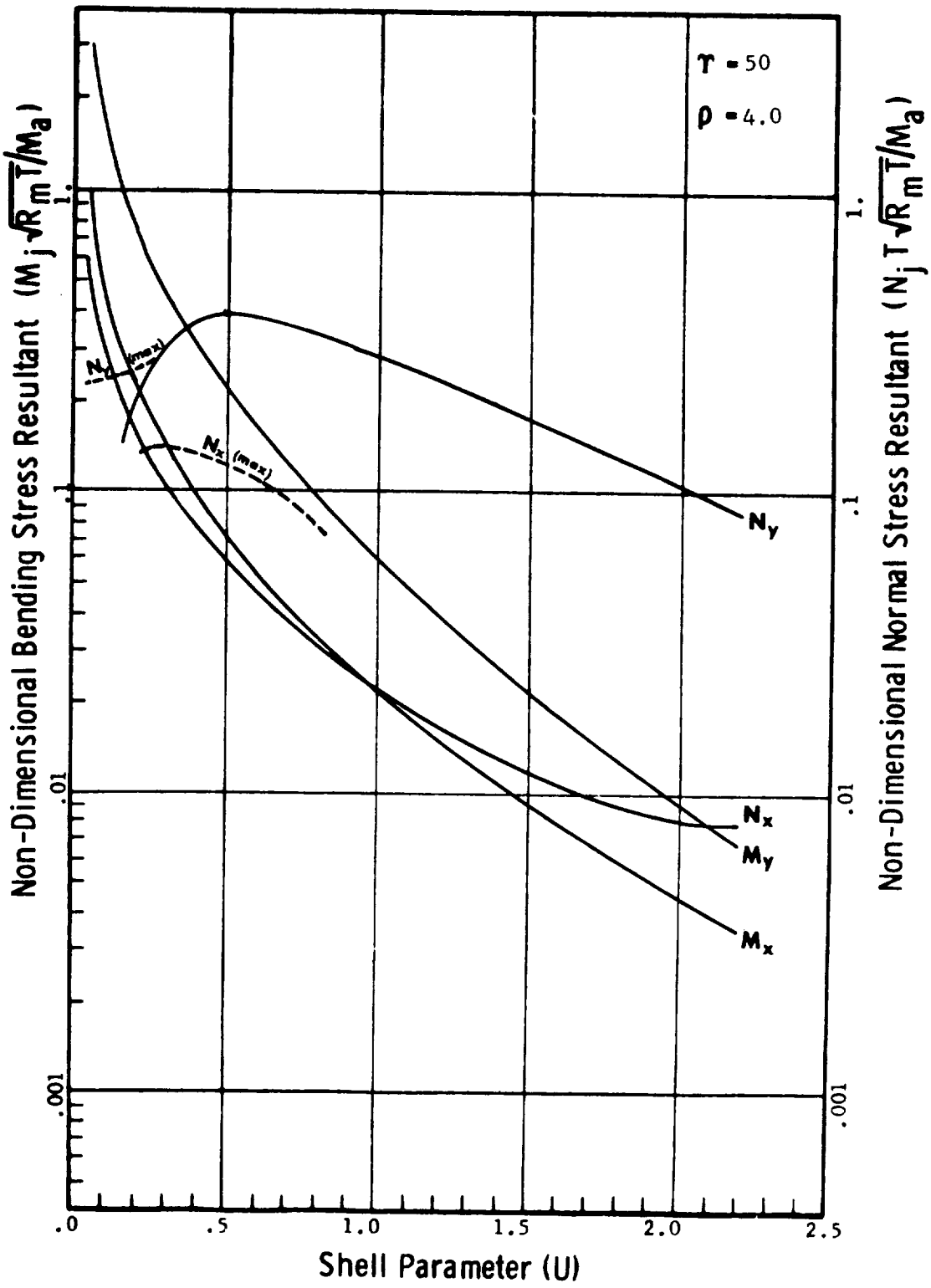

Figure B7.2.1.5-21 Non-Dimensional Stress Resultants for Overturning Moment (M_a) Hollow Attachment $\Upsilon = 50$ and $\rho = 4.0$

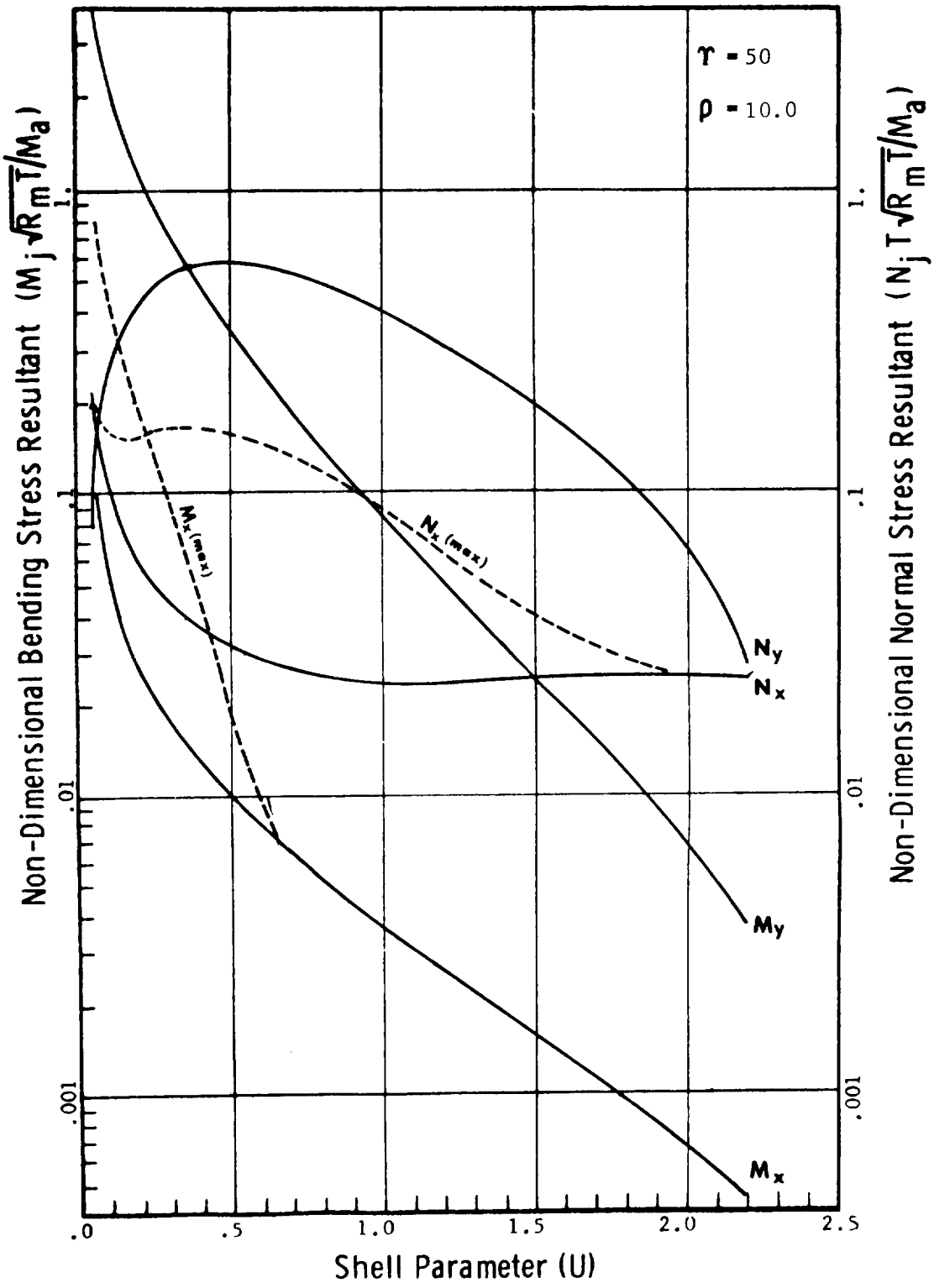

Figure B7.2.1.5-22 Non-Dimensional Stress Resultants for Overturning Moment (M_a) Hollow Attachment $\Upsilon = 50$ and $\rho = 10.0$

B7.2.1.6 EXAMPLE PROBLEM

A spherical bulkhead with a welded hollow attachment is subjected to the force and moments shown in Figure B7.2.1.6-1. Shell and attachment geometry are shown in Figures B7.2.1.6-1 and B7.2.1.6-2.

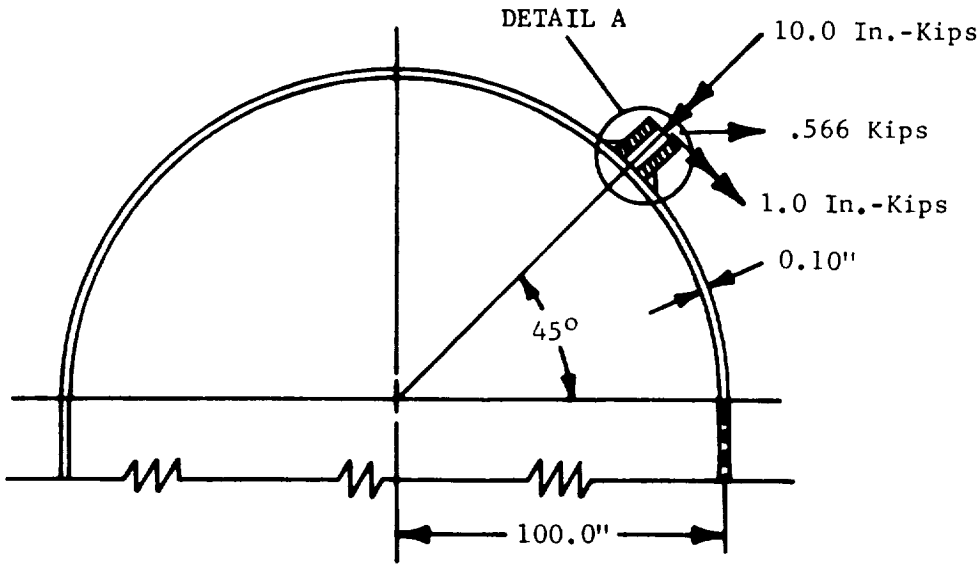

Fig. B7.2.1.6-1 Spherical Bulkhead

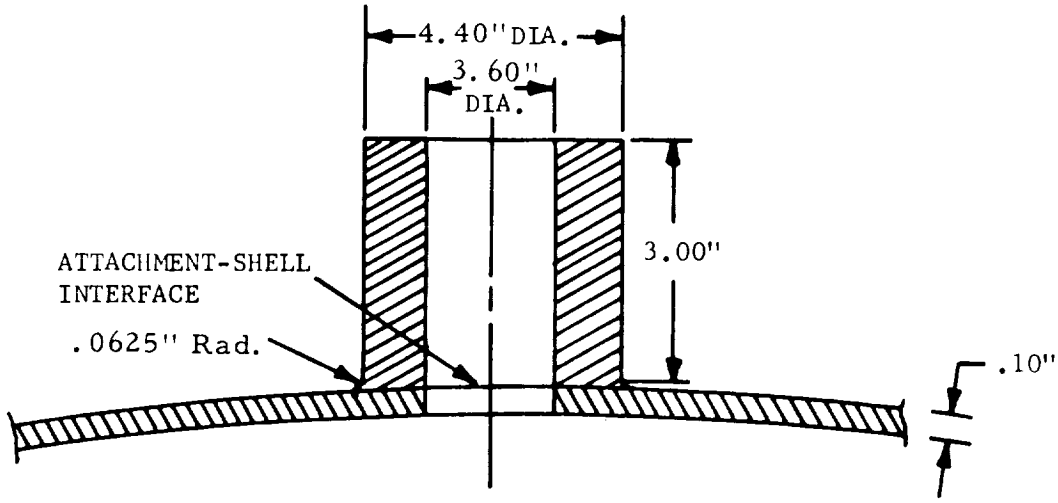

Fig. B7.2.1.6-2 Welded Hollow Attachment (Detail A)

1. Establish a local coordinate system (Figs. B7.2.1.1-1 and B7.2.1.6-3) on the center line of the attachment at the attachment-shell interface, so that the loading in Figure B7.2.1.6-1 is in the 2-3 plane.

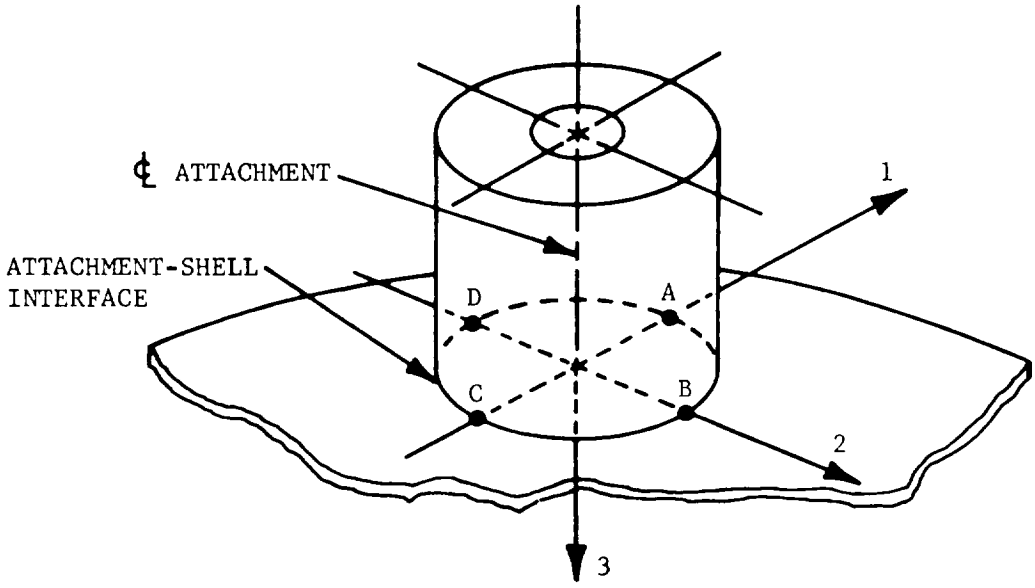

Fig. B7.2.1.6-3 Local Coordinate System

2. Resolve the load system into components (Figs. B7.2.1.1-1 and B7.2.1.6-4) and enter results on the appropriate stress calculation sheet (Figs. B7.2.1.2-2 for hollow attachments and B7.2.1.2-3 for solid attachments). Figure B7.2.1.6-5 shows the stress calculation sheet for the example problem.

3. Establish the appropriate shell geometric properties (Figure B7.2.1.1-2) and enter results on the stress calculation sheet. All dimensions are in inches.

$R_m = 100.0$

$T = 0.10$

$r_0 = 2.20$

$r_m = 2.00$

$t = 0.40$

$a = 0.0625$

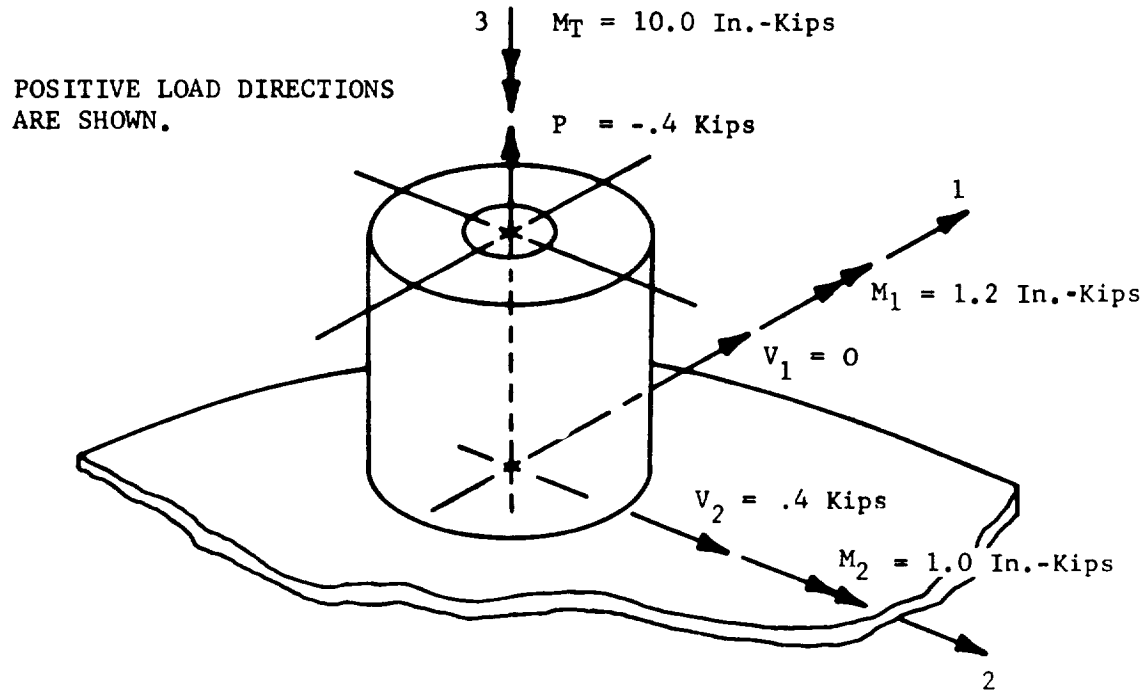

Fig. B7.2.1.6-4 Arbitrary Load System Components

4. Determine the appropriate parameters according to paragraph B7.2.1.2-II, and enter results on the stress calculation sheet.

$$U = r_0/(R_m T)^{\frac{1}{2}} = 2.20/(100 \times 0.1)^{\frac{1}{2}} = 0.695$$

For hollow attachment:

$$\Upsilon = r_m/t = 2.00/0.40 = 5.0$$

$$\rho = T/t = 0.10/0.40 = 0.25$$

For a brittle material (weld) at the attachment-to-shell juncture:

$$K_n = 1 + (T/5.6\,a)^{0.65} = 1 + (0.1/5.6 \times .0625)^{0.65} = 1.44$$

$$K_b = 1 + (T/9.4\,a)^{0.80} = 1 + (0.1/9.4 \times .0625)^{0.80} = 1.70$$

5. Determine the stresses according to paragraph B7.2.1.2-III through VI and enter results on the stress calculation sheet. The nondimensional stress resultants are obtained from Figure B7.2.1.5-3 (Hollow Attachment- $\Upsilon = 5$ and $\rho = 0.25$) for the radial load and from Figure B7.2.1.5-13 (Hollow Attachment - $\Upsilon = 5$ and $\rho = 0.25$) for the overturning moments.

STRESS CALCULATION SHEET FOR STRESSES IN SPHERICAL SHELLS CAUSED BY LOCAL LOADS
(HOLLOW ATTACHMENT)

APPLIED LOADS

P = −.4 kips
V_1 = 0 "
V_2 = .4 "
M_T = 10.0 in-kips
M_1 = 1.2 "
M_2 = 1.0 "

SHELL GEOMETRY

T = .10
t = .40
R_m = 100.
r_m = 2.00
r_o = 2.20
a = .0625

PARAMETERS

U = .695
T = 5.0
β = .25
K_n = 1.44
K_b = 1.70

STRESS	LOAD	NON-DIMENSIONAL STRESS RESULTANT	ADJUSTING FACTOR	STRESS COMPONENT	STRESSES* A_1	A_o	B_1	B_o	C_1	C_o	D_1	D_o
MERIDIONAL STRESS (f_x)	P	$\frac{N_x T}{P}$ = (.061) −.056	$\frac{K_n P}{T^2}$ = −57.6	$\frac{K_n N_x}{T}$ =	(+3.5) −3.2	(+3.5) −3.2	(+3.5) −3.2	(+3.5) −3.2	(+3.5) −3.2	(+3.5) −3.2	(+3.5) −3.2	(+3.5) −3.2
		$\frac{M_x}{P}$ = .064	$\frac{6K_b P}{T^2}$ = −408	$\frac{6K_b M_x}{T^2}$ =	−26.1 +26.1	+26.1 −26.1	−26.1 +26.1	+26.1 −26.1	−26.1 +26.1	+26.1 −26.1	−26.1 +26.1	+26.1 −26.1
	M_1	$\frac{N_x T\sqrt{R_m T}}{M_1}$ = .067	$\frac{K_n M_1}{T^2\sqrt{R_m T}}$ = 54.7	$\frac{K_n N_x}{T}$ =			−3.7	−3.7			+3.7	+3.7
		$\frac{M_x\sqrt{R_m T}}{M_1}$ = .15	$\frac{6K_b M_1}{T^2\sqrt{R_m T}}$ = 387.3	$\frac{6K_b M_x}{T^2}$ =			+58.1	−58.1			−58.1	+58.1
	M_2	$\frac{N_x T\sqrt{R_m T}}{M_2}$ = .067	$\frac{K_n M_2}{T^2\sqrt{R_m T}}$ = 46.6	$\frac{K_n N_x}{T}$ =	+3.1	+3.1			−3.1	−3.1		
		$\frac{M_x\sqrt{R_m T}}{M_2}$ = .15	$\frac{6K_b M_2}{T^2\sqrt{R_m T}}$ = 322.8	$\frac{6K_b M_x}{T^2}$ =	−48.4	+48.4			+48.4	−48.4		
	TOTAL MERIDIONAL STRESSES (f_x)				−68.2	81.1	31.8	−32.5	22.7	−22.2	−77.3	91.4
CIRCUMFERENTIAL STRESS (f_y)	P	$\frac{N_y T}{P}$ = .087	$\frac{K_n P}{T^2}$ = −57.6	$\frac{K_n N_y}{T}$ =	+5.0	+5.0	+5.0	+5.0	+5.0	+5.0	+5.0	+5.0
		$\frac{M_y}{P}$ = .019	$\frac{6K_b P}{T^2}$ = −408	$\frac{6K_b M_y}{T^2}$ =	−7.8 +7.8	+7.8 −7.8	−7.8 +7.8	+7.8 −7.8	−7.8 +7.8	+7.8 −7.8	−7.8 +7.8	+7.8 −7.8
	M_1	$\frac{N_y T\sqrt{R_m T}}{M_1}$ = (.11) .087	$\frac{K_n M_1}{T^2\sqrt{R_m T}}$ = 54.7	$\frac{K_n N_y}{T}$ =			(6.0) −4.8	(6.0) 4.8			(6.0) +4.8	(6.0) +4.8
		$\frac{M_y\sqrt{R_m T}}{M_1}$ = (.042) .045	$\frac{6K_b M_1}{T^2\sqrt{R_m T}}$ = 387.3	$\frac{6K_b M_y}{T^2}$ =			(18.6) 17.4	(18.6) 17.4			(18.6) 17.4	(18.6) 17.4
	M_2	$\frac{N_y T\sqrt{R_m T}}{M_2}$ = (.11) .087	$\frac{K_n M_2}{T^2\sqrt{R_m T}}$ = 46.6	$\frac{K_n N_y}{T}$ =	(5.0) +4.0	(5.0) +4.0			(5.0) −4.0	(5.0) −4.0		
		$\frac{M_y\sqrt{R_m T}}{M_2}$ = (.048) .045	$\frac{6K_b M_2}{T^2\sqrt{R_m T}}$ = 322.8	$\frac{6K_b M_y}{T^2}$ =	(15.5) 14.5	(15.5) 14.5			(15.5) +14.5	(15.5) −14.5		
	TOTAL CIRCUMFERENTIAL STRESS (f_y)				−14.3	33.3	11.0	−11.8	8.7	−7.7	−16.6	37.4
SHEAR STRESS (f_{xy})	V_1	0	$\pi r_o T$ = .69	$\frac{V_1}{\pi r_o T}$ = 0			− 0	− 0			+ 0	+ 0
	V_2	.40	$\pi r_o T$ = .69	$\frac{V_2}{\pi r_o T}$ = .6	− .6	− .6			+ .6	+ .6		
	M_T	10.0	$2\pi r_o^2 T$ = 3.04	$\frac{M_T}{2\pi r_o^2 T}$ = 3.3	−3.3	−3.3	+3.3	+3.3	−3.3	−3.3	+3.3	+3.3
	TOTAL SHEAR STRESS (f_{xy})				−3.9	−3.9	3.3	3.3	−2.7	−2.7	3.3	3.3
PRINCIPAL STRESSES**	f_{max}	$\frac{f_x + f_y}{2} + \sqrt{\left(\frac{f_x - f_y}{2}\right)^2 + f_{xy}^2}$ ***			−68.5	81.4	32.3	−33.0	23.2	−22.9	−77.5	91.6
	f_{min}	$\frac{f_x + f_y}{2} - \sqrt{\left(\frac{f_x - f_y}{2}\right)^2 + f_{xy}^2}$ ***			−14.0	33.0	10.5	−11.3	8.2	−7.0	−16.4	37.2
	$f_{xy\,max}$	$\pm\sqrt{\left(\frac{f_x - f_y}{2}\right)^2 + f_{xy}^2}$			27.2	24.2	10.9	10.9	7.5	8.0	30.5	27.2

* IF LOAD IS OPPOSITE TO THAT SHOWN IN FIGURE B7.2.1.1-1 THEN REVERSE THE SIGN SHOWN.
** SEE SECTION A3.1.0.
*** CHANGE SIGN OF THE RADICAL IF ($f_x + f_y$) IS NEGATIVE.

Figure B7.2.1.6-5 Stress Calculation Sheet (Example Problem)

B7.2.2.0 LOCAL LOADS ON CYLINDRICAL SHELLS

This section presents a method to obtain cylindrical shell membrane and bending stresses at an attachment-to-shell juncture resulting from arbitrary loads induced through rigid attachments on pressurized or unpressurized shells. Shell geometry and loading conditions are used to obtain normal and bending stress resultants and deflections from a computer program for radial-type loads (P and M_a). Membrane shear stresses caused by shearing loads (V_a) and twisting moments (M_T) can be calculated directly without the computer program. Deflections are not calculated for shearing loads and twisting moments.

Local load stresses reduce rapidly at points removed from the attachment-to-shell juncture. Boundaries of that region of the shell influenced by the local loads can be determined for those load cases calculated with the computer program by investigation of the stresses and deflections at points removed from the attachment.

The additional stiffness of the shell caused by internal pressure (pressure coupling) is taken into account by the computer program for determination of local load stress resultants and deflections. The stress resultants induced in the shell by the internal pressure are not included in the computer program results and must be superimposed upon the local load stress resultants calculated by the method contained in this section.

B7.2.2.1 GENERAL

I NOTATION

The notations presented in this section are not applicable to the computer program. The computer program variables are defined in the Astronautics Computer Utilization Handbook.

- a - fillet radius at attachment-to-shell juncture or longitudinal half diameter of elliptical load pad, in.
- b - x-coordinate distance to center of attachment ($b = L/2$) or circumferential half diameter of elliptical load pad, in.
- c - half length of square attachment, in.
- c_1 - longitudinal half length of rectangular attachment, in.
- c_2 - circumferential half length of rectangular attachment, in.
- E - modulus of elasticity, psi
- f_x - normal longitudinal stress, psi
- f_y - normal circumferential stress, psi
- f_{xy} - shear stress, psi
- K_n, K_b - stress concentration parameters for normal stresses and bending stresses, respectively
- L - length of cylinder
- M_a - applied overturning moment, in.-lb.
- M_T - applied twisting moment, in.-lb.
- M_j - internal bending moment stress resultant per unit length of shell, in.-lb/in.
- n - number of equally spaced attachments in the circumferential direction
- N_j - internal normal force stress resultant per unit length of shell, lb/in.
- p - uniform load intensity, psi
- P - radial load or total distributed radial load, lb.
- q - internal pressure, psi

B7.2.2.1 GENERAL (Concluded)

I NOTATION (Concluded)

r - radius of circular attachment, in.

R - radius of cylindrical shell, in.

s - circumferential arc length, in.

T - thickness of cylindrical shell, in.

u - longitudinal displacement, in.

v - circumferential displacement, in.

V_a - applied concentrated shear load or total distributed shear load, lb.

w - radial displacement, in.

x - longitudinal coordinate, in.

y - circumferential coordinate, in.

z - radial coordinate, in.

θ - polar coordinate

ν - Poisson's ratio

ϕ - circumferential cylindrical coordinate

Subscripts

a - applied (a = 1 or a = 2)
b - bending
i - inside
j - internal (j = x or j = y)
m - mean (average of outside and inside)
n - normal
o - outside
x - longitudinal
y - circumferential
z - radial

1 - longitudinally directed applied load vector or longitudinal direction
2 - circumferentially directed applied load vector or circumferential direction

B7.2.2.1 GENERAL

II SIGN CONVENTION

Local loads applied at an attachment-to-shell induce a biaxial state of stress on the inside and outside surfaces of the shell. The longitudinal stress (f_x), circumferential stress (f_y), shear stress (f_{xy}), the positive directions of the applied loads (M_a*, M_T, P, q, and V_a), the stress resultants (M_j and N_j), and the positive directions of the displacements (u, v, and w) are indicated in Figure B7.2.2.1-1.

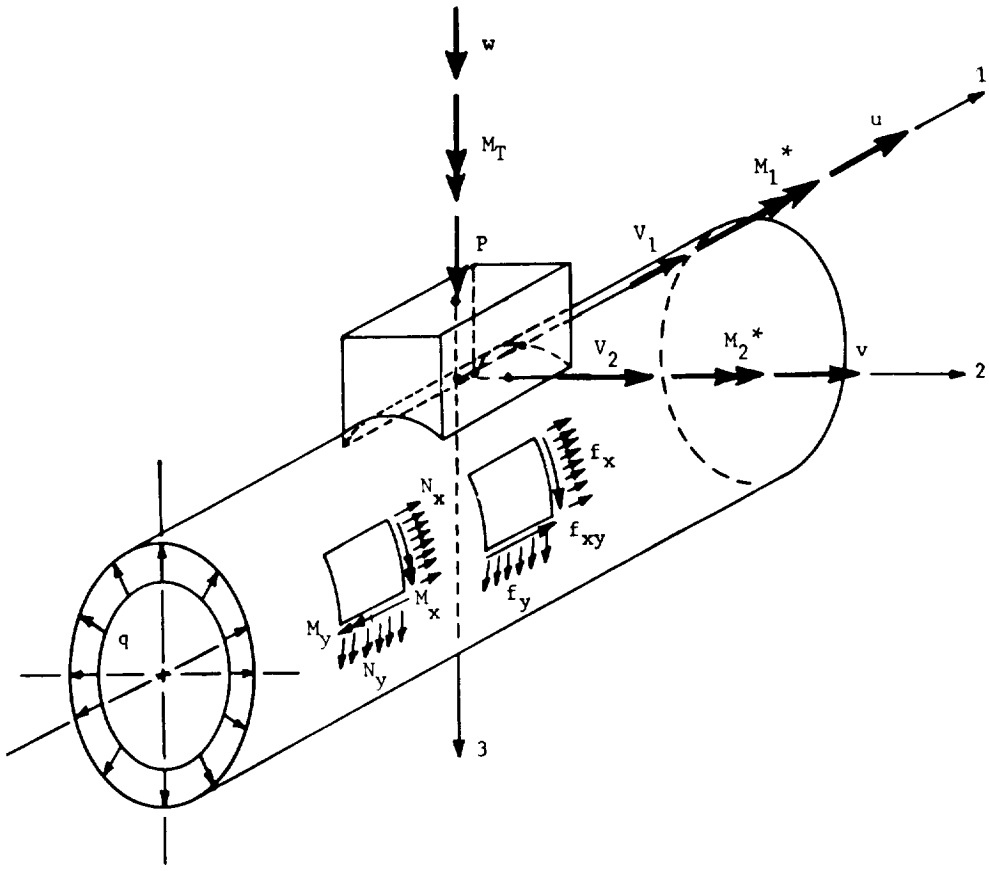

Fig. B7.2.2.1-1 Stresses, Stress Resultants, Loads, and Displacements

* The applied overturning moment M_1 (M_2) is represented by a longitudinally (circumferentially) directed vector but is defined as an applied circumferential (longitudinal) overturning moment since its effect is in the circumferential (longitudinal) direction.

The geometry of the shell and attachment, the local coordinate system at the attachment, and the coordinate system of the shell are indicated in Figure B7.2.2.1-2.

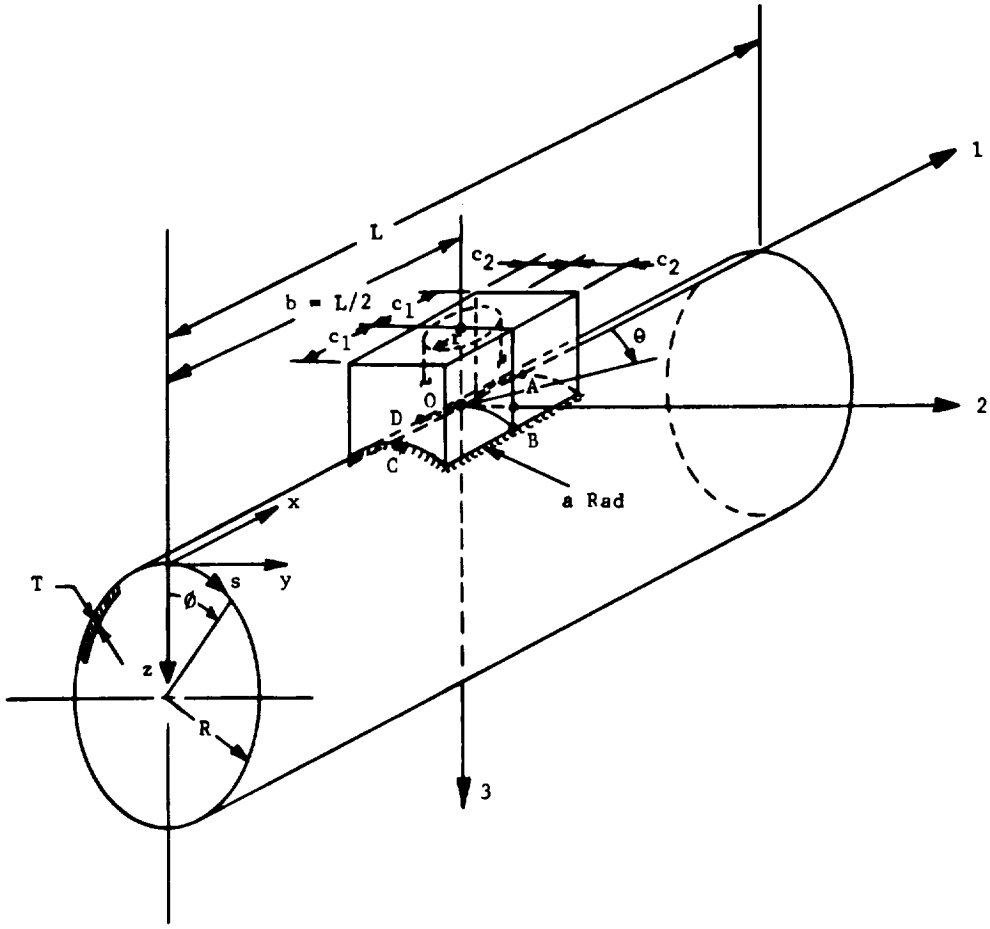

Fig. B7.2.2.1-2 Shell and Attachment Geometry

It is possible to predict the sign of the induced stress, tensile (+) or compressive (-), by considering the deflections of the shell resulting from various loading modes.

Mode I (radial load), Figure B7.2.2.1-3, shows a positive radial load (P) transmitted to the shell by a rigid attachment. The load (P) causes compressive membrane stresses and local bending stresses adjacent to the

attachment. The compressive membrane stresses are similar to the stresses induced by an external pressure. The local bending stresses result in tensile bending stresses on the inside of the shell and compressive bending stresses on the outside of the shell at points A, B, C and D.

Modes II (circumferential moment) and III (longitudinal moment), Figure B7.2.2.1-3, show negative overturning moments (M_a) transmitted to the shell by rigid attachments. The overturning moments (M_a) cause compressive and tensile membrane stresses and local bending stresses adjacent to the attachment. Tensile membrane stresses are induced in the shell at B or C, similar to the stresses caused by an internal pressure. Compressive membrane stresses are induced in the shell at D or A, similar to the stresses caused by an external pressure. The local bending stresses cause tensile bending stresses in the shell at B or C on the outside and at D or A on the inside, and cause compressive bending stresses in the shell at B or C on the inside and at D or A on the outside.

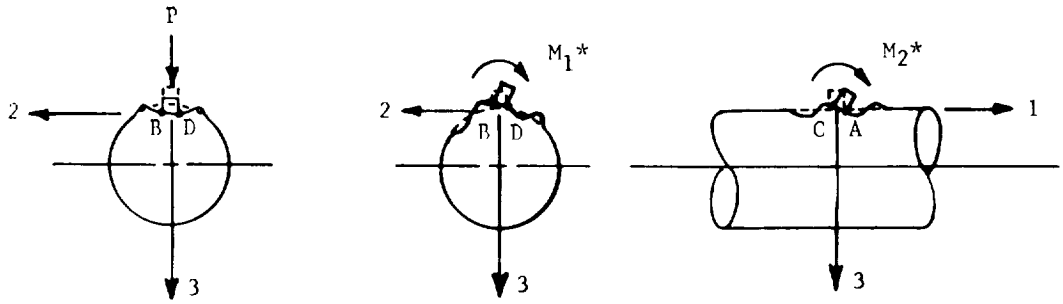

MODE I — RADIAL LOAD

MODE II — CIRCUMFERENTIAL MOMENT *

MODE III — LONGITUDINAL MOMENT *

Fig. B7.2.2.1-3 Loading Modes

* The applied overturning moment M_1 (M_2) is represented by a longitudinally (circumferentially) directed vector but is defined as an applied circumferential (longitudinal) overturning moment since its effect is in the circumferential (longitudinal) direction.

The signs of the stresses induced in the shell adjacent to the attachment by positive applied loads for rigid attachments are shown in Figure B7. 2. 2. 2-1 "Stress Calculation Sheet". The figure or parts thereof can be reproduced and used as calculation sheets.

B7.2.2.1 GENERAL

III LIMITATIONS OF ANALYSIS

Considerable judgment must be used in the interpretation of the results of this section and in the establishment of the geometry and loadings used in the analysis.

Six general areas must be considered for limitations: attachment and shell size, attachment location, shift in maximum stress location, stresses caused by shear loads, geometry and loading.

A Size of Attachment with Respect to Shell Size

The analysis is applicable to small attachments relative to the shell size and to thin shells. The limitations on these conditions are shown by the shaded area of Figure B7.2.2.1-4.

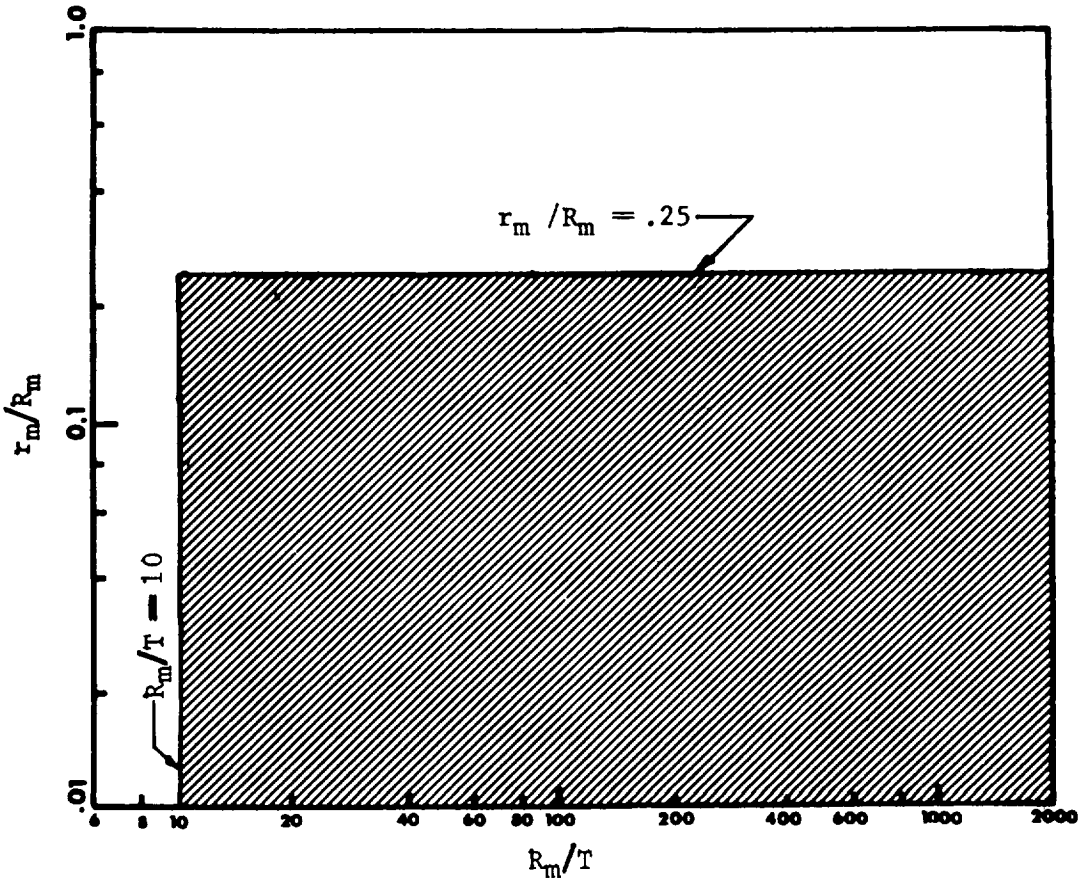

Fig. B7.2.2.1-4

B Location of Attachment with Respect to Boundary Conditions to Shell

The analysis is applicable when there are no stress perturbations caused by other loadings in the area influenced by the local loads. These perturbations can be caused by discontinuity, thermal loading, liquid level loading, change in section and material change. The area influenced by the local loading can be determined by an investigation of the stresses and deflections at points removed from the attachment.

C Shift in Maximum Stress Locations

Under certain conditions the stresses in the shell may be higher at points removed from the attachment-to-shell juncture than at the juncture. The following conditions should be carefully considered:

1. Stresses can be higher in the attachment than in the shell. This is most likely when the attachment is not reinforced, when reinforcement is placed on the shell and not on the attachment, and when very thin attachments are used.
2. For some load conditions certain stress resultants peak at points slightly removed from the attachment-to-shell juncture. The load conditions that cause this peaking are in most cases the same load cases that cause peaking for local loads on spherical shells. The extent of the peaking can be evaluated by an investigation of the stresses and deflections at points slightly removed from the attachment.
3. Comparison of analytical and experimental results [3] for membrane stresses shows that membrane stress resultants can be calculated at the point where stresses are desired. Comparison of analytical and experimental results [2, 3] for bending stress resultants at loaded attachments shows that the bending stress resultants must be calculated at the center of the attachment and

then shifted to the edge for the determination of stresses at the edge of the attachment. The determination of bending stresses at other points requires that the bending stress resultants be calculated at a distance $C_{1/2}$ or $C_{2/2}$ closer to the attachment.

D Stresses Caused by Shear Loads

An accurate stress distribution caused by a shear load (V_a) applied to a cylindrical shell is not available. The actual stress distribution consists of varying shear and membrane stresses around the rigid attachment. The method [2] presented here assumes that the shell resists the shear load by shear only. If this assumption appears unreasonable, it can be assumed that the shear load is resisted totally by membrane stresses or by some combination of membrane and shear stresses.

E Shell and Attachment Geometry

The analysis assumes that the cylindrical shell has simply supported end conditions or is of sufficient length that simply supported end conditions can be assumed.

The computer program requires that circular and elliptical attachments be converted to equivalent square and rectangular attachments, respectively. The equivalent attachment must have an area equal to the area of the actual attachment for a radially applied force. The equivalent attachment must have a moment of inertia about the bending axis equal to the moment of inertia about the bending axis of the actual attachment for bending loads. In both cases the aspect ratios (a/b and c_1/c_2) of the attachments (actual and equivalent, respectively) must be equal. If the attachment is welded, the weld size must be added to the attachment when determining equivalent attachments.

L/R_m is a secondary parameter and has little effect on the solution of $1.0 \leq L/R_m \leq 5.0$. The attachment coordinate system, defined by Figure B7.2.2.1-2, must be located at $x = L/2$.

F Shell Loading

The computer program accounts for pressure coupling (that is, the increase in shell stiffness caused by internal pressure). The internal pressure (q) must be positive or a positive differential. The stresses caused by the internal pressure must be calculated separately and superimposed upon the local loads stresses calculated by the method presented here.

The shell deflections must be small, approximately equal to the cylindrical shell thickness, for the analysis to be valid and to allow superposition of stresses.

B7.2.2.2 STRESSES

I GENERAL

Stress resultants and displacements caused by radial load (P) and overturning moment (M_a) are obtained from the computer program given in the Computer Handbook. Stresses caused by shear load (V_a) and twisting moment (M_T) are calculated directly from attachment geometry and loading.

The stress resultants (M_j and N_j) and displacements (u, v, and w) determined by the computer program are for a specific location. The location is specified by x and ϕ input values determined according to the coordinate system (x, ϕ, z) defined in Figure B7.2.2.1-2.

The computer program will calculate stress resultants and displacements for configurations (see Computer Utilization Handbook):

Case 1 - One Uniformly Distributed Radial Load

Case 2 - "n" Equally Spaced Uniformly Distributed Radial Loads

Case 3 - One Concentrated Radial Load

Case 4 - "n" Equally Spaced Concentrated Radial Loads

Case 5 - Longitudinal Overturning Moment

Case 6 - Circumferential Overturning Moment

The general equation for stresses in a shell at a rigid attachment juncture in terms of the stress resultants is of the form:

$$f_j = K_n (N_j/T) \pm K_b (6M_j/T^2)$$

The stress concentration parameters (K_n and K_b) are defined and can be evaluated from Paragraph B7.2.1.2, Sections I and IIB.

Figure B7.2.2.2-1 "Stress Calculation Sheet" can be used for the calculation of all stresses caused by an arbitrary local loading. The sheet automatically accounts for signs.

STRESS CALCULATION SHEET FOR STRESSES IN CYLINDRICAL SHELLS CAUSED BY LOCAL LOADS

APPLIED LOADS

P = _____
P = _____
V_1 = _____
V_2 = _____
M_T = _____
M_1 = _____
M_2 = _____

SHELL GEOMETRY

T = _____
R_m = _____
L = _____
c_1 = _____
c_2 = _____
a = _____
r_o = _____

CO-ORDINATES

	x	φ
O =	_____	_____
A =	_____	_____
B =	_____	_____
C =	_____	_____
D =	_____	_____

PARAMETERS

K_n = _____
K_b = _____

STRESS	LOAD	STRESS RESULT.	ADJUST. FACTOR	CALC. STRESS	STRESSES* A_i	A_o	C_i	C_o	STRESS RESULT.	ADJUST. FACTOR	CALC. STRESS	STRESSES* B_i	B_o	D_i	D_o
LONGITUDINAL STRESS (f_x)	P case I thru IV	N_x (A)**	$\frac{K_n}{T}$ =		+	+	+	+	N_x (B)**	$\frac{K_n}{T}$ =		+	+	+	+
		M_x (O)=	$\frac{6K_b}{T^2}$ =		+	−	+	−	M_x (O)=	$\frac{6K_b}{T^2}$ =		+	−	+	−
	M_1 case VI	N_x (A)=	$\frac{K_n}{T}$ =						N_x (B)=	$\frac{K_n}{T}$ =		+	+	−	−
		M_x (A)=	$\frac{6K_b}{T^2}$ =						M_x (B)=	$\frac{6K_b}{T^2}$ =		+	−	+	−
	M_2 case V	N_x (A)=	$\frac{K_n}{T}$ =		−	−	+	+	N_x (B)=	$\frac{K_n}{T}$ =					
		M_x (A)=	$\frac{6K_b}{T^2}$ =		−	+	+	−	M_x (B)=	$\frac{6K_b}{T^2}$ =					
	TOTAL LONGITUDINAL STRESSES (f_x)														
CIRCUMFERENTIAL STRESS (f_y)	P	N_y (A)**	$\frac{K_n}{T}$ =		+	+	+	+	N_y (B)**	$\frac{K_n}{T}$ =		+	+	+	+
		M_y (O)=	$\frac{6K_b}{T^2}$ =		+	−	+	−	M_y (O)=	$\frac{6K_b}{T^2}$ =		+	−	+	−
	M_1	N_y (A)=	$\frac{K_n}{T}$ =						N_y (B)=	$\frac{K_n}{T}$ =		+	+	−	−
		M_y (A)=	$\frac{6K_b}{T^2}$ =						M_y (B)=	$\frac{6K_b}{T^2}$ =		+	−	+	−
	M_2	N_y (A)=	$\frac{K_n}{T}$ =		−	−	+	+	N_y (B)=	$\frac{K_n}{T}$ =					
		M_y (A)=	$\frac{6K_b}{T^2}$ =		−	+	+	−	M_y (B)=	$\frac{6K_b}{T^2}$ =					
	TOTAL CIRCUMFERENTIAL STRESSES (f_y)														
SHEAR STRESS (f_{xy})	V_1	V_1 =	$\frac{1}{\pi r_o T}$ =									−	−	+	+
	V_2	V_2 =	$\frac{1}{\pi r_o T}$ =		−	−	+	+							
	M_T	M_T =	$\frac{1}{2\pi r_o^2 T}$ =		−	−	−	−				+	+	+	+
	TOTAL SHEAR STRESS (f_{xy})														
PRINCIPAL STRESSES	f_{max}	$\frac{f_x + f_y}{2} + \sqrt{\left(\frac{f_x - f_y}{4}\right)^2 + f_{xy}^2}$ ***													
	f_{min}	$\frac{f_x + f_y}{2} - \sqrt{\left(\frac{f_x - f_y}{4}\right)^2 + f_{xy}^2}$ ***													
	$f_{xy\ max}$	$\pm\sqrt{\left(\frac{f_x - f_y}{4}\right)^2 + f_{xy}^2}$													

* CHANGE SIGN OF CALCULATED STRESS WHERE NEGATIVE SIGNS ARE INDICATED.

** LETTER IN PARENTHESIS DESIGNATES THE POINT (A, B, OR O) AT WHICH THE STRESS RESULTANTS SHOULD BE COMPUTED BY THE COMPUTER PROGRAM. THE STRESSES FOR POINTS (A, B, C, AND D) CAN BE OBTAINED FROM THESE STRESS RESULTANTS USING THE SIGNS INDICATED.

*** CHANGE SIGN OF THE RADICAL IF $(f_x + f_y)$ IS NEGATIVE.

Fig. B7.2.2.2-1 Stress Calculation Sheet

B7.2.2.2 STRESSES

II STRESSES RESULTING FROM A RADIAL LOAD

Radial load configuration Cases I and II (Computer Utilization Handbook) cause membrane and bending stress components in both the longitudinal and circumferential directions.

A Longitudinal Stress (f_x)

Step 1. Determine the required load and geometric load input for the computer program.

Step 2. Determine the bending stress resultant (M_x) at point O and the normal stress resultant (N_x) at points A and B with the computer program. See Figure B7.2.2.1-2 for the location of points A, B and O.

Step 3. Using the criteria in Paragraph B7.2.1.2, Section I, obtain values for the stress concentration parameters (K_n and K_b).

Step 4. Using the bending stress resultant (M_x) at point O and the normal stress resultant (N_x) at point A as determined in Step 2, and the stress concentration parameters as determined in Step 3, determine the longitudinal stresses (f_x) at point A using the following equation:

$$f_x = K_n(N_x/T) \pm K_b(6M_x/T^2)$$

Proper consideration of the sign will give the values for the longitudinal stress at the inside and outside surfaces of the shell.

Step 5. Repeat Step 4, but use the normal stress resultant (N_x) as determined for point B and the bending stress resultant (M_x) as determined for point O to determine the longitudinal stresses (f_x) at point B.

B Circumferential Stresses (f_y)

The circumferential stresses (f_y) can be determined by following the five steps outlined in Paragraph A, above, except for determining M_y and N_y instead of M_x and N_x in Step 2 and using the following stress equation in Step 4.

$$f_y = K_n(N_y/T) \pm K_b(6M_y/T^2)$$

C Concentrated Load Stresses

Points A, B, C and D in Figure B7.2.2.1-2 do not exist for Load Cases III and IV. Longitudinal and circumferential membrane and bending stress caused by concentrated loads (Cases III and IV) is determined from stress resultants calculated at point O. The stresses are calculated using Paragraph A, above, after applying proper modifications to the equations.

B7.2.2.2 STRESSES

III STRESSES RESULTING FROM AN OVERTURNING MOMENT

Overturning moment load configurations, Cases V and VI (Computer Utilization Handbook), will cause membrane and bending stress components in both the longitudinal and circumferential directions.

A Longitudinal Stress (f_x)

Step 1. Determine load and geometric input for the computer program.

Step 2. Determine the bending stress resultant (M_x) and normal stress resultant (N_x) at points A for Load Case V and B for Load Case VI with the computer program.

Step 3. Using the criteria in Paragraph B7.2.1.2, Section I, obtain the values for the stress concentration parameters (K_n and K_b).

Step 4. Using the bending stress resultant (M_x) and the normal stress resultant (N_x) at point A as determined in Step 2 and the stress concentration parameters as determined in Step 3, determine the longitudinal stress (f_x) at point A using the following equation:

$$f_x = K_n(N_x/T) \pm K_b(6M_x/T^2)$$

Proper consideration of the sign will give the values for longitudinal stresses at the inside and outside surfaces of the shell.

Step 5. Repeat Step 4, but use stress resultants as determined for point B to determine the longitudinal stresses at point B.

B Circumferential Stress (f_y)

The circumferential stresses (f_y) can be determined by following the five steps outlined in Paragraph A, above, except for determining M_y and N_y instead of M_x and N_x in Step 2, and using the following stress equation in Step 4:

$$f_y = K_n (N_y/T) \pm K_b (6M_y/T^2)$$

B7.2.2.2 STRESSES

IV STRESSES RESULTING FROM A SHEAR LOAD

A shear load (V_a) will cause a shear stress (f_{xy}) in the shell at the attachment-to-shell juncture. The shear stress is determined as follows:

A Round Attachment

$$f_{xy} = \frac{V_a}{\pi r_0 T} \sin \theta \qquad \text{for } V_a = V_1$$

$$f_{xy} = \frac{V_a}{\pi r_0 T} \cos \theta \qquad \text{for } V_a = V_2$$

B Rectangular Attachment

$$f_{xy} = \frac{V_a}{4c_1 T} \qquad \text{for } V_a = V_1$$

$$f_{xy} = \frac{V_a}{4c_2 T} \qquad \text{for } V_a = V_2$$

B7.2.2.2 STRESSES

V STRESSES RESULTING FROM A TWISTING MOMENT

A Round Attachment

A twisting moment (M_T) applied to a round attachment will cause a shear stress (f_{xy}) in the shell at the attachment-to-shell juncture. The shear stress is pure shear and is constant around the juncture. The shear stress is determined as follows:

$$f_{xy} = M_T/2\pi r_0 T$$

B Square Attachment

A twisting moment applied to a square attachment will cause a complex stress field in the shell. No acceptable methods for analyzing the loading are available.

B7.2.2.3 STRESS RESULTING FROM ARBITRARY LOADING

I CALCULATION OF STRESSES

Most loadings that induce loads on cylindrical shells are of an arbitrary nature. Stresses are determined by the following procedure:

Step 1. Resolve the arbitrary applied load (forces and/or moments) into axial force, shear forces, overturning moments and twisting moment components. See Paragraph B7.2.1.6 Example Problem. The positive directions of the components and the point of application of the load components (intersection of centerline of attachment with attachment-shell interface) are indicated in Figure B7.2.2.1-1.

Step 2. Evaluate inside and outside stresses at desired points (such as A, B, C and D) around the attachment for each component of the arbitrary applied loading by the methods in Paragraph B7.2.2.2.

Step 3. Obtain the stresses for the arbitrary loading by combining the longitudinal, circumferential and shear stresses evaluated by Step 2 for each of the points selected on the inside and outside of the shell. Proper consideration of signs is necessary.

B7. 2. 2. 3 STRESSES RESULTING FROM ARBITRARY LOADING

II LOCATION AND MAGNITUDE OF MAXIMUM STRESS

The location and magnitude of the maximum stresses caused by an arbitrary load require a consideration of the following:

A. The determination of principal stresses (f_{max}, f_{min}, $f_{xy} = 0$, or $f_{xy} = max$) for the determined stresses (f_x, f_y, and f_{xy}) at a specific point.

B. The proper selection of points for determining the stresses.

B7.2.2.4 DISPLACEMENTS

Shell displacements caused by radial load configurations and overturning moments are obtained from the computer program described in the Computer Handbook. Shell displacements caused by twisting moment and shear loads are not determined.

Comparison of experimental and theoretical deflections indicate that deflections are sensitive to the detailed conditions of the attachment. In general, however, the experimental and theoretical values are of the same order of magnitude.

REFERENCES:

1. Bijlaard, P. P., "Stresses From Local Loadings in Cylindrical Pressure Vessels," Transactions ASME, Vol. 77, 1955, PP. 805-816.

2. Wichman, K. R.; Hopper, A. G.; and Mershon, J. L., "Local Stresses in Spherical and Cylindrical Shells due to External Loadings," Welding Research Council Bulletin, Bulletin No. 107, August 1965.

3. Lowry, J. K., "Stresses and Deflections in Pressurized Cylindrical Shells, Due to the Application of Asymmetric Local Loadings," General Dynamics/Astronautics, San Diego, California, Report No. GD/A-DDG64-019, September 1, 1964.

BIBLIOGRAPHY:

1. Timoshenko, S., Woinowsky-Krieger, S., "Theory of Plates and Shells," McGraw-Hill Book Co., Inc., Second Ed., New York, N. Y., 1959.

2. The Astronautic Computer Utilization Handbook, NASA.

SECTION B7.3

BENDING ANALYSIS OF

TABLE OF CONTENTS

B7.3.0 BENDING ANALYSIS OF THIN SHELLS

In this section some of the theories discussed in Section B7.0 will be applied to solve shell problems. Section B7.0 defined the structural shell and several shell theories, with their limitations and ramifications. It was pointed out that the thickness-to-radius-of-curvature ratio, material behavior, type of construction (e.g., honeycomb sandwich or ring-stiffened shells), types of loading, and other factors all play a role in establishing which theory is applicable. Furthermore, shallow versus nonshallow shells required different approaches even though they fell into the same thin shell theory.

In this section, differential equations and their solutions will be tabulated for simple and complex rotationally symmetric geometries subjected to arbitrary rotationally symmetric loads. There are certain restraining conditions, called edge restraints, that the solution must satisfy. The edge restraints are reduced to unit loads and, by making the solution of the differential equations satisfy these unit edge restraints, the influence coefficients for the geometry are obtained. These influence coefficients, etc., are then used to solve problems that involve determining stresses, strains, and displacements in simple and complex geometries.

The procedure for bending analysis of thin shells will be as follows: The surface loads, inertia loads, and thermally induced loads are included in the equilibrium equations and will be part of the "membrane solution" using Section B7.1. The solution due to edge restraints alone is then found and the results superimposed over the membrane solution. The results obtained will be essentially identical to those obtained by using the complete, exact bending theory.

B7.3.1 GENERAL

The geometry, coordinates, stresses, and stress resultants for a shell of revolution are the same as given in Paragraph B7.1.1.0. Also, the notations and sign conventions are generally the same as those given in Paragraph B7.1.1.1 and Paragraph B7.1.1.2, respectively. The limitations of analysis are the same as given in Paragraph B7.1.1.3, except that in this section flexural strains, stresses, and stress resultants are no longer zero. Boundaries of the shell need not be free to rotate and deflect normal to the shell middle surface.

B7. 3. 1. 1 Equations

I Equilibrium Equations

A shell element with the stress resultants as given in Section B7. 1. 1. 0 will now be considered and the conditions for its equilibrium under the influence of all external and internal loads will be determined. The equations arising by virtue of the demands of equilibrium and the compatibility of deformations will be derived by considering an individual differential element.

The external loads are comprised of body forces that act on the element and surface forces (stresses) that act on the upper and lower boundaries of the element, which are sections of the curved surfaces bounding the shell. The internal forces will be stress resultants acting on the faces of the shell element.

For the following equations, external forces are replaced by statically equivalent stresses distributed at the middle surfaces. The middle surface is thus loaded by forces as well as moments.

Now, instead of considering the equilibrium of an element of a shell one may study the equilibrium of the corresponding element of the middle surface. The stresses, in general, vary from point to point in the shell, and as a result the stress resultants will also vary.

Consider the stress resultants of concern applied to the middle surface of the shell as shown in Figures B7. 3. 1-1 and B7. 3. 1-2.

The equilibrium of the shell, in the θ, ϕ, and z coordinate directions respectively, is given by the following equations:

$$\frac{\partial \alpha_2 N_\theta}{\partial \theta} + \frac{\partial \alpha_1 N_{\phi\theta}}{\partial \phi} + N_{\theta\phi}\frac{\partial \alpha_1}{\partial \phi} - N_\phi \frac{\partial \alpha_2}{\partial \theta} + Q_\theta \frac{\alpha_1 \alpha_2}{R_1} + \alpha_1 \alpha_2 p_1 = 0$$

$$\frac{\partial \alpha_1 N_\phi}{\partial \phi} + \frac{\partial \alpha_2 N_{\theta\phi}}{\partial \theta} + N_{\phi\theta}\frac{\partial \alpha_2}{\partial \theta} - N_\theta \frac{\partial \alpha_1}{\partial \phi} + Q_\phi \frac{\alpha_1 \alpha_2}{R_2} + \alpha_1 \alpha_2 p_2 = 0$$

$$\frac{\partial \alpha_2 Q_\theta}{\partial \theta} + \frac{\partial \alpha_1 Q_\phi}{\partial \phi} - \alpha_1 \alpha_2 \left(\frac{N_\theta}{R_1} + \frac{N_\phi}{R_2}\right) + \alpha_1 \alpha_2 q = 0 \quad , \qquad (1a)$$

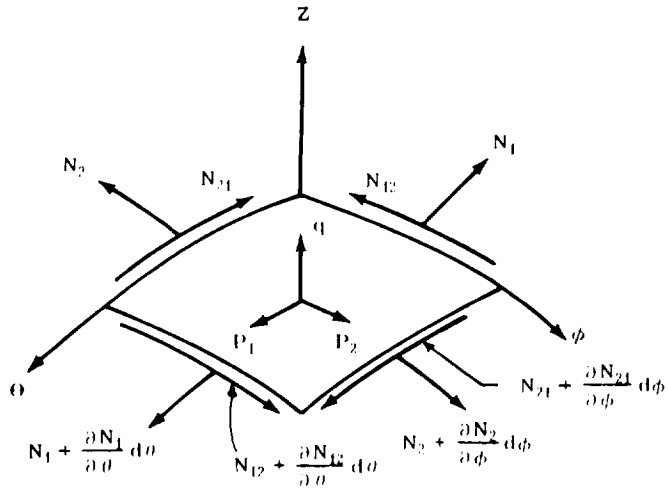

FIGURE B7.3.1-1 TYPICAL SHELL REFERENCE ELEMENT WITH AXIAL AND IN-PLANE SHEAR FORCES

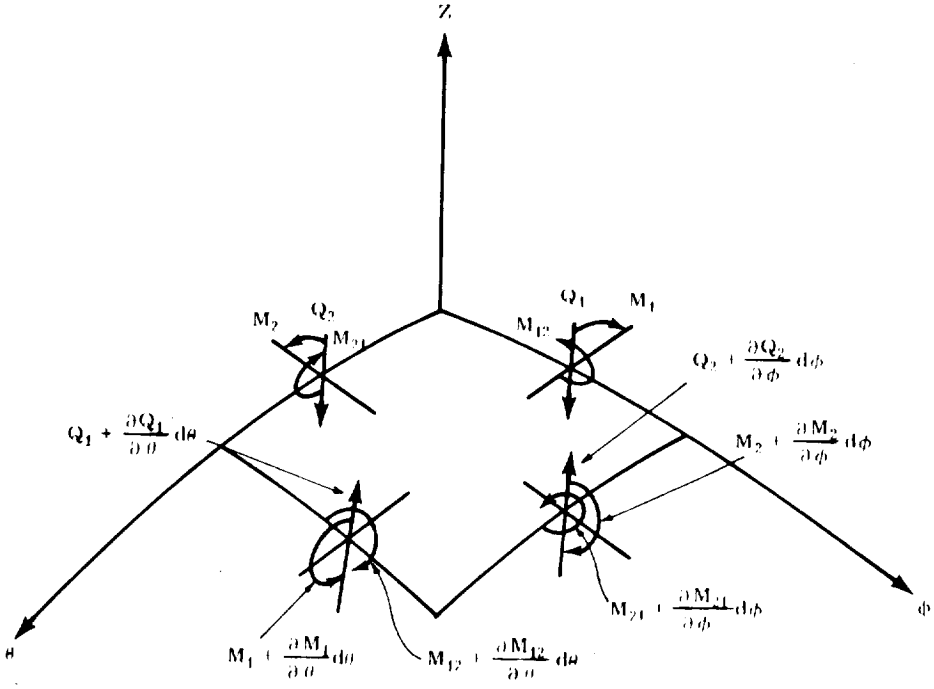

FIGURE B7.3.1-2 TYPICAL SHELL REFERENCE ELEMENT WITH TRANSVERSE SHEAR, BENDING, AND TWISTING ELEMENTS

where p_1, p_2, and q are components of the effective external force per unit area applied to the middle surface of the shell.

The equilibrium of moments about the θ, ϕ, and z coordinates results in the following moment equilibrium expressions:

$$\frac{\partial \alpha_2}{\partial \theta} M_{\theta\phi} + \frac{\partial \alpha_1 M_{\phi}}{\partial \phi} - M_{\theta} \frac{\partial \alpha_1}{\partial \phi} + M_{\phi\theta} \frac{\partial \alpha_2}{\partial \theta} - Q_{\phi} \alpha_1 \alpha_2 = 0$$

$$\frac{\partial \alpha_1}{\partial \phi} M_{\phi\theta} + \frac{\partial \alpha_2 M_{\theta}}{\partial \theta} - M_{\phi} \frac{\partial \alpha_2}{\partial_{\theta}} + M_{\theta\phi} \frac{\partial \alpha_1}{\partial \phi} - Q_{\theta} \alpha_1 \alpha_2 = 0 \qquad (1b)$$

$$N_{\theta\phi} - N_{\phi\theta} + \frac{M_{\theta\phi}}{R_1} - \frac{M_{\phi\theta}}{R_2} = 0 \quad .$$

The force components of the last equilibrium expression are due to warping of the faces, and result from in-plane shears and twisting moments.

Now, for shells of revolution the resultant forces ($N_{\phi\theta}$, Q_{θ}) and moments ($M_{\phi\theta}$) vanish and $\alpha_1 = R_1$; $\alpha_2 = R_2 \sin \phi$. Therefore, the equilibrium equations become:

$$\frac{d(N_{\phi} R)}{d\phi} - N_{\theta} R_1 \cos \phi + Q_{\phi} R_1 + Rp = 0$$

$$\frac{d(Q_{\phi} R)}{d\phi} - N_{\phi} R_1 - N_{\theta} R_1 \sin \phi + R_1 R_q = 0 \qquad (2)$$

$$\frac{d(M_{\phi} R)}{d\phi} - M_{\theta} R_1 \cos \phi - R_1 R Q_{\phi} = 0$$

where the second, fourth, and sixth equations of (1) have been identically satisfied.

In the equilibrium equations presented here, changes in the dimensions and in the shape of the element of the middle surface arising from its deformation have been neglected. This simplification arises from the assumption of small deformations.

II Strain Displacement

For the particular case of axisymmetric deformations, the displacement (V) is zero, and all derivatives of displacement components with respect to θ vanish. In this case the middle surface strain-displacement equations become:

$$\epsilon_1^o = \epsilon_\phi^o = \frac{1}{R_1}\frac{du}{d\phi} + \frac{w}{R_1}$$

$$\epsilon_2^o = \epsilon_\theta^o = \frac{u\cot\phi}{R_1} + \frac{u dR_2}{R_1 R_2 d\phi} + \frac{w}{R_2} \qquad (3)$$

$$\gamma_{12}^o = \gamma_{\phi\theta}^o = 0$$

and the curvature and twist expressions become

$$\kappa_1 = \kappa_\phi = -\frac{1}{R_1}\frac{d}{d\phi}\left(\frac{1}{R_1}\frac{dw}{d\phi} - \frac{u}{R_1}\right)$$

$$\kappa_2 = \kappa_\theta = -\frac{1}{R_1^2}\left[\cot\phi + \frac{1}{R_2}\frac{dR_2}{d\phi}\right]\left[\frac{dw}{d\phi} - u\right] \qquad (4)$$

$$\kappa_{12} = \kappa_{\phi\theta} = 0$$

for general surface of revolution, the expressions $\frac{dR}{d\phi}$ and $\frac{dR_2}{d\phi}$ are as follows for $R = R_2 \sin \phi$:

$$\frac{dR}{d\phi} = R_1 \cos \phi$$

$$\frac{dR_2}{d\phi} = (R_1 - R_2) \cot \phi \qquad (5)$$

inserting equation (5) into equation (3) yields

$$\epsilon_2 = \frac{u \cot \phi}{R_2} + \frac{w}{R_2}$$

$$\kappa_2 = -\frac{\cot \phi}{R_1 R_2}\left[\frac{dw}{d\phi} - u\right] \qquad (6)$$

while remaining strain-displacement equations of (3) and (4) are unchanged.

III Stress-Strain Equations

For an isotropic shell, the following constitutive equations relate stress resultants and couples to components of strain:

$$N_1 = \frac{Et}{1-\mu^2}\left(\epsilon_1^o + \mu\epsilon_2^o\right) \qquad M_1 = D[\kappa_1 + \mu\kappa_2]$$

$$N_2 = \frac{Et}{1-\mu^2}\left(\epsilon_2^o + \mu\epsilon_1^o\right) \qquad M_2 = D[\kappa_2 + \mu\kappa_1] \qquad (7)$$

$$N_{12} = N_{21} = \frac{Et}{2(1+\mu)}\gamma_{12}^o \qquad M_{12} = M_{21} = \frac{(1-\mu)}{2} D \kappa_{12}$$

where

$$D = \frac{Et^3}{12(1-\mu^2)}$$

and where (middle surface) strains (ϵ_1^o, ϵ_2^o, γ_{12}^o) are given in equation (3) and change in curvature and twist terms (κ_1, κ_2, κ_{12}) are given in equation (4).

IV Solution of Equations

By eliminating Q_ϕ from the first and last equilibrium equations (2) and determining the force resultants from equation (7), two second-order ordinary differential equations in the two unknown displacement components u and w are obtained. Rather than obtain equations in this manner, however, a transformation of dependent variables can be performed leading to a more manageable pair of equations, which for shells of constant meridional curvature and constant thickness, combine into a single fourth-order equation solvable in terms of a hypergeometric series.

The transformation to the Reissner-Meissner equations is accomplished by introducing, two new variables, the angular rotation

$$\tilde{V} = \frac{1}{R_1}\left(u - \frac{dw}{d\phi}\right)$$

and the quantity

$$\tilde{U} = R_2 Q_\phi \quad .$$

This substitution of variables leads to two second-order differential equations in $\tilde{U}$ and $\tilde{V}$ replacing the corresponding two equations in u and w. The details of this transformation are illustrated in Reference 1.

For shells of constant thickness and constant meridional curvature or, in fact, for any shell of revolution satisfying the Meissner condition, the transformed pair of equations can be combined into a single fourth-order equation, the solution of which is determined from the solution of a second-order complex equation. For shells of the description above, the shell equations can be represented in the simplified form:

$$L\left(\tilde{U} + \frac{u}{R_1}\,\tilde{U}\right) = Et\,\tilde{V}$$

$$L\left(\tilde{V}\right) - \frac{u}{R_1}\,\tilde{V} = -\frac{\tilde{U}}{D}$$

where the operator

$$L(\quad) = \frac{R_2}{R_1^2}\,\frac{d^2(\quad)}{d\phi^2} + \frac{1}{R_1}\left[\frac{d}{d\phi}\left(\frac{R_2}{R_1}\right) + \frac{R_2}{R_1}\cot\phi\right]\frac{d(\quad)}{d\phi} - \frac{R_1\cot^2\phi}{R_2 R_1}\ .$$

From the system shown above of two simultaneous differential equations of second order, an equation of fourth order is obtained for each unknown. Following operations described in Reference 1 yield an equation of the form

$$LL(\tilde{U}) + r^4\tilde{U} = 0$$

$$\Gamma^4 = \frac{Et}{D} - \frac{u^2}{R_1^2}\ .$$

The solution of the fourth-order equation can be considered the solution of two second-order complex equations of the form

$$L(\tilde{U}) \pm i\ \Gamma^2\,\tilde{U} = 0\ .$$

Reissner-Meissner type equations are the most convenient and most widely employed forms of the first approximation theory for axisymmetrically loaded shells of revolution. They follow exactly from the relations of Love's first approximation when the meridional curvature and thickness are constant, as they are for cylindrical, conical, spherical, and toroidal shells of uniform thickness. Furthermore, they follow directly from Love's equations in the more general case, provided that special restraints on the variation of thickness and geometry are satisfied.

B7.3.1.2 Unit Loading Method

Generally a shell is a statically indeterminate structure. The internal forces of the shell are determined from six equations of equilibrium, which are derived from the three-force and three-moment equilibrium conditions.

There are ten unknowns that make the problem internally statically indeterminate because determination of the unknowns does not depend on the supports. The situation is similar to one that occurs in a truss which, as used in practice, is a highly statically indeterminate system. If reactions to the applied loading can be found with the help of known equations of statical equilibrium, the system is externally determinate; however, a truss is a statically indeterminate system internally because, instead of the assumed simplification (which introduces hinges at the joints), all joints are welded or riveted together. This introduces the moment into the members. However, this additional influence is usually negligible. To find the statically indeterminate values, deformations must be considered.

The main objective of the following sections is to bypass the elaborate calculations by replacing the classical methods of elasticity theory with the simplified but accurate procedure called the unit loading method. This is accomplished by enforcing the conditions of equilibrium, compatibility in displacement, and rotations at the junctions.

I Comparison of Membrane and Bending Theories for Nonshallow Shells

As discussed in Sections B7.0 and B7.1, the bending theory is more general than the membrane theory because it permits use of all possible boundary conditions. To compare the two theories, assume a nonshallow spherical shell with some axisymmetrical loading built in along the edges. When the results are compared, the following conclusions can be made:

1. The stresses and deformations are almost identical for all locations of the shell with the exception of a narrow strip on the shell surface which is adjacent to the boundary. This narrow strip is generally no wider than $\sqrt{Rt}$, where R is the radius and t is the thickness of the spherical shell.

2. Except for the strip along the boundary, all bending moments, twisting moments, and vertical shears are negligible; this causes the entire solution to be practically identical to the membrane solution.

3. Disturbances along the supporting edge are very significant; however, the local bending and shear decrease rapidly along the meridian, and may become negligible outside of the narrow strip, as described in item 1.

Since the bending and membrane theories give practically the same results, except for a strip adjacent to the boundary, the simple membrane theory can be used; then, at the edges, the influence of moment and shear can be applied to bring the displaced edge of the shell into the position prescribed by boundary conditions. The bending theory is used for this operation. Consequently, once the solutions are obtained, they can be used later without any special derivation. The results obtained from application of both theories can be superimposed, which will lead to the final results being almost identical to those obtained by using the exact bending theory.

II Unit-Loading Method Applied to the Combined Theory

The solution of a shell of revolution under axisymmetrical loading can be conducted in a simplified way, known as the unit-loading method.

1. Assume that the shell under consideration is a free membrane. Obtain a solution for the overall stresses and distortions of the edges by using Section B7.1. This is the primary solution.

2. Apply the following edge loadings:

   a. Moment in inch-pounds per inch along the edge

   b. Horizontal shear in pounds per inch along the edge

   c. Vertical shear in pounds per inch along the edge

These loadings should be of such magnitude as to be able to return the distorted edge of the membrane into a position prescribed by the nature of supports (edge condition). The third edge loading in the majority of cases is not necessary. The amount of applied corrective loadings depends on the magnitude of edge deformations due to the primary solution. The exact magnitude will be determined by the interaction procedure to be explained in Section B7.3.2. However, to start the interaction process, formulas will be necessary for deformations due to the following:

a. Unit-edge moment: M = 1 pound per inch

b. Unit-edge horizontal shear: Q = 1 pound per inch

c. Unit-edge vertical shear: V = 1 pound per inch.

These solutions will be referred to as unit-edge influences, or as secondary solutions.

3. Having the primary and unit-edge solutions, one can enter these into the interaction process. This process will determine the correct amount of corrective loadings (M, Q, and V); all stresses and distortions due to these loadings can consequently be determined.

4. Superposition of stresses and distortions obtained by primary solution and corrective loadings lead to the final solution.

B7.3.2 INTERACTION ANALYSIS

Missiles, space vehicles, and pressure vessels are examples of structural configurations usually consisting of various combinations of shell elements. For analysis, such complex shell configurations generally can be broken down into simple elements. However, at the intersection of these elements a discontinuity (point of abrupt change in geometry or loading) usually exists; that is, unknown shears and moments are introduced. The common shapes that a complex shell may be broken down to include spherical, elliptical, conical, toroidal; these shapes also occur in compound bulkheads. Figure

B7.3.2-1, for example, illustrates a compound bulkhead which consists of the spherical transition between the conical and cylindrical sections. For analysis of such a shell, the analyst must choose between two methods, depending on the accuracy required: (1) he can consider such a system as an irregular one and use some approximation, or (2) he can calculate it as a compound shell, using the method of interaction.

In this section, the interaction method is presented which is applicable not only to monocoque shells but also to sandwich and orthotropic shells. The interacting elements are often constructed from different materials. The loading can also vary considerably. The most frequently used loadings are internal or external pressure, axial tension or compression load, thermally induced loads, and the thrust loads.

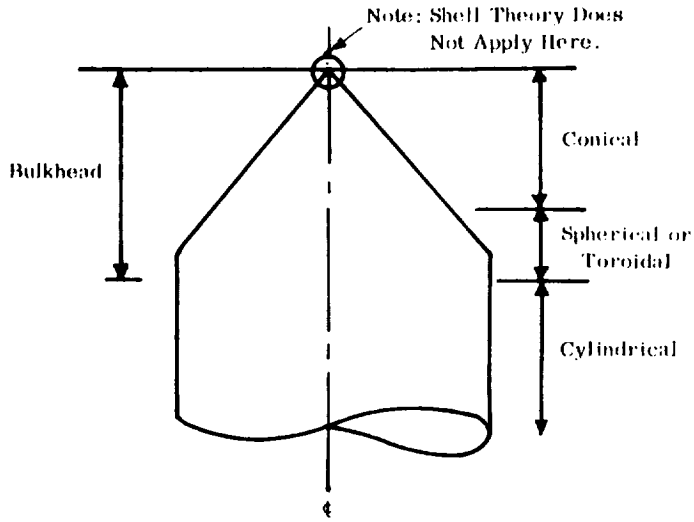

FIGURE B7.3.2-1 COMPOUND BULKHEAD

B7.3.2.1 Interaction Between Two Shell Elements

For simplicity, the interaction between two structural elements will be described first. The more general case of interaction of several elements, as is usually the case when the combined bulkhead is under consideration, will be described second. For the purpose of presentation, a system consisting of a bulkhead and cylinder, pressurized internally, is selected. The bulkhead can be considered as a unit element of some defined shape and will not be subdivided into separate portions in the great majority of cases. For example, assume the pressurized container to be theoretically separated into two main parts, the cylindrical shell and dome, as shown in Figure B7.3.2-2. Stresses and deformations introduced by internal pressure (or another external loading) can be determined for each part separately.

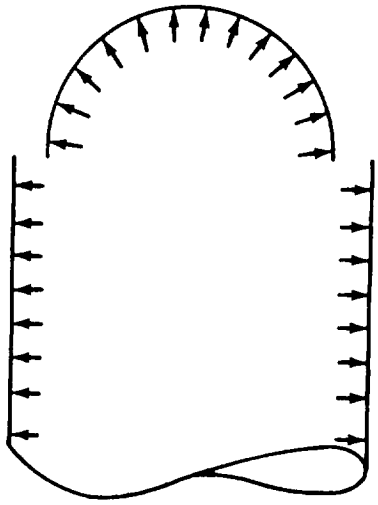

FIGURE B7.3.2-2 CYLINDRICAL SHELL AND DOME

Assume that the membrane analysis (primary solution) supplied the radial displacement ($\Delta r \doteq \delta_c$) and rotation (β_c) for the cylinder along the discontinuity line and $\Delta r = \delta_d$ and β_d for the dome. Since the structure is separated into two elements,

$$\delta_c \neq \delta_d$$

$$\beta_c \neq \beta_d \quad .$$

Consequently, there exists the discontinuity as follows:

(a) in displacement $\quad \delta_c - \delta_d$

(b) in slope $\quad \beta_c - \beta_d$.

To close this gap, unknown forces (Q and M) will be introduced around the juncture to hold the two pieces together.

Displacements and rotation of the cylinder due to unit values of Q and M are defined as follows:

$$Q_c^{\delta}, \; Q_c^{\beta} \text{ and } M_c^{\delta}, \; M_c^{\beta} \quad .$$

The corresponding values for the dome for the same unit loadings will be:

$$Q_d^{\delta}, \; Q_d^{\beta} \text{ and } M_d^{\delta}, \; M_d^{\beta} \quad .$$

These unit deformations and unit loadings at the junctions are presented in Figure B7.3.2-3.

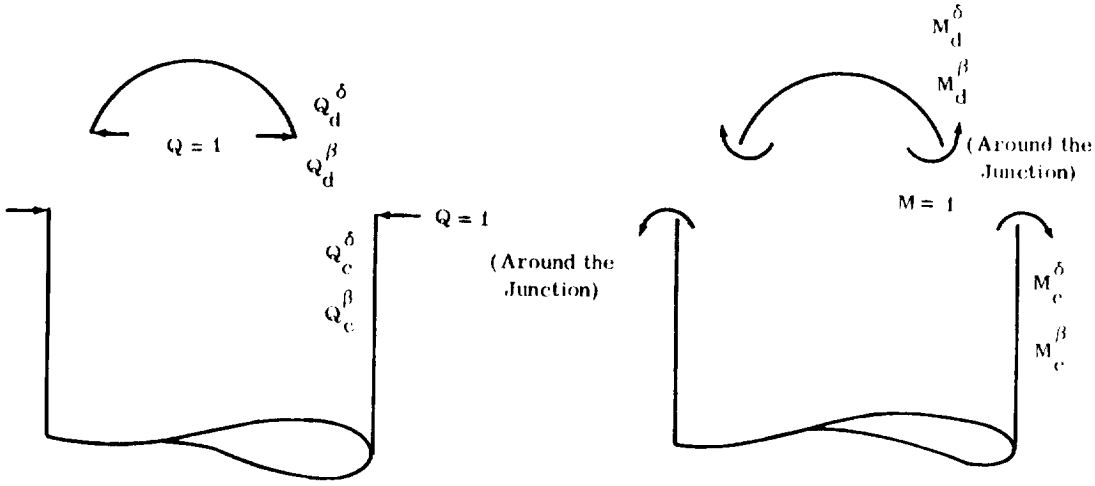

FIGURE B7.3.2-3 UNIT DEFORMATIONS AND UNIT LOADINGS

To close the gap, the following equations can be written:

$$\left(Q_c^\delta + Q_d^\delta\right)Q + \left(M_c^\delta + M_d^\delta\right)M = \delta_c - \delta_d$$

$$\left(Q_c^\beta + Q_d^\beta\right)Q + \left(M_c^\beta + M_d^\beta\right)M = \beta_c - \beta_d \quad .$$

Thus, with the two equations, the two unknowns (Q and M) can be determined.

It is noted that one cut through the shell leads to two algebraic equations with two unknowns.

The following sign convention is adopted:

1. Horizontal deflection, δ, is positive outward
2. Shears are positive if they cause deflection outward
3. Moments are positive if they cause tension on the inside fibers of the shell

4. Rotations are positive if they correspond to a positive moment.

In general, this sign convention is arbitrary. Any rule of signs may be adopted if it does not conflict with logic and is used consistently.

Observe that in addition to M and Q, there is an axial force distribution around the junction between the cylinder and dome (reaction of bulkhead), but the effect of this force on the displacement due to M and Q is negligible.

B7.3.2.2 Interaction Between Three or More Shell Elements

In practice, most cases are similar to the two-member interaction described in the previous paragraph. However, at times it may be convenient to consider interaction of more than two elements. This can be performed in two ways:

1. Interact first the two elements; then, when this combination is solved, interact it with the third element, etc.

2. Simultaneously interact all elements.

The first method is self-explanatory. The second method requires further explanation. If the shape of the bulkhead is such that its meridian cannot be approximated with one definite analytical curve, such a bulkhead is called a compound bulkhead and can be approximated with many curves as shown in Figure B7.3.2-1.

In this case, two or more imaginary cuts through the shell will be required to separate the compound bulkhead into component shells of basic shape. This is shown in Figure B7.3.2-4, where the compound shell has two imaginary cuts separating the three elementary shells (spherical, toroidal, and cylindrical). Figure B7.3.2-4 also illustrates the loading and discontinuity influences that belong to each cut. The discontinuity influences will restore the continuity of the compound shell.

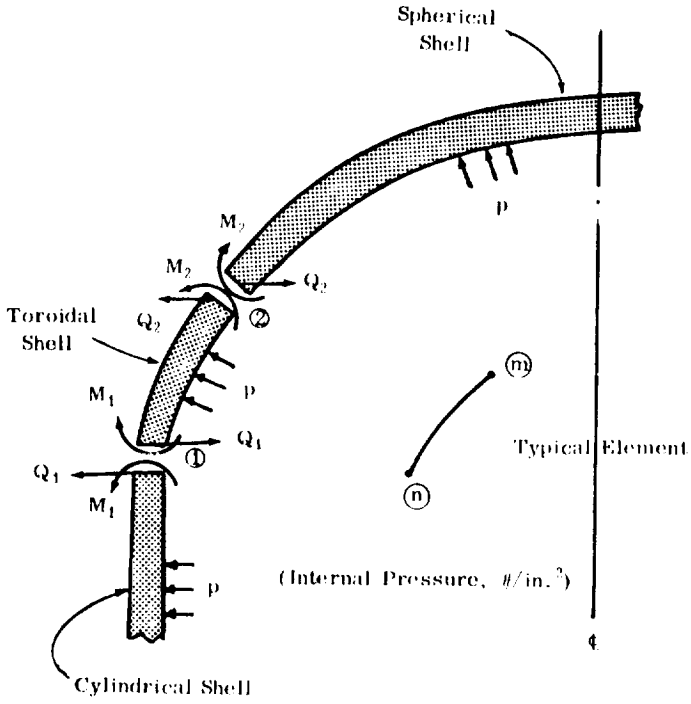

FIGURE B7.3.2-4 DISCONTINUITY LOADS

The symbols used for the two successive cuts m and n are also shown in Figure B7.3.2-4.

M_{nn}^{β}, Q_{nn}^{β} = rotation at point n due to a unit moment M or unit horizontal shear Q at point n

M_{nn}^{δ}, Q_{nn}^{δ} = horizontal displacement due to the same loading in application points as above

M^{β}_{nm}, Q^{β}_{nm} = rotation at point n due to a unit moment M or unit horizontal shear Q acting at point m

M^{δ}_{nm}, Q^{δ}_{nm} = horizontal displacement due to the same loading in application points as above.

Designating n = 1 and m = 2, the nomenclature above can be considered proper indices for the toroidal portion (1) and (2) as shown in Figure B7.3.2-4.

Additional nomenclature needed to cover the spherical shell portion of Figure B7.3.2-4 is as follows:

M^{β}_{s}, Q^{β}_{s} = rotations at point (2) on the spherical shell due to a unit moment or unit shear at the same point

M^{δ}_{s}, Q^{δ}_{s} = horizontal displacements due to the same conditions as stated above.

Similarly, displacements and rotations of point (1) on the cylindrical shell are defined by using subscript c (cylinder) instead of subscript s (sphere).

Due to the primary loading (internal pressure), the rotations and displacements will be indicated with β and $\Delta r = \Delta$. As before, the subscripts c and s refer to the cylinder and sphere. The subscripts 1t and 2t will be used to denote the toroidal shell at the edges (1) and (2).

Now the equations for the total rotation and displacement can be formed.

Spherical Shell:

$$\delta_s = M^{\delta}_{s} M_2 + Q^{\delta}_{s} Q_2 + \Delta_s p$$

$$\beta_s = M^{\beta}_{s} M_2 + Q^{\beta}_{s} Q_2 + \beta_s p$$

Toroidal Shell:

$$\delta_{2t} = M_{22}^{\delta} M_2 + Q_{22}^{\delta} Q_2 + M_{21}^{\delta} M_1 + Q_{21}^{\delta} Q_1 + \Delta_{2t} p$$

$$\beta_{2t} = M_{22}^{\beta} M_2 + Q_{22}^{\beta} Q_2 + M_{21}^{\beta} M_1 + Q_{21}^{\beta} Q_1 + \beta_{2t} p$$

$$\delta_{1t} = M_{12}^{\delta} M_2 + Q_{12}^{\delta} Q_2 + M_{11}^{\delta} M_1 + Q_{11}^{\delta} Q_1 + \Delta_{1t} p$$

$$\beta_{1t} = M_{12}^{\beta} M_2 + Q_{12}^{\beta} Q_2 + M_{11}^{\beta} M_1 + Q_{11}^{\beta} Q_1 + \beta_{1t} p$$

Cylindrical Shell:

$$\delta_c = M_c^{\delta} M_1 + Q_c^{\delta} Q_1 + \Delta_c p$$

$$\beta_c = M_c^{\beta} M_1 + Q_c^{\beta} Q_1 + \beta_c p$$

The following compatibility equations must be satisfied:

$$\delta_s = \delta_{2t} \qquad \beta_s = \beta_{2t}$$

$$\delta_c = \delta_{1t} \qquad \beta_c = \beta_{1t} \quad .$$

Following considerations of the relations above and some mathematical rearrangements, a system of four linear equations with four unknowns will finally be obtained. In matrix form they are:

$$\begin{bmatrix} M_{21}^{\delta} & \left(M_{22}^{\delta} - M_s^{\delta}\right) & Q_{21}^{\delta} & \left(Q_{22}^{\delta} - Q_s^{\delta}\right) \\ \left(M_{11}^{\delta} - M_c^{\delta}\right) & M_{12}^{\delta} & \left(Q_{11}^{\delta} - Q_c^{\delta}\right) & Q_{12}^{\delta} \\ M_{21}^{\beta} & \left(M_{22}^{\beta} - M_s^{\beta}\right) & Q_{21}^{\beta} & \left(Q_{22}^{\beta} - Q_s^{\beta}\right) \\ \left(M_{11}^{\beta} - M_c^{\beta}\right) & M_{12}^{\beta} & \left(Q_{11}^{\beta} - Q_c^{\beta}\right) & Q_{12}^{\beta} \end{bmatrix} \begin{bmatrix} M_1 \\ M_2 \\ Q_1 \\ Q_2 \end{bmatrix} + \begin{bmatrix} \Delta_{2t} - \Delta_s \\ \Delta_{1t} - \Delta_c \\ \beta_{2t} - \beta_s \\ \beta_{1t} - \beta_c \end{bmatrix} p = 0 \quad .$$

It is noted that two imaginary cuts lead to four equations with four unknowns: M_1, M_2, Q_1, and Q_2.

Previously, when considering only one imaginary cut, only two equations with two unknowns were obtained. Consequently, if n imaginary cuts are introduced simultaneously, 2n linear equations with 2n unknowns can be obtained.

It can be concluded that the problem of interaction is reduced to the problem of finding rotation (β) and displacements ($\Delta r = \delta$) of interacting structural elements due to the primary loadings and the secondary loadings ($M = Q = 1$) (around the junction). The rotations and displacements then will be introduced into a set of linear equations and statically indeterminate values (M and Q) will be found.

B7.3.3 EDGE INFLUENCE COEFFICIENTS

The shells considered in this section are homogeneous isotropic monocoque shells of revolution. Thin shells are considered and all loadings are axisymmetrical. Paragraph B7.3.4 will present necessary modifications of derived formulas for nonhomogeneous material and nonmonocoque shells.

B7.3.3.1 General Discussion

Unit loadings (defined in Paragraph B7.3.1.2) are the loadings acting on upper or lower edge of shell:

$M = 1$ lb-in./in.

$Q = 1$ lb/in.

Unit influences are deformations and forces in a shell of revolution due to unit loadings. Influences of this nature are of load character and do not progress very far into the shell from the disturbed edge. Various differently shaped shells are covered at this location. Of special interest is a shell that represents a bulkhead, which is characterized with $\phi_{max} = 90^\circ$; such bulkheads

are very common in aerospace vehicles and pressure vessels. The bulkhead shells are tangent to the cylindrical body of the vehicle.

When the values of deformations due to the unit loadings are available, the deformations, along with the primary deformations, can be used to determine discontinuity stresses (Paragraph B7.3.2).

The bending theory is used to obtain the influence coefficients due to unit loadings. The fundamentals of this procedure were explained previously.

It has been mentioned that deflections and internal loads due to unit loadings are of local importance. It can be concluded that disturbances due to edge-unit loadings will disappear completely for $\alpha \geqq 20^\circ$ and will become negligible for $\alpha \geqq 10^\circ$, as shown in Table B7.3.3-1, for a spherical shell.

TABLE B7.3.3-1 UNIT-EDGE LOADING SOLUTIONS

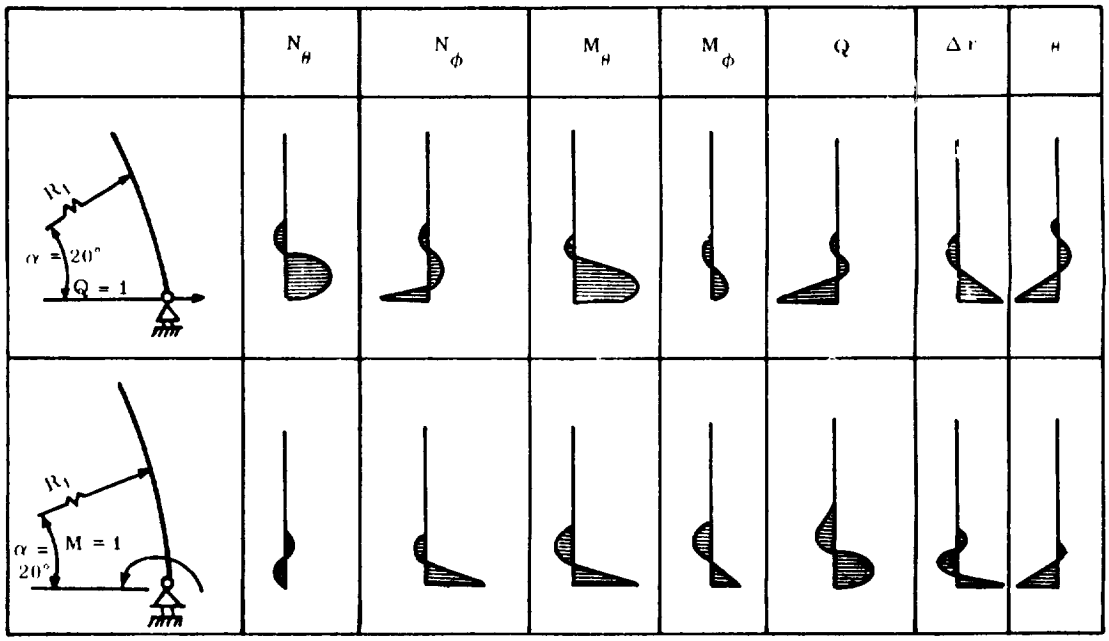

Table B7.3.3-1 illustrates a very important conclusion: due to the unit-edge loadings, practically all parts of the shell satisfying the condition $\alpha \geq 20^\circ$ will remain unstressed and undisturbed. These parts will not be needed for satisfying equilibrium. They do not affect the stresses and deformations in the disturbed zone $0 < \alpha < 20^\circ$ in any way. The material above $\alpha = 20^\circ$ can be deleted because this material does not contribute to the stresses or strains, which are computed for the zone defined by $0 < \alpha < 20^\circ$. No values of stresses or deformations will be changed in the zone $0 < \alpha < 20^\circ$ if we replace the removed material with any shape of shell (Figure B7.3.3-1) which illustrates imaginary operations. Consequently, cases (A), (B), and (C) of Figure B7.3.3-1 are statically equivalent. This discussion leads to the following conclusions:

1. The spherical shell of revolution, loaded with the unit loadings ($M = Q = 1$), acts as a lower segment would act under the same loading (segment defined with $\alpha = 20^\circ$). Consequently, it does not matter what shape the rest of the shell has (Figure B7.3.3-2).

2. If any shell at the lower portion (which is adjusted to the load edge) can be approximated with the spherical shell to a satisfactory degree, the solution obtained for the spherical shell which is loaded with $M = Q = 1$ all around the edges (Figures B7.3.3-2 and B7.3.3-3) can be used for the actual shell.

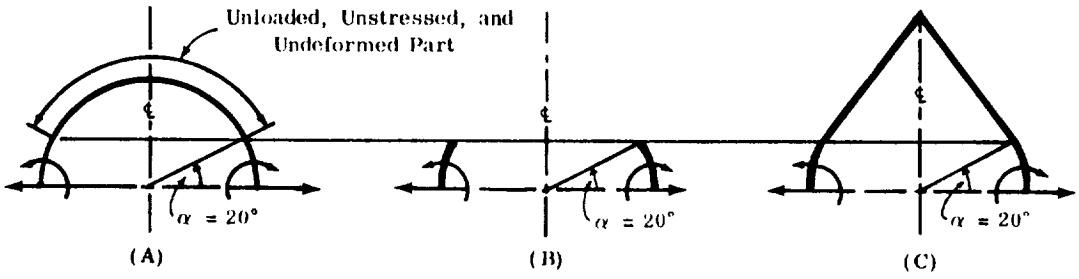

FIGURE B7.3.3-1 STATICALLY ANALOGICAL SHELLS

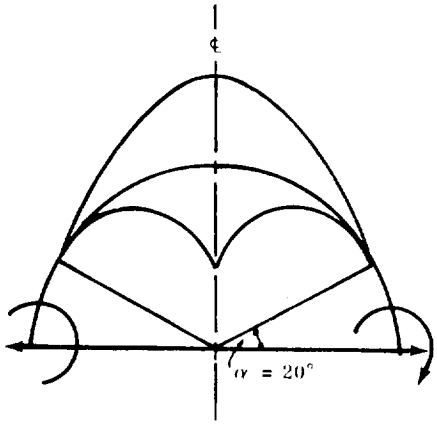

FIGURE B7.3.3-2 DIFFERENT VARIANTS FOR UNSTRESSED PORTION

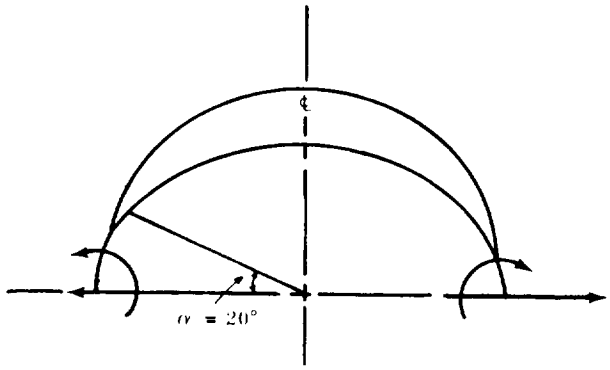

FIGURE B7.3.3-3 APPROXIMATION WITH THE SPHERE

3. When accuracy requirements are relaxed, $\alpha = 10^\circ$ may be used in place of $\alpha = 20^\circ$.

Another approximation, known as Geckeler's assumption, may be useful; i.e., if the thickness of the shell (t) is small in comparison with equatorial radius ($r_1 = a$) and limited by the relation ($a/t > 50$), the bending stresses at the edge may be determined by cylindrical shell theory. Meissner even recommends $a/t > 30$. This means that the bulkhead shell can be approximated with a cylinder for finding unit influences. Many solutions can be presented for various shaped shells due to the unit loading action. This is done in the following paragraphs.

B7.3.3.2 Definition of F-Factors

The general solution of the homogeneous differential equation

$$w'''' + 4K^4 w = 0$$

can be represented with the following combination of trigonometric and hyperbolic functions:

$\cosh k L\xi \cos k L\xi$ $\quad$ $\sinh k L\xi \cos k L\xi$

$\cosh k L\xi \sin k L\xi$ $\quad$ $\sinh k L\xi \sin k L\xi$

where kL is a dimensionless parameter and ξ is a dimensionless ordinate.

In the sections which follow, F-factors will be used that simplify the analysis. Definitions of the F-factors in Table B7.3.3-2 are taken from Reference 2. As a special parameter for determining the F-factors, η is considered as follows:

$$F = F(\eta) \quad \text{i.e.,} \quad F_1 = \sinh^2\eta + \sin^2\eta$$

For a cylindrical shell

$$\eta = kL \text{ or } \eta = kL\xi \text{ and } k = \frac{\sqrt[4]{3(1-\mu^2)}}{\sqrt{Rt}}$$

For a conical shell

$$\eta = kL \text{ or } \eta = kL \text{ and } k = \frac{\sqrt[4]{3(1-\mu^2)}}{\sqrt{t x_m \cot\alpha_0}}$$

For a spherical shell

$$\eta = k \text{ for } F_i;\ \eta = k\alpha \text{ for } F_i(\alpha) \text{ and } k = \sqrt[4]{3(1-\mu^2)\ (R/t)^2} \quad .$$

Graphs of the functions are presented in Reference 2.

TABLE B7. 3. 3-2 $F_i(\xi)$ AND F_i FACTORS

i	$F_i(\xi)$	F_i
1	$\sinh^2 kL\xi - \sin^2 kL\xi$	$\sinh^2 kL - \sin^2 kL$
2	$\sinh^2 kL\xi + \sin^2 kL\xi$	$\sinh^2 kL + \sin^2 kL$
3	$\sinh kL\xi \cosh kL\xi + \sin kL\xi \cos kL\xi$	$\sinh kL \cosh kL + \sin kL \cos kL$
4	$\sinh kL\xi \cosh kL\xi - \sin kL\xi \cos kL\xi$	$\sinh kL \cosh kL - \sin kL \cos kL$
5	$\sin^2 kL\xi$	$\sin^2 kL$
6	$\sinh^2 kL\xi$	$\sinh^2 kL$
7	$\cosh kL\xi \cos kL\xi$	$\cosh kL \cos kL$
8	$\sinh kL\xi \sin kL\xi$	$\sinh kL \sin kL$
9	$\cosh kL\xi \sin kL\xi - \sinh kL\xi \cos kL\xi$	$\cosh kL \sin kL - \sinh kL \cos kL$
10	$\cosh kL\xi \sin kL\xi + \sinh kL\xi \cos kL\xi$	$\cosh kL \sin kL + \sinh kL \cos kL$
11	$\sin kL\xi \cos kL\xi$	$\sin kL \cos kL$
12	$\sinh kL\xi \cosh kL\xi$	$\sinh kL \cosh kL$
13	$\cosh kL\xi \cos kL\xi - \sinh kL\xi \sin kL\xi$	$\cosh kL \cos kL - \sinh kL \sin kL$
14	$\cosh kL\xi \cos kL\xi + \sinh kL\xi \sin kL\xi$	$\cosh kL \cos kL + \sinh kL \sin kL$
15	$\cosh kL\xi \sin kL\xi$	$\cosh kL \sin kL$
16	$\sinh kL\xi \cos kL\xi$	$\sinh kL \cos kL$
17	$\exp(-kL\xi \cos kL\xi)$	$\exp(-kL \cos kL)$
18	$\exp(-kL\xi \sin kL\xi)$	$\exp(-kL \sin kL)$
19	$\exp[-kL\xi(\cos kL\xi + \sin kL\xi)]$	$\exp[-kL(\cos kL + \sin kL)]$
20	$\exp[-kL\xi(\cos kL\xi - \sin kL\xi)]$	$\exp[-kL(\cos kL - \sin kL)]$

B7.3.3.3 Spherical Shells

The boundaries of the shells considered herein must be free to rotate and deflect vertically and horizontally because of the action of unit loadings. Abrupt discontinuities in the shell thickness must not be present. Thickness of the shell must be uniform in the range in which the stresses exist.

I Nonshallow Spherical Shells

Formulas will be tabulated for closed and open spherical shells. Open shells are shells that have an axisymmetrical circular opening at the apex. Unit-edge loadings may act at the lower or upper edge of the open shell. Linear bending theory was employed for derivation of the formulas presented.

The following designations will be used:

$$k = \sqrt[4]{(R/t)^2\, 3(1-\mu^2)}\ ;\ \alpha = \phi_1 - \phi \quad .$$

Tables B7.3.3-3, B7.3.3-4, B7.3.3-5, and B7.3.3-6 are presented.

II Shallow Spherical Shells

This section presents, for shallow spherical shells, the solutions which satisfy the relation

$$\cot \phi \cong \frac{1}{\phi}$$

which is characteristic for the category of shallow spherical shells. Physically, this means that for shallow shells the disturbances resulting from unit-edge loadings will not decay before reaching the apex. Consequently, from diametrically opposite edge loadings, disturbances will be superimposed in some area around the apex.

Tables B7.3.3-7 and B7.3.3-8 are presented.

TABLE B7. 3. 3-3 CLOSED SPHERICAL SHELL

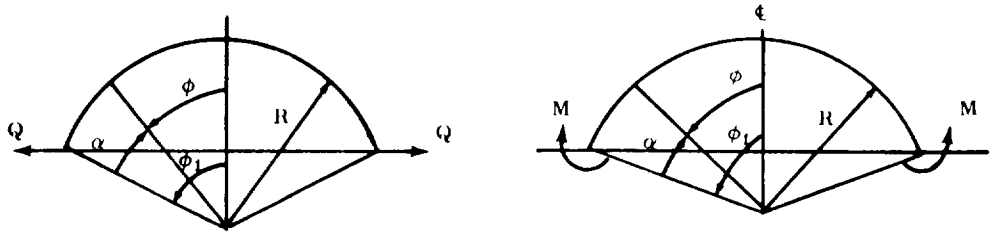

Q_ϕ	$-\sqrt{2}Q \sin \phi_1 e^{-k\alpha} \cos\left(k\alpha + \frac{\pi}{4}\right)$	$+\frac{2Mk}{R} e^{-k\alpha} \sin k\alpha$
N_ϕ	$-Q_\phi \cot \phi$	$-Q_\phi \cot \phi$
N_θ	$2Qk \sin \phi_1 e^{-k\alpha} \cos k\alpha$	$2\sqrt{2}\ \frac{Mk^2}{R} e^{-k\alpha} \cos\left(k\alpha + \frac{\pi}{4}\right)$
M_ϕ	$\frac{RQ}{k} \sin \phi_1 e^{-k\alpha} \sin k\alpha$	$\sqrt{2}\, Me^{-k\alpha} \sin\left(k\alpha + \frac{\pi}{4}\right)$
M_θ	$-\frac{RQ}{k^2\sqrt{2}} \sin \phi_1 (\cot \phi) e^{-k\alpha} \sin\left(k\alpha + \frac{\pi}{4}\right) + \mu M_\phi$	$\frac{M}{k} \cot \phi\ e^{-k\alpha} \cos k\alpha + \mu M_\phi$
$Et\beta$	$-2\sqrt{2}\,Qk^2 \sin \phi_1 e^{-k\alpha} \sin\left(k\alpha + \frac{\pi}{4}\right)$	$-\frac{4k^3M}{R} e^{-k\alpha} \cos k\alpha$
$Et(\Delta r)$	$RQ \sin \phi_1 e^{-k\alpha}\left[2k \sin \phi \cos k\alpha - \sqrt{2}\mu \cos \phi \cos\left(k\alpha + \frac{\pi}{4}\right)\right]$	$R \sin \phi\left(N_\theta - \mu N_\phi\right)$

For $\alpha = 0$, $\phi = \phi_1$		
$Et\beta$	$-2Qk^2 \sin \phi_1$	$-\frac{4k^3M}{R}$
$Et(\Delta r)$	$QR \sin \phi_1\left(2k \sin \phi_1 - \mu \cos \phi_1\right)$	$2Mk^2 \sin \phi_1$

For $\phi_1 = 90^\circ$, $\alpha = 0$		
$Et\beta$	$-2k^2Q$	$-\frac{4k^3}{R} M$
$Et(\Delta r)$	$2RkQ$	$2k^2M$

TABLE B7.3.3-4 OPEN SPHERICAL SHELL

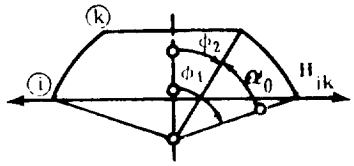

Boundary Conditions

$\alpha = 0 (\phi = \phi_1)$: $M_\phi = 0$

$H_{ik} = Q_{ik} \sin \phi_1 + N_{ik} \cos \phi_1$

$\alpha = \alpha_0 (\phi = \phi_2)$ $M_\phi = 0$

$Q = 0$

Internal Forces and Deformations

N_ϕ	$H_{ik} \sin \phi \cot \phi \left[F_7(\alpha) - \frac{F_4}{F_1} F_{10}(\alpha) + \frac{F_2}{F_1} F_8(\alpha)\right]$
N_θ	$-H_{ik} k \sin \phi_1 \left[-F_9(\alpha) - 2 \frac{F_4}{F_1} F_7(\alpha) + \frac{F_2}{F_1} F_{10}(\alpha)\right]$
Q_ϕ	$H_{ik} \sin \phi_1 \left[F_7(\alpha) - \frac{F_4}{F_1} F_{10}(\alpha) + \frac{F_2}{F_1} F_8(\alpha)\right]$
M_ϕ	$-H_{ik} \frac{R}{2k} \sin \phi_1 \left[-F_{10}(\alpha) + 2 \frac{F_4}{F_1} F_8(\alpha) - \frac{F_2}{F_1} F_9(\alpha)\right]$
M_θ	$H_{ik} \frac{R}{2k} \sin \phi_1 \left\{ -\left[\frac{\cot \phi}{k} F_8(\alpha) - \mu F_{10}(\alpha)\right] + \frac{F_4}{F_1} \left[\frac{\cot \phi}{k} F_9(\alpha) - 2\mu F_8(\alpha)\right] + \frac{F_2}{F_1} \left[\frac{\cot \phi}{k} F_7(\alpha) + \mu F_9(\alpha)\right] \right\}$
Δr	$-H_{ik} \frac{Rk}{Et} \sin \phi \sin \phi_1 \left[-F_9(\alpha) - 2 \frac{F_4}{F_1} F_7(\alpha) + \frac{F_2}{F_1} F_{10}(\alpha)\right]$
β	$-H_{ik} \frac{2k^2}{Et} \sin \phi_1 \left[-F_8(\alpha) - \frac{F_4}{F_1} F_9(\alpha) + \frac{F_2}{F_1} F_7(\alpha)\right]$

TABLE B7.3.3-4 OPEN SPHERICAL SHELL (Continued)

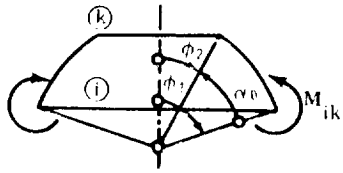

Boundary Conditions

$\alpha = 0$	$M_\phi = -M_{ik}$
	$Q_\phi = 0$
$\alpha = \alpha_0$	$M_\phi = 0$
	$Q_\phi = 0$

Internal Forces and Deformations

N_ϕ	$M_{ik} \cot\phi \frac{2k}{R}\left[\frac{F_6}{F_1} F_{15}(\alpha) + \frac{F_5}{F_1} F_{16}(\alpha) - \frac{F_3}{F_1} F_8(\alpha)\right]$
N_θ	$-M_{ik} \frac{2K^2}{R}\left[\frac{F_6}{F_1} F_{14}(\alpha) + \frac{F_5}{F_1} F_{13}(\alpha) - \frac{F_3}{F_1} F_{10}(\alpha)\right]$
Q_ϕ	$M_{ik} \frac{2k}{R}\left[\frac{F_6}{F_1} F_{15}(\alpha) + \frac{F_5}{F_1} F_{16}(\alpha) - \frac{F_3}{F_1} F_8(\alpha)\right]$
M_ϕ	$M_{ik}\left\{\frac{F_6}{F_1}\left[\frac{\cot\phi}{k} F_{16}(\alpha) - \mu F_{13}(\alpha)\right] - \frac{F_5}{F_1}\left[\frac{\cot\phi}{k} F_{15}(\alpha) - \mu F_{14}(\alpha)\right] - \frac{F_3}{F_1}\left[\frac{\cot\phi}{k} F_7(\alpha) + \mu F_9(\alpha)\right]\right\}$
M_θ	$-M_{ik}\left[\frac{F_6}{F_1} F_{13}(\alpha) - \frac{F_5}{F_1} F_{14}(\alpha) + \frac{F_3}{F_1} F_9(\alpha)\right]$
Δr	$-M_{ik} \frac{2k^2}{Et} \sin\phi\left[\frac{F_6}{F_1} F_{14}(\alpha) + \frac{F_5}{F_1} F_{13}(\alpha) - \frac{F_3}{F_1} F_{10}(\alpha)\right]$
β	$-M_{ik} \frac{4k^3}{EtR}\left[\frac{F_6}{F_1} F_{16}(\alpha) - \frac{F_5}{F_1} F_{15}(\alpha) - \frac{F_3}{F_1} F_7(\alpha)\right]$

TABLE B7. 3. 3-4 OPEN SPHERICAL SHELL (Continued)

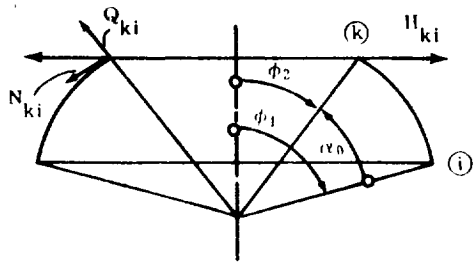

Boundary Conditions

$\alpha = 0 (\phi = \phi_1)$	$M_\phi = 0$
	$Q_\phi = 0$
$\alpha = \alpha_0 (\phi = \phi_2)$	$M_\phi = 0$
	$H_{ki} = -Q_{ki} \sin \phi_2 - N_{ki} \cos \phi_2$

Internal Forces and Deformations

N_ϕ	$H_{ki} \cot \phi \sin \phi_2 \left[\frac{F_9}{F_1} F_{10}(\alpha) - 2 \frac{F_8}{F_1} F_8(\alpha) \right]$
N_θ	$H_{ki}\, 2k \sin \phi_2 \left[- \frac{F_9}{F_1} F_7(\alpha) + \frac{F_8}{F_1} F_{10}(\alpha) \right]$
Q_o	$H_{ki} \sin \phi_2 \left[\frac{F_9}{F_1} F_{10}(\alpha) - \frac{2F_8}{F_1} F_8(\alpha) \right]$
M_o	$H_{ki} \frac{R}{k} \sin \phi_2 \left[\frac{F_9}{F_1} F_8(\alpha) - \frac{F_8}{F_1} F_9(\alpha) \right]$
M_θ	$H_{ki} \frac{R}{2k} \sin \phi_2 \left\{ \frac{F_9}{F_1} \left[- \frac{\cot \phi}{k} F_9(\alpha) + \mu 2 F_8(\alpha) \right] - \frac{2F_8}{F_1} \left[\frac{\cot \phi}{k} F_7(\alpha) + \mu F_9(\alpha) \right] \right\}$
Δr	$-H_{ki} \sin \phi_2 \frac{Rk}{Et} 2 \sin \phi \left[\frac{F_9}{F_1} F_7(\alpha) - \frac{F_8}{F_1} F_{10}(\alpha) \right]$
β	$H_{ki} \sin \phi_2 \frac{2k^2}{Et} \left[\frac{F_9}{F_1} F_9(\alpha) + \frac{2F_8}{F_1} F_7(\alpha) \right]$

TABLE B7.3.3-4 OPEN SPHERICAL SHELL (Concluded)

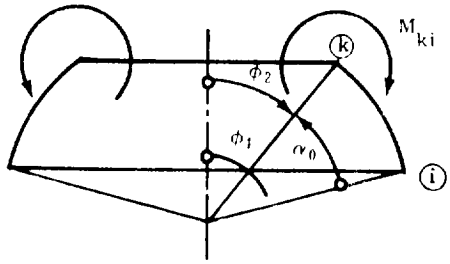

Boundary Conditions

$\alpha = 0 (\phi = \phi_1)$	: M_ϕ	0
	Q_ϕ	0
$\alpha = \alpha_0 (\phi = \phi_2)$	: M_ϕ	M_{ki}
	Q_ϕ	0

Internal Forces and Deformations

N_ϕ	$M_{ki} \frac{2k}{R} \cot\phi \left[\frac{F_8}{F_1} F_{10}(\alpha) - \frac{F_{10}}{F_1} F_8(\alpha)\right]$
N_θ	$M_{ki} \frac{2k^2}{R} \left[-2 \frac{F_8}{F_1} F_7(\alpha) + \frac{F_{10}}{F_1} F_{10}(\alpha)\right]$
Q_ϕ	$-M_{ki} \frac{2k}{R} \left[-\frac{F_8}{F_1} F_{10}(\alpha) + \frac{F_{10}}{F_1} F_8(\alpha)\right]$
M_ϕ	$M_{ki} \left[2 \frac{F_8}{F_1} F_8(\alpha) - \frac{F_{10}}{F_1} F_9(\alpha)\right]$
M_θ	$-M_{ki} \left\{\frac{F_8}{F_1} \left[\frac{\cot\phi}{k} F_9(\alpha) - \mu 2 F_8(\alpha)\right] + \frac{F_{10}}{F_1} \left[\frac{\cot\phi}{k} F_7(\alpha) + F_7(\alpha)\right]\right\}$
Δr	$M_{ki} \frac{2k^2}{Et} \sin\phi \left[-2 \frac{F_8}{F_1} F_7(\alpha) + \frac{F_{10}}{F_1} F_{10}(\alpha)\right]$
β	$M_{ki} \frac{4k^3}{EtR} \left[\frac{F_8}{F_1} F_9(\alpha) + \frac{F_{10}}{F_1} F_7(\alpha)\right]$

TABLE B7.3.3-5 SPHERICAL SEGMENT WITH FREE EDGES, EDGE DISTORTIONS RESULTING FROM SECONDARY LOADINGS

Loading Condition \ Edge Distortions	Δr_{ik}	β_{ik}	Δr_{ki}	β_{ik}
H_{ik}	$+H_{ik}\frac{2Rk}{Et}\sin^2\phi_1\frac{F_4}{F_1}$	$-H_{ik}\frac{2k^2}{Et}\sin\phi_1\frac{F_2}{F_1}$	$-H_{ik}\frac{2Rk}{Et}\sin\phi_1\sin\phi_2\frac{F_9}{F_1}$	$-H_{ik}\frac{2k^2}{Et}\sin\phi_1\frac{2F_8}{F_1}$
M_{ik}	$-M_{ik}\frac{2k^2}{Et}\sin\phi_2\frac{F}{F_1}$	$-M_{ik}\frac{2k^3}{EtR}\frac{2F_3}{F_1}$	$-M_{ik}\frac{2k^2}{Et}\sin\phi_2\frac{2F_8}{F_1}$	$+M_{ik}\frac{2k^3}{EtR}\frac{2F_{10}}{F_1}$
H_{ki}	$-H_{ki}\frac{2Rk}{Et}\sin\phi_2\sin\phi_1\frac{F_2}{F_1}$	$-H_{ki}\frac{2k^2}{Et}\sin\phi_2\frac{2F_8}{F_1}$	$-H_{ki}\frac{2Rk}{Et}\sin^2\phi_2\frac{F_4}{F_1}$	$-H_{ki}\frac{2k^2}{Et}\sin\phi_2\frac{F_2}{F_1}$
M_{ki}	$-M_{ki}\frac{2k^2}{Et}\sin\phi_1\frac{2F_2}{F_1}$	$-M_{ki}\frac{2k^3}{EtR}\frac{2F_{10}}{F_1}$	$-M_{ki}\frac{2k^2}{Et}\sin\phi_2\frac{F}{F_1}$	$+M_{ki}\frac{2k^3}{EtR}\frac{2F_3}{F_1}$

TABLE B7.3.3-6 OPEN (OR CLOSED) SPHERICAL SHELL EXPOSED TO UNIT DISTORTIONS AT LOWER EDGE

Rotation β_{ik}

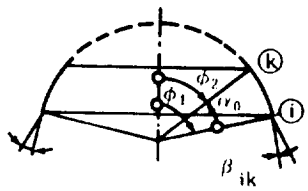

Boundary Conditions

$\alpha = 0 (\phi = \phi_1)$: $\Delta r = 0 : \beta = \beta_{ik}$

$\alpha = \alpha_0 (\phi = \phi_2)$: $\Delta r = 0 : \beta = 0$

Internal Forces and Deformations

N_ϕ	$\beta_{ik} \cot\phi \frac{Et}{2k^2} \left[\frac{F_2}{F_1} F_7(\alpha) + \frac{F_4}{F_1} F_9(\alpha) - F_8(\alpha) \right]$
N_θ	$-\beta_{ik} \frac{Et}{2k} \left[-\frac{F_2}{F_1} F_9(\alpha) + 2 \frac{F_4}{F_1} F_8(\alpha) - F_{10}(\alpha) \right]$
Q_ϕ	$\beta_{ik} \frac{Et}{2k^2} \left[\frac{F_2}{F_1} F_7(\alpha) + \frac{F_4}{F_1} F_9(\alpha) - F_8(\alpha) \right]$
M_ϕ	$-\beta_{ik} \frac{REt}{4k^3} \left[-\frac{F_2}{F_1} F_{10}(\alpha) + 2 \frac{F_4}{F_1} F_7(\alpha) + F_9(\alpha) \right]$
M_θ	$\beta_{ik} \frac{REt}{4k^3} \left\{ -\frac{F_2}{F_1} \left[\frac{\cot\phi}{k} F_8(\alpha) - \mu F_{10}(\alpha) \right] + \frac{F_4}{F_1} \left[\frac{\cot\phi}{k} F_{10}(\alpha) - 2\mu F_7(\alpha) \right] - \left[\frac{\cot\phi}{k} F_7(\alpha) + \mu F_9(\alpha) \right] \right\}$
Δr	$-\beta_{ik} \frac{R}{2k} \sin\phi \left[-\frac{F_2}{F_1} F_9(\alpha) + 2 \frac{F_4}{F_1} F_8(\alpha) - F_{10}(\alpha) \right]$
β	$-\beta_{ik} \left[-\frac{F_2}{F_1} F_8(\alpha) + \frac{F_4}{F_1} F_{10}(\alpha) - F_7(\alpha) \right]$

TABLE B7.3.3-6 OPEN (OR CLOSED) SPHERICAL SHELL EXPOSED TO UNIT DISTORTIONS AT LOWER EDGE (Continued)

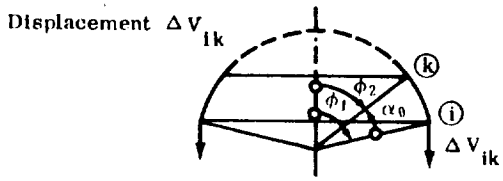

Boundary Conditions

$\alpha = (\phi = \phi_1)$: $\beta = 0$, $\Delta V = \Delta V_{ik}$
$\alpha = \alpha_0 (\phi = \phi_2)$: $\beta = 0$, $\Delta V = 0$

Internal Forces and Deformations

N_ϕ	$\dfrac{\Delta V_{ik}\, Et \cot \phi}{R\left[(1+\mu) \sin \phi_1 F_3 + k \cos \phi_1 F_1\right]} \left[- F_3 F_7(\alpha) - F_5 F_{15}(\alpha) + F_6 F_{16}(\alpha)\right]$
N_θ	$\dfrac{-\Delta V_{ik}\, Et\, k}{R\left[(1+\mu) \sin \phi_1 F_3 + k \cos \phi_1 F_1\right]} \left[F_3 F_9(\alpha) - F_5 F_{14}(\alpha) + F_6 F_{13}(\alpha)\right]$
Q_ϕ	$\dfrac{\Delta V_{ik}\, Et}{R\left[(1+\mu) \sin \phi_1 F_3 + k \cos \phi_1 F_1\right]} \left[- F_3 F_7(\alpha) - F_5 F_{15}(\alpha) + F_6 F_{16}(\alpha)\right]$
M_ϕ	$\dfrac{-\Delta V_{ik}\, Et}{2k\left[(1+\mu) \sin \phi_1 F_3 + k \cos \phi_1 F_1\right]} \left[F_3 F_{10}(\alpha) - F_5 F_{13}(\alpha) - F_6 F_{14}(\alpha)\right]$
M_θ	$\dfrac{\Delta V_{ik}\, Et}{2k\left[(1+\mu) \sin \phi_1 F_3 + k \cos \phi_1 F_1\right]} \left\{ F_3 \left[\dfrac{\cot \phi}{k} F_8(\alpha) - \mu F_{10}(\alpha)\right] - F_5 \left[\dfrac{\cot \phi}{k} F_{16}(\alpha) - \mu F_{13}(\alpha)\right] - F_6 \left[\dfrac{\cot \phi}{k} F_{15}(\alpha) - \mu F_{14}(\alpha)\right]\right\}$
Δr	$\dfrac{-\Delta V_{ik}\, k \sin \phi}{\left[(1+\mu) \sin \phi_1 F_3 + k \cos \phi_1 F_1\right]} \left[F_3 F_9(\alpha) - F_5 F_{14}(\alpha) + F_6 F_{13}(\alpha)\right]$
β	$\dfrac{2k^2\, \Delta V_{ik}}{R\left[(1+\mu) \sin \phi_1 F_3 + k \cos \phi_1 F_1\right]} \left[F_3 F_8(\alpha) - F_5 F_{16}(\alpha) - F_6 F_{15}(\alpha)\right]$

TABLE B7. 3. 3-6 OPEN (OR CLOSED) SPHERICAL SHELL EXPOSED TO UNIT DISTORTIONS AT LOWER EDGE (Concluded)

Displacement Δr_{ik}

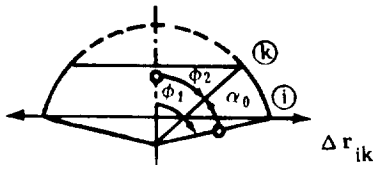

Boundary Conditions

$\alpha = 0 (\phi = \phi_1)$: $\Delta r = \Delta r_{ik}$, $\beta = 0$
$\alpha = 0 (\phi = \phi_2)$: $\Delta r = 0$, $\beta = 0$

Internal Forces and Deformations

N_ϕ	$\Delta r_{ik} \cot \phi \frac{Et}{Rk \sin \phi} \left[\frac{F_3}{F_1} F_7(\alpha) + \frac{F_5}{F_1} F_{15}(\alpha) - \frac{F_6}{F_1} F_{16}(\alpha)\right]$
N_θ	$\Delta r_{ik} \frac{Et}{R \sin \phi_1} \left[\frac{F_3}{F_1} F_9(\alpha) - \frac{F_5}{F_1} F_{14}(\alpha) + \frac{F_6}{F_1} F_{13}(\alpha)\right]$
Q_ϕ	$\Delta r_{ik} \frac{Et}{Rk \sin \phi_1} \left[\frac{F_3}{F_1} F_7(\alpha) \frac{F_5}{F_1} F_{15}(\alpha) - \frac{F_6}{F_1} F_{16}(\alpha)\right]$
M_ϕ	$\Delta r_{ik} \frac{Et}{2k^2 \sin \phi_1} \left[\frac{F_3}{F_1} F_{10}(\alpha) - \frac{F_5}{F_1} F_{13}(\alpha) - \frac{F_6}{F_1} F_{14}(\alpha)\right]$
M_θ	$\Delta r_{ik} \frac{Et}{2k^2 \sin \phi} \left\{ - \frac{F_3}{F_1} \left[\frac{\cot \phi}{k} F_8(\alpha) - \mu F_{10}(\alpha)\right] + \frac{F_5}{F_1} \left[\frac{\cot \phi}{k} F_{16}(\alpha) - \mu F_{13}(\alpha)\right] + \frac{F_6}{F_1} \left[\frac{\cot \phi}{k} F_{15}(\alpha) - \mu F_{14}(\alpha)\right] \right\}$
Δr	$\Delta r_{ik} \frac{\sin \phi}{\sin \phi_1} \left[\frac{F_3}{F_1} F_9(\alpha) - \frac{F_5}{F_1} F_{14}(\alpha) + \frac{F_6}{F_1} F_{13}(\alpha)\right]$
β	$\Delta r_{ik} \frac{2k}{R \sin \phi_1} \left[\frac{F_3}{F_1} F_8(\alpha) - \frac{F_5}{F_1} F_{16}(\alpha) - \frac{F_6}{F_1} F_{15}(\alpha)\right]$

TABLE B7.3.3-7 EDGE-LOADED SHALLOW SPHERICAL SHELLS

Complete (or "Long") Spherical Cap, Shallow, Constant t, Edge Moment M	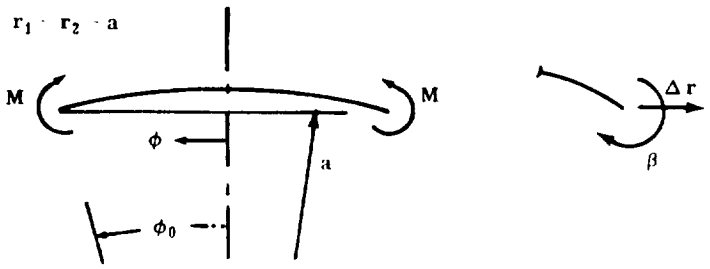
Basis	**Esslinger's Approximation**
Differential Equation and Boundary Conditions	$\frac{d^4Q_\phi}{d\phi^4} + \frac{2}{\phi}\frac{d^3Q_\phi}{d\phi^3} - \frac{3}{\phi^2}\frac{d^2Q_\phi}{d\phi^2} + \frac{3}{\phi^3}\frac{dQ_\phi}{d\phi} - \frac{3}{\phi^4}Q_\phi + 4k^4Q_\phi = 0$ where $k^4 = 3(1-\mu^2)\frac{a^2}{t^2}$ $Q_\phi\Big\|_{\phi=\phi_0} = 0 \qquad M_\phi\Big\|_{\phi=\phi_0} = M$
Solution	$Q_\phi = \left[\frac{C_{1M}}{k}\,\mathrm{Ber}'(k\sqrt{2}\phi) - \frac{C_{2M}}{k}\,\mathrm{Bei}'(k\sqrt{2}\phi)\right]\frac{M}{t}$
Forces	$N_\phi = (n_1 C_{1M} + n_2 C_{2M})\frac{M}{t}$ $N_\theta = (\eta_1 C_{1M} + \eta_2 C_{2M})\frac{M}{t}$ $M_\phi = (m_1 C_{1M} + m_2 C_{2M})M$ $M_\theta = \mu M_\phi + (k_1 C_{1M} + k_2 C_{2M})M$
Edge Influence Coefficients	$C_{VM} = -\frac{X_b}{Et^2\phi_0} \qquad C_{wM} = \frac{X_a}{Et\phi_0}$

Notes: Approximate useful range: $\phi_0 < 20°$.

For $\mathrm{Ber}'(k\sqrt{2}\phi)$, $\mathrm{Bei}'(k\sqrt{2}\phi)$ see Reference 3.

For C_{1M}, C_{2M}, X_a, and X_b as functions of $\sqrt{2}\phi_0$ see Table B7.3.3-8.

For n_1, n_2, ... etc. as function of $k\sqrt{2}\phi$ see Table B7.3.3-8

TABLE B7.3.3-7 EDGE-LOADED SHALLOW SPHERICAL SHELLS (Continued)

Complete (or "Long") Spherical Cap, Shallow, Constant t, Edge Force H	$r_1 \quad r_2 = a$ 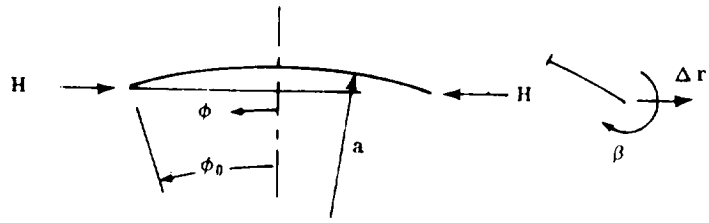
Basis	Esslinger's Approximation
Differential Equation and Boundary Conditions	$\frac{d^4Q_\phi}{d\phi^4} + \frac{2}{\phi}\frac{d^3Q_\phi}{d\phi^3} - \frac{3}{\phi^2}\frac{d^2Q_\phi}{d\phi^2} + \frac{3}{\phi^3}\frac{dQ_\phi}{d\phi} - \frac{3}{\phi^4}Q_\phi + k^4 Q_\phi = 0$ where $k^4 = 3(1-\mu^2)\frac{a^2}{t^2}$ $Q_\phi\Big\|_{\phi=\phi_0} = -H\cos\phi_0 \qquad M_\phi\Big\|_{\phi=\phi_0} = 0$
Solution	$Q_\phi = \left[\frac{C_{1H}}{k}\,\mathrm{Ber}'(k\sqrt{2}\phi) - \frac{C_{2H}}{k}\,\mathrm{Bei}'(k\sqrt{2}\phi)\right] H$
Forces	$N_\phi = (n_1 C_{1H} + n_2 C_{2H})\, H$ $N_\vartheta = (\eta_1 C_{1H} + \eta_2 C_{2H})\, H$ $M_\phi = (m_1 C_{1H} + m_2 C_{2H})\, Ht$ $M_\theta = \mu M_\phi + (k_1 C_{1H} + k_2 C_{2H})\, Ht$
Edge Influence Coefficients	$C_{VH} = \frac{X_a}{Et\phi_0} \qquad C_{wH} = -\frac{W_a}{E\phi_0}$

Notes: Approximate useful range: $\phi_0 < 20^\circ$.

For $\mathrm{Ber}'(k\sqrt{2}\phi)$, $\mathrm{Bei}'(k\sqrt{2}\phi)$ see Reference 3.

For C_{1H}, C_{2H}, W_a, and X_a as functions of $k\sqrt{2}\phi_0$ see Table B7.3.3-8.

For n_1, n_2, ... etc., as functions of $k\sqrt{2}\phi$ see Table B7.3.3-8.

TABLE B7.3.3-7 EDGE-LOADED SHALLOW SPHERICAL SHELLS (Continued)

Complete (or "Long") Spherical Shell, Shallow Opening, Constant t, Edge Moment M	$r_1 = r_2 = a$ 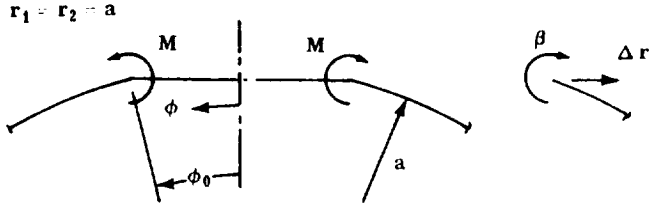
Basic	Esslinger's Approximation
Differential Equation and Boundary Conditions	$\frac{d^4Q_\phi}{d\phi^4} + \frac{2}{\phi}\frac{d^3Q_\phi}{d\phi^3} - \frac{3}{\phi^2}\frac{d^2Q_\phi}{d\phi^2} + \frac{3}{\phi^3}\frac{dQ_\phi}{d\phi} - \frac{3}{\phi^4}Q_\phi + 4k^4Q_\phi = 0$ where $k^4 = 3(1-\mu^2)\frac{a^2}{t^2}$ $Q_\phi\Big\|_{\phi=\phi_0} = 0 \qquad M_\phi\Big\|_{\phi=\phi_0} = M$
Solution	$Q_\phi = -\frac{2}{\pi}\left[\frac{C_{3M}}{k}\,\mathrm{Kei}'(k\sqrt{2}\phi) + \frac{C_{4M}}{k}\,\mathrm{Ker}'(k\sqrt{2}\phi)\right]\frac{M}{t}$
Forces	$N_\phi = (n_3 C_{3M} + n_4 C_{4M})\frac{M}{t}$ $N_\theta = (\eta_3 C_{3M} + \eta_4 C_{4M})\frac{M}{t}$ $M_\phi = (m_3 C_{3M} + m_4 C_{4M})M$ $M_\theta = \mu M_\phi + (k_3 C_{3M} + k_4 C_{4M})M$
Edge Influence Coefficients	$C_{VM} = \frac{X_d}{Et^2\phi_0}$ $C_{wM} = \frac{X_c}{Et\phi_0}$

Notes: Approximate useful range: $\phi_0 < 20°$.

For $\mathrm{Ker}'(k\sqrt{2}\phi)$, $\mathrm{Kei}'(k\sqrt{2}\phi)$ see Reference 3.

For C_{3M}, C_{4M}, X_c, and X_d as functions of $k\sqrt{2}\phi_0$ see Table B7.3.3-8.

For n_3, n_4, ... etc. as functions of $k\sqrt{2}\phi$ see Table B7.3.3-8.

TABLE B7.3.3-7 EDGE-LOADED SHALLOW SPHERICAL SHELLS (Concluded)

Complete (or "Long") Spherical Shell, Shallow Opening, Constant t, Edge Force H	$r_1 = r_2 = a$ 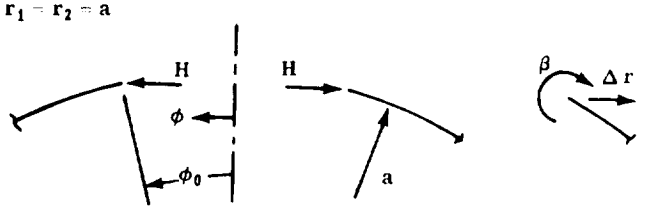
Basis	**Esslinger's Approximation**
Differential Equation and Boundary Conditions	$\frac{d^4Q_\phi}{d\phi^4} + \frac{2}{\phi}\frac{d^3Q_\phi}{d\phi^3} - \frac{3}{\phi^2}\frac{d^2Q_\phi}{d\phi^2} + \frac{3}{\phi^3}\frac{dQ_\phi}{d\phi} - \frac{3}{\phi^4}Q_\phi + 4k^4Q_\phi = 0$ where $k^4 = 3(1-\mu^2)\frac{a^2}{t^2}$ $Q_\phi\Big\|_{\phi=\phi_0} = -H\phi_0$ $\qquad$ $M_\phi\Big\|_{\phi=\phi_0} = 0$
Solution	$Q_\phi = -\frac{2}{\pi}\left[\frac{C_{3H}}{k}\,\mathrm{Ker}'(k\sqrt{2}\phi) + \frac{C_{4H}}{k}\,\mathrm{Kei}'(k\sqrt{2}\phi)\right]H$
Forces	$N_\phi = (n_3 C_{3H} + n_4 C_{4H})\,H$ $N_\theta = (\eta_3 C_{3H} + \eta_4 C_{4H})\,H$ $M_\phi = (m_3 C_{3H} + m_4 C_{4H})\,Ht$ $M_\theta = \mu M_\phi + (k_3 C_{3H} + k_4 C_{4H})\,Ht$
Edge Influence Coefficients	$C_{VH} = \frac{X_c}{Et\phi_0}$ $\qquad$ $C_{wH} = \frac{W_c}{E\phi_0}$

Notes: Approximate useful range: $\phi_0 < 20°$.

For $\mathrm{Ker}'(k\sqrt{2}\phi)$, $\mathrm{Kei}'(k\sqrt{2}\phi)$ see Reference 3

For C_{3H}, C_{4H}, W_c, and X_c as functions of $k\sqrt{2}\phi_0$ see Table B7.3.3-8.

For n_3, n_4, ... etc. as functions of $k\sqrt{2}\phi$ see Table B7.3.3-8.

TABLE B7.3.3-8 SHALLOW SPHERICAL SHELL COEFFICIENTS

Equations for the Eselinger Coefficients for Table B7.3.3-7

$$C_{1H} = \frac{K_{12}}{\sqrt{2}}\left[k\sqrt{2}\phi_0\,\psi_2 - (1-\mu)\psi_1'\right]$$

$$C_{2H} = -\frac{K_{12}}{2}\left[k\sqrt{2}\phi_0\,\psi_1 + (1-\mu)\psi_2'\right]$$

$$C_{1M} = -K_{12}\,\psi_2'\sqrt{6(1-\mu^2)} \qquad C_{2M} = K_{12}\,\psi_1'\sqrt{6(1-\mu^2)}$$

$$W_a = -\frac{K_{12}}{\sqrt{12(1-\mu^2)}}\left[(k\sqrt{2}\phi_0)^3(\psi_1^2+\psi_2^2) - 2(k\sqrt{2}\phi_0)^2(\psi_1'\psi_2 - \psi_2'\psi_1) + (1-\mu^2)k\sqrt{2}\phi_0(\psi_1'^2+\psi_2'^2)\right]$$

$$X_a = -K_{12}\left[(k\sqrt{2}\phi_0)^2(\psi_1\psi_1' + \psi_2\psi_2')\right]$$

$$X_b = -K_{12}\sqrt{12(1-\mu^2)}\left[(k\sqrt{2}\phi_0)(\psi_1'^2+\psi_2'^2)\right]$$

$$\bar{K}_{12} = \left[\psi_1\psi_2' - \psi_2\psi_1' + \frac{1-\mu}{k\sqrt{2}\phi_0}(\psi_1'^2+\psi_2'^2)\right]^{-1}$$

$$n_1 = \sqrt{2}\,\frac{\psi_1'}{k\sqrt{2}\phi} \qquad n_2 = \sqrt{2}\,\frac{\psi_2'}{k\sqrt{2}\phi}$$

$$\eta_1 = -\sqrt{2}\left[-\psi_2 + \frac{\psi_1'}{k\sqrt{2}\phi}\right] \qquad \eta_2 = -\sqrt{2}\left[\psi_1 + \frac{\psi_2'}{k\sqrt{2}\phi}\right]$$

$$m_1 = -\frac{1}{\sqrt{6(1-\mu^2)}}\left[\psi_1 + (1-\mu)\frac{\psi_2'}{k\sqrt{2}\phi}\right]$$

$$m_2 = -\frac{1}{\sqrt{6(1-\mu^2)}}\left[\psi_2 - (1-\mu)\frac{\psi_1'}{k\sqrt{2}\phi}\right]$$

$$k_1 = \sqrt{\frac{1-\mu^2}{12}}\,n_2 \qquad k_2 = -\sqrt{\frac{1-\mu^2}{12}}\,n_1$$

ψ_1, ψ_2, ψ_1', ψ_2' are Schleicher functions and their derivatives for the argument $k\sqrt{2}\phi$ and are related to Bessel-Kelvin functions by $\psi_1 = \text{ber}$, $\psi_2 = -\text{bei}$, $\psi_1' = \text{ber}'$, and $\psi_2' = -\text{bei}'$.

(Reference 1, pages 491-494, and 6-17, 6-20, and 6-32)

TABLE B7. 3. 3-8 SHALLOW SPHERICAL SHELL COEFFICIENTS (Concluded)

Equations for the Esslinger Coefficients for Table B7. 3. 3-7

$$C_{3H} = \frac{K_{34}}{\sqrt{2}}\left[k\sqrt{2}\phi_0\,\psi_4 - (1-\mu)\,\psi_3'\right]$$

$$C_{4H} = -\frac{K_{34}}{\sqrt{2}}\left[k\sqrt{2}\phi_0\,\psi_3 + (1-\mu)\,\psi_4'\right]$$

$$C_{3M} = -K_{34}\,\psi_4'\sqrt{6(1-\mu^2)} \qquad C_{4M} = K_{34}\,\psi_3'\sqrt{6(1-\mu^2)}$$

$$W_c = \frac{K_{34}}{\sqrt{12(1-\mu^2)}}\left[(k\sqrt{2}\phi_0)^3(\psi_3^2+\psi_4^2) - 2(k\sqrt{2}\phi_0)^2(\psi_3'\psi_4 - \psi_4'\psi_3) + (1-\mu^2)\,k\sqrt{2}\phi_0\,(\psi_3'^2+\psi_4'^2)\right]$$

$$X_c = -K_{34}\left[(k\sqrt{2}\phi_0)^2(\psi_3\psi_3' + \psi_4\psi_4')\right]$$

$$X_d = K_{34}\sqrt{12(1-\mu^2)}\left[(k\sqrt{2}\phi_0)(\psi_3'^2+\psi_4'^2)\right]$$

$$K_{34} = \left[\psi_3\psi_4' - \psi_4\psi_3' + \frac{1-\mu}{k\sqrt{2}\phi_0}(\psi_3'^2+\psi_4'^2)\right]^{-1}$$

$$n_3 = \sqrt{2}\,\frac{\psi_3'}{k\sqrt{2}\phi} \qquad n_4 = \sqrt{2}\,\frac{\psi_4'}{k\sqrt{2}\phi}$$

$$\eta_3 = -\sqrt{2}\left[-\psi_4 + \frac{\psi_3'}{k\sqrt{2}\phi}\right] \qquad \eta_4 = -\sqrt{2}\left[\psi_3 + \frac{\psi_4'}{k\sqrt{2}\phi}\right]$$

$$m_3 = -\frac{1}{\sqrt{6(1-\mu^2)}}\left[\psi_3 + (1-\mu)\,\frac{\psi_4'}{k\sqrt{2}\phi}\right]$$

$$m_4 = -\frac{1}{\sqrt{6(1-\mu^2)}}\left[\psi_4 - (1-\mu)\,\frac{\psi_3'}{k\sqrt{2}\phi}\right]$$

$$k_3 = \sqrt{\frac{1-\mu^2}{12}}\,n_4 \qquad k_4 = -\sqrt{\frac{1-\mu^2}{12}}\,n_3$$

ψ_3, ψ_4, ψ_3', ψ_4', are Schleicher functions and their derivatives for the argument $k\sqrt{2}\phi$ and are related to Bessel-Kelvin functions by $\psi_3 = -\frac{2}{\pi}\,\mathrm{kei}$, $\psi_4 = -\frac{2}{\pi}\,\mathrm{ker}$, $\psi_3' = -\frac{2}{\pi}\,\mathrm{kei}'$, and $\psi_4' = -\frac{2}{\pi}\,\mathrm{ker}'$.

(Reference 1, pages 491-494, and 6-17, 6-20, and 6-32)

B7.3.3.4 Cylindrical Shells

This paragraph presents the solutions for long and short cylinders, loaded along the boundary with the unit-edge loadings (moments, shear, forced horizontal displacement, and forced rotation at the boundary). All disturbances in the cylindrical wall caused by edge loading will become, for practical purposes, negligible at distance $x = \sqrt{Rt}$. If the height of the cylinder is less than x, the analyst is dealing with a circular ring instead of a shell. Further, to be conservative, the following precautions should be taken.

a. If $kL \leq 5$, the more exact theory is used, and such cylinders are designated as short cylinders.

b. If $kL \geq 5$, the simplified formula is used; this is a special case of the more general case a.

The constant k is defined as follows:

$$k^4 = 3(1 - \mu^2)/R^2 t^2 \quad .$$

The primary solutions (membrane theory) will not be affected by the length of the cylinder. The boundaries must be free to rotate and deflect because of the action of the unit-edge loadings. The shell thickness must be uniform in the range where the stresses are present.

I Long Cylinders

The formulas for the disturbances caused by unit-edge loadings are presented in Table B7.3.3-9. In this table,

$$D = \frac{Et^3}{12(1 - \mu^2)} \quad .$$

TABLE B7.3.3-9 LONG CYLINDRICAL SHELLS, UNIT-EDGE LOADING SOLUTIONS

	Q = 1	M = 1
	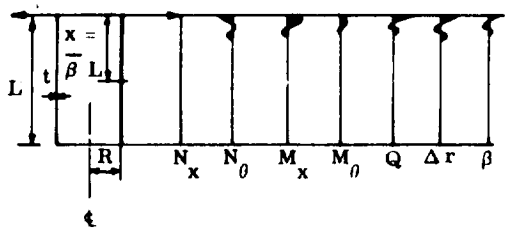	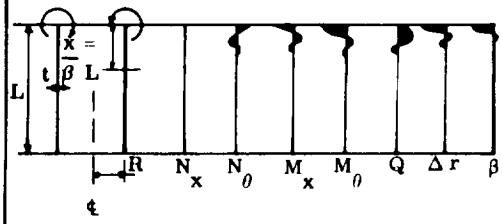
N_x	0	0
N_θ	$-\frac{2Rk}{L} e^{-k\bar{\beta}} \cos k\bar{\beta}$	$\frac{2\sqrt{2} \cdot Rk^2}{L^2} e^{-k\bar{\beta}} \cos\left(k\bar{\beta} + \frac{\pi}{4}\right)$
M_x	$\frac{L}{k} e^{-k\bar{\beta}} \sin k\bar{\beta}$	$-\sqrt{2} \cdot e^{-k\bar{\beta}} \sin\left(k\bar{\beta} + \frac{\pi}{4}\right)$
M_θ	μM_x	μM_x
Q	$\sqrt{2} \cdot e^{-k\bar{\beta}} \cos\left(k\bar{\beta} + \frac{\pi}{4}\right)$	$\frac{2k}{L} e^{-k\bar{\beta}} \sin k\bar{\beta}$
β	$\frac{L^2}{\sqrt{2} \cdot k^2 D} e^{-k\bar{\beta}} \sin\left(k\bar{\beta} + \frac{\pi}{4}\right)$	$-\frac{L}{Dk} e^{-k\bar{\beta}} \cos k\bar{\beta}$
Δr	$-\frac{R}{Et}\left(N_\theta - \mu N_x\right) = \frac{L^3}{2Dk^3} e^{-k\bar{\beta}} \cos k\bar{\beta}$	$-\frac{R}{Et}\left(N_\theta - \mu N_x\right) = -\frac{L^3}{\sqrt{2}Dk^2} e^{-k\bar{\beta}} \cos\left(k\bar{\beta} + \frac{\pi}{4}\right)$

For the Case $\bar{\beta} = 0$

β	$\frac{L^2}{2k^2D}$	$\frac{-L}{Dk}$
Δr	$\frac{L^3}{2k^3D}$	$\frac{-L^2}{2Dk^2}$

II Short Cylinders

The following constants are used for Tables B7. 3. 3-10 and B7. 3. 3-11:

$k^4 = 3(1-\mu^2)/R^2 t^2$

$\rho = \sinh^2 \beta L - \sin^2 \beta L$

$K_1 = (\sinh \beta L \cosh \beta L - \sin \beta L \cos \beta L)/\rho$

$K_2 = (\sin \beta L \cosh \beta L - \cos \beta L \sinh \beta L)/\rho$

$K_3 = (\sinh^2 \beta L + \sin^2 \beta L)/\rho$

$K_4 = 2 \sinh \beta L \sin \beta L/\rho$

$K_5 = 2(\sin \beta L \cos \beta L + \sinh \beta L \cosh \beta L)/\rho$

$K_6 \quad 2(\sin \beta L \cosh \beta L + \cos \beta L \sinh \beta L)/\rho$

The formulas for unit-edge loading disturbances are presented in Tables B7. 3. 3-10 and B7. 3. 3-11. To use these formulas the relation $\beta L \leq 5$ must be satisfied.

A summary of edge distortions resulting from edge loadings is given in Table B7. 3. 3-12.

B7. 3. 3. 5 Conical Shells

This paragraph presents the solutions for nonshallow open or closed conical shells in which α_0 is not small. There is no exact information about limiting angle α_0. It is recommended that consideration be limited to the range of $\alpha_0 \geq 45°$. If $\alpha_0 = 90°$, the cone degenerates into a cylinder.

TABLE B7.3.3-10 CYLINDRICAL SHELLS, EXACT FORMULAS FOR UNIT-EDGE LOADING SOLUTIONS

	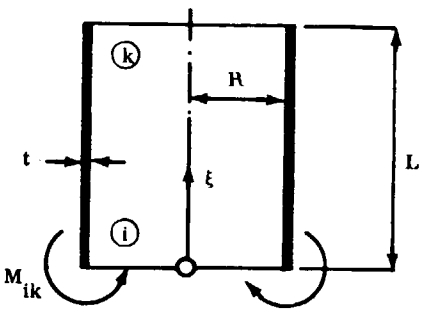	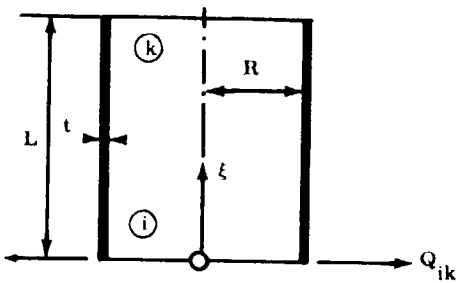
N_θ	$M_{ik}\, 2k^2R \left[-\frac{F_2}{F_1} F_7(\xi) + \frac{F_3}{F_1} F_{10}(\xi) - F_8(\xi) \right]$	$Q_{ik}\, 2kR \left[\frac{F_4}{F_1} F_7(\xi) - \frac{F_5}{F_1} F_{15}(\xi) - \frac{F_6}{F_1} F_{16}(\xi) \right]$
M_x	$M_{ik} \left[\frac{F_2}{F_1} F_8(\xi) - \frac{F_3}{F_1} F_9(\xi) - F_7(\xi) \right]$	$\frac{Q_{ik}}{k} \left[-\frac{F_4}{F_1} F_8(\xi) - \frac{F_5}{F_1} F_{16}(\xi) + \frac{F_6}{F_1} F_{15}(\xi) \right]$
Q_x	$-kM_{ik} \left[\frac{F_2}{F_1} F_{10}(\xi) - \frac{2F_3}{F_1} F_8(\xi) + F_8(\xi) \right]$	$Q_{ik} \left[\frac{F_4}{F_1} F_{10}(\xi) + \frac{F_5}{F_1} F_{13}(\xi) - \frac{F_6}{F_1} F_{14}(\xi) \right]$
Δr	$\frac{M_{ik}}{2Dk^2} \left[-\frac{F_2}{F_1} F_7(\xi) + \frac{F_3}{F_1} F_{10}(\xi) - F_8(\xi) \right]$	$\frac{Q_{ik}}{2Dk^3} \left[\frac{F_4}{F_1} F_7(\xi) - \frac{F_5}{F_1} F_{15}(\xi) - \frac{F_6}{F_1} F_{16}(\xi) \right]$
β	$\frac{M_{ik}}{2Dk} \left[\frac{F_2}{F_1} F_9(\xi) + \frac{2F_3}{F_1} F_7(\xi) - F_{10}(\xi) \right]$	$-\frac{Q_{ik}}{2Dk^2} \left[\frac{F_4}{F_1} F_9(\xi) + \frac{F_5}{F_1} F_{14}(\xi) + \frac{F_6}{F_1} F_{13}(\xi) \right]$

TABLE B7.3.3-11 CYLINDRICAL SHELLS, EXACT FORMULAS FOR UNIT-EDGE DEFORMATIONS

	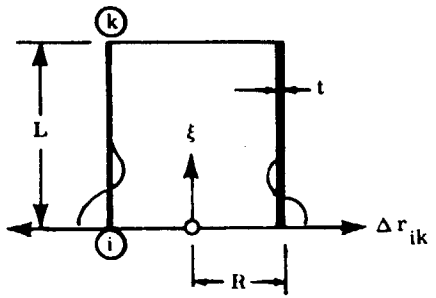	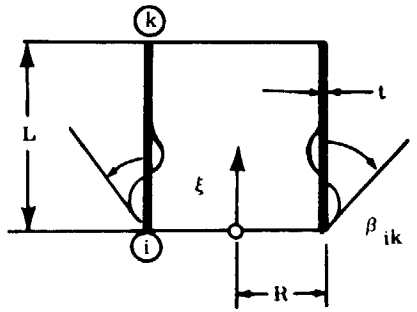
N_θ	$\Delta r_{ik} \frac{Et}{R}\left[F_7(\xi) + \frac{F_3}{F_1}F_9(\xi) - \frac{F_2}{F_1}F_8(\xi)\right]$	$\frac{\beta_{ik}}{k}\frac{Et}{R}\left[\frac{F_6}{F_1}F_{15}(\xi) - \frac{F_5}{F_1}F_{16}(\xi) - \frac{F_4}{F_1}F_8(\xi)\right]$
M_x	$\Delta r_{ik}\, 2Dk^2\left[-F_8(\xi) + \frac{F_3}{F_1}F_{10}(\xi) - \frac{F_2}{F_1}F_7(\xi)\right]$	$\beta_{ik}\, 2Dk\left[\frac{F_6}{F_1}F_{16}(\xi) + \frac{F_5}{F_1}F_{15}(\xi) - \frac{F_4}{F_1}F_7(\xi)\right]$
Q_x	$\Delta r_{ik}\, 2Dk^3\left[-F_{10}(\xi) + 2\frac{F_3}{F_1}F_7(\xi) + \frac{F_2}{F_1}F_9(\xi)\right]$	$-\beta_{ik}\, 2Dk^2\left[\frac{F_6}{F_1}F_{13}(\xi) + \frac{F_5}{F_1}F_{14}(\xi) + \frac{F_4}{F_1}F_9(\xi)\right]$
Δr	$\Delta r_{ik} k\left[F_7(\xi) + \frac{F_3}{F_1}F_9(\xi) - \frac{F_2}{F_1}F_8(\xi)\right]$	$\frac{\beta_{ik}}{k}\left[\frac{F_6}{F_1}F_{15}(\xi) - \frac{F_5}{F_1}F_{16}(\xi) - \frac{F_4}{F_1}F_8(\xi)\right]$
β	$\Delta r_{ik} k\left[-F_9(\xi) + 2\frac{F_3}{F_1}F_8(\xi) - \frac{F_2}{F_1}F_{10}(\xi)\right]$	$\beta_{ik}\left[\frac{F_6}{F_1}F_{14}(\xi) - \frac{F_5}{F_1}F_{13}(\xi) - \frac{F_4}{F_1}F_{10}(\xi)\right]$

TABLE B7. 3. 3-12 CYLINDRICAL SHELLS EDGE DISTORTIONS RESULTING FROM EDGE LOADINGS

Loading Condition \ Edge Distortions	ΔH_{ik}	β_{ik}	ΔH_{ki}	β_{ki}
Q_{ik}	$-Q_{ik} \frac{2R^2k}{Et} \frac{F_4}{F_1}$	$Q_{ik} \frac{2R^2k^2}{Et} \frac{F_2}{F_1}$	$Q_{ki} \frac{2R^2k}{Et} \frac{F_9}{F_1}$	$Q_{ik} \frac{2R^2k^2}{Et} \frac{2F_8}{F_1}$
M_{ik}	$M_{ik} \frac{2R^2k^2}{Et} \frac{F_2}{F_1}$	$-M_{ik} \frac{2R^2k^3}{Et} \frac{2F_3}{F_1}$	$-M_{ik} \frac{2R^2k^2}{Et} \frac{2F_8}{F_1}$	$-M_{ik} \frac{2R^2k^3}{Et} \frac{2F_{10}}{F_1}$
Q_{ki}	$-Q_{ki} \frac{2R^2k}{Et} \frac{F_9}{F_1}$	$Q_{ki} \frac{2R^2k^2}{Et} \frac{2F_3}{F_1}$	$Q_{ki} \frac{2R^2k}{Et} \frac{F_4}{F_1}$	$Q_{ki} \frac{2R^2k^2}{Et} \frac{F_2}{F_1}$
M_{ki}	$-M_{ki} \frac{2R^2k^2}{Et} \frac{2F_8}{F_1}$	$M_{ki} \frac{2R^2k^3}{Et} \frac{2F_{10}}{F_1}$	$M_{ki} \frac{2R^2k^2}{Et} \frac{F_2}{F_1}$	$M_{ki} \frac{2R^2k^3}{Et} \frac{2F_3}{F_1}$

Another limitation must be applied to the height of the cone. As in the case of the sphere, the disturbances due to unit-edge loadings will decay at a short distance from the disturbed edge (for practical purposes, approximately at $\sqrt{R_0 t}$). Consequently, a "high" cone is characterized by an undisturbed edge (or apex) as a result of unit-loading influences on the respective opposite edge.

The boundaries must be free to rotate and deflect vertically and horizontally as a result of the action of the unit-edge loadings. Abrupt discontinuities in the shell thickness must not be present. The thickness of the shell must be uniform in the range in which the stresses exist.

The formulas are assembled for closed and open conical shells. Open conical shells are characterized by removal of the upper part above some circumference in the plane parallel to the base.

Linear bending theory was used to derive the following formulas. If the height of the segment is less than $\sqrt{Rt}$, the analyst is practically dealing with a circular ring instead of a shell. The following constants are important:

$$k = \frac{h}{\sqrt{R_0 t \sin \phi}} \qquad \sqrt[4]{3(1-\mu^2)} \quad , \quad R_0 = \text{MAX } R$$

$$D = \frac{Et^3}{12(1-\mu^2)} \quad .$$

Additional designations are indicated in Figure B7.3.3-4.

R is variable and is perpendicular to the meridian. Angle (ϕ) is constant. Table B7.3.3-13 presents the formulas for a closed conical shell.

I Open Conical Shell, Unit Loading at Lower Edge

Since unit influences are not progressing very far from the edge into the cone, the formulas presented in Table B7.3.3-13 can be used for the cone with opening at vertex (Figure B7.3.3-5).

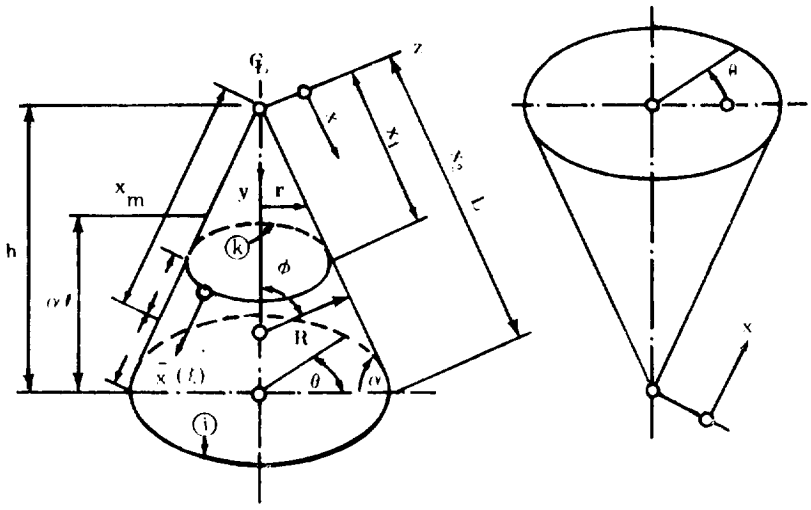

FIGURE B7.3.3-4 CONE NOMENCLATURE

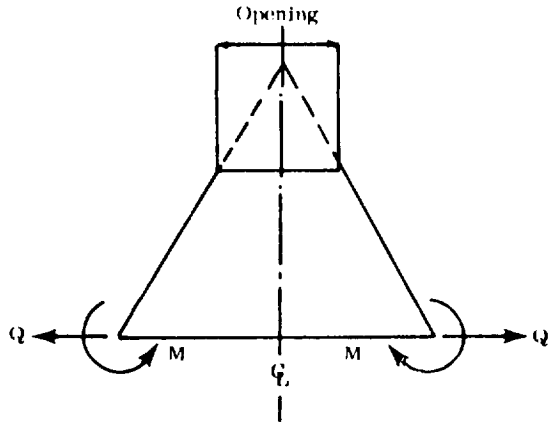

FIGURE B7.3.3-5 OPEN CONICAL SHELL LOADING AT LOWER EDGE

TABLE B7. 3. 3-13 CONICAL SHELL, UNIT-EDGE LOADING SOLUTIONS

Horizontal Unit Load

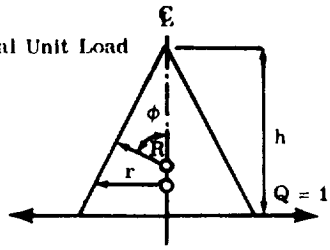

Unit Moment Loading

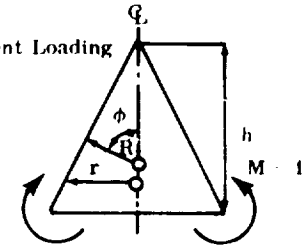

N_ϕ	$-\sqrt{2}\cos\phi \cdot e^{-k\alpha}\cos\left(k\alpha+\frac{\pi}{4}\right)$	$-\frac{2k\cos\phi}{h}e^{-k\alpha}\sin k\alpha$
N_θ	$-\frac{2R^2k\sin^2\phi}{h}e^{-k\alpha}\cos k\alpha$	$\frac{2\sqrt{2}Rk^2\sin^2\phi}{h^2}e^{-k\alpha}\cos\left(k\alpha+\frac{\pi}{4}\right)$
M_ϕ	$\frac{h}{k}e^{-k\alpha}\sin k\alpha$	$-\sqrt{2}e^{-k\alpha}\sin\left(k\alpha+\frac{\pi}{4}\right)$
M_θ	$\frac{h^2}{\sqrt{2}Rk^2}\frac{\cot\phi}{\sin\phi}e^{-k\alpha}\sin\left(k\alpha+\frac{\pi}{4}\right)+\mu M_\phi$	$-\frac{h\cot\phi\,e^{-k\alpha}\cos k\alpha}{Rk\sin\alpha}+\mu M_\phi$
Q	$-\sqrt{2}\sin\phi \cdot e^{-k\alpha}\cos\left(k\alpha+\frac{\pi}{4}\right)$	$-\frac{2k\sin\phi}{h}e^{-k\alpha}\sin k\alpha$
Deformations		
Δr	$\frac{h^2e^{-k\alpha}}{2Dk^2\sin\phi}\left[\cos k\alpha-\frac{h}{\sqrt{2}Rk}\frac{\cos\phi}{\sin\phi}\cos\left(k\alpha+\frac{\pi}{4}\right)\right]$	$\frac{-h^2e^{-k\alpha}}{2Dk^2\sin\phi}\left[\sqrt{2}\cos\left(k\alpha-\frac{\pi}{4}\right)+\mu\frac{h}{R}\frac{\cos\phi\sin k\alpha}{k\sin^2\phi}\right]$
β	$-\frac{h^2e^{-k\alpha}\sin\left(k\alpha+\frac{\pi}{4}\right)}{\sqrt{2}Dk^2\sin\phi}$	$\frac{he^{-k\alpha}\cos k\alpha}{Dk\sin\phi}$
For $\alpha = 0$		
Δr	$\frac{h^3}{2Dk^3\sin\phi}\left[1-\frac{\mu n\cot\phi}{2Rk\sin\phi}\right]$	$-\frac{h^2}{2Dk^2\sin\phi}$
β	$-\frac{n^2}{2Dk^2\sin\phi}$	$\frac{h}{Dk\sin\phi}$

II Open Conical Shell, Unit Loading at Upper Edge

If it is imagined that the shell, loaded as shown in Figure B7.3.3-6(A), is replaced with shell as shown in Figure B7.3.3-6(B), the result is a conical shell loaded with unit loading at the lower edge. The same formulas are used for determining edge influence, but it is noted that $\phi > 90°$.

An additional set of formulas for open conical shells (that can be also used for closed cone) is presented in Table B7.3.3-14. These formulas are expressed with the functions F_i and $F_i(\xi)$, which are tabulated in Paragraph B7.3.3.2. The following constant is used for k:

$$k = \frac{\sqrt[4]{3(1-\mu^2)}}{\sqrt{t x_m \cot \alpha_0}}$$

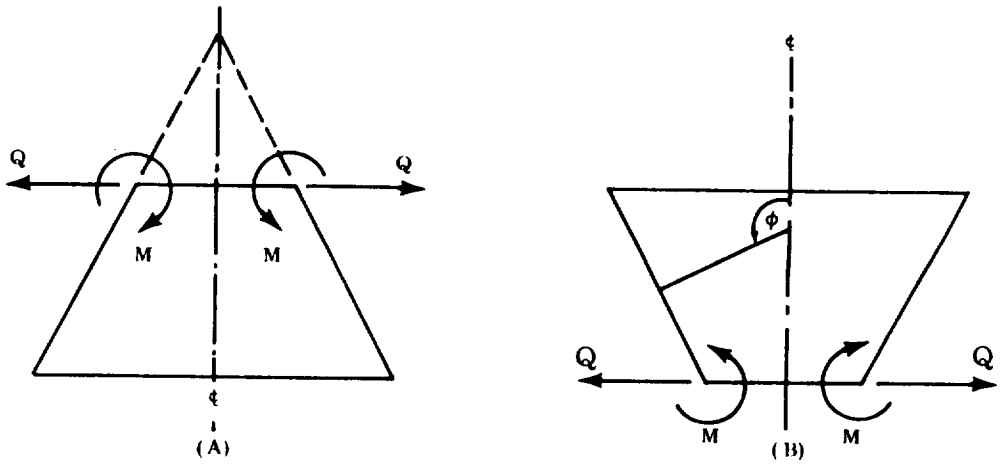

FIGURE B7.3.3-6 OPEN CONICAL SHELL LOADING AT UPPER EDGE

TABLE B7. 3. 3-14 OPEN CONICAL SHELL, UNIT-EDGE LOADING SOLUTIONS

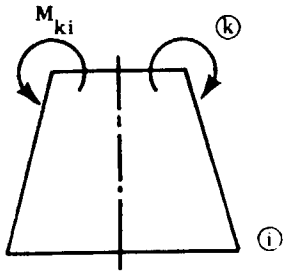

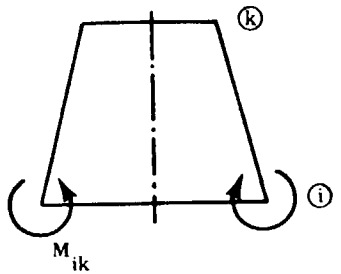

N_x	$M_{ki}\ 2k \cot \alpha_0 \left[\frac{F_6}{F_1} F_{15}(\xi) + \frac{F_5}{F_1} F_{16}(\xi) - \frac{F_3}{F_1} F_8(\xi)\right]$	$M_{ik}\ 2k \cot \alpha_0 \left[\frac{F_8}{F_2} F_{10}(\xi) - \frac{F_{10}}{F_1} F_8(\xi)\right]$
N_θ	$M_{ki}\ 2k^2 x_m \cot \alpha_0 \left[\frac{F_6}{F_1} F_{14}(\xi) + \frac{F_5}{F_1} F_{13}(\xi) - \frac{F_3}{F_1} F_{10}(\xi)\right]$	$M_{ik}\ 2k^2 x_m \cot \alpha_0 \left[\frac{2F_8}{F_1} F_7(\xi) - \frac{F_{10}}{F_1} F_{10}(\xi)\right]$
M_x	$M_{ki}\left[\frac{F_6}{F_1} F_{13}(\xi) - \frac{F_5}{F_1} F_{11}(\xi) + \frac{F_3}{F_1} F_9(\xi)\right]$	$-M_{ik}\left[\frac{2F_8}{F_1} F_8(\xi) - \frac{F_{10}}{F_1} F_9(\xi)\right]$
Q_x	$M_{ki}\ 2k\left[\frac{F_6}{F_1} F_{15}(\xi) - \frac{F_5}{F_1} F_{16}(\xi) - \frac{F_3}{F_1} F_8(\xi)\right]$	$M_{ik}\ 2k\left[\frac{F_8}{F_1} F_{10}(\xi) - \frac{F_{10}}{F_1} F_8(\xi)\right]$
Δr	$M_{ki} \frac{\sin \alpha_0}{2Dk^2}\left[\frac{F_6}{F_1} F_{14}(\xi) + \frac{F_5}{F_1} F_{13}(\xi) - \frac{F_3}{F_1} F_{10}(\xi)\right]$	$M_{ik} \frac{\sin \alpha_0}{2Dk^2}\left[\frac{2F_8}{F_1} F_7(\xi) - \frac{F_{10}}{F_1} F_{10}(\xi)\right]$
β	$-\frac{M_{ik}}{Dk}\left[\frac{F_6}{F_1} F_{16}(\xi) - \frac{F_5}{F_1} F_{15}(\xi) - \frac{F_3}{F_1} F_7(\xi)\right]$	$M_{ik} \frac{1}{Dk}\left[\frac{F_8}{F_1} F_9(\xi) + \frac{F_{10}}{F_1} F_7(\xi)\right]$

TABLE B7. 3. 3-14 OPEN CONICAL SHELL, UNIT-EDGE LOADING SOLUTIONS (Concluded)

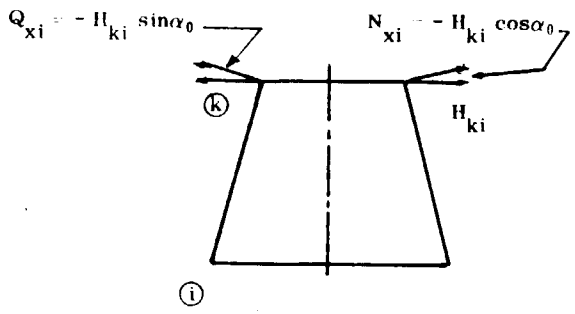

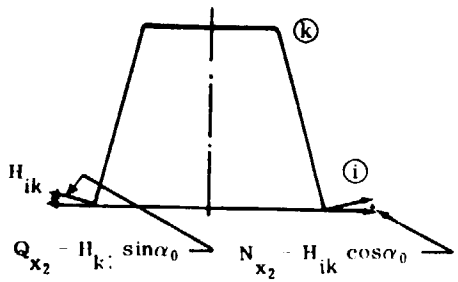

N_x	$-H_{ki} \cos\alpha_0 \left[F_7(\xi) - \frac{F_4}{F_1} F_{10}(\xi) + \frac{F_2}{F_1} F_8(\xi)\right]$	$H_{ki} \cos\alpha_0 \left[-\frac{F_9}{F_1} F_{10}(\xi) + \frac{2F_8}{F_1} F_8(\xi)\right]$
N_θ	$H_{ki} x_m k \cos\alpha_0 \left[F_9(\xi) + \frac{2F_4}{F_1} F_7(\xi) - \frac{F_2}{F_1} F_{10}(\xi)\right]$	$2H_{ik} x_m \cos\alpha_0 \left[-\frac{F_9}{F_1} F_7(\xi) + \frac{F_8}{F_1} F_{10}(\xi)\right]$
M_x	$H_{ki} \frac{\sin\alpha_0}{2} \left[F_{10}(\xi) - \frac{2F_4}{F_1} F_8(\xi) + \frac{F_2}{F_1} F_9(\xi)\right]$	$H_{ik} \frac{\sin\alpha_0}{k} \left[\frac{F_9}{F_1} F_8(\xi) - \frac{F_8}{F_1} F_9(\xi)\right]$
Q_x	$-H_{ki} \sin\alpha_0 \left[F_7(\xi) - \frac{F_4}{F_1} F_{10}(\xi) + \frac{F_2}{F_1} F_8(\xi)\right]$	$H_{ik} \sin\alpha_0 \left[-\frac{F_9}{F_1} F_{10}(\xi) + \frac{2F_8}{F_1} F_8(\xi)\right]$
Δr	$H_{ki} \frac{\sin^2\alpha_0}{4Dk^3} \left[F_9(\xi) + \frac{2F_4}{F_1} F_7(\xi) - \frac{F_2}{F_1} F_{10}(\xi)\right]$	$H_{ik} \frac{\sin^2\alpha_0}{2Dk^3} \left[-\frac{F_9}{F_1} F_7(\xi) + \frac{F_8}{F_1} F_{10}(\xi)\right]$
β	$H_{ki} \frac{\sin\alpha_0}{2Dk^2} \left[-F_8(\xi) + \frac{F_4}{F_1} F_9(\xi) + \frac{F_2}{F_1} F_7(\xi)\right]$	$-H_{ik} \frac{\sin\alpha_0}{2Dk^2} \left[+\frac{F_9}{F_1} F_9(\xi) + \frac{2F_8}{F_1} F_7(\xi)\right]$

In connection with some problems, it may be of interest to know the stresses and displacements in the conical shell (closed or open), if unit displacements at the edges are acting instead of M and Q:

At lower boundary i

- Δr_{ik} = unit displacement in horizontal direction
- β_{ik} = unit rotation.

At upper boundary k

- Δr_{ik} = unit displacement in horizontal direction
- β_{ik} = unit rotation.

Table B7. 3. 3-15(a) supplies the answer to this problem. Table B7. 3. 3-15(b) presents a summary of edge distortions resulting from secondary loading of a conical segment with free edges.

B7. 3. 3. 6 Circular Plates

A collection of solutions for circular plates with different axisymmetrical loading conditions is presented in this section. Circular plates with and without a central circular hole are considered. These solutions can be used individually or in the process of interaction with more complicated structures. The following nomenclature will be used:

- w = deflection
- β = rotation
- E = Young's modulus
- μ = Poisson's ratio
- t = thickness of plate
- $D = \frac{Et^3}{12(1-\mu^2)}$

TABLE B7. 3. 3-15(a) OPEN CONICAL SHELL, UNIT-EDGE LOADING SOLUTIONS

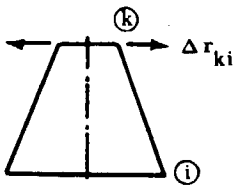

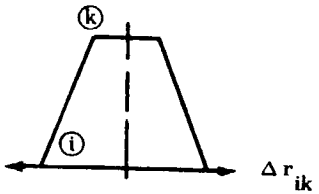

N_x	$\frac{4Dk^3 \cot \alpha_0 \, \Delta r_{ki}}{\sin \alpha_0} \left[- \frac{F_3}{F_1} F_7(\xi) - \frac{F_5}{F_1} F_{15}(\xi) + \frac{F_6}{F_1} F_{16}(\xi) \right]$	$\frac{4Dk^3 \cot \alpha_0 \, \Delta r_{ik}}{\sin \alpha_0} \left[\frac{F_{10}}{F_1} F_7(\xi) + \frac{F_8}{F_1} F_9(\xi) \right]$
N_θ	$\frac{Et \, \Delta r_{ki}}{x_m \cos \alpha_0} \left[\frac{F_3}{F_1} F_9(\xi) - \frac{F_5}{F_1} F_{14}(\xi) + \frac{F_6}{F_1} F_{13}(\xi) \right]$	$\frac{Et \, \Delta r_{ik}}{x_m \cos \alpha_0} \left[- \frac{F_{10}}{F_1} F_9(\xi) + \frac{2F_8}{F_1} F_8(\xi) \right]$
M_x	$\frac{2Dk^2 \, \Delta r_{ki}}{\sin \alpha_0} \left[\frac{F_3}{F_1} F_{10}(\xi) - \frac{F_5}{F_1} F_{13}(\xi) - \frac{F_6}{F_1} F_{14}(\xi) \right]$ $M_\phi = \mu M_x$	$\frac{2Dk^2 \, \Delta r_{ik}}{\sin \alpha_0} \left[- \frac{F_{10}}{F_1} F_{10}(\xi) + \frac{2F_8}{F_1} F_7(\xi) \right]$
Q_x	$\frac{4Dk^3 \, \Delta r_{ki}}{\sin \alpha_0} \left[- \frac{F_3}{F_1} F_7(\xi) - \frac{F_5}{F_1} F_{15}(\xi) + \frac{F_6}{F_1} F_{16}(\xi) \right]$	$\frac{4Dk^3 \, \Delta r_{ik}}{\sin \alpha_0} \left[\frac{F_{10}}{F_1} F_9(\xi) + \frac{F_8}{F_1} F_9(\xi) \right]$
Δr	$\Delta r = \Delta r_{ki} \left[\frac{F_3}{F_1} F_9(\xi) - \frac{F_5}{F_1} F_{14}(\xi) + \frac{F_6}{F_1} F_{13}(\xi) \right]$	$\Delta r_{ik} \left[- \frac{F_{10}}{F_1} F_9(\xi) + \frac{2F_8}{F_1} F_8(\xi) \right]$
β	$- \frac{2k}{\sin \alpha_0} \Delta r_{ki} \left[\frac{F_3}{F_1} F_8(\xi) - \frac{F_5}{F_1} F_{16}(\xi) - \frac{F_6}{F_1} F_{15}(\xi) \right]$	$\frac{2k \, \Delta r_{ik}}{\sin \alpha_0} \left[\frac{F_{10}}{F_1} F_8(\xi) - \frac{F_8}{F_1} F_{16}(\xi) - \frac{F_8}{F_1} F_{15}(\xi) \right]$

TABLE B7. 3. 3-15(a) OPEN CONICAL SHELL, UNIT-EDGE LOADING SOLUTIONS (Concluded)

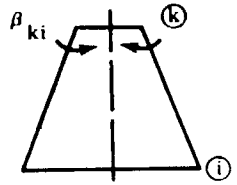

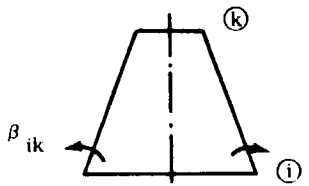

N_x	$2Dk^2 \cot \alpha_0 \beta_{ki} \left[\frac{F_2}{F_1} F_7(\xi) + \frac{F_4}{F_1} F_9(\xi) - F_8(\xi)\right]$	$2Dk^2 \cot \alpha_0 \beta_{ik} \left[\frac{2F_8}{F_1} F_7(\xi) + \frac{F_9}{F_1} F_9(\xi)\right]$
N_θ	$2Dk^3 x_m \cot \alpha_0 \beta_{ki} \left[-\frac{F_2}{F_1} F_9(\xi) + \frac{2F_4}{F_1} F_8(\xi) - F_{10}(\xi)\right]$	$4Dk^3 x_m \cot \alpha_0 \beta_{ik} \left[-\frac{F_8}{F_1} F_9(\xi) + \frac{F_9}{F_1} F_8(\xi)\right]$
M_x	$Dk \beta_{ki} \left[-\frac{F_2}{F_1} F_{10}(\xi) + \frac{2F_4}{F_1} F_7(\xi) + F_9(\xi)\right]$	$2Dk \beta_{ik} \left[-\frac{F_8}{F_1} F_{10}(\xi) + \frac{F_9}{F_1} F_7(\xi)\right]$
Q_x	$2Dk^2 \beta_{ki} \left[\frac{F_2}{F_1} F_7(\xi) + \frac{F_4}{F_1} F_9(\xi) - F_8(\xi)\right]$	$2Dk^2 \beta_{ik} \left[\frac{2F_8}{F_1} F_7(\xi) + \frac{F_9}{F_1} F_9(\xi)\right]$
Δr	$\frac{\sin \alpha_0}{2k} \beta_{ki} \left[-\frac{F_2}{F_1} F_9(\xi) + \frac{2F_4}{F_1} F_8(\xi) - F_{10}(\xi)\right]$	$\frac{\sin \alpha_0}{k} \beta_{ik} \left[-\frac{F_8}{F_1} F_9(\xi) + \frac{F_9}{F_1} F_9(\xi)\right]$
β	$\beta_{ki} \left[\frac{F_2}{F_1} F_8(\xi) - \frac{F_4}{F_1} F_{10}(\xi) + F_7(\xi)\right]$	$\beta_{ik} \left[\frac{2F_8}{F_1} F_8(\xi) - \frac{F_9}{F_1} F_{10}(\xi)\right]$

TABLE B7. 3. 3-15(b) CONICAL SEGMENT WITH FREE EDGES. EDGE DISTORTIONS RESULTING FROM SECONDARY LOADINGS

Loading Condition \ Edge Distortion	Δr_{ik}	β_{ik}	Δr_{ki}	β_{ki}
H_{ik}	$-H_{ik}\frac{\sin^2\alpha_0}{2Dk^3}\frac{F_4}{F_1}$	$+H_{ik}\frac{\sin\alpha_0}{2Dk^2}\frac{F_2}{F_1}$	$+H_{ik}\frac{\sin^2\alpha_0}{2Dk^3}\frac{F_8}{F_1}$	$+H_{ik}\frac{\sin\alpha_0}{2Dk^2}\frac{2F_8}{F_1}$
M_{ik}	$+M_{ik}\frac{\sin\alpha_0}{2Dk^2}\frac{F_2}{F_1}$	$-M_{ik}\frac{1}{2Dk}\frac{2F_3}{F_1}$	$-M_{ik}\frac{\sin\alpha_0}{2Dk^2}\frac{2F_8}{F_1}$	$-M_{ik}\frac{1}{2Dk}\frac{2F_{10}}{F_1}$
H_{ki}	$-H_{ki}\frac{\sin^2\alpha_0}{2Dk^3}\frac{F_9}{F_1}$	$+H_{ki}\frac{\sin\alpha_0}{2Dk^2}\frac{2F_8}{F_1}$	$+H_{ki}\frac{\sin^2\alpha_0}{2Dk^3}\frac{F_4}{F_1}$	$+H_{ki}\frac{\sin\alpha_0}{2Dk^2}\frac{F_2}{F_1}$
M_{ki}	$-M_{ki}\frac{\sin\alpha_0}{2Dk^2}\frac{2F_8}{F_1}$	$+M_{ki}\frac{1}{2Dk}\frac{2F_{10}}{F_1}$	$+M_{ki}\frac{\sin\alpha_0}{2Dk^2}\frac{F_2}{F_1}$	$+M_{ki}\frac{1}{2Dk}\frac{2F_3}{F_1}$

M_r = radial moment

M_t = tangential moment

Q_r = radial shear.

Other designations are indicated in tables presented in this section.

The formulas presented were derived by using the linear bending theory. The "primary" solution is presented first; then "secondary" solutions are presented in the same way as for the shells. Finally, special cases (fixed boundary conditions) will be given.

I Primary Solutions

Primary solutions are assembled in Tables B7. 3. 3-16 and B7. 3. 3-17.

II Secondary Solutions

The only unit-edge loading of importance is a unit moment loading along the edges (Figure B7.3.3-7). Table B7.3.3-18 presents solutions for this loading for different cases of circular plate with and without the circular opening at the center. Table B7. 3. 3-19 presents the stresses in circular plates resulting from edge elongation.

III Special Cases

Special cases and solutions for circular plates that occur commonly in practice are presented in this paragraph. The geometry, boundary conditions, and loadings for special circular plates (with and without a central hole) are shown in Tables B7. 3. 3-20, B7. 3. 3-21, and B7. 3. 3-22.

TABLE B7. 3. 3-16 SIMPLY SUPPORTED CIRCULAR PLATES

Loading Constant	Parabolic Distribution
$p = \text{const.}$; $p = pa^2 w$ $A = \frac{P}{2aw}$; $Q_r = \frac{P\rho}{2aw}$	$p = p_o(1-\rho^2)$; $P = p_o a^2 \frac{w}{2}$ $A = \frac{P}{2aw}$; $Q_r = \frac{P\rho(2-\rho^2)}{2wa}$
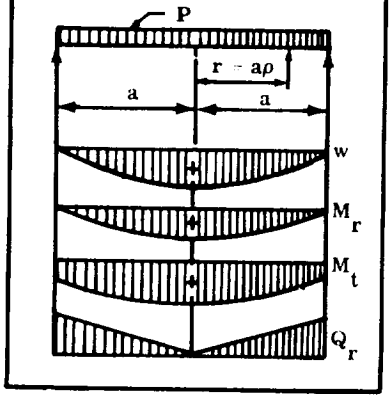	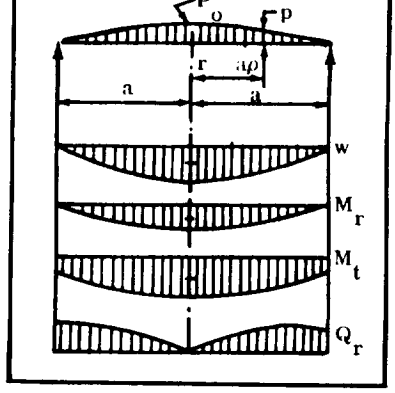

w	$\frac{Pa^2(1-\rho)}{64D\pi}\left(\frac{5+\mu}{1+\mu} - \rho^2\right)$	$\frac{Pa^2}{288D\pi}\left(\frac{31+7\mu}{1+\mu} - \frac{39+15\mu}{1+\mu} - \rho^2 + 9\rho^4 - \rho^6\right)$
β	$\frac{Pa\rho}{16D\pi}\left(\frac{3+\mu}{1+\mu} - \rho^2\right)$	$\frac{Pa\rho}{48D\pi}\left(\frac{13+5\mu}{1+\mu} - 6\rho^2 + \rho^4\right)$
M_r	$\frac{P}{16\pi}(3+\mu)(1-\rho^2)$	$\frac{P}{48\pi}\left[13+5\mu - 6(3+\mu)\rho^2 + (5+\mu)\rho^4\right]$
M_t	$\frac{P}{16\pi}\left[3+\mu - (1+3\mu)\rho^2\right]$	$\frac{P}{48\pi}\left[13+5\mu - 6(1+3\mu)\rho^2 + (1+5\mu)\rho^4\right]$

TABLE B7.3.3-16 SIMPLY SUPPORTED CIRCULAR PLATES (Continued)

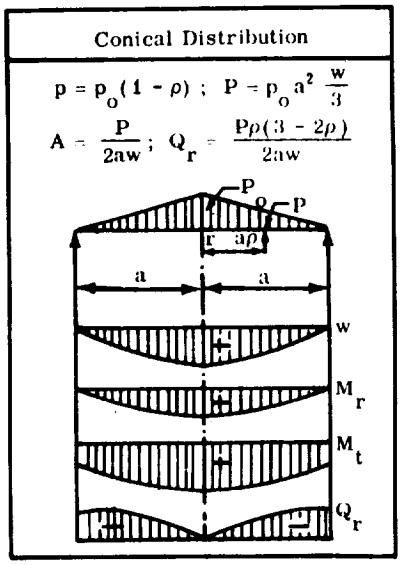

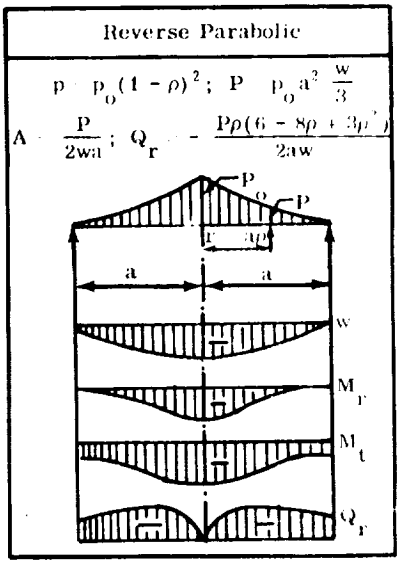

w	$\frac{Pa^2}{4800D\pi}\left[\frac{3(183+43\mu)}{1+\mu}\rho^2 - \frac{10(71+29\mu)}{1+\mu}\rho^4 + 225\rho^4 - 64\rho^5\right]$	$\frac{Pa^2}{2400D\pi}\left[\frac{323+83\mu}{1+\mu} - \frac{5(89+41\mu)}{1+\mu}\rho^2 + 225\rho^4 - 128\rho^5 + 25\rho^6\right]$
β	$\frac{Pa\rho}{240D\pi}\left(\frac{71+29\mu}{1+\mu} - 45\rho^2 + 16\rho^3\right)$	$\frac{Pa\rho}{240D\pi}\left(\frac{89+41\mu}{1+\mu} - 90\rho^2 + 64\rho^3 - 15\rho^4\right)$
M_r	$\frac{P}{240D\pi}\left[71+29\mu - 45\rho^2(3+\mu) + 16\rho^3(4+\mu)\right]$	$\frac{P}{240D\pi}\left[89+41\mu - 90\rho^2(3+\mu) + 64\rho^3(4+\mu) - 15\rho^4(5+\mu)\right]$
M_r	$\frac{P}{240D\pi}\left[71+29\mu - 45\rho^2(1+3\mu) + 16\rho^3(1+4\mu)\right]$	$\frac{P}{240D\pi}\left[89+41\mu - 90\rho^2(1+3\mu) + 64\rho^3(1+4\mu) - 15\rho^4(1+5\mu)\right]$

TABLE B7.3.3-16 SIMPLY SUPPORTED CIRCULAR PLATES (Continued)

Circumferential Loading (Linear)		
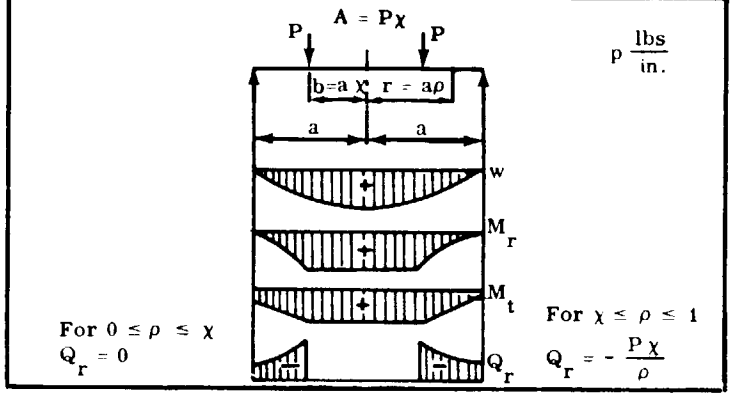		
w	$\frac{Pa^3}{8D}\frac{\chi}{1+\mu}\left\{(3+\mu)(1+\chi^2)+(1+\mu)\chi^2 \ln\chi - \left[(1-\mu)(1-\chi^2)-2(1+\mu)\ln\chi\right]\rho^2\right\}$	$\frac{Pa^3}{8D}\frac{\chi}{1+\mu}\left\{\left[3+\mu-(1-\mu)\chi^2\right]-(1-\rho^2)+2(1+\mu)(\chi^2+\rho^2)\ln\rho\right\}$
β	$\frac{Pa^2}{8D}\frac{\chi}{1+\mu}\rho\left[(1-\mu)(1-\chi^2)-2(1+\mu)\ln\chi\right]$	$\frac{Pa^2}{4D}\frac{\chi}{1+\mu}\rho\left[2-(1-\mu)\chi^2-(1+\mu)\frac{\chi^2}{\rho^2}-2(1+\mu)\ln\rho\right]$
M_r	$\frac{Pa\chi}{4}\left[(1-\mu)(1-\chi^2)-2(1+\mu)\ln\chi\right]$	$\frac{Pa\chi}{4}\left[(1-\mu)\chi^2\left(\frac{1}{\rho^2}-1\right)-2(1+\mu)\ln\rho\right]$
M_t	$\frac{Pa\chi}{4}\left[(1-\mu)(1-\chi^2)-2(1+\mu)\ln\chi\right]$	$\frac{Pa\chi}{4}\left\{(1-\mu)\left[2-\chi^2\left(\frac{1}{\rho^2}+1\right)\right]-2(1+\mu)\ln\rho\right\}$
Q_r	0	$-P\chi\frac{1}{\rho}$

TABLE B7. 3. 3-16 SIMPLY SUPPORTED CIRCULAR PLATES (Continued)

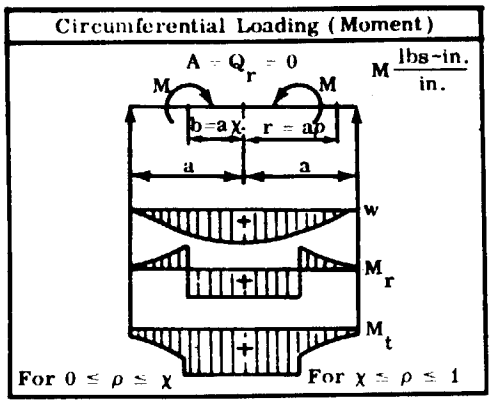

w	$\frac{Ma^2}{4D}\frac{1}{1+\mu}\left\{2\chi^2\left[1-(1+\mu)\ln\chi\right]-\left[1+\mu+(1-\mu)\chi^2\right]\rho^2\right\}$	$\frac{Ma^2}{4D}\frac{\chi^2}{1+\mu}\left[(1-\mu)(1-\rho^2)-2(1+\mu)\ln\rho\right]$
β	$\frac{Ma\rho}{2D(1+\mu)}\left[1+\mu+(1-\mu)\chi^2\right]$	$\frac{Ma\chi^2}{2D(1+\mu)}\left[(1-\mu)\rho+\frac{1+\mu}{\rho}\right]$
M_r	$\frac{M}{2}\left[1+\mu+(1-\mu)\chi^2\right]$	$\frac{M}{2}(1-\mu)\chi^2\left(1-\frac{1}{\rho^2}\right)$
M_t	$\frac{M}{2}\left[1+\mu+(1-\mu)\chi^2\right]$	$\frac{M}{2}(1-\mu)\chi^2\left(1+\frac{1}{\rho^2}\right)$
Q_r	0	0

TABLE B7. 3. 3-16 SIMPLY SUPPORTED CIRCULAR PLATES (Continued)

Partially Equal Loading

$p = \text{Const.}$; $P = pb^2 w = pa^2\ w\chi^2$; $A = \frac{P}{2aw}$

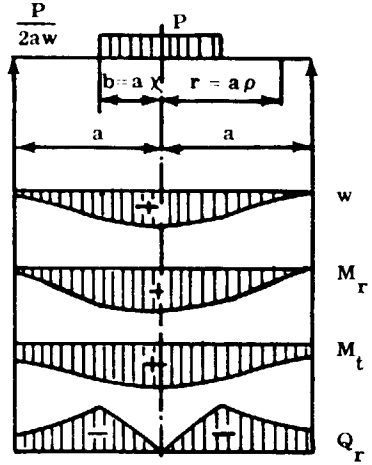

For $0 \le \rho \le \chi$ $\quad Q_r = -\frac{P\rho}{2a\chi^2 w}$

For $\chi \le \rho \le 1$ $\quad Q_r = -\frac{P}{2aw\rho}$

w	$\frac{Pa^2}{64D\pi}\frac{1}{1-\mu}\left\{4(3-\mu)-(7-3\mu)\chi^2+4(1+\mu)\chi^2\cdot\ln\chi - 2\left[4-(1-\mu)\chi^2\right]-4(1+\mu)\ln\chi\cdot\rho^2+(1+\mu)\frac{\rho^4}{\chi^2}\right\}$	$\frac{Pa^2}{32D\pi}\frac{1}{1+\mu}\left\{\left[2(3+\mu)-(1-\mu)\chi^2\right](1-\rho^2)+2(1+\mu)\chi^2\ln\rho+4(1+\mu)\rho^2\ln\rho\right\}$
β	$\frac{Pa}{16\pi D}\frac{1}{1-\mu}\rho\left[4-(1-\mu)\chi^2-4(1-\mu)\ln\chi-\frac{1+\mu}{\chi^2}\rho^2\right]$	$\frac{Pa}{16D\pi}\frac{1}{1-\mu}\left\{\left[4-(1-\mu)\chi^2\right]\rho-(1+\mu)\frac{\chi^2}{\rho}-4(1+\mu)\rho\ln\rho\right\}$
M_r	$\frac{P}{16\pi}\left[4-(1-\mu)\chi^2-4(1+\mu)\ln\chi-3-\mu\right]$	$\frac{P}{16\pi}\left[(1-\mu)\chi^2\left(\frac{1}{\rho^2}-1\right)-4(1+\mu)\ln\rho\right]$
M_t	$\frac{P}{16\pi}\left[4-(1+\mu)\chi^2-4(1+\mu)\ln\chi-\frac{1+3\mu}{\chi^2}\rho^2\right]$	$\frac{P}{16\pi}\left\{(1-\mu)\left[4-\chi^2\left(\frac{1}{\rho^2}+1\right)\right]-4(1+\mu)\ln\rho\right\}$

TABLE B7.3.3-16 SIMPLY SUPPORTED CIRCULAR PLATES (Concluded)

Concentrated Loading

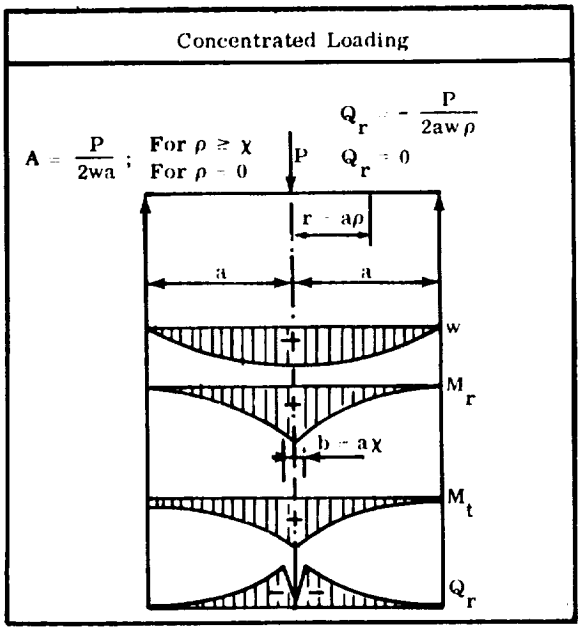

w	$\frac{Pa^2}{16D\pi}\left[\frac{3+\mu}{1+\mu}(1-\rho^2)+2\rho^2 \ln\rho\right]$
β	$\frac{Pa}{4D\pi}\rho\left(\frac{1}{1+\rho}-\ln\rho\right)$
M_r	For $\rho \geq \chi$, $-\frac{P}{4\pi}(1+\mu)\ln\rho$ For $\rho = 0$, $\frac{P}{4\pi}\left[1-(1+\mu)\ln\chi\right]$
M_t	For $\rho \geq \chi$, $\frac{P}{4\pi}\left[1-\mu-(1+\mu)\ln\rho\right]$ For $\rho = 0$, $\frac{P}{4\pi}\left[1-(1+\mu)\ln\chi\right]$

TABLE B7.3.3-17 SIMPLY SUPPORTED CIRCULAR PLATES WITH CENTRAL HOLE

Equally Distributed Loading (lb/in.^{2})

$$Q_r = \frac{-pa}{2}\left(\rho - \chi^2 \frac{1}{\rho}\right); \quad A = \frac{pa}{2}(1-\chi^2); \quad \chi < 1;$$

$$A = \frac{pa}{2}(\chi^2 - 1); \quad \chi > 1; \quad k_2 = \chi^2\left[3+\mu+4(1+\mu)\frac{\chi^2}{1+\chi^2}\ln\chi\right]$$

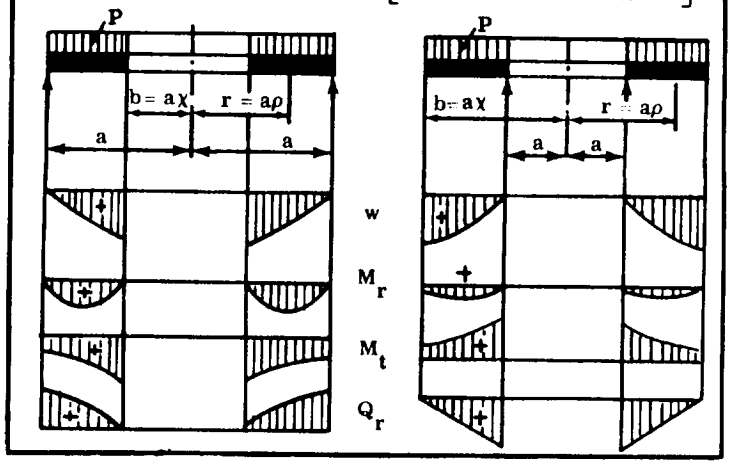

w	$\frac{pa^4}{64D}\left\{\frac{2}{1+\mu}\left[(3+\mu)(1-2\chi^2)+k_2\right](1-\rho^2) - (1-\rho^4) - \frac{4k_2 \ln\rho}{1-\mu} - 8\chi^2\rho^2 \ln\rho\right\}$
β	$\frac{pa^3}{16D}\left[\frac{1}{1+\mu}(3+\mu-4\chi^2+k_2)\rho - \rho^3 + \frac{k_2}{1-\mu}\frac{1}{\rho} + 4\chi^2\rho\ln\rho\right]$
M_r	$\frac{pa^2}{16}\left[(3+\mu)(1-\rho^2) + k_2\left(1-\frac{1}{\rho^2}\right) + 4(1+\mu)\chi^2 \ln\rho\right]$
M_t	$\frac{pa^2}{16}\left[2(1-\mu)(1-2\chi^2) + (1+3\mu)(1-\rho^2) + k_2\left(1+\frac{1}{\rho^2}\right) + 4(1+\mu)\chi^2 \ln\rho\right]$

TABLE B7. 3. 3-17 SIMPLY SUPPORTED CIRCULAR PLATES WITH CENTRAL HOLE (Concluded)

Concentrated Edge Loading (lb/in.)

$Q_r = P\chi/\rho$; $A = P\chi$ for $\chi < 1$; $A = -P\chi$ for $\chi > 1$

$k_4 = 1 + \mu \dfrac{\chi^2}{1+\chi^2} 1n\chi$

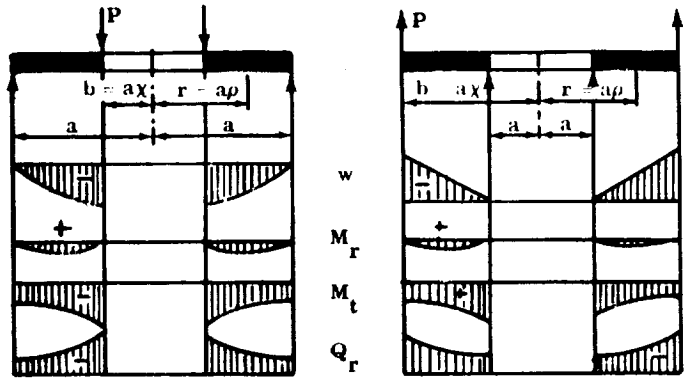

w	$\dfrac{Pa^3\chi}{8D}\left[\dfrac{3+\mu-2k_4}{1+\mu}(1-\rho^2) + 4\dfrac{k_4}{1-\mu} 1n\rho + 2\rho^2 1n\rho\right]$
β	$\dfrac{Pa^2\chi}{8D}\left[\dfrac{1-k_4}{1+\mu}\rho - \dfrac{k_4}{1-\mu}\cdot\dfrac{1}{\rho} - \rho 1n\rho\right]$
M_r	$\dfrac{Pa\chi}{2}\left[k_4\left(\dfrac{1}{\rho^2}-1\right) - (1+\mu) 1n\rho\right]$
M_t	$\dfrac{Pa\chi}{2}\left[1-\mu-k_4\left(\dfrac{1}{\rho^2}+1\right) - (1+\mu) 1n\rho\right]$

TABLE B7. 3. 3-18 SIMPLY SUPPORTED CIRCULAR PLATES WITH CENTRAL HOLE

Equally Distributed Edge Moment ($\rho = \chi$)

M is in lb-in./in.; $Q_r = 0$; A = 0; $k_6 = \chi^2/(1 - \chi^2)$

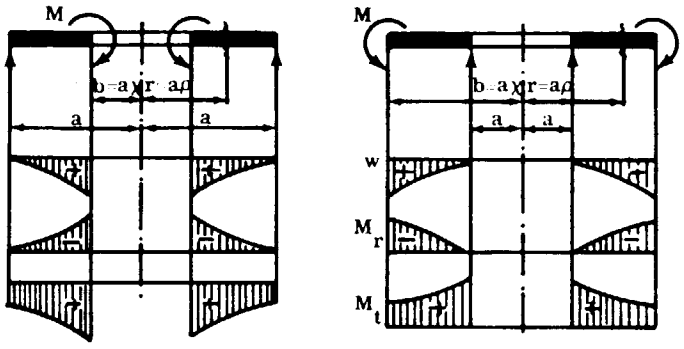

Equally Distributed Edge Moment ($\rho = 1$)

M is in lb-in./in.; $Q_r = 0 = A$; $k_7 = 1/(1 - \chi^2)$

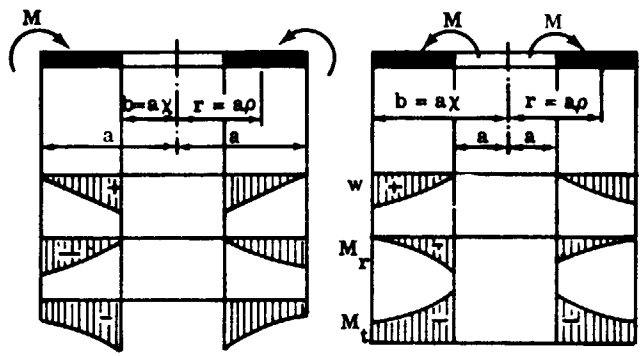

w	$\frac{Ma^2}{2D}\,\frac{k_6}{1+\mu}\left(1 - \rho^2 - 2\,\frac{1+\mu}{1-\mu}\,\ln\rho\right)$	$\frac{Ma^2}{2D}\,\frac{k_7}{1+\mu}\left(1 - \rho^2 - 2\,\frac{1+\mu}{1-\mu}\,\chi^2 \cdot \ln\rho\right)$
β	$\frac{Ma}{D}\,\frac{k_6}{1+\mu}\left(\rho + \frac{1+\mu}{1-\mu} \cdot \frac{1}{\rho}\right)$	$\frac{Ma}{D}\,\frac{k_7}{1+\mu}\left(\rho + \frac{1+\mu}{1-\mu}\,\chi^2 \cdot \frac{1}{\rho}\right)$
M_r	$Mk_6\left(1 - \frac{1}{\rho^2}\right)$	$M\chi^2\,k_7\left(\frac{1}{\chi^2} - \frac{1}{\rho^2}\right)$
M_t	$Mk_6\left(1 + \frac{1}{\rho^2}\right)$	$M\chi^2\,k_7\left(\frac{1}{\chi^2} + \frac{1}{\rho^2}\right)$

TABLE B7. 3. 3-19 CIRCULAR PLATES, STRESSES IN PLATES RESULTING FROM EDGE ELONGATION

Stress / Elongation		
	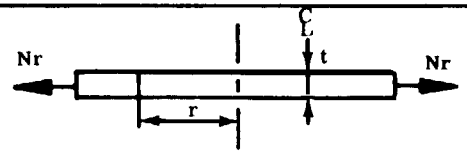	
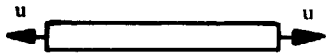	$\frac{uEt}{a(1-\mu)}$	
Stress / Elongation	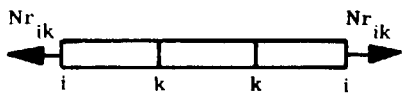	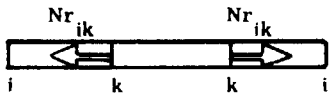
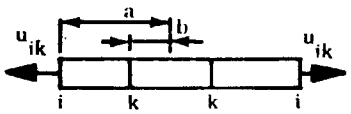	$u_{ik}\ \frac{Et(1-\lambda^{-2})}{a[1-\mu+\lambda^{-2}(1+\mu)]}$	$u_{ik}\ \frac{Et(\lambda^2-1)}{2a}$
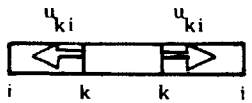	$u_{ki}\ \frac{Et(1-\lambda^{-2})}{2b}$	$u_{ki}\ \frac{Et(\lambda^2-1)}{b[1-\mu+\lambda^2(1+\mu)]}$
Note: $\lambda = \frac{a}{b}$		

TABLE B7. 3. 3-20 CIRCULAR PLATE WITH CENTRAL HOLE

Equally Distributed Loading over the Surface Area

$$k_1 = \chi^2 \cdot \frac{-\mu)\chi^2 + (1+\mu)\ (1+4\chi^2\ 1n\chi)}{1-\mu+(1+\mu)\chi^2}$$

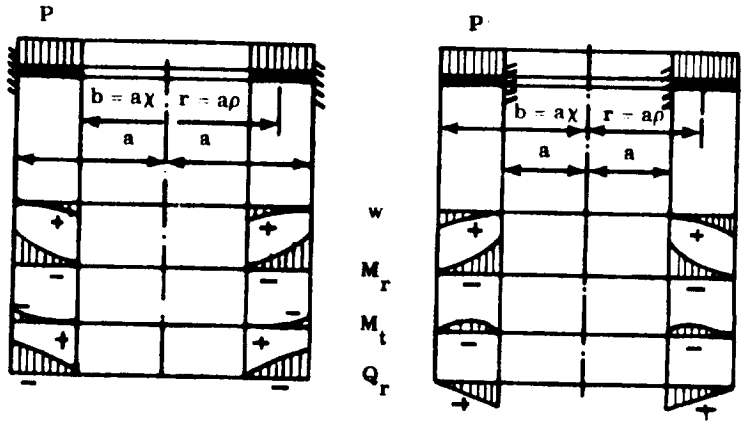

w	$\frac{pa^4}{64D}\left[-1+2(1-k_1-2\chi^2)\ (1-\rho^2)+\rho^4-4k_1\ 1n\rho-8\chi^2\ \rho^2\ 1n\rho\right]$
β	$\frac{pa^3}{16D}\left[(1-k_1)\rho-\rho^3+k_1\cdot\frac{1}{\rho}+4\chi^2\rho\ 1n\rho\right]$
M_r	$\frac{pa^2}{16}\left[(1+\mu)\ (1-k_1)+4\chi^2-(3+\mu)\rho^2-(1-\mu)k_1\cdot\frac{1}{\rho^2}+4\chi^2\ (1+\mu)\ 1n\rho\right]$
M_t	$\frac{pa^2}{16}\left[(1+\mu)\ (1-k_1)+4\mu\ \chi^2-(1+3\mu)\rho^2+(1-\mu)\frac{k_1}{\rho^2}+4(1+\mu)\chi^2\ 1n\rho\right]$
Q_r	$-\frac{pa}{2}\left(\rho-\chi^2\frac{1}{\rho}\right)$

TABLE B7. 3. 3-20 CIRCULAR PLATE WITH CENTRAL HOLE (Continued)

Equally Distributed Loading over the Edge Circumference

$$k_3 = \chi^2 \frac{1 + (1+\mu) \ln \chi}{1 - \mu + (1+\mu) \chi^2} \qquad P \frac{\text{lbs}}{\text{in.}}$$

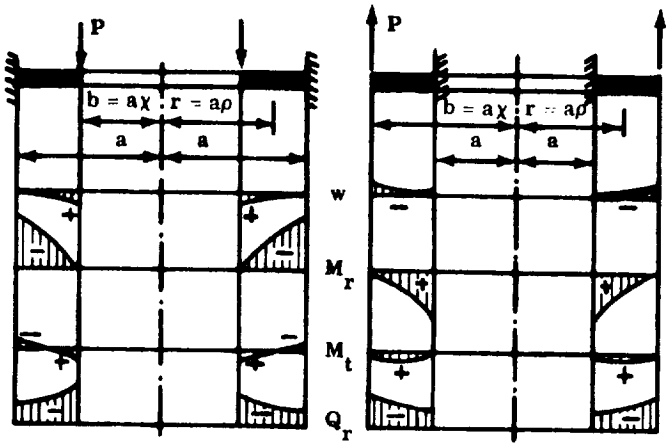

w	$\frac{Pa^3\chi}{8D} \left[(1 - 2k_3)(1 - \rho^2) + 4k_3 \ln\rho + 2\rho^2 \ln\rho \right]$
β	$\frac{Pa^2\chi}{2D} \left[k_3 \left(\rho - \frac{1}{\rho} \right) - \rho \ln\rho \right]$
M_r	$\frac{Pa\chi}{2} \left[-1 + (1+\mu) k_3 + (1-\mu) k_3 \frac{1}{\rho^2} - (1+\mu) \ln\rho \right]$
M_t	$\frac{Pa\chi}{2} \left[-\mu + (1+\mu) k_3 - (1-\mu) \frac{k_3}{\rho^2} - (1+\mu) \ln\rho \right]$
Q_r	$-P\chi \frac{1}{\rho}$

TABLE B7. 3. 3-20 CIRCULAR PLATE WITH CENTRAL HOLE (Concluded)

Equally Distributed Edge Moment

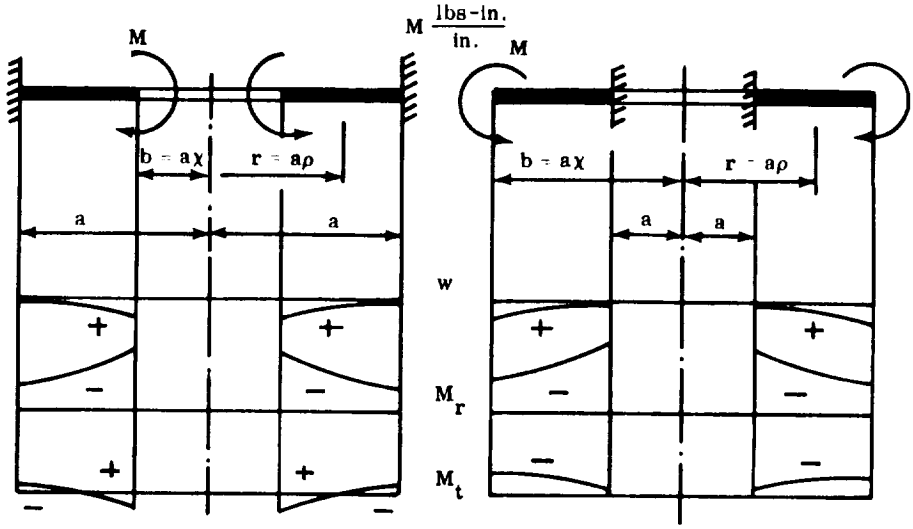

$$k_5 = \frac{\chi^2}{1 - \mu + (1 + \mu)\chi^2}$$

$$w = \frac{Ma^2}{2D} k_5(-1 + \rho^2 - 2 \cdot \ln \rho)$$

$$\beta = \frac{Ma}{D} \cdot k_5 \left(\frac{1}{\rho} - \rho\right)$$

$$M_r = -M k_5 \left[1 + \mu + (1 - \mu)\frac{1}{\rho^2}\right]$$

$$M_t = -M k_5 \left[1 + \mu - (1 - \mu)\frac{1}{\rho^2}\right]$$

$$Q_r = 0$$

TABLE B7. 3. 3-21 CIRCULAR PLATES WITH CLAMPED EDGES

Loading Constant

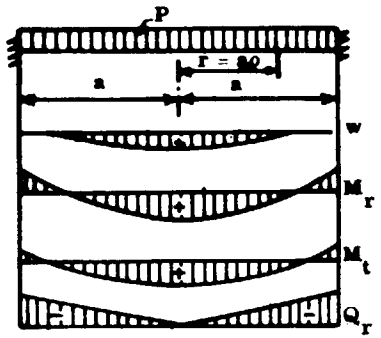

p = const. P = pa² w

Parabolic Distribution

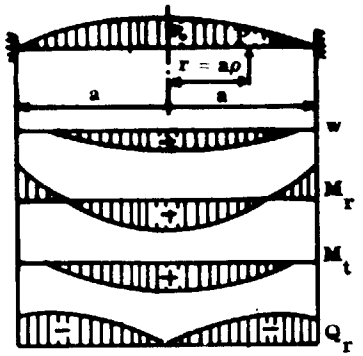

p = P o (1 - ρ) P = ½ P o a² w

w	$\frac{Pa^2}{64\pi D}(1-\rho^2)^2$	$\frac{Pa^2}{288D\pi}(7-15\rho^2+9\rho^4-\rho^6)$
β	$\frac{Pa}{16D\pi}\cdot\rho(1-\rho^2)$	$\frac{Pa\rho}{48D\pi}(5-6\rho^2+\rho^4)$
M_r	$\frac{P}{16\pi}\left[1+\mu-(3+\mu)\rho^2\right]$	$\frac{P}{48\pi}\left[5(1+\mu)-6(3+\mu)\rho^2+\rho^4(5+\mu)\right]$
M_t	$\frac{P}{16\pi}\left[1+\mu-(1+3\mu)\rho^2\right]$	$\frac{P}{48\pi}\left[5(1+\mu)-6(1+3\mu)\rho^2+(1+5\mu)\rho^4\right]$
Q_r	$-\frac{P}{2a\pi}\cdot\rho$	$-\frac{P}{2a\pi}\cdot\rho(2-\rho^2)$

TABLE B7.3.3-21 CIRCULAR PLATES WITH CLAMPED EDGES (Continued)

Conical Distribution

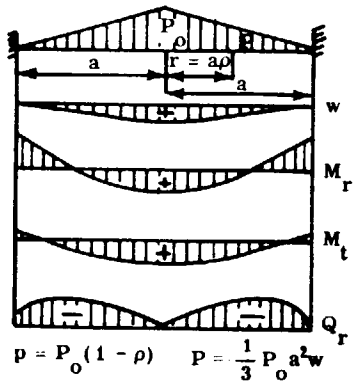

Reverse Parabolic

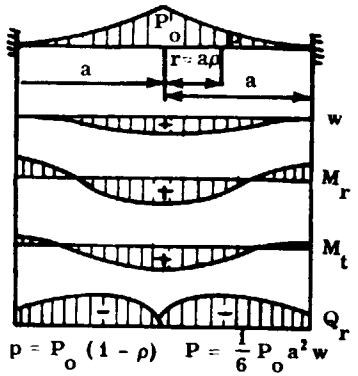

w	$\frac{Pa^2}{4800D\pi}(129 - 290\rho^2 + 225\rho^4 - 64\rho^5)$	$\frac{Pa^2}{4800D\pi}(83 - 205\rho^2 + 225\rho^4 - 128\rho^5 + 25\rho^6)$
β	$\frac{Pa\rho}{240D\pi}(29 - 45\rho^2 + 16\rho^3)$	$\frac{Pa\rho}{240D\pi}\left[(41 - 90\rho^2 + 64\rho^3 - 15\rho^4)\right]$
M_r	$\frac{P}{240\pi}\left[29(1+\mu) - 45(3+\mu)\rho^2 + 16(4+\mu)\rho^3\right]$	$\frac{P}{240\pi}\left[41(1+\mu) - 90(3+\mu)\rho^2 + 64(4+\mu)\rho^3 - 15(5+\mu)\rho^4\right]$
M_t	$\frac{P}{240\pi}\left[29(1+\mu) - 45(1+3\mu)\rho^2 + 16(1+4\mu)\rho^3\right]$	$\frac{P}{240\pi}\left[41(1+\mu) - 90(1+3\mu)\rho^2 + 64(1+4\mu)\rho^3 - 15(1+5\mu)\rho^4\right]$
Q_r	$-\frac{P}{2a\pi}\cdot\rho(3 - 2\rho)$	$-\frac{P}{2a\pi}\rho(6 - 8\rho + 3\rho^2)$

TABLE B7.3.3-21 CIRCULAR PLATES WITH CLAMPED EDGES (Continued)

Partially Equally Distributed Loading

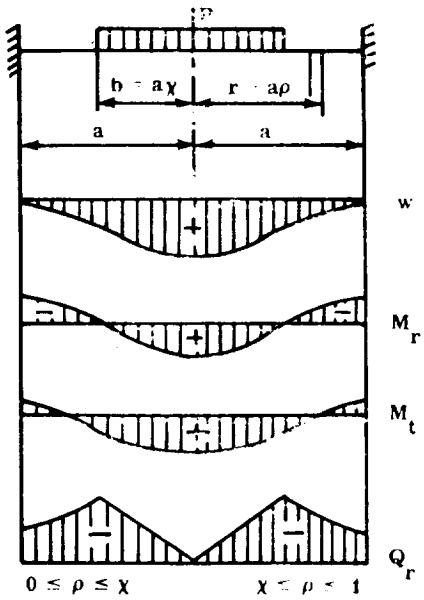

w	$\frac{Pa^2}{64D\pi}\left[4 - 3\chi^2 + 4\chi^2 \ln\chi - 2(\chi^2 - 4\ln\chi)\rho^2 + \frac{1}{\chi^2}\rho^4\right]$	$\frac{Pa^2}{32D\pi}\left[(2-\chi^2)(1-\rho^2) + 2(\chi^2 - \chi^2)\ln\rho\right]$
β	$\frac{Pa\rho}{16D\pi}\left[\chi^2 - 4\ln\chi - \frac{1}{\chi^2}\rho^2\right]$	$\frac{Pa}{16D\pi}\rho\left[\chi^2\left(1 - \frac{1}{\rho^2}\right) - 4\ln\rho\right]$
M_r	$\frac{P}{16\pi}\left[(1+\mu)(\chi^2 - 4\ln\chi) - \frac{3+\mu}{\chi^2}\rho^2\right]$	$\frac{P}{16\pi}\left[-4 + (1-\mu)\frac{\chi^2}{\rho^2} + (1+\mu)(\chi^2 - 4\ln\rho)\right]$
M_t	$\frac{P}{16\pi}\left[(1+\mu)(\chi^2 - 4\ln\chi) - \frac{1+3\mu}{\chi^2}\rho^2\right]$	$\frac{P}{16\pi}\left[-4\mu - (1-\mu)\frac{\chi^2}{\rho^2} + (1+\mu)(\chi^2 - 4\ln\rho)\right]$
Q_r	$-\frac{P}{2a\chi^2\pi}\cdot\rho$	$-\frac{P}{2a\pi}\frac{1}{\rho}$

TABLE B7.3.3-21 CIRCULAR PLATES WITH CLAMPED EDGES (Continued)

Concentrated Loading

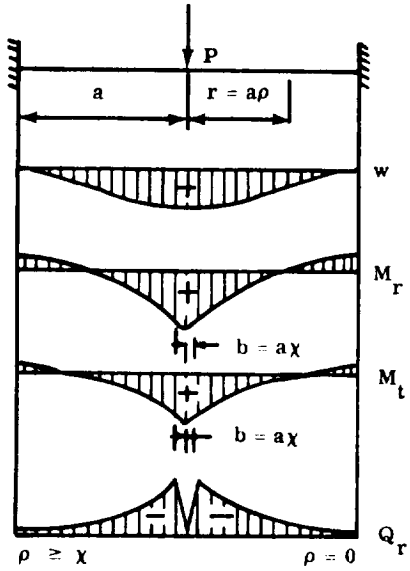

w	$\frac{Pa^2}{16D\pi}\ (1 - \rho^2 + 2\rho^2 \ln \rho)$	
β	$-\frac{Pa}{4D\pi}\ \rho \ln \rho$	
M_r	$-\frac{P}{4\pi}\left[1 + (1 + \mu) \ln \rho\right]$	$-\frac{P}{4\pi}\ (1 + \mu) \ln \chi$
M_t	$-\frac{P}{4\pi}\left[\mu + (1 + \mu) \ln \rho\right]$	$-\frac{P}{4\pi}\ (1 + \mu) \ln \chi$
Q_r	$-\frac{P}{2a\pi}\ \frac{1}{\rho}$	0

TABLE B7. 3. 3-21 CIRCULAR PLATES WITH CLAMPED EDGES (Continued)

Circumferential Loading (Linear)

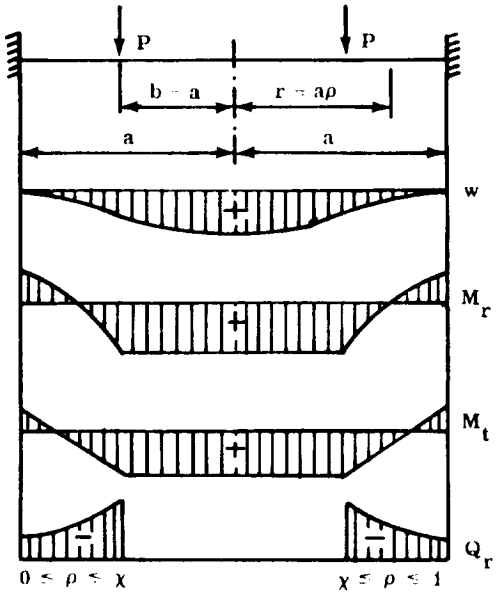

w	$\frac{Pa^3\chi}{8D}\left[1 - \chi^2 + 2\chi^2 \ln\chi + (1 - \chi^2 + 2\ln\chi)\rho^2\right]$	$\frac{Pa^3\chi}{8D}\left[(1 + \chi^2)(1 - \rho^2) + 2(\chi^2 + \rho^2)\ln\rho\right]$
β	$-\frac{Pa^2\chi\rho}{4D}(1 + \chi^2 + 2\ln\chi)$	$\frac{Pa^2\chi\rho}{4D}\left[\chi^2\left(1 - \frac{1}{\rho^2}\right) - 2\ln\rho\right]$
M_r	$-\frac{Pa}{4}\chi(1 + \mu) - (1 - \chi^2 + 2\ln\chi)$	$-\frac{Pa\chi}{4}\left[2 - (1 - \mu)\frac{\chi^2}{\rho^2} - (1 + \mu)(\chi^2 - 2\ln\rho)\right]$
M_t	$-\frac{Pa\chi}{4}(1 + \mu) - (1 - \chi^2 + 2\ln\chi)$	$-\frac{Pa\chi}{4}\left[2\mu + (1 - \mu)\frac{\chi^2}{\rho^2} - (1 + \mu)(\chi^2 - 2\ln\rho)\right]$
Q_r	0	$-P\chi\frac{1}{\rho}$

TABLE B7. 3. 3-21 CIRCULAR PLATES WITH CLAMPED EDGES (Concluded)

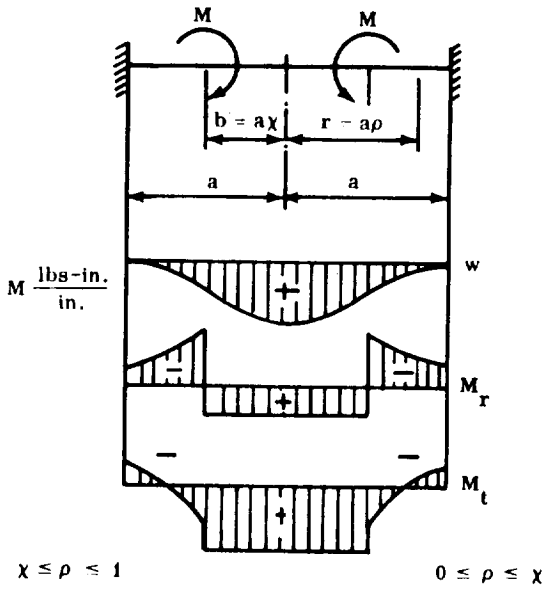

w	$-\frac{Ma^2\chi^2}{4D}(1-\rho^2+2\ln\rho$	$-\frac{Ma^2}{4D}\left[2\chi^2\ln\chi+\rho^2(1-\chi^2)\right]$
β	$\frac{Ma\chi^2}{2D}\left(\frac{1}{\rho}-\rho\right)$	$\frac{Ma\rho}{2D}(1-\chi^2)$
M_r	$-\frac{M\chi^2}{2}\left[1+\mu+(1-\mu)\frac{1}{\rho^2}\right]$	$\frac{M}{2}(1+\mu)(1-\chi^2)$
M_t	$-\frac{M\chi^2}{2}\left[1+\mu-(1-\mu)\frac{1}{\rho^2}\right]$	$\frac{M}{2}(1+\mu)(1-\chi^2)$
Q_r	0	0

TABLE B7. 3. 3-22 SYMMETRICALLY LOADED CIRCULAR RINGS

Item	Loading Condition	n > 1		n = 1		n = 0	
		Stresses	Displacements	Stresses	Displacements	Stresses	Displacements
1	**Radial Loading** $p = p_n \cos n\theta$, where n is an integer: $n = 1, 2, 3, \ldots$ 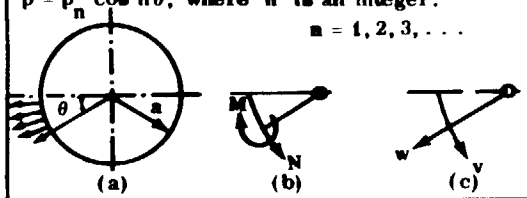 (a) (b) (c)	$N = \frac{p_n a}{n^2 - 1} \cos n\theta$ $M = \frac{p_n a^2}{n^2 - 1} \cos n\theta$	$v = -\frac{p_n a^2}{n(n^2-1)}\left(\frac{a^2}{(n^2-1)EI_z} + \frac{1}{EA}\right)\cos n\theta$ $w = \frac{p_n a^4}{(n^2-1)^2 EI_z} \cos n\theta$	Problem Does Not Exist Because the Loading Is Not in Self-Equilibrium		$N = pa$ $M = 0$	$v = 0$ $w = \frac{pa^2}{EA}$
2	**Tangential Loading** $p = p_n \sin n\theta$ 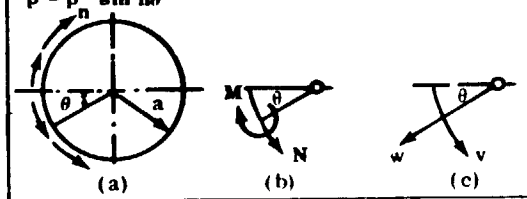 (a) (b) (c)	$N = \frac{p_n a}{n^2 - 1} \cos n\theta$ $M = \frac{p_n a^2}{n(n^2 - 1)} \cos n\theta$	$v = \frac{p_n a^2}{n^2 - 1}\left[\frac{a^2}{n(n^2-1)EI_z} + \frac{1}{EA}\right]\sin n\theta$ $w = -\frac{p_n a^4}{n(n^2-1)^2 EI_z} \cos n\theta$	Problem Does Not Exist Because the Loading Is Not in Self-Equilibrium		Problem Does Not Exist Because the Loading Is Not in Self-Equilibrium	
3	**Loading Normal to the Plane of the Ring** $p = p_n \cos n\theta$ 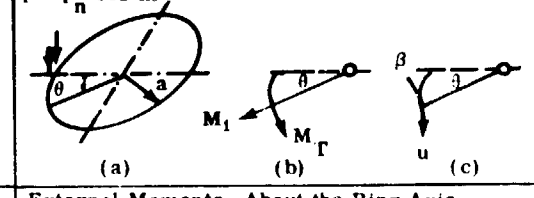 (a) (b) (c)	$N = \frac{p_n a^2}{n^2 - 1}$ $M_1 = -\frac{p_n a^2}{n(n^2-1)} \sin n\theta$	$u = \frac{p_n a^3}{(n^2-1)^2}\left[\frac{2}{EI_1} + \frac{1}{GJ}\right]\cos n\theta$ $\beta = \frac{p_n a^2}{(n^2-1)^2}\left[\frac{2}{EI_1} + \frac{1}{GJ}\right]\cos n\theta$	Problem Does Not Exist Because the Loading Is Not in Self-Equilibrium		Problem Does Not Exist Because the Loading Is Not in Self-Equilibrium	
4	**External Moments, About the Ring Axis** $m = m_n \cos n\theta$ 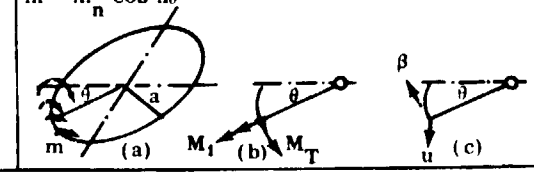 m (a) (b) (c)	$M_1 = \frac{m_n a}{n^2 - 1} \cos n\theta$ $M_T = \frac{m_n a}{n^2 - 1} \cos n\theta$	$u = \frac{m_n a^3}{(n^2-1)^2}\left[\frac{1}{EI_1} + \frac{1}{GJ}\right]\cos n\theta$ $\beta = \frac{m_n a^2}{(n^2-1)^2}\left[\frac{1}{EI_1} + \frac{n^2}{GJ}\right]\cos n\theta$	Problem Does Not Exist Because the Loading Is Not in Self-Equilibrium		$M_1 = ma$ $M_T = 0$	u = May Assume Any Desired Value $\beta = \frac{ma^2}{EI_1}$

$$w = \frac{Ma^2}{2D(1+\mu)}(1-\rho^2)$$

$$\beta = \frac{Ma}{D(1+\mu)} \cdot \rho$$

$$M_r = M_t = M$$

$$Q_r = 0$$

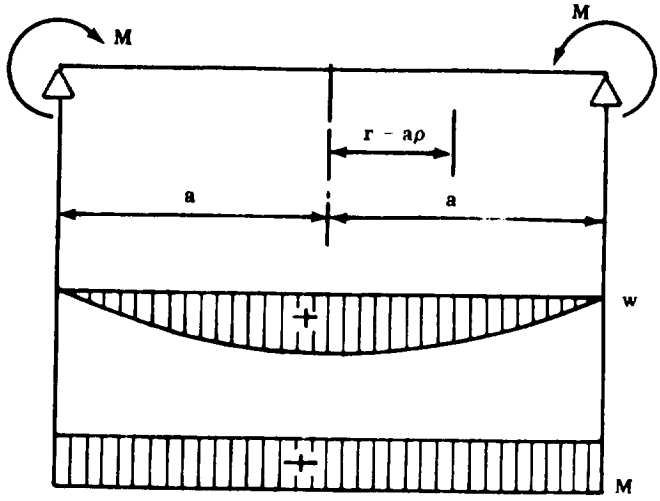

FIGURE B7.3.3-7 FORMULAS OF INFLUENCES FOR A SIMPLY SUPPORTED CIRCULAR PLATE LOADED WITH EQUALLY DISTRIBUTED END MOMENT

B7. 3. 3. 7 Circular Rings

Circular rings are important structural elements which often interact with shells. The theory of shells would not be complete without information about circular rings. In this section, such information is summarized and presented for symmetrical loading with respect to the center of the ring.

Nomenclature employed is as follows:

A = area of the cross section

I_1, I_2 = moment of inertia for the centroidal axis in the plane or normal to the plane of the ring

J = torsional rigidity factor of the section.

Table B7. 3. 3-22 presents the solutions for different loads on rings.

B7. 3. 4 STIFFENED SHELLS

Up to this point, only homogeneous, isotropic, monocoque shells have been considered.

It is known that certain rearrangements of the material in the section increase the rigidity; consequently, less material is needed, and this affects the efficiency of design. Therefore, to obtain a more efficient and economical structure, the material in the section should be arranged to make the section most resistant to certain predominant stresses. Based on this premise, stiffened structures were developed.

B7. 3. 4. 1 General

Stiffened shells are commonly used in the aerospace and civil engineering fields. The shell functions more efficiently if the meridional system, circumferential system, or a combination of both systems of stiffeners is used. The meridional stiffeners usually have all the characteristics of beams and are designed to take compressional and bending influences more effectively than the monocoque section. The circumferential stiffeners provided most of the lateral support for the meridional stiffeners. However, circumferential stiffeners are capable of withstanding moments, shears, and axial stresses.

If the stiffeners are located relatively close together, it appears logical to replace the stiffened section with an equivalent monocoque section having the corresponding ideal modulus of elasticity. Then the shell under discussion can be analyzed as a monocoque shell. More details on this approach will be given in later sections. The geometry included is for cylindrical, spherical, and conical shells.

I Cylindrical Shell

This shell may have longitudinal stiffening, circumferential stiffening, or both. Stiffening may be placed on the internal or external side of the surface, or it may be located on both sides. If cut-outs are needed, they will usually be located between the stiffeners.

II Spherical Shell

This shell, if stiffened, will usually be stiffened in both meridional and circumferential directions. The problem may be slightly more complicated in the meridional direction because, obviously, the section that corresponds to this direction will decrease in size toward the apex. This leads to the non-uniform ideal thickness.

III Conical Shell

This configuration structurally lies between cases I and II.

IV Approach for Analysis

The approach for analysis is similar for all shells. If only circumferential stiffening exists, the structure can be cut into simple elements consisting of cylindrical, conical, or spherical elements and rings as shown in Figure B7.3.4-1 and, considering the primary loading, the interaction will be performed as given in Paragraph B7.3.2. If only longitudinal stiffeners are present, interaction of cylindrical panels with longitudinal beams (stiffeners) will be performed, as shown in Figure B7.3.4-2.

If both circumferential and longitudinal stiffeners are present, the panel will be supported on all four sides. The ratio of circumferential to longitudinal distances between the stiffeners is very important. These panels loaded with pressure (external or internal) will transmit the reactions to the circumferential and longitudinal stiffeners.

There are no fixed formulas in existence for stiffened shells in general. If the stiffeners are close together, the structure can be analyzed as a shell. Then the stiffened section, for the purpose of analysis, should be replaced with the equivalent monocoque section, which is characterized with the equivalent modulus of elasticity. This replacement has to be done for both meridional and circumferential directions. Both sections will possess ideal monocoque properties, the same thickness, but different ideal moduli of elasticity. This leads to the idea of orthotropic material. The concept of orthotropy will be studied in detail in a later section, and a proper analysis procedure will be suggested.

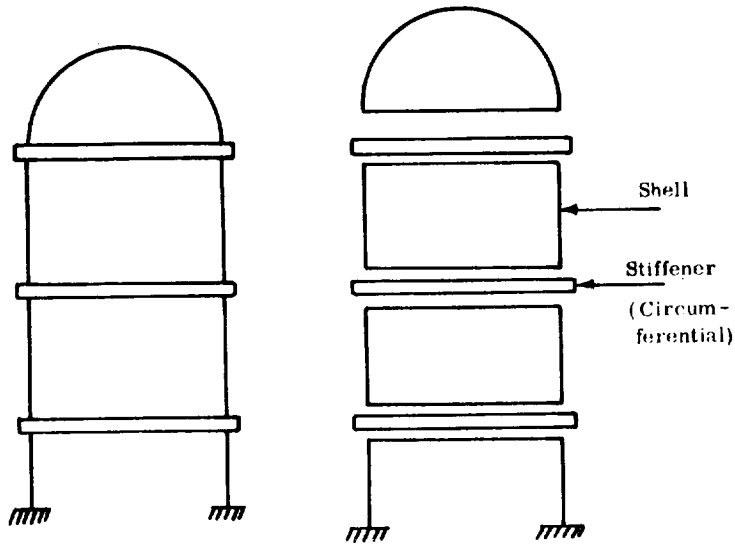

FIGURE B7. 3. 4-1 CIRCUMFERENTIALLY STIFFENED SHELL

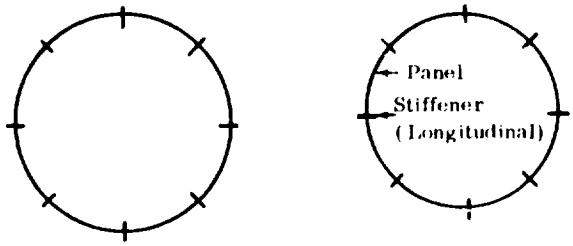

FIGURE B7. 3. 4-2 LONGITUDINALLY STIFFENED SHELL

V Method of Transformed Section

This approximate method covers all variations of stiffened (and sandwich) construction, regardless of the kind of elements that make up the section. This method shows how the combined section can be substituted with an equivalent monocoque section of the same stiffness. This idealized section should be determined for the circumferential and meridional directions of the

shell. Then the analyst deals with an orthotropic, monocoque shell. The analysis of orthotropic shells is similar to the analysis of monocoque shells discussed previously, if certain corrections are entered into the formulas cited at that time. The analysis for shells where the shear distortions cannot be neglected is more complicated and will be explained in detail in the following sections.

Assume a composite section (stiffened, sandwich, etc.) which consists of different layers of material, as shown in Figure B7.3.4-3. Each layer (i) is characterized by a modulus of elasticity (E_i) and a cross-sectional area (A_i). First select one convenient modulus of elasticity (E^*) as a basis for the equivalent monocoque section which is to be established. Accordingly, all layers will be modified and reduced to one equivalent material which is characterized with E^*. In this manner, the ideal transformed section (Figure B7.3.4-4) is determined. It should be noted that, for the convenience of design, the thickness (t_i) of individual layers was not changed, but areas A_i become A_i^*. The same modulus of elasticity (E^*) now corresponds to every A_i^*, thus making the entire section homogeneous.

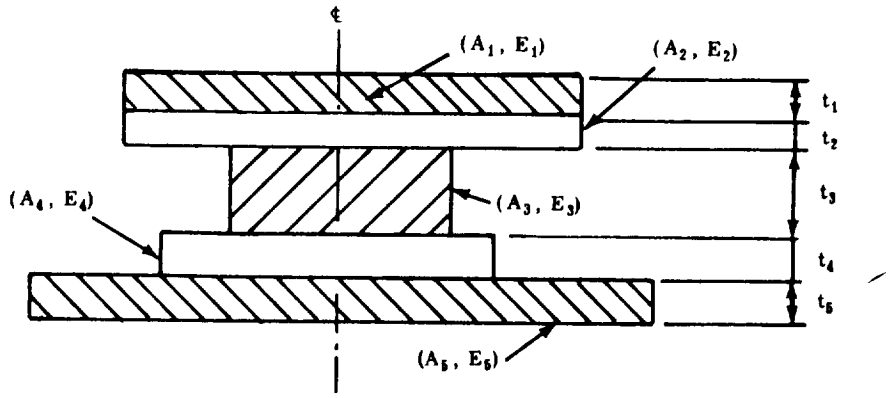

FIGURE B7.3.4-3 ORIGINAL COMPOSITE SECTION

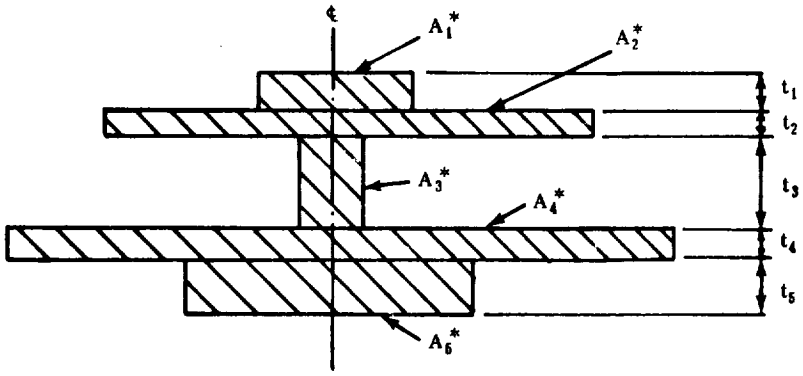

FIGURE B7. 3. 4-4 TRANSFORMED SECTION

The necessary computations are presented in Table B7. 3. 4-1. Designations are given on the sketch included in the table.

The computations lead to the determination of the moment of inertia of an equivalent section. The ideal monocoque rectangular section can be determined as having the same bending resistance as the original section. For example, if the section is symmetrical about the neutral axis, the thickness (t) can be found for the new monocoque rectangular section of the same resistance as follows:

$$I = \frac{bt^3}{12} = I^*; \qquad t = 2.29 \sqrt[3]{\frac{I^*}{b}}$$

where b is the selected width of the new section.

B7. 3. 4. 2 Sandwich Shells

The basic philosophy which the analyst applies to a sandwich structure is precisely the same as he would apply to any structural element. This procedure consists of determining a set of design allowables with which the set of applied loads is compared.

TABLE B7. 3. 4-1 TRANSFORMED SECTION METHOD

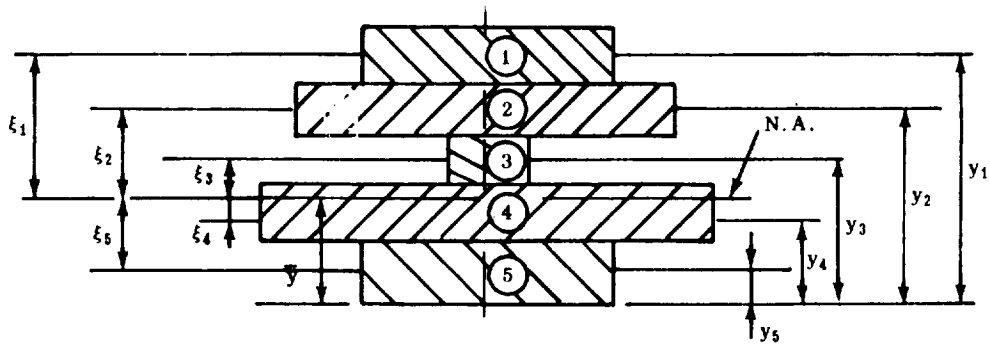

Element	A_i	E_i	$n_i = \frac{E_i}{E^*}$	$A_i^* = n_i A_i$	y_i	$A_i^* y_i$	ξ_i	$A_i^* \xi_i^2$	$A_i^* t_i^2$
①									
②									
③									
.									
.									
.									
				ΣA_i^*		$\Sigma A_i^* y_i$		$\Sigma A_i^* \xi_i^2$	$\Sigma A_i^* t_i^2$

$$\bar{y} = \frac{\Sigma A_i^* y_i}{\Sigma A_i}$$

$$I^* = \Sigma A_i^* \xi^2 + \frac{1}{12} \Sigma A_i^* t_i^2$$

Generally, two types of "allowables" data exist. The first type is determined by simple material tests and is associated with material more than with geometry, and the second type is dependent upon the geometry of the element. If, in a sandwich construction, the materials of construction are considered to be the core, facings, and bonding media, the basic material properties would be associated with the properties of these three independent elements.

The second class of allowables data is distinguished by being dependent upon configuration as well as upon the basic properties of the facings, core, and bond media. This class of failure modes may be further subdivided into modes of failure that include the entire configuration, and those modes that are localized to a portion of the structure but still limit the overall load-carrying capacity.

The most important local modes of failure are dimpling, wrinkling, and crimping. These modes of failure are dependent upon the local geometry and upon the basic properties of the materials of the sandwich. The general modes of failure generally are associated with the buckling strength of sandwich structural elements. This will be discussed in Section B7. 4.

In this paragraph, the general design of sandwich shells under pure static conditions will be presented. Two fundamental cases will be recognized:

1. Shear deformations can be neglected.

2. Shear deformations are extensive; however, shear can be taken by the core. No new basic theories are required, only the application of established theory. Once the shear deformation is properly included in the analysis, the analysis is complete.

The first logical approximation would be to replace actual sandwich with orthotropic material. The concepts of orthotropy actually may cover not only the large family of sandwiches, but also other materials such as corrugated shells, etc.

To give a systematical description of orthotropic analysis, attention will again be directed to the mathematical structure of the analytical formulas for the monocoque shells presented earlier in this section. This will make clear what kind of modifications can be made to apply the same formulas (that were derived for monocoque material) to the orthotropic shells.

B7. 3. 4. 3 Orthotropic Shells

A material is orthotropic if the characteristics of the materials are not the same in two mutually orthogonal directions (two-dimensional space). Such material has different values for E, G, and μ for each direction. Poisson's ratio, μ, also may be different in the case of bending and axial stresses. In the majority of cases this difference is negligible, but to distinguish one from the other, μ will be designated for Poisson's ratio which corresponds to bending stresses, and μ' for axial stresses. The behavior of the shell under loading is a function of certain constants that depend upon the previously mentioned material constants and geometry. The special case of orthotropy is isotropy (the material characteristics in both directions of two-dimensional space are the same). To see the dependence of stresses and deformations in shells upon previously mentioned constants, a short review of isotropic concepts of shells is provided. These constants are designated with extensional and bending rigidities.

I Extensional and Bending Rigidities

In the past, only isotropic monocoque shells were considered, and numerous formulas were presented. The definitions for isotropic shells are as follows:

Extensional rigidity

$$B = \frac{Et}{1 - \mu^2}$$

Bending rigidity

$$D = \frac{Et^3}{12(1 - \mu^2)}$$

B and D have appeared in many previous formulas.

The following characteristic stress formulas apply for rotationally symmetric thin shells:

$$N_\phi = B\left(\epsilon_\phi + \mu\epsilon_\theta\right)$$

$$N_\theta = B\left(\epsilon_\theta + \mu\epsilon_\phi\right) \quad .$$

The bending loads are

$$M_\phi = -D\left(\frac{1}{R_\phi}\frac{d}{d\phi} + \mu\frac{\beta}{R_\theta}\cot\phi\right)$$

$$M_\theta = D\left(\frac{\beta}{R_\theta}\cos\phi + \mu\frac{1}{R_\phi}\frac{d\beta}{d\phi}\right) \quad .$$

The final stresses can be obtained as follows:

$$\sigma_\phi = \frac{E}{1-\mu^2}\left(\frac{N_\phi}{B} + \frac{M_\phi}{D}z\right) \qquad (1)$$

$$\sigma_\theta = \frac{E}{1-\mu^2}\left(\frac{N_\theta}{B} - \frac{M_\theta}{D}z\right) \quad .$$

For a monocoque section of rectangular shape

$$\sigma_\phi = \frac{N_\phi}{t} + \frac{M_\phi}{\frac{t^3}{12}}z \qquad (2)$$

$$\sigma_\theta = \frac{N_\theta}{t} - \frac{M_\theta}{\frac{t^3}{12}} \quad .$$

The physical meaning of D and B is obvious if equations (1) and (2) are compared.

The componental stresses due to membrane forces are

$$1\sigma_{\phi} = \frac{EN_{\phi}}{(1-\mu^2)B} = \frac{E}{1-\mu^2} \cdot N_{\phi} \frac{1-\mu^2}{Et} = \frac{N_{\phi}}{1 \times t} = \frac{N_{\phi}}{A}$$

$$1\sigma_{\theta} = \frac{EN_{\theta}}{(1-\mu^2)B} = \frac{E}{1-\mu^2} \cdot N_{\theta} \frac{1-\mu^2}{Et} = \frac{N_{\theta}}{1 \times t} = \frac{N_{\theta}}{A}$$

where

$$A = 1 \times t \quad .$$

It is convenient to choose the width of the section strip that is equal to unity.

The componental stresses due to bending:

$$2\sigma_{\phi} = \frac{M_{\phi} z}{D} \cdot \frac{E}{1-\mu^2} = M_{\phi} z \frac{E}{(1-\mu^2)} \frac{12(1-\mu^2)}{Et^3} = \frac{12M_{\phi} z}{1 \times t^3} = \frac{M\phi z}{I}$$

$$2\sigma_{\theta} = \frac{M_{\theta} z}{D} \cdot \frac{E}{1-\mu^2} = M_{\theta} z \frac{E}{(1-\mu^2)} \frac{12(1-\mu^2)}{Et^3} = \frac{12M_{\theta} z}{1 \times t^3} = \frac{M_{\phi} z}{I}$$

where

$$I = \frac{1 \times t^3}{12} \quad .$$

Evidently, if stiffened or sandwich shell is being used, a modified B and D shall be used in the equations, then all previously derived equations for monocoque shells may be used for stiffened and sandwich shells. If the values from the "transformed section" are used, then

$$B = \frac{A^* E^*}{1-\mu^2} \quad ; \quad D = \frac{I^* E^*}{1-\mu^2} \quad .$$

In the preceding formulas $\mu' \approx \mu$ is assumed.

II Orthotropic Characteristics

Now the orthotropy is defined if, for two mutually orthogonal main directions, 1 and 2, the following constants are known or determined:

D_1, B_1, μ_1, μ_1' and shear rigidity D_{Q_1}

D_2, B_2, μ_2, μ_2' and shear rigidity D_{Q_2} .

To use the previously given formulas (for the isotropic case) for the analysis of the orthotropic structures, the formulas must be modified. For this purpose, a systematical modification of the primary and secondary solutions will be provided in the following paragraph to make possible the use of the unit-edge loading method for the orthotropic case. In the analysis of monocoque shells, the shear distortions usually are neglected. With sandwich, in most cases, such neglect is justified. The previously collected formulas for the isotropic case do not include the shear distortion. Consequently, orthotropic analyses which neglect the shear distortions will be examined first. Later, an additional study will be presented which considers the distortions due to the shear.

III Orthotropic Analysis, If Shear Distortions Are Neglected

A. Primary Solutions

It was previously stated that in most cases, the primary solutions are membrane solutions. For the purpose of interaction, the following set of values is needed (considering axisymmetrically loaded shells of revolution).

N_θ - membrane load in circumferential direction

N_ϕ - membrane load in meridional direction

u - displacement in the direction of tangent to the meridian

w - displacement in the direction of the normal-to-the-middle surface.

Actually, having u and w, any componental displacements can be obtained from the pure geometric relations if only the axisymmetrical cases are considered. Consequently, for this purpose, it will be adequate to investigate u and w.

To determine N_θ and N_ϕ, all formulas that were presented for the isotropic case can be used, because the membrane is a statically determinate system and independent of the material properties.

When N_θ and N_ϕ are obtained, u and w can be obtained in the following manner.

First determine the strains components (ϵ_ϕ and ϵ_θ). For the isotropic case, the correspondent formulas are

$$\epsilon_\phi = \frac{1}{Et}(N_\phi - \mu' N_\theta)$$

$$\epsilon_\theta = \frac{1}{Et}(N_\theta - \mu' N_\phi) \quad .$$

For the orthotropic case the same formulas may be written

$$\epsilon_\phi = \frac{1}{B_\phi(1 - \mu'_\phi \mu'_\theta)}(N_\phi - \mu'_\theta N_\theta)$$

$$\epsilon_\theta = \frac{1}{B_\theta(1 - \mu'_\theta \mu'_\phi)}(N_\theta - \mu'_\phi N_\phi) \quad .$$

Note: $D = B\frac{t^2}{12}$.

Displacement can now be obtained from the following differential equation:

$$\frac{du}{d\phi} - u \cot \phi = R_1 \epsilon_\phi - R_2 \epsilon_\theta = f(\phi) \quad .$$

The solution of the equation above is

$$u = \sin \phi \left(\int \frac{f(\phi)}{\sin \phi} \, d\phi + C \right)$$

where C is the constant of integration to be determined from the condition at the support. Then, the displacement (w) is obtained from the following equation:

$$\epsilon_\theta = \frac{u}{R_2} \cot \phi - \frac{w}{R_2} \quad .$$

Consequently, for every symmetrically loaded shell of revolution the stresses and deformations are determined for the orthotropic case.

B. Secondary Solutions

To obtain the secondary solutions, the formulas that were derived for the isotropic case can be used and then, using the substitution of proper constants, they can be transformed into formulas for the orthotropic case. Generally, due to any edge disturbance (unit loading) the formulas give direct solutions for

N_ϕ, N_θ, M_ϕ, M_θ, Q, β, and Δr

in the form of:

Solution = (edge disturbance) × (function of significant constant) × (function of geometry).

Cylindrical Shell - All formulas given in Tables B7. 3. 3-9 and B7. 3. 3-10 can be modified if the following replacement is made:

$$k = \frac{L}{\sqrt{Rt}} \sqrt[4]{3(1-\mu^2)} \rightarrow \frac{L}{2R} \sqrt{\frac{B_y\left(1-\mu_x\mu_\theta\right)}{D_x}}$$

$$D = \frac{Et^3}{12(1-\mu^2)} \rightarrow D_x = \frac{E_x t^3}{12(1-\mu_1\mu_2)}$$

$$B = \frac{Et}{1-\mu^2} \rightarrow B_y = \frac{E_y t}{1-\mu_x'\mu_y'}$$

$$D = B\frac{t^2}{12} \quad .$$

E_x = the modulus of elasticity in longitudinal direction.

E_y = the modulus of elasticity in circumferential direction.

IV Orthotropic Analysis, If Shear Distortions Are Included

For this more complicated case, the solution may be found in Reference 4, which was considered as the basis for Paragraphs IV and V. Cylinders and spheres only are are considered herein.

A. Cylindrical Shell

In the case of a cylinder constructed from a sandwich with relatively low traverse shear rigidity, the shear distortion may not be negligible; therefore, an analysis is presented which includes shear distortion for a symmetrically loaded orthotropic sandwich cylinder.

The following nomenclature is used:

D_x, D_y = Flexural stiffnesses of the shell wall per inch of width of orthotropic shell in axial and circumferential directions, respectively (in. -lb).

D_{Q_x} = Shear stiffness in x-z plane per inch of width (lb/in.)

B_x, B_y = Extensional stiffnesses of orthotropic shell wall in axial and circumferential directions, respectively (lb/in.).

M_x = Moment acting in x direction (in.-lb/in.).

Q_x = Transverse shear force acting in x-z plane (lb/in.).

μ_x, μ_y = Poisson's ratio associated with bending in x and y directions, respectively.

μ_x', μ_y' = Poisson's ratio associated with extension in x and y directions, respectively.

The derived solutions are presented in Tables B7.3.4-2 and B7.3.4-3.

B. Half Spheres

Based on Geckler's assumption for the half sphere, all formulas derived for cylinders can be adapted for the spherical shell as well.

V Influence of Axial Forces on Bending in Cylinder

Usually it is assumed that the contribution of the axial force (N_0) to the bending deflection is negligible; however, for a cylinder with a relatively large radius, the axial force may significantly contribute to the bending deflection. Therefore, the preceding analysis was extended by the same author (Reference 4) to include the effect of the axial force on the deflections. This leads to modification of the formulas (Tables B7.3.4-2 and B7.3.4-3) in the manner shown in Table B7.3.4-4. The constants are slightly modified as follows:

$$\alpha^2 = \frac{\left[\frac{B_y\left(1-\mu_x'\mu_y'\right)}{D_{Q_x}}\frac{1}{R^2} + \frac{N_0}{D_x}\right]}{4\left[1+\frac{N_0}{D_{Q_x}}\right]}$$

TABLE B7. 3. 4–2 INFLUENCE COEFFICIENTS DUE TO EDGE LOADING M_0 IN ORTHOTROPIC CYLINDER

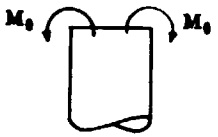

Constants

$$\alpha^2 = \frac{B_y\left(1 - \mu'_x\mu'_y\right)}{4D_{Q_x}R^2} \qquad \beta^4 = \frac{B_y\left(1 - \mu'_x\mu'_y\right)}{4D_xR^2} \qquad D = D_x$$

	$\alpha^4 - \beta^4 > 0$	N0*	$\alpha^4 - \beta^4 = 0$	N0*	$\alpha^4 - \beta^4 < 0$	N0*
w	$\frac{M_0}{D(A_2 - A_1)}\left[\frac{A_2}{4\alpha^2 - A_1^2}\,e^{-A_1x} + \frac{A_1}{A_2^2 - 4\alpha^2}\,e^{-A_2x}\right]$	1	$\left[\frac{e^{mx}}{2\alpha^2} + \frac{xe^{mx}}{m}\right]\left(-\frac{M_0}{D}\right)$	4	$\frac{e^{-Vx}}{2D\beta^4}M_0\left(-\beta^2\cos Px + \frac{V}{P}\beta^2\sin Px\right)$	7
M_x	$M_0\left(\frac{A_2e^{-A_1x} - A_1e^{-A_2x}}{A_2 - A_1}\right)$	2	$e^{mx}M_0(1 - mx)$	5	$\frac{e^{-Vx}}{P}M_0(P\cos Px + V\sin Px)$	8
Q_x	$M_0\left(\frac{-A_1A_2e^{-A_1x} + A_1A_2e^{-A_2x}}{A_2 - A_1}\right)$	3	$-2\alpha^2e^{mx}xM_0$	6	$-\frac{e^{-Vx}}{P}M_0\sin Px(V^2 + \mu^2)$	9
Constants:	$A_1 = \left[2\alpha^2 + 2(\alpha^4 - \beta^4)^{1/2}\right]^{1/2}$ $A_2 = \left[2\alpha^2 - 2(\alpha^4 - \beta^4)^{1/2}\right]^{1/2}$		$m = -(2)^{1/2}\alpha$		$V = (\beta^2 + \alpha^2)^{1/2}$ $P = (\beta^2 - \alpha^2)^{1/2}$	
	Influence Coefficients for the Displacements and Rotation at the Edge of the Shell					
$w_x = 0$	$-M_0/2\beta^2D$					10
$\left[\frac{dw}{dx}\right]_{x=0}$	$(M_0/D^2)(\alpha^2 + \beta^2)^{1/2}$					11

TABLE B7.3.4-3 INFLUENCE COEFFICIENTS DUE TO EDGE LOADING Q_0 IN ORTHOTROPIC CYLINDER

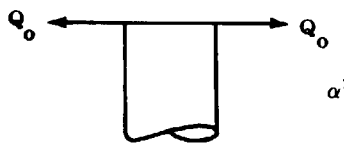

Constants

$$\alpha^2 = \frac{B_y\left(1 - \mu'_x \mu'_r\right)}{4D_{Q_x} R^2} \; ; \quad \beta^4 = \frac{B_y\left(1 - \mu'_x \mu'_y\right)}{4D_x R^2} \; ; \quad D = D_x$$

	$\alpha^4 - \beta^4 > 0$	N_0*	$\alpha^4 - \beta^4 = 0$	N_0*	$\alpha^4 - \beta^4 < 0$	N_0*
w	$\frac{Q_0}{D(A_2 - A_1)}\left[\frac{e^{-A_1 x}}{4\alpha^2 - A_1^2} + \frac{e^{-A_2 x}}{A_2^2 - 4\alpha^2}\right]$	12	$\frac{Q_0}{D\alpha^2}\left[\frac{e^{mx}}{m} + \frac{xe^{mx}}{2}\right]$	15	$\frac{e^{-Vx}}{2D\beta^4} Q_0 \left(\frac{\alpha^2}{P} \sin Px - V \cos Px\right)$	18
M_x	$Q_0\left[\frac{e^{-A_1 x} - e^{-A_2 x}}{A_2 - A_1}\right]$	13	$e^{mx} x Q_0$	16	$\frac{e^{-Vx}}{P} Q_0 \sin Px$	19
Q_x	$Q_0\left[\frac{-A_1 e^{-A_1 x} + A_2 e^{-A_2 x}}{A_2 + A_1}\right]$	14	$e^{mx} Q_0\left[1 + mx\right]$	17	$\frac{e^{-Vx}}{P} Q_0\left[P \cos Px - V \sin Px\right]$	20
Constants	$A_1 = \left[2\alpha^2 + 2(\alpha^4 - \beta^4)^{1/2}\right]^{1/2}$ $A_2 = \left[2\alpha^2 - 2(\alpha^4 - \beta^4)^{1/2}\right]^{1/2}$		$m = -(2)^{1/2} \alpha$		$V = (\beta^2 + \alpha^2)^{1/2}$ $P = (\beta^2 - \alpha^2)^{1/2}$	
Influence Coefficients for the Displacements and Rotation at the Edge of the Shell						
$w_x = 0$	$-Q_0 \frac{(\beta^2 + \alpha^2)^{1/2}}{2\beta^4 D}$					21
$\left[\frac{dw}{dx}\right]_{x=0}$	$Q_0 \frac{2\alpha^2 + \beta^2}{2D\beta^4}$					22

TABLE B7.3.4-4 MODIFICATION OF TABLES B7.3.4-2 AND -3 TO INCLUDE THE EFFECTS OF AXIAL FORCES ON BENDING

Formula	Quantities: (Formulas in Tables B7.3.4-2 and -3)	Substitute
1	$(4\alpha^2 - A_1^2)$	$(4\gamma^2 - A_1^2)$
	$(A_2^2 - 4\alpha^2)$	$(A_2^2 - 4\gamma^2)$
4	Whole Formula	$w = \frac{e^{mx} M_0}{D(m^2 - 4\gamma^2)^2}\left[(4\gamma^2 - 3m^2) + (m^2 - 4\gamma^2)mx\right]$
6	$2\alpha^2 M_0 x$	$m^2 M_0$
7	Whole Formula	$w = \frac{M_0 e^{-sx}}{2VD}\left[(S^2 + \gamma^2)\cos Px + \frac{S}{P}(\gamma^2 + P^2)\sin Px\right]$
8	V	S
9	V	S
10	Whole Formula	$w_{x=0} = (-M_0/2VD)(2\alpha^2 + \beta^2 - 2\gamma^2)$
11	Whole Formula	$\left[\frac{dw}{dx}\right]_{x=0} = (M_0/P^2/VD)(\alpha^2 + \beta^2)^{1/2}$
12	$(4\alpha^2 - A_1^2)$	$(4\gamma^2 - A_1^2)$
	$(A_2^2 - 4\alpha^2)$	$(A_2^2 - 4\gamma^2)$
15	Whole Formula	$w = \frac{e^{mx} Q_0}{D(m^2 - 4\gamma^2)^2}\left[2m - (m^2 - 4\gamma^2)x\right]$
18	Whole Formula	$w = \frac{Q_0 e^{-sx}}{2VD}\left[\frac{\gamma^2}{P}\sin Px - S\cos Px\right]$
19	V	S
20	V	S
21	Whole Formula	$(-Q_0/2VD)(\alpha^2 + \beta^2)^{1/2}$
22	Whole Formula	$\left(\frac{dw}{dx}\right)_{x=0} = \frac{Q_0}{2VD}(\beta^2 + 2\gamma^2)$

$$\beta^4 = \frac{B_y\left(1 - \mu'_x \mu'_y\right)}{4 D_x R^2 \left[1 + \frac{N_0}{D_{Q_x}}\right]}$$

$$\gamma^2 = \frac{B_y\left(1 - \mu'_x \mu'_y\right)}{4 D_{Q_x} R^2} \quad ; \quad V = 4\gamma^4 - 4\gamma^2 \alpha^2 + \beta^4$$

$$S = (\beta^2 + \alpha^2)^{1/2}$$

$$D = D_x$$

B7. 3. 5 UNSYMMETRICALLY LOADED SHELLS

Until now, the axisymmetrical cases have been treated with respect to the geometry, material, and loading. The "unit-load method" was exclusively used for the solution. It was shown that the most complex solutions are applied to the shells without symmetry, loaded unsymmetrically. The first level of simplification of the complex procedures would be the usage of axisymmetric shell loaded unsymmetrically.

The scope of this manual does not permit presentation of the actual derivations, but solutions for the most commonly appearing cases in engineering will be presented in the remaining tables.

The shells are assumed to be thin enough to use the membrane theory. These tables of solutions also provide the necessary information about the loading and geometry.

B7. 3. 5. 1 Shells of Revolution

The first level of simplification of the complex procedures would be axisymmetric shells loaded unsymmetrically. Similarly, symmetrical shells may have unsymmetrical boundaries, which will cause the symmetrical loading to be no longer symmetrical.

Table B7. 3. 5-1 presents some solutions for certain loadings for spherical, conical, and cylindrical shells loaded unsymmetrically.

B7. 3. 5. 2 Barrel Vaults

This paragraph presents the collection of different solutions for curved panels of simple beam system. The geometry of curved panels is circular, elliptical, cycloidal, parabolic, catenary, and special shape. The solutions for different loadings are given in Tables B7. 3. 5-2, B7. 3. 5-3, and B7. 3. 5-4. The shells under consideration are thin, and linear theory was the basis for the derived formulas.

TABLE B7.3.5-1 SPHERE, CONE, AND CYLINDER LOADED BY WIND LOADING

	$Z = P_w \sin\phi \cos\theta$	$Z = P_w \sin\phi \cos\theta$	$Z = P_w \sin\phi \cos\theta$ Conical Shell Supported at the Vertex of the Cone with Free Edge	$Z = P_w \cos\theta$
	Circumferential Direction N_ϕ	$N_{\theta\phi}$	N_θ	Differential Element N_ϕ, N_θ, $N_{\theta\phi}$
N_{ϕ}	$-p_w \frac{R}{3} \frac{\cos\theta\cos\phi}{\sin^3\phi}\left[3(\cos\phi_0 - \cos\phi) - (\cos^3\phi_0 - \cos^3\phi)\right]$ For $\phi_0 = 0$ (No Opening) $-p_w \frac{R}{3} \frac{\cos\theta\cos\phi}{\sin^3\phi}(2 - 3\cos\phi + \cos^3\phi)$	$-p_w \frac{x}{2}\left[\cos\phi - \frac{1}{3\cos\phi} - \frac{x_0^3}{x^3}\cdot\left(\cos\phi - \frac{1}{\cos\phi}\right) - \frac{x_0^3}{x^3}\frac{2}{3\cos\phi}\right]\cos\theta$ For $\phi_0 = 0$ (Complete Cone) $-p_w \frac{x}{2}\left(\cos\phi - \frac{1}{3\cos\phi}\right)\cos\theta$	$p_w\left[\frac{\ell^3 - x^3}{3x^3} - \frac{\ell^2 - x^2}{2x}\sin^2\phi\right]\frac{\cos\theta}{\cos\phi}$	$p_w \frac{x}{2R}\cos\theta$
N_{θ}	$-p_w \frac{R}{3} \frac{\sin\theta}{\sin^3\phi}\left[3(\cos\phi_0 - \cos\phi) - (\cos^3\phi_0 - \cos^3\phi)\right]$ For $\phi_0 = 0$ (No Opening) $-p_w \frac{R}{3} \frac{\sin\theta}{\sin^2\phi}(2 - 3\cos\phi + \cos^3\phi)$	$-p_w \frac{x^3 - x_0^3}{3x^2}\sin\theta$ For $x_0 = 0$ (Complete Cone) $-p_w \frac{x}{3}\sin\theta$	$p_w \frac{\ell^3 - x^3}{3x^2}\sin\theta$	$-p_w x \sin\theta$
N_{θ}	$p_w \frac{R}{3} \frac{\cos\theta}{\sin^3\phi}\left[\cos\phi(3\cos\phi_0 - \cos^3\phi_0) - 3\sin^2\phi - 2\cos^4\phi\right]$ For $\phi_0 = 0$ (No Opening) $p_w \frac{R}{3} \frac{\cos\theta}{\sin^3\phi}(2\cos\phi - 3\sin^2\phi - 2\cos^4\phi)$	$-p_w x \cos\phi\cos\theta$ For $x_0 = 0$ (Complete Cone) $-p_w x \cos\phi\cos\theta$	$-p_w x \cos\phi\cos\theta$	$-p_w R \cos\theta$

TABLE B7.3.5-2 CURVED CIRCULAR PANELS, BARREL VAULTS

Deadweight Loading (q) $X = 0$, $Y = q \sin \phi$, $Z = q \cos \phi$

Uniform Load on Projected Area

Loading $X = 0$, $Y = p \sin \phi \cos \phi$, $Z = p \cos^2 \phi$

Internal Forces

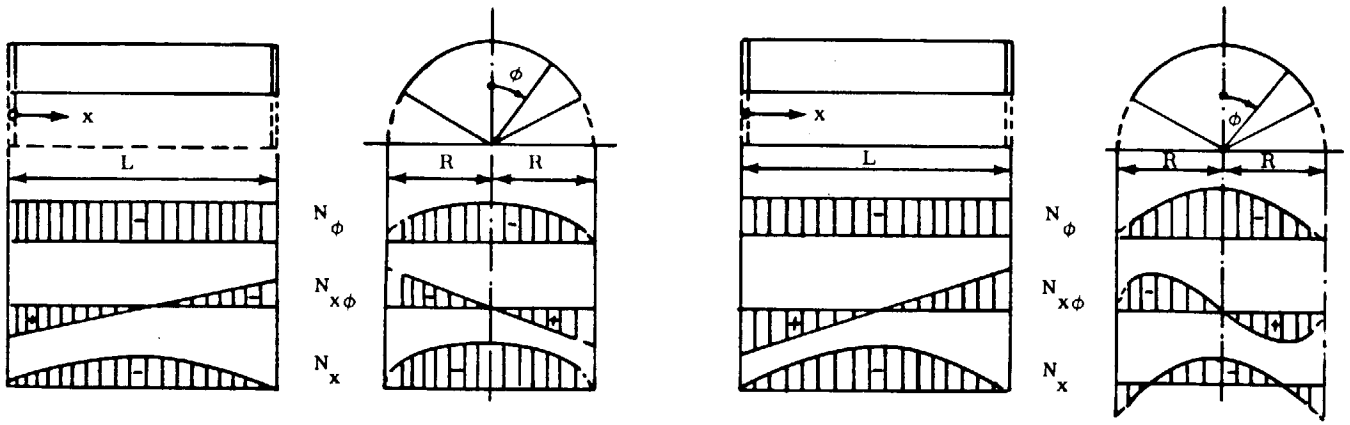

N_ϕ	$-qR\cos\phi$	$-pR\cos^2\phi$	At $\phi = 45°$
$N_{x\phi}$	$q(L-2x)\sin\phi = N_{\phi x}$	$N_{\phi x} = \frac{3}{4}p(L-2x)\sin 2\phi$	$N_x = 0$
N_x	$-\frac{qx}{R}(L-x)\cos\phi$	$-\frac{3p}{2R}\times(L-x)\cos 2\phi$	$N_{x\phi}$ = max

TABLE B7. 3. 5-3 CURVED ELLIPTICAL AND CYCLOIDAL PANELS, BARREL VAULTS

Elliptical Panel, Deadweight Loading	Cycloidal Panel, Deadweight Loading
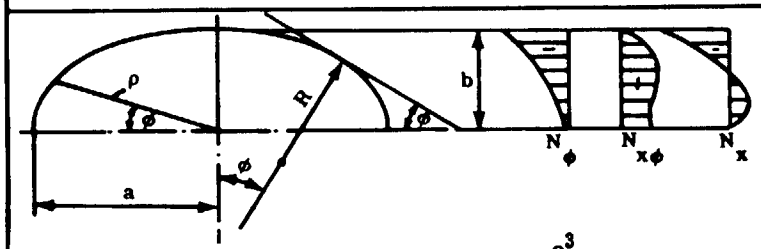	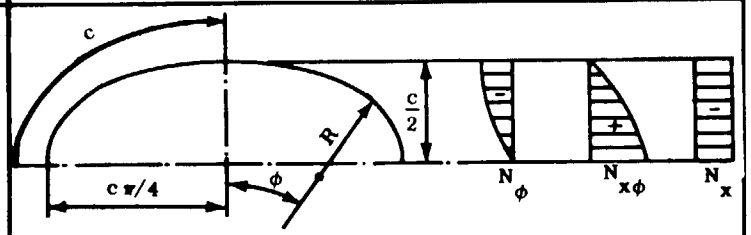
The Radius of Curvature: $R = \frac{\rho^3}{ab}$ Where $\rho = ab/(a^2 \sin^2 \phi + b^2 \cos^2 \phi)^{1/2}$ Loading Components: $X = O,\ Y = q \sin \phi,\ Z = q \cos \phi$ (For x and L, See Ref. 2)	The Radius of Curvature $R = c \cos \phi$ Loading Components: $X = O,\ Y = q \sin \phi,$ $Z = q \cos \phi$
N_ϕ $-\frac{q\rho^3}{ab} \cos \phi$	$-q\,c \cos^2 \phi$
$N_{x\phi}$ $\frac{q}{2}(L - 2x)\left(2 + 3\frac{a^2 - b^2}{a^2b^2}\rho^2 \cos^2 \phi\right)\sin \phi$	$\frac{3}{2}q(L - 2x) \sin \phi$
N_x $-\frac{q}{2}x(L - x)\frac{ab}{\rho^3}\left[2 + 3\frac{a^2 - b^2}{a^2b^2}\rho^2\left(\cos^2 \phi - 2\frac{\rho^2}{b^2}\sin^2 \phi\right)\right]\cos \phi$	$-\frac{3q}{2c}x(L - x)$

TABLE B7.3.5-4 BARREL VAULTS

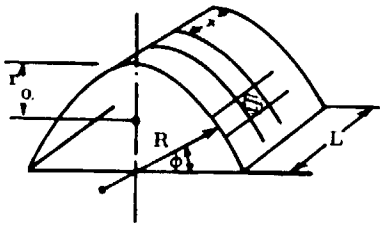

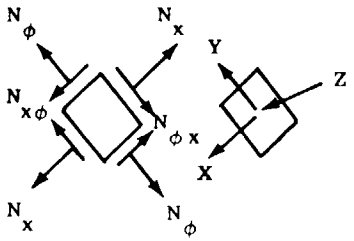

N_x, N_ϕ Unit Normal Forces

$N_{\phi x}$ Unit Central Shear

X, Y, Z Surface Load Components

Boundary Conditions: $N_x = 0$ for $x = 0$ and $x = L$

Shell	Loading	M_x	N_ϕ	$N_{\phi x}$
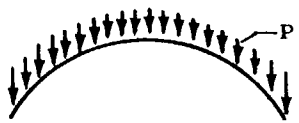 Circle	$Y = -p \cos \phi$ $Z = p \sin \phi$	$-p \frac{x}{R} (L - x) \sin \phi$	$-p R \sin \phi$	$-p(L - 2x) \cos \phi$
 Circle	$Z = p_w \cos \phi$	$-p_w \frac{x}{2R} (L - x) \cos \phi)$	$-p_w R \cos \phi$	$p_w\left(\frac{L}{2} - x\right) \sin \phi$
 Parabola	$Y = -p \cos \phi$ $Z = p \sin \phi$	$p \frac{x}{2r_0} (L - x) \sin^4 \phi$	$-p \frac{r_0}{\sin^2 \phi}$	$p\left(\frac{L}{2} - x\right) \cos \phi$

TABLE B7. 3. 5-4 BARREL VAULTS (Continued)

Shell	Loading	N_x	N_ϕ	$N_{x\phi}$
Parabola 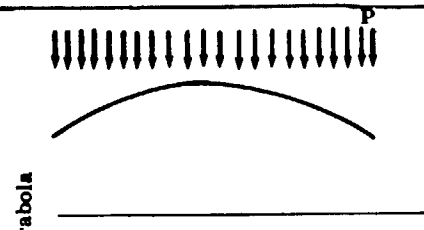	$Y = p \sin\phi \cos\phi$ $Z = p \sin^2\phi$	0	$-p \frac{r_\theta}{\sin\phi}$	0
Parabola 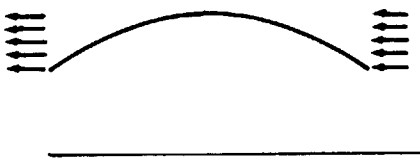	$Z = p_w \cos\phi$	$p_w \frac{x}{2r_\theta}(L - x) \sin\phi \cos\phi \times (3 + 2\sin^2\phi)$	$-p_w r_\theta \frac{\cos\phi}{\sin^3\phi}$	$p_w\left(\frac{L}{2} - x\right)\frac{1 + 2\cos^2\phi}{\sin\phi}$
Cycloid 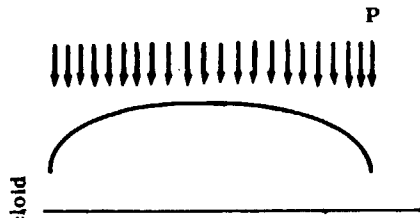	$Y = -p \sin\phi \cos\phi$ $Z = p \sin^2\phi$	$p \frac{2x}{r_\theta}(L - x) \frac{1 - 2\sin^2\phi}{\sin\phi}$	$-p r_\theta \sin^2\phi$	$-p\left(\frac{L}{2} - x\right) 4 \sin\phi \cos\phi$
Cycloid 	$Z = p_w \cos\phi$	$-p_w \frac{x}{r_\theta}(L - x) \times (1 - \cos\phi) \frac{\cos\phi}{\sin^2\phi}$	$-p_w r_\theta \sin\phi \cos\phi$	$-p_w\left(\frac{L}{2} - x\right)\frac{1 - 2\sin^2\phi}{\sin\phi}$

TABLE B7.3.5-4 BARREL VAULTS (Continued)

Shell	Loading	N_x	N_ϕ	$N_{x\phi}$
Elliptic: 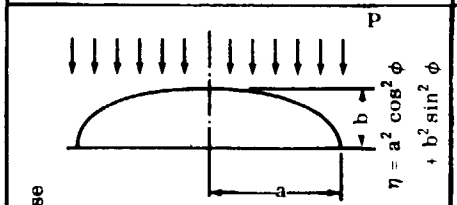	$Y = -p \sin \phi \cos \phi$ $Z = p \sin^2 \phi$	$-p \frac{3\pi (L-x)}{2a^2 b^2 \eta^{1/2}} \times$ $\left[b^2 (a^2 \cos^2 \phi - b^2 \sin^2 \phi) + 2\eta^2 (\sin^2 \phi - \cos^2 \phi)\right]$	$-p a^2 b^2 \frac{\sin^2 \phi}{\eta^{3/2}}$	$p\left(\frac{L}{2} - x\right) \times$ $\frac{3 \sin \phi \cos \phi}{\eta} (b^2 - 2\eta)$
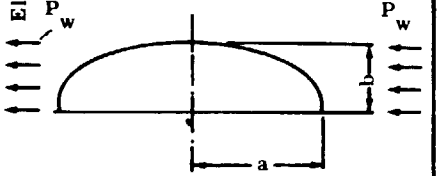	$Z = p_w \cos \phi$	$-p_w \frac{x}{2} \frac{(L-x) \cos \phi}{a^2 b^2 \eta^{1/2}} \left[\eta^2 + 3\eta(b^2 - a^2)(1 - 3 \sin^2 \phi) - 6(b^2 - a)^2 \sin^2 \phi \cos^2 \phi\right]$	$-p_w a^2 b^2 \frac{\cos \phi}{\eta^{3/2}}$	$p_w\left(\frac{L}{2} - x\right) 3 \frac{b^2 - a^2}{\eta} \times$ $(1 + \cos^2 \phi) \sin \phi$
Catenary: 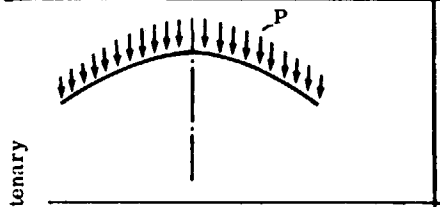	$Y = -p \cos \phi$ $Z = p \sin \phi$	0	$-p \frac{r_\theta}{\sin \phi}$	0
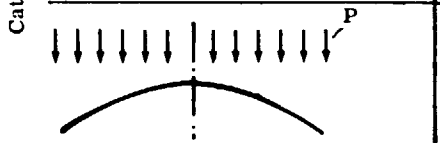	$Y = -p \sin \phi \cos \phi$ $X = p \sin^2 \phi$	$p \frac{x}{2r_\theta} (L - x) \sin^2 \phi \times$ $(1 - 2 \sin^2 \phi)$	$-pr_\theta$	$-p\left(\frac{L}{2} - x\right) \sin \phi \cos \phi$

TABLE B7.3.5-4 BARREL VAULTS (Concluded)

Shell	Loading	N_x	N_ϕ	$N_{x\phi}$
Catenary 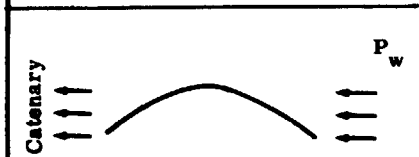	$Z = p_w \cos\phi$	$p_w \frac{x}{2r_\theta}(L - x)(2 + \sin^2\phi)\cos\phi$	$-p_w r_\theta \frac{\cos\phi}{\sin^2\phi}$	$p_w\left(\frac{L}{2} - x\right)\frac{1 + \cos^2\phi}{\sin\phi}$
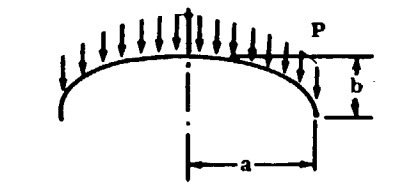	$Y = -p\cos\phi$ $Z = p\sin\phi$	$p\frac{x(L-x)(\gamma + \pi/4)}{2a(\gamma + \sin\phi)^3}\cdot\left[\gamma(1 - 6\sin^2\phi) - (2\gamma^2 + 3\sin^2\phi)\sin\phi\right]$	$-p\frac{a}{\gamma + \pi/4}(\gamma + \sin\phi)\sin\phi$	$p\left(x - \frac{L}{2}\right)\frac{(2\gamma + 3\sin\phi)\cos\phi}{\gamma + \sin\phi}$
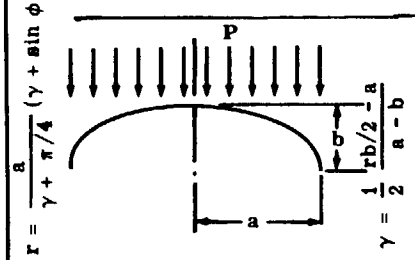	$Y = -p\sin\phi\cos\phi$ $Z = p\sin^2\phi$	$p\frac{x(L-x)(\gamma + \pi/4)}{2a(\gamma + \sin\phi)^3}\cdot\left[\gamma(8 - 15\sin^2\phi)\sin\phi + (3\gamma^2 + 4\sin^2\phi) - (1 - 2\sin^2\phi)\right]$	$p\frac{a}{\gamma + \pi/4}(\gamma + \sin\phi)\sin^2\phi$	$p\left(x - \frac{L}{2}\right)\frac{(3\gamma + 4\sin\phi)\sin\phi\cos\phi}{\gamma + \sin\phi}$
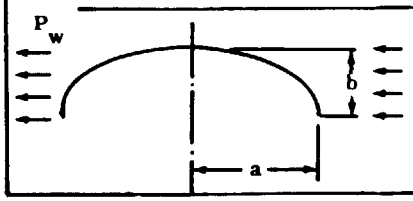	$Z = p_w\cos\phi$	$-p_w\frac{x(L-x)(\gamma + \pi/4)}{2a(\gamma + \sin\phi)^3}\cos\phi(1 + \gamma^2 + \sin^2\phi + 4\gamma\sin\phi)$	$-p_w\frac{a}{\gamma + \pi/4}(\gamma + \sin\phi)\cos\phi$	$p_w\left(x - \frac{L}{2}\right)\frac{1 + 2\sin^2\frac{L}{2} + 2\sin\phi}{\gamma + \sin\phi}$

REFERENCES

1. Timoshenko, S. P., and Woinowsky-Krieger, S., Theory of Plates and Shells. New York, McGraw-Hill Book Co., Inc., 1959.

2. Baker, E. H., Cappelli, A. P., Kovalevsky, L., Rish, F. L., and Verette, R. M., Shell Analysis Manual. North American Aviation, Inc., SID 66-398, June 1966.

3. Lowell, H. H., Tables of the Bessel-Kelvin Functions Ber, Bei, Ker, Kei, and their Derivatives for the Argument Range 0(0.01) 107.50. NASA Technical Report R-32, 1959.

4. Baker, E. H., Analysis of Symmetrically Loaded Sandwich Cylinders. American Institute of Aeronautics and Astronautics.

SECTION B8

TORSION

B8.0.0 TORSION

Sections under B8 deal with the torsional analysis of straight structural elements that have longitudinal dimensions much greater than their cross-sectional dimensions. Such an element is called a bar.

The first division, Section B8.1, provides a common ground for the analytical divisions which follow: the solid cross section, treated in Section B8.2; the thin-walled closed cross section treated in Section B8.3; and the thin-walled open cross section, treated in Section B8.4.

In each of the divisions, the cross section under consideration will be defined, described, and pictorially represented. Particular conditions which are pertinent to the approach, such as restraints, will be stated; the basic theory, and limitations, if any, will be given.

SECTION B8.1

GENERAL

TABLE OF CONTENTS

B8.1.0 GENERAL

Section B8.1 presents the notation and sign convention for local coordinate systems, applied twisting moments, internal resisting moments, stresses, deformations, and derivations of angle of twist. These conventions will be followed in Sections B8.2, B8.3, and B8.4.

Restrained torsion and unrestrained torsion are considered for the thin-walled open and thin-walled closed cross sections, and unrestrained torsion is considered for the solid cross section. Restrained torsion requires that no relative longitudinal displacement shall occur between two similar points on any two similar cross sections. Warping is restrained.

Restrained torsion of solid cross sections is not considered because it is a localized stress condition and attenuates rapidly. The stresses and deformations determined by the methods contained in this section can be superimposed upon stresses and deformations caused by other types of loading if the deformations are small and the maximum combined stress does not exceed the yield stress of the material.

B8.1.1 NOTATION

All general terms used in this section are defined herein. Special terms are defined in the text as they occur.

a	Width of rectangular section, in.
A	Enclosed area of mean periphery of thin-walled closed section, $in.^2$
b	Length of element, width of flange, in.
b'	Width of flange minus thickness of web, in.
C	Length of wall centerline (circumference), in.
d	Total section depth, in.
D	Diameter of circular bar, in.
E	Young's modulus, $lb/in.^2$
G	Shear modulus of elasticity, $lb/in.^2$
h	Distance between flange centerlines, in.
I	Moment of inertia, $in.^4$
J	Polar moment of inertia, $in.^4$
K	Torsional constant, $in.^4$
L	Length of bar, in.
L_x	Arbitrary distance along x-axis from origin, in.
m_t	Applied uniform twisting moment or maximum value of varying applied twisting moment, in.-lb/in.
M_i	Internal twisting moment, in.-lb.
M_t	Applied concentrated twisting moment, in.-lb.
$M_{(x)}$	Internal twisting moment at point x along bar, written as function of x
p	Pressure, $lb/in.^2$

P	Arbitrary point on cross section
q	Shear flow, lb/in.
r	Radius of circular cross section, in.
R	Radius of circular fillet, in.
s	Distance measured along thin-walled section from origin, in.
S_t	Torsional modulus, $in.^3$
$S_w(s)$	Warping statical moment, $in.^4$
t	Thickness of element, in.
t_w	Thickness of web, in.
T	Tensile force per unit length, $lb/in.^2$
u	Displacement in the x direction, in.
v	Displacement in the y direction, in.
w	Displacement in the z direction, in.
$W_n(s)$	Normalized warping function, $in.^2$
V	Volume, $in.^3$
α	Defined in Section B8.4.1-IV
β	Defined in Section B8.4.1-IV
Γ	Warping constant, $in.^6$
γ	Shear strain
θ	Unit twist, rad/in. ($\theta = d\phi/dx = \phi'$)
μ	Poisson's ratio
ρ	Radial distance from the centroid of the cross section to arbitrary point P, in.
ρ_o	Radial distance to tangent line of arbitrary point P from shear center, in.

σ_x	Longitudinal normal stress, lb/in.^{2}
τ	Total shear stress, lb/in.^{2}
τ_t	Torsional shear stress, lb/in.^{2}
τ_ℓ	Longitudinal shear stress, lb/in.^{2}
τ_w	Warping shear stress, lb/in.^{2}
ϕ	Angle of twist, rad ($\phi = \int_0^{L_x} \theta dx$)
ϕ', ϕ'', ϕ'''	First, second, and third derivatives of angle of twist with respect to x, respectively
Φ	Saint-Venant stress function

Subscripts:

i	inside
l	longitudinal
n	normal
o	outside
s	point s
t	torsional or transverse
w	warping
x	longitudinal direction

The equation for β in terms of (b/d) is

$$\beta = \left[0.333 - \frac{0.21}{(b/d)}\left(1.0 - \frac{0.0833}{(b/d)^4}\right)\right] .$$

TABLE B8.2.2-1

b/d	1.0	1.5	2.0	2.5	3.0	4.0	6.0	10.0	100	∞
α	0.208	0.238	0.256	0.269	0.278	0.290	0.303	0.314	0.331	0.333
β	0.141	0.195	0.229	0.249	0.263	0.281	0.298	0.312	0.331	0.333

The stress distributions on different radial lines are shown in Figure B8.2.2-2A, and the resulting warping deformation at an arbitrary cross section located at distance L_x from the origin is shown in Figure B8.2.2-2B.

IV Elliptical Section

The maximum torsional shear stress occurs at point A (Fig. B8.2.2-3) and is determined by

$$\tau_t(\max) = M_t/S_t$$

where

$$S_t = \frac{\pi\, bd^2}{16} .$$

The torsional shear stress at point B is determined by

$$\tau_t(B) = \tau_t(\max)\left(\frac{b}{d}\right) .$$

The total angle of twist is determined by the following equation:

$$\phi(\max) = \frac{M_t L}{KG}$$

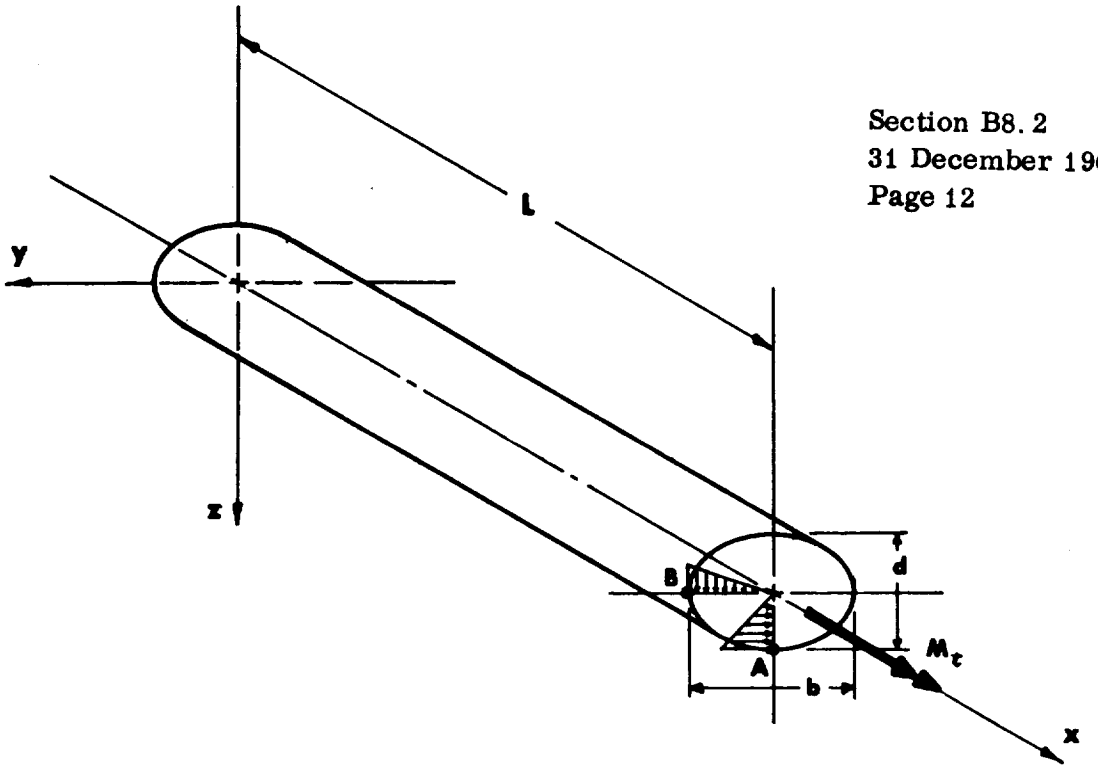

FIGURE B8.2.2-3 ELLIPTICAL CROSS SECTION

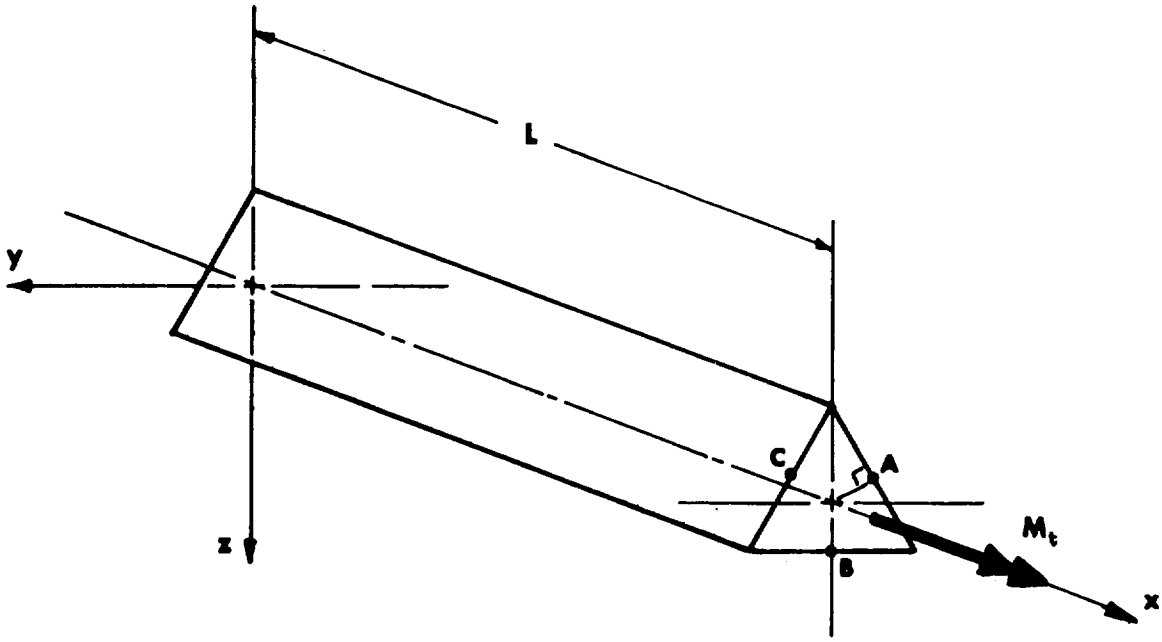

FIGURE B8.2.2-4 EQUILATERAL TRIANGULAR CROSS SECTION

where

$$K = \frac{\pi b^3 d^3}{16 (b^2 + d^2)} .$$

V Equilateral Triangular Section

The maximum torsional shear stress occurs at points A, B, and C (Figure B8.2.2-4) and is determined by

$$\tau_t(\max) = \frac{M_t}{S_t}$$

where

$$S_t = b^3/20.$$

The total angle of twist is determined by

$$\phi \max = \frac{M_t L}{KG}$$

where

$$K = \frac{b^4\sqrt{3}}{80} .$$

VI Regular Hexagonal Section

The approximate maximum torsional shear stress is determined by

$$\tau_t(\max) = M_t/S_t$$

where

$$S_t = 0.217Ad$$

and is located at the midpoints of the sides (Fig. B8.2.2-5). A is the cross-sectional area and d is the diameter of the inscribed circle.

The approximate total angle of twist is determined by

$$\phi \text{ (max)} = \frac{M_t L}{KG}$$

where

$$K = 0.133Ad^2 .$$

VII Regular Octagonal Section

The approximate maximum torsional shear stress is determined by

$$\tau_t(\text{max}) = M_t/S_t$$

where

$$S_t = 0.223Ad$$

and is located at the midpoints of the sides (Fig. B8.2.2-6). A is the cross-sectional area and d is the diameter of the inscribed circle.

The approximate total angle of twist is determined by

$$\phi \text{ (max)} = \frac{M_t L}{KG}$$

where

$$K = 0.130Ad^2 .$$

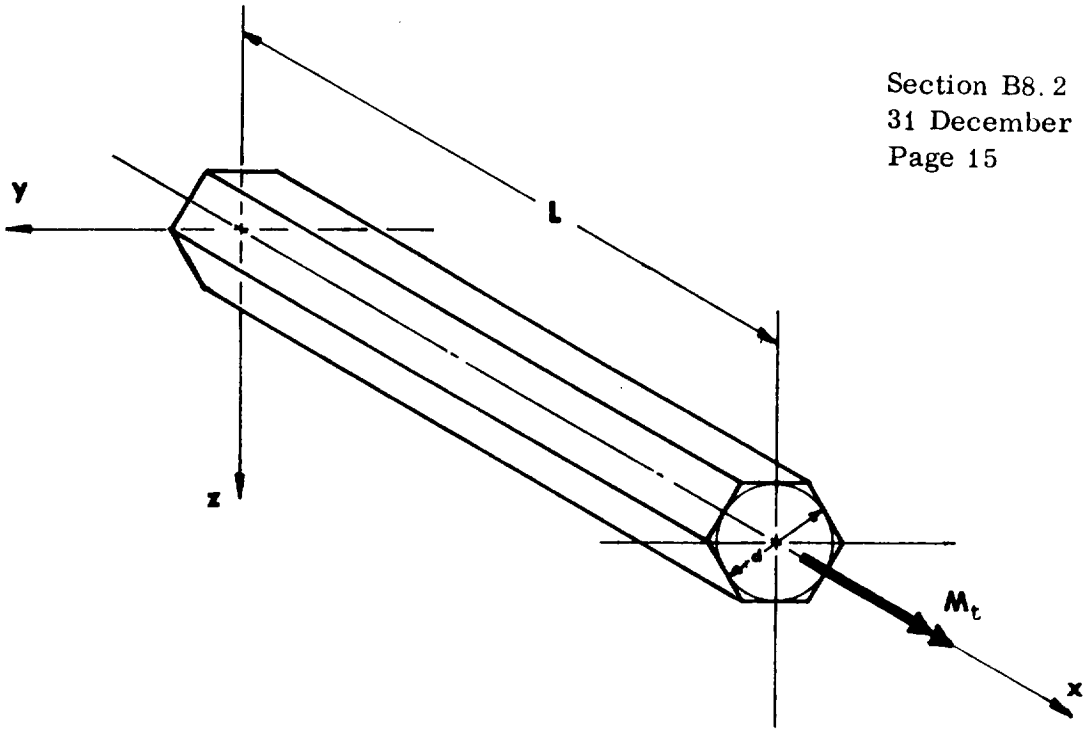

FIGURE B8.2.2-5 REGULAR HEXAGONAL CROSS SECTION

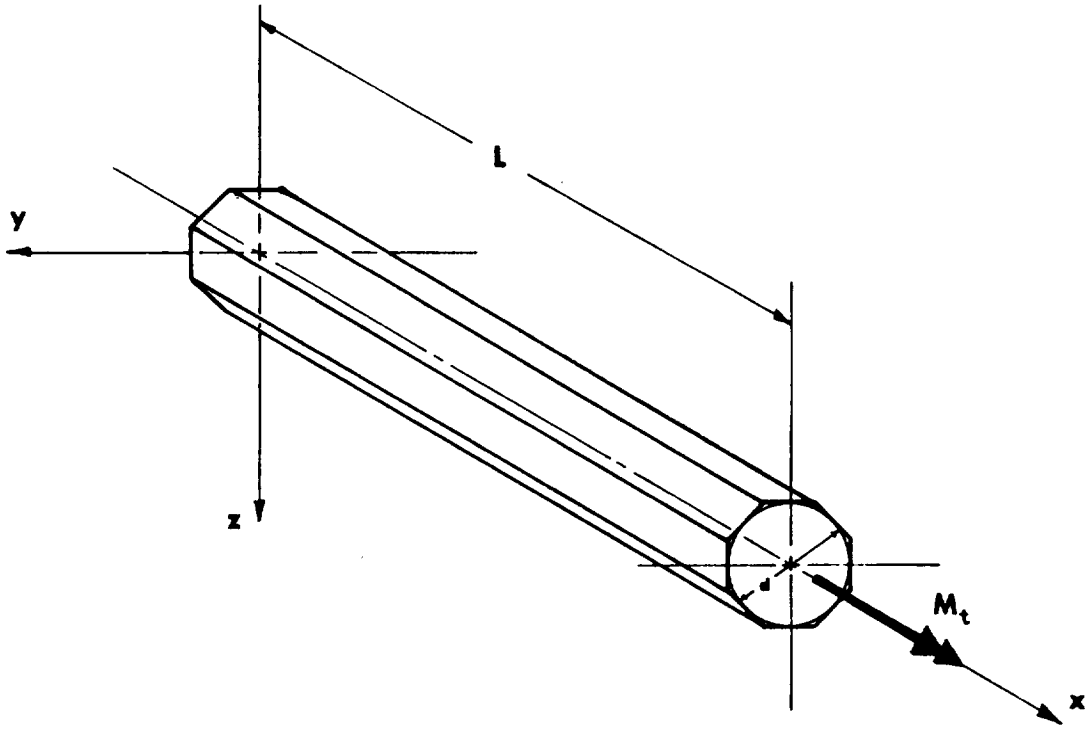

FIGURE B8.2.2-6 REGULAR OCTAGONAL CROSS SECTION

VIII Isosceles Trapezoidal Section

The approximate maximum torsional shear stress and total angle of twist can be determined for an isosceles trapezoid when the trapezoid is replaced by an equivalent rectangle. The equivalent rectangle is obtained by drawing perpendiculars to the sides of the trapezoid (CB and CD) from the centroid C and then forming rectangle EFGH using points B and D (Fig. B8.2.2-7).

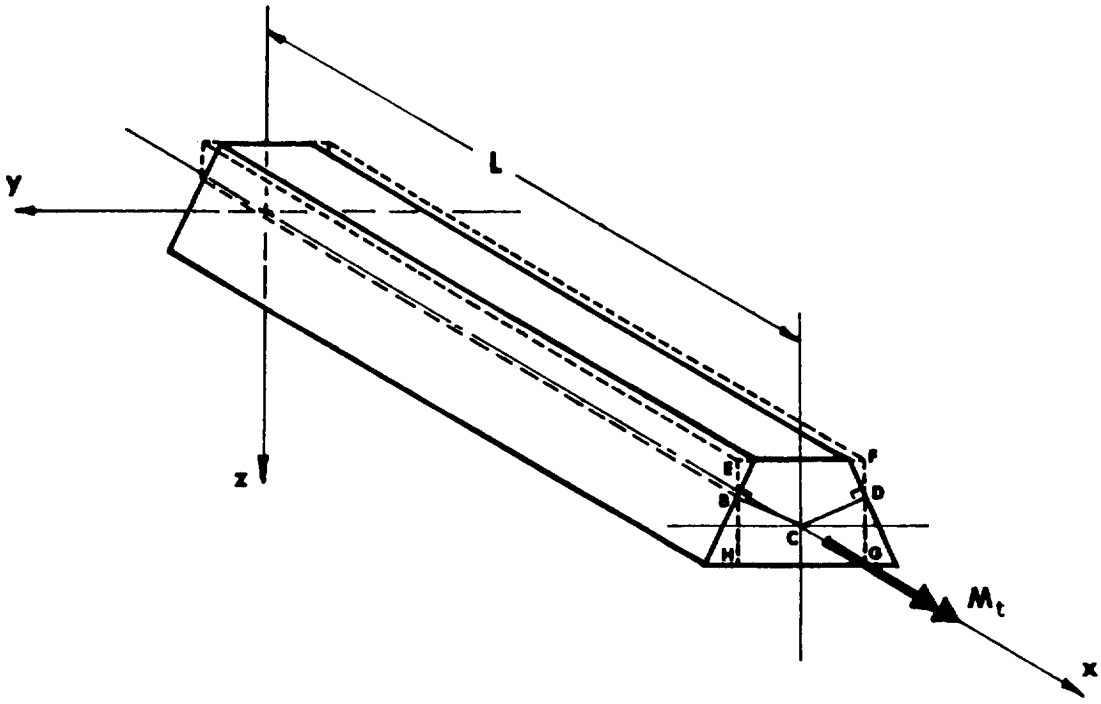

FIGURE B8.2.2-7 ISOSCELES TRAPEZOIDAL SECTION

B8.2.3 EXAMPLE PROBLEMS FOR TORSION OF SOLID SECTIONS

I Example Problem 1

Find the maximum torsional shear stress and the total angle of twist for the solid rectangular cross section shown in Figure B8.2.3-1.

Solution: From Table B8.2.2-1, $\alpha = -0.256$ and $\beta = 0.229$ for b/d = 2.0. The maximum stress will occur at point A in Figure B8.2.3-1.

The torsion section modulus (S_t) is

$$S_t = \alpha bd^2$$

$$= 0.256\,(5)\,(2.5)^2$$

$$= 8.00 \text{ in}^3$$

The torsional shear stress (τ_t) at point A is

$$\tau_t = M_t/S_t$$

$$= 100,000/8.00$$

$$\tau_t = 12,500 \text{ psi.}$$

The torsional constant (K) is

$$K = \beta bd^2$$

$$= 0.229\,(5)\,(2.5)^2$$

$$= 7.156 \text{ in}^4 .$$

The total angle of twist (ϕ) is

$$\phi = M_t L/GK$$

$$= 100,000\,(32)/4,000,000\,(7.156)$$

$$= 0.1118 \text{ rad.}$$

II Example Problem 2

Find the maximum torsional shear stress (τ_t) and the angle of twist (ϕ) at point B for the tapered bar shown in Figure B8.2.3-2 with a constant distributed torque.

Solution:

The radius (r) of the tapered bar as a function of the x-coordinate is:

$$r = 2.5 - 0.005x$$

The internal twisting moment M(x) as a function of the x-coordinate is:

$$M(x) = m_t x = 200x \, .$$

The torsional section modulus (S_t) of the bar as a function of the x-coordinate is

$$S_t(x) = 0.5 \, \pi \, r^3$$

$$= 1.5708 \, [2.5 - 0.005x]^3$$

The maximum torsional shear stress (τ_t) at point B is

$$\tau_t = \frac{M(x)}{S_t(x)}$$

$$= \frac{200x}{1.5708 \, (2.50 - 0.005x)^3} \, .$$

For $x = L_x = 300$,

$$\tau_t = 38,197 \text{ psi} \, .$$

Since both the internal twisting moment and the torsional stiffness vary with the x-coordinate, the angle of twist is obtained from

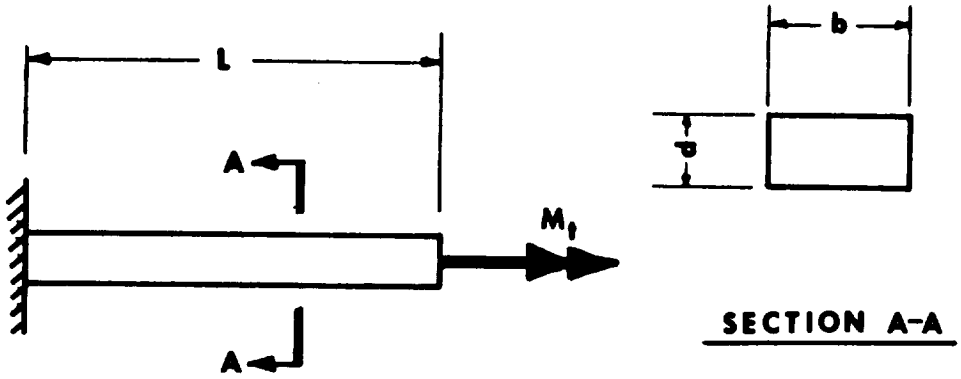

b = 5.0"
d = 2.5"

M_t = 100,000 in. lb.
G = 4,000,000 psi.

L = 32"

FIGURE B8.2.3-1

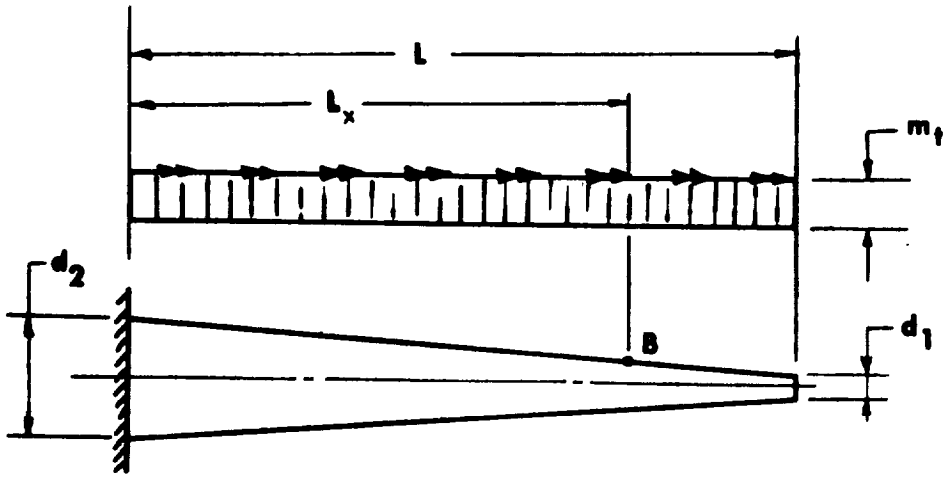

L = 400"
L_x = 300"

d_1 = 1"
d_2 = 5"

m_t = 200 in. lb./in.
G = 4,000,000 psi.

FIGURE B8.2.3-2

$$\phi = \frac{1}{G} \int_0^{L_x} \frac{M(x)}{K(x)} \, dx \, .$$

The torsional stiffness (K) of the bar as a function of the x-coordinate is

$$K = 0.5 \, \pi r^4$$

$$= 1.5708 (2.5 - 0.005x)^4 \, .$$

The angle of twist (ϕ) in radians between the origin and point B can be obtained by evaluating the following integral.

$$\phi = \frac{1}{4x10^6} \int_0^{300} \frac{200x}{(2.5 - 0.005x)} \, dx \, .$$

III Example Problem 3

Find the total angle of twist (ϕ) at points A, B, C, and D for the bar loaded as shown in Figure B8.2.3-3.

Solution:

The internal moments at points A, B, C, and D are:

$$M(D) = 0$$

$$M(C) = \int_{35}^{50} \left(6,670 - \frac{x}{7500}\right) dx = 15.0 \text{ in.-Kips}$$

$$M(B) = 15,000 + \int_{20}^{35} 1000 \, dx = 30.0 \text{ in.-Kips}$$

$$M(A) = 30,000 + \int_{0}^{20} 3000 \, \frac{x}{20} \, dx = 60.0 \text{ in.-Kips} \, .$$

The equation for angle of twist is

$$\phi = \int_0^{L_x} \frac{M_t}{GK} dx,$$

which is also the area under the M_t/GK diagram (Fig. B8.2.3-4).

Using the moment-area analogy from beam theory, the following statement can be made.

"The total angle of twist between any two cross sections of a bar which is loaded with an arbitrary torsional load is equal to the area under the M_t/GK diagram between the two cross sections."

Using the moment-area principle above, the angles of twist are

ϕ (A) = 0 fixed end.

$$\phi \text{ (B)} = 30,000(20) + 2/3(30,000)(20) = \frac{1,000,000}{GK} = 0.100 \text{ rad}$$

$$\phi \text{ (C)} = 1,000,000 + 15,000(15) + 1/2\,(15,000)(15) = \frac{1,337,500}{GK}$$

$$= 0.13375 \text{ rad}$$

$$\phi \text{ (D)} = 1,337,500 + 1/3\,(15,000)(15) = \frac{1,412,500}{GK} = 0.14125 \text{ rad.}$$

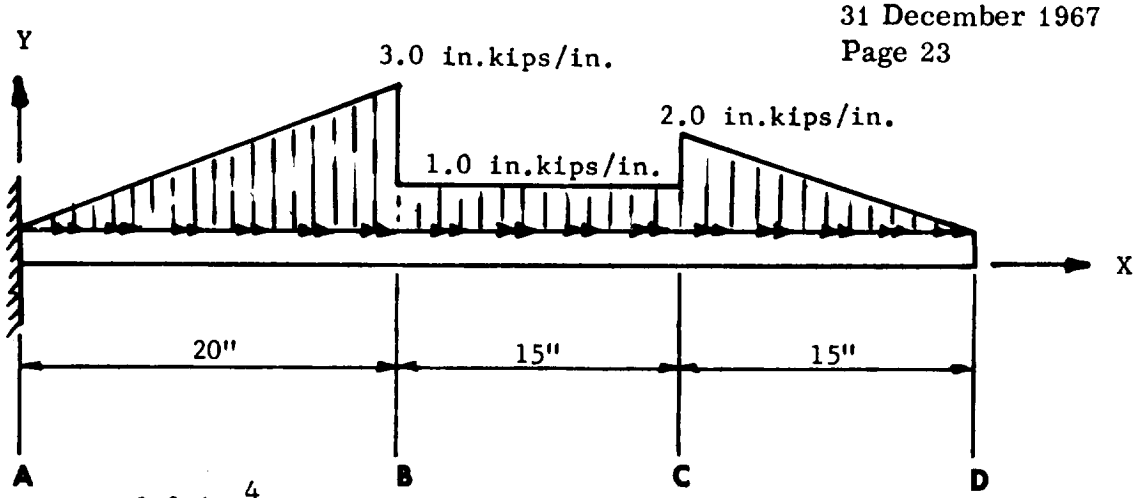

$K = 2.0 \text{ in.}^4$

$G = 5{,}000{,}000 \text{ psi.}$

FIGURE B8.2.3-3

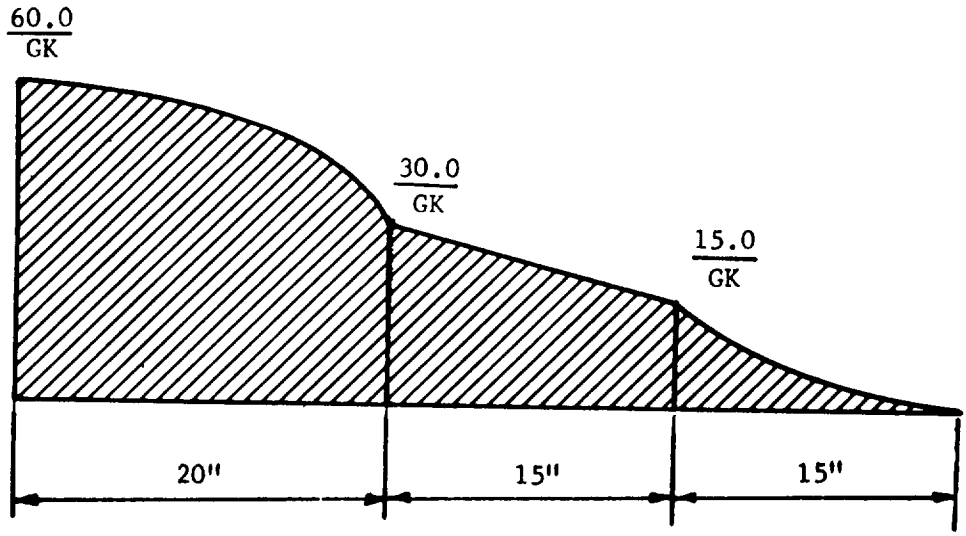

FIGURE B8.2.3-4

SECTION B8.3

TORSION OF THIN-WALLED CLOSED SECTIONS

TABLE OF CONTENTS

B8.3.0 TORSION OF THIN-WALLED CLOSED SECTIONS

A closed section is any section where the center line of the wall forms a closed curve.

The torsional analyses of thin-walled closed sections for unrestrained and restrained torsion are included. Torsional shear stress, angle of twist, and warping stresses are determined for restrained torsion. Torsional shear stress, angle of twist, and warping deformations are considered for unrestrained torsion.

Analysis of multicell closed sections is beyond the scope of this analysis. The analysis of multicell closed sections can be found in References 11 and 13.

B8.3.1 GENERAL

I. Basic Theory

The torsional analysis of thin-walled closed sections requires that stresses and deformations be determined. The torsional shear stress (τ_t), plus warping normal stress (σ_w) for restrained torsion, should be determined at any point (P) on a thin-walled closed section at an arbitrary distance (L_x) from the origin. The angle of twist (ϕ) should be determined between an arbitrary cross section and the origin plus the warping deformation (w) at any point (P) on an arbitrary cross section for unrestrained torsion.

As was the case for solid sections (see Section B8.2.1-I), two unique coefficients exist that characterize the geometry of each cross section. These coefficients are called the torsional constant (K) and the torsional section modulus (S_t) and are functions of the dimensions of the cross section.

The torsional shear stress distribution varies along any radial line emanating from the geometric centroid of the thin-walled closed section. Since

the thickness of the thin-walled section is small compared with the radius, the stress varies very little through the thickness of the cross section and is assumed to be constant through the thickness at that point.

Figure B8.3.1-1A shows a typical thin-walled cross section and Figure B8.3.1-1B shows a typical element of this cross section. Equilibrium of forces in the x direction (longitudinal) will give the following equation:

$$\tau_{L_{x^1}} t_1 \Delta X = \tau_{L_{x^2}} t_2 \Delta X ,$$

or, since shear stresses are equal in the longitudinal and circumferential directions,

$$\tau_{t1} t_1 = \tau_{t2} t_2 .$$

This equation indicates that the product of the torsional shear stress and the thickness at any point around the cross section is constant. This constant is called the "shear flow" (q). Therefore:

$$q = \tau_t t .$$

The internal forces are related to the applied twisting moment by the following equation:

$$\tau_t = \frac{M_t}{2At} = \frac{M_t}{S_t}$$

where

$$S_t = 2At$$

and A is the enclosed area of the mean periphery of the thin-walled closed section.

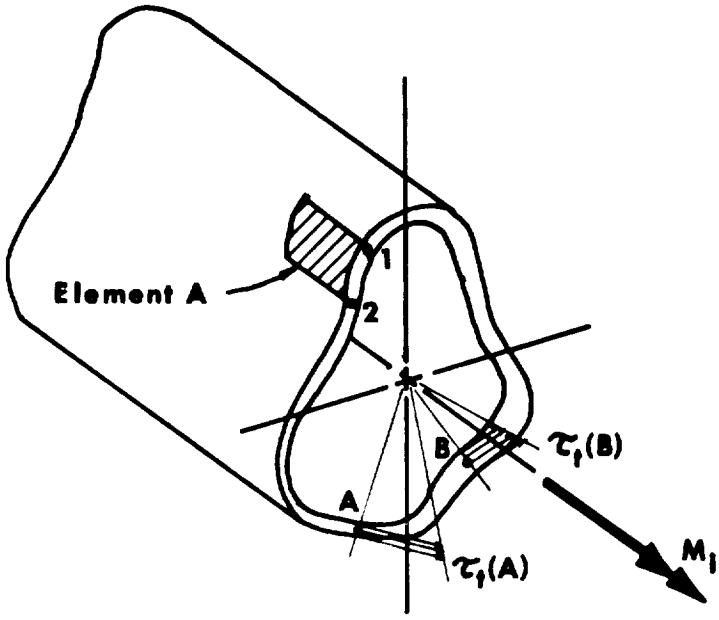

A. Stress Distribution and Internal Moment for Thin-Walled Cross Section

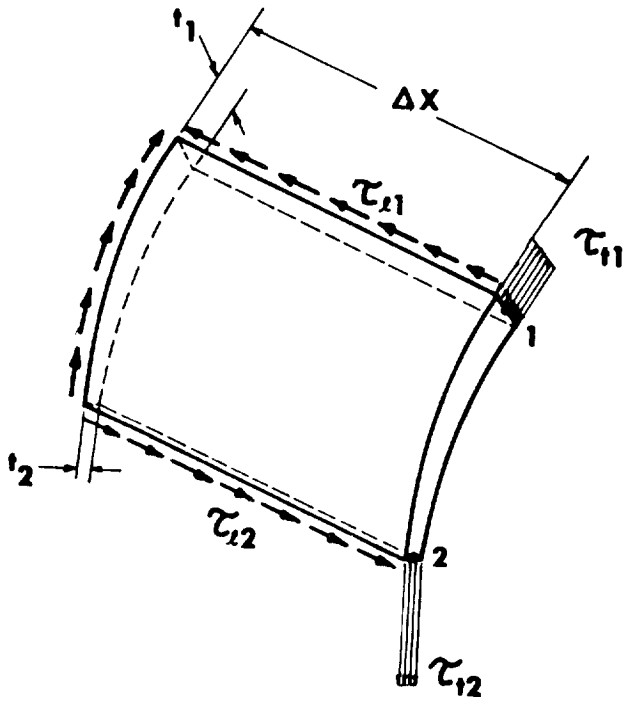

B. Stresses on Element A

FIGURE B8.3.1-1 TYPICAL THIN-WALLED CLOSED CROSS SECTION

Written in terms of shear flow, this equation becomes:

$$q = \frac{M_t}{2A} \quad .$$

II. Limitations

The torsional anslysis of thin-walled closed cross sections is subject to the following limitations:

A. The material is homogeneous and isotropic.

B. The cross section must be thin-walled, but not necessarily of constant thickness.

C. Variations in thickness must not be abrupt except at reentrant corners (see Section B8.3.3-III).

D. No buckling occurs.

E. The stresses calculated at points of constraint and at abrupt changes of applied twisting moment are not exact.

F. The applied twisting moment cannot be an impact load.

G. The bar cannot have abrupt changes in cross section.

H. The shear stress does not exceed the shearing proportional limit and is proportional to the shear strain (elastic analysis).

III. Membrane Analogy

The same use can be made of the stress function represented by the surface ABDE (Fig. B8.3.1-2) in solving the problem of the torsional resistance of a thin-walled tube as was made of the function in Section B8.2.1-III for the solid bar. These uses are as follows:

A. The twisting moment (M_t) to which the thin-walled tube is subjected is equal to twice the volume underneath the surface ABDE and is, therefore, given approximately by the equation

$$M_t = 2AH$$

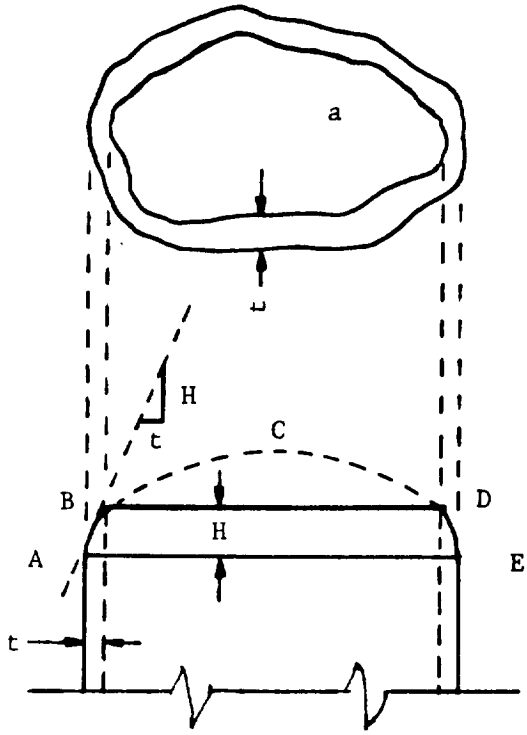

FIGURE B8.3.1-2 MEMBRANE ANALOGY FOR TORSION OF THIN-WALLED CLOSED CROSS SECTION

where A is defined as in Section B8.3.1-I and H is the height of the plane BD above the cross section.

B. The slope of the surface at any point is equal to the stress in the bar in a direction perpendicular to the direction in which the slope is taken. Hence, the slope at any point along the arcs AB or DE may be taken as H/t. The maximum shearing stress in a hollow bar at any point is, therefore,

$$\tau_t = H/t \ .$$

It can be seen that H is the same quantity as "shear flow," defined in Section B8.3.1-I.

IV. Basic Torsion Equations For Thin-Walled Closed Sections

A. Torsional Shear Stress

The basic equation for determining the torsional shear stress at an arbitrary cross section is:

$$\tau_t = \frac{M(x)}{S_t(x,s)} = \frac{M(x)}{2A(x)\,t(x,s)} = \frac{q(x)}{t(x,s)}$$

where

$$S_t(x,s) = 2A(x)\ t\ (x,s)$$

$$Q(x) = \frac{M(x)}{2A(x)}$$

and A is defined as in Section B8.3.1-I.

M(x) or q(x) is evaluated for $x = L_x$ at the arbitrary cross section where the torsional shear stress is to be determined, and t(x,s) is evaluated at the arbitrary cross section at the point (s) on the circumference of the arbitrary cross section.

If a constant torque is applied to the end of the bar and the cross section is constant along the length of the bar, the equations reduce to:

$$\tau_t = \frac{M_t}{S_t(s)} = \frac{M_t}{2At(s)} = \frac{q}{t(s)}$$

where

$$q = \frac{M_t}{2A} \quad .$$

In the equations for torsional shear stress in Sections B8.3.2 and B8.3.3, which follow, M(x) is equal to M_t and A(x) is constant and equal to A. The equations in these sections determine the shear stress at any point (s) around the cross section.

B. Angle of Twist

The basic equation for determining the angle of twist between the origin and any cross section located at a distance L_x from the origin is:

$$\phi = \frac{1}{G}\int_0^{L_x} \frac{M(x)}{K(x,s)}\,dx = \frac{1}{4G}\int_0^{L_x}\left\{\frac{M(x)}{A^2(x)}\left[\int_0^C \frac{ds}{t(s)}\right](x)\right\}dx$$

where C is equal to the length of the wall center line (circumference) and

$$K(x,s) = 4A^2(x)\Big/\int_0^C \frac{ds}{t(s)} \quad .$$

When M(x) is a constant torsional moment applied at the end of the bar, A is a constant, and t is not a function of x, the equation reduces to:

$$\phi = \frac{M_t l}{GK(s)}$$

where

$$K(s) = 4A^2\Big/\int_0^C \frac{ds}{t(s)} \quad .$$

When t is a constant, the equation reduces to:

$$\phi = \frac{M_t l}{GK}$$

where

$$K = \frac{4A^2 t}{C} \quad .$$

The total twist of the bar is:

$$\phi\ (\max) = \frac{M_t l}{GK}$$

where

$$K = \frac{4A^2 t}{C} \quad .$$

C. Warping Deformation

The basic equation for determining the warping deformation (w) at any point (P) on an arbitrary cross section located at a distance $x = L_x$ from the origin is:

$$w(s) - w_o = \frac{M_t}{2AG} \int_0^s \left[\frac{1}{t(s)} - r(s) \left(\frac{\int_0^C \frac{ds}{t(s)}}{2A} \right) \right] ds$$

where w(s) is the warping deformation at point (s) measured from the x-y plane through the origin of the s coordinate system; w_o is the distance from the x-y plane through the origin of the mean displacement plane; and r(s) is the normal distance to a line parallel to the increment of arc length ds (see Example Problem 2, Section B8.3.4-II).

The mean displacement plane, which is located at the same z coordinate as the undeformed cross section, will pass through those points on the cross section that lie on axes of symmetry (see Example Problem 2, Section B8.3.4-II). For unsymmetrical sections, the point (s), measured from an assumed arc length origin through which the mean displacement plane passes, is determined by evaluating the following integral for s.

$$\int_0^s \left[\frac{1}{t(s)} - r(s) \left(\frac{\int_0^C \frac{ds}{t(s)}}{2A} \right) \right] ds = 0 \quad .$$

D. Warping Stresses

Warping stress calculations are very complicated and cannot be put into a generalized form. Techniques for evaluating these stresses can be found in Reference 1.

Warping stresses for a rectangular section are included in section B8.3.3-II.

B8.3.2 CIRCULAR SECTIONS

I. Constant-Thickness Circular Sections

A constant-thickness, circular, thin-walled closed section experiences no warping for unrestrained torsion and develops no warping normal stresses for restrained torsion.

The torsional shear stress is determined by the following equation:

$$\tau_t = \frac{M_t}{S_t}$$

where

$$S_t = 2At \ .$$

The torsional shear stress defined in terms of shear flow is determined by the following equation:

$$\tau_t = q/t$$

where

$$q = \frac{M_t}{2A} \ .$$

The total angle of twist is determined by the following equation:

$$\phi \ (\max) = \frac{M_t L}{GK}$$

where

$$K = \frac{4A^2t}{C} \ .$$

II. Varying Thickness Circular Sections

A circular thin-walled closed section with varying thickness will warp for unrestrained torsion, and warping normal stresses are developed for restrained torsion. The warping normal stresses and warping deformations are negligible and can be neglected when the change in thickness is small and gradual.

The torsion shear stress is calculated in the same manner as for constant-thickness circular sections, except that t is now a function of s.

The total angle of twist for a circular thin-walled closed section with varying thickness is determined by the following equation:

$$\phi \text{ (max)} = \frac{M_t L}{GK}$$

where

$$K = \frac{4A^2}{\int_0 \frac{ds}{t(s)}} \quad .$$

B8.3.3 NONCIRCULAR SECTIONS

I. Unrestrained Torsion

Noncircular sections experience warping for unrestrained torsion, except for the case noted below, and develop no warping normal stresses.

Note that no warping occurs in a cross section that has a constant value for the product rt around the circumference of the cross section.

Longitudinal warping deformations are usually not of concern and are not evaluated. The use of the basic equation for determining warping deformations for closed sections (see Section B8.3.1-IVC) is used in Example Problem II (see Section B8.3.4-III).

A. Elliptical Section

The torsional shear stress for constant thickness is determined by the following equation:

$$\tau_t = \frac{M_t}{S_t}$$

where

$$S_t = 2At$$

and

$$A = \pi \left[ab - \frac{t}{2} (a + b) + \frac{t^2}{4} \right] \quad .$$

The values of a, b, and t are defined in Figure B8.3.3.-1.

The torsional shear stress defined in terms of shear flow is determined by the following equation:

$$\tau_t = \frac{q}{t}$$

where

$$q = \frac{M_t}{2A}$$

and A is defined as above.

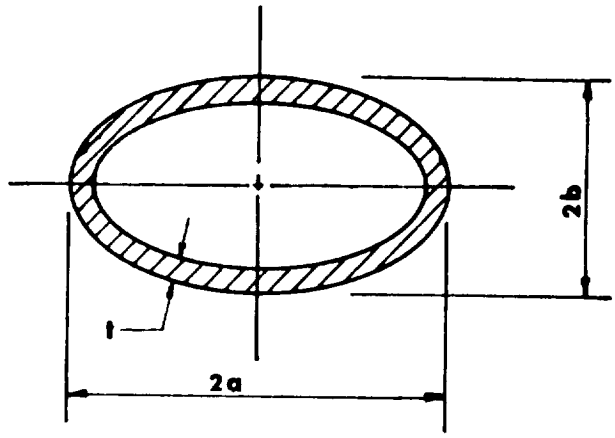

FIGURE B8.3.3-1 ELLIPTICAL SECTION

The torsional shear stress for varying thickness is calculated in the same manner as constant thickness, except that it is now a function of s, t(s).

The total angle of twist for constant thickness is determined by the following equation:

$$\phi \text{ (max)} = \frac{M_t L}{GK}$$

where

$$K = \frac{4A^2 t}{C}$$

A is defined above, and the equation for C is, approximately,

$$C = \pi(a + b - t)\left[1 + 0.27\,\frac{(a-b)^2}{(a+b)^2}\right] .$$

The total angle of twist for varying thickness is determined by the following equation:

$$\phi\ (\max) = \frac{M_t L}{GK}$$

where

$$K = \frac{4A^2}{\int_0^C \frac{ds}{t(s)}}$$

and the area is as defined in Section B8.3.1-I.

B. Rectangular Section (Constant Thickness)

The torsional shear stress for constant thickness is determined at points A and B (Fig. B8.3.3-2) by the following equation:

$$\tau_t = \frac{M_t}{S_t}$$

where

$$S_t = 2At$$

and $$A = ab - t(a+b) + t^2 .$$

The values of a, b, and t are defined in Figure B8.3.3-2.

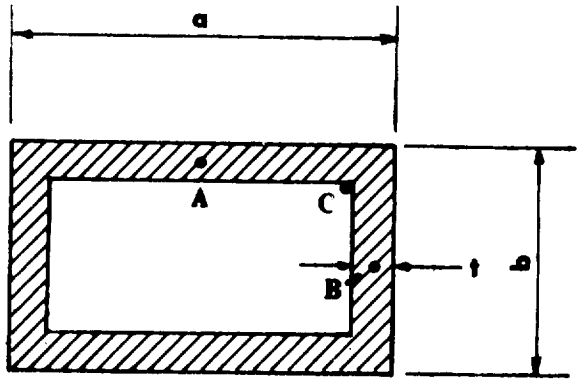

FIGURE B8.3.3-2 RECTANGULAR SECTION (CONSTANT THICKNESS)

The torsional shear stress defined in terms of shear flow is determined by the following equation:

$$\tau_t = \frac{q}{t}$$

where

$$q = \frac{M_t}{2A}$$

and A is defined as above.

The stresses at the inner corners (points C on Fig. B8.3.3-2) will be higher than the stresses calculated at points A and B unless the ratio of the radius of the fillet to thickness is greater than 1.5. For small radius rectangular section stresses see Section B8.3.3-III.

The total angle of twist for constant thickness is determined by the following equation:

$$\phi(\max) = \frac{M_t L}{GK}$$

where

$$K = \frac{4A^2 t}{C} \quad .$$

A is defined above, and $C = 2(a + b - 2t)$.

C. Rectangular Sections (Different Thickness)

The torsional shear stress for different but nonvarying thickness is determined at points A and B (Fig. B8.3.3-3) by the following equation:

$$\tau_t = \frac{M_t}{S_t}$$

where

$$S_t = 2At_1$$

for point A,

$$S_t = 2At_2$$

for point B, and

$$A = (a - t_2)(b - t_1) \quad .$$

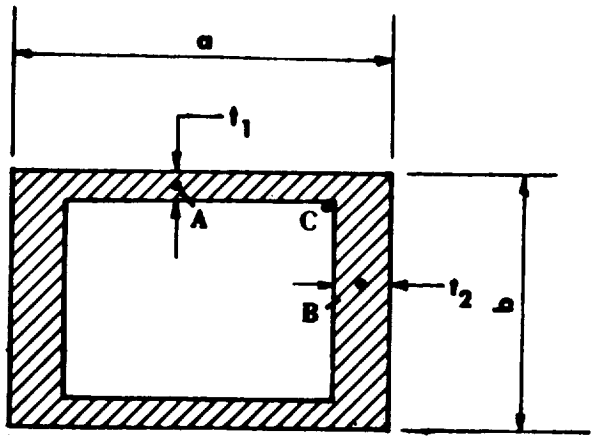

FIGURE B8.3.3-3 RECTANGULAR SECTION (DIFFERENT THICKNESSES)

The torsional shear stress defined in terms of shear flow is determined by the following equation:

$$\tau_t = \frac{q}{t_1}$$

for point A,

$$\tau_t = \frac{q}{t_2}$$

for point B, and

$$q = \frac{M_t}{2A}$$

where A is defined as above.

The stress at the inner corners (points C) will be higher than the stresses calculated at points A and B unless the ratio of the radius of the fillet to the thickness is greater than 1.5. For small radius rectangular section stresses see Section B8.3.3-III.

The total angle of twist for different but nonvarying thickness is determined by the following equation:

$$\phi \text{ (max)} = \frac{M_t L}{GK}$$

where

$$K = \frac{2t_1t_2(a - t_2)^2 (b - t_1)^2}{at_1 + bt_2 - t_1^2 - t_2^2}$$

D. Arbitrary Section (Constant Thickness)

The torsional shear stress for an arbitrary section with constant thickness (Fig. B8.3.3-4) is determined by the following equation:

$$\tau_t = \frac{M_t}{S_t}$$

where

$$S_t = 2At$$

and A is defined in Section B8.3.1-I.

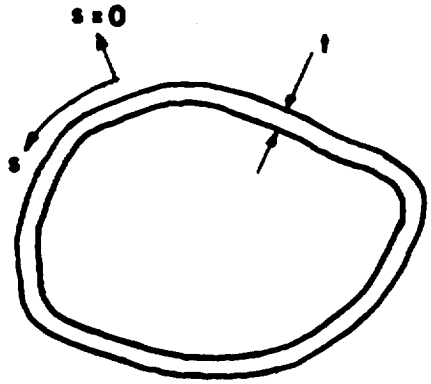

FIGURE B8.3.3-4 ARBITRARY SECTION (CONSTANT THICKNESS)

The torsional shear stress defined in terms of shear flow is determined by the following equation:

$$\tau_t = \frac{q}{t}$$

where

$$q = \frac{M_t}{2A}$$

and A is defined as above.

The total angle of twist is determined by the following equation:

$$\phi \text{ (max)} = \frac{M_t L}{GK}$$

where

$$K = \frac{4A^2t}{C} \quad .$$

A is defined as above, and C, the circumference, is defined as follows:

$$C = \int_0^C ds \quad .$$

E. Arbitrary Section (Varying Thickness)

The torsional shear stress for an arbitrary section with varying thickness (Fig. B8.3.3-5) is determined by the following equation:

$$\tau_t = \frac{M_t}{S_t}$$

where

$$S_t = 2At$$

and A is defined in Section B8.3.1-I. The shear flow is determined by the following equation:

$$\tau_t = \frac{q}{t}$$

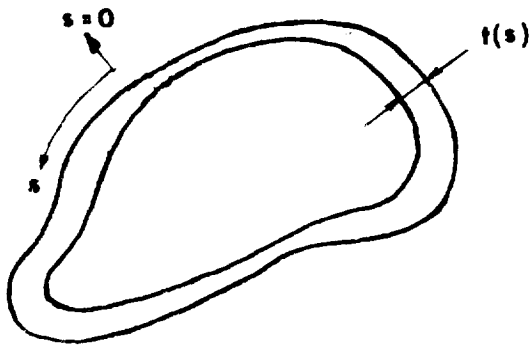

FIGURE B8.3.3-5 ARBITRARY SECTION (VARYING THICKNESS)

where

$$q = \frac{M_t}{2A}$$

and A is defined as above.

Note that the maximum shear stress occurs at the point of least thickness. The total angle of twist is determined by the following equation:

$$\phi(\max) = M_t \frac{L}{GK}$$

where

$$K = 4A^2 / \int_0^C \frac{ds}{t(s)}$$

and A is defined as above.

II. Restrained Torsion

Restrained torsion of noncircular closed sections occurs at fixed ends and at points of abrupt change in torque.

The warping normal stresses associated with the restrained torsion attenuate rapidly, and their analytical determination is extremely difficult.

Torsional shear stresses associated with these restraints are calculated as in Section B8.3.3-I. The warping normal stress for the rectangular section shown in Figure B8.3.3-2 is determined by the following equation:

$$\sigma_w(\max) = \frac{m}{K}$$

where

$$K = \frac{tG}{4M_t}(a+b)^2 \left(\frac{1-\mu^2}{E}\right)\left(\frac{2}{1-\mu}\right)^{\frac{1}{2}}$$

and m is obtained from Figure B8.3.3-6.

III. Stress Concentration Factors

The curve in Figure B8.3.3-7 gives the ratio of the stress at the re-entrant corners to the stress along the straight sections at points A and B shown in Figure B8.3.3-2.

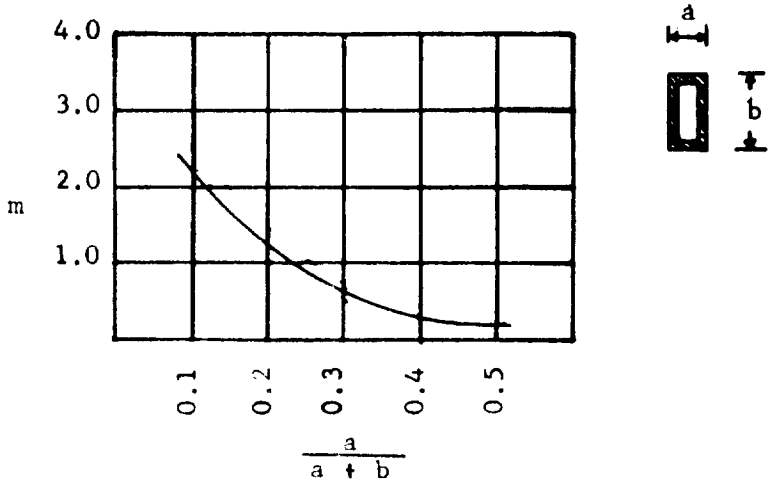

FIGURE B8.3.3-6 VALUE OF m FOR RECTANGULAR SECTION

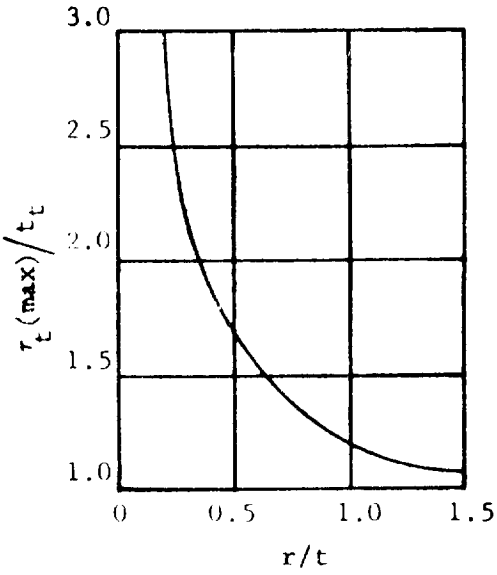

FIGURE B8.3.3-7 STRESS CONCENTRATION FACTORS AT REENTRANT CORNERS

B8.3.4 EXAMPLE PROBLEMS FOR TORSION OF THIN-WALLED CLOSED SECTIONS

I. Example Problem 1

For the problem shown in Figure B8.3.4-1, it is required to find the following:

A. Shear stresses at points A, B, and C on the cross section and maximum angle of twist caused by the torsional load.

B. Local normal stresses caused by restraint at the fixed end.

Solution:

A. From Section B8.3.3-IB, the shear stress at points A and B is

$$\tau_t = \frac{M_t}{2At}$$

where $A = ab - t(a + b) + t^2$.

Therefore, $A = 6(3) - 0.2(6 + 3) + (0.2)^2$

$$A = 16.24 \text{ in.}^2$$

and $$\tau_t = \frac{100,000}{2(16.24)(0.2)}$$

$$\tau_t = 15,394 \text{ psi} \quad .$$

For the maximum shear stress at point C, refer to Figure B8.3.3-7 for the ratio of the stress at point C to the stress at points A and B.

$$\frac{\tau_t(\max)}{\tau_t(A)} = 1.7$$

$$\tau_t(\max) = 1.7\ (15,394)$$

$$\tau_t(\max) = 26,170 \text{ psi}$$

The maximum angle of twist is determined by the following equation from Section B8.3.3-IB:

$$\phi(\max) = \frac{M_t L}{GK}$$

where

$$K = \frac{4A^2 t}{C}$$

and $C = 2(a + b - 2t)$.

Therefore, $C = 2(6 + 3 - 2(0.2))$

$$C = 17.2$$

$$K = \frac{4(16.24)^2 0.2}{17.2}$$

$$K = 12.27$$

$$\phi(\max) = \frac{100,000(60)}{4 \times 10^6 (12.27)}$$

$$\phi(\max) = 0.122 \text{ radians} .$$

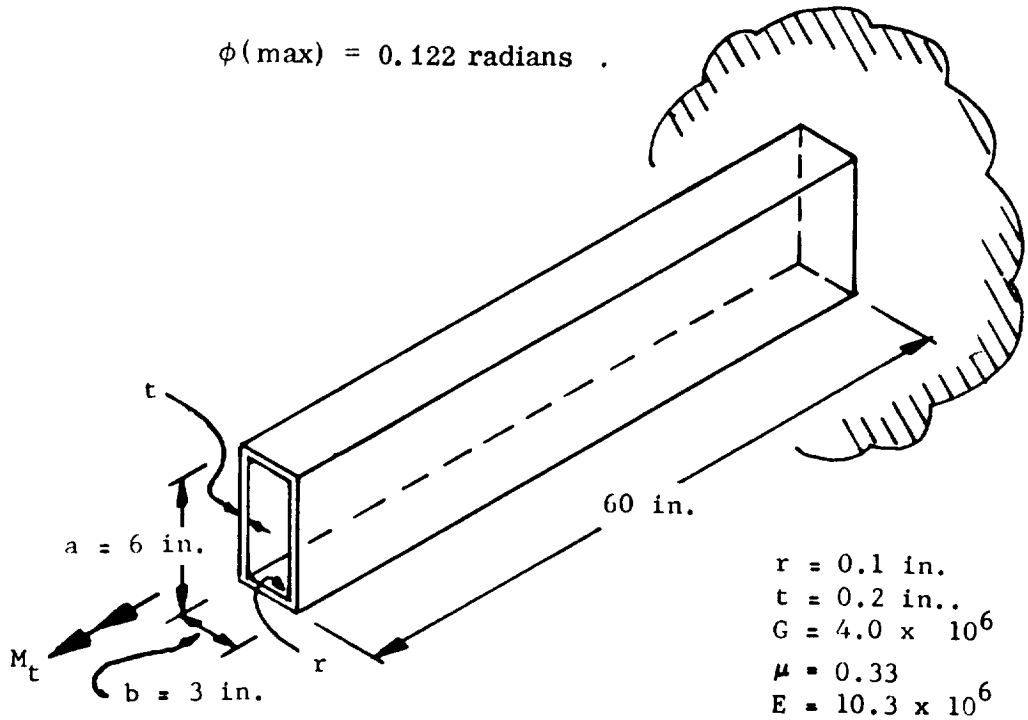

FIGURE B8.3.4-1

B. To find the normal stress at the fixed end, use the equations in Section B8.3.3-II.

From Figure B8.3.3-6,

$$m = 0.3$$

$$K = \frac{tG}{4M_t}(a+b)^2\left(\frac{1-\mu^2}{E}\right)\left(\frac{2}{1-\mu}\right)^{\frac{1}{2}}$$

$$K = \frac{(0.2)(4 \times 10^6)}{4 \times 10^5}(3+6)^2\sqrt{\frac{2}{1-0.33}}\left(\frac{1-0.33^2}{10.3 \times 10^6}\right)$$

$$K = 24.217 \times 10^{-6}$$

$$\sigma = \frac{0.33}{24.217 \times 10^{-6}} = 13{,}620 \text{ psi}$$

II. Example Problem 2

For the cross section shown in Figure B8.3.4-2, it is required to find the warping deformations of the points shown.

(dimensions are in inches)

$M_t = 1 \times 10^5$ in.-lb.

$G = 4.0 \times 10^6$

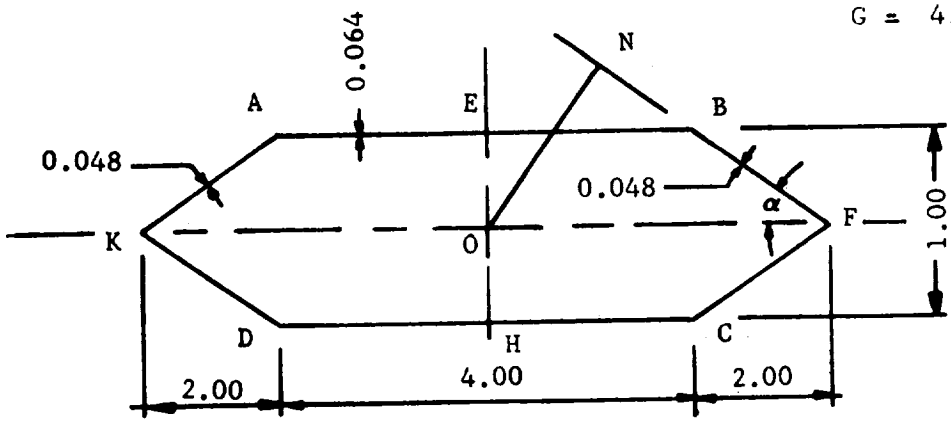

Determine the distribution of warping

$\sin \alpha = 0.2425 \quad \therefore \quad ON = 0.97$

FIGURE B8.3-4-2

From Section B8.3.1-IVC,

$$w(s) - w_o = \frac{M_t}{2AG} \int_0^s \left[\frac{1}{t(s)} - r(s) \left(\frac{\int_0^C \frac{ds}{t(s)}}{2A} \right) \right] ds$$

or

$$\frac{G}{M_t} [w(s) - w_o] = \frac{1}{2A} \int_0^s \left[\frac{1}{t(s)} - r(s) \left(\frac{\int_0^C \frac{ds}{t(s)}}{2A} \right) \right] ds \quad .$$

A = enclosed area of section = 6.0 in.^{2}

$$\int_0^C \frac{ds}{t(s)} = 2 \left\{ \frac{KD}{0.048} + \frac{DC}{0.064} + \frac{CF}{0.048} \right\} = 2 \left\{ \frac{2.062}{0.048} + \frac{4}{0.064} + \frac{2.062}{0.048} \right\}$$

$$= 296.8 \quad .$$

Choose point D as the origin and measure s from point D. For sector DC:
r = 0.5 t = 0.064

$$\frac{2AG}{M_t} \left[w_C - w_D \right] = \int_0^4 \left[\frac{1}{0.064} - \frac{0.5(296.8)}{2(6)} \right] ds$$

$$= 3.26(4)$$

$$= \underline{13.04}$$

For sector CF: r = 0.97 t = 0.048

$$\frac{2AG}{M_t} \left[w_F - w_C \right] = \int_0^{2.062} \left[\frac{1}{0.048} - \frac{0.97(296.8)}{2(6)} \right] ds$$

$$= - (3.16)(2.062)$$

$$= - 6.52 \quad .$$

For sector FB: r = 0.97 t = 0.048 (Same as sector CF)

$$\frac{2AG}{M_t}\left[w_B - w_F\right] = \underline{-6.52}$$

For sector BA: (same as sector DC)

$$\frac{2AG}{M_t}\left[w_A - w_B\right] = \underline{13.04}\ .$$

For sector AK: (same as sector CF)

$$\frac{2AG}{M_t}\ w_K - w_A = \underline{-6.52}\ .$$

For sector KD: (same as sector CF)

$$\frac{2AG}{M_t}\left[w_D - w_K\right] = \underline{-6.52}\ .$$

Hence, the summation of warping deflections around the section from D back to D equals zero.

Now it is desired to find the mean displacement plane (see Fig. B8.3.4-3). From symmetry, points E_1, F_1, H_1, and K_1 will lie on the mean displacement plane and will not deform from their original positions. Therefore the distance

from point D to the mean displacement plane is

$$\frac{2AG}{M_t}\left[w_D - w_0\right] = \underline{6.52} \quad .$$

Therefore the warping deformations are

$$w_D = w_C = w_B = w_A = \frac{6.52\ M_t}{2AG}$$

$$= \frac{6.52(1 \times 10^5)}{2(6)(4 \times 10^6)} = 0.0136 \text{ inch}$$

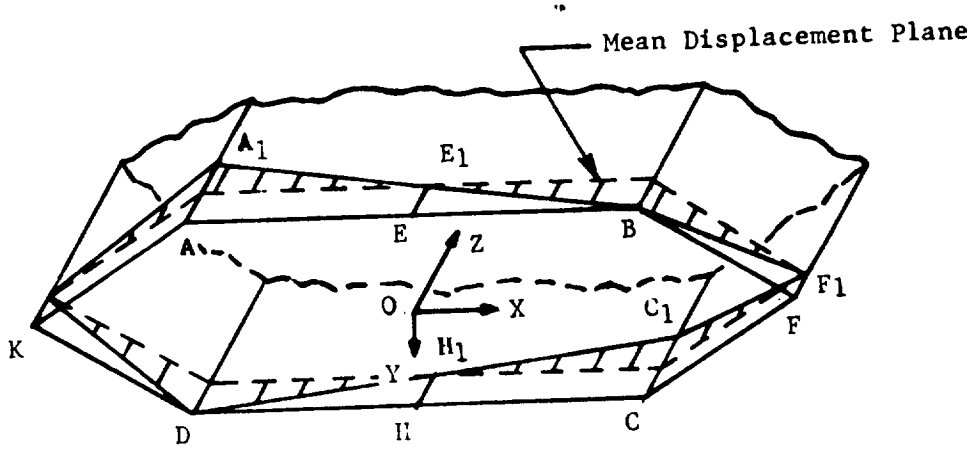

FIGURE B8.3.4-3

III. Example Problem 3

For the problem shown in Figure B8.3.4-4, it is required to find the following:

A. Maximum torsional shear stress at $L_x = 0$, $L_x = \frac{L}{2}$, and $L_x = L$.

B. Maximum angle of twist.

Solution:

A. The formula for shear stress as obtained by Section B8.3.1-IVA is

$$\tau_t = \frac{M(x)}{2A(x)\, t(x,s)} \quad .$$

Therefore, at $L_x = 0$, since $M(x) = 0$, $\tau_t = 0$ at $L_x = \frac{L}{2}$, $M(x) = \frac{M_0}{2}$

$$A(x) = \pi r_0^2 \left(1 + \frac{1}{2}\right)^2$$

$$= \pi r_0^2 \frac{9}{4} \quad .$$

The shear stress will be maximum at thickness of t_0. Therefore

$$\tau(\max) = \frac{4M_0}{2(2)\pi r_0^2 9 t_0}$$

$$= \frac{M_0}{9\pi r_0^2 t_0} = \frac{100,000}{9\pi(5)^2 0.1} = 1,414 \text{ psi} \quad .$$

Where $L_x = L$

$$M(x) = M_0$$

$$A(x) = 4\pi r_0^2$$

$$\tau(\max) = \frac{M_0}{2(4)\pi r_0^2 t_0} = 1,591 \text{ psi} \quad .$$

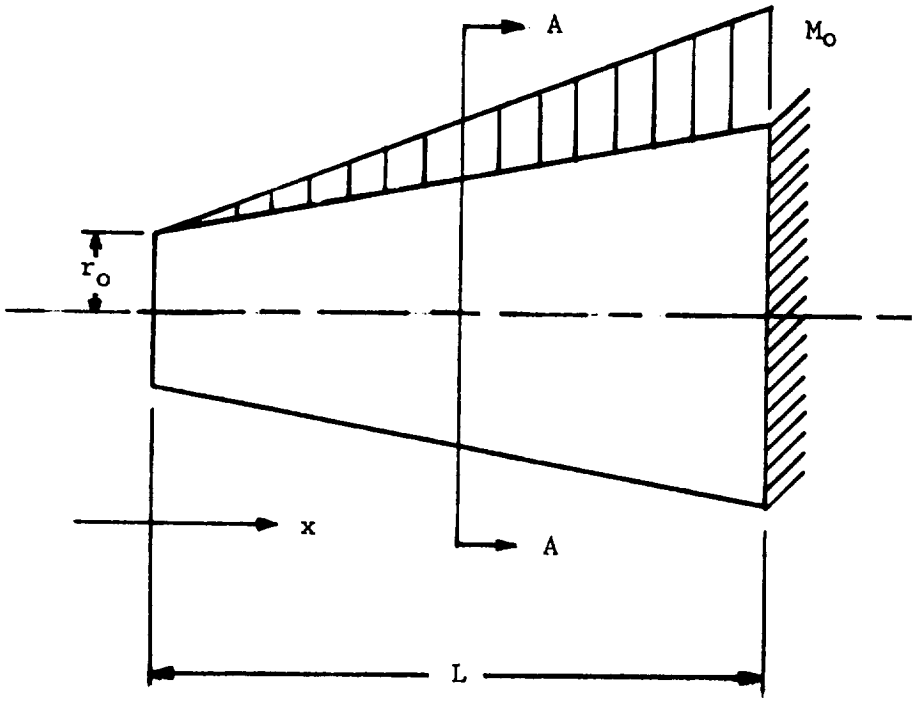

$M(x) = M_o x / L$

$G = 4 \times 10^6$
$t_o = 0.1$ in.
$r_o = 5.0$ in.
$M_o = 1 \times 10^5$ in.-lb.
$L = 30.0$ in.

$t(s) = to(1 + \sin\theta)$
$r(x) = r_o (1 + x/L)$

$A(x) = \pi r^2 (x)$

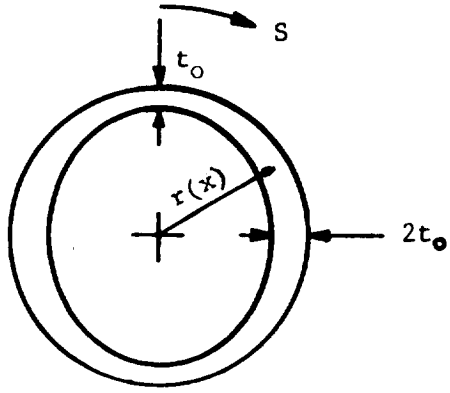

SECTION A-A

FIGURE B8.3.4-4

B. The formula for angle of twist is obtained from Section B8.3.1-IVB.

$$\phi = \frac{1}{G} \int_0^{L_x} \left\{ \frac{M(x)}{A^2(x)} \left[\int_0^C \frac{ds}{t(s)} \right](x) \right\} dx$$

$$\left[\int_0^C \frac{ds}{t(s)} \right](x) = 4 \int_0^{90} \frac{r(x)\, d\theta}{t_0(1 + \sin\theta)}$$

$$= \frac{4r(x)}{t_0} \left[-\tan\left(\frac{\pi}{4} - \frac{\theta}{2}\right) \right]_0^{90}$$

$$= \frac{4r(x)}{t_0}$$

Therefore, for maximum angle of twist

$$4G\phi = \frac{4}{t_0} \int_0^L \frac{M_0\left(\frac{x}{L}\right) r_0 \left(1 + \left(\frac{x}{L}\right)\right.}{\pi^2 r_0^4 \left(1 + \frac{x}{4}\right)^4} dx$$

$$G\phi = \frac{M_0}{\pi^2 r_0^3 t_0 L} \int_0^L \frac{x\, dx}{\left(1 + \frac{x}{L}\right)^3}$$

$$G\phi = \frac{M_0 L^2}{\pi^2 r_0^3 t_0 L} \left[\frac{-1}{\left(1 + \frac{x}{L}\right)} + \frac{1}{2\left(1 + \frac{x}{L}\right)^2} \right]_0^L$$

$$G\phi = \frac{M_0 L}{\pi^2 r_0^3 t_0} \left(\frac{1}{8}\right)$$

$$\phi = \frac{M_0 L}{8\pi^2 r_0^3 t_0 G} = \frac{1 \times 10^5 \times 30}{8\pi^2 (5)^3 (0.1) 4 \times 10^6}$$

ϕ (max) = 0.76×10^{-3} radians .

SECTION B8.4

TORSION OF THIN-WALLED OPEN SECTIONS

TABLE OF CONTENTS

B8.4.0 TORSION OF THIN-WALLED OPEN SECTIONS

An open section is a section in which the centerline of the wall does not form a closed curve. Channels, angles, I-beams, and wide-flange sections are among many common structural shapes characterized by combinations of thin-walled rectangular elements; a variety of thin-walled curved sections is used in aircraft and missile structures. The basic characteristic of these sections is that the thickness of the component element is small in comparison with the other dimensions.

The torsional analysis of thin-walled open sections for both unrestrained and restrained torsion is included in this section. Torsional shear stress, angle of twist, and warping deformations are determined for unrestrained torsion. Torsional shear stress, warping shear stress, warping normal stress, angle of twist, and the first, second, and third derivatives of angle of twist are determined for restrained torsion.

B8.4.1 GENERAL

The stresses and deformations determined by the equations in this section can be superimposed with bending and axial load stress and deformations if the limitations of Section B8.4.1-II are not exceeded and proper consideration of stress and deformation sign convention is taken into account.

B8.4.1 GENERAL

I. BASIC THEORY

If a member of open cross section is twisted by couples applied at the ends in the plane perpendicular to the axis of the bar and the ends are free to warp, we have the case of unrestrained torsion (Fig. B8.4.1-1).

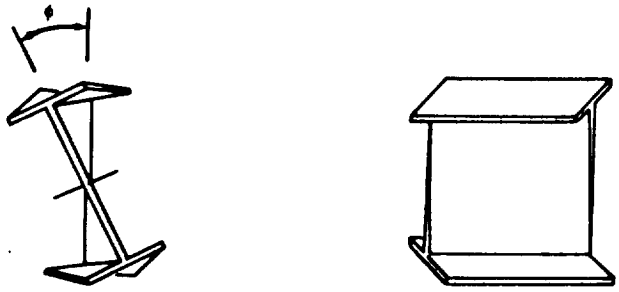

A. Rotated Section B. Warped Section

Figure B8.4.1-1. Warping

However, if cross sections are not free to warp or if the torque varies along the length of the bar, warping varies along the bar and torsion is accompanied by tension or compression of longitudinal fibers. Also, the rate of change of the angle of twist along the bar's longitudinal axis varies. This case is called restrained torsion.

These two types of torsion will be discussed separately in the following sections.

A. Unrestrained Torsion

The twisting moment on thin-walled open sections is resisted only by the torsional shear stress for unrestrained torsion. However, the manner in

which a thin-walled open section carries a torsional moment differs from the manner in which the thin-walled closed section carries a torsional moment. This difference can be seen by comparison of Figures B8.2.1-1A, B8.2.2-2A, and B8.3.1-1A to Figure 8.4.1-2. The thin-walled closed section carries the load by a shear flow that goes around the section, while the open section carries the load by a shear flow which goes around the perimeter of the section. From Figure B8.4.1-2, it can be seen that the shear stress distribution across the thickness of the section is linear and that the maximum stress on one edge is equal to the negative of the maximum stress on the other edge. (Ref. 1).

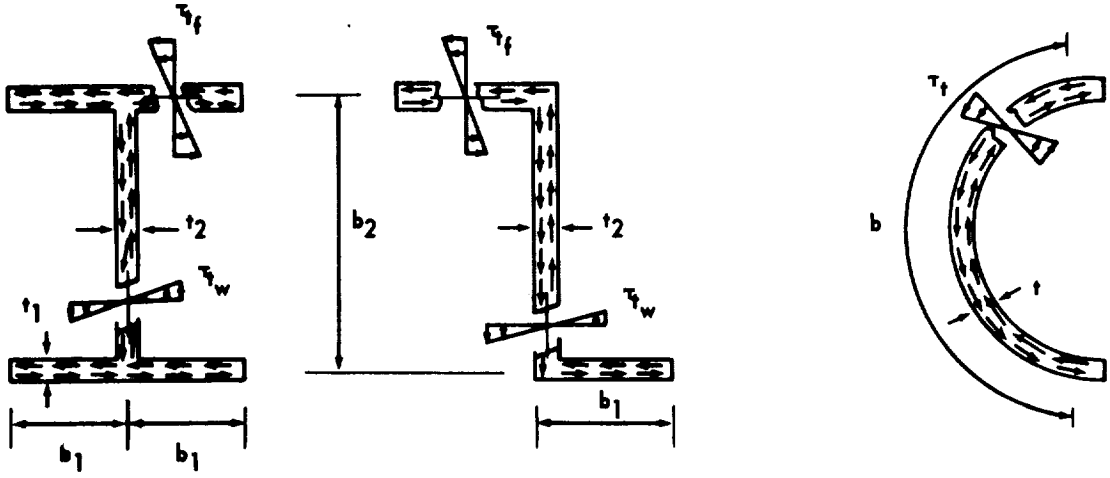

Figure B8.4.1-2. Pure Torsion Shear Stress Distribution

The torsional analysis of thin-walled open sections for unrestrained torsion will require that the torsional shear stress (τ_t) be determined at any point (P) on the section. Because of the definition of unrestrained torsion, the torsional shear stress at any point on the section will remain constant throughout the length of the member.

The angle of twist of the cross section (ϕ) should also be determined, plus the warping deformation (w) at any point (P) on the cross section.

As was the case for solid sections and thin-walled closed sections, two unique coefficients exist that characterize the geometry of each cross section. These coefficients are called the torsional constant (K) and the torsional modulus (S_t) and are functions of the dimensions of the cross section. These coefficients are discussed in detail below (Section B8.4.1-IV).

B. Restrained Torsion

When a member with a thin-walled open cross section is restrained against warping a complex distribution of longitudinal stresses is developed that cannot be evaluated using elementary theories. The assumption that plane sections remain plane during deformation is no longer valid, and applications of Saint-Venant's principle may lead to serious errors. In thin-walled open sections, stresses produced by restrained warping diminish very slowly from their points of application and may constitute the primary stress system developed in the member.

Obviously, if one section is restrained in such a way that it cannot warp, a system of normal stresses must be developed to eliminate this warping. In general, these normal stresses vary from point to point along the member and, hence, they are accompanied by a nonuniform shearing stress distribution. This, in turn, alters the twist of the section. As a result, the twisting moment developed on each section is no longer proportional to the rate of twist, and final shearing stresses cannot be obtained by those that were produced by unrestrained torsion.

Therefore, three types of stresses must be evaluated for the case of restrained torsion. These are: (1) pure torsional shear stress, (2) warping shear stress, and (3) warping normal stress. These stress distributions are shown for several common sections in Figures B8.4.1-3, B8.4.1-4, and B8.4.1-5. It will be required to evaluate these stresses at any point (P) on the cross section and at any arbitrary distance (L_x) from the origin. Also, the angle of twist (ϕ) should be determined between an arbitrary cross section and the origin along with the warping deformation (w) at any point (P) on an arbitrary cross section. **(Ref. 2).**

It was shown previously that two coefficients were necessary to characterize the geometry of the cross section for unrestrained torsion. These were the torsional constant (K) and the torsional section modulus (S_t). For restrained torsion, three additional coefficients are required to characterize fully the geometry of the cross section and the point where the stresses are to be determined. These coefficients are called the warping constant (Γ) — a function of the dimensions of the cross section, the normalized warping function (W_n), and warping statical moment (S_w). The latter two are functions of both the dimensions of the cross section and a specific point on the cross section. These coefficients are discussed in detail in Section B8.4.1-IV.

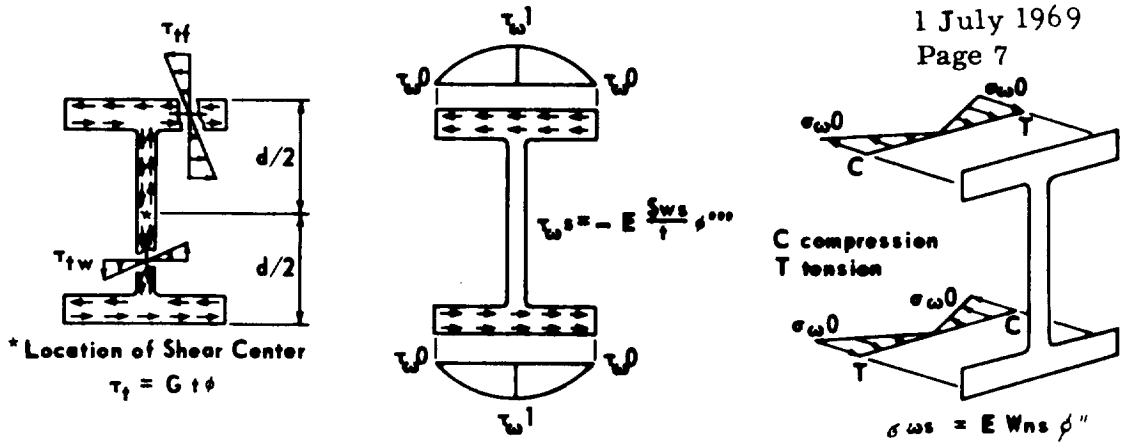

Figure B8.4.1-3. Restrained Warping Stress in I-Section

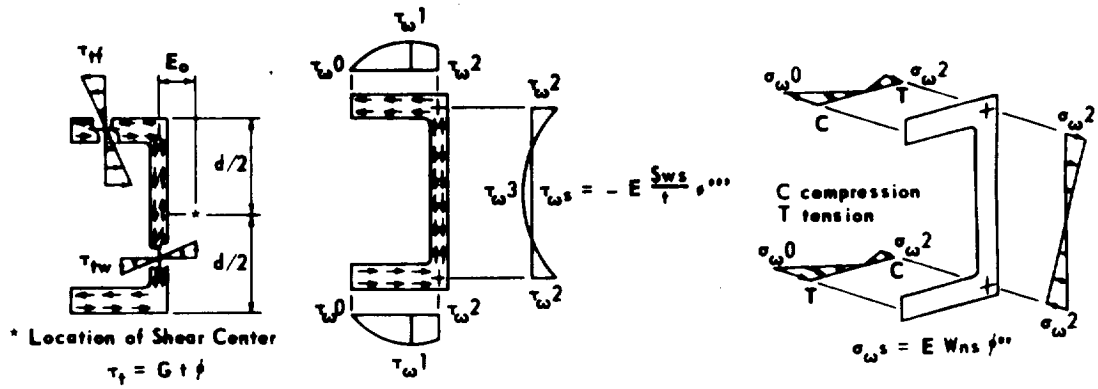

Figure B8.4.1-4. Restrained Warping Stresses in Channel Section

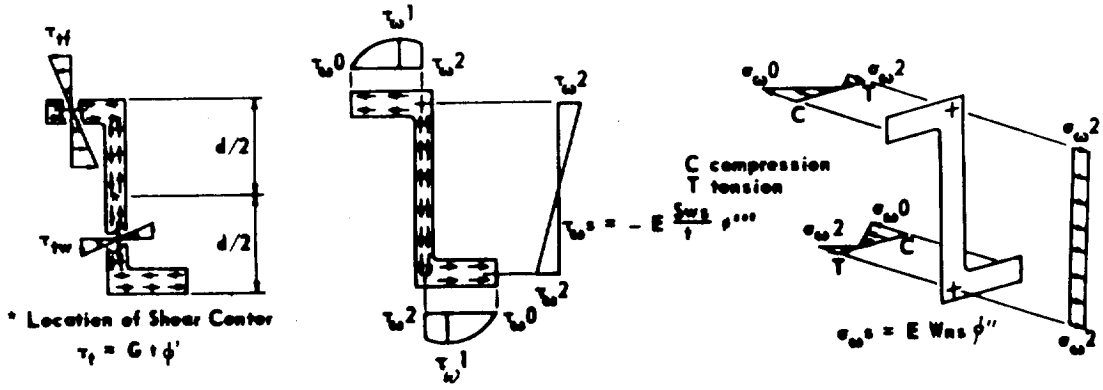

Figure B8.4.1-5. Restrained Warping Stresses in Z-Section

B8.4.1 GENERAL

II. LIMITATIONS

The torsional analysis of thin-walled open sections is subject to the following limitations:

A. Homogeneous and isotropic material

B. Thin-walled cross section not necessarily of constant thickness

C. No abrupt variations in thickness except at reentrant corners

D. No buckling

E. Inexact calculations of stresses at points of constraint and at abrupt changes of applied twisting moment

F. Applied twisting moment cannot be impact load

G. No abrupt changes can occur in cross section

H. Shear stress is within shearing proportional limit and proportional to the shear strain (elastic analysis).

I. Points of constraint are fully fixed, and no partial fixity is allowed.

B8.4.1 GENERAL

III. MEMBRANE ANALOGY

In the case of a narrow rectangular cross section, the membrane analogy gives a very simple solution to the torsional problem. Neglecting the effect of the short sides of the rectangle and assuming that the surface of the slightly deflected membrane is cylindrical (Figure B8.4.1-6), the deflection is

$$H = \frac{pt^2}{8T}$$

and the maximum slope is $\frac{pt}{2T}$. The volume bounded by the deflected membrane and the xy plane is (Ref. 3):

$$V = \frac{pbt^3}{12T} .$$

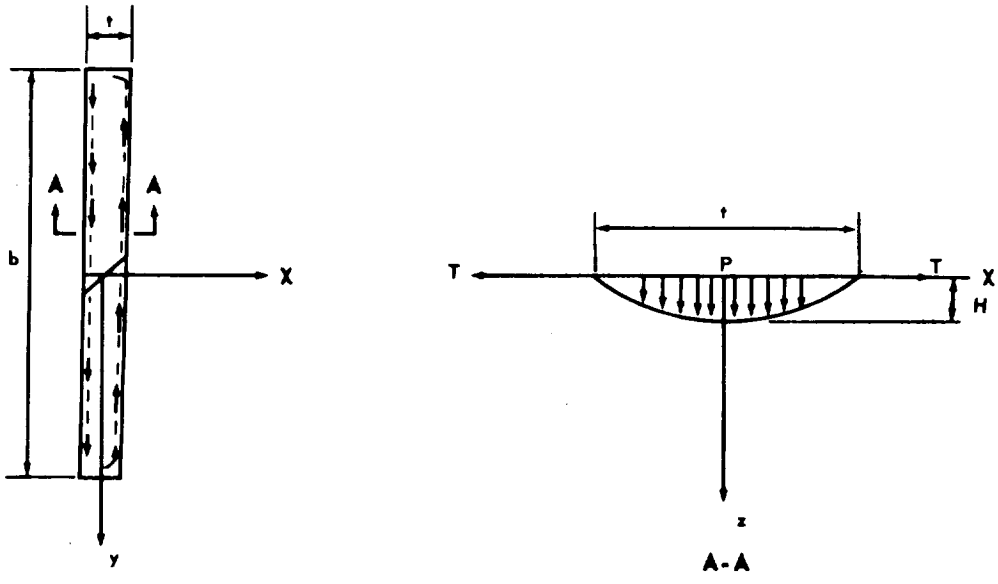

Figure B8.4.1-6. Membrane Analogy for Torsion of Thin Rectangular Section

Now using membrane analogy and substituting $2G\theta$ for p/T in the previous equations, the twisting moment (M_t) is given by

$$M_t = \frac{1}{3} bt^3 G\theta$$

or

$$\theta = M_t / 1/3bt^3G = \frac{M_t}{S_t G t}$$

and the maximum shearing stress is

$$\tau_{max} = tG\theta = \frac{M_t}{\frac{1}{3} bt^2} = \frac{M_t}{S_t}$$

where

$$S_t = 1/3bt^2 .$$

The equations for M_t and τ_{max}, obtained for a thin rectangle can also be used for cross sections, such as those shown in Figure B8.4.1-2, by simply adding the expression $1/3bt^3$ for each element of the section (neglecting a small error at corners or points of intersection of the elements). In the general case of a section with N elements:

$$K = 1/3 \sum_{i=1}^{n} b_i t_i^3 .$$

The maximum shearing stress on any element i is given by

$$(\tau_{max})_i = \frac{M_t (t_i)_{max}}{S_t} .$$

The maximum stress on the entire section is given by

$$\tau_{max} = \frac{M_t t_{max}}{S_t} .$$

B8.4.1 GENERAL

IV. TORSIONAL COEFFICIENTS

In the development of the formulas for the torsional analysis of open cross sections, it is convenient to designate certain terms as torsional coefficients for the cross section. The terms K and Γ are properties of the entire cross section, while the terms S_t, S_w, and W_n apply to specific points on the cross section.

A. Torsional Constant (K)

The torsional coefficient (K) is called the torsional constant, and its value depends upon the geometry of the cross section.

Torsional constants for thin-walled open sections are based on formulas for the thin rectangle.

Section B8.2.2-III contains an expression for the torsional constant for a general rectangular section. Since we are concerned with a thin-walled section, it can be seen that when the length-to-thickness ratio is approximately ten, the value of the torsion constant is

$$K \cong 1/3bt^3 .$$

This value is also verified by the membrane analogy in Section B8.4.1-III. The torsional constant for curved elements is the same as that for a rectangle with b denoting the length of the curved element, as shown in Figure B8.4.1-2.

Therefore, for a section composed of many thin rectangular, or thin curved elements, the torsional constant can be evaluated by the following expression:

$$K = 1/3 \sum_{i}^{n} b_i t_i^3 \quad .$$

If a section has any element with a length-to-thickness ratio less than ten, the value of K for that element should be determined by the equations in Section B8.2.2-III.

More accurate torsional constant expressions are determined for some standard sections by considering the junctions of the rectangles and rounded fillets at the junctions.

Some K values for frequently used sections are **(Ref. 2)**:

1. For I sections with uniform flanges (Fig. B8.4.1-7A):

$$K = 2/3bt_f^3 + 1/3(d-2t_f)\, t_w^3 + 2\,\alpha\, D^4 - 0.42016t_f^4$$

where

$$\alpha = 0.094 + 0.07\,\frac{R}{t_f}$$

$$D = \frac{(t_f + R)^2 + t_w\left(R + \frac{t_w}{4}\right)}{2R + t_f}$$

2. For I sections with sloping flanges (Fig. B8.4.1-7B):

$$K = \frac{b - t_w}{6}\,(t_f + a)\,(t_f^2 + a^2) + 2/3\, t_w a^3 + 1/3(d - 2a)\, t_w^3$$

$$+ 2\,\alpha\, D^4 - Et_f^4$$

where

$$D = \frac{(F + c)^2 + t_w \left(R + \frac{t_w}{4}\right)}{F + R + c}$$

and for 5-percent flange slope

$$\alpha = 0.066 + 0.021 \frac{t_w}{a} + 0.072 \frac{R}{a}$$

$$E = 0.44104$$

$$F = \frac{R}{20} \left(19.0250 - \frac{t_w}{2R}\right)$$

and for 2-percent flange slope

$$\alpha = 0.084 + 0.007 \frac{t_w}{a} + 0.071 \frac{R}{a}$$

$$E = 0.42828$$

$$F = \frac{R}{50} \left(49.01 - \frac{t_w}{2R}\right) .$$

3. For channels with sloping flanges (Fig. B8.4.1-7C):

$$K = 1/3\ t_w^3 d + \frac{b'}{6} (a + t_f) (a^2 + t_f^2) .$$

4. For Tee section (Fig. B8.4.1-7D):

$$K = \frac{bt_f^3}{3} + \frac{ht_w^3}{3} + \alpha D^4$$

where

$$\alpha = 0.094 + 0.07 R/t_f$$

$$D = \frac{(t + R)^2 + t_w \left(R + \frac{t_w}{4}\right)}{2R + t_f}$$

5. Angle section (Fig. B8.4.1-7E):

$$K = 1/3bt_1^3 + 1/3\ dt_2^3 + \alpha D^4$$

where

$$\alpha = \frac{t_2}{t_1}\left(0.07 + 0.076 \frac{R}{t_1}\right) \qquad t_1 \geqq t_2$$

$$D \cong \frac{(t_1 + R)^2 + t_2 \left(R + \frac{t_2}{4}\right)}{2R + t_1}$$

6. Zee section and channel section with uniform flanges (Fig. B8.4.1-7F).

K values for these sections can be calculated by summing the K's of the constituent angle sections computed in case 5.

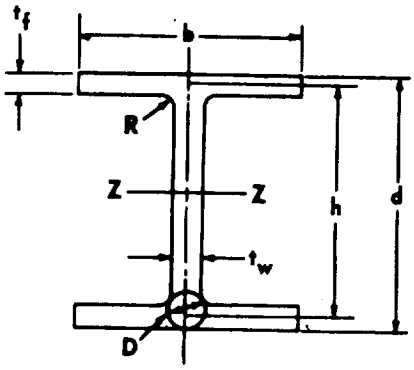

A. Uniform Flanges

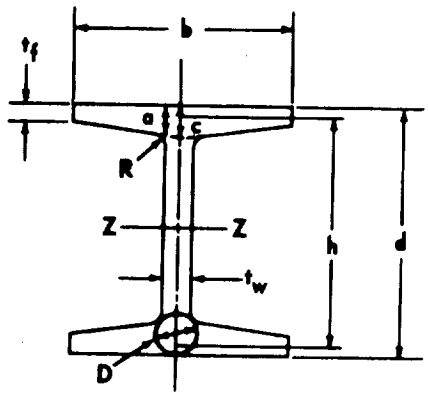

B. Sloping Flanges

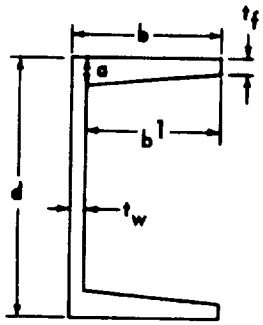

C. Channel with Sloping Flanges

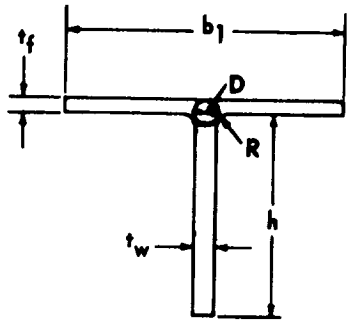

D. Tee Section

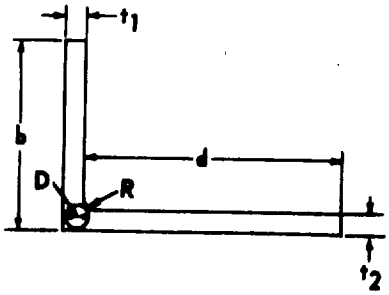

E. Angle

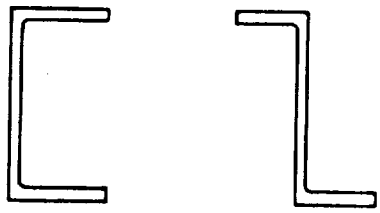

F. Zee and Uniform Channel

Figure B8.4.1-7. Frequently Used Sections

It should be noted that the K formulas for these frequently used sections are based on membrane analogy and on reasonably close approximations giving results that are rarely as much as 10 percent in error.

B. Torsional Modulus (S_t)

The torsional coefficient (S_t) is called the torsional modulus. Its value for any point on the section depends upon the geometry of the cross section.

The basic equation for determining the torsional modulus at an arbitrary point (s) on a cross section is:

$$S_t(s) = \frac{K}{t(s)}$$

where K is as defined in Section B8.4.1-IVA and t(s) is the thickness of the section at point (s).

Because the torsional modulus is necessary for the calculation of the torsional shear stress in the equation

$$t = \frac{M(x)}{S_t(x,s)}$$

it is often required to find the minimum value of $S_t(s)$ in order to make τ_t a maximum.

Therefore:

$$S_t(\min) = \frac{K}{t_{max}}$$

where t_{max} is the maximum thickness in the cross section.

C. Normalized Warping Function (W_n)

The torsional coefficient (W_n) is called the normalized warping function. Its value depends upon the geometry of the cross section and upon specific points on the cross section.

For the generalized section shown in Figure B8.4.1-8, the following equation is used for calculating $W_n(s)$ at any point (s) on the section:

$$W_n(s) = \frac{1}{A} \int_0^b W_{os}\, tds - w_{os}$$

where

$$A = \int_0^b tds$$

$$W_{os} = \int_0^s \rho_o\, ds.$$

Some W_n values for frequently used sections include:

1. For symmetrical wide flange and I-shapes (Fig. B8.4.1-9A):

$$W_{no} = \frac{bh}{4}$$

2. For channel sections (Fig. B8.4.1-9B):

$$W_{no} = \frac{uh}{2}$$

$$W_{n2} = \frac{E_o h}{2}$$

ρ Perpendicular distance to tangent line from centroid
ρ_o Perpendicular distance to tangent line from shear center
cg Centroid of cross section
sc Shear center of cross section
z,y Coordinates referred to the principal centroidal axes
ϕ Angle of twist

[All directions are shown positive. ρ and ρ_o are positive if they are on the left side of an observer at P (z,y) facing the positive direction of s.]

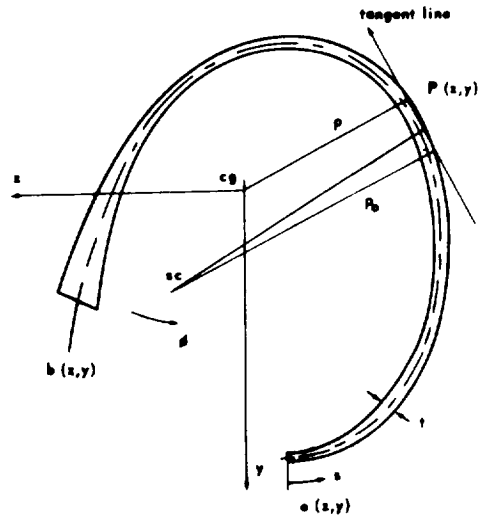

Figure B8.4.1-8. General Thin-Walled Open Cross Section

where

$$E_o = \frac{(b')^2 t}{2b't + h t_w/3}$$

and

$$u = b' - E_o .$$

3. For zee sections (Fig. B8.4.1-9C):

$$W_{no} = \frac{uh}{2}$$

$$W_{n2} = \frac{u'h}{2}$$

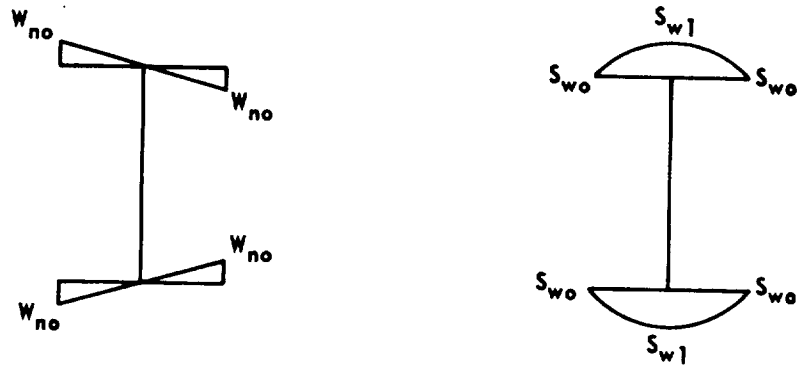

A. Symmetrical H-and I-Sections

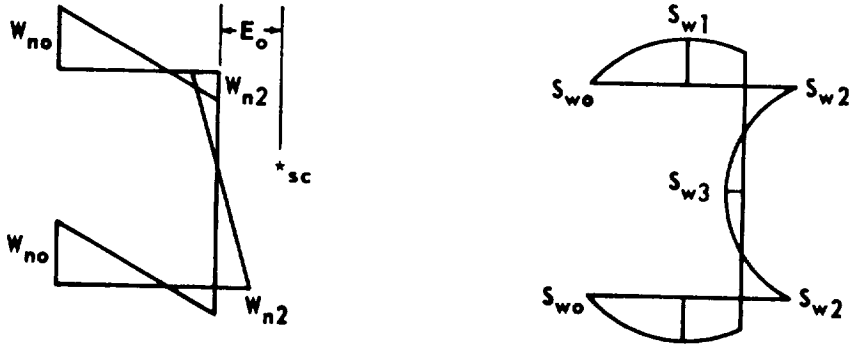

B. Channel Sections

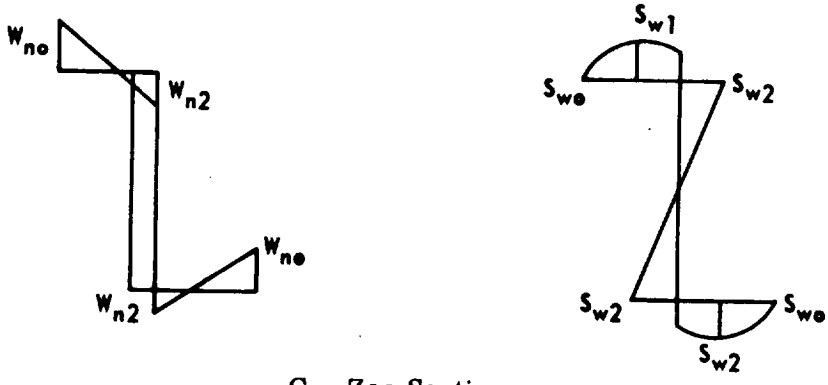

C. Zee Sections

Figure B8.4.1-9. Distribution of W_n and S_w for Standard Sections

where

$$u = b' - u'$$

$$u' = \frac{(b')^2 t}{h_{tw} + 2b't} \quad .$$

In the foregoing expressions:

h = distance between centerlines of flanges, in.

b = flange width, in.

b' = distance between toe of flange and centerline of web, in.

t = average thickness of flange, in.

t_w = thickness of web, in.

D. Warping Statical Moments (S_w)

The torsional coefficient (S_w) is called the warping statical moment. Its value depends upon the geometry of the cross section and upon specific points on the cross section.

For the generalized section shown in Figure B8.4.1-8, the following equation is used for calculating $S_w(s)$ at any point (s) on the section:

$$S_w(s) = \int_o^s W_n(s)\, t\, ds.$$

The value of $W_n(s)$ is determined from the previous subsection (B8.4.1-IVC). Some S_w values for frequently used sections include:

1. For symmetrical wide flange and I-shapes (Figure B8.4.1-9A):

$$S_{w1} = \frac{hb^2t}{16}$$

2. For channel sections (Figure B8.4.1-9B):

$$S_{w1} = \frac{u^2ht}{4}$$

$$S_{w2} = \frac{(b' - 2E_o)hb't}{4}$$

$$S_{w3} = \frac{(b' - 2E_o)hb't}{4} - \frac{E_o h^2 t_w}{8}$$

3. For zee sections (Fig. B8.4.1-9C):

$$S_{w1} = \frac{(ht_w + b't)^2 h(b')^2 t}{4(ht_a + 2b't)^2}$$

$$S_{w2} = \frac{h^2 t_w (b')^2 t}{4(ht_w + 2b't)}$$

where u, h, t, b, b', E_o, and t_w are defined in the previous section.

E. Warping Constant (Γ)

The torsional coefficient (Γ) is called the warping constant. Its value depends only on the geometry of the cross section. For the generalized section shown in Figure B8.4.1-8, the following equation is used for calculating Γ:

$$\Gamma = \int_0^b W_n(s)\, t^2 ds \ .$$

The value of $W_n(s)$ is determined from Section B8.4.1-IVC. Some values for frequently used sections are:

1. For symmetrical wide flange and I-shapes (Fig. B8.4.1-9A):

$$\Gamma = \frac{h^2 b^3 t}{24} = \frac{I_y h^2}{4} \ .$$

2. For channel sections (Fig. B8.4.1-9B):

$$\Gamma = 1/6\ (b'3E_o) h^2(b')\ t + F_o^2\, I_x \ .$$

3. For zee sections:

$$\Gamma = \frac{(b')^3 t h^2}{12} \ \frac{b't + 2ht_w}{nt_w + 2b't}$$

where h, b, t, t_w, b', and E_o are defined in Section B8.4.1-IVC, I_x = the moment of inertia of the entire section about the xx axis, and I_y = the moment of inertia of the entire section about the yy axis.

B8.4.2 UNRESTRAINED TORSION

The formulas given in this section apply only to members of open cross section twisted by couples applied at the ends in the plane perpendicular to the longitudinal axis of the bar, and the ends are free to warp as shown in Figure B8.4.1-1.

B8.4.2 UNRESTRAINED TORSION

I. ANGLE OF TWIST

For the case of unrestrained torsion, the torsional moment resisted by the cross section is

$$M_1 = GK\,\phi'$$

where

M_1 = resisting moment of unrestrained cross section, in.-lb
$= M_t$

G = shear modulus of elasticity, psi

K = torsional constant for the cross section, $in.^4$

$\phi' = \frac{d\phi}{dX}$ = angle of twist per unit of length.

This is the first derivative of the angle of rotation ϕ with respect to X, the distance measured along the length of the member from the left (Fig. B8.4.2-1).

Therefore, the basic equation for determining the angle of twist between the origin and an arbitrary cross section at a distance L_x from the origin is:

$$\phi(x) = \frac{1}{G} \int_o^{L_x} \frac{M(x)}{K(x)}\, dx$$

where $K(x)$ is the torsion constant at L_x. If the cross section does not vary and $M(x)$ is taken as M_t applied at the end of the member, the angle of twist is determined from the equation:

$$\phi(x) = \frac{M_t L x}{GK} \quad .$$

The total twist of the bar is:

$$\phi(max) = \frac{M_t L}{GK} \quad .$$

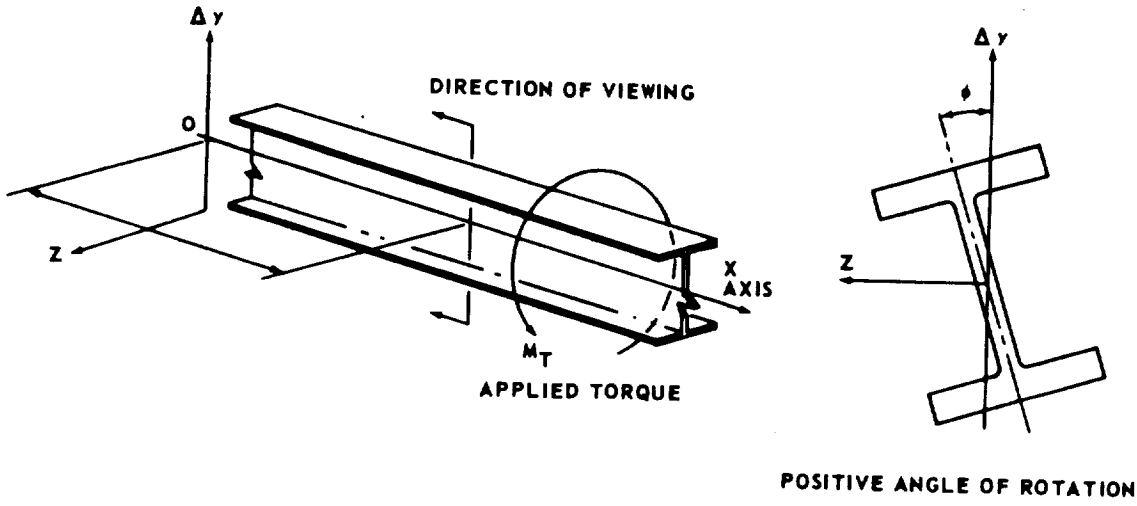

Figure B8.4.2-1. General Orientation

B8.4.2 UNRESTRAINED TORSION

II. STRESSES

The twisting moment (M_t) on thin-walled open sections is resisted only by the torsional shear stress for unrestrained torsion. The torsional shear stress at the edge of an element is determined by the formula:

$$\tau_t = Gt\,\phi' \ .$$

Because $\phi = \frac{M(x)}{GK}$ the basic equation for determining the torsional shear stress at an arbitrary point (s) on an arbitrary cross section is:

$$\tau_t = \frac{M(x)}{S_t(x,s)}$$

where

$$S_t(x,s) = \frac{K(x)}{t(x,s)} \ .$$

$K(x)$ is evaluated at $x = L_x$ where the torsional shear stress is to be determined, and $t(x,s)$ is evaluated at the arbitrary cross section and at the point(s) on the arbitrary cross section.

If the member has uniform cross section and $M(x)$ is taken as M_t, applied to the end of the bar, the equation reduces to:

$$\tau_t = \frac{M_t}{S_t(s)}$$

where

$$S_t(s) = \frac{K}{t(s)} \quad .$$

The maximum stress τ_t will occur on the thickest element; $t(s)$ is maximum.

B8.4.2 UNRESTRAINED TORSION

III. WARPING DEFORMATION

The basic equation for determining the warping deformation w(s) at any point on an arbitrary cross section at a distance $x = L_x$ from the origin is

$$w(s) - w_o = \phi' \int_o^s r ds$$

where w(s) is the warping deformation at point (s) on the middle line of the cross section in the x direction; w_o is the displacement in the x-direction of the point from which s is measured; r(s) is the distance of the tangent of arc length ds from point o, taken positive if a vector along the tangent and pointing in the direction of increasing s gives a positive moment with respect to the axis of rotation (Fig. B8.4.2-2); ϕ' is determined from Section B8.4.2-I.

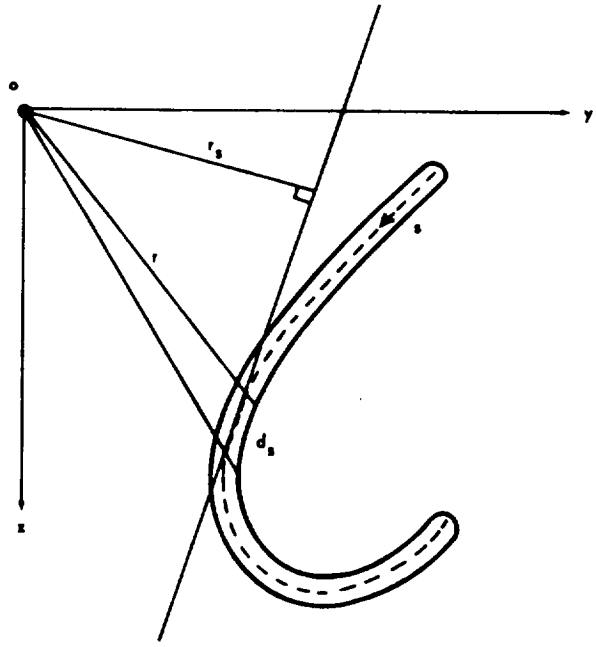

Figure B8.4.2-2. General Section

For the case of unrestrained torsion, the point 0 can be located arbitrarily.

The warping of the cross section with respect to the plane of average w has been found to be

$$w(s) = \phi' W_n(s)$$

where $W_n(s)$ is the normalized warping function found in Section B8.4.1-IVC.

B8.4.2 UNRESTRAINED TORSION

IV. STRESS CONCENTRATION FACTORS

Stress concentrations occur in composite cross sections at any reentrant corner; that is, at the intersection of the web and either of the flanges in the I-section or at the interior angle joining the two legs of the angle section. Exact analysis of stress concentrations at these points is very difficult and must be carried out experimentally, usually by membrane analogy.

For many common sections, the maximum stress at the concave or reentrant point is

$$\tau_{max} = K_3 \, G \, \phi'$$

where (Ref. 4)

$$K_3 = \frac{D}{1 + \frac{\pi^2 D^4}{16 A^2}} \left\{ 1 + \left[0.118 \ln \left(1 + \frac{D}{2\rho} \right) + 0.238 \frac{D}{2\rho} \right] \tanh \frac{2\theta}{\pi} \right\}$$

D = diameter of largest inscribed circle (Section B8.4.1-IVA)

A = cross-sectional area

ρ = radius of concave boundary at the point (positive)

θ = angle through which a tangent to the boundary rotates in rolling around the concave portion, rad.

For angles with legs of equal thickness, the percentage increase of stress in fillets is shown on Figure B8.4.2-3.

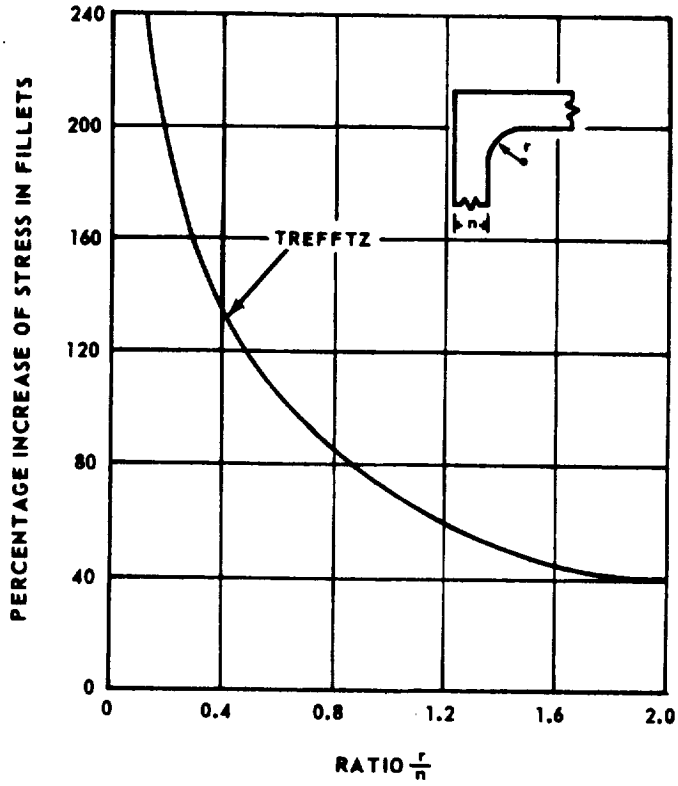

Figure B8.4.2-3. Stress Increase in Fillets of Angles

B8.4.4 EXAMPLE PROBLEMS

I. UNRESTRAINED TORSION

A member with an unsymmetrical section shown in Figure B8.4.4-1 is loaded by an end moment and is free to warp. If M_t = 100 in.-lbs and L = 41 in., determine the maximum angle of twist, torsional shear stress, and warping deformations.

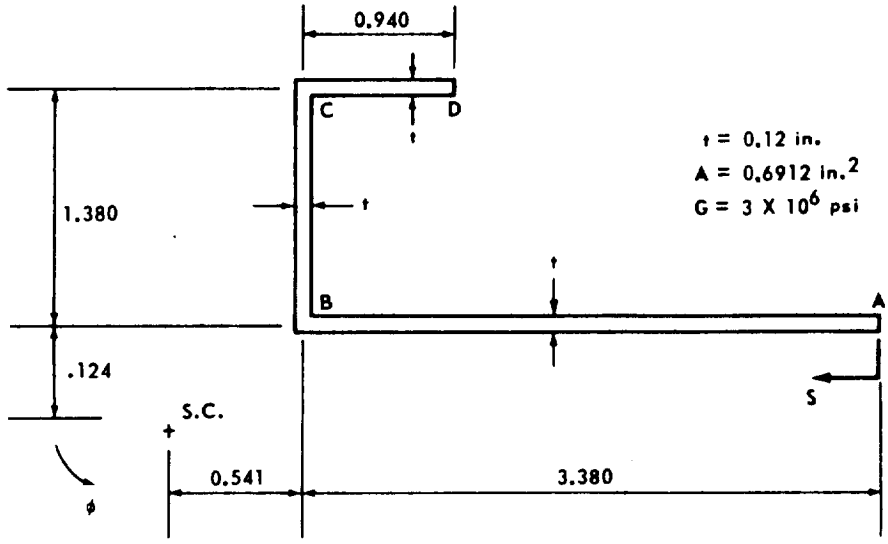

Figure B8.4.4-1. Cross Section for Example Problem I

Evaluate $W_{os} = \int_0^s \rho_o \, ds$:

$W_{os} = 0.124s$ for $s < 3.380$

$W_{os} = 0.419 + 0.541s$ for $4.760 > s > 3.380$

$W_{os} = 1.166 - 1.504s$ for $s > 4.760$

Evaluate $W_n(s)$:

$$W_n(s) = \frac{1}{A}\int_o^b W_{os}\,tds - W_{os}$$

$$\frac{1}{A}\int_o^b W_{os}\,tds = \frac{0.12}{0.6912}\left\{\int_o^{3.38} 0.124s\,ds + \int_o^{1.38} (0.419 + 0.541s)\,ds\right.$$

$$\left. + \int_o^{0.94} (1.166 - 1.504s)\,ds = 0.388.\right.$$

Then:

$W_n(s) = 0.388 - 0.124s$ for $s < 3.380$

$W_n(s) = -0.031 - 0.541s$ for $4.760 > s > 3.380$

$W_n(s) = -0.778 + 1.504s$ for $s > 4.76$.

Therefore, at points on the cross section:

$W_n(A) = 0.388$

$W_n(B) = -0.031$

$W_n(C) = -0.778$

$W_n(D) = 0.636$.

The distribution of $W_n(s)$ is shown in Figure B8.4.4-2.

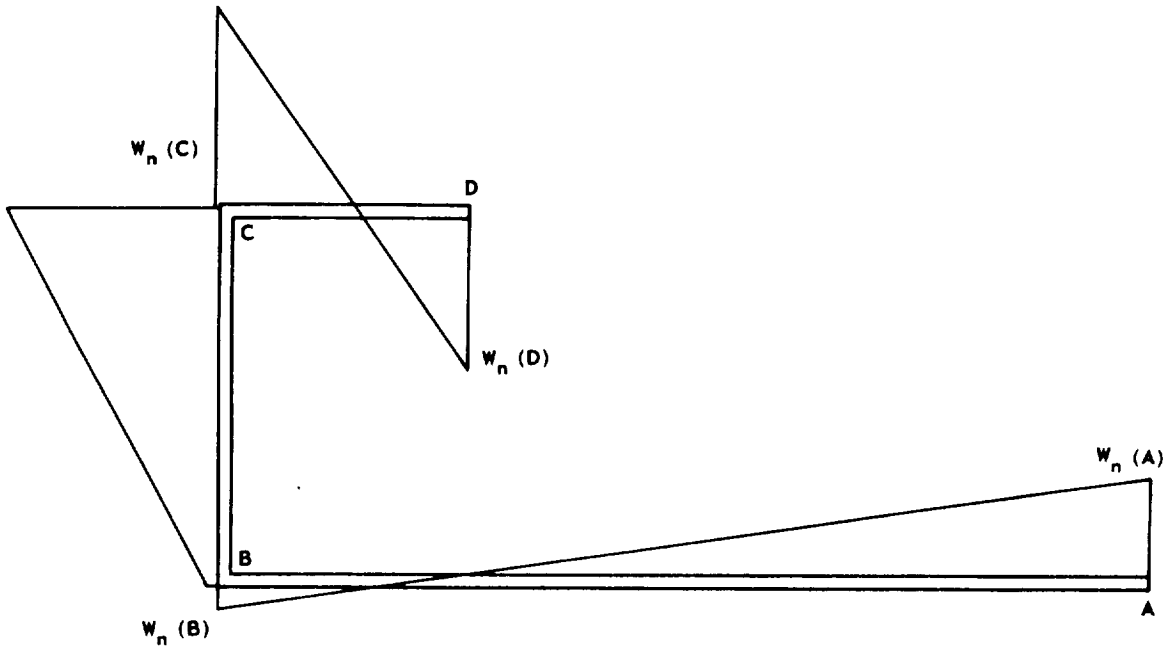

Figure B8.4.4-2. Distribution of $W_n(s)$

Warping Deformations (measured from mean displacement plane):

$$W(s) = \phi' W_n(s) \qquad \text{(Section B8.4.2-III)}$$

$$W(s) = \frac{M}{GK} W_n(s)$$

$$W(A) = \frac{100\ (0.388)}{3 \times 10^6 \times 3.285 \times 10^{-3}}$$

$$W(A) = 0.0039 \text{ in.}$$

$$W(B) = -0.0003 \text{ in.}$$

$$W(C) = -0.0079 \text{ in.}$$

$$W(D) = 0.0065 \text{ in.}$$

Evaluate K:

$$K = 1/3\ bt^3$$

$$K = 1/3(3.38 + 1.38 + 0.94)\ (0.12)^3$$

$$K = 3.285 \times 10^{-3}\ \text{in.}^4$$

Maximum angle of twist:

$$\phi\ (\max) = \frac{M_t L}{GK} \qquad \text{(Section B8.4.2-I)}$$

$$\phi\ (\max) = \frac{100 \times 41}{3 \times 10^6 \times 3.285 \times 10^{-3}}$$

$$\phi\ (\max) = 0.416 \text{ radian}.$$

Torsional Shear Stress:

$$\tau_t = \frac{M_t}{S_t(s)} \qquad \text{(Section B8.4.2-II)}$$

where

$$S_t(s) = \frac{K}{t}$$

$$\tau_t = \frac{100 \times 0.12}{3.285 \times 10^{-3}} = 3655 \text{ psi}.$$

B8.4.3 RESTRAINED TORSION

I. ANGLE OF TWIST AND DERIVATIVES

It was shown that for unrestrained torsion, the torsional moment resisted by the section is $M_1 = GK\phi'$ (Section B8.4.2-I).

Longitudinal bending occurs when a section is restrained from free warping. This bending is accompanied by shear stresses in the plane of the cross section, and these stresses resist the external applied torsional moment according to the following relationship:

$$M_2 = - E \Gamma \phi'''$$

where

M_2 = resisting moment caused by restrained warping of the cross section, in.-lb

E = modulus of elasticity, psi

Γ = warping constant for the cross section (Section B8.4.1-IVB), $in.^6$

ϕ''' = third derivative of the angle of rotation with respect to x.

Therefore, the total torsional moment resisted by the section is the sum of M_1 and M_2. The first of these is always present; the second depends on the resistance to warping. Denoting the total torsional resisting moment by M, the following expression is obtained.

$$M = M_1 + M_2 = GK\phi' - E\Gamma\phi'''$$

or

$$\frac{1}{a^2}\phi' - \phi''' = \frac{M}{E\Gamma}$$

where

$$a^2 = \frac{E\Gamma}{GK} \ .$$

The solution of this equation depends upon the distribution of applied torque (M) and the boundary or end restraints of the member. Numerical evaluation of this equation for ϕ, ϕ', ϕ'', and ϕ''' is obtained from a computer program in the Astronautics Computer Utilization Handbook for many loading and end conditions.

It is necessary to evaluate the foregoing expressions for the angle of twist and its derivatives before a complete picture of stress distribution and warping can be defined.

B8.4.3 RESTRAINED TORSION

II. STRESSES

A. Pure Torsional Shear Stress

The equation for torsional shear stress is the same as given in Section B8.4.2-II; however, now the angle of twist varies along the member and must be determined from the previous section.

Neglecting stress concentrations at reentrant corners, the pure torsional shear stress equation is

$$\tau_t = Gt\ \phi'.$$

This stress will be largest in the thickest element of the cross section. For distribution of this stress for common sections, see Figures B8.4.1-3, B8.4.1-4, and B8.4.1-5. This stress can be calculated by a computer program from the Astronautics Computer Utilization Handbook for many loading and end conditions.

B. Warping Shear Stress

When the cross section is restrained from warping freely along the entire length of the member, warping shear stresses are induced. These stresses are essentially uniform over the thickness (t), but the magnitude varies at different locations of the cross section (Figs. B8.4.1-3, B8.4.1-4, and B8.4.1-5). These stresses are determined from the equation:

$$\tau_{ws} = -\frac{ES_{ws}}{t}\ \phi'''$$

where

τ_{ws} = warping shear stress at point s, psi

E = modulus of elasticity, psi

S_{ws} = warping statical moment at point s (Section B8.4.1-IVD), $in.^4$

t = thickness of the element, in.

ϕ''' = third derivative of the angle of twist with respect to x, distance measured along the length of the member.

This stress can be calculated by a computer program from the Astronautic Computer Utilization Handbook for many loading and end conditions.

C. Warping Normal Stress

Warping normal stresses are caused when the cross section is restrained from warping freely along the entire length of the member. These stresses act perpendicular to the surface of the cross section and are constant across the thickness of an element but vary in magnitude along the length of the element. The magnitude of these stresses is determined by the equation:

$$\sigma_{ws} = E W_{ns} \phi''$$

where

σ_{ws} = warping normal stress at point s, psi

E = modulus of elasticity, psi

W_{ns} = normalized warping function at point s (Sec.B8.4.1-IVC), $in.^2$

ϕ' = record derivative of the angle of twist with respect to x, distance measured along the length of the member.

This stress can be calculated by a computer program from the Astronautic Computer Utilization Handbook for many loading and end conditions.

B8.4.3 RESTRAINED TORSION

III. WARPING DEFORMATIONS

Warping deformations can be calculated by using the same equation that was given in Section B8.4.2-III, except that now ϕ' will vary along the length of the member. The expression for ϕ' can be obtained from Section B8.4.3-I or values can be obtained from a program given in the Astronautic Computer Utilization Handbook. It should be noted that the warping normal stresses are proportional to corresponding warping displacements; hence, by knowing the warping displacements, a picture of distribution of the warping stresses is evident.

References

1. Oden, J. T.: Mechanics of Elastic Structures. McGraw-Hill Book Co., Inc., 1967.

2. Heins, C. P., Jr., and Seaburg, D. A.: Torsion Analysis of Rolled Steel Design File/Design Data. Bethlehem Steel AIA File No. 13-A-1.

3. Flügge, W.: Handbook of Engineering Mechanics. McGraw-Hill Book Co., Inc., 1962.

4. Roark, R. J.: Formulas for Stress and Strain. McGraw-Hill Book Co., Inc., 1965.

Bibliography

The Astronautics Computer Utilization Handbook, NASA.

Files, J. H.: Restrained Torsion of Thin-Walled Open Sections. IN-P&VE-S-67-1, August 20, 1967.

SECTION B9

PLATES

TABLE OF CONTENTS

TABLE OF CONTENTS (Continued)

TABLE OF CONTENTS (Concluded)

B9 PLATES

B9.1 INTRODUCTION

Plate analysis is important in aerospace applications for both lateral applied loads and also for sheet buckling problems. The plate can be considered as a two-dimensional counterpart of the beam except that the plate bends in all planes normal to the plate, whereas the beam bends in one plane only.

Because of the varied behavior of plates, they have been classified into four types, as follows:

Thick Plates — Thick plate theory considers the stress analysis of plates as a three-dimensional elasticity problem. The analysis becomes, consequently, quite involved and the problem is completely solved only for a few particular cases. In thick plates, shearing stresses become important, similar to short, deep beams.

Medium-Thick Plates — In medium-thick plates, the lateral load is supported entirely by bending stresses. Also, the deflections, w, of the plate are small compared to its thickness, t, ($w < t/3$). Theory is developed by making the following assumptions:

1. There is no in-plane deformation in the middle plane of the plate.
2. Points of the plate lying initially on a normal-to-the-middle plane of the plate remain on the normal-to-the-middle surface of the plate after bending.
3. The normal stresses in the direction transverse to the plate can be disregarded.

Thin Plates — The thin plate supports the applied load by both bending and direct tension accompanying the stretching of the middle plane. The deflections of the plate are not small compared to the thickness ($1/3t < w < 10t$) and bending of the plate is accompanied by strain in the middle surface. These supplementary tensile stresses act in opposition to the given lateral load and the given load is now transmitted partly by the flexural rigidity and partly by a membrane action of the plate. Thus, nonlinear equations can be obtained and the solution of the problem becomes much more complicated. In the case of large deflections, one must distinguish between immovable edges and edges free to move in the plane of the plate, which may have a considerable bearing upon the magnitude of deflections and stresses in the plate.

Membranes — For membranes, the resistance to lateral load depends exclusively on the stretching of the middle plane and, hence, bending action is not present. Very large deflections would occur in a membrane ($w > 10t$).

In the literature on plates, the greatest amount of information is available on medium-thick plates. Many solutions have been obtained for plates of various shapes with different loading and boundary conditions [1, 2]. However, in the aerospace industry, thin plates are the type most frequently encountered. Some approximate methods of analysis are available for thin plates for common shapes and loads.

This section includes some of the solutions for both medium-thick plates and thin plates. Plates subjected to thermal loadings are covered in Section D3.0.7. Plates constructed from composite materials are covered in Section F.

B9.2 PLATE THEORY

This section contains the theoretical solutions for medium-thick plates (small deflection), membranes, and thin plates (large deflection). Solutions for thick plates will not be given here as this type plate is seldom used in the industry.

B9.2.1 Small Deflection Theory

Technical literature on the small deflection analysis of plates contains many excellent derivations of the plate bending equations (References 1 and 2, for instance). Therefore, only key equations will be presented here.

Figure B9-1 shows the differential element of an initially flat plate acted upon by bending moments (per unit length) M_x and M_y about axes parallel to the y and x directions, respectively. Sets of twisting couples $M_{xy} (= -M_{yx})$ also act on the element.

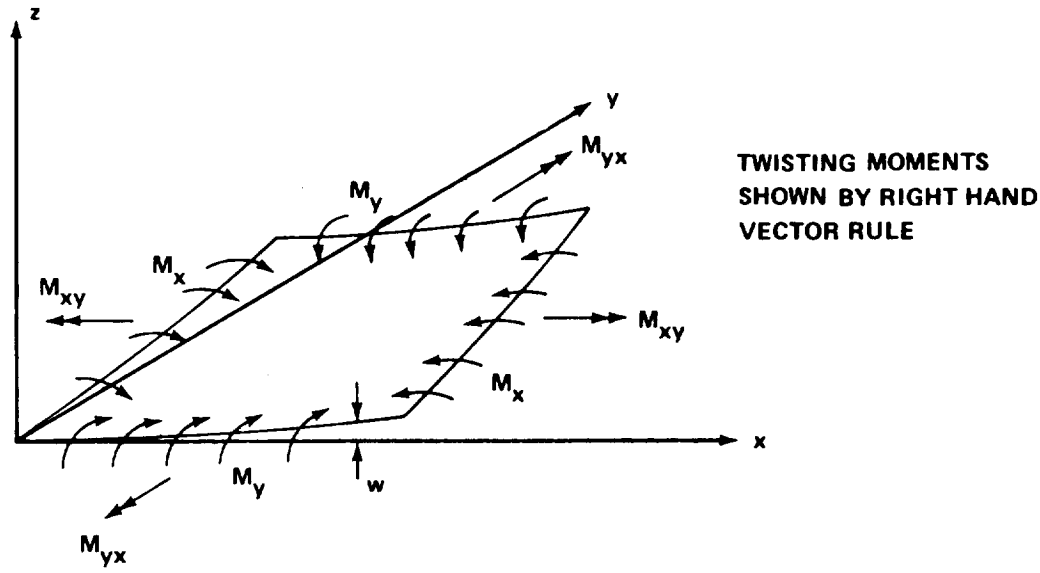

FIGURE B9-1. DIFFERENTIAL PLATE ELEMENT

As in the case of a beam, the curvature in the x, z plane, $\frac{\partial^2 w}{\partial x^2}$, is proportional to the moment M_x applied. The constant of proportionality is $\frac{1}{EI}$, the reciprocal of the bending stiffness. For a unit width of beam, $I = \frac{t^3}{12}$. In the case of a plate, due to the Poisson effect, the moment M_y also produces a (negative) curvature in the x, z plane. Thus, with both moments acting, one has

$$\frac{\partial^2 w}{\partial x^2} = \frac{12}{Et^3}\left(M_x - \mu M_y\right) \quad ,$$

where μ is Poisson's ratio. Likewise, the curvature in the y, z plane is

$$\frac{\partial^2 w}{\partial y^2} = \frac{12}{Et^3}\left(M_y - \mu M_x\right) \quad .$$

Rearranging these two equations in terms of curvature yields

$$M_x = D\left(\frac{\partial^2 w}{\partial x^2} + \mu \frac{\partial^2 w}{2y^2}\right) \qquad (1)$$

$$M_y = D\left(\frac{\partial^2 w}{\partial y^2} + \mu \frac{\partial^2 w}{\partial x^2}\right) \qquad (2)$$

where

$$D = \frac{Et^3}{12(1-\mu^2)} \quad .$$

The twist of the element, $\partial^2 w/\partial x \partial y$ $(=\partial^2 w/\partial y \partial x)$ is the change in x-direction slope per unit distance in the y-direction (and vice versa). It is proportional to the twisting couple M_{xy}. A careful analysis (see References 1 and 2) gives the relation as

$$M_{xy} = D(1-\mu)\frac{\partial^2 w}{\partial x \partial y} \quad . \qquad (3)$$

Equations (1), (2), and (3) relate the applied bending and twisting couples to the distortion of the plate in much the same way as does $M = EId^2y/dx^2$ for a beam.

Figure B9-2 shows the same plate elements as the one in Fig. B9-1, but with the addition of internal shear forces Q_x and Q_y (corresponding to the "v" of beam theory) and a distributed transverse pressure load q(psi). With the presence of these shears, the bending and twisting moments now vary along the plate as indicated in Fig. B9-2a.

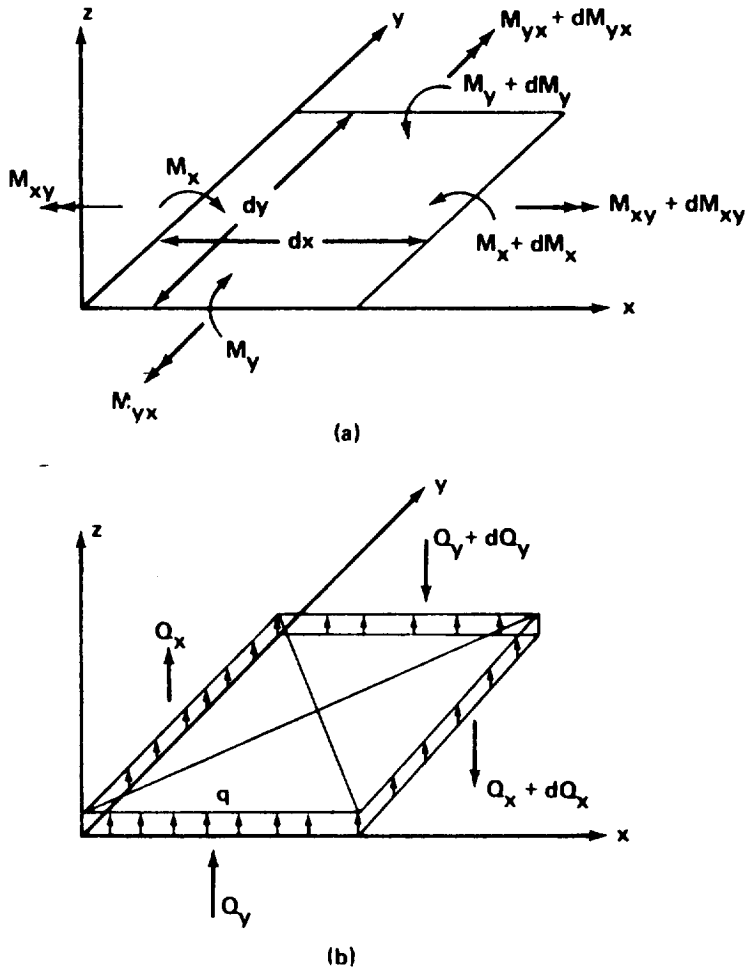

FIGURE B9-2. DIFFERENTIAL PLATE ELEMENT WITH LATERAL LOAD

By summing moments of the two loading sets of Figs. B9-2a and B9-2b about the y axis, one obtains

$$M_x dy + (M_{yx} + dM_{yx})dx + (Q_x + dQ_x)dxdy = (M_x + dM_x)dy + M_{yx}dx \quad .$$

Dividing by dxdy and discarding the term of higher order yields

$$Q_x = \frac{\partial M_x}{\partial x} - \frac{\partial M_{yx}}{\partial y} \quad , \qquad (4)$$

or,

$$Q_x = \frac{\partial M_x}{\partial x} + \frac{\partial M_{xy}}{\partial y} \quad . \qquad (4a)$$

In a similar manner, a moment summation about the x-axis yields

$$Q_y = \frac{\partial M_y}{\partial y} + \frac{\partial M_{xy}}{\partial x} \quad . \qquad (5)$$

[Equations (4) and (5) correspond to V = dM/dx in beam theory.]

One final equation is obtained by summing forces in the z-direction on the element:

$$q = \frac{\partial Q_x}{\partial y} + \frac{\partial Q_y}{\partial y} \quad . \qquad (6)$$

Equations (4), (5), and (6) provide three additional equations in the three additional quantities Q_x, Q_y, and q. The plate problem is, thus, completely defined. A summary of the quantities and equations obtained above are presented in Table B9-1. For comparison, the corresponding items from the engineering theory of beams are also listed.

Table B9-1. Tabulation of Plate Equations

Class	Item	Plate Theory	Beam Theory
Geometry	Coordinates	$x \quad y$	x
	Deflections	w	y
	Distortions	$\frac{\partial^2 w}{\partial x^2}, \frac{\partial^2 w}{\partial y^2}, \frac{\partial^2 w}{\partial x \partial y}$	$\frac{d^2 y}{dx^2}$
Structural Characteristic	Bending Stiffness	$D = \frac{Et^3}{12(1 - \mu^2)}$	EI
Loadings	Couples	M_x, M_y, M_{xy}	M
	Shears	Q_x, Q_y	V
	Lateral	q	q or w
Hooke's Law	Moment	$M_x = D\left(\frac{\partial^2 w}{\partial x^2} + \mu \frac{\partial^2 w}{\partial y^2}\right)$	$M = EI\frac{d^2 y}{dx^2}$
	Distortion	$M_y = D\left(\frac{\partial^2 w}{\partial y^2} + \mu \frac{\partial^2 w}{\partial x^2}\right)$	
	Relation	$M_{xy} = D(1 - \mu)\frac{\partial^2 w}{\partial x \partial y}$	
Equilibrium	Moments	$Q_x = \frac{\partial M_x}{\partial x} + \frac{\partial M_{xy}}{\partial y}$ $Q_y = \frac{\partial M_y}{\partial y} + \frac{\partial M_{xy}}{\partial x}$	$V = \frac{dM}{dx}$
	Forces	$q = \frac{\partial Q_x}{\partial x} + \frac{\partial Q_y}{\partial y}$	$q = \frac{dV}{dx}$

Finally, one very important equation is obtained by eliminating all internal forces (M_x, M_y, M_{xy}, Q_x, Q_y) between the six equations above. The result is a relation between the lateral loading q and the deflections w (for a beam, $q/EI = d^4y/dx^4$):

$$\frac{\partial^4 w}{\partial x^4} + 2\frac{\partial^4 w}{\partial x^2 \partial y^2} + \frac{\partial^4 w}{\partial y^4} = \frac{q}{D} \quad . \tag{7}$$

The plate bending problem is thus reduced to an integration of equation (7). For a given lateral loading $q(x,y)$, a deflection function $w(x,y)$ is sought which satisfies both equation (7) and the specified boundary conditions. Once found, $w(x,y)$ can be used in equations (1) through (5) to determine the internal forces and stresses. Often, various approximate methods are used to solve equation (7). One of the most powerful is the finite difference technique, presented in Reference 1.

It must be emphasized that in deriving the plate-bending equations it was assumed that no stresses acted in the middle (neutral) plane of the plate (no membrane stresses). Thus, in summing forces to derive equation (6), no membrane stresses were present to help support the lateral load. In the solutions to the great majority of all plate-bending problems, the deflection surface found is a nondevelopable surface, i.e., a surface which cannot be formed from a flat sheet without some stretching of the sheet's middle surface. But, if appreciable middle surface strains must occur, then large middle surface stresses will result, invalidating the assumption from which equation (6) was derived.

Thus, practically all loaded plates deform into surfaces which induce some middle surface stresses. It is the necessity for holding down the magnitude of these very powerful middle surface stretching forces that results in the more severe rule-of-thumb restriction that plate bending formulae apply accurately only to problems in which deflections are a few tenths of the plate's thickness.

B9.2.1.1 Orthotropic Plates

In the previous discussion it was assumed that the elastic properties of the material of the plate were the same in all directions. It will now be assumed that the material of the plate has three planes of symmetry with respect to the elastic properties. Such plates are generally called orthotropic plates. The bending of plates with more general elastic properties (anisotropic plates) is considered in Section F.

For orthotropic plates the relationship between stress and strain components for the case of plane stress in the x, y plane is presented by the following equations:

$$\sigma_x = E'_x \epsilon_x + E'' \epsilon_y$$

$$\sigma_y = E'_y \epsilon_y + E'' \epsilon_x$$

$$\tau_{xy} = G\gamma_{xy} \qquad (8)$$

Following procedures outlined in Reference 1, the expression for bending and twisting moments are

$$M_x = D_x \frac{\partial^2 w}{\partial x^2} + D_1 \frac{\partial^2 w}{\partial y^2} \qquad (9)$$

$$M_y = D_y \frac{\partial^2 w}{\partial y^2} + D_1 \frac{\partial^2 w}{\partial x^2} \qquad (10)$$

$$M_{xy} = 2D_{xy} \frac{\partial^2 w}{\partial x \partial y} \qquad (11)$$

in which

$$D_x = \frac{E'_x t^3}{12}, \quad D_y = \frac{E'_y t^3}{12}, \quad D_1 = \frac{E'' t^3}{12}, \quad D_{xy} = \frac{G t^3}{12} .$$

The relationship between the lateral loading q and the deflections w becomes:

$$D_x \frac{\partial^4 w}{\partial x^4} + 2\left(D_1 + 2D_{xy}\right)\frac{\partial^4 w}{\partial x^2 \partial y^2} + D_y \frac{\partial^4 w}{\partial y^4} = q \qquad . \qquad (12)$$

Equation (12) can be used in the investigation of plate bending for many various types of orthotropic construction which have different flexural rigidities in two mutually perpendicular directions. Specific solutions will be given in Subsection B9.5, Orthotropic Plates.

B9.2.2 Membrane Theory

Before large deflection theory of plates is discussed, one should consider the limiting case of the flat membrane which cannot support any of the lateral load by bending stresses and, hence, has to deflect and stretch to develop both the necessary curvatures and membrane stresses.

The two-dimensional membrane problem is a nonlinear one whose solution has proven to be very difficult [3]. However, we can study a simplified version whose solution retains the desired general features. The one-dimensional

analysis of a narrow strip cut from an originally flat membrane whose length in the y-direction is very large (Fig. B9-3).

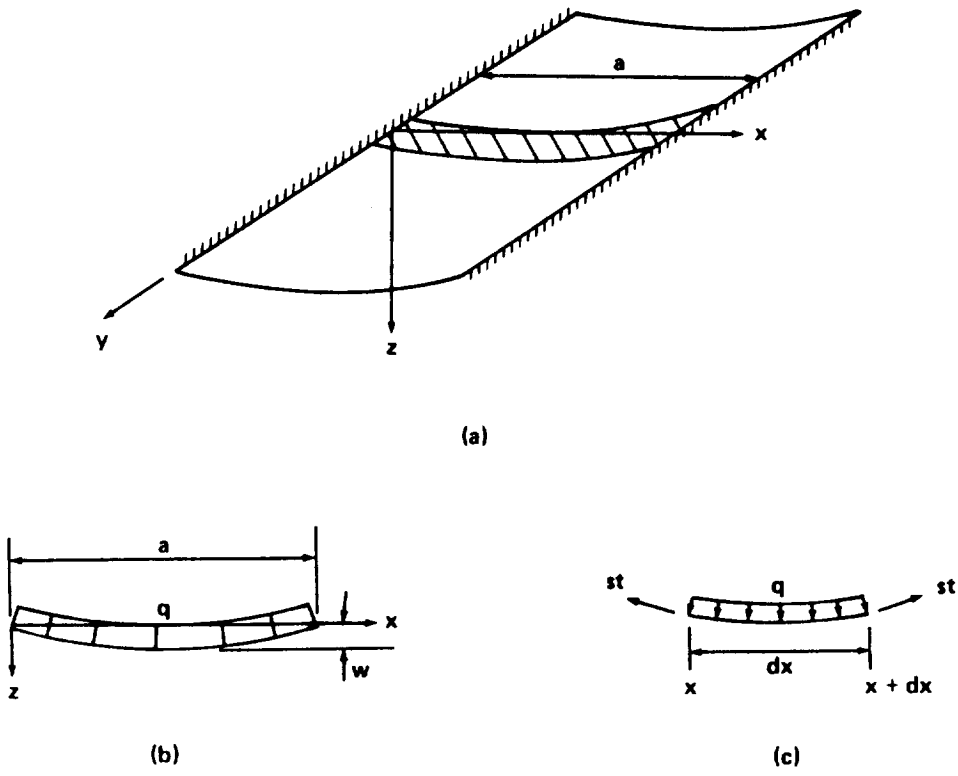

FIGURE B9-3. ONE-DIMENSIONAL MEMBRANE

Figure B9-3 shows the desired one-dimensional problem which now resembles a loaded cable. The differential equation of equilibrium is obtained by summing vertical forces on the element of Fig. B9-3c.

$$st\left(\frac{dw}{dx}\bigg|_{x+dx} - \frac{dw}{dx}\bigg|_{x}\right) + qdx = 0$$

or

$$\frac{d^2w}{dx^2} = -\frac{q}{st} \quad , \tag{13}$$

where s is the membrane stress in psi. Equation (13) is the differential equation of a parabola. Its solution is

$$w = \frac{qx}{2st}(a-x) \quad . \tag{14}$$

The unknown stress in equation (14) can be found by computing the change in length of the strip as it deflects. From Reference 3, this stretch δ is

$$\delta = \frac{1}{2}\int_0^a \left(\frac{dw}{dx}\right)^2 dx \quad .$$

Substituting through the use of equation (14) and integrating yields

$$\delta = \frac{q^2a^3}{24s^2t^2} \quad ,$$

and consideration of the stress-strain relationship yields

$$s = \frac{\delta}{a} E \quad .$$

By equating and solving for s one finds

$$s = 0.347 \left[E\left(\frac{qa}{t}\right)^2\right]^{\frac{1}{3}} \quad . \tag{15}$$

If equation (15) is substituted into equation (14), the maximum deflection at $x = a/2$ is

$$w_{max} = 0.360\, a \left(\frac{qa}{Et}\right)^{\frac{1}{3}} \quad . \tag{16}$$

Solutions of the complete two-dimensional nonlinear membrane problem have been obtained in Reference 4, the results being expressed in forms identical to those obtained above for the one-dimensional problem.

$$w_{max} = n_1 a \left(\frac{qa}{Et}\right)^{\frac{1}{3}} \qquad (17)$$

$$s_{max} = n_2 \left[E\left(\frac{qa}{t}\right)^2\right]^{\frac{1}{3}} . \qquad (18)$$

Here a is the length of the long side of the rectangular membrane, and n_1 and n_2 are given in Table B9-2 as functions of the panel aspect ratio a/b.

Table B9-2. Membrane Stress and Deflection Coefficients

a/b	1.0	1.5	2.0	2.5	3.0	4.0	5.0
n_1	0.318	0.228	0.16	0.125	0.10	0.068	0.052
n_2	0.356	0.37	0.336	0.304	0.272	0.23	0.205

The maximum membrane stress (s_{max}) occurs at the middle of the long side of the panel.

Experimental results reported in Reference 4 show good agreement with the theory for square panels in the elastic range.

B9.2.3 Large Deflection Theory

The theory has been outlined for the analysis of the two extreme cases of sheet panels under lateral loads. At one extreme, sheets whose bending stiffness is great relative to the loads applied (and which therefore deflect only slightly) may be analyzed satisfactorily by the plate bending solutions. At the other extreme, very thin sheets, under lateral loads great enough to cause large deflections, may be treated as membranes whose bending stiffness is ignored.

As it happens, the most efficient plate designs generally fall between these two extremes. On the one hand, if the designer is to take advantage of the presence of the interior stiffening (rings, bulkheads, stringers, etc.), which is usually present for other reasons anyway, then it is not necessary to make the skin so heavy that it behaves like a "pure" plate. On the other hand, if the skin is made so thin that it requires supporting of all pressure loads by stretching and developing membrane stresses, then permanent deformation results, producing "quilting" or "washboarding."

The exact analysis of the two-dimensional plate which undergoes large deflections and thereby supports the lateral loading partly by its bending resistance and partly by membrane action is very involved. As shown in Reference 1, the investigation of large deflections of plates reduces to the solution of two nonlinear differential equations. The solution of these equations in the general case is unknown, but some approximate solutions of the problem are known and are discussed in Reference 1.

An approximate solution of the large deflection plate problem can be obtained by adding the small deflection membrane solutions in the following way:

The expression relating deflection and uniform lateral load for small deflection of a plate can be found to be

$$w_{max} = \alpha \frac{q' a^4}{Et^3} \quad , \qquad (19)$$

where α is a coefficient dependent upon the geometry and boundary conditions of the plate.

The similar expression for membrane plates is equation (17)

$$w_{max} = n_1 a \left(\frac{q''a}{Et}\right)^{\frac{1}{3}} \quad . \tag{20}$$

Solving equations (19) and (20) for q' and q'' and adding the results yields

$$q = q' + q''$$

$$q = \frac{1}{\alpha} \frac{Et^3}{a^4\left(\frac{b}{a}\right)^4} w_{max} + \frac{1}{n_1^3} \frac{Et}{a^4} w_{max}^3 \quad . \tag{21}$$

Obviously, equation (21) is based upon summing the individual stiffnesses of the two extreme behavior mechanisms by which a flat sheet can support a lateral load. No interaction between stress systems is assumed and, since the system is nonlinear, the result can be an approximation only.

Equation (21) is best rewritten as

$$\frac{qa^4}{Et^4} = \frac{1}{\alpha}\left(\frac{w_{max}}{t}\right)\left(\frac{a}{b}\right)^4 + \frac{1}{n_1^3}\left(\frac{w_{max}}{t}\right)^3 \quad . \tag{22}$$

Figure B9-4 shows equation (22) plotted for a square plate using values of α =0.0443, and n_1 = 0.318. Also plotted are the results of an exact analysis [1]. As may be seen, equation (22) is somewhat conservative inasmuch as it gives a deflection which is too large for a given pressure.

The approximate large-deflection method outlined above has serious shortcomings insofar as the prediction of stresses is concerned. For simply supported edges, the maximum combined stresses are known to occur at the panel midpoint. Figure B9-5 shows plots of these stresses for a square panel

as predicted by the approximate method (substituting q' and q'' into appropriate stress equations).

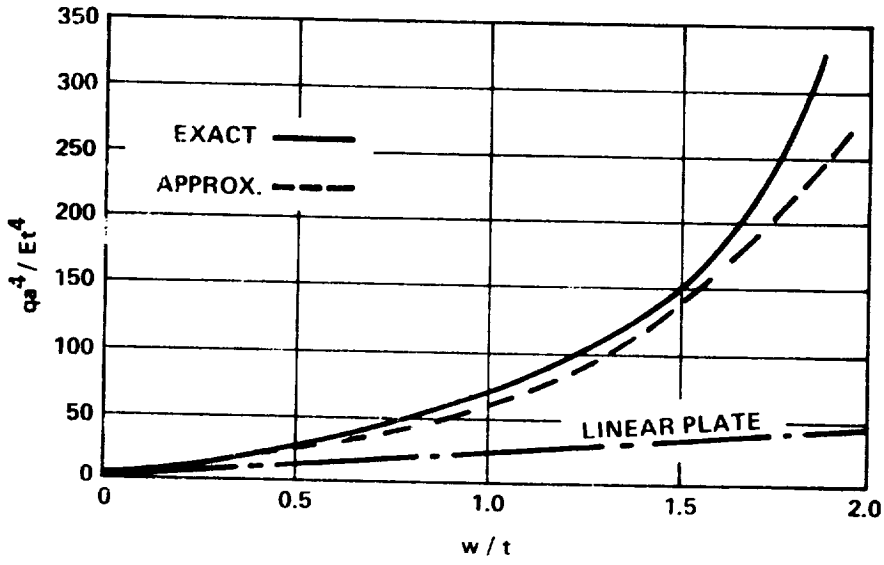

FIGURE B9-4. DEFLECTIONS AT THE MIDPOINT OF A SIMPLY SUPPORTED SQUARE PANEL BY TWO LARGE-DEFLECTION THEORIES

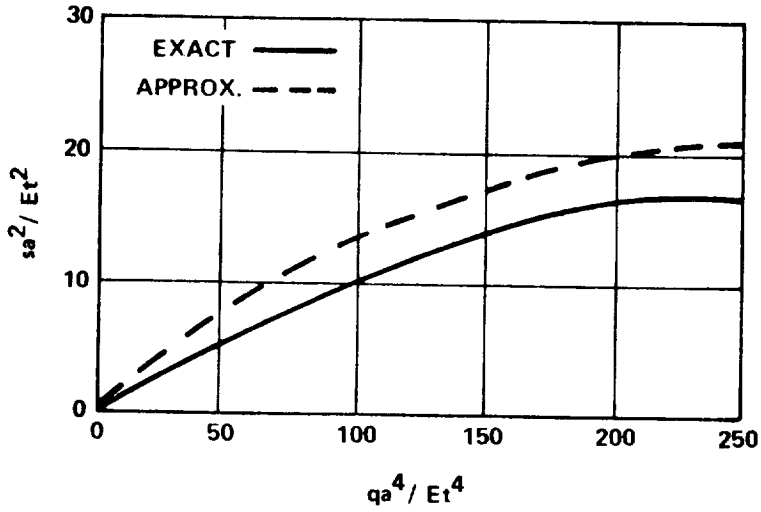

FIGURE B9-5. LARGE DEFLECTION THEORIES' MIDPANEL STRESSES; SIMPLY SUPPORTED PANEL

B9.3 MEDIUM-THICK PLATES (SMALL DEFLECTION THEORY)

This section includes solutions for stress and deflections for plates of various shapes for different loading and boundary conditions. All solutions in this section are based on small deflection theory as described in Paragraph B9.2.1.

B9.3.1 Circular Plates

For a circular plate it is naturally convenient to express the governing differential equations in polar coordinate form. The deflection surface of a laterally loaded plate in polar coordinate form is

$$\left(\frac{\partial^2}{\partial r^2} + \frac{1}{r}\frac{\partial}{\partial r} + \frac{1}{r^2}\frac{\partial^2}{\partial \theta^2}\right)\left(\frac{\partial^2 w}{\partial r^2} + \frac{1}{r}\frac{\partial w}{\partial r} + \frac{1}{r^2}\frac{\partial^2 w}{\partial \theta^2}\right) = \frac{q}{D} \quad . \tag{23}$$

If the load is symmetrically distributed with respect to the center of the plate, w is independent of θ and the equation becomes

$$\frac{1}{r}\frac{d}{dr}\left\{r\frac{d}{dr}\left[\frac{1}{r}\frac{d}{dr}\left(r\frac{dw}{dr}\right)\right]\right\} = \frac{q}{D} \quad . \tag{24}$$

The bending and twisting moments are

$$M_r = D\left[\frac{\partial^2 w}{\partial r^2} + \mu\left(\frac{1}{r}\frac{\partial w}{\partial r} + \frac{1}{r^2}\frac{\partial^2 w}{\partial \theta^2}\right)\right] \tag{25}$$

$$M_t = D\left(\frac{1}{r}\frac{\partial w}{\partial r} + \frac{1}{r^2}\frac{\partial^2 w}{\partial \theta^2} + \mu\frac{\partial^2 w}{\partial r^2}\right) \tag{26}$$

$$M_{rt} = (1-\mu)D\left(\frac{1}{r}\frac{\partial^2 w}{\partial r \partial \theta} - \frac{1}{r^2}\frac{\partial w}{\partial \theta}\right) \tag{27}$$

B9.3.1.1 Solid, Uniform-Thickness Plates

Solutions for solid circular plates have been tabulated for many loadings and boundary conditions. The results are presented in Table B9-3.

Table B9-3. Solutions for Circular Solid Plates

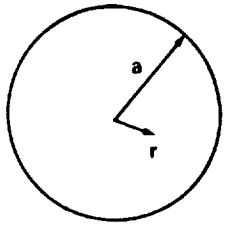

Case	Formulas For Deflection And Moments
Supported Edges, Uniform Load 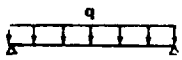	$w = \frac{qa^2}{16D(1+\mu)}(a^2-r^2)$ $\quad w_{max} = \frac{(5+\mu)}{64(1+\mu)}\frac{qa^4}{D}$ $M_r = \frac{q}{16}(3+\mu)(a^2-r^2)$ $\quad (M_r)_{max} = (M_t)_{max} = \frac{3+\mu}{16}qa^2$ $M_t = \frac{q}{16}[a^2(3+\mu) - r^2(1+3\mu)]$ At Edge $\theta = \frac{Pa}{8\pi(1+\mu)}$
Clamped Edges, Uniform Load 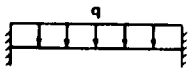	$w = \frac{q}{64D}(a^2-r^2)$ $\quad w_{max} = \frac{qa^4}{64D}$ $M_r = \frac{q}{16}[a^2(1+\mu) - r^2(3+\mu)]$ $(M_r)_{max}$ at $r=a = \frac{-qa^2}{8}$ $M_t = \frac{q}{16}[a^2(1+\mu) - r^2(1+3\mu)]$ $(M_r)_{r=0} = \frac{qa^2}{16}(1+\mu)$
Supported Edges, Uniform Load Over Concentric Circular Area of Radius, c 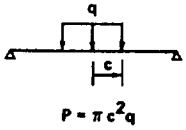 $P = \pi c^2 q$	$w = \frac{P}{16\pi D}\left\{\frac{3+\mu}{1+\mu}(a^2-r^2) + 2r^2\log\frac{r}{a} + c^2\left[\log\frac{r}{a} - \frac{1-\mu}{2(1+\mu)}\frac{a^2-r^2}{a^2}\right]\right\}$ $w_{r=0} = \frac{P}{16\pi D}\left[\frac{3+\mu}{1+\mu}a^2 + c^2\log\frac{c}{a} - \frac{7+3\mu}{4(1+\mu)}c^2\right]$ At Center $M_{max} = \frac{P}{4\pi}\left[(1+\mu)\log\frac{a}{c} + 1 - \frac{(1-\mu)c^2}{4a^2}\right]$ At Edge $\theta = \frac{Pa}{4\pi(1+\mu)}$

Table B9-3. (Continued)

Case	Formulas For Deflection And Moments
Simply Supported, Uniform Load On Concentric Circular Ring Of Radius, b 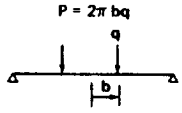 	$(w)_{r=b} = \frac{P}{8\pi D}\left[(a^2-b^2)\left(1 + \frac{1}{2}\frac{1-\mu}{1+\mu}\frac{a^2-b^2}{a^2}\right) + 2b^2 \log \frac{b}{a}\right]$ $\max(w)_{r=0} = \frac{P}{8\pi D}\left[b^2 \log \frac{b}{a} + (a^2-b^2)\frac{(3+\mu)}{2(1+\mu)}\right]$ $M_{r=b} = \frac{(1+\mu)P(a^2-b^2)}{8\pi a^2} - \frac{(1+\mu)\,P \log \frac{b}{a}}{4\pi}$
Fixed Edges, Uniform Load On Concentric Circular Ring Of Radius, b 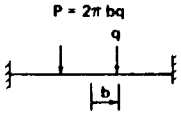 	$(w)_{r=b} = \frac{P}{8\pi D}\left(\frac{a^4-b^4}{2a^2} + 2b^2 \log \frac{b}{a}\right)$ $\max(w)_{r=0} = \frac{P}{8\pi D}\left[b^2 \log \frac{b}{a} + \frac{(a^2-b^2)}{2}\right]$ $M_{r=a} = \frac{P}{4\pi}\frac{a^2-b^2}{a^2}$
Simply Supported, Concentrated Load At Center 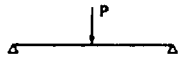 	$w = \frac{P}{16\pi D}\left[\frac{3+\mu}{1+\mu}(a^2-r^2) + 2r^2 \log \frac{r}{a}\right]$ $w_{max} = \frac{(3+\mu)}{16\pi(1+\mu)}\frac{Pa^2}{D}$ $M_r = \frac{P}{4\pi}(1+\mu) \log \frac{a}{r}$ $M_t = \frac{P}{4\pi}\left[(1+\mu) \log \frac{a}{r} + 1 - \mu\right]$
Fixed Edges, Concentrated Load At Center 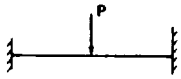 	$w = \frac{Pr^2}{8\pi D} \log \frac{r}{a} + \frac{P}{16\pi D}(a^2-r^2)$ $w_{max} = \frac{3}{48\pi}\frac{Pa^2}{D}$ $M_r = \frac{P}{4\pi}\left[(1+\mu) \log \frac{a}{r} - 1\right]$ $M_t = \frac{P}{4\pi}\left[(1+\mu) \log \frac{a}{r} - \mu\right]$
Clamped Edges, Uniform Load Over Concentric Circular Area Of Radius, c 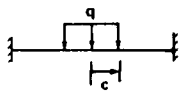 $P = \pi c^2 q$	$w_{max}(r=0) = \frac{P}{64\pi D}\left(1a^2 - 4c^2 \log \frac{a}{c} - 3c^2\right)$ At r=a $M_r = \frac{P}{4\pi}\left(1 - \frac{c^2}{2a^2}\right) \qquad M_t = \mu M_r$ At r=0 $M_r = M_t = \frac{P(1+\mu)}{4\pi}\left(\log \frac{a}{c} + \frac{c^2}{4a^2}\right)$

Table B9-3. (Continued)

Case	Formulas For Deflection And Moments
Supported By Uniform Pressure Over Entire Lower Surface, Uniform Load Over Concentric Circular Area Of Radius, c 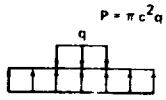	At r=0 $w = \frac{P}{64\pi D}\left[4c^2 \log\frac{a}{c} + 2c^2\left(\frac{3+\mu}{1+\mu}\right) + \frac{c^4}{a^2} - a^2\left(\frac{7+3\mu}{1+\mu}\right) + \frac{(a^2-c^2)c^2}{a^2}\right]$ $M_r = M_t = \frac{P}{4\pi}\left[(1+\mu)\log\frac{a}{c} + \frac{1}{4}(1-\mu)\left(1-\frac{c^2}{a^2}\right)\right]$ If c→0 $w = \frac{Pa^2}{64\pi D}\frac{(7+3\mu)\mu}{(1+\mu)}$
No Support, Uniform Edge Moment 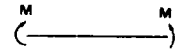	$w = \frac{M(a^2-r^2)}{2D(1+\mu)}$ $\qquad w_{r=0} = \frac{Ma^2}{2D(1+\mu)}$ Edge Rotation $\theta = \frac{Ma}{D(1+\mu)}$
Edges Supported, Central Couple (Trunnion Loading) 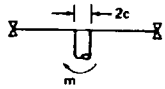	At r=c $M = \frac{9m}{2\pi c}\left[1 + (1+\mu)\log\frac{2(a-c)}{Ka}\right]$ where $K = \frac{0.49\,a^2}{(c+0.7a)^2}$
Edges Clamped, Central Couple (Trunnion Loading) 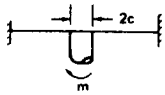	At r=c $M = \frac{9m}{2\pi c}\left[1 + (1+\mu)\log\frac{2(0.45\,a-c)}{0.45\,ka}\right]$ where $k = \frac{0.1\,a^2}{(c+0.28\,a)^2}$
Edges Supported, Uniform Load Over Small Eccentric Circular Area Of Radius, r_o 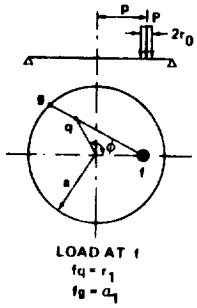	At Point of Load: $M_r = M_t = \frac{P}{4\pi}\left\{1 + (1+\mu)\log\frac{a-p}{r_o} - (1-\mu)\left[\frac{r_o^2}{4(a-p)^2}\right]\right\}$ At Point q: $w = K_0(r^3-b_0ar^2+c_0a^3) + K_1(r^4-b_1ar^3+c_1a^3r)\cos\phi + K_2(r^4-b_2ar^3+c_2a^2r^2)\cos\phi$ where $K_0 = \frac{2(1+\mu)P(p^4-b_0ap^2+c_0a^3)}{9(5+\mu)K\pi a^4}$, $K = \frac{Et^3}{12(1-\mu^2)}$ $K_1 = \frac{2(3+\mu)P(p^4-b_1ap^3+c_1a^3p)}{3(9+\mu)K\pi a^6}$, $b_0 = \frac{3(2+\mu)}{2(1+\mu)}$ $K_2 = \frac{(4+\mu)^2P(p^4-b_2ap^3+c_2a^2p^2)}{(9+\mu)(5+\mu)K\pi a^6}$, $b_1 = \frac{3(4+\mu)}{2(3+\mu)}$ $b_2 = \frac{2(5+\mu)}{4+\mu}$, $c_0 = \frac{4+\mu}{2(1+\mu)}$, $c_1 = \frac{6+\mu}{2(3+\mu)}$, $c_2 = \frac{6+\mu}{4+\mu}$

Table B9-3. (Concluded)

Case	Formulas For Deflection and Moments
Edges Fixed, Uniform Load Over Small Eccentric Circular Area of Radius, r_0 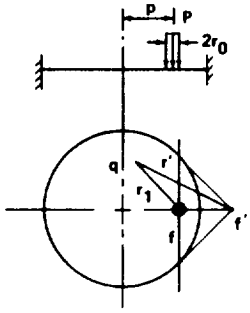	At Point of Load: $M_r = \frac{P}{4\pi}\left[(1+\mu)\log\frac{a-p}{r_0} + (1+\mu)\frac{r_0^2}{4(a-p)^2}\right] =$ max M when $r_0<0.6(a-p)$ $w = \frac{3P(1-\mu^2)(a^2-p^2)^2}{4\pi Et^3a^2}$ At Point q: $w = \frac{3P(1-\mu^2)}{2\pi Et^3}\left[\frac{1}{2}\left(\frac{p^2r'^2}{a^2} - r_1^2\right) - r_1^2\log\frac{pr'}{ar_1}\right]$ At Edge: $M_r = \frac{P}{4\pi}\left[1 - \frac{r_0^2}{2(a-p)^2}\right] =$ max M when $r_0 > 0.6(a-p)$
Supported At Several Points Along The Boundary 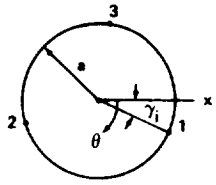	<u>Supported At Two Points</u>: ($\gamma_1 = 0$, $\gamma_2 = \pi$) Load P at Center: $w_{r=0} = 0.116\frac{Pa^2}{D}$ $w_{r=a,\ \theta=\pi/2} = 0.118\frac{Pa^2}{D}$ Uniformly Loaded Plate: $w_{r=0} = 0.269\frac{qa^4}{D}$ $w_{r=a,\ \theta=\pi/2} = 0.371\frac{qa^4}{D}$ <u>Supported At Three Points 120 Deg Apart:</u> Load P at Center $w_{r=0} = 0.0670\frac{Pa^2}{D}$ Uniformly Loaded $w_{r=0} = 0.1137\frac{qa^4}{D}$
Edge Supported, Linearly Distributed Load Symmetrical About Diameter 	max $M_r = \frac{qa^2(5+\mu)}{72\sqrt{3}}$ at r = 0.577 a max $M_t = \frac{qa^2(5+\mu)(1+3\mu)}{72(3+\mu)}$ at r = 0.675 a max edge reaction per linear inch = $\frac{1}{4}$ qa max w = $0.042\frac{qa^4}{Et^3}$ at r = 0.503 a ($\mu = 0.3$)

B9.3.1.2 Annular, Uniform-Thickness Plates

Solutions for annular circular plates with a central hole are tabulated in Table B9-4.

B9.3.1.3 Solid, Nonuniform-Thickness Plates

For the plates treated here, the thickness is a function of the radial distance, and the acting load is symmetrical with respect to the center of the plate.

I. Linearly Varying Thickness:

The plate of this type is shown in Fig. B9-6.

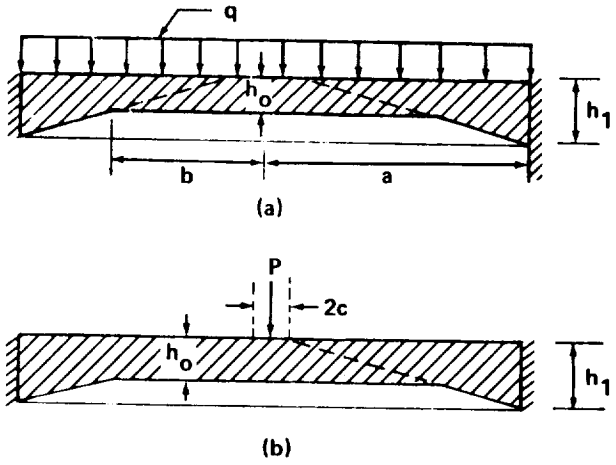

FIGURE B9-6. CIRCULAR PLATE WITH LINEARLY VARYING THICKNESS

Tables B9-5 and B9-6 give the deflection w_{max} and values of bending moments of the plate in two cases of loading. To calculate the bending moment at the center in the case of a central load P, one may assume a uniform distribution of that load over a small circular area of a radius c. The moment $M_r = M_t$ at r = 0 can be expressed in the form

$$M_{max} = \frac{P(1+\mu)}{4\pi}\left(\log\frac{a}{c} + \frac{c^2}{4a^2}\right) + \gamma_1 P \quad . \qquad (28)$$

Table B9-4. Solutions For Annular, Uniform-Thickness Plates

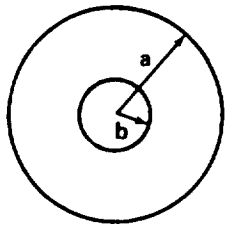

Case	Formulas For Deflection And Moments
Outer Edge Supported, Uniform Load Over Entire Actual Surface 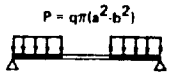 	At Inner Edge: $\max M = M_t = \frac{q}{8(a^2-b^2)}\left[a^4(3+\mu) + b^4(1-\mu) - 4a^2b^2 - 4(1+\mu)a^2b^2 \log \frac{a}{b}\right]$ When b Is Very Small $\max M = M_t = \frac{qa^2}{8}(3+\mu)$ $\max w = \frac{q}{8D}\left[\frac{a^4(5+\mu)}{8(1+\mu)} + \frac{b^4(7+3\mu)}{8(1+\mu)} - \frac{a^2b^2(3+\mu)}{2(1+\mu)} + \frac{a^2b^2(3+\mu)}{2(1-\mu)} \log \frac{a}{b} - \frac{2a^2b^4(1+\mu)}{(a^2-b^2)(1-\mu)}\left(\log \frac{a}{b}\right)^2\right]$
Outer Edge Clamped, Uniform Load Over Entire Actual Surface 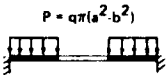 	At Outer Edge: $\max M_r = \frac{q}{8}\left[a^2 - 2b^2 + \frac{b^4(1-\mu) - 4b^4(1+\mu)\log \frac{a}{b} + a^2b^2(1+\mu)}{a^2(1-\mu) + b^2(1+\mu)}\right]$ $\max w = \frac{q}{64D}\left\{a^4 + 5b^4 - 6a^2b^2 + 8b^4 \log \frac{a}{b} - \frac{[8b^6(1+\mu) - 4a^2b^2(3+\mu) - 4a^2b^2(1+\mu)]\log \frac{a}{b} + 16a^2b^4(1+\mu)\left(\log \frac{a}{b}\right)^2}{a^2(1-\mu) + b^2(1+\mu)} + \frac{4a^2b^4 - 2a^4b^2(1+\mu) + 2b^6(1-\mu)}{a^2(1-\mu) + b^2(1+\mu)}\right\}$
Outer Edge Supported, Uniform Load Along Inner Edge 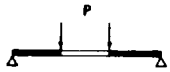 	At Inner Edge: $\max M = M_t = \frac{P}{4\pi}\left[\frac{2a^2(1+\mu)}{a^2-b^2}\log \frac{a}{b} + (1-\mu)\right]$ $\max w = \frac{P}{16\pi D}\left[\frac{(a^2-b^2)(3+\mu)}{(1+\mu)} + \frac{4a^2b^2(1+\mu)}{(1-\mu)(a^2-b^2)}\left(\log \frac{a}{b}\right)^2\right]$

Table B9-4. (Continued)

Case	Formulas For Deflection And Moments
Outer Edge Clamped, Uniform Load Along Inner Edge 	At Outer Edge: $\max M_r = \frac{P}{4\pi}\left[1 - \frac{2b^2 - 2b^2(1+\mu)\log\frac{a}{b}}{a^2(1-\mu) + b^2(1+\mu)}\right] = \max M$ when $\frac{a}{b} < 2.4$ At Inner Edge: $\max M_t = \frac{P\mu}{4\pi}\left[1 + \frac{a^2(1-\mu) - b^2(1+\mu) - 2(1-\mu^2)a^2\log\frac{a}{b}}{\mu a^2(1-\mu) + b^2(1+\mu)}\right]$ $= \max M$ when $\frac{a}{b} > 2.4$ $\max w = \frac{P}{16\pi D}\left[a^2 - b^2 + \frac{2b^2(a^2-b^2) - 8a^2b^2\log\frac{a}{b} + 4a^2b^2(1+\mu)\left(\log\frac{a}{b}\right)^2}{a^2(1-\mu) + b^2(1+\mu)}\right]$
Supported Along Concentric Circle Near Outer Edge, Uniform Load Along Concentric Circle Near Inner Edge 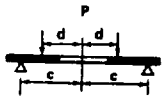	At Inner Edge: $\max M = M_t = \frac{P}{4\pi}\left[\frac{2a^2(1+\mu)}{a^2-b^2}\log\frac{c}{\alpha} + (1-\mu)\frac{c^2-d^2}{a^2-b^2}\right]$
Inner Edge Supported, Uniform Load Over Entire Actual Surface 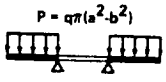	At Inner Edge: $\max M = M_t = \frac{q}{8(a^2-b^2)}\left[4a^4(1+\mu)\log\frac{a}{b} + 4a^2b^2 + b^4(1-\mu) - a^4(1+3\mu)\right]$ At Outer Edge: $\max w = \frac{q}{64D}\left[a^4(7+3\mu) + b^4(5+\mu) - a^2b^2(12+4\mu) - \frac{4a^2b^2(3+\mu)(1+\mu)}{(1-\mu)}\log\frac{a}{b} + \frac{16a^4b^2(1+\mu)^2}{(a^2-b^2)(1-\mu)}\left(\log\frac{a}{b}\right)^2\right]$
Outer Edge Fixed And Supported, Inner Edge Fixed, Uniform Load Over Entire Actual Surface 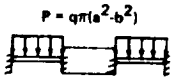	At Outer Edge: $\max M_r = \frac{q}{8}\left[(a^2 - 3b^2) + \frac{4b^4}{a^2-b^2}\left(\log\frac{a}{b}\right)^2\right]$ At Inner Edge: $M_r = \frac{q}{8}\left[(a^2+b^2) - \frac{4a^2b^2}{(a^2-b^2)}\left(\log\frac{a}{b}\right)\right]$ $\max w = \frac{q}{64D}\left[a^4 + 3b^4 - 4a^2b^2 - 4a^2b^2\log\frac{a}{b} + \frac{16a^2b^2}{a^2-b^2}\left(\log\frac{a}{b}\right)^2\right]$

Table B9-4. (Continued)

Case	Formulas For Deflection And Moments
Outer Edge Fixed And Supported, Inner Edge Fixed, Uniform Load Along Inner Edge 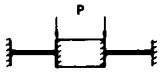	At Outer Edge: $M_r = \frac{P}{4\pi}\left[1 - \frac{2b^2}{a^2-b^2}\left(\log \frac{a}{b}\right)\right]$ At Inner Edge: $\max M_r = \frac{P}{4\pi}\left[1 - \frac{2a^2}{a^2-b^2}\left(\log \frac{a}{b}\right)\right]$ $\max w = \frac{P}{16\pi D}\left[a^2 - b^2 - \frac{4a^2b^2}{a^2-b^2}\left(\log \frac{a}{b}\right)^2\right]$
Inner Edge Fixed And Supported, Uniform Load Over Entire Actual Surface 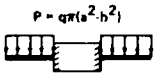	At Inner Edge: $\max M_r = \frac{q}{8}\left[\frac{4a^4(1+\mu)\log\frac{a}{b} - a^4(1+3\mu) + b^4(1-\mu) + 4a^2b^2\mu}{a^2(1+\mu)+b^2(1-\mu)}\right]$ At Outer Edge: $\max w = \frac{q}{64D}\left\{\frac{a^6(7+3\mu) + b^6(1-\mu) - a^4b^2(1+7\mu) - a^2b^4(7-5\mu)}{a^2(1+\mu)+b^2(1-\mu)} - \frac{4a^2b^2[a^2(5-\mu)+b^2(1+\mu)]\log\frac{a}{b} + 16a^4b^2(1+\mu)\left(\log\frac{a}{b}\right)^2}{a^2(1+\mu)+b^2(1-\mu)}\right\}$
Inner Edge Fixed And Supported, Uniform Load Along Outer Edge 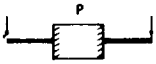	At Inner Edge: $\max M_r = \frac{P}{4\pi}\left[\frac{2a^2(1+\mu)\log\frac{a}{b} + a^2(1-\mu) - b^2(1-\mu)}{a^2(1+\mu)+b^2(1-\mu)}\right]$ At Outer Edge: $\max w = \frac{P}{16\pi D}\left[\frac{a^4(3+\mu) - b^4(1-\mu) - 2a^2b^2(1+\mu) - 8a^2b^2\log\frac{a}{b}}{a^2(1+\mu)+b^2(1-\mu)} - \frac{4a^2b^2(1+\mu)\left(\log\frac{a}{b}\right)^2}{a^2(1+\mu)+b^2(1-\mu)}\right]$
Outer Edge Fixed, Uniform Moment Along Inner Edge 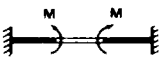	At Inner Edge: $\max w = \frac{M}{2D}\left[\frac{a^2b^2 - b^4 - 2a^2b^2\log\frac{a}{b}}{a^2(1-\mu)+b^2(1+\mu)}\right]$ At Outer Edge: $\max M_r = M\left[\frac{2b^2}{(1+\mu)b^2+(1-\mu)a^2}\right]$
Inner Edge Fixed, Uniform Moment Along Outer Edge 	At Inner Edge: $\max M_r = M\left[\frac{2a^2}{(1+\mu)a^2+(1-\mu)b^2}\right]$ At Outer Edge: $\max w = \frac{M}{2D}\left[\frac{a^4 - a^2b^2 - 2a^2b^2\log\frac{a}{b}}{a^2(1+\mu)+b^2(1-\mu)}\right]$

Table B9-4. (Continued)

Case	Formulas For Deflection and Moments
Outer Edge Supported, Unequal Uniform Moments Along Edges 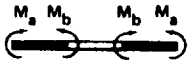	$M_r = \frac{1}{a^2 - b^2}\left[a^2M_a - b^2M_b - \frac{a^2b^2}{r^2}(M_a - M_b)\right]$ $w = \frac{1}{D(a^2 - b^2)}\left\{\frac{a^2 - r^2}{2}\left(\frac{a^2M_a - b^2M_b}{1+\mu}\right) + \log\frac{a}{r}\left[\frac{a^2b^2(M_a - M_b)}{(1-\mu)}\right]\right\}$
Outer Edge Supported, Inner Edge Fixed, Uniform Load Over Entire Actual Surface 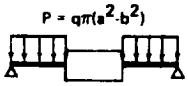	At Inner Edge: $\max M_r = \frac{q}{8}\left[\frac{4a^2b^2(1+\mu)\log\frac{a}{b} - a^4(3+\mu) + a^2b^2(5+\mu)}{a^2(1+\mu) + b^2(1-\mu)} - b^2\right]$ $\max w = \frac{q}{64D}\left\{a^4 - 3b^4 + 2a^2b^2 - 8a^2b^2\log\frac{a}{b} - \frac{16(1+\mu)a^2b^2\log^2\frac{a}{b} + [4(7+3\mu)a^2b^4 - 4(5+3\mu)]\log\frac{a}{b}}{a^2(1+\mu) + b^2(1-\mu)} - \frac{4(4+\mu)a^4b^2 - 2(3+\mu)a^6 - 2(5+\mu)a^2b^4}{a^2(1+\mu) + b^2(1-\mu)}\right\}$
Both Edges Fixed, Balanced Loading (Piston) 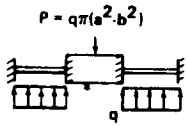	At Inner Edge: $\max M_r = \frac{q}{8}\left(\frac{4a^4}{a^2 - b^2}\log\frac{a}{b} - 3a^2 + b^2\right)$ $\max w = \frac{q}{64D}\left[3a^4 - 4a^2b^2 + b^4 + 4a^2b^2\log\frac{a}{b} - \frac{16a^4b^2}{a^2 - b^2}\left(\log\frac{a}{b}\right)^2\right]$
Outer Edge Supported, Inner Edge Free, Uniform Load On Concentric Circular Ring of Radius, r_0 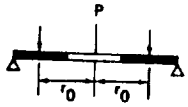	At Inner Edge: $\max M_t = \frac{P}{4\pi}\left[\frac{1}{2}(1-\mu) + (1+\mu)\log\frac{a}{r_0} - (1-\mu)\frac{r_0^2}{2a^2}\right] - \frac{c(a^2+b^2)}{(a^2-b^2)}$ $\max w = \frac{P}{8\pi D}\left[\frac{(a^2-b^2)(3+\mu)}{2(1+\mu)} - (b^2 + r_0^2)\log\frac{a}{b} - \frac{r_0^2(a^2-b^2)(1-\mu)}{2a^2(1+\mu)}\right] - \frac{c}{2D}\left[\frac{b^2}{(1+\mu)} + \frac{2a^2b^2}{(a^2-b^2)(1-\mu)}\log\frac{a}{b}\right]$ where $c = \frac{P}{8\pi}\left[(1-\mu) + 2(1+\mu)\log\frac{a}{r_0} - (1-\mu)\frac{r_0^2}{a^2}\right]$

Table B9-4. (Concluded)

<table>
<tr><th>Case</th><th>Formulas For Deflection and Moments</th></tr>
<tr><td>Outer Edge Fixed, Inner Edge Free, Uniform Load Of Concentric Circular Ring Of Radius, r_0
 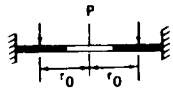
</td><td>At Inner Edge:
$\max M_t = \frac{P}{8\pi}\left[(1+\mu)\left(2\log\frac{a}{r_0} + \frac{r_0^2}{a^2} - 1\right)\right] - c\left[\frac{a^2(1-\mu) - b^2(1+\mu)}{a^2(1-\mu) + b^2(1+\mu)}\right]$
At Outer Edge:
$M_r = \frac{P}{8\pi}\left(1 - \frac{r_0^2}{a^2}\right) + c\left[\frac{2b^2}{a^2(1-\mu) + b^2(1+\mu)}\right]$
$\max w = \frac{P}{8\pi D}\left[\frac{(a^2 + r_0^2)(a^2 - b^2)}{2a^2} - (b^2 + r_0^2)\log\frac{a}{b}\right] - \frac{c}{2D}\left[\frac{b^4 + 2a^2b^2\log\frac{a}{b} - a^2b^2}{b^2(1+\mu) + a^2(1-\mu)}\right]$
where
$c = \frac{P}{8\pi}\left[(1+\mu)\left(2\log\frac{a}{r_0} + \frac{r_0^2}{a^2} - 1\right)\right]$</td></tr>
<tr><td>Central Couple Balanced By Linearly Distributed Pressure
 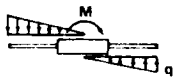

$q = 4M/\pi a^3$</td><td>At Inner Edge:
$\max M_r = \beta\frac{M}{6a}$ where
<table><tr><td>$\frac{a}{b}$</td><td>1.25</td><td>1.50</td><td>2</td><td>3</td><td>4</td><td>5</td></tr><tr><td>β</td><td>0.1625</td><td>0.456</td><td>1.105</td><td>2.25</td><td>3.385</td><td>4.470</td></tr></table>($\mu = 0.3$)</td></tr>
<tr><td>Concentrated Load Applied At Outer Edge
 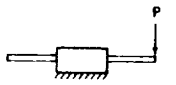
</td><td>At Inner Edge:
$\max M_r = \beta\frac{P}{6}$ where
<table><tr><td>$\frac{a}{b}$</td><td>1.25</td><td>1.50</td><td>2</td><td>3</td><td>4</td><td>5</td></tr><tr><td>β</td><td>3.7</td><td>4.25</td><td>5.2</td><td>6.7</td><td>7.9</td><td>8.8</td></tr></table>for $\mu = 0.3$</td></tr>
</table>

Table B9-5. Deflections and Bending Moments of Clamped Circular Plates Loaded Uniformly (Fig. B9-6a) ($\mu = 0.25$)

$\frac{b}{a}$	$w_{max} = \alpha \frac{qa^4}{Eh_0^3}$	$M_r = \beta qa^2$			$M_t = \beta_1 qa^2$		
	α	r=0 β	r=b β	r=a β	r=0 β_1	r=b β_1	r=a β_1
0.2	0.008	0.0122	0.0040	-0.161	0.0122	0.0078	-0.040
0.4	0.042	0.0332	0.0007	-0.156	0.0332	0.0157	-0.039
0.6	0.094	0.0543	-0.0188	-0.149	0.0543	0.0149	-0.037
0.8	0.148	0.0709	-0.0591	-0.140	0.0709	0.0009	-0.035
1.0	0.176	0.0781	-0.125	-0.125	0.0781	-0.031	-0.031

Table B9-6. Deflections and Bending Moments of Clamped Circular Plates Under a Central Load (Fig. B9-6b) ($\mu = 0.25$)

$\frac{b}{a}$	$w_{max} = \alpha \frac{Pa^2}{Eh_0^3}$	$M_r = M_t$	$M_r = \beta P$		$M_t = \beta_1 P$	
	α	r = 0 γ_1	r = b β	r = a β	r = b β_1	r = a β_1
0.2	0.031	-0.114	-0.034	-0.129	-0.028	-0.032
0.4	0.093	-0.051	-0.040	-0.112	-0.034	-0.028
0.6	0.155	-0.021	-0.050	-0.096	-0.044	-0.024
0.8	0.203	-0.005	-0.063	-0.084	-0.057	-0.021
1.0	0.224	0	-0.080	-0.080	-0.020	-0.020

The last term is due to the nonuniformity of the thickness of the plate and the coefficient γ_1 is given in Table B9-6.

Symmetrical deformation of plates such as those shown in Fig. B9-7 have been investigated and some results are given in Tables B9-7, B9-8, and B9-9.

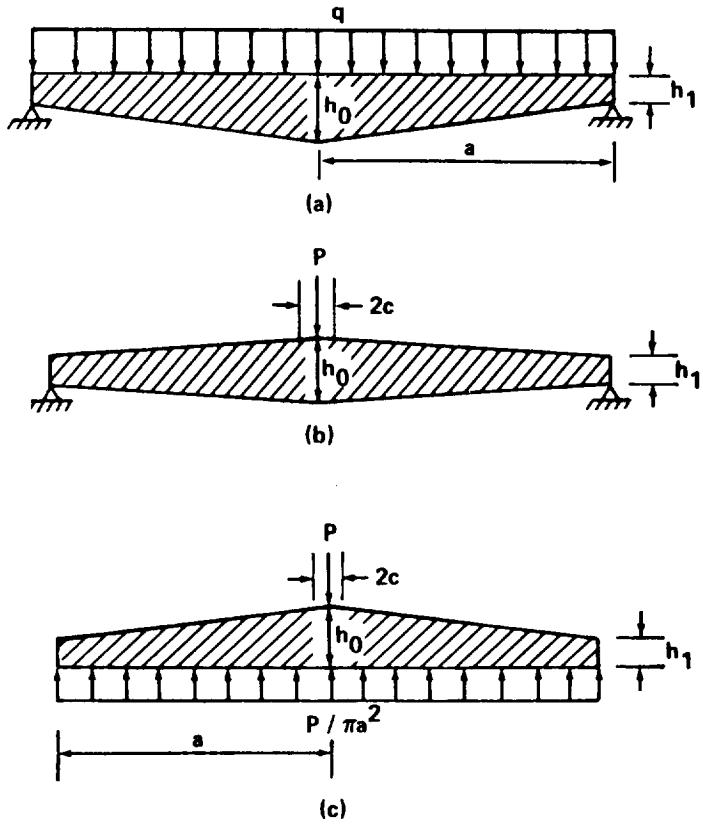

FIGURE B9-7. TAPERED CIRCULAR PLATE

For bending moments under central load P (Fig. B9-7b) the following equation is true (γ_2 is given in Table B9-8):

$$M_{max} = \frac{P}{4\pi}\left[(1+\mu)\log\frac{a}{c} + 1 - \frac{(1-\mu)c^2}{4a^2}\right] + \gamma_2 P \quad . \qquad (29)$$

Table B9-7. Deflections and Bending Moments of Simply Supported Plates Under Uniform Load (Fig. B9-7a) ($\mu = 0.25$)

$\frac{h_0}{h_1}$	$w_{max} = \alpha \frac{qa^4}{Eh_0^3}$	$M_r = \beta qa^2$		$M_t = \beta_1 qa^2$		
	α	$r = 0$	$r = \frac{a}{2}$	$r = 0$	$r = \frac{a}{2}$	$r = a$
		β	β	β_1	β_1	β_1
1.00	0.738	0.203	0.152	0.203	0.176	0.094
1.50	1.26	0.257	0.176	0.257	0.173	0.054
2.33	2.04	0.304	0.195	0.304	0.167	0.029

Table B9-8. Deflections and Bending Moments of Simply Supported Circular Plates Under Central Load (Fig. B9-7b) ($\mu = 0.25$)

$\frac{h_0}{h_1}$	$w_{max} = \alpha \frac{Pa^2}{Eh_0^3}$	$M_r = M_t$	$M_r = \beta P$	$M_t = \beta_1 P$	
	α	$r = 0$	$r = \frac{a}{2}$	$r = \frac{a}{2}$	$r = a$
		γ_2	β	β_1	β_1
1.00	0.582	0	0.069	0.129	0.060
1.50	0.93	0.029	0.088	0.123	0.033
2.33	1.39	0.059	0.102	0.116	0.016

Table B9-9. Bending Moments of a Circular Plate With Central Load And Uniformly Distributed Reacting Pressure (Fig. B9-7c) ($\mu = 0.25$)

$\frac{h_0}{h_1}$	$M_r = M_t$	$M_r = \beta P$	$M_t = \beta_1 P$	
	$r = 0$	$r = \frac{a}{2}$	$r = \frac{a}{2}$	$r = a$
	γ_2	β	β_1	β_1
1.00	-0.065	0.021	0.073	0.030
1.50	-0.053	0.032	0.068	0.016
2.33	-0.038	0.040	0.063	0.007

Of practical interest is a combination of loadings shown in Figs. B9-7a and b. For this case the γ_2 to be used in equation (29) is given in Table B9-9.

II. Nonlinear Varying Thickness:

In many cases the variation of the plate thickness can be represented with sufficient accuracy by the equation

$$y = e^{-\beta x^2/6} \tag{30}$$

in which β is a constant that must be chosen in each particular case so that it approximates as closely as possible the actual proportions of the plate. The variation of thickness along a diameter of a plate corresponding to various values of the constant β is shown in Fig. B9-8.

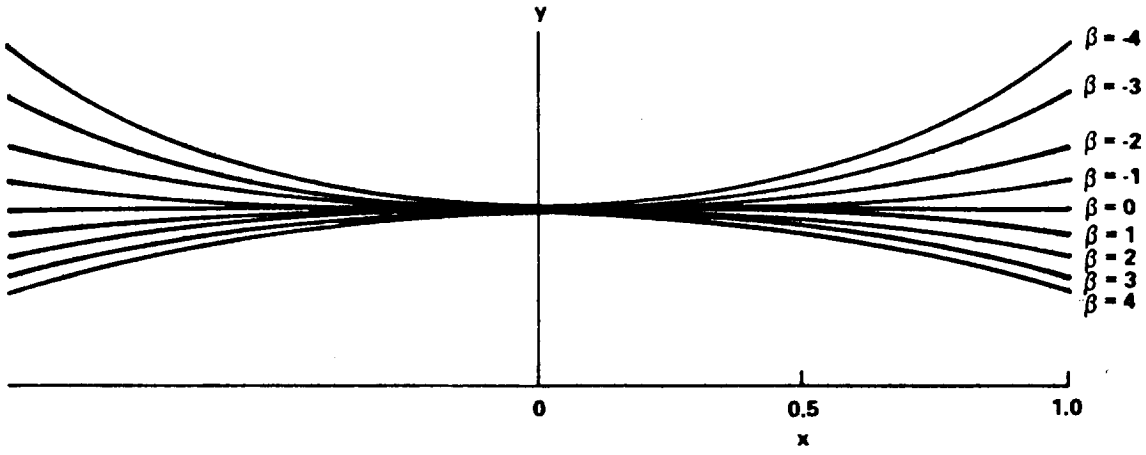

FIGURE B9-8. VARIATION OF PLATE THICKNESS FOR CIRCULAR PLATES

Solutions for this type of variation for uniformly loaded plates with both clamped edges and simply supported edges are given in Reference 1, pages 301-302.

B9.3.1.4 Annular Plates with Linearly Varying Thickness

Consider the case of a circular plate with a concentric hole and a thickness varying as shown in Fig. B9-9.

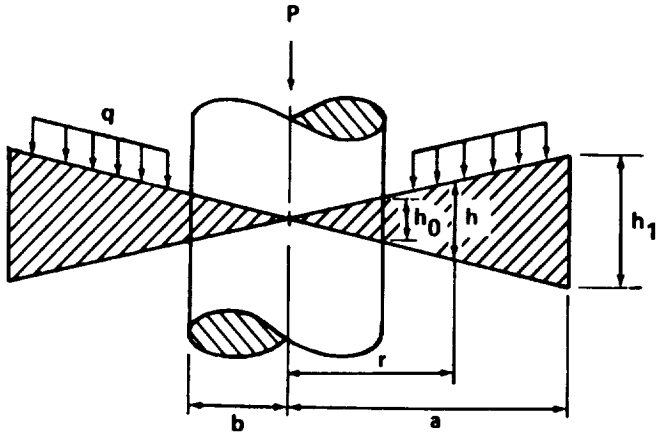

FIGURE B9-9. ANNULAR PLATE WITH LINEARLY VARYING THICKNESS

The plate carries a uniformly distributed surface load q and a line load $p = P/2\pi b$ uniformly distributed along the edge of the hole.

Table B9-10 gives values of coefficients k and k_1, to be used in the following expressions for the numerically largest stress and the largest deflection of the plate:

$$(\sigma_r)_{max} = k\frac{qa^2}{h_1^2} \quad \text{or} \quad (\sigma_r)_{max} = k\frac{P}{h_1^2}$$

$$w_{max} = k_1\frac{qa^4}{Eh_1^3} \quad \text{or} \quad w_{max} = k_1\frac{Pa^2}{Eh_1^3} \qquad (31)$$

Table B9-10. Values of Coefficients in Equations (31) for Various Values of the Ratio $\frac{a}{b}$ (Fig. B9-9) ($\mu = \frac{1}{3}$)

Case	Coef-ficient	$\frac{a}{b}$ = 1.25	1.5	2	3	4	5	Boundary Conditions
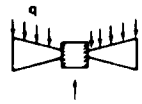	k	0.249	0.638	3.96	13.64	26.0	40.6	$P = \pi q(a^2 - b^2)$ $\phi_b = 0$
	k_1	0.00372	0.0453	0.401	2.12	4.25	6.28	$M_a = 0$
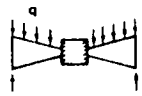	k	0.149	0.991	2.23	5.57	7.78	9.16	$P = 0$ $\phi_b = 0$
	k_1	0.00551	0.0564	0.412	1.673	2.79	3.57	$M_a = 0$
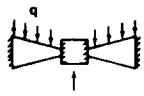	k	0.1275	0.515	2.05	7.97	17.35	30.0	$P = \pi q(a^2 - b^2)$ $\phi_b = 0$
	k_1	0.00105	0.0115	0.0931	0.537	1.261	2.16	$\phi_a = 0$
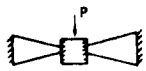	k	0.159	0.396	1.091	3.31	6.55	10.78	$q = 0$ $\phi_b = 0$
	k_1	0.00174	0.0112	0.0606	0.261	0.546	0.876	$\phi_a = 0$
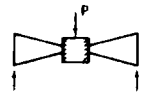	k	0.353	0.933	2.63	6.88	11.47	16.51	$q = 0$ $\phi_b = 0$
	k_1	0.00816	0.0583	0.345	1.358	2.39	3.27	$M_a = 0$
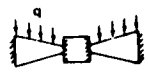	k	0.0785	0.208	0.52	1.27	1.94	2.52	$P = 0$ $\phi_b = 0$
	k_1	0.00092	0.008	0.0195	0.193	0.346	0.482	$\phi_a = 0$

B9.3.1.5 Sector of a Circular Plate

The general solution developed for circular plates can also be adapted for a plate in the form of a sector (Fig. B9-10), the straight edges of which are simply supported. For a uniformly loaded plate simply supported along the straight and circular edges the expressions for the deflections and bending moments at a given point can be represented in each particular case by the following formulas:

$$w = \alpha \frac{qa^4}{D}, \quad M_r = \beta\, qa^2, \quad M_t = \beta_1\, qa^2, \qquad (32)$$

in which α, β, and β_1 are numerical factors. Several values of these factors for points taken on the axis of symmetry of a sector are given in Table B9-11.

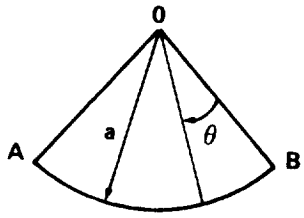

FIGURE B9-10. SECTOR OF A CIRCULAR PLATE

The coefficients for the case of a sector clamped along the circular boundary and simply supported along the straight edges are given in Table B9-12. It can be seen that in this case the maximum bending stress occurs at the midpoint of the unsupported circular edge. The following equation is used for the case when $\pi/k = \pi/2$

$$w_{max} = 0.0633 \frac{qa^4}{D}.$$

The bending moment at the same point is

$$M_t = 0.1331\, qa^2.$$

Table B9-11. Values of the Factors α, β, and B_1 for Various Angles $\frac{\pi}{k}$ of a Sector Simply Supported at the Boundary ($\mu = 0.3$)

$\frac{\pi}{k}$	$\frac{r}{a} = \frac{1}{4}$			$\frac{r}{a} = \frac{1}{2}$			$\frac{r}{a} = \frac{3}{4}$			$\frac{r}{a} = 1$		
	α	β	β_1	α	β	β_1	α	β	β_1	α	β	β_1
$\frac{\pi}{4}$	0.00006	-0.0015	0.0093	0.00033	0.0069	0.0183	0.00049	0.0161	0.0169	0	0	0.0025
$\frac{\pi}{3}$	0.00019	-0.0025	0.0177	0.00080	0.0149	0.0255	0.00092	0.0243	0.0213	0	0	0.0044
$\frac{\pi}{2}$	0.00092	0.0036	0.0319	0.00225	0.0353	0.0352	0.00203	0.0381	0.0286	0	0	0.0088
π	0.00589	0.0692	0.0357	0.00811	0.0868	0.0515	0.00560	0.0617	0.0468	0	0	0.0221

Table B9-12. Values of the Coefficients α and β for Various Angles $\frac{\pi}{k}$ of a Sector Clamped Along the Circular Boundary and Simply Supported Along the Straight Edges ($\mu = 0.3$)

$\frac{\pi}{k}$	$\frac{r}{a} = \frac{1}{4}$		$\frac{r}{a} = \frac{1}{2}$		$\frac{r}{a} = \frac{3}{4}$		$\frac{r}{a} = 1$	
	α	β	α	β	α	β	α	β
$\frac{\pi}{4}$	0.00005	-0.0008	0.00026	0.0087	0.00028	0.0107	0	-0.025
$\frac{\pi}{3}$	0.00017	-0.0006	0.00057	0.0143	0.00047	0.0123	0	-0.034
$\frac{\pi}{2}$	0.00063	0.0068	0.00132	0.0272	0.00082	0.0113	0	-0.0488
π	0.00293	0.0472	0.00337	0.0446	0.00153	0.0016	0	-0.0756

In the general case of a plate having the form of a circular sector with radial edges clamped or free, one must apply approximate methods. Another problem which allows an exact solution is that of bending of a plate clamped along two circular arcs. Data regarding the clamped semicircular plate are given in Table B9-13.

Table B9-13. Values of the Factors α, β, and β_1 for a Semicircular Plate Clamped Along the Boundary ($\mu = 0.3$)

Load Distribution	$\frac{r}{a} = 0$ β	$\frac{r}{a} = 0.483$ β_{max}	$\frac{r}{a} = 0.486$ α_{max}	$\frac{r}{a} = 0.525$ β_{1max}	$\frac{r}{a} = 1$ β
Uniform Load q	-0.0731	0.0355	0.00202	0.0194	-0.0584
Hydrostatic Load $q\frac{y}{a}$	-0.0276	—	—	—	-0.0355

I. Annular Sectored Plate:

For a semicircular annular sectored plate with outer edge supported and the other edges free, with uniform load over the entire actual surface as shown in Fig. B9-11, the equations for maximum moment and deflection are:

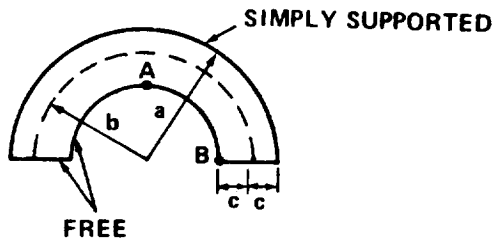

FIGURE B9-11. ANNULAR SECTORED PLATE

At A

$$M_t = qcb\left(\frac{b}{c} - \frac{1}{3}\right)\left[c_1\left(1 - \gamma_1^2\frac{c}{b}\right) + c_2\left(1 - \gamma_2^2\frac{c}{b}\right) + \frac{c}{b}\right]K \quad ,$$

At B

$$w = \frac{24qc^2b^2}{Et^3}\left(\frac{b}{c} - \frac{1}{3}\right)\left[c_1 \cosh\frac{\gamma_1\pi}{2} + c_2 \cosh\gamma_2\frac{\pi}{2} + \frac{c}{b}\right] ,$$

where

$$c_1 = \frac{1}{\left(\frac{b}{c} - \gamma_1^2\right)(\lambda - 1)\cosh\gamma_1\frac{\pi}{2}} , \quad c_2 = \frac{1}{\left(\frac{b}{c} - \gamma_2^2\right)\left(\frac{1}{\lambda} - 1\right)\cosh\gamma_2\frac{\pi}{2}} ,$$

$$\gamma_1 = \frac{\gamma}{\sqrt{2}}\sqrt{1 + \sqrt{1 - \frac{4b^2}{c^2\gamma^4}}} , \quad \gamma_2 = \frac{\gamma}{\sqrt{2}}\sqrt{1 - \sqrt{1 - \frac{4b^2}{c^2\gamma^4}}} ,$$

$$\gamma = \sqrt{\frac{2b}{c} + 4\left(1 - \frac{0.625t}{2c}\right)\frac{G}{E}\left(1 + \frac{b}{c}\right)^2} ,$$

$$\lambda = \frac{\gamma_1\left(\frac{b}{c} - \gamma_1^2 + \lambda_1\right)\left(\frac{b}{c} - \gamma_2^2\right)\tanh\gamma_1\frac{\pi}{2}}{\gamma_2\left(\frac{b}{c} - \gamma_2^2 + \lambda_1\right)\left(\frac{b}{c} - \gamma_1^2\right)\tanh\gamma_2\frac{\pi}{2}} ,$$

$$\lambda_1 = 4\left(1 - \frac{0.625t}{2c}\right)\frac{G}{E}\left(1 + \frac{b}{c}\right)^2 .$$

K is a function of $\frac{b-c}{b+c}$ and has the following values:

$\frac{b-c}{b+c}$ =	0.05	0.10	0.2	0.3	0.4	0.5	0.6	0.7	0.8	0.9	1.0
K =	2.33	2.20	1.95	1.75	1.58	1.44	1.32	1.22	1.13	1.06	1.0

B9.3.2 Rectangular Plates

Solutions for many rectangular plate problems with various loadings and boundary conditions are given in Tables B9-14 through 18. For loads and boundary conditions not covered here, solutions can be found by applying the various theoretical, approximate, or complete solutions discussed in

Table B9-14. Solutions for Rectangular Plates

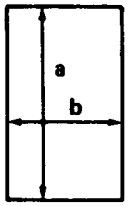

$b/a = \alpha$

P is load

All Edges Supported, Uniform Load Over Entire Surface

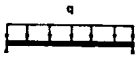

At Center:

$$M_a = (0.0375 + 0.0637\alpha^2 - 0.0533\alpha^4)qb^2$$

$$M_b = \frac{0.125qb^2}{(1 + 1.61\alpha^4)} = \max M$$

$$\max w = \frac{0.1422}{(1 + 2.21\alpha^4)} \frac{qb^4}{Et^3}$$

All Edges Supported, Uniform Load Over Small Concentric Circular Area Of Radius, r_0

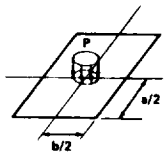

At Center:

$$M_b = \frac{P}{4\pi}\left[(1+\mu)\log\frac{b}{2r_0} + (1+k)\right]$$

where

$$k = \frac{0.914}{1 + 1.6\alpha^2} - 0.6$$

$$\max w = \frac{0.203Pb^2}{12D(1 + 0.462\alpha^4)}$$

All Edges Supported, Uniform Load Over Central Rectangular Area Shown Shaded

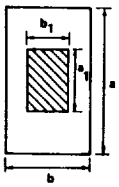

At Center: $\max \sigma = \sigma_b = \beta \frac{P}{t^2}$ where β is found in the following ($\mu = 0.3$):

b_1/b \ a_1/b	a = b					
	0	0.2	0.4	0.6	0.8	1.0
0		1.82	1.38	1.12	0.93	0.76
0.2	1.82	1.28	1.08	0.90	0.76	0.63
0.4	1.39	1.07	0.84	0.72	0.62	0.52
0.6	1.12	0.90	0.72	0.60	0.52	0.43
0.8	0.92	0.76	0.62	0.51	0.42	0.36
1.0	0.76	0.63	0.52	0.42	0.35	0.30

b_1/b \ a_1/b	a = 1.4b					
	0	0.2	0.4	0.8	1.2	1.4
0		2.0	1.55	1.12	0.84	0.75
0.2	1.78	1.43	1.23	0.95	0.74	0.64
0.4	1.39	1.13	1.00	0.80	0.62	0.55
0.6	1.10	0.91	0.82	0.68	0.53	0.47
0.8	0.90	0.76	0.68	0.57	0.45	0.40
1.0	0.75	0.62	0.57	0.47	0.38	0.33

b_1/b \ a_1/b	a = 2b					
	0	0.4	0.8	1.2	1.6	2.0
0		1.64	1.20	0.97	0.78	0.64
0.2	1.73	1.31	1.03	0.84	0.68	0.57
0.4	1.32	1.08	0.88	0.74	0.60	0.50
0.6	1.04	0.90	0.76	0.64	0.54	0.44
0.8	0.87	0.76	0.63	0.54	0.44	0.38
1.0	0.71	0.61	0.53	0.45	0.38	0.30

Table B9-14. (Continued)

All Edges Supported, Distributed Load Varying Linearly Along Length

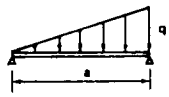

$\max \sigma = \beta \frac{qb^2}{t^2}$, $\max w = \delta \frac{qb^4}{Et^3}$ where β and δ are found in the following:

$\frac{a}{b}$	1	1.5	2.0	2.5	3.0	3.5	4.0
β	0.16	0.26	0.34	0.38	0.43	0.47	0.49
δ	0.022	0.043	0.060	0.070	0.078	0.086	0.091

All Edges Supported, Distributed Load Varying Linearly Along Breadth

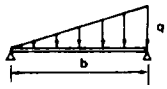

$\max \sigma = \beta \frac{qb^2}{t^2}$, $\max w = \delta \frac{qb^4}{Et^3}$ where β and δ are found as follows:

$\frac{a}{b}$	1	1.5	2.0	2.5	3.0	3.5	4.0
β	0.16	0.26	0.32	0.35	0.37	0.38	0.38
δ	0.022	0.042	0.056	0.063	0.067	0.069	0.070

All Edges Fixed, Uniform Load Over Entire Surface

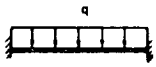

At Centers of Long Edges:

$$M_b = \frac{qb^2}{12(1 + 0.623\alpha^6)} = \max M$$

At Centers of Short Edges:

$$M_a = \frac{qb^2}{24}$$

At Center

$$M_b = \frac{qb^2}{8(3 + 4\alpha^4)} \quad , \quad M_a = 0.009qb^2(1 + 2\alpha^2 - \alpha^4)$$

$$\max w = \frac{0.0284}{(1 + 1.056\alpha^4)} \frac{qb^4}{Et^3} \quad , \quad \text{formulas for } M_b,\ \mu = 0.3;\ \text{others } \mu = 0$$

One Long Edge Fixed, Other Free, Short Edges Supported, Uniform Load Over Entire Surface

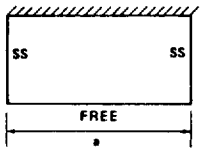

At Center of Fixed Edge:

$$\max M = M_b = \frac{qb^2}{2(1 + 3.2\alpha^3)}$$

At Center of Free Edge:

$$M_a = \frac{8qa^2}{\left(1 + \frac{0.285}{\alpha^4}\right)} \quad , \quad \max w = \frac{1.37qb^4}{Et^3(1 + 10\alpha^3)}$$

$(\mu = 0.3)$

One Long Edge Clamped, Other Three Edges Supported, Uniform Load Over Entire Surface

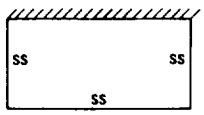

Max Stress $\sigma = \beta \frac{qb^2}{t^2}$, $\max w = \frac{\alpha qb^4}{Et^3}$

where β and α may be found from the following:

$\frac{a}{b}$	1.0	1.5	2.0	2.5	3.0	3.5	4.0
β	0.50	0.67	0.73	0.74	0.74	0.75	0.75
α	0.03	0.046	0.054	0.056	0.057	0.058	0.058

$(\mu = 0.3)$

Table B9-14. (Continued)

One Short Edge Clamped, Other Three Edges Supported, Uniform Load Over Entire Surface

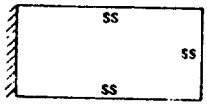

Max Stress $\sigma = \beta \frac{qb^2}{t^2}$, max $w = \frac{\alpha q b^4}{Et^3}$

where β and α may be found from the following:

$\frac{a}{b}$	1.0	1.5	2.0	2.5	3.0	3.5	4.0
β	0.50	0.67	0.73	0.74	0.75	0.75	0.75
α	0.03	0.071	0.101	0.122	0.132	0.137	0.139

($\mu = 0.3$)

One Short Edge Free, Other Three Edges Supported, Uniform Load Over Entire Surface

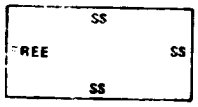

max $\sigma = \frac{\beta q b^2}{t^2}$, max $w = \frac{\alpha q b^4}{Et^3}$

where β and α are found from the following:

$\frac{a}{b}$	1.0	1.5	2.0	4.0
β	0.67	0.77	0.79	0.80
α	0.14	0.16	0.165	0.167

($\mu = 0.3$)

One Short Edge Free, Other Three Edges Supported, Distributed Load Varying Linearly Along Length

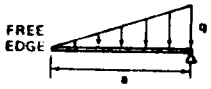

max $\sigma = \frac{\beta q b^2}{t^2}$, max $w = \frac{\alpha q b^4}{Et^3}$

where β and α are found from the following:

$\frac{a}{b}$	1.0	1.5	2.0	2.5	3.0	3.5	4.0
β	0.2	0.28	0.32	0.35	0.36	0.37	0.37
α	0.04	0.05	0.058	0.064	0.067	0.069	0.070

($\mu = 0.3$)

One Long Edge Free, Other Three Edges Supported, Uniform Load Over Entire Surface

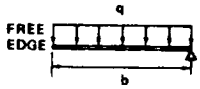

max $\sigma = \frac{\beta q b^2}{t^2}$, max $w = \frac{\alpha q b^4}{Et^3}$

where β and α are found from the following:

$\frac{a}{b}$	1.0	1.5	2.0
β	0.67	0.45	0.36
α	0.14	0.106	0.080

($\mu = 0.3$)

One Long Edge Free, Other Three Edges Supported, Distributed Load Varying Linearly Along Length

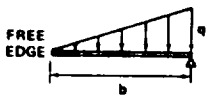

max $\sigma = \frac{\beta q b^2}{t^2}$, max $w = \frac{\alpha q b^4}{Et^3}$

where β and α are found from the following:

$\frac{a}{b}$	1.0	1.5	2.0
β	0.2	0.16	0.11
α	0.04	0.033	0.026

($\mu = 0.3$)

Table B9-14. (Continued)

All Edges Fixed, Uniform Load Over Small Concentric Circular Area Of Radius, r_0

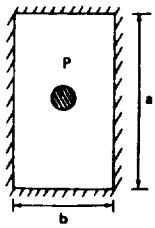

At Center:

$$M_b = \frac{P}{4\pi}\left[(1+\mu)\log\frac{b}{2r_0} + 5(1-\alpha)\right] = \max M \quad , \quad w = \beta\frac{Pb^2}{12}$$

where β has values as follows:

$\frac{a}{b}$	4	2	1
β	0.072	0.0816	0.0624

Long Edges Fixed, Short Edges Supported, Uniform Load Over Entire Surface

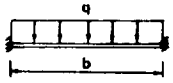

At Centers of Long Edges:

$$\max M = M_b = \frac{qb^2}{12(1+0.2\alpha^4)}$$

At Center:

$$M_b = \frac{qb^2}{24(1+0.8\alpha^4)} \quad , \quad M_a = \frac{qb^2(1+0.3\alpha^2)}{80}$$

$(\mu = 0)$

Short Edges Fixed, Long Edges Supported, Uniform Load Over Entire Surface

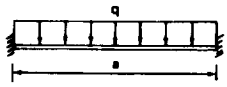

At Centers of Short Edges:

$$\max M = M_a = \frac{qb^2}{8(1+0.8\alpha^4)}$$

At Center:

$$M_b = \frac{qb^2}{8(1+0.8\alpha^2+6\alpha^4)} \quad , \quad M_a = \frac{0.015qb^2(1+3\alpha^2)}{(1+\alpha^4)}$$

$(\mu = 0)$

All Edges Supported, Distributed Load in Form of Triangular Prism

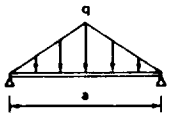

$$\max M = \beta qb^2 \quad , \quad \max w = \frac{\alpha qb^4}{D}$$

β and α found from the following:

$\frac{a}{b}$	1.0	1.5	2.0	3.0	∞
β	0.034	0.0548	0.0707	0.0922	0.1250
α	0.00263	0.00308	0.00686	0.00868	0.01302

$(\mu = 0.3)$

Table B9-14. (Continued)

All Edges Supported, Uniformly Distributed Edge Moment

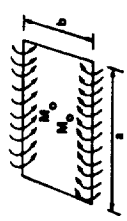

At Center:

$M_a = \beta M_0$, $M_b = \beta_1 M_0$, $w = \frac{\alpha M_0 b^2}{D}$

β, β_1, and α are found from the following:

$\frac{b}{a}$	α	β	β_1
0	0.1250	0.300	1.000
0.5	0.0964	0.387	0.770
0.75	0.0620	0.424	0.476
1.00	0.0368	0.394	0.236
1.50	0.0280	0.264	0.046
2.00	0.0174	0.153	-0.010

One Edge Fixed, Opposite Edge Free, Other Edges Supported, Concentrated Load On Center Of Free Edge

On Free Edge: $w = \frac{\alpha P b^2}{D}$ where

x	0	$\frac{b}{4}$	$\frac{b}{2}$	b	2b
α	0.168	0.150	0.121	0.068	0.016

At Center of Fixed Edge: $M = \beta P$ where

$\frac{b}{a}$	4	2	1.5	1	$\frac{2}{3}$	0.5	0.25
β	-0.000039	-0.0117	-0.0455	-0.163	-0.366	-0.436	-0.507

Table B9-15. Coefficients For Maximum Moments For Various Loads, Plate With Three Sides Fixed, One Free ($\mu = 0.2$)

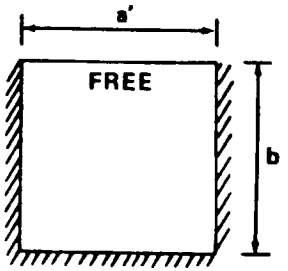

Load / a/b	q, b	q, 2/3 b	q, b/3	q, b	q, 2/3b	q, b/3	q, b/6	M, b	P, b
1/4	0.0052 qb^2	0.0051 qb^2	0.0044 qb^2	0.0038 qb^2	0.0032 qb^2	0.0017 qb^2	0.0004 qb^2	1.000 M	0.0471 Pb
1/2	0.0209 qb^2	0.0184 qb^2	0.0105 qb^2	0.0114 qb^2	0.0084 qb^2	0.0040 qb^2	0.0009 qb^2	1.000 M	0.1522 Pb
3/4	0.0476 qb^2	0.0330 qb^2	0.0140 qb^2	0.0208 qb^2	0.0131 qb^2	0.0051 qb^2	0.0013 qb^2	1.1461 M	0.2723 Pb
1	0.0852 qb^2	0.0433 qb^2	0.0131 qb^2	0.0277 qb^2	0.0165 qb^2	0.0050 qb^2	0.0012 qb^2	1.3643 M	0.3938 Pb
3/2	0.1788 qb^2	0.0617 qb^2	0.0140 qb^2	0.0433 qb^2	0.0190 qb^2	0.0042 qb^2	0.0010 qb^2	1.6292 M	0.6266 Pb
2	0.2613 qb^2	0.0757 qb^2	0.0136 qb^2	0.0644 qb^2	0.0208 qb^2	0.0039 qb^2	0.0008 qb^2	1.7779 M	0.8094 Pb
3	0.3304 qb^2	0.1036 qb^2	0.0146 qb^2	0.0857 qb^2	0.0270 qb^2	0.0038 qb^2	0.0006 qb^2	1.7980 M	0.9388 Pb

Table B9-16. Coefficients For Maximum Moments For Various Loads, Plate With Three Sides Fixed, One Hinged ($\mu = 0.2$)

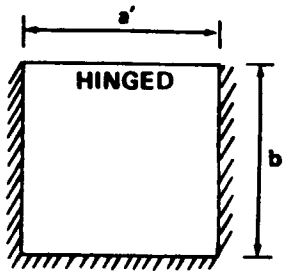

Load / a/b	q, b	q, 2/3 b	q, b/3	q, b	q, 2/3b	q, b/3	q, b/6	M, b
1/4	0.0052 qb^2	0.0051 qb^2	0.0044 qb^2	0.0038 qb^2	0.0032 qb^2	0.0017 qb^2	0.0014 qb^2	1.00 M
1/2	0.0201 qb^2	0.0185 qb^2	0.0105 qb^2	0.0114 qb^2	0.0084 qb^2	0.0040 qb^2	0.0025 qb^2	1.00 M
3/4	0.0403 qb^2	0.0329 qb^2	0.0132 qb^2	0.0207 qb^2	0.0131 qb^2	0.0051 qb^2	0.0027 qb^2	1.00 M
1	0.0572 qb^2	0.0425 qb^2	0.0131 qb^2	0.0269 qb^2	0.0163 qb^2	0.0050 qb^2	0.0032 qb^2	1.00 M
3/2	0.0695 qb^2	0.0472 qb^2	0.0132 qb^2	0.0302 qb^2	0.0176 qb^2	0.0041 qb^2	0.0036 qb^2	1.00 M
2	0.0664 qb^2	0.0451 qb^2	0.0120 qb^2	0.0289 qb^2	0.0161 qb^2	0.0035 qb^2	0.0038 qb^2	1.00 M
3	-0.0704 qb^2	-0.0477 qb^2	-0.0111 qb^2	-0.0297 qb^2	-0.0154 qb^2	-0.0029 qb^2	0.0039 qb^2	1.00 M

B8.1.2 SIGN CONVENTION

The local coordinate system for a bar subjected to an applied twisting moment and the sign conventions for applied twisting moments, internal resisting moments, stresses, displacements, and derivatives of displacements are defined so that there is continuity throughout the equations presented in this section.

B8.1.2 SIGN CONVENTION

I. LOCAL COORDINATE SYSTEM

The local coordinate system is applied to either end of a bar unless specific limitations are stated. The x axis is placed along the length of the bar. The y and z axes are the axes of maximum inertia when the cross section is unsymmetrical, as may be seen in the solid cross section shown in Figure B8.1.2-1. The coordinate system and sign convention shown apply to thin-walled open and thin-walled closed cross sections also.

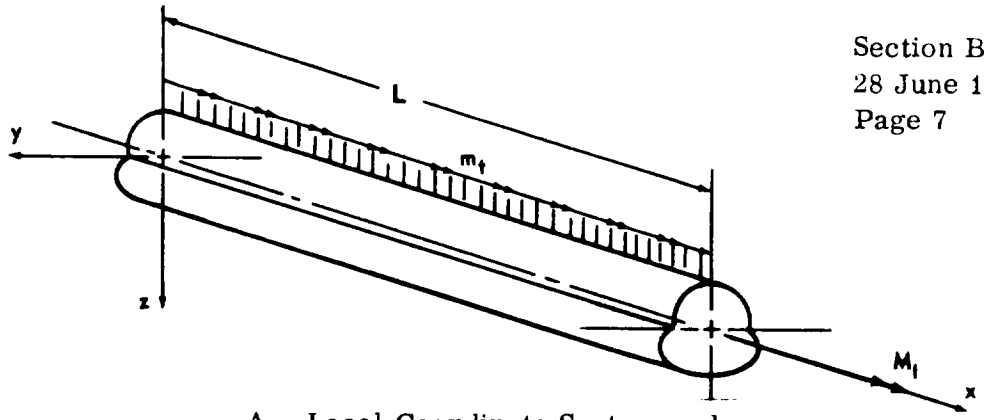

A. Local Coordinate System and Positive Applied Twisting Moments

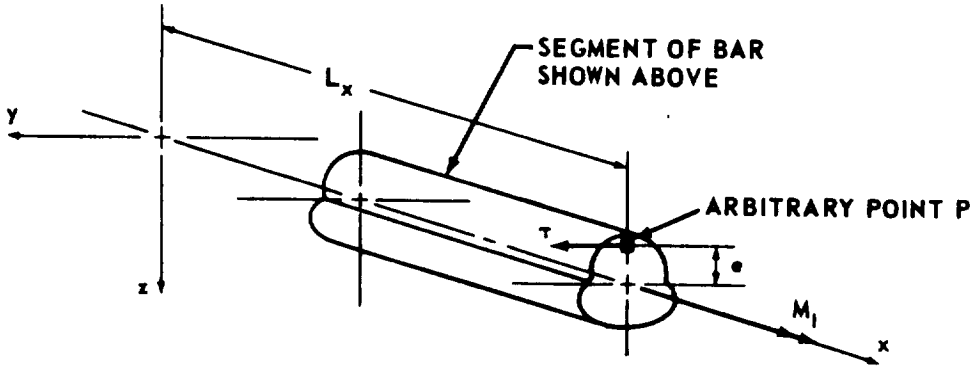

B. Positive Internal Resisting Moment and Shear Stresses

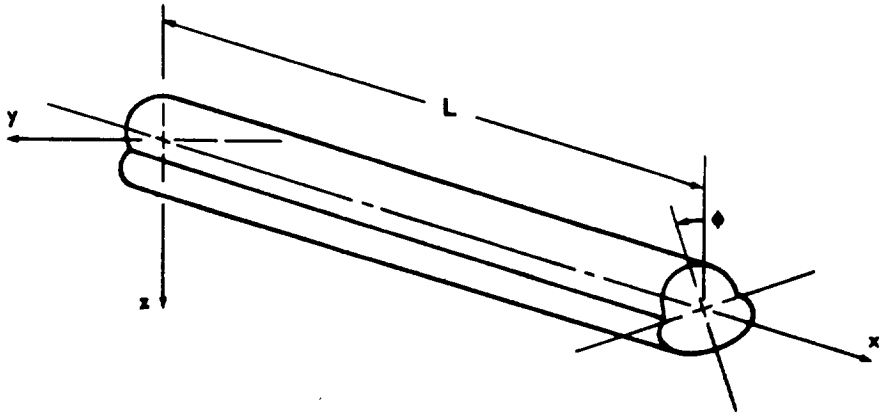

C. Positive Angle of Twist

Figure B8.1.2-1. Local Coordinate System and Positive Sign Convention

B8.1.2 SIGN CONVENTION

II. APPLIED TWISTING MOMENTS

The applied twisting moments (m_t or M_t) are twisting moments about the x axis. The applied twisting moments are positive if they are clockwise when viewed from the origin or are in the positive x direction when represented vectorially. (See Fig. B8.1.2-1A.)

B8.1.2 SIGN CONVENTION

III. INTERNAL RESISTING MOMENTS

The internal resisting moments (M_i) are about the x axis and have the same sign convention as the applied twisting moment when they are evaluated on the y-z plane of a bar segment that is farthest from the origin. (See Fig. B8.1.2-1B.)

B8.1.2 SIGN CONVENTION

IV. STRESSES

Tensile normal stresses (σ_x) are positive, and compressive normal stresses are negative. Shear stresses (τ) are positive when they are equivalent to positive internal resisting moments. (See Fig. B8.1.2-1B.)

B8.1.2 SIGN CONVENTION

V. DEFORMATIONS

An applied twisting moment induces a rotation or angle of twist (ϕ) about the x axis. The rotation is positive if it is clockwise when viewed from the origin. (See Fig. B8.1.2-1C.) An applied twisting moment also induces a longitudinal displacement (u) in the x direction for unrestrained torsion. (See Fig. B8.2.2-2B.) The longitudinal displacement is positive when in the direction of the positive x axis.

B8.1.2 SIGN CONVENTION

VI. DERIVATIVES OF ANGLE OF TWIST

The first (ϕ'), second (ϕ''), and third (ϕ''') derivatives of the angle of twist with respect to the positive x coordinate are positive, positive, and negative, respectively, when the rotation is positive and a concentrated applied twisting moment (M_t) is applied at the ends of the bar.

SECTION B8.2

TORSION OF SOLID SECTIONS

TABLE OF CONTENTS

B8.2.0 TORSION OF SOLID SECTIONS

The torsional analysis of solid sections is restricted to unrestrained torsion and does not consider warping deformations.

B8.2.1 General

I Basic Theory

The torsional analysis of solid sections requires that stresses and deformations be determined. The torsional shear stress (τ_t) is determined at any point (P) on a cross section at an arbitrary distance (L_x) from the origin. The resulting angle of twist (ϕ) is determined between an arbitrary cross section and the origin. These shear stresses and the resulting angles of twist can be determined when the material properties of the bar, geometry of the bar, and the applied twisting moment are known.

Two unique coefficients characterize the geometry of each cross section, the torsional constant (K) and the torsional section modulus (S_t). These coefficients are functions of the dimensions of the cross section. These constants are used for calculating deformations and stresses, respectively. For a circular section, the torsional constant reduces to the polar moment of inertia (J), and the torsional section modulus reduces to J/ρ; but for all other cross sections they are more complex functions.

The torsional shear stress distribution on any cross section of a circular bar will vary linearly along any radial line emanating from the geometric centroid, and will have the same distribution on all radial lines (Fig. B8.2.1-1A). The longitudinal shear stress (τ_x), which is equal to the torsional shear stress (τ_t), produces no warping of the cross section when the stress distribution is the same on adjacent radial lines (Figs. B8.2.1-1B and B8.2.1-1C). For noncircular sections, the torsional shear stress distribution is nonlinear (except

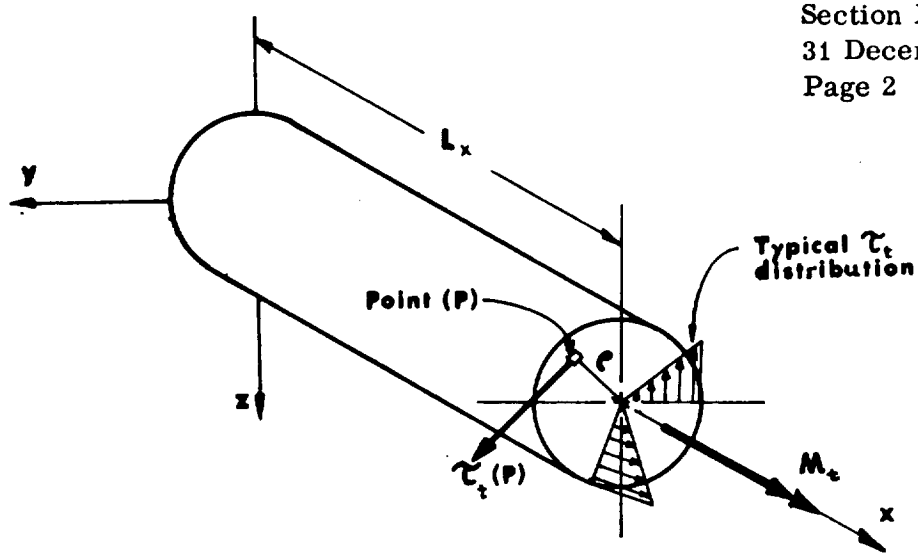

A. Circular Bar Shear Stress Distribution

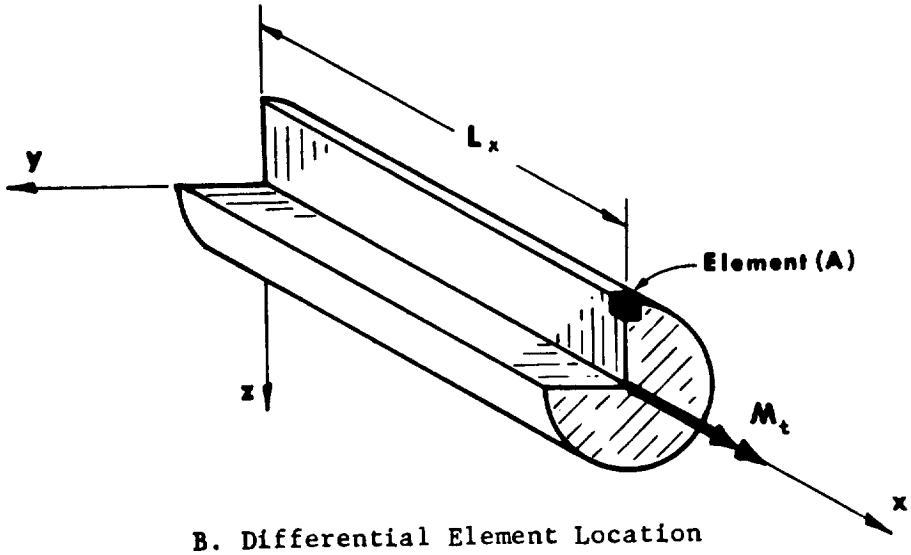

B. Differential Element Location

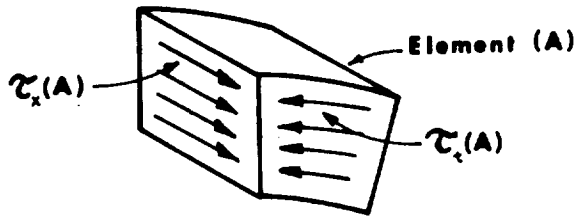

C. Differential Element

FIGURE B8.2.1-1 SHEAR STRESS DISTRIBUTION

along lines of symmetry where the cross section contour is normal to the radial line) and will be different on adjacent radial lines (Fig. B8.2.2-2A). When the torsional and longitudinal shear stress is different on adjacent radial lines, warping of the cross section will occur (Fig. B8.2.2-2B).

When the warping deformation induced by longitudinal shear stresses is restrained, normal stresses (σ) are induced to maintain equilibrium. These normal stresses are neglected in the torsional analysis of solid sections since they are small, attenuate rapidly, and have little effect on the angle of twist.

Restraints to the warping deformation occur at fixed ends and at points where there is an abrupt change in the applied twisting moment.

II Limitations

The torsional analysis of solid cross sections is subject to the following limitations.

A. The material is homogeneous and isotropic

B. The shear stress does not exceed the shearing proportional limit and is proportional to the shear strain (elastic analysis).

C. The stresses calculated at points of constraint and at abrupt changes of applied twisting moment are not exact.

D. The applied twisting moment cannot be an impact load.

E. The bar cannot have an abrupt change in cross section.*

III Membrane Analogy

The torsional analysis of solid bars with irregularly shaped cross sections is usually complex, and for some cases unsolvable. The membrane analogy can be used to visualize the solution for these cross sections.

The basic differential equation for a torsional analysis, written in terms of the St. Venant's stress function, is:

---

* Stress concentration factors must be used at abrupt changes in the cross section.

$$\frac{\partial^2 \Phi}{\partial y^2} + \frac{\partial^2 \Phi}{\partial z^2} = -2G\theta.$$

This equation is similar to the basic differential equation used for the analysis of a deflected membrane, which is:

$$\frac{\partial^2 \mu}{\partial y^2} + \frac{\partial^2 \mu}{\partial z^2} = -p/T \ .$$

The following analogies exist between the solutions of these two analyses when the membrane has the same boundaries as the cross section of a twisted bar.

A. The volume under the deflected membrane for any pressure (p) is equal to one-half the applied twisting moment (M_t), when $2G\theta = p/T$ numerically.

B. The tangent to a contour line of deflected membrane at any point is in the same direction as the maximum torsional shear stress at the same point on the cross section.

C. The slope at any point in the deflected membrane normal to the contour at that point is proportional to the magnitude of the torsional shear stress at that point on the cross section.

IV Basic Torsion Equations for Solid Sections

A. Torsional Shear Stress

The basic equation for determining the torsional shear stress at an arbitrary point (P) on an arbitrary cross section is:

$$\tau_t = \frac{M(x)}{S_t}$$

where M(x) is evaluated at $x = L_x$ for the arbitrary cross section where the torsional shear stress is to be determined.

If a constant torque is applied to the end of the bar, the equation reduces to:

$$\tau_t = \frac{M_t}{S_t} .$$

S_t will vary along the length of the bar for a varying cross section and, in this case, the equation is:

$$\tau_t = \frac{M(x)}{S_t(x)} .$$

For the case of varying moment and varying cross section, both M(x) and $S_t(x)$ must be evaluated at the cross section where the torsional shear stress is to be determined.

In the equations for torsional shear stress determinations in sections B8.2.2-III through B8.2.2-VIII, M(x) is equal to M_t and the stress is determined at the point of maximum torsional shear stress. The resulting equations determine maximum shear stress only.

B. Angle of Twist

The basic equation for determining the angle of twist between the origin and any cross section located at a distance L from the origin is:

$$\phi = \frac{1}{GK} \int_0^{L_x} M(x)\, dx.$$

When M(x) is a constant torsional moment applied at the end of the bar, the equation reduces to:

$$\phi = \frac{1}{GK} \int_0^{L_x} M_t \, dx = \frac{M_t L_x}{GK} \quad ,$$

and the total twist of the bar is:

$$\phi \, (\max) = \frac{M_t L}{GK} \quad .$$

When the cross section varies along the length of the bar, the torsional constant becomes a function of x and must be included within the integral as follows:

$$\phi = \frac{1}{G} \int_0^{L_x} \frac{M(x)}{K(x)} \, dx \, .$$

The moment-area technique (numerical integration) is very useful in calculating angle of twist between any two sections when a M(x)/GK(x) - Diagram is used. See Section B8.2.3, example problem 3.

B8.2.2 TORSIONAL SHEAR STRESS AND ANGLE OF TWIST FOR SOLID SECTIONS

The equations presented in this section for torsional shear stress are for points of maximum torsional shear stress. For some cross sections, torsional shear stress equations are presented for more than one location.

The equations presented for angle of twist are for the total angle of twist developed over the full length of the bar.

The applied load in all cases is a concentrated twisting moment (M_t) applied at the end of the bar.

I Circular Section

The maximum torsional shear stress occurs at the outside surface of the circular cross section (Fig. B8.2.1-1A) and is determined by

$$\tau_t(\max) = \frac{M_t}{S_t}$$

where

$$S_t = \frac{J}{\rho} = \frac{\pi r^4}{2}\left(\frac{1}{r}\right) = \frac{\pi r^3}{2} \quad .$$

Since the torsional shear stress varies linearly from the centroid of the section, the stress at any point (P) on the cross section is determined by

$$\tau_t(P) = \frac{M_t \rho}{J} \quad .$$

The total angle of twist is determined by

$$\phi(\max) = \frac{M_t L}{GK}$$

where

$$K = \frac{\pi r^4}{2} \quad .$$

The angle of twist between the origin and an arbitrary cross section located at a distance L_x from the origin is determined by

$$\phi = \frac{M_t L_x}{GK} \quad .$$

II Hollow Circular Section

The torsional shear stress and angle of twist for a thick-walled hollow cylinder can be determined from the equations in Section B8.2.2.-I when the torsional constant and the torsional section modulus are determined by the following equations.

$$K = \frac{\pi}{2}\left(r_o^4 - r_i^4\right)$$

$$S_t = \frac{\pi}{2}\left(r_o^3 - r_i^3\right)$$

where r_o and r_i are defined by Figure B8.2.2-1.

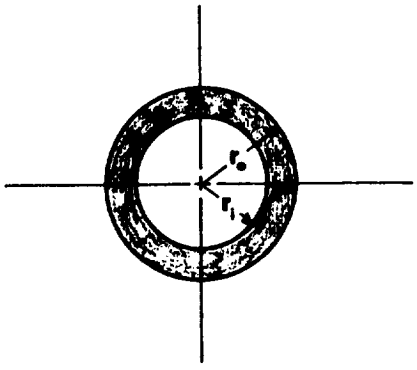

FIGURE B8.2.2-1 HOLLOW CIRCULAR CROSS SECTION

III Rectangular Section

The maximum torsional shear stress occurs at point A (Fig. B8.2.2-2A) and is determined by the following equation.

$$\tau_t\,(\max) = M_t/S_t$$

where

$$S_t = \alpha\, b\, d^2 \ .$$

Some typical values of α are shown in Table B8.2.2-1.

The equation for α in terms of (b/d) is

$$\alpha = \frac{1}{\left[3.0 + \frac{1.8}{(b/d)}\right]} \ .$$

The torsional shear stress at point (B) is determined by

$$\tau_t(B) = \tau_t(\max)\left(\frac{b}{d}\right) .$$

The total angle of twist is determined by

$$\phi\ (\max) = \frac{M_t L}{GK}$$

where

$$K = \beta\, b\, d^3 \ .$$

Some typical values of β are shown in Table B8.2.2-1.

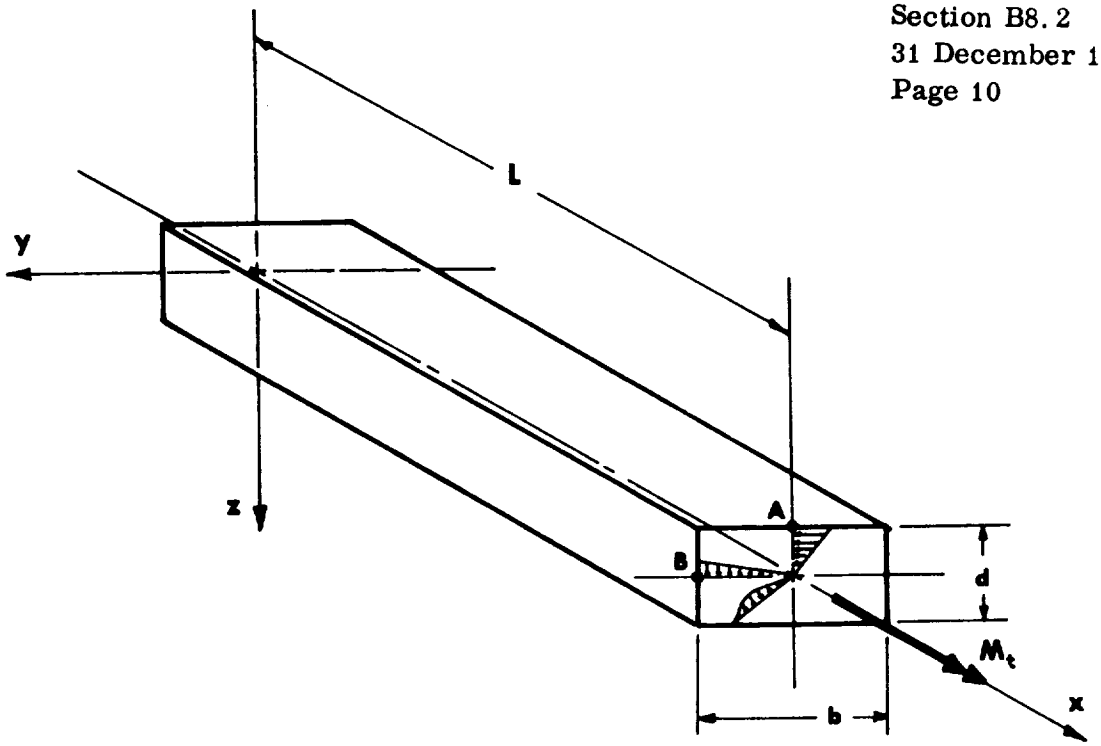

A. Stress Distribution on Rectangular Cross Section

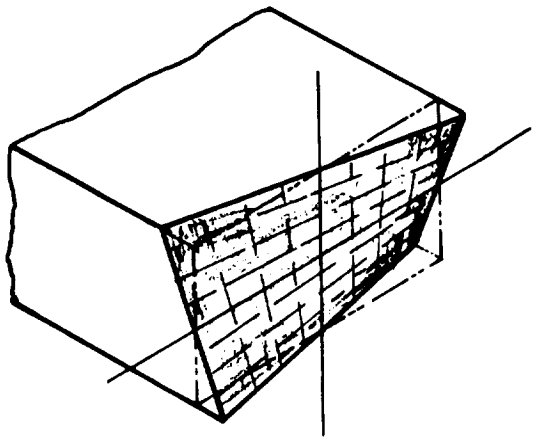

B. Warping Deformation of a Rectangular Cross Section

FIGURE B8.2.2-2 RECTANGULAR CROSS SECTION

Table B9-17. Coefficients For Maximum Moments For Various Loads, Plate Fixed Along One Edge, Free On Opposite Edge And Hinged On Other Two Edges (μ = 0.2)

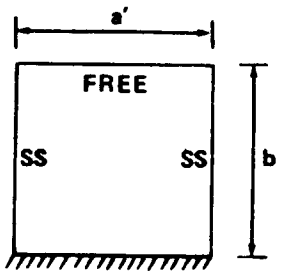

Load / a/b	q, b	q, 2/3 b	q, b/3	q, b	q, 2/3b	q, b/3	q, b/6	M, b	P, b
1/4	-0.0080 qb^2	0.0073 qb^2	0.0066 qb^2	0.0061 qb^2	0.0055 qb^2	0.0038 qb^2	0.0020 qb^2	1.0 M	-0.0534 Pb
1/2	-0.0317 qb^2	0.0269 qb^2	0.0177 qb^2	0.0199 qb^2	0.0156 qb^2	0.0080 qb^2	0.0030 qb^2	1.0 M	-0.1300 Pb
3/4	-0.0644 qb^2	0.0497 qb^2	0.0250 qb^2	0.0353 qb^2	0.0243 qb^2	0.0101 qb^2	0.0032 qb^2	1.0 M	-0.2007 Pb
1	0.1108 qb^2	0.0757 qb^2	0.0317 qb^2	0.0535 qb^2	0.0333 qb^2	0.0122 qb^2	0.0036 qb^2	1.0 M	-0.2590 Pb
3/2	0.2136 qb^2	0.1216 qb^2	0.0406 qb^2	0.0871 qb^2	0.0471 qb^2	0.0147 qb^2	0.0040 qb^2	1.0 M	-0.3114 Pb
2	0.3007 qb^2	0.1552 qb^2	0.0461 qb^2	0.1128 qb^2	0.0565 qb^2	0.0161 qb^2	0.0043 qb^2	1.0 M	0.4831 Pb
3	0.4084 qb^2	0.1929 qb^2	0.0516 qb^2	0.1426 qb^2	0.0666 qb^2	0.0175 qb^2	0.0045 qb^2	1.0 M	0.7513 Pb

Table B9-18. Coefficients For Maximum Moments For Various Loads, Plate Fixed On Two Adjacent Sides, Free On Other Sides ($\mu = 0.2$)

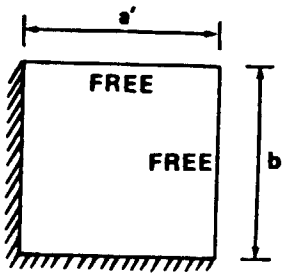

Load / a/b	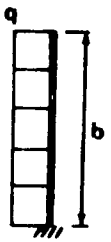	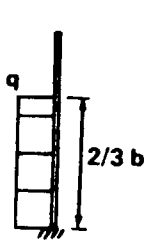	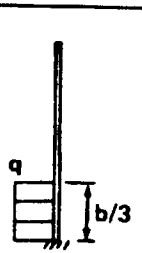	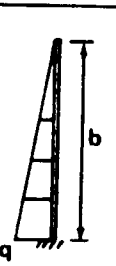		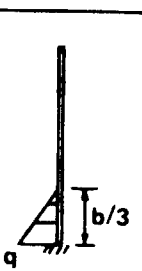	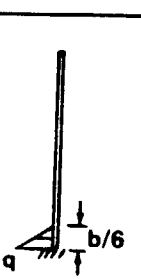
1/8	0.0083 qb^2	0.0083 qb^2	0.0057 qb^2	0.0072 qb^2	0.0066 qb^2	0.0041 qb^2	0.0027 qb^2
1/4	0.0313 qb^2	0.0289 qb^2	0.0165 qb^2	0.0221 qb^2	0.0181 qb^2	0.0087 qb^2	0.0036 qb^2
3/8	0.0664 qb^2	0.0495 qb^2	0.0238 qb^2	0.0354 qb^2	0.0257 qb^2	0.0118 qb^2	0.0038 qb^2
1/2	0.1074 qb^2	0.0775 qb^2	0.0310 qb^2	0.0546 qb^2	0.0358 qb^2	0.0140 qb^2	0.0043 qb^2
3/4	0.2076 qb^2	0.1262 qb^2	0.0402 qb^2	0.0896 qb^2	0.0507 qb^2	0.0167 qb^2	0.0048 qb^2
1	0.2949 qb^2	0.1605 qb^2	0.0456 qb^2	0.1157 qb^2	0.0603 qb^2	0.0181 qb^2	0.0050 qb^2

B9.3.3 Elliptical Plates

For plates whose boundary is the shape of an ellipse, solutions have been found for some common loadings. Table B9-19 presents the available solutions for elliptical plates. For additional information as to method of solution to the plate differential equations see Reference 1.

B9.3.4 Triangular Plates

Solutions for several loadings on triangular shaped plates are presented in Table B9-20.

B9.3.5 Skew Plates

Solutions have been obtained for skew plates in References 1 and 5. The significant results from these references are presented in Table B9-21.

Table B9-19. Solutions For Elliptical, Solid Plates

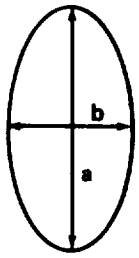

$b/a = \alpha$

Edge Supported, Uniform Load Over Entire Surface	At Center: $\text{max stress} = \sigma_b = \frac{-0.3125(2-\alpha)qb^2}{t^2}$ $\text{max } w = \frac{(0.146 - 0.1\alpha)qb^4}{Et^3} \quad (\text{for } \mu = \frac{1}{3})$
Edge Supported, Uniform Load Over Small Concentric Circular Area of Radius, r_0	At Center: $\text{max } M = M_b = \frac{P}{4\pi}\left[(1+\mu)\log\frac{b}{2r_0} + 6.57\mu - 2.57\alpha\mu\right]$ $\text{max } w = \frac{Pb^2}{Et^3}(0.19 - 0.045\alpha) \quad (\mu = \frac{1}{4})$
Edge Fixed, Uniform Load Over Entire Surface	At Edge: $M_a = \frac{qb^2\alpha^2}{4(3+2\alpha^2+3\alpha^4)}, \quad M_b = \frac{qb^2}{4(3+2\alpha^2+3\alpha^4)}$ At Center: $M_a = \frac{qb^2(\alpha^2+\mu)}{8(3+2\alpha^2+3\alpha^4)}, \quad M_b = \frac{qb^2(1+\alpha^2\mu)}{8(3+2\alpha^2+3\alpha^4)}$ $\text{max } w = \frac{qb^4}{64D(6+4\alpha^2+6\alpha^4)}$
Edge Fixed, Uniform Load Over Small Concentric Circular Area of Radius, r_0	At Center: $M_b = \frac{P(1+\mu)}{4\pi}\left(\log\frac{b}{r_0} - 0.317\alpha - 0.376\right)$ $\text{max } w = \frac{Pb^2(0.0815 - 0.026\alpha)}{Et^3} \quad (\mu = 0.25)$

Table B9-20. Solutions For Triangular Plates

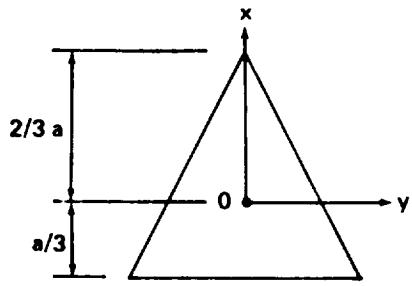

Equilateral Triangle, Edges Supported, Distributed Load Over Entire Surface

$$\max \sigma_x = 0.1488 \frac{qa^2}{t^2} \text{ at } y = 0, \quad x = -0.062a \qquad (\mu = 0.3)$$

$$\max \sigma_y = 0.1554 \frac{qa^2}{t^2} \text{ at } y = 0, \quad x = 0.129a \qquad (\mu = 0.3)$$

$$\max w = \frac{qa^4}{342D} \text{ at point 0}$$

Edges Supported, Load P Concentrated At 0 On Small Circular Area Of Radius, r_0

$$\max \sigma_y = \frac{3(1+\mu)P}{2\pi t^2}\left[\log \frac{0.378a}{\sqrt{1.6r_0^2 + t^2} - 0.675t} - 0.379 + \frac{(1-\mu)}{2(1+\mu)}\right]$$

$$\max w = 0.06852 \frac{Pa^2(1-\mu^2)}{Et^3} \text{ at point 0}$$

Right-Angle Isosceles Triangle, Edges Supported, Distributed Load Over Entire Surface

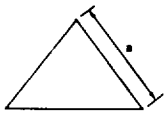

$$\max \sigma_x = 0.131 \frac{qa^2}{t^2}, \qquad \max \sigma_y = 0.1125 \frac{qa^2}{t^2}$$

$$\max w = 0.0095 \frac{qa^4}{Et^3} \qquad (\mu = 0.3)$$

Equilateral Triangle With Two Or Three Edges Clamped, Uniform Or Hydrostatic Load

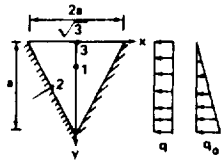

$M = \beta_1 q a^2$ or $M = \beta_1 q_0 a^2$ where

Load Distribution	Edge y = 0 Supported				Edge y = 0 Clamped			
	M_{x_1}	M_{y_1}	M_{n_2}	M_{y_2}	M_{x_1}	M_{y_1}	M_{n_2}	M_{y_2}
Uniform β	0.0126	0.0147	-0.0285	0	0.0113	0.0110	-0.0238	-0.0238
Hydrostatic β_1	0.0053	0.0035	-0.0100	0	0.0051	0.0034	-0.0091	-0.0060

($\mu = 0.2$)

Table B9-21. Solutions for Skew Plates

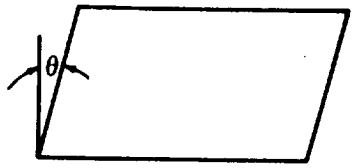

All Edges Supported, Distributed Load Over Entire Surface

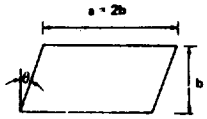

$\max \sigma = \sigma_b = \frac{\beta q b^2}{t^2}$ where β is

θ	0 deg	30 deg	45 deg	60 deg	75 deg
β	0.501	0.50	0.45	0.40	0.16

($\mu = 0.2$)

Edges b Supported, Edges a Free, Uniform Distributed Load Over Entire Surface

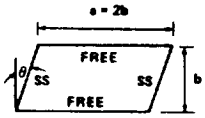

$\max \sigma = \sigma_b = \frac{\beta q b^2}{t^2}$ where β is

θ	0 deg	30 deg	45 deg	60 deg
β	0.762	0.615	0.437	0.250

All Edges Clamped, Uniform Distributed Load Over Entire Surface

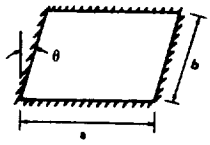

At Center: $M = \beta q a^2$ $w = \frac{\beta_1 q a^4}{D}$

where β and β_1 are

Skew Angle θ (deg)	$\frac{a}{b} = 1$		$\frac{a}{b} = 1.25$		$\frac{a}{b} = 1.5$		$\frac{a}{b} = 2.0$	
	β	β_1	β	β_1	β	β_1	β	β_1
15	0.024	0.001123	0.019	0.00066	0.015	0.00038	0.0097	0.00014
30	0.020	0.00077	0.016	0.00045	0.0125	0.00026	0.0075	0.00009
45	0.015	0.00038	0.011	0.00022	0.014	0.00012	0.005	0.00004
60	0.0085	0.00011	0.0062	0.00006	0.0048	0.00003	0.0025	0.00001
75	0.0025	0.000009	0.0027	0.000005	0.00125	0.000002	0.00125	

Along Fixed Edge:

The coefficient β_2 for maximum bending moment along the edge at a distance fa from the acute corner is

($M = \beta_2 q a^2$ for $\frac{a}{b} = 1$)

Skew Angle (deg)	β_2	f
15	-0.0475	0.6
30	-0.0400	0.69
45	-0.0299	0.80

B9.4 ISOTROPIC THIN PLATES — LARGE DEFLECTION ANALYSIS

Large deflection theory of plates was discussed in Paragraph B9.2.3. It was determined that the region covered by the classification of large deflection analysis was approximately $\frac{1}{3}\,t < w/t > 10t$. In this region, the load resistance of plates is a combination of bending and direct tensile stress. Solutions for available plate geometries and loads will be given in this subsection. Figure B9-7 gave a guide as to the regimes of membrane plates, medium-thick plates, and thin plates. Curves are given in Fig. B9-12 for membrane plates and for medium-thick plates. Between these two regimes is the regime of thin plates, which generally includes most of the plate dimensions and pressures encountered in aerospace design.

B9.4.1 Circular Plates — Uniformly Distributed Load

A circular plate whose edge is clamped so that rotation and radial displacement are prevented at the edge is shown in Fig. B9-13. The plate, loaded by a uniformly distributed load, has a maximum deflection which is large relative to the thickness of the plate as shown in Fig. B9-13c. In Fig. B9-13d a diametral strip of one unit width cut from the plate shows the bending moments per unit of width and the direct tensile forces which act in this strip at the edge and at the center of the plate. The direct tensile forces arise from two sources. First, the fixed support at the edge prevents the edge at opposite ends of a diametral strip from moving radially, thereby causing the strip to stretch as it deflects. Second, if the plate is not clamped at its edge but is simply supported

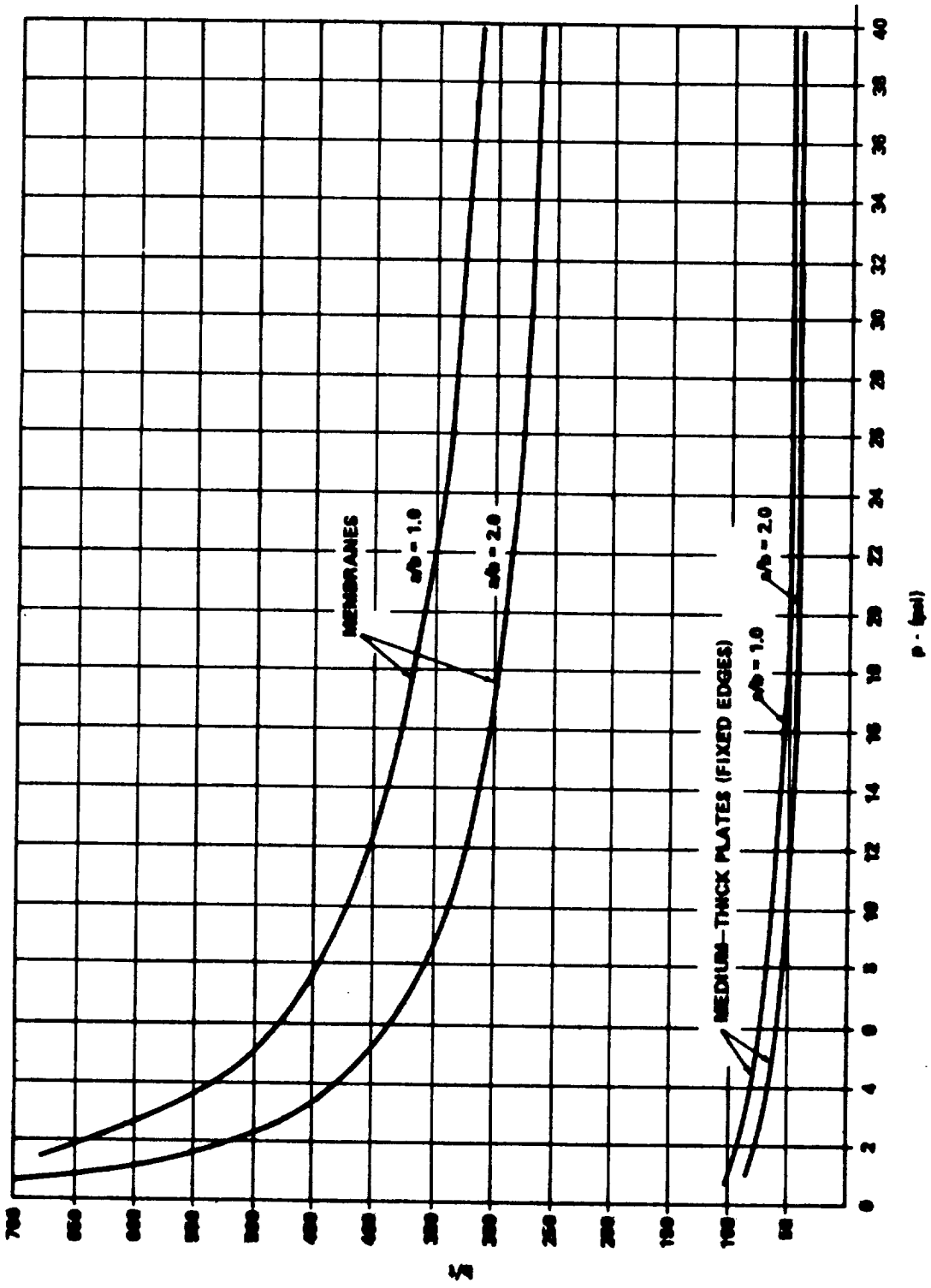

FIGURE B9-12. LIMITING REGIONS FOR RECTANGULAR MEMBRANE AND THICK PLATE THEORIES

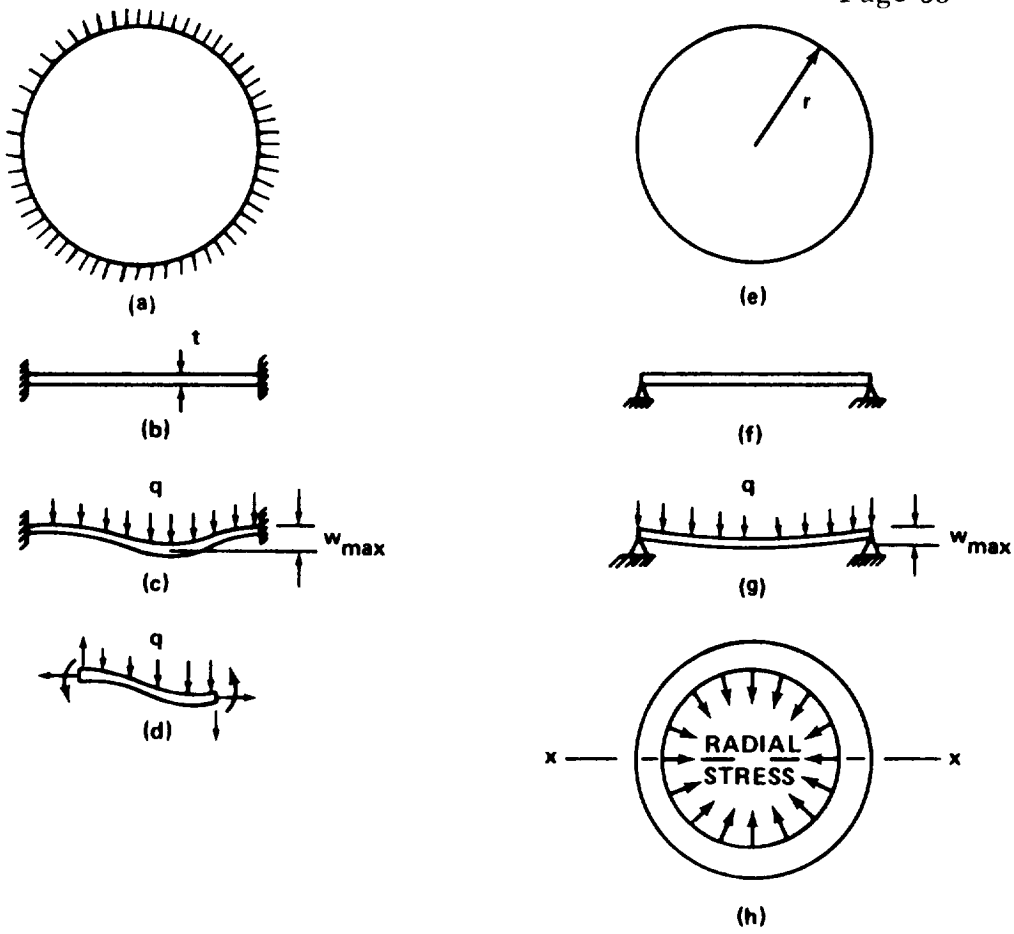

FIGURE B9-13. BEHAVIOR OF THIN CIRCULAR PLATE

as shown in Figs. B9-13e and f, radial stresses arise out of the tendency for outer concentric rings of the plate (such as shown in Fig. B9-13h) to retain their original diameter as the plate deflects. In Fig. B9-13h the concentric ring at the outer edge is shown cut from the plate. This ring tends to retain the original outside diameter of the unloaded plate; the radial tensile stresses acting on the inside of the ring, as shown in Fig. B9-13h, cause the ring diameter to decrease, and in doing so they introduce compressive stresses on every

diametral section such as xx . These compressive stresses in the circumferential direction sometimes cause the plate to wrinkle or buckle near the edge, particularly if the plate is simply supported. The radial stresses are usually larger in the central portion of the plate than they are near the edge.

Stresses have been determined for a thin circular plate with clamped edges and the results are plotted in Fig. B9-14, where σ_{be} and σ_{bc} are the bending

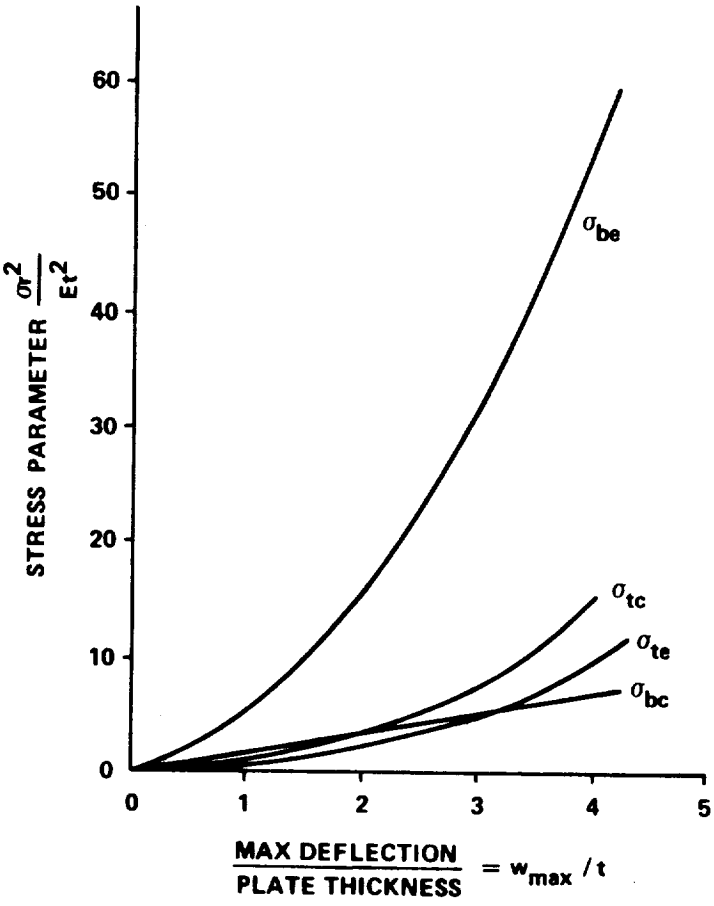

FIGURE B9-14. STRESSES IN THIN PLATES HAVING LARGE DEFLECTIONS, CIRCULAR PLATE WITH CLAMPED EDGES

stresses in a radial plane at the edge and center of the plate, and σ_{te} and σ_{tc} are corresponding direct tensile stresses. It is noted that the bending stress σ_{be} at the fixed edge is the largest of these four stresses. The direct tensile stresses become relatively larger as the deflection increases.

Figure B9-15 presents a set of curves which show the relationship between load, deflection, and stress for a thin circular plate with clamped edges. For example, if the dimensions and the modulus of elasticity of the plate and the load q are given, the quantity qr^4/Et^4 can be computed. The value of w_{max}/t corresponding to this value of qr^4/Et^4 is found from the curve on the left. By projecting across to stress curves, corresponding stress parameters $\sigma_{max} r^2/Et^2$ are read at the center and at the edge of the plate.

Figure B9-16 presents curves similar to those of Fig. B9-15 for a plate whose edges are simply supported.

Also, Table B9-22 presents data for the calculation of approximate values of deflections and stresses in uniformly loaded circular plates, both clamped and simply supported. The deflection at the center w_0 is given by the equation,

$$\frac{w_0}{t} + A\left(\frac{w_0}{t}\right)^3 = B\ \frac{q}{E}\left(\frac{r}{t}\right)^4 \quad . \tag{33}$$

Also, the stresses in the middle plane are given by

$$\sigma_r = \alpha_r E\left(\frac{w_0}{r}\right)^2 \quad , \quad \sigma_t = \alpha_T E\left(\frac{w_0}{r}\right)^2 \quad , \tag{34}$$

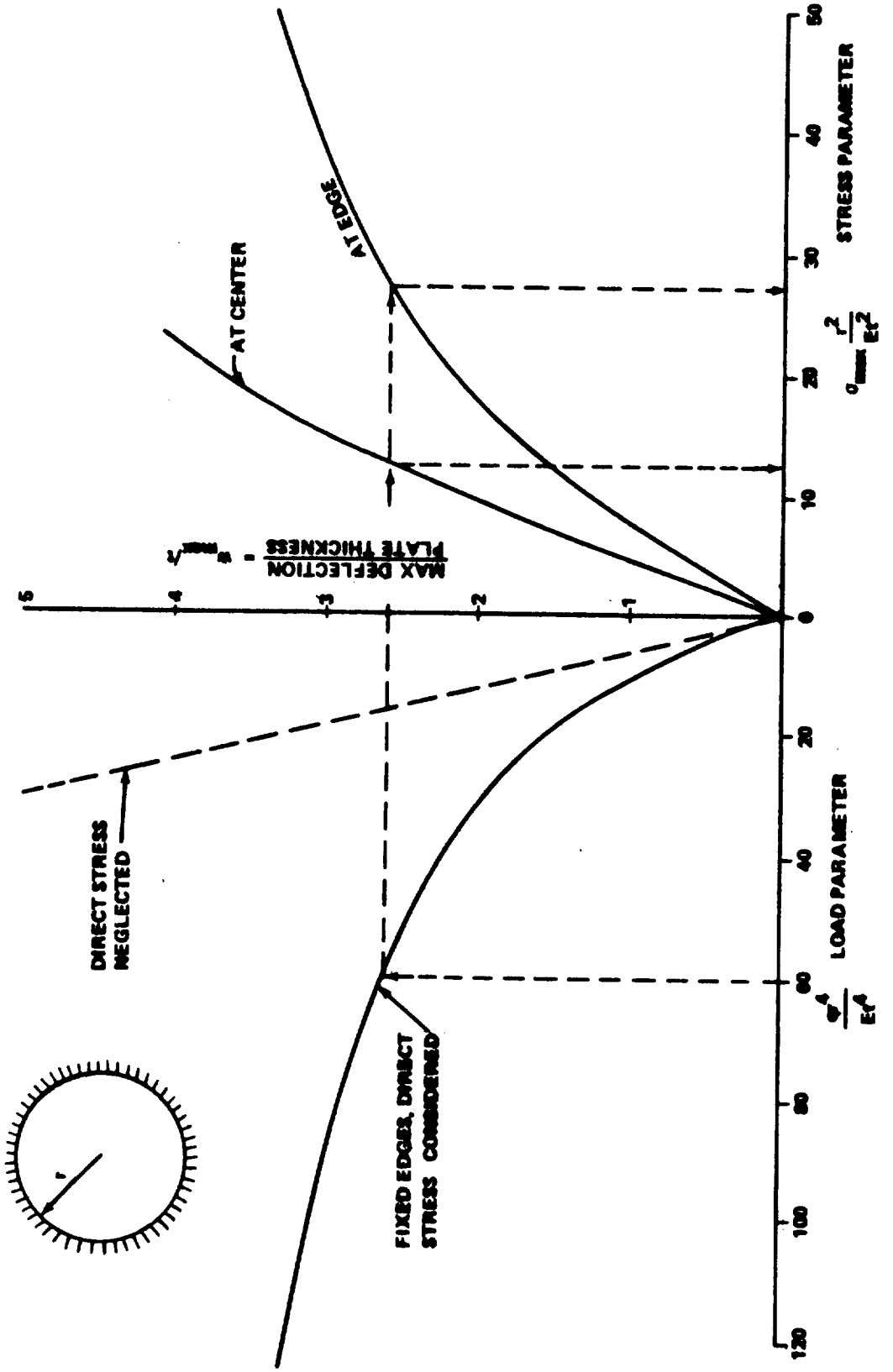

FIGURE B9-15. MAXIMUM STRESSES AND DEFLECTIONS IN THIN CIRCULAR PLATE WITH CLAMPED EDGES

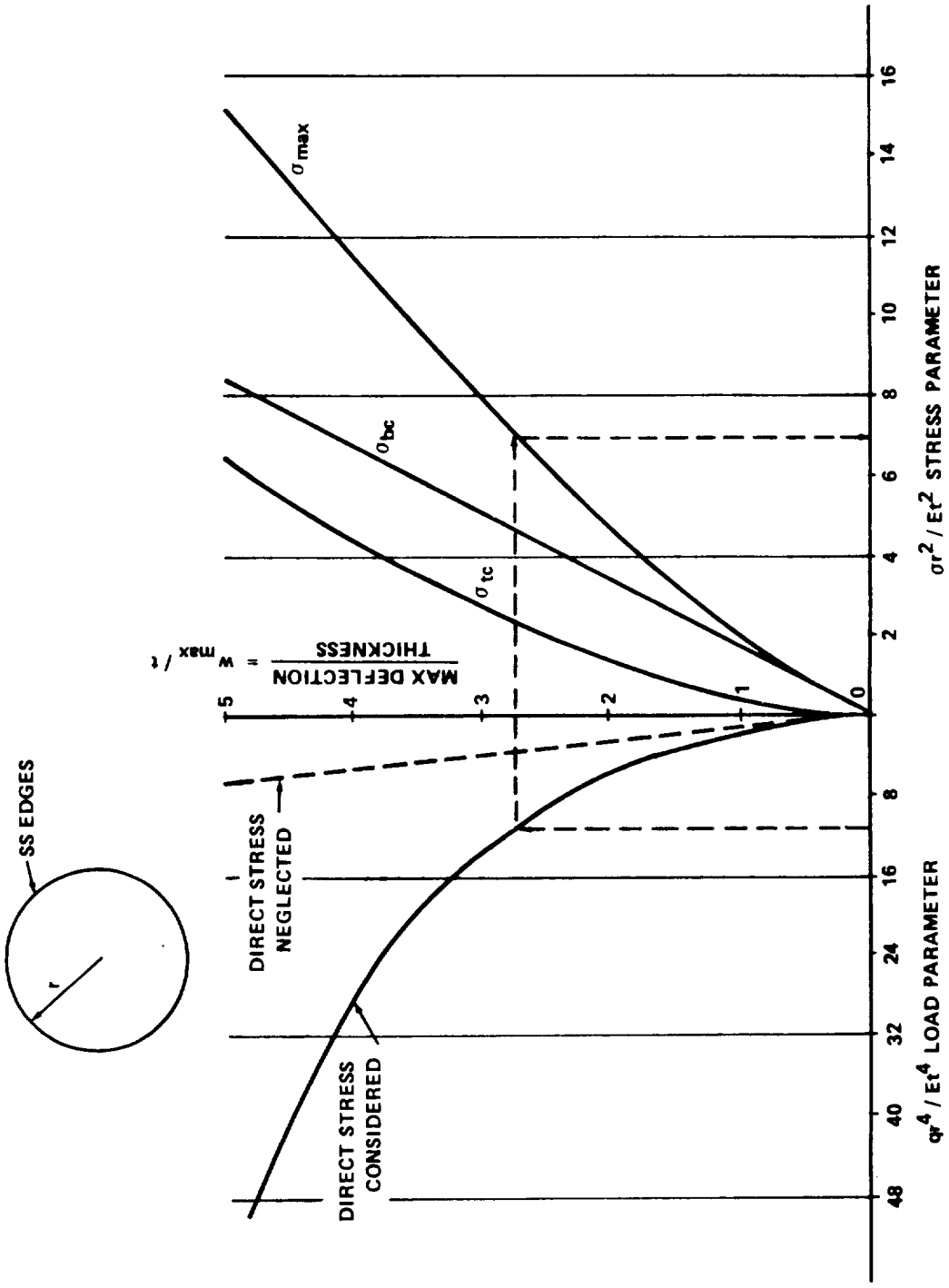

FIGURE B9-16. MAXIMUM STRESSES AND DEFLECTIONS IN THIN CIRCULAR PLATE WITH SIMPLY SUPPORTED EDGES

Table B9-22. Data for Calculation of Approximate Values of Deflections w_0 and Stresses in Uniformly Loaded Plates ($\mu = 0.3$)

Boundary Conditions		A	B	Center		Edge			
				$\alpha_r = \alpha_t$	$\beta_r = \beta_t$	α_r	α_t	β_r	β_t
Plate Clamped	Edge Immovable	0.471	0.171	0.976	2.86	0.476	0.143	-4.40	-1.32
	Edge Free To Move	0.146	0.171	0.500	2.86	0	-0.333	-4.40	-1.32
Plate Simply Supported	Edge Immovable	1.852	0.696	0.905	1.778	0.610	0.183	0	0.755
	Edge Free To Move	0.262	0.696	0.295	1.778	0	-0.427	0	0.755

and the extreme fiber bending stresses are given by

$$\sigma_r' = \beta_r E \frac{w_0 t}{r^2} \quad , \quad \sigma_t' = \beta_t E \frac{w_0 t}{r^2} \quad . \tag{35}$$

B9.4.2 Circular Plates – Loaded at the Center

An approximate solution of the problem of a circular plate loaded at the center with either clamped or simply supported edges has been obtained in Reference 1. Table B9-23 contains the coefficients necessary for solution of the center deflection w_0 from equations (33), (34), and (35).

B9.4.3 Rectangular Plates – Uniformly Loaded

For the case of a plate with clamped edges, an approximate solution has been obtained [1]. Numerical values of all the parameters have been computed for various intensities of the load q and for three different shapes of the plate b/a = 1, b/a = 2/3, and b/a = 1/2 for $\mu = 0.3$. The maximum deflections at the center of the plate are graphically represented in Fig. B9-17, in which

Table B9-23. Data for Calculation of Approximate Values of Deflections w_0 and Stresses in Centrally Loaded Plates ($\mu = 0.3$)

Boundary Conditions		A	B	Center	Edge			
				$\alpha_r = \alpha_t$	α_r	α_t	β_r	β_t
Plate Clamped	Edge Immovable	0.443	0.217	1.232	0.357	0.107	-2.198	-0.659
	Edge Free To Move	0.200	0.217	0.875	0	-0.250	-2.198	-0.659
Plate Simply Supported	Edge Immovable	1.430	0.552	0.895	0.488	0.147	0	0.606
	Edge Free To Move	0.272	0.552	0.407	0	-0.341	0	0.606

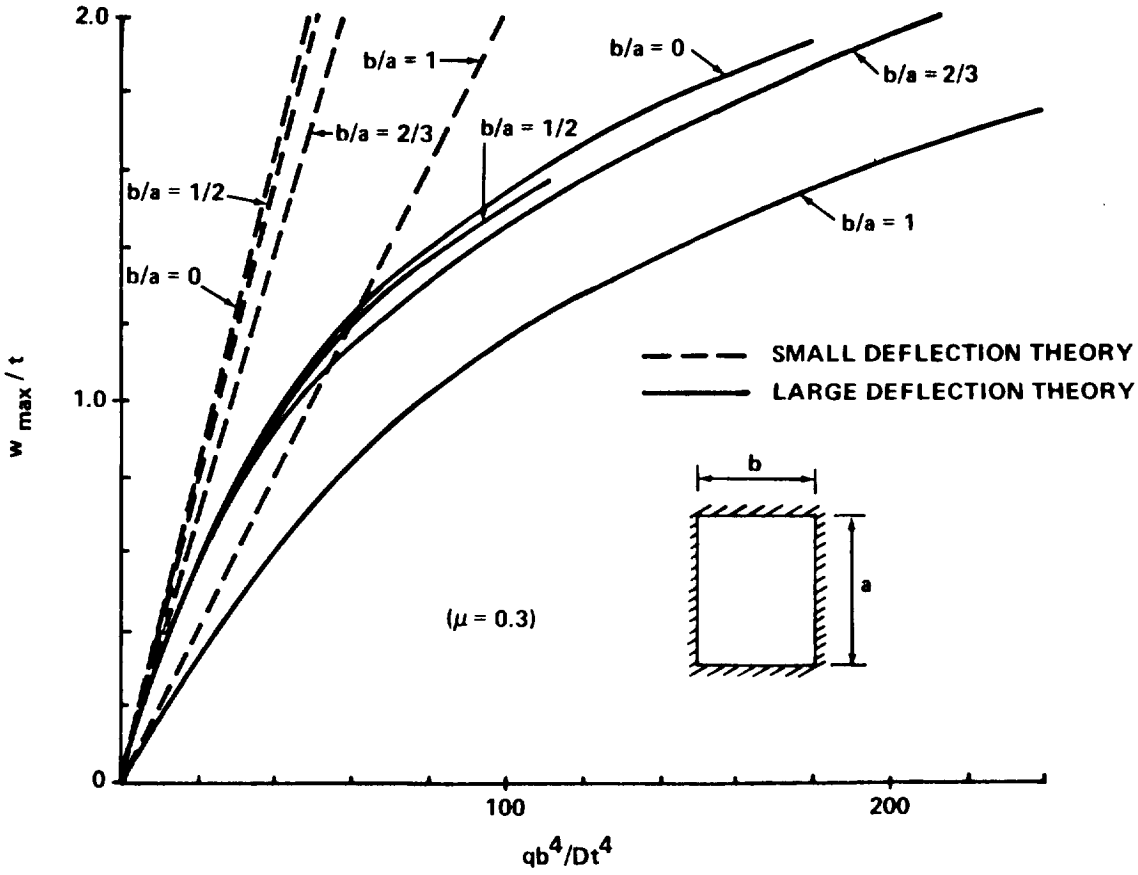

FIGURE B9-17. MAXIMUM DEFLECTIONS AT CENTER FOR RECTANGULAR PLATE WITH CLAMPED EDGES

w_{max}/t is plotted against qb^4/Dt^4. For comparison, the figure also includes the use of the theory of small deflections. Also included is the curve for $b/a = 0$, which represents deflections of an infinitely long plate. It can be seen that the deflections of finite plates with $b/a < 2/3$ are very close to those obtained for an infinitely long plate. The maximum values of the combined membrane and bending stress are at the middle of the long sides of the plate. They are given in graphical form in Fig. B9-18.

For the case of a rectangular plate, uniformly loaded with immovable, simply supported edges, a solution has been obtained [1]. Values for membrane stresses and extreme fiber bending stresses are given in Figs. B9-19 and B9-20, respectively. An approximate equation for maximum deflection, w_0, at the center of the plate in terms of the load q is given by:

$$q = \frac{w_0 E t^3}{a^4}\left[1.37 + 1.94\left(\frac{w_0}{t}\right)^2\right]. \qquad (36)$$

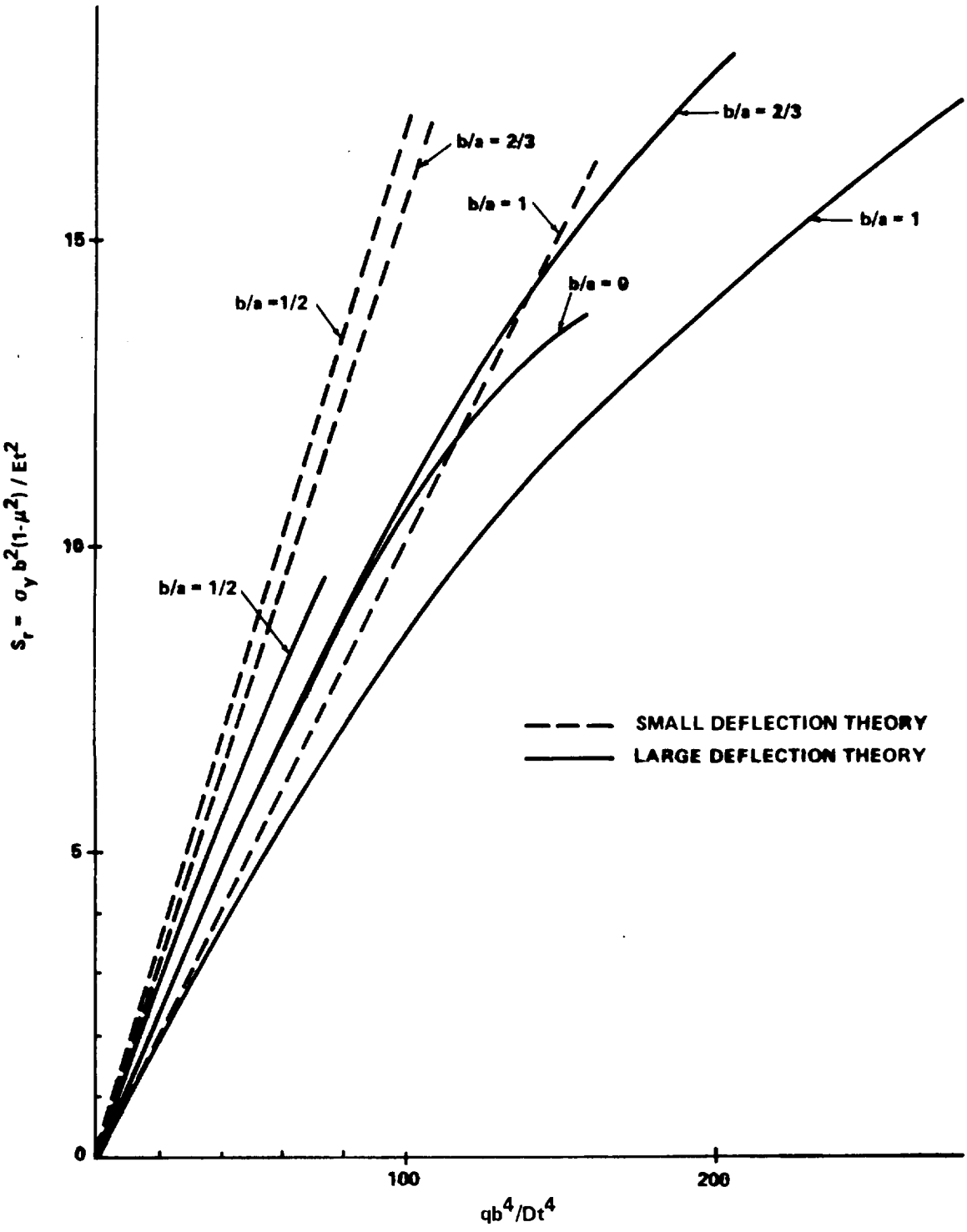

FIGURE B9-18. MAXIMUM STRESS AT CENTER OF LONG EDGE FOR RECTANGULAR PLATE WITH CLAMPED EDGES

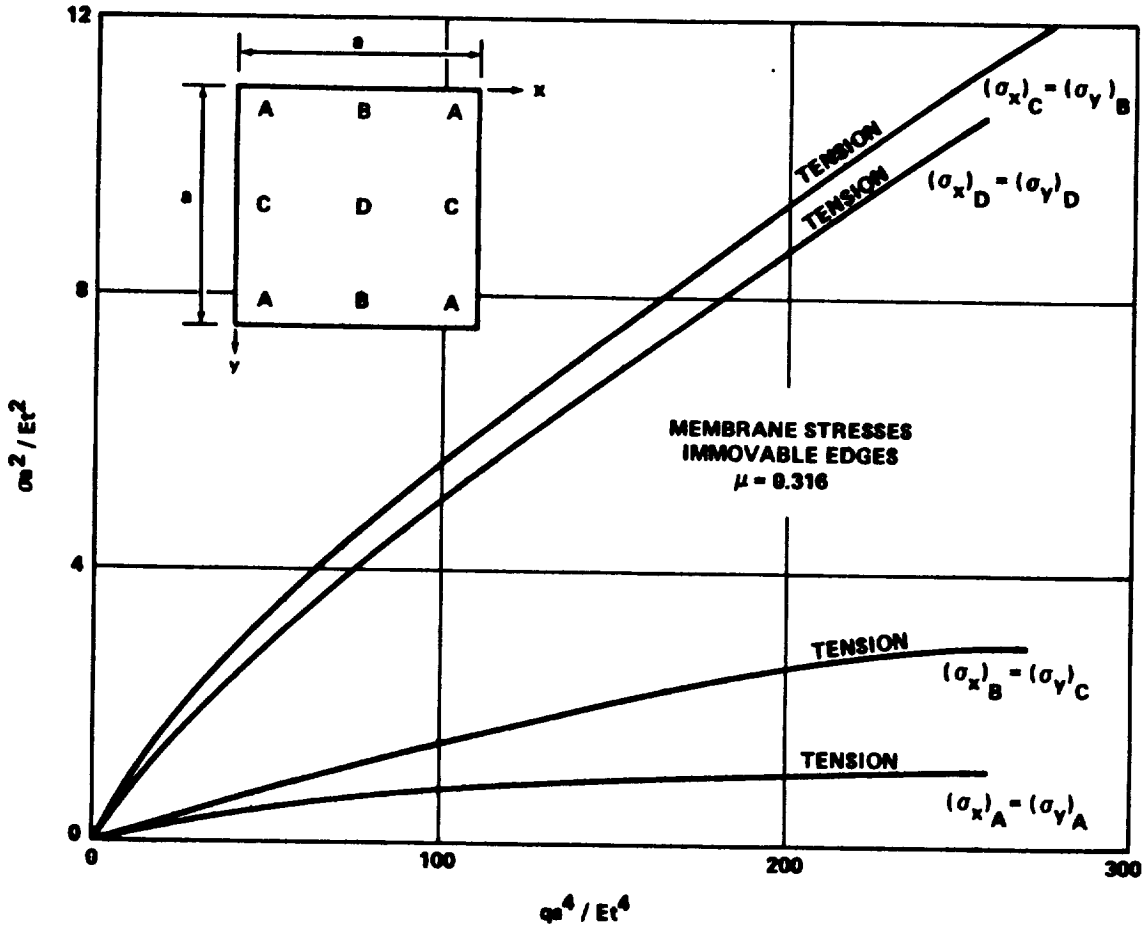

FIGURE B9-19. MEMBRANE STRESSES IN SQUARE PLATE, UNIFORMLY LOADED

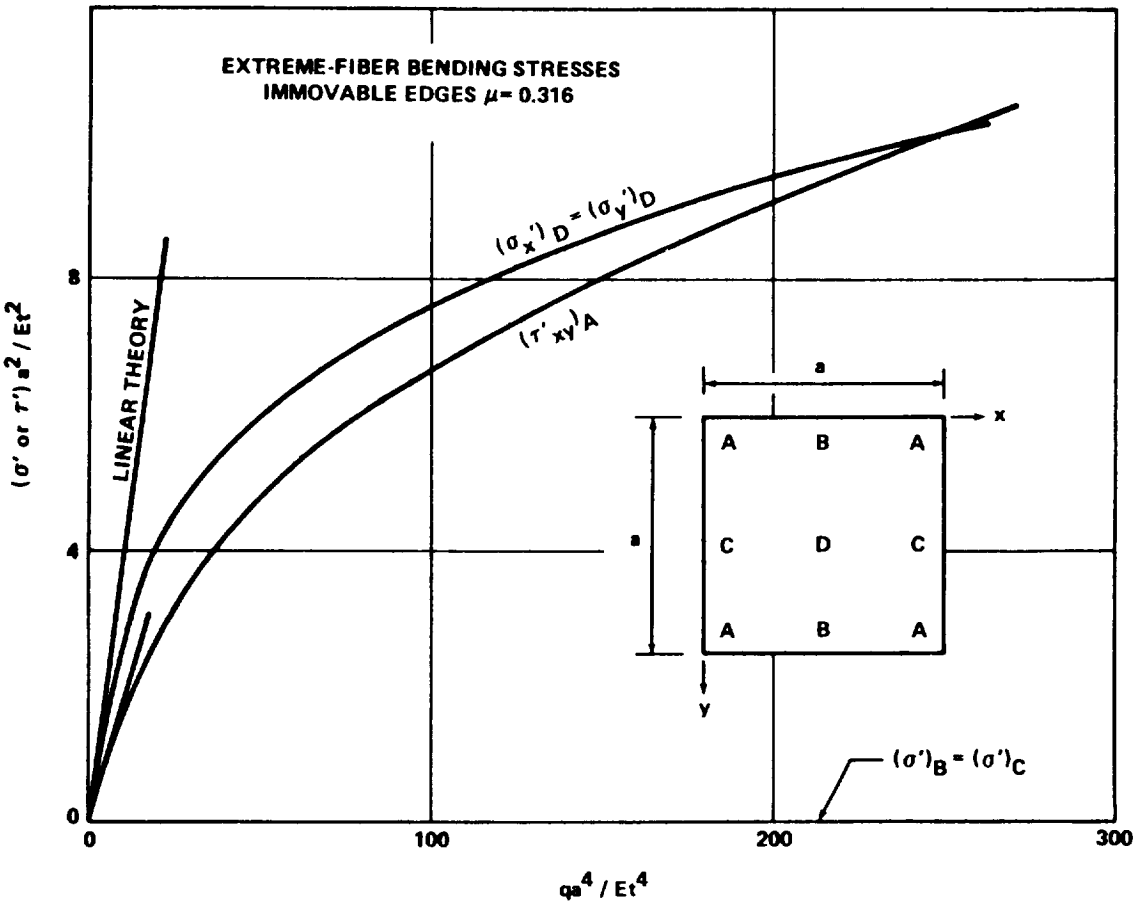

FIGURE B9-20. BENDING STRESSES IN SQUARE PLATE, UNIFORMLY LOADED

B9.5 ORTHOTROPIC PLATES

B9.5.1 Rectangular Plate

The deflection and the bending moments at the center of an orthotropic rectangular plate can be calculated from the following equations obtained from Reference 1.

$$w = \alpha \frac{q_0 b^4}{D_y} \quad , \tag{37}$$

$$M_x = \left(\beta_1 + \beta_2 \frac{E''}{E'_x} \sqrt{\frac{D_x}{D_y}}\right) \frac{q_0 a^2}{\epsilon} \quad , \tag{38}$$

$$M_y = \left(\beta_2 + \beta_1 \frac{E''}{E'_y} \sqrt{\frac{D_y}{D_x}}\right) q_0 b^2 \quad , \tag{39}$$

where α, β_1, and β_2 are numerical coefficients given in Table B9-24 and

$$\epsilon = \frac{a}{b} \sqrt[4]{\frac{D_y}{D_x}} \quad . \tag{40}$$

The four constants E'_x, E'_y, E'', and G in equations (37), (38), and (39) are needed to characterize the elastic properties of a material in the case of plane stress. These four constants are defined by equations (8) of Section B9.2.1.1. Equations (41) through (44) are expressions for rigidities and are subject to modifications according to the nature of the material and the geometry of the stiffening.

$$D_x = \frac{E'_x h^3}{12} \tag{41}$$

$$D_y = \frac{E'_y h^3}{12} \tag{42}$$

$$D_1 = \frac{E'' h^3}{12} \qquad (43)$$

$$D_{xy} = \frac{Gh^3}{12} \qquad (44)$$

Table B9-24. Constants α, β_1, and β_2 for A Simply Supported Rectangular Orthotropic Plate with $H = \sqrt{D_x D_y}$

ϵ	α	β_1	β_2
1.0	0.00407	0.0368	0.0368
1.1	0.00438	0.0359	0.0447
1.2	0.00565	0.0344	0.0524
1.3	0.00639	0.0324	0.0597
1.4	0.00709	0.0303	0.0665
1.5	0.00772	0.0280	0.0728
1.6	0.00831	0.0257	0.0785
1.7	0.00884	0.0235	0.0837
1.8	0.00932	0.0214	0.0884
1.9	0.00974	0.0191	0.0929
2.0	0.01013	0.0174	0.0964
2.5	0.01150	0.0099	0.1100
3.0	0.01223	0.0055	0.1172
4.0	0.01282	0.0015	0.1230
5.0	0.01297	0.0004	0.1245
∞	0.01302	0.0	0.1250

All values of rigidities based on purely theoretical considerations should be regarded as a first approximation and tests are recommended to obtain more reliable values. Usual values of the rigidities for three cases of practical interest are given below.

1. Plate Reinforced By Equidistant Stiffeners In One Direction: Consider a plate reinforced symmetrically with respect to its middle plane as shown in Fig. B9-21. The elastic constants of the material of the plating are E and ν, E' the Young's modulus, and I the moment of inertia of a stiffener, taken with respect to the middle axis of the cross section of the plate. The rigidity values are stated by equations (45) and (46):

$$D_x = \frac{Eh^3}{12(1-\nu^2)} = H \quad , \tag{45}$$

$$D_y = \frac{Eh^3}{12(1-\nu^2)} + \frac{E'I}{a_1} \quad , \tag{46}$$

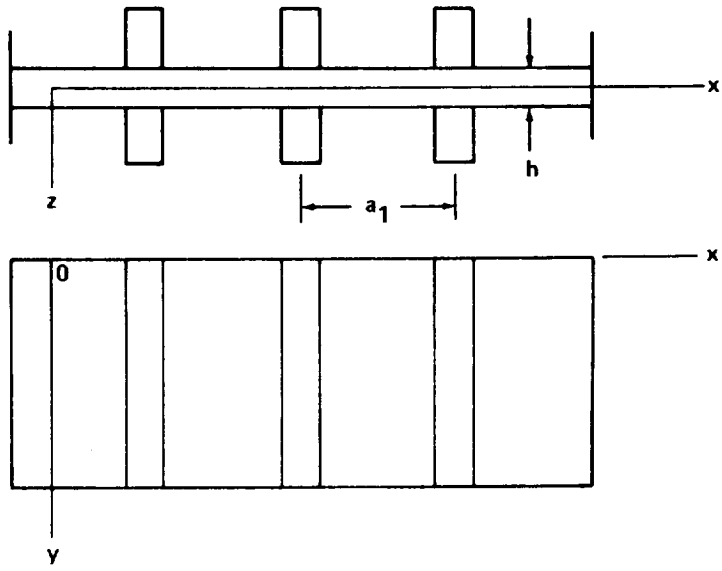

FIGURE B9-21. ORTHOTROPIC PLATE WITH EQUIDISTANT STIFFENERS

2. Plate Cross-Stiffened By Two Sets Of Equidistant Stiffeners: Assume the reinforcement to remain symmetrical about the plating. The moment of

inertia of one stiffener is I_1, and b_1 is the spacing of the stiffeners in the x-direction. The corresponding values for stiffeners in the y-direction are I_2 and a_1. The rigidity values for this case are stated by equations (47), (48), and (49):

$$D_x = \frac{Eh^3}{12(1-\nu^2)} + \frac{E' I_1}{b_1} \quad , \tag{47}$$

$$D_y = \frac{Eh^3}{12(1-\nu^2)} + \frac{E' I_2}{a_1} \quad , \tag{48}$$

$$H = \frac{Eh^3}{12(1-\nu^2)} \quad . \tag{49}$$

3. Plate Reinforced By A Set Of Equidistant Ribs: Refer to Fig. B9-22 and let E be the modulus of the material, I the moment of inertia of a T-section of width a_1, and $\alpha = h/H$. Then, the rigidities are expressed by equations (50), (51), and (52):

$$D_x = \frac{Ea_1h^3}{12(a_1 - t + \alpha^3 t)} \quad , \tag{50}$$

$$D_y = \frac{EI}{a_1} \quad , \tag{51}$$

$$D_1 = 0 \quad . \tag{52}$$

The effect of the transverse contraction is neglected in the foregoing equations. The torsional rigidity may be calculated by means of equation (53):

$$D_{xy} = D'_{xy} + \frac{C}{2a_1} \quad , \tag{53}$$

in which D'_{xy} is the torsional rigidity of the plate without the ribs and C the torsional rigidity of one rib.

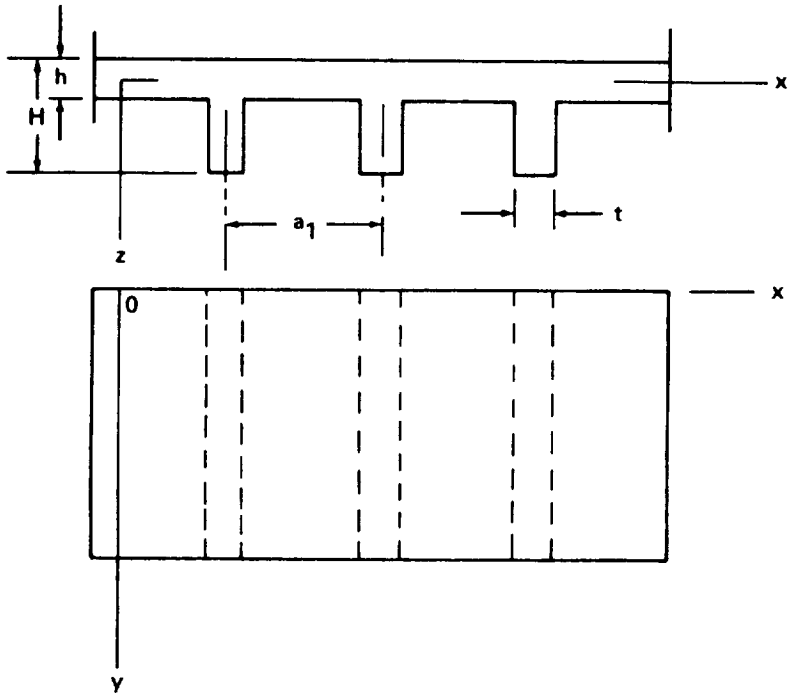

FIGURE B9-22. ORTHOTROPIC PLATE WITH STIFFENERS ON ONE SIDE

Formulas for the elastic constants of plates with integral waffle-like stiffening can be found in Reference 6.

B9.6 STRUCTURAL SANDWICH PLATES

B9.6.1 Small Deflection Theory

The information presented for the small deflection theory was obtained from Reference 7.

Structural sandwich is a layered composite formed by bonding two thin facings to a thick core. The main difference in design procedures for sandwich structural elements and those of homogeneous material is the inclusion of the effects of core shear properties on deflection, buckling, and stress for the sandwich. The basic design principles for a sandwich can be summarized into four conditions as follows:

1. Sandwich facings shall be at least thick enough to withstand chosen design stresses under design ultimate loads.
2. The core shall be thick enough and have sufficient shear rigidity and strength so that overall sandwich buckling, excessive deflection, and shear failure will not occur under design ultimate loads.
3. The core shall have high enough moduli of elasticity and the sandwich shall have great enough flatwise tensile and compressive strength so that wrinkling of either facing will not occur under design ultimate loads.
4. If the core is made of cellular or corrugated material and dimpling of the facings is not permissible, the cell size or corrugation spacing shall be small enough so that dimpling of either facing into the core spaces will not occur under design ultimate loads.

B9.6.1.1 Basic Principles for Design of Flat Sandwich Panels under Uniformly Distributed Normal Load

Assuming that a design begins with chosen design stresses and deflections and a given load to transmit, a flat rectangular or circular panel of sandwich construction under uniformly distributed normal load shall be designed to comply with the four basic design principles.

Detailed procedures giving theoretical formulas and graphs for determining dimensions of the facings and core, as well as necessary core properties, for simply supported panels are given in the following paragraphs. Double formulas are given, one formula for sandwich with isotropic facings of different materials and thicknesses and another formula for sandwich with each isotropic facing of the same material and thickness. Facing moduli of elasticity, $E_{1,2}$, and stress values, $F_{1,2}$, shall be compression or tension values at the condition of use; that is, if application is at elevated temperature, then facing properties at elevated temperature shall be used in design. For many combinations of facing materials it will be advantageous to choose thicknesses such that $E_1t_1 = E_2t_2$. The following procedures are restricted to linear elastic behavior.

B9.6.1.2 Determining Facing Thickness, Core Thickness , and Core Shear Modulus for Simply Supported Flat Rectangular Panels

This section gives procedures for determining sandwich facing and core thicknesses and core shear modulus so that chosen design facing stresses and allowable panel deflections will not be exceeded. The facing stresses, produced by bending moment, are maximum at the center of a simply supported panel

under uniformly distributed normal load. If restraint exists at panel edges, a redistribution of stresses may cause higher stresses near panel edges. The procedures given apply only to panels with simply supported edges. Because facing stresses are caused by bending moment, they depend not only upon facing thickness but also upon the distance the facings are spaced, hence core thickness. Panel stiffness, hence deflection, is also dependent upon facing and core thickness.

If the panel is designed so that facing stresses are at chosen design levels, the panel deflection may be larger than allowable, in which case the core or facings must be thickened and the design facing stress lowered to meet deflection requirements. A solution is presented in the form of charts with which, by iterative process, the facing and core thicknesses and core shear modulus can be determined.

The average facing stress, F(stress at facing centroid) , is given by the theoretical formulas:

$$F_{1,2} = K_2 \frac{pb^2}{ht_{1,2}} \qquad \text{(for unequal facings)} \quad , \tag{54}$$

and

$$F = K_2 \frac{pb^2}{ht} \qquad \text{(for equal facings)} \quad , \tag{55}$$

where p is the intensity of the distributed load; b is the panel width; h is the distance between facing centroids; t is facing thickness; 1 and 2 are subscripts denoting facings 1 and 2; and K_2 is a theoretical coefficient dependent on panel aspect ratio and sandwich bending and shear rigidities. If the core is isotropic (shear moduli alike in the two principal directions), K_2 values depend only upon panel aspect ratio. The values of K_2 for sandwich with orthotropic core are dependent not only on panel aspect ratio but also upon sandwich bending and shear rigidities as incorporated in the parameter $V = \frac{\pi^2 D}{b^2 U}$ which can be written as:

$$V = \frac{\pi^2 t_c E_1 t_1 E_2 t_2}{\lambda b^2 G_c (E_1 t_1 + E_2 t_2)} \qquad (56)$$

$$V = \frac{\pi^2 t_c E t}{2\lambda b^2 G_c} \qquad \text{(for equal facings)} \quad , \qquad (57)$$

where U is sandwich shear stiffness; E is modulus of elasticity of facing; $\lambda = 1 - \mu^2$; μ is Poisson's ratio of facings [in formula (56) it is assumed that $\mu = \mu_1 = \mu_2$]; and G_c is the core shear modulus associated with axes parallel to panel side of length a and perpendicular to the plane of the panel. The core shear modulus associated with axes parallel to panel side of width b and perpendicular to the plane of the panel is denoted by (RG_c).

Solving equations (54) and (55) for h/b gives

$$\frac{h}{b} = \sqrt{K_2}\ \frac{\sqrt{\frac{p}{F_{1,2}}}}{\sqrt{\frac{t_{1,2}}{h}}} \qquad (58)$$

$$\frac{h}{b} = \sqrt{K_2}\,\frac{\sqrt{\frac{p}{F}}}{\sqrt{\frac{t}{h}}} \qquad \text{(for equal facings)} \quad . \qquad (59)$$

A chart for solving formulas (58) and (59) graphically is given in Fig. B9-23. The formulas and charts include the ratio t/h, which is usually unknown, but by iteration satisfactory ratios of t/h and h/b can be found.

The deflection, δ, of the panel center is given by the theoretical formula:

$$\delta = \frac{K_1}{K_2} \cdot \frac{\lambda F_{1,2}}{E_{1,2}} \left(1 + \frac{E_{1,2}t_{1,2}}{E_{2,1}t_{2,1}}\right)\frac{b^2}{h} \qquad (60$$

$$\delta = 2\,\frac{K_1}{K_2} \cdot \frac{\lambda F}{E} \cdot \frac{b^2}{h} \qquad \text{(for equal facings)} \quad , \qquad (61)$$

where K_1 is a coefficient dependent upon panel aspect ratio and the value of V.

Solving equations (60) and (61) for h/b gives

$$\frac{h}{b} = \frac{\sqrt{\frac{K_1}{K_2}}\sqrt{\frac{\lambda F_{1,2}}{E_{1,2}}}\sqrt{1 + \frac{E_{1,2}t_{1,2}}{E_{2,1}t_{2,1}}}}{\sqrt{\frac{\delta}{h}}} \qquad (62)$$

$$\frac{h}{b} = \frac{\sqrt{\frac{2K_1}{K_2}}\sqrt{\frac{\lambda F}{E}}}{\sqrt{\frac{\delta}{h}}} \qquad \text{(for equal facings)} \quad . \qquad (63)$$

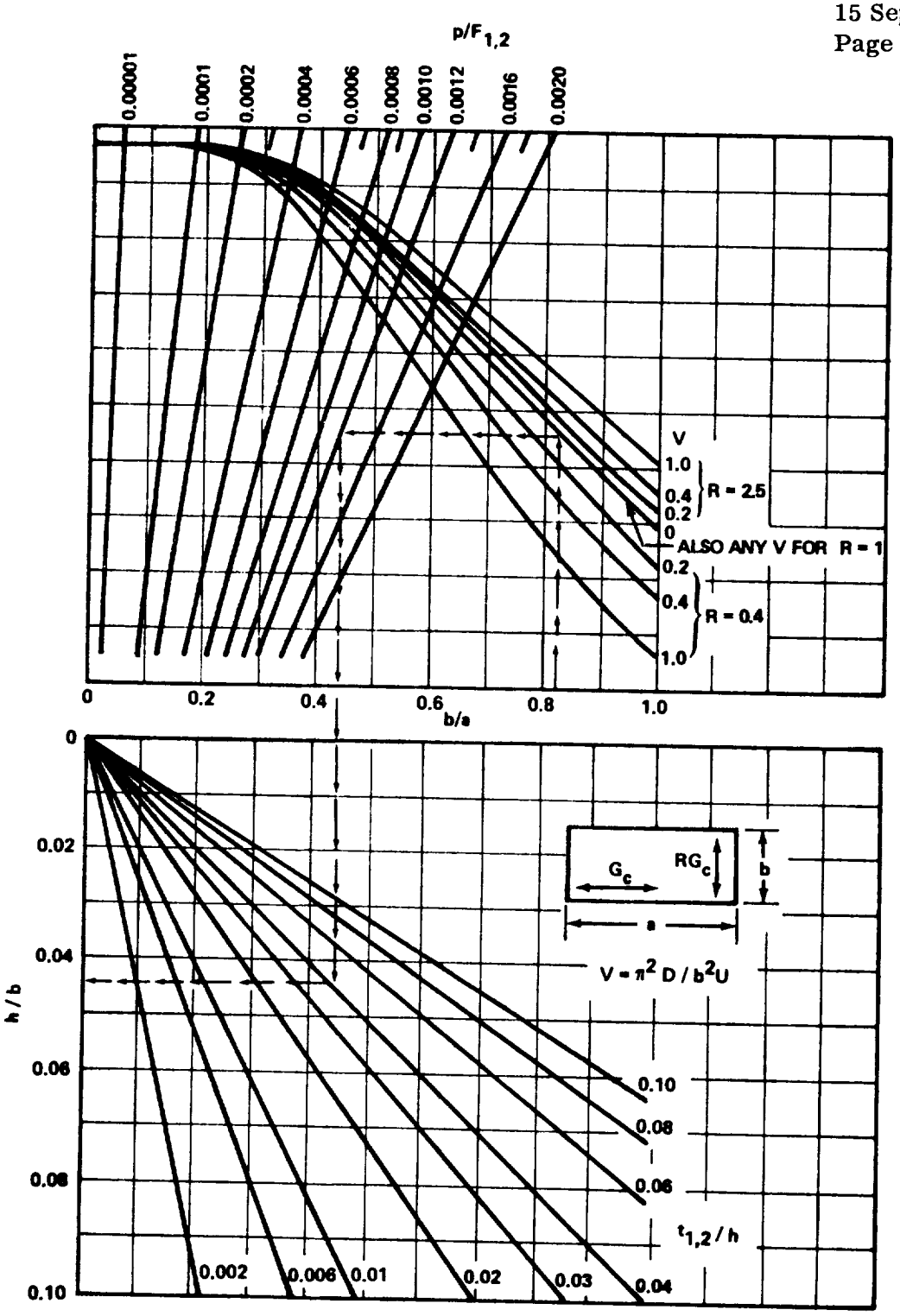

FIGURE B9-23. CHART FOR DETERMINING h/b RATIO FOR FLAT RECTANGULAR SANDWICH PANEL, WITH ISOTROPIC FACINGS, UNDER UNIFORMLY DISTRIBUTED NORMAL LOAD SO THAT FACING STRESS WILL BE $F_{1,2}$

Charts for solving formulas (62) and (63) are given in Figs. B9-24, B9-25, and B9-26. Use of the equations and charts beyond $\delta/h = 0.5$ is not recommended.

B9.6.1.3 Use of Design Charts

The sandwich must be designed by iterative procedures; these charts enable rapid determination of the various quantities sought. The charts were derived for a Poisson's ratio of the facings of 0.3 and can be used with small error for facings having other values of Poisson's ratio.

As a first approximation, it will be assumed that $V = 0$. If the design is controlled by facing stress criteria, as may be determined, this assumption will lead to an exact value of h if the core is isotropic, to a minimum value of h if the core is orthotropic with a greater core shear modulus across the panel width than across the length, and to too large a value of h if the core is orthotropic with a smaller core shear modulus across the panel width than across the length. If the design is controlled by deflection requirements, the assumption that $V = 0$ will produce a minimum value of h. The value of h is minimum because $V = 0$ if the core shear modulus is infinite. For any actual core, the shear modulus is not infinite; hence a thicker core must be used.

The following procedure is suggested:

1. Enter Fig. B9-23 with desired values for the parameters b/a and $p/F_{1,2}$, using the curve for $V = 0$. Assume a value for $t_{1,2}/h$ and determine

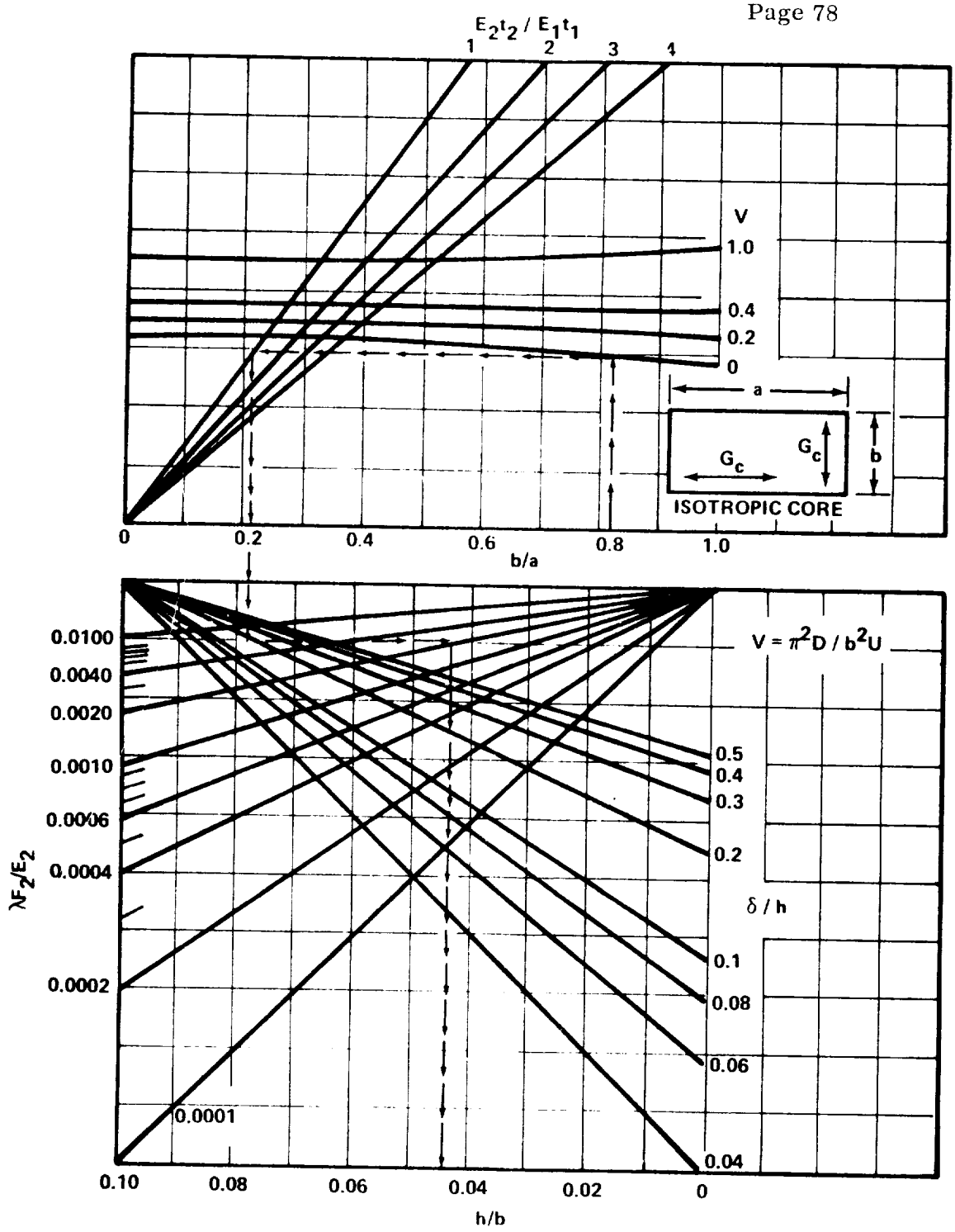

FIGURE B9-24. CHART FOR DETERMINING h/b RATIO FOR FLAT RECTANGULAR SANDWICH PANEL, WITH ISOTROPIC FACINGS AND ISOTROPIC CORE, UNDER UNIFORMLY DISTRIBUTED NORMAL LOAD PRODUCING DEFLECTION RATIO δ/h

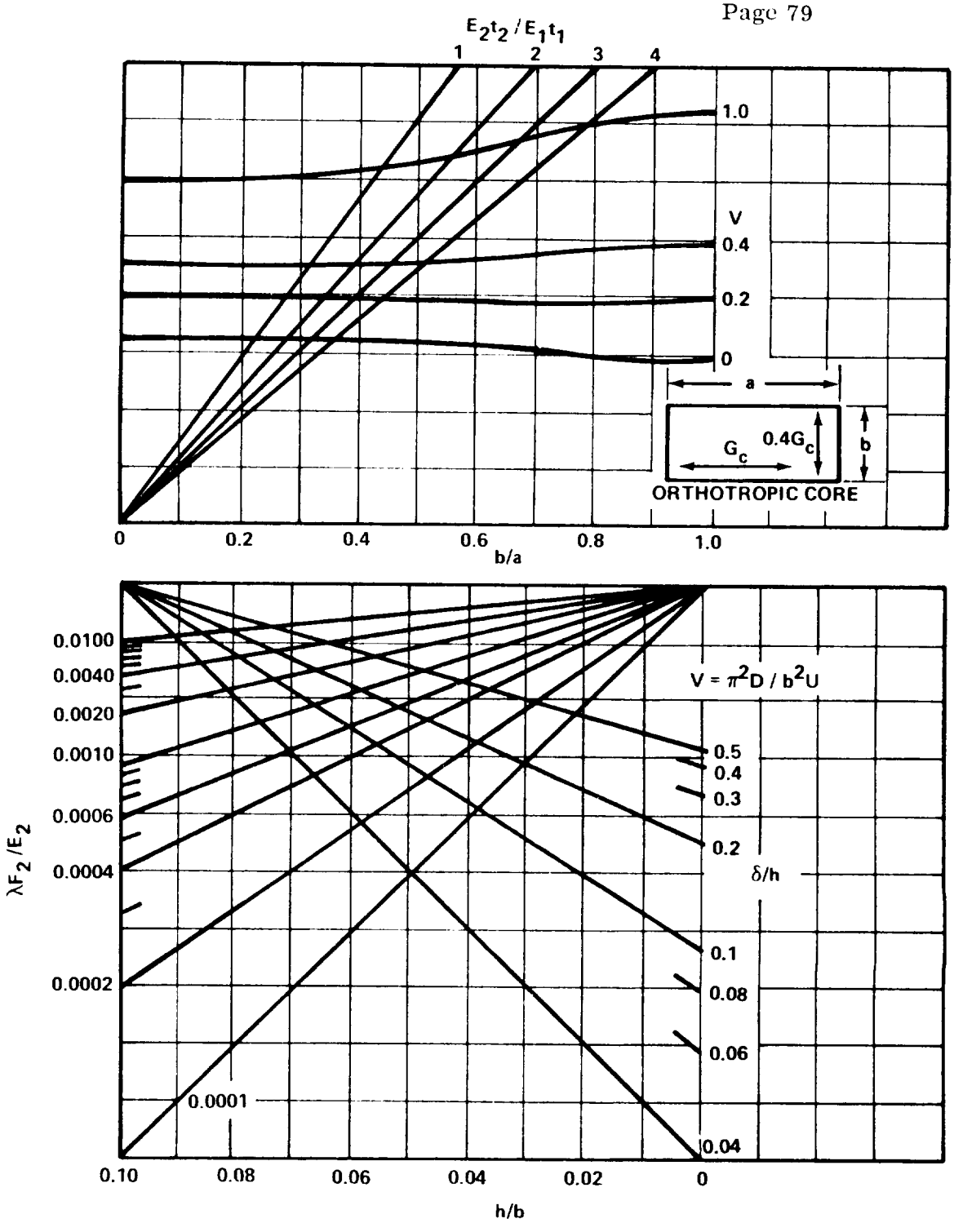

FIGURE B9-25. CHART FOR DETERMINING h/b RATIO FOR FLAT RECTANGULAR SANDWICH PANEL, WITH ISOTROPIC FACINGS AND ORTHOTROPIC (SEE SKETCH) CORE, UNDER UNIFORMLY DISTRIBUTED NORMAL LOAD PRODUCING DEFLECTION RATIO δ/h

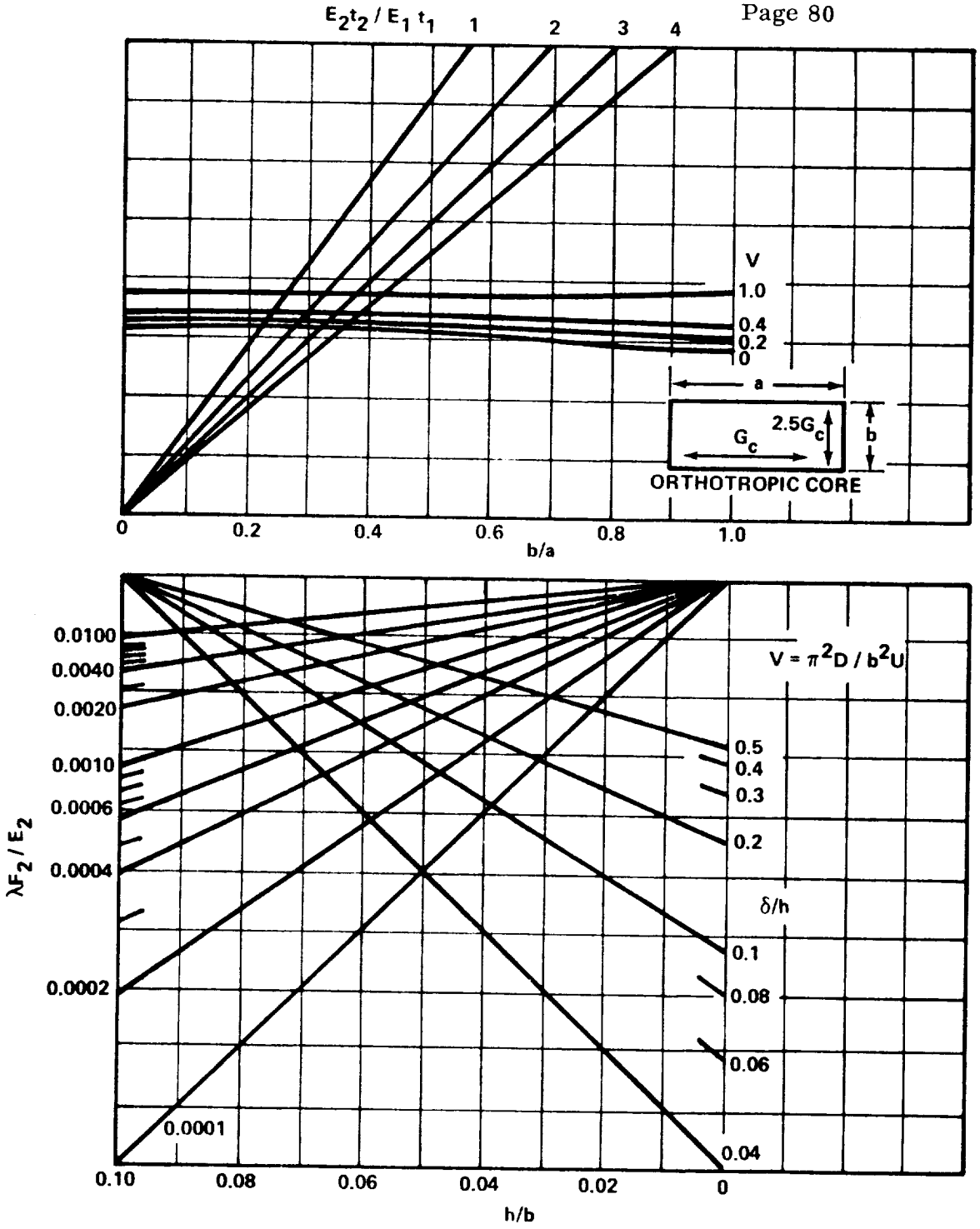

FIGURE B9-26. CHART FOR DETERMINING h/b RATIO FOR FLAT RECTANGULAR SANDWICH PANEL, WITH ISOTROPIC FACINGS AND ORTHOTROPIC (SEE SKETCH) CORE, UNDER UNIFORMLY DISTRIBUTED NORMAL LOAD PRODUCING DEFLECTION RATIO δ/h

h/b . Compute h and $t_{1,2}$. Modify ratio $t_{1,2}/h$ if necessary and determine more suitable values for h and $t_{1,2}$.

2. Enter Fig. B9-24 with desired values for the parameters b/a , E_2t_2/E_1t_1 , and $\lambda F_2/E_2$, using the curve for V = 0 . Assume a value of δ/h and determine h/b . Compute h and δ . Modify ratio δ/h if necessary and determine more suitable values for h and δ .

3. Repeat steps 1 and 2 using lower chosen design facing stresses until h determined by step 2 is equal to, or a bit less than, h determined by step 1.

4. Compute the core thickness, t_c , using the following formulas:

$$t_c = h - \frac{t_1 + t_2}{2} \qquad (64)$$

$$t_c = h - t \qquad \text{(for equal facings)} \quad . \qquad (65)$$

This first approximation was based on a core with an infinite shear modulus. Since actual core shear modulus values are not very large, a value of t_c somewhat larger must be used. Successive approximations can be made by entering Figs. B9-23 and B9-24, B9-25, or B9-26 with values of V as computed by equations (56) and (57). Figure B9-23 includes curves for sandwich with isotropic and certain orthotropic cores. Figure B9-24 applies to sandwich with isotropic core (R = 1) . Figure B9-25 applies to sandwich with orthotropic cores for which the shear modulus associated with the panel width is 0.4 of the shear modulus associated with the panel length (R = 0.4) . Figure B9-26 applies to sandwich with orthotropic cores for which the shear modulus associated with

the panel width is 2.5 times the shear modulus associated with the panel length ($R = 2.5$).

NOTE: For honeycomb cores with core ribbon parallel to panel length a, $G_c = G_{TL}$ and the shear modulus parallel to panel width b is G_{TW}. For honeycomb cores with core ribbons parallel to panel width b, $G_c = G_{TW}$ and the shear modulus parallel to panel length a is G_{TL}.

In using Figs. B9-23 through B9-26 for $V \neq 0$, it is necessary to iterate because V is directly proportional to the core thickness t_c. As an aid to finally determine t_c and G_c, Fig. B9-27 presents a number of lines representing V for various values of G_c with V ranging from 0.01 to 2 and G_c ranging from 1000 to 1 000 000 psi. The following procedure is suggested:

1. Determine a core thickness using a value of 0.01 for V.

2. Compute the constant relating V to G_c:

$$\left[\frac{\pi^2 t_c E_1 t_1 E_2 t_2}{\lambda b^2 (E_1 t_1 + E_2 t_2)}\right] \text{ or } \left(\frac{\pi^2 t_c E t}{2\lambda b^2}\right) \quad \text{(for equal facings)} = VG_c .$$

3. With this constant, enter Fig. B9-27 and determine necessary G_c.

4. If the shear modulus is outside the range of values for materials available, follow the appropriate line of Fig. B9-27 and pick a new value of V, for reasonable value of core shear modulus.

5. Reenter Figs. B9-23 through B9-26 with the new value of V and repeat all previous steps.

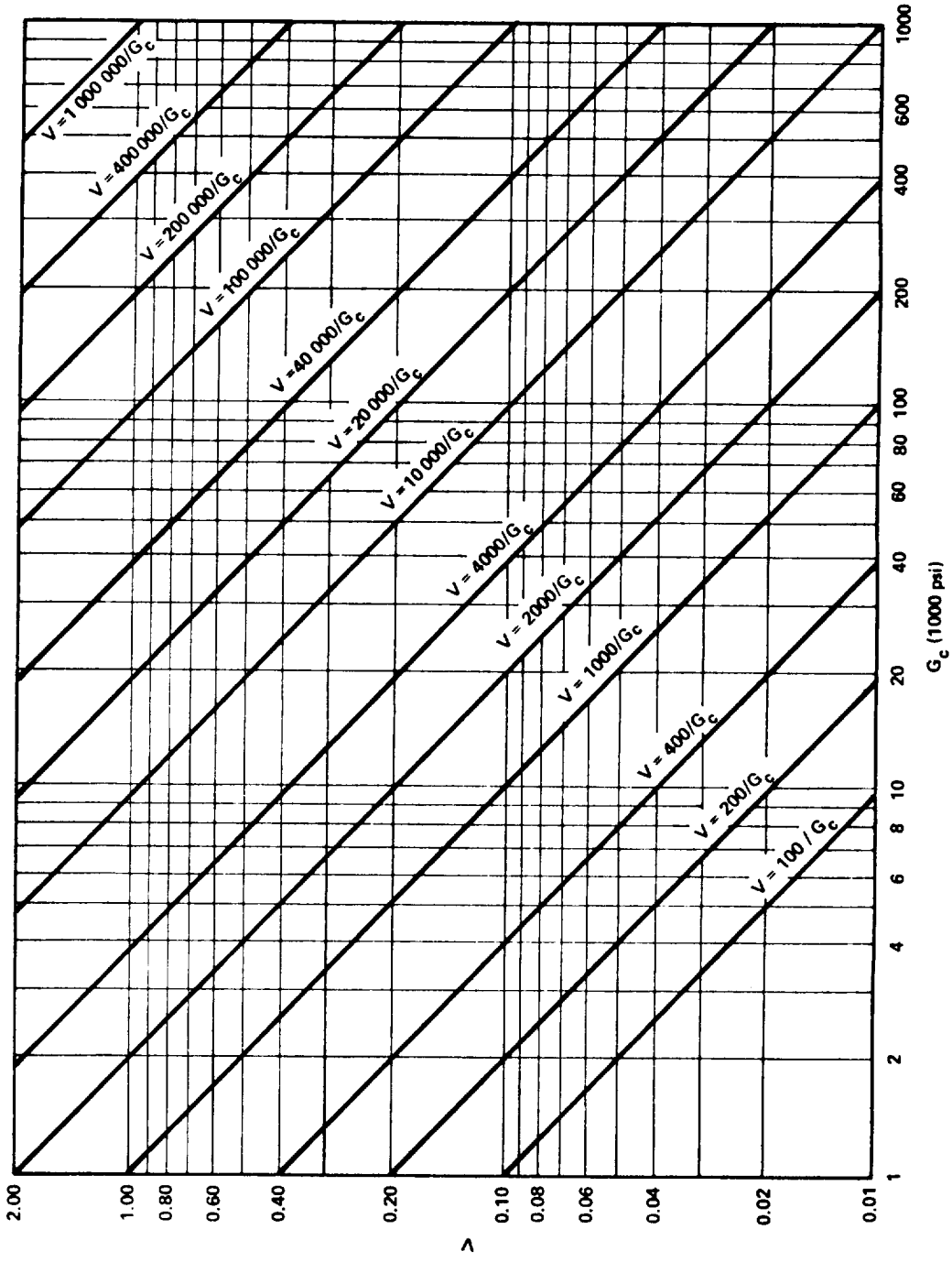

FIGURE B9-27. CHART FOR DETERMINING V AND G_c FOR SANDWICH PANELS UNDER UNIFORMLY DISTRIBUTED NORMAL LOAD

B9.6.1.4 Determining Core Shear Stress

This section gives the procedure for determining the maximum core shear stress of a flat rectangular sandwich panel under uniformly distributed normal load. The core shear stress is maximum at the panel edges, at mid-length of each edge. The maximum shear stress, F_{cs}, is given by the formula:

$$F_{cs} = K_3 p \frac{b}{h} \quad , \tag{66}$$

where K_3 is a theoretical coefficient dependent upon panel aspect ratio and the parameter V. If the core is isotropic, values of V do not affect the core shear stress.

The chart of Fig. B9-28 presents a graphical solution of formula (66). The chart should be entered with values of thicknesses and other parameters previously determined.

B9.6.1.5 Checking Procedure

The design shall be checked by using the graphs of Figs. B9-29, B9-30, and B9-31 to determine theoretical coefficients K_2, K_1, and K_3 to compute facing stresses, deflection, and core shear stresses.

B9.6.1.6 Determining Facing Thickness, Core Thickness, and Core Shear Modulus for Simply Supported Flat Circular Panels

This section gives procedures for determining sandwich facing and core thicknesses and core shear modulus so that chosen design facing stresses and allowable panel deflections will not be exceeded. The facing stresses, produced

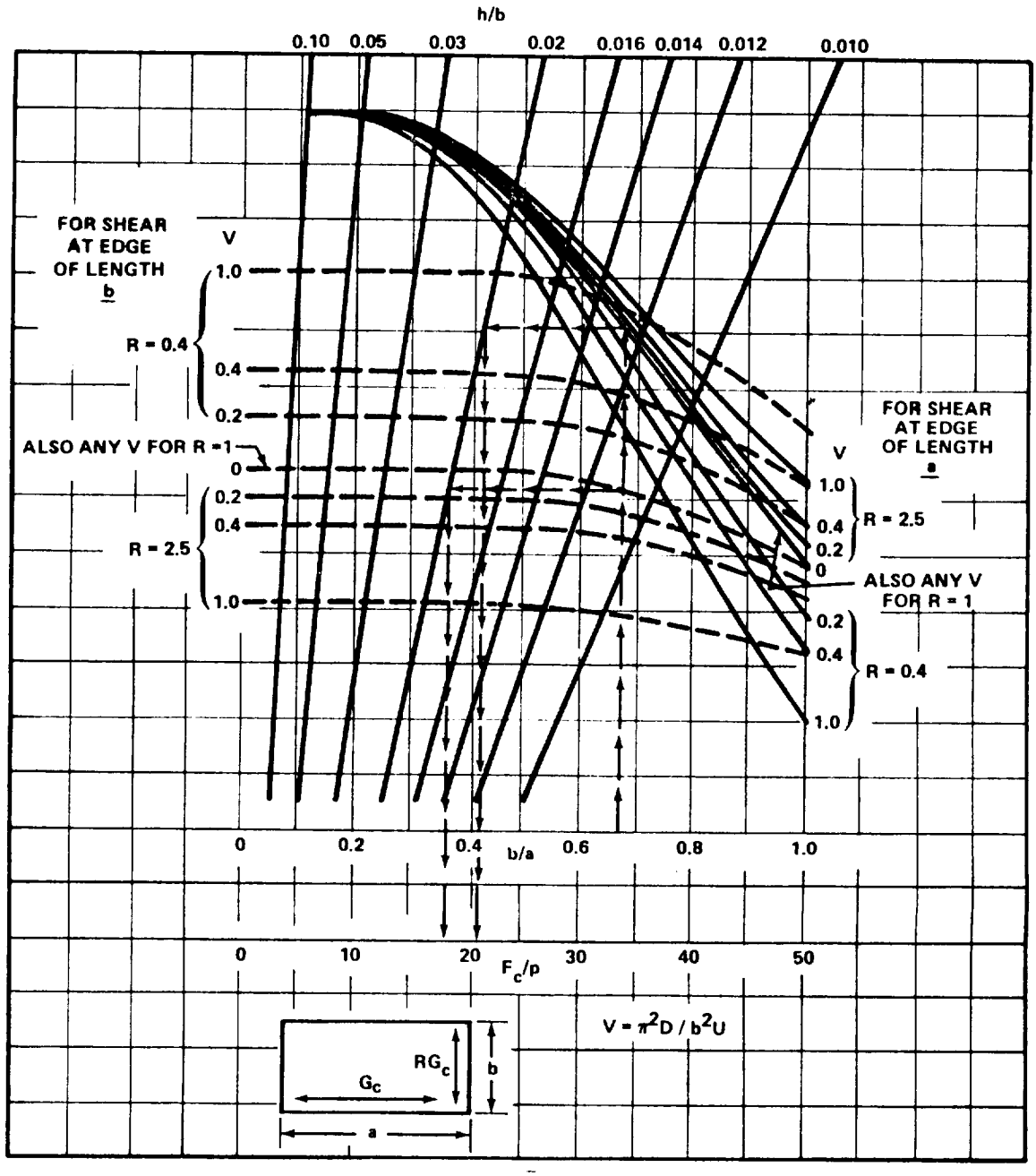

FIGURE B9-28. CHART FOR DETERMINING CORE SHEAR STRESS RATIO $\frac{F_{sc}}{p}$ FOR FLAT RECTANGULAR SANDWICH PANEL, WITH ISOTROPIC FACINGS, UNDER UNIFORMLY DISTRIBUTED NORMAL LOAD

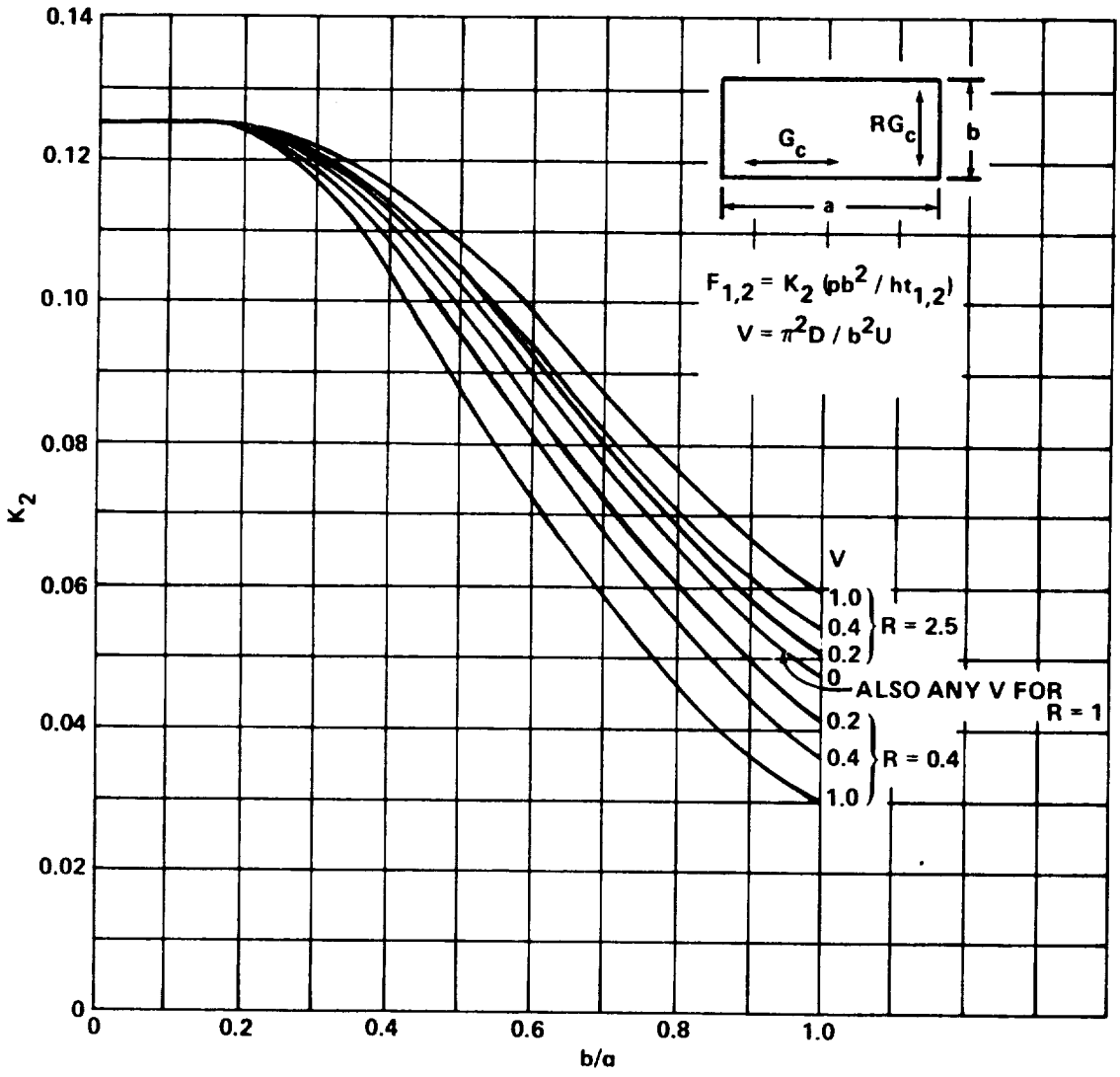

FIGURE B9-29. K_2 FOR DETERMINING FACING STRESS, F, OF FLAT RECTANGULAR SANDWICH PANELS WITH ISOTROPIC FACINGS AND ISOTROPIC OR ORTHOTROPIC CORE (SEE SKETCH) UNDER UNIFORMLY DISTRIBUTED NORMAL LOAD

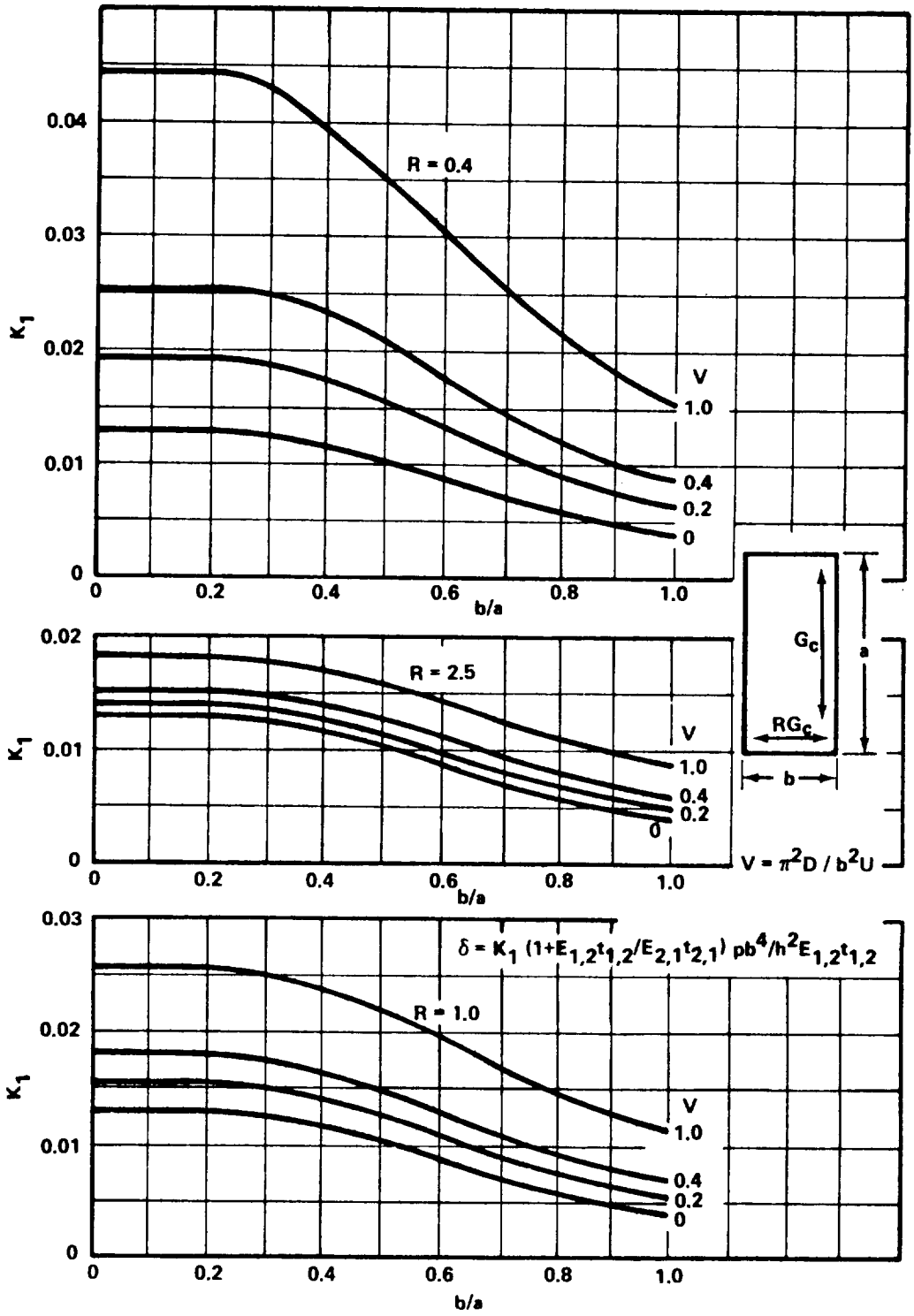

FIGURE B9-30. K_1 FOR DETERMINING MAXIMUM DEFLECTION, δ, OF FLAT RECTANGULAR SANDWICH PANELS WITH ISOTROPIC FACINGS AND ISOTROPIC OR ORTHOTROPIC CORE (SEE SKETCH) UNDER UNIFORMLY DISTRIBUTED NORMAL LOAD

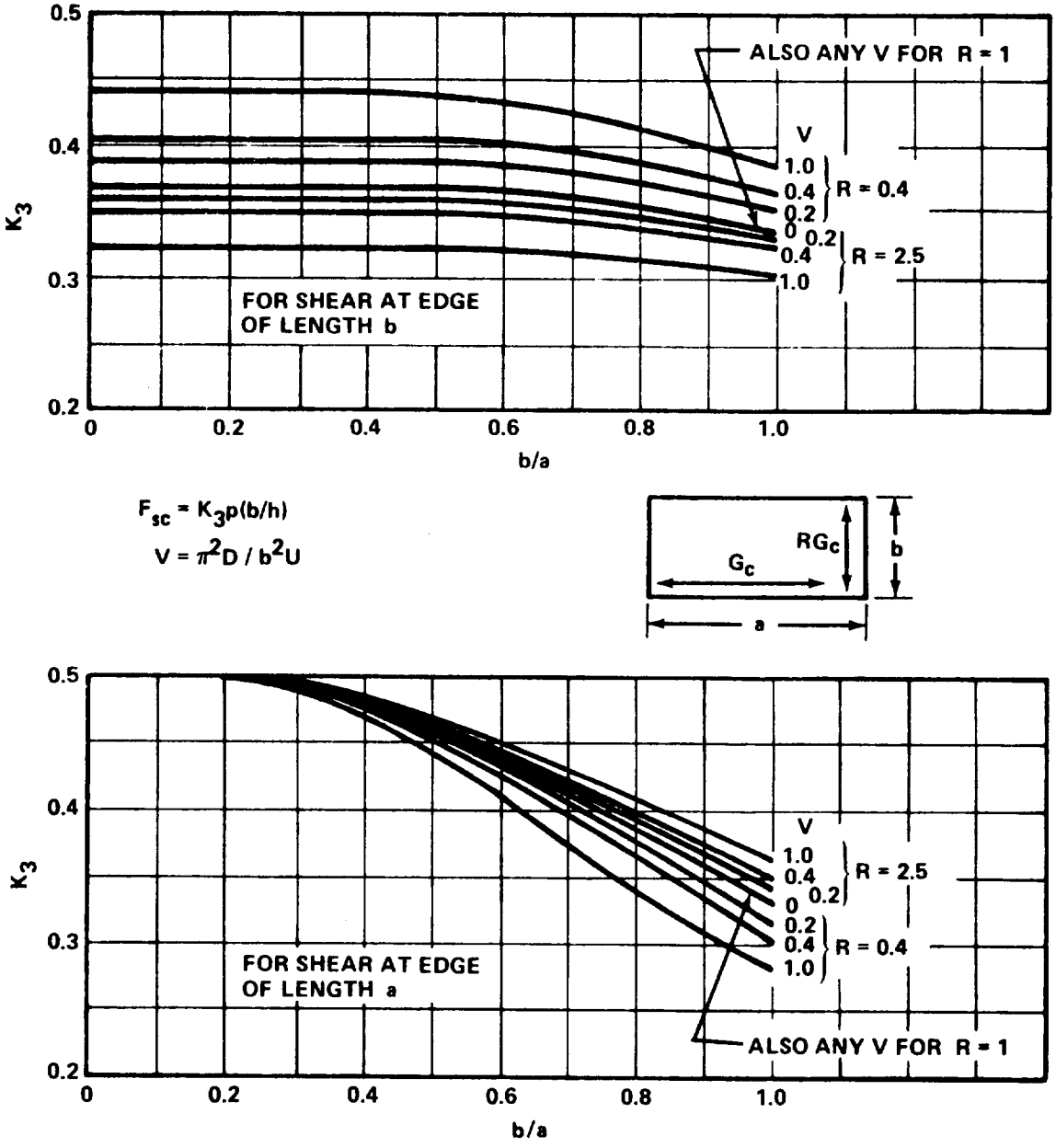

FIGURE B9-31. K_3 FOR DETERMINING MAXIMUM CORE SHEAR STRESS, F_{sc}, FOR FLAT RECTANGULAR SANDWICH PANELS WITH ISOTROPIC FACINGS AND ISOTROPIC OR ORTHOTROPIC CORE (SEE SKETCH) UNDER UNIFORMLY DISTRIBUTED NORMAL LOAD

by bending moment, are maximum at the center of a simply supported circular panel under uniformly distributed normal load. If restraint exists at panel edges, a redistribution of stresses may cause higher stresses near panel edges. The procedures given apply only to panels with simply supported edges, isotropic facings, and isotropic cores. A solution is presented in the form of charts with which, by iterative process, the facing and core thicknesses and core shear modulus can be determined.

The average facing stress, F (stress at facing centroid), is given by the theoretical formula:

$$F_{1,2} = \frac{3+\mu}{16} \frac{pr^2}{t_{1,2}h} \tag{67}$$

$$F = \frac{3+\mu}{16} \frac{pr^2}{th} \quad \text{(for equal facings)} \quad , \tag{68}$$

where μ is Poisson's ratio of facings [in formula (67), it is assumed that $\mu = \mu_1 = \mu_2$]; r is the radius of the circular panel; and other quantities are as previously defined (see Section B9.6.1.2).

Solving equations (67) and (68) for $\frac{h}{r}$ gives

$$\frac{h}{r} = \frac{\sqrt{3+\mu}\sqrt{\frac{p}{F_{1,2}}}}{4\sqrt{\frac{t_{1,2}}{h}}} \tag{69}$$

$$\frac{h}{r} = \frac{\sqrt{3+\mu}\sqrt{\frac{p}{F}}}{4\sqrt{\frac{t}{h}}} \quad \text{(for equal facings)} \quad . \tag{70}$$

A chart for solving formulas (69) and (70) graphically is given in Fig. B9-32. The formulas and chart include the ratio t/h, which is usually unknown, but by iteration satisfactory ratios of t/h and h/r can be found.

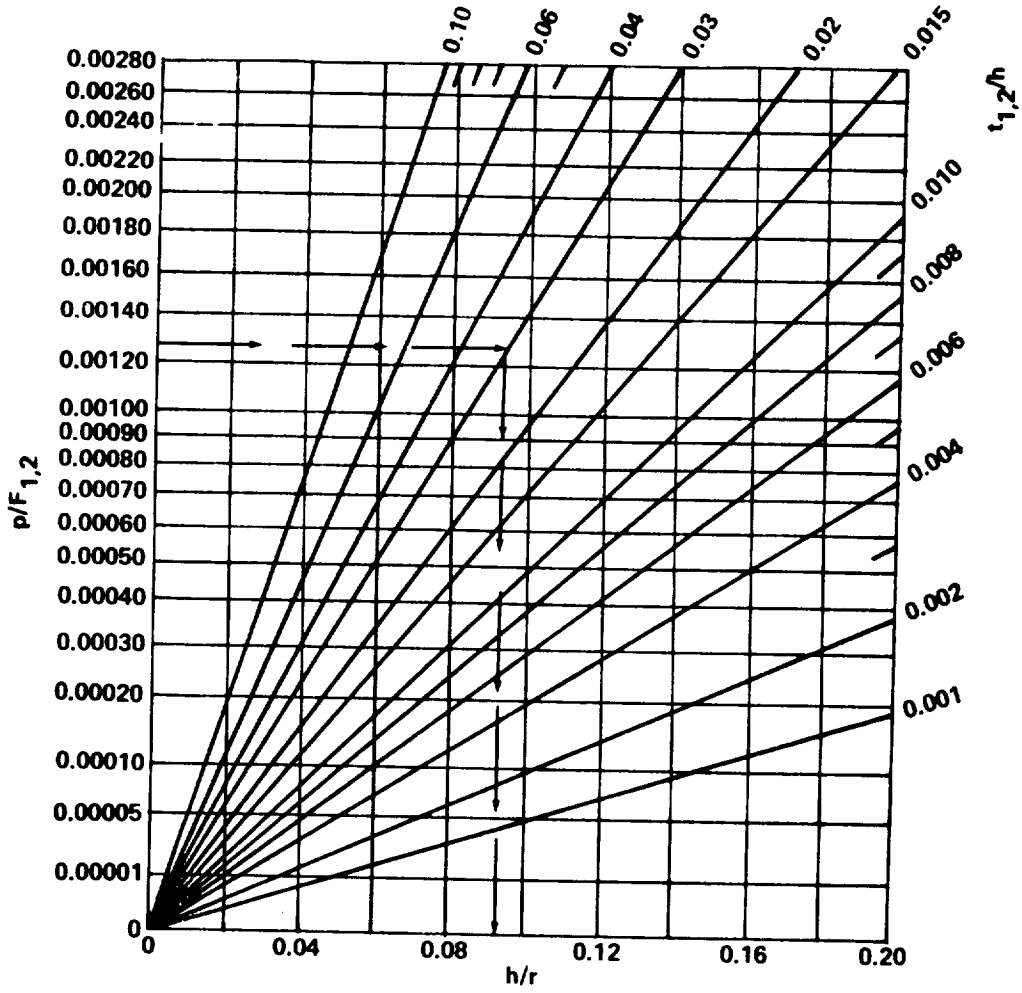

FIGURE B9-32. CHART FOR DETERMINING h/r RATIO FOR FLAT CIRCULAR SANDWICH PANEL, WITH ISOTROPIC FACINGS AND CORE, UNDER UNIFORMLY DISTRIBUTED NORMAL LOAD SO THAT FACING STRESS WILL BE $F_{1,2}$; $\mu = 0.3$

The deflection, δ, of the panel center is given by the theoretical formula:

$$\delta = K_4\left(1 + \frac{E_{1,2}t_{1,2}}{E_{2,1}t_{2,1}}\right)\frac{\lambda F_{1,2}r^2}{E_{1,2}h} \qquad (71)$$

$$\delta = 2K_4\frac{\lambda F}{E}\frac{r^2}{h} \quad \text{(for equal facings)} \quad , \qquad (72)$$

where K_4 depends on the sandwich bending and shear rigidities as incorporated in the parameter $V = \frac{\pi^2 D}{(2r)^2 U}$ which can be written as

$$V = \frac{\pi^2 t_c E_1 t_1 E_2 t_2}{4\lambda r^2 G_c (E_1 t_1 + E_2 t_2)} \qquad (73)$$

$$V = \frac{\pi^2 t_c E t}{8\lambda r^2 G_c} \quad \text{(for equal facings)} \quad , \qquad (74)$$

where r is panel radius and all other terms are as previously defined in Section B9.6.1.2

Solving equations (71) and (72) for $\frac{h}{r}$, gives

$$\frac{h}{r} = \frac{\sqrt{K_4}\sqrt{\frac{\lambda F_{1,2}}{E_{1,2}}}\sqrt{1 + \frac{E_{1,2}t_{1,2}}{E_{2,1}t_{2,1}}}}{\sqrt{\frac{\delta}{h}}} \qquad (75)$$

$$\frac{h}{r} = \frac{\sqrt{2K_4}\sqrt{\frac{\lambda F}{E}}}{\sqrt{\frac{\delta}{h}}} \quad \text{(for equal facings)} \quad . \qquad (76)$$

A chart for solving formulas (75) and (76) is given in Fig. B9-33. Use of the equations and charts beyond $\delta/h = 0.5$ is not recommended.

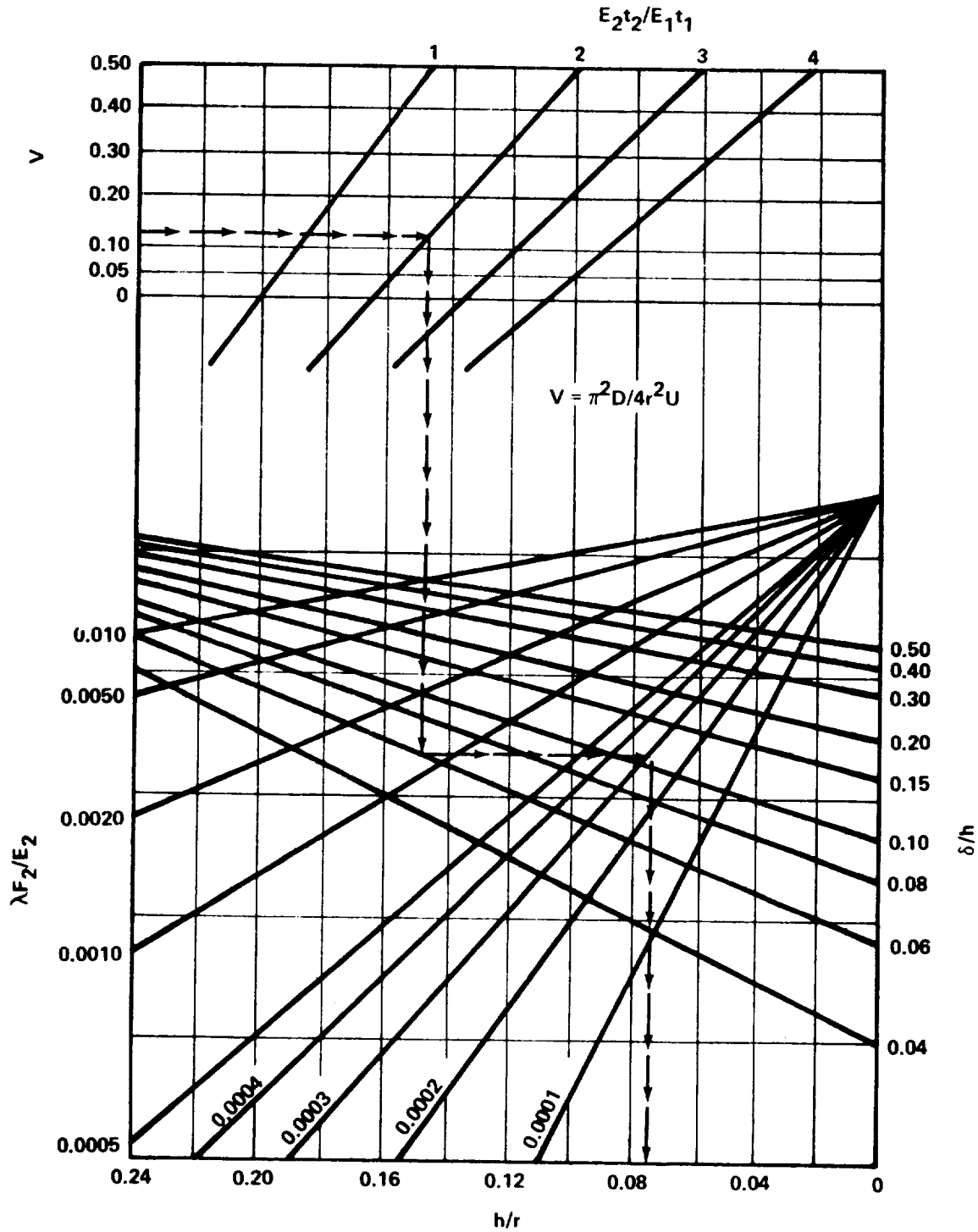

FIGURE B9-33. CHART FOR DETERMINING h/r RATIO FOR FLAT CIRCULAR SANDWICH, WITH ISOTROPIC FACINGS AND CORE, UNDER UNIFORMLY DISTRIBUTED NORMAL LOAD PRODUCING CENTER DEFLECTION RATIO δ/h

B9.6.1.7 Use of Design Charts

The sandwich must be designed by iterative procedures and the charts enable rapid determination of the various quantities sought. The charts were derived for Poisson's ratio of the facings of 0.3 and can be used with small error for facings having other values of Poisson's ratio.

As a first approximation, it will be assumed that $V = 0$. If the design is controlled by facing stress criteria, as may be determined, this assumption will lead to an exact value of h. If the design is controlled by deflection requirements, the assumption that $V = 0$ will produce a minimum value of h. The value of h is minimum because $V = 0$ if the core shear modulus is infinite. For any actual core, the shear modulus is not infinite; hence a thicker core must be used.

The following procedure is suggested:

1. Enter Fig. B9-28 with the desired value for the parameter $\frac{p}{F_{1,2}}$. Assume a value for $\frac{t_{1,2}}{h}$ and determine h/r. Compute h and $t_{1,2}$. Modify ratio $\frac{t_{1,2}}{h}$ if necessary and determine more suitable values for h and $t_{1,2}$.
2. Enter Fig. B9-33 with desired values of the parameters $\frac{E_2 t_2}{E_1 t_1}$ and $\frac{\lambda F_2}{E_2}$ and assume $V = 0$. Assume a value for δ/h and determine h/r. Compute h and δ. Modify ratio δ/h if necessary and determine more suitable values for h and δ.

3. Repeat steps 1 and 2, using lower chosen design facing stresses, until h determined by step 2 is equal to, or a bit less than, h determined by step 1.

4. Compute the core thickness t_c, using the following formulas:

$$t_c = h - \frac{t_1 + t_2}{2}$$

$$t_c = h - t \quad \text{(for equal facings)} \quad .$$

This first approximation was based on a core with an infinite shear modulus. Since actual core shear modulus values are not very large, a value of t_c somewhat larger must be used. Successive approximations can be made by entering Fig. B9-33 with values of V as computed by equations (73) and (74).

In using Fig. B9-33 for $V \neq 0$ it is necessary to iterate because V is directly proportional to the core thickness t_c. As an aid to finally determine t_c and G_c, Fig. B9-27 can again be used. The constant relating V to G_c may be computed from the formula

$$VG_c = \left[\frac{\pi^2 t_c E_1 t_1 E_2 t_2}{4\lambda r^2 (E_1 t_1 + E_2 t_2)} \right] \text{ or } \left(\frac{\pi^2 t_c E t}{8\lambda r^2} \right) \quad \text{(for equal facings)} \quad .$$

With this constant, Fig. B9-27 may be entered. Use of the figure is as described in Section B9.6.1.3.

B9.6.1.8 Determining Core Shear Stress

This section gives the procedure for determining the maximum core shear stress of a flat circular sandwich panel under uniformly distributed

normal load. The core shear stress is maximum at the panel edge. The maximum shear stress, F_{cs}, is given by the formula

$$F_{cs} = \frac{pr}{2h} \quad . \tag{77}$$

B9.6.1.9 Checking Procedure

The design shall be checked by computing the facing stresses using equation (67) and the deflection using equation (71). The value of K_4 to be used in equation (71) is given by

$$K_4 = \frac{16}{\pi^2(3 + \mu)} \left[\frac{(5 + \mu)\pi^2}{64(1 + \mu)} + V \right] \quad , \tag{78}$$

which reduces $K_4 = 0.309 + 0.491V$ when $\mu = 0.3$. Values of V may be computed using equation (73).

An alternate method for computing the deflection at the panel center is given by the formula

$$\delta = K_5 \left(1 + \frac{E_{1,2}t_{1,2}}{E_{2,1}t_{2,1}} \right) \frac{\lambda pr^4}{\pi^2 E_{1,2}t_{1,2}h^2} \tag{79}$$

$$\delta = 2K_5 \frac{\lambda pr^4}{\pi^2 Eth^2} \tag{80}$$

where

$$K_5 = \frac{(5 + \mu)\pi^2}{64(1 + \mu)} + V$$

which reduces to $K_5 = 0.629 + V$ when $\mu = 0.3$.

The core selected for the panel should be checked to be sure that it has a core shear modulus value, G_c, at least as high as that assumed in computing

the deflection in equation (71) and that the core shear strength is sufficient to withstand the maximum core shear stress calculated from equation (77).

B9.6.2 Large Deflection Theory

Most of the literature classifies large deflection theory as having a deflection-to-plate thickness ratio greater than 0.50. In Figs. B9-34, B9-35, B9-36, and B9-37, a small difference is noted between the linear and nonlinear theory for deflection-to-plate ratios less than 0.50.

B9.6.2.1 Rectangular Sandwich Plate with Fixed Edge Conditions

The curves of Fig. B9-34 were obtained from Reference 8 with the following corresponding nomenclature for a rectangular sandwich plate with fixed edge conditions (shear deformations are not included):

w_o	Center deflection of plate
h	Thickness of the core layer
a, b	Half length of panel in x and y directions
λ	a/b
E	Elastic constant of the face layers
ν	Poisson's ratio of the core layer
p	External load per unit area
t	Thickness of the face layer
Q	$12a^3(1 - \nu^2)\, p/th^2E$

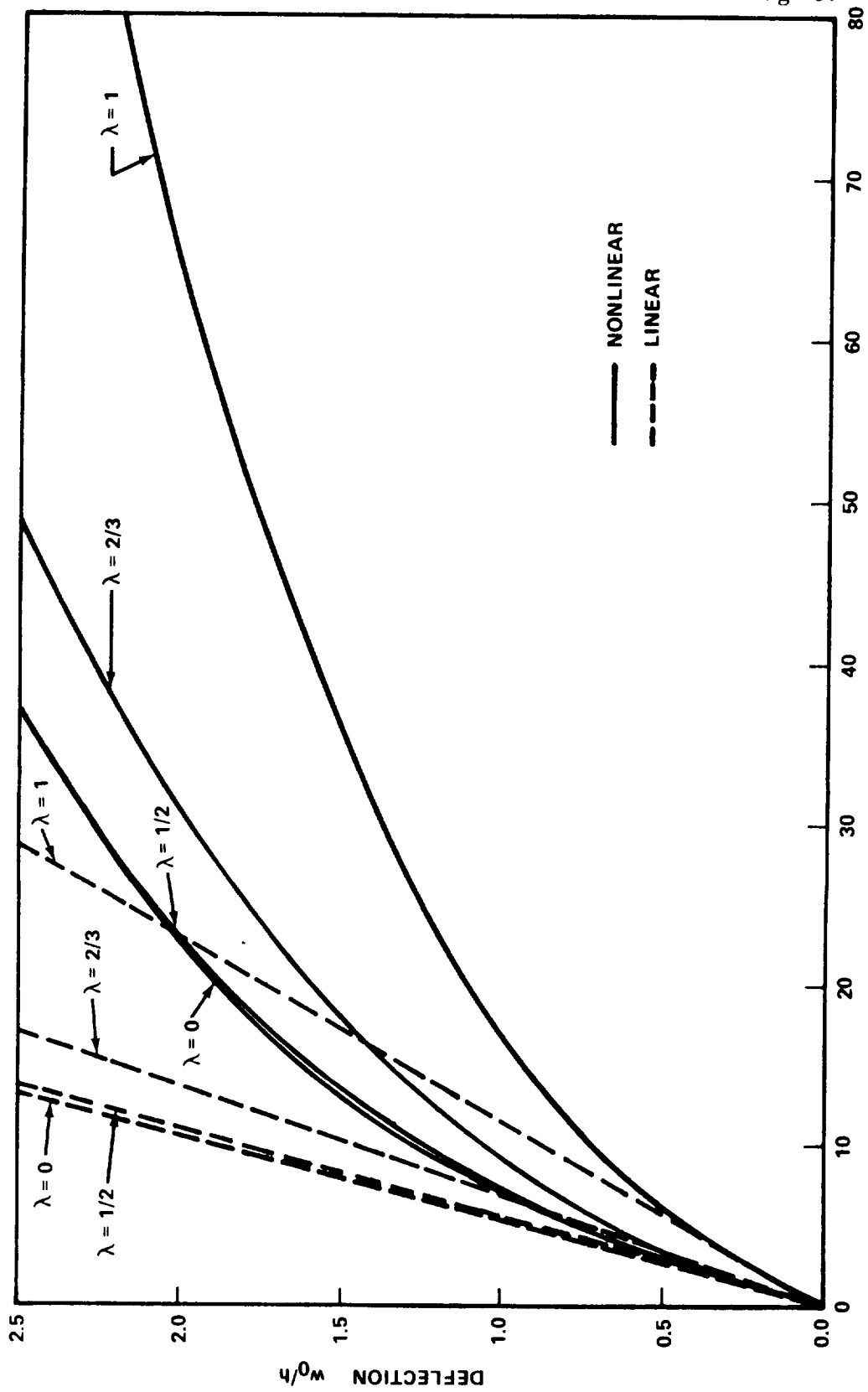

FIGURE B9-34. DEFLECTION OF RECTANGULAR SANDWICH PLATES WITH THE EDGES CLAMPED

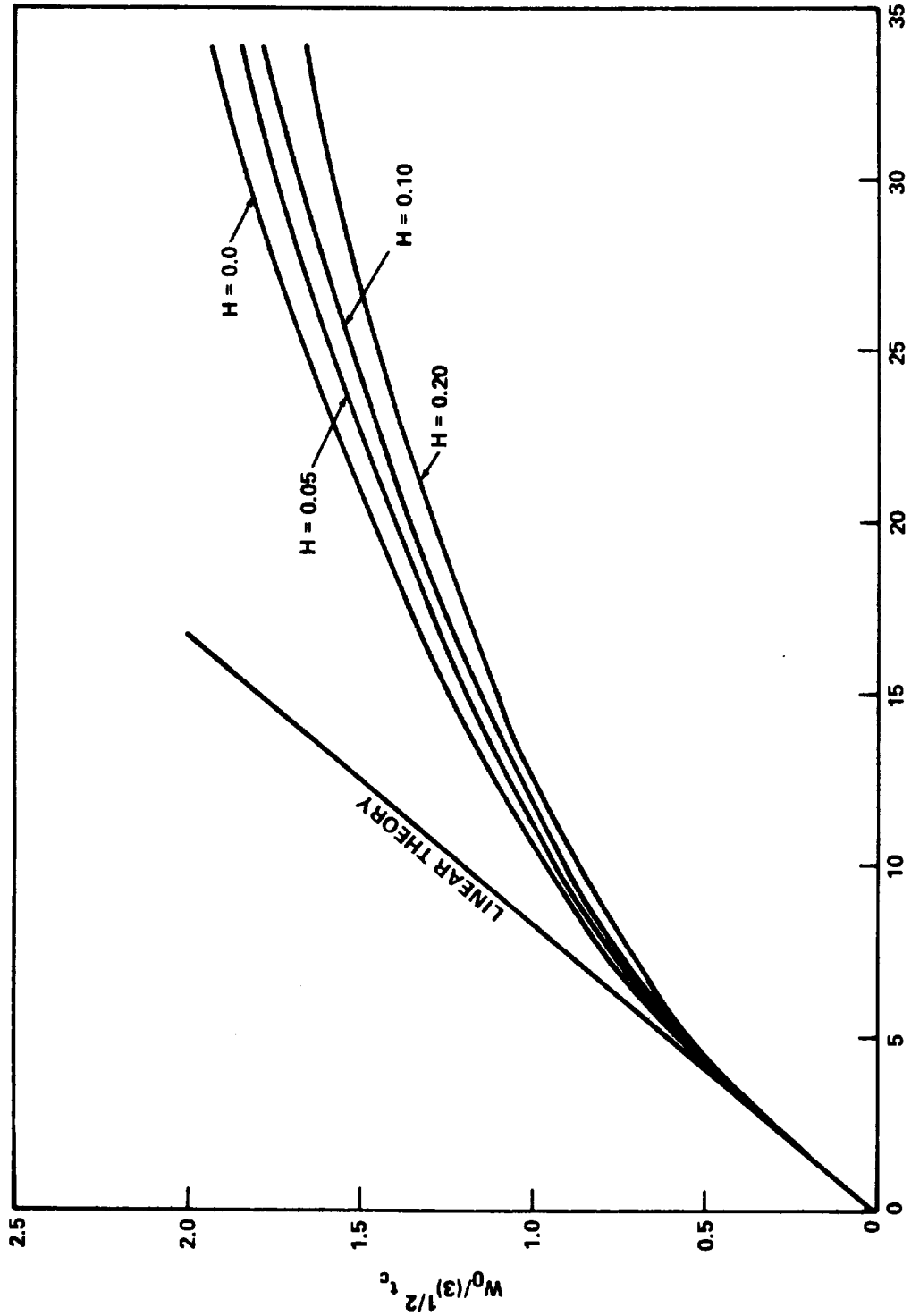

FIGURE B9-35. CENTER DEFLECTION w_o VERSUS APPLIED EDGE MOMENT M_0 FOR $\nu_f = 0.25$

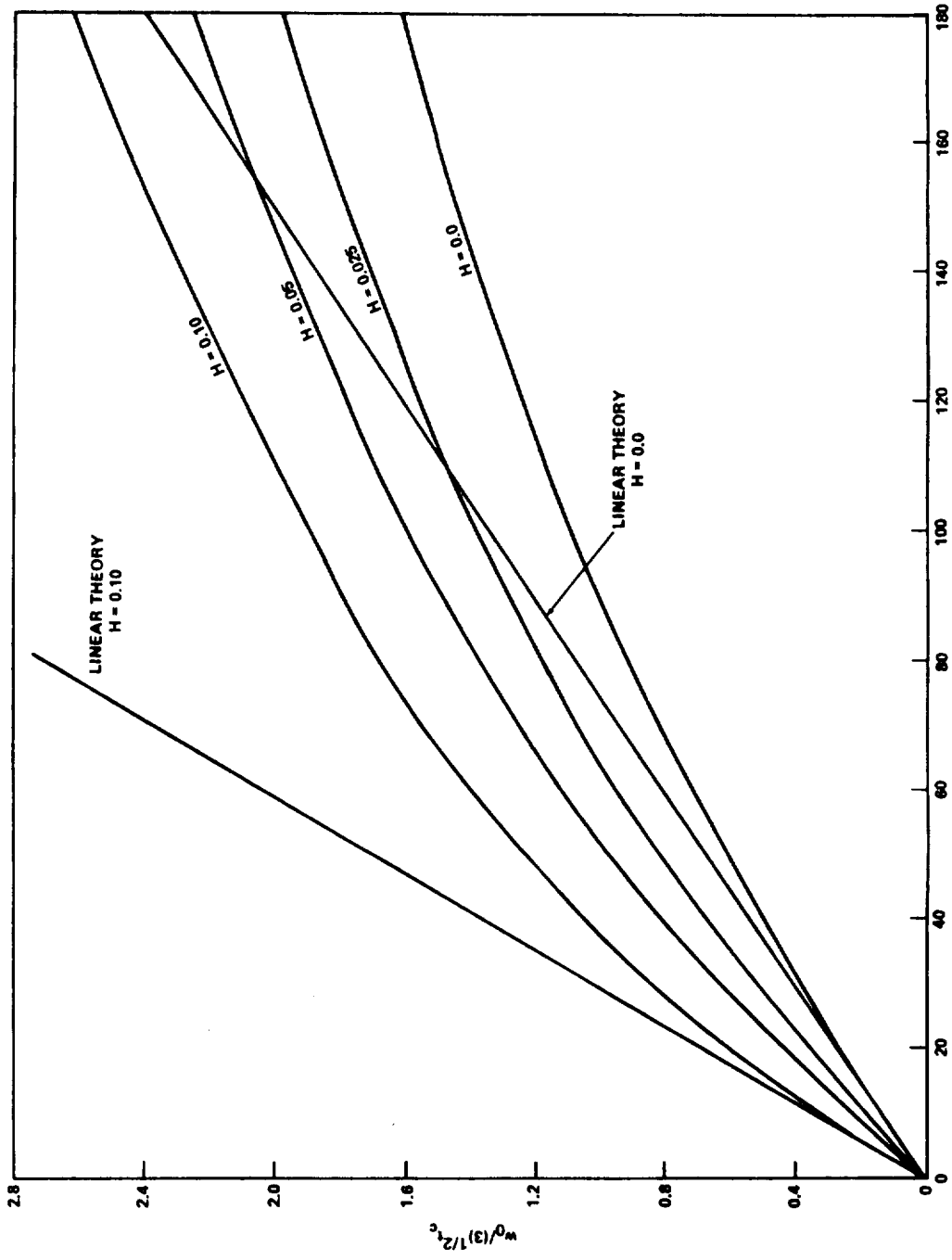

FIGURE B9-36. CENTER DEFLECTION w_o VERSUS APPLIED LOAD q FOR A CIRCULAR PLATE WITH CLAMPED, MOVABLE EDGE

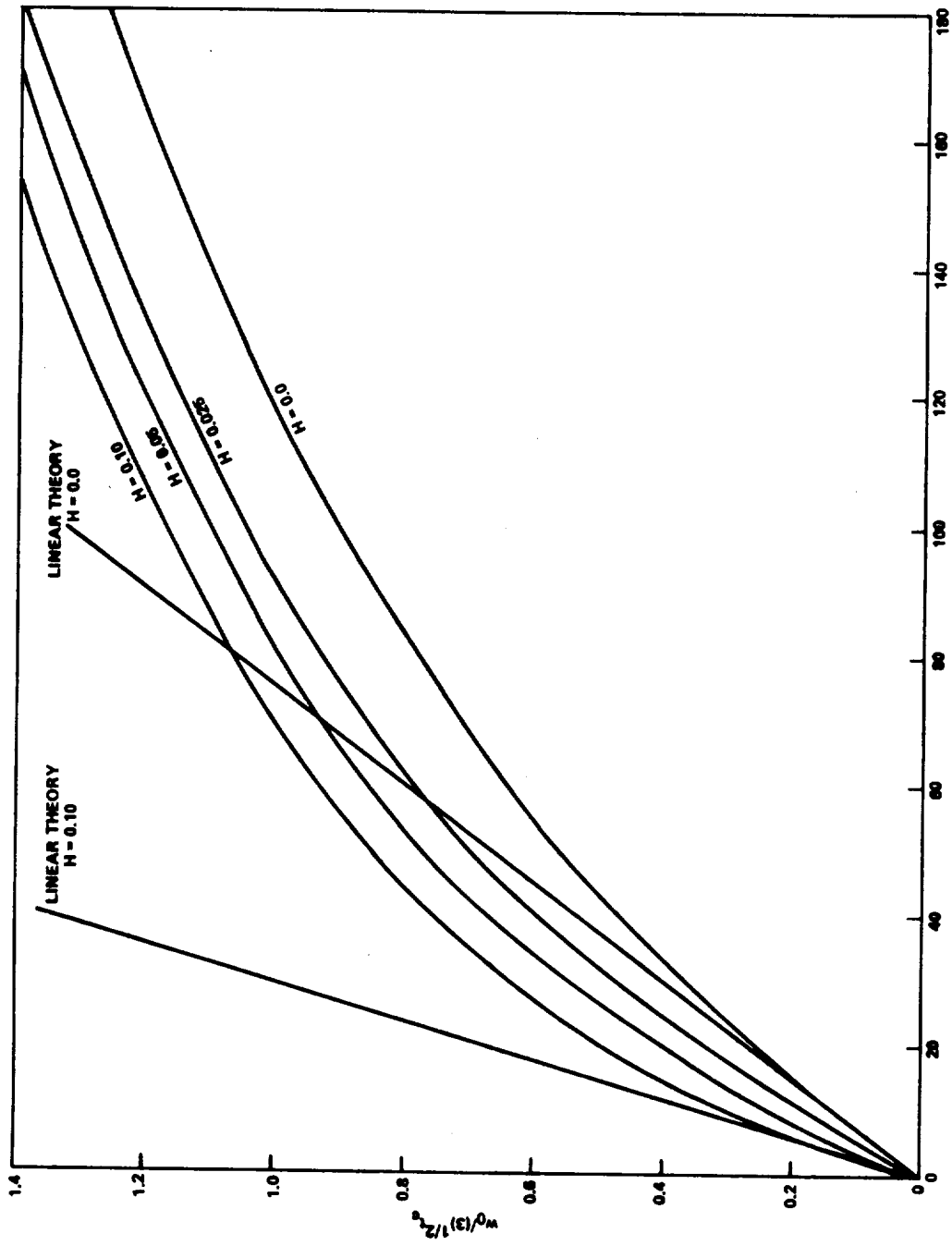

FIGURE B9-37. CENTER DEFLECTION w_o VERSUS APPLIED LOAD q FOR A CIRCULAR PLATE WITH CLAMPED IMMOVABLE EDGE ($\nu_f = 0.25$)

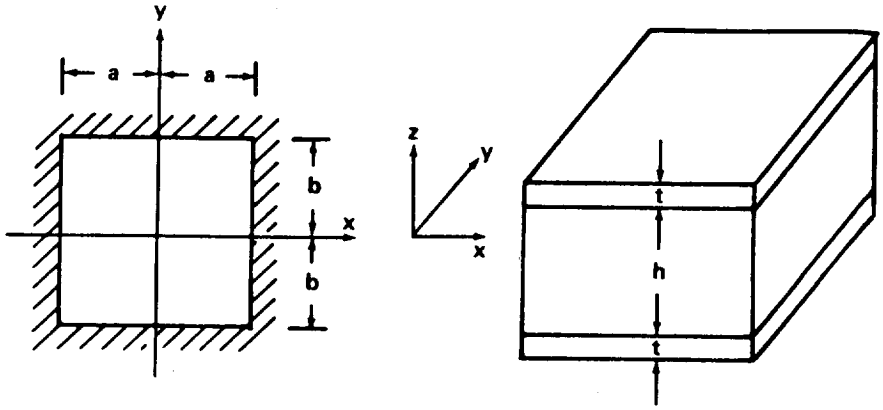

B9.6.2.2 Circular Sandwich Plate with Simply Supported Movable, Clamped Movable, and Clamped Immovable Boundary Conditions

The curves of Figs. B9-35, B9-36, and B9-37 were obtained from Reference 9 for a circular sandwich plate for the following states of loading and boundary conditions:

1. Moments uniformly distributed around a simply supported, radially movable boundary,
2. Uniformly loaded plate with a clamped, radially movable boundary, and
3. Uniformly loaded plate with a clamped, radially immovable boundary.

The equations are nondimensionalized for each state of loading. The effect of shear deformation is characterized by the nondimensional parameter H. If H = 0, then shear deformation is neglected; a nonzero value of H signifies shear distortion in the core. Nomenclature of the symbols is as follows:

w_o Normal deflection at the plate center

t_c Thickness of the core

H Measure of effect of core shear deformation = $\frac{D}{BR^2}$

M_o Applied edge moment

R Radius of a circular plate

C In-plane rigidity = $2E_f t_{f_2}$

D Bending rigidity = $E_f t_f t_c / 2(1 - \nu_f^2)$

q Applied, transverse load

ν_f Poisson's ratio of face sheet

B Transverse shear rigidity = $G_c t_c$

G_c Shear modulus of the core

E_f Modulus of elasticity of the face sheet

t_f Thickness of the face sheet

REFERENCES

1. Timoshenko, S. and Woinowsky-Krieger, S.: Theory of Plates and Shells. McGraw-Hill, New York, 1959.

2. Den Hartog, J. P.: Advanced Strength of Materials. McGraw-Hill, New York, 1952.

3. Bruhn, E. F.: Analysis and Design of Flight Vehicle Structures. Tri-State Offset Company, Cincinnati, Ohio, 1965.

4. Heuhert, M. and Sommer, A.: Rectangular Shell Plating Under Uniformly Distributed Hydrostatic Pressure. NACA TM 965.

5. Iyengar, K. T. and Srinivasan, R. S.: Clamped Skew Plate Under Uniform Normal Loading. Journal of the Royal Aeronautical Society, February 1967.

6. Dow, N. F. and Hubka, R. F.: Formulas for the Elastic Constants of Plates with Integral Waffle-Like Stiffening. NACA Report 1195, 1954.

7. MIL-HDBK-23, Structural Sandwich Composites. Department of Defense, Washington, D. C., July 1968.

8. Kan, Han-Pin and Huang, Ju-Chin: Large Deflection of Rectangular Sandwich Plates. Tennessee Technological University, Cookeville, Tennessee, February 1967.

9. Smith, C. V.: Large Deflections of Circular Sandwich Plates. Georgia Institute of Technology, Atlanta, Georgia, October 1967.

BIBLIOGRAPHY

Roark, R. J.: Formulas for Stress and Strain. McGraw-Hill, New York, Third Edition, 1954.

SECTION B10

HOLES & CUTOUTS IN PLATES

B10 HOLES AND CUTOUTS IN PLATES

The magnitude of stress concentrations around holes in plates used as components of structures has long been an important design consideration. The localized stress around a hole is usually obtained by multiplying the nominal stress by a factor called a stress concentration factor. For example, the localized stress or stress concentration σ_{max} at the edge of a relatively small hole, at the center of a wide plate that resists an axial tensile load P is

$$\sigma_{max} = K \frac{P}{A} = K\sigma_o \quad , \tag{1}$$

or

$$K = \frac{\sigma_{max}}{\sigma_o} \quad , \tag{2}$$

in which K is the stress concentration factor and $\sigma_o = \frac{P}{A}$ is the (nominal) stress that would occur at the same point if the bar did not contain the hole; that is, in this illustration the cross section area is the gross area including the area which is removed at the hole. If the diameter of the hole is relatively large, the net area of cross section is frequently used in calculating the nominal stress σ_o, hence the value of the stress concentration factor for a given discontinuity will depend on the method of calculating the nominal stress.

If σ_{max} in a member is the theoretical value of the localized stress, as found from the mathematical theory of elasticity, or the photoelasticity method, etc., K is given the subscript t, and K_t is called the theoretical stress concentration factor. If, on the other hand, the value of K is found from tests of the actual material under the conditions of use, K is given the subscript e, and K_e is called the effective or significant stress concentration factor.

10.1 SMALL HOLES

Solutions in this subsection will be limited to small holes in plates, that is, holes which are relatively small in comparison to the plate size such that boundary conditions do not affect the results. An exception to this is the case when holes are near a free edge of a plate.

10.1.1 Unreinforced Holes

This paragraph contains information on holes of various shapes in plates with no reinforcement around the hole, such as increased thickness, rings, or doublers.

10.1.1.1 Circular Holes

The case of a circular hole in an infinite plate in tension has been solved by many investigators. The stress concentration factor, based on gross area, is $K_t = \frac{\sigma_{max}}{\sigma} = 3$.

Strictly speaking, $K_t = 3$ applies only for a plate which is very thin relative to the hole diameter. When these dimensions are of the same order, K_t is somewhat greater than 3 at the midplane of the plate and is less than 3 at the surface of the plate [1]. For a ratio of plate thickness to hole diameter of three-fourths, $K_t = 3.1$ at the midplane and 2.8 at the surface.

For the case of a finite-width plate with a transverse hole, a solution has been obtained [2] and the corresponding K_t values are given in Fig. B10-1. These values are in good agreement with photoelastic results.

The case of a hole near the edge of a semi-infinite plate in tension has been solved and results are shown in Fig. B10-2. The load carried by the section between the hole and the edge of the plate has been shown to be

$$P = \sigma c h \sqrt{1 - \left(\frac{r}{c}\right)^2} \quad , \tag{3}$$

where

σ = stress applied to semi-infinite plate.

c = distance from center of hole to edge of plate.

r = radius of hole.

h = thickness of plate.

In Fig. B10-2, the upper curve gives values of $\frac{\sigma_B}{\sigma}$, where σ_B is the maximum stress at the edge of the hole nearest the edge of the plate. Although the factor $\frac{\sigma_B}{\sigma}$ may be used directly in design, it was thought desirable to compute also a "stress concentration factor" on the basis of the load carried by the minimum net section. This K_t factor will then be comparable with the stress concentration factors for other cases; this is

important in analysis of experimental data. Based on the actual load carried by the minimum section, the average stress on the net section A-B is:

$$\sigma_{\text{net A-B}} = \frac{\sigma ch \sqrt{1 - \left(\frac{r}{c}\right)^2}}{(c - r)\, h} = \frac{\sigma \sqrt{1 - \left(\frac{r}{c}\right)^2}}{1 - \frac{r}{c}} , \qquad (4)$$

$$K_t = \frac{\sigma_B}{\sigma_{\text{net A-B}}} = \frac{\sigma_B \left(1 - \frac{r}{c}\right)}{\sigma \sqrt{1 - \left(\frac{r}{c}\right)^2}} . \qquad (5)$$

The case of a tension plate of finite width having an eccentrically located hole is shown in Fig. B10-3. When the hole is centrally located $\left(\frac{e}{c} = 1 \text{ in Fig. B10-3}\right)$, the load carried by section A-B is σch. As $\frac{e}{c}$ is increased to infinity, the load carried by Section A-B is $\sigma ch \sqrt{1 - \left(\frac{r}{c}\right)^2}$. Assuming a linear relation between the foregoing end conditions results in the following expression for the load carried by section A-B :

$$P_{A-B} = \frac{\sigma ch \sqrt{1 - \left(\frac{r}{c}\right)^2}}{1 - \frac{c}{e}\left[1 - \sqrt{1 - \left(\frac{r}{c}\right)^2}\right]} . \qquad (6)$$

The stress on the net section A-B is

$$\sigma_{\text{net A-B}} = \frac{\sigma ch \sqrt{1 - \left(\frac{r}{c}\right)^2}}{h\,(c - r)\left\{1 - \frac{c}{e}\left[1 - \sqrt{1 - \left(\frac{r}{c}\right)^2}\right]\right\}} , \qquad (7)$$

$$K_t = \frac{\sigma_{max}}{\sigma_{net}} = \frac{\sigma_{max}}{\sigma} \frac{\left(1 - \frac{r}{c}\right)}{\sqrt{1 - \left(\frac{r}{c}\right)^2}} \left\{1 - \frac{c}{e}\left[1 - \sqrt{1 - \left(\frac{r}{c}\right)^2}\right]\right\} . \qquad (8)$$

It is seen in the lower part of Fig. B10-3 that this relation brings all the K_t curves rather closely together, so that for all practical purposes the curve for the centrally located hole $\left(\frac{e}{c} = 1\right)$ is, under these circumstances, a reasonable approximation for all eccentricities.

I. Biaxial Tension:

For the case of a hole in an infinite plate stressed biaxially results are given in Fig. B10-4. For a circular hole,

$$\sigma_{max} = 3\,\sigma_1 - \sigma_2 \quad . \qquad (9)$$

For σ_2 equal in magnitude to σ_1, $K_t = 2$, when both are of the same sign. When σ_1 and σ_2 are equal but of opposite sign, $K_t = 4$.

II. Bending:

For bending of a plate the following results have been obtained. For a infinitely wide plate with a hole, mathematical results have been obtained in terms of $\frac{a}{h}$ (Fig. B10-5). Values for finite widths and various valves of $\frac{a}{h}$ are shown in Fig. B10-6.

10.1.1.2 Elliptical Holes

I. Axial Loading:

The stress distribution associated with an elliptical hole in an infinitely wide plate subjected to uniformly distributed axial load has been obtained, and the stress concentration factor as a function of the ratio of the major width (b) to the minor width (a) is given in Fig. B10-7.

$$K_t = 1 + \frac{2b}{a} \quad . \tag{10}$$

A photoelastic solution of the distribution of stresses around a centrally located elliptical hole in a plate of finite width and subjected to uniform axial loading has been obtained in Ref. 3, and the stress concentration factors are presented in Fig. B10-8.

For the case of a biaxially stressed plate with an elliptical hole $\left(\frac{b}{a} = 2\right)$, the results are given in Fig. B10-4.

$$\sigma_{max} = \sigma_1 \left(1 + \frac{2b}{a}\right) - \sigma_2 \quad . \tag{11}$$

II. Bending:

Stress concentration values for an elliptical hole in an infinitely wide plate are given in Fig. B10-9.

10.1.1.3 Rectangular Holes with Rounded Corners

Stress concentration factors for an unreinforced rounded rectangular hole in an infinite sheet in tension have been evaluated in Ref. 4. Variation

of the stress concentration factor for various values of side length to corner radius is shown in Fig. B10-10.

10.1.1.4 Oblique Holes

An oblique or skew hole may be defined as one having its axis at an angle with respect to the normal to a surface. At the intersection with a plane surface a skew cylindrical hole gives rise to an elliptical trace and produces an acute-angled edge which, for large angles of obliquity with respect to the normal, may be very sharp.

Stress concentration factors have been determined for oblique holes in flat plates by a photoelasticity method in Ref. 5. Results of their analysis are presented in Fig. B10-11 along with theoretical curves for elliptical holes in infinite and finite widths.

The stress-concentration factor based on net area is relatively insensitive to the radius of the acute-angled tip. However, in a relatively narrow plate, the maximum stress may actually be increased by the addition of a radius because of the loss of load-carrying area.

It should be noted that the results of Ref. 5 apply only to plates with a ratio of hole diameter d to plate width w of 0.1. Additional information on oblique holes in plates can also be found in Ref. 6.

10.1.1.5 Multiple Holes

I. Two Holes:

Stress concentration factors for two holes of the same diameter in an infinite plate has been documented in Ref. 2. For the case of uniaxial tension perpendicular to the line of holes, Fig. B10-12 gives the factors; and for the case of biaxial tension, the results are given in Fig. B10-13.

The solution for stress concentration factors of two holes of different diameters in an infinite plate loaded by an equal biaxial stress has been obtained by Ref. 7 and the results are given in Fig. B10-14.

Reference 8 contains the solution for a plate containing a circular hole with a circular notch, as shown in Fig. B10-15. Figure B10-16 shows the stress concentration factor at the bottom of notch (point A) when the tension load is in the y direction. The smaller or deeper the notch is, the greater are the values of maximum stress.

II. Single Row of Holes:

For a single row of holes in an infinite plate, Figures B10-17 and B10-18 give stress concentration factors for tension perpendicular to the line of holes and for biaxially stressed holes respectively.

III. Double Row of Holes:

For a double row of staggered holes, the stress concentration factor is given in Fig. B10-19. For the staggered holes, a problem arises in basing

K_t on net section, since for a given $\frac{b}{a}$ the relation of net sections A-A and B-B depends on θ. For $\theta < 60$ deg, A-A is the minimum section and the following formula is used:

$$K_{t_A} = \frac{\sigma_{max}}{\sigma} \left[1 - 2\left(\frac{a}{b}\right) \cos\theta\right] , \qquad (12)$$

for $\theta > 60$ deg, B-B is the minimum section and the formula is based on the net section in the row:

$$K_{t_B} = \frac{\sigma_{max}}{\sigma} \left[1 - \frac{a}{b}\right] . \qquad (13)$$

IV. Arrays of Holes:

Stress concentration factors in a plate containing a large number of uniformly spaced perforations in regular triangular or square arrays under biaxial loading was investigated by photoelastic methods in Ref. 9. Four configurations of perforation were considered as shown in Fig. B10-20.

Stress concentration factors for several combinations of configuration and loading are plotted against $\frac{\rho}{p}$ in Figs. B10-21 through B10-26.

In these figures, the stress concentration factor is defined as the ratio of the peak value of σ_θ at point A, A', B' on the hole boundary to σ_1 namely $K = \frac{\sigma_{\theta\,max}}{\sigma_1}$. σ_1 is the algebraically larger one of the principal

stresses that would be produced in the plate by the combination of the biaxial loads applied if there were no holes. The stress concentrations factors at angular positions on the boundary are shown by subscripts to K .

On these figures, the primary tendency is the rise of K with $\frac{\rho}{p}$. Among the four types of hole configuration, the diagonal-square type is always of disadvantage for it produces the highest stress concentration factor for every type of biaxial loading throughout the range of $\frac{\rho}{p}$, while the parallel-square type gives the lowest factor, and the perpendicular and parallel-triangular types lie in between. For example, a list of K for a comparatively large value of $\frac{\rho}{p} = 0.92$ for each hole configuration and biaxial-load is given in Table B10-1.

Where strength is the main consideration, the above results show that the parallel-square type of hole configuration is most desirable, especially when $\frac{\rho}{p}$ is large. The triangular hole configuration, both perpendicular and parallel, which is usually used is unfavorable contrary to expectation.

10.1.2 Reinforced Holes

This paragraph contains information on holes which have an increased thickness around the hole in order to reduce the stress concentration factors. Information will be divided into two categories: when the reinforcement is of constant cross section and when the reinforcement cross section varies around the hole.

10.1.2.1 Constant Reinforcement

Stress concentration at a hole can be reduced by providing a region of increased thickness around the hole, sometimes called a "boss" or "bead." Values of stress concentration factor for beads of various cross-sectional areas for a plate having a hole diameter one-fifth the plate width $\frac{a}{w} = 0.2$ are obtained in Ref. 2. Also, the stress concentration factors were obtained on the basis of the radial dimension $\frac{a_b - a}{2}$ being small compared to the hole diameter.

To account for other values of $\frac{a}{w}$, an approximate method has been obtained:

$$K_{tB}^{*} = B\left(K_t - 1\right) + 1 \quad , \tag{14}$$

where

K_{tB}^{*} = stress concentration factor for plate with hole and bead, for the particular value of $\frac{a}{w}$ desired.

B = Bead factor = $\frac{K_{tB} - 1}{1.51}$ (Fig. B10-27).

K_t = stress concentration factor for plate with hole and without bead (Fig. B10-1) for the particular value of $\frac{a}{w}$ desired.

It is pointed out in Ref. 10 that the maximum cross-sectional area of a bead, $\frac{a_b - a}{2} h_b$, should be about $\frac{ah}{4}$. Above this value the theory from which the stress concentration values were obtained no longer holds.

Studies by Dhir on stresses around two equal reinforced circular openings in a thin plate [11] have shown that the most effective amount of reinforcement appears to be near 40 percent area replacement (percent of area replaced to area removed by hole). Any additional amount of reinforcement did not produce a proportionate reduction of the stresses. The interaction between the two holes was not significant if the distance between the inner edges of the two holes was one diameter or greater. For tension load perpendicular to the line of the two holes, a 40 percent area replacement lowered the stress concentration factor from 3.0, for an unreinforced hole, to 1.75.

Additional work in the area of reinforced holes has been done in Refs. 12 and 13; however, these references do not give design data in usable form, as a solution must be obtained from a computerized analysis.

I. Asymmetrically Reinforced:

The previous discussion has only concerned holes with symmetrical reinforcement, that is, with reinforcement on both sides of the plate.

In practice, however, these are frequent cases where one surface of the plate must be kept smooth and the reinforcement can be attached to the

other surface only. This problem is treated in Refs. 13 and 14; however, because of the interaction between bending and stretching, the problem is highly nonlinear and has only been solved for certain limiting cases. It is found that the asymmetry of the reinforcement introduces bending stresses in the plate and reinforcement because of the eccentricity of the reinforcement. Careful consideration of the parameters must be employed, as in some cases the addition of reinforcement causes a stress concentration factor greater than what would have been present if no reinforcement were added. The work of Ref. 15 shows that for a given loading condition a size of reinforcement can be chosen to minimize the stress concentration factor.

10.1.2.2 Variable Reinforcement

In some cases the design of the reinforcement around a hole may be important when the weight of the structure must be as low as possible. Reinforcement may then be of variable cross section around the hole. Hicks [16, 17] has considered the problem of variably reinforced circular holes and arrived at expressions for stresses for different loading systems. He has shown that when the reinforcement has a given weight, the effect of varying its cross section is to reduce the stress concentration in the plate. One disadvantage of the variable reinforcement is that it may be undesirable from a manufacturing point of view.

10.2 LARGE HOLES AND CUTOUTS

Some designs may occur in which it is necessary or desirable to have relatively large holes or cutouts in a plate, such as lightening holes in the web of a beam or cutouts in a plate structure. A limited amount of data is available for problems of this type; however, available solutions will be discussed in this section.

10.2.1 Bending of Plates with Circular Holes

Solutions have been obtained in Ref. 18 for a uniformly loaded square plate either simply supported or clamped along the outer boundary with a central circular hole as shown in Fig. B10-28. Results for deflections and bending moments for each boundary condition are given in Tables B10-2 and -3.

10.2.2 Holes in Beam Webs

Holes are frequently cut in the webs of beams to provide for passage of pipes and ducts, for access to the inside of a box beam, or for weight saving. Little information is available on the stress distribution around holes in beam webs.

An analytical method for calculating stresses around holes in the web of wide flange beams shown in Fig. B10-29 is presented in Ref. 19. The applicability of the analysis depends on the size of the hole and on the magnitude of the moment-shear ratio at the hole. The analysis is primarily applicable to circular holes; as for elliptic holes, limits of applicability of the analysis technique were not established.

An empirical technique for the analysis of webs with round lightening holes having formed 45 deg flanges is presented in Ref. 20.

Table B10-1. Stress Concentration in a Plate Due to Uniformly Spaced Circular Holes

$\frac{\rho}{p} = 0.92$

Biaxial loads \ Configuration	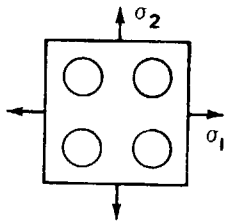	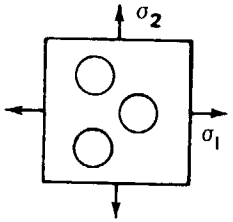	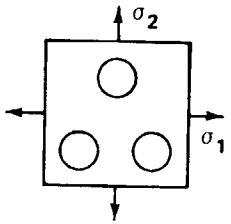	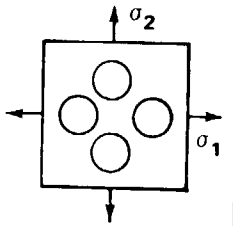
$\sigma_1 \neq 0$, $\sigma_2 = 0$ Uniaxial Tension	12.5	19.4	23.0	37.0
$\sigma_2 = 0.5\,\sigma_1$	12.6	14.0	17.4	23.4
$\sigma_2 = \sigma_1$ hydrostatic tension	12.6	13.5	13.5	12.6
$\sigma_2 = -\sigma_1$ pure shear	12.6	39.0	39.0	64.4

Table B10-2. Maximum Deflections and Moments in Simply Supported Square Plate With a Circular Hole Subjected to Uniform Load

R/b	W_{max}	Max M_θ
	$\frac{qb^4}{D}$	qb^2
0	0.649	0.192
1/6	0.0719	0.344
1/3	0.0697	0.276
1/2	0.0530	0.207
2/3	0.0303	0.143
5/6	0.0119	0.085
1	0.00268	0.036

Table B10-3. Maximum Deflections and Moments in a Clamped Square Plate With a Circular Hole Subjected to Uniform Load

R/b	W_{max}	Max M_θ along the hole	Max M_n along the edge
	$\frac{qb^4}{D}$	qb^2	qb^2
0	0.02025	0.0916	-0.2055
1/6	0.02148	0.1451	-0.2032
1/3	0.01648	0.0907	-0.1837
1/2	0.00858	0.0522	-0.1374
2/3	0.00307	0.0310	-0.0780
5/6	0.00081	0.0176	-0.0410
1	0.00025	0.0067	-0.0215

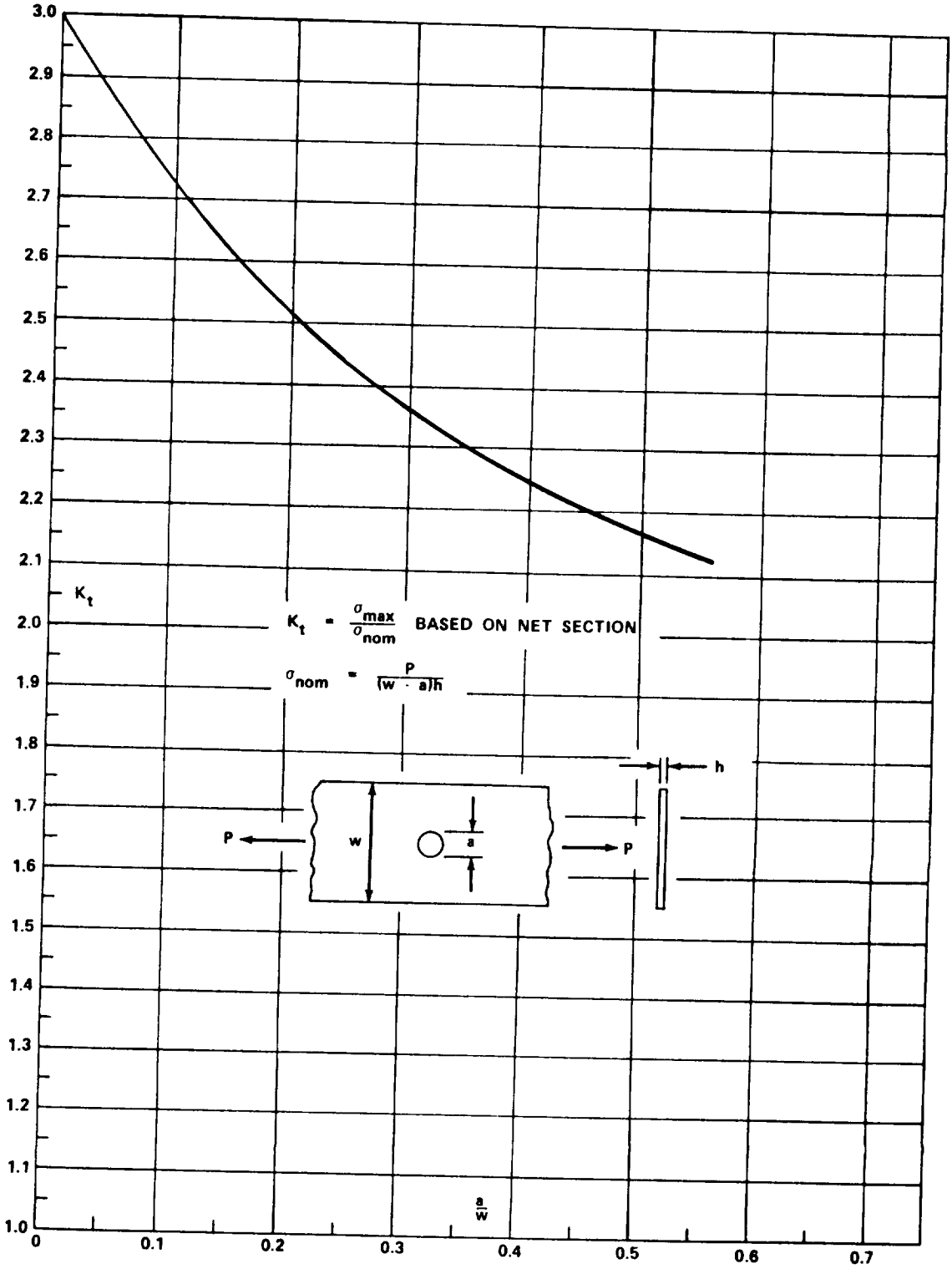

FIGURE B10-1. STRESS CONCENTRATION FACTOR, K_t, FOR AXIAL LOADING CASE OF A FINITE-WIDTH PLATE WITH A TRANSVERSE HOLE.

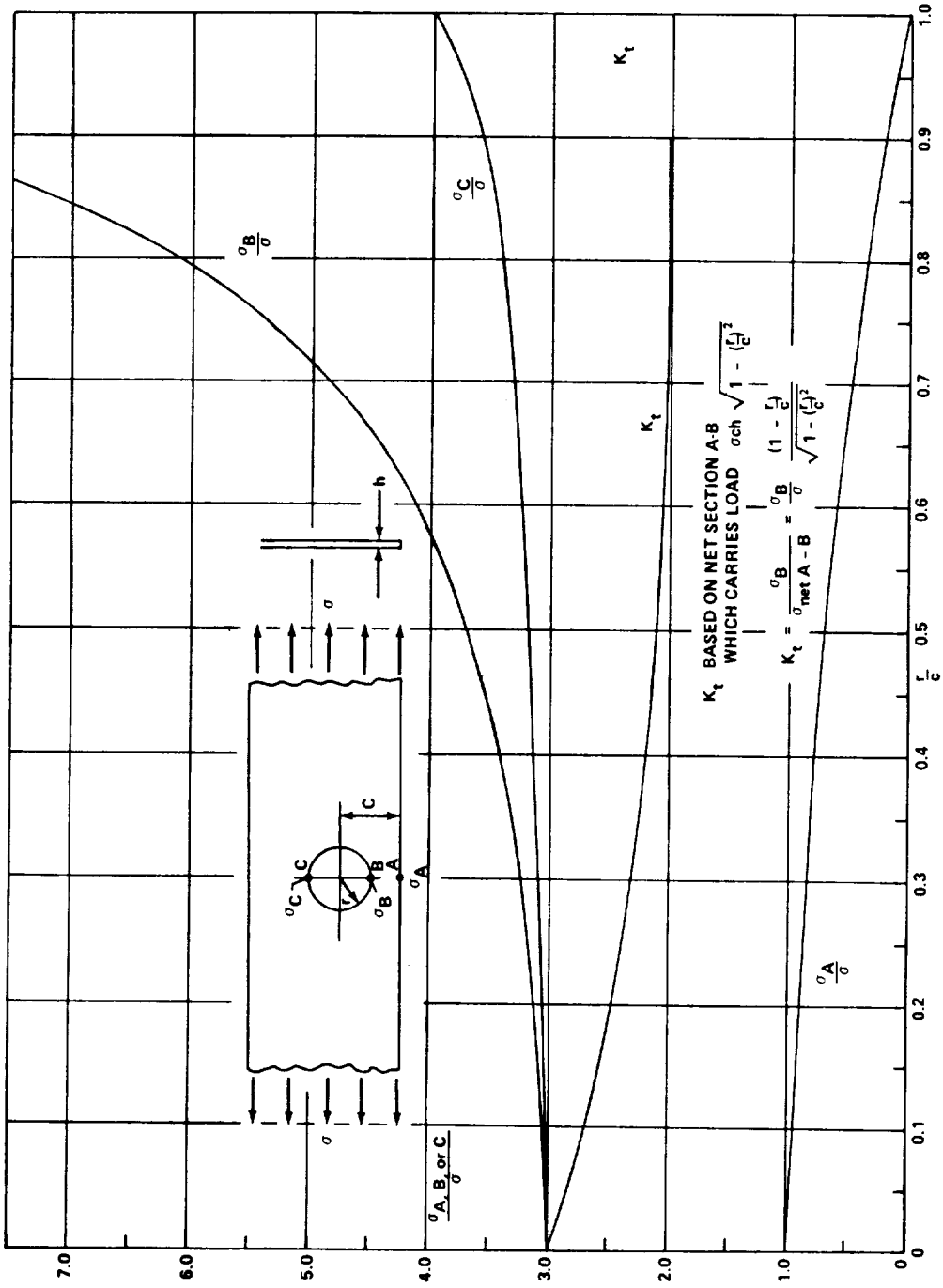

FIGURE B10-2. STRESS CONCENTRATION FACTOR, K_t, FOR THE TENSION CASE OF A SEMI-INFINITE PLATE WITH A CIRCULAR HOLE NEAR THE EDGE.

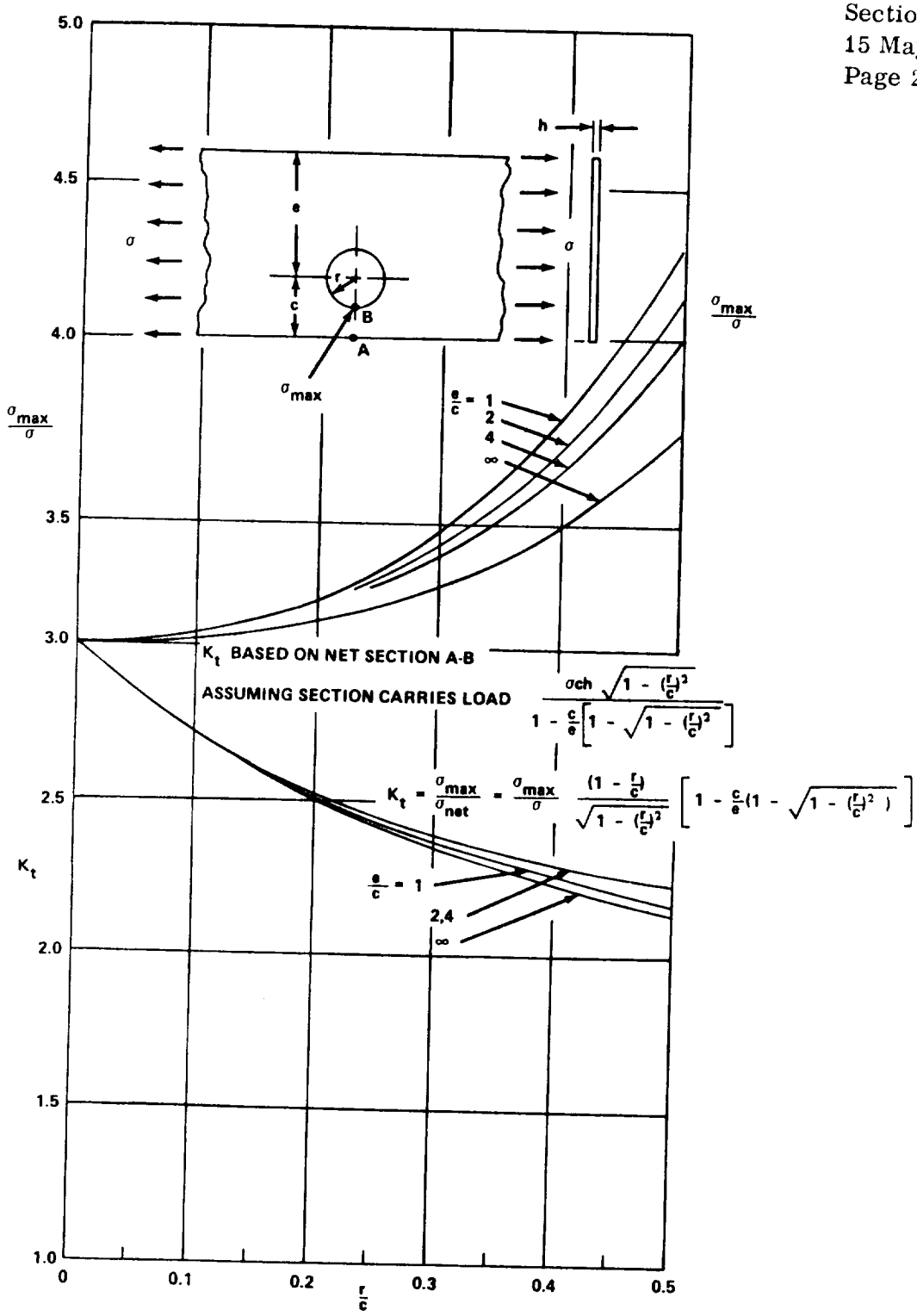

FIGURE B10-3. STRESS CONCENTRATION FACTOR, K_t, FOR TENSION CASE OF A FLAT BAR WITH A CIRCULAR HOLE DISPLACED FROM CENTER LINE.

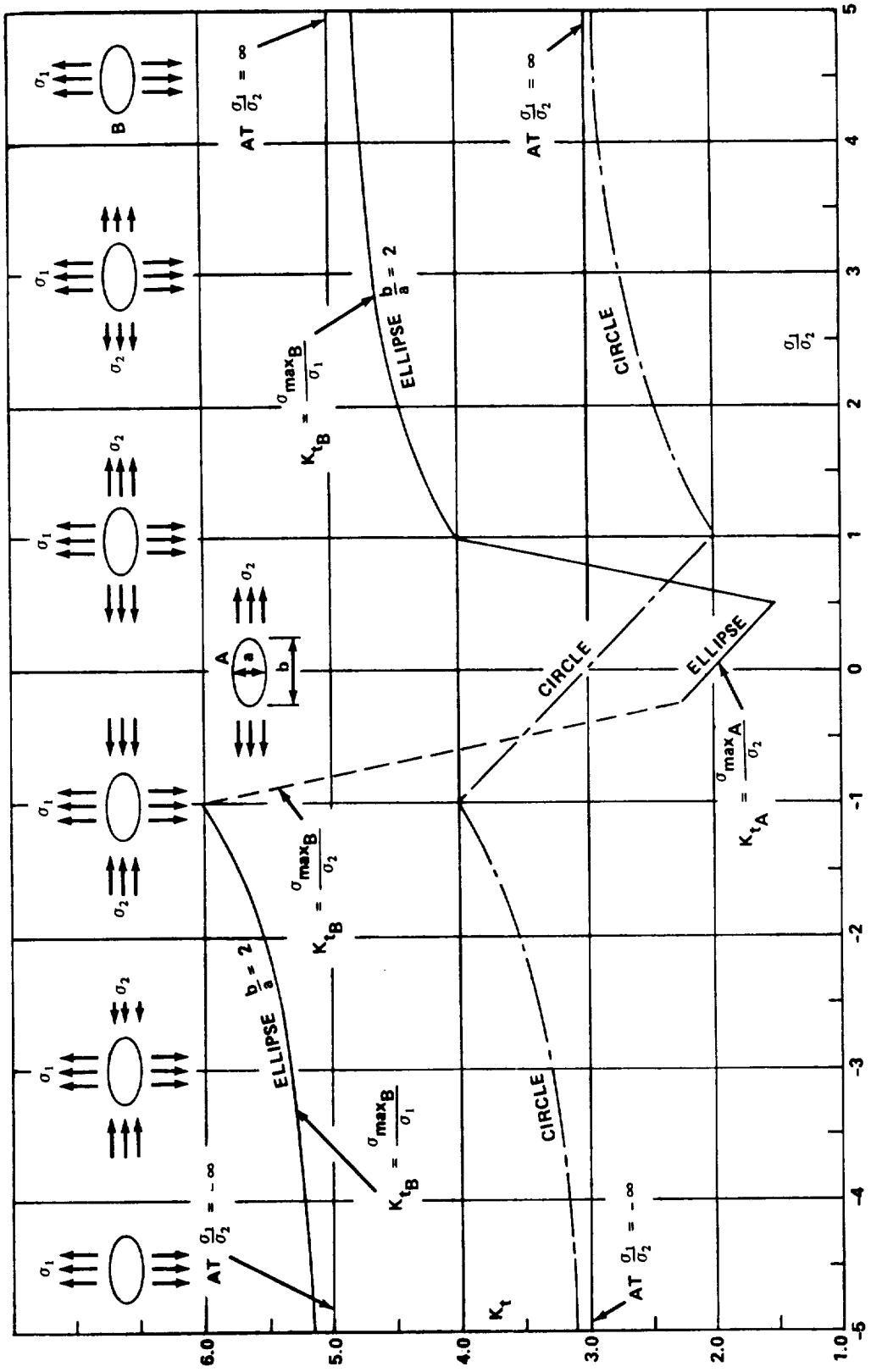

FIGURE B10-4. STRESS CONCENTRATION FACTOR, K_t, FOR AN ELLIPTICAL HOLE $\frac{b}{a} = 2$ AND FOR A CIRCULAR HOLE IN A PLATE SUBJECTED TO BIAXIAL STRESS.

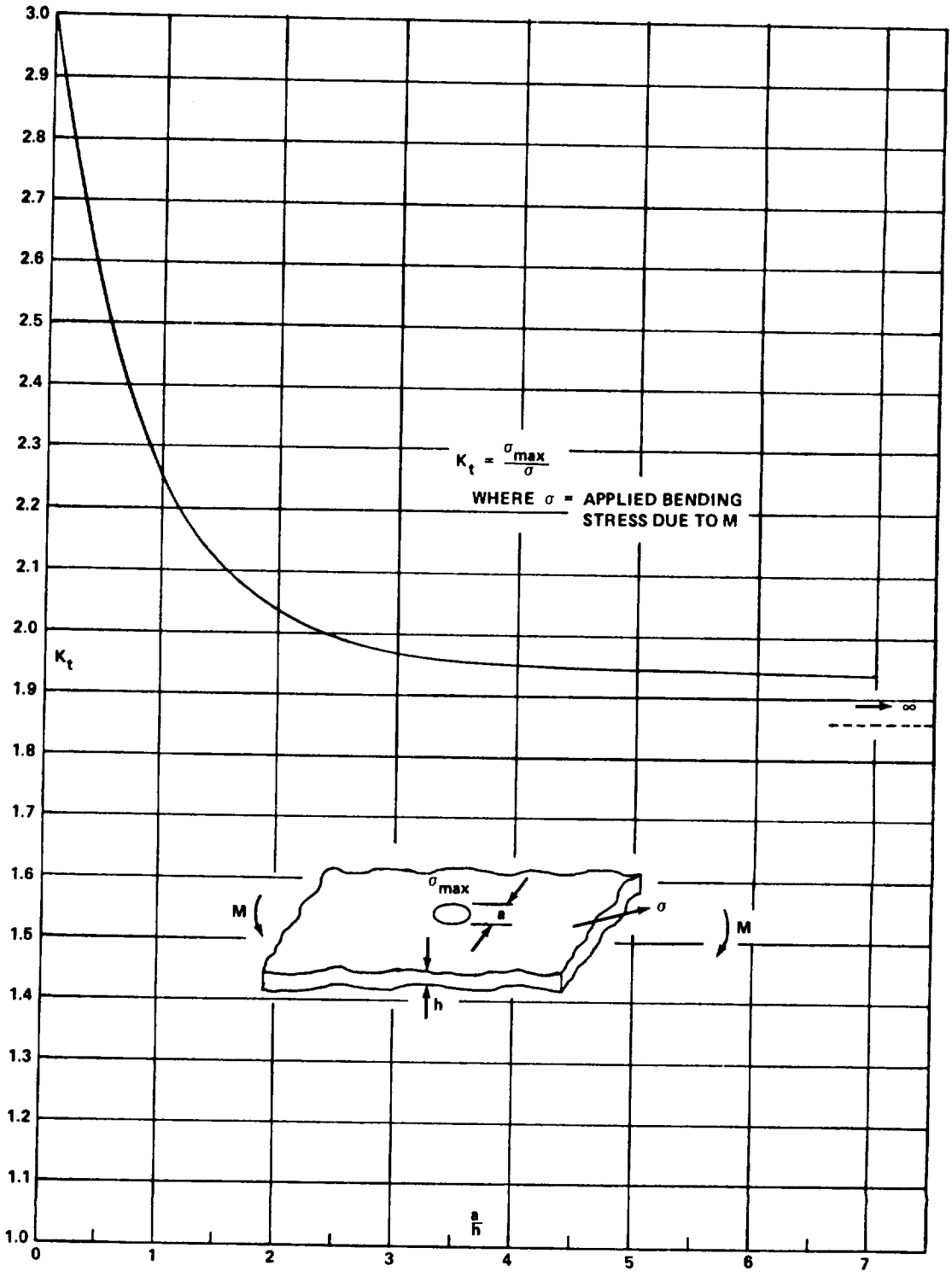

FIGURE B10-5. STRESS CONCENTRATION FACTOR, K_t, FOR BENDING CASE OF AN INFINITELY WIDE PLATE WITH A TRANSVERSE HOLE.

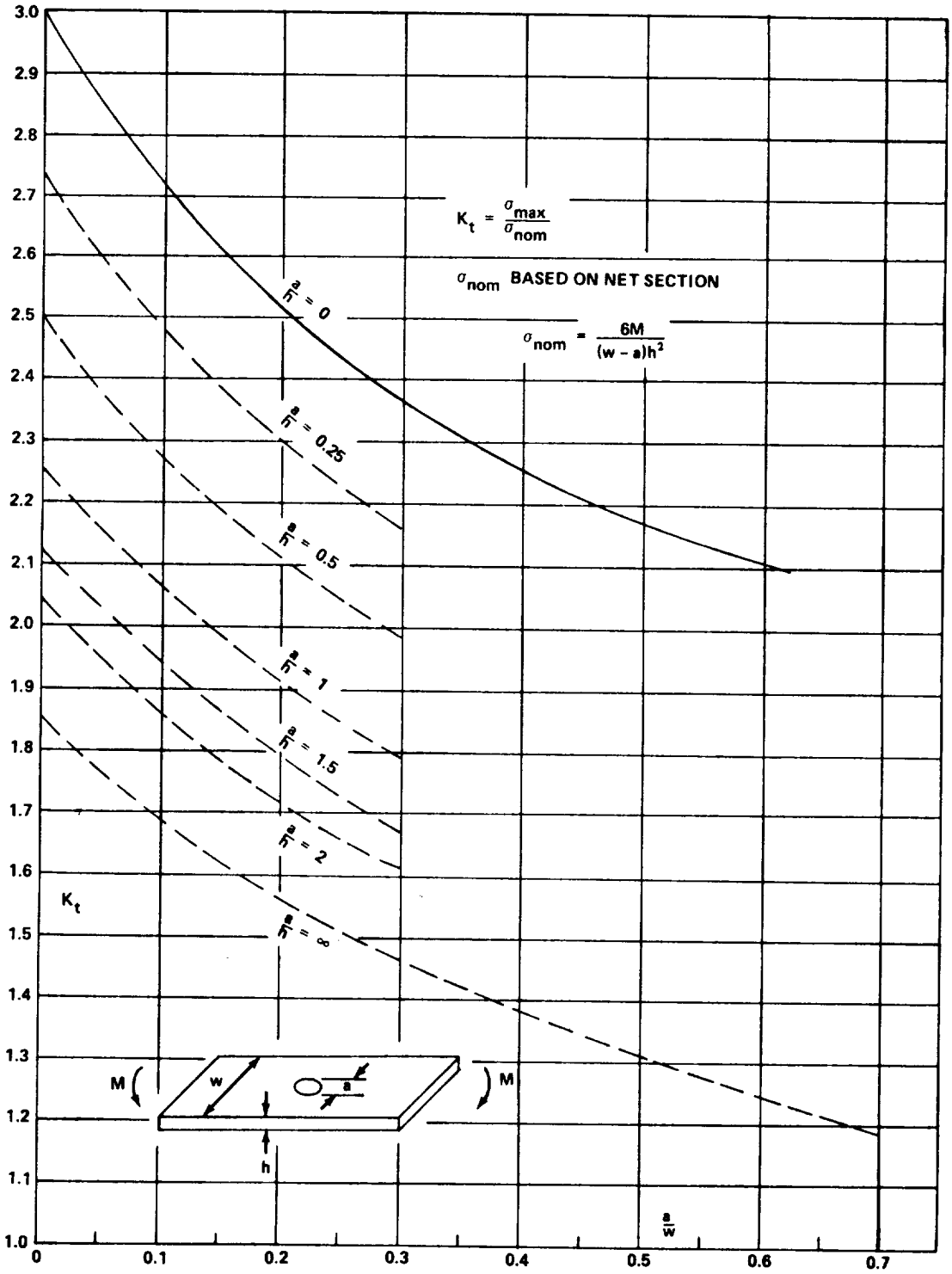

FIGURE B10-6. STRESS CONCENTRATION FACTOR, K_t, FOR BENDING CASE OF FINITE-WIDTH PLATE WITH A TRANSVERSE HOLE.

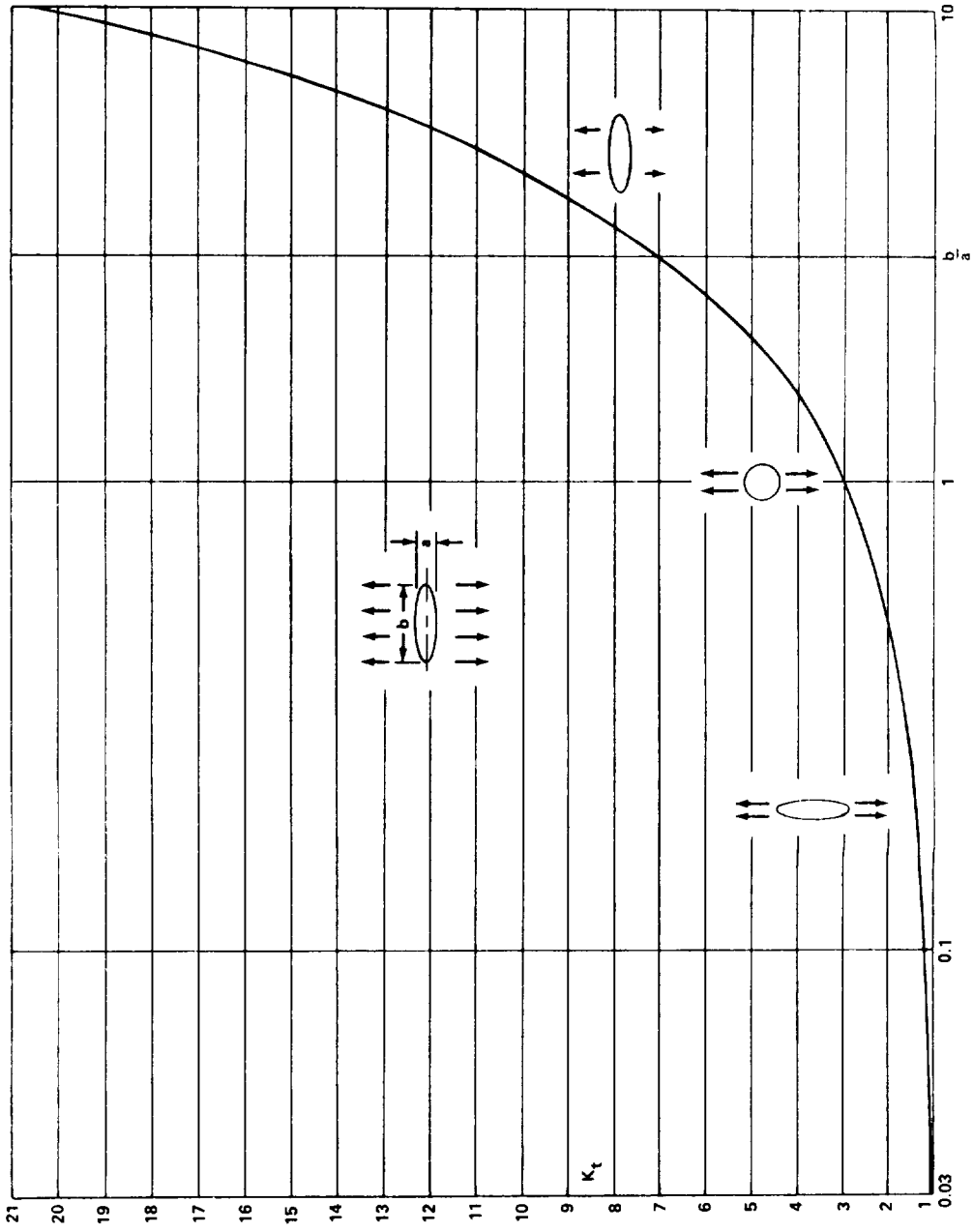

FIGURE B10-7. STRESS CONCENTRATION FACTOR, K_t, FOR AN ELLIPTICAL HOLE IN AN INFINITE PLATE IN TENSION.

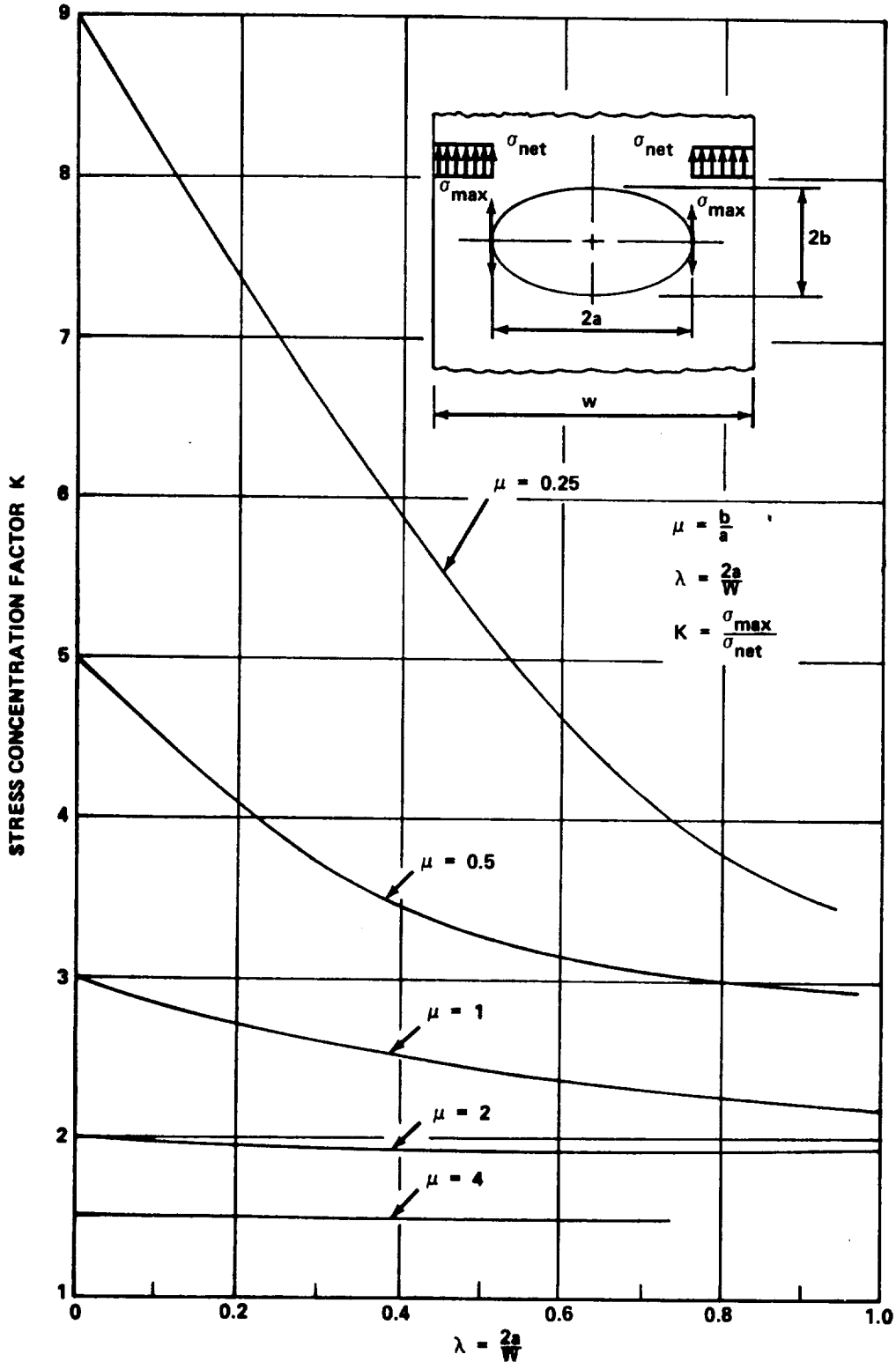

FIGURE B10-8. STRESS CONCENTRATION FACTOR FOR POINTS UNDER MAXIMUM TENSION IN A FINITE PLATE WITH AN ELLIPTICAL HOLE.

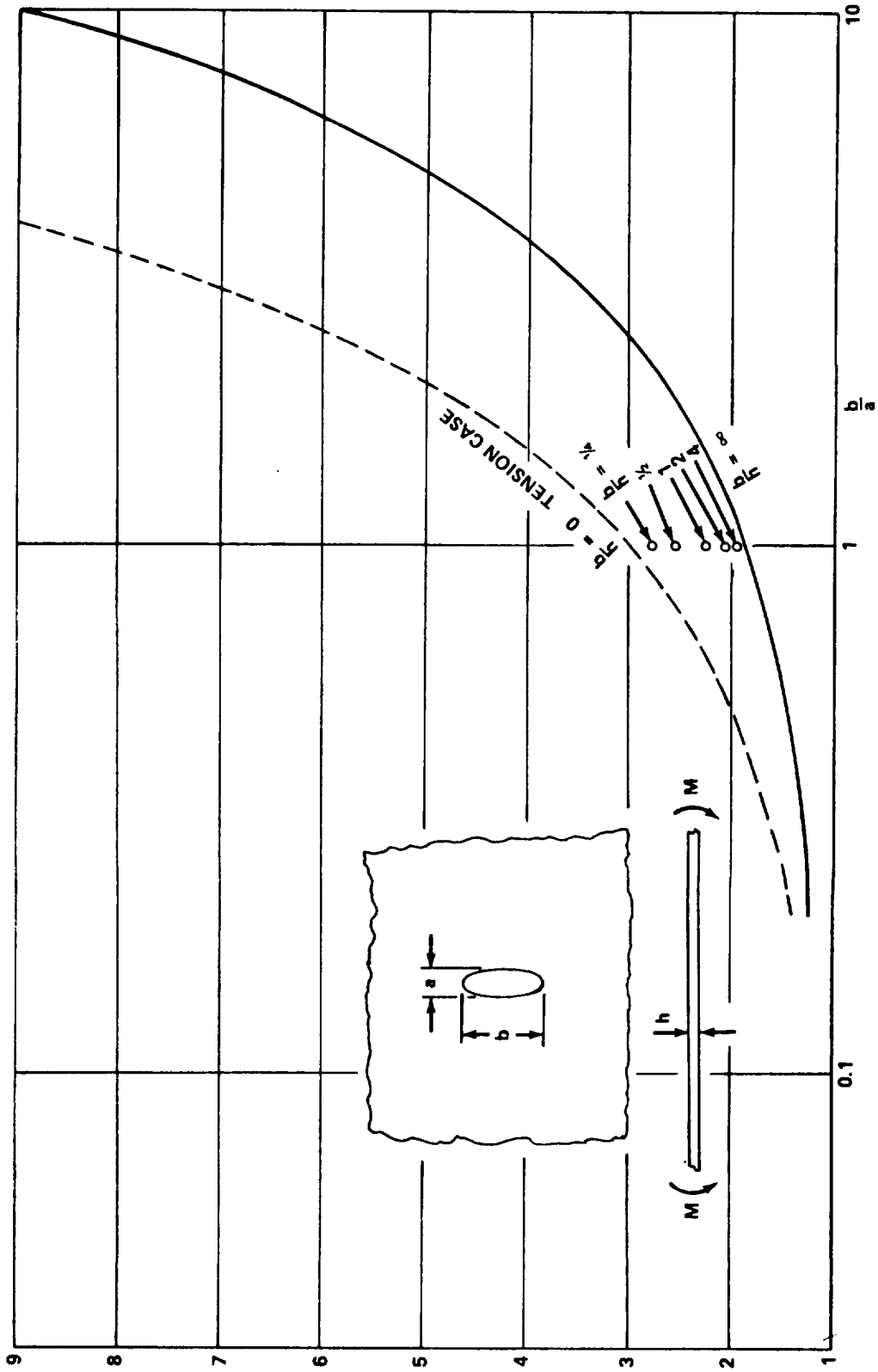

FIGURE B10-9. STRESS CONCENTRATION FACTOR, K_t, FOR THE TRANSVERSE BENDING CASE OF AN INFINITELY WIDE SHEET CONTAINING AN ELLIPTICAL HOLE.

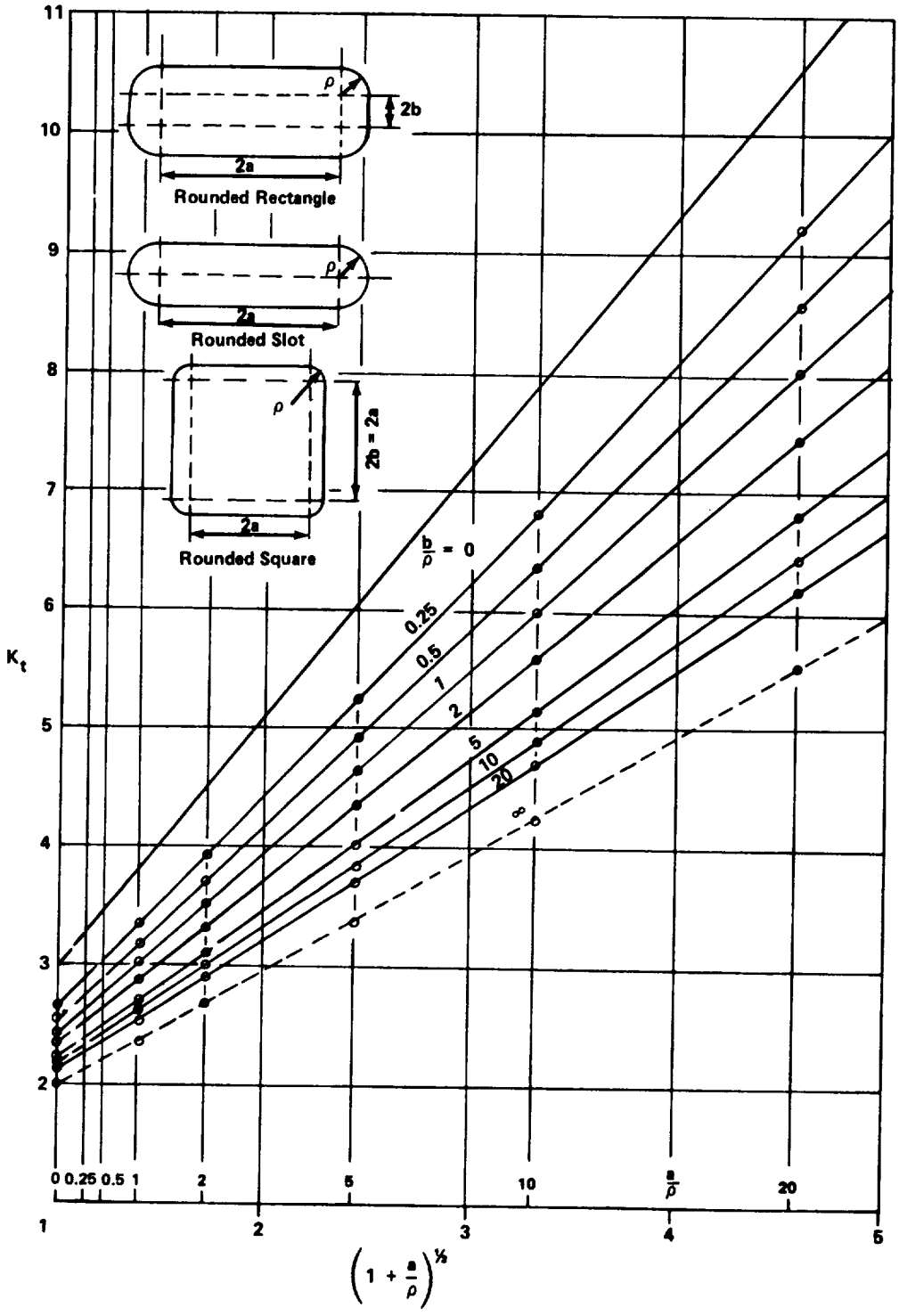

FIGURE B10-10. VARIATION OF K_t WITH $\frac{a}{\rho}$ FOR CONSTANT $\frac{b}{\rho}$ WITH TENSILE LOADING TENDING TO OPEN THE SLOT.

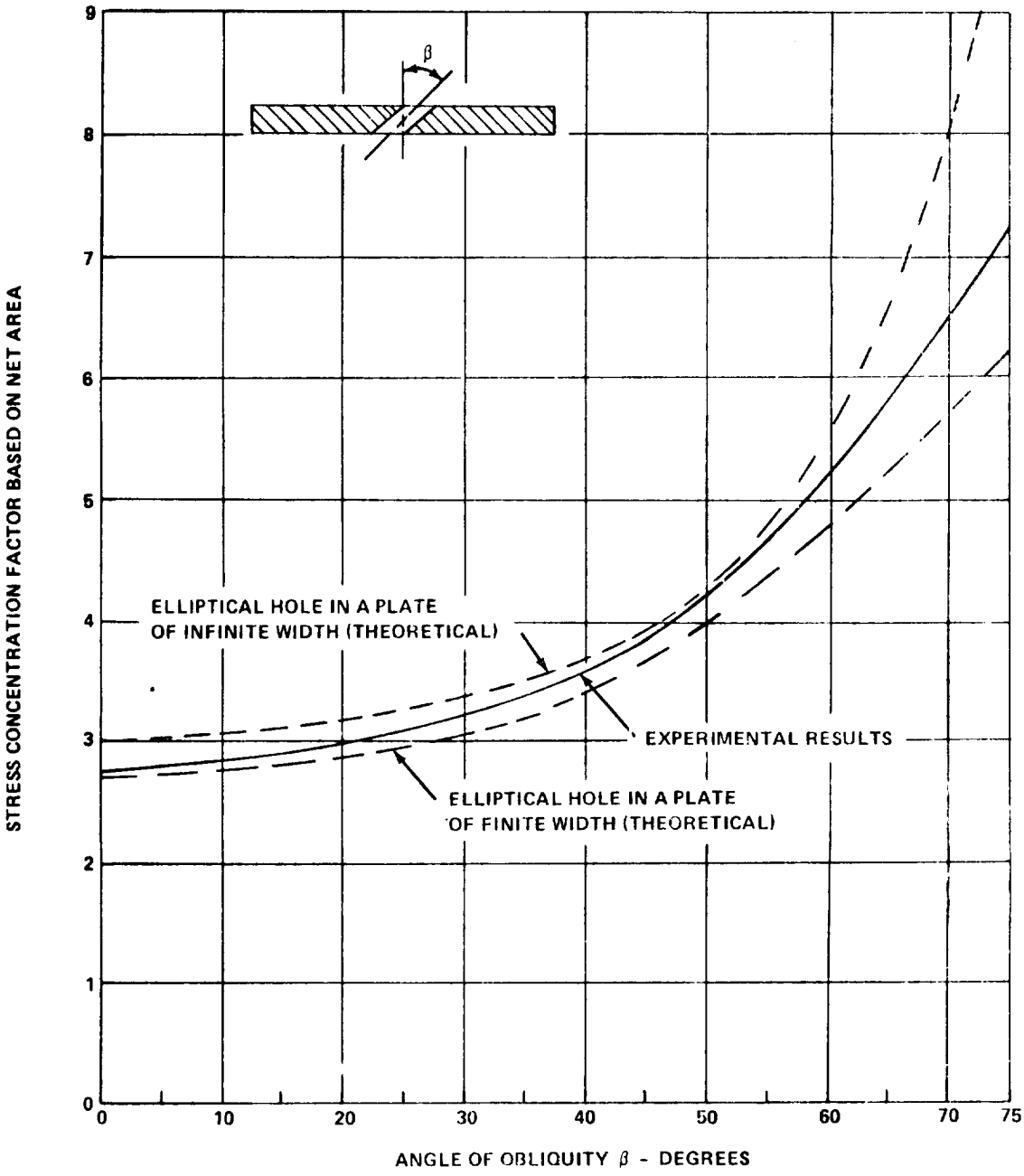

FIGURE B10-11. STRESS CONCENTRATION FACTOR BASED ON NET AREA AS A FUNCTION OF ANGLE OF OBLIQUITY β.

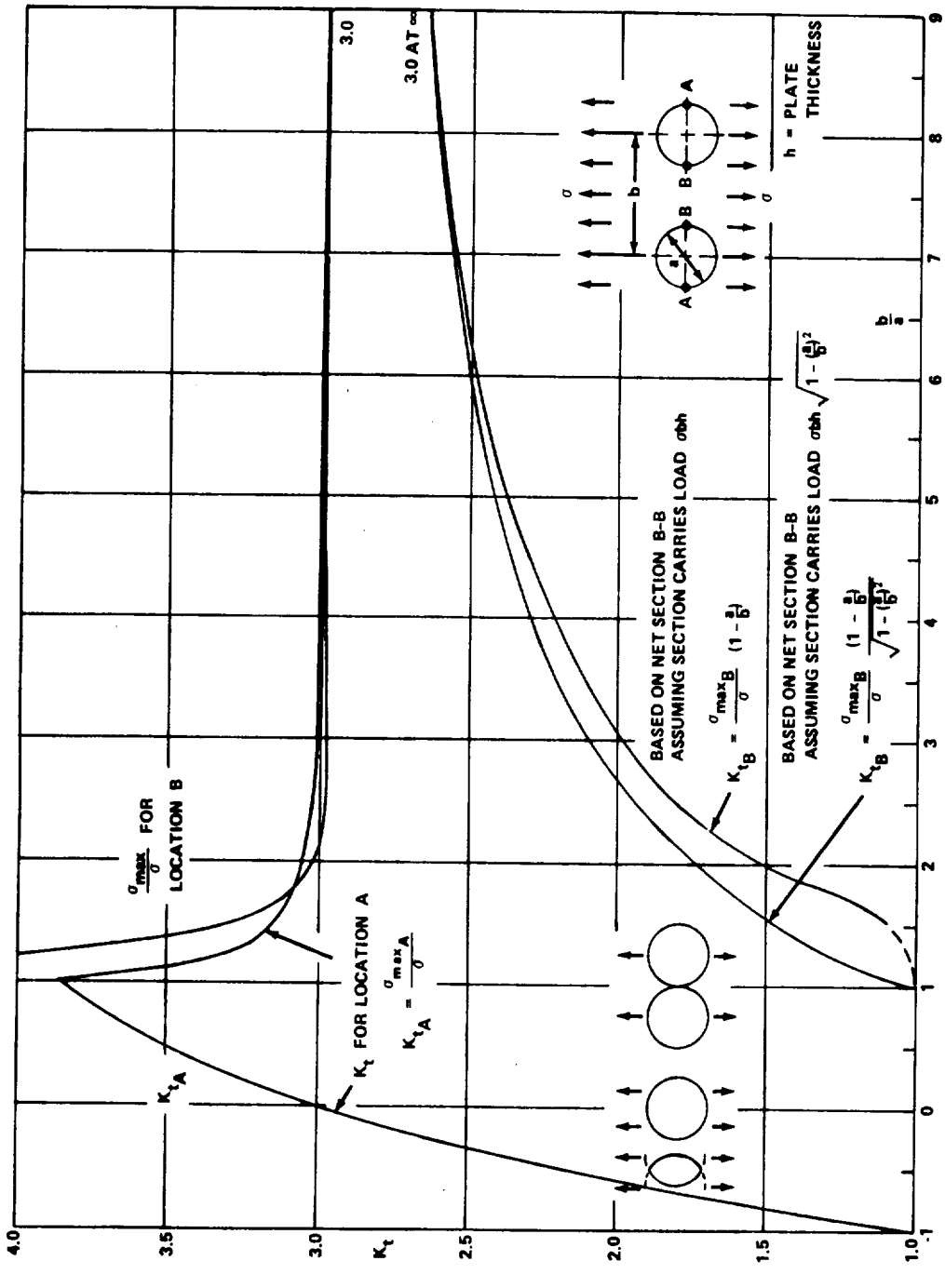

FIGURE B10-12. STRESS CONCENTRATION FACTOR, K_t, FOR TENSION CASE OF AN INFINITE PLATE WITH TWO CIRCULAR HOLES (TENSION PERPENDICULAR TO LINE OF HOLES).

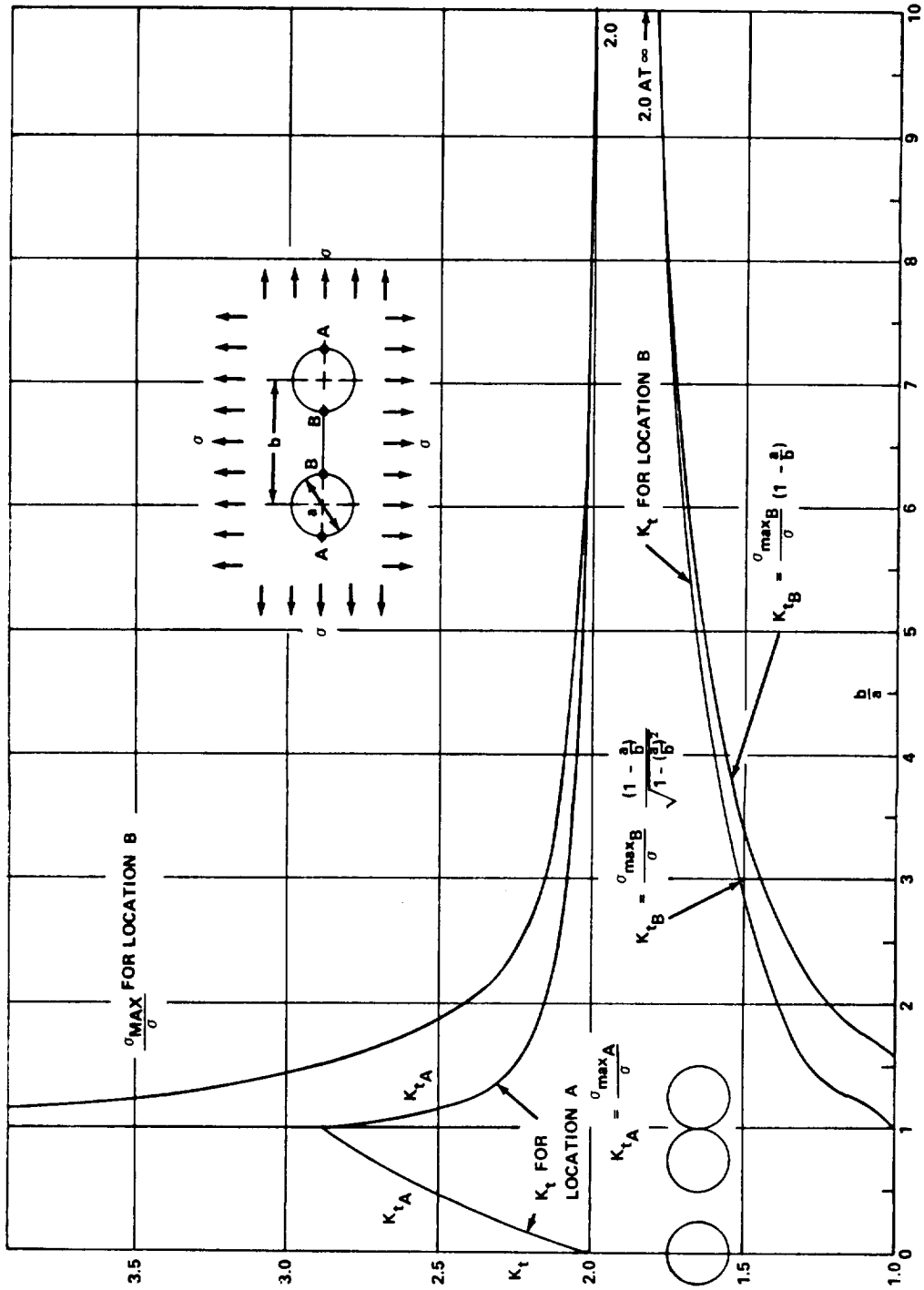

FIGURE B10-13. STRESS CONCENTRATION FACTOR, K_t, FOR BIAXIAL TENSION CASE OF AN INFINITE PLATE WITH TWO CIRCULAR HOLES.

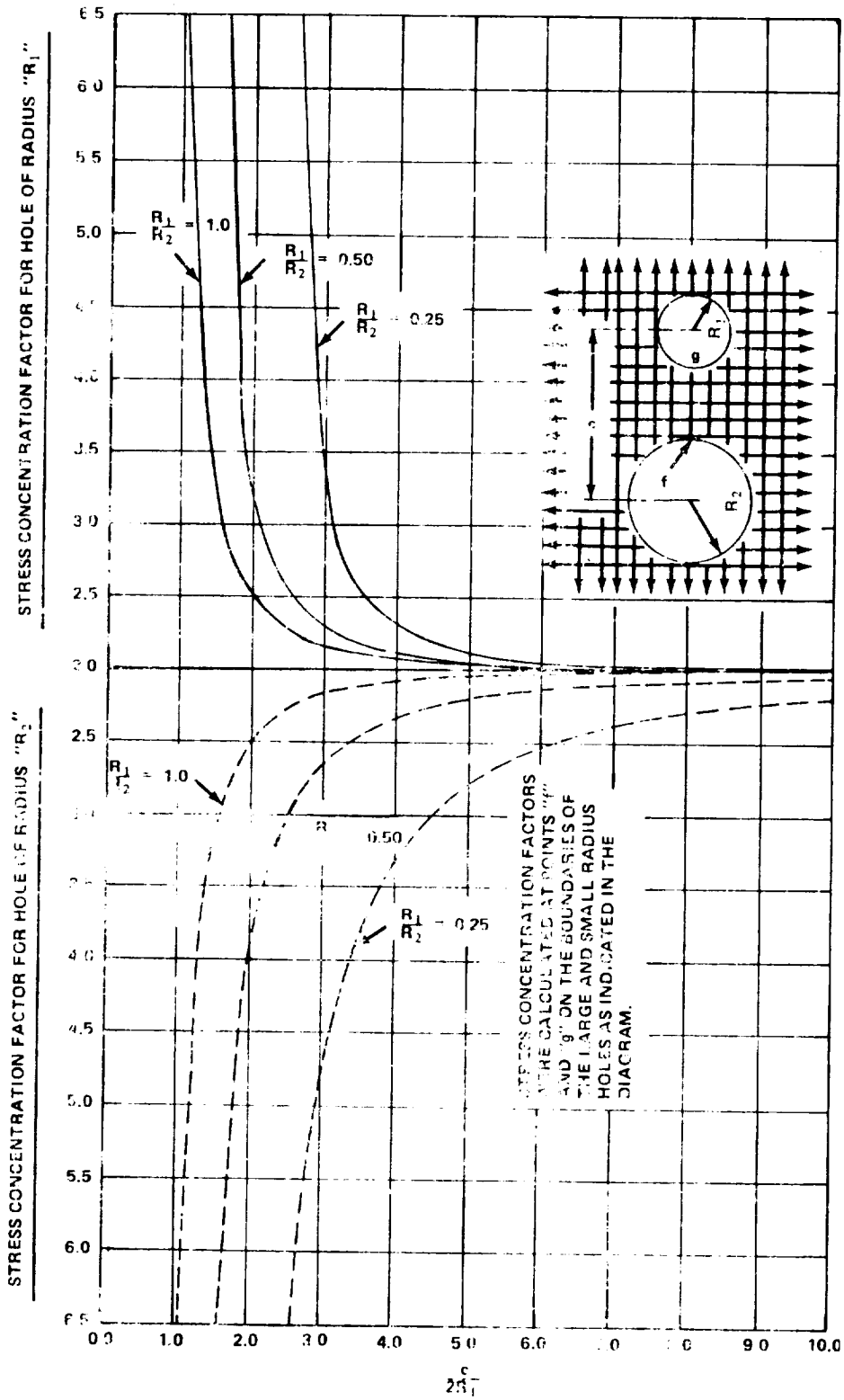

FIGURE B10-14. STRESS CONCENTRATION FACTORS FOR TWO UNEQUAL-SIZED HOLES IN BIAXIAL FIELD OF STRESS.

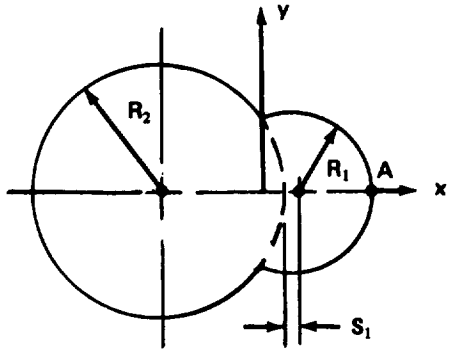

FIGURE B10-15. HOLE WITH CIRCULAR NOTCH.

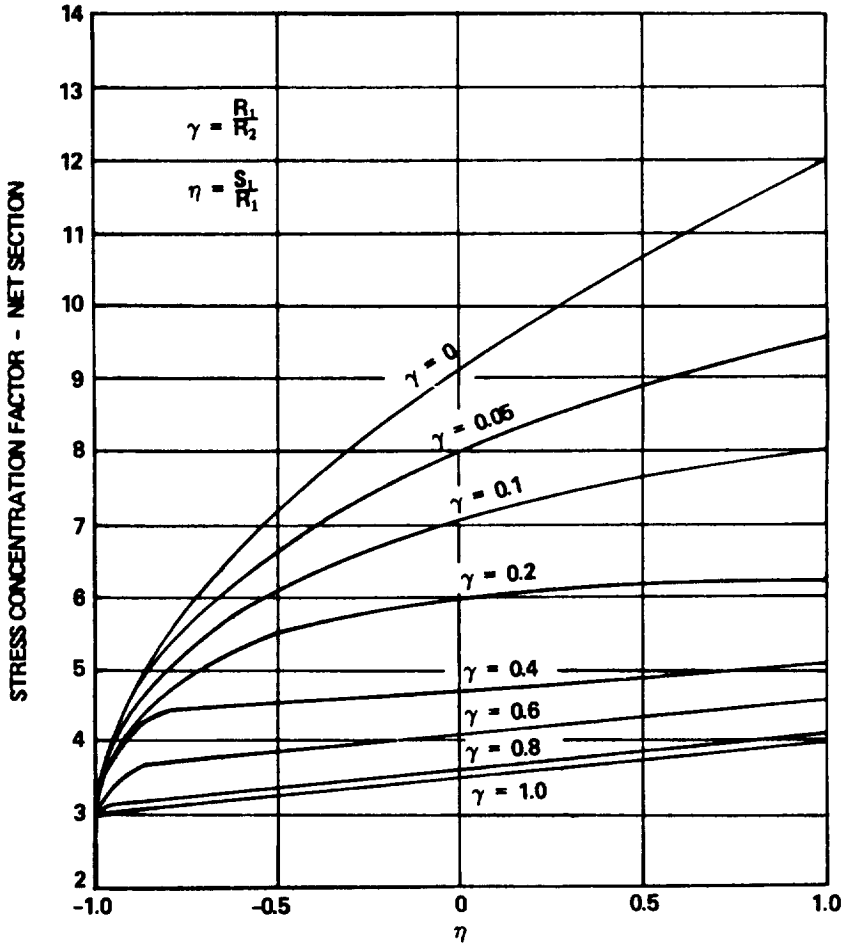

FIGURE B10-16. STRESS CONCENTRATION FACTOR AT POINT A UNDER TENSION IN Y-DIRECTION.

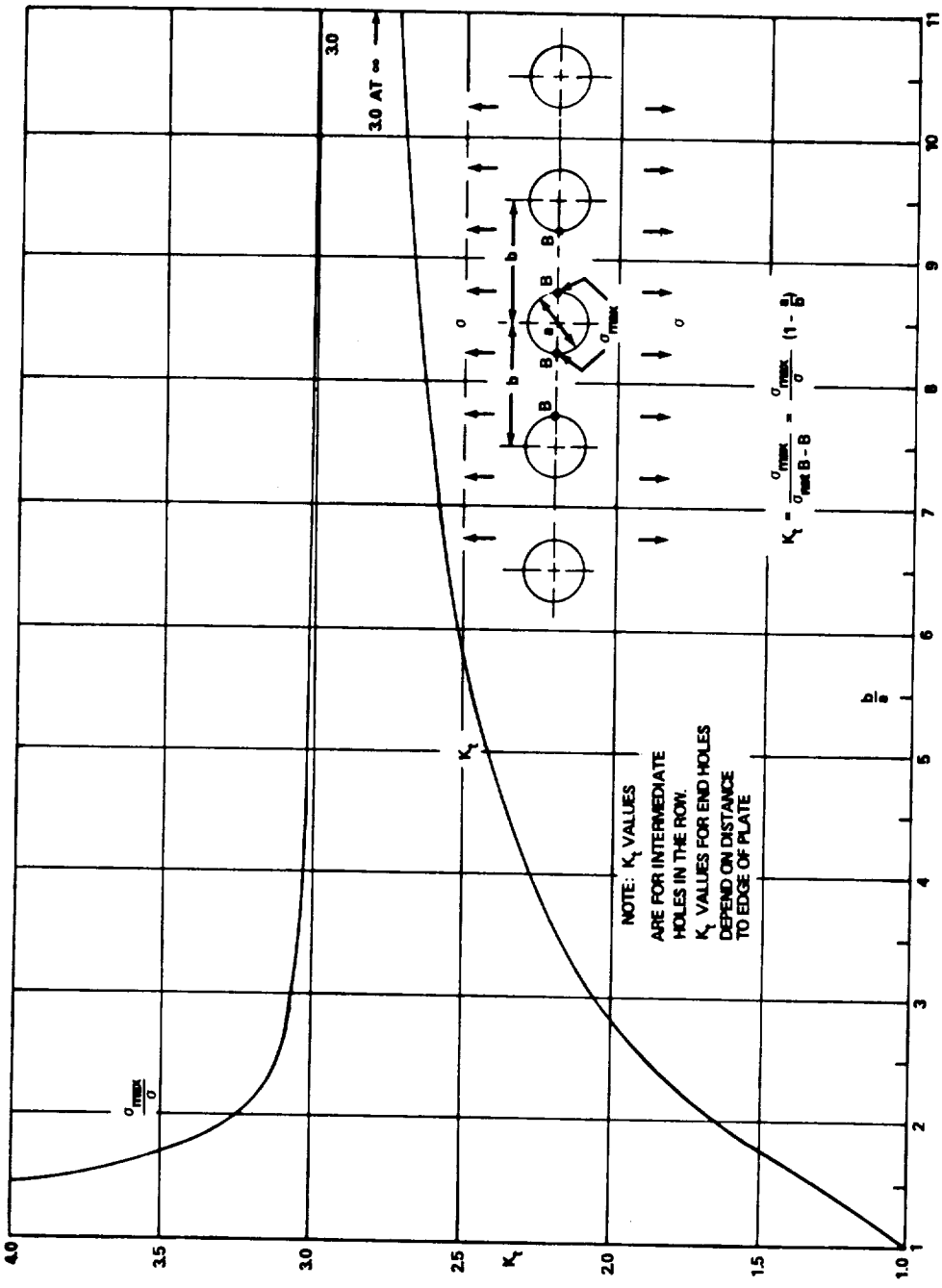

FIGURE B10-17. STRESS CONCENTRATION FACTOR, K_t, FOR TENSION CASE OF A SHEET WITH A SINGLE ROW OF HOLES. (TENSION PERPENDICULAR TO LINE OF HOLES.) K_t BASED ON NET SECTION.

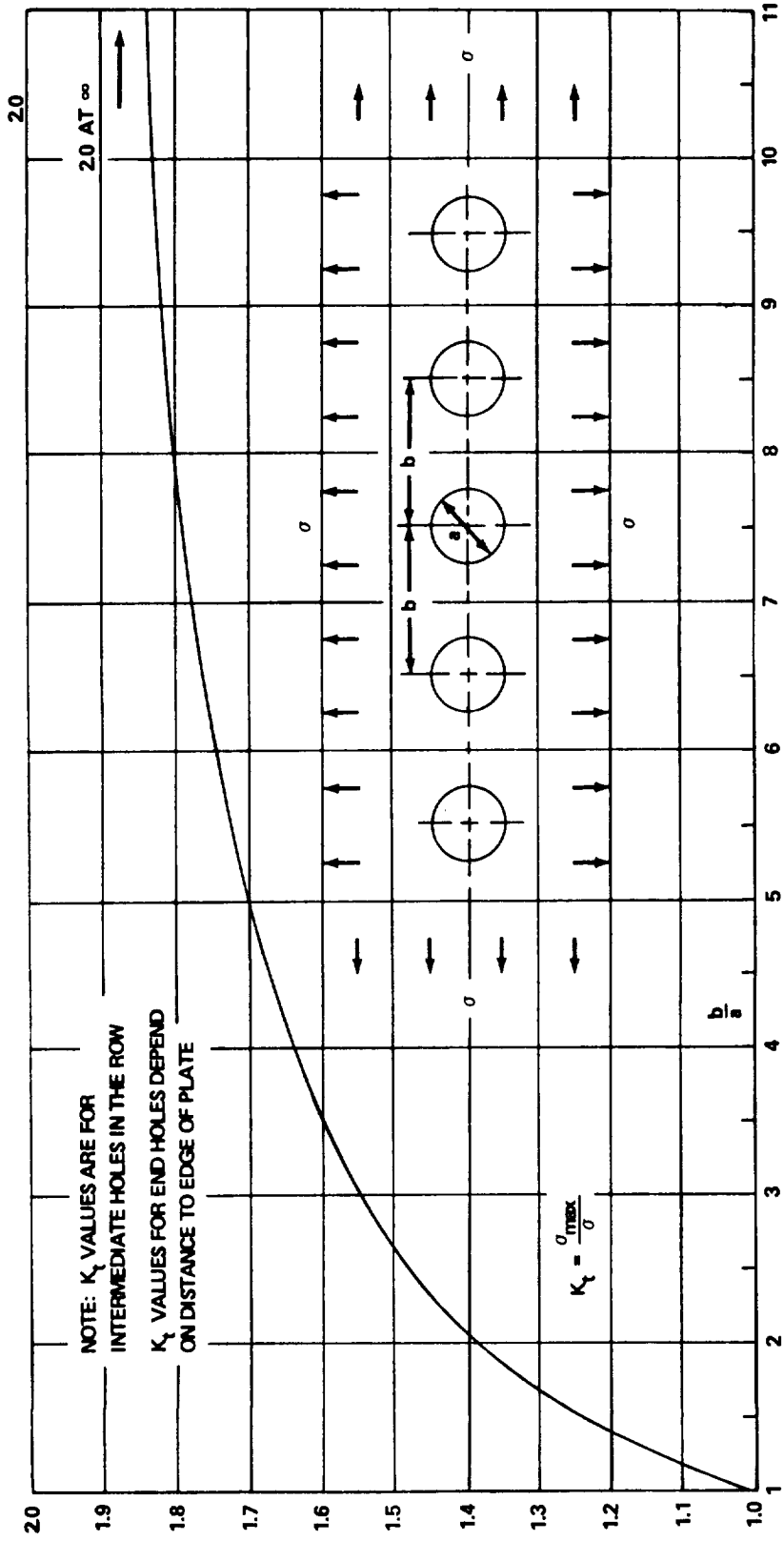

FIGURE B10-18. STRESS CONCENTRATION FACTOR, K_t, FOR A BIAXIALLY STRESSED INFINITELY WIDE PLATE CONTAINING A ROW OF HOLES.

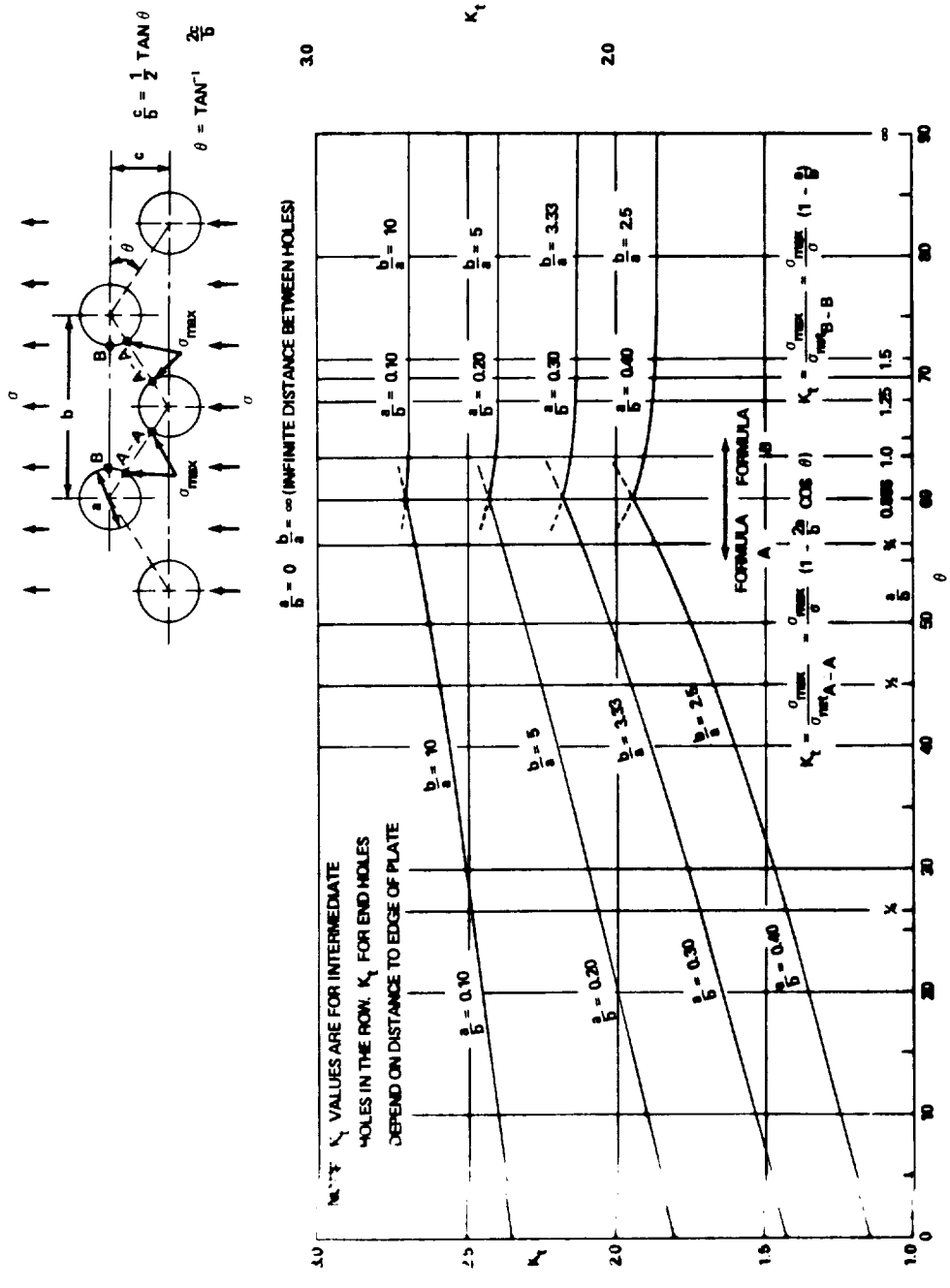

FIGURE B10-19. STRESS CONCENTRATION FACTOR, K_t, FOR TENSION CASE OF A SHEET WITH DOUBLE ROW OF HOLES. K_t BASED ON MINIMUM NET SECTION.

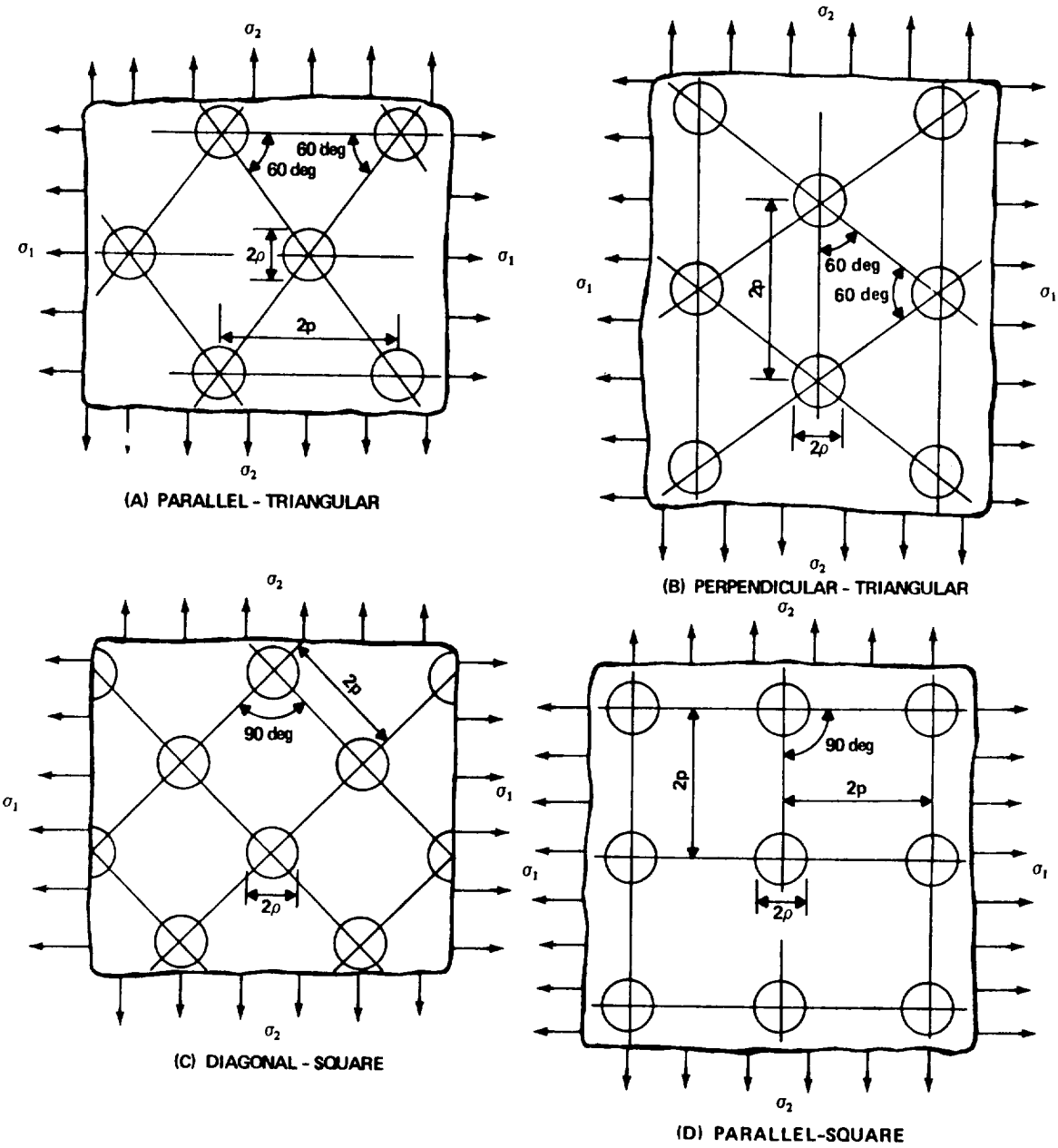

FIGURE B10-20. HOLE CONFIGURATIONS.

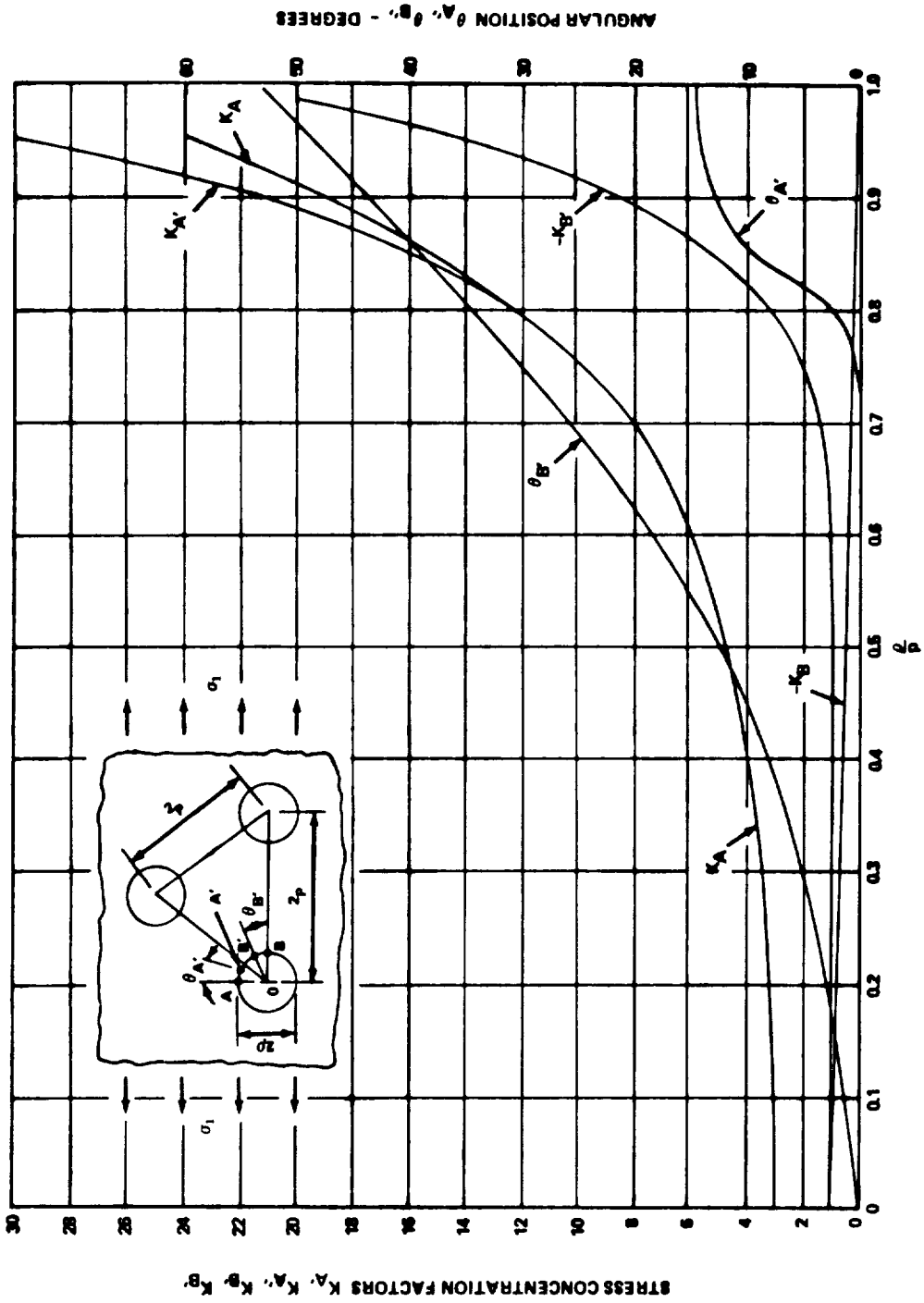

FIGURE B10-21. STRESS CONCENTRATION FACTORS FOR UNIAXIAL TENSION AND PARALLEL-TRIANGULAR HOLE CONFIGURATION.

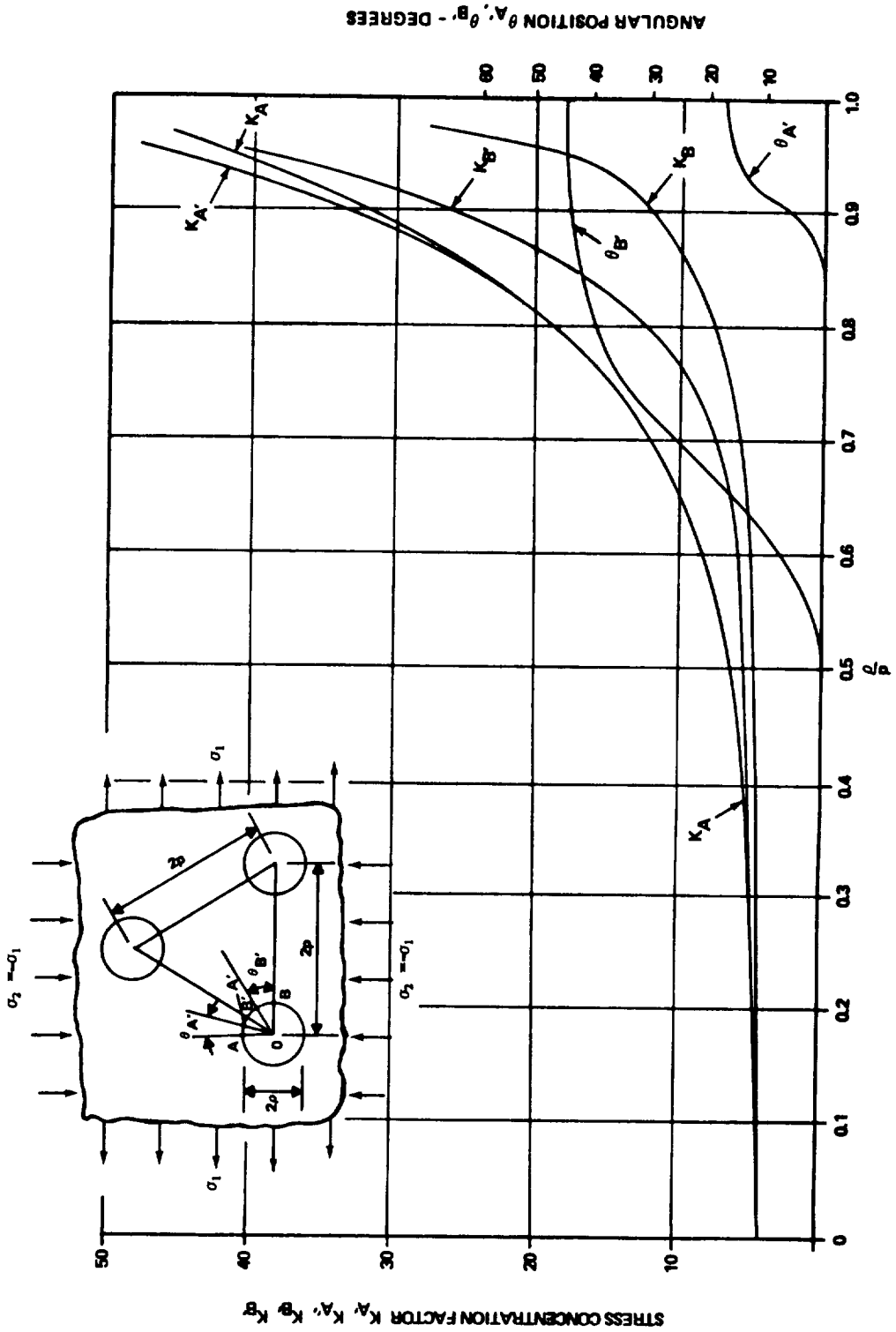

FIGURE B10-22. STRESS CONCENTRATION FACTORS FOR PURE SHEAR AND PARALLEL-TRIANGULAR HOLE CONFIGURATION.

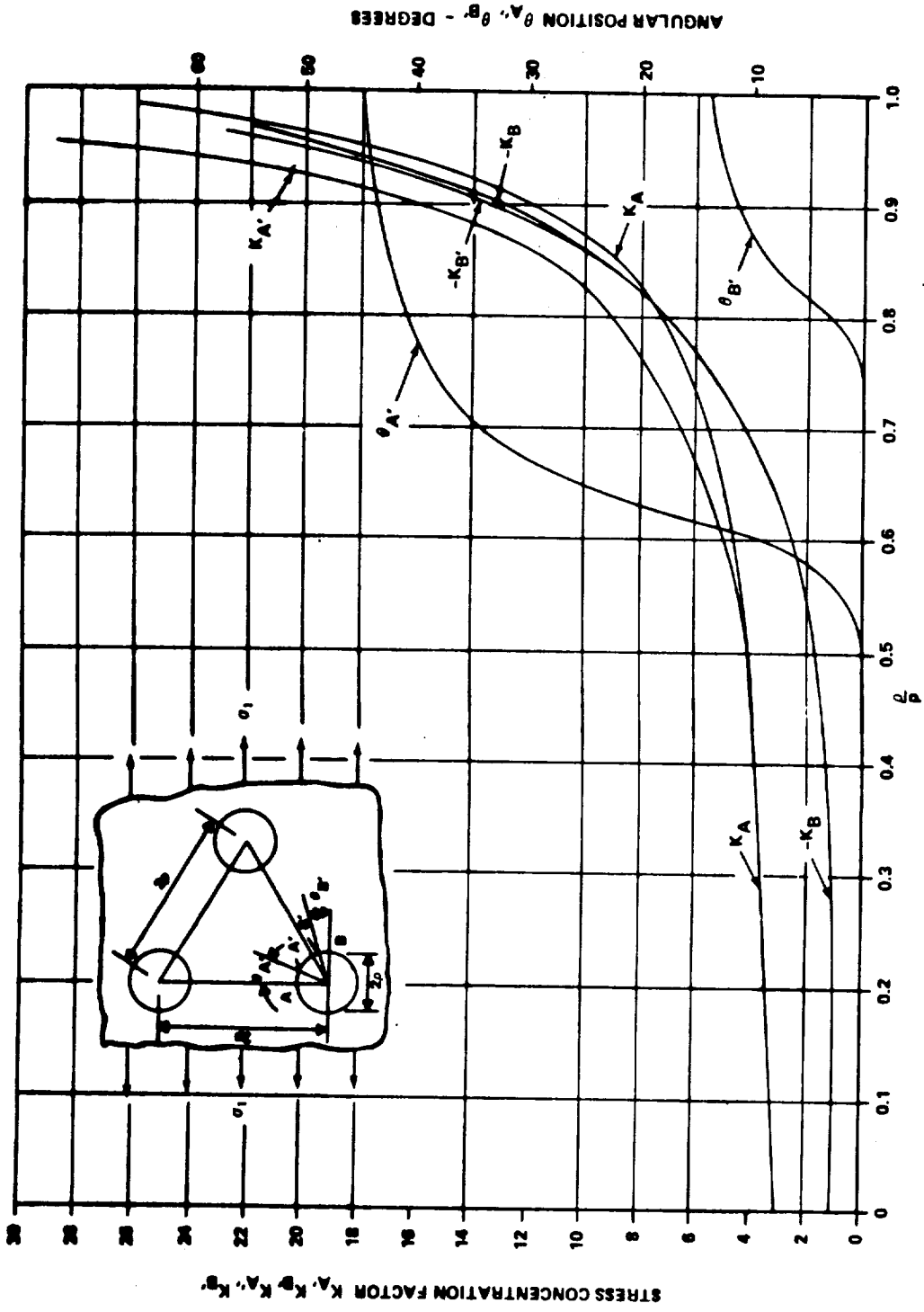

FIGURE B10-23. STRESS CONCENTRATION FACTORS FOR UNIAXIAL TENSION AND PERPENDICULAR-TRIANGULAR HOLE CONFIGURATION.

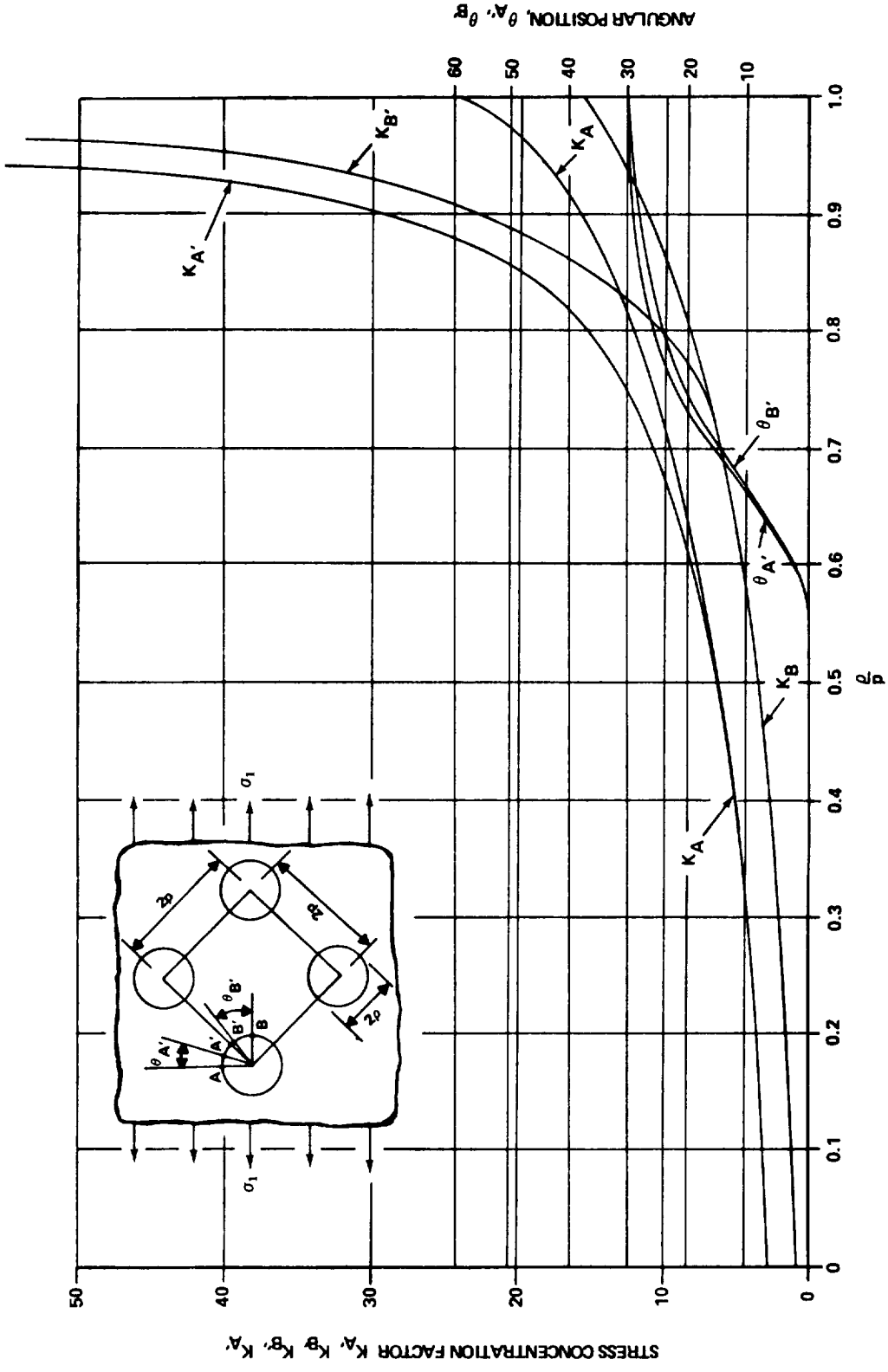

FIGURE B10-24. STRESS CONCENTRATION FACTORS FOR UNIAXIAL TENSION AND DIAGONAL-SQUARE HOLE CONFIGURATION.

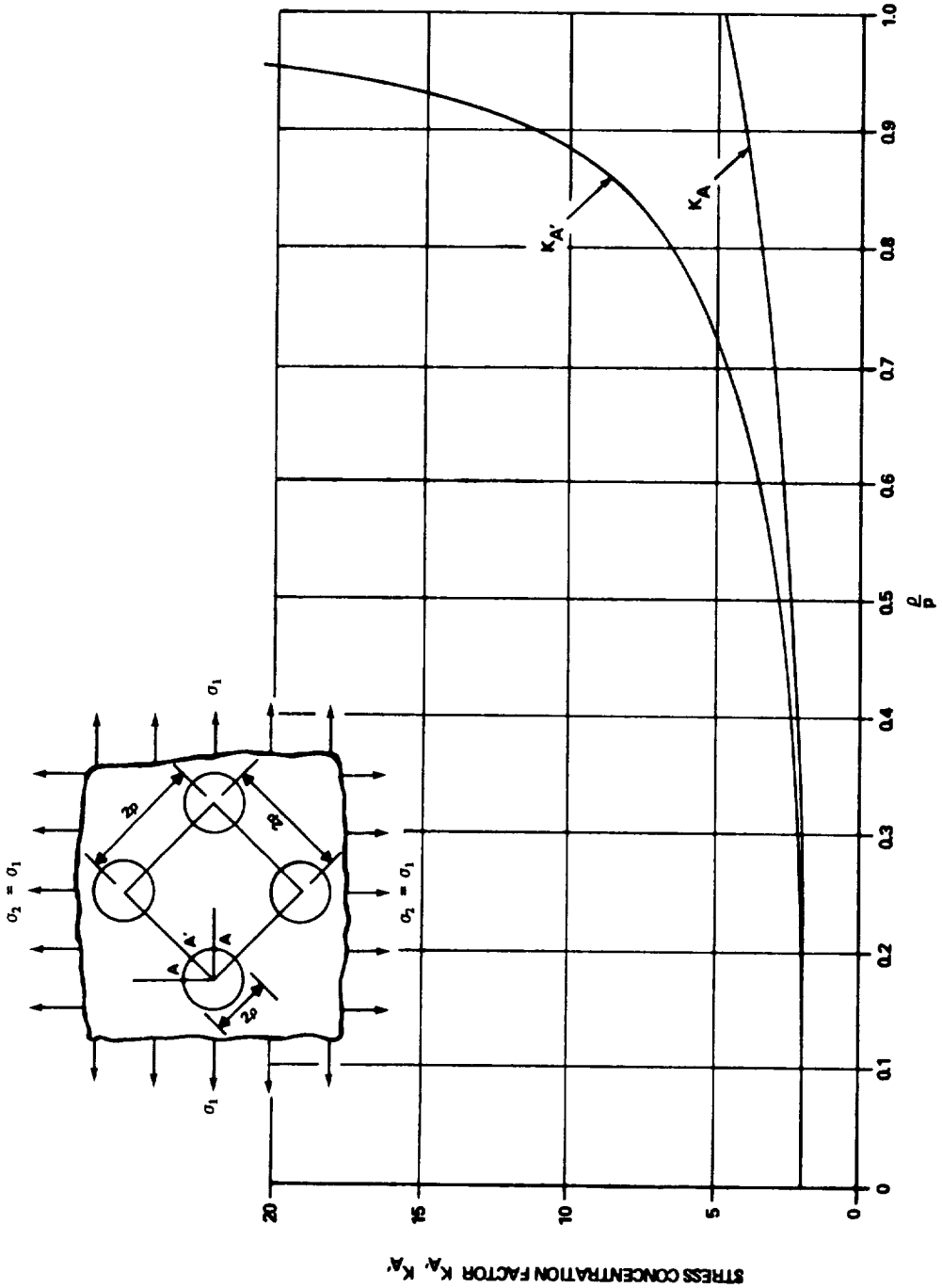

FIGURE B10-25. STRESS CONCENTRATION FACTORS FOR HYDROSTATIC TENSION FOR DIAGONAL-SQUARE HOLE CONFIGURATION.

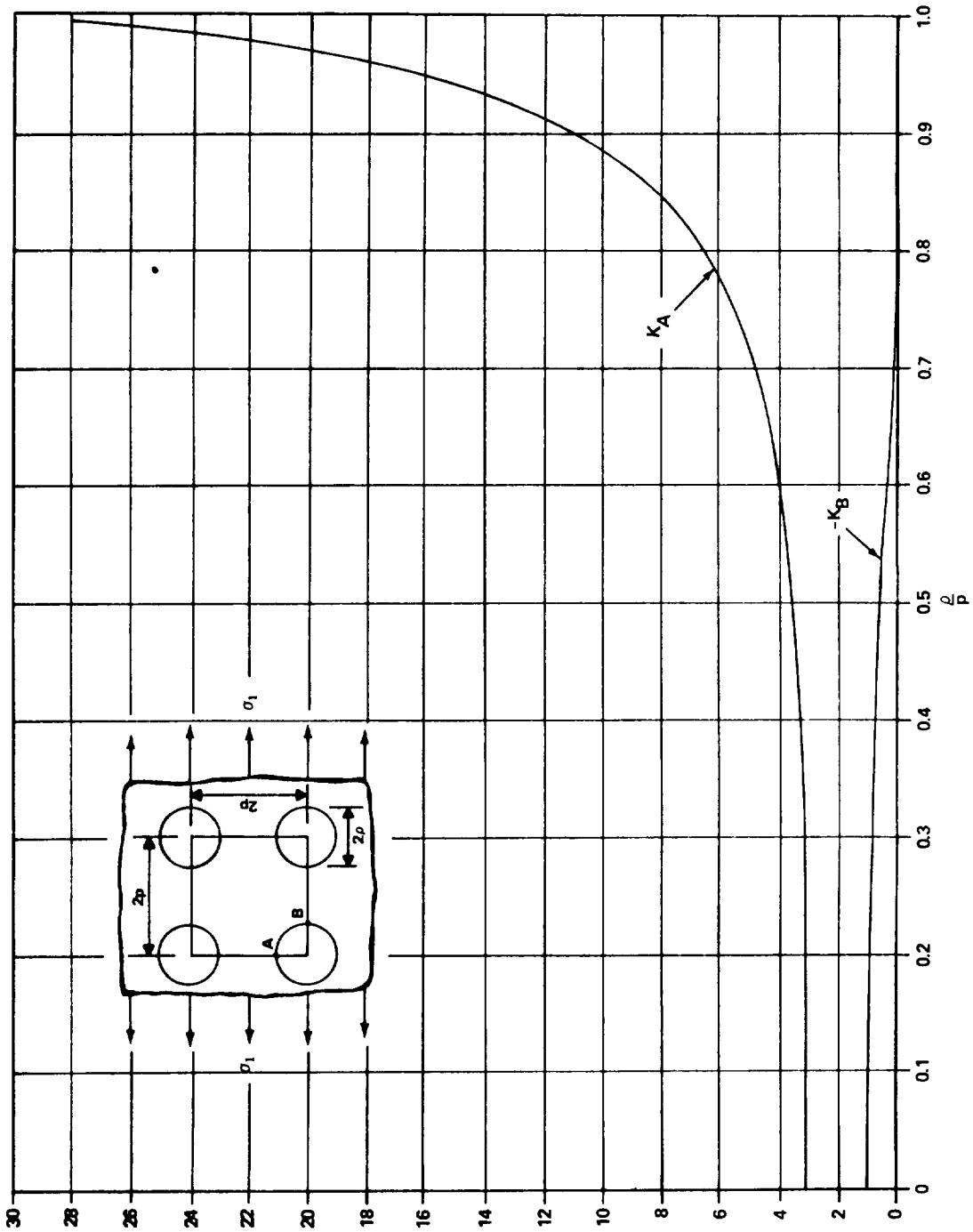

FIGURE B10-26. STRESS CONCENTRATION FACTORS FOR UNIAXIAL TENSION FOR PARALLEL-SQUARE HOLE CONFIGURATION.

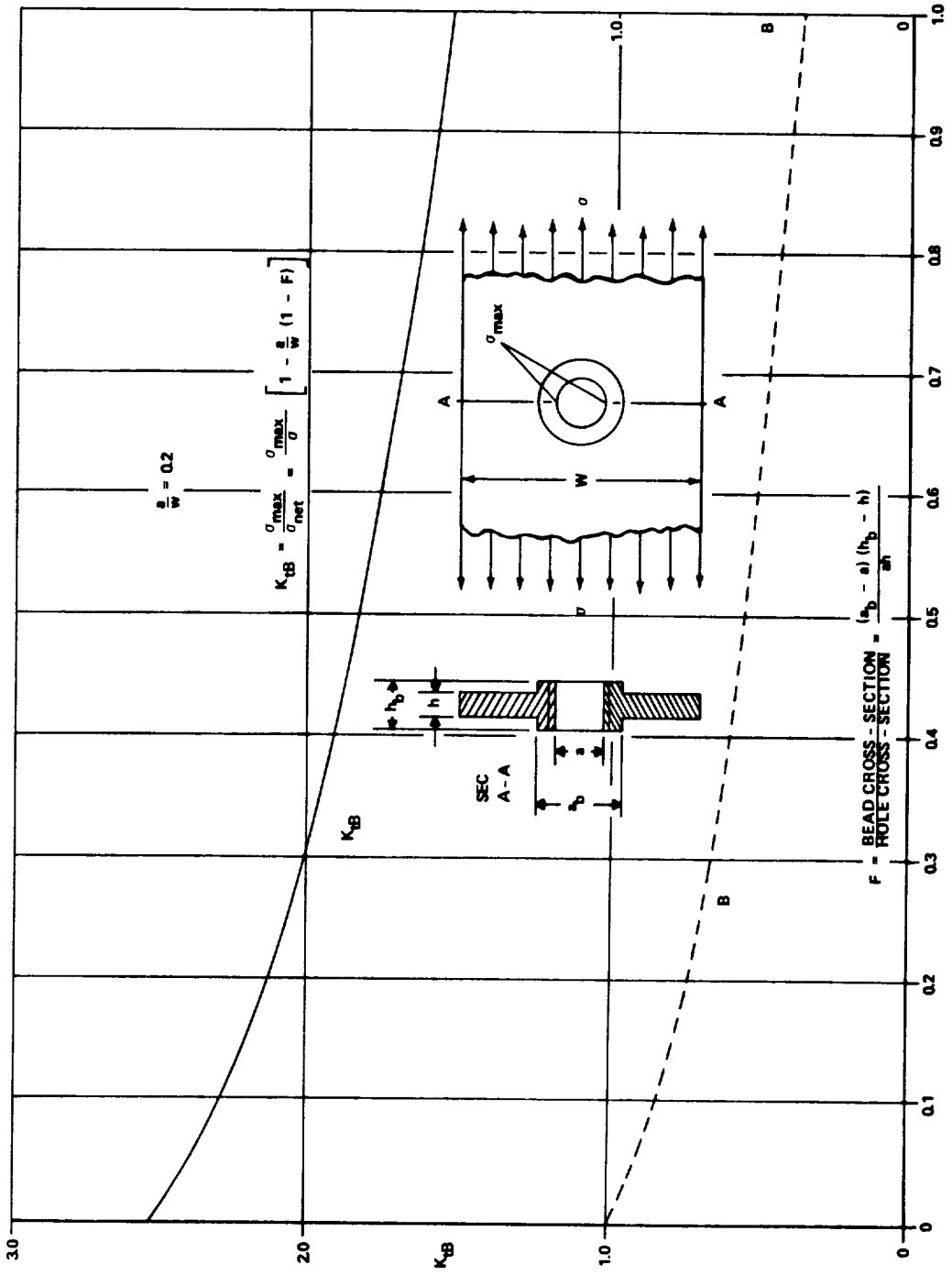

FIGURE B10-27. STRESS CONCENTRATION FACTOR, K_{tB}, FOR A TENSION PLATE WITH A BEADED HOLE.

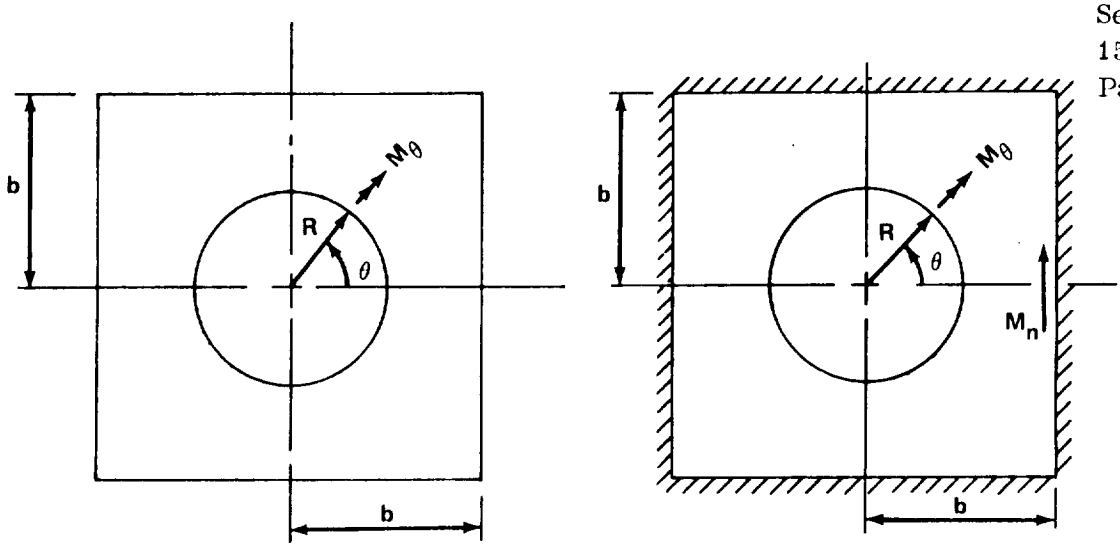

FIGURE B10-28. SQUARE PLATE WITH A CIRCULAR HOLE.

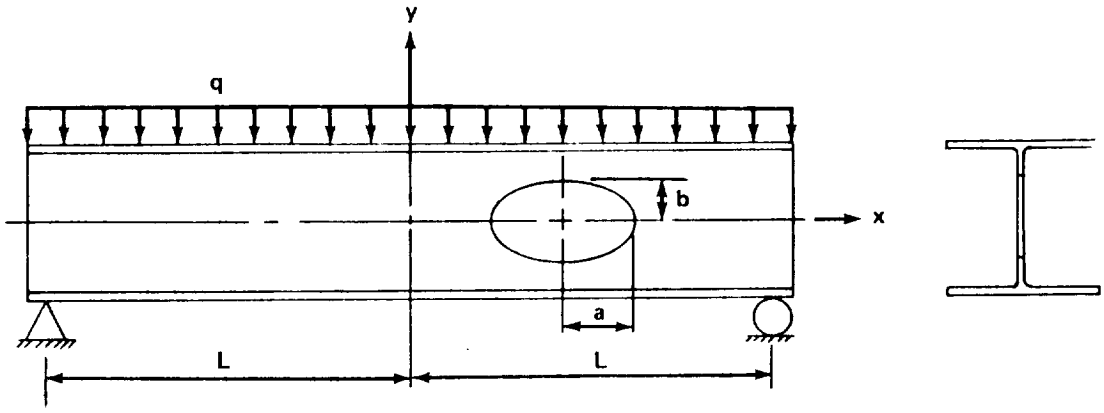

FIGURE B10-29. WIDE-FLANGE BEAM WITH A WEB HOLE.

BIBLIOGRAPHIES

Davies, G. A. O.: Stresses in a Square Plate Having a Central Circular Hole. Journal of the Royal Aeronautical Society, June 1965.

Hoddon, R. A. W.: Stresses in an Infinite Plate With Two Unequal Circular Holes. Quarterly Journal of Mechanics and Applied Mathematics, Vol. 20, Part 3, 1967.

Lerchenthal, C. H., and Talmor, R.: Reduction of Stress Concentration Near Circular Cutouts in a Tension Field Without Sheet Reinforcement.

Low, E. F., and Chang, W. F.: Stress Concentration Around Shaped Holes. Journal of the Engineering Mechanics Division, Proceedings of the American Society of Civil Engineers, June 1967.

Savin, G. N.: Elastic Stresses Around Holes in Wide-Flange Beams. Journal of the Structural Division, Proceedings of the American Society of Civil Engineers, April 1966.

REFERENCES

1. Sternberg, E., and Sadowsky, M. A.: Three-Dimensional Solution for the Stress Concentration Around a Circular Hole in a Plate of Arbitrary Thickness. Transactions of the ASME, Vol. 71, Applied Mechanics Section, 1949, p. 27.

2. Peterson, R. E.: Stress Concentration Design Factors. John Wiley and Sons, Inc., New York, 1959.

3. Durelli, A. J., Parks, V. J., and Feng, H. C.: Stresses Around an Elliptical Hole in a Finite Plate Subjected to Axial Loading. Journal of Applied Mechanics, Transactions of the ASME, March 1966.

4. Sobey, A. J.: Stress Concentration Factors for Rounded Rectangular Holes in Infinite Sheets. Royal Aircraft Establishment Report No. Structures 292, November 1963.

5. McKenzie, H. W., and White, D. J.: Stress Concentration Caused by an Oblique Round Hole in a Flat Plate Under Uniaxial Tension. Journal of Strain Analysis, Vol. 3, No. 2, 1968.

6. Ellyin, F., and Sherbourne, A. N.: Effect of Skew Penetration on Stress Concentration. Journal of the Engineering Mechanics Division, Proceedings of the ASCE, December 1968.

7. Salemo, V. L., and Mahoney, J. B.: Stress Solution for an Infinite Plate Containing Two Arbitrary Circular Holes Under Equal Biaxial Stresses. Journal of Engineering for Industry, Transactions of the ASME, November 1968.

REFERENCES (Continued)

8. Miyao, K.: Stresses in a Plate Containing a Circular Hole With a Notch. Journal of the JSME, Vol. 13, No. 58, 1970.

9. Nisida, M., and Shirota, Y.: Stress Concentration in a Plate due to Uniformly Spaced Circular Holes, Proceedings of the Fourteenth Japan National Congress for Applied Mechanics, 1965.

10. Davies, G. A. O.: Plate-Reinforced Holes. The Aeronautical Quarterly, February 1967.

11. Dhir, S. K.: Stresses Around Two Equal Reinforced Circular Openings in a Thin Plate. International Journal of Solids and Structures, Vol. 4, 1968.

12. Howard, I. C., and Morley, L. S. D.: The Stresses Around Holes in Plane Sheets. The Aeronautical Quarterly, November 1967.

13. Wittrick, W. H.: Analysis of Stress Concentration at Reinforced Holes in Infinite Sheets. The Aeronautical Quarterly, August 1960.

14. Hicks, R.: Asymmetrical Plate-Reinforced Circular Hole in a Uniformly End-Load Flat Plate. The Aeronautical Quarterly, May 1959.

15. Wittrick, W. H.: On the Axisymmetrical Stress Concentration at an Eccentrically Reinforced Circular Hole in a Plate. The Aeronautical Quarterly, February 1965.

REFERENCES (Concluded)

16. Hicks, R.: Variably Reinforced Circular Holes in Stressed Plates. The Aeronautical Quarterly, August 1958.

17. Hicks, R.: Reinforced Elliptical Holes in Stressed Plates. Journal of the Royal Aeronautical Society, October 1957.

18. Lo, C. C., and Leissa, A. W.: Bending of Plates With Circular Holes. Acta Mechanica, Vol. 4, No. 1, 1967.

19. Bower, J. F.: Elastic Stresses Around Holes in Wide-Flange Beams. Journal of the Structural Division, Proceedings of the American Society of Civil Engineers, April 1966.

20. Bruhn, E. F.: Analysis and Design of Flight Vehicle Structures. Tri-state Offset Company, Cincinnati, Ohio, 1965.

* U.S. Government Printing Office: 1972 — 745-386/4112 Region No. 4

SECTION C

STABILITY ANALYSIS

SECTION C1

COLUMNS

TABLE OF CONTENTS

C 1.0.0 COLUMNS

C 1.1.0 Introduction

In general, column failure may be classed under two headings:

(1) Primary failure (general instability)

(2) Secondary failure (local instability)

Primary or general instability failure is any type of column failure, whether elastic or inelastic, in which the cross-sections are translated and/or rotated but not distorted in their own planes. Secondary or local instability failure of a column is defined as any type of failure in which cross-sections are distorted in their own planes but not translated or rotated. However, the distinction between primary and secondary failure is largely theoretical because most column failures are a combination of the two types.

Fig. C 1.1.0-1 illustrates the curves for several types of column failure.

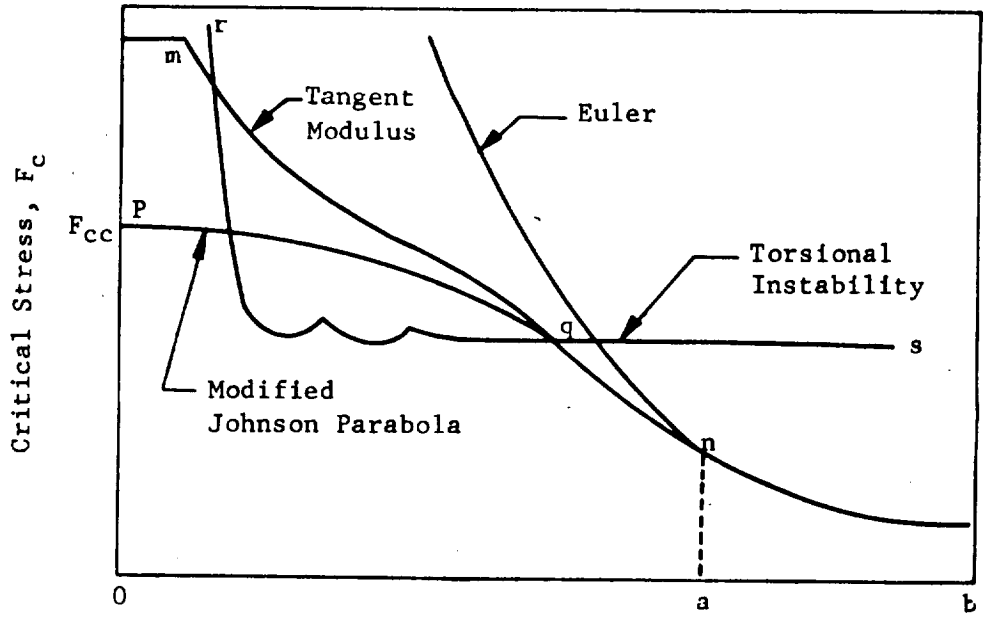

Fig. C 1.1.0-1

L' represents the effective length of the column and is dependent upon the manner in which the column is constrained, and ρ is the minimum radius of gyration of the cross-sectional area of the column.

For a value of L'/ρ in the range "a" to "b", the column buckles in the classical Euler manner. If the slenderness ratio, L'/ρ , is in

C 1.1.0 Introduction (Cont'd)

the range of "0" to "a", a column may fail in one of the three following ways:

(1) Inelastic bending failure. This is a primary failure described by the Tangent Modulus equation, curve mn. This type of failure depends only on the mechanical properties of the material.

(2) Combined inelastic bending and local instability. The elements of a column section may buckle, but the column can continue to carry load until complete failure occurs. This failure is predicted by a modified Johnson Parabola, "pq", a curve defined by the crippling strength of the section. At low values of L'/ρ the tendency to cripple predominates; while at L'/ρ approaching the point "q", the failure is primarily inelastic bending. Geometry of the section, as well as material properties, influences this combined type of failure.

(3) Torsional instability. This failure is characterized by twisting of the column and depends on both material and section properties. The curve "rs" is superimposed on Fig. C 1.1.0-1 for illustration. Torsional instability is presented in Section C 1.5.0.

These curves are discussed in detail in Sections C 1.3.0, C1.3.2, and C 1.5.0. For a given value of L'/ρ between (0) and (a), the critical column stress is the minimum stress predicted by these three failure curves.

Each of the Tangent Modulus curves has a cutoff stress at low L'/ρ values (point "m"). This cutoff stress has been chosen as $F_{0.2}$ for ductile material, and is the stress for which $E_t/E = 0.2$. E_t is the Tangent Modulus and E is the Modulus of Elasticity.

C 1.2.0 Long Columns (elastic buckling)

A column with a slenderness ratio (L'/ρ) greater than the critical slenderness ratio (point "a" Fig. C 1.1.0-1) is called a long column. This type of column fails through lack of stiffness instead of a lack of strength.

The critical column load, P_c, as given by the Euler formula for a pin ended column ($L' = L$) of constant cross section, is

$$P_c = \frac{\pi^2 EI}{(L)^2} \qquad \text{..... (1)}$$

where

E = Young's Modulus
I = Least moment of inertia
L = Length of the column

End conditions - The strength of a column is in part dependent on the end conditions; in other words, the degree of end-fixity or constraint. A column supported at the ends so that there can be neither lateral displacement nor change of slope at either end is called fixed-ended. A column, one end of which is fixed and the other end neither laterally supported nor otherwise constrained, is called free-ended. A column, both end-surfaces of which are flat and normal to the axis, and bear evenly against rigid loading surfaces, is called flat-ended. A column, the ends of which bear against transverse pins, is called pin-ended.

The critical load for long columns with various end conditions as shown in Fig. C 1.2.0-1 are:

$$\text{(a)}\quad P_c = \frac{\pi^2 EI}{4L_1^2} \qquad \text{..... (2)}$$

$$\text{(b)}\quad P_c = \frac{2.05\pi^2 EI}{L_2^2} \qquad \text{..... (3)}$$

$$\text{(c)}\quad P_c = \frac{4\pi^2 EI}{L_3^2} \qquad \text{..... (4)}$$

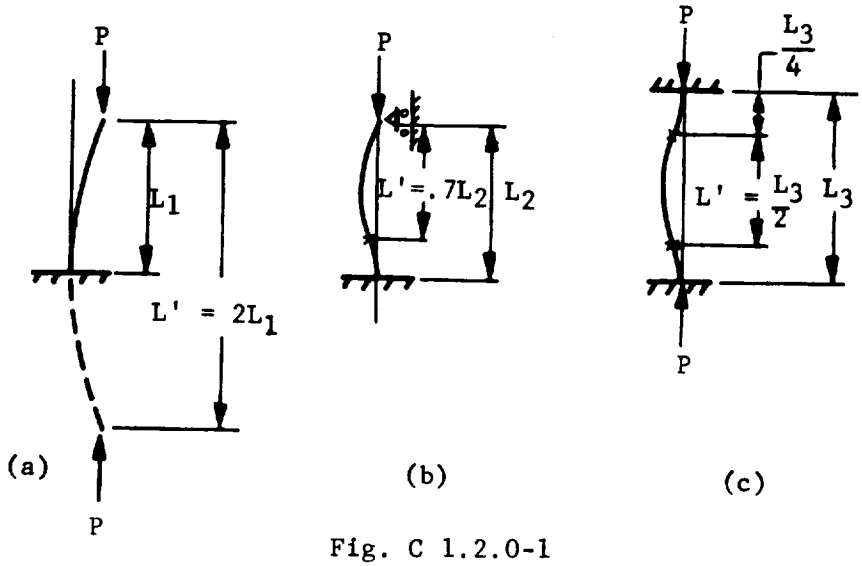

Fig. C 1.2.0-1

The effective column lengths L' for Fig. C 1.2.0-1 are $2L_1$, 0.7 L_2, and 0.5 L_3 respectively. For the general case, $L' = L/\sqrt{c}$, where c is a constant dependent on end restraints.

Fixity coefficients (c) for several types of elastically restrained columns are given in Figs. C 1.2.0-2 through C 1.2.0-4.

Limitations of the Euler Formulas. The elastic modulus (E) was used in the derivation of the Euler formulas. Therefore, all the reasoning is applicable while the material behaves elastically. To bring out this significant limitation, Eq. 1 will be written in a different form. By definition, $I = A\rho^2$, where A is the cross-sectional area and ρ is its radius of gyration. Substitution of this relation into Eq. 1 gives

$$P_c = \frac{\pi^2 EI}{(L')^2} = \frac{\pi^2 EA\rho^2}{(L')^2} \qquad \text{---------- (5)}$$

$$F_c = \frac{P_c}{A} = \frac{\pi^2 E}{\left(\frac{L'}{\rho}\right)^2} \qquad \text{---------- (6)}$$

The critical stress (F_c) for a column is defined as an average stress over the cross-sectional area of a column at the critical load (P_c).

C 1.2.0 Long Columns (Cont'd)

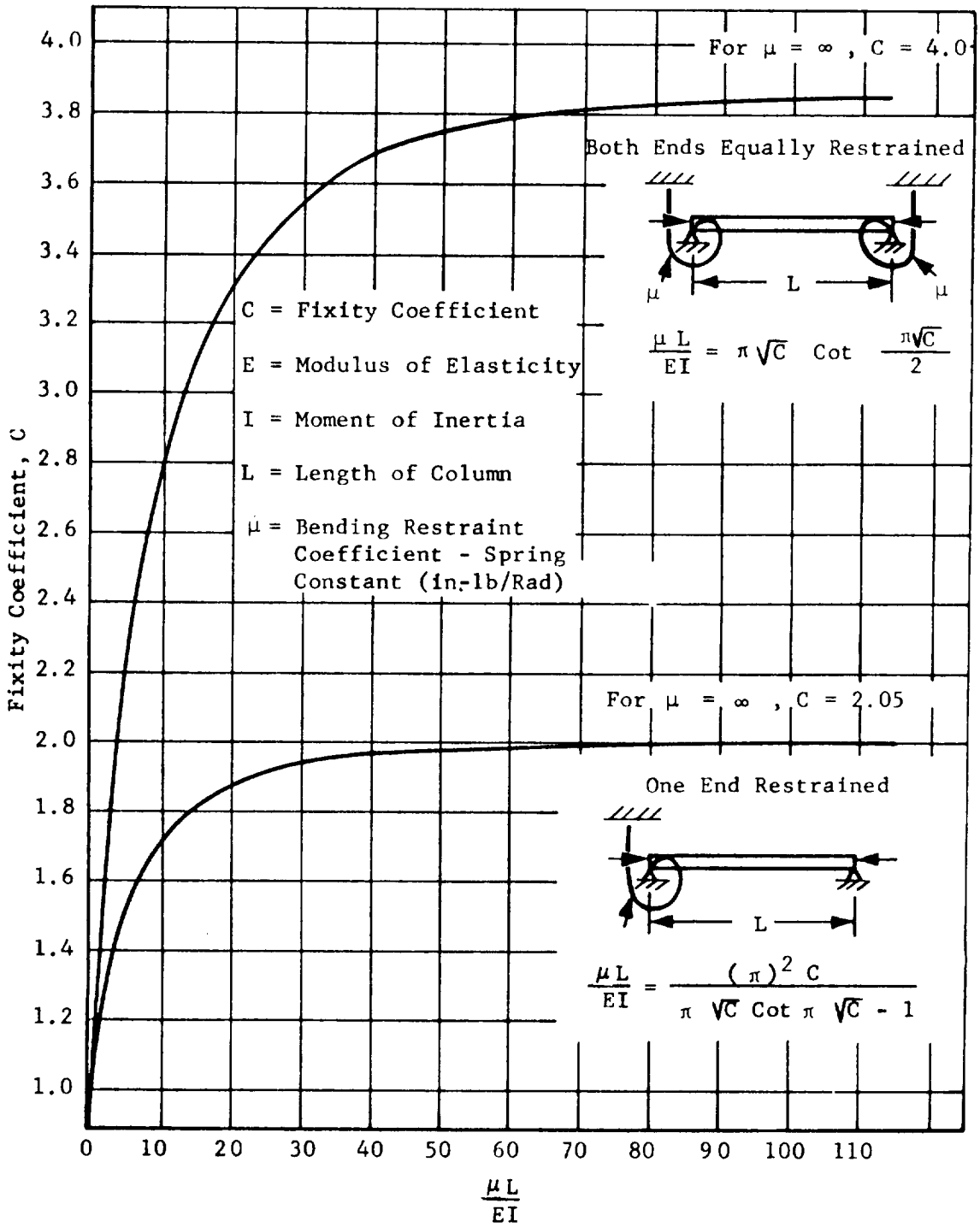

Fig. C1.2.0-2 Fixity Coefficient for a Column with End Supports Having a Known Bending Restraint

C 1.2.0 Long Columns (Cont'd)

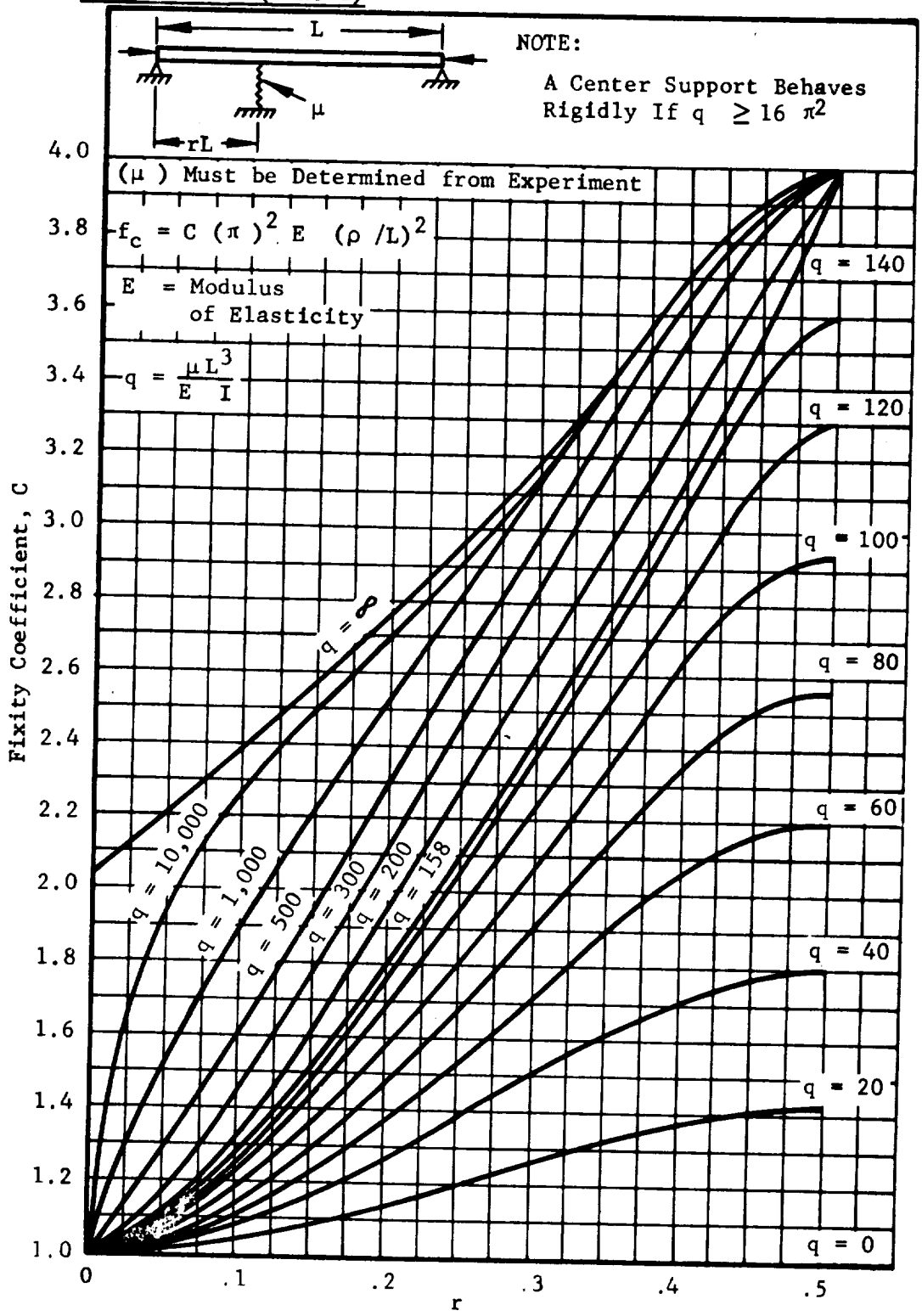

Fig. C1.2.0-3 Fixity Coefficient for a Column with Simply Supported Ends and an Intermediate Support of Spring Constant, μ

C 1.2.0 Long Columns (Cont'd)

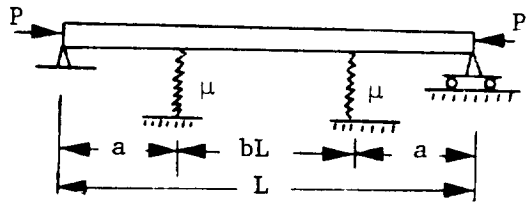

$$P_c = \frac{C\pi^2 EI}{L^2} \text{ or } f_c = \frac{C\pi^2 E}{(L/\rho)^2}$$

$$q = \frac{\mu L^3}{8EI}$$

Where (μ) = Spring Constant Which Is Equal To The Number of Pounds Necessary To Deflect The Spring One Inch Extrapolated to Zero Deflection.

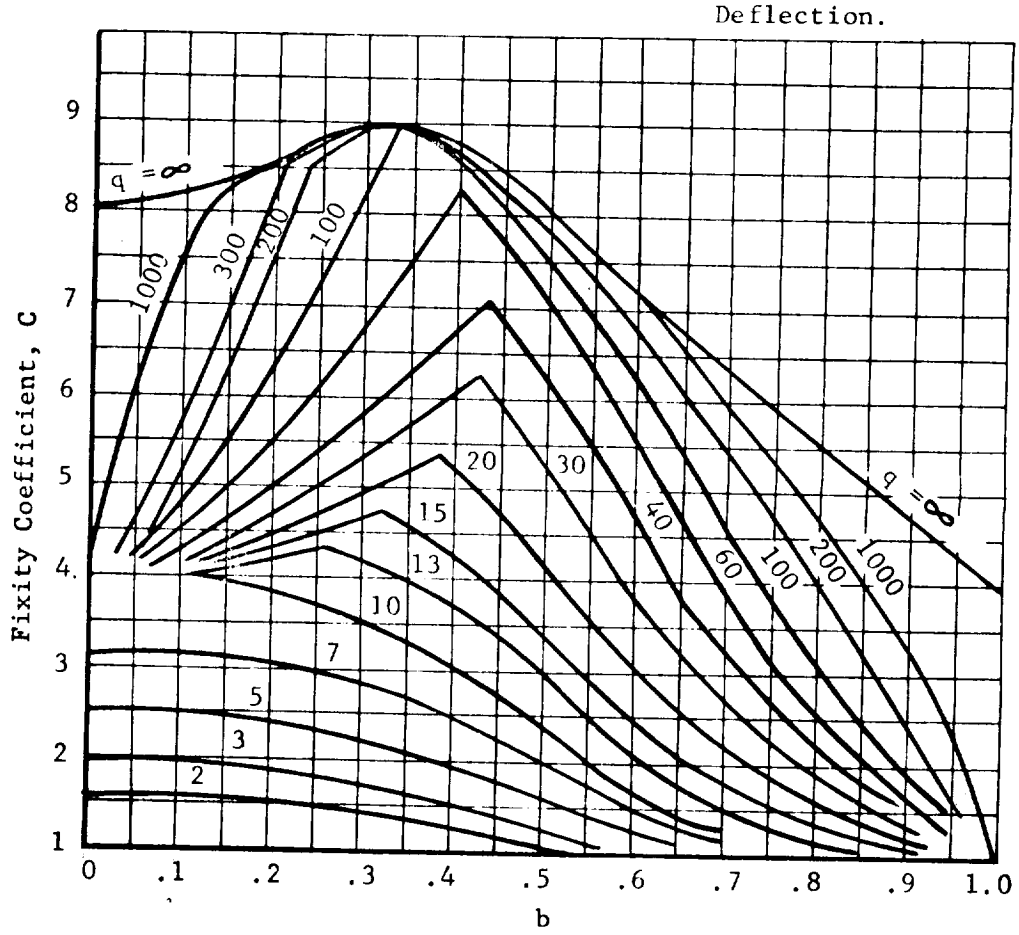

Fig. C1.2.0-4 Fixity of a Column with Two Elastic, Symmetrically Placed Supports Having Spring Constants, μ

C 1.3.0 Short Columns

Most columns fall into the range generally described as the short column range. With reference to Fig. C 1.1.0-1 of Section C 1.1.0, this may be described by $0 < L'/\rho < a$. This distinction is made on the basis that column behavior departs from that described by the classical Euler equation, Eq. (6). The average stress on the cross-section at buckling exceeds the stress defined by the proportional limit of the material. The slenderness ratio corresponding to the stress at the proportional limit defines the transition.

In the short column range a torsionally stable column may fail by crippling or inelastic bending, or a combination of both, as described in Sections C 1.3.1 and C 1.3.2.

C 1.3.1 Crippling Stress

When the corners of a thin-walled section in compression are restrained against any lateral movement, the corner material can continue to be loaded even after buckling has occurred in the section. When the stress in the corners exceeds its critical stress, the section loses its ability to support any additional load and fails. The average stress on the section at the failure load is called the crippling stress F_{cc}. Fig. C 1.3.1-1a shows the cross-sectional distortion occurring over one wave length in a typical thin-walled section. Fig. C 1.3.1-1b shows the stress distribution over the cross-section just before crippling.

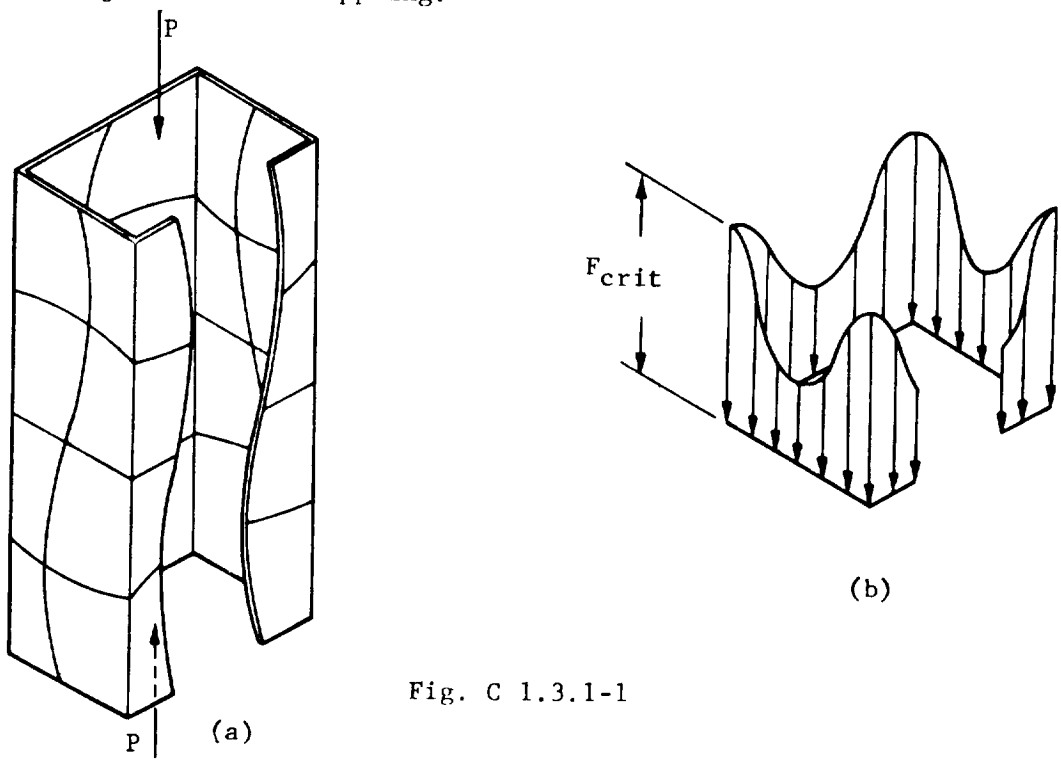

Fig. C 1.3.1-1

The empirical method for predicting the crippling stress of extruded and sheet metal elements is presented in this section. This crippling stress, F_{cc}, applies to extremely short column lengths and indicates the beginning of short column failure. It constitutes the column cut-off stress for sections composed of thin elements.

The crippling load of a member is equal to the product of the crippling stress and the actual area of the member; however, in calculating the crippling stress, the summation of the element areas is not equal to the actual area of the member.

A common structural component is composed of an angle, tee, zee, etc. attached to a thin skin. The buckling stress of the skin panel is less than the crippling stress of the stiffener. Taking a thin

C 1.3.1 Crippling Stress (Cont'd)

panel plus angle stiffeners at spacing, b, as shown on Fig. C 1.3.1-2, apply a compressive load. Up to the critical buckling load for the skin, the direct compressive stress is uniformly distributed. After the skin buckles, the central portion of the plate can carry little or no additional load; however, the edges of the plate, being restrained by the stiffeners, can and do carry an increasing amount of load. The stress distribution is shown in Fig. C 1.3.1-2.

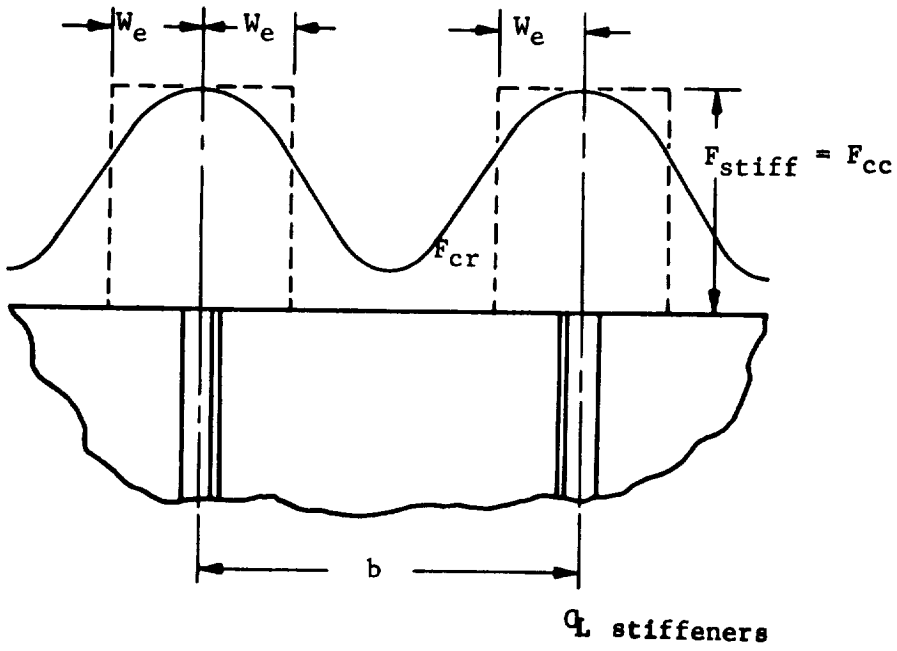

Fig. C 1.3.1-2

For the purpose of analysis, the true stress distribution shown by the solid line in Fig. C 1.3.1-2 is replaced by a uniform distribution as shown by the dotted lines. Essentially, an averaging process is used to determine the effective width, W_e, in which the stress, F_{cc}, is held constant.

Notation

F_{cc} = the crippling stress of a section.
f_{ccn} = the crippling stress of an element.
b_n = effective width of an element.
b_{fn} = flat portion of effective width of an element.
t_n = thickness of an element.
R = bend radius of formed stiffeners measured to the centerline.
R_b = extruded bulb radius.
W_e = effective width of skin.
E = Modulus of Elasticity.

C 1.3.1 Crippling Stress (Cont'd)

Use of the crippling curves

I. The crippling stress, F_{cc}, at a stiffener is computed by the following expression

$$F_{cc} = \frac{\Sigma b_n t_n f_{ccn}}{\Sigma b_n t_n} \qquad \text{..... (1)}$$

II. The method for dividing formed sheet and extruded stiffeners into elements is shown in Fig. C 1.3.1-3.

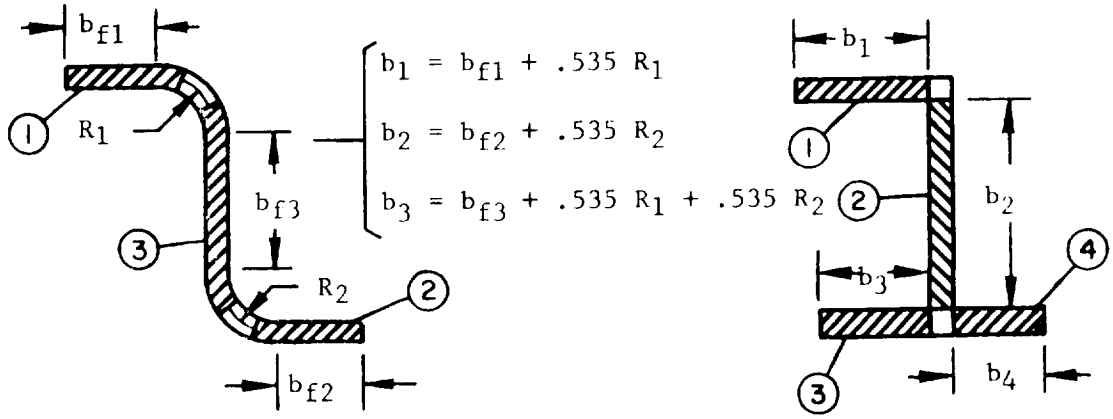

Fig. C 1.3.1-3

III. Angle stiffeners have low crippling stresses as each leg is in the one-edge-free condition and offers little support to the other leg. The method of dividing such stiffeners into effective elements is shown in Fig. C 1.3.1-4.

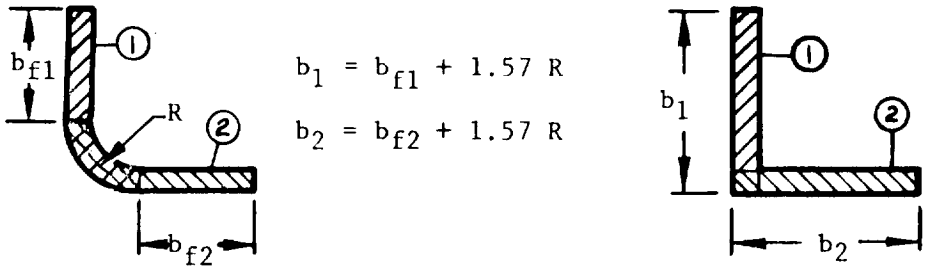

Fig. C 1.3.1-4

C 1.3.1 Crippling Stress (Cont'd)

IV. Certain types of formed stiffeners, as shown in **Figures** C 1.3.1-5, C 1.3.1-6, and C 1.3.1-7, whose radii are equal and **whose** centers are on the same side of the sheet, require special consideration. Table C 1.3.1-1 explains the handling of these cases.

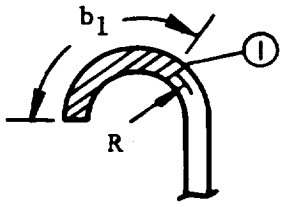

Fig. C 1.3.1-5

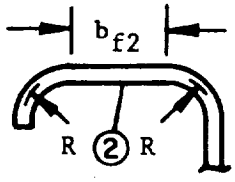

Fig. C 1.3.1-6

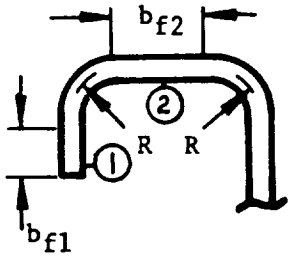

Fig. C 1.3.1-7

When b_{f2}	And b_{f1}	As shown in Fig.	Use
= 0	= 0	C 1.3.1-5	b_1 = 2.10R (one edge free)
< R	= 0	C 1.3.1-6	b_2 = 2.10R (one edge free)
≥ R	= 0	C 1.3.1-6	$b_2 = b_{f2}$ + 1.07R (Avg. one & no edge free)
< R	< R	C 1.3.1-7	b_2 = 2.10R (one edge free, neglect b_1)
≥ R	< R	C 1.3.1-7	$b_2 = b_{f2}$ + 1.07R (Avg. one & no edge free, neglect b_1)
≥ 0	≥ R	C 1.3.1-7	$b_1 = b_{f1}$ + 1.07R (one edge free) $b_2 = b_{f2}$ + 1.07R (no edge free)

Table C 1.3.1-1

V. Special conditions for extrusions

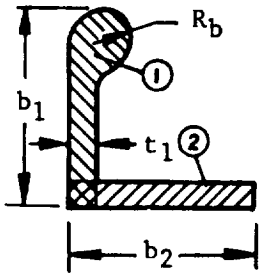

(a)

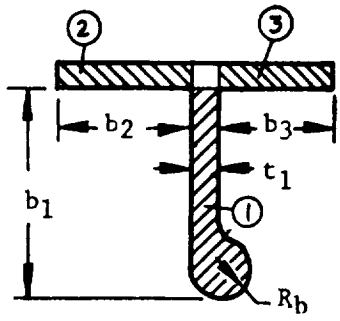

(b)

Fig. C 1.3.1-8

The crippling stress of an outstanding leg with bulb is 0.7 of the value for the no-edge-free condition if R_b is greater than or equal to the thickness of the adjacent leg (t_1 Fig. C 1.3.1-8). When $R_b < t_1$, the outstanding leg shall be considered as having one edge free.

C 1.3.1 Crippling Stress (Cont'd)

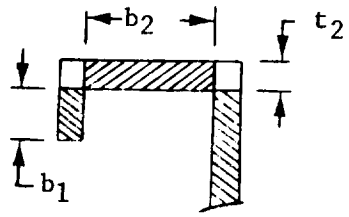

Fig. C 1.3.1-9

for $b_1 > t_2$ and $\leq 3t_2$ neglect b_1; and F_{cc2} = Avg. of no edge free and one edge free.

for $b_1 > 3t_2$ Regular method.

VI. The effective width of sheet, in a sheet-stiffener combination under compression, is determined from the plot of $2W_e/t$ versus f_{stiff} (Fig. C 1.3.1-12).

Note the following special cases

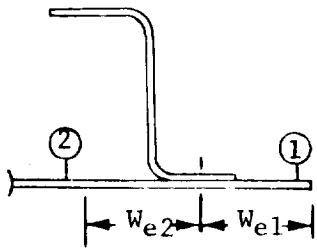

One-Edge-Free Sheet

Fig. C 1.3.1-10

one edge free

$$\frac{W_{e1}}{t} = .382\left(\frac{2W_e}{t}\right)_{\text{chart}} \text{ (no edge free)}$$

no edge free

$$\frac{2W_{e2}}{t} = \left(\frac{2W_e}{t}\right)_{\text{chart}}$$

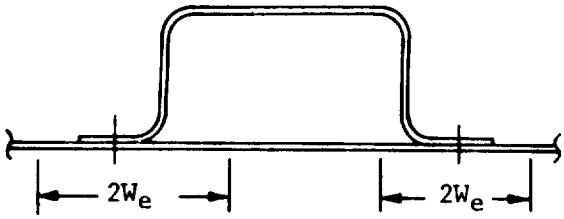

Effective Sheet with Large Hat Stiffener

Fig. C 1.3.1-11

(a) If effective widths overlap, reduce accordingly.

(b) Calculate as one or no edge free as necessary.

C 1.3.1 Crippling Stress (Cont'd)

Effective width of stiffened sheet.

The effective width, (W_e), is the width of skin on either or both sides of the stiffener acting at the stiffener stress level. This stress level for the skin is obtainable only if there is no inter spot-weld, or inter rivet buckling.

For calculating the effective width of sheet acting with the stiffener the following equation is graphed on Fig. C 1.3.1-12

$$\frac{2W_e}{t} = \frac{K\ (E_s)\ \text{skin}}{\sqrt{(E_s)\ \text{stiff}}} \sqrt{\frac{1}{f_{stiff}}} \qquad \ldots\ldots\ldots\ldots\ldots\ldots\ (2)$$

Where

W_e = effective width of skin (in.)
t = thickness of skin (in.)
E_s = secant modulus at stress level of stiffener (ksi)
f = stress (KSI)
K = 1.7 for simply supported case (no edge free)
K = 1.3 for one edge free.

For a sheet-stiffener combination of the same material, Eq. 2 becomes

$$\frac{2W_e}{t} = K \sqrt{\frac{E_s}{f_{stiff}}} \qquad \ldots\ldots\ldots\ldots\ldots\ldots\ (3)$$

The procedure for determining the crippling stress for a sheet-stiffener compression panel is

(1) Determine approximate stress level of stiffener.

$$f_{stiff} = \frac{\text{Load}}{\text{Area}} = \frac{P}{A_{stiff}}$$

(2) Determine (W_e) by using f_{stiff} and Fig. C 1.3.1-12. This procedure is not applicable if the sheet is subjected to inter spot-weld or inter rivet buckling.

(3) The crippling stress for the composite section is then calculated by Eq. 1.

C 1.3.1 Crippling Stress (Cont'd)

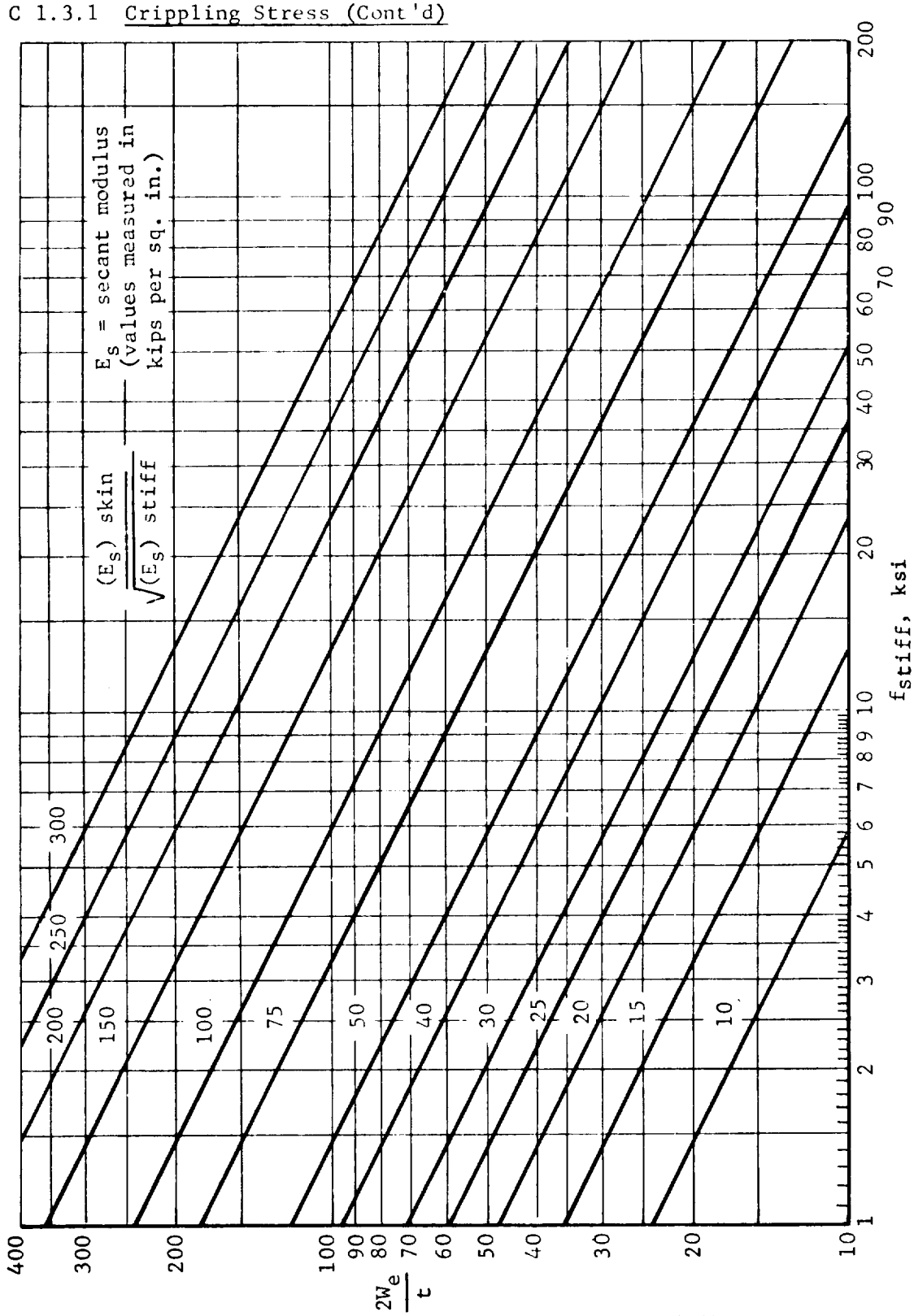

Fig. C1.3.1-12a Effective Width of Stiffened Sheet

C 1.3.1 Crippling Stress (Cont'd)

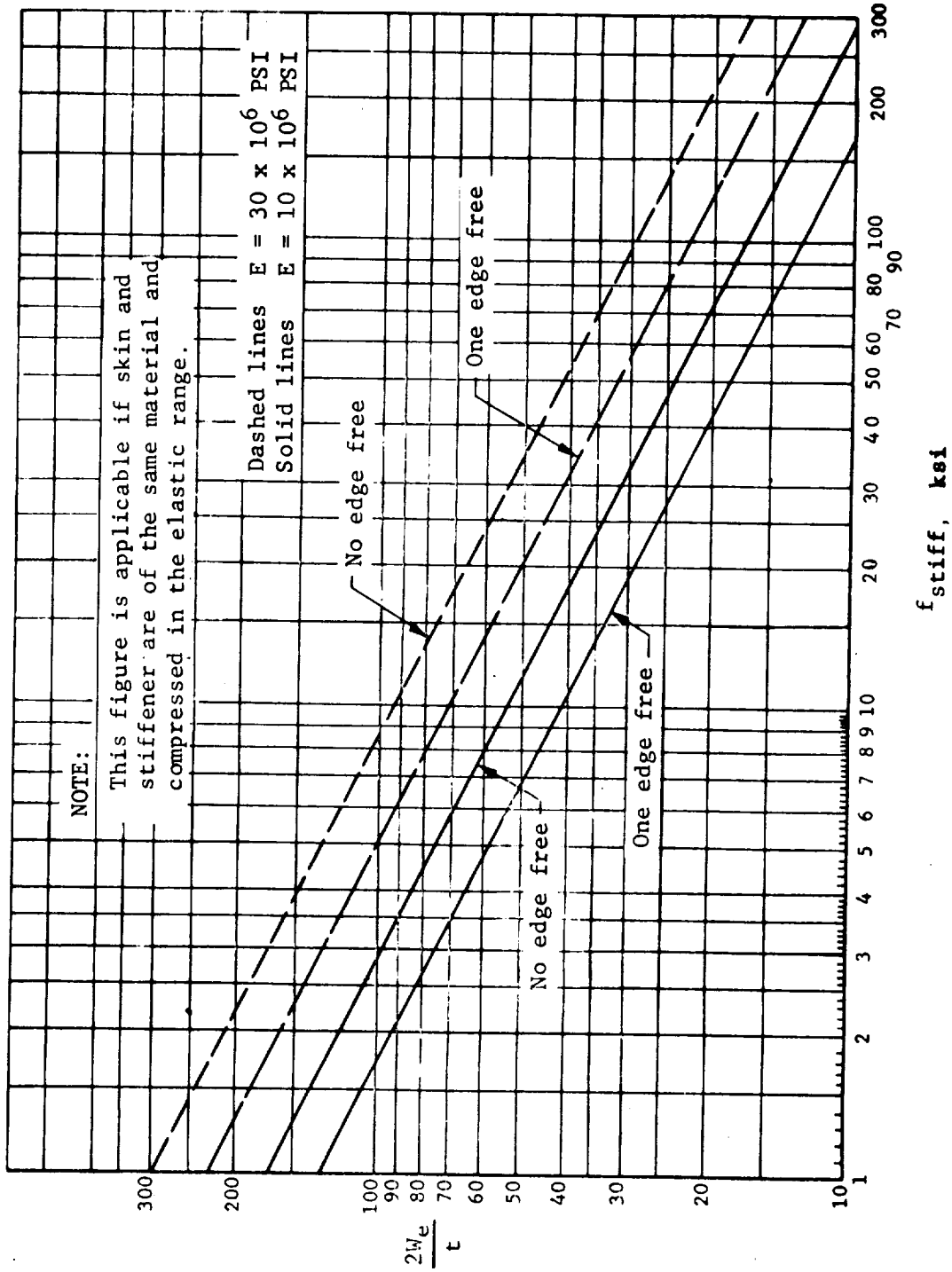

Fig. C 1.3.1-12b Effective Width of Stiffened Sheet

C 1.3.1 Crippling Stress (Cont'd)

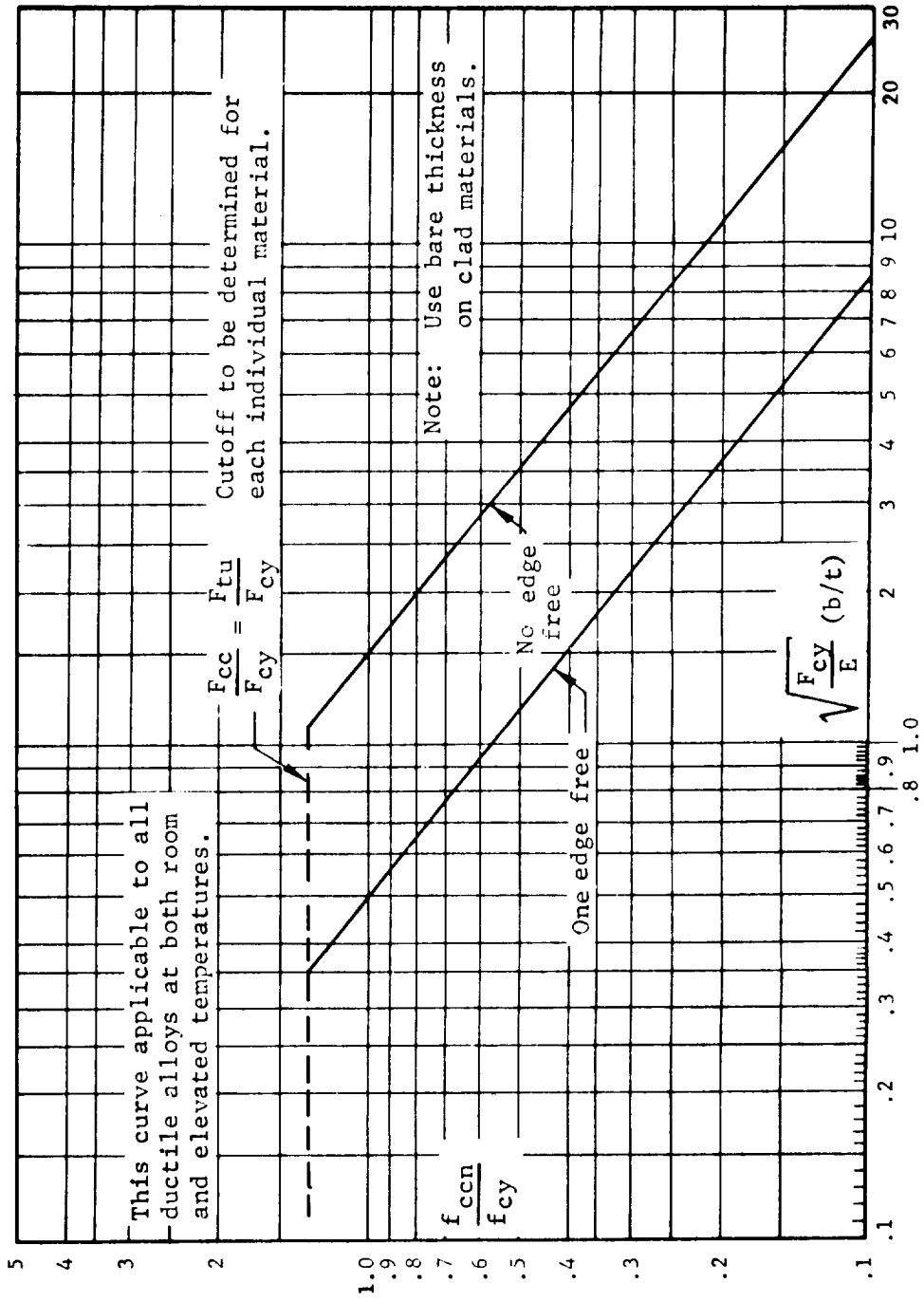

Fig. C 1.3.1-13 Nondimensional Crippling Curves

C 1.3.2 Column Curve for Torsionally Stable Sections

The column curves in Fig. C 1.3.2-3 are presented for the determination of the critical column stress for torsionally stable sections. The modes of failure are discussed in sections C 1.2.0 and C 1.3.0.

These curves are Euler's long column curve and Johnson's modified 2.0 parabolas. They are to be used to determine the critical stress, F_c, for columns at both room and elevated temperatures. It is noted that the modulus of elasticity, E, corresponds to the temperature at which the critical stress is desired.

The following sample problem is used to illustrate the use of Fig. C 1.3.2-3 to determine the critical stress, F_c.

Illustrative problem

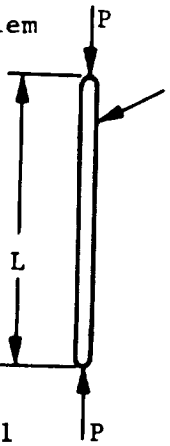

Fig. C 1.3.2-1

6061-T6 Square tubing 3.00 x .065

L = 60 inches (pin ended)
Temperature, T = 500° F (exposed ½ hr)

$E = 7.9 \times 10^6$ psi @ 500° F
F_{cy} = 26.6 ksi @ 500° F
ρ = 1.730 in.

Determine the critical stress for the column.

Solution

Determine the crippling stress of the section by the method outlined in Section C 1.3.1.

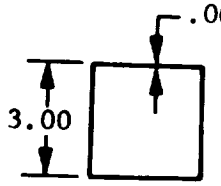

Fig. C 1.3.2-2

b = 3 - .065 = 2.935 (Center line values used here)

t = .065

$$\frac{b}{t}\sqrt{\frac{F_{cy}}{E}} = \left(\frac{2.935}{.065}\right)\sqrt{\frac{26.6 \times 10^3}{7.9 \times 10^6}} = 2.62$$

From Fig. C 1.3.1-13

$$\frac{f_{ccn}}{f_{cy}} = .64$$

C 1.3.2 Column Curve for Torsionally Stable Sections (Cont'd)

Use Eq. 1 Section C 1.3.1

$$\frac{F_{cc}}{F_{cy}} = \frac{\Sigma f_{ccn} b_n t_n}{F_{cy} \Sigma b_n t_n} = \frac{4(.64)\ (2.935)\ (.065)}{4(2.935)\ (.065)} = .64$$

$$F_{cc} = .64(26.6) = 17{,}030 \text{ psi}$$

The critical stress for the column is obtained from Fig. C 1.3.2-3.

$$\frac{F_{cc}}{E} = \frac{17{,}030}{7.9 \times 10^6} = 2.16 \times 10^{-3}$$

For pin-ended column

$$L = L' = 60 \text{ in.}$$

$$\frac{L'}{\rho} = \frac{60}{1.73} = 34.7$$

Then from Fig. C 1.3.2-3

$$\frac{F_c}{E} = 2.02 \times 10^{-3}$$

Giving a critical stress of

$$F_c = 2.02 \times 10^{-3}\ (7.9 \times 10^6) = 15{,}960 \text{ psi}$$

C 1.3.2 Column Curves for Torsionally Stable Columns (Cont'd)

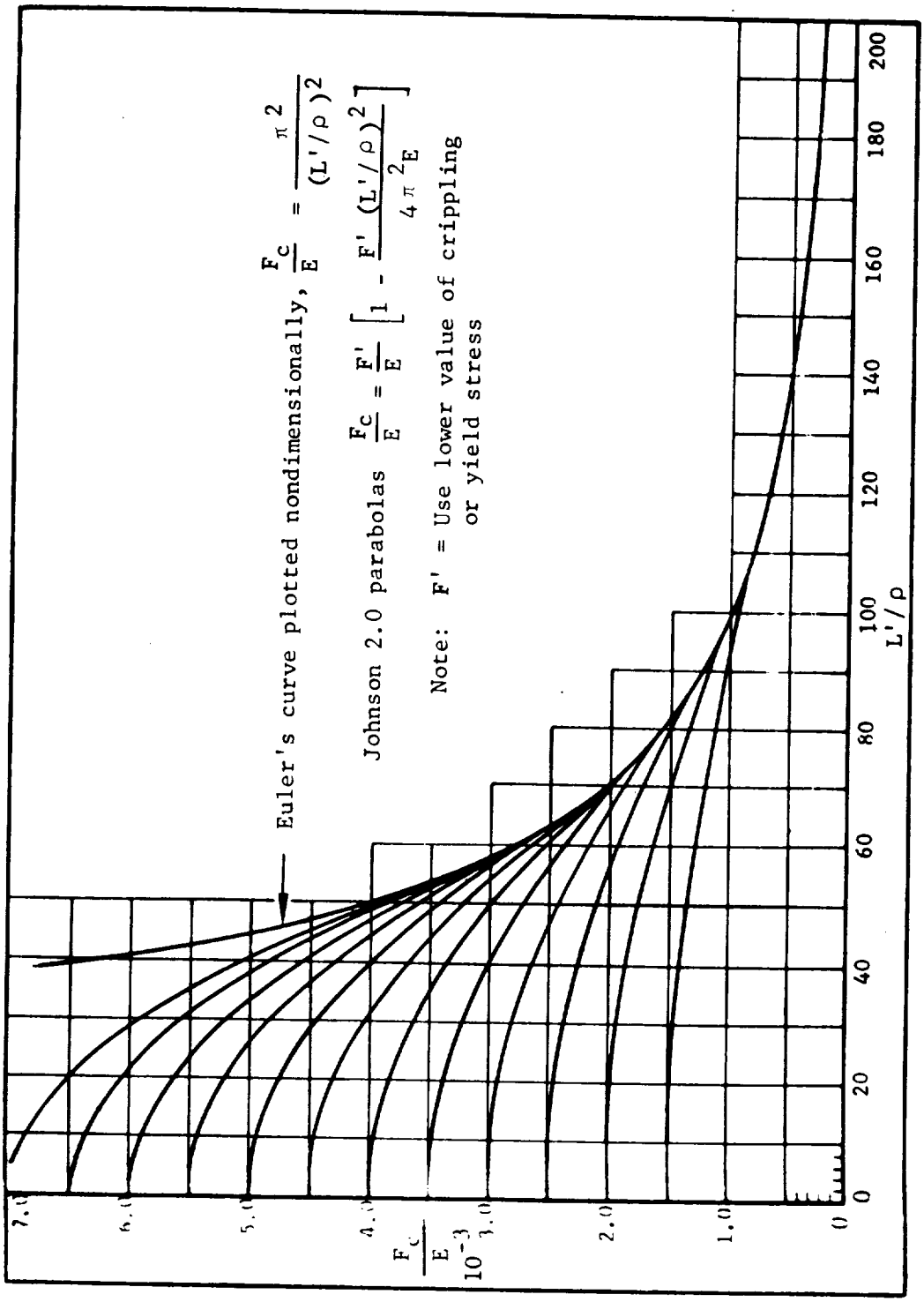

Fig. C 1.3.2-3 Critical Stress for Torsionally Stable Columns

C 1.3.3 Sheet Stiffener Combinations

Flat panel

Sheet-stiffener combinations of flat compression panels may be analyzed as columns. Each stiffener of the panel plus an effective width of sheet acting at the stiffener stress constitutes an individual column that is free to bend about an axis parallel to the panel sheet. The sheet between stiffeners is continuous and offers considerable restraint against stiffener failure about an axis perpendicular to the sheet even though the sheet itself has buckled between stiffeners.

The stress distribution over the panel section after the sheet has buckled is shown by the solid curve in Fig. C 1.3.3-1. The dotted curve is the assumed stress distribution using the concept of effective widths. The effective widths (W_e) for torsionally stable and unstable sections are given in Section C 1.3.1.

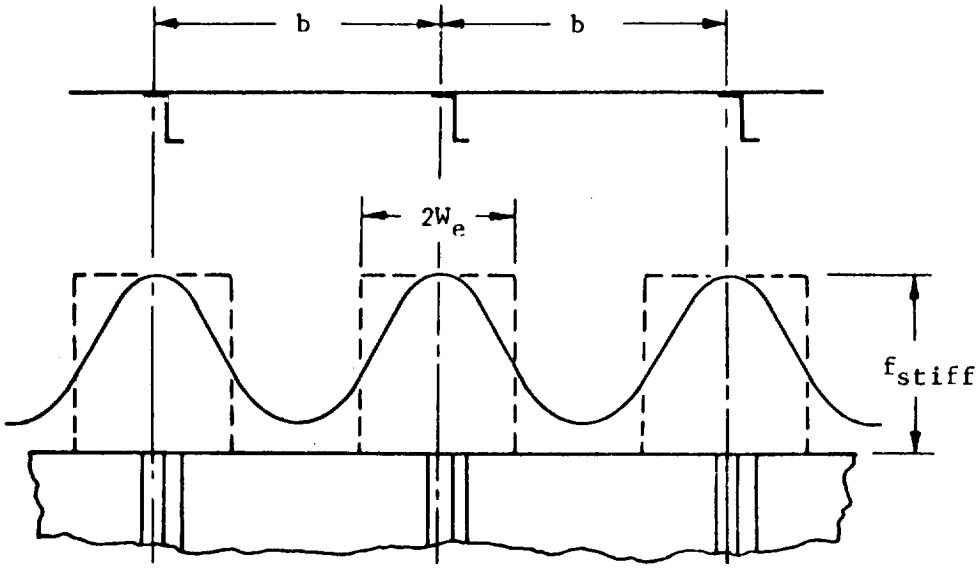

Fig. C 1.3.3-1

The procedure for determination of the critical stress and load on a sheet-stiffener compression panel is

(1) Determine the slenderness ratio L'/ρ of the stiffener alone where ρ is the radius of gyration of the stiffener cross-section about a centroidal axis parallel to the sheet.

(2) From the crippling curve (Fig. C 1.3.1-13) determine F_{cc} of the stiffener cross-section. The value F_{cc}/E is given by F_c/E at $L'/\rho = 0$ in Fig. C 1.3.2-3.

C 1.3.3 Sheet Stiffener Combinations (Cont'd)

(3) Using the column curves (Fig. 1.3.2-3), with L'/ρ and F_{cc} determined in steps (1) and (2), record the value of F_c. (Interpolate between curves as required)

(4) Determine the effective widths of sheet by using Fig. C 1.3.1-12 where $f_{stiff} = F_c$.

(5) Use Fig. C 1.3.3-3 to compute ρ of the stiffener plus effective sheet.

(6) Re-enter the column curve (Fig. C 1.3.2-3) with new L'/ρ and record the value of F_c.

(7) Repeat steps (4), (5), and (6) until satisfactory convergence to a final stress, F_c, is obtained. Convergence generally occurs after two trials. F_c is the critical stress of the stiffened sheet.

(8) The critical load, P_c, is

$$P_c = F_c \left[A_{st} + t_s \Sigma W_e \right] \quad \ldots\ldots\ldots\ldots\ldots\ldots\ldots \quad (1)$$

Where A_{st} is the cross-sectional area of the stiffener.

Curved panels

Analysis of curved stiffened panels requires but a slight extension in procedure beyond that described for flat panels. Fig. C 1.3.3-2 shows a curved panel with the effective widths of sheet that act with the stiffeners.

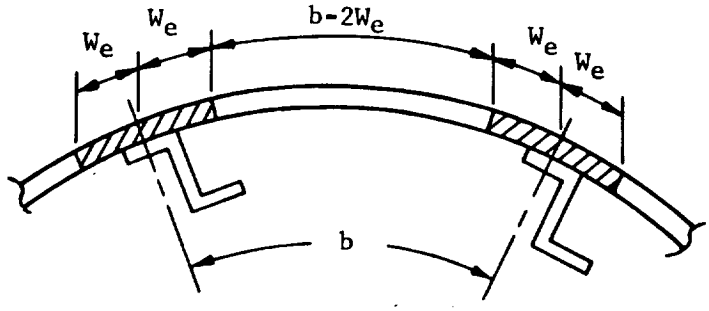

Fig. C 1.3.3-2

The load-carrying capacity of such a panel is equal to that of a flat panel plus an additional load attributable to the effect of the curvature of the sheet between the stiffeners. The critical load is

$$P_c = P_{flat} + P_{curved}$$

C 1.3.3 Sheet Stiffener Combinations (Cont'd)

or for Fig. C 1.3.3-2

$$P_c = (F_c)_{\text{column}} (A_{st} + 4t_s W_e) + (F_{cr})_{\substack{\text{curved} \\ \text{panel}}} (b - 2W_e)\, t_s$$

The critical stress (F_{cr}) of the curved panel is calculated by the equations of section C 3.0.0. Note that in computing this stress the entire width "b" of the curved panel is used. Only the reduced width, $b - 2W_e$, is used in calculating the load that is contributed by the curved panel.

C 1.3.3 Sheet Stiffener Combinations (Cont'd)

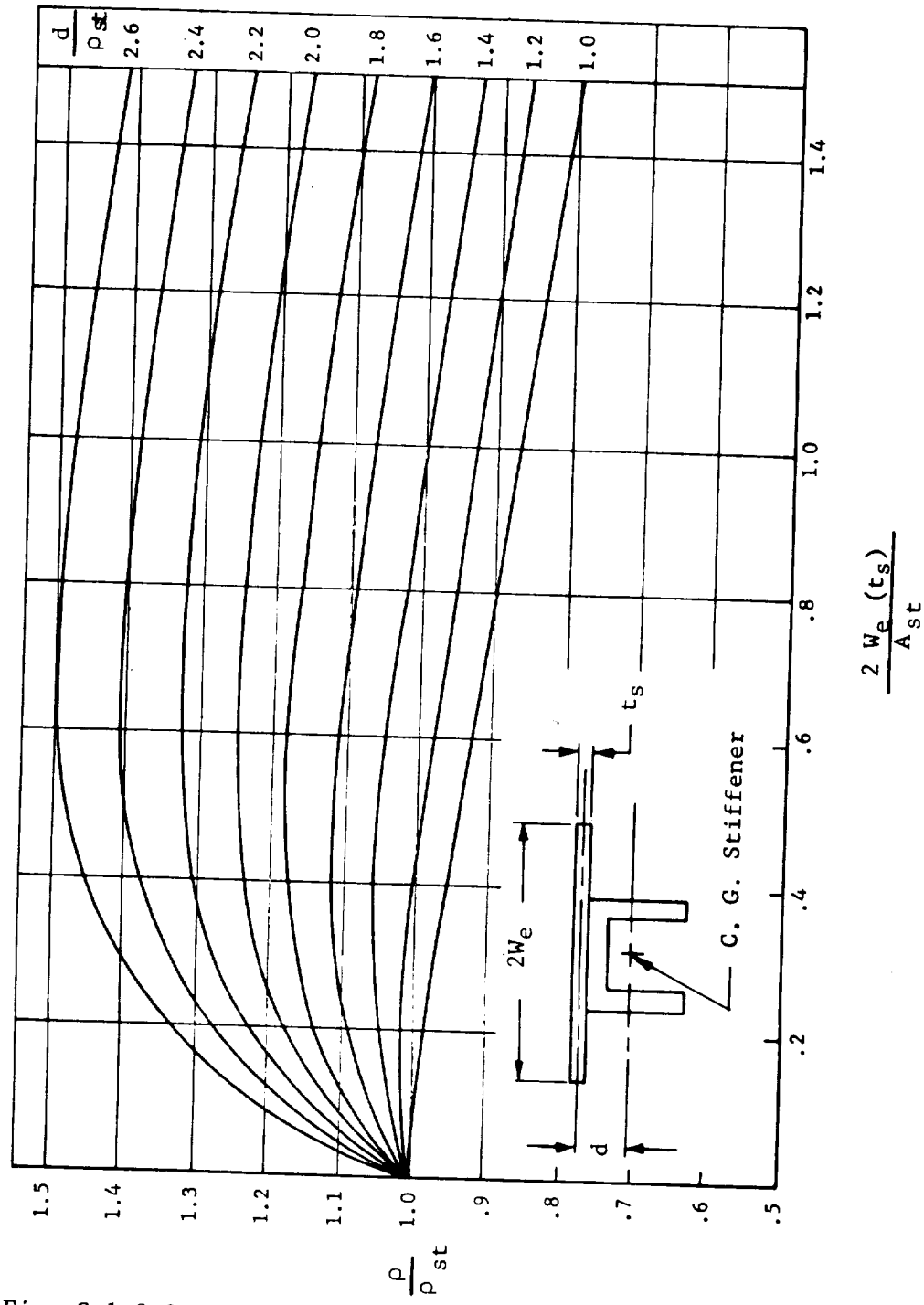

Fig. C 1.3.3-3 Variation of Radius of Gyration for Sheet Stiffener Combinations

C 1.4.0 Columns with Variable Cross Sections

The modified Euler equation (tangent modulus) used to determine the critical load of a prismatic, torsionally stable column not subjected to crippling failure is

$$P_c = \frac{c\pi^2 E_t I}{(L')^2} \quad \text{..... (1)}$$

This section gives appropriate column buckling coefficients (m) and formulas for computing the Euler loads for varying cross-section columns. Where $m = \frac{1}{c}$ in Eq. 1.

The following example is typical for calculating the critical load of a stepped column.

Example

Given:

$E_1 = 10 \times 10^6$ **psi** (aluminum)
$I_1 = .30$ in^4
$E_2 = 30 \times 10^6$ **psi** (steel)
$I_2 = .50$ in^4
$A_1 = 1.94$ in^2

Determine critical buckling load, P_c

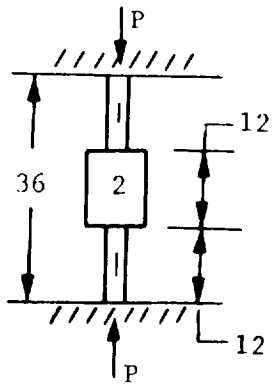

Fig. C 1.4.0-1

Solution:

$$\frac{a}{L} = \frac{12}{36} = .33 \qquad \frac{E_1 I_1}{E_2 I_2} = \frac{10 \times 10^6\ (.30)}{30 \times 10^6\ (.50)} = .20$$

From Fig. C 1.4.0-2, m = .545

$$P_c = \frac{\pi^2 (E_t I)_1}{mL^2} = \frac{(3.14)^2}{.545} \quad \frac{(10)10^6\ (.30)}{(36)^2} = 41{,}800 \text{ lb}$$

Stress level of aluminum section (max. of column)

$$f_1 = \frac{P_c}{A_1} = \frac{41800}{1.94} = 21{,}600 \text{ psi}$$

If f_1 is below the proportional limit of the material in question, then P_c is the critical load of the column. However, if f_1 is above the stress at the proportional limit, the tangent modulus (E_t) at the stress level must be used. This leads to a trial process to determine the critical load of the column.

C 1.4.0 Columns with Variable Cross Sections (Cont'd)

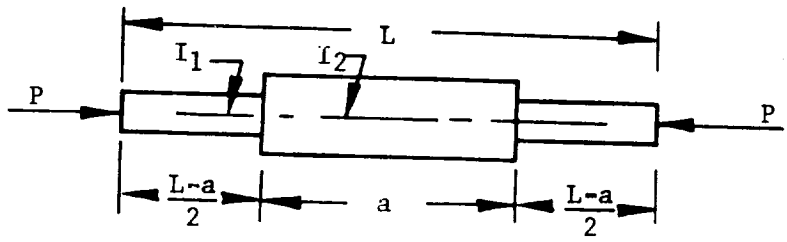

$$P_c = \frac{\pi^2}{m} \frac{(E_t I)_1}{L^2}$$

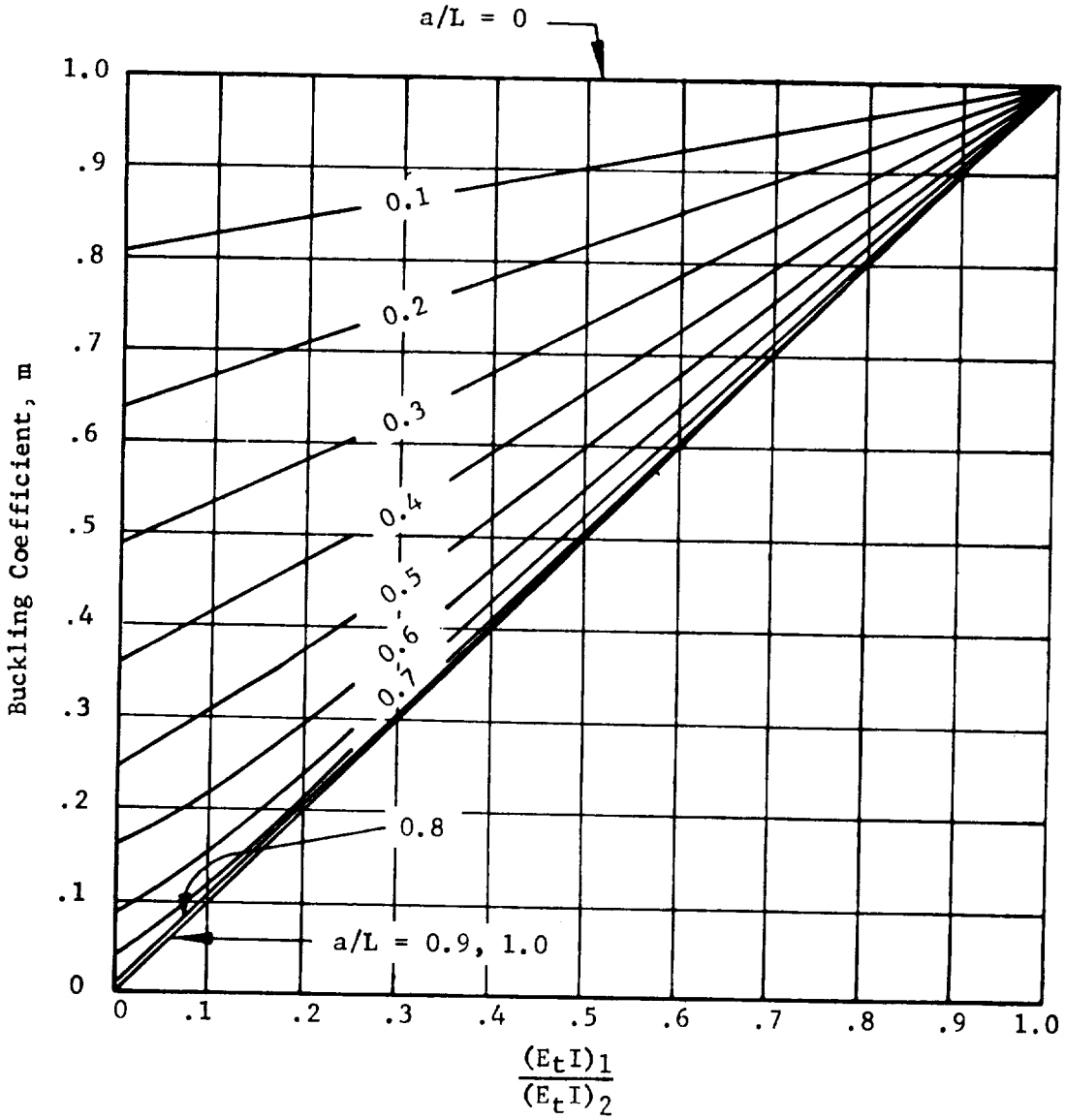

Fig. C1.4.0-2 Buckling Coefficient

C 1.4.0 Columns With Variable Cross Sections (Cont'd)

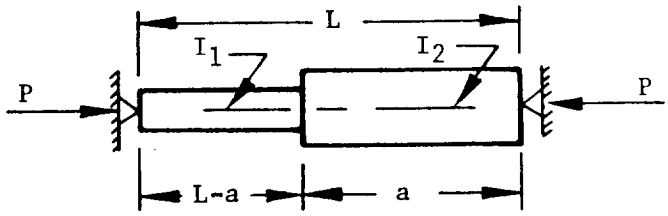

$$P_c = \frac{\pi^2}{m} \frac{(E_t I)_1}{L^2}$$

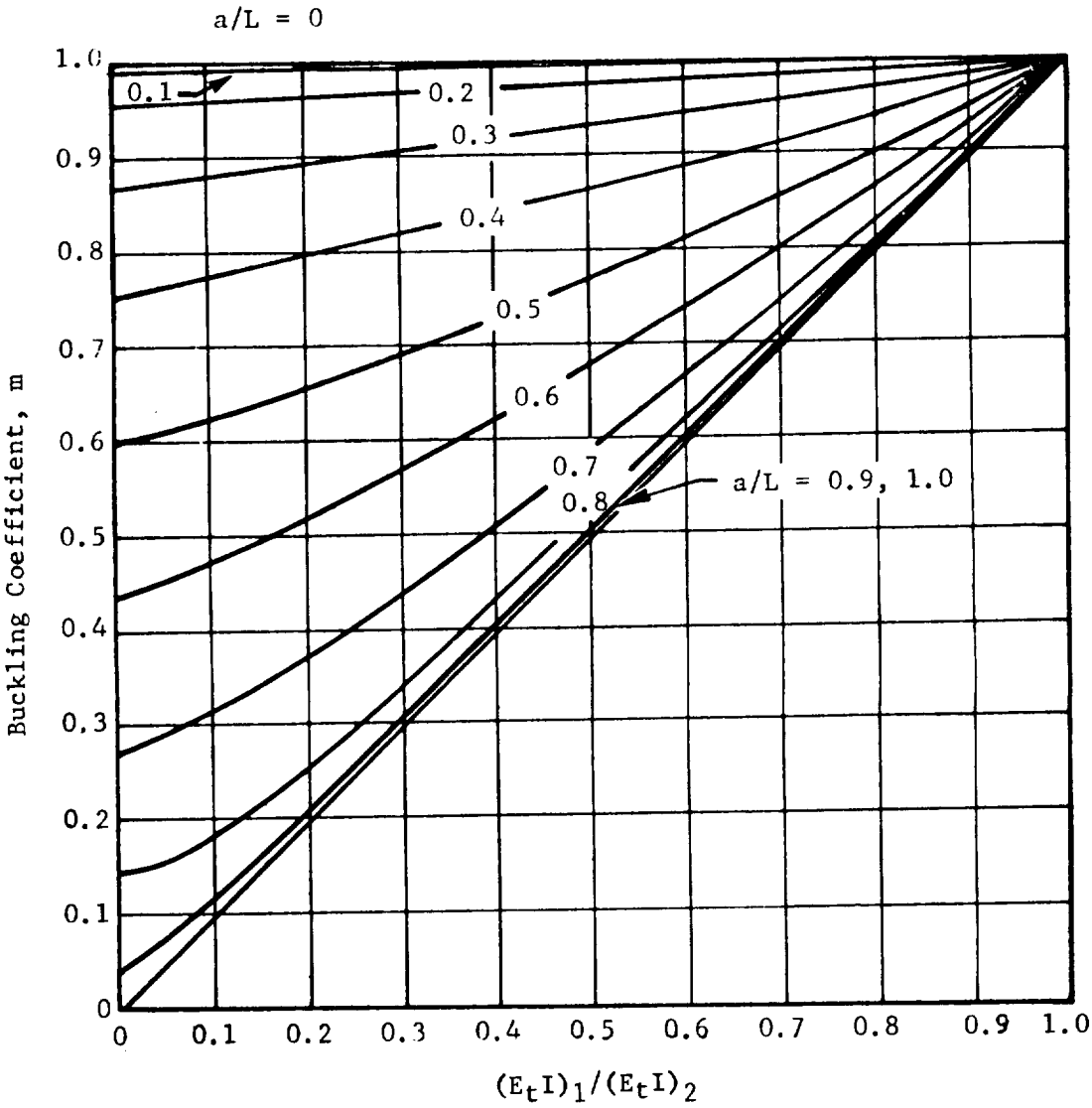

Fig. C1.4.0-3 Buckling Coefficient

C 1.4.0 Columns with Variable Cross Sections (Cont'd)

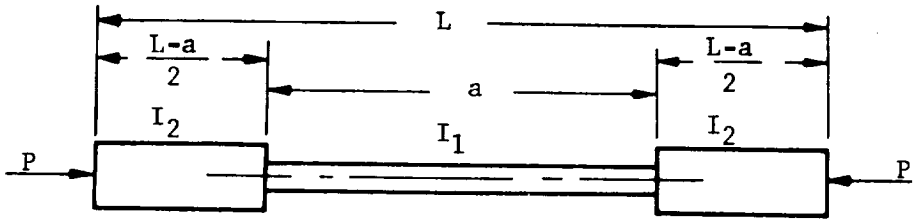

$$P_c = \frac{\pi^2}{m} \frac{(E_t I)_1}{L^2}$$

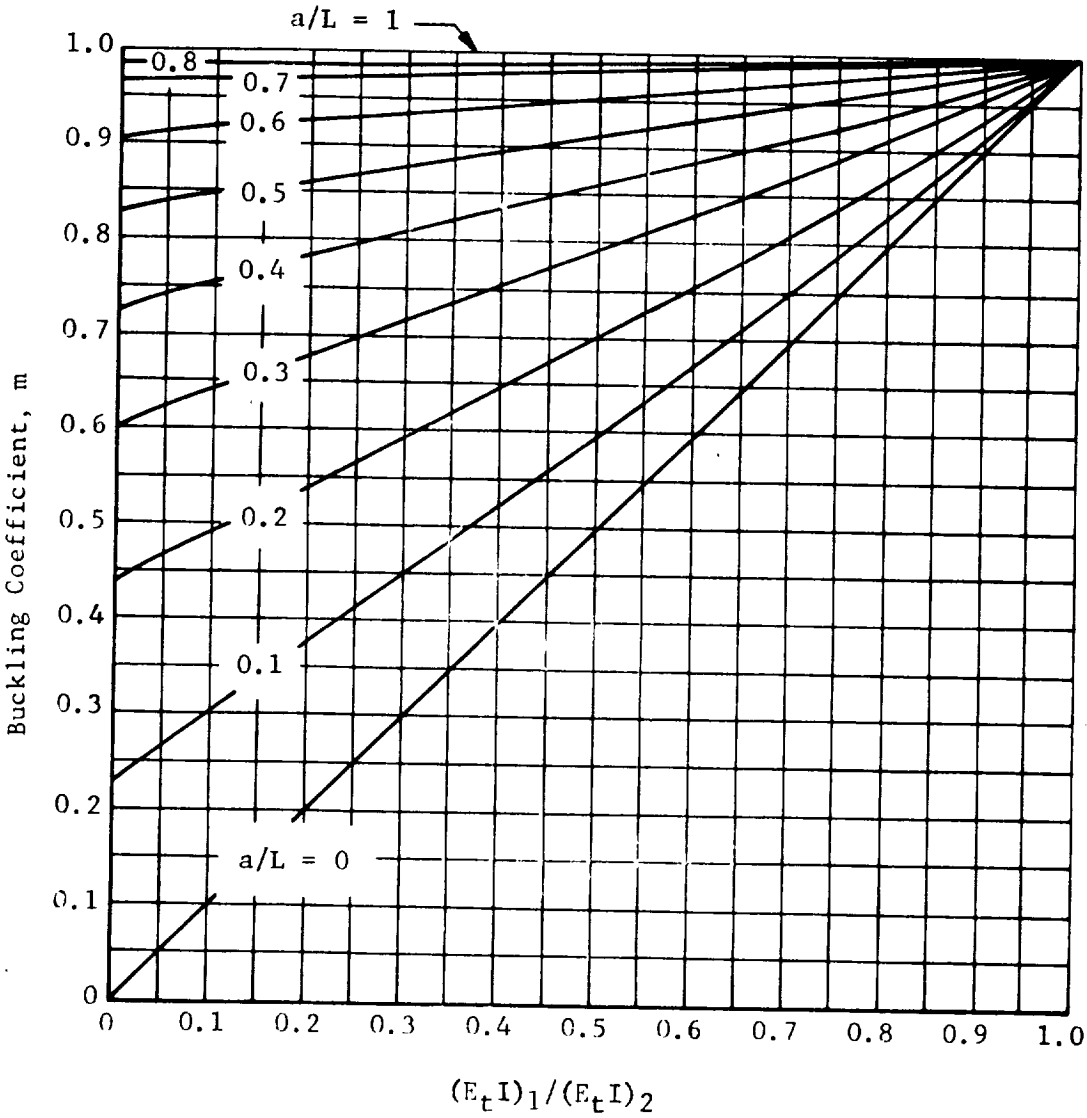

Fig. C1.4.0-4 Buckling Coefficient

C 1.5.0 Torsional Instability of Columns

The critical torsional stress or load for a column is to be determined by use of the following references until this section of the Manual is completed.

1. Argyris, John H., Flexure-Torsion Failure of Panels, Aircraft Engineering, June, 1954.

2. Kappus, Robert, Twisting Failure of Centrally Loaded Open-Section Columns in the Elastic Range, T.M.851, N.A.C.A. 1938.

3. Niles, Alfred S. and J. S. Newell, Airplane Structures, Vol. II Third Edition, John Wiley & Sons, Inc., New York, 1943.

4. Sechler, Ernest E. and L. G. Dunn, Airplane Structural Analysis and Design, John Wiley & Sons, Inc., New York, 1942.

BIBLIOGRAPHY

Text books

1. Timoshenko, S. Strength of Materials, Part I and II, Third Edition, D. Van Nostrand Company, Inc., New York, 1957.

2. Seely, Fred B., and J. O. Smith, Advanced Mechanics of Materials, Second Edition, John Wiley & Sons, Inc., New York, 1957.

3. Popov, E. P., Mechanics of Materials, Prentice-Hall, Inc., New York, 1954.

4. Sechler, Ernest E. and L. G. Dunn, Airplane Structural Analysis and Design, John Wiley & Sons, Inc., New York, 1942.

5. Steinbacher, Franz R. and G. Gerard, Aircraft Structural Mechanics, Pitman Publishing Corporation, New York, 1952.

6. Niles, Alfred S. and J. S. Newall, Airplane Structures, Vol. II, Third Edition, John Wiley & Sons, Inc., New York, 1943.

Manuals

1. Convair Div. of General Dynamics Corp.

2. Chrysler Corp. Missile Div.

3. North American Aviation

4. Martin

5. Grumman Aircraft

6. McDonnell Aircraft

SECTION C1.5

TORSIONAL INSTABILITY OF COLUMNS

TABLE OF CONTENTS

C1.5.0 TORSIONAL INSTABILITY OF COLUMNS

In the previous sections, it was assumed that the column was torsionally stable; i.e., the column would either fail by bending in a plane of symmetry of the cross section, by crippling, or by a combination of crippling and bending. However, there are cases in which a column will buckle either by twisting or by a combination of bending and twisting. Such torsional buckling failures occur if the torsional rigidity of the section is very low, as for a bar of thin-walled open cross section. Since the difference in behavior of an open cross section is that the torsional rigidity varies roughly as the cube of its wall thickness, thin-walled open sections can buckle by twisting at loads well below the Euler load. Another factor that makes torsional buckling important in thin-walled open sections is the frequent lack of double symmetry. In such sections, centroid and shear center do not coincide and, therefore, torsion and flexure interact.

In this section, it will be assumed that the plane cross sections of the column warp, but their geometric shape does not change during buckling; i.e., the theories consider primary failure of columns as opposed to secondary failure, characterized by distortion of the cross sections.

Separate investigation of primary and local buckling can necessarily give only approximate results because, in general, there will be coupling of primary and secondary buckling. For torsionally stable sections, approximate equations have been developed which include this coupling (Johnson-Euler curves, Section C1.3.2). However, no attempt has been made to formulate a theory which would include coupling of torsion and flexure and local buckling, therefore, an analysis would be extremely complicated.

C1.5.1 CENTRALLY LOADED COLUMNS

Centrally loaded columns can buckle in one of three possible modes: (1) They can bend in the plane of one of the principal axes; (2) they can twist about the shear center axis; or (3) they can bend and twist simultaneously. For any given member, depending on its length and the geometry of its cross section, one of these three modes will be critical. Mode (1) has been discussed in the previous sections. Modes (2) and (3) will be discussed below.

I Two Axes of Symmetry

When the cross section has two axes of symmetry or is point symmetric, the shear center and centroid will coincide. In this case, the purely torsional buckling load about the shear center axis is given by Reference 8.

$$P_\phi = \frac{1}{r_o^2}\left[GJ + \frac{E\Gamma\pi^2}{\ell^2}\right]$$

where:

r_o = polar radius of gyration of the section about its shear center

G = shear modulus of elasticity

J = torsion constant (See Section B8.4.1-IV A)

E = Young's modulus of elasticity

Γ = warping constant of the section (See Section B8.4.1-IV E)

ℓ = effective length of member

Thus, for a cross section with two axes of symmetry there are three critical values of the axial load. They are the flexural buckling loads about the principal axes, P_x and P_y, and the purely torsional buckling load, P_ϕ. Depending on the shape of cross section and length of member, one of these loads will have the lowest value and will determine the mode of buckling. In this case there is no interaction, and the column fails either in pure bending or in pure twisting. Shapes in this category include I-sections, Z-sections, and cruciform sections.

II General Cross Section

In the general case of a column of thin-walled open cross section, buckling occurs by a combination of torsion and bending. Purely flexural or purely torsional buckling cannot occur. To investigate this type of buckling, consider the unsymmetrical cross section shown in Figure C1.5-1. The x and y axes are the principal centroidal axes of the cross section and x_o and y_o are the coordinates of the shear center. During buckling, the cross section will undergo translation and rotation. The translation is defined by the deflections u and v in the x and y directions, respectively, of the shear center o. Thus, during translation of the cross section, point o moves to o' and point c to c'. The rotation of the cross section about the shear center is denoted by the angle ϕ, and the final position of the centroid is c''. Equilibrium of a longitudinal element of a column deformed in this manner leads to three simultaneous differential equations (Reference 8). The solution of these equations yields the following cubic equation for calculating the critical value of buckling load:

$$r_o^2\left(P_{cr}-P_y\right)\left(P_{cr}-P_x\right)\left(P_{cr}-P_\phi\right) - P_{cr}^2 y_o^2\left(P_{cr}-P_x\right) - P_{cr}^2 x_o^2\left(P_{cr}-P_y\right) = 0$$

where

$$P_x = \frac{\pi^2 EI_x}{\ell^2}, \quad P_y = \frac{\pi^2 EI_y}{\ell^2},$$

and

$$P_\phi = \frac{1}{r_o^2}\left(GJ + \frac{E\Gamma\pi^2}{\ell^2}\right).$$

Solution of the cubic equation then gives three values of the critical load, P_{cr}, of which the smallest will be used in practical applications. The lowest value of P_{cr} can always be shown to be less than the lowest of the three parameters, P_x, P_y, and P_ϕ. This is to be expected, noting that it represents an interaction of the three individual modes. By use of the effective length, ℓ, various end conditions can be incorporated in the solution above.

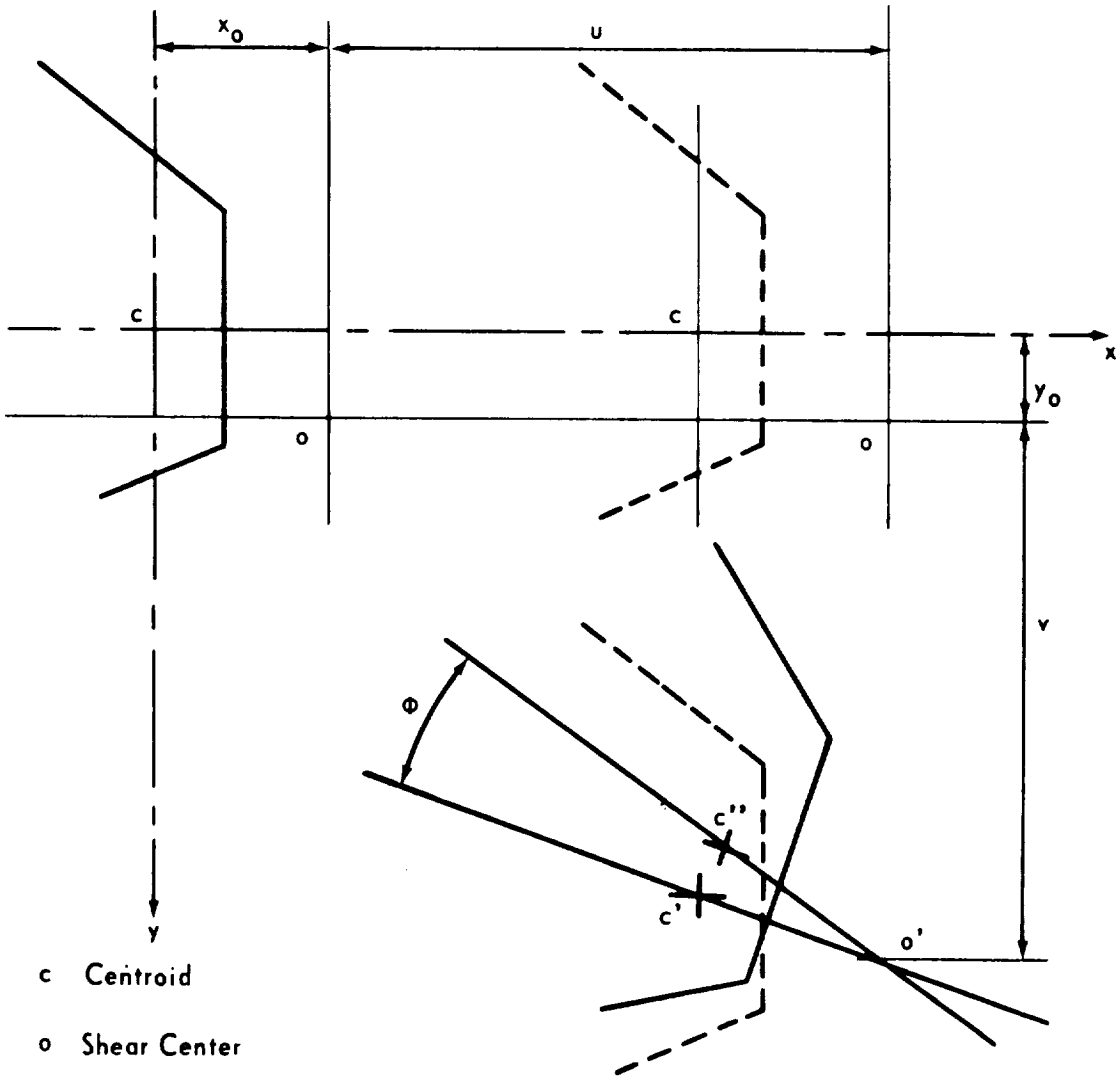

FIGURE C1. 5-1. DISPLACEMENT OF SECTION DURING TORSIONAL – FLEXURAL BUCKLING

III One Axis of Symmetry

If the x-axis is an axis of symmetry, then $y_o = 0$ and the equation for a general section reduces to

$$\left(P_{cr}-P_y\right)\left[r_o^2\left(P_{cr}-P_x\right)\left(P_{cr}-P_\phi\right)-P_{cr}^2 x_o^2\right] = 0 \quad . \qquad (1)$$

There are again three solutions, one of which is $P_{cr} = P_y$ and represents purely flexural buckling about the y-axis. The other two are the roots of the quadratic term inside the square brackets equated to zero, and give two torsional-flexural buckling loads. The lowest torsional-flexural load will always be below P_x and P_ϕ. It may, however, be above or below P_y. Therefore, a singly symmetrical section (such as an angle, channel, or hat) can buckle in either of two modes, by bending, or in torsional-flexural buckling. Which of these two actually occurs depends on the dimensions and shape of the given section.

The evaluation of the buckling load from equation (1) is often lengthy and tedious. Chajes and Winter (Reference 7) have devised a simple and efficient procedure for evaluating the torsional-flexural buckling load from equation (1) for singly symmetrical sections shown in Figure C1.5-2. In their approach, the essential parameters and their effect on the critical load are clearly evident. Since most shapes used for compression members are singly symmetric, their method is quite useful as described below.

A. Critical Mode of Failure

Failure of singly symmetrical sections can occur either in pure bending or in simultaneous bending and twisting. Because the evaluation of the torsional-flexural buckling load, regardless of the method used, can never be made as simple as the determination of the Euler load, it would be convenient to know if there are certain combinations of dimensions for which torsional-flexural buckling need not be considered at all. To obtain this information, a method of delineating the regions governed by each of the two possible modes of failure has been developed. The method is applicable to any set of boundary conditions. For the purpose of this investigation, however, it will be limited to members with compatible end conditions; i.e., supports that offer equal restraint to bending about the principal axes and to warping.

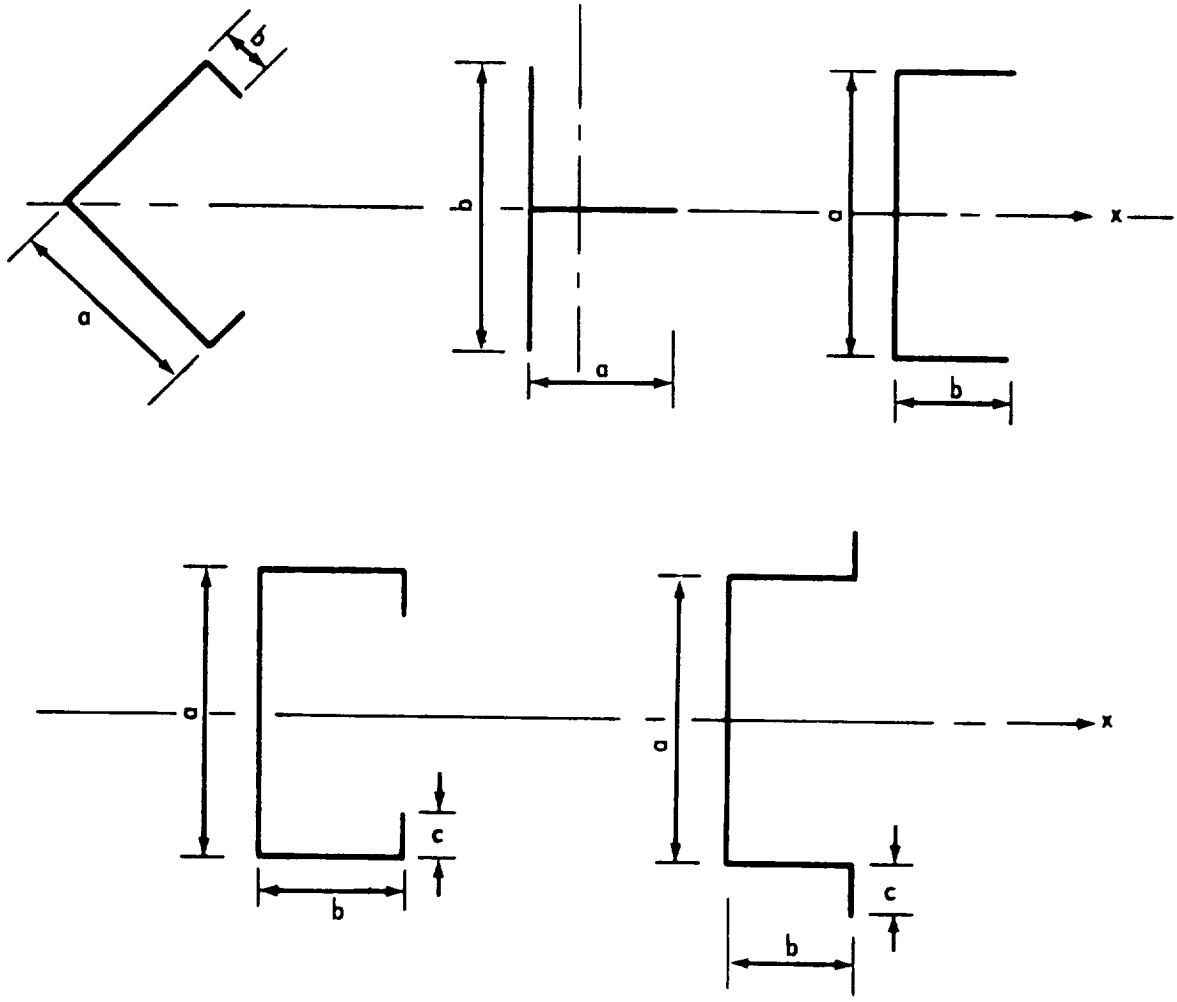

FIGURE C1.5-2 SINGLY SYMMETRICAL SECTIONS

For sections symmetrical about the x axis, the critical buckling load is given by equation (1). According to this equation, the load at which the member actually buckles is either P_y or the smaller root of the quadratic equation, whichever is smaller.

The buckling domain can be visualized as being composed of three regions. These are shown schematically in Figure C1.5-3 for a section whose shape is defined by the width ratio, b/a. Region 1 contains all sections for which $I_y > I_x$.

In this region, only torsional-flexural buckling can occur. Sections for which $I_x > I_y$ fall into Regions 2 or 3. In Region 2, the mode of buckling depends on the parameter $t\ell/a^2$. The $(t\ell/a^2)_{min}$ curve represents the boundary between the two possible modes of failure. It is a plot of the value of $t\ell/a^2$ at which the buckling mode changes from purely flexural to torsional-flexural. The boundary between Regions 2 and 3 is located at the intersection of the $(t\ell/a^2)_{min}$ curve with the b/a axis. Sections in Region 3 will always fail in the flexural mode regardless of the value of $t\ell/a^2$.

Figure C1.5-4 defines these curves for angles, channels, and hat sections. In this figure, members that plot below and to the right of the curve fail in the torsional-flexural mode, whereas those to the left and above fail in the pure bending mode. The curves in Figure C1.5-4 also give the location of the boundaries between the various buckling domains. Each of the curves approaches a vertical asymptote, indicated as a dashed line in the figure. The asymptote, which is the boundary between Regions 1 and 2, is located at b/a corresponding to sections for which $I_x = I_y$. Sections with b/a larger than the transition value at the asymptote will always fail in torsional-flexural buckling, regardless of their other dimensions. If b/a is smaller than the value for the asymptote, then the section falls in Region 2 and failure can be either by pure flexural buckling or in the torsional-flexural mode. In this region, the parameter, $t\ell/a^2$, will determine which of the two possible modes of failure is critical. In the case of the plain and lipped channel section, there is a lower boundary Region 2. This transition occurs where the $(t\ell/a^2)_{lim}$ curve intersects the b/a axis. Sections for which b/a is less than the value at this intersection are located in Region 3. These sections will always fail in the flexural mode, regardless of the value of $t\ell/a^2$. For the lipped angle and hat sections the $(t\ell/a^2)_{lim}$ curve does not intersect the b/a axis. Region 3, where only flexural buckling occurs, does not exist for these sections.

B. Interaction Equation

The critical buckling load for singly symmetrical sections (x-axis is the axis of symmetry) that buckle in the torsional-flexural mode is given by the lowest root of

$$r_o^2\left(P_{cr}-P_x\right)\left(P_{cr}-P_\phi\right) - P_{cr}^2 x_o^2 = 0 \ . \qquad (2)$$

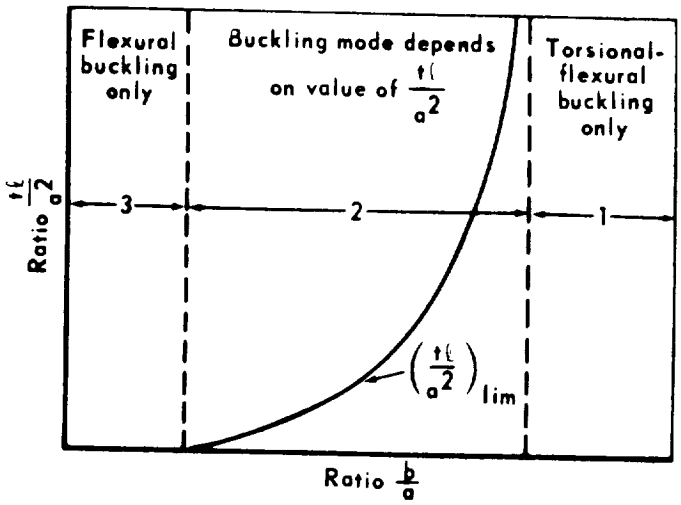

FIGURE C1.5-3 BUCKLING REGIONS

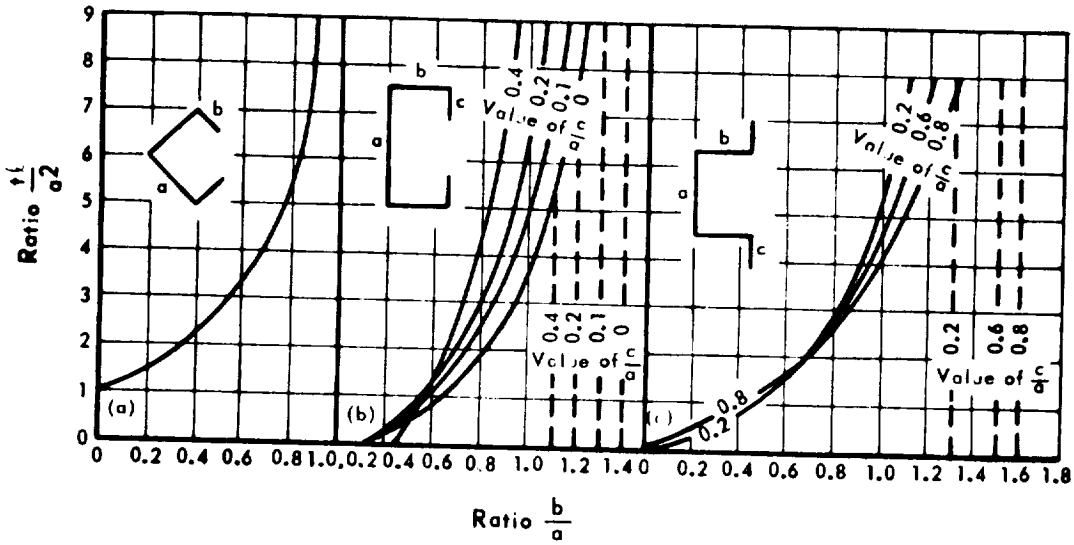

FIGURE C1.5-4 BUCKLING MODE OF SINGLY SYMMETRICAL SECTIONS

Dividing this equation by $P_x P_\phi r_o^2$, and rearranging results in the following interaction equation:

$$\frac{P}{P_\phi} + \frac{P}{P_x} - K\left(\frac{P^2}{P_\phi P_x}\right) = 1 \qquad (3)$$

in which

$$K = 1 - \left(\frac{x_o}{r_o}\right)^2 \qquad (4)$$

is a shape factor that depends on geometrical properties of the cross section.

Figure C1.5-5 is a plot of equation (3). This plot provides a simple method for checking the safety of a column against failure by torsional-flexural buckling.

To determine if a given member can safely carry a certain load, P, it is only necessary to compute P_x and P_ϕ for the section in question and then, knowing K, use the correct curve to check whether the point determined by the arguments P/P_x and P/P_ϕ falls below (safe) or above (unsafe) the pertinent curve. If it is desired to determine the critical load of a member instead of ascertaining whether it can safely carry a given load, use

$$P_{cr} = \frac{1}{2K}\left[\left(P_\phi + P_x\right) - \sqrt{\left(P_\phi + P_x\right)^2 - 4KP_\phi P_x}\right] \qquad (5)$$

which is another form of equation (3).

The interaction equation (eq. 3) indicates that P_{cr} depends on three factors: the loads, P_x and P_ϕ, and the shape factor, K. P_x and P_ϕ are the two factors which interact, while K determines the extent to which they interact. The reason bending and twisting interact is that the shear center and the centroid do not coincide. A decrease in x_o, the distance between these points, therefore causes a decrease in the interaction.

To evaluate the torsional-flexural buckling load by means of the interaction equation, it is necessary to know P_ϕ and K. A convenient method for determining these two parameters is therefore an essential part of the procedure.

C. Evaluation of K

For any given section, K is a function of certain parameters that define the shape of the section. Starting with equation (4) and substituting for

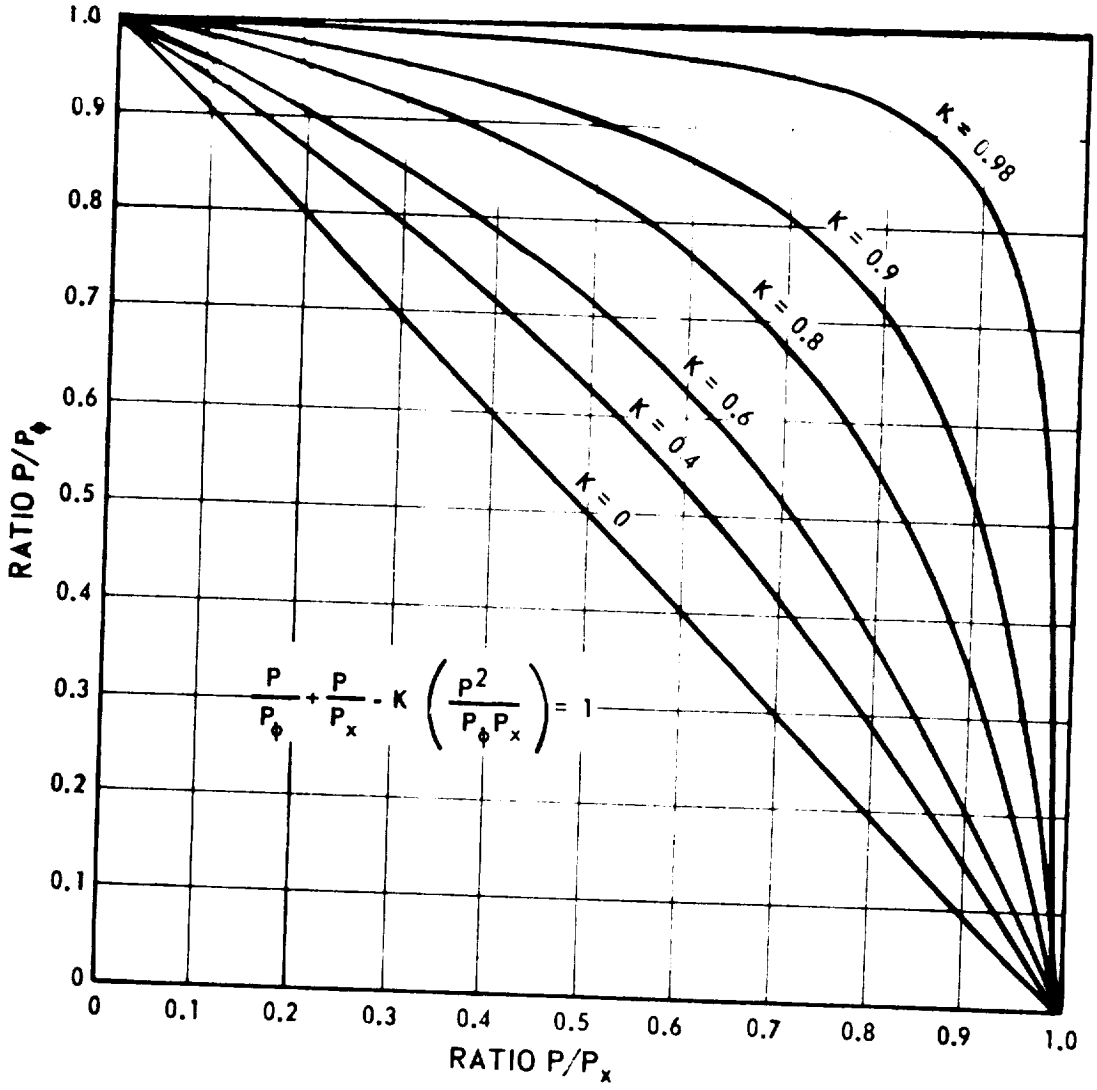

FIGURE C1.5-5 INTERACTION CURVES

x_o and r_o, K can be reduced to an expression in terms of one or more of these parameters. If the thickness of the member is uniform, the parameters will be of the form b/a, in which a and b are the widths of two of the flat components of the section. In the case of a tee section, for example, equation (4) can be reduced to

$$K = 1 - \frac{4}{[1 + b/a]\,[(b/a)^3 + 1]} \qquad (6)$$

in which b/a is the ratio of the flange to the leg width (Fig. C1.5-2).

In general, the number of elements of which a section is composed and the number of width ratios required to define its shape will determine the complexity of the relation for K. Because all equal-legged angles without lips have the same shape, K is a constant for this section. For channels and lipped angles, K is a function of a single variable, b/a, while lipped channels and hat sections require two parameters, b/a and c/a, to define K (Fig. C1.5-2).

Curves for determination of K have been obtained for angles, channels, and hat sections. These curves are shown in Figures C1.5-6 and C1.5-7. A single curve covers all equal-legged lipped angle sections. The value of K for all plain equal-legged angles, K = 0.625, is given by the point b/a = 0 on this curve (Fig. C1.5-6). For hats and channels (Figure C1.5-7), a series of curves is given.

D. Evaluation of P_ϕ

The evaluation of P_ϕ follows the same scheme as that used to determine K. Starting with the equation for P_ϕ, given in Paragraph C1.5.1-I, and substituting for r_o, J, and Γ yields

$$P_\phi = EA\left[C_1(t/a)^2 + C_2(a/\ell)^2\right] \qquad (7)$$

a general relation for P_ϕ, in which, E = Young's modulus, A = cross-sectional area; t = the thickness of the section; ℓ = effective length of the member; a = the width of one of the elements of the section; and C_1 and C_2 = functions of b/a and c/a, in which b and c are the widths of the remaining elements.

Equation (4) indicates the important parameters in torsional buckling and their effect on the buckling load. Similar to Euler buckling, P_ϕ varies directly with E and A. The term inside the bracket consists of two parts, the St. Venant torsional resistance and the warping resistance. In the first of these, the parameter, t/a, indicates the decrease in torsional resistance with decreasing relative wall thickness; whereas, in the second the parameter a/ℓ shows the decrease in warping resistance with increasing slenderness.

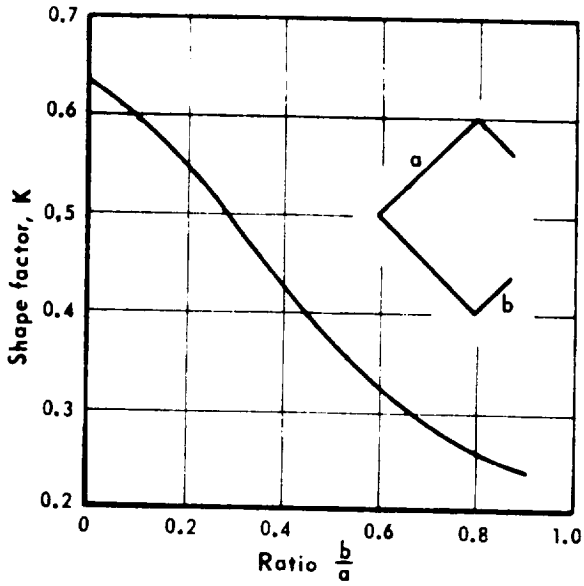

FIGURE C1.5-6 SHAPE FACTOR K FOR EQUAL-LEGGED ANGLES

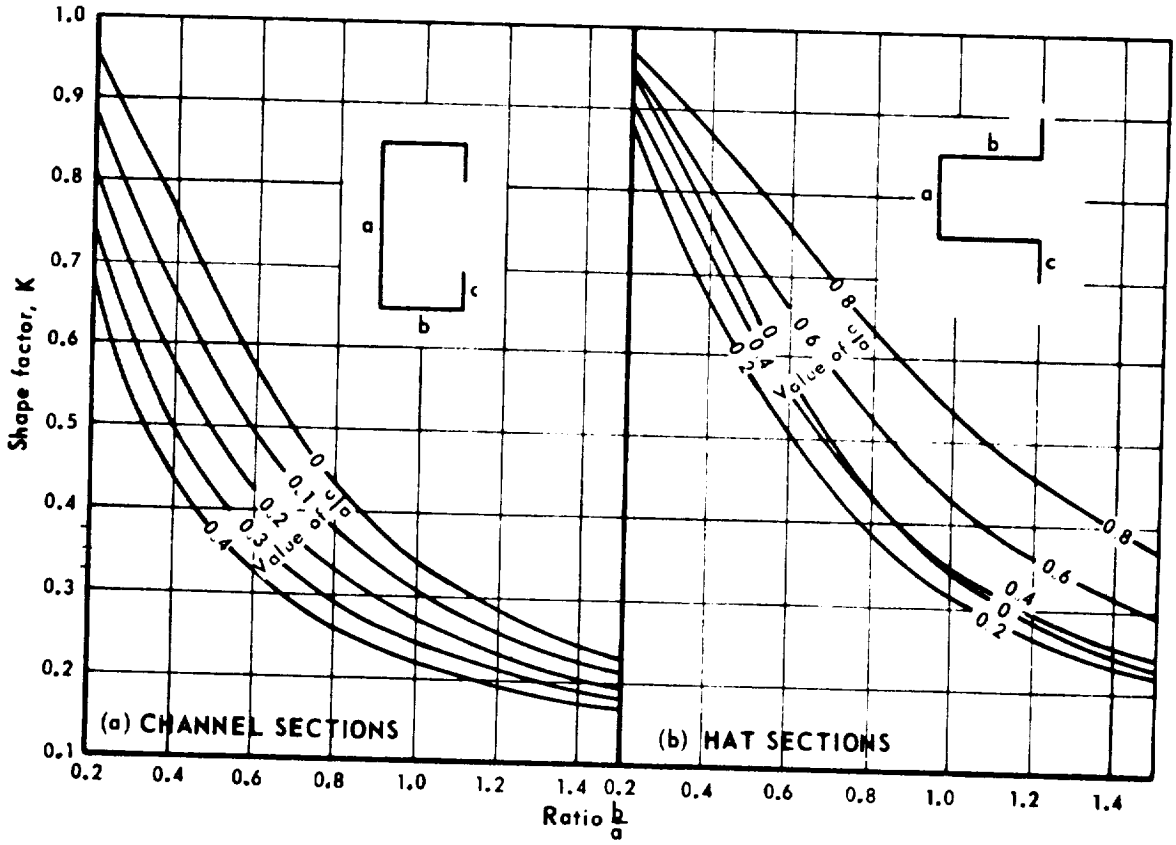

FIGURE C1.5-7 SHAPE FACTOR K

The coefficients, C_1 and C_2, in the St. Venant and warping terms are functions of b/a and c/a, respectively. These terms therefore indicate the effect that the shape of the section has on P_ϕ.

Sections composed of thin rectangluar elements whose middle lines intersect at a common point have negligible warping stiffness; i.e., $\Gamma = 0$. Because C_2 is proportional to Γ, the torsional buckling load of these sections reduces to

$$P_\phi = EAC_1(t/a)^2 \quad . \tag{8}$$

For the plain equal-legged angle, which falls into this category, P_ϕ can be further reduced to

$$P_\phi = AG(t/a)^2 \tag{9}$$

in which G is the shear modulus of elasticity, and a is the length of one of the legs.

In general, however, C_1 and C_2 must be evaluated. Curves for these values are given in Figures C1.5-8, C1.5-9, and C1.5-10 for angles, hats, and channels.

For other cross sections values of the warping constant, Γ, and location of shear center are given in Table 1.

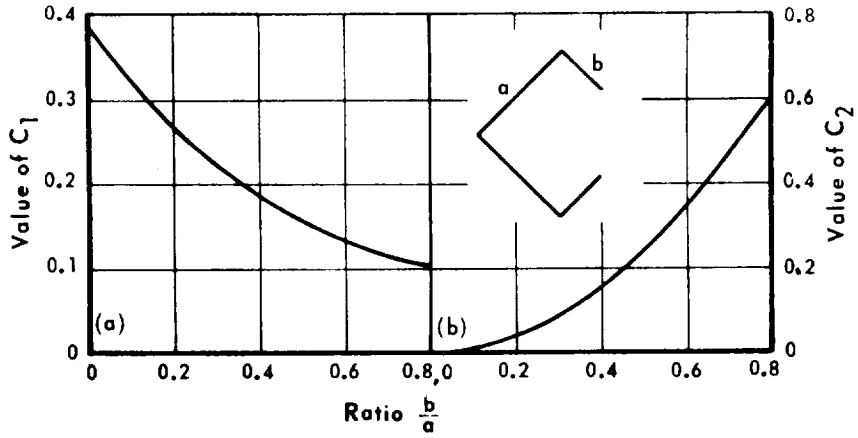

FIGURE C1.5-8 TORSIONAL BUCKLING LOAD COEFFICIENTS, C_1 AND C_2, FOR EQUAL-LEGGED ANGLES

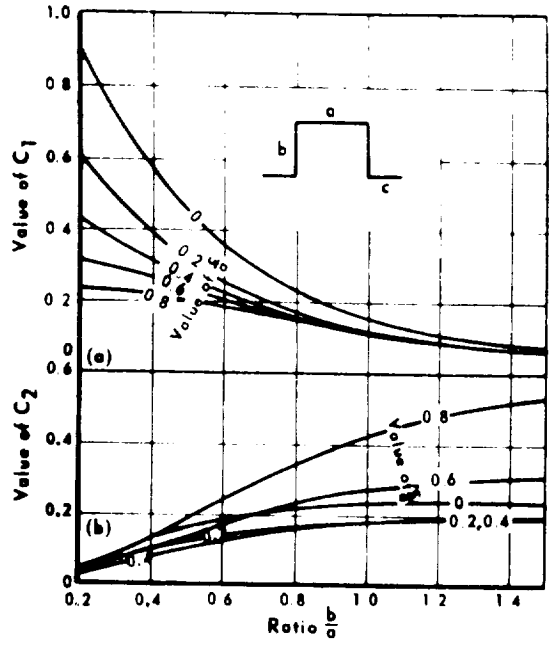

FIGURE C1.5-9 TORSIONAL BUCKLING LOAD COEFFICIENTS, C_1 AND C_2, FOR HAT SECTIONS

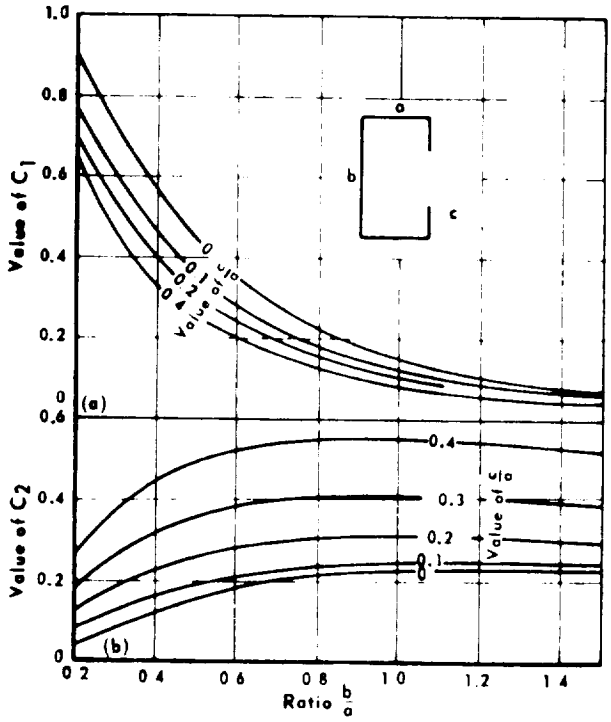

FIGURE C1.5-10 TORSIONAL BUCKLING LOAD COEFFICIENTS, C_1 AND C_2, FOR CHANNEL SECTIONS

TABLE I. SHEAR CENTER LOCATIONS AND WARPING CONSTANTS FOR VARIOUS CROSS SECTIONS

s = shear center
c = centroid
Γ = warping constant

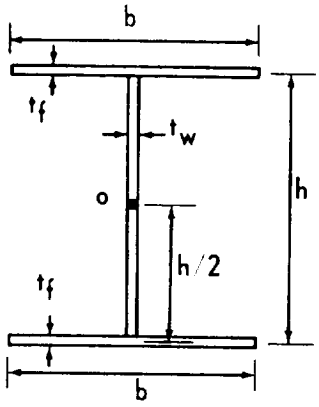

$$\Gamma = \frac{t_f h^2 b^3}{24}$$

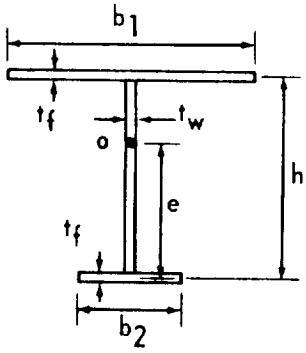

$$e = h\,\frac{b_1^3}{b_1^3 + b_2^3}$$

$$\Gamma = \frac{t_f h^2}{12}\,\frac{b_1^3\, b_2^3}{b_1^3 + b_2^3}$$

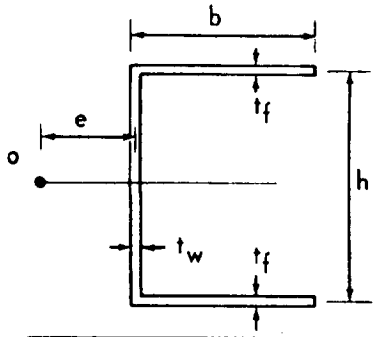

$$e = \frac{3b^2 t_f}{6bt_f + ht_w}$$

$$\Gamma = \frac{t_f b^3 h^2}{12}\,\frac{3bt_f + 2ht_w}{6bt_f + ht_w}$$

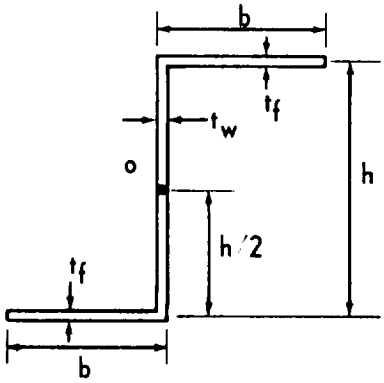

$$\Gamma = \frac{b^3 h^2}{12\,(2b + h)^2}\left[\,2t_f(b^2 + bh + h^2) + 3\,t_w bh\,\right]$$

TABLE I (Continued)

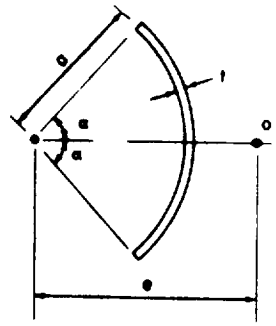

$$e = 2a\,\frac{\sin\alpha - \alpha\cos\alpha}{\alpha - \sin\alpha\cos\alpha}$$

$$I = \frac{2ta^5}{3}\left[\alpha^3 - \frac{6(\sin\alpha - \alpha\cos\alpha)^2}{\alpha - \sin\alpha\cos\alpha}\right]$$

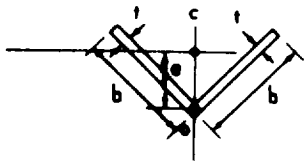

o is located at the intersection of the two legs

$I = \frac{A^3}{144}$ A = cross-sectional area of the angle

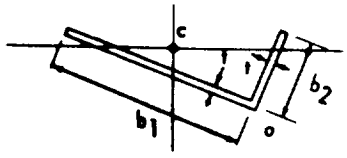

o is located at the intersection of the two legs

$I = \frac{t^3}{36}(b_1^3 + b_2^3)$

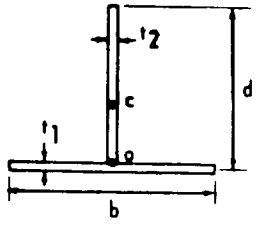

o is located at the intersection of flange and web

$$I = \frac{t_1^3 b}{144} + \frac{t_2^3 d^3}{36}$$

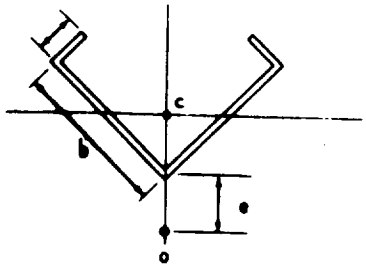

$$e = \frac{b(b_1)^2(3b-2b_1)}{\sqrt{2}\left[2b^3 - (b-b_1)^3\right]}$$

TABLE 1 (Concluded)

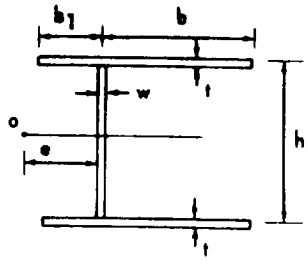

$$e = \frac{3(b^2 - b_1^2)}{(w - t)h + 6(b + b_1)} \quad ; \; b_1 < b$$

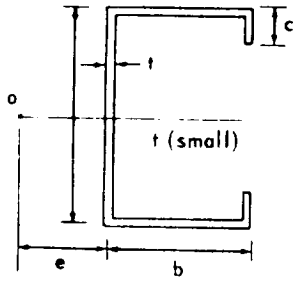

Values of e/h					
c/h \ b/h	1.0	0.8	0.6	0.4	0.2
0	0.430	0.330	0.236	0.141	0.055
0.1	0.477	0.380	0.280	0.183	0.087
0.2	0.530	0.425	0.325	0.222	0.115
0.3	0.575	0.470	0.365	0.258	0.138
0.4	0.610	0.503	0.394	0.280	0.155
0.5	0.621	0.517	0.405	0.290	0.161

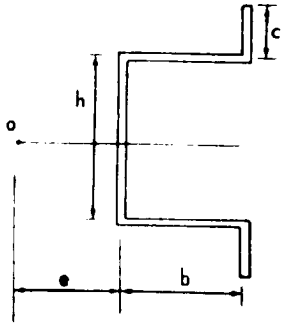

Values of e/h					
c/h \ b/h	1.0	0.8	0.6	0.4	0.2
0	0.430	0.330	0.236	0.141	0.055
0.1	0.464	0.367	0.270	0.173	0.080
0.2	0.474	0.377	0.280	0.182	0.090
0.3	0.453	0.358	0.265	0.172	0.085
0.4	0.410	0.320	0.235	0.150	0.072
0.5	0.355	0.275	0.196	0.123	0.056
0.6	0.300	0.225	0.155	0.095	0.040

C1.5.2 SPECIAL CASES

I Continuous Elastic Supports

Consider the stability of a centrally compressed bar which is supported elastically throughout its length and defined by coordinates h_x and h_y (Fig. C1.5-11).

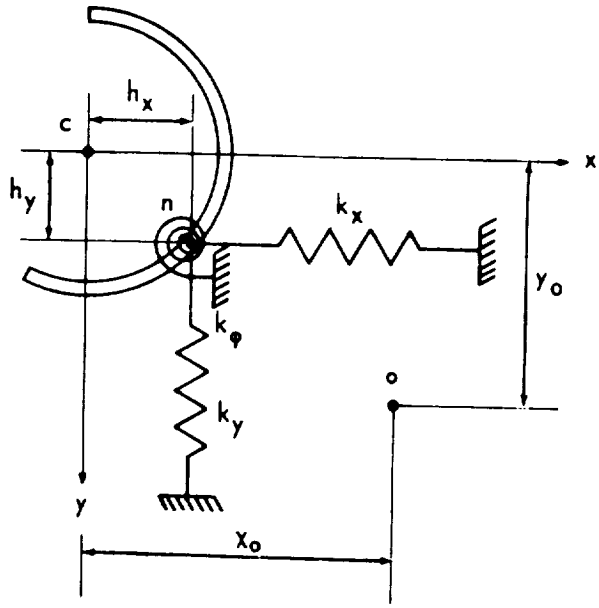

FIGURE C1.5-11 SECTION WITH CONTINUOUS ELASTIC SUPPORTS

For this case, three simultaneous differential equations can be obtained (Reference 8). They are:

$$EI_y \frac{d^4u}{dz^4} + P\left(\frac{d^2u}{dz^2} + y_o \frac{d^2\phi}{dz^2}\right) + k_x\left[u + \left(y_o - h_y\right)\phi\right] = 0$$

$$EI_x \frac{d^4v}{dz^4} + P\left(\frac{d^2v}{dz^2} - x_o \frac{d^2\phi}{dz^2}\right) + k_y\left[v - \left(x_o - h_x\right)\phi\right] = 0$$

$$E\Gamma \frac{d^4\phi}{dz^4} - \left(GJ - \frac{I_o}{A} P\right)\frac{d^2\phi}{dz^2} - P\left(x_o \frac{d^2v}{dz^2} - y_o \frac{d^2u}{dz^2}\right)$$
$$+ k_x\left[u + \left(y_o - h_y\right)\phi\right]\left(y_o - h_y\right) - k_y\left[v - \left(x_o - h_x\right)\phi\right]\left(x_o - h_x\right)$$
$$+ k_\phi \phi = 0 \quad .$$

If the ends of the bar are simply supported, that is, free to warp and to rotate about the x and y axes but with no rotation about the z axis, we can take the solution of the equations above in the form

$$u = A_1 \sin \frac{n\pi z}{\ell} \qquad v = A_2 \sin \frac{n\pi z}{\ell} \qquad \phi = A_3 \sin \frac{n\pi z}{\ell}$$

Substitution of these expressions into the differential equations leads to the evaluation of a determinant and hence to a cubic equation for the critical loads, in the same manner as described in Paragraph C1.5.3-I. The cubic equation is

$$A_3 P^3 + A_2 P^2 + A_1 P + A_0 = 0$$

where

$$A_3 = -\left(\frac{n\pi}{\ell}\right)^6 \frac{\left(I_x + I_y\right)}{A}$$

$$A_2 = E\left[\frac{\left(I_x + I_y\right)^2}{A} + I_y y_o^2 + I_x x_o^2 + \Gamma\right]\left(\frac{n\pi}{\ell}\right)^8 + GJ\left(\frac{n\pi}{\ell}\right)^6$$
$$+\left[k_x h_y^2 + k_y h_x^2 + k_\phi + \left(k_x + k_y\right)\frac{\left(I_x + I_y\right)}{A}\right]\left(\frac{n\pi}{\ell}\right)^4$$

$$A_1 = -E^2\left[\frac{I_x I_y I_o}{A} + \left(I_x + I_y\right)\Gamma\right]\left(\frac{n\pi}{\ell}\right)^{10} - EGJ\left(I_x + I_y\right)\left(\frac{n\pi}{\ell}\right)^8$$
$$-E\left[I_y k_x \left(y_o - h_y\right)^2 + I_y k_y \left(x_o - h_x\right)^2 + I_x k_x h_y^2 + I_x k_y h_x^2\right.$$
$$\left.+\frac{I_y k_x I_o}{A} + I_x k_x \frac{\left(I_x + I_y\right)}{A} + \left(I_x + I_y\right)k_\phi + \left(I_x + I_y\right)\Gamma\right]\left(\frac{n\pi}{\ell}\right)^6$$
$$-GJ\left(k_x + k_y\right)\left(\frac{n\pi}{\ell}\right)^4 - \left[k_x k_y\left(\frac{I_x + I_y}{A} + h_x^2 + h_y^2\right)\right.$$
$$\left.+ k_\phi\left(k_x + k_y\right)\right]\left(\frac{n\pi}{\ell}\right)^2$$

$$A_0 = E^3 I_x I_y \Gamma \left(\frac{n\pi}{\ell}\right)^{12} + E^2 I_x I_y GJ \left(\frac{n\pi}{\ell}\right)^{10} - E^2 \left[I_x I_y k_x \left(y_o - h_y\right)^2 + I_x I_y k_y \left(x_o - h_x\right)^2 + I_x I_y k_\phi + \left(I_y k_y + I_x k_x\right)\Gamma \right] \left(\frac{n\pi}{\ell}\right)^8 + EI_x GJ \left(k_x + k_y\right) \left(\frac{n\pi}{\ell}\right)^6 + E \left[I_y k_x k_y \left(y_o - h_y\right)^2 + I_x k_x k_y \left(x_o - h_x\right)^2 + \left(I_y k_y + I_x k_x\right) k_\phi + k_x k_y \Gamma \right] \left(\frac{n\pi}{\ell}\right)^4 + k_x k_y GJ \left(\frac{n\pi}{\ell}\right)^2 + k_x k_y k_\phi \quad .$$

It can be seen that the values of the coefficients to the cubic equation depend on n. The value of n which minimizes the lowest positive root of the cubic equation must be found. The complexity of this solution may necessitate the use of a computer.

II Prescribed Axis of Rotation

Using the same differential equations given in the previous paragraph, we can investigate buckling of a bar for which the axis is prescribed about which the cross sections rotate during buckling. To obtain a rigid axis of rotation, we have only to assume that $k_x = k_y = \infty$. Then the n axis (Fig. C1.5-11) will remain straight during buckling and the cross sections will rotate with respect to this axis. The resulting differential equation is:

$$\left[E\Gamma + EI_y \left(y_o - h_y\right)^2 + EI_x \left(x_o - h_x\right)^2 \right] \frac{d^4\phi}{dz^4} - \left[GJ - \frac{I_o P}{A} + P\left(x_o^2 + y_o^2\right) - P\left(h_x^2 + h_y^2\right) \right] \frac{d^2\phi}{dz^2} + k_\phi \phi = 0 \quad .$$

Taking the solution of this equation in the form $\phi = A_3 \sin \frac{n\pi x}{\ell}$

$$P_{cr} = \frac{\left[E\Gamma + EI_y \left(y_o - h_y\right)^2 + EI_x \left(x_o - h_x\right)^2 \right] \left(\frac{n\pi}{\ell}\right)^2 + GJ + k_\phi \frac{\ell^2}{n^2\pi^2}}{\frac{I_o}{A} - \left(x_o^2 + y_o^2\right) + \left(h_x^2 + h_y^2\right)} \quad ,$$

we can calculate the critical buckling load in each particular case.

If the bar has two planes of symmetry, the solution is:

$$P_{cr} = \frac{\left(E\Gamma + EI_y h_y^2 + EI_x h_x^2\right)\left(\frac{n^2\pi^2}{\ell^2}\right) + GJ + k_\phi\left(\frac{\ell^2}{n^2\pi^2}\right)}{h_x^2 + h_y^2 + \left(\frac{I_o}{A}\right)} .$$

In each particular case, the value of n which makes P_{cr} a minimum must be found.

If the fixed axis of rotation is the shear-center axis, the solution becomes

$$P_{cr} = \frac{E\Gamma\left(\frac{n^2\pi^2}{\ell^2}\right) + GJ + k_\phi\left(\frac{\ell^2}{n^2\pi^2}\right)}{\frac{I_o}{A}} .$$

This expression is valid for all cross-sectional shapes.

III Prescribed Plane of Deflection

In practical design of columns, the situation arises in which certain fibers of the bar deflect in a known direction during buckling. For example, if a bar is welded to a thin sheet, as in Figure C1.5-12, the fibers of the bar in contact with the sheet cannot deflect in the plane of the sheet. Instead, the fibers along the contact plane nn must deflect only in the direction perpendicular to the sheet. In problems of this type, it is advantageous to take the centroidal axes, x and y, parallel and perpendicular to the sheet. Usually this means that the axes are no longer principal axes of the cross section.

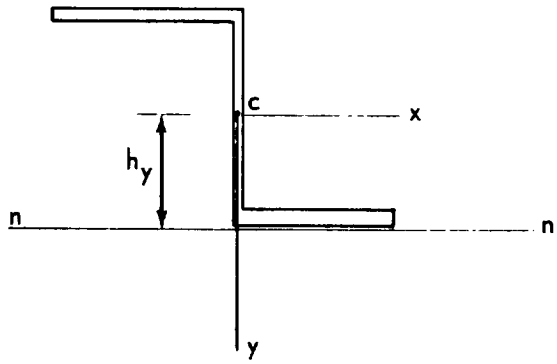

FIGURE C1.5-12 SECTION WITH PRESCRIBED PLANE OF DEFLECTION

For this case, two simultaneous differential equations can be obtained (Reference 8).

They are

$$EI_x \frac{d^4v}{dz^4} + P\frac{d^2v}{dz^2} - EI_{xy}\left(y_o - h_y\right)\frac{d^4\phi}{dz^4} - Px_o \frac{d^2\phi}{dz^2} = 0$$

$$\left[E\Gamma + EI_y\left(y_o - h_y\right)^2\right]\frac{d^4\phi}{dz^4} - \left(GJ - \frac{I_o}{A}P + Py_o^2 - Ph_y^2\right)\frac{d^2\phi}{dz^2}$$

$$- EI_{xy}\left(y_o - h_y\right)\frac{d^4v}{dz^4} - Px_o\frac{d^2v}{dz^2} = 0$$

These equations can be used to find the critical buckling loads for a given case. As before, taking simple supports and a solution in the form

$$v = A_2 \sin\frac{\pi z}{\ell} \qquad \phi = A_3 \sin\frac{\pi z}{\ell}$$

The following determinant can be obtained:

$$\begin{vmatrix} \left(EI_x\frac{\pi^2}{\ell^2} - P\right) & -\left[EI_{xy}\left(y_o - h_y\right)\frac{\pi^2}{\ell^2} - Px_o\right] \\ \left[-EI_{xy}\left(y_o - h_y\right)\frac{\pi^2}{\ell^2} + Px_o\right] & \left[E\Gamma\frac{\pi^2}{\ell^2} + EI_y\left(y_o - h_y\right)^2\frac{\pi^2}{\ell^2} + GJ - \frac{I_o}{A}P + Py_o^2 - Ph_y^2\right] \end{vmatrix} = 0$$

From this determinant a quadratic equation for P is obtained from which the critical load can be calculated in each particular case.

$$A_2P^2 + A_1P + A_0 = 0$$

where

$$A_2 = \frac{I_o}{A} - y_o^2 - x_o^2 + h_y^2$$

$$A_1 = -\frac{I_o}{A}P_x + P_x y_o^2 - P_x h_y^2 - \frac{I_o}{A}P_\phi - P_y\left(y_o - h_y\right)^2 + 2x_o P_{xy}\left(y_o - h_y\right)$$

$$A_0 = \frac{I_o}{A}P_\phi P_x + P_x P_y\left(y_o - h_y\right)^2 - P^2_{xy}\left(y_o - h_y\right)^2$$

$$P_x = EI_x\frac{\pi^2}{\ell^2}$$

$$P_y = EI_y\frac{\pi^2}{\ell^2}$$

$$P_{xy} = EI_{xy}\frac{\pi^2}{\ell^2}$$

$$P_\phi = \frac{A}{I_o}\left(GJ + E\Gamma\frac{\pi^2}{\ell^2}\right)$$

$$I_o = I_x + I_y + A\left(x_o^2 + y_o^2\right)$$

If the bar is symmetrical with respect to the y axis, as in the case of a channel, the x axis and the y axis become the principal axes. Then, with the substitution of $I_{xy} = 0$ and $x_o = 0$, the two equations become independent. The first of these equations gives the Euler load for buckling in the plane of symmetry. The second equation gives

$$P_{y\phi} = \frac{E\Gamma\left(\frac{\pi^2}{\ell^2}\right) + EI_y\left(y_o - h_y\right)^2\left(\frac{\pi^2}{\ell^2}\right) + GJ}{\left(\frac{I_o}{A}\right) - y_o^2 + h_y^2}$$

which represents the torsional buckling load for this case.

C1.5.3 ECCENTRICALLY LOADED COLUMNS

I General Cross Section

In the previous sections we have considered the buckling of columns subjected to centrally applied compressive loads only. The case when the force, P, is applied eccentrically (Fig. C1.5-13) will not be considered.

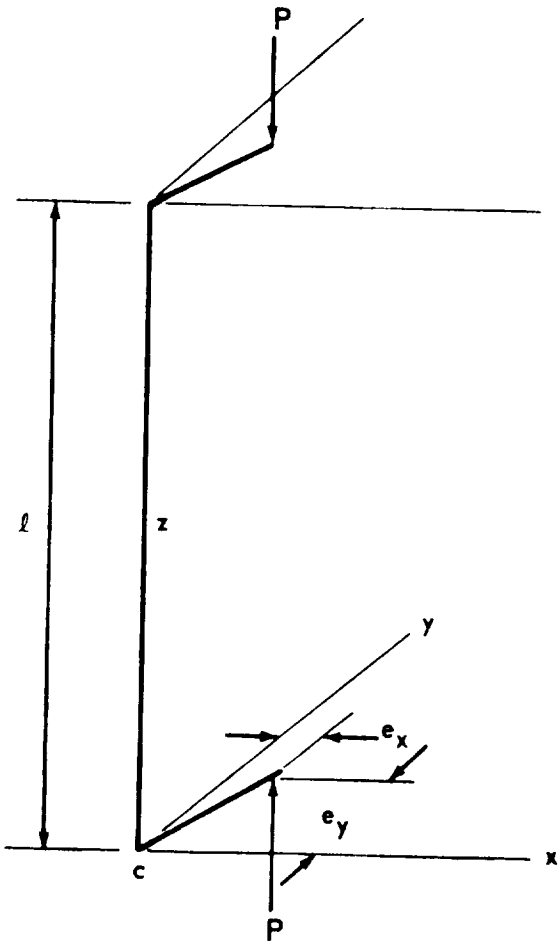

FIGURE C1.5-13 ECCENTRICALLY APPLIED LOAD

In investigating the stability of the deflected form of equilibrium, and considering the case of simply supported ends, the following determinant for calculation of the critical loads is obtained (Reference 8).

$$\begin{vmatrix} (P - P_y) & o & P(y_o - e_y) \\ o & (P - P_x) & P(e_x - x_o) \\ P(y_o - e_y) & P(e_x - x_o) & Pe_y\beta_1 + Pe_x\beta_2 + P\frac{I_o}{A} - \frac{I_o}{A}P_\phi \end{vmatrix} = 0$$

The solution of this determinant gives the following cubic equation for calculating P_{cr}:

$$A_3P^3 + A_2P^2 + A_1P + A_0 = 0$$

where

$$A_3 = \frac{A}{I_o}\left[e_x\beta_2 + e_y\beta_1 - (e_y - y_o)^2 - (e_x - x_o)^2\right] + 1$$

$$A_2 = \frac{A}{I_o}\left[P_x(y_o - e_y)^2 + P_y(x_o - e_x)^2 - e_x\beta_2(P_x + P_y) - e_y\beta_1(P_x + P_y)\right] - (P_x + P_y + P_\phi)$$

$$A_1 = \frac{A}{I_o}\left[P_xP_ye_x\beta_2 + P_xP_ye_y\beta_1\right] + (P_xP_y + P_yP_\phi + P_xP_\phi)$$

$$A_0 = -P_xP_yP_\phi$$

$$P_x = EI_x\frac{\pi^2}{\ell^2}$$

$$P_y = EI_y\frac{\pi^2}{\ell^2}$$

$$P_\phi = \frac{A}{I_o}\left(GJ + E\Gamma\frac{\pi^2}{\ell^2}\right)$$

$$I_o = I_x + I_y + A\left(x_o^2 + y_o^2\right)$$

$$\beta_1 = \frac{1}{I_x}\left(\int_A y^3 dA + \int_A x^2 y dA\right) - 2y_o$$

$$\beta_2 = \frac{1}{I_y}\left(\int_A x^3 dA + \int_A x y^2 dA\right) - 2x_o \quad .$$

In the general case, buckling of the bar occurs by combined bending and torsion. In each particular case, the three roots of the cubic equation can be evaluated numerically for the lowest value of the critical load.

The solution becomes very simple if the thrust, P, acts along the shear-center axis. We then have

$$e_x = x_o \quad , \quad e_y = y_o$$

and the buckling loads become independent of each other. In this case, lateral buckling in the two principal planes and torsional buckling may occur independently. Thus, the critical load will be the lowest of the two Euler loads, P_x, P_y, and the load corresponding to purely torsional buckling, which is:

$$P = \frac{\frac{I_o}{A} P_p}{e_y\beta_1 + e_x\beta_2 + \frac{I_o}{A}} \quad .$$

II One Axis of Symmetry

Another special case occurs when the bar has one plane of symmetry (which is true for many common sections). Assuming that the yz plane is the plane of symmetry (Fig. C1.5-13), the x_o β_2 0. The solution for the critical buckling loads is obtained in the same manner as in Paragraph I.

A case of common interest occurs when the load, P, acts in the plane of symmetry; then $e_x = 0$. When this happens, buckling in the plane of symmetry takes place independently and the corresponding critical load is the same as the Euler load. However, lateral buckling in the xz plane and torsional buckling are coupled, and the corresponding critical loads are obtained from the following quadratic equation:

$$\left(P_y - P\right)\left[\frac{I_o}{A}P_\phi - P\left(e_y\beta_1 + \frac{I_o}{A}\right)\right] - P^2\left(y_o - e_y\right)^2 = 0 \quad .$$

III Two Axes of Symmetry

If the cross section of the bar has two axes of symmetry, the shear center and the centroid coincide. Then $y_o = x_o = \beta_1 = \beta_2 = 0$, which simplifies the solutions of Paragraphs I and II somewhat.

C1.5.4 EXAMPLE PROBLEMS FOR TORSIONAL-FLEXURAL INSTABILITY OF COLUMNS

I Example Problem 1

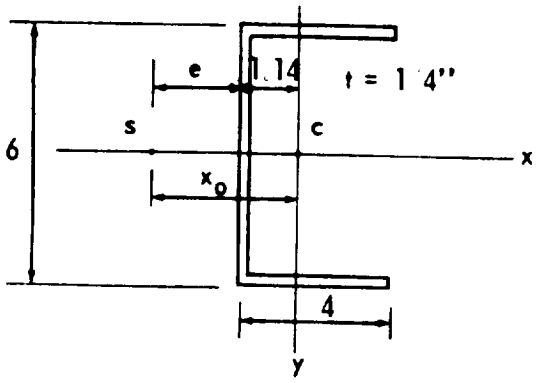

c - centroid

s - shear center

Given:

L = 60 in.

A = 3.5 in.^{2}

I_x = 22.5 in.^{4}

I_y = 6.05 in.^{4}

E = 10.5 x 10^6 psi

G = 4.0 x 10^6 psi

J = .073 in.^{4}

Find critical load applied at centroid, c, and the mode of buckling. Use general method and also use method of Section C1.5.1-III.

A. Method 1

From Section C1.5.1-III, equation (5),

$$P_{cr} = \frac{1}{2K}\left[\left(P_\phi + P_x\right) - \sqrt{\left(P_\phi - P_x\right)^2 - 4KP_\phi P_x}\right]$$

where $K = 1 - \left(\frac{x_o}{r_o}\right)^2$.

From Table I,

$$e = \frac{3b^2t_f}{6bt_f + ht_w} = \frac{3(4)^2(\frac{1}{4})}{6(4)(\frac{1}{4}) + 6(\frac{1}{4})} = 1.6 \text{ in.}$$

and

$$\Gamma = \frac{t_f b^3 h^2}{12}\,\frac{3bt_f + 2ht_w}{6bt_f + ht_w}$$

$$\Gamma + \frac{(\frac{1}{4})(4)^3(6)^2}{12}\left[\frac{3(4)(\frac{1}{4}) + 2(6)(\frac{1}{4})}{6(4)(\frac{1}{4}) + 6(\frac{1}{4})}\right]$$

$$\Gamma = 38.4 \text{ in.}^6$$

$$I = I_x + I_y + A X_o^2$$

$$I_o = 22.5 + 6.05 + 3.5\,(2.74)^2$$

$$I_o = 54.75 \text{ in.}^4$$

$$r_o^2 = \frac{I_o}{A} = \frac{54.75}{3.5} = 15.65 \text{ in.}^2$$

$$P_x = \frac{\pi^2 E I_x}{\ell^2} = \frac{\pi^2 10.5 \times 10^6 \times 22.5}{(60)^2} = 647,691 \text{ lbs}$$

$$P_y = \frac{\pi^2 E J_y}{\ell^2} = \frac{\pi^2 10.5 \times 10^6 \times 6.05}{(60)^2} = 174,000 \text{ lbs}$$

$$P_\phi = \frac{1}{r_o^2}\left[GJ + \frac{E\Gamma\pi^2}{\ell}\right]$$

$$P_\phi = \frac{1}{15.65}\left[4 \times 10^6 (.073) + \frac{10.5 \times 10^6 (38.4)\pi^2}{(60)^2}\right]$$

$$P_\phi = 89,200 \text{ lbs}$$

$$K = 1 - \left(\frac{x_o}{r_o}\right)^2 = 1 - \frac{(2.74)^2}{15.65} = 0.55$$

$$P_{cr} = \frac{1}{2(0.55)}\left[(89,200 + 647,691) - \sqrt{(89,200 + 647,691)^2 - 4(0.55)(89,200)(647,691)}\right]$$

$P_{cr} = 82,727$ lbs ,

therefore, critical load is 82,727 pounds and the mode is torsional-flexural buckling.

B. Method 2

Check Figure C1.5-4(b) for critical mode of buckling with

$$b/a = 4/6 = 0.66 \quad , \quad c/a = 0 \quad , \quad \frac{t\ell}{a^2} = 0.416 \quad .$$

Since the point plots are below the curve for $c/a = 0$, the critical mode of buckling will be torsional-flexural buckling.

From Figure C1.5-7(a), $K = 0.53$

From Figure C1.5-10, $C_1 = 0.31$ and $C_2 = 0.20$.

From Section C1.5.1-III, equation (7),

$$P_\phi = EA\left[C_1 (t/a)^2 + C_2(a/\ell)^2\right]$$

$$P_\phi \quad 10.5 \times 10^6(3.5)\left[0.31\left(\frac{0.25}{6}\right)^2 + 0.2\left(\frac{6}{60}\right)^2\right]$$

$$P_\phi = 93,500 \text{ lbs}$$

$$P_x \quad \frac{\pi^2 EI_x}{\ell^2} = 647,691 \text{ lbs}$$

$$P_{cr} = \frac{1}{2(0.53)}\left[(93,500 + 647,691)\right.$$

$$\left. -\sqrt{(93,500 + 647,691) - 4(0.53)(93,500)(647,691)}\right]$$

$P_{cr} = 86,668$ lbs

II Example Problem 2

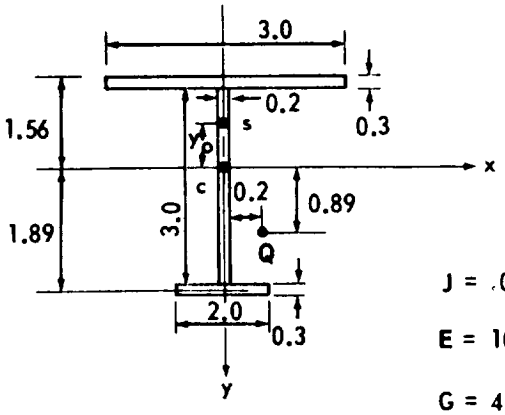

c = centroid

s = shear center

Q = point of load application

Given: $A = 2.1$ in.^{2}

$J = .053$ in.^{4} $\quad I_x = 4.43$ in.^{4}

$E = 10.5 \times 10^6$ psi $\quad I_y = .88$ in.^{4}

$G = 4.0 \times 10^6$ psi $\quad L = 50$ in.

Find: Critical load applied at point Q.

To locate shear center and evaluate the warping constant, refer to Table I.

$$e = \frac{hb_1^3}{b_1^3 + b_2^3} = \frac{3.3(3.0)^3}{(3.0)^3 + (2.0)^3} = -2.546$$

$$y_o = -2.546 + 1.89 = -0.656$$

$$\Gamma = \frac{t_f h^2}{12} \frac{b_1^3 b_2^3}{b_1^3 + b_2^3}$$

$$\Gamma = \frac{0.3(3.3)^2}{12} \frac{(3)^3(2)^3}{(3)^3 + (2)^3}$$

$$\Gamma = 1.68 \text{ in.}^6$$

To calculate I_o, β_1, β_2 refer to Paragraph C1.5.3-I:

$$I_o = I_x + I_y A(y_o)^2$$

$$I_o = 4.43 + 0.88 + (2.1)(-0.656)^2$$

$$I_o = 6.21 \text{ in.}^4$$

$$\beta_1 = \frac{1}{I_x}\left(\int_A y^3 da + \int x^2 y da\right) - 2y_o$$

$$\beta_1 = \frac{1}{4.43}\left[(3.0)(0.3)(-1.41)^3 + 3.0(0.2)(0.24)^3 + 2.0(0.3)(1.89)^3\right]$$

$$-2(-0.656)$$

$$\beta_1 = 1.66 \text{ in.}$$

$$\beta_2 = 0$$

$$P_x = \frac{\pi^2 EI_x}{\ell^2} = \frac{\pi^2 10.5 \times 10^6 (4.43)}{(50)^2} \quad 183,633 \text{ lbs}$$

$$P_y = \frac{\pi^2 EI_y}{\ell^2} \quad 36,477 \text{ lbs}$$

$$P_\varphi = \frac{A}{I_o}\left[GJ + \frac{E\Gamma\pi^2}{\ell^2}\right] = \frac{2.1}{6.21}\left[1 \times 10^6(0.053) + \frac{10.5 \times 10^6(1.68)\pi^2}{(50)^2}\right]$$

$$P_\varphi \quad 95,239 \text{ lbs} \quad .$$

Now calculate the coefficients to the cubic equation in Paragraph C1.5.3-I:

$$A_3 = \frac{A_o}{I_o}\left[e_x\beta_2 + e_y\beta_1 - (e_y - y_o)^2 - (e_x - y_o)^2\right] + 1$$

$$A_3 = \frac{2.1}{6.21}\left[(0.2)(0) + (0.89)(1.66) - (0.89 + 0.655)^2 - (0.2-0)^2\right] + 1$$

$$A3 = 0.6789$$

$$A_2 = \frac{A}{I_o}\left[P_x\left(y_o - e_y\right)^2 + P_y\left(x_o - e_x\right)^2 - e_x\beta_2\left(P_x + P_y\right) - e_y\beta_1\left(P_x + P_y\right)\right]$$

$$-\left(P_x + P_y + P_\varphi\right)$$

$$A_2 = \frac{2.1}{6.21}\left[183,633(-0.655-0.89)^2 + 36,477(0-0.2)^2\right.$$

$$\left.-0.2(0)(183,633 + 36,477) - (0.89)(1.66)(183,633 + 36,477)\right]$$

$$A_2 = -276,596$$

$$A_1 = \frac{A}{I_o}\left[P_x P_y e_x\beta_2 + P_x P_y e_y\beta_1\right] + \left(P_x P_y + P_y P_\phi + P_x P_\varphi\right)$$

$$A_1 = \frac{2.1}{6.21}\left[183,633(36,477)(0.2)(0) + 183,633(36,477)(0.89)(1.66)\right]$$

$$+\left[183,633(36,477) + 36,477(95,394) + (183,633)(95,394)\right]$$

$$A_1 = 31.042 \times 10^9$$

$$A_0 = -P_x P_y P_\varphi$$

$$A_0 = -(183,633)(36,477)(95,394)$$

$$A_0 = -638.985 \times 10^{12}$$

$$A_3P^3 + A_2P^2 + A_1P + A_0 = 0 \quad .$$

Dividing by A_3, $P^3 + \frac{A_2}{A_3}P + \frac{A_1}{A_3}P + \frac{A_0}{A_3} = 0$

let $k = \frac{A_2}{A_3}$, $q = \frac{A_1}{A_3}$, $r = \frac{A_0}{A_3}$

$k = -4.0742 \times 10^5$

$q = 4.5725 \times 10^{10}$

$r = -9.4123 \times 10^{14}$.

For solution of cubic, let $P = X - k/3$, then the cubic reduces to

$$X^3 + aX + b = 0$$

where

$a = 1/3(3q - k^2)$

$b = \frac{1}{27}(2k^3 - 9kq + 27r)$

$a = -0.9605 \times 10^{10}$

$b = 0.259 \times 10^{15}$

$Q = \frac{b^2}{4} + \frac{a^3}{27} = -0.01605 \times 10^{30}$.

Since $Q < 0$, we have three real, unequal roots given by

$$X_k = -2\sqrt{-\frac{a}{3}} \cos\left(\frac{\phi}{3} + 120K\right) , \quad K = 0, 1, 2$$

where

$$\phi = \text{arc cos}\sqrt{\frac{b^2}{4} \div \left(-\frac{a^3}{27}\right)} \qquad \phi = 45°39'$$

$X_o = -109,200$

$X_1 = 80,324$

$X_2 = 28,876$.

Substitute these roots into $P = x - k/3$ for critical load values.

$P_1 = X_1 - 1/3$

$$P_1 = -109,200 - \frac{(-4.0742 \times 10^5)}{3}$$

$P_1 = 26,606$ lbs

$P_2 = 80,324 + 135,806$

$P_2 = 216,130$ lbs

$P_3 = 28,876 + 135,806$

$P_3 = 164,682$ lbs .

Therefore, the critical load is $P_1 = 26,606$ pounds.

III Example Problem 3

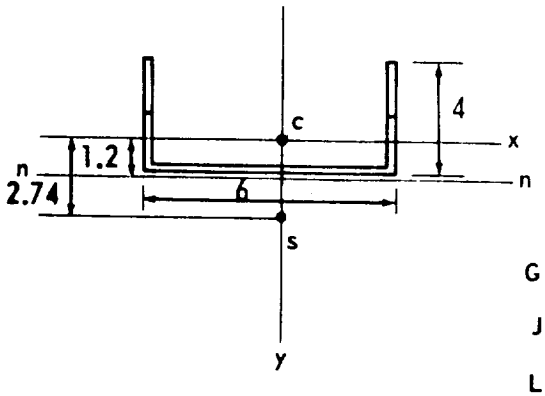

c = centroid

s = shear center

$I = 38.4 \text{ in}^6$

$A = 2.1 \text{ in.}^2$

$G = 4 \times 10^6 \text{ psi}$ $\quad I_{xx} = 6.05 \text{ in.}^4$

$J = .073$ $\quad I_y = 22.5 \text{ in.}^4$

$L = 60 \text{ in.}$ $\quad E = 10.5 \times 10^6 \text{ psi}$

Find the critical load applied at point c (centroid) with prescribed deflection normal to plane n-n (refer to Section C1.5.2-III). For Euler buckling about the x axis the critical load is

$$P_x = \frac{\pi^2 E I_x}{\ell^2} = \frac{\pi^2 10.5 \times 10^6 (6.05)}{(60)^2} = 174,157 \text{ lbs} .$$

The torsional buckling load is

$$P_{y\phi} = \frac{E\Gamma\left(\frac{\pi^2}{\ell^2}\right) + EI_y\left(y_o - h_y\right)^2\left(\frac{\pi^2}{\ell^2}\right) + GJ}{\frac{I_o}{A} - y_o^2 + h_y^2}$$

$$P_{y\phi} = \frac{10.5\text{x}10^6(38.4)\left(\frac{\pi}{60}\right)^2 + 10.5\text{x}10^6(22.5)(2.74-1.2)^2\left(\frac{\pi}{60}\right)^2 + 4\text{x}10^6(0.073)}{\frac{54.75}{2.1} - (2.74)^2 + (1.2)^2}$$

$$P_{y\phi} = 146,672 \text{ lbs} .$$

Therefore, the critical load is $P_{y\phi}$ (146,672 lbs) and the mode of failure is **torsional buckling, assuming no local failures.**

REFERENCES

1. Timoshenko, S.: Strength of Materials. Part I and II, Third Edition, D. Van Nostrand Company, Inc., New York, 1957.

2. Seely, F. B., and Smith, J. O.: Advanced Mechanics of Materials. Second Edition, John Wiley & Sons, Inc., New York, 1957.

3. Popov, E. P.: Mechanics of Materials. Prentice-Hall, Inc., New York, 1954.

4. Sechler, E. E., and Dunn, L. G.: Airplane Structural Analysis and Design. John Wiley & Sons, Inc., New York, 1942.

5. Steinbacher, F. R., and Gerard, G.: Aircraft Structural Mechanics. Pitman Publishing Corporation, New York, 1952.

6. Niles, A. S., and Newall, J. S.: Airplane Structures. Vol. II, Third Edition, John Wiley & Sons, Inc., New York, 1943.

7. Chajes, A., and Winter, G.: Torsional-Flexural Buckling of Thin-Walled Numbers. Journal of Structural Division, ASCE Proceedings, August 1965, p. 103.

8. Timoshenko, S. P., and Gere, J. M.: Theory of Elastic Stability. McGraw-Hill Book Company, Inc., New York, 1961.

9. Bleich, F.: Buckling Strength of Metal Structures. McGraw-Hill Book Company, Inc., New York, 1952.

SECTION C2

STABILITY OF PLATES

TABLE OF CONTENTS

TABLE OF CONTENTS (Continued)

TABLE OF CONTENTS(Concluded)

SECTION C2. STABILITY OF PLATES

2.1 BUCKLING OF FLAT PLATES.

This section contains design information for predicting the buckling of flat plates. Various geometrical shapes under several types of loading common to aerospace structures are considered. In most cases the methods presented may be used in either the elastic or plastic stress range. For plates subjected to thermal gradients which may cause buckling, reference should be made to Section D4.0.2, "Thermal Buckling of Plates."

2.1.1 UNSTIFFENED PLATES.

With few exceptions, plate critical stress equations take the following form:

$$F_{cr} = \eta \bar{\eta} \frac{k \pi^2 E}{12(1 - \nu_e^2)} \left(\frac{t}{b}\right)^2 \qquad (1)$$

where the terms are defined as follows:

F_{cr} buckling stress which includes the effects of plasticity and cladding (psi)

η plasticity reduction factor

$\bar{\eta}$ cladding reduction factor

k buckling coefficient

E Young's Modulus (elasticity) (psi)

ν_e elastic Poisson's ratio

t plate thickness (in.)

b dimension of plate (usually short dimension, in.)

The buckling constant, k, depends only on the plate dimensions, excluding its thickness, and upon the condition of support at the edges. For the material, temperature, and stress level used, the proper values of E, ν_e, η, and $\bar{\eta}$ must be substituted into the equation above.

Buckling curves are used to find values of the buckling coefficient, k, for numerous loading conditions and various boundary conditions. By knowing only the plate aspect ratio, a/b, values of k can be read directly.

The wavelength of the buckled surface is an important factor in establishing the critical buckling stress. A plate will buckle into a "natural" wavelength corresponding to a minimum load. This principle has been applied to advantage in structures to increase the efficiency of the flat sheet. That is, if by any structural means the natural wavelength of buckling can be prevented, the plate will carry more load.

I. Plasticity Reduction Factor

A tremendous amount of theoretical and experimental work has been done relative to the value of the so-called plasticity correction factor. Possibly the first values used by design engineers were $\eta = E_t/E$ or $\eta = E_{sec}/E$. Whatever the expression for η, it must involve a measure of the stiffness of the material in the inelastic stress range; and, since the stress-strain relation in the plastic range is nonlinear, a resort must be made to the

stress-strain curve to obtain a plasticity correction factor. This complication is greatly simplified by using the Ramberg and Osgood equations for the stress-strain curve which involves three simple parameters:

$$\frac{E\epsilon}{F_{0.7}} = \frac{f}{F_{0.7}} + \left(\frac{f}{F_{0.7}}\right)^n \qquad (2)$$

where $n = 1 + \log_e(17/7) \Big/ \log_e (F_{0.7}/F_{0.85})$, and the terms are defined as follows:

$F_{0.7}$ secant yield stress taken as the intersection of the curve and a slope $0.7E$ drawn from origin

n a parameter which describes the shape of the stress-strain curve on the yield region

$F_{0.85}$ stress at the intersection of the curve by a line of slope of $0.85E$ through the origin

Reference 1 gives values for $F_{0.7}$, $F_{0.85}$, and many flight vehicle materials; some of these are given in Table C2-1.

There is usally a maximum, or "cutoff" stress, above which it is considered unsafe to stress the material. The value of this cutoff stress differs with the type of loading, and may vary according to the design criteria established for each design. Suggested values of the cutoff stress are presented in Table C2-2. A check should be made to ensure that the buckling stress is equal to, or less than, the cutoff stress.

With the use of the Ramberg-Osgood parameters, plasticity reduction factors will be given for various types of loading in the paragraphs which follows.

II. Cladding Reduction Factors

Aluminum alloy sheets are available with a thin covering of practically pure aluminum and is widely used in aircraft structures. Such material is referred to as alclad or clad aluminum alloy. The mechanical strength properties of this clad material is considerably lower than the core material. Since the clad is located at the extreme fibers of the alclad sheet, it is located where the strains attain their value when buckling takes place. Figure C2-1 shows the makeup of an alclad sheet and Fig. C2-2 shows the stress-strain curves for cladding, core, and combinations. Thus, a further correction must be made for alclad sheets because of the lower strength clad covering material. Reference 1 gives simplified cladding reduction factors as summarized in Table C2-3.

2.1.1.1 Rectangular Plates.

Rectangular plates subjected to loads which cause instability constitute one of the major elements encountered in the structural design of space vehicles. Rectangular plate simulation occurs in such areas as beam webs, panels, and flanges.

I. Compressive Buckling

Figure C2-3 shows the change in buckled shape of rectangular plates as the boundary conditions are changed on the unloaded edges from free to restrained. In Fig. C2-3(a) the sides are free; thus, the plate acts as a

column. In Fig. C2-3(b) one side is restrained and the other side is free; such a restrained plate is referred to as a flange. In Fig. C2-3(c) both sides are restrained; this restrained element is referred to as a plate.

Critical compressive stress for buckling of plate columns (free at two unloaded edges) can be obtained from Fig. C2-4. As can be seen from this figure, a transition occurs with changing $b/L\sqrt{c}$ values as evidenced by the varying value of ψ between the limits $(1-\nu_e^2) < \psi < 1$. The increased load-carrying capacity of a wide plate column, $\psi = 1$, is due to antielastic bending effects in the plate at buckling. For narrow columns, $\psi = 1 - \nu_e^2$, the equation reduces to the Euler equation.

Figure C2-5 gives curves for finding the buckling coefficient, k, to use in equation (1) for various boundary, or edge, conditions and a/b ratio of the plate. The letter C on an edge means clamped or fixed against rotation. The letter F means a free edge and SS means simply supported or hinged. From these curves it can be seen that for long plates, $(a/b) > 4$, the effect of the loaded edge support condition is negligible.

The buckling of a rectangular plate compressed by two equal and opposite forces located at the midpoint of its long side (Fig. C2-6) is given in Reference 2. For simply supported sides, the following equation is true:

$$P_{cr} = \frac{\pi^2 D}{2b}\left[\frac{1}{\frac{\pi}{8}\left(\tanh\frac{\pi\beta}{2} - \frac{\frac{\pi\beta}{2}}{\cosh^2\frac{\pi\beta}{2}}\right)}\right] \qquad (3)$$

For long plates, (a/b) > 2, this reduces to

$$P_{cr} = \frac{4\pi D}{b} \quad . \tag{4}$$

If the long sides of the plate are clamped, the solution reduces to

$$P_{cr} = \frac{8\pi D}{b} \quad . \tag{5}$$

Figure C2-7 shows curves for k_c for various degrees of restraint (μ) along the sides of the sheet panel, where μ is the ratio of rotational rigidity of the plate. Figure C2-8 shows curves for k_c for a flange that has one edge free and the other with various degrees of edge restraint.

Figure C2-9 gives the k_c factor for a long sheet panel with two extremes of edge stiffener, namely a zee-stiffener which is a torsionally weak stiffener and a hat section which is a closed section and, therefore, a relatively strong stiffener torsionally.

To account for buckling in the inelastic range, one must obtain the plasticity reduction factor. By using the Ramberg-Osgood parameters of Paragraph 2. 1. 1 along with Figs. C2-10 and C2-11, one can find the compression buckling stress for flat plates with various boundary conditions.

Cladding reduction factors should be obtained from Paragraph 2. 1. 1.

II. Shear Buckling

The critical elastic shear buckling stress for flat plates with various boundary conditions is given by the following equation:

$$F_{s_{cr}} = \frac{\pi^2 k_s E}{12(1-\nu_e^2)} \left(\frac{t}{b}\right)^2 \qquad (6)$$

where b is always the shorter dimension of the plate, as all edges carry shear. The shear buckling coefficient, k_s, is plotted as a function of the plate aspect ratio a/b in Fig. C2-12 for simply supported edges and clamped edges.

It is interesting to note that a long rectangular plate subjected to pure shear produces internal compressive stresses on planes at 45 degrees with the plate edges. Thus, these compressive stresses cause the long panel to buckle in patterns at an angle to the plate edges as illustrated in Fig. C2-13; the buckle patterns have a half-wave length of 1.25 b.

Shear buckling of rectangular plates with mixed boundary conditions has been investigated by Cook and Rockey [3]. The results are tabulated in Table C2-4.

If buckling occurs at a stress above the proportional limit stress, a plasticity correction factor should be included in equation (6). This factor can be taken as $\eta_s = G_s/G$ where G is the shear modulus and G_s the shear secant modulus as obtained from a shear stress-strain diagram

for the material. Also, Fig. C2-14 can be used for panels with edge rotational restraint if the values of $\sigma_{0.7}$ and n are known.

III. Bending Buckling

The critical elastic bending buckling stress for flat plates is

$$F_{b_{cr}} = \frac{\pi^2 k_b E}{12(1-\nu_e^2)} \left(\frac{t}{b}\right)^2 \quad . \qquad (7)$$

When a plate buckles in bending, it involves relatively short wavelength buckles equal to (2/3)b for long plates with simply supported edges (Fig. C2-15). Thus, the smaller buckle patterns cause the buckling coefficient k_b to be larger than k_c or k_s.

Figure C2-16 gives the critical stress coefficients for a plate in bending in the plane of the plate with all edges simply supported. Figure C2-17 gives the coefficients for the case when the plate tension side is simply supported and the compression side is fixed. Figure C2-18 gives the coefficients as a function of a/b for various degrees of edge rotational restraint.

The plasticity reduction factor can be obtained from Fig. C2-10 using simply supported edges.

IV. Buckling Under Combined Loads

Practical design of plates usually involves a combined load system. The buckling strength of plates under combined loads will be determined by use of interaction equations.

A. Combined Bending and Longitudinal Compression

The interaction equation that is accepted for combined bending and longitudinal compression is

$$R_b^{1.75} + R_c = 1.0 \qquad (8)$$

This equation is plotted in Fig. C2-19. Also shown are curves for various margin-of-safety (M. S.) values.

B. Combined Bending and Shear

The interaction equation for combined bending and shear is

$$R_b^2 + R_s^2 = 1.0 \quad , \qquad (9)$$

and the expression for margin of safety is

$$\text{M. S.} = \frac{1}{\sqrt{R_b^2 + R_s^2}} - 1 \qquad (10)$$

Figure C2-20 is a plot of equation (9). Curves showing various M. S. values are also shown. R_s is the stress ratio due to torsional shear stress and R_s is the stress ratio for transverse or flexural shear stress.

C. Combined Shear and Longitudinal Direct Stress (Tension or Compression)

The interaction equation for this combination of loads is

$$R_L + R_s^2 = 1.0 \quad , \qquad (11)$$

and the expression for margin of safety is

$$\text{M. S.} = \frac{2}{\left(R_L + \sqrt{R_L^2 + 4R_s^2}\right)} - 1 \quad . \qquad (12)$$

Figure C2-21 is a plot of equation (11). If the direct stress is tension, it is included on the figure as negative compression using the compression allowable.

D. Combined Compression, Bending, and Shear

The conditions for buckling under combined compression, bending, and shear are represented by the interaction curves of Fig. C2-22. This figure tells whether or not the plate will buckle but will not give the margin of safety. Given the ratios R_c, R_s, and R_b: If the value of the R_c curve defined by the given value of R_b and R_s is greater numerically than the given value of R_c, then the panel will buckle.

The margin of safety of elastically buckled flat plates may be determined from Fig. C2-23. The dashed lines indicate a typical application where $R_c = 0.161$, $R_s = 0.23$, and $R_b = 0.38$. Point 1 is the first determined for the specific value of R_s and R_b. The dashed diagonal line from the origin 0 through point 1, intersecting the related R_c/R_s curve at point 2, yields the allowable shear and bending stresses for the desired margin of safety calculations. (Note: When R_c is less than R_s use the right half of the figure; in other cases use the left half.)

E. Combined Longitudinal Bending, Longitudinal Compression, and Transverse Compression

A theoretical investigation by Noel [4] has been performed on the buckling of simply supported flat rectangular plates under critical

combinations of longitudinal bending, longitudinal compression, and lateral compression. Interaction curves for these loadings are presented in Fig. C2-24 for various plate aspect ratios. These curves can be used for the limiting case of two loading conditions by setting one stress ratio equal to zero. The results of the studies leading up to (and verified by) these curves indicate that the reduction in the allowable bending stress due to the additon of lateral compression is greatly magnified by the further addition of only a small longitudinal compressive load.

F. Combined Bending, Shear, and Transverse Compression

Interaction surfaces for combined bending, shear, and transverse compression have been established by Johnston and Buckert [5] for infinitely long plates. The two types of support considered were simple support along both long edges, and simple support along the tension (due to bending) edge with clamping along the compression (due to bending) edge. The resulting curves are shown in Fig. C2-25 and C2-26.

In the case of transverse compression and shear acting alone, Batdort and Houbolt [6] examined long plates with edges elastically restrained. It was found that an appreciable fraction of the critical stress in pure shear may be applied to the plate without any reduction in the transverse compressive stress necessary to produce buckling. Batdorf and Stein [7] examined simply supported plates of finite aspect ratio and found that the curve for infinitely long plates required modification for finite aspect ratios. This condition is shown in Fig. C2-27.

G. Combined Longitudinal Compression, Transverse Compression, and Shear

Johnson [8] has examined critical combinations of longitudinal compression, transverse compression, and shear for simply supported flat rectangular plates. The calculated data are presented graphically in Figs. C2-28 through C2-32. To make use of these curves, the following procedure must be observed:

1. Calculate the ratios $k_x/k_s = N_x/N_s$ and $k_y/k_s = N_y/N_s$.

2. On the curve corresponding to the plate a/b, lay off a straight line from the origin of k_x/k_s.

3. At the intersection of this line and the curve corresponding to the k_y/k_s ratio of step 1, read k_y and/or k_s.

4. Determine required plate thickness from

$$N_x = (f_x)_{appl.}(t) = \frac{k_x \pi^2 E}{12(1 - \nu_e^2)} \frac{t^3}{b^2}$$

or

$$t^3_{req'd.} = \frac{(N_x)_{appl.} B}{k_x} = \frac{(N_y)_{appl.} B}{k_y} = \frac{(N_s)_{appl.} B}{k_s}$$

where

$$B = \frac{12(1 - \nu_e^2) b^2}{\pi^2 E}$$

If desired, the value of k_y may be determined from k_s and k_y/k_s.

5. Determine the margin of safety. Assuming that the loads increase at the same rate and are therefore in the same proportion to each other at all load levels, the margin of safety based on load is given by

$$M.S. = \left(\frac{N_{cr}}{N_{appl.}}\right) - 1 = \left(\frac{t_d}{t_{req'd.}}\right)^3 - 1$$

where t_d is the design thickness. Margin of safety based on stress is given by

$$M.S. = \left(\frac{f_{cr}}{f_{appl.}}\right) - 1 = \left(\frac{t_d}{t_{req'd.}}\right)^2 - 1 \quad .$$

EXAMPLE:

Consider a simply supported plate with $a = 10$ in., $b = 5$ in., $t = 0.051$ in., $\nu_e = 0.30$, $E = 10^7$ lb/in.^{2}, $N_x = 100$ lb/in., $N_y = 32$ lb/in., and $N_s = 80$ lb/in. Determine the margin of safety.

Calculate the stress ratios and load ratios:

$$k_y/k_s = N_y/N_s = 32/80 = 0.4$$

$$k_x/k_s = N_x/N_s = 100/80 = 1.25$$

On Fig. C2-33, the interaction curves for $a/b = 2$, lay off a line from the origin of slope $k_x/k_s = 1.25$. The intersection of this line with the curve $k_y/k_s = 0.4$ determines the critical buckling coefficients for three loads. From Fig. C2-33, the following values are obtained:

$$k_x = 2.5 \quad , \quad k_s = 2.0 \quad , \quad \text{and} \quad k_y/k_s = 0.4 \quad ;$$

therefore, $k_y = 0.8$.

To determine the plate thickness required to sustain these loads, any one of the three buckling coefficients determined may be used. Using k_x, the following value is obtained:

$$t_{req'd.} = \left[\frac{N_x \, 12(1 - \nu_e^2) \, b^2}{k_x \pi^2 E} \right]^{1/3} = 0.048 \text{ in.}$$

Since the actual design thickness is 0.051 in., the margin of safety based on stress is

$$\text{M. S.} = \left[\frac{t_d}{t_{req'd.}} \right]^2 - 1 = \left(\frac{0.051}{0.048} \right)^2 - 1 = +0.1289.$$

The margin of safety based on load is

$$\text{M. S.} = \left(\frac{t_d}{t_{req'd.}} \right)^3 - 1 = +0.1995 \; .$$

H. Combined Shear and Nonuniform Longitudinal Compression

Bleich [9] presents a solution for buckling of a plate subjected to combined shear and nonuniform longitudinal compression as shown in Fig. C2-33. The critical buckling coefficient is for

$$\alpha \geq 1: \quad k = 3.85 \, \gamma^2 \beta \sqrt{\beta^2 + 3} \left(-1.0 + \sqrt{1 + \frac{4}{\beta^2 \gamma^2}} \right) \qquad (13)$$

where

$$\gamma = \frac{5.34 + \frac{4}{\alpha^2}}{7.7} \quad ;$$

$$\frac{1}{2} \leq \alpha \leq 1: \quad k = 3.85\,\gamma^2\beta\sqrt{\beta^2+3}\left(-1+\sqrt{1+\frac{4}{\gamma^2\beta^2}}\right) \qquad (14)$$

where

$$\gamma = \frac{4 + \frac{5.34}{\alpha^2}}{7.7 + 33\,(1-\alpha)^3}$$

V. Special Cases

A. Efficiently Tapered Plate

When a tapered plate has attained the state of unstable equilibrium, instability is characterized by deflections out of the plane of the plate in one region only. The other portions of the plate remain essentially free of such deflections. This condition of instability constitutes an inefficient design, since the same loading distribution presumably could be sustained by a lighter plate tapered in such a manner that instability under the specified loading will be characterized by deflections throughout the entire plate. For this reason Pines and Gerard [10] have examined an exponentially tapered simply supported plate subjected to compressive loads as shown in Fig. C2-34. The load variation along the plate was assumed to be produced by shear stresses small enough to have negligible influence upon the buckling characteristics of the plate. The resulting buckling coefficient versus the plate aspect ratio is plotted in Fig. C2-34 for various amounts of plate taper.

B. Compressed Plate with Variable Loading

The problem of determining the buckling stress of an axially compressed flat rectangular plate was investigated by Libove, Ferdman, and Reusch [11] for a simply supported plate with constant thickness and a linear axial load gradient. The curves appearing in Fig. C2-35 depict their results. (Long plates will buckle at the end where the maximum load is applied.)

C. Elastic Foundation

Seide [12] has obtained a solution for the problem of the compressive buckling of infintely long, flat, simply supported plates resting on an elastic foundation. It is shown that the effect of nonattachment of the plate and foundation reduces drastically the buckling load of the plate as compared to a plate with attached foundation.

2.1.1.2 Parallelogram Plates.

Parallelogram plates may exist in beam webs or in an oblique panel pattern. The technology of analysis with respect to such plates is not very well developed. However, several solutions are available which present buckling coefficients for some basic loading conditions and boundary conditions.

I. Compression

Wittrick [13] has examined the buckling stress of a parallelogram plate with clamped edges for the case of uniform compression in one direction. Results in the form of buckling curves are shown in Fig. C2-36. Comparison of these curves with those for rectangular plates shows that for compressive

loads, parallelogram plates are move efficient than equivalent area rectangular plates of the same length. References 14 and 15 contain solutions for simply supported parallelogram plates subjected to longitudinal compression.

A stability analysis of a continuous flat sheet divided by nondeflecting supports into parallelogram-shaped areas (Fig. C2-37) under compressive loads has been performed by Anderson [16]. The results show that, over a wide range of panel aspect ratios, such panels are decidedly more stable than equivalent rectangular panels of the same area. Buckling coefficients are plotted in Fig. C2-37 for both transverse compression and longitudinal compression. An interaction curve for equal-sided skew panels is shown in Fig. C2-38.

Listed in Table C2-5 is a completion of critical plate buckling parameters obtained by Durvasula [17].

II. Shear

The buckling stress of a parallelogram with clamped edges subjected to shear loads has also been investigated by Wittrick [18]. It is worth noting that the shear loads are applied in such a manner that every infinitesimal rectangular element is in a state of pure shear. For such a condition to exist, the plate must be loaded as shown in Fig. C2-39. To signify this condition, the shear stresses are drawn along the y-axis in Fig. C2-40. As might be expected, unlike a rectangular plate it was found that a reversal of the

direction of the shear load causes a change in its critical value. The lower shear stress value occurs when the shear is tending to increase the obliquity of the plate.

The smaller critical shear stress values are plotted in Fig. C2-40. Table C2-5 presents critical shear stress parameters for both directions of shear for several plate geometries.

2.1.1.3 Triangular Plates.

Several investigations have been performed on triangular plates. Cox and Klein [19] analyzed buckling for normal stress alone in isosceles triangles of any vertex angle. The results are shown in Fig. C2-41. The buckling of a right-angled isosceles triangular plate subjected to shear along the two perpendicular edges together with uniform compression in all directions has been considered by Wittrick [20-23]. Four combinations of boundary conditions were considered, and the buckle is assumed to be symmetrical about the bisector for the right angle. Figure C2-42 depicts the interaction curve in terms of shear and compressive stresses. In the limiting cases, these results agree with those of Cox and Klein. In Wittrick's study it was shown that for a plate subjected to shear only, the critical stress is changed considerably upon reversal of the shear. Because of this, the interaction curve is unsymmetrical and the critical compressive stress can be appreciably increased by the application of a suitable amount of shear.

2.1.1.4 Trapezoidal Plates.

Klein [24] has determined the elastic buckling loads of simply supported flat plates of isosceles trapezoidal planform loaded in compression along the parallel edges. Shear loads are assumed to act along the sloping edges so that any ratio of axial loads may act along the parallel edges of the given plate. A collocation method was used to obtain his results. The deflection function assumed does not satisfy the boundary condition for moment along the sloping edges. However, the results are accurate enough for practical purposes. (His results appear to be more incorrect for long plates where the sides comprise a large percent of the plate edges.) Buckling curves obtained are shown in Fig. C2-43 and C2-44.

Pope [25] has analyzed the buckling of a plate of constant thickness tapered symmetrically in planform and subjected to uniform compressive loading on the parallel ends. Two cases are considered:

1. Different uniform stresses applied normal to the ends, equilibrium being maintained by shear flows along the sides (Figs. C2-45 through C2-56).

2. Equal uniform stresses applied to the ends, with displacement of the sides prevented normal to the direction of taper (Figs. C2-57 through C2-60).

Boundary conditions are such that opposite pairs of edges are either simply supported or clamped. Pope has used a more rigorous analysis than Klein;

and for comparable plates, Pope's results (which represent an upper bound) are more correct and will give buckling values lower than Klein's. However, the range of applicability of Pope's curves is limited to taper angles, θ, of less than 15 degrees.

2.1.1.5 Circular Plates.

The buckling values of circular plates subjected to radial compressive loads (Fig. C2-61) have been investigated [2].

It has been shown that the critical buckling stress for a circular plate with clamped edges as shown in Fig. C2-61 is

$$f_{r_{cr}} = \frac{14.68\ D}{a^2 t} \qquad (15)$$

Similarly, for the case of a plate with a simply supported edge, the critical stress is

$$f_{r_{cr}} = \frac{4.20\ D}{a^2 t} \qquad (16)$$

The case of a circular plate subjected to unidirectional compression with clamped edges has been investigated [26] and found to be

$$N_o = \frac{32\ D}{a^2} \qquad (17)$$

Circular plates with a cutout center hole of radius, b, subjected to radial compressive forces have also been investigated. The critical buckling stress for these plates is

$$f_{r_{cr}} = \frac{k\,D}{a^2 t} \qquad (18)$$

where the values of k are given in Fig. C2-62.

2.1.2 STIFFENED PLATES.

Critical values of load for plate buckling are dependent upon the flexural rigidity of the plate. The stability of the plate can be increased by increasing its thickness, but such a design will not be economical with respect to the weight of material used. A more economical solution is obtained by keeping the thickness of the plate as small as possible and increasing the stability by introducing reinforcing ribs. For rectangular plates with longitudinal stiffeners, the stiffeners not only carry a portion of the compressive load but subdivide the plate into smaller panels, thus considerably increasing the critical stress at which the plate will buckle.

Stability analysis of flat, stiffened plates should account for both general and local modes of instability. The general mode of instability is characterized by deflection of the stiffeners while, for local instability, buckling occurs with nodes along (or nearly along) the stiffener-skin juncture. Some coupling between these two modes exists, but this effect is usually small, and, therefore, neglected. The local instability of conventionally stiffened plates and integrally stiffened plates is presented in Section C4, "Local Buckling of Stiffened Plates."

This section is concerned with the critical buckling load of the plate. It should be emphasized, however, that the problem of finding the ultimate load is distinctly different from that of finding the buckling load, and the two must not be confused. Ultimate loads of sheet-stringer combinations should be calculated using Section C1.

2. 1. 2. 1 Conventionally Stiffened Plates in Compression.

Buckling resulting from general instability of a conventionally stiffened plate may be determined from the general equation

$$F_{cr} = \frac{k \pi^2 E_c}{12(1-\nu^2)} \left(\frac{t}{b}\right)^2 \quad . \qquad (19)$$

In this case, k is a function of several of the parameters of the stiffened plate and t is the thickness of the skin. Design tables and charts will be presented for the evaluation of k for both the case where the stiffeners are parallel to the load and the case where the stiffeners are perpendicular to the load.

I. Stiffeners Parallel to Load

A. Simply Supported Plate with One Stiffener or Centerline

Consider a rectangular plate of length a, width b, and thickness t, which is reinforced by a longitudinal stiffener on the centerline (Fig. C2-63). The area of the cross section of the stiffener is A, and its moment of inertia is I, taken with respect to the axis coinciding with the

outer surface of the flange. The torsional rigidity of the stiffener is regarded as small and will be neglected. Also, the following notation is used:

$$\gamma = \frac{EI}{Db} = \frac{12(1-\nu^2)\, I}{b\, t^3} \tag{20}$$

$$\delta = \frac{A}{bt} \tag{21}$$

The coefficient γ is the ratio of the flexural rigidity of the stiffener to that of the plate of width b, and δ is the ratio of the cross-sectional area of the stiffener to the area bt of the plate.

If the stiffener remains straight the buckling mode is antisymmetric as shown in Fig. C2-63(c). This antisymmetric displacement form will occur when the rigidity ratio γ is larger than a certain value γ_o. For values of γ below γ_o, the symmetric displacement form in which the stiffener deflects with the plate will occur. At the ratio γ_o both configurations are equally possible.

Bleich [9] has derived the following formula for γ_o:

$$\gamma_o = 11.4\,\alpha + (1.25 + 16\,\delta)\,\alpha^2 - 5.4\sqrt{\alpha} \tag{22}$$

where $\alpha = a/b$ and $0 \le \delta \le 0.20$. Using this, the required moment of inertia, I_o, to keep the stiffener straight is

$$I_o = 0.092\, b\, t^3\, \gamma_o \quad . \tag{23}$$

Timoshenko [2] gives values of k to be used in equation (19) for various parameters, α, δ, and γ. These results are given in Table C2-6. The values of k above the horizontal lines in Table C2-6 indicate those proportions of the stiffener and plate for which the stiffener remains straight when the plate buckles.

B. Simply Supported Plates Having One Stiffener Eccentrically Located

Bleich [9] obtains solutions for a rectangular plate stiffened with one eccentrically located stiffener as shown in Fig. C2-64. For the particular case of $b_1/b = 1/3$, he determines a value for the moment of inertia of the stiffener required to remain undeflected during buckling. It is

$$I = 1.85\, b t^3 + 0.4\, A t^2 \qquad (\alpha \leq 1) \quad . \qquad (24)$$

Also, with this (or greater) value of I, the critical buckling coefficient, k, is equal to 10.42.

C. Simply Supported Plates Having Two Equidistant Stiffeners

For the case of two stiffeners subdividing the plate into three equal panels, Timoshenko has obtained values for the coefficient k; these are given in Table C2-7 for various values of the parameters, α, δ, and γ. Bleich has obtained formulas for values of stiffener rigidity necessary for the stiffener to remain undeflected during buckling. They are

$$\gamma_o = 96 + 610\,\delta + 975\,\delta^2 \qquad (25)$$

for $0 < \delta < 0.20$ and

$$I_o = 0.092\, bt^3 \gamma_o \quad , \tag{26}$$

with the critical stress for the plate given by

$$F_{cr} = 32.5\, E \left(\frac{t}{b}\right)^2 \quad . \tag{27}$$

D. Plates Having More Than Two Stiffeners

When the number of stiffeners is equal to or greater than three, the stiffened plate can be treated as an orthotropic plate. This results in the following equation for the compression buckling coefficient:

$$k = \frac{2\left\{\left[1 + \frac{N-1}{N}\left(\frac{E I_s}{bD}\right)\left(1 + \frac{\frac{A\bar{z}^2}{I_s}}{1 + \frac{0.88A}{bt}}\right)\right]^{1/2} + 1\right\}}{N^2\left[\frac{N-1}{N}\left(\frac{A}{bt}\right) + 1\right]} \tag{28}$$

where the terms are defined as follows:

N	number of bays
A	area of stiffener cross section
I_s	bending moment of inertia of stiffener cross section taken about the stiffener centroidal axis
$\bar{z}$	distance from midsurface of skin to stiffener centroidal axis
D	flexural rigidity of skin per inch of width, $E\, t^3/12(1 - \nu^2)$
b	spacing of stiffeners

II. Stiffeners Transverse to Load

Timoshenko [2] has studied plates with stiffeners transverse to the applied load. He has obtained several limiting values of γ at which the stiffener remains straight during buckling of the plate. These values are given in Table C2-8 for various values of α for one, two, and three transverse stiffeners.

For the case of a large number of equal and equidistant stiffeners, the plate is considered to have two different flexural rigidities in the two perpendicular directions. The critical stress is given as

$$F_{cr} = \frac{2\pi^2}{b^2 t}\left(\sqrt{D_1 D_2} + D_3\right) \qquad (29)$$

where

$D_1 = (EI)_x/(1 - \nu_x \nu_y)$, flexural rigidity in longitudinal direction;

$D_2 = (EI)_y/(1 - \nu_x \nu_y)$, flexural rigidity in transverse direction;

$D_3 = 1/2\,(\nu_x D_2 + \nu_y D_1) + 2(GI)_{xy}$; and

$2(GI)_{xy}$ is the average torsional rigidity.

2. 1. 2. 2 Conventionally Stiffened Plates in Shear.

The simple cases of simply supported rectangular plates with one and two stiffeners have been investigated by Timoshenko. Tables C2-9 and C2-10 give the limiting values of the ratio γ in the case of one stiffener and two stiffeners, respectively.

Additional analysis of stiffened plates in shear is given in Section C4. 4. 0 and in Section B4. 8. 1.

2. 1. 2. 3 Conventionally Stiffened Plates in Bending.

The case of a rectangular plate reinforced with a longitudinal stiffener under bending load is common in the design of webs for shear beams. For this case, reference should be made to Section B4. 8. 1. 1.

2. 1. 2. 4 Plates Stiffened With Corrugations in Compression.

A method is presented below for the analysis of corrugated plates subjected to a compressive load applied parallel to the corrugations. Both general and local instability modes of failure are treated. General instability results in complete failure of a corrugated plate, since the corrugations are unable to develop post-buckling strength. In the case of local instability, however, the corrugations can usually develop some post-buckling strength. However, it is recommended that the lower compression buckling stress calculated for these two modes of failure be considered ultimate. It is assumed that the corrugated edges are supported in such a manner that the load is uniformly applied along these edges. All edges are assumed to be simply supported.

The compression buckling stress for the general instability mode of failure may be found by orthotropic plate analysis to be

$$F_{cr} = \eta \frac{k_o \pi^2 E_c}{12(1-\nu^2)} \left(\frac{t}{a}\right)^2 \qquad (30)$$

where $k_o = (1 - \nu^2)\left\{ \frac{12I}{t^3 L} \left(\frac{a}{b}\right)^2 + \left(\frac{d}{L}\right)^2 \left[2\nu + 2\left(\frac{L}{d}\right)^2 + \left(\frac{b}{a}\right)^2\right] \right\}$ and other terms are defined as follows:

E_c modulus of elasticity in compression

a length of the loaded edge of the plate

b plate dimension in the direction parallel to the load

d centerline to centerline spacing of corrugations

L developed length per width d

I moment of inertia of width d about neutral axis

When the plate aspect ratio a/b is greater than approximately 1/3, the computations above may be simplified since the corrugated plate behaves approximately as a wide column. For these cases, the following equation applies:

$$F_c = \eta \frac{\pi^2 E_c I}{L t b^2} \qquad (31)$$

The compression buckling stress for the local instability mode of failure may be found from the following equation when the corrugation is composed of flat elements:

$$F_{c_{cr}} = \eta \frac{k_o \pi^2 E_c}{12(1 - \nu^2)} \left(\frac{t}{b}\right)^2 \qquad (32)$$

where k_c represents simply supported edge conditions and is taken from Fig. C2-5, t is the thickness of the plate, and b is the width of the widest flat plate element of the corrugation form. The latter dimension may best be described by presenting some typical examples such as those shown in Fig. C2-65.

In the case of Fig. C2-65(d), the compression buckling stress for local instability should be based on the buckling of an axially load cylinder of radius R (see Section C3. 1).

2. 1. 2. 5 Plates Stiffened With Corrugations in Shear.

Plates stiffened with corrugations may provide a structural weight advantage for light shear loading conditions. Both local and general instability modes of failure are treated in the following methods of analysis. It is assumed in these methods that support for the corrugated edges of the plate is such that the unbuckled form of the corrugation cannot be distorted. This condition means that in the unbuckled state an externally applied shearing force will produce only shearing stresses in the corrugated plate (i. e., no bending or torsion). In practice, this condition may be met by welding or brazing, or by rigorous mechanical joining of the corrugated plate to, for instance, a spar cap on the inner surface of a wing skin.

General instability results in the complete failure of the corrugated plate because the corrugations are unable to redistribute stresses in this mode for the development of post-buckling stress. In contrast, local

instablility of the corrugations does not necessily mean failure, since some post-buckling strength can be developed for that case. It is recommended, however, that the lower shear buckling stress calculated here for these two modes of failure be considered ultimate.

The shear buckling stress for the general instability mode of failure is from Reference 1:

$$F_{s_{cr}} = \eta \frac{4k}{b^2 t} \sqrt[4]{D_1 (D_2)^3} \quad \text{when } H > 1 \tag{33}$$

$$F_{s_{cr}} = \eta \frac{4k}{b^2 t} \sqrt{D_2 D_3} \quad \text{when } H < 1 \tag{34}$$

where D_1 and D_2 are the flexural stiffnesses of the plate in the x and y directions, respectively; D_3 is a function of the torsional rigidity of the plate, and H is equal to $\sqrt{D_1 D_2}/D_3$. The values for k are taken from Fig. C2-66 or C2-67.

For general instability analysis, the optimum orientation of the corrugations for a reversible shear flow is parallel to the short side of the plate. For this orientation, the plate flexural stiffnesses may be expressed as follows:

$$D_1 = \frac{E_c t^3 d}{12 L} \tag{35}$$

$$D_2 = \frac{E_c I}{d} \tag{36}$$

$$D_3 = \nu D_1 + \frac{E_c t^3 L}{12 d} \qquad (37)$$

The shear buckling stress for the local instability mode of failure may be found from the following equation when the corrugation form is composed of flat elements:

$$F_{s_{cr}} = \eta \frac{k_s \pi^2 E_c}{12(1 - \nu^2)} \left(\frac{t}{b}\right)^2 . \qquad (38)$$

Here k_s represents simply supported edge conditions and is taken from Fig. C2-5. The latter dimension may best be described by referring to some typical examples such as those presented in Fig. C2-65. In the case of Fig. C2-65(d), the shear buckling stress for local instability should be based on the torsional buckling of a cylinder of radius R (see Section C3.1).

2.1.2.6 Sandwich Plates.

Procedures for the design and analysis of sandwich plates can be found in Reference 27 which contains the latest information in structural sandwich technology. It contains many formulas and charts necessary to select and check designs and its use is quite widespread in the aerospace industry.

2.1.2.7 Plates of Composite Material.

The buckling of plates constructed of composite materials is presented in Section F and in Reference 28.

2. 2 CURVED PLATES.

Design information is presented in this section for the prediction of buckling in plates of single curvature which are both stiffened and unstiffened.

2. 2. 1 UNSTIFFENED CURVED PLATES.

2. 2. 1. 1 Compression Buckling.

The behavior of curved plates uniformly compressed along their curved edges is similar in many respects to that of a circular cylinder under axial compression (e. g. , both buckle at stresses considerably below the predictions of small deflection theory, and it is necessary to resort to semi-empirical methods to show agreement with the available test results).

It is recommended that the methods for predicting buckling of axially compressed monocoque cylinders (Section C3. 1. 1) be used to predict buckling of curved plates.

2. 2. 1. 2 Shear Buckling.

Critical shear buckling stresses for curved plates are calculated by the following formula:

$$F_{s_{cr}} = \frac{k_s \eta \pi^2 E}{12(1-\nu_e^2)} \left(\frac{t}{b}\right)^2 \qquad (39)$$

where k is determined from Fig. C2-68, and $\eta = \sqrt{E_T/E_c}$

2. 2. 2 STIFFENED CURVED PLATES IN COMPRESSION.

Information is presented in the following paragraphs for stiffened plates of single curvature in compression where the stiffening members are either axial or circumferential. In these considerations, both the local and general modes of instability must be considered.

2. 2. 2. 1 Curved Plates With Axial Stiffeners.

A method for predicting buckling of simply supported curved plates with a single central axial stiffener has been developed in Reference 29. This method is similar to that presented in Paragraph 2. 1. 2. 1 for stiffened flat plates in compression, in that the same basic equation is used in conjunction with specified buckling coefficients. However, in the present case, the buckling coefficients for the local and the general modes of instability are shown on the same chart. Figures C2-69a through C2-69d present these coefficients, which may be used with the following equation to predict buckling when $Z_b \leq 0.25$:

$$F_{c_{cr}} = \frac{k_c \pi^2 E}{12(1 - \nu_e^2)} \left(\frac{t}{b}\right)^2 \qquad (40)$$

This equation may also be written as

$$F_{c_{cr}} = \frac{k_c \pi^2 E}{12\sqrt{1 - \nu_e^2}\; Z_b \left(\frac{R}{t}\right)} \qquad (41)$$

where Z_b is the plate curvature parameter, $\frac{b^2}{Rt}\sqrt{1-\nu_e^2}$; R is the plate radius of curvature; and b is the half-width of the loaded (curved) edge of plate.

Figures C2-69a through C2-69d yield buckling coefficients as a function of Z_b, A/bt, and EL_s/bD for values of the ratio a/b equal to 4/3, 2, 3, and 4, respectively, where terms are defined as follows:

- I_s bending moment of inertia of the stiffener cross section taken about the stiffener centroidal axis
- D flexural stiffness of the plate per inch of width, $Et^3/12(1-\nu_e^2)$
- a length of plate

The sloping portions of the curves to the left in each of the charts of Figs. C2-69a through C2-69d represent designs wherein the general mode of instability is critical. Local instability is represented by the horizontal lines to the right in each chart. The intersection of these curves represents efficient design, since less moment-of-inertia in the stiffener induces general instability and a lowering of the buckling stress, while more moment-of-inertia in the stiffener has no effect on the buckling stress of the stiffened plate.

Although not specifically shown in Fig. C2-69a through C2-69d, the increase in the curved-plate buckling stress, due to the addition of a central axial stiffener, is negligible when $Z_b > 2.5$. Thus, plates with a

large degree of curvature are not benefited by stiffening with a central axial member. In this case, buckling stress should be determined by the techniques in Section C3. 1. 1.

Also, the methods cited above should not be applied with two or more axial stiffeners, since the stiffener geometrical requirements needed to satisfy the general mode of instability are sensitive to the number of stiffeners when the number is small. With multiple stiffeners, the methods described for orthotropic cylinders in Section C3. 1. 2 should be used.

2. 2. 2. 2 Curved Plates With Circumferential Stiffeners.

Curved plates stiffened with a single central circumferential stiffener have been considered by Batdorf and Schildcrout [30]. They determined analytically that the addition of a single central circumferential stiffener increases the buckling stress of a curved plate but only within a rather restricted range of plate geometries. This range is a function of both the ratio a/b (where a is the half-length of the plate, b is the width of the curved, loaded edge) and the geometric parameter Z_b. For the buckling stress of the curved plate to increase with the addition of a single central circumferential stiffener, a/b must be 0. 6 or less. The parameter Z_b imposes further restrictions as a function of a/b which are shown in Fig. C2-70. For a given value of a/b, Z_b for the design must be equal to or smaller than that value read from the chart. If Z_b for the design is larger than the value read from the chart, no gain in the buckling stress results from the addition of the stiffener to the curved plate.

Small deflection theory was used in Reference 30 to predict the buckling stress of curved plates with circumferential stiffeners. Consequently, the results are presented in terms of a gain factor which indicates the gain in buckling stress for a stiffened curved plate over an unstiffened curved plate, where the gain is based on theoretical predictions of the buckling stress for both configurations. The information presented here, therefore, may be applied by multiplying the gain factor by the buckling stress for an unstiffened curved plate of the same overall dimensions by methods given in Paragraph 2. 2. 1. 1.

Maximum gain factors are presented as a function of a/b and Z_b in Fig. C2-71. The term "maximum" implies that the stiffener has sufficient bending rigidity to enforce a buckle node at the stiffener line.

The required stiffener bending rigidity needed to enforce a buckle node at the stiffener line is defined in Fig. C2-72 when the figure is entered with a maximum gain factor obtained from Fig. C2-71.

Figure C2-72 may also be used to determine gain factors when an existing stiffener has either more or less bending rigidity than that required to enforce a node along the stiffener line. In this case, the same geometrical limitations stipulated in Fig. C2-70 apply and must be observed. (Note that the gain factors obtained here may not be maximum; therefore, the ordinate of Fig. C2-72 is labeled to take this possibility into account.)

After first referring to Fig. C2-70 to ascertain whether or not a gain is indeed possible, find the gain factor (from Fig. C2-72) based on the properties of the existing stiffener. Now plot this gain factor on Fig. C2-71. If the point is below and to the left of the a/b curve to which it relates, then the gain factor is less than the maximum permissible and the bending rigidity of the stiffener is less than the minimum required. In this case, general instability of the curved plate represents the critical mode, and buckling may be predicted using the gain factor obtained from Fig. C2-70. When the point is above and to the right of the a/b curve in Fig. C2-71 to which it relates, the contrary is true, and local instability of the curved plate represents the critical mode. In this case, buckling may be predicted using the maximum gain factor obtained from the a/b, Z_b intersection in Fig. C2-71.

The methods of this section should not be applied to curved plates with two or more circumferential stiffeners. The general instability stresses predicted by the design charts are sensitive to the number of stiffeners when their total number is small. In this case, recourse should be had to Section C3. 1. 2.

2. 2. 3 STIFFENED CURVED PLATES IN SHEAR.

Methods are presented in the following paragraphs for predicting the buckling stress of plates of single curvature in shear having a single stiffener in either the axial or circumferential direction. The methods account for both the local and general modes of instability, and charts are

given that present the buckling coefficient k_s versus EI/bD, where at low values of EI/bD the general mode of instability is critical. As EI/bD increases, the local mode of instability becomes critical and is signified by a constant value of k_s. Thus, to enforce a node at the stiffener, the design must have an EI/bD which falls on the horizontal portion of the design curve. Note that the EI/bD value representing the extreme left point of the horizontal line yields the most efficient design; local and general instability are both critical here.

2. 2. 3. 1 Curved Plates With Axial Stiffeners.

The buckling stress for curved plates with a single, central stiffener may be determined from the equation:

$$F_{c_{cr}} = \eta \frac{k_s \pi^2 E}{12(1 - \nu_e^2)} \left(\frac{t}{b}\right)^2 \qquad (42)$$

where k_s is taken from Fig. C2-73, b is the overall dimension of the curved plate, and t is the thickness of the curved plate. Figure C2-73(a) applies when axial length is greater than circumferential width, and Fig. C2-73(b) applies when axial length is less than circumferential width. Note that in both cases, b is denoted the short overall dimension of the plate. Curves are presented as a function of the aspect ratio of the plate, a/b, as well as of the plate curvature parameter, Z_b. Note also that the data of Fig. C2-73 are based on small deflection theory and agree satisfactorily

with experimental results except in the case of cylinders for which a 16 percent reduction is recommended.

The preceding method should not be extended to apply to curved plates with multiple axial stiffeners. The bending rigidity required of each stiffener to support general instability is sensitive to the total number of stiffeners when this number is small.

2. 2. 3. 2 Curved Plates With Circumferential Stiffeners.

The buckling stress for curved plates stiffened circumferentially with a single central stiffener may be determined from equation (42) with the buckling coefficients, k_s, taken from Fig. C2-74. As in Fig. C2-73 for a cylinder, a 16 percent reduction of the horizontal portions of the curves (the portion signifying local instability) is recommended.

The data above should not be applied to curved plates with multiple circumferential stiffeners for the reasons noted previously in Paragraph 2. 2. 3. 1.

2. 2. 4 CURVED PLATES UNDER COMBINED LOADING.

Interaction relations for longitudinal compression combined with normal pressure, shear combined with normal pressure, and longitudinal compression combined with shear are presented in the following paragraphs for unstiffened, curved plates. Interaction relations for stiffened, curved plates are presently unavailable; however, techniques discussed in Section C3. 1. 2 may be used. The normal pressure in the first two cases is

applied to the concave face of the curved plate. The interaction relations apply only to elastic stress conditions, since verification of their application to plastic stress conditions is lacking at present.

2. 2. 4. 1 Longitudinal Compression Plus Normal Pressure.

The interaction equation for longitudinal compression plus normal pressure applied to the concave face of an unstiffened curved plate is

$$R_c^2 - R_p = 1 \qquad (43)$$

where $R_c = F_c/F_{c_{cr}}$ and $R_p = p/p_{cr}$, where the following definitions apply:

F_c applied longitudinal compression stress

$F_{c_{cr}}$ buckling stress of the curved plate where subjected to simple axial compression, determined by the methods of Section 2. 2. 1. 1

p absolute value of the applied normal pressure

p_{cr} absolute value of the external pressure which would buckle the cylinder of which the plate is a section, determined by the methods of Section C3. 1. 1. 5

Note that absolute values of the quantities p and p_{cr} are substituted into the interaction equation since their difference in sign is already accounted for in the equation. It can be seen that normal pressure applied to the concave face of the unstiffened, curved plate increases the axial compression load which may be carried by the plate prior to buckling.

2. 2. 4. 2 Shear Plus Normal Pressure.

When an unstiffened curved plate is subjected to shear combined with normal pressure acting on the concave face of the plate, the following interaction equation applies:

$$R_s^2 - R_p = 1 \qquad (44)$$

where $R = F_s/F_{s_{cr}}$ (F_s is applied shear stress and $F_{s_{cr}}$ is buckling stress of the curved plate when subjected to simple in-plane shear, determined by the methods of Section 2. 2. 1. 2), and R_p is as previously defined.

2. 2. 4. 3 Longitudinal Compression Plus Shear.

The interaction equation for an unstiffened curved plate subjected to longitudinal compression and shear is

$$R_c + R_s^2 = 1 \qquad (45)$$

where R_c and R_s are as defined in previous paragraphs. This relationship represents approximately an average curve through the available experimental results while the lower bound of the test results may be represented by a linear relation between R_c and R_s.

Table C2-1. Values of Material Properties

Material	Temp Exp (hr)	Temp (°F)	e (%)	F_{T_U} (ksi)	F_{cy} (ksi)	E_c 10^6 ksi	$F_{0.7}$ (ksi)	$F_{0.85}$ (ksi)	n
Stainless Steel									
AISI 301 1/2 Hard Sheet									
Longitudinal Compression	1/2	R. T.	15	150	58	26.0	48	37	4.4
AISI 301 Full Hard									
Longitudinal Compression	1/2	R. T.	8	185	85	26.0	77.5	63	5.2
17-7 PH (TH1050) Sheet, Plate and Strip									
t = 0.01 - 0.125	1/2	R. T.		180	162	29.0	166	145	7.4
Low Carbon and Alloy Steels									
AISI 4130, 4140, 4340									
Heat Treated	1/2	R. T.	18.5	150	145	29.0	145	140	25
Heat Resistant Alloys									
A-286 (AMS 5725A)	1/2	R. T.	15	140	95	29.0	93	87	14
Sheet, Plate and Strip	1/2	1000		115	81.7	19.8	81	75	12.5
Inconel-X	1/2	R. T.	20	155	105	31.0	104	100	23.5
	1/2	1200		104	83	23.2	82	78.6	21
Aluminum Alloys									
2014-T6 Extrusions	2	R. T.	7	60	53	10.7	53	50.3	18.5
T ≤ 0.499 in.	2	450		28	21	9.2	20.5	19.5	25

Table C2-1. (Concluded)

Material	Temp Exp (hr)	Temp (°F)	e (%)	F_{T_U} (ksi)	F_{cy} (ksi)	$\frac{E_c}{10^3}$ ksi	$F_{0.7}$ (ksi)	$F_{0.85}$ (ksi)	n
2024-T81 Clad Sheet Heated Treated, t < 0.064	2	R. T.	5	62	55	10.7	56	51.6	11.2
6061-T6 Sheet, Heat Treated Annealed, t < 0.25	1/2	R. T.	10	42	35	10.1	35	34	31
	1/2	450			20.5	8.5	19.3	17.7	10.9
7075-T6 Bare Sheet and Plate, t ≤ 0.50	2	R. T.	7	76	67	10.5	70	63	9.2
	2	425			25.5	8.1	25.4	23.5	12.1
7075-T6 Extrusions, t ≤ 0.25	2	R. T.	7	75	70	10.5	72	68	16.6
	2	600			8	5.3	6.5	4.3	3.2
7075-T6 Clad Sheet and Plate, t ≤ 0.5	2	R. T.	8	70	64	10.5	64.5	61.6	19.5
Magnesium Alloys									
HK31A-0 Sheet, t = 0.016 - 0.25	1/2	R. T.	12	30	12	6.5	10	8.4	6
	1/2	500		15	9.3	4.94	7.5	5.6	4.2
Titanium Alloys									
Ti-6Al-4V Annealed Bar and Sheet, t ≤ 0.187 in.	1/2	R. T.	10	130	126	16	127	124.5	43
	1/2	600		99	84.5	13	85.5	82	22
	1/2	1000		70	60.6	7.7	61	59.5	36

Table C2-2. Cutoff Stresses for Buckling of Flat Unstiffened Plates

Material	Cutoff Stress: Compression Buckling	Cutoff Stress: Bending Buckling	Cutoff Stress: Shear Buckling F_{cy}
2024-T	$F_{cy}\left(1+\frac{F_{cy}}{200\,000}\right)$	$F_{cy}\left(1+\frac{F_{cy}}{200\,000}\right)$	0.61
2014-T			0.61
6061-T			0.61
7075-T	$1.075\,F_{cy}$	$1.075\,F_{cy}$	0.61
18-8(1/2 H)[a]	$0.835\,F_{cy}$	$0.835\,F_{cy}$	0.51
(3/4 H)	$0.875\,F_{cy}$	$0.875\,F_{cy}$	0.53
(FH)	$0.866\,F_{cy}$	$0.866\,F_{cy}$	0.53
All Other Materials	F_{cy}	F_{cy}	0.61

a. Cold-rolled, with grain, based on MIL-HDBK-5 properties.

Table C2-3. Summary of Simplified Cladding Reduction Factors

Loading	$\sigma_{cl} < \bar{\sigma}_{cr} < \sigma_{pl}$	$\bar{\sigma}_{cr} > \sigma_{pl}$
Short Plate Columns	$\frac{1+\left(\frac{3\beta f}{4}\right)}{1+3f}$	$\frac{1}{1+3f}$
Long Plate Columns	$\frac{1}{1+3f}$	$\frac{1}{1+3f}$
Compression and Shear Panels	$\frac{1+3\beta f}{1+3f}$	$\frac{1}{1+3f}$

Table C2-4. Shear Buckling Coefficients for Rectangular Plates with Mixed Boundary Conditions

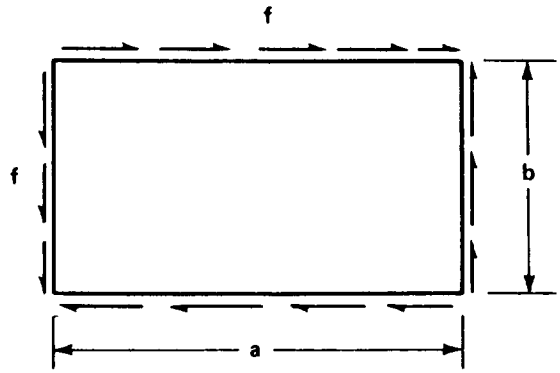

$$\frac{f_{cr}}{\eta} = k_s \frac{\pi^2 E}{12\,(1-\nu_e^2)} \left(\frac{t}{b}\right)^2$$

NOTE: b IS SMALLER DIMENSION ALWAYS

Edge Conditions	Two Short Edges Clamped, Two Long Edges Simply Supported	One Short Edge Clamped, Three Edges Simply Supported	One Long Edge Clamped, Three Edges Simply Supported
Aspect Ratio b/a	k_s	k_s	k_s
0	5.35	5.35	7.07
0.2	5.58	5.58	
0.333	6.13		7.96
0.5	6.72	6.72	8.43
0.667	7.83	7.59	9.31
0.80	9.34	8.57	9.85
0.90	10.83	9.66	10.38
1.00	12.60	10.98	10.98

Table C2-5. Critical Plate Buckling Parameters for Parallelogram Plates, all Edges Clamped

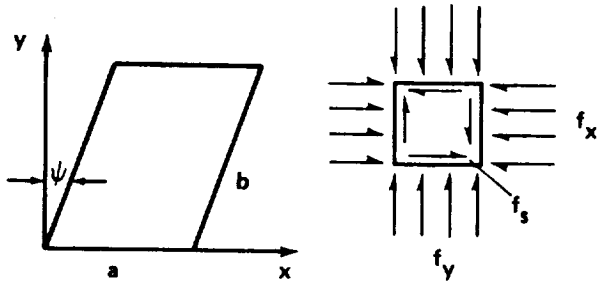

a/b	ψ	k_x	k_y	k_s	
0.5	0	19.35	32.13	- 42.28	+ 42.28
	15	21.63	34.09	- 34.58	+ 55.36
	30	30.38	39.72	- 31.58	+ 76.90
	45	55.26	53.22	- 40.54	+ 128.3
	60	130.5	86.20	- 85.0	531.5
0.6	0	14.92			
	15	16.49			
	30	22.55			
	45	39.73			
	60	90.50			
0.75	0	11.70			
	15	12.76			
	30	16.71			
	45	27.06			
	60	60.59			
1.0	0	10.08	10.08	- 14.83	14.83
	15	10.87	10.43	- 14.39	17.24
	30	13.58	11.76	- 16.66	23.64
	45	20.44	15.26	- 24.08	32.56
	60	42.14	25.78	- 46.58	69.86
1.25	0	9.25			
	15	9.92			
	30	12.32			
	45	18.50			
	60	38.01			
1.50	0	8.33	5.78	- 11.56	11.56
	15	8.91	6.151	- 12.01	12.73
	30	11.16	7.271	- 14.05	15.19
	45	17.10	10.10	- 20.21	22.37
	60	36.84	18.54	- 40.24	45.83
2.0	0	8.033	4.838	- 10.57	10.57
	15	8.70	5.132	- 10.84	11.10
	30	10.53	6.208	- 13.34	13.73
	45	15.74	8.938	- 19.24	20.35
	60	39.35	17.08	- 39.38	44.40

Table C2-6. Values of k for a Plate Stiffened by One Longitudinal Stiffener

α	$\gamma = 5$			$\gamma = 10$			$\gamma = 15$			$\gamma = 20$			$\gamma = 25$		
	$\delta = 0.05$	$\delta = 0.10$	$\delta = 0.20$	$\delta = 0.05$	$\delta = 0.10$	$\delta = 0.20$	$\delta = 0.05$	$\delta = 0.10$	$\delta = 0.20$	$\delta = 0.05$	$\delta = 0.10$	$\delta = 0.20$	$\delta = 0.05$	$\delta = 0.10$	$\delta = 0.20$
0.6	16.5	16.5	16.5	16.5	16.5	16.5	16.5	16.5	16.5	16.5	16.5	16.5	16.5	16.5	16.5
0.8	15.4	14.6	13.0	16.8	16.8	16.8	16.8	16.8	16.8	16.8	16.8	16.8	16.8	16.8	16.8
1.0	12.0	11.1	9.72	16.0	16.0	15.8	16.0	16.0	16.0	16.0	16.0	16.0	16.0	16.0	16.0
1.2	9.83	9.06	7.88	15.3	14.2	12.4	16.5	16.5	16.5	16.5	16.5	16.5	16.5	16.5	16.5
1.4	8.62	7.91	6.82	12.9	12.0	10.3	16.1	15.7	13.6	16.1	16.1	16.1	16.1	16.1	16.1
1.6	8.01	7.38	6.32	11.4	10.5	9.05	14.7	13.6	11.8	16.1	16.1	14.4	16.1	16.1	16.1
1.8	7.84	7.19	6.16	10.6	9.70	8.35	13.2	12.2	10.5	15.9	14.7	12.6	16.2	16.2	14.7
2.0	7.96	7.29	6.24	10.2	9.35	8.03	12.4	11.4	9.80	14.6	13.4	11.6	16.0	15.4	13.3
2.2	8.28	7.58	6.50	10.2	9.30	7.99	12.0	11.0	9.45	13.9	12.7	10.9	15.8	14.5	12.4
2.4	8.79	8.06	6.91	10.4	9.49	8.15	11.9	10.9	9.37	13.5	12.4	10.6	15.1	13.8	11.9
2.6	9.27	8.50	7.28	10.8	9.86	8.48	12.1	11.1	9.53	13.5	12.4	10.6	14.8	13.6	11.6
2.8	8.62	7.91	6.31	11.4	10.4	8.94	12.5	11.5	9.85	13.7	12.6	10.8	14.8	13.6	11.6
3.0	8.31	7.62	6.53	12.0	11.1	9.52	13.1	12.0	10.3	14.1	13.0	11.1	15.2	13.9	11.9
3.2	8.01	7.38	6.32	11.4	10.5	9.05	13.9	12.7	10.9	14.8	13.5	11.6	15.6	14.3	12.3
3.6	7.84	7.19	6.16	10.6	9.70	8.35	13.2	12.2	10.5	15.9	14.7	12.6	16.2	15.7	13.5
4.0	7.96	7.29	6.24	10.2	9.35	8.03	12.4	11.4	9.8	14.6	13.4	11.6	16.0	15.4	13.3

Table C2-7. Values of k for Two Longitudinal Stiffeners Dividing the Plate into Three Equal Parts

α	$\gamma = \frac{10}{3}$		$\gamma = 5$		$\gamma = \frac{20}{3}$		$\gamma = 10$	
	$\delta = 0.05$	$\delta = 0.10$	$\delta = 0.05$	$\delta = 0.10$	$\delta = 0.05$	$\delta = 0.10$	$\delta = 0.05$	$\delta = 0.10$
0.6	26.8	24.1	36.4	33.2	36.4	36.4	36.4	36.4
0.8	16.9	15.0	23.3	20.7	29.4	26.3	37.2	37.1
1.0	12.1	10.7	16.3	14.5	20.5	18.2	28.7	25.6
1.2	9.61	8.51	12.6	11.2	15.5	13.8	21.4	19.0
1.4	8.32	7.36	10.5	9.32	12.7	11.3	17.2	15.2
1.6	7.70	6.81	9.40	8.31	11.1	9.82	14.5	12.8
1.8	7.51	6.64	8.85	7.83	10.2	9.02	12.9	11.4
2.0	7.61	6.73	8.70	7.69	9.78	8.65	11.9	10.6

Table C2-8. Limiting Values of γ For One, Two, and Three Transverse Stiffeners

α	0.5	0.6	0.7	0.8	0.9	1.0	1.2	$\sqrt{2}$
One Rib	12.8	7.25	4.42	2.82	1.84	1.19	0.435	0
Two Ribs	65.5	37.8	23.7	15.8	11.0	7.94	4.43	2.53
Three Ribs	177	102	64.4	43.1	30.2	21.9	12.6	7.44

Table C2-9. Limiting Values of the Ratio γ For Plate With One Stiffener Under Shearing Stress

a/b	1	1.25	1.5	2
γ = EI/Da	15	6.3	2.9	0.83

Table C2-10. Limiting Values of the Ratio γ For Plate With Two Stiffeners Under Shearing Stress

a/b	1.2	1.5	2	2.5	3
γ = EI/Da	22.6	10.7	3.53	1.37	0.64

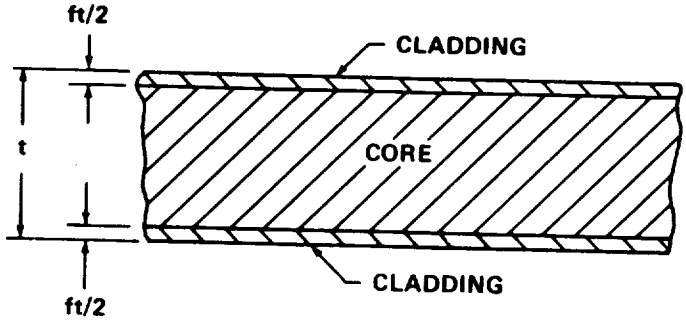

FIGURE C2-1. ALUMINUM CLADDING

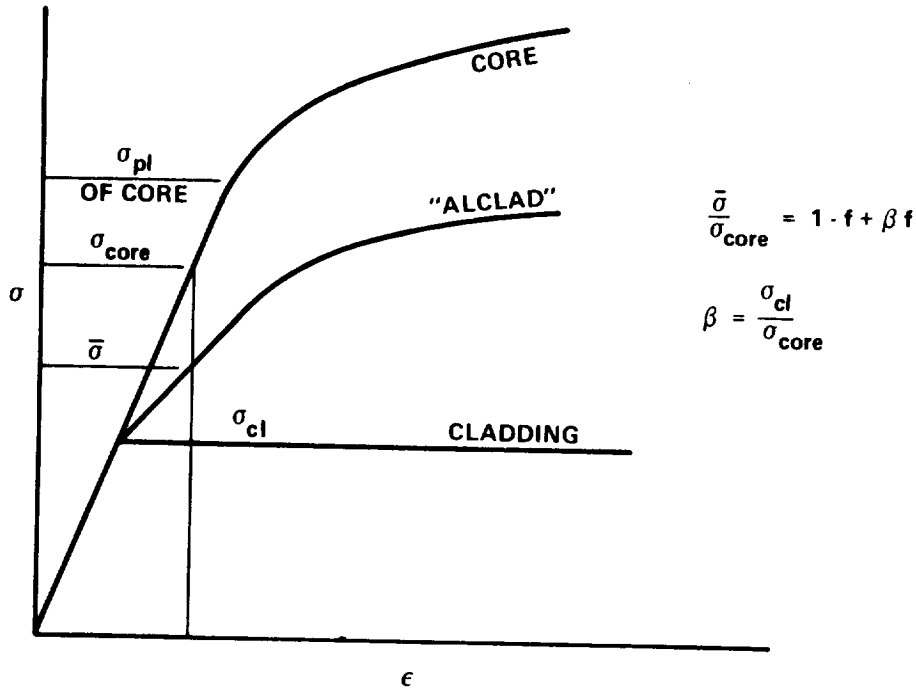

FIGURE C2-2. STRESS-STRAIN CURVES FOR CLADDING, CORE, AND "ALCAD" COMBINATIONS

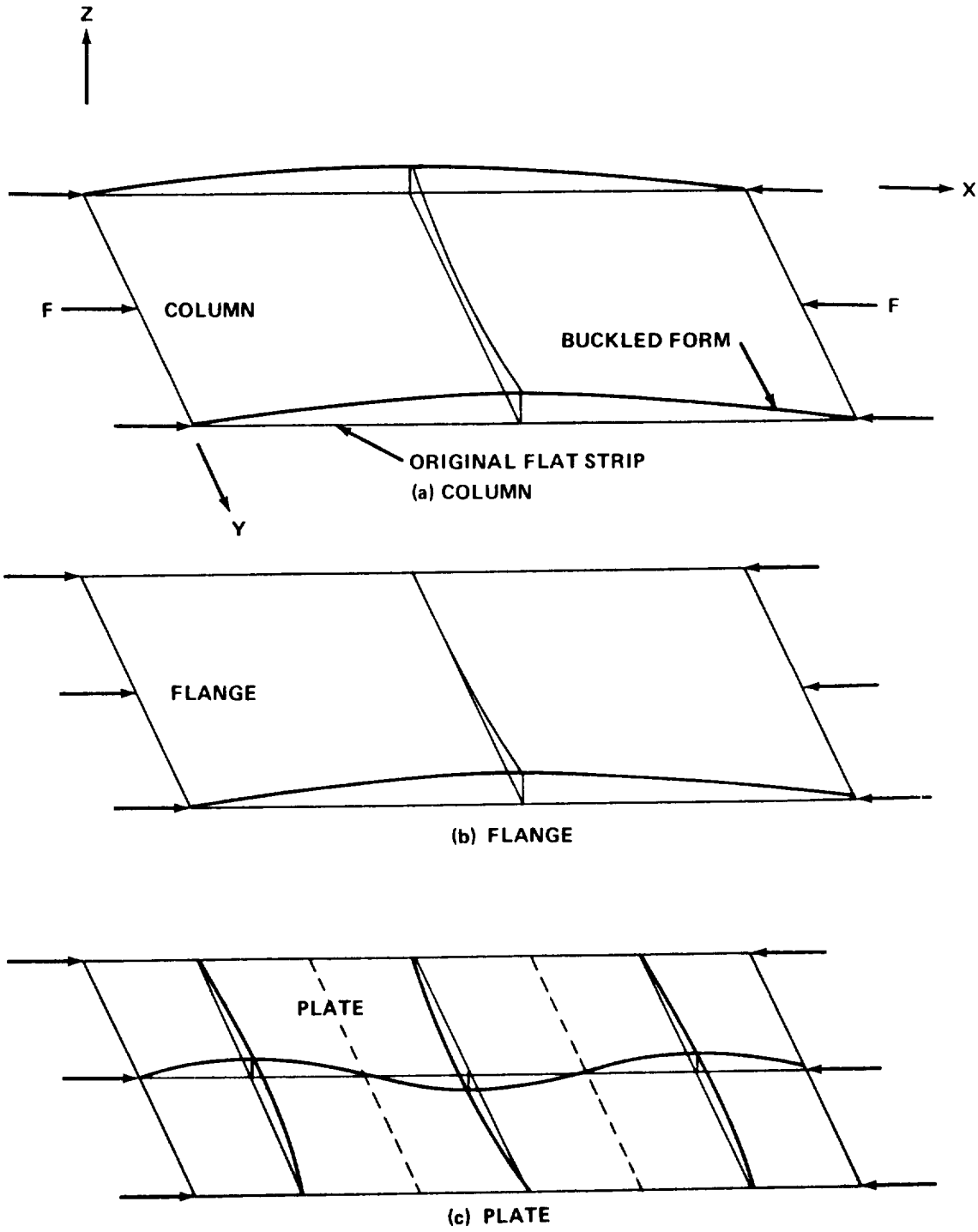

FIGURE C2-3. TRANSITION FROM COLUMN TO PLATE AS SUPPORTS ARE ADDED ALONG UNLOADED EDGES (Note changes in buckle configurations.)

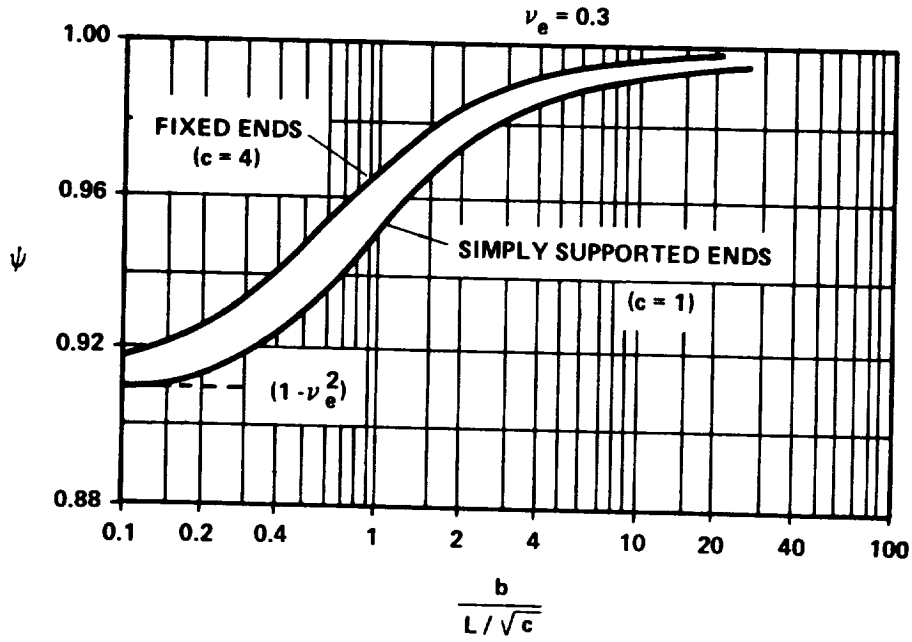

$$\frac{f_{cr}}{\eta} = c\,\frac{\psi}{1-\nu_e^2}\,\frac{\pi^2 E}{12}\left[\frac{t}{L}\right]^2$$

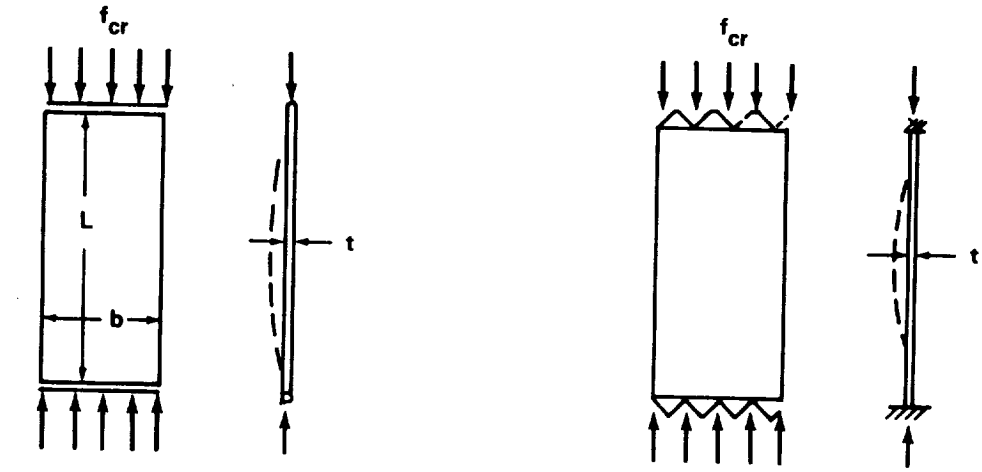

FIGURE C2-4. CRITICAL COMPRESSIVE STRESS FOR PLATE COLUMNS

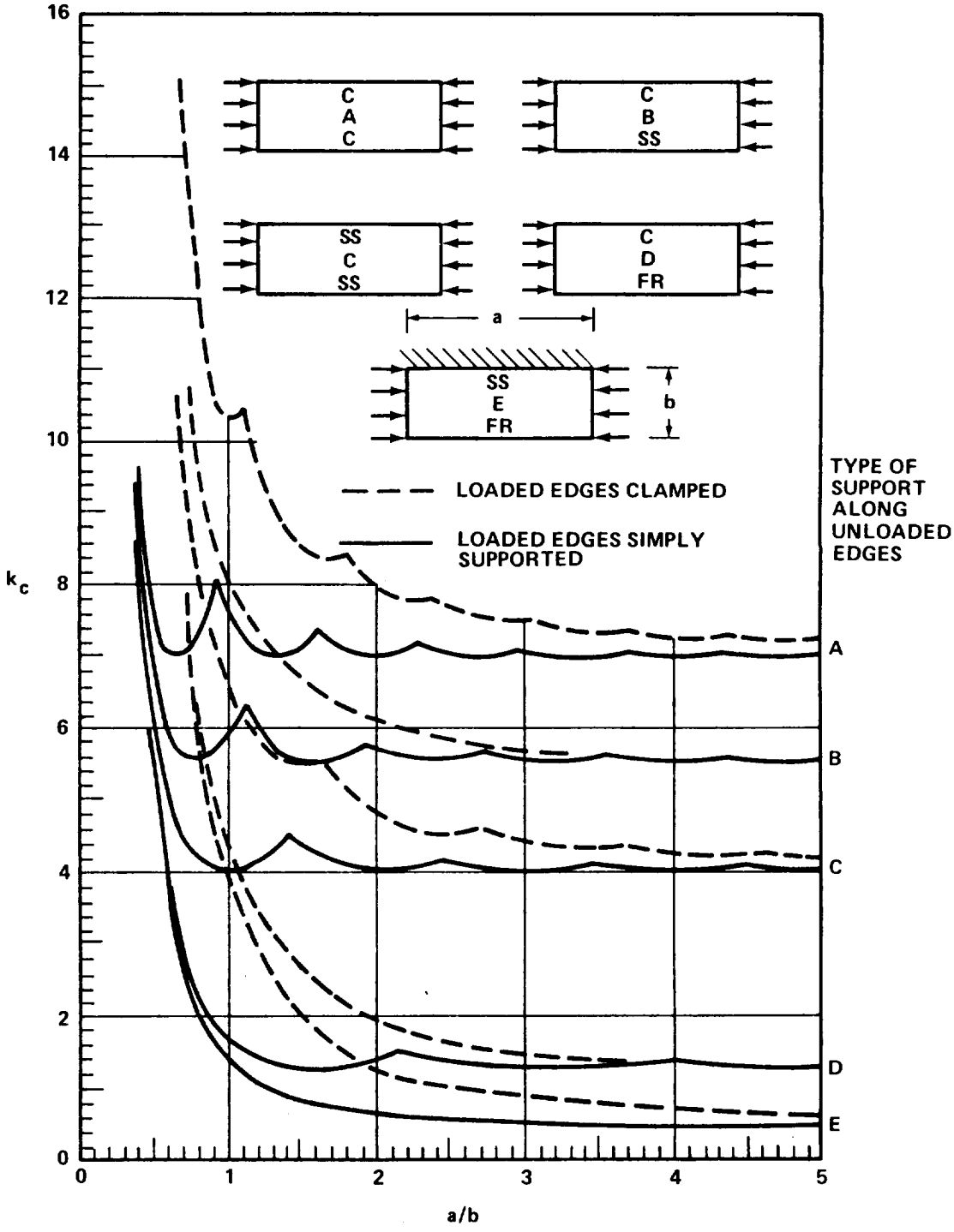

FIGURE C2-5. COMPRESSIVE-BUCKLING COEFFICIENTS FOR FLAT RECTANGULAR PLATES

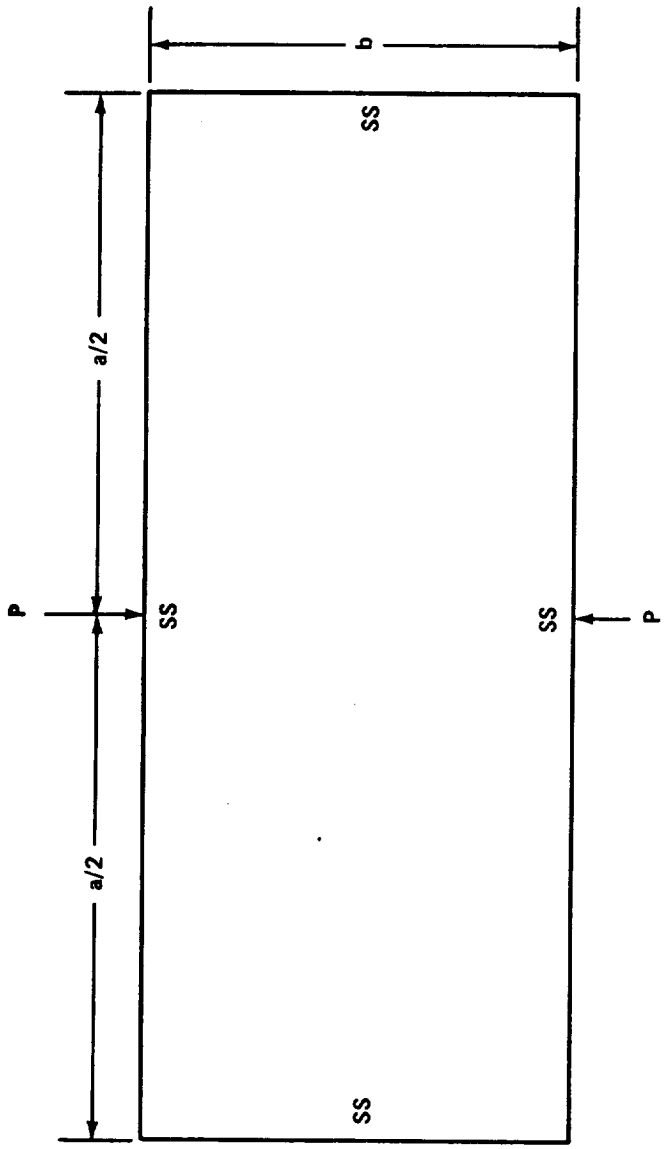

FIGURE C2-6. PLATE WITH CONCENTRATED LOAD

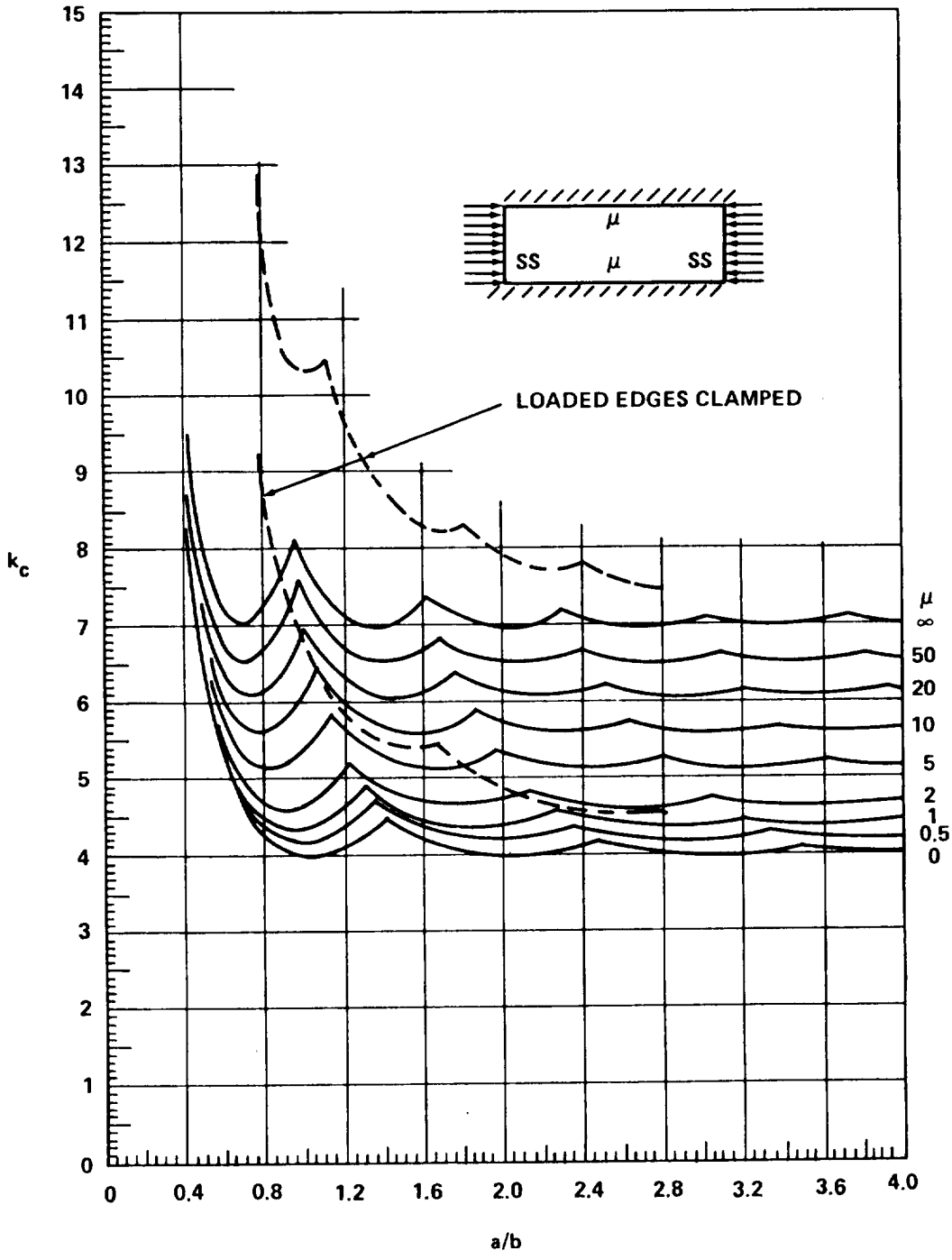

FIGURE C2-7. COMPRESSIVE-BUCKLING-STRESS COEFFICIENT OF PLATES AS A FUNCTION OF a/b FOR VARIOUS AMOUNTS OF EDGE ROTATIONAL RESTRAINT

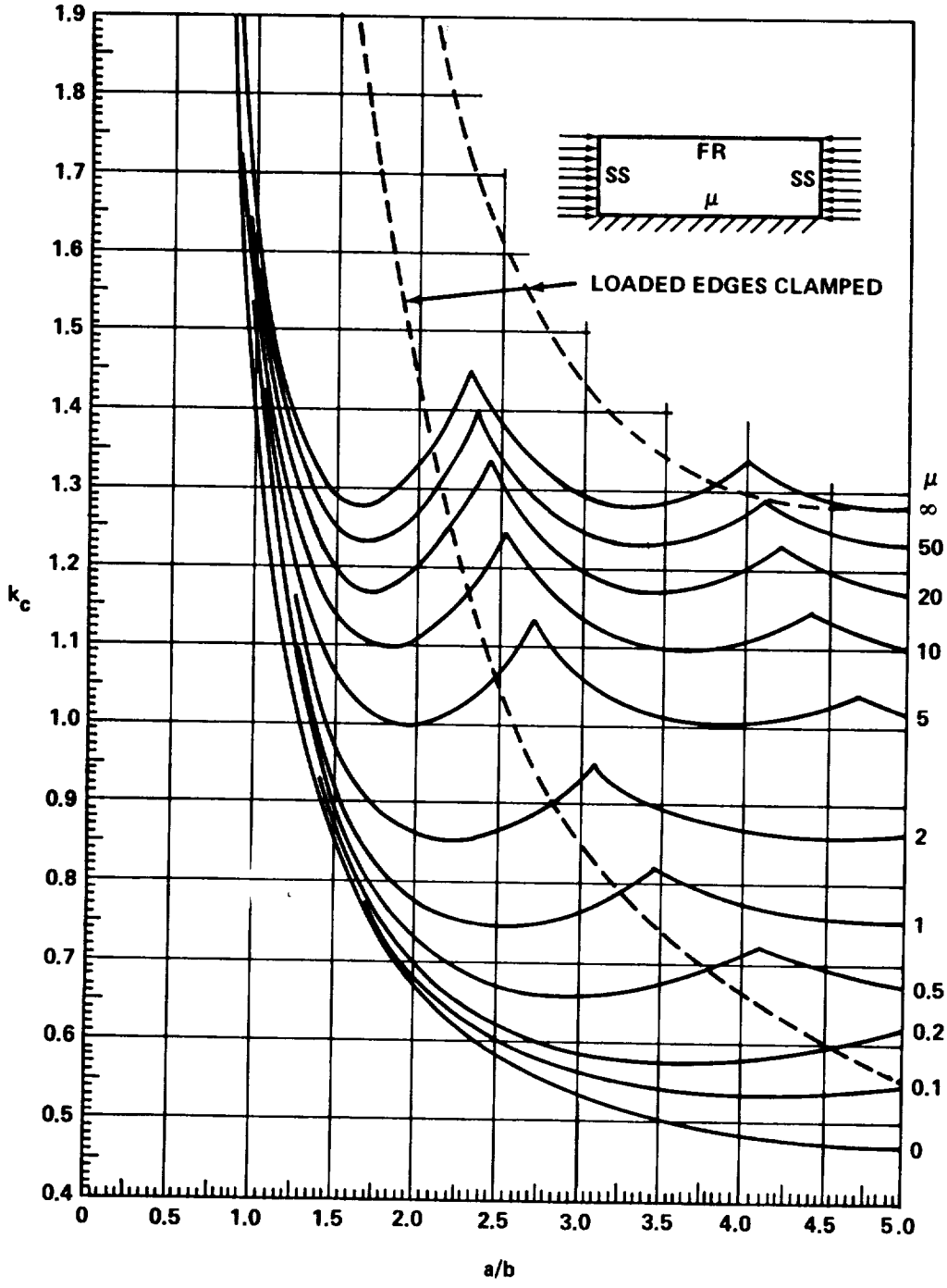

FIGURE C2-8. COMPRESSIVE-BUCKLING-STRESS COEFFICIENT OF FLANGES AS A FUNCTION OF a/b FOR VARIOUS AMOUNTS OF EDGE ROTATIONAL RESTRAINT

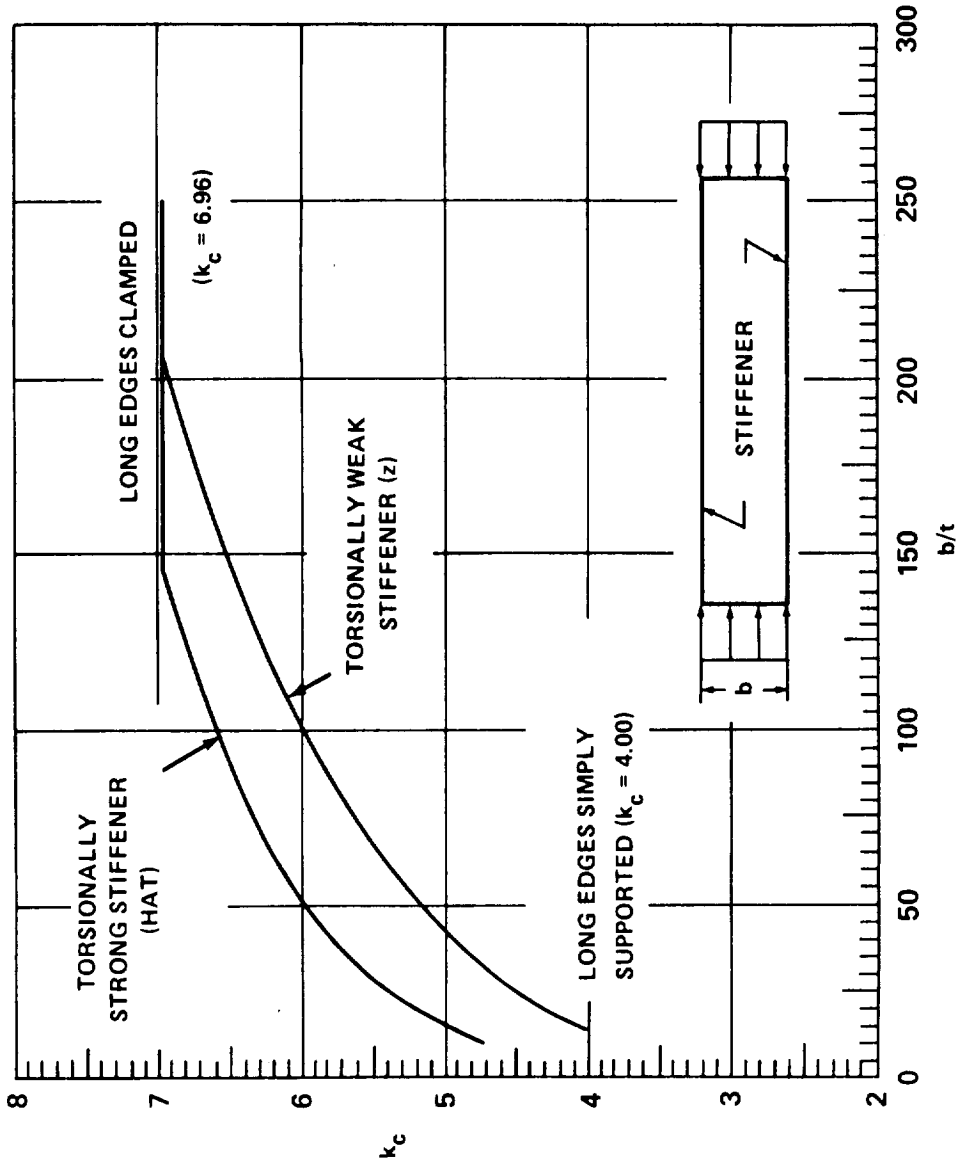

FIGURE C2-9. COMPRESSIVE-BUCKLING COEFFICIENT FOR LONG RECTANGULAR STIFFENED PANELS AS A FUNCTION OF b/t AND STIFFENER TORSIONAL RIGIDITY

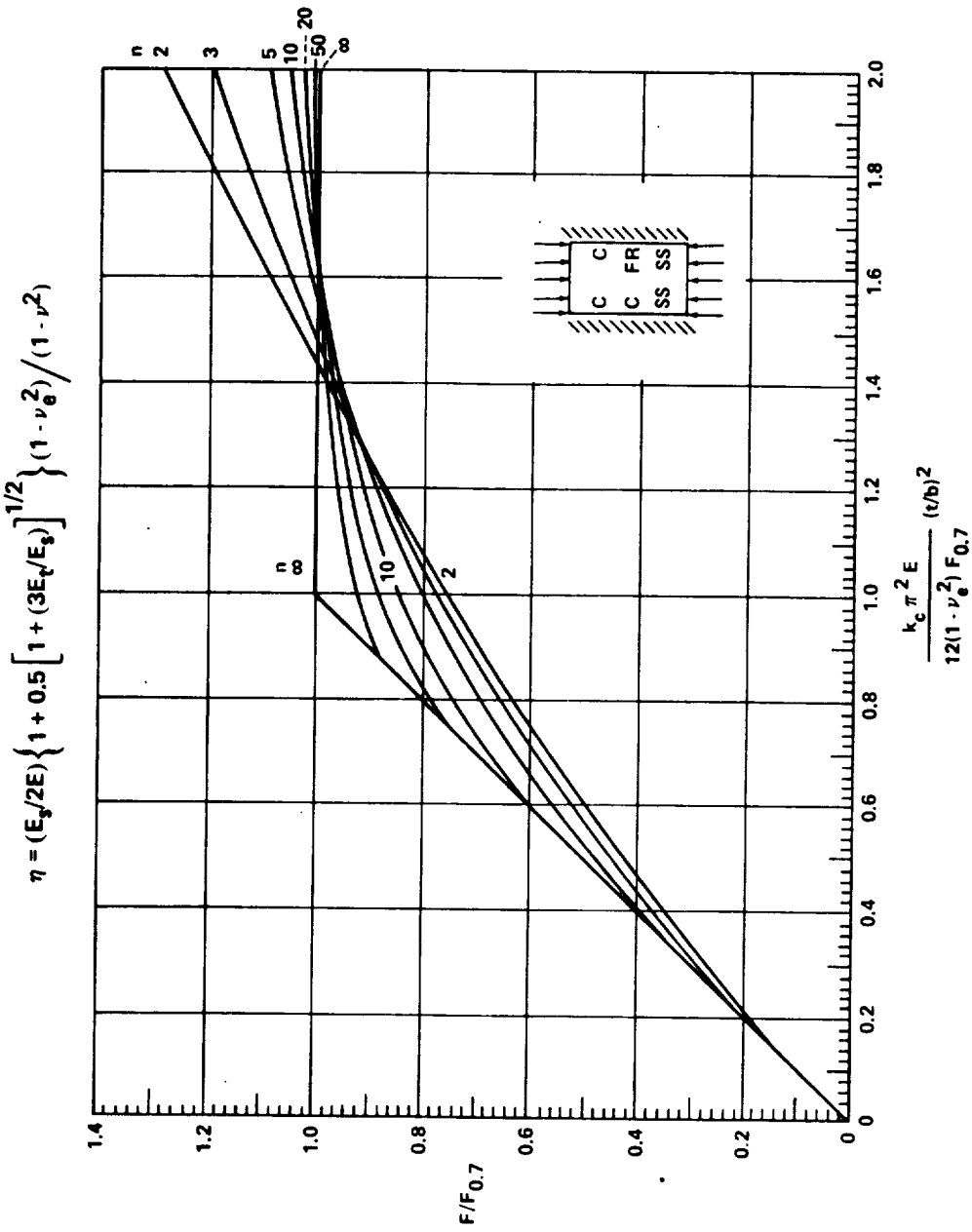

FIGURE C2-10. CHART OF NONDIMENSIONAL COMPRESSIVE BUCKLING STRESS FOR LONG CLAMPED FLANGES AND FOR SUPPORTED PLATES WITH EDGE ROTATIONAL RESTRAINT

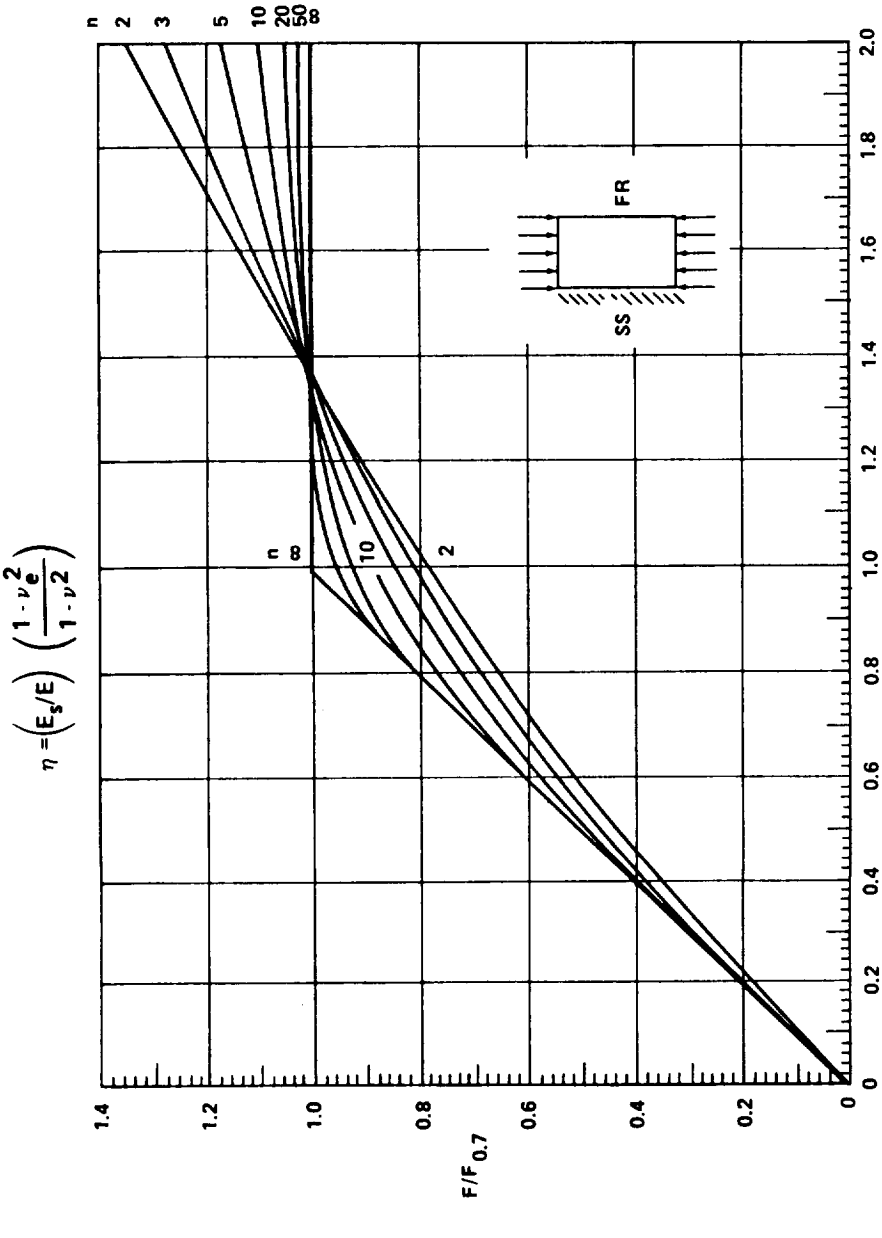

FIGURE C2-11. CHART OF NONDIMENSIONAL COMPRESSIVE BUCKLING STRESS FOR LONG HINGED FLANGES

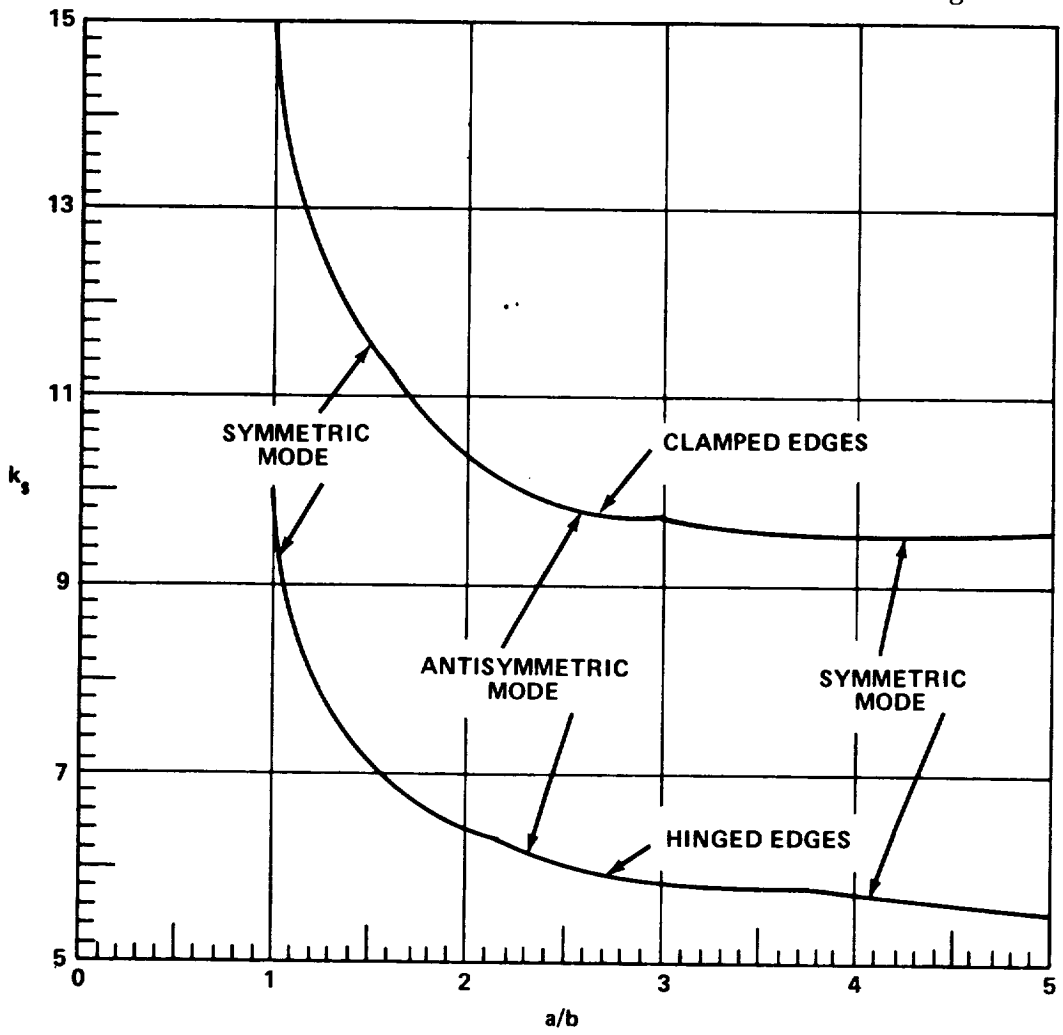

FIGURE C2-12. SHEAR-BUCKLING-STRESS COEFFICIENT OF PLATES AS A FUNCTION OF a/b FOR CLAMPED AND HINGED EDGES

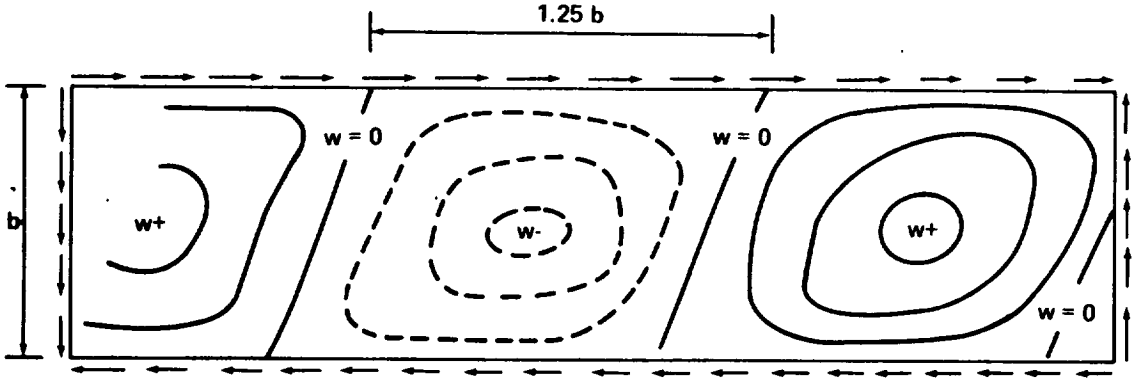

FIGURE C2-13. SHEAR BUCKLING PATTERN FOR RECTANGULAR PLATE

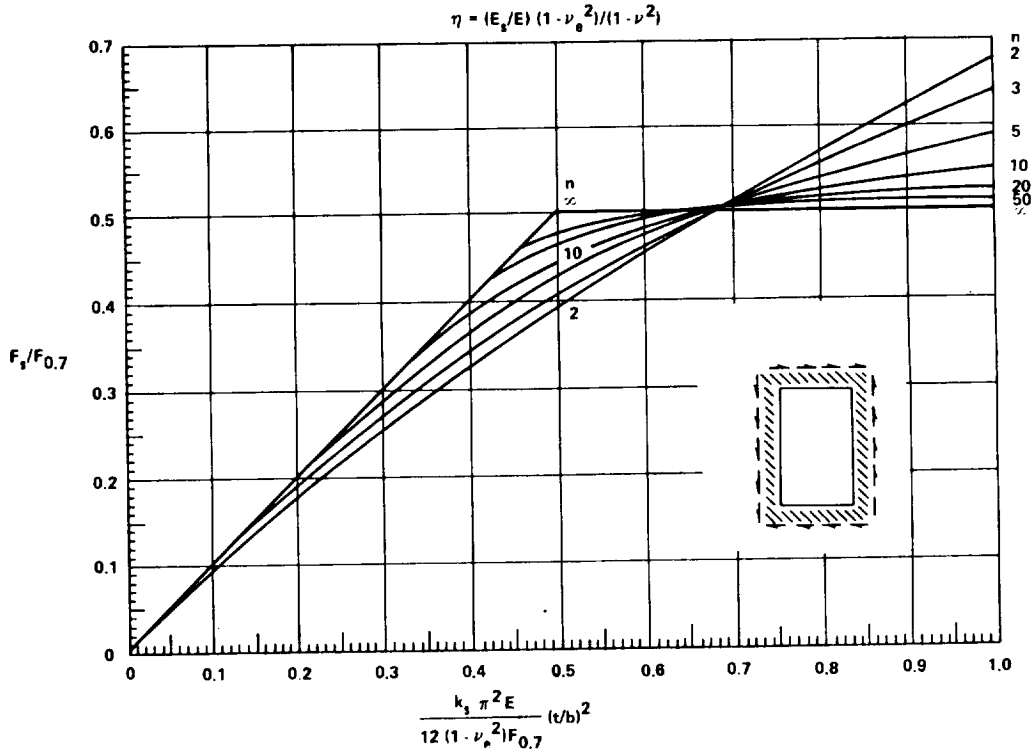

FIGURE C2-14. CHART OF NONDIMENSIONAL SHEAR BUCKLING STRESS FOR PANELS WITH EDGE ROTATIONAL RESTRAINT

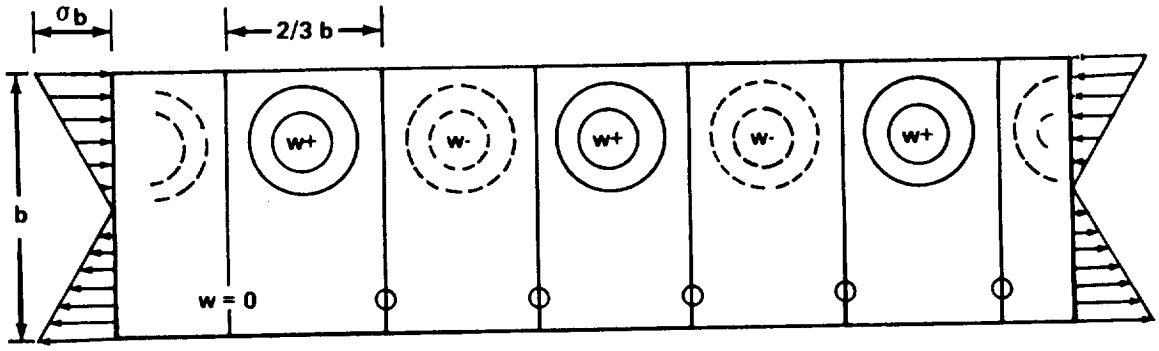

FIGURE C2-15. BUCKLE PATTERN FOR BENDING OF RECTANGULAR PLATE

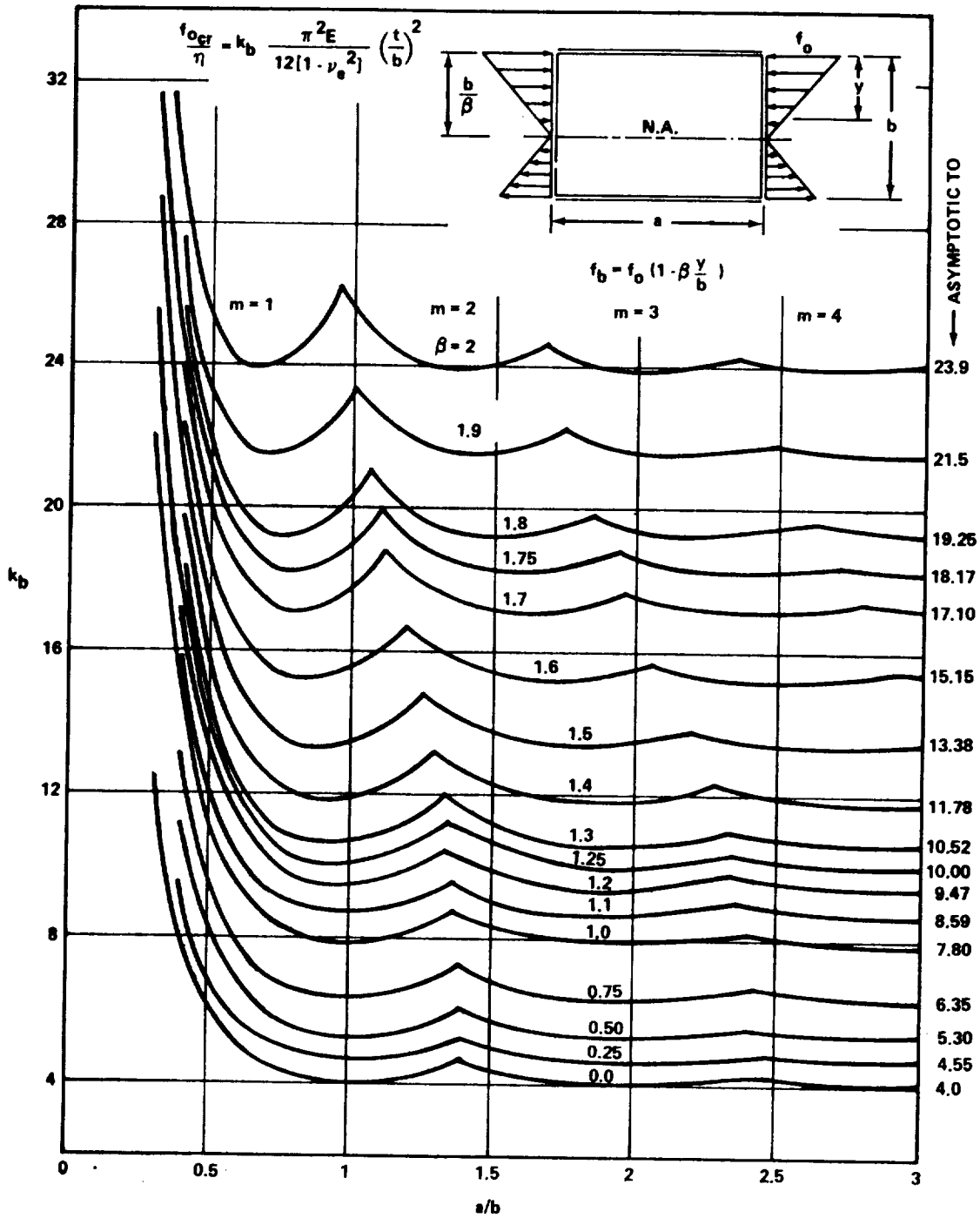

FIGURE C2-16. CRITICAL STRESS COEFFICIENTS FOR A FLAT PLATE IN BENDING IN THE PLANE OF THE PLATE, ALL EDGES SIMPLY SUPPORTED

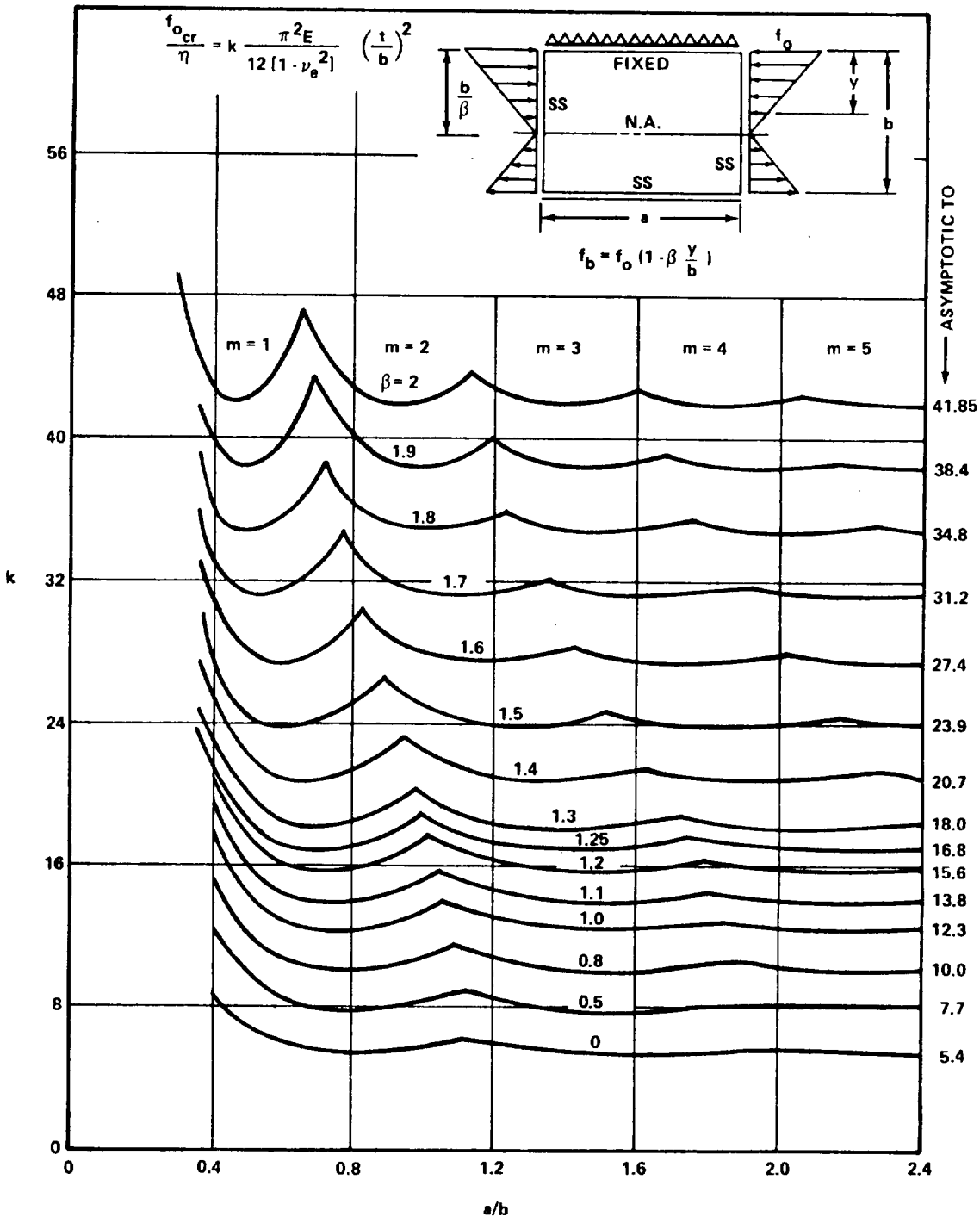

FIGURE C2-17. CRITICAL STRESS COEFFICIENTS FOR A PLATE IN BENDING IN THE PLANE OF THE PLATE, TENSION SIDE SIMPLY SUPPORTED AND COMPRESSION SIDE FIXED

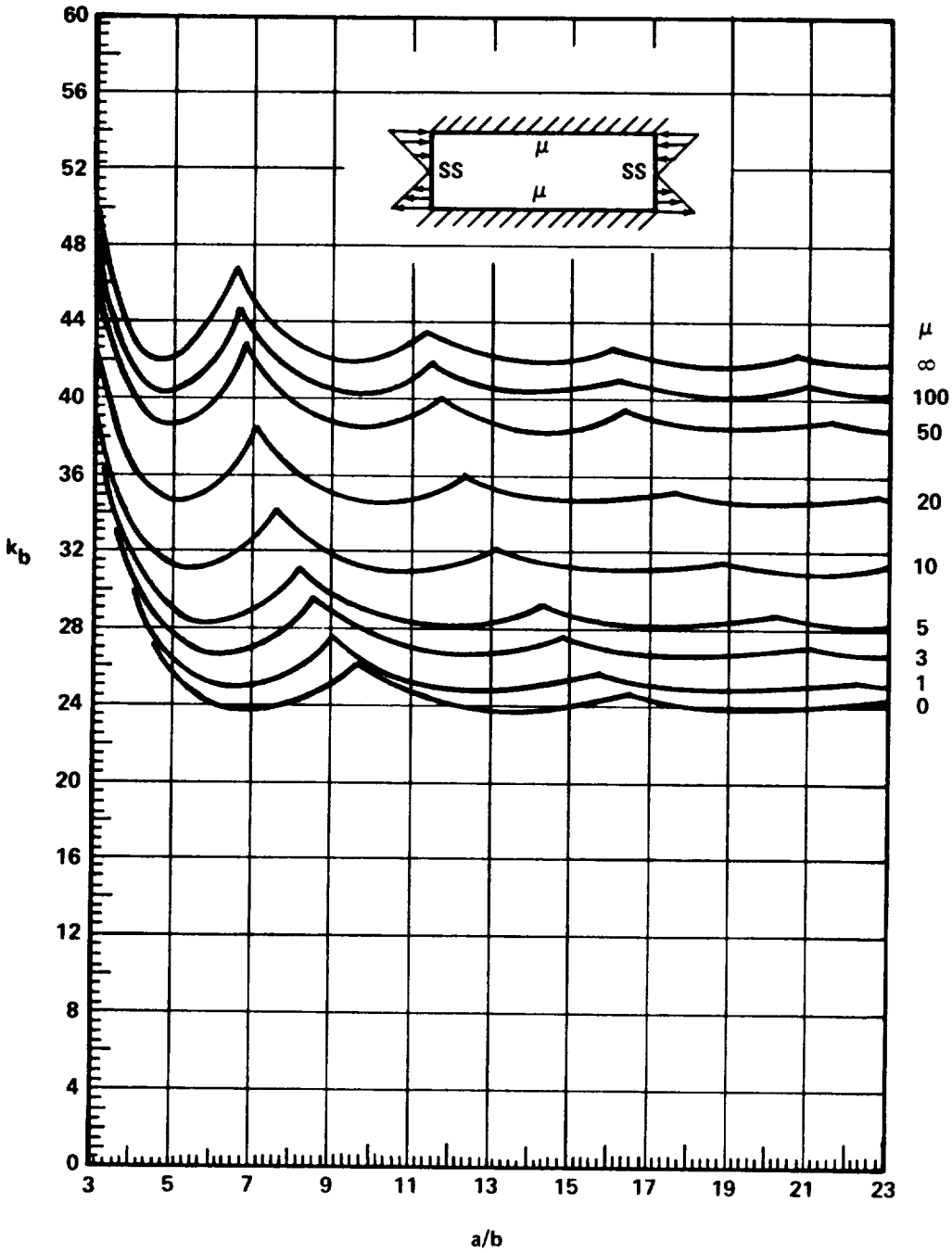

FIGURE C2-18. BENDING-BUCKLING COEFFICIENT OF PLATES AS A FUNCTION OF a/b FOR VARIOUS AMOUNTS OF EDGE ROTATIONAL RESTRAINT

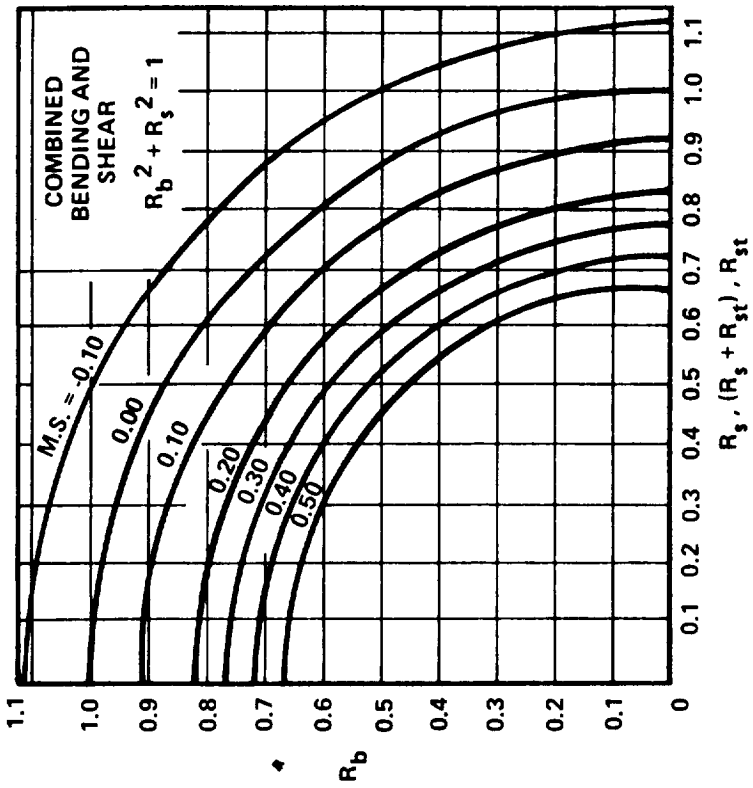

FIGURE C2-20. INTERACTION OF COMBINED BENDING AND SHEAR

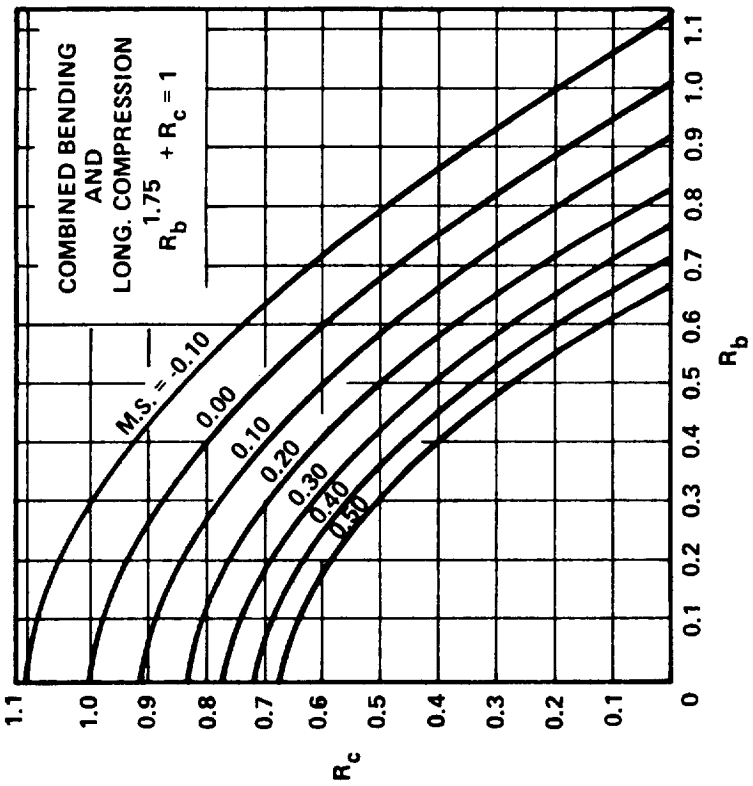

FIGURE C2-19. INTERACTION OF COMBINED BENDING AND LONGITUDINAL COMPRESSION OF PLATES

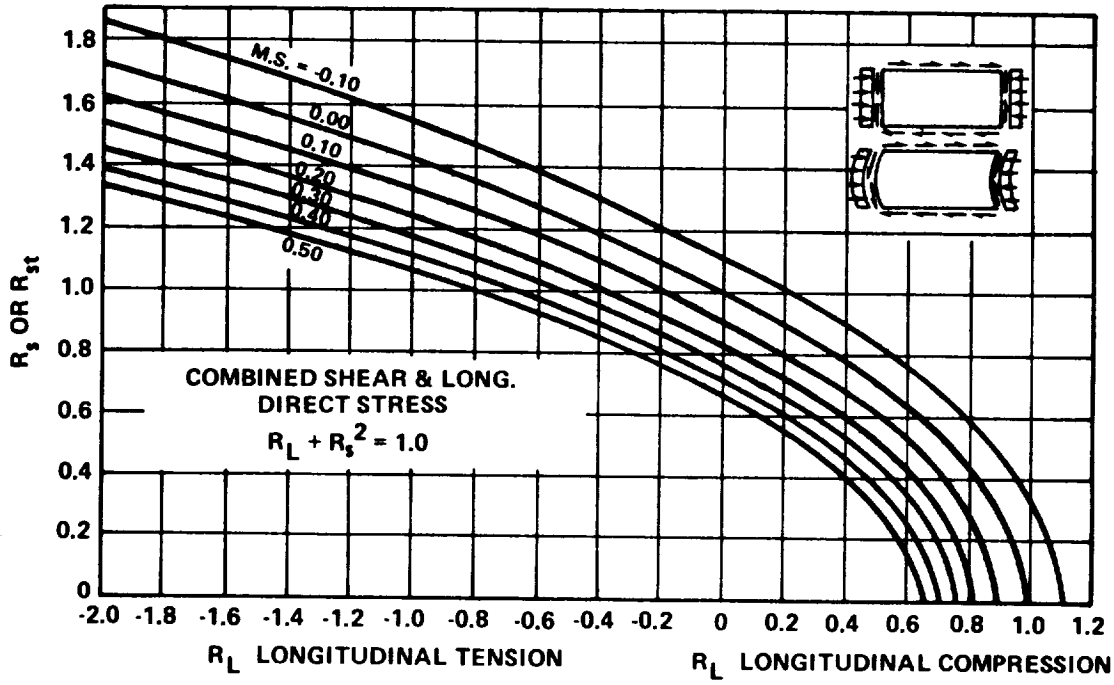

FIGURE C2-21. INTERACTION OF COMBINED SHEAR AND LONGITUDINAL DIRECT STRESS

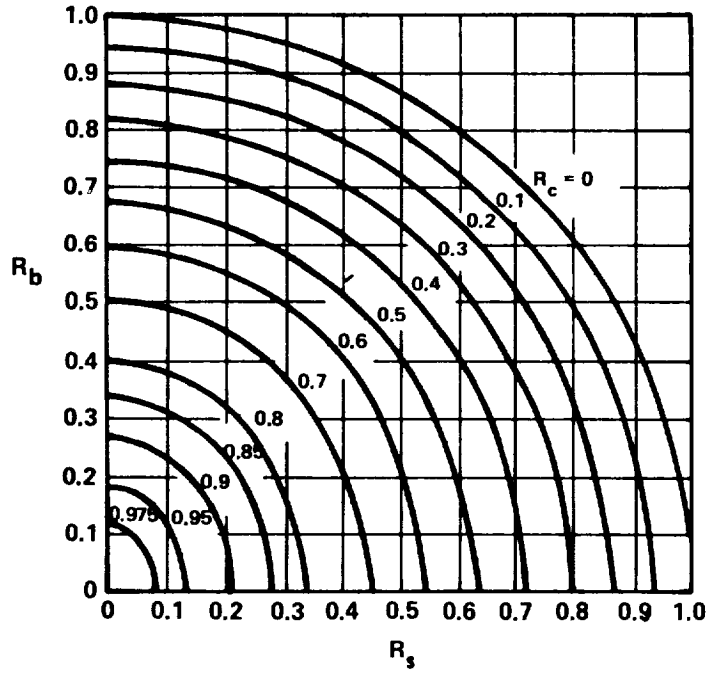

FIGURE C2-22. INTERACTION OF COMBINED COMPRESSION, BENDING, AND SHEAR

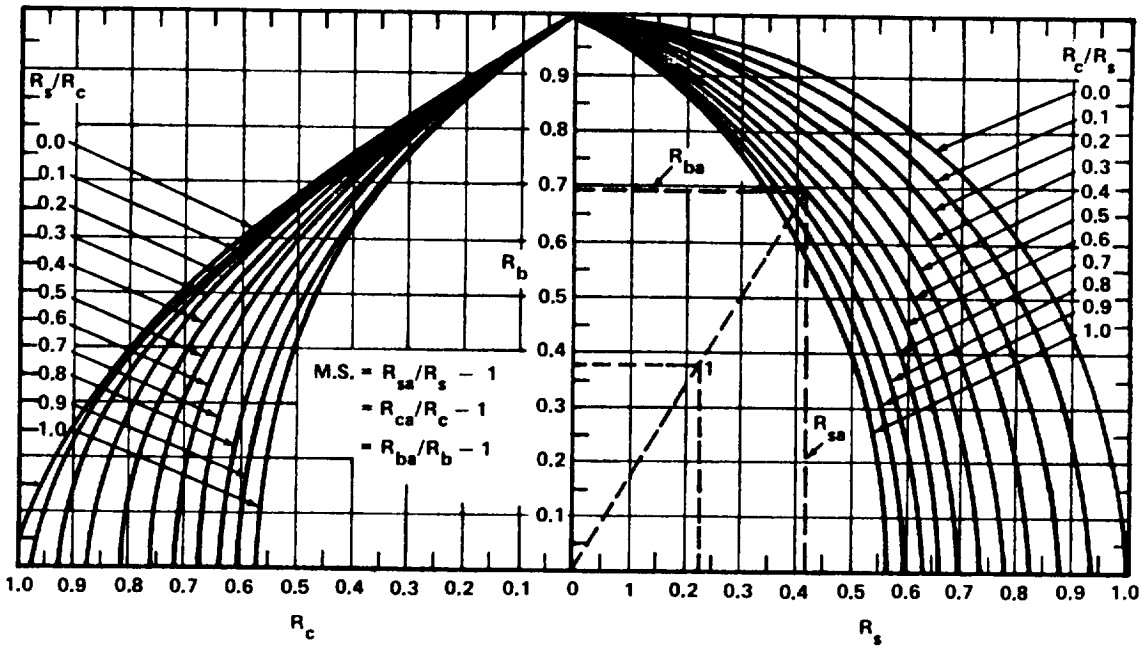

FIGURE C2-23. MARGIN OF SAFETY DETERMINATION FOR COMBINED COMPRESSION BENDING AND SHEAR

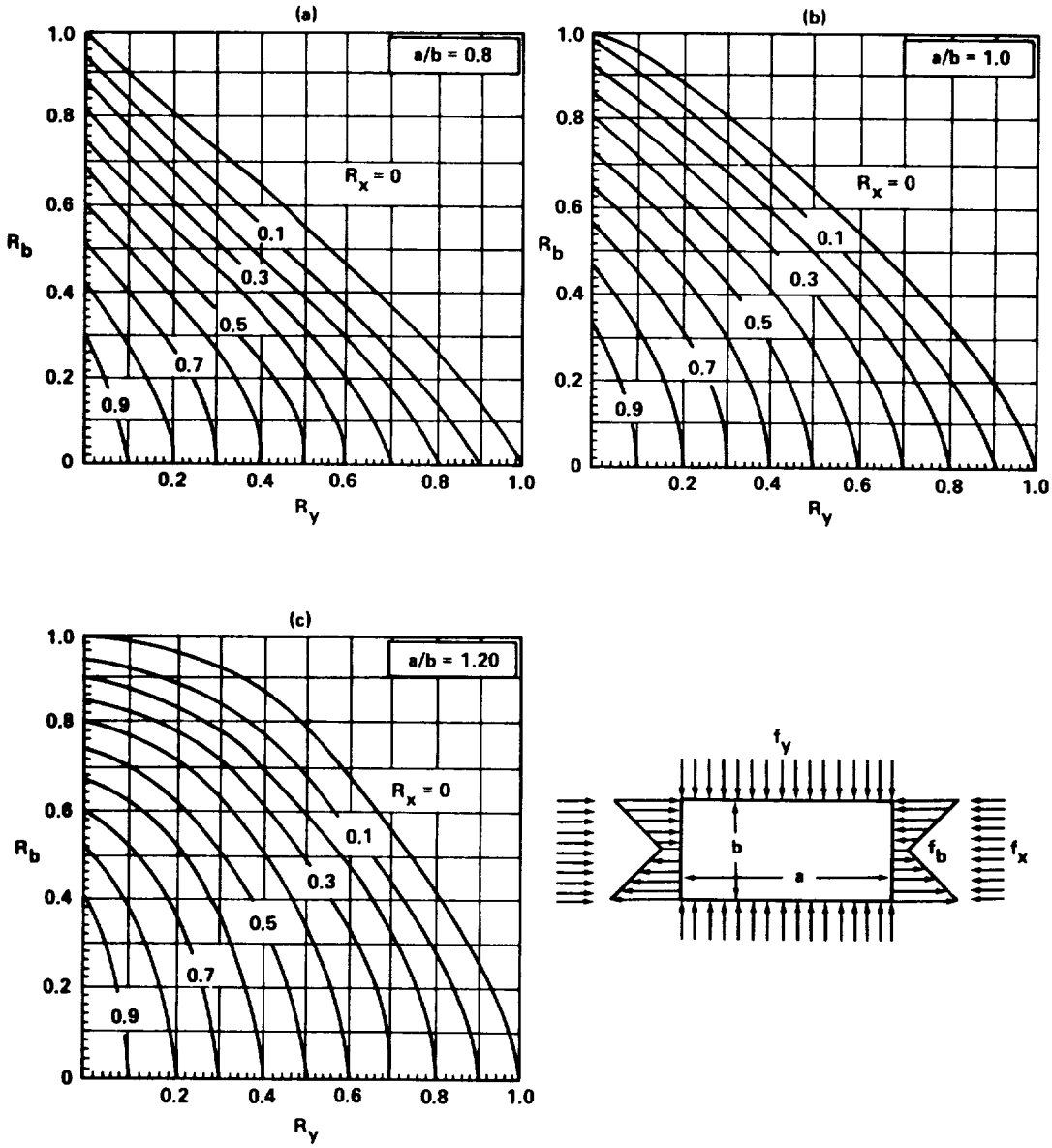

FIGURE C2-24. INTERACTION CURVES FOR SIMPLY SUPPORTED FLAT RECTANGULAR PLATES UNDER COMBINED BIAXIAL COMPRESSION AND LONGITUDINAL BENDING LOADINGS

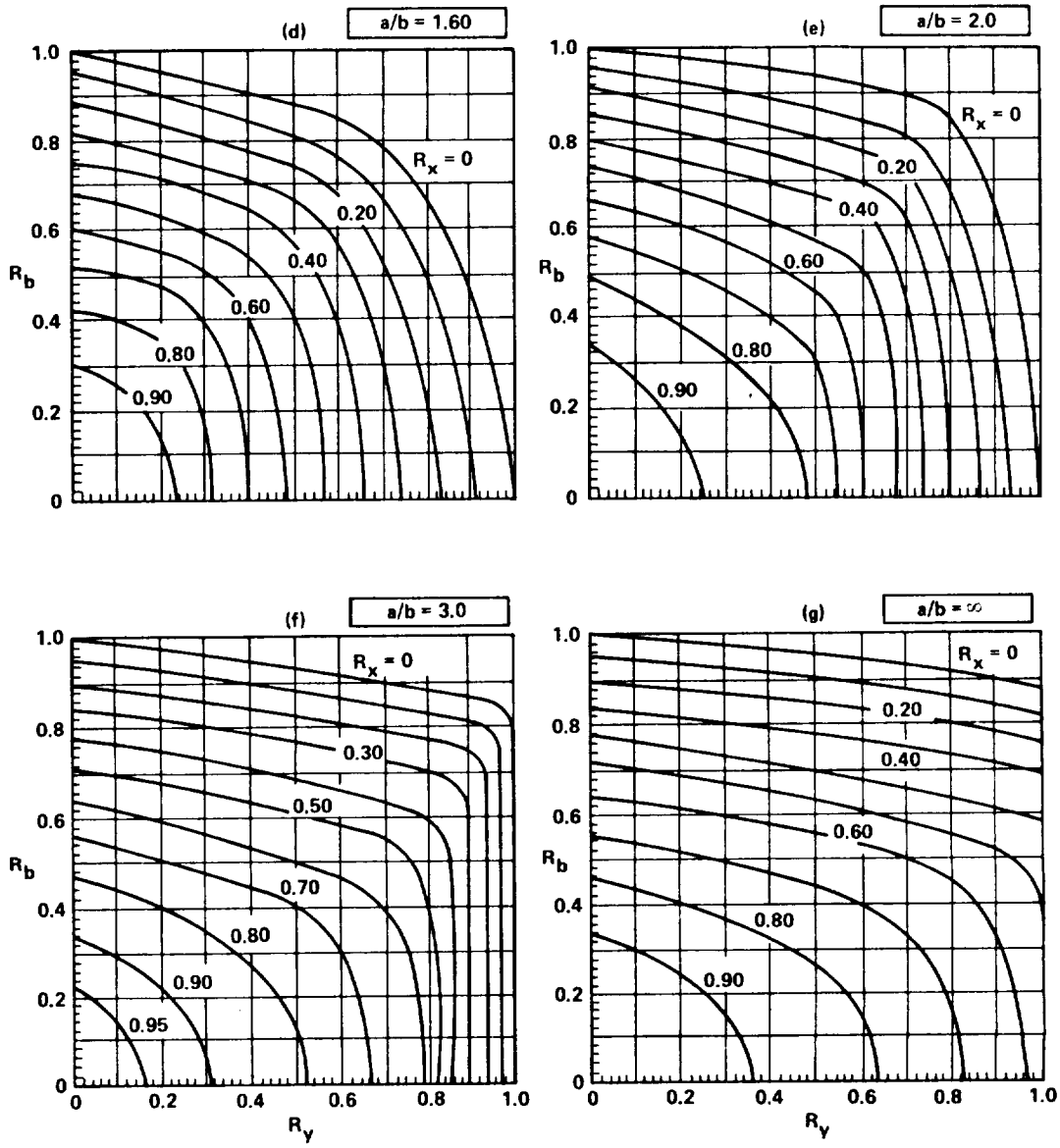

FIGURE C2-24. Concluded

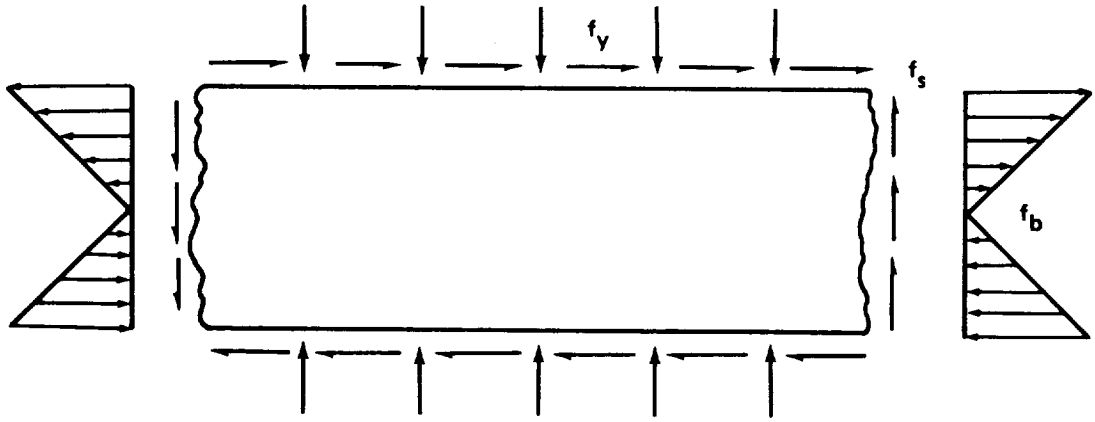

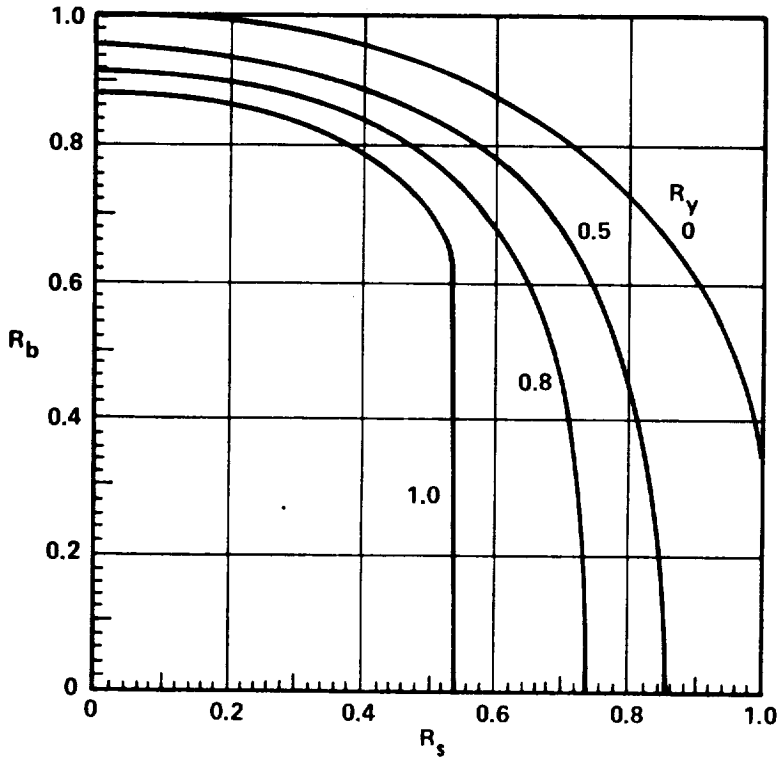

FIGURE C2-25. INTERACTION CURVES FOR SIMPLY SUPPORTED, LONG FLAT PLATES UNDER VARIOUS COMBINATIONS OF SHEAR, BENDING, AND TRANSVERSE COMPRESSION

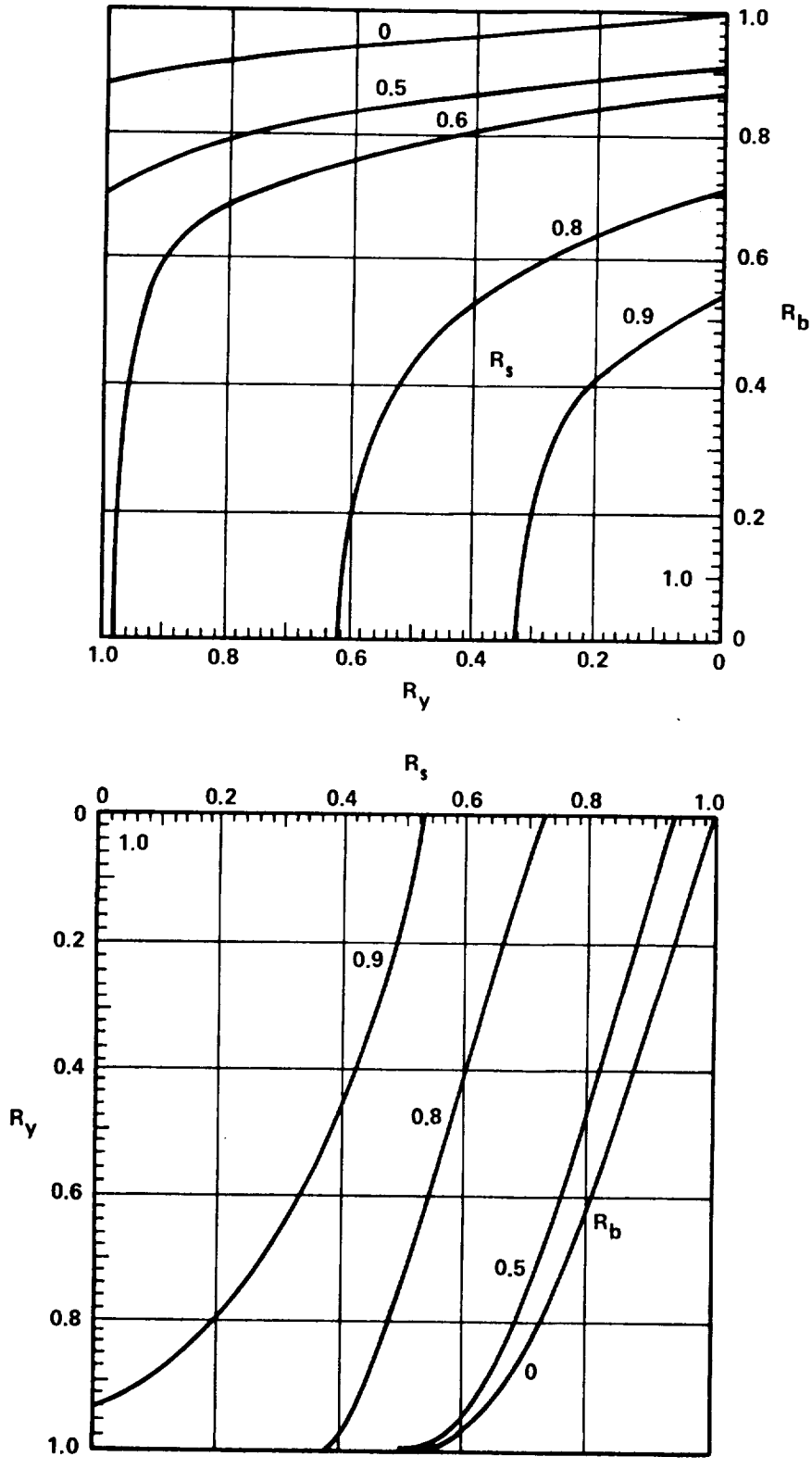

FIGURE C2-25. Concluded

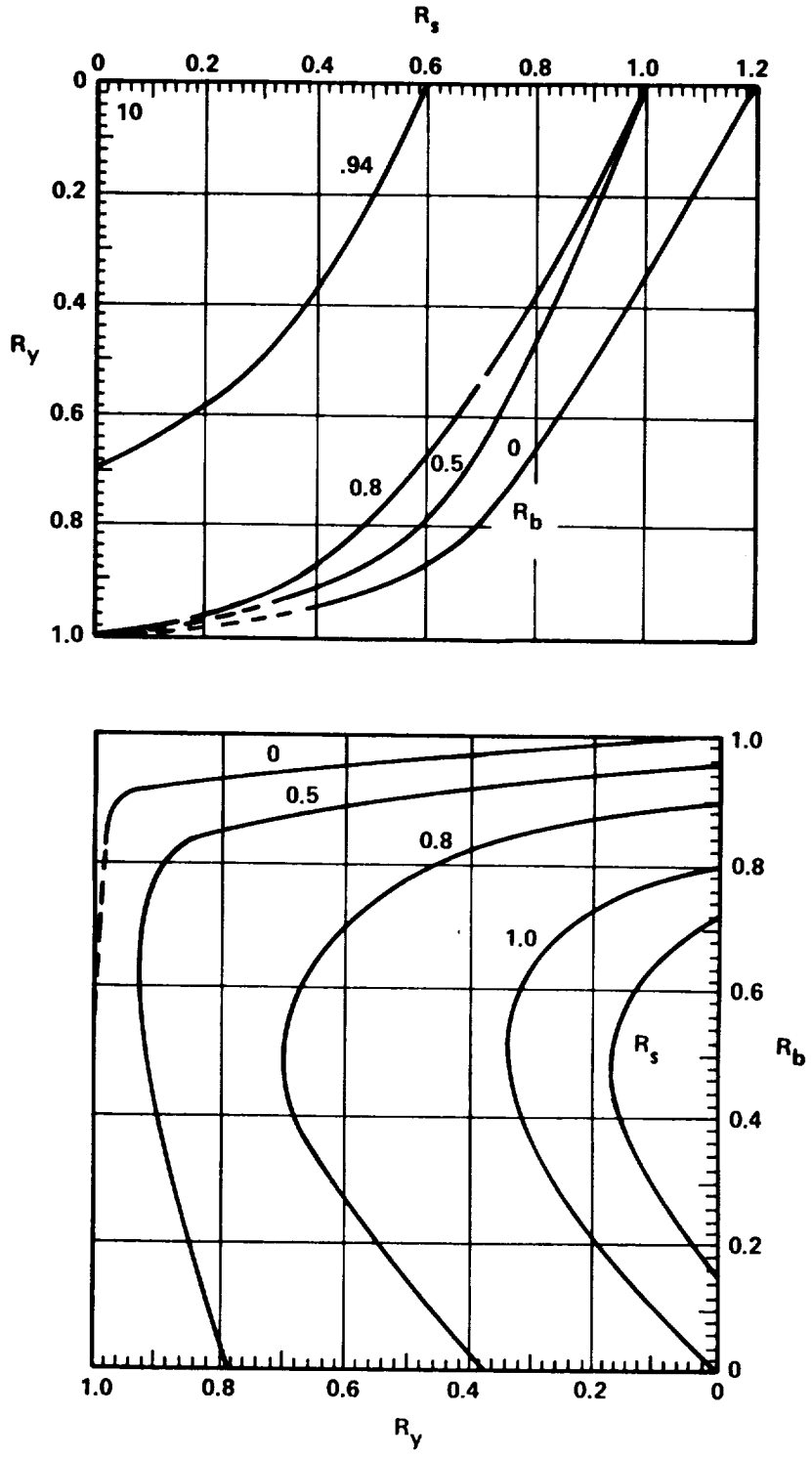

FIGURE C2-26. INTERACTION CURVES FOR UPPER EDGES SIMPLY SUPPORTED, LOWER EDGES CLAMPED, LONG PLATES UNDER VARIOUS COMBINATIONS OF SHEAR, BENDING, AND TRANSVERSE COMPRESSION

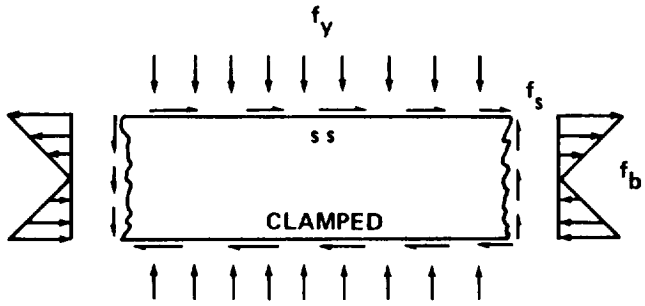

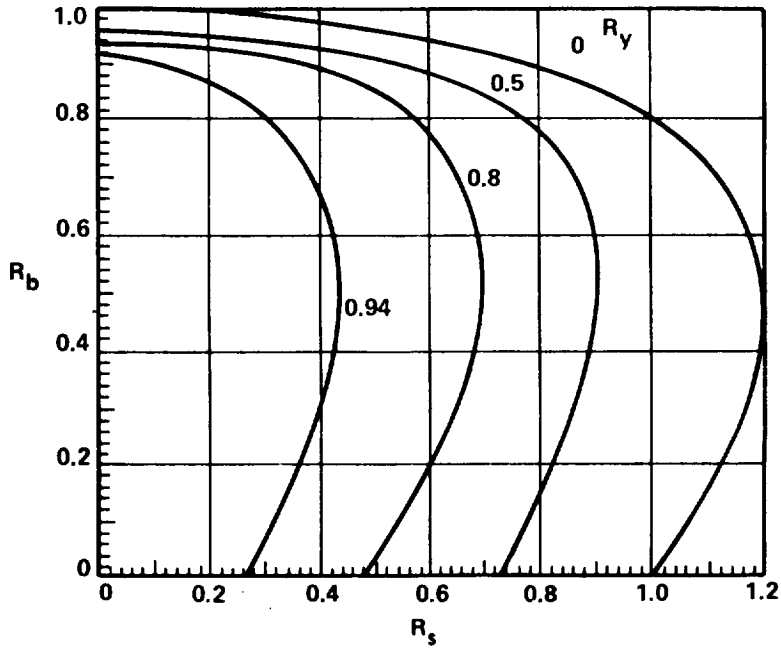

FIGURE C2-26. Concluded

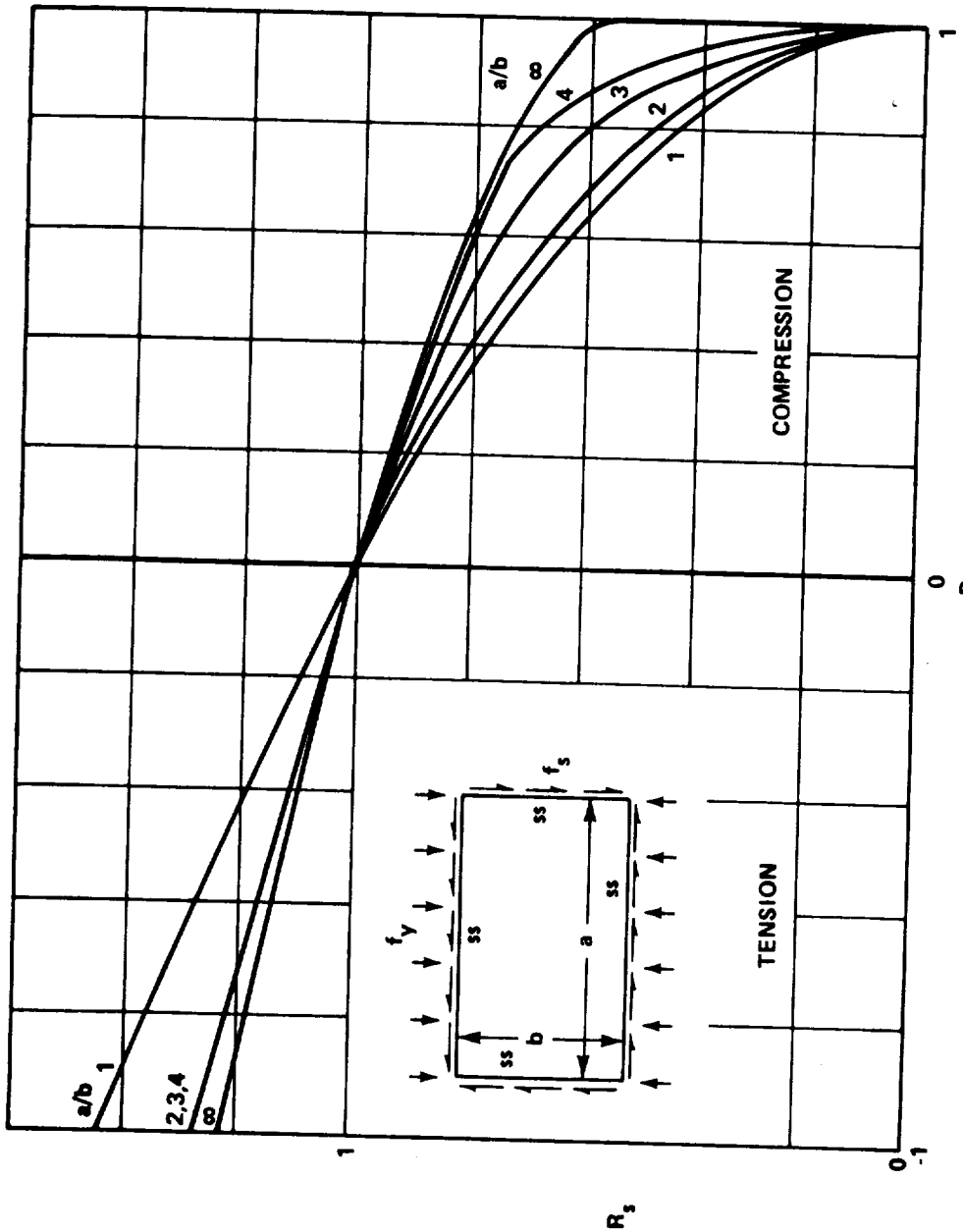

FIGURE C2-27. TRANSITION IN THE FORM OF INTERACTION CURVE FOR SHEAR AND TRANSVERSE DIRECT STRESS FOR A SIMPLY SUPPORTED RECTANGULAR FLAT PLATE AS THE LENGTH-WIDTH RATIO CHANGES FROM 1 TO ∞ IN TERMS OF R_s AND R_y. $\left(R_s = f_s / f_{s_{cr}},\ R_y = f_y / f_{y_{cr}}\right)$

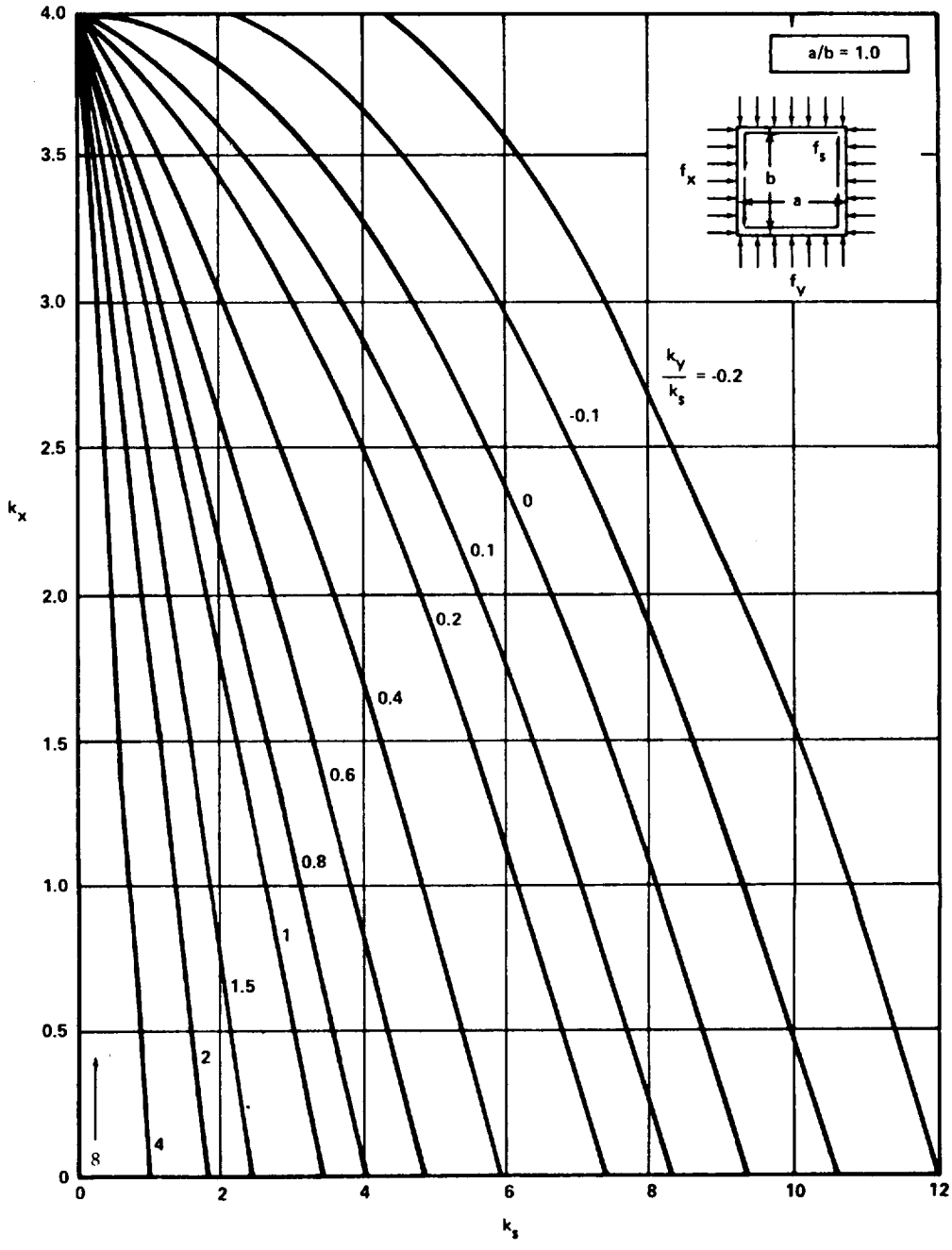

FIGURE C2-28. CRITICAL STRESS COEFFICIENTS FOR SIMPLY SUPPORTED FLAT PLATES UNDER LONGITUDINAL COMPRESSION, TRANSVERSE COMPRESSION, AND SHEAR

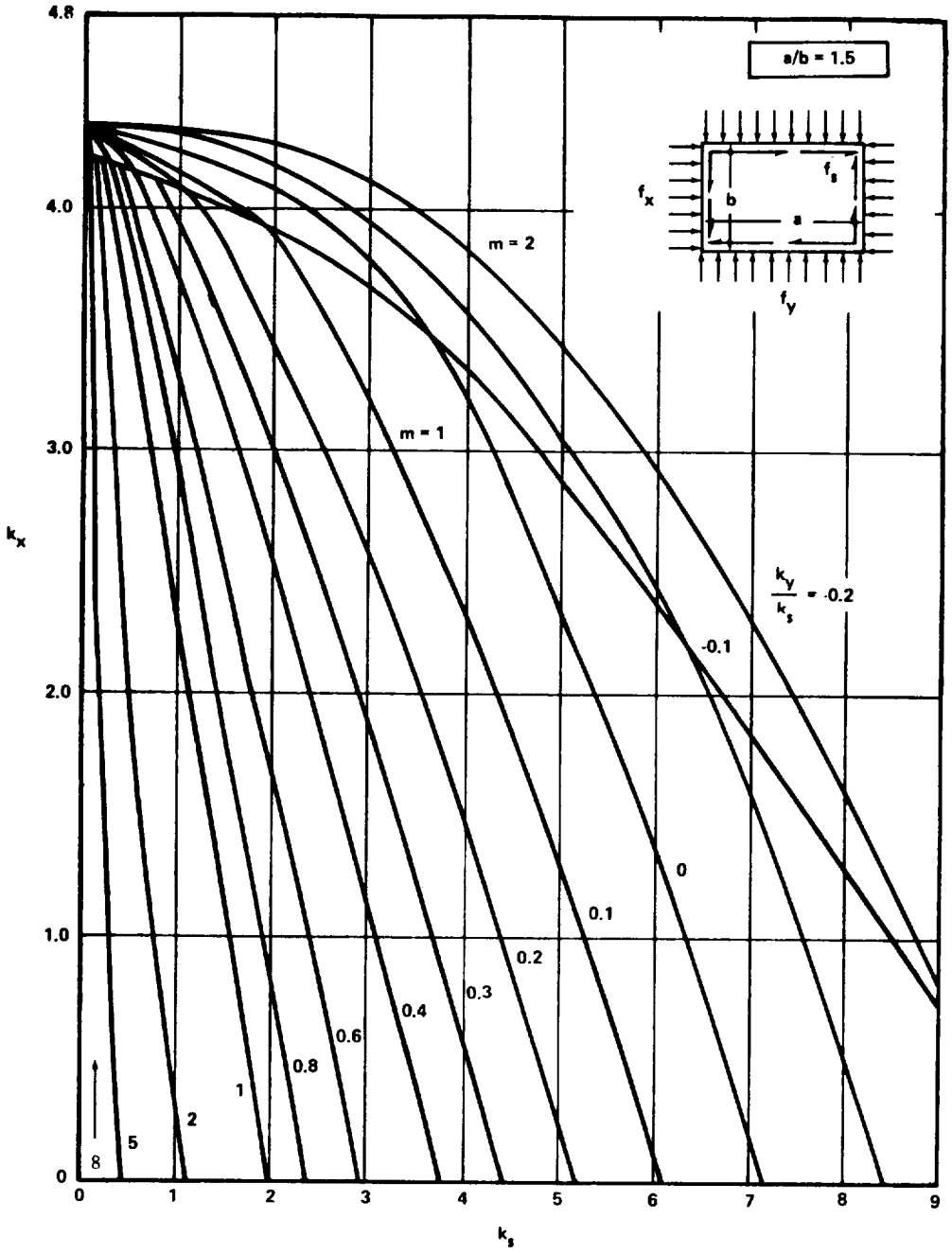

FIGURE C2-29. CRITICAL STRESS COEFFICIENTS FOR SIMPLY SUPPORTED FLAT PLATES UNDER LONGITUDINAL COMPRESSION, TRANSVERSE COMPRESSION, AND SHEAR

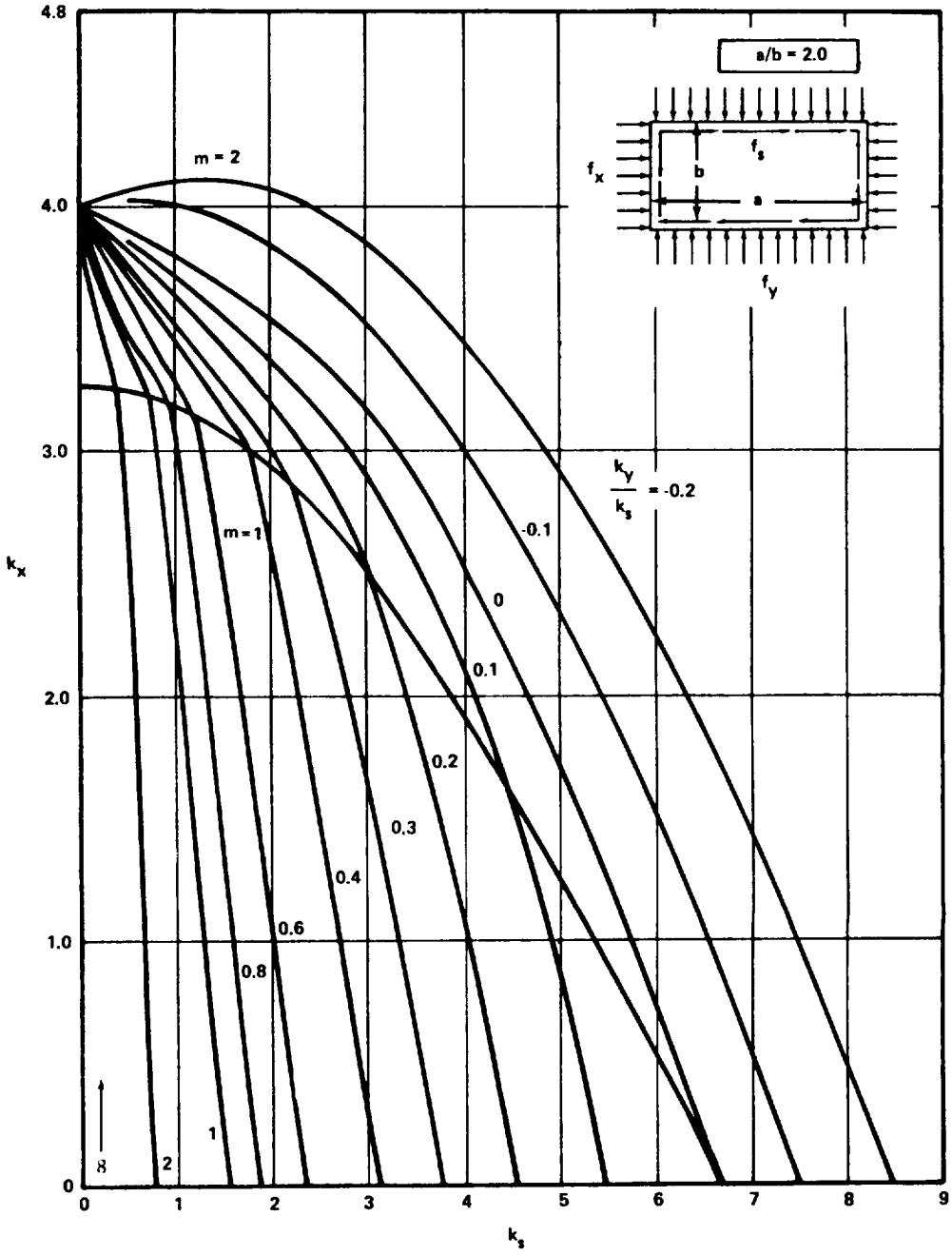

FIGURE C2-30. CRITICAL STRESS COEFFICIENTS FOR SIMPLY SUPPORTED FLAT PLATES UNDER LONGITUDINAL COMPRESSION, TRANSVERSE COMPRESSION, AND SHEAR

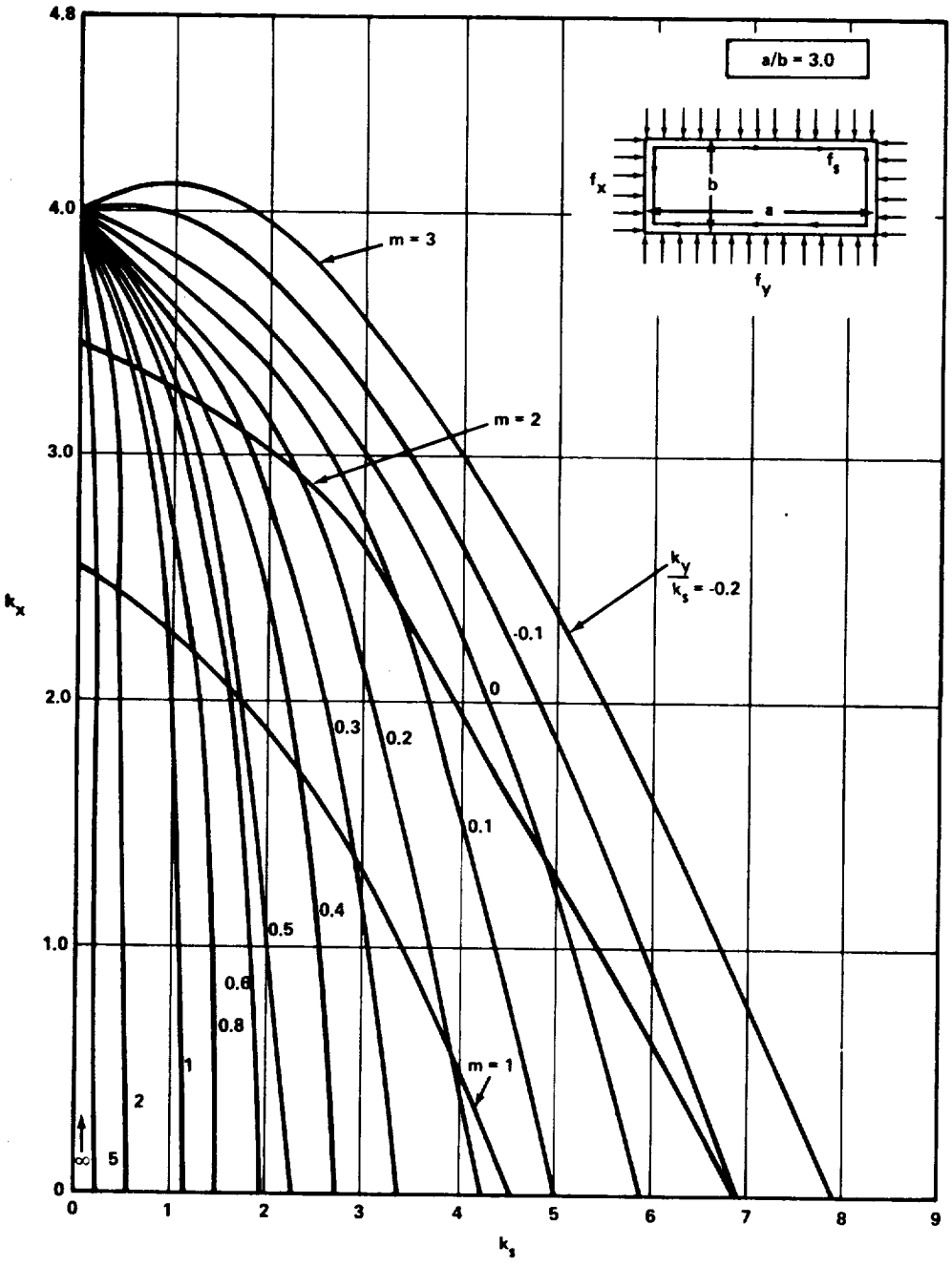

FIGURE C2-31. CRITICAL STRESS COEFFICIENTS FOR SIMPLY SUPPORTED FLAT PLATES UNDER LONGITUDINAL COMPRESSION, TRANSVERSE COMPRESSION, AND SHEAR

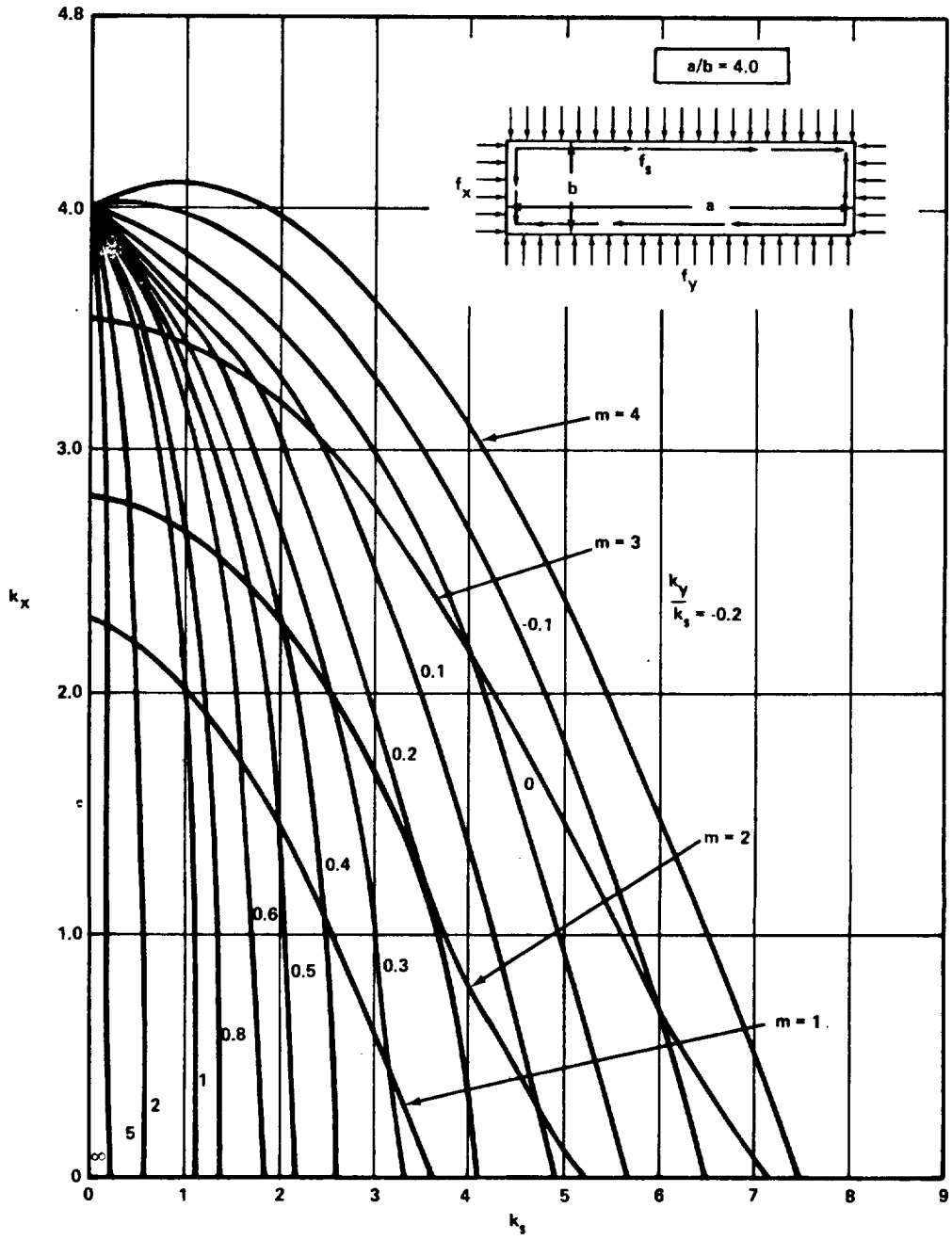

FIGURE C2-32. CRITICAL STRESS COEFFICIENTS FOR SIMPLY SUPPORTED FLAT PLATES UNDER LONGITUDINAL COMPRESSION, TRANSVERSE COMPRESSION, AND SHEAR

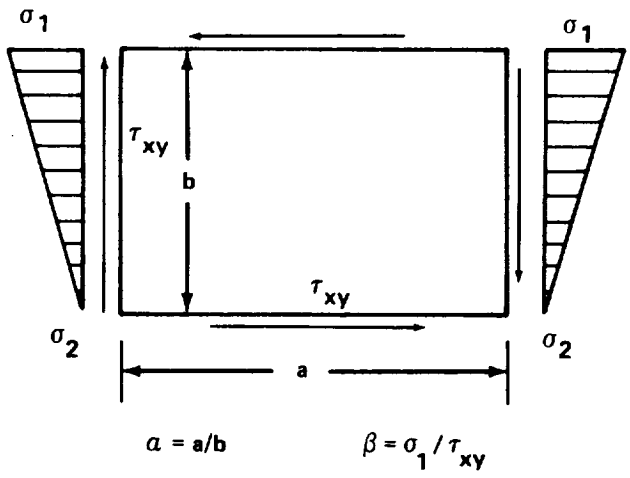

FIGURE C2-33. RECTANGULAR PLATE UNDER COMBINED SHEAR AND NONUNIFORM LONGITUDINAL COMPRESSION

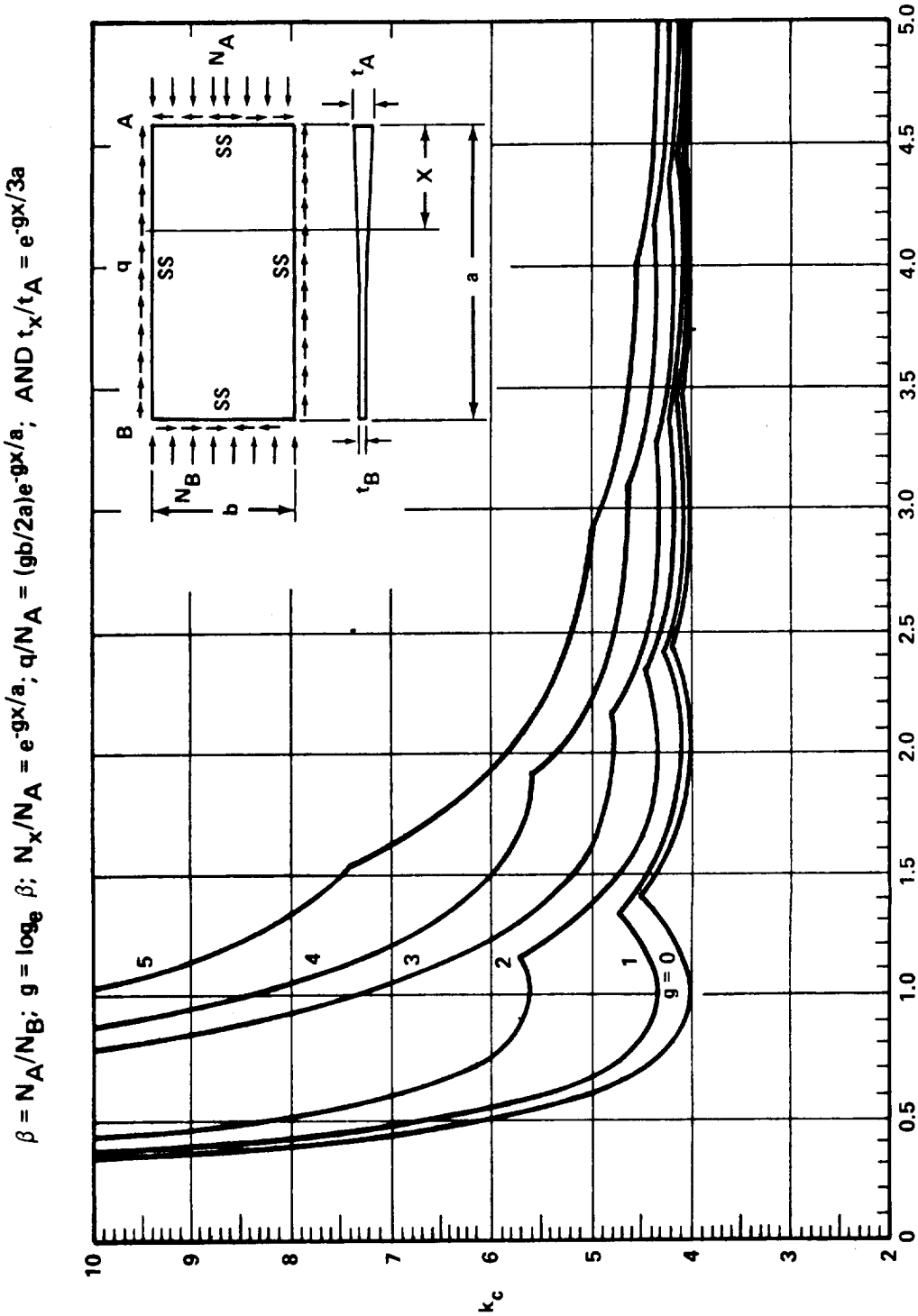

FIGURE C2-34. COMPRESSIVE-BUCKLING-STRESS COEFFICIENT FOR A SIMPLY SUPPORTED RECTANGULAR FLAT PLATE OF MINIMUM WEIGHT
(Thickness and loading vary exponentially along length.)

$$F_{av} = \frac{k_{c_{av}} \pi^2 E}{12(1 - \nu_e^2)} (t/b)^2$$

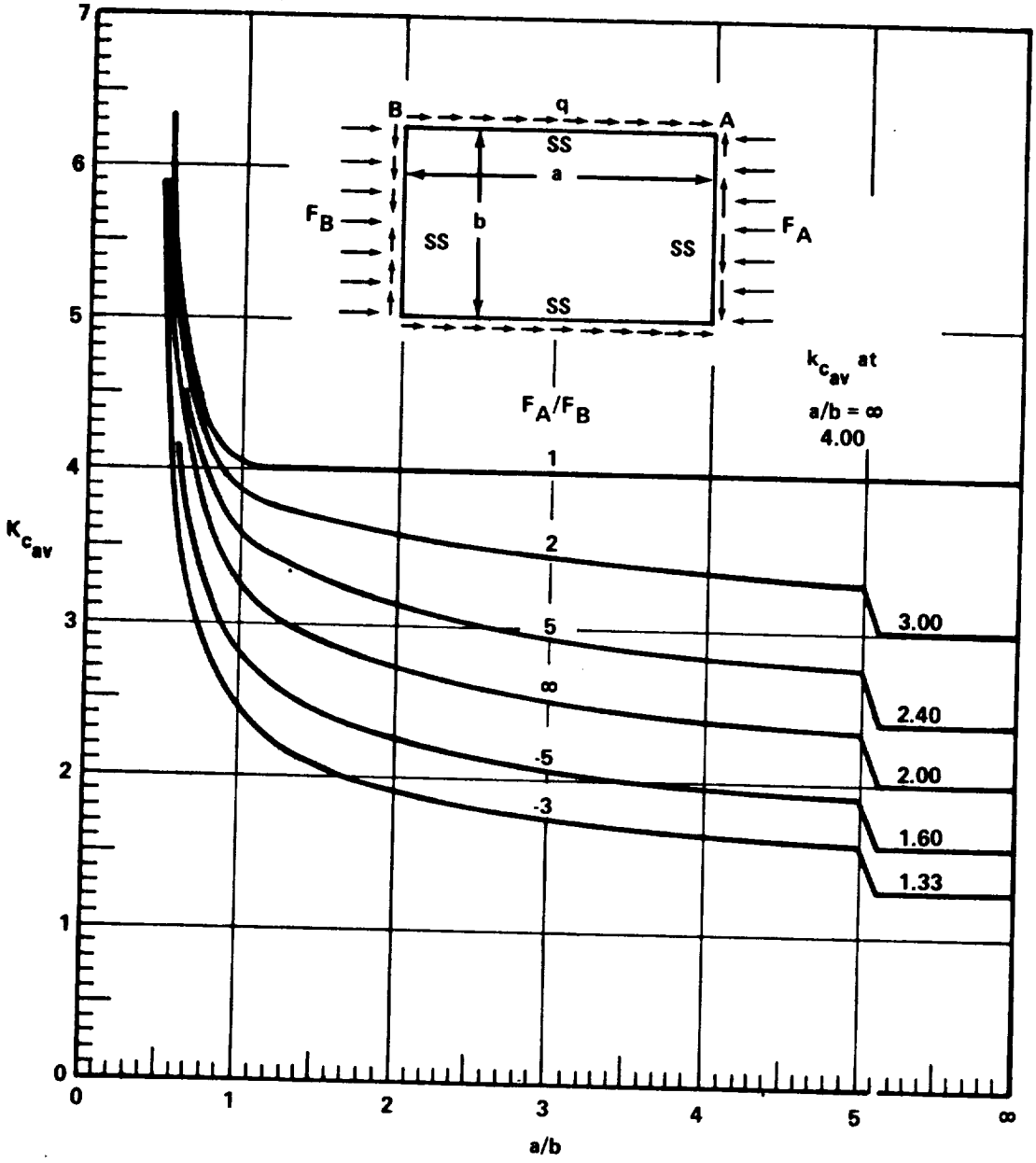

FIGURE C2-35. AVERAGE COMPRESSIVE-BUCKLING-STRESS COEFFICIENT FOR RECTANGULAR FLAT PLATE OF CONSTANT THICKNESS WITH LINEARLY VARYING AXIAL LOAD

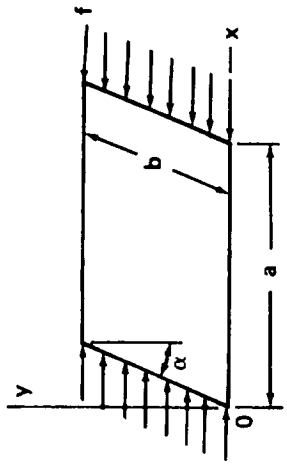

$$\frac{f_{cr}}{\eta} = \frac{k}{\cos^4 \alpha} \quad \frac{\pi^2 E}{12(1-\nu_e^2)} \quad \left[\frac{t}{b}\right]^2$$

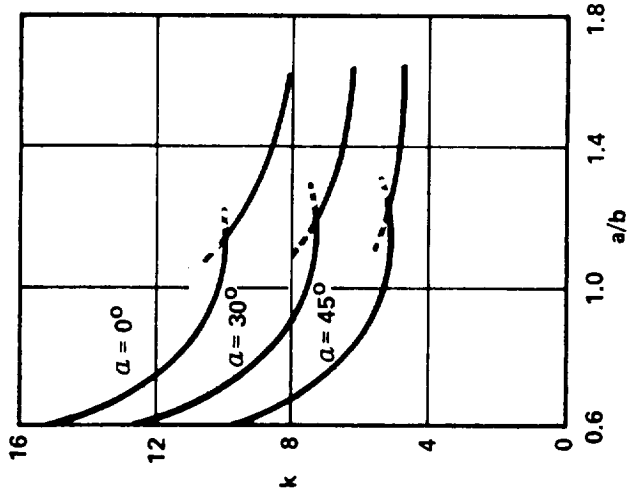

FIGURE C2-36. BUCKLING COEFFICIENTS OF CLAMPED OBLIQUE FLAT PLATES IN COMPRESSION

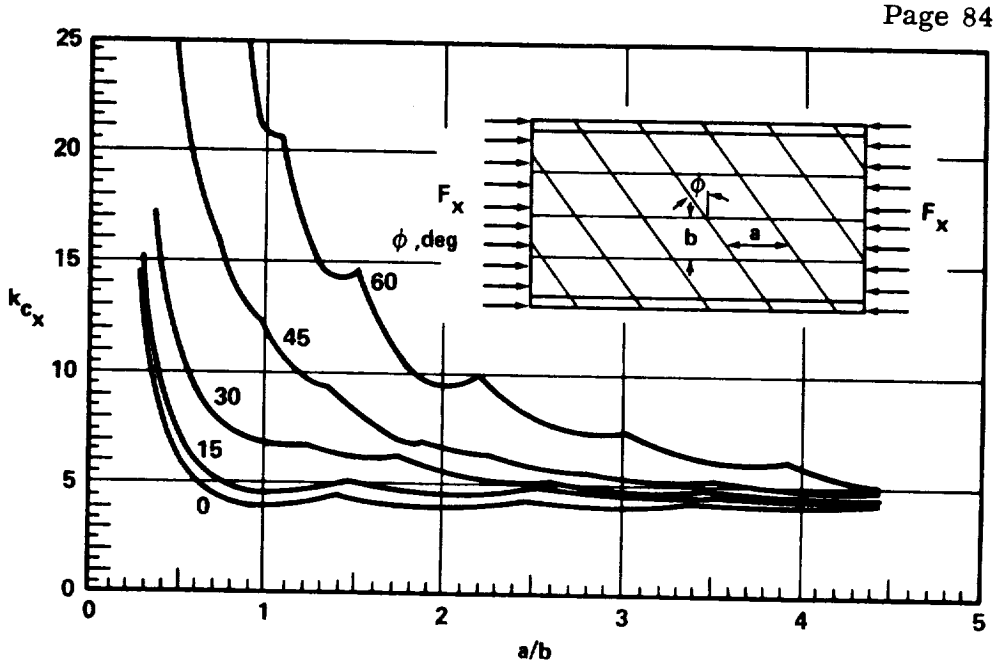

(a) LOADING IN x-DIRECTION

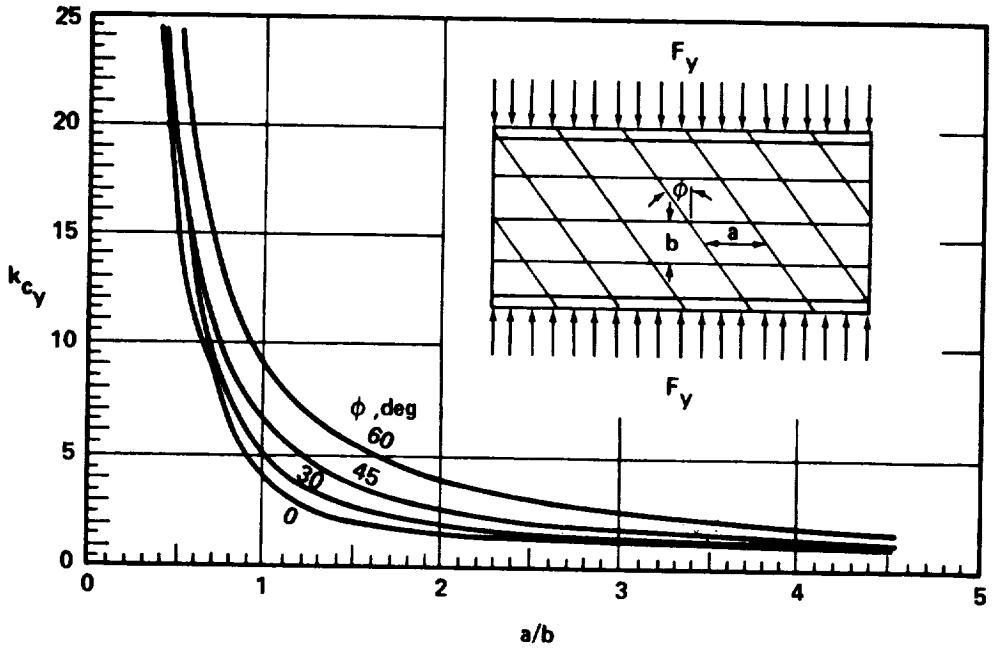

(b) LOADING IN y-DIRECTION

FIGURE C2-37. COMPRESSIVE-BUCKLING COEFFICIENTS FOR FLAT SHEET ON NONDEFLECTING SUPPORTS DIVIDED INTO PARALLELOGRAM-SHAPED PANELS
(All panels sides are equal.)

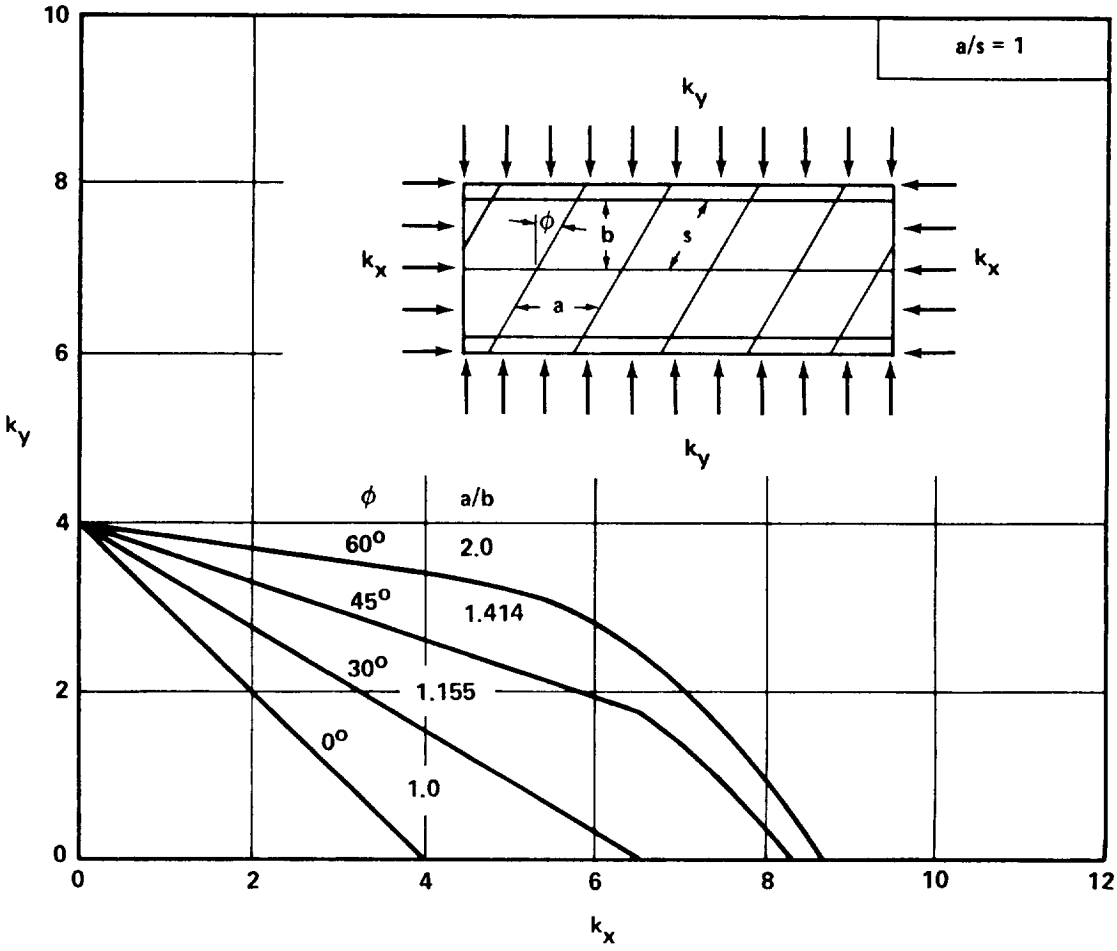

FIGURE C2-38. INTERACTION CURVES FOR COMBINED AXIAL AND TRANSVERSE LOADING OF SKEW PANELS

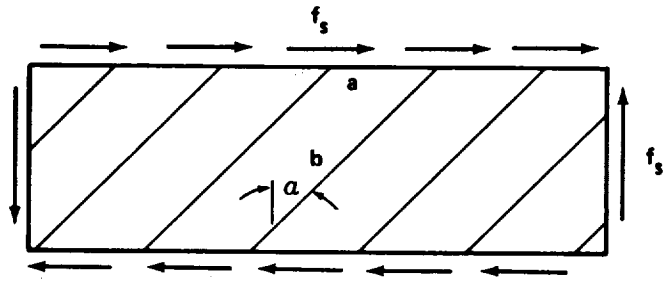

FIGURE C2-39. SHEAR LOADING OF PARALLELOGRAM PLATE

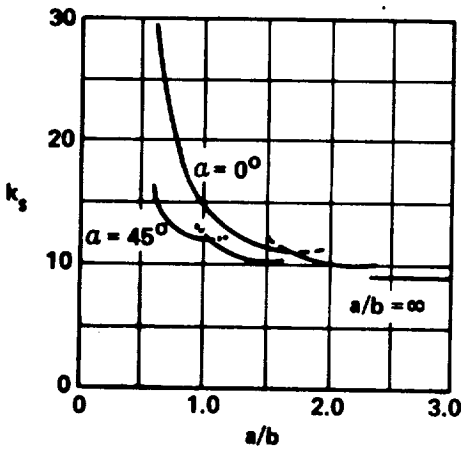

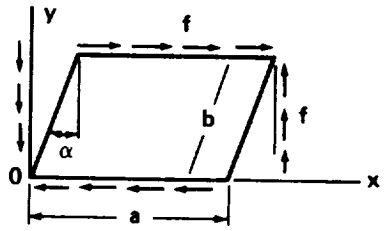

$$\frac{f_{cr}}{\eta} = k \frac{1}{\cos^2 \alpha} \frac{\pi^2 E}{12 (1 - \upsilon_e^2)} \left[\frac{t}{b}\right]^2$$

FIGURE C2-40. BUCKLING COEFFICIENTS OF CLAMPED OBLIQUE FLAT PLATES IN SHEAR

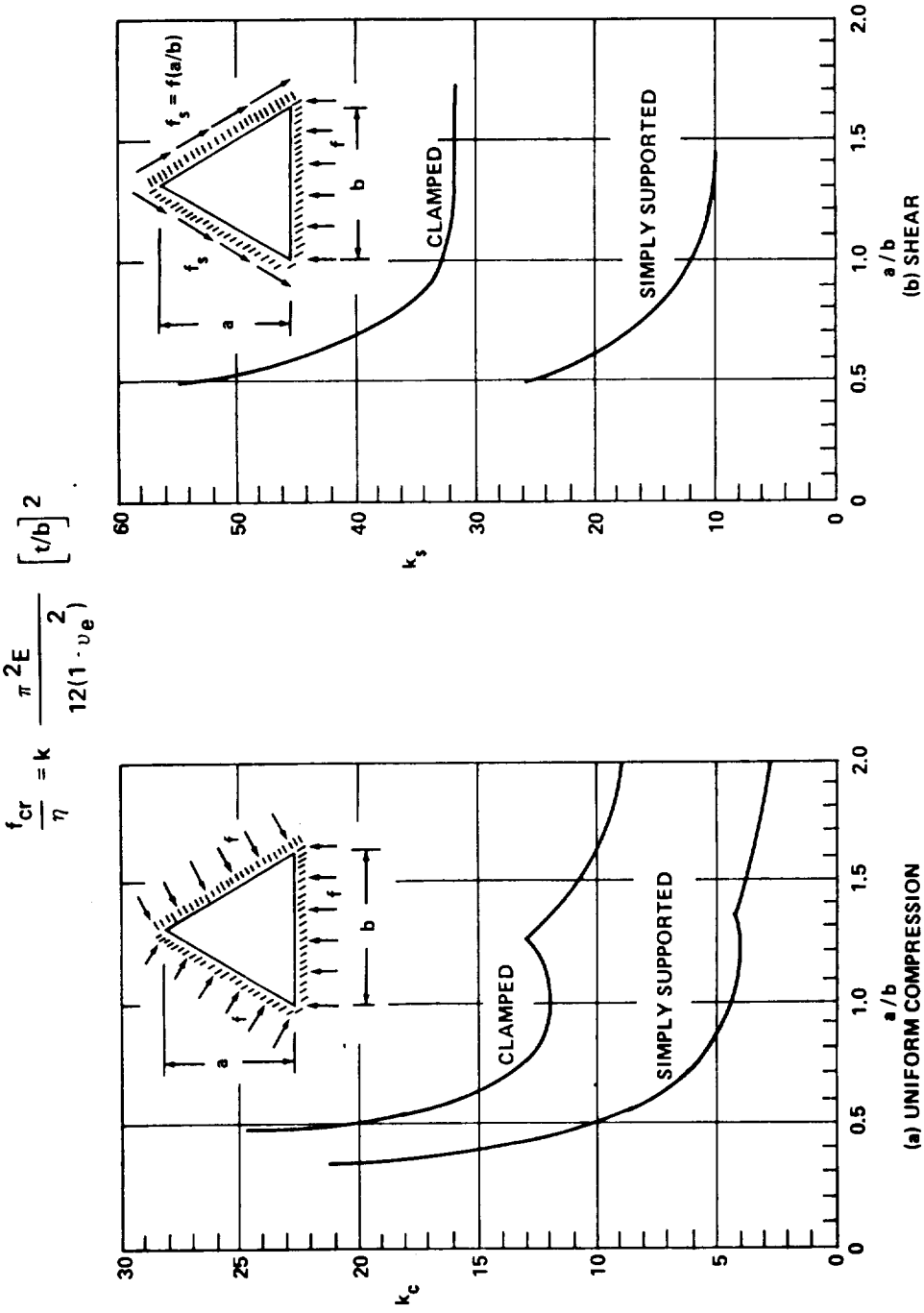

FIGURE C2-41. BUCKLING COEFFICIENTS FOR ISOSCELES TRIANGULAR PLATES

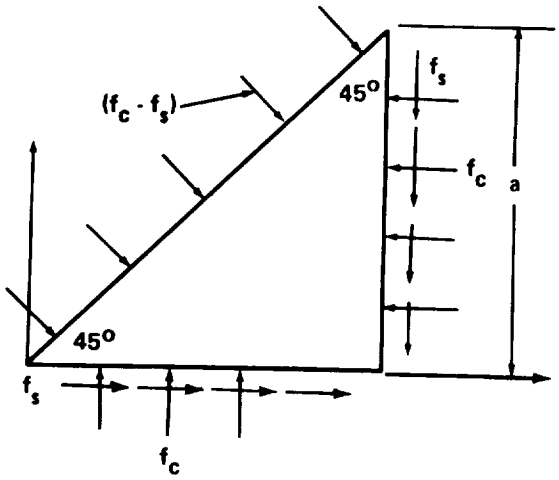

$$\frac{f_{cr}}{\eta} = k \frac{\pi^2 E}{12(1-\nu_e^2)} t^2/a^2$$

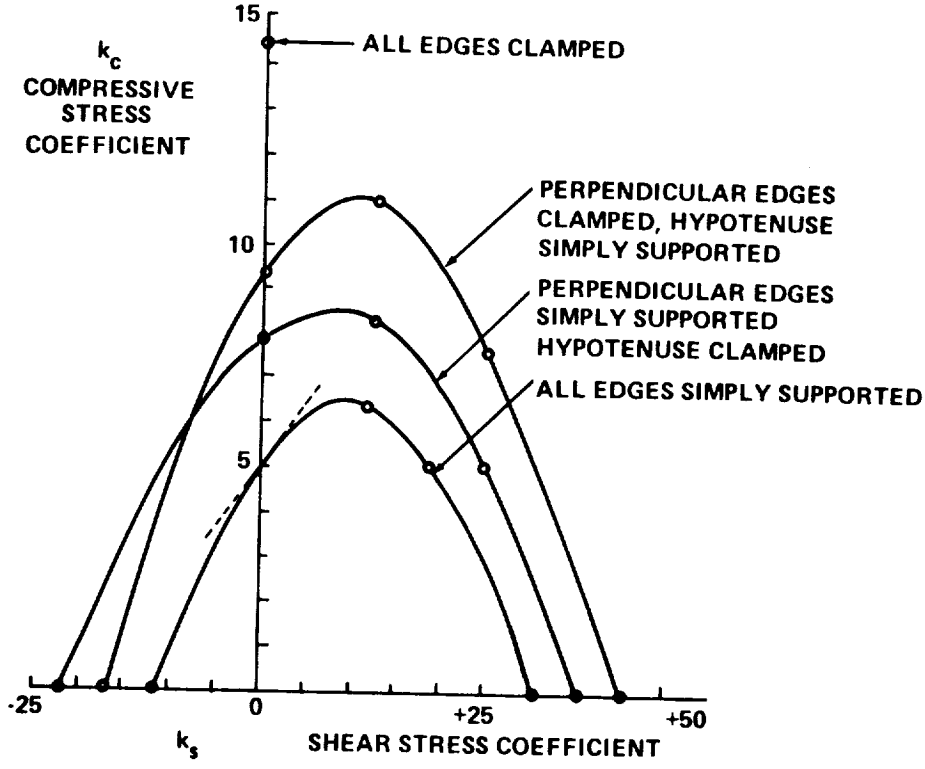

FIGURE C2-42. INTERACTION CURVES FOR BUCKLING OF RIGHT-ANGLED ISOSCELES TRIANGULAR PLATE

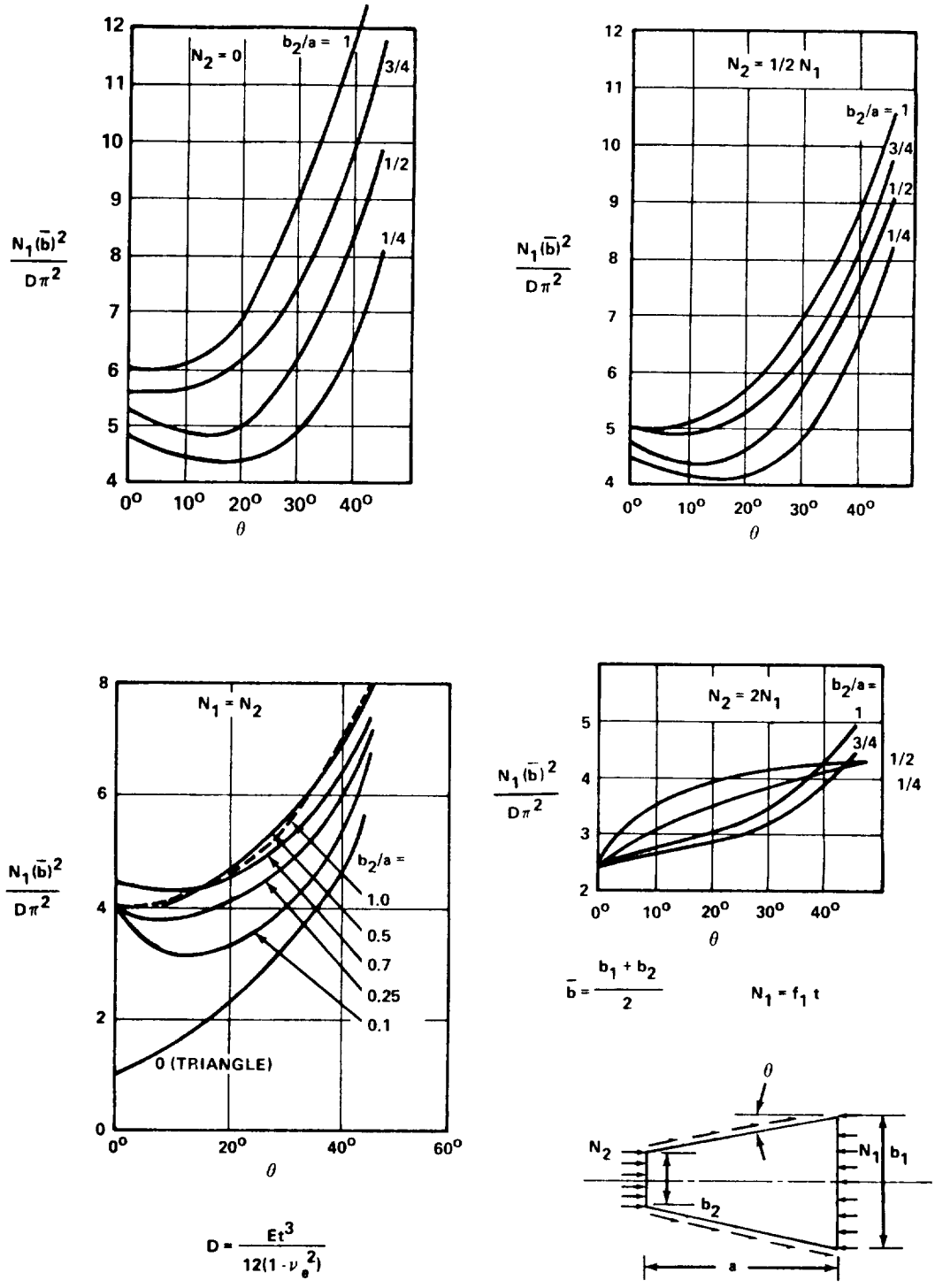

FIGURE C2-43. BUCKLING CURVES FOR TRAPEZOIDAL PLATES

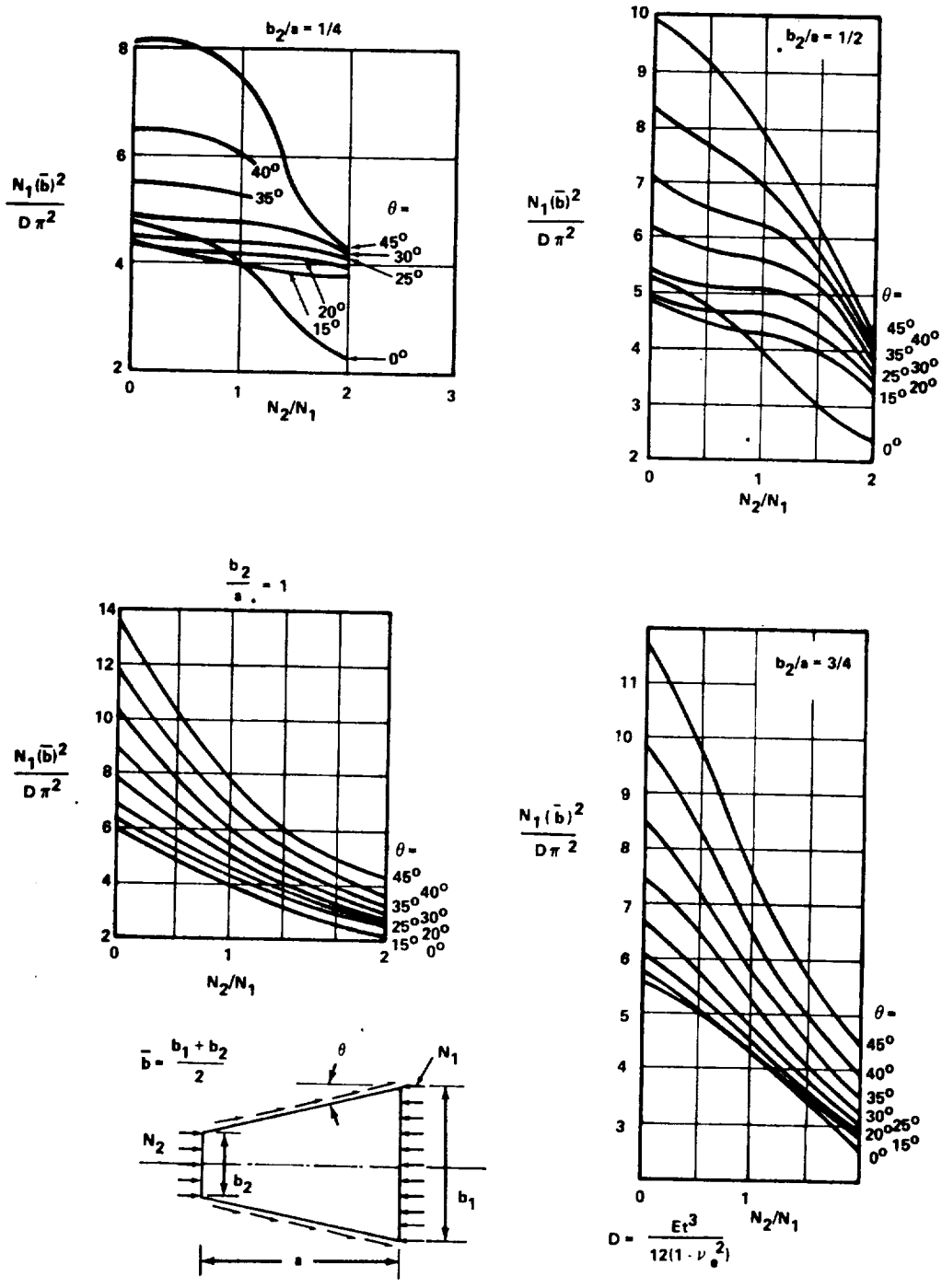

FIGURE C2-44. BUCKLING CURVES FOR TRAPEZOIDAL PLATES

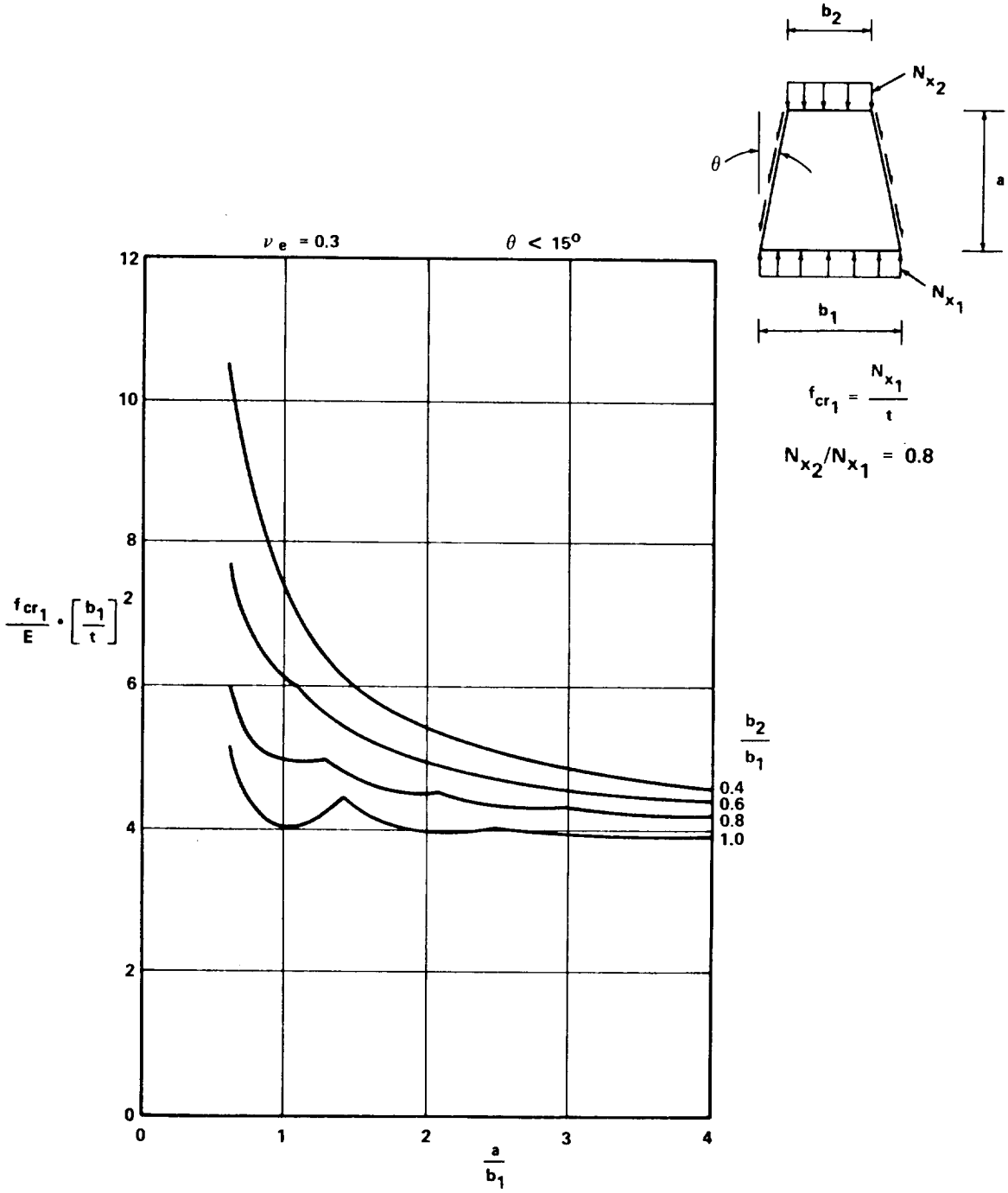

FIGURE C2-45. BUCKLING STRESS DIAGRAM (Sides and ends simply-supported. No stress normal to sides.)

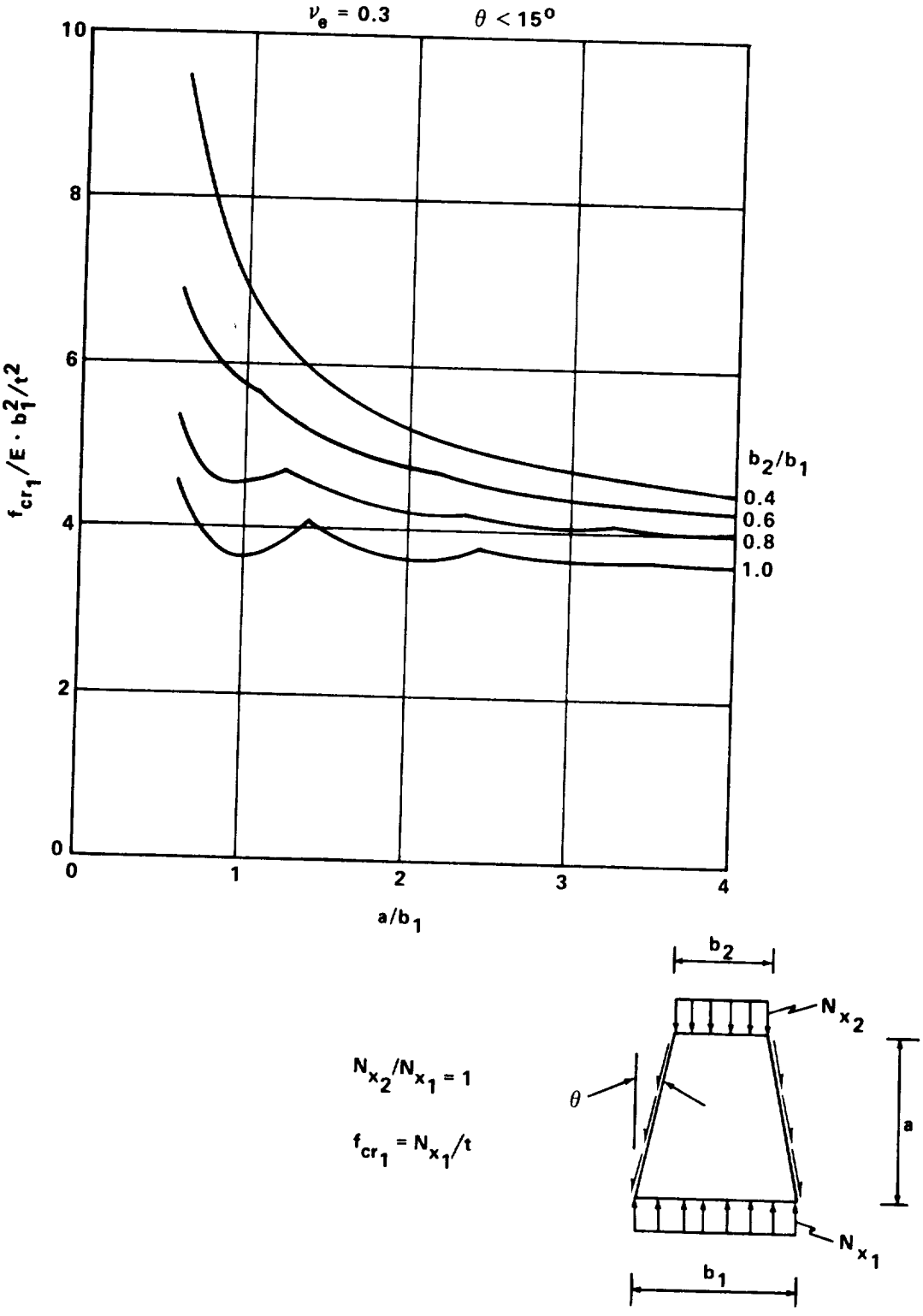

FIGURE C2-46. BUCKLING STRESS DIAGRAM (Sides and ends simply-supported. No stress normal to sides.)

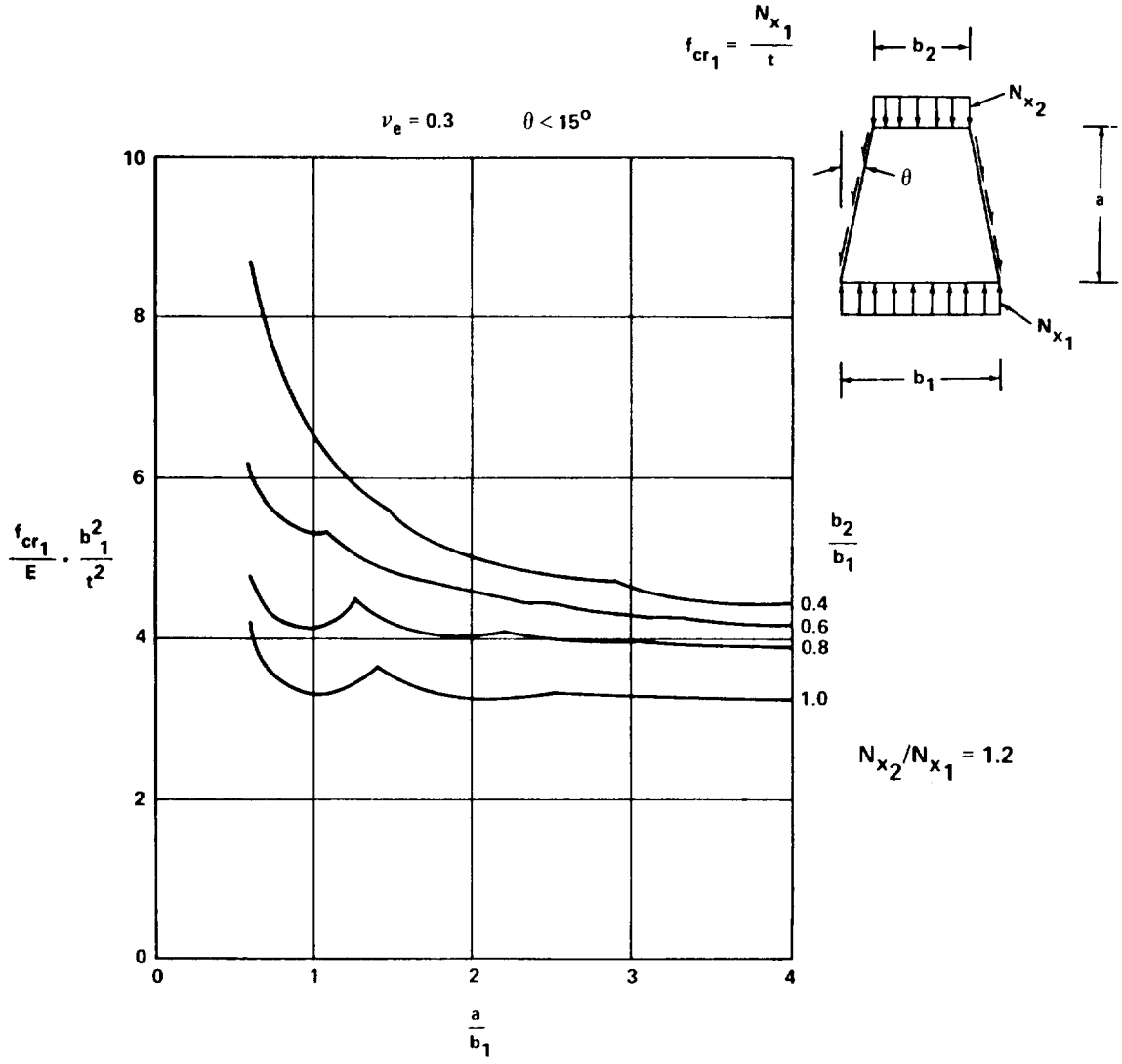

FIGURE C2-47. BUCKLING STRESS DIAGRAM (Sides and ends simply-supported. No stress normal to sides.)

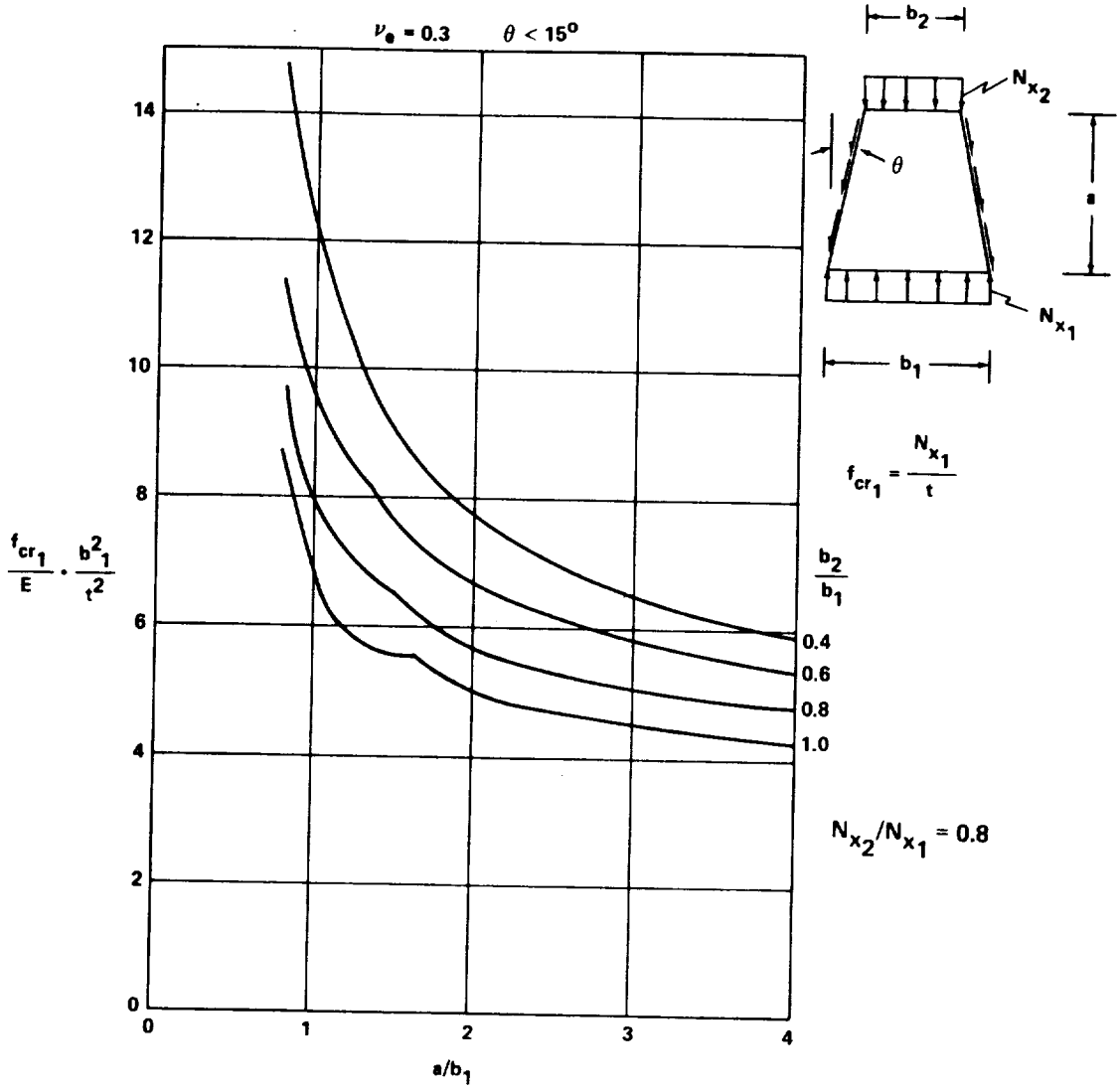

FIGURE C2-48. BUCKLING STRESS DIAGRAM (Sides simply-supported. Ends clamped. No stress normal to sides.)

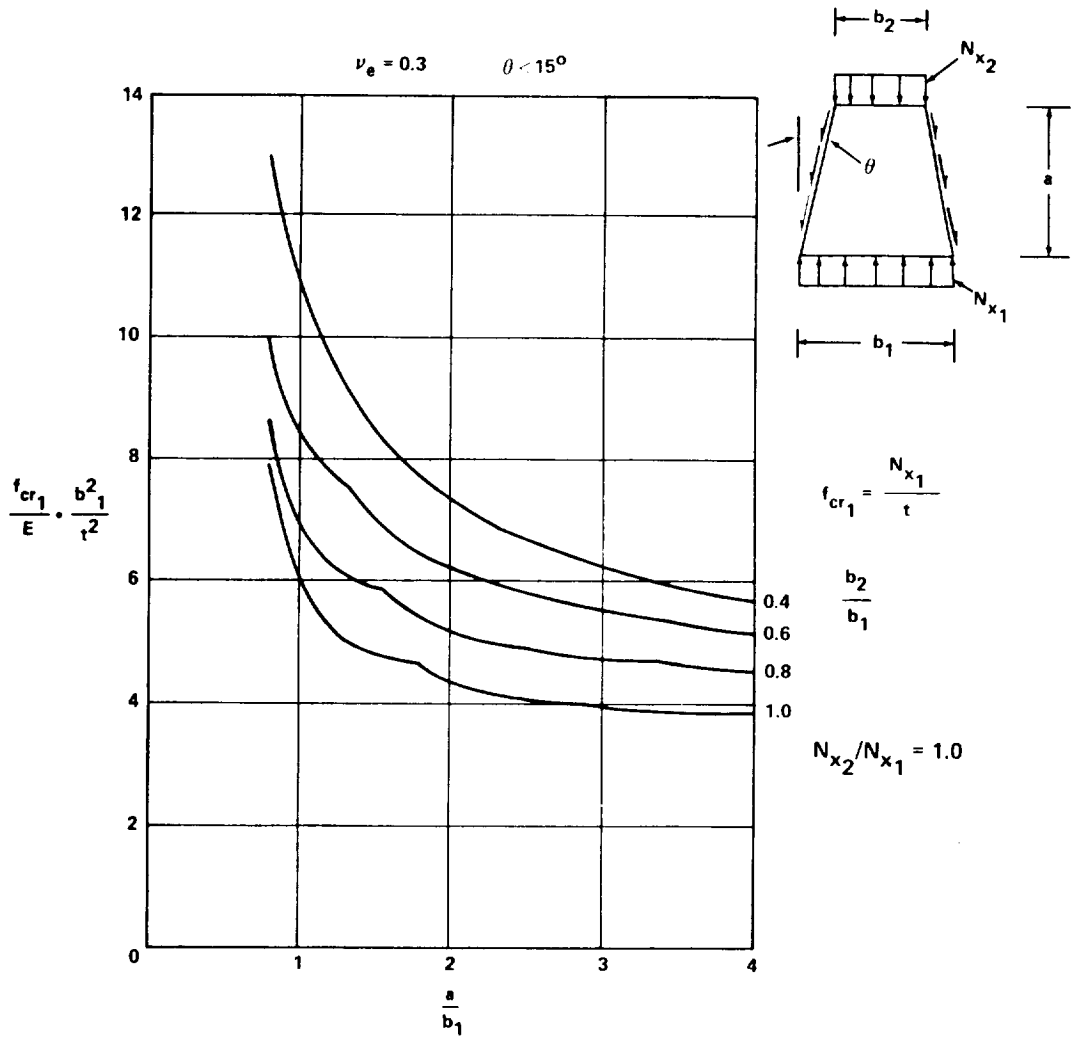

FIGURE C2-49. BUCKLING STRESS DIAGRAM (Sides simply-supported. Ends clamped. No stress normal to sides.)

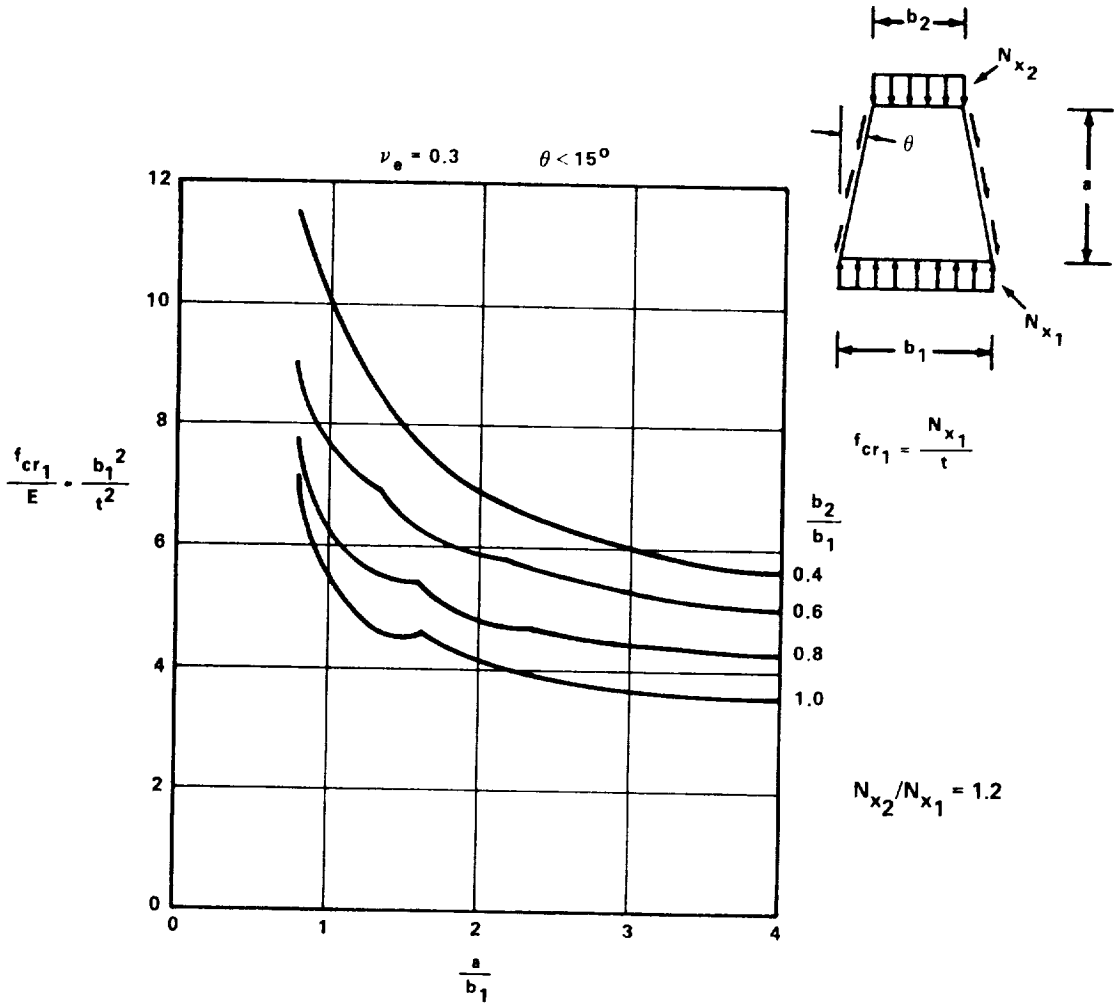

FIGURE C2-50. BUCKLING STRESS DIAGRAM (Sides simply-supported. Ends clamped. No stress normal to sides.)

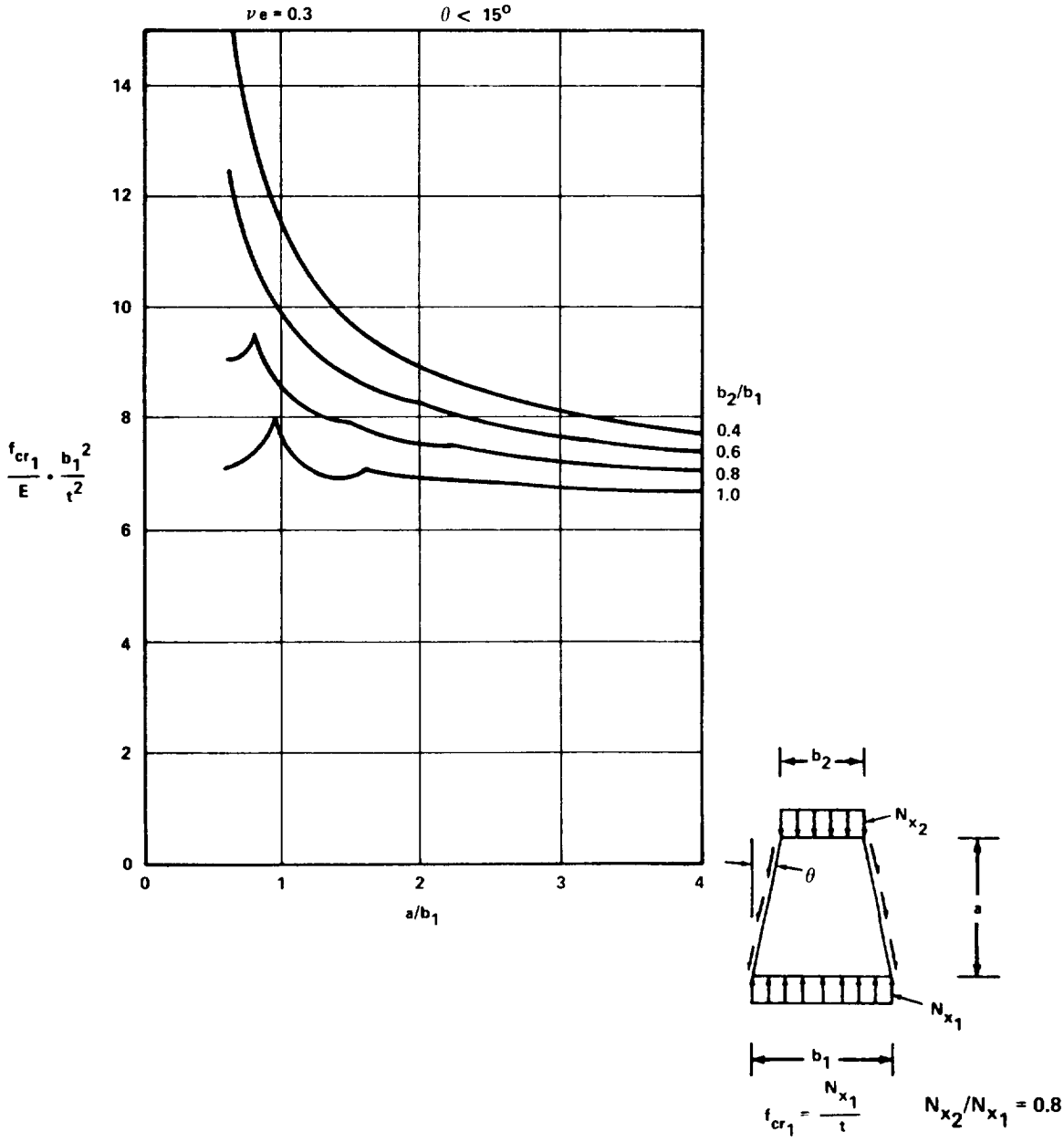

FIGURE C2-51. BUCKLING STRESS DIAGRAM (Sides clamped. Ends simply-supported. No stress normal to sides.)

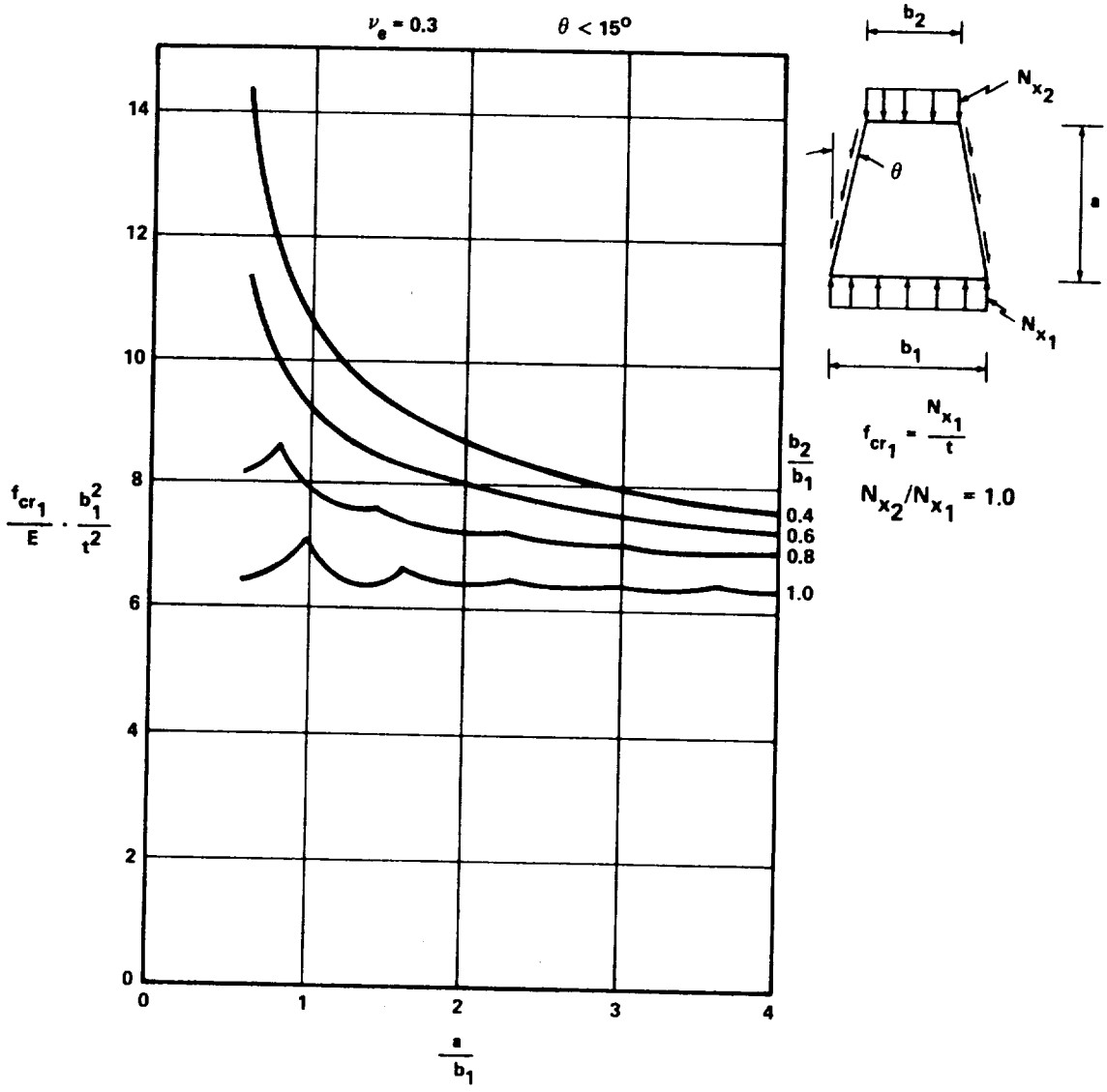

FIGURE C2-52. BUCKLING STRESS DIAGRAM (Sides clamped. Ends simply-supported. No stress normal to sides.)

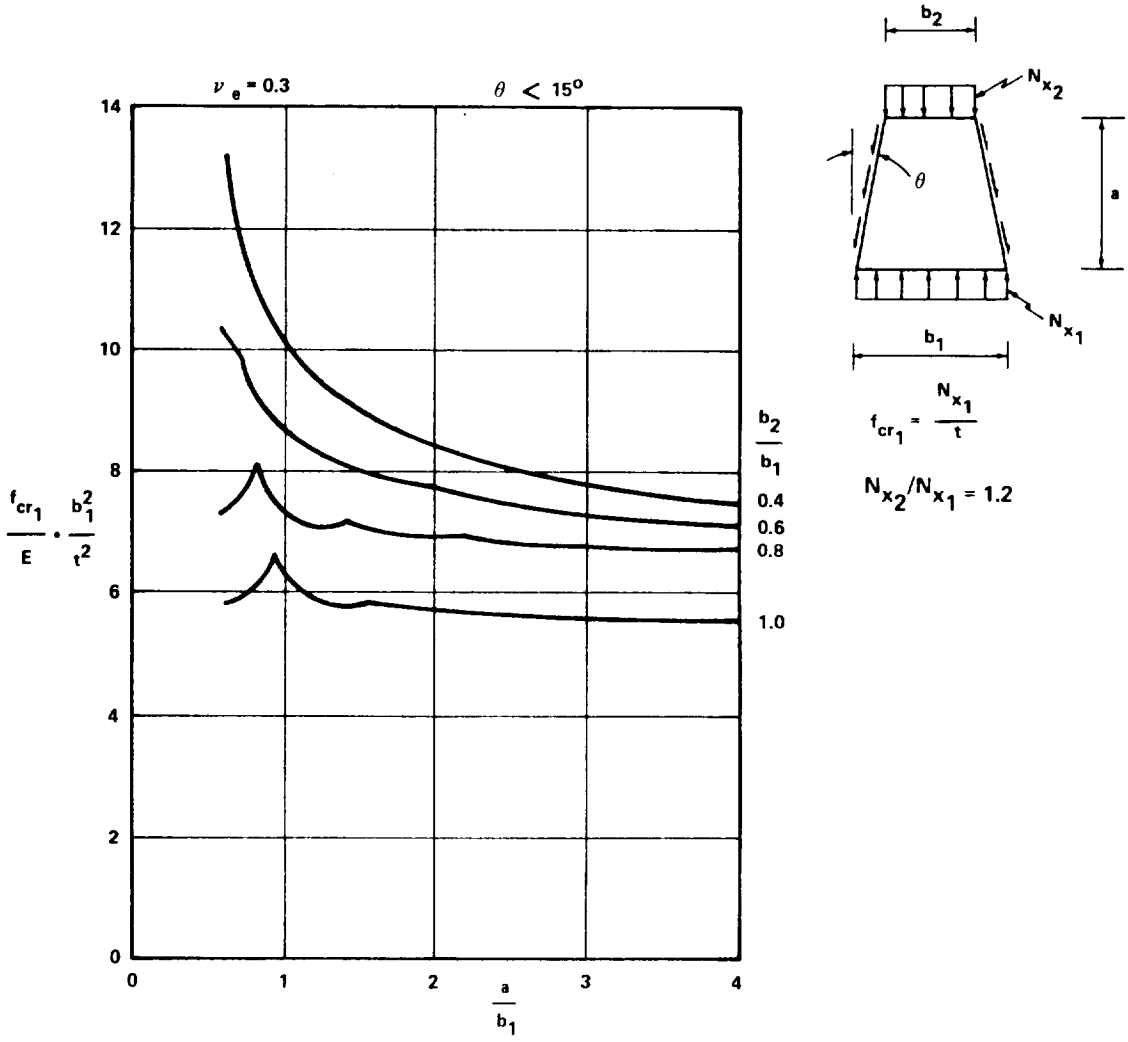

FIGURE C2-53. BUCKLING STRESS DIAGRAM (Sides clamped. Ends simply-supported. No stress normal to sides.)

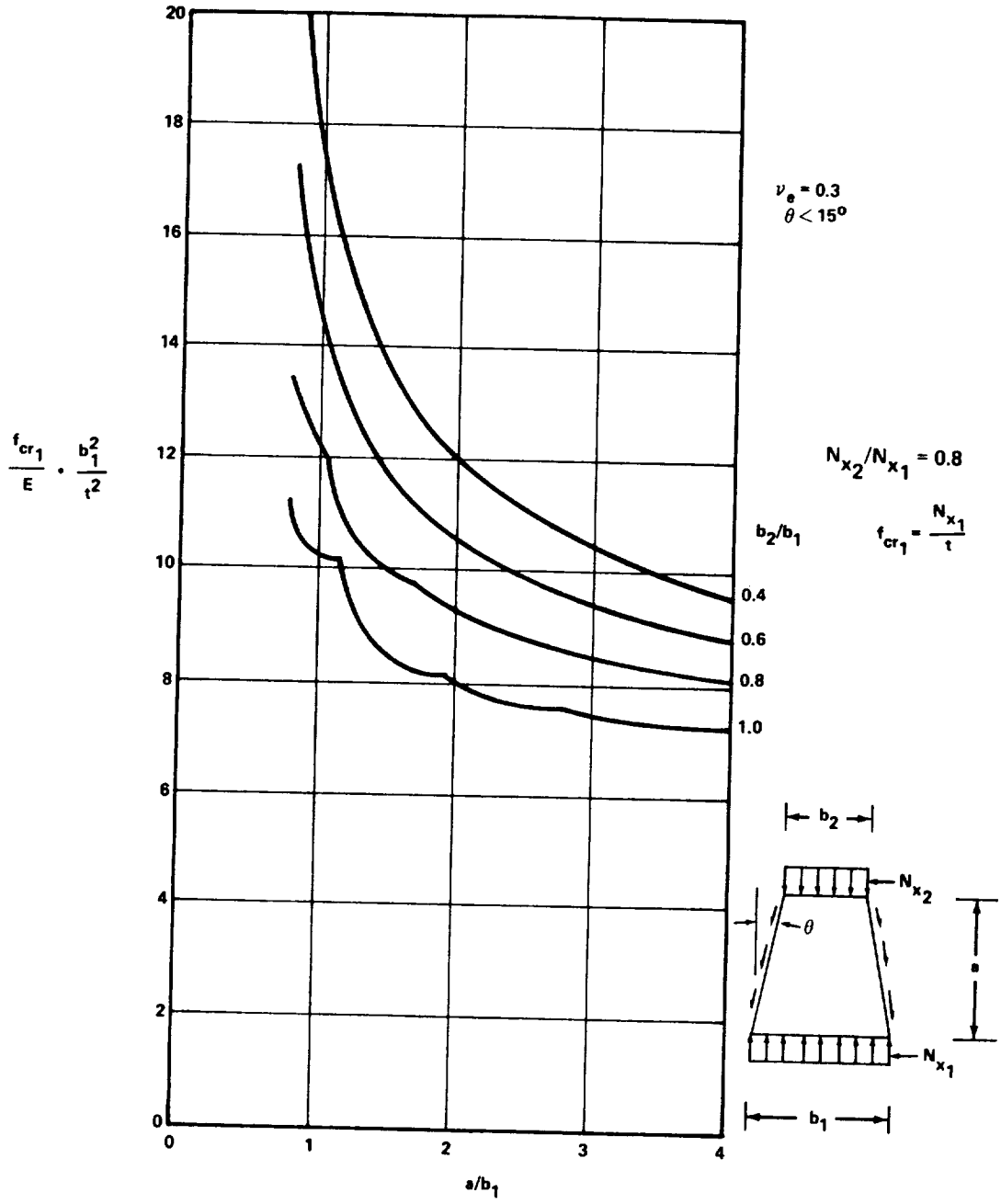

FIGURE C2-54. BUCKLING STRESS DIAGRAM (Sides and ends clamped. No stress normal to sides.)

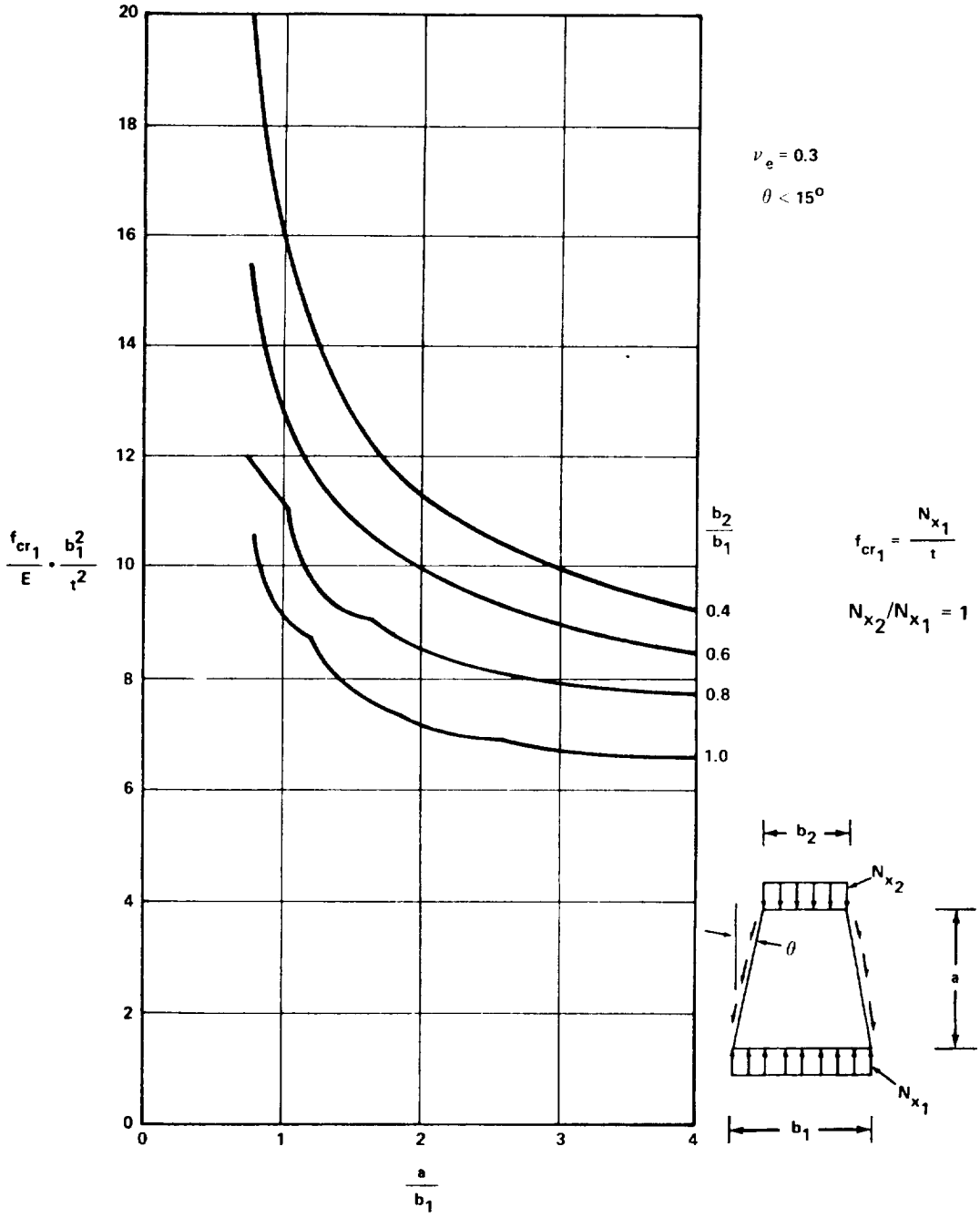

FIGURE C2-55. BUCKLING STRESS DIAGRAM (Sides and ends clamped. No stress normal to sides.)

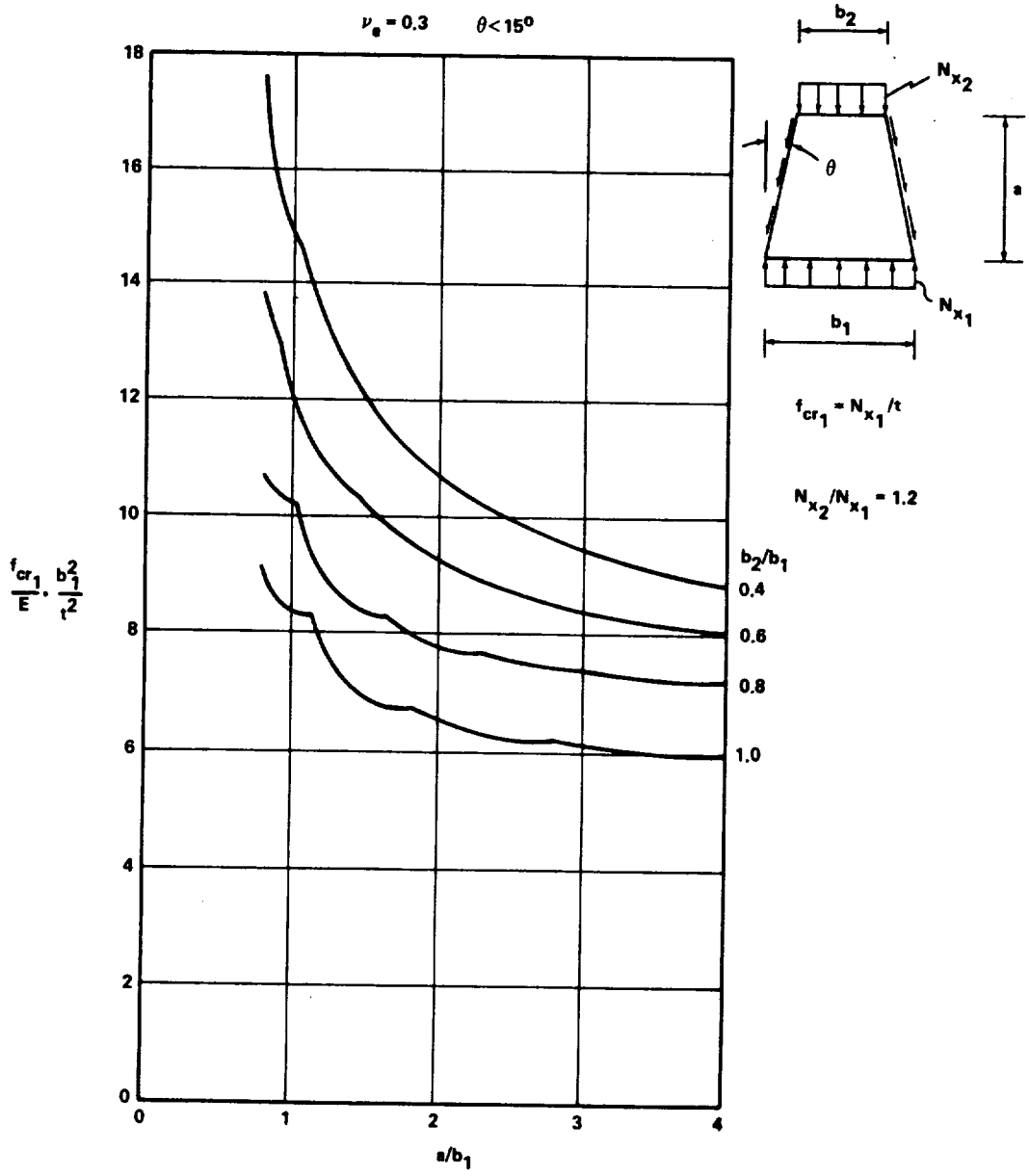

FIGURE C2-56. BUCKLING STRESS DIAGRAM (Sides and ends clamped. No stress normal to sides.)

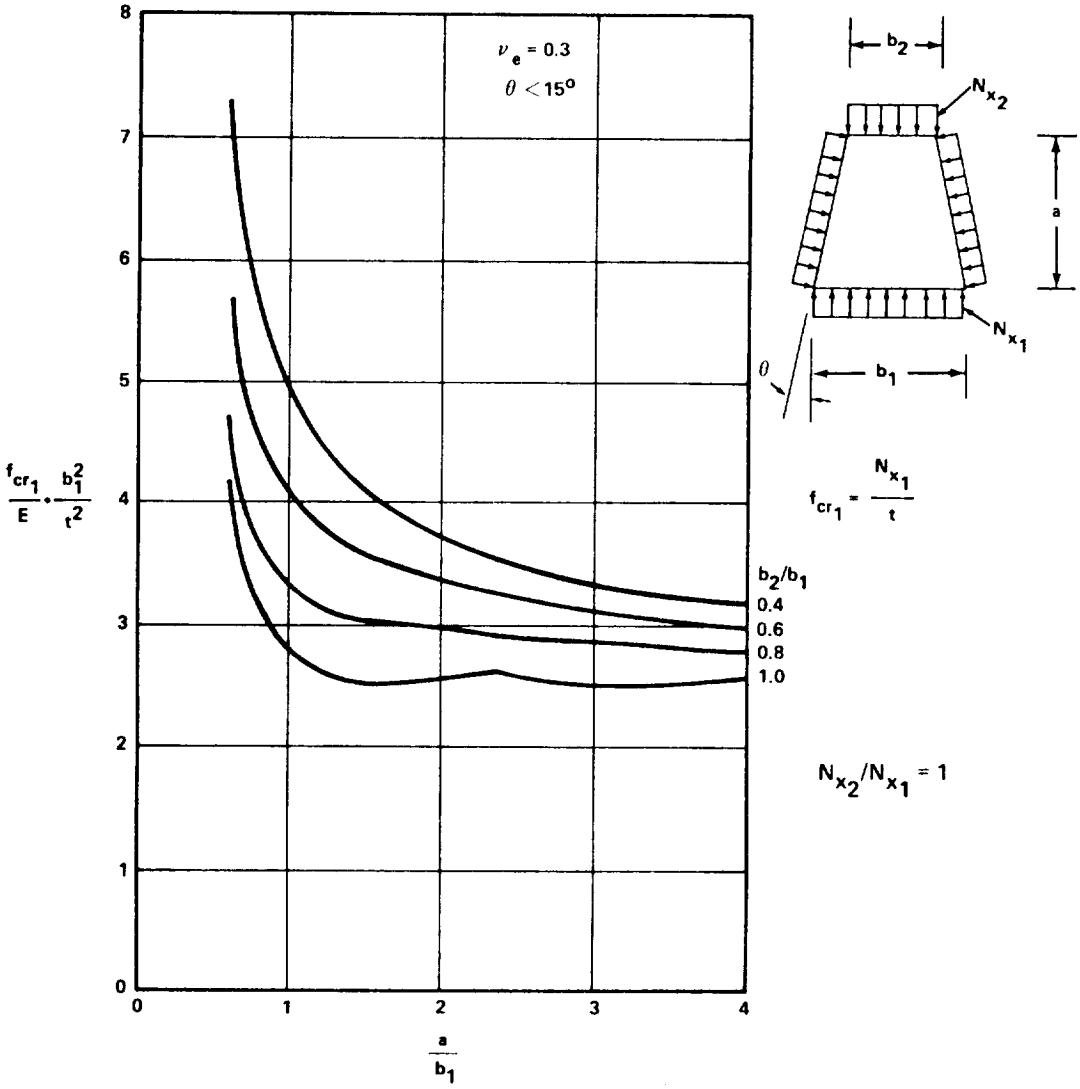

FIGURE C2-57. BUCKLING STRESS DIAGRAM (Sides and ends simply-supported. No displacement of the sides normal to the direction of taper.)

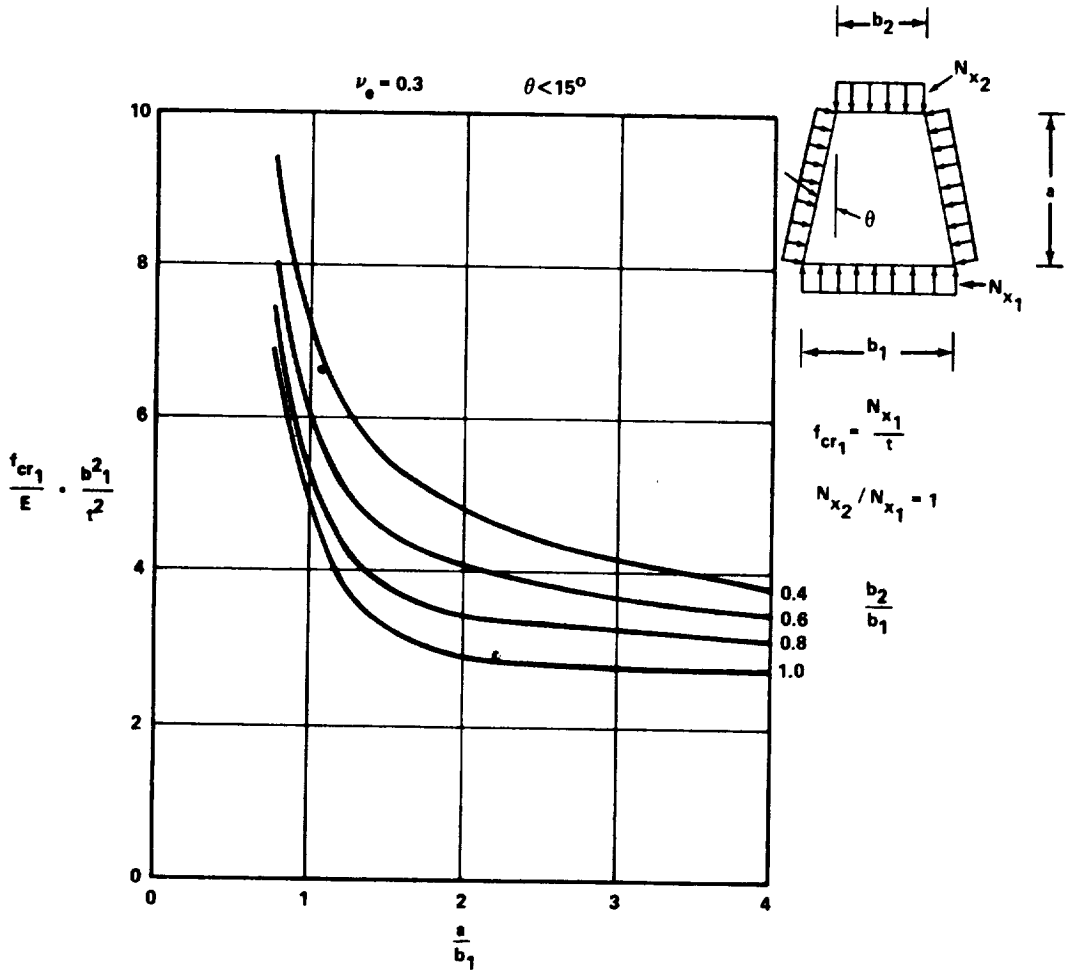

FIGURE C2-58. BUCKLING STRESS DIAGRAM (Sides simply-supported. Ends clamped. No displacement of the sides normal to the direction of taper.)

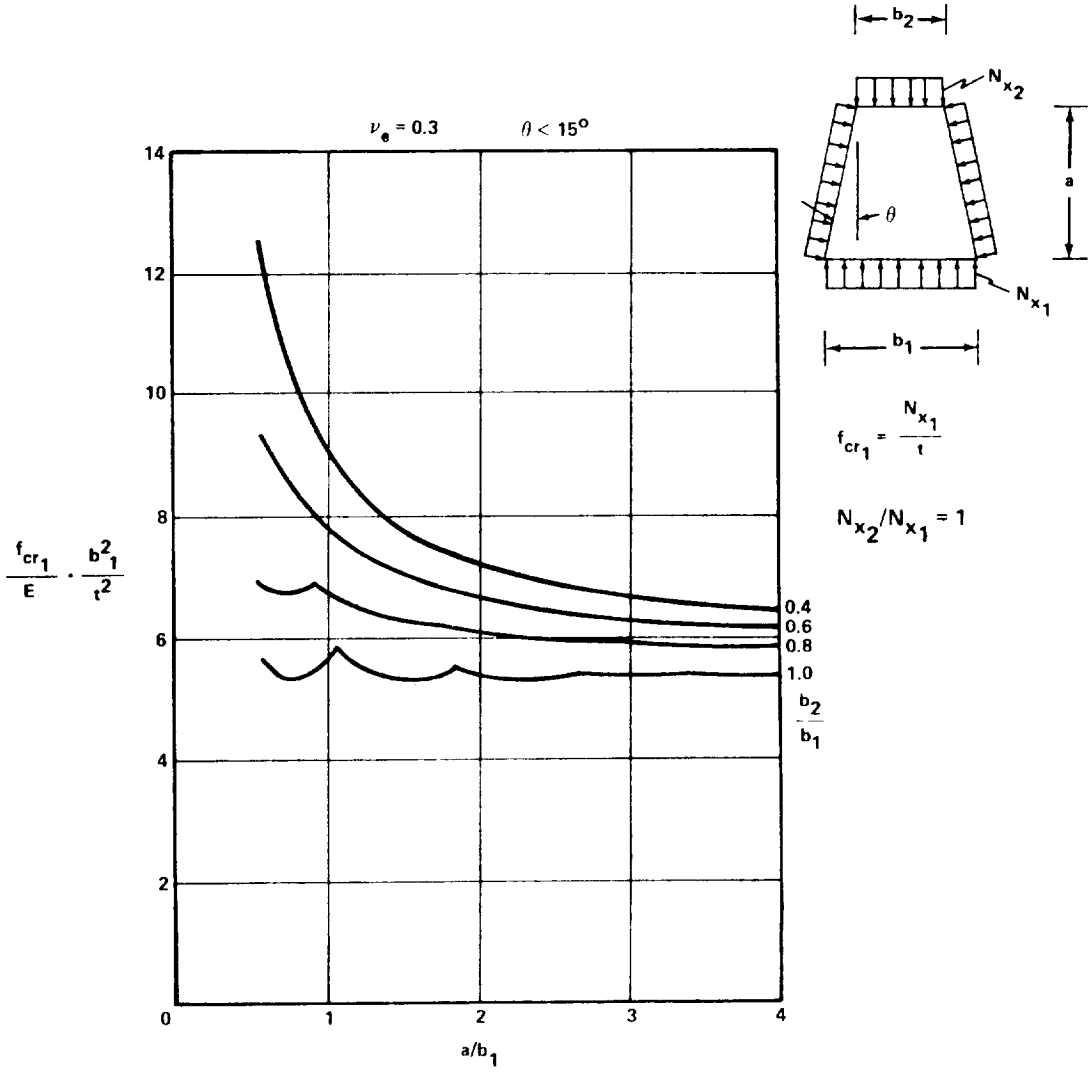

FIGURE C2-59. BUCKLING STRESS DIAGRAM (Sides clamped. Ends simply-supported. No displacement of the sides normal to the direction of taper.)

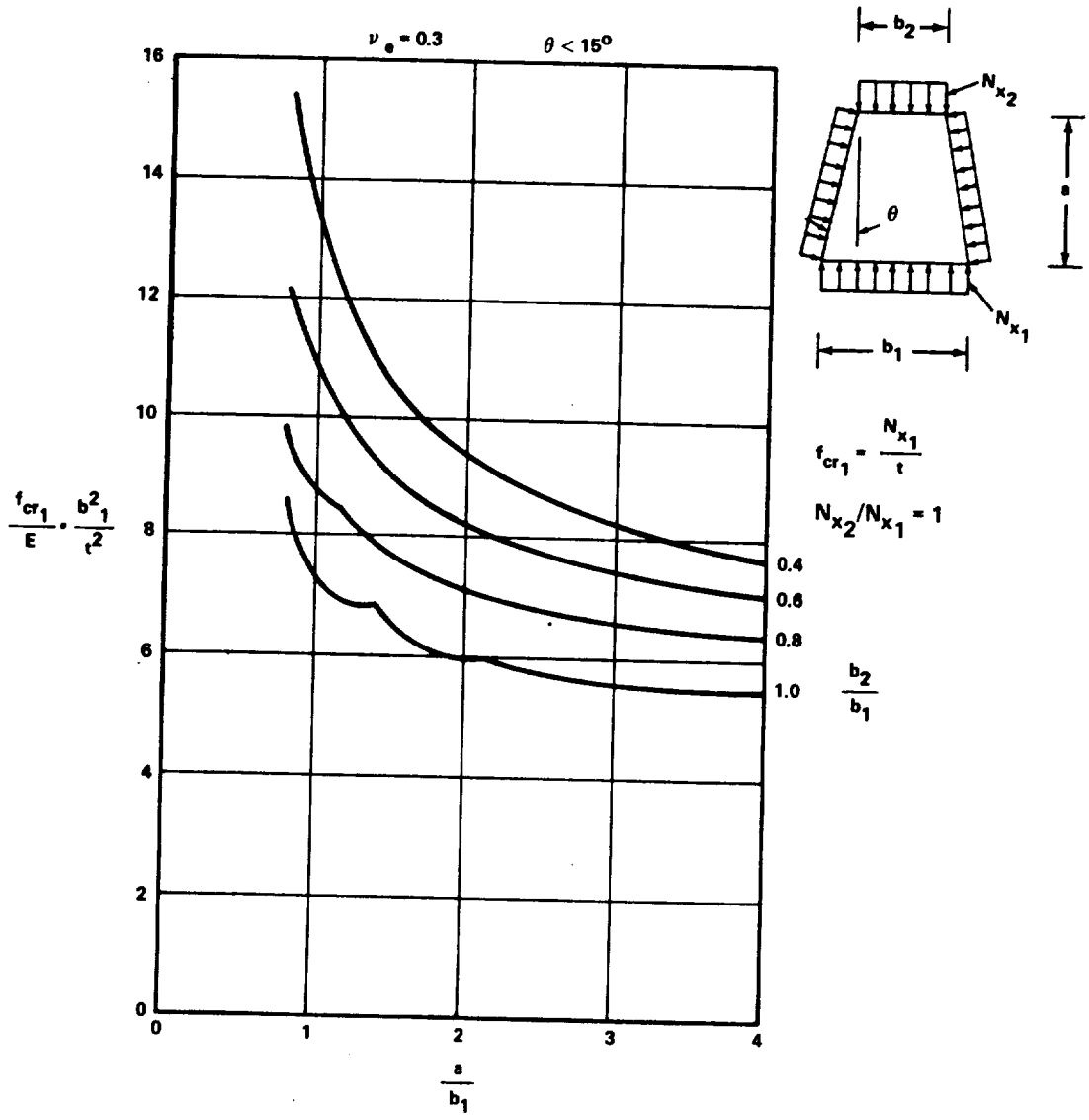

FIGURE C2-60. BUCKLING STRESS DIAGRAM (Sides and ends clamped. No displacement of the sides normal to the direction of taper.)

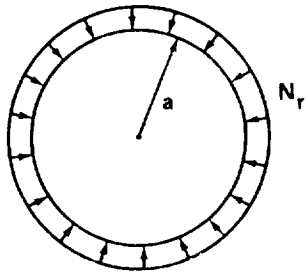

FIGURE C2-61. CIRCULAR PLATE SUBJECTED TO RADIAL LOAD

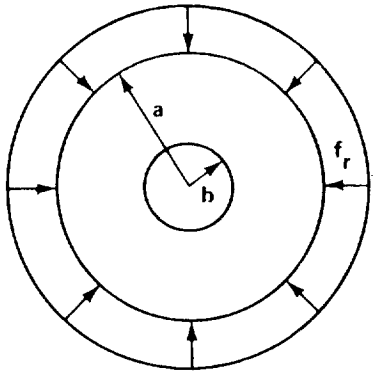

$$\frac{f_{r_{cr}}}{\eta} = k \frac{E}{12\,(1-\nu_e^2)} \frac{t^2}{a^2}$$

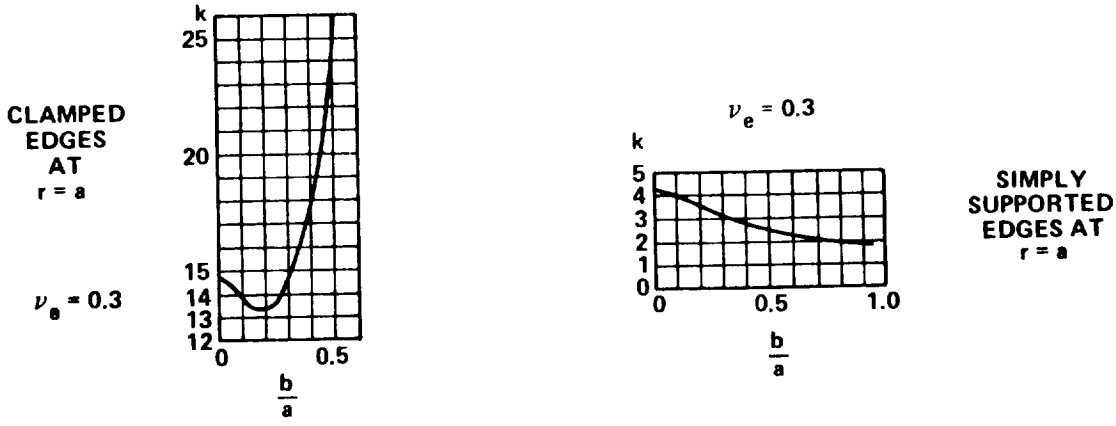

FIGURE C2-62. BUCKLING COEFFICIENTS FOR ANNULAR PLATE

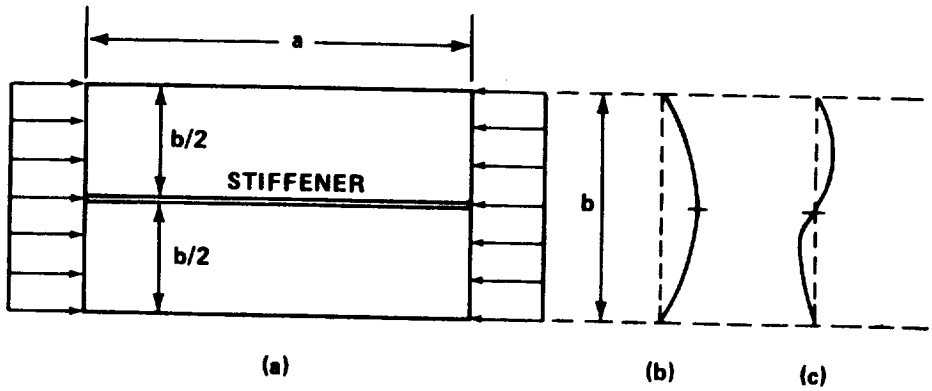

FIGURE C2-63. RECTANGULAR PLATE WITH CENTRAL LONGITUDINAL STIFFENER UNDER COMPRESSIVE LOAD

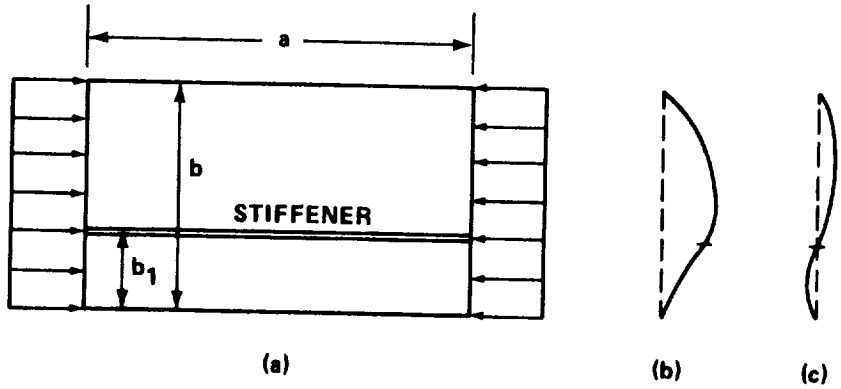

FIGURE C2-64. RECTANGULAR PLATE WITH ONE STIFFENER ECCENTRICALLY LOCATED UNDER COMPRESSION

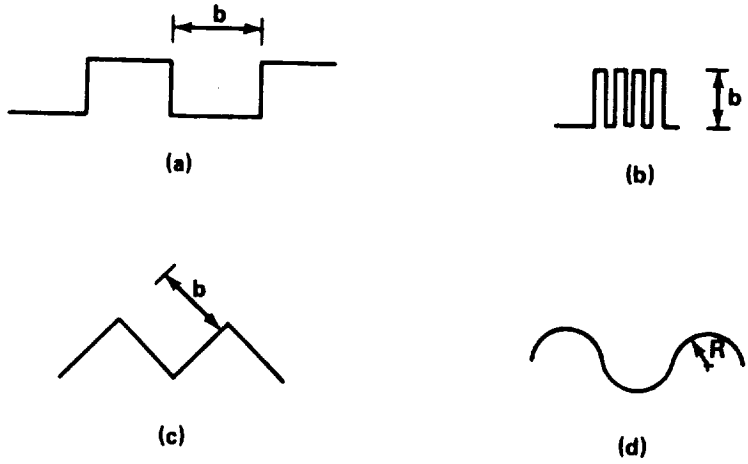

FIGURE C2-65. TYPICAL CORRUGATIONS

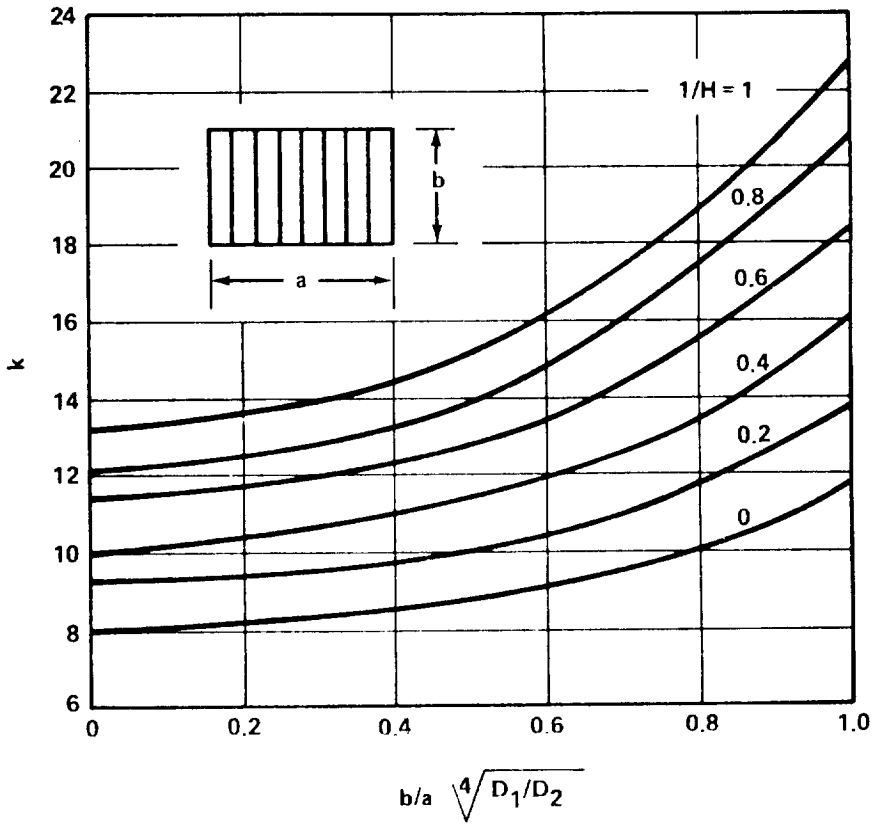

FIGURE C2-66. SHEAR BUCKLING COEFFICIENTS FOR FLAT SIMPLY SUPPORTED CORRUGATED PLATES WHEN H>1

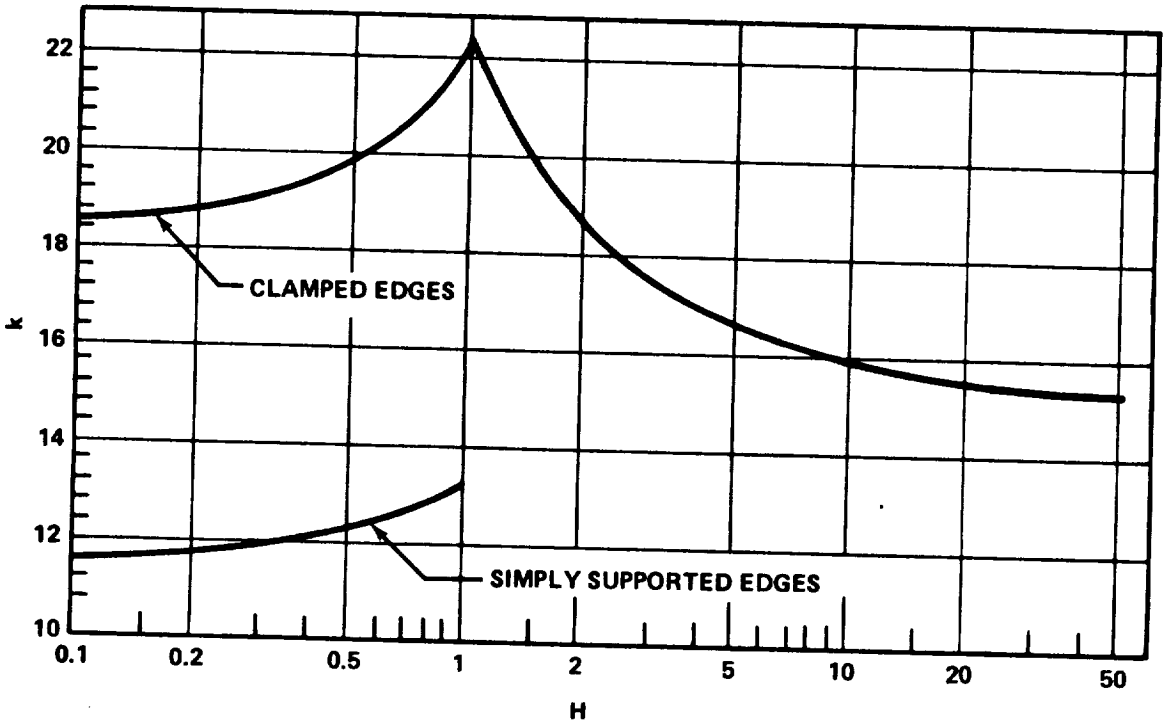

FIGURE C2-67. SHEAR BUCKLING COEFFICIENTS FOR FLAT INFINITELY LONG CORRUGATED PLATES: SIMPLY SUPPORTED EDGES, H<1 AND CLAMPED EDGES

$$F_{s_{cr}} = \frac{k_s \pi^2 E}{12 (1 - \nu_e^2)} (t/b)^2 \; ; \; Z_b = b^2/rt \; (1 - \nu_e^2)^{1/2}$$

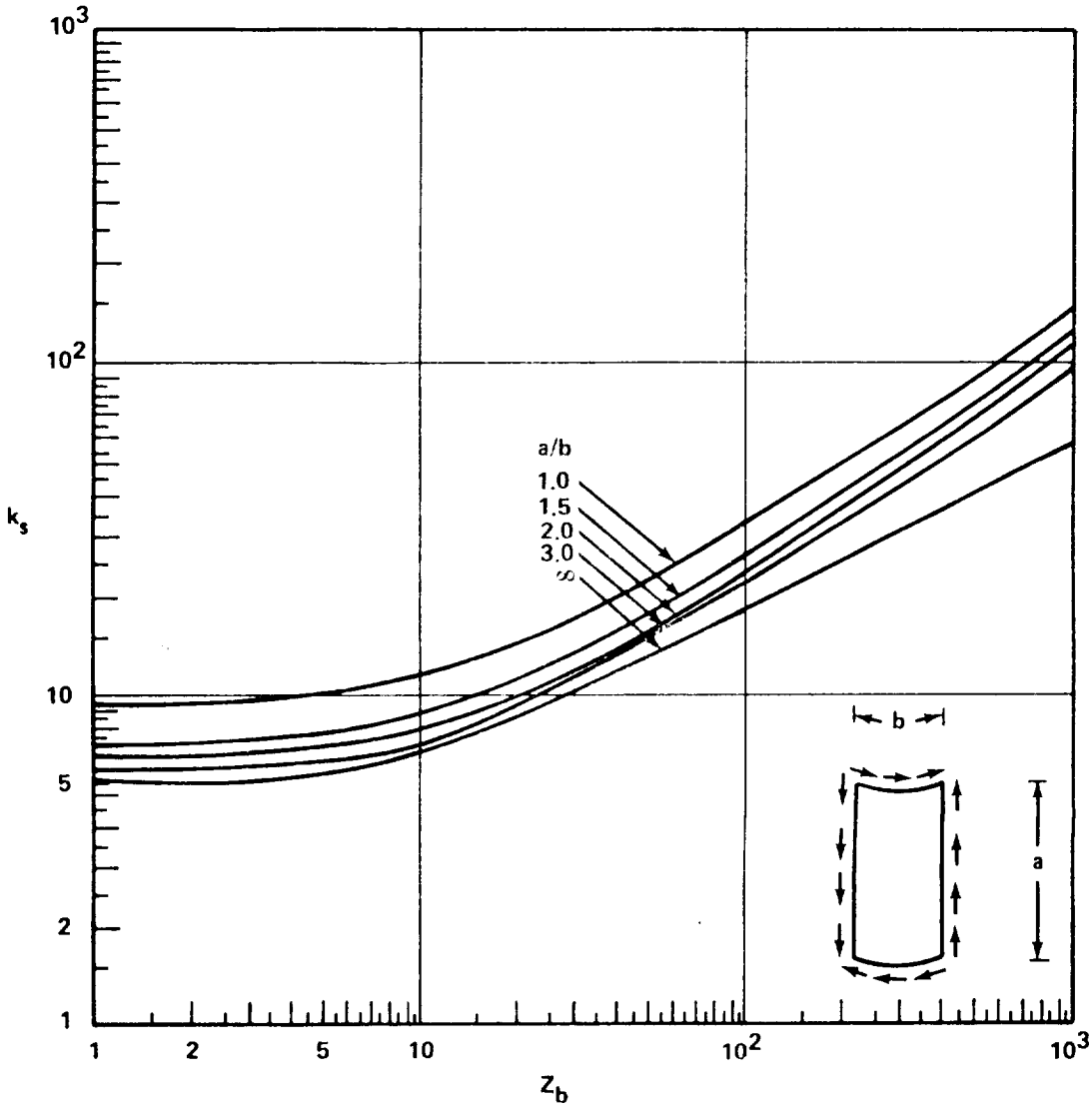

(a) LONG SIMPLY SUPPORTED PLATES

FIGURE C2-68. SHEAR BUCKLING COEFFICIENTS FOR VARIOUS CURVED PLATES

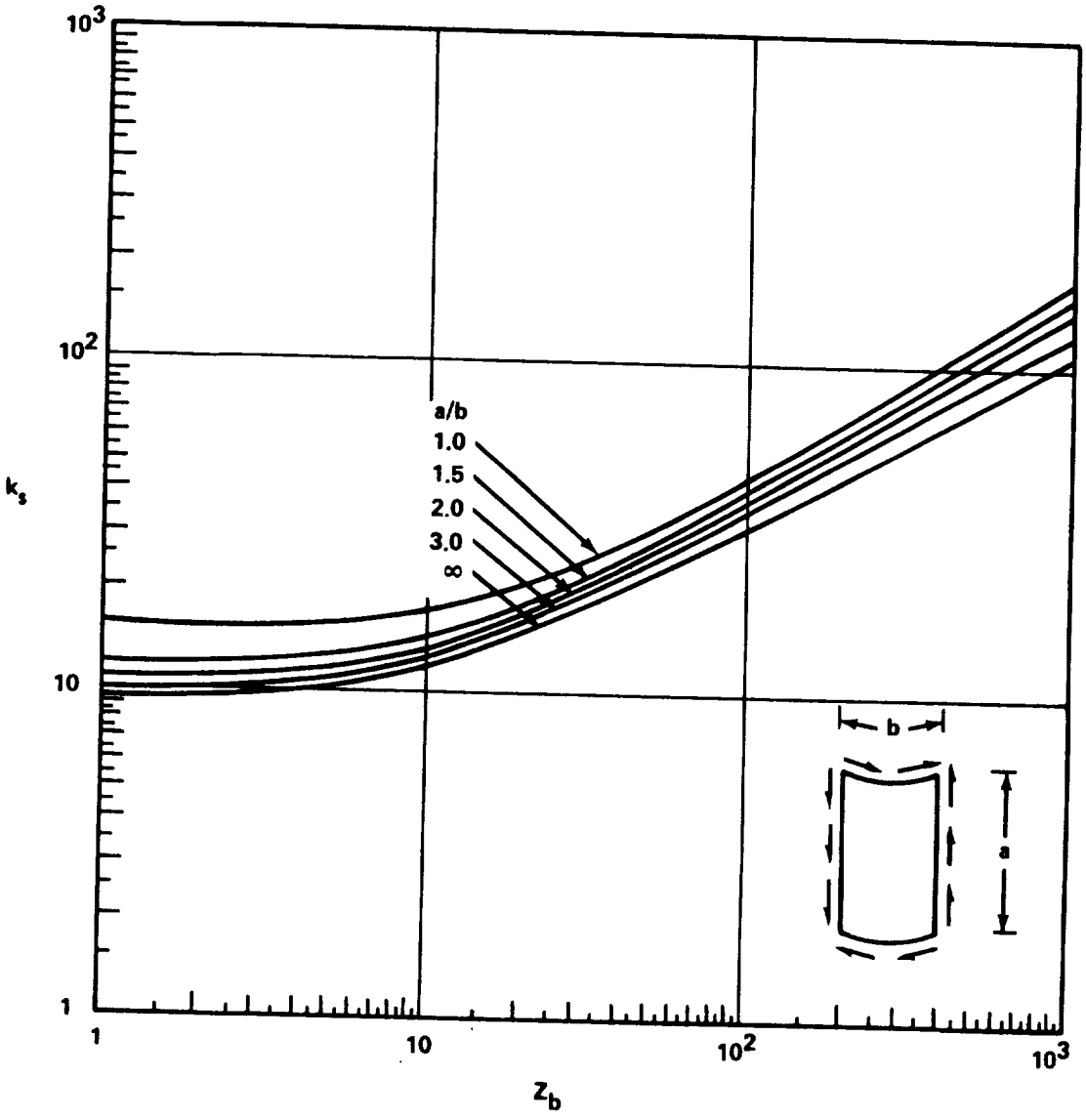

(b) LONG CLAMPED PLATES

FIGURE C2-68. (Continued)

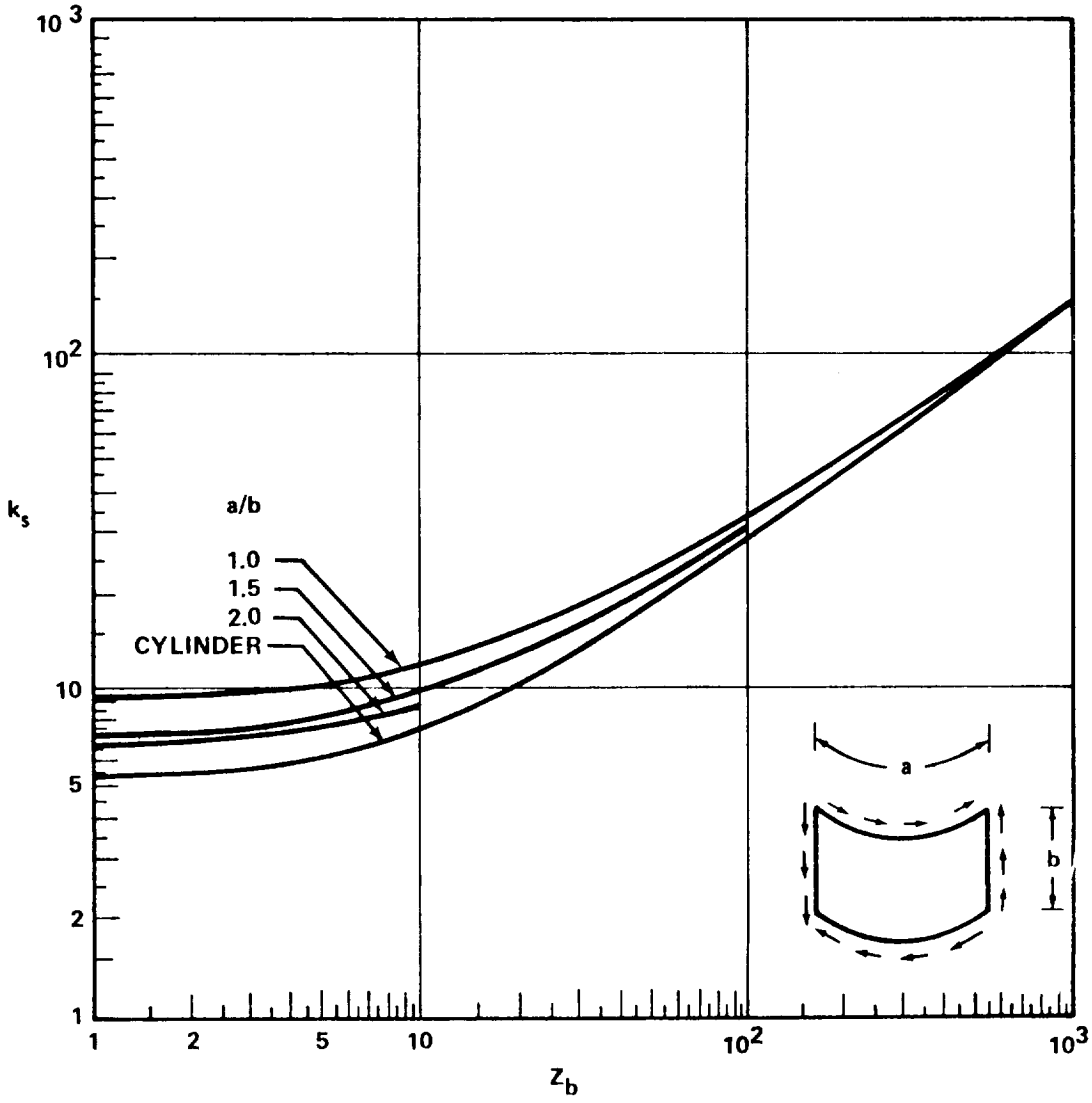

(c) WIDE, SIMPLY SUPPORTED PLATES

FIGURE C2-68. (Continued)

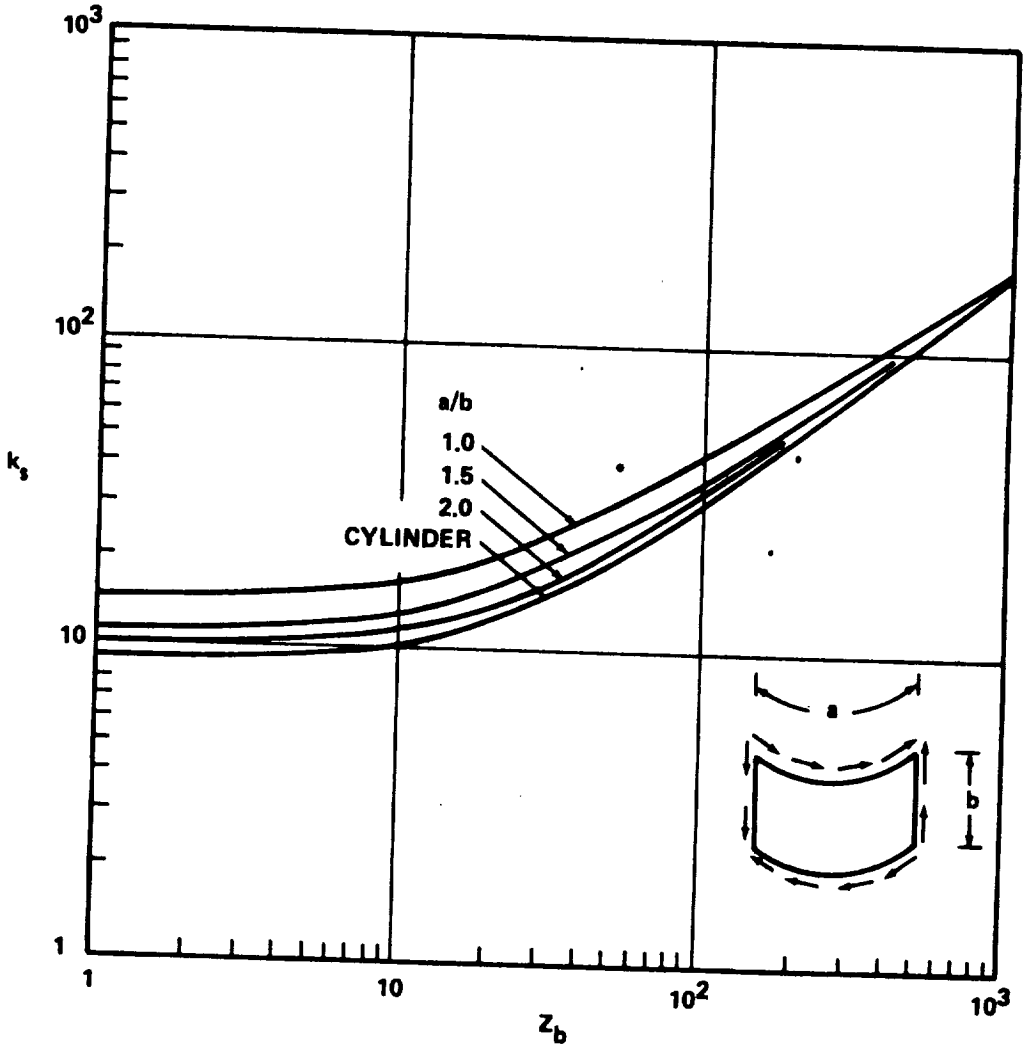

(d) WIDE CLAMPED PLATES

FIGURE C2-68. (Concluded)

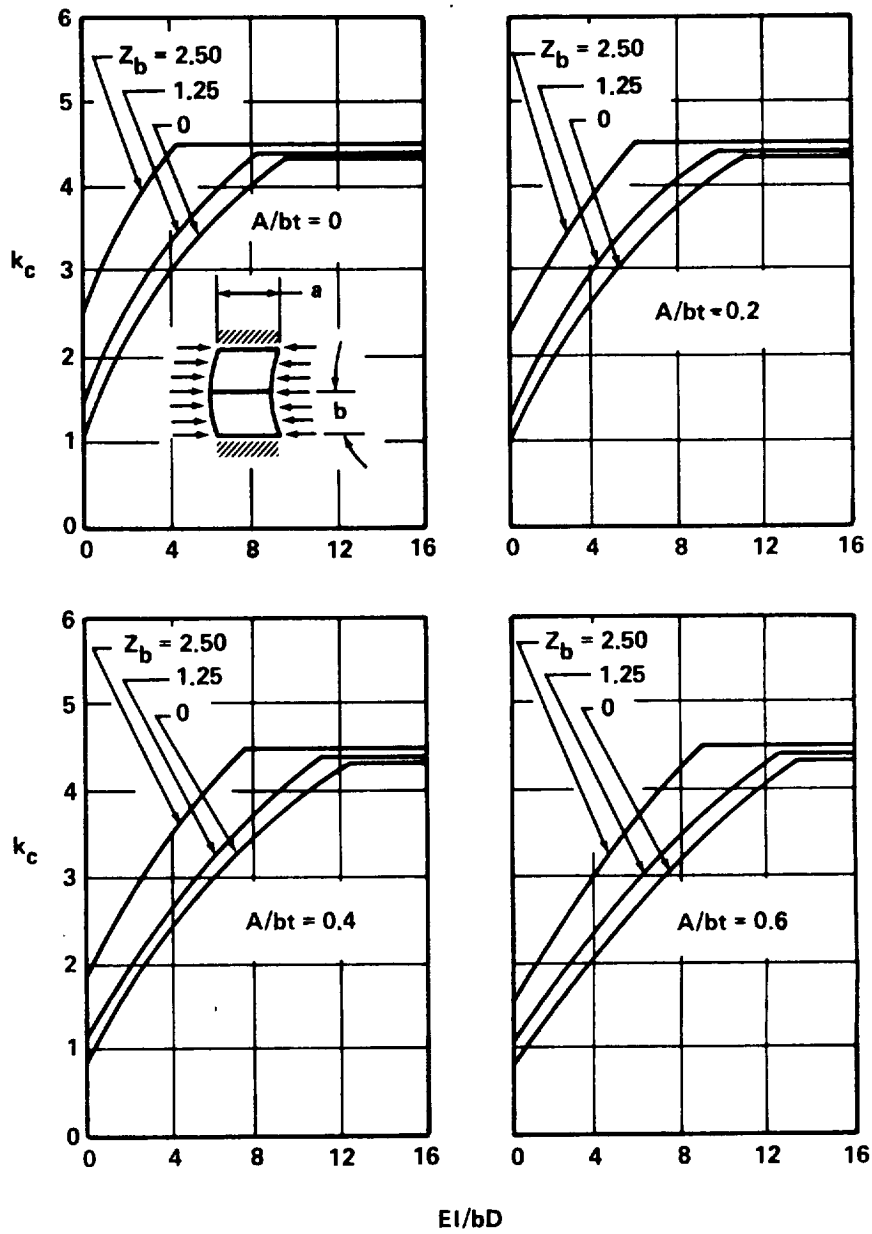

(a) a/b = 4/3

FIGURE C2-69. COMPRESSIVE-BUCKLING COEFFICIENTS FOR SIMPLY SUPPORTED CURVED PLATES WITH CENTER AXIAL STIFFENER

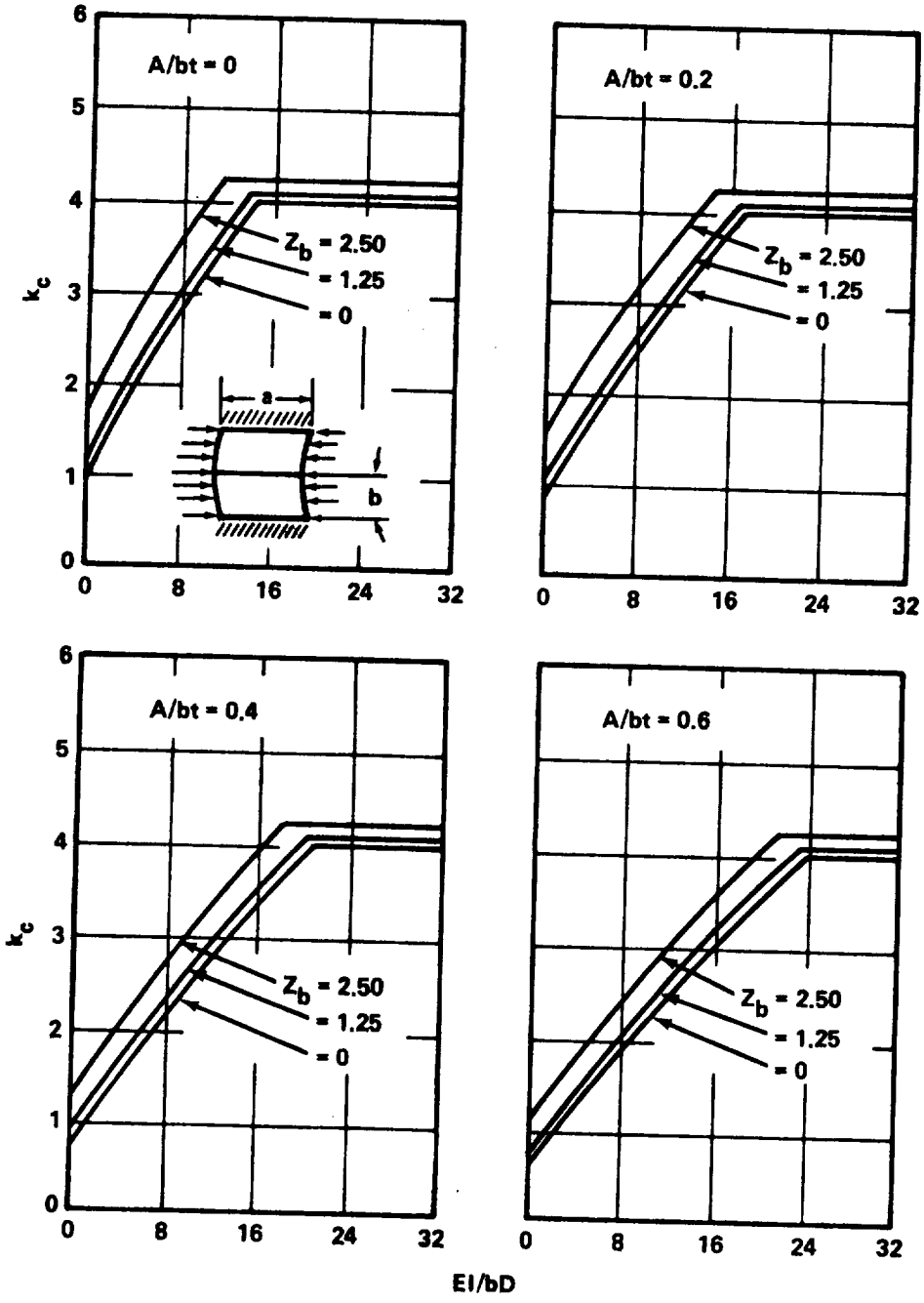

(b) a/b = 2

FIGURED C2-69. (Continued)

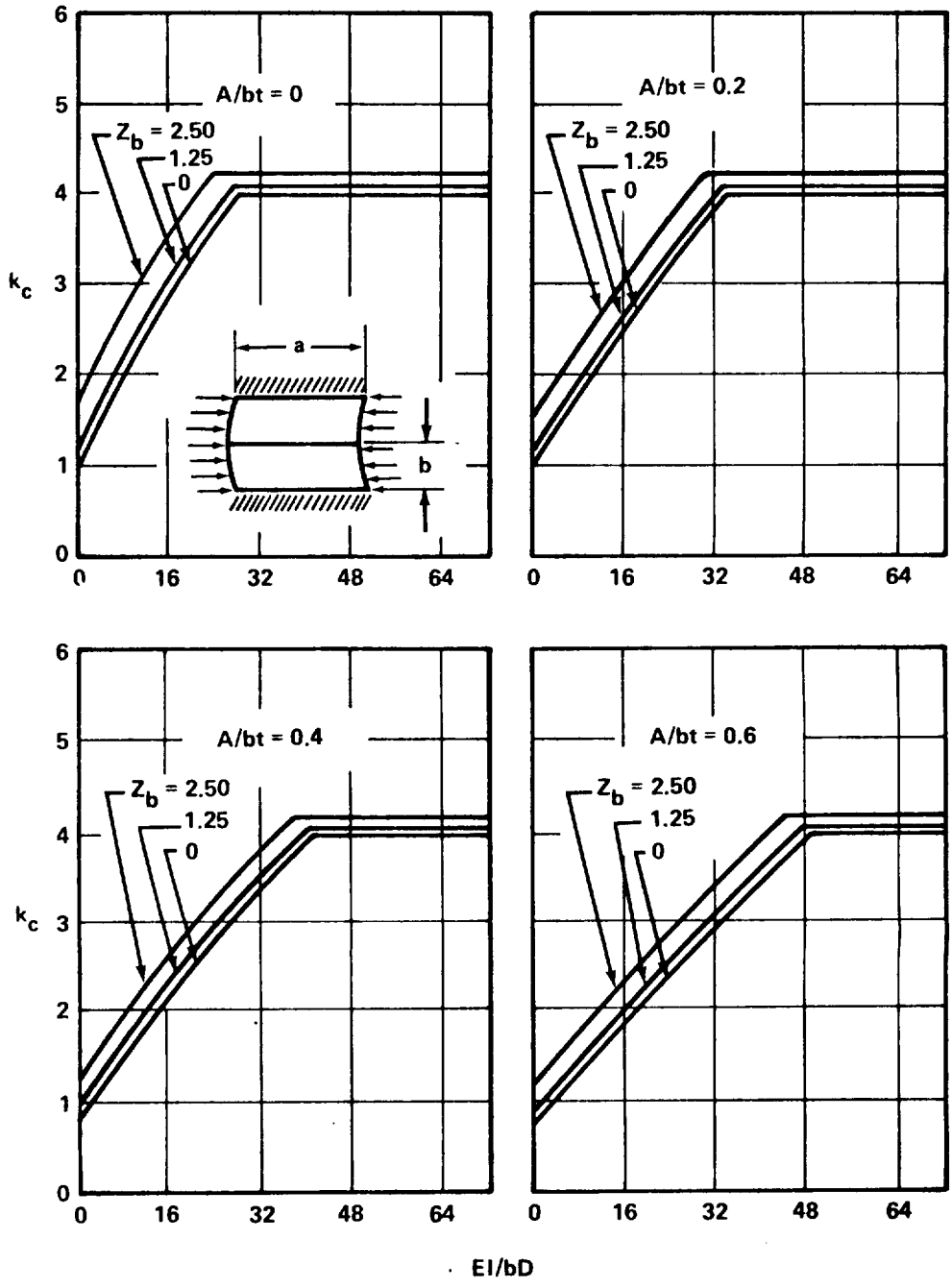

(c) a/b = 3

FIGURE C2-69. (Continued)

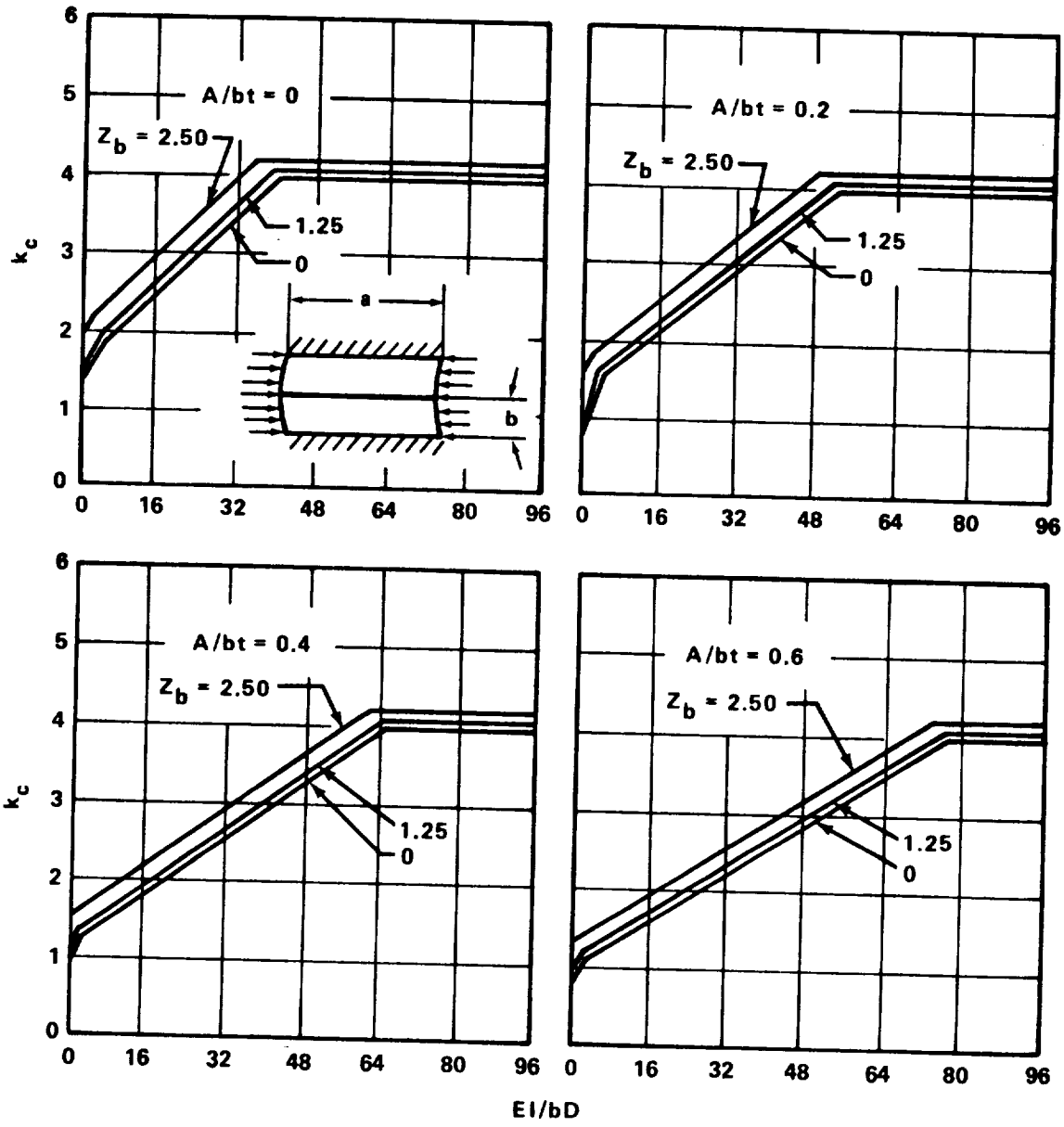

(d) a/b = 4

FIGURE C2-69. (Concluded)

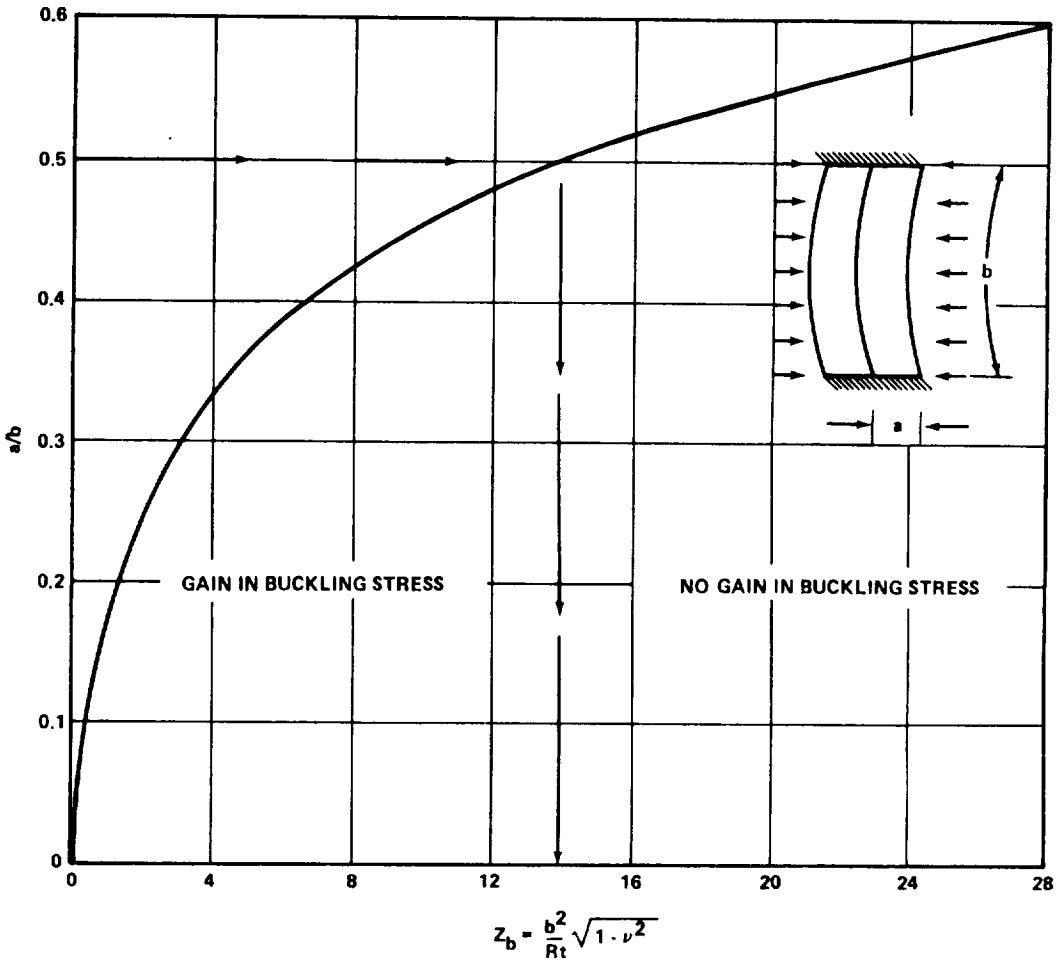

FIGURE C2-70. DEFINITION OF a/b VS Z_b RELATIONSHIP FOR GAIN IN BUCKLING STRESS OF AXIALLY COMPRESSED CURVED PLATES DUE TO ADDITION OF SINGLE CENTRAL CIRCUMFERENTIAL STIFFENER

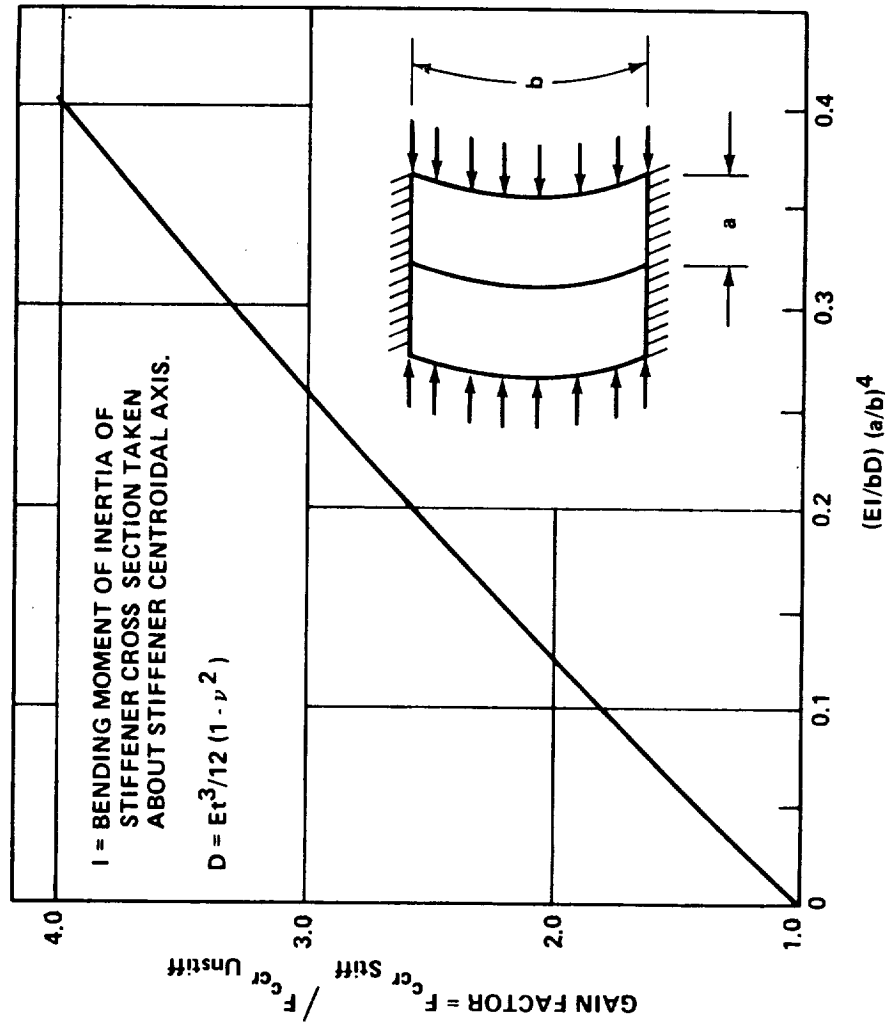

FIGURE C2-72. STIFFNESS REQUIREMENTS AS A FUNCTION OF GAIN FACTOR FOR SIMPLY SUPPORTED CURVED PLATES WITH A SINGLE CENTRAL CIRCUMFERENTIAL STIFFENER

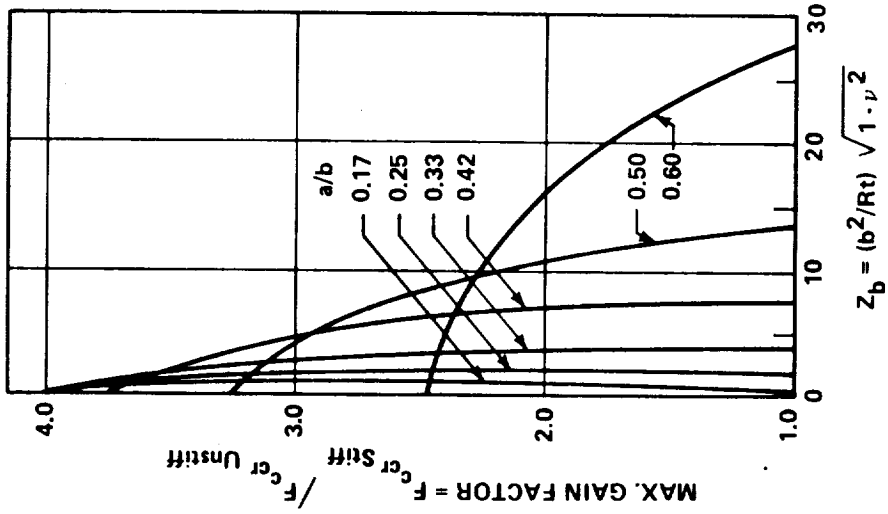

FIGURE C2-71. MAXIMUM GAIN FACTORS FOR SIMPLY SUPPORTED CURVED PLATES WITH A SINGLE, CENTRAL, CIRCUMFERENTIAL STIFFENER

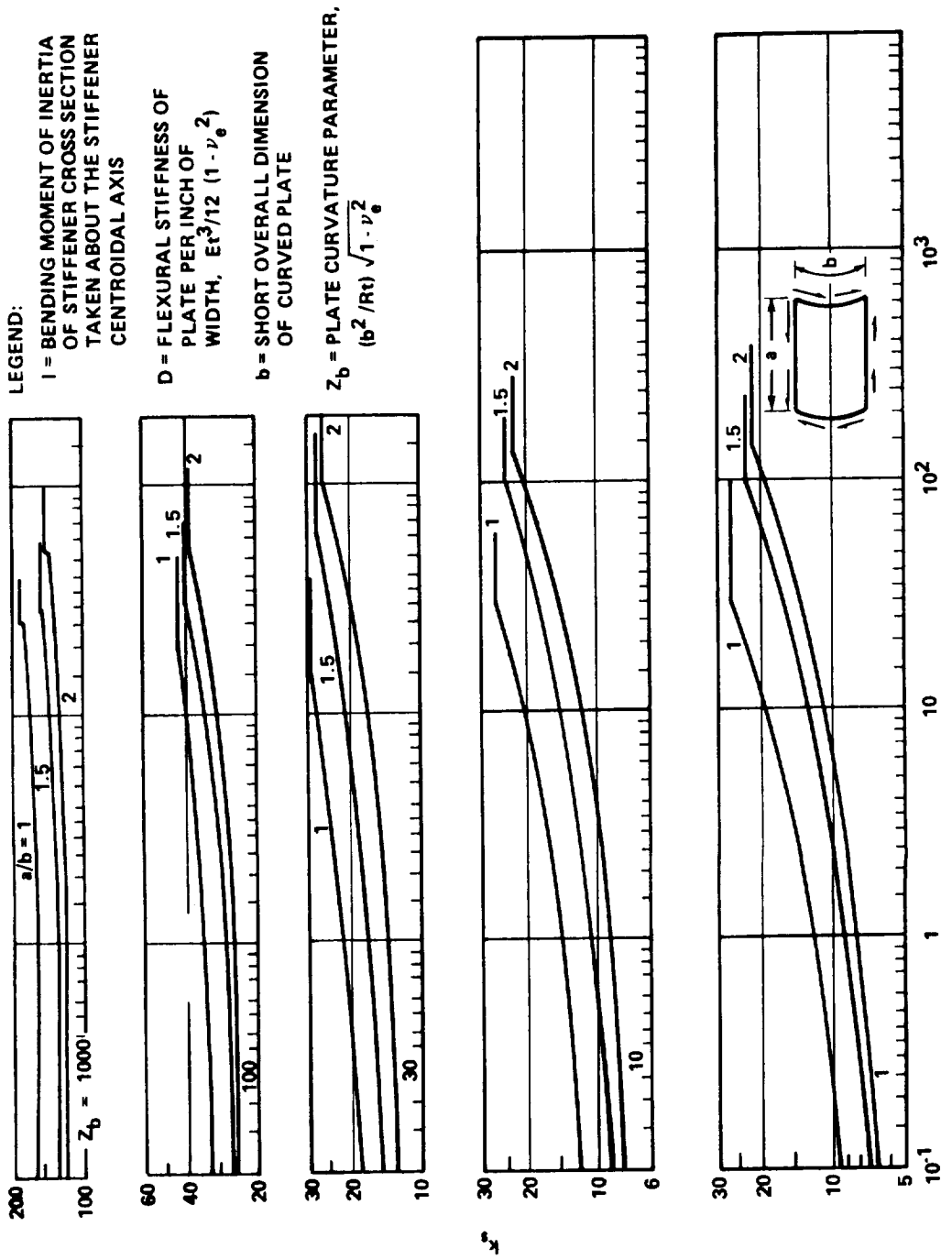

FIGURE C2-73a. SHEAR BUCKLING COEFFICIENTS FOR SIMPLY SUPPORTED CURVED PLATES WITH CENTER AXIAL STIFFENER, AXIAL LENGTH GREATER THAN CIRCUMFERENTIAL WIDTH

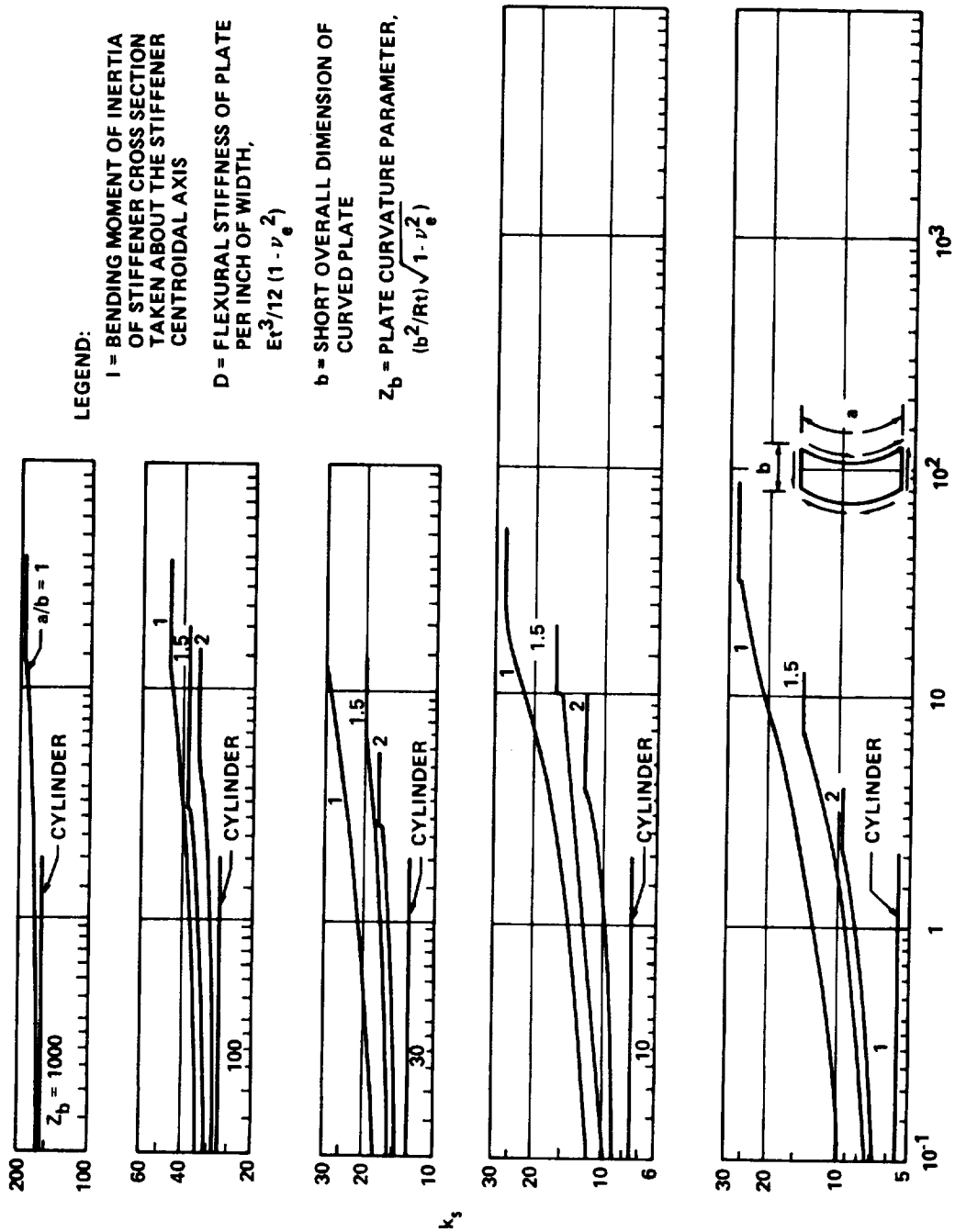

FIGURE C2-73b. SHEAR BUCKLING COEFFICIENTS FOR SIMPLY SUPPORTED CURVED PLATES WITH CENTER AXIAL STIFFENER, AXIAL LENGTH LESS THAN CIRCUMFERENTIAL WIDTH

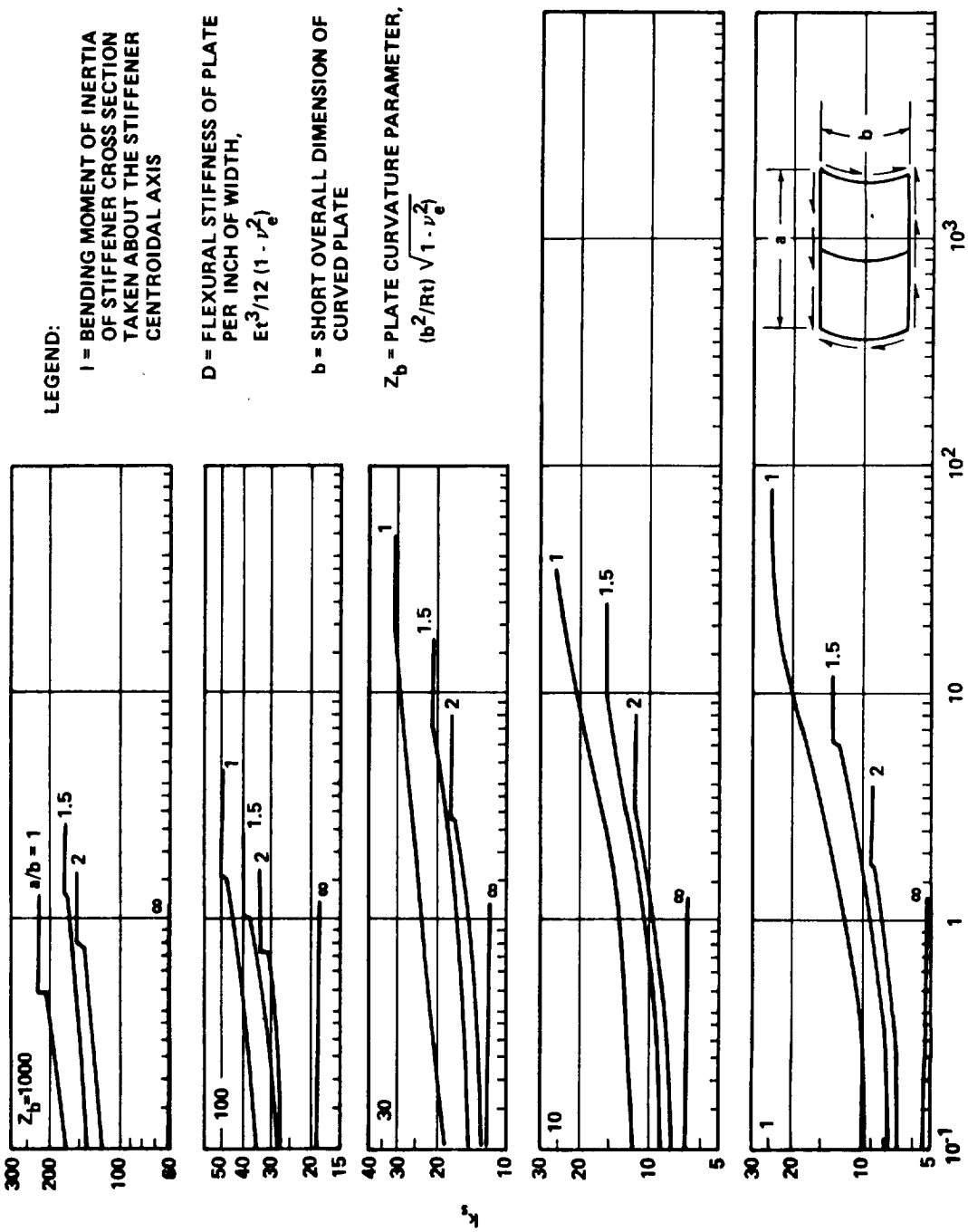

FIGURE C2-74a. SHEAR BUCKLING COEFFICIENTS FOR SIMPLY SUPPORTED CURVED PLATES WITH CENTER CIRCUMFERENTIAL STIFFENER, AXIAL LENGTH GREATER THAN CIRCUMFERENTIAL WIDTH

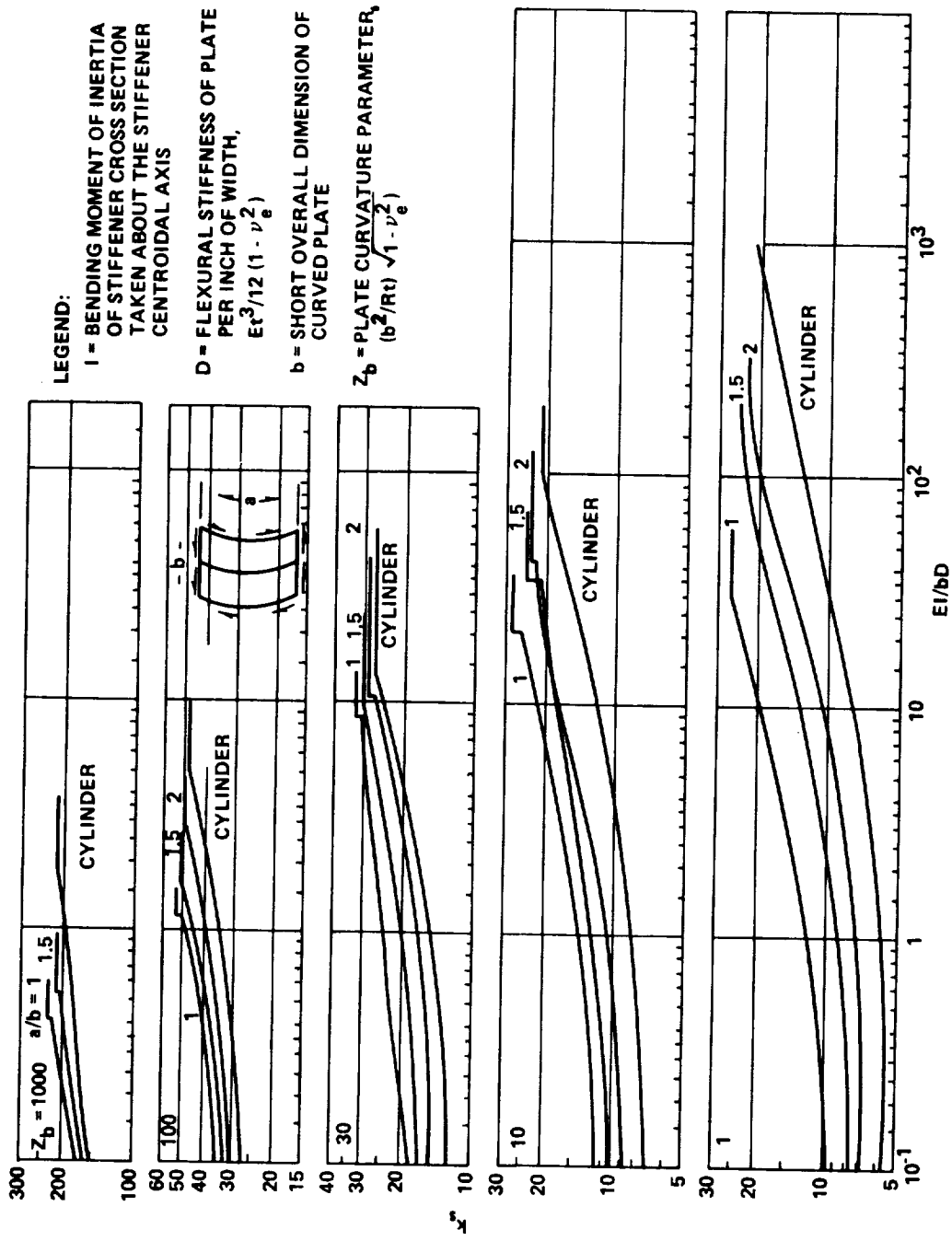

FIGURE C2-74b. SHEAR BUCKLING COEFFICIENTS FOR SIMPLY SUPPORTED CURVED PLATES WITH CENTER CIRCUMFERENTIAL STIFFENER, AXIAL LENGTH LESS THAN CIRCUMFERENTIAL WIDTH

REFERENCES

1. Bruhn, E. F.: Analysis and Design of Flight Vehicle Structures. Tri-State Offset Printing Company, Cincinnati, Ohio, 1965.

2. Timoshenko, S. P., and Gere, J. M.: Theory of Elastic Stability. McGraw-Hill Book Company, Inc., New York, 1961.

3. Cook, I. T., and Rockey, K. C.: Shear Buckling of Rectangular Plates with Mixed Boundary Conditions. Aeron. Quart., Nov. 1963.

4. Noel, R. G.: Elastic Stability of Simply Supported Flat Rectangular Plates Under Critical Combinations of Longitudinal Bending, Longitudinal Compression, and Lateral Compression. J. Aeron. Sci., vol. 19, no. 12, Dec. 1952.

5. Johnston, A. E., Jr., and Buckert, K. P.: Critical Combinations of Bending, Shear, and Transverse Compressive Stresses for Buckling of Infinitely Long Flat Plates. NACA TN 2536, Dec. 1951.

6. Batdorf, S. B., and Houbolt, J. C.: Critical Combinations of Shear and Transverse Direct Stress for an Infinitely Long Flat Plate with Edges Elastically Restrained Against Rotation. NACA Report 847, 1946.

7. Batdorf, S. B., and Stein, M.: Critical Combinations of Shear and Direct Stress for Simply Supported Rectangular Flat Plates. NACA TN 1223, Mar. 1947.

8. Johnson, J. H., Jr.: Critical Buckling Stresses of Simply Supported Flat Rectangular Plates Under Combined Longitudinal Compression, Transverse Compression, and Shear. J. Aeron. Sci., June 1954.

9. Bleich, F.: Buckling Strength of Metal Structures. McGraw-Hill Book Company, Inc., New York, 1952.

10. Pines, S., and Gerard, G.: Instability Analysis and Design of an Efficiently Tapered Plate Under Compressive Loading. J. Aeron. Sci., vol. 14, no. 10, Oct. 1947.

11. Libove, C. L., Ferdman, S., and Reusch, J. J.: Elastic Buckling of a Simply Supported Plate Under a Compressive Stress that Varies Linearly in the Direction of the Loading. NACA TN 1891, 1949.

REFERENCES (Continued)

12. Seide, P.: Compression Buckling of a Long Simply Supported Plate on an Elastic Foundation. J. Aeron. Sci., June 1958.

13. Wittrick, W. H.: Buckling of Oblique Plates with Clamped Edges Under Uniform Compression. Aeron. Quart., vol. 4, pt. II, Feb. 1953.

14. Guest, J.: The Compressive Buckling of a Parallelogram Plate Simply Supported Along all Four Edges. Rep. SM 199, Aero. Res. Labs., Dept. Supply (Melbourne), Sept. 1952.

15. Guest J., and Silberstein, J. P. O.: A Note on the Buckling of Simply Supported Parallelogram Plates, Structures and Materials. Note 204, Aero. Res. Labs., Dept. Supply (Melbourne), May 1953.

16. Anderson, R. A.: Charts Giving Critical Compressive Stress of Continuous Flat Sheet Divided into Parallelogram-Shaped Panels. NACA TN 2392, July 1951.

17. Durvasula, S.: Buckling of Clamped Skew Plates. AIAA Journal, vol. 8, no. 1, Jan. 1970.

18. Wittrick, W. H.: Buckling of Oblique Plates with Clamped Edges Under Uniform Shear. Aeron. Quart., vol. V, May 1954.

19. Cox, H. L., and Klein, B.: The Buckling of Isosceles Triangular Plates. J. Aeron. Sci., vol. 22, no. 5, May 1955.

20. Wittrick, W. H.: Buckling of a Right-Angled Isosceles Triangular Plate in Combined Compression and Shear (Perpendicular Edges Clamped, Hypotenuse Simply Supported). Rep. SM 211, Aero. Res. Labs., Dept. Supply (Melbourne), June 1953.

21. Wittrick, W. H.: Buckling of a Right-Angled Isosceles Triangular Plate in Combined Compression and Shear (Perpendicular Edges Simply Supported, Hypotenuse Clamped). Rep. SM 220, Aero. Res. Labs., Dept. Supply (Melbourne), Nov. 1953.

22. Wittrick, W. H.: Buckling of a Simply Supported Triangular Plate in Combined Compression and Shear. Rep. SM 197, Aero. Res. Labs., Dept. Supply (Melbourne), July 1952.

*REFERENCES (Concluded)

23. Wittrick, W. H.: Symmetrical Buckling of Right-Angled Isosceles Triangular Plates. Aeron. Quart., vol. V, Aug. 1954.

24. Klein, B.: Buckling of Simply Supported Plates Tapered in Planform. J. Appl. Mech., June 1956.

25. Pope, G. G.: The Buckling of Plates Tapered in Planform. Royal Aircraft Establishment, Report No. Structures 274, Apr. 1962.

26. Tang, S.: Elastic Stability of a Circular Plate Under Unidirectional Compression. J. Spacecraft, vol. 6, no. 1, Jan. 1969.

27. MIL-HDBK-23, Structural Sandwich Composites, July 1968.

28. Structural Design Guide for Advanced Composite Application. Prepared by the Los Angeles Division of the North American Rockwell Corporation for Wright-Patterson Air Force Base, Ohio, Aug. 1969.

29. Schildcrout, M., and Stein, M.: Critical Axial-Compressive Stress of a Curved Rectangular Panel With a Central Longitudinal Stiffener. NACA TN 1879, 1949.

30. Batdorf, S. B., and Schildcrout, M.: Critical Axial-Compressive Stress of a Curved Rectangular Panel With a Central Chordwise Stiffener. NACA TN 1661, 1948.

SECTION C3

STABILITY OF SHELLS

TABLE OF CONTENTS

TABLE OF CONTENTS (Continued)

TABLE OF CONTENTS (Continued)

TABLE OF CONTENTS (Continued)

TABLE OF CONTENTS (Concluded)

DEFINITION OF SYMBOLS

Symbol	Definition
A_s , A_r	Stiffener area, and ring area, respectively
A, B	Lengths of semiaxes of ellipsoidal shells
a	Radius of curvature of circular toroidal-shell cross section
B_1	Extensional stiffness of isotropic sandwich wall
b	Stiffener spacing; also, distance from center of circular cross section of circular toroidal shell cross section to axis of revolution
b_e	Effective width of skin between stiffeners
C_{ij}	Coefficients of constitutive equations
$\overline{C}_x$, $\overline{C}_y$, $\overline{C}_{xy}$, $\overline{K}_{xy}$	Coupling constants for orthotropic cylinders
c	Coefficient of fixity in Euler column formula
D	Wall flexural stiffness per unit width, $\frac{Et^3}{12(1-\mu^2)}$
D_q	Transverse shear-stiffness parameter for isotropic sandwich wall, $G_{xz} \frac{h^2}{h - \frac{1}{2}(t_1 + t_2)}$
$\overline{D}_x$, $\overline{D}_y$	Bending stiffness per unit width of wall in x- and y-directions, respectively; $\overline{D}_x = \overline{D}_y = D$ for isotropic cylinder

DEFINITION OF SYMBOLS (Continued)

Symbol	Definition
$\overline{D}_{xy}$	Modified twisting stiffness of wall; $\overline{D}_{xy} = 2D$ for isotropic cylinder
D_f	Flexural stiffness of isotropic sandwich wall, $\frac{E_s th^2}{2(1-\mu^2)}$
d	Ring spacing
E	Young's modulus
E_R	Reduced modulus
E_S , E_f	Young's moduli: face sheet; sandwich, respectively
E_c	Young's modulus of elastic core
E_r , E_s	Young's moduli: rings; stiffeners, respectively
E_s , E_θ	Young's moduli of orthotropic material in the s- and θ-directions, respectively
E_{sec}	Secant modulus for uniaxial stress-strain curve
E_{tan}	Tangent modulus for uniaxial stress-strain curve
E_x , E_y	Young's modulus of orthotropic material in x- and y-directions, respectively
E_z	Young's modulus of sandwich core in direction perpendicular to face sheet of sandwich
E_1 , E_2	Young's moduli of the face sheets for isotropic sandwich shell

DEFINITION OF SYMBOLS (Continued)

Symbol	Definition
$\overline{E}$	Equivalent Young's modulus for isotropic sandwich shell
$\overline{E}_s$, $\overline{E}_\theta$	Equivalent Young's moduli of orthotropic material in the s- and θ-directions, respectively
$\overline{E}_x$, $\overline{E}_y$, $\overline{E}_{xy}$	Extensional stiffness of wall in x- and y-directions, respectively; $\overline{E}_x = \overline{E}_y = \frac{Et}{1-\mu^2}$, $\overline{E}_{xy} = \frac{\mu Et}{1-\mu^2}$ for isotropic cylinder
e_r	Distance of the centroid of the ring-shell combination from the middle surface
f	Ratio of minimum to maximum principal compressive stress in face sheets
G	Shear modulus
G_s , G_r	Shear moduli: stiffeners; rings, respectively
G_{sz}	Shear modulus of core of sandwich wall in s-z plane
G_{xy}	Inplane shear modulus of orthotropic material
G_{xz} , G_{yz}	Shear moduli of core of sandwich wall in x-z and y-z planes, respectively
$\overline{G}$	Equivalent shear modulus
$\overline{G}_{xy}$	Shear stiffness of orthotropic or sandwich wall in x-y plane; $\overline{G}_{xy} = Gt$ for isotropic cylinder

DEFINITION OF SYMBOLS (Continued)

Symbol	Definition
h	Depth of sandwich wall measured between centroids of two face sheets
$\bar{I}$	Moment of inertia per unit width of corrugated cylinder
I_r , I_s	Moments of inertia of rings and stiffeners, respectively, about their centroid
J_r , J_s	Beam torsion constants of rings and stiffeners, respectively
k_p	Buckling coefficient of cylinder subject to hydrostatic pressure, $pr\,\ell^2/\pi^2 D$
k_{pc}	Buckling coefficient of cylinder with an elastic core subject to lateral pressure, pr^3/D
k_x	Buckling coefficient of cylinder subject to axial compression, $N_x\ell^2/\pi^2 D$ or $N_x\ell^2/\pi^2 D_1$
k_{xy}	Buckling coefficient of cylinder subjected to torsion, $N_{xy}\ell^2/\pi^2 D$ or $N_{xy}\ell^2/\pi^2 D_1$
k_y	Buckling coefficient of cylinder subject to lateral pressure, $N_y\ell^2/\pi^2 D$ or $N_y\ell^2/\pi^2 D_1$
L	Slant length of cone
L_o	Ring spacing measured along cone generator
ℓ	Length of cylinder, axial length of cone, or length of toroidal-shell segment

DEFINITION OF SYMBOLS (Continued)

Symbol	Definition
M	Bending moment on cylinder or cone
M_{cr}	Critical bending moment on cone or cylinder
M_{press}	Bending moment at collapse of a pressurized cylinder or cone
$M_{p=0}$	Bending moment at collapse of a nonpressurized cylinder
M_t	Twisting moment on cylinder
M_1 , M_2 , M_{12}	Moment resultants per unit of middle surface length
m	Number of buckle half-waves in the axial direction
N	Axial tension force per unit circumference applied to a toroidal segment
N_o	$\frac{2\gamma E}{\sqrt{1-\mu^2}} \frac{h}{r} \sqrt{t_1 t_2}$
N_x	Axial load per unit width of circumference for cylinder subjected to axial compression
N_{xy}	Shear load per unit width of circumference for cylinder subjected to torsion
N_y	Circumferential load per unit width of circumference for cylinder subjected to lateral pressure
N_1 , N_2 , N_{12}	Force resultants per unit of middle surface length
n	Number of buckle waves in the circumferential direction

DEFINITION OF SYMBOLS (Continued)

Symbol	Definition
P	Axial load on cylinder or cone; concentrated load at apex of spherical cap
P_{cr}	Critical axial load on cone; critical concentrated load at apex of spherical cap
$P_{p=0}$	Axial load on nonpressurized cylinder at buckling
P_{press}	Axial load on pressurized cylinder at buckling
p	Applied uniform internal or external hydrostatic pressure
p_{cl}	Classical uniform buckling pressure for a complete spherical shell
p_{cr}	Critical hydrostatic (uniform) pressure
R	Shear flexibility coefficient, $\frac{\pi^2 D}{\ell^2 D_q}$
R_A	Effective radius of a thin-walled oblate spheroid, $\frac{B}{A}$
R_b	Ratio of bending moment on cylinder or cone subjected to more than one type of loading to the allowable bending moment for the cylinder or cone when subjected only to bending
R_c	Ratio of axial load in cylinder or cone subjected to more than one type of loading to the allowable axial load for the cylinder or cone when subjected only to axial compression

DEFINITION OF SYMBOLS (Continued)

Symbol	Definition
R_m	Maximum radius of torispherical shell
R_p	Ratio of external pressure on cylinder or cone subjected to more than one type of loading to the allowable external pressure for the cylinder or cone when subjected only to external pressure
R_s	Radius of spherical shell
R_t	Ratio of torsional moment on cylinder or cone subjected to more than one type of loading to the allowable torsional moment for the cylinder or cone when subjected only to torsion
R_{tr}	Toroidal radius of torispherical shell
r	Radius of cylinder, equivalent cylindrical shell or equator of toroidal shell segment
r_1	Radius of small end of the cone
r_2	Radius of large end of the cone
S	Cell size of honeycomb core
s	Distance along cone generator measured from vertex of cone
s_1	Distance along cone generator measured from vertex of cone to small end of cone
T	Torsional moment on cone

DEFINITION OF SYMBOLS (Continued)

Symbol	Definition
T_{cr}	Critical torsional moment on cone
t	Skin thickness of isotropic cylinder or cone; thickness of corrugated cylinder
$\bar{t}$	Effective thickness of corrugated cylinder; area per unit width of circumference; effective skin thickness of isotropic sandwich cone
t_f	Face thickness of sandwich cylinder having faces of equal thickness
t_k	Skin thickness of k^{th} layer of layered cylinder
t_1 , t_2	Facing-sheet thicknesses for sandwich construction having faces of unequal thickness
x, y, z	Coordinates in the axial, circumferential, and radial directions, respectively
Z	Curvature parameter: $\frac{\ell^2}{rt}\sqrt{1-\mu^2}$ for isotropic cylinder and toroidal-shell segment; $2\frac{\ell^2}{rh}\sqrt{1-\mu^2}$ for isotropic sandwich cylinder
$\tilde{z}_k$	Distance of center of k^{th} layer of layered cylinder from reference surface (positive outward)
$\tilde{z}_s$, $\tilde{z}_r$	Distance of centroid of stiffeners and rings, respectively, from reference surface (positive when stiffeners or rings are on outside)

DEFINITION OF SYMBOLS (Continued)

Symbol	Definition
α	Semivertex angle of cone
β	Buckle aspect ratio $\left(\frac{n\ell}{\pi rm}\right)$
γ	Correlation factor to account for difference between classical theory and predicted instability loads
Δ	Distance of reference surface from inner surface of layered wall
$\Delta\gamma$	Increase in buckling correlation factor resulting from internal pressure
δ	Ratio of core density of honeycomb sandwich plate to density of face sheet of sandwich plate
δ_k	Distance of centroid of k^{th} layer of layered cylinder from inner surface
ϵ_1 , ϵ_2 , ϵ_{12}	Reference-surface strains
η	Plasticity reduction factor
η_o	Ring-geometry parameter
θ	Coordinate in the circumferential direction
λ	Spherical-cap geometry parameter
μ	Poisson's ratio
μ_c	Poisson's ratio of core material
μ_s , μ_θ	Poisson's ratios associated with stretching of an orthotropic material in the s- and θ-directions, respectively

DEFINITION OF SYMBOLS (Continued)

Symbol	Definition
μ_x , μ_y	Poisson's ratios associated with stretching of an orthotropic material in x- and y-directions, respectively
$\bar{\mu}_s$, $\bar{\mu}_\theta$	Equivalent Poisson's ratios in the s- and θ-directions, respectively
$\bar{\rho}$	Average radius of curvature of cone, $\frac{r_1 + r_2}{2 \cos \alpha}$
ρ_1	Radius of curvature at small end of cone, $\frac{r_1}{\cos \alpha}$
ρ_2	Radius of curvature at large end of cone, $\frac{r_2}{\cos \alpha}$
σ_N	Normal stress
σ_{max}	Maximum membrane compressive stress
σ_p	Critical axial stress for a cylinder with an elastic core
σ_s	Local failure stress
$\sigma_{x_{cr}}$	Axial stress, critical
σ_y	Circumferential stress
τ	Shear stress
τ_{cr}	Torsional buckling stress of an unfilled cylinder; critical shear stress
$\tau_{xy_{cr}}$	Shear stress in the x-y plane, critical
ϕ	Half the included angle of spherical cap

DEFINITION OF SYMBOLS (Concluded)

Symbol	Definition
$\bar{\phi}_2$	Half the included angle of spherical cap portion of torispherical closure
$\kappa_1, \kappa_2, \kappa_3$	Reference-surface curvature changes
ψ_1, ψ_2	[See eq. (17).]

C3. 0 STABILITY OF SHELLS.

The buckling load of a shell structure is defined as the applied load at which an infinitesimal increase in that load results in a large change in the equilibrium configuration of the shell. The change in equilibrium configuration is usually a large increase in the deflections of the shell, which may or may not be accompanied by a change in the basic shape of the shell from the prebuckled shape. For most types of shells and loading conditions, the buckling load is quite pronounced and easily identified.

The load-carrying capability of the shell may or may not decrease after buckling depending on the type of loading, the geometry of the shell, the stress levels of the buckled shell, etc. Only the buckling load will be discussed in this section because the information available on collapse load is very limited. In general, the buckling load and collapse load are nearly the same, but if they are different the deformations before the collapse are often very large.

The magnitude of the critical static load of a structure generally depends on its geometric proportions, the manner in which it is stiffened and supported, the bending and extensional stiffnesses of its various components, or other reasonably well-defined characteristics. For thin-walled shell structures less certain characteristics, such as small deviations of the structure from its nominal unloaded shape, may also have quite important effects on the load at which buckling will occur. Other factors that affect buckling, such as nonuniform stiffnesses, and variation of loading with time are not considered here.

For columns and flat plates, the classical small deflection theory predicts the buckling load quite well; in general, the theoretical buckling load is used as the design allowable buckling load. However, this method of analysis cannot be used generally for shell structures. The

buckling load for some types of shells and loadings may be much less than the load predicted by classical small deflection theory and, in addition, the scatter of the test data may be quite large. Explanations for these discrepancies are discussed in References 1 through 5. When sufficient data exist, a statistical reduction of the test data may be useful in determining a design allowable buckling load. This method has been used to determine most of the design curves presented in this section.

One of the primary shortcomings of this method of obtaining design curves is that the test specimens and boundary conditions used to obtain the design curves may not be typical of the particular structure which the design curves are being used to analyze. However, until additional information on shell stability is obtained, a statistical analysis has been used whenever possible to obtain design curves.

Whenever sufficient data do not exist to obtain a statistical design allowable buckling load, design recommendations are made on available information. Usually this involves recommending correction factors or "knockdown" factors to reduce the theoretical buckling loads. Such a recommendation may be too conservative in some cases; nevertheless, further theoretical and experimental investigations are necessary to justify raising the design curves.

Most analysis procedures presented in this section are for shells with simply supported edges. For most applications simply supported edges should be assumed unless test results are obtained which indicate the effects of the actual boundary condition of the design.

An attempt has been made to simplify the analysis procedures so that the design allowable buckling loads may be obtained from hand computations and graphs. The analyses which have been presented are sometimes quite long (orthotropic cylinders, for instance) but, in general,

results can be obtained quickly with a few simple computations. In many cases, computer programs are available for a more sophisticated analysis. The applicable programs are described, and their limitations and availability are noted. They can generally be obtained from COSMIC or from the Computer Utilization Manual.

As more information on shell stability becomes available, revisions to this section will be made. However, the analyst should attempt to keep abreast of the changes in current technology because of recent theoretical and experimental investigations.

3.1 CYLINDERS.

A better understanding of the theory of buckling of circular cylindrical shells has been made possible by use of electronic digital computers. This understanding has been aided both by more rigorous formulations of the theory and by reliance on experimental investigation.

Most of the available information on buckling of circular cylindrical shells is restricted to unstiffened shells of uniform thickness or to stiffened shells with uniform stiffness and properties, subjected to axisymmetric loading states which have certain simple longitudinal distributions, generally uniform. Problems involving surface loadings and thickness or stiffness variations that are axisymmetric but nonuniform longitudinally have been solved, but detailed investigations of the effects of various parameters have not been made. Also, available information is inadequate for the analysis of loadings that are nonuniform circumferentially. Problems of this type can be treated by digital computer programs and will be discussed in Subsection 3.4.

The application of theory to the design of actual cylindrical shells has been complicated by apparent discrepancies between theory and experiment. For shells in which longitudinal compression of the cylinder wall predominates, the discrepancies can be quite large. For shells in which shear or circumferential compression predominates, the discrepancies are generally less severe but still large enough to require experimental programs to establish design data. The causes of such discrepancies are generally understood.

The primary source of error is the dependence of the buckling load of cylindrical shells on small deviations from the nominal circular cylindrical shape of the structure. Because the unloaded shape of a test specimen usually has not been stringently controlled, most test results for

nominally identical specimens have larger scatter and fall below the theoretical values.

Another source of discrepancy is the dependence of buckling loads of cylindrical shells on edge values of longitudinal and circumferential displacements or forces. Also, because tangential edge conditions have not usually been precisely controlled in buckling tests, some of the scatter of test results can be attributed to this source. Current methods of establishing design data tend to treat both initial imperfections and edge conditions as random effects. Results from all available tests are considered together without regard to specimen construction or methods of testing and are analyzed to yield lower bound or statistical correction factors to be applied to simplified versions of the theoretical results. This technique has proved satisfactory to date for design purposes.

Within the limitations imposed by the state of the art, acceptable procedures for the estimation of critical loads on circular cylindrical shells are described in this section.

3.1.1 ISOTROPIC UNSTIFFENED CYLINDERS.

Unstiffened isotropic circular cylinders subjected to various conditions of loading are considered below.

3.1.1.1 Axial Compression — Unpressurized.

The design allowable buckling stress for a circular cylinder subjected to axial compression is given by

$$\frac{\sigma_{x_{cr}}}{\eta} = \frac{\gamma E\, t/r}{\sqrt{3\,(1-\mu^2)}} \qquad (1)$$

$$\frac{\sigma_{x_{cr}}}{\eta} = 0.6\,\gamma\,\frac{Et}{r} \quad (\text{for } \mu = 0.3) \quad ,$$

where the factor γ should be taken as

$$\gamma = 1.0 - 0.901\ (1-e^{-\phi}) \qquad (2)$$

where

$$\phi = \frac{1}{16}\sqrt{\frac{r}{t}} \quad \text{for} \quad \left(\frac{r}{t} < 1500\right) .$$

Equation (2) is shown graphically in Figure 3.1-1 and provides a good lower bound for most test data [6]. The information in Figure 3.1-1 should be used with caution for cylinders with length-radius ratios greater than about five since the correlation has not been verified by experiment in this range. Very long cylinders should be checked for Euler-column buckling.

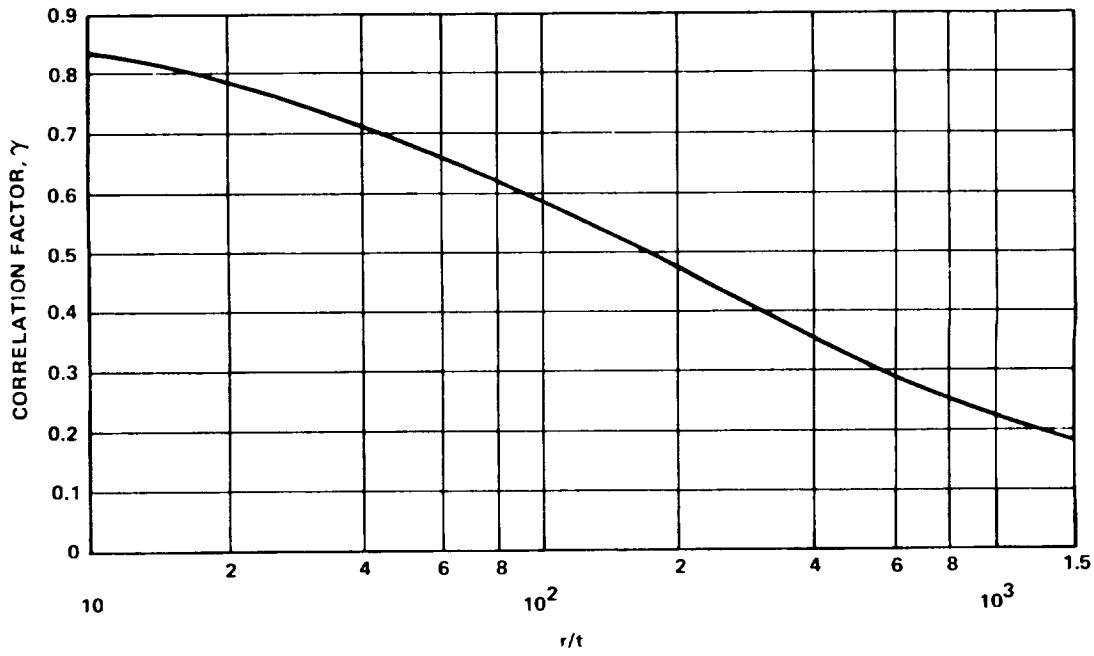

FIGURE 3.1-1. CORRELATION FACTORS FOR ISOTROPIC CIRCULAR CYLINDERS SUBJECTED TO AXIAL COMPRESSION

When geometric and material properties are such that the computed buckling stress $\frac{\sigma_{x_{cr}}}{\eta}$ is in the plastic range, the actual buckling stress $\sigma_{x_{cr}}$ should be calculated by applying the plasticity coefficient, η. This calculation is facilitated by the use of the curves of Paragraph 3.1.6. For moderately long cylinders the critical stress $\sigma_{x_{cr}}$ should be determined by using curve E_1 in Paragraph 3.1.6. For extremely short cylinders ($Z \rightarrow 0$) curve G should be used.

For a cylinder having a length between those lengths for which curves E_1 and G apply, a plasticity factor is not available. Presumably, a linear interpolation should provide satisfactory results. Such a factor would be a function of cylinder geometry as well as of the usual material stress-strain curve.

3.1.1.2 Axial Compression — Pressurized

Buckling and collapse coincide for internally pressurized circular cylinders in axial compression, just as in the case of the unpressurized cylinder. Pressurization increases the buckling load in the following ways:

1. The total compressive load must be greater than the tensile pressurization load $p \pi r^2$ before buckling can occur.

2. The destabilizing effect of initial imperfections is reduced. The circumferential tensile stress induced by the pressurization inhibits the diamond buckling pattern, and, at sufficiently high pressurization, the cylinder buckles in the classical axisymmetric mode at approximately the classical buckling stress.

It is recommended that the total load for buckling, unless substantiated by testing, be obtained by the addition of the pressurization load $p \pi r^2$, the buckling load for the unpressurized cylinder [equation (1)], and an increase in the buckling load caused by pressurization; that is:

$$P_{press} = 2 \pi Et^2 \left(\frac{\gamma}{\sqrt{3\,(1-\mu^2)}} + \Delta\gamma \right) + p \pi r^2 \qquad (3)$$

where $\Delta\gamma$ is obtained from Figure 3.1-2.

For $\mu = 0.3$,

$$P_{press} = 2 \pi Et^2 \,(0.6\gamma + \Delta\gamma) + p \pi r^2 \quad . \qquad (4)$$

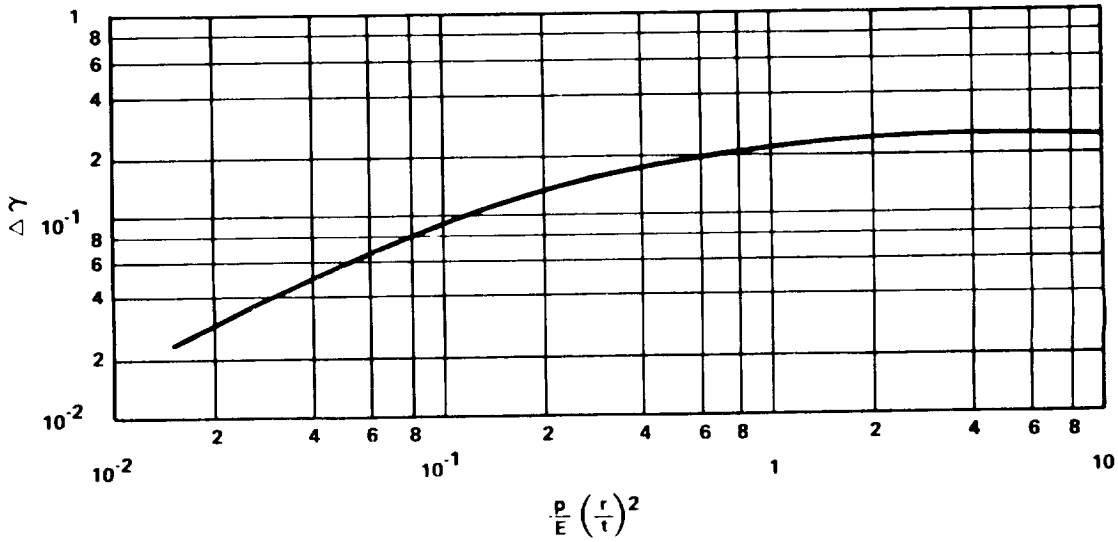

FIGURE 3.1-2. INCREASE IN AXIAL-COMPRESSIVE BUCKLING-STRESS COEFFICIENT OF CYLINDERS RESULTING FROM INTERNAL PRESSURE

3.1.1.3 Bending — Unpressurized.

Buckling and collapse coincide for isotropic, unpressurized circular cylinders in bending. The procedure given for isotropic cylinders in axial compression may be used also to obtain the critical maximum stress for isotropic cylinders in bending, except that a correlation factor based on bending tests should be used in place of the factor given by equation (2) for cylinders in axial compression. The correlation factor for the cylinder in bending is taken as

$$\gamma = 1.0 - 0.731\ (1-e^{-\phi}) \qquad (5)$$

where

$$\phi = \frac{1}{16}\sqrt{\frac{r}{t}}$$

Equation (5) is presented graphically in Figure 3.1-3. This equation should be used with caution for $r/t > 1500$ because experimental data are not available in this range [7]. Although the theoretical critical stress for axial compression and that for bending are the same, the correlation factor for bending is greater than that for compression. This is primarily because the buckling of a cylinder in compression can be triggered by any imperfection on the shell surface, whereas in bending, buckling is generally initiated in the region of the greatest compressive stress.

For inelastic buckling the critical stress may be found by using curves E_1 in Paragraph 3.1.6. If the stresses are elastic the allowable moment is

$$M_{cr} = \pi r^2 \sigma_{x_{cr}} t \qquad (6)$$

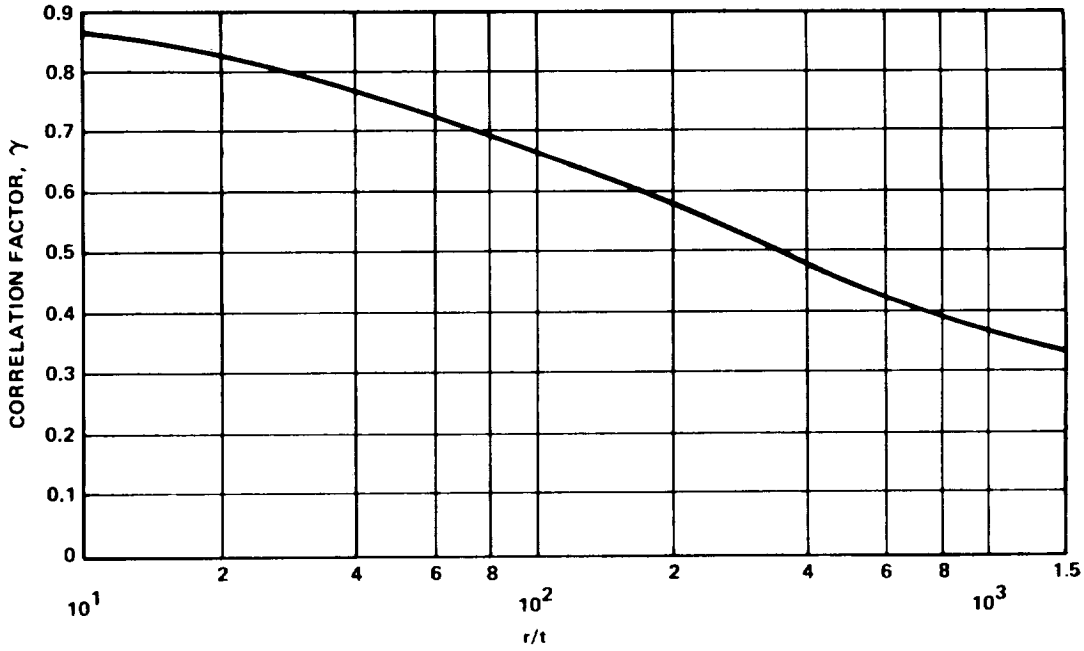

FIGURE 3.1-3. CORRELATION FACTORS FOR ISOTROPIC CIRCULAR CYLINDER SUBJECTED TO BENDING

3.1.1.4 Bending — Pressurized.

For thin-walled cylinders subjected to bending and internal pressure, it is recommended that the buckling moment be obtained by adding the moment-carrying capability of a pressurized membrane cylinder the buckling moment for the unpressurized cylinder [equations (1) and (5)], and an increase in the critical moment caused by pressurization. Then

$$M_{press} = \pi r Et^2 \left(\frac{\gamma}{\sqrt{3\,(1-\mu^2)}} + \Delta\gamma \right) + 0.5\, p\, \pi\, r^3 \quad , \qquad (7)$$

where $\Delta\gamma$ is obtained from Figure 3.1-2.

For $\mu = 0.3$,

$$M_{press} = \pi r Et^2 (0.6\gamma + \Delta\gamma) + 0.5 p \pi r^3 \quad . \qquad (8)$$

3.1.1.5 External Pressure.

The term "lateral pressure" designates an external pressure which acts only on the curved walls of the cylinder and not on the ends. The load in the cylinder wall is given by

$$N_y = \sigma_y t = pr \quad . \qquad (9)$$

The term "hydrostatic pressure" designates an external pressure which acts on both the curved walls and the ends of the cylinder. The cylinder wall loads are given by

$$N_y = \sigma_y t = pr \quad ,$$

$$N_x = \sigma_x t = \frac{pr}{2} \quad . \qquad (10)$$

Except for unusually short cylinders, the critical pressures for the two types of loads are not significantly different.

An approximate buckling equation for supported cylinders loaded by lateral pressure is given as

$$N_{y_{cr}} = k_y \frac{\pi^2 D}{r \ell^2} \quad . \qquad (11)$$

The buckling equation for cylinders loaded by hydrostatic pressure is obtained by replacing k_y by k_p in the formula above.

As shown in Figure 3.1-4, except for unusually short cylinders, the critical pressures for the two types of loads are not significantly different. For short cylinders equations suitable for design solutions to the hydrostatic ($Z < 30$) and lateral ($Z < 70$) cases respectively are:

$$k_y = 1.853 + .141714\ Z^{.83666} \tag{12a}$$

and

$$k_y = 3.980 + .02150\ Z^{1.125} \quad . \tag{12b}$$

The solutions for intermediate length cylinders ($100 \leq Z \leq 4000$) converge to an equation given by

$$k_y = .780\sqrt{Z} \tag{13a}$$

or the critical pressure is given by

$$p = \frac{.04125}{(1-\mu^2)^{3/4}} \quad \frac{E}{\left(\frac{r}{t}\right)^{5/2}\left(\frac{\ell}{r}\right)} \quad . \tag{13b}$$

The family of curves for long cylinders ($Z > 3000$) is dependent upon the radius-thickness ratio of the cylinder and corresponds to buckling of the cylinder into an oval shape, as given by

$$k_y = \frac{2.70}{\pi^2} \quad \frac{Z}{\frac{r}{t}\sqrt{1-\mu^2}} \tag{14a}$$

or

$$p = \frac{E}{4(1-\mu^2)} \left(\frac{t}{r}\right)^3 \tag{14b}$$

and applies for $20 \leq \frac{r}{t}\sqrt{1-\mu^2} \leq 100$.

☆U.S. GOVERNMENT PRINTING OFFICE 1976-641-255/391 REGION NO. 4

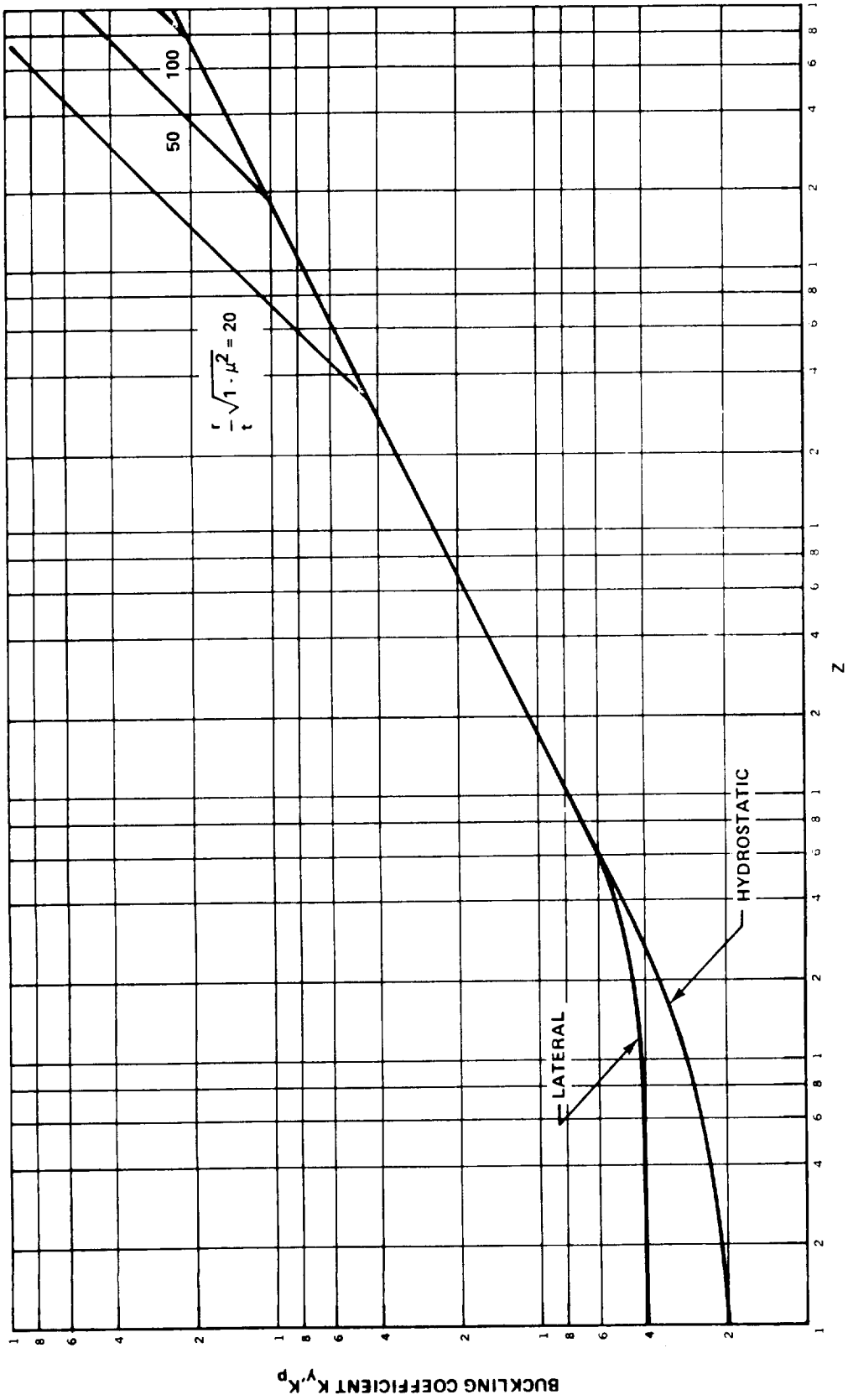

FIGURE 3.1-4. BUCKLING COEFFICIENTS FOR SIMPLY SUPPORTED ISOTROPIC CIRCULAR CYLINDERS SUBJECTED TO EXTERNAL PRESSURE

For inelastic stresses the plasticity correction factor should be obtained from Paragraph 3.1.6. For short cylinders ($\gamma Z < 5$) the C curves should be used. For moderate length cylinders ($5 < \gamma Z < 4000$) the E_1 curve should be used. For long cylinders ($\gamma Z > 4000$) the E curve should be used.

3.1.1.6 Shear or Torsion — Unpressurized.

The theoretical buckling coefficient for cylinders in torsion can be obtained from Figure 3.1-5. The straight-line portion of the curve is given by the equation

$$k_{xy} = \frac{N_{xy}\, \ell^2}{\pi^2 D} = 0.85\, (\gamma Z)^{3/4} \qquad (15)$$

and applies for $50 < \gamma Z < 78\, (\frac{r}{t})^2\, (1-\mu^2)$. Equation (15) can be written as

$$\tau_{xy_{cr}} = \frac{0.747\, \gamma^{3/4}\, E}{(\frac{r}{t})^{5/4}\, (\frac{\ell}{r})^{1/2}} \qquad (16)$$

For $\gamma Z > 78\, (\frac{r}{t})^2\, (1-\mu^2)$, the cylinder buckles with two circumferential waves. The buckling coefficient is then given by

$$k_{xy} = \frac{2\sqrt{2}\, \gamma Z}{\pi^2\, (\frac{r}{t})^{1/2}\, (1-\mu^2)^{1/4}} \qquad (17)$$

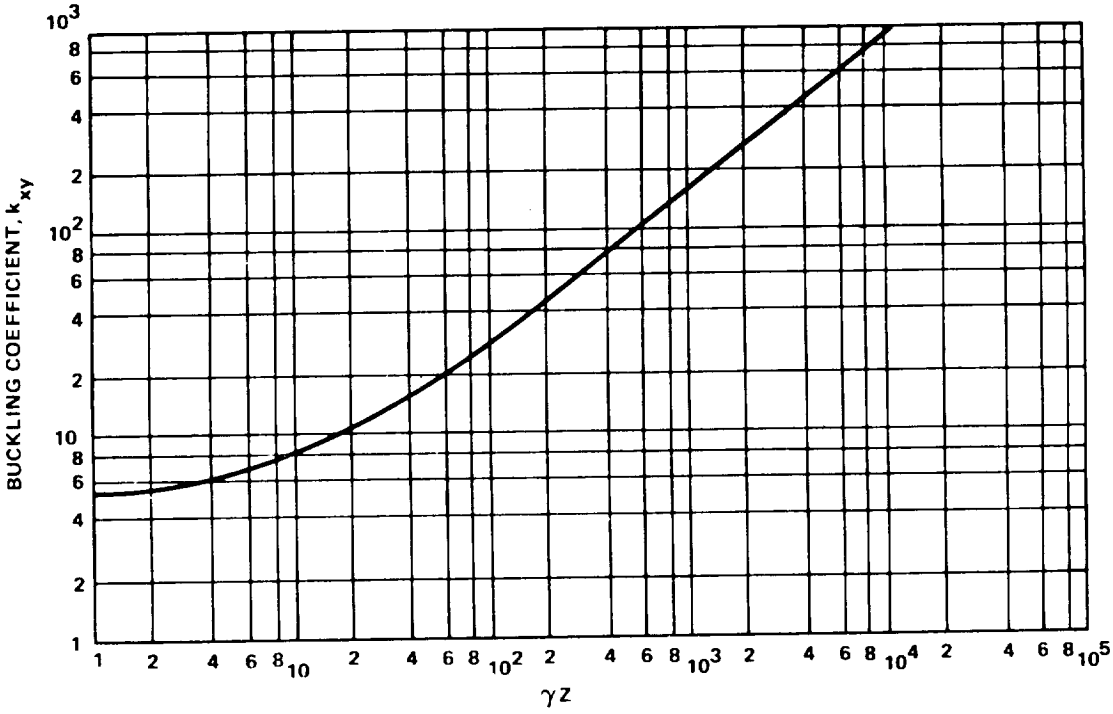

FIGURE 3.1-5. BUCKLING COEFFICIENTS FOR SIMPLY SUPPORTED ISOTROPIC CIRCULAR CYLINDERS SUBJECTED TO TORSION

or

$$\tau_{xy_{cr}} = \frac{\gamma E}{3\sqrt{2}\,(1-\mu^2)^{3/4}} \left(\frac{t}{r}\right)^{3/2} . \qquad (18)$$

To approximate the lower limit of most data, the value

$$\gamma^{3/4} = 0.67 \qquad (19)$$

is recommended for moderately long cylinders.

Plasticity should be accounted for by using curves A in Paragraph 3.1.6.

3.1.1.7 Shear or Torsion — Pressurized.

The increase in buckling stress caused by internal pressure may be calculated by using the curves in Reference 1.

3.1.1.8 Combined Loading.

The criterion for structural failure of a member under combined loading is frequently expressed in terms of a stress-ratio equation, $R_1^x + R_2^y + R_3^z = 1$. The subscripts denote the stress caused by a particular kind of loading (compression, shear, etc.), and the exponents (usually empirical) express the general relationship of the quantities for failure of the member. Simply stated, the term "stress-ratio" is used to denote the ratio of applied to allowable stress.

I. Axial Compression and Bending.

The recommended interaction equation for combined compressive load and bending is

$$R_c + R_b = 1 \quad . \tag{20}$$

The quantities R_c and R_b are, respectively, the compressive and bending load or stress ratios. The denominators of the ratios are the allowable loads or stresses given by equations (1) and (2) for cylinders in axial compression and by equations (1) and (5) for cylinders in bending.

Equation (20) is also recommended for internally pressurized circular cylinders in combined axial compression and bending by using equations (3) or (4) and (7) or (8).

II. Axial Compression and External Pressure.

The recommended interaction equation for combined compressive load and hydrostatic or lateral pressure is

$$R_c + R_p = 1 \quad . \tag{21}$$

The quantities R_c and R_p are, respectively, the compressive and hydrostatic or lateral pressure load or stress ratios. The denominators of the ratios are the allowable stresses given by equations (1) and (2) for cylinders in axial compression and by equations (11) or (12) for cylinders subjected to external pressure.

III. Axial Compression and Torsion.

For cylindrical shells under torsion and axial compression, the analytical interaction curve is a function of Z and varies from a parabolic shape at low-Z values to a straight line at high-Z values. The scatter of experimental data suggests the use of a straight-line interaction formula. Therefore, the recommended interaction equation is

$$R_c + R_t = 1 \quad . \tag{22}$$

The quantities R_c and R_t are, respectively, the compressive and torsion load or stress ratios. The denominators of the ratios are the allowable stresses given by equations (1) and (2) for cylinders in axial compression and by equations (16) or (18) for cylinders in torsion.

IV. Bending and Torsion.

A conservative estimate of the interaction for cylinders under combined bending and torsion is

$$R_b + R_t^2 = 1 \quad . \tag{23}$$

The quantities R_b and R_t are, respectively, the bending and torsion load or stress ratios. The denominators of the ratios are the allowable stresses given by equations (1) and (5) for cylinders in bending and by equations (16) or (18) for cylinders in torsion.

3.1.2 ORTHOTROPIC CYLINDERS.

The term "orthotropic cylinders" covers a wide variety of cylinders. In its strictest sense, it denotes cylinders made of a single orthotropic material or of orthotropic layers. It also denotes types of stiffened cylinders for which the stiffener spacing is small enough for the cylinder to be approximated by a fictitious sheet whose orthotropic bending and extensional properties include those of the individual stiffening elements averaged out over representative widths or areas. Generally, the directions of the axes of orthotropy are taken to coincide with the longitudinal and circumferential directions of the cylinder.

The behavior of the various types of orthotropic cylinders may be described by a single theory, the elements of which are equations of equilibrium for the buckled structure, relationships between force and moment resultants, and extensional and bending strains. For cylinders of a single orthotropic material, it is generally permissible to neglect the coupling between force resultants and bending strains and between moment resultants and extensional strains. The theory is then similar to that for isotropic cylinders.' For stiffened cylinders or for cylinders having orthotropic layers, however, neglect of the coupling terms can lead to serious errors. For example, the inclusion of coupling terms yields a significant difference in theoretical results for stiffened cylinder configurations having stiffeners on the inner surface or the outer surface. The difference vanishes when coupling is omitted.

Theoretical and experimental results for stiffened shells are generally in better agreement than those for unstiffened shells. The possibility of local buckling of the cylinder between stiffening elements should be checked.

In general, the complexity of the analysis for orthotropic cylinders necessitates the use of a computer solution. Applicable computer solutions are discussed in Subsection 3.4.

3.1.2.1 Axial Compression.

A buckling equation for stiffened orthotropic cylinders in compression [8] is given by:

$$N_x = \left(\frac{\ell}{m\pi}\right)^2 \frac{\begin{vmatrix} A_{11} & A_{12} & A_{13} \\ A_{21} & A_{22} & A_{23} \\ A_{31} & A_{32} & A_{33} \end{vmatrix}}{\begin{vmatrix} A_{11} & A_{12} \\ A_{21} & A_{22} \end{vmatrix}} \quad \text{for} \quad (n \geq 4) \quad , \qquad (24)$$

in which

$$A_{11} = \overline{E}_x \left(\frac{m\pi}{\ell}\right)^2 + \overline{G}_{xy} \left(\frac{n}{r}\right)^2 \quad . \qquad (25)$$

$$A_{22} = \overline{E}_y \left(\frac{n}{r}\right)^2 + \overline{G}_{xy} \left(\frac{m\pi}{\ell}\right)^2 \quad . \qquad (26)$$

$$A_{33} = \overline{D}_x \left(\frac{m\pi}{\ell}\right)^4 + \overline{D}_{xy} \left(\frac{m\pi}{\ell}\right)^2 \left(\frac{n}{r}\right)^2 + \overline{D}_y \left(\frac{n}{r}\right)^4$$

$$+ \frac{\overline{E}_y}{r^2} + \frac{2\overline{C}_y}{r} \left(\frac{n}{r}\right)^2 + \frac{2\overline{C}_{xy}}{r} \left(\frac{m\pi}{\ell}\right)^2 \quad . \qquad (27)$$

$$A_{12} = A_{21} = \left(\overline{E}_{xy} + \overline{G}_{xy}\right) \frac{m\pi}{\ell} \frac{n}{r} \quad . \qquad (28)$$

$$A_{23} = A_{32} = \left(\overline{C}_{xy} + 2\overline{K}_{xy}\right) \left(\frac{m\pi}{\ell}\right)^2 \frac{n}{r} + \frac{\overline{E}_y n}{r^2} + \overline{C}_y \left(\frac{n}{r}\right)^3 \quad . \qquad (29)$$

$$A_{31} = A_{13} = \frac{\overline{E}_{xy}}{r} \frac{m\pi}{\ell} + \overline{C}_x \left(\frac{m\pi}{\ell}\right)^3 + \left(\overline{C}_{xy} + 2\overline{K}_{xy}\right) \frac{m\pi}{\ell} \left(\frac{n}{r}\right)^2 \quad . \qquad (30)$$

Values of stiffeners to be used for various types of construction are given in Paragraph 3.1.2.6. Prebuckling deformations are not taken into account in the derivation of the equation. The cylinder edges are assumed to be supported by rings that are rigid in their own plane but offer no resistance to rotation or bending out of their plane. The equation can be specialized for various types of cylinders which have been treated separately in the literature; for example, unstiffened or stiffened orthotropic cylinders with eccentricity effects neglected and stiffened or stiffened orthotropic cylinders with eccentricity effects taken into account. For ring-stiffened corrugated cylinders, a similar but not identical theory is given in References 9 and 10. For given cylinder and stiffener dimensions, the values of m and n to be used are those which minimize $\overline{N}_x$.

The unusually large number of parameters in equation (24) does not permit any definitive numerical results to be shown. The computer programs discussed in Subsection 3.4 should be used for solution of the critical axial compressive load for a given design. It has been shown that for combinations of parameters representative of stiffened shells, calculations indicate that external stiffening, whether stringers or rings or both, can be more effective than internal stiffening for axial compression. Generally, calculations neglecting stiffener eccentricity yield unconservative values of the buckling load for internally stiffened cylinders and conservative values of the buckling load for externally stiffened cylinders. An extensive investigation of the variation of the buckling load with various stiffener parameters is reported in Reference 11. The limited experimental data [9-17] for stiffened shells are in reasonably good agreement with the theoretical results for the range of parameters investigated.

On the basis of available data, it is recommended that the buckling loads [calculated from equation (24)] of cylinders having closely spaced, moderately large stiffeners be multiplied by a factor of 0.75. The correlation coefficients covering the transition from unstiffened cylinders to stiffened cylinders with closely spaced stiffeners have not been fully investigated. Although theory and experiment [16] indicate that restraint against edge rotation and longitudinal movement significantly increases the buckling load, not enough is known about the edge restraint of actual cylinders to warrant taking advantage of these effects unless such effects are substantiated by tests.

For layered or unstiffened orthotropic cylindrical shells, the available test data are quite meager [18, 19]. For configurations where the coupling coefficients $\overline{C}_x$, $\overline{C}_y$, $\overline{C}_{xy}$, and $\overline{K}_{xy}$ can be neglected,

it is recommended that the buckling load be calculated from the equation

$$\frac{N_x \ell^2}{\pi^2 \bar{D}_x} = m^2 \left(1 + 2 \frac{\bar{D}_{xy}}{\bar{D}_x} \beta^2 + \frac{\bar{D}_y}{\bar{D}_x} \beta^4 \right) + \frac{\gamma^2 \ell^4}{\pi^4 m^2 \bar{D}_x r^2} \frac{\bar{E}_x \bar{E}_y - \bar{E}^2_{xy}}{\bar{E}_x + \left(\frac{\bar{E}_x \bar{E}_y - \bar{E}^2_{xy}}{\bar{G}_{xy}} - 2\bar{E}_{xy} \right) \beta^2 + \bar{E}_y \beta^4} . \quad (31)$$

The correlation factor γ is taken to be of the same form as the correlation factor for isotropic cylinders [equation (2)] with the thickness replaced by the geometric mean of the radii of gyration for the axial and circumferential directions. Thus

$$\gamma = 1.0 - 0.901 \, (1 - e^{-\phi}) \quad (32)$$

where

$$\phi = \frac{1}{29.8} \left[\frac{r}{\sqrt[4]{\frac{\bar{D}_x \bar{D}_y}{\bar{E}_x \bar{E}_y}}} \right]^{1/2} . \quad (33)$$

3.1.2.2 Bending.

Theoretical and experimental results [10, 20-23], indicate that the critical maximum load per unit circumference of a stiffened cylinder

in bending can exceed the critical unit load in axial compression. In the absence of an extensive investigation, it is recommended that the critical maximum load per unit circumference of a cylinder with closely spaced stiffeners be taken as equal to the critical load in axial compression, which is calculated from equation (24) multiplied by a factor of 0.75.

For layered or unstiffened orthotropic cylinders with negligible coupling coefficients, it is recommended that the maximum unit load be calculated by equation (31) with γ replaced by

$$\gamma = 1.0 - 0.731\ (1-e^{-\phi}) \tag{34}$$

where

$$\phi = \frac{1}{29.8}\left[\frac{r}{\sqrt[4]{\frac{\bar{D}_x\,\bar{D}_y}{\bar{E}_x\,\bar{E}_y}}}\right]^{1/2} . \tag{35}$$

3.1.2.3 External Pressure.

The counterpart of equation (24) for stiffened orthotropic cylinders under lateral pressure is given by

$$p = \frac{r}{n^2}\,\frac{\begin{vmatrix} A_{11} & A_{12} & A_{13} \\ A_{21} & A_{22} & A_{23} \\ A_{31} & A_{32} & A_{33} \end{vmatrix}}{\begin{vmatrix} A_{11} & A_{12} \\ A_{21} & A_{22} \end{vmatrix}} . \tag{36}$$

For hydrostatic pressure, the quantity n^2 shown in equation (36) is replaced by

$$n^2 + 1/2 \left(\frac{m \pi r}{\ell}\right)^2 \quad .$$

In the case of lateral pressure, m is equal to unity, whereas n must be varied to yield a minimum value of the critical pressure but not less than 2. In the case of hydrostatic pressure, the value of m should be varied as well as n. For long cylinders, equation (36) is replaced by

$$p = \frac{3\left(\overline{D}_y - \frac{\overline{D}_y^2}{\overline{E}_y}\right)}{r^3} \quad . \tag{37}$$

If the coupling coefficients $\overline{C}_x$, $\overline{C}_y$, $\overline{C}_{xy}$, and $\overline{K}_{xy}$ can be neglected, the critical buckling pressure can be approximated by [24]:

$$p \approx \frac{5.513}{\ell r^{3/2}} \left[\frac{\overline{D}_y^3\left(\overline{E}_x \overline{E}_y - \overline{E}_{xy}^2\right)}{\overline{E}_y}\right]^{1/4} \tag{38}$$

for

$$\left(\frac{\overline{D}_y}{\overline{D}_x}\right)^{3/2} \left(\frac{\overline{E}_x \overline{E}_y - \overline{E}_{xy}^2}{12\,\overline{E}_y \overline{D}_x}\right)^{1/2} \frac{\ell^2}{r} > 500 \quad . \tag{39}$$

Equation (36) has been investigated primarily for isotropic cylinders with ring stiffeners [25-27]. For closely spaced ring stiffening, References 25 and 26 show that the effectiveness of inside or outside rings depends on the shell and ring geometries. Generally, for shells with values of Z less than 100, outside rings are more effective than inside rings, whereas for values of Z greater than 500, the reverse is true. As the ring geometry varies, the effectiveness of outside stiffening tends to increase as the stiffness of the rings relative to the shell increases. Somewhat lower buckling pressures are given by the extremely complex but more accurate theory of Reference 28, but the differences are not so significant as to warrant its use.

The experimental results for ring-stiffened cylinders described in Reference 29 are in reasonably good agreement with the theoretical results of equation (36). However, for cylinders of all types, it is recommended that the buckling pressure calculated from equation (36) be multiplied by a factor of 0.75 for use in design, as has been recommended for unstiffened isotropic cylinders of moderate length.

3.1.2.4 Torsion.

The problem of torsional buckling of orthotropic cylinders has been treated in References 24 and 30, which do not take into account coupling between bending and extension, and in Reference 31, which does. If coupling effects are negligible, the critical torque of moderately long cylinders can be estimated from the relationship [24]:

$$M_t \approx 21.75\, \overline{D}_y^{5/8} \left(\frac{\overline{E}_x \overline{E}_y - \overline{E}_{xy}^2}{\overline{E}_y} \right)^{3/8} \frac{r^{5/4}}{\ell^{1/4}} \qquad (40)$$

for

$$\left(\frac{\bar{D}_y}{\bar{D}_x}\right)^{5/6}\left(\frac{\bar{E}_x\bar{E}_y - \bar{E}_{xy}^2}{12\,\bar{E}_y\bar{D}_x}\right)^{1/2}\frac{\ell^2}{r} \geq 500 \quad . \qquad (41)$$

Reference 31, however, shows that coupling effects are quite important for cylinders stiffened by closely spaced rings. For long shells internal rings are generally more effective than outside rings; for short shells the reverse is true. In the absence of general formulas or graphs to cover the entire range of parameters that should be considered, the equations of Reference 31 should be solved for each specific case considered.

The test data of Reference 32 are in good agreement with theoretical predictions but are insufficient to provide an adequate test of the theory. It is therefore recommended that theoretical critical torques be multiplied by a factor of 0.67 for moderately long cylinders.

3.1.2.5 Combined Bending and Axial Compression.

On the basis of theory [10, 20, 21] and limited experimental data [9-10], a straight-line interaction curve is recommended for orthotropic cylinders subjected to combined bending and axial compression. The critical combinations of loading are thus given by

$$R_c + R_b = 1 \quad . \qquad (42)$$

3.1.2.6 Elastic Constants.

The values of the various elastic constants used in the theory of buckling of orthotropic cylinders are different for different types of construction.

I. Stiffened Multilayered Orthotropic Cylinders.

Some widely used expressions for this type of cylinder are:

$$\overline{E}_x = \sum_{k=1}^{N} \left(\frac{E_x}{1 - \mu_x \mu_y} \right)_k t_k + \frac{E_s A_s}{b} \quad . \tag{43}$$

$$\overline{E}_y = \sum_{k=1}^{N} \left(\frac{E_y}{1 - \mu_x \mu_y} \right)_k t_k + \frac{E_r A_r}{d} \quad . \tag{44}$$

$$\overline{E}_{xy} = \sum_{k=1}^{N} \left(\frac{\mu_x E_y}{1 - \mu_x \mu_y} \right)_k t_k = \sum_{k=1}^{N} \left(\frac{\mu_y E_x}{1 - \mu_x \mu_y} \right)_k t_k \quad . \tag{45}$$

$$\overline{G}_{xy} = \sum_{k=1}^{N} \left(G_{xy} \right)_k t_k \quad . \tag{46}$$

$$\overline{D}_x = \sum_{k=1}^{N} \left(\frac{E_x}{1 - \mu_x \mu_y} \right)_k \left(\frac{1}{12} t_k^3 + t_k \tilde{z}_k^2 \right) + \frac{E_s I_s}{b} + \tilde{z}_s^2 \frac{E_s A_s}{b} \quad . \tag{47}$$

$$\overline{D}_y = \sum_{k=1}^{N} \left(\frac{E_y}{1 - \mu_x \mu_y} \right)_k \left(\frac{1}{12} t_k^3 + t_k \tilde{z}_k^2 \right) + \frac{E_r I_r}{b} + \tilde{z}_r^2 \frac{E_r A_r}{d} \quad , \tag{48}$$

$$\overline{D}_{xy} = \sum_{k=1}^{N} \left(4G_{xy} + \frac{\mu_x E_y}{1 - \mu_x \mu_y} + \frac{\mu_y E_x}{1 - \mu_x \mu_y} \right)_k \frac{1}{12} t_k^3 + t_k \tilde{z}_k^2$$

$$+ \frac{G_s J_s}{b} + \frac{G_r J_r}{d} \quad , \tag{49}$$

$$\overline{C}_x = \sum_{k=1}^{N} \left(\frac{E_x}{1 - \mu_x \mu_y} \right)_k t_k \tilde{z}_k + \tilde{z}_s \frac{E_s A_s}{b} \quad , \tag{50}$$

$$\overline{C}_y = \sum_{k=1}^{N} \left(\frac{E_y}{1 - \mu_x \mu_y} \right)_k t_k \tilde{z}_k + \tilde{z}_r \frac{E_r A_r}{d} \quad , \tag{51}$$

$$\overline{C}_{xy} = \sum_{k=1}^{N} \left(\frac{\mu_y E_x}{1 - \mu_x \mu_y} \right)_k t_k \tilde{z}_k = \sum_{k=1}^{N} \left(\frac{\mu_x E_y}{1 - \mu_x \mu_y} \right)_k t_k \tilde{z}_k \quad , \tag{52}$$

$$\overline{K}_{xy} = \sum_{k=1}^{N} \left(G_{xy} \right)_k t_k \tilde{z}_k \quad , \tag{53}$$

where the subscript k refers to the material and geometry of the k^{th} layer of an N-layered shell (Fig. 3.1-6). A proper choice of the reference surface can make at least one of the coupling coefficients vanish. For example, if Δ is taken as

$$\Delta = \frac{\sum_{k=1}^{N} \left(\frac{\mu_y E_x}{1 - \mu_x \mu_y} \right)_k t_k \delta_k}{\overline{E}_{xy}} , \qquad (54)$$

the coefficient $\overline{C}_{xy}$ vanishes, and if

$$\Delta = \frac{\sum_{k=1}^{N} \left(G_{xy} \right)_k t_k \delta_k}{\overline{G}_{xy}} , \qquad (55)$$

the coefficient $\overline{K}_{xy}$ vanishes.

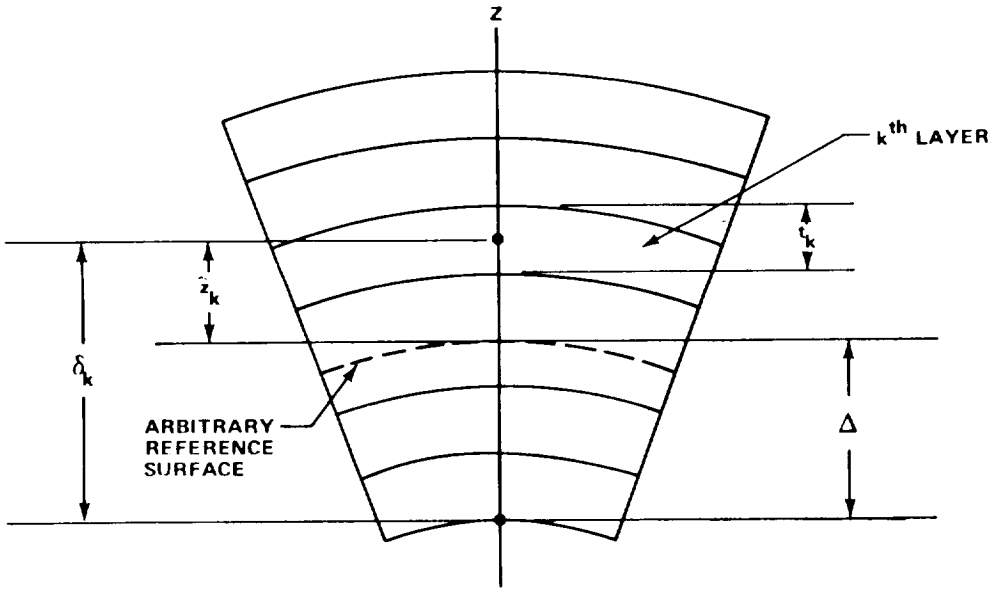

FIGURE 3.1-6. MULTILAYERED ORTHOTROPIC CYLINDRICAL SHELL GEOMETRY

II. Isotropic Cylinders with Stiffeners and Rings.

For a cylinder consisting of a stiffened single isotropic layer and for a reference surface at the center of the layer, equations (43) to (53) reduce to

$$\overline{E}_x = \frac{Et}{1-\mu^2} + \frac{E_s A_s}{b} \quad . \tag{56}$$

$$\overline{E}_y = \frac{Et}{1-\mu^2} + \frac{E_r A_r}{d} \quad . \tag{57}$$

$$\overline{E}_{xy} = \frac{\mu Et}{1-\mu^2} \quad . \tag{58}$$

$$\overline{G}_{xy} = \frac{Et}{2(1+\mu)} \quad . \tag{59}$$

$$\overline{D}_x = \frac{Et^3}{12(1-\mu^2)} + \frac{E_s I_s}{b} + \tilde{z}_s^2 \frac{E_s A_s}{b} \quad . \tag{60}$$

$$\overline{D}_y = \frac{Et^3}{12(1-\mu^2)} + \frac{E_r I_r}{d} + \tilde{z}_r^2 \frac{E_r A_r}{d} \quad . \tag{61}$$

$$\overline{D}_{xy} = \frac{Et^3}{6(1+\mu)} + \frac{G_s J_s}{b} + \frac{G_r J_r}{d} \quad . \tag{62}$$

$$\overline{C}_x = \tilde{z}_s \frac{E_s A_s}{b} \quad . \tag{63}$$

$$\bar{C}_y = \tilde{z}_r \frac{E_r A_r}{d} \quad . \tag{64}$$

$$\bar{C}_{xy} = \bar{K}_{xy} = 0 \quad . \tag{65}$$

III. Ring-Stiffened Corrugated Cylinders.

The following formulas are commonly used to calculate the required stiffnesses of ring-stiffened corrugated cylinders, with the choice of formula depending on the different assumptions which may be made:

$$\bar{E}_x = E\bar{t}\,, \quad \bar{E}_y = \frac{E_r A_r}{d} \quad , \tag{66}$$

$$\bar{G}_{xy} = Gt\left(\frac{t}{\bar{t}}\right) \quad . \tag{67}$$

$$\bar{D}_x = E\bar{I} \quad . \tag{68}$$

$$\bar{D}_y = \frac{E_r I_r}{d} + \tilde{z}_r^2 \frac{E_r A_r}{d} \quad . \tag{69}$$

$$\bar{D}_{xy} = \frac{G_r J_r}{d} \quad . \tag{70}$$

$$\bar{C}_y = \tilde{z}_r \frac{E_r A_r}{d} \quad . \tag{71}$$

$$\overline{E}_{xy} = \overline{C}_{x} = \overline{C}_{xy} = \overline{K}_{xy} = 0 \qquad (72)$$

Slightly different stiffnesses are given in Reference 22.

IV. Waffle-Stiffened Cylinders.

Stiffnesses for cylinders with waffle-like walls are described in References 33 to 35.

V. Special Considerations.

In some designs of stiffened cylinders, the skin may buckle before failure of the cylinder. Buckled sheet is less stiff than unbuckled sheet. The decreased stiffness can be calculated by methods similar to those presented in References 13, 23, and 36.

3.1.3 ISOTROPIC SANDWICH CYLINDERS.

The term "isotropic sandwich" designates a layered construction formed by bonding two thin facings to a thick core. Generally, the thin facings provide nearly all the bending rigidity of the construction. The core separates the facings and transmits shear so that the facings bend about a neutral axis. The core provides the shear rigidity of the sandwich construction.

Sandwich construction should be checked for two possible modes of instability failure: (1) general instability failure where the shell fails with core and facings acting together, and (2) local instability taking the form of dimpling of the faces or wrinkling of the faces (Fig. 3.1-7).

If the isotropic sandwich shell has thin facings and the core has relatively little bending stiffness, then for unequal thickness facings the bending stiffness is given by

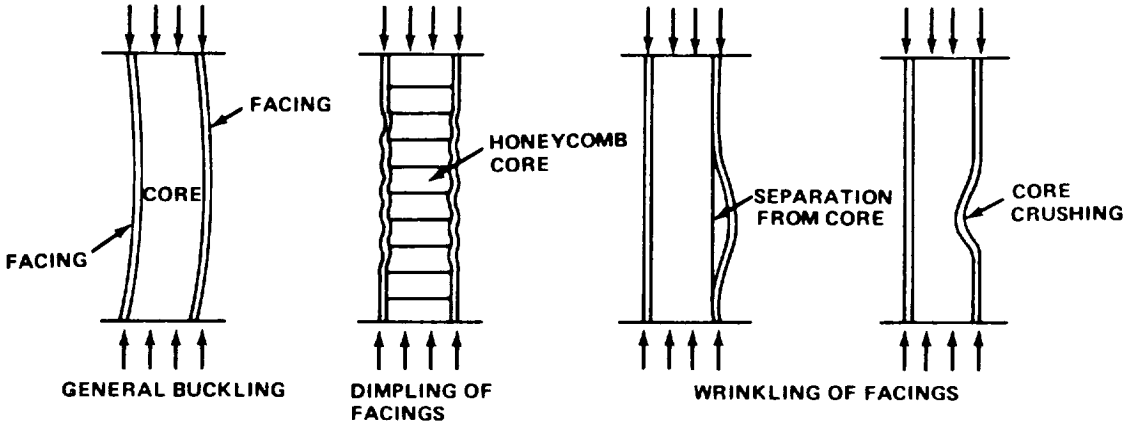

FIGURE 3.1-7. TYPES OF FAILURE OF SANDWICH SHELLS

$$D_1 = \frac{E t_1 t_2 h^2}{(1 - \mu^2)(t_1 + t_2)} \tag{73}$$

and for equal thickness facings,

$$D_1 = \frac{E t_f h^2}{2(1 - \mu^2)} \tag{74}$$

The extensional stiffness for unequal thickness facings is given by

$$B_1 = \frac{E}{(1 - \mu^2)} (t_1 + t_2) \tag{75}$$

and for equal thickness,

$$B_1 = \frac{2 E t_f}{(1 - \mu^2)} \tag{76}$$

The transverse shear stiffness for an isotropic core is given by

$$D_q = G_{xz} \frac{h^2}{h - \frac{t_1 + t_2}{2}} \tag{77}$$

and for equal thickness,

$$D_q = G_{xz} \frac{h^2}{h - t_f} \tag{78}$$

The stiffness of other types of sandwich construction is given in References 37, 38, and 39.

3.1.3.1 Axial Compression.

Investigations of the buckling behavior of isotropic sandwich circular cylinders in axial compression are reported in References 40 and 41. Design information from these references is given in Figures 3.1-8 and 3.1-9.

Figure 3.1-9 is the more convenient of the two figures to use and is applicable to all but unusually short cylinders [$\gamma Z < \pi^2/(1 + R)$]. Figures 3.1-8 and 3.1-9 are based on the small-deflection buckling theory and should be used in conjunction with the correlation factor of Figure 3.1-10 to predict buckling loads. Figure 3.1-10 is based on equation (32), given for orthotropic cylinders. For the present application the parameter ϕ becomes

$$\phi = \frac{\sqrt{2}}{29.8} \sqrt{\frac{r}{h}} \tag{79}$$

This procedure is consistent with the procedures given earlier for other types of construction when shearing of the core does not contribute significantly to the buckling deformations, that is, when N_o/D_q of Figure 3.1-9 is small.

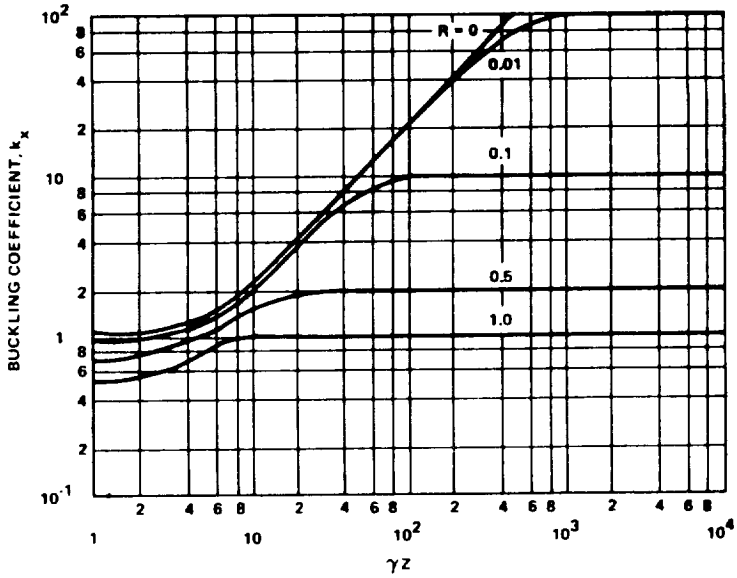

FIGURE 3.1-8. BUCKLING COEFFICIENTS FOR SIMPLY SUPPORTED ISOTROPIC SANDWICH CIRCULAR CYLINDERS SUBJECTED TO AXIAL COMPRESSION $G_{xz}/G_{yz} = 1.0$

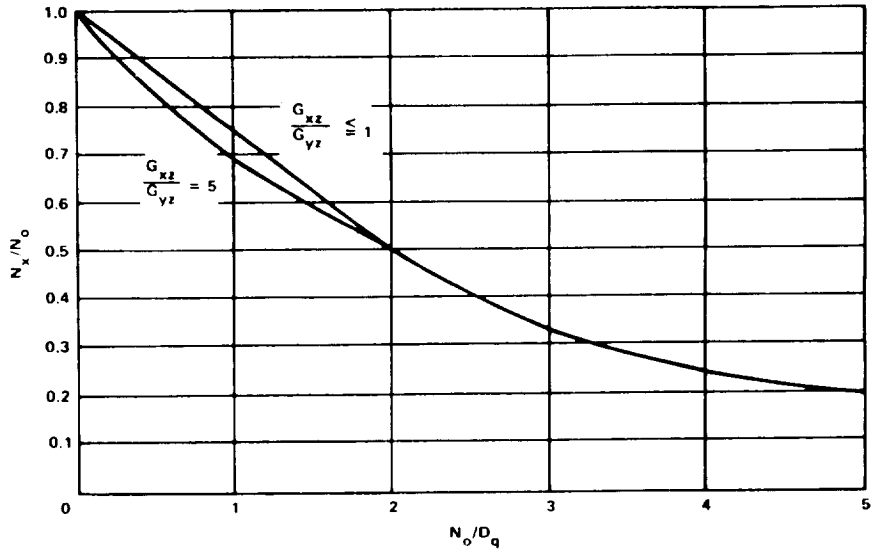

FIGURE 3.1-9. BUCKLING OF MODERATELY LONG, SIMPLY SUPPORTED, ISOTROPIC SANDWICH CIRCULAR CYLINDERS SUBJECTED TO AXIAL COMPRESSION

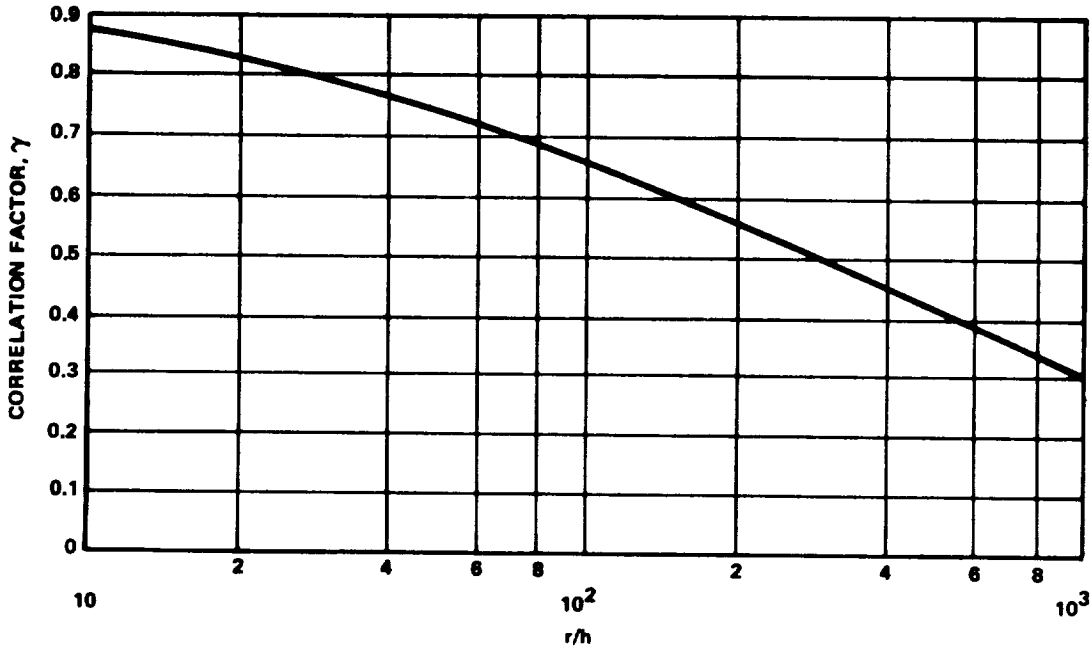

FIGURE 3.1-10. CORRELATION FACTORS FOR ISOTROPIC SANDWICH CIRCULAR CYLINDERS SUBJECTED TO AXIAL COMPRESSION

As shearing deformations become more pronounced, the correction resulting from application of the factor γ, as prescribed above, decreases and becomes zero in the limiting condition of buckling from a weak core $[(N_o/D_q) > 2]$.

A weight-strength study based on Figure 3.1-9 and published values for the shear stiffness of honeycomb cores [42] indicate that unusually lightweight cores are more desirable than heavier cores. Until adequate test data are obtained to substantiate this indication, however, designs should be limited to sandwiches with rather heavy cores ($\delta \geq 0.03$). Also, it has been found that sandwich plates with light honeycomb cores are susceptible to additional modes of deformation, and failure may result from intracell

buckling, face wrinkling, or an interaction of one or both of these modes with a cylinder-buckling mode. In addition, small buckle-like deformations have occurred in actual structures long before the theoretical buckling load was reached (see, for example, Ref. 43, p. 217). This behavior requires that the structure be capable of resisting internal moments and shears in addition to the directly applied loads. In the case of sandwich cylinders, the moments and shears may cause core buckling or shear failure of the core.

The only known method of preventing these core failures is to use relatively heavy cores which have considerable strength in crushing and shear. Honeycomb cores with a density ratio $\delta = 0.03$ should be adequate to prevent these core failures. Large margins against failure in intracell buckling and wrinkling can be obtained with rather heavy cores with little or no weight penalty. Moreover, when heavy cores are used approximate equations are adequate for predicting failures in the intracell buckling and face-wrinkling modes. The following equations may be used for this purpose. For intracell buckling:

$$\sigma_x = 2.5\, E_R\, (t/S)^2 \tag{80}$$

where S is the core cell size expressed as the diameter of the largest inscribed circle and

$$E_R = \frac{4\, E\, E_{tan}}{\left(\sqrt{E} + \sqrt{E_{tan}}\right)^2} \tag{81}$$

where E and E_{tan} are the elastic and tangent moduli of the face-sheet material. If initial dimpling is to be checked, the equation

$$\sigma_x = 2.2\, E_R\, (t/S)^2 \qquad (82)$$

should be used. The sandwich will still carry load if initial dimpling occurs.

Critical wrinkling stresses are predicted by

$$\sigma_x = 0.50\, (E_{sec}\, E_z\, G_{xz})^{1/3} \qquad (83)$$

where E_z is the modulus of the core in a direction perpendicular to the core, and G_{xz} is the shear modulus of the core in the x-z plane. If biaxial compressive stresses are applied to the sandwich, then the coefficients of the equations must be reduced by the factor $(1 + f^3)^{-1/3}$ where

$$f = \frac{\text{minimum principal compressive stress in facings}}{\text{maximum principal compressive stress in facings}} \quad . \qquad (84)$$

Wrinkling and intracell-buckling equations which consider strength of bond, strength of foundation, and initial waviness of the facings are given in References 39, 44, and 45.

The plasticity correction factor given for isotropic cylinders in axial compression also may be applied to isotropic sandwich cylinders. The factor is applicable to sandwich cylinders with stiff cores and becomes somewhat conservative as the shear stiffness of the core is decreased [46].

3.1.3.2 Bending.

The buckling equations given in Paragraph 3.1.3.1 for circular cylinders in axial compression may be used for cylinders in bending, provided that the correlation factor γ is taken from Figure 3.1-11 instead of from Figure 3.1-10. Figure 3.1-11 is based on equation (34), given earlier for orthotropic cylinders in bending.

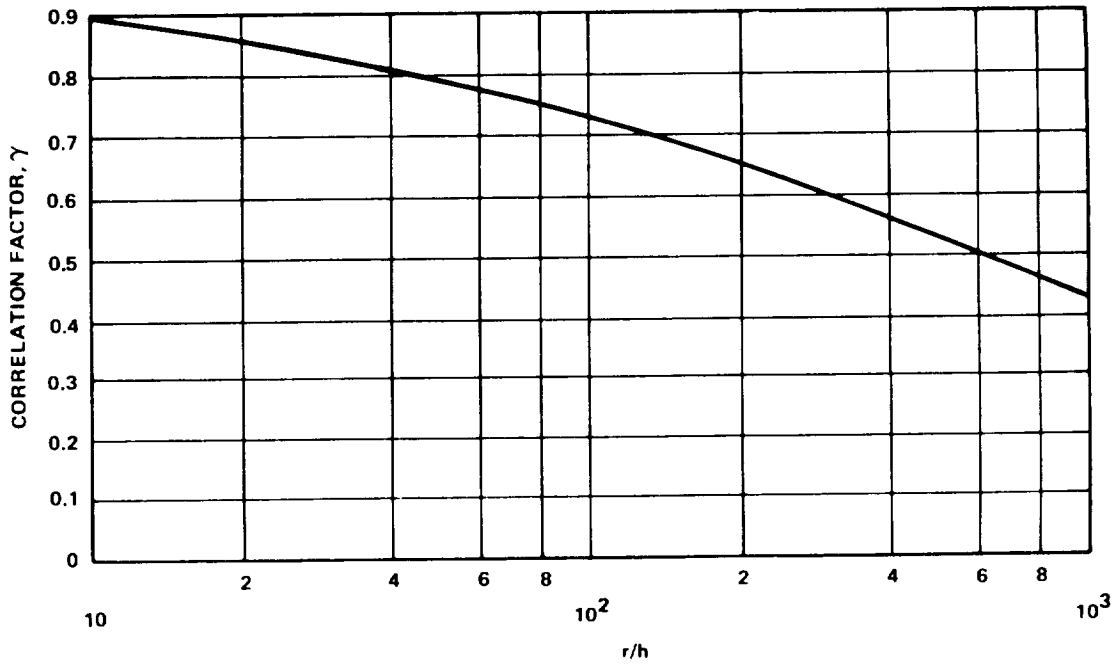

FIGURE 3.1-11. CORRELATION FACTORS FOR ISOTROPIC SANDWICH CIRCULAR CYLINDERS SUBJECTED TO BENDING

3.1.3.3 Lateral Pressure.

A plot of k_y against γZ, constructed from the data of Reference 47, is given in Figure 3.1-12. The straight-line portion of the curve of Figure 3.1-12 for a sandwich cylinder with a rigid core ($\delta=0$) is given by the equation

$$k_y = \frac{N_y \ell^2}{\pi D_1} = 0.56 \sqrt{\gamma Z} \qquad (85)$$

There are no experimental data to substantiate Figure 3.1-12. From experience with isotropic cylinders, however, it is suggested that a factor γ equal to 0.56 be used with this figure.

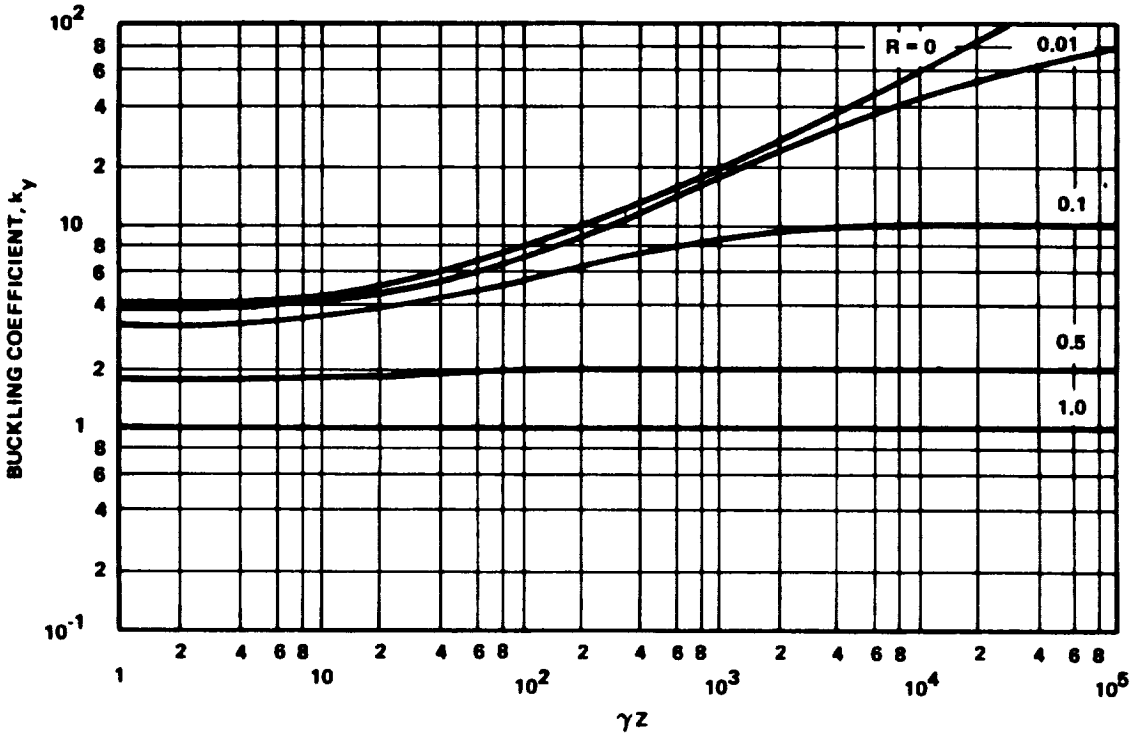

FIGURE 3.1-12. BUCKLING COEFFICIENTS FOR SIMPLY SUPPORTED ISOTROPIC SANDWICH CIRCULAR CYLINDERS SUBJECTED TO LATERAL PRESSURE $G_{xz}/G_{yz} = 1.0$

Here, as with sandwich cylinders in axial compression or bending, designs should be limited to sandwich cylinders for which the density ratio δ is 0.03 or greater, unless the design is substantiated by adequate tests.

For inelastic stresses the plasticity correction factor should be obtained from Paragraph 3.1.6. For short cylinders ($\gamma Z < 5$) the C curves should be used. For moderate-length cylinders $5 < \gamma Z < 4000$ the E_1 curve should be used. For long cylinders $\gamma Z > 4000$, the E curve should be used.

3.1.3.4 Torsion.

Isotropic sandwich cylinders in torsion have not received the same attention as cylinders in compression, although both rigid- and weak-core criteria are reasonably well defined. Whereas the transition region between

rigid and weak cores is not as well defined, the methods presented are probably sufficient for design purposes. Information on the transition region is given in References 37 and 47; the latter was used to construct the plot of Figure 3.1-13, which applies to sandwich cylinders with cores exhibiting isotropic shear behavior $G_{xz}/G_{yz} = 1$. The curves of this figure are discontinuous at the value of γZ where the buckling coefficient k_{xy} becomes equal to $1/R$, indicating a change of mode of buckling at that point.

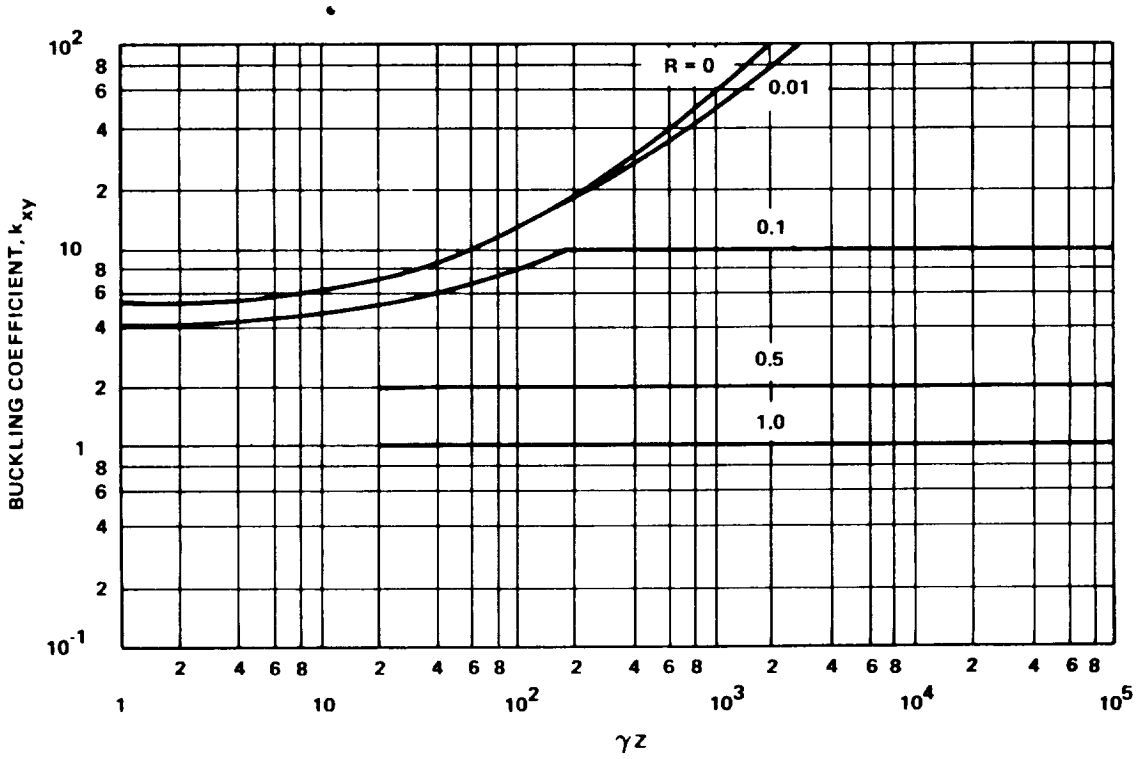

FIGURE 3.1-13. BUCKLING COEFFICIENTS FOR SIMPLY SUPPORTED ISOTROPIC SANDWICH CIRCULAR CYLINDERS SUBJECTED TO TORSION $G_{xz}/G_{yz} = 1.0$

Reference 37 does not support this behavior, but it does not cover a sufficiently wide range of geometric proportions to be used in the construction of the figure. In addition, Reference 37 indicates that there was some scatter in the calculated results used to construct the charts of that reference. In the ranges where comparisons between the data of References 37 and 47 could be made, only rather small discrepancies were noted. The straight-line portion ($\gamma Z > 170$) of the curve of Figure 3.1-13 for a rigid core ($R=0$) is given by the equation

$$k_{xy} = \frac{N_{xy}\, \ell^2}{\pi^2 D_1} = 0.34\ (\gamma Z)^{3/4} \quad . \qquad (86)$$

Experimental data are not available to substantiate Figure 3.1-13 for most sandwich cylinders. From experience with isotropic cylinders, it is indicated that 0.586 is the factor γ to be used with the figure. Here, as with sandwich cylinders for which the density ratio of δ is 0.03 or greater, the same factor should be used unless the design is substantiated by adequate tests. Plasticity may be taken into account by using the A curves of Paragraph 3.1.6.

3.1.4 CYLINDERS WITH AN ELASTIC CORE.

The term "cylinder with an elastic core" defines a thin cylindrical shell enclosing an elastic material that can be either solid or have a hole in its center. This type of shell closely approximates a propellant-filled missile structure. The propellant is generally of a viscoelastic material and therefore is strain-rate sensitive. The core modulus should be obtained from tension or compression tests of the core material simulating its expected strain rate.

Although there are some analytical data for orthotropic shells [48], design curves are given only for isotropic shells and cores. The inverse problem of a core or cushion on the outside of the cylindrical shell is analyzed in Reference 49. Not enough data are available, however, to recommend design curves for this problem.

3.1.4.1 Axial Compression.

The buckling behavior of cylindrical shells with a solid elastic core in axial compression is given in Reference 50. Analytical results obtained from this reference are shown graphically in Figure 3.1-14. For small values of ϕ_1

$$\sigma_p = (1 + \phi_1)\, \sigma_{x_{cr}} \tag{87}$$

where

$$\phi_1 = \frac{\sqrt[4]{12\,(1-\mu^2)}}{4\,(1-\mu_c^2)}\, \frac{E_c}{E} \left(\frac{r}{t}\right)^{3/2} \tag{88}$$

and $\sigma_{x_{cr}}$ is the critical value of axial compression for an isotropic circular cylinder, as found in Paragraph 3.1.1.1. This approximation is accurate for ϕ_1 less than one-half. For larger values of ϕ_1, for example, ϕ_1 greater than 3,

$$\sigma_p = 3/2\, \phi_1^{3/2}\, \sigma_{x_{cr}} \tag{89}$$

The plasticity correlation factors should be determined as in Paragraph 3.1.1.1.

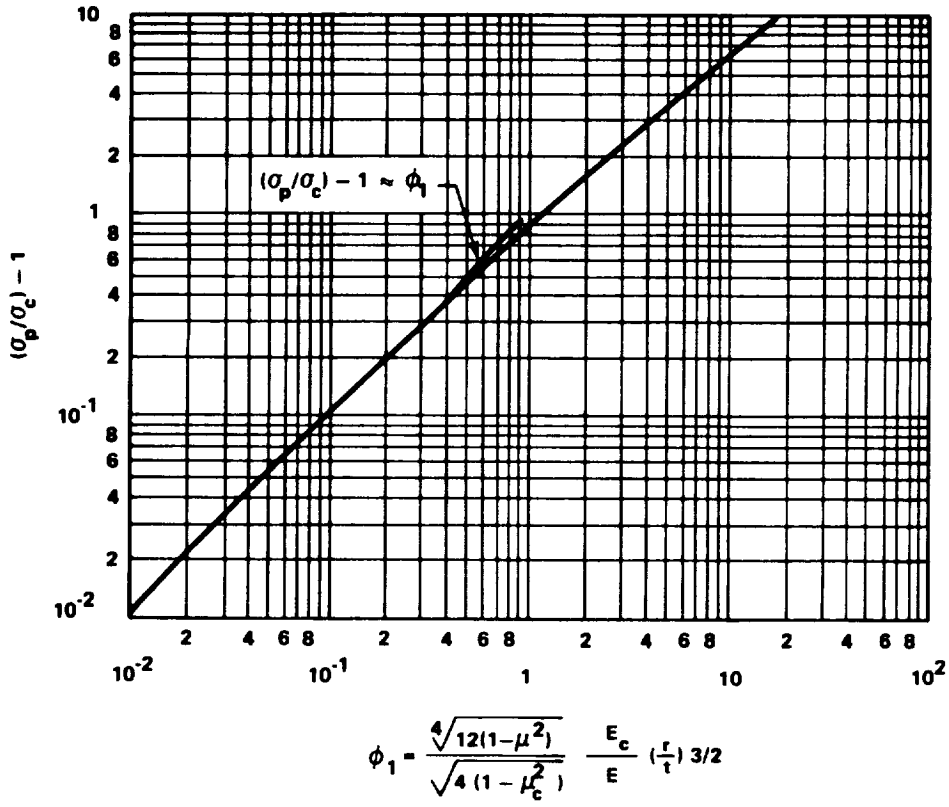

FIGURE 3.1-14. VARIATION OF COMPRESSIVE BUCKLING STRESS WITH CORE STIFFNESS PARAMETER

3.1.4.2 External Pressure.

Analytical curves for the lateral pressure core are presented in Reference 50. A plot of k_{pc} against $\frac{\pi r}{\ell}$ for $\frac{r}{t}$ = 100, 200, 500, or 1000 is shown graphically in Figure 3.1-15. The parameter k_{pc} is expressed by

$$k_{pc} = \frac{pr^3}{D} \quad . \tag{90}$$

These curves are to be used for finite cylinders loaded by lateral pressures.

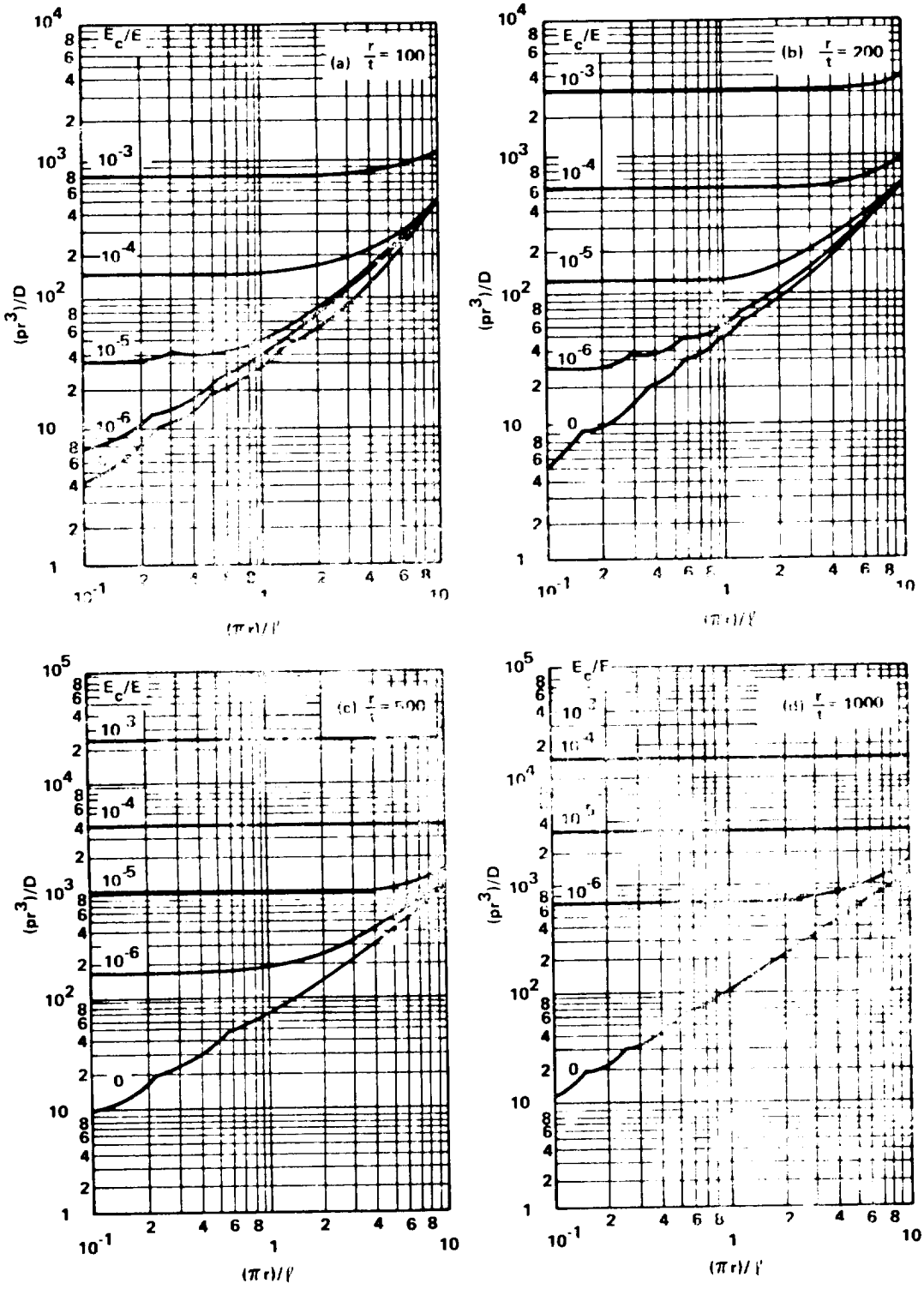

FIGURE 3.1-15. VARIATION OF BUCKLING PRESSURE COEFFICIENT WITH LENGTH AND MODULUS RATIO ($\mu = 0.3$, $\mu_c = 0.5$)

Some cylinders are long enough for the critical pressure to be independent of length; the single curve shown in Figure 3.1-16 can then be used. The straight-line portion of the curve can be approximated by the equation

$$\frac{k_{pc}}{1 + \frac{E_c r}{Et\,(1 - \mu_c)}} = 3\,(\phi_2)^{3/2} \qquad (91)$$

where

$$\phi_2 = \frac{3\,(1 - \mu^2)}{1 - \mu_c^2}\ \frac{E_c}{E}\ \left(\frac{r}{t}\right)^3 \qquad (92)$$

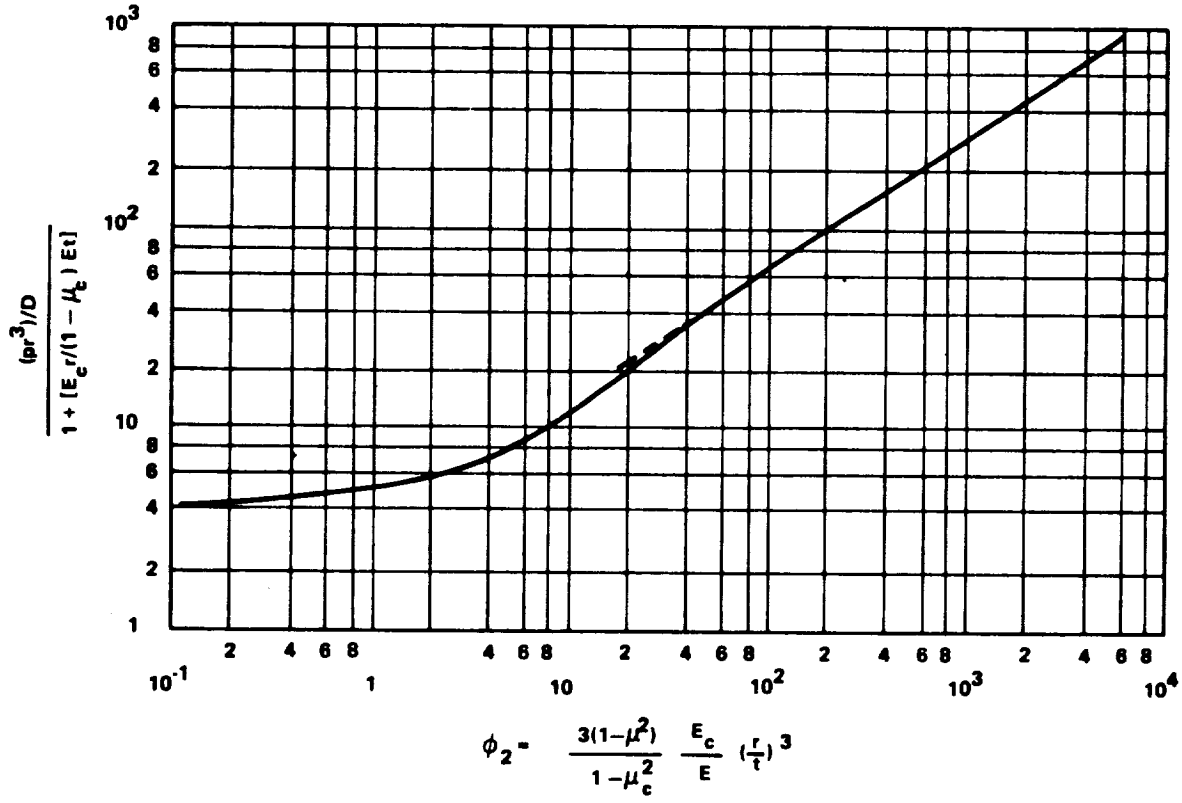

FIGURE 3.1-16. BUCKLING PRESSURE COEFFICIENTS FOR LONG CYLINDER WITH A SOLID CORE

The few experimental data points available indicate good agreement between analysis and experiment, but one test point falls 4 percent below theory. Hence, a correlation factor of 0.90 is recommended for use in conjunction with the curves in Figures 3.1-15 and 3.1-16. A reinvestigation of the factor may be warranted as more data become available. Plasticity should be accounted for by using curves A in Paragraph 3.1-6.

3.1.4.3 Torsion.

The buckling behavior of cylindrical shells with an elastic core is analytically described in Reference 51 and is shown graphically in Figure 3.1-17.

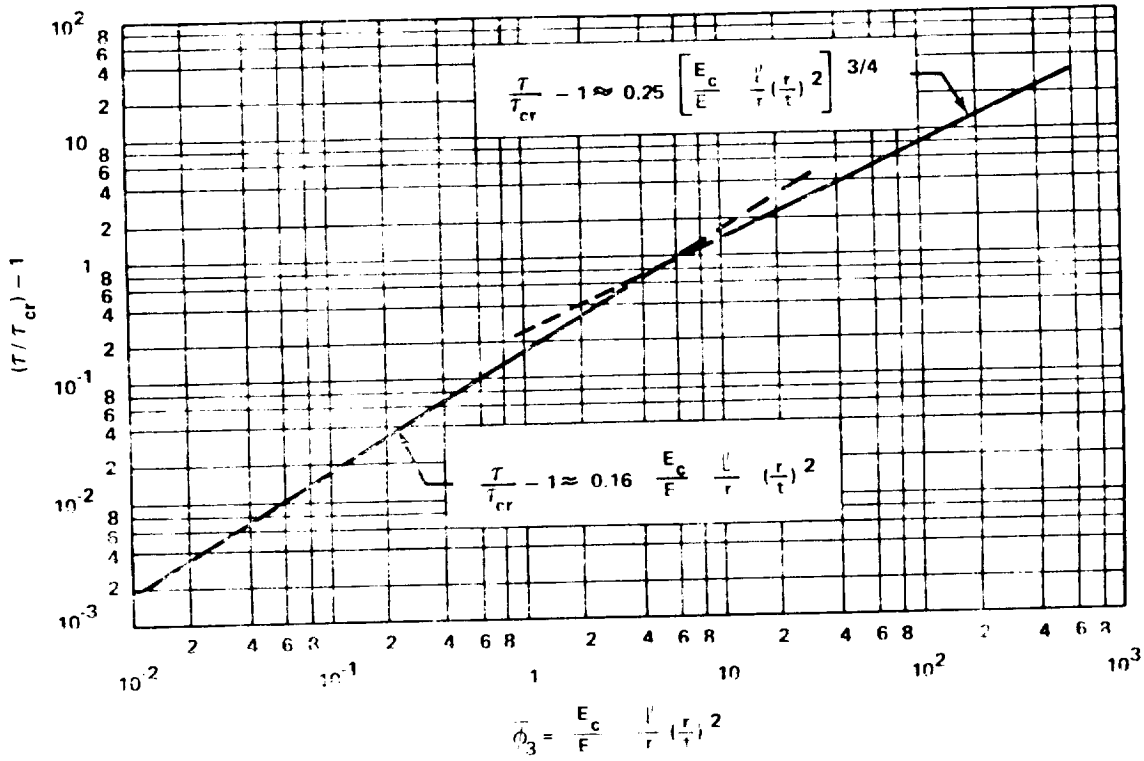

FIGURE 3.1-17. TORSIONAL BUCKLING COEFFICIENTS FOR CYLINDERS WITH AN ELASTIC CORE

For small values of ϕ_3 ($\phi_3 < 7$), the analytical results can be approximated by

$$\frac{\tau}{\tau_{xy_{cr}}} = 1 + 0.16\,\phi_3 \qquad (93)$$

where

$$\phi_3 = \frac{E_c}{E}\left(\frac{\ell}{r}\right)\left(\frac{r}{t}\right)^2 \qquad (94)$$

and $\tau_{xy_{cr}}$ is the torsional buckling stress given by equation (16), with γ equal to unity. When ϕ_3 is greater than 10, the analytical results follow the curve

$$\frac{\tau}{\tau_{xy_{cr}}} = 1 + 0.25\,(\phi_3)^{3/4} \qquad (95)$$

Experimental data are not available for this loading condition. The experimental points obtained from cylinders with an elastic core for axial compression and external pressure, however, show better correlation with theory than the corresponding experimental results for the unfilled cylinder. Hence, conservative-design curves can be obtained by calculating $\tau_{xy_{cr}}$ in equations (93) and (95) with the correlation factor given by equation (19) and the plasticity factor given by curves A in Paragraph 3.1-6.

3.1.4.4 Combined Axial Compression and Lateral Pressure.

Interaction curves for cylinders with an elastic core subjected to combined axial compression and lateral pressure are shown in Figure 3.1-18.

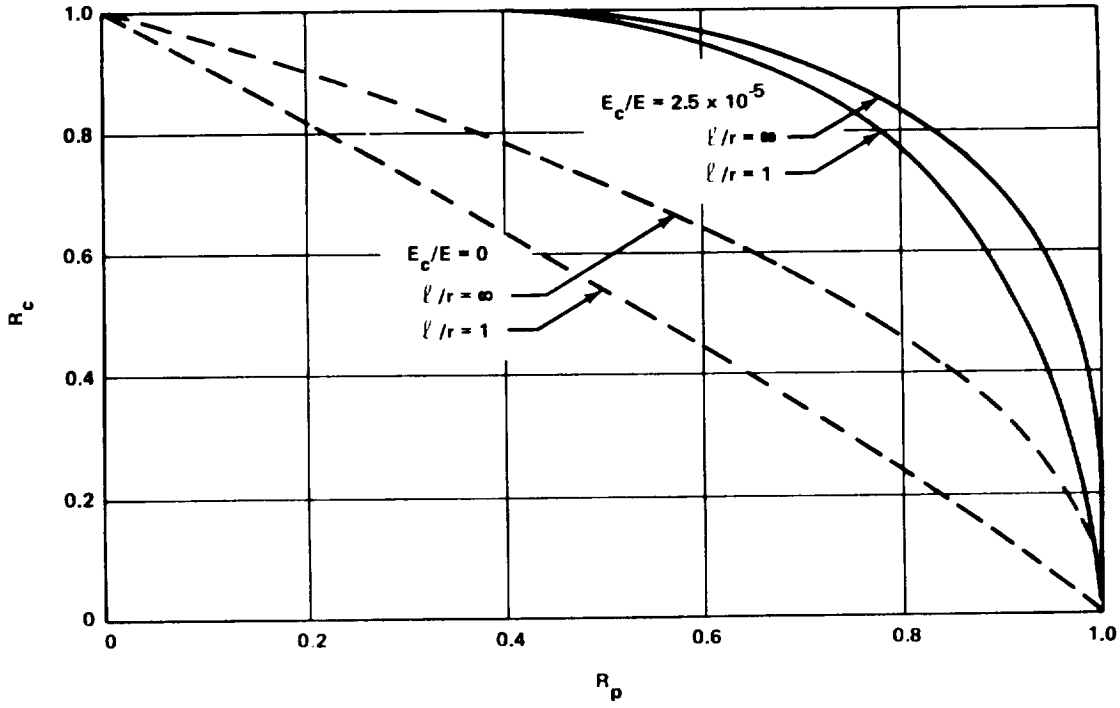

FIGURE 3.1-18. INTERACTION CURVES FOR CYLINDERS (r/t = 300) WITH AN ELASTIC CORE

These curves were obtained analytically in Reference 50 and indicate that for a sufficiently stiff core, the critical axial compressive stress is insensitive to lateral pressure, and similarly, the critical lateral pressure is insensitive to axial compression. Until more experimental data become available, the use of a straight-line interaction curve is recommended for conservative design.

3.1.5 DESIGN OF RINGS.

Little information is available on which to base the design of rings for cylinders to exclude general instability failures. The criterion of Reference 52 is frequently cited as applicable to cylinders subjected to bending or compression. Unfortunately, this criterion is empirical and based on data from

test cylinders with proportions of little interest in contemporary design. A few checks made on cylinders in use have indicated that the criterion usually is conservative, but this may not be so in certain cases [10, 53].

A less direct procedure for designing rings may be used. It consists simply of calculating the failing load of the cylinder in the so-called general-instability mode, which involves failure of the rings, as well as calculation of the failing load of the cylinder for wall failure between rings. Both calculations are made for several ring weights. If such calculations are plotted against ring weight, the weight necessary to force failure in the desired mode can be ascertained. In addition, the amount of error in weight from uncertainties in the calculations can be judged. Presumably, there may be some interaction between failing modes; thus, somewhat heavier rings than those indicated by the calculations should be used.

This method of designing rings is, of course, applicable to all types of loading and all types of wall construction. It also has the advantage of giving the designer some feeling for the influence of the various factors which determine ring weight.

A study of References 53 and 54, which present general linear analyses of ring-stiffened isotropic cylinders in torsion and of orthotropic cylinders in compression, indicates that the recommended procedure gives the same result as general theory for all cylinders except those with a single ring dividing the cylinder into two equal bays.

3.1.6 PLASTICITY CORRECTION FACTOR.

The effect of plasticity on the buckling of shells can be accounted for by the use of the plasticity coefficient, η. This coefficient is defined by the ratio

$$\eta = \frac{\sigma_{cr}}{\sigma_e}$$

where

σ_{cr} = the actual buckling stress.

σ_e = the elastic buckling stress (the stress at which buckling would occur if the material remained elastic at any stress level).

The elastic buckling stress, therefore, is given by the equation

$$\sigma_e = \frac{\sigma_{cr}}{\eta} \quad .$$

The definition of η depends on σ_{cr}/σ_e, which is a function of the loading, the type of shell, the boundary conditions, and the type of construction. For example, the η recommended for homogeneous isotropic cylindrical shells with simply supported edges subjected to axial compression is

$$\eta = \frac{\sqrt{E_t E_s}}{E} \left[\frac{1 - \mu_e^2}{1 - \mu^2} \right]^{1/2}$$

where E_t, E_s and μ are the tangent modulus, secant modulus and Poisson's ratio, respectively, at the actual buckling stress, and μ_e is the elastic Poisson's ratio.

For a given material, temperature, and η, a chart may be prepared for σ_{cr}/η versus σ_{cr}. By first calculating the elastic buckling stress, σ_{cr}/η, the actual buckling stress σ_{cr} can be read from the chart of σ_{cr}/η versus σ_{cr}. This method eliminates an iterative procedure which would otherwise be necessary.

Figures 3.1-19 through 3.1-25 present curves of σ_{cr}/η versus σ_{cr} for some materials and temperatures commonly encountered in the aerospace industry. In many cases, the curves are so close together that they are drawn as one curve.

The η used to determine each curve is defined as follows:

Curve	η	
A	E_s/E	
B	$\frac{E_s}{E}\left[0.330 + 0.670\sqrt{\mu^2 + (1-\mu^2)\frac{E_t}{E_s}}\right]$	
C	$\frac{E_s}{E}\left[1/2 + 1/2\sqrt{\mu^2 + (1-\mu^2)\frac{E_t}{E_s}}\right]$	
D	$\frac{E_s}{E}\left[0.352 + 0.648\sqrt{\mu^2 + (1-\mu^2)\frac{E_t}{E_s}}\right]$	
E	$\mu^2 E_s/E + (1-\mu^2) E_t/E$	
F	$0.046 E_s/E + 0.954 E_t/E$	$(\mu = 0.33)$
G	E_t/E	
E_1	$\frac{\sqrt{E_t E_s}}{E}\left[\frac{1-\mu_e^2}{1-\mu^2}\right]^{1/2}$	

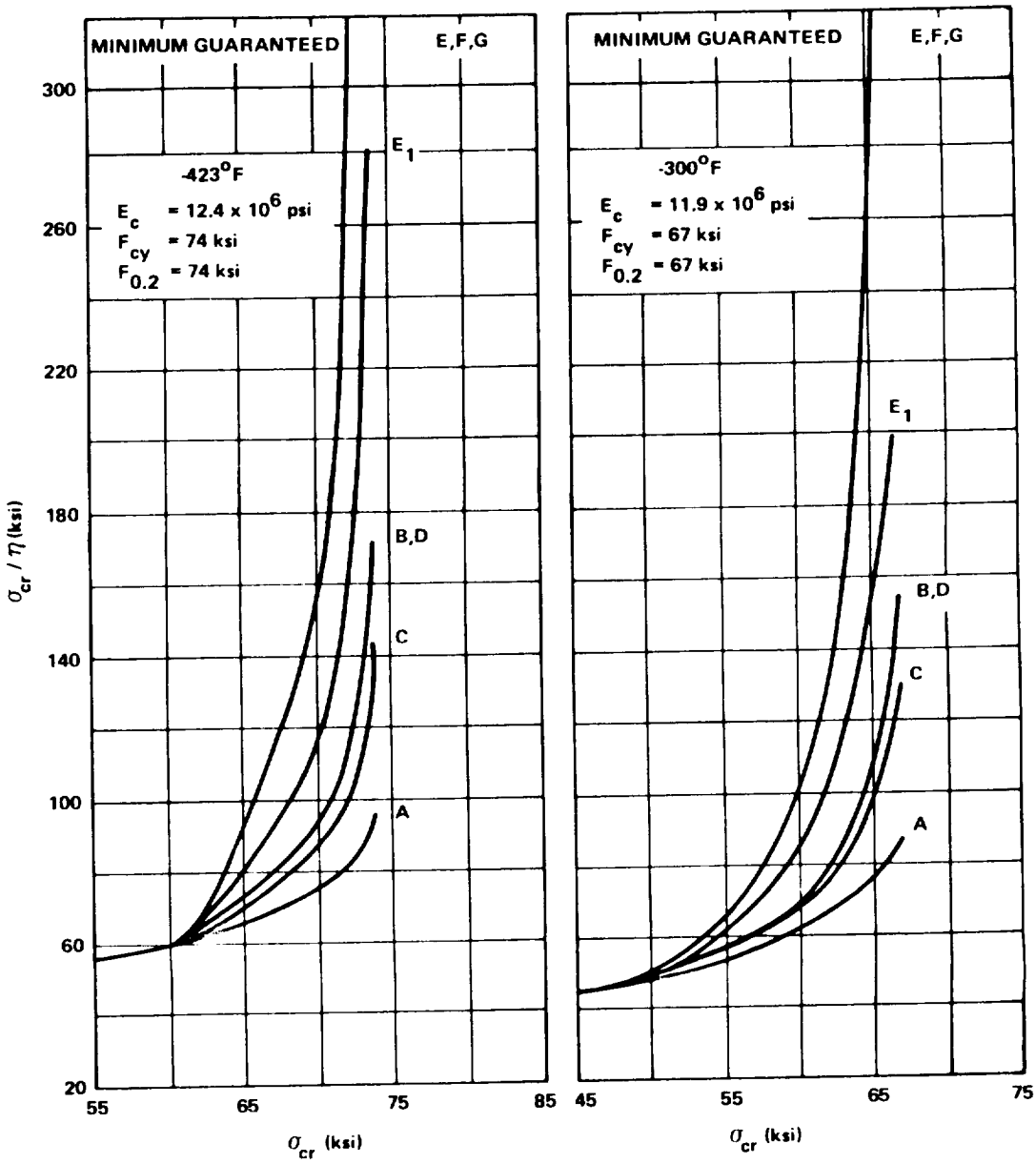

FIGURE 3.1-19. PLASTICITY CORRECTION CURVES FOR 2014-T6, -T651 ALUMINUM ALLOY SHEET AND PLATE (-423° F, -300° F)

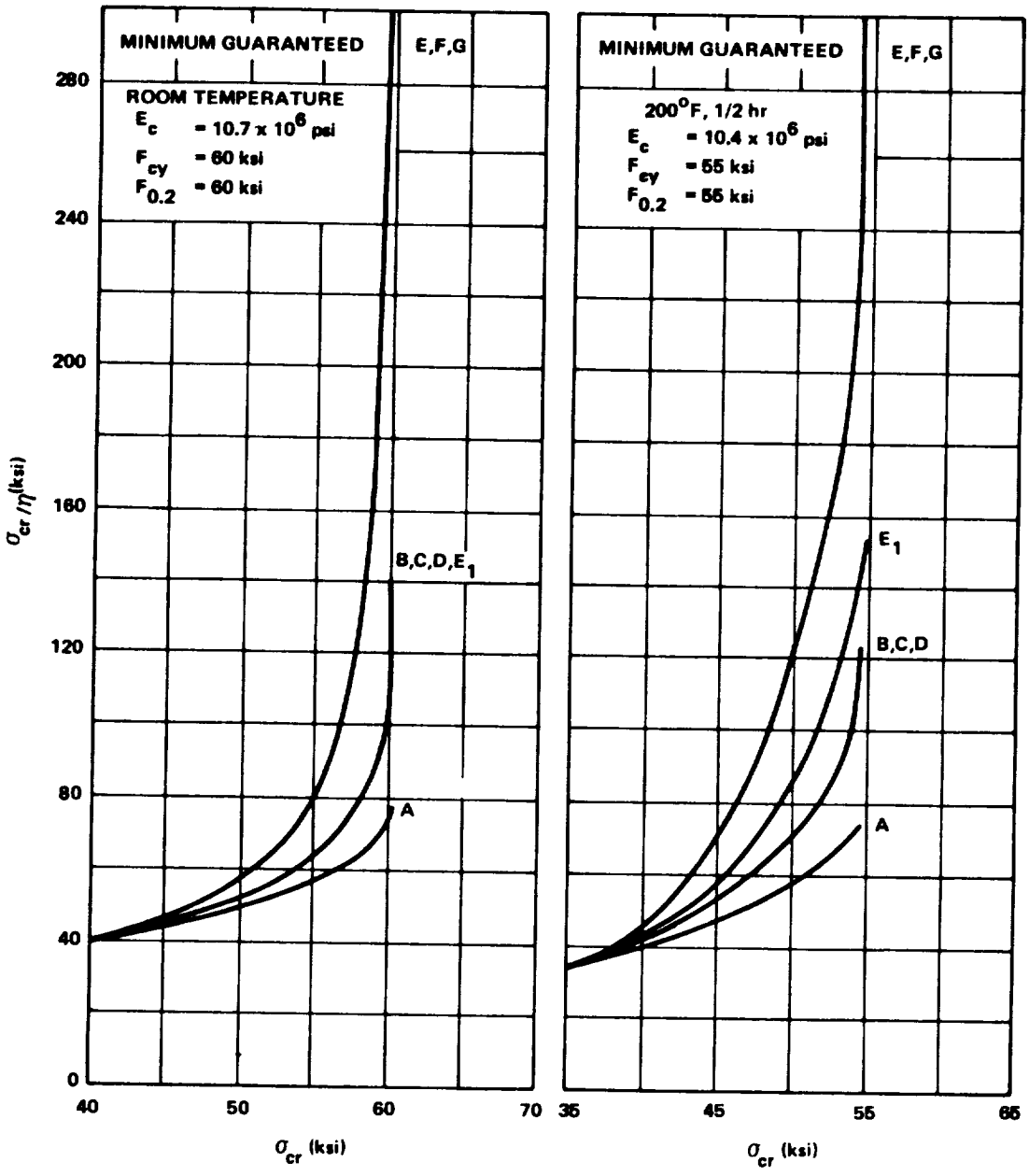

FIGURE 3.1-20. PLASTICITY CORRECTION CURVES FOR 2014-T6, -T651 ALUMINUM ALLOY SHEET AND PLATE (room temp.; 200°F, 1/2 hr)

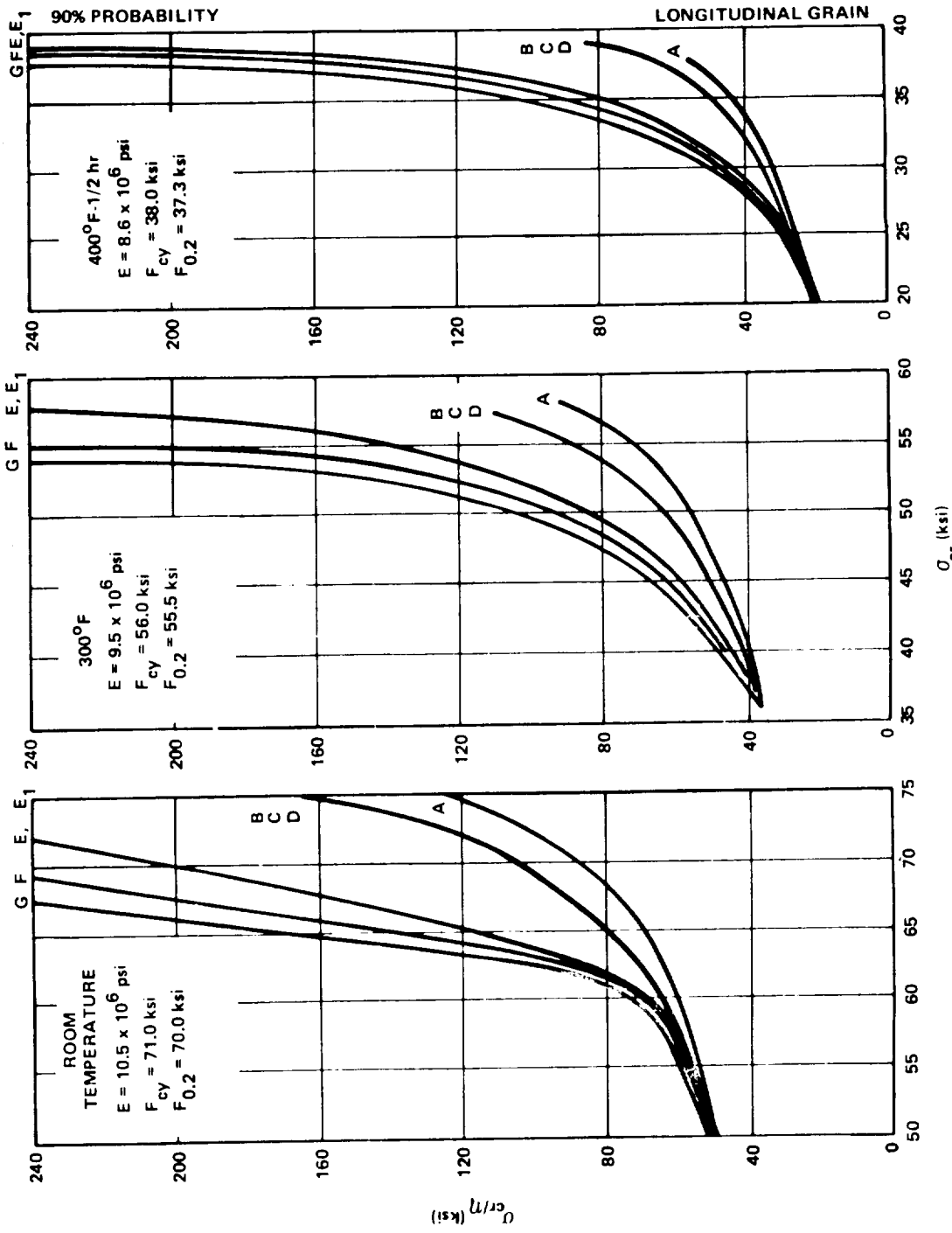

FIGURE 3.1-21. PLASTICITY CORRECTION CURVES FOR BARE 7075-T6 ALUMINUM ALLOY SHEET

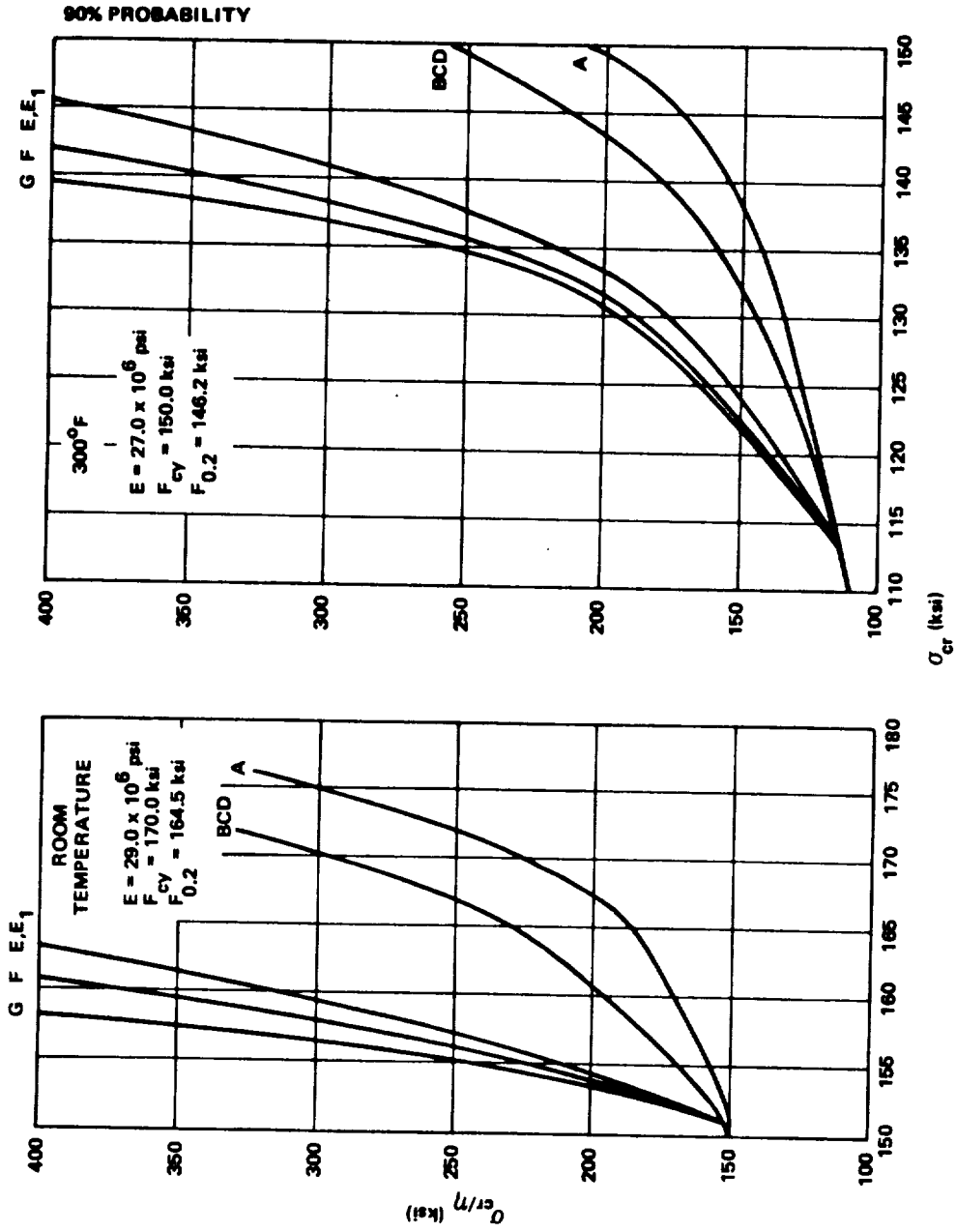

FIGURE 3.1-22. PLASTICITY CORRECTION CURVES FOR ALLOY STEEL 4130, 4140, AND 4340 (180 000 psi)

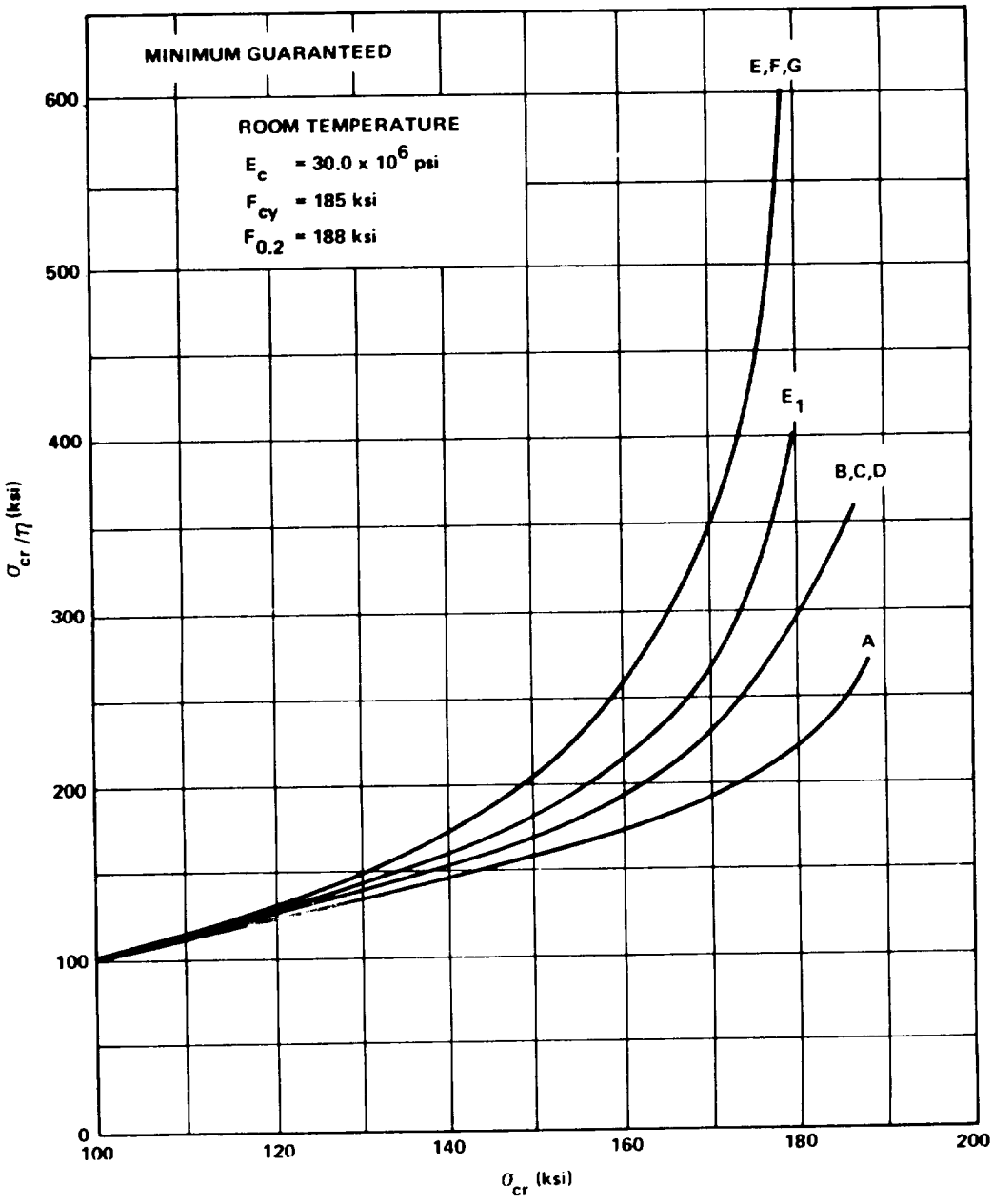

FIGURE 3.1-23. PLASTICITY CORRECTION CURVES FOR PH 15-7 Mo STAINLESS STEEL SHEET AND PLATE — RH 1050, FH 1075 (room temp.)

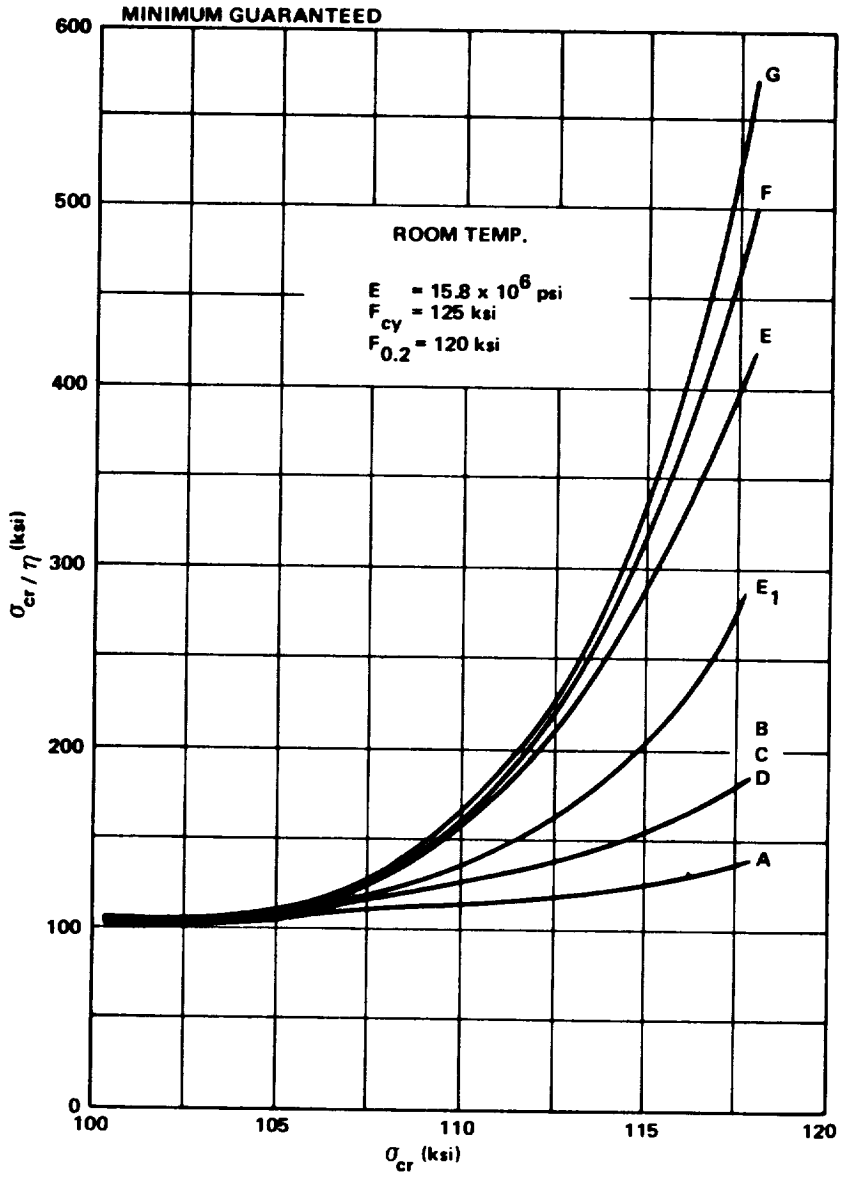

FIGURE 3.1-24. PLASTICITY CORRECTION CURVES FOR TITANIUM ALLOY SHEET < 0.25 6AL-4V ANNEALED LB0170-113

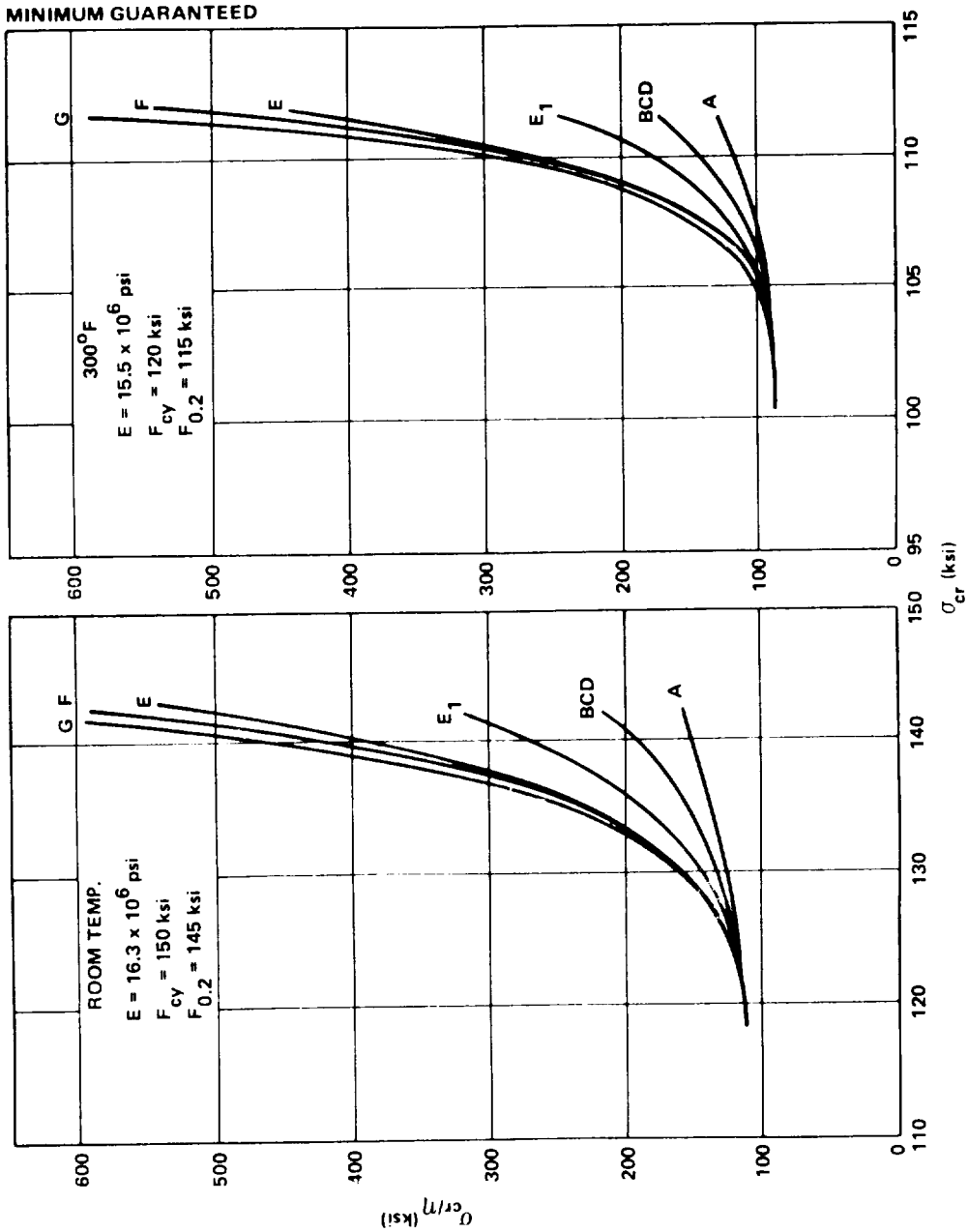

FIGURE 3.1-25. PLASTICITY CORRECTION CURVES FOR TITANIUM ALLOY SHEET < 0.25 6AL-4V CONDITION (SOLUTION-TREATED AND ANNEALED)

Although the value of μ is a function of the stresses for stresses in excess of the proportional limit, the plasticity curves were obtained assuming the conservative value of $\mu = 1/3$. The difference between using the value of $\mu = 1/3$ and $\mu = 1/2$ is small except for curves E and F.

It is worth noting that for curve A, $\eta = E_s/E$; for curve G, $\eta = E_t/E$ and, on the remaining curves, η is a function of both E_t and E_s. It can be seen that curves A and G bound the range of η. Curve G is the most conservative, whereas curve A results in the smallest possible reduction in the buckling load due to plasticity.

3.2 CONICAL SHELLS.

This section recommends practices for predicting buckling of uniform stiffened and unstiffened circular conical shells under various types of static loading and suggests procedures that yield estimates of static buckling loads which are considered to be conservative.

Many studies have been conducted of the buckling of conical shells under various loading conditions. Knowledge of the elastic stability of conical shells, however, is not as extensive as that of cylindrical shells. Whereas the behavior of the two types of shells appears to be similar, significant differences in experimental results remain unexplained. Frequently, there are insufficient data to cover the wide range of conical-shell geometric parameters. In addition, some important loading cases and the effects of edge conditions remain to be studied. Some of these problems can be treated by digital computers. One such program is given in References 1 and 2.

3.2.1 ISOTROPIC CONICAL SHELLS.

The following are the recommended design procedures for isotropic conical shells under axial compression, bending, uniform hydrostatic pressure, and torsion, along with those for combined loads.

3.2.1.1 Axial Compression.

For conical shells under axial compression, there is considerable disagreement between experimental loads and the loads predicted by theory. These discrepancies have been attributed to the effects of imperfections of the structure and of edge-support conditions different from those assumed in the analysis, as well as to shortcomings of the small-deflection theory used.

A theoretical analysis [3] indicates that the critical axial load for long conical shells can be expressed as

$$P_{cr} = \gamma \frac{2\pi Et^2 \cos^2 \alpha}{\sqrt{3(1-\mu^2)}} \qquad (1)$$

with the theoretical value of γ equal to unity. Experiments [4,5] indicate that within the range of the geometries of the tested specimens, there is no apparent effect of conical-shell geometry on the correlation factor. Therefore, γ can be taken as a constant. At present, it is recommended that γ be taken as the constant value.

$$\gamma = 0.33 \qquad (10 \text{ deg} < \alpha < 75 \text{ deg}) \quad , \qquad (2)$$

which gives a lower bound to the experimental data. Buckling-load coefficients for cone semivertex angles greater than 75 deg must be verified by experiment because data are not available in this range. For $\alpha < 10$ deg the buckling load coefficient can be taken as that of a cylindrical shell having the same wall thickness as the cone and a length and radius equal to the slant height and average radius of curvature of the cone, respectively.

No studies have been published on the compressive buckling of conical shells in the yield region. Because the nominal stress level in a conical shell varies along its length, the effects of plasticity in conical shells are likely to differ from those in cylindrical shells. A conservative estimate of plasticity effects in conical shells could be obtained, however, if the reduction factors for cylindrical shells are used (Paragraph 3.1.1.1). The secant and tangent moduli should correspond to the maximum membrane compressive stress

$$\sigma_{max} = \frac{P}{2\pi \rho_1 t \cos^2 \alpha} \qquad (3)$$

Figure 3.2-1 is an alignment chart devised to determine the critical axial force (P_{cr}) from equation (1) where the shell thickness (t) and the semivertex angle (α) are known. This nomograph is applicable in the elastic range for aluminum alloy.

From equations (1) and (3) the maximum membrane compressive stress is

$$\sigma_{cr} = \gamma E \frac{t}{r_1} \cos \alpha \quad . \tag{4}$$

Figure 3.2-2a is a nomograph of equation (4) to determine the critical axial stress when the shell thickness, small radius, and semivertex angle are known. The following example shows the use of the nomograph. A conical shell has a thickness (t) of 0.06 in., a small radius (r_1) of 40 in., and a semivertex angle of 60 deg. Determine the critical compressive stress resulting from an axial force. On the nomograph of Figure 3.2-2 join 40 on the r_1 scale with 0.06 on the t scale and extend the line until it meets line QR. From this point draw a line to 60 deg on the scale. This line intersects the σ_{cr} scale at 2600 psi, which is the critical buckling stress.

Figure 3.2-2b is useful if the stress falls into the plastic range for the three materials shown.

3.2.1.2 Bending.

For conical shells in bending, buckling occurs when the maximum compressive stress at the small end of the cone is equal to the critical compressive stress of a cylinder having the same wall thickness and the same local radius of curvature. The buckling moment is given by

$$M_{cr} = \frac{\gamma \pi E t^2 r_1 \cos^2 \alpha}{[3(1-\mu^2)]^{1/2}} \tag{5}$$

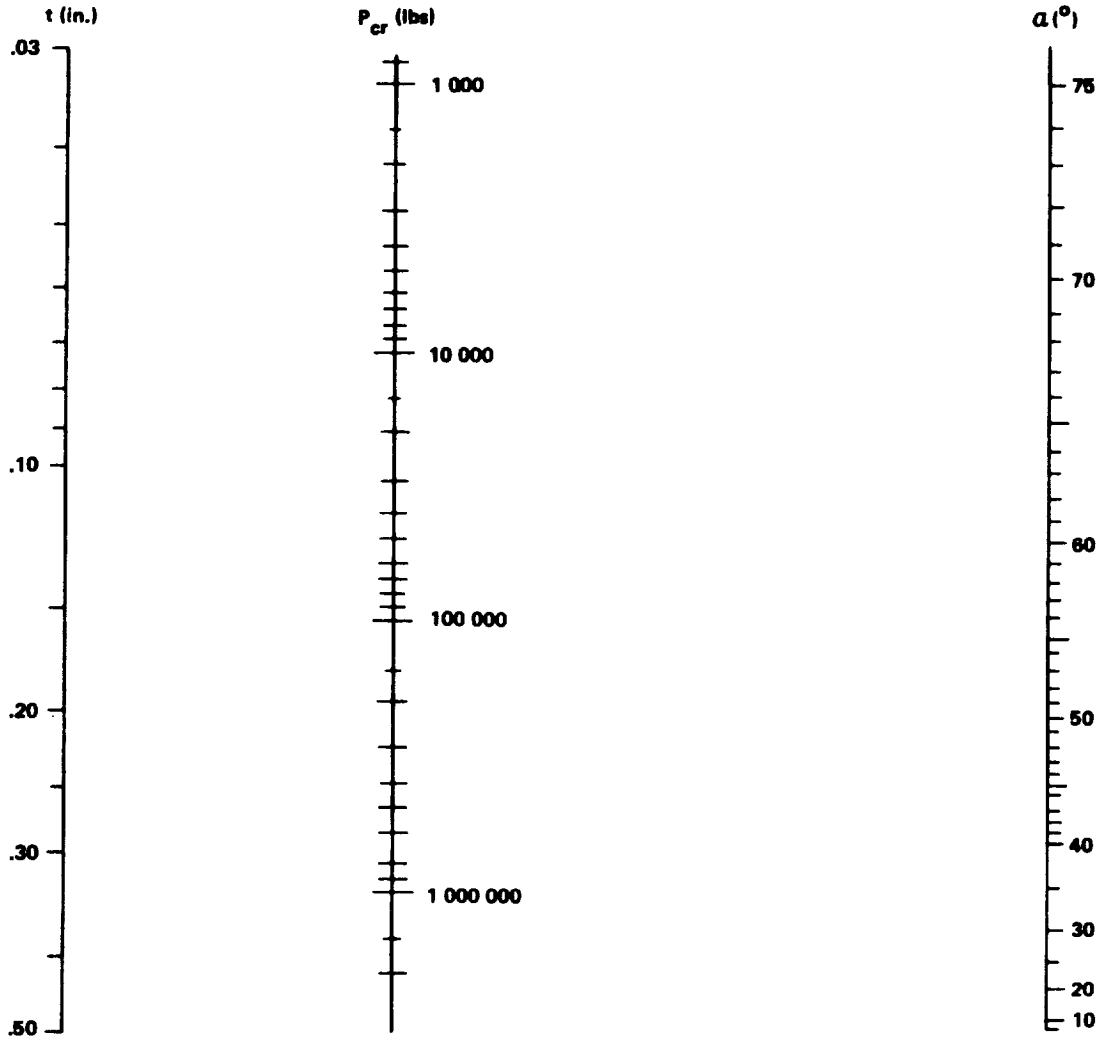

FIGURE 3.2-1. CRITICAL AXIAL LOAD FOR LONG CONICAL SHELL (ALUMINUM ALLOY MATERIAL), $E = 10.4 \times 10^6$ psi

with the theoretical value of γ equal to unity. Based on experimental data [6] it is recommended that the coefficient γ be taken as the constant value,

$$\gamma = 0.41 \qquad (10 \text{ deg} < \alpha < 60 \text{ deg}) \qquad . \qquad (6)$$

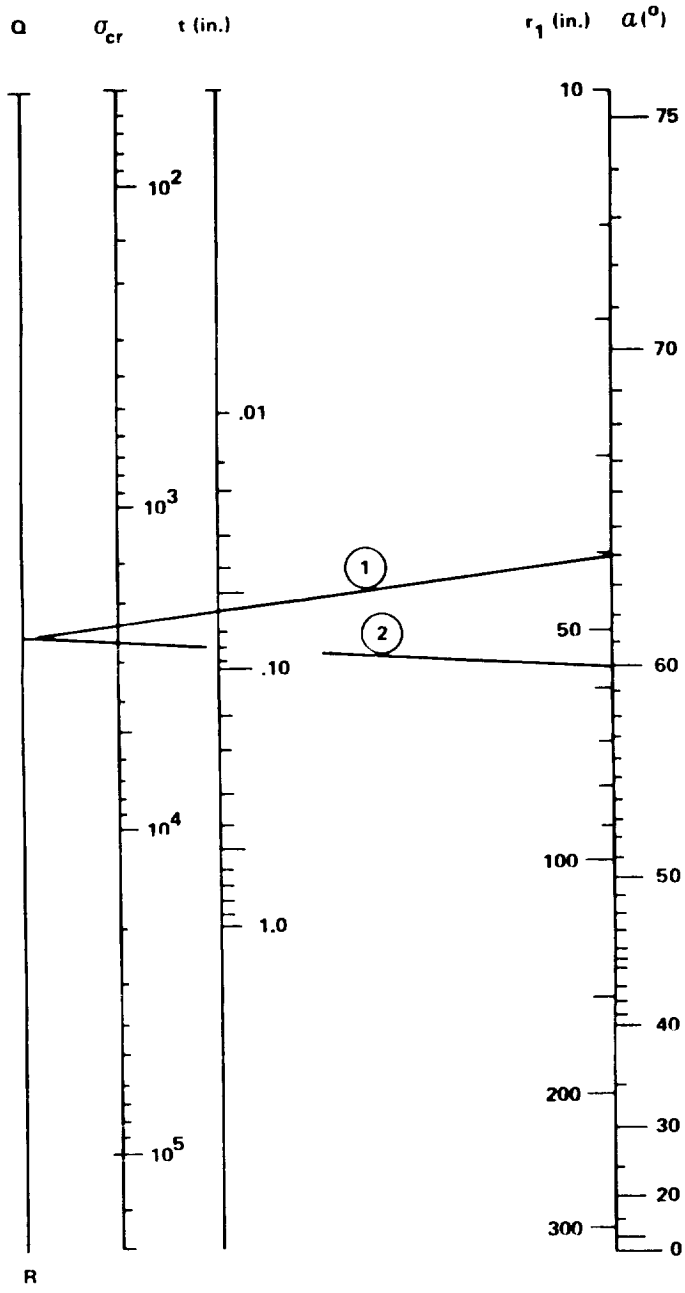

FIGURE 3.2-2a. CRITICAL COMPRESSIVE STRESS FOR LONG CONICAL SHELL (ALUMINUM ALLOY MATERIAL), $E = 10.4 \times 10^6$ psi

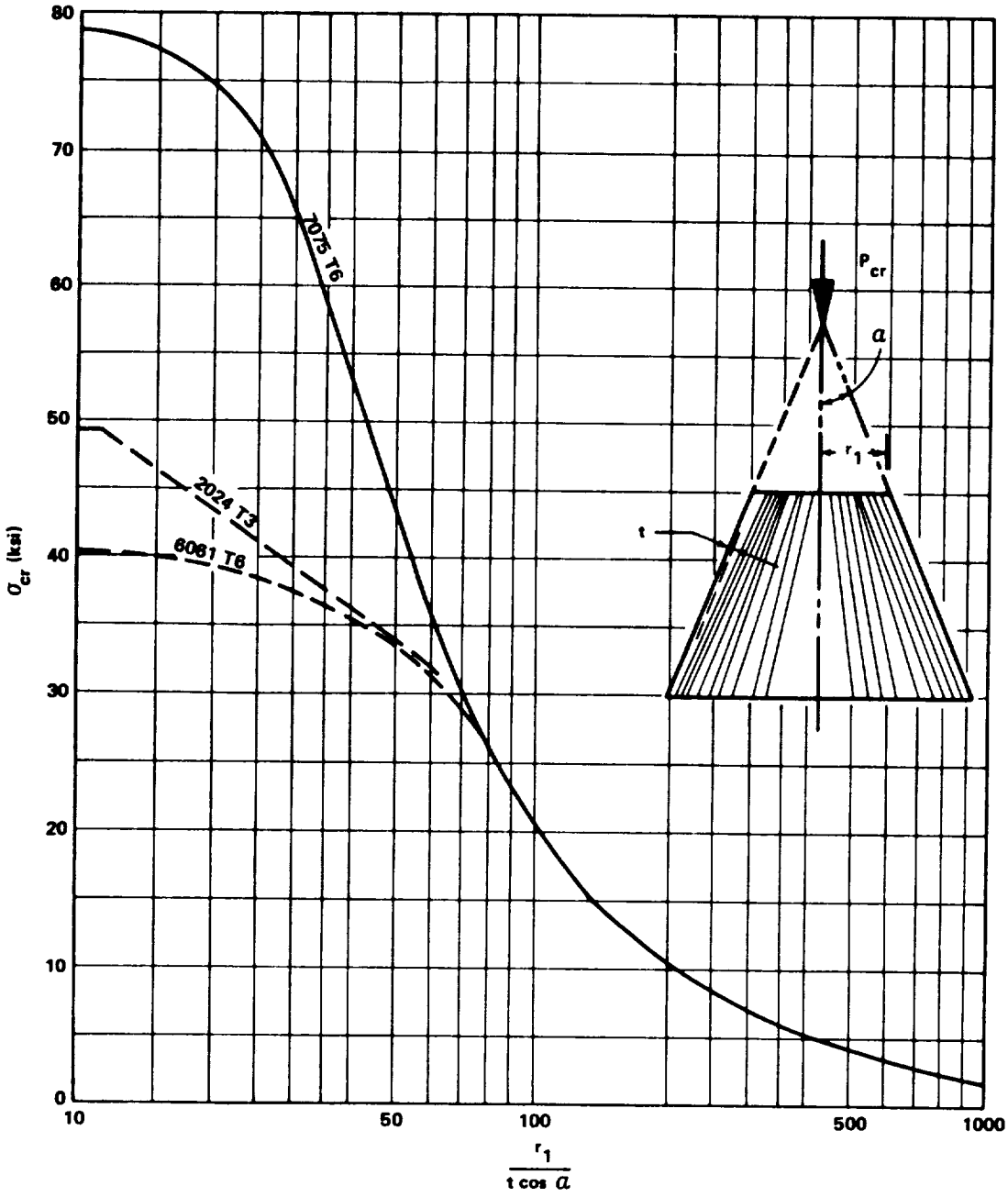

FIGURE 3.2-2b. BUCKLING OF ISOTROPIC CONICAL SHELL UNDER AXIAL COMPRESSION

Buckling load coefficients for cone semivertex angles greater than 60 deg must be verified by test. Buckling coefficients for equivalent cylindrical shells in bending can be used with semivertex angles less than 10 deg. For conical shells subjected to plastic stresses, the correction suggested for conical shells in axial compression may be used.

The buckling moment M_{cr} may be obtained from the nomograph of Figure 3.2-3, when the shell thickness t, the small radius r_1, and the semivertex angle α are known. The lines 1 and 2 on Figure 3.2-3 show the proper sequence of parameter alignment. This illustration can also be used for design purposes when a moment is given and a required thickness is needed.

3.2.1.3 Uniform Hydrostatic Pressure.

The theoretical buckling pressure of a conical shell which buckles into several circumferential waves $(n > 2)$ can be expressed [7] in the approximate form

$$p_{cr} = \frac{0.92\, E\, \gamma}{\left(\frac{L}{\bar{\rho}}\right)\left(\frac{\bar{\rho}}{t}\right)^{5/2}} \quad . \tag{7}$$

Experiments [8, 9] show a relatively wide scatter band for the value of γ but indicate that the constant value

$$\gamma = 0.75 \tag{8}$$

should provide a lower bound for the available data. Figure 3.2-4 gives the solution to equation (7) for values of $\bar{\rho}/t$ and $L/\bar{\rho}$. The curves are applicable in the elastic range only.

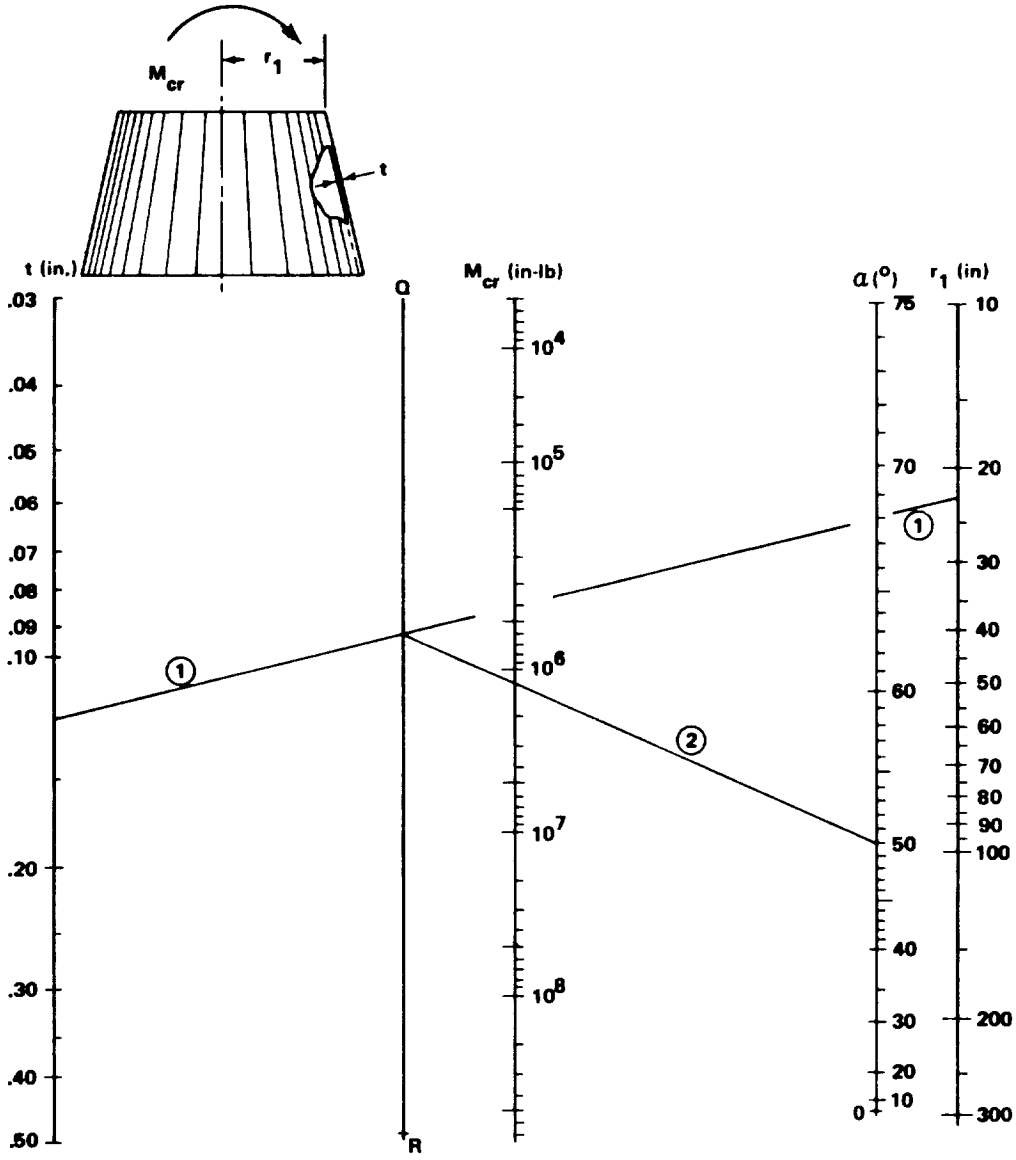

FIGURE 3.2-3. BUCKLING MOMENT FOR CONICAL TRUNCATED SHELL (ALUMINUM ALLOY MATERIAL), $E = 10.4 \times 10^6$ psi

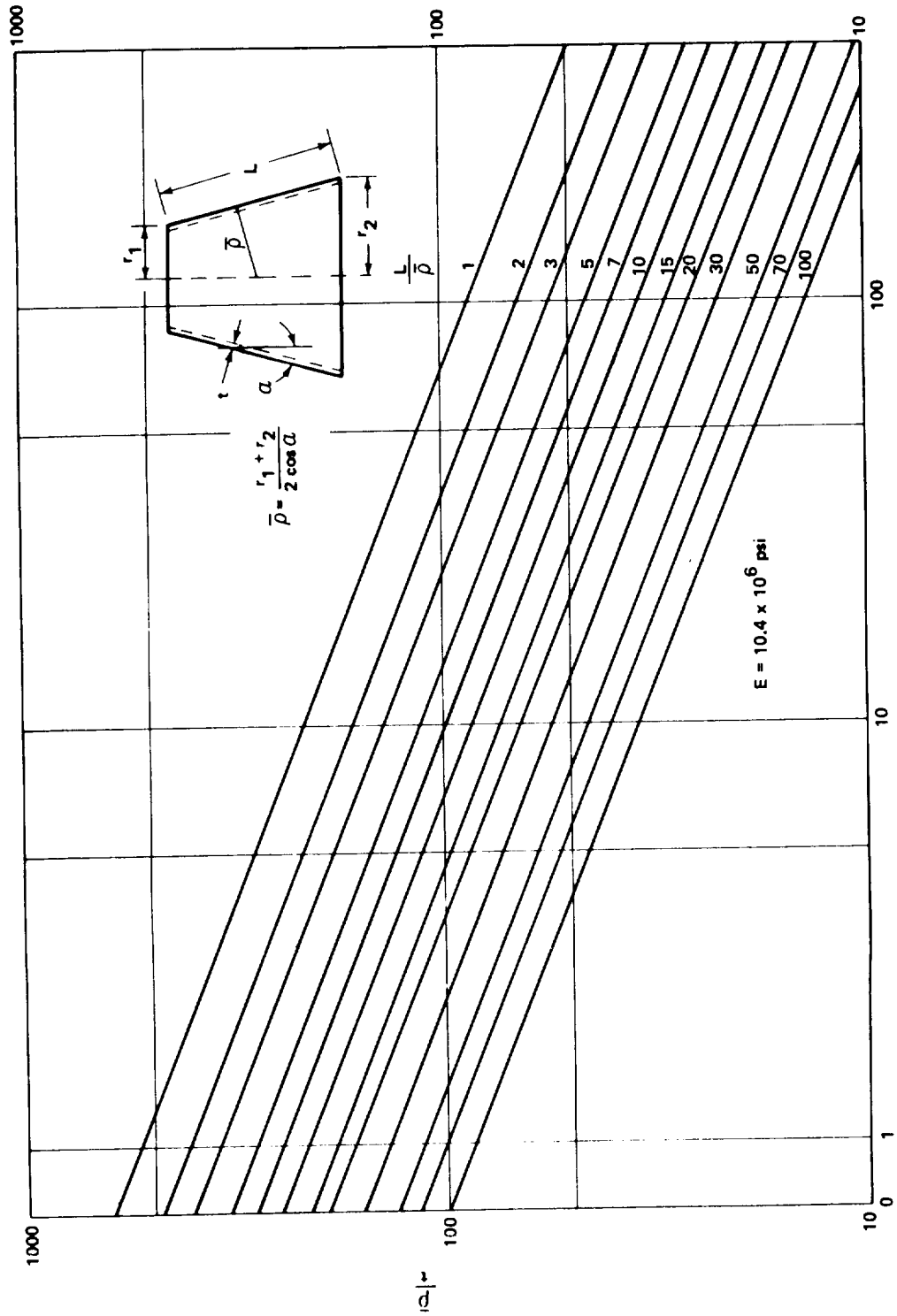

FIGURE 3.2-4. BUCKLING ALLOWABLE PRESSURES OF ISOTROPIC CONICAL SHELL UNDER UNIFORM EXTERNAL HYDROSTATIC PRESSURE

For conical shells which buckle in the plastic range, the plasticity correction for moderate-length cylindrical shells may be used for the range of the conical shell geometries considered. The procedure is to use the E_1 curves in Paragraph 3.1.6. The moduli should correspond to the maximum circumferential compressive stress at the large end of the conical shell:

$$\sigma_{max} = p_{cr} (\rho_2/t) \quad . \tag{9}$$

3.2.1.4 Torsion.

An approximate equation for the critical torque of a conical shell [10] is

$$T_{cr} = 52.8 \gamma D \left(\frac{t}{\ell}\right)^{1/2} \left(\frac{r}{t}\right)^{5/4} \tag{10}$$

where

$$r = r_2 \cos \alpha \left\{1 + \left[1/2\left(1 + \frac{r_2}{r_1}\right)\right]^{1/2} - \left[1/2\left(1 + \frac{r_2}{r_1}\right)\right]^{-1/2}\right\} \frac{r_1}{r_2} \quad . \tag{11}$$

The variation of $r/r_2 \cos \alpha$ with r_1/r_2 is shown in Figure 3.2-5. For design purposes it is recommended that the torsional-moment coefficient in equation (10) be taken as the constant value

$$\gamma = 0.67 \quad . \tag{12}$$

Figure 3.2-6 is a nomograph devised to determine the buckling torque of a conical shell (equation 10) when t, t/ℓ, and r/t are known.

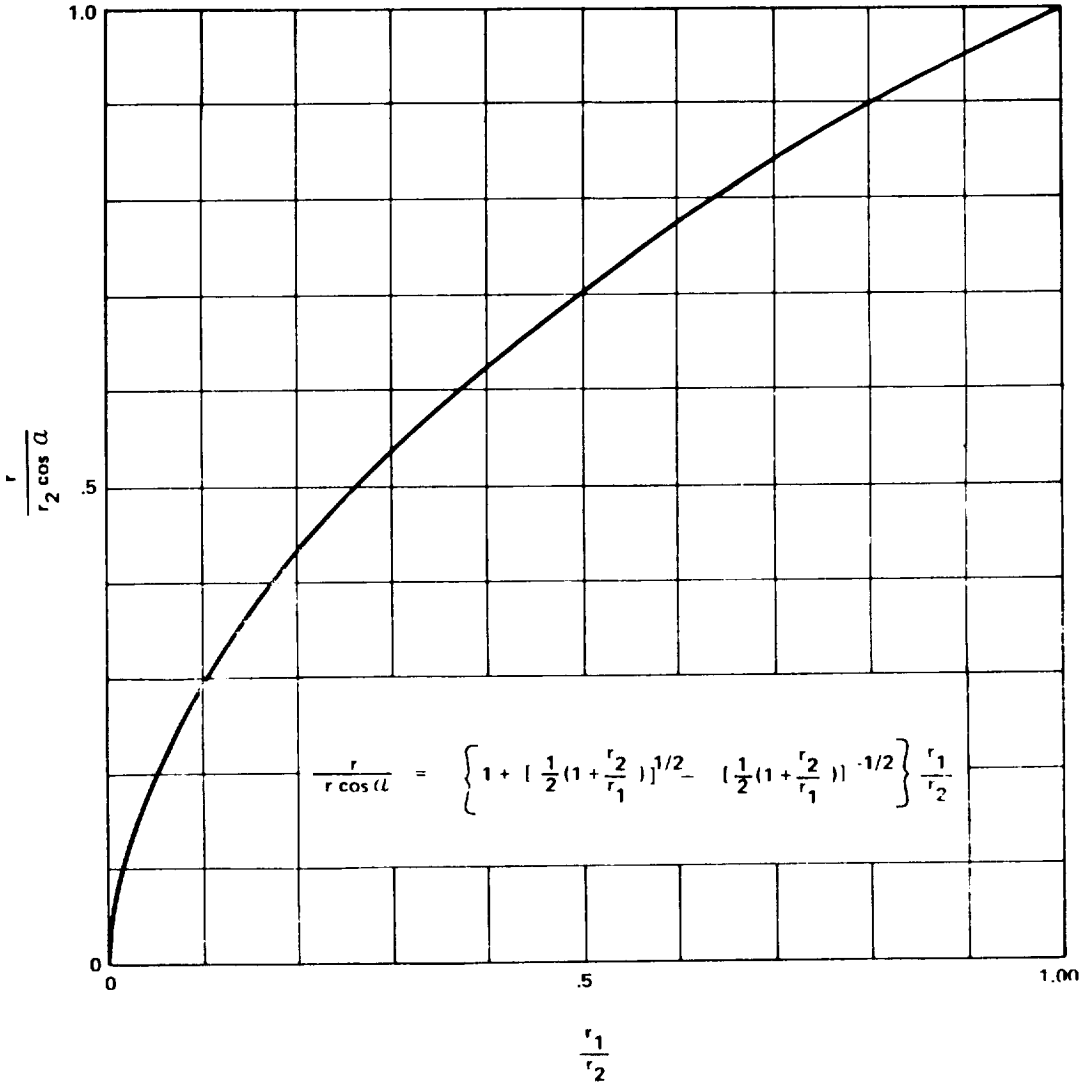

FIGURE 3.2-5. VARIATION OF $r/r_2 \cos \alpha$ WITH r_1/r_2

No data are available for the plastic buckling of conical shells in torsion. The plasticity factor used for cylindrical shells in torsion should, however, give conservative results. The secant modulus should correspond to the maximum shear stress at the small end of the cone, given by

$$\tau_{cr} = \frac{T_{cr}}{2\pi r_1^2 t} \qquad (13)$$

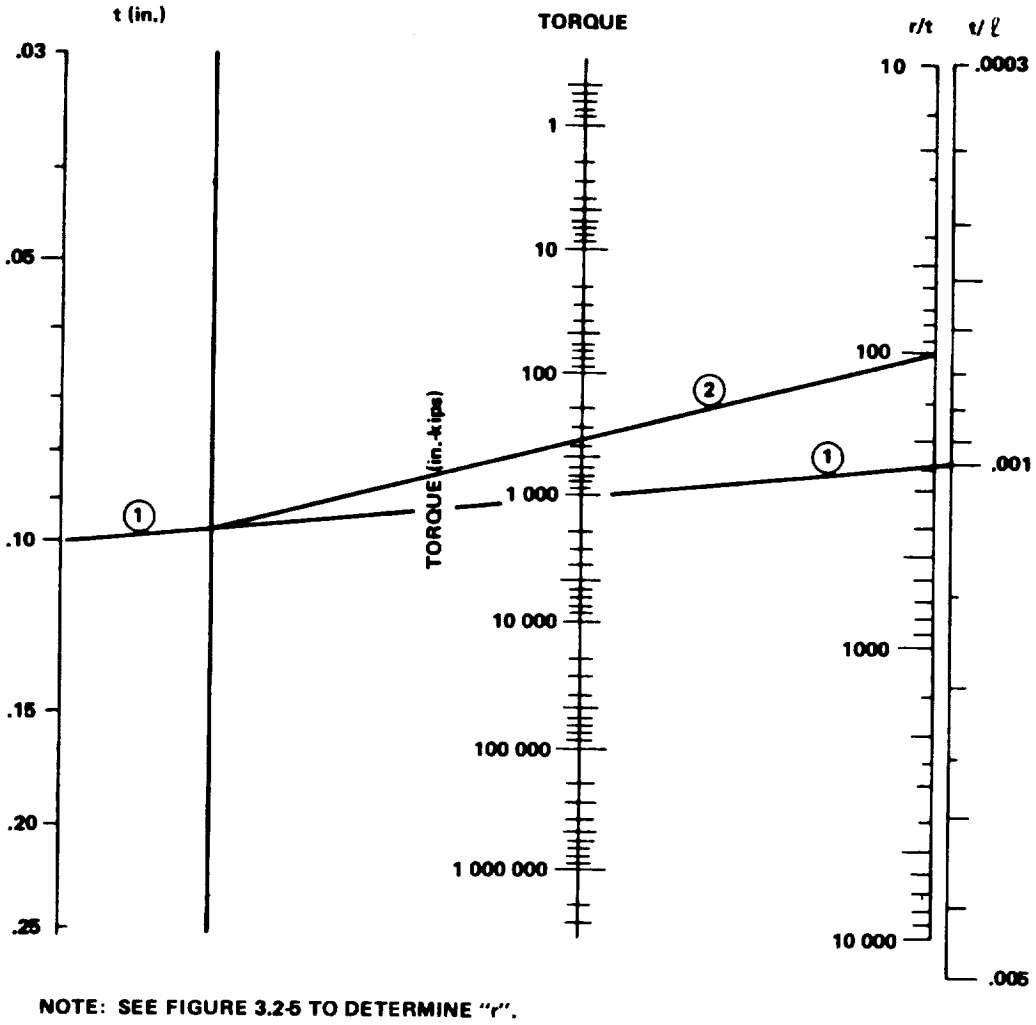

NOTE: SEE FIGURE 3.2-5 TO DETERMINE "r".

FIGURE 3.2-6. ALLOWABLE TORQUE FOR CONICAL SHELL
($E = 10.4 \times 10^6$)

3.2.1.5 Combined Loads.

I. Pressurized Conical Shells in Axial Compression.

The theory for predicting buckling of internally pressurized conical shells under axial compression [11] differs from that for cylindrical shells in two respects. First, the axial load-carrying capacity is a function of internal

pressure and exceeds the sum of the load-carrying capacity of the unpressurized shell and the pressure load at the small end of the cone. Second, results of analyses for conical shells indicate that edge conditions at the small end have a significant effect on the axial load-carrying capacity. The results are independent of edge conditions at the large end for long cones.

There are insufficient data to warrant design use of the entire increase in load-carrying capacity of internally pressurized conical shells. It is therefore recommended that the critical axial compressive load for a pressurized conical shell be determined by adding the pressurization load $\pi r_1^2 p$ at the small end of the cone to the compressive buckling load at the conical shell. Then

$$p_{cr} = \left[\frac{\gamma}{\sqrt{3(1-\mu^2)}} + \Delta\gamma \right] (2\pi Et^2 \cos^2 \alpha) + \pi r_1^2 p \quad . \qquad (14)$$

The unpressurized compressive-buckling coefficient γ is equal to 0.33, and the increase in the buckling coefficient $\Delta\gamma$ for the equivalent cylindrical shell is given in Figure 3.2-7. The critical axial load may be increased above the value given by equation (14), however, if the increase is justified by test.

II. Pressurized Conical Shells in Bending.

As in the case of unpressurized conical shells subjected to pure bending, no theory has yet been developed for pressurized conical shells under bending. For conservative design, therefore, the design moment of the pressurized conical shell is written as

$$M_{press} = \left[\frac{\gamma}{\sqrt{3\ 1-\mu^2}} + \Delta\gamma \right] \pi E r_1 (t \cos \alpha)^2 + \frac{p \pi r_1^3}{2} \quad . \qquad (15)$$

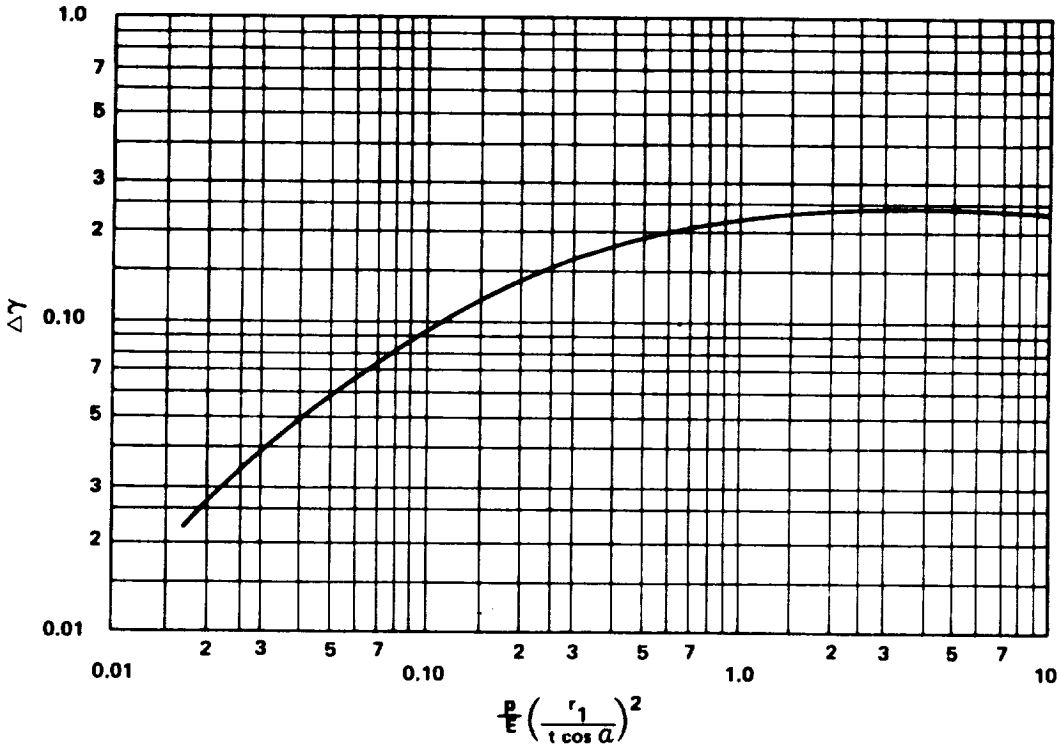

FIGURE 3.2-7. INCREASE IN AXIAL COMPRESSIVE BUCKLING-STRESS COEFFICIENTS OF CONICAL SHELLS RESULTING FROM INTERNAL PRESSURE

The unpressurized compressive-buckling coefficient γ is equal to 0.41, and the increase in buckling coefficient $\Delta\gamma$ for the equivalent cylindrical shell can be obtained from Figure 3.2-7.

III. Combined Axial Compression and Bending for Unpressurized and Pressurized Conical Shells.

Some experimental interaction curves have been obtained for unpressurized and pressurized conical shells under combined axial compression and bending [6]. These investigations indicate that the following straight-line

interaction curve for conical shells is adequate for design purposes:

$$R_c + R_b = 1 \tag{16}$$

where

$$R_c = \frac{P}{P_{cr}} \tag{17}$$

and

$$R_b = \frac{M}{M_{cr}} \tag{18}$$

For equations (17) and (18),

P = applied compressive load.

P_{cr} = critical compressive load for cone not subjected to bending, obtained from equations (1) and (2) for unpressurized shells, and from equation (14) for pressurized shells.

M = applied bending moment.

M_{cr} = critical moment for cone not subjected to axial compression, as obtained from equations (5) and (6) for unpressurized shells, and from equation (15) for pressurized shells.

If actual test values of P_{cr} and M_{cr} are used, the straight-line interaction curve may no longer be conservative, and the entire interaction curve must be substantiated by test.

IV. Combined External Pressure and Axial Compression.

For a conical shell subjected to combined external pressure and axial compression, the relationship

$$R_c + R_p = 1 \tag{19}$$

is recommended for design purposes. Where

$$R_p = \frac{P}{P_{cr}} \tag{20}$$

P_{cr} is given by equation (7) and (8), and R_c is given by equation (17).

V. Combined Torsion and External Pressure or Axial Compression.

For conical shells under combined torsion and external hydrostatic pressure the following interaction formula is recommended for design purpose:

$$R_t + R_p = 1 \tag{21}$$

with

$$R_t = \frac{T}{T_{cr}} \tag{22}$$

where T_{cr} is given by equations (10), (11), and (12), and R_p is given by equation (20).

For conical shells under combined torsion and axial compression, the following interaction formula is recommended for design purposes:

$$R_t + R_c = 1 \tag{23}$$

where R_t is given by equation (22) and R_c by equation (17).

3.2.2 ORTHOTROPIC CONICAL SHELLS.

The theory of buckling of orthotropic conical shells is valuable in determining adequate buckling criteria for shells which are geometrically orthotropic because of closely spaced meridional or circumferential stiffening, as well as for shells constructed of a material whose properties differ in the two directions. An extension of the Donnell-type isotropic conical shell theory to conical shells with material orthotropy is given in Reference 12, whereas buckling of conical shells with geometric orthotropy is considered in Reference 13. Numerical results are limited to only a few values of the many parameters, but these provide the basis for tentative generalizations. Few experiments have been conducted. Following are the design recommendations based on the limited data available. The computer programs discussed in Subsection 3.4 are also recommended.

3.2.2.1 Uniform Hydrostatic Pressure.

I. Constant-Thickness Orthotropic Material.

A limited investigation [14] indicates that the relationship between the theoretical buckling pressures of an orthotropic conical shell and of the so-called equivalent orthotropic cylinder is similar to that between the buckling pressures of an isotropic conical shell and of the equivalent isotropic cylinder. In both cases the equivalent cylinder is defined as one having a length equal to the slant length, L, of the conical shell; a radius equal to the average radius of curvature, $\bar{\rho}$, of the conical shell, and the same thickness. Thus, the theoretical hydrostatic buckling pressures for supported moderate-length orthotropic conical shells [15, 16] can be expressed as

$$P_{cr} = \frac{0.86\,\gamma}{\left(1 - \mu_s \mu_0\right)^{3/4}} E_s^{1/4} E_0^{3/4} \left(\frac{\bar{\rho}}{L}\right) \left(\frac{t}{\bar{\rho}}\right)^{5/2} , \qquad (24)$$

which reduces to the corresponding expression for the isotropic cone when

$$E_s = E_\theta = E \quad ,$$
$$\mu_s = \mu_\theta = \mu \quad . \tag{25}$$

Only limited experimental data exist for conical shells constructed for an orthotropic material [17]. In the absence of a more extensive range of test results, it is recommended that the value of the correlation coefficient γ be taken as 0.75 for both orthotropic and isotropic cones.

II. Stiffened Conical Shells.

The stability of conical shells stiffened by rings under uniform hydrostatic pressure has also been investigated [13, 18]. In these investigations, all rings were assumed to have the same cross-sectional shape and area but could have variable spacing. The approximate buckling formulas given in these references are not recommended for use in design until a larger amount of substantiating test data becomes available.

3.2.2.2 Torsion.

I. Constant-Thickness Orthotropic Material.

The investigation reported in Reference 19 indicates that the theoretical buckling torque of an orthotropic conical shell is approximated by that of an equivalent orthotropic cylinder having a length equal to the height, ℓ, of the conical shell and having the same thickness and radius given in equation (11). Refer to Figure 3.2-5 for the variation of $\frac{r}{r_2 \cos \alpha}$ with $\frac{r_1}{r_2}$.

The critical torque of a moderate-length orthotropic conical shell may then be approximated by the expression

$$T_{cr} = 4.57\,\gamma\,\frac{E_{\theta}^{5/8}\,E_{s}^{3/8}\,r^{2}t}{\left(1-\mu_{\theta}\mu_{s}\right)^{5/8}}\left(\frac{t}{r}\right)^{5/4}\left(\frac{r}{\ell}\right)^{1/2} \qquad (26)$$

A reduction factor of $\gamma = 0.67$ (the value given for isotropic conical shells) is recommended. The few data points available for fiberglass-reinforced epoxy conical shells [17] yield a larger value of γ but fall within the scatter band for the isotropic shell of constant thickness.

II. Ring-Stiffened Conical Shells.

Although no accurate theoretical calculations have been made for ring-stiffened conical shells in torsion, a few tests [17] indicate that when the rings are equally spaced and have the same cross-sectional shape and area, a procedure similar to that for the materially orthotropic conical shell will yield adequate results. The critical torque of such a ring-stiffened conical shell may thus be approximated by the critical torque of a ring-stiffened cylinder having the radius, length, and thickness described above. The critical torque of a ring-stiffened cone with uniformly spaced rings is then given by

$$T_{cr} = 4.57\,\gamma\,\frac{E\,r^{2}t}{\left(1-\mu_{s}\mu_{\theta}\right)^{5/8}}\left(\frac{t}{r}\right)^{5/4}\left(\frac{r}{\ell}\right)^{1/2}\left(1+\eta_{\theta}\right)^{5/8} \qquad (27)$$

where (Fig. 3.2-8)

$$\eta_{\theta} = 12(1-\mu^{2})\,\frac{E_{r}}{E}\left[\frac{I_{r}}{L_{o}t^{3}} + \frac{A_{r}}{L_{o}t}\left(\frac{\tilde{z}_{r}-e_{r}}{t}\right)^{2}\right] + 12\left(\frac{e_{r}}{t}\right)^{2} \qquad (28)$$

and the factor γ is recommended to be taken equal to 0.67. The few available test results also indicate a larger value of γ, but these again fall within the scatter band for the isotropic conical shell of constant thickness.

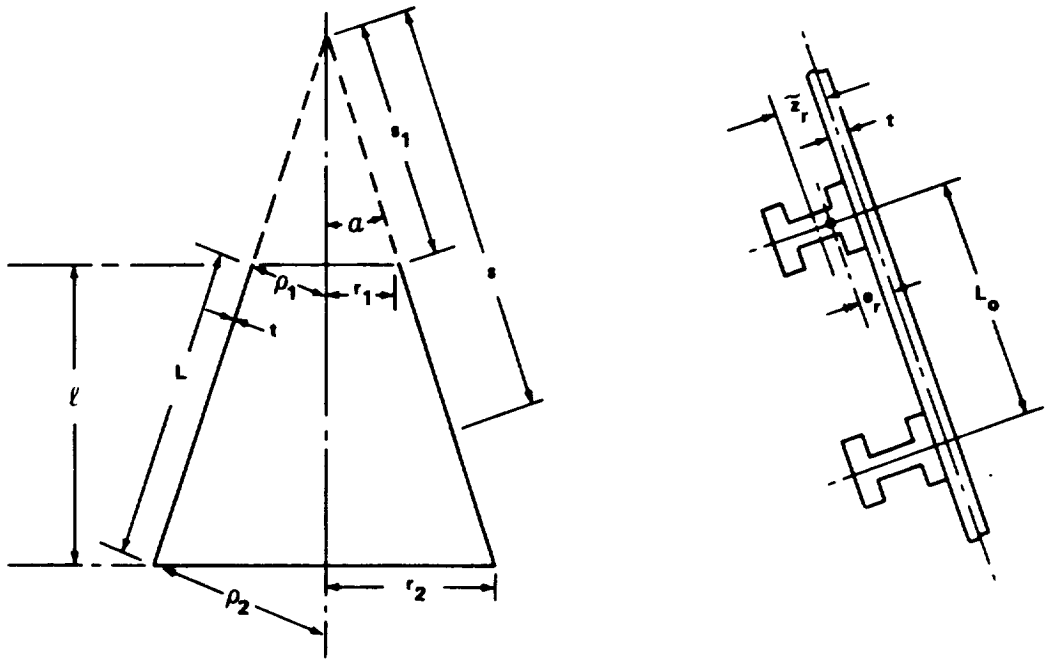

FIGURE 3.2-8. NOTATION FOR RING-STIFFENED CONICAL SHELLS

3.2.3 SANDWICH CONICAL SHELLS.

If the sandwich core is resistant to transverse shear so that its shear stiffness can be assumed to be infinite, the previous results for isotropic and orthotropic conical shells may readily be adapted to the analysis of sandwich conical shells by the following method.

3.2.3.1 Isotropic Face Sheets.

If the core is assumed to have infinite transverse shear stiffness and no load-carrying capacity in the meridional or circumferential directions, the analysis for isotropic conical shells of constant thickness may be used for isotropic sandwich conical shells of constant thickness. An equivalent modulus and thickness must be defined for the sandwich shell. The face sheets may be

of different thicknesses and of different materials, subject to the restriction that the Poisson's ratios of the two materials be identical. If the stretching and bending stiffnesses of such an isotropic sandwich shell are equated to the stretching and bending stiffnesses of an equivalent constant-thickness isotropic shell having the same neutral surface dimensions, then

$$\overline{E}\ \overline{t} = E_1 t_1 + E_2 t_2 \quad . \tag{29a}$$

$$\frac{\overline{E}(\overline{t})^3}{12} = \frac{h^2}{\frac{1}{E_1 t_1} + \frac{1}{E_2 t_2}} \quad . \tag{29b}$$

Then the modulus and the thickness of the equivalent constant-thickness isotropic shell are

$$\overline{t} = \frac{h\sqrt{12}}{\sqrt{\frac{E_1 t_1}{E_2 t_2}} + \sqrt{\frac{E_2 t_2}{E_1 t_1}}} \quad . \tag{30a}$$

$$\overline{E} = \frac{E_1 t_1 + E_2 t_2}{\overline{t}} \quad . \tag{30b}$$

The buckling loads of the isotropic sandwich shell may now be taken as the buckling loads of the equivalent isotropic shell of constant thickness as listed below.

Load	Paragraph Reference
Axial Compression	3.2.1.1
Bending	3.2.1.2
Uniform hydrostatic pressure	3.2.1.3

Load	Paragraph Reference
Torsion	3.2.1.4
Pressurized conical shells in axial compression	3.2.1.5-I
Pressurized conical shells in bending	3.2.1.5-II
Combined axial compression and bending for unpressurized and pressurized conical shells	3.2.1.5-III
Combined external pressure and axial compression	3.2.1.5-IV
Combined torsion and external pressure or axial compression	3.2.1.5-V

In the absence of experimental data, the reduction or correlation factors for isotropic shells of constant thickness are recommended for isotropic sandwich shells.

3.2.3.2 Orthotropic Face Sheets.

If the core is assumed to have infinite transverse shear stiffness and no load-carrying capacity in the meridional or circumferential directions, the available results for conical shells of constant-thickness orthotropic material may be used for sandwich conical shells having orthotropic faces. The face sheets may be of different thicknesses but of the same orthotropic material as long as their principal axes are oriented in the same direction. The same procedure as for sandwich shells having isotropic face sheets leads to the following thickness and material properties of the equivalent materially orthotropic conical shells of constant thickness:

$$\bar{t} = \frac{\sqrt{12}\, h}{\sqrt{\frac{t_1}{t_2}} + \sqrt{\frac{t_2}{t_1}}} \qquad (31a)$$

$$\frac{\bar{E}_s}{\bar{E}_s} = \frac{\bar{E}_\theta}{\bar{E}_\theta} = \frac{\bar{G}}{G} = \frac{t_1 + t_2}{\bar{t}} \quad . \tag{31b}$$

$$\frac{\bar{\mu}_s}{\mu_s} = \frac{\bar{\mu}_\theta}{\mu_\theta} = 1 \quad . \tag{31c}$$

The buckling load of the orthotropic sandwich conical shell is then the buckling load of the equivalent conical shell of orthotropic material having constant thickness. The reduction or correlation factors for isotropic shells of constant thickness are recommended for use for sandwich shells with orthotropic face sheets.

3.2.3.3 Local Failure.

Thus far, only overall buckling has been considered as a criterion of failure. Other modes of failure are possible, however. For honeycomb-core sandwich shells, failure may occur because of core crushing, intracell buckling, and face wrinkling. The use of relatively heavy cores ($\delta > 0.03$) will usually prevent core crushing. Lighter cores may prove to be justified as data become available. No studies have been conducted that predict localized buckling failures under stress states that are a function of position. If we assume, however, that the stress state varies only slightly over the buckled region, the following approximate equations developed for cylindrical shells can be used to predict failure from intracell buckling and face wrinkling of heavy honeycomb-core sandwich conical shells with equal-thickness face sheets under uniaxial loading. For intracell buckling

$$\sigma_s = 2.5\, E_R \left(\frac{t_f}{s}\right)^2 \tag{32}$$

where S is the core cell size expressed as the diameter of the largest inscribed circle and

$$E_R = \frac{4\, E_f\, E_{tan}}{\left(\sqrt{E_f} + \sqrt{E_{tan}}\right)^2} \tag{33}$$

where E_f and E_{tan} are the elastic and tangent moduli of the face-sheet material. If initial dimpling is to be checked, the equation

$$\sigma_s = 2.2\, E_R \left(\frac{t_f}{S}\right)^2 \tag{34}$$

should be used. The sandwich will still carry loads if initial dimpling occurs. For wrinkling

$$\sigma_s = 0.50\, (E_{sec}\, E_z\, G_{sz})^{1/3} \tag{35}$$

where E_z is the modulus of the core in a direction perpendicular to the plane of the core, and G_{sz} is the transverse shear modulus of the core. If biaxial compressive stresses are applied to the sandwich, the coefficients of equations must be reduced by the factor $(1 + f^3)^{-1/3}$, where f is the ratio of minimum to maximum principal compressive stress in the face sheets.

Wrinkling and intracell-buckling equations which consider strength of bond, strength of foundation, and initial waviness of the face sheets are given in References 20, 21, and 22.

The plasticity correction factor given for isotropic conical shells in axial compression may be applied also to isotropic sandwich conical shells. The factor is applicable to sandwich cones with stiff cores and becomes somewhat conservative as the shear stiffness of the core is decreased [23].

3.3 DOUBLY CURVED SHELLS.

Doubly curved shells are frequently used in space vehicles as external closures of fuel tanks or entry vehicles or an internal common bulkheads. When doubly curved shells develop compressive membrane forces in reaction to externally applied loads, their load-carrying capacity is often limited by structural instability, or buckling.

The buckling strength of a doubly curved shell depends upon its curvature, its geometric proportions (including the stiffening, when present), the elastic properties of its materials, the manner in which its edges are supported, and the nature of the applied loading. Initial, although small, geometric deviations of the shell from its ideal shape can have a significant adverse effect on the buckling strength of doubly curved shells and can cause large scatter of experimental results.

This paragraph recommends practices for design of compressively loaded doubly curved shells. Included are practices recommended for the design of complete spheres, ellipsoids, and toroids, as well as bulkheads. Most of the data are for shells subjected to uniform pressure loads, although data are also given for point loads on spheres.

The reduction of critical buckling loads caused by imperfections, small dynamic oscillations, boundary conditions, and the like is usually accounted for by multiplying the theoretical buckling loads by a correlation factor to obtain a lower-bound conservative estimate. However, when insufficient data are available to obtain correlation factors, testing is recommended to verify the design. Experimental verification is also recommended for shells of arbitrary shape and for shells of revolution having cutouts, joints, plasticity effects, and nonuniform shell stiffness. The effect of small oscillations in applied loading is considered to be accounted for by the correlation factor.

For doubly curved shells, considerable capability for theoretical analysis is available although experimental investigations of the stability of doubly curved shells lag far behind analytical capabilities; the shallow spherical cap under external pressure is the only problem which has been investigated extensively.

The growing use of digital computers for analysis of shell structures has greatly improved the available analyses which can be performed. For example, a comprehensive computer program, BOSOR 3, [1] performs a stability analysis of segmented, ring-stiffened shells of revolution. The program is quite general with respect to types of loading, geometry, boundary conditions, and wall stiffness variation. All the programs for doubly curved shells, including both finite-difference and finite-element, treat only those cases in which the shell does not become plastic before buckling.

Although the capability for stability analysis has increased, parametric optimization studies for problems of interest are lacking. This may well be because of the relative newness of most computer programs. To date, most computer programs have been used for spot checks of approximate solutions and for comparisons with experimental data.

The designer is advised to be alert to new developments in shell-stability analysis.

3.3.1 ISOTROPIC DOUBLY CURVED SHELLS.

Unstiffened isotropic doubly curved shells subjected to various conditions of loadings are considered in this paragraph. Solutions are limited to spherical, ellipsoidal, and toroidal shells.

3.3.1.1 Spherical Caps Under Uniform External Pressure.

The buckling of a spherical cap under uniform external pressure (Fig. 3.3-1) has been treated extensively. The theoretical results are presented in References 2 and 3 for axisymmetric snap-through of shallow spherical

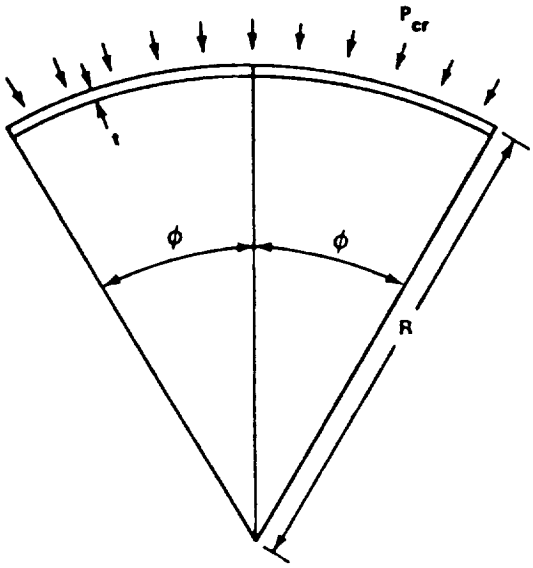

FIGURE 3.3-1. GEOMETRY OF SPHERICAL CAP UNDER UNIFORM EXTERNAL PRESSURE

shells with edges that are restrained against translation but are either free to rotate or are clamped. Results for asymmetric buckling are given in References 4 and 5 for the same boundary conditions. The results reported in these references are presented as the ratio of the buckling pressure p_{cr} for the spherical cap and the classical buckling pressure $p_{c\ell}$ for a complete spherical shell as a function of a geometry parameter λ :

$$\frac{p_{cr}}{p_{c\ell}} = f(\lambda) \qquad (1)$$

with

$$p_{c\ell} = \frac{2}{[3(1-\mu^2)]^{1/2}} \; E\left(\frac{t}{r}\right)^2 \quad , \qquad (2)$$

$$\lambda = [12(1-\mu^2)]^{1/4} \; (R/t)^{1/2} \; 2 \sin\frac{\phi}{2} \qquad (3)$$

where ϕ is half the included angle of the spherical cap (Fig. 3.3-1). The function $f(\lambda)$ depends on the boundary conditions imposed on the shell.

Most of the available test data apply to spherical shells, and the values are lower than the theoretically predicted buckling pressures. The discrepancy between theory and experiment can be attributed largely to initial deviations from the ideal spherical shape [3, 6, 7] and to differences between the actual and assumed edge conditions [8, 9]. Most of the available data are

summarized in Reference 10; some other test results are given in References 6 and 11. A lower bound to the data for clamped shells is given by

$$\frac{p_{cr}}{p_{c\ell}} = 0.14 + \frac{3.2}{\lambda^2} \quad (\lambda > 2) \qquad (4)$$

This curve is plotted in Figure 3.3-2. Whereas the λ parameter is used in shallow-shell analysis, Figure 3.3-2 may be applied to deep shells as well as to shallow shells.

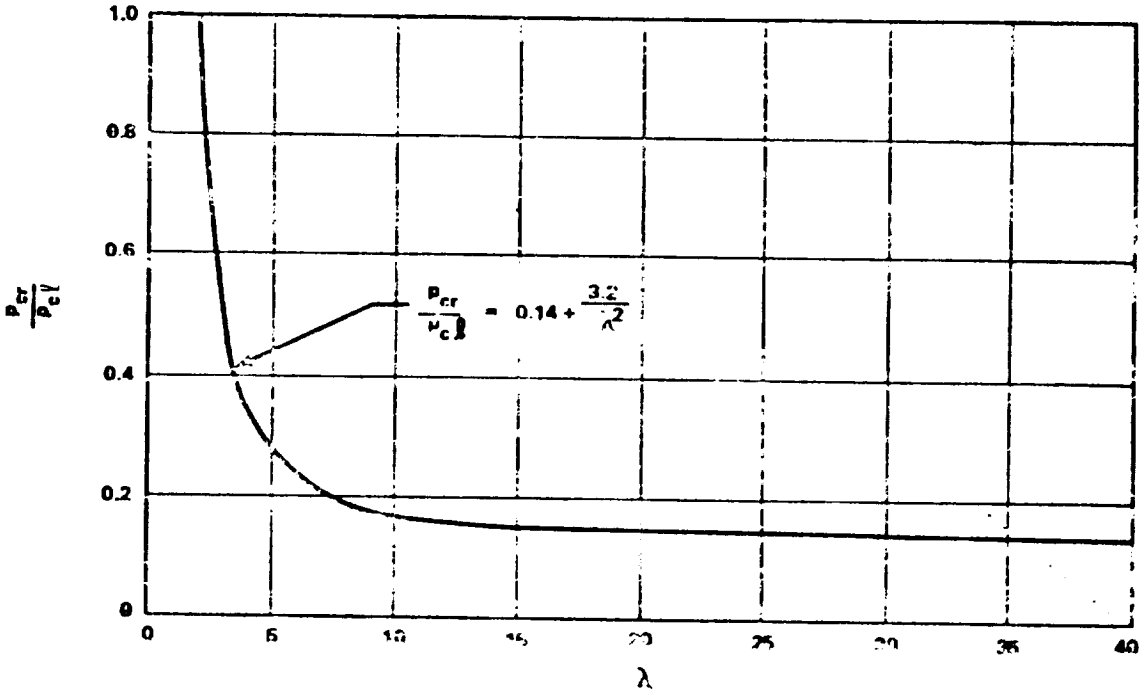

FIGURE 3.3-2. RECOMMENDED DESIGN BUCKLING PRESSURE OF SPHERICAL CAPS

3.3.1.2 Spherical Caps Under Concentrated Load at the Apex.

Spherical caps under concentrated load at the apex (Fig. 3.3-3) will buckle under certain conditions. The theoretical results for edges that are free to rotate and to expand in the direction normal to the axis of revolution,

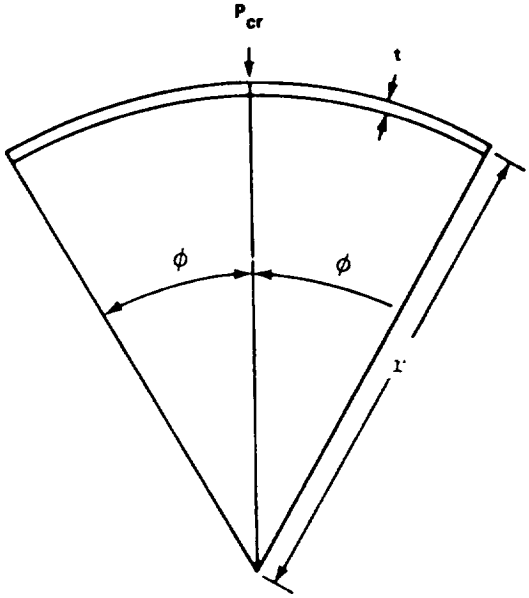

FIGURE 3.3-3. GEOMETRY OF SPHERICAL CAP UNDER CONCENTRATED LOAD AT THE APEX

and for clamped edges, are given in Reference 12 for axisymmetric snap-through and in References 13 and 14 for asymmetric buckling. Experimental results for loads which approximate concentrated loading are described in References 15 to 19.

For shells with unrestrained edges, buckling will not occur if λ is less than about 3.8. In this range of shell geometry, deformation will increase with increasing load until collapse resulting from plasticity effects occurs. For shells with values of λ greater than 3.8, theoretical and experimental results are in good agreement for axisymmetric snap-through but disagree when theory indicates that asymmetric buckling should occur first. In this case, buckling and collapse are apparently not synonymous, and only collapse loads have been measured. A lower-bound relationship between the collapse-load parameter and the geometry parameter for the data of References 13, 15, and 16 for shells with unrestrained edges is given by

$$\frac{P_{cr}\, r}{Et^3} = \frac{1}{24}\,\lambda^2 \quad (4 \leq \lambda \leq 18) \qquad . \qquad (5)$$

For spherical caps with clamped edges, theory indicates that buckling will not occur if λ is less than about 8. For values of λ between 8 and 9, axisymmetric snap-through will occur, with the shell continuing to carry an increasing load. For larger values of λ, asymmetrical buckling

will occur first, but the shell will continue to carry load. Although imperfections influence the initiation of symmetric or asymmetric buckling, few measurements have been made of the load at which symmetric or asymmetric deformations first occur. Experimental results indicate that the collapse loads of clamped spherical caps loaded over a small area are conservatively estimated by the loads calculated in Reference 13 and shown in Figure 3.3-4. When the area of loading becomes large, large buckling may occur at a lower level.

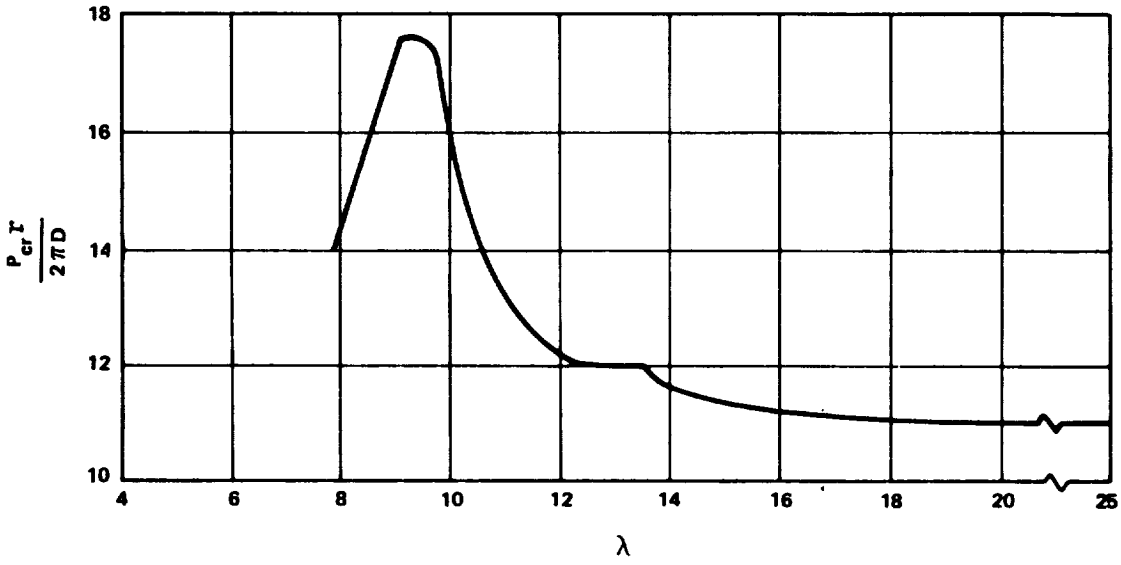

FIGURE 3.3-4. THEORETICAL BUCKLING LOADS FOR CLAMPED SPHERICAL CAP UNDER CONCENTRATED LOAD

3.3.1.3 Spherical Caps Under Uniform External Pressure and Concentrated Load at the Apex.

Clamped spherical caps subjected to combinations of uniform external pressure and concentrated load at the apex are discussed in Reference 20. The experimental and theoretical data given there are insufficient, however,

to yield conclusive results. A straight-line interaction curve is recommended:

$$\frac{P}{P_{cr}} + \frac{p}{p_{cr}} = 1 \qquad (6)$$

where P is the applied concentrated load, p is the applied uniform pressure, P_{cr} the critical concentrated load given in Paragraph 3.3.1.2, and p_{cr} the critical uniform external pressure given in Paragraph 3.3.1.1.

3.3.1.4 Complete Ellipsoidal Shells Under Uniform External Pressure.

Ellipsoidal shells of revolution subjected to uniform external pressure, as shown in Figure 3.3-5, are treated in Reference 21. Calculated theoretical results for prolate spheroids are shown in Figures 3.3-6a and 3.3-6b. Experimental results given in Reference 22 for prolate spherical shells with $4 > A/B > 1.5$ are in reasonably close agreement with the theoretical results of Reference 21. For $A/B \geq 1.5$, the theoretical pressure should be multiplied by the factor 0.75 to provide a lower bound to the data. The results given in Reference 23 for half of a prolate spheroidal shell $(A/B = 3)$ closed by an end plate are in good agreement with those for the complete shell.

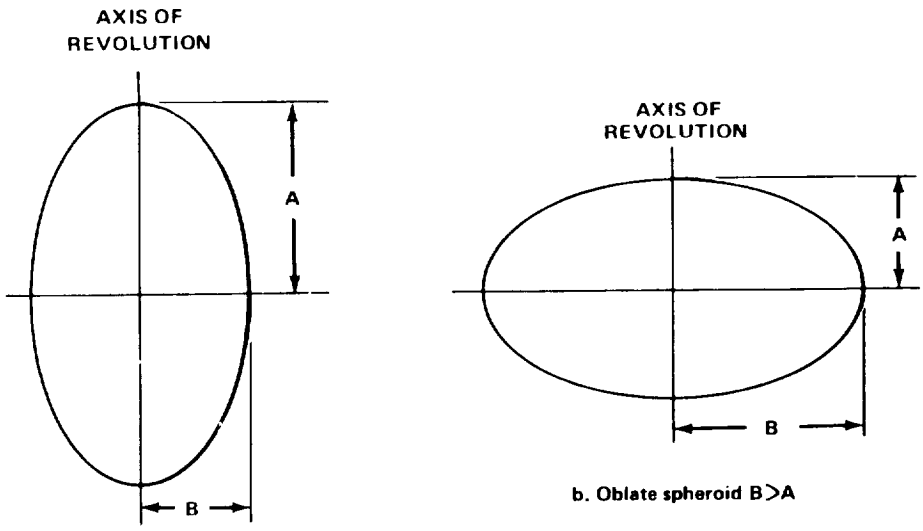

a. Prolate spheroid A>B

b. Oblate spheroid B>A

FIGURE 3.3-5. GEOMETRY OF ELLIPSOIDAL SHELLS

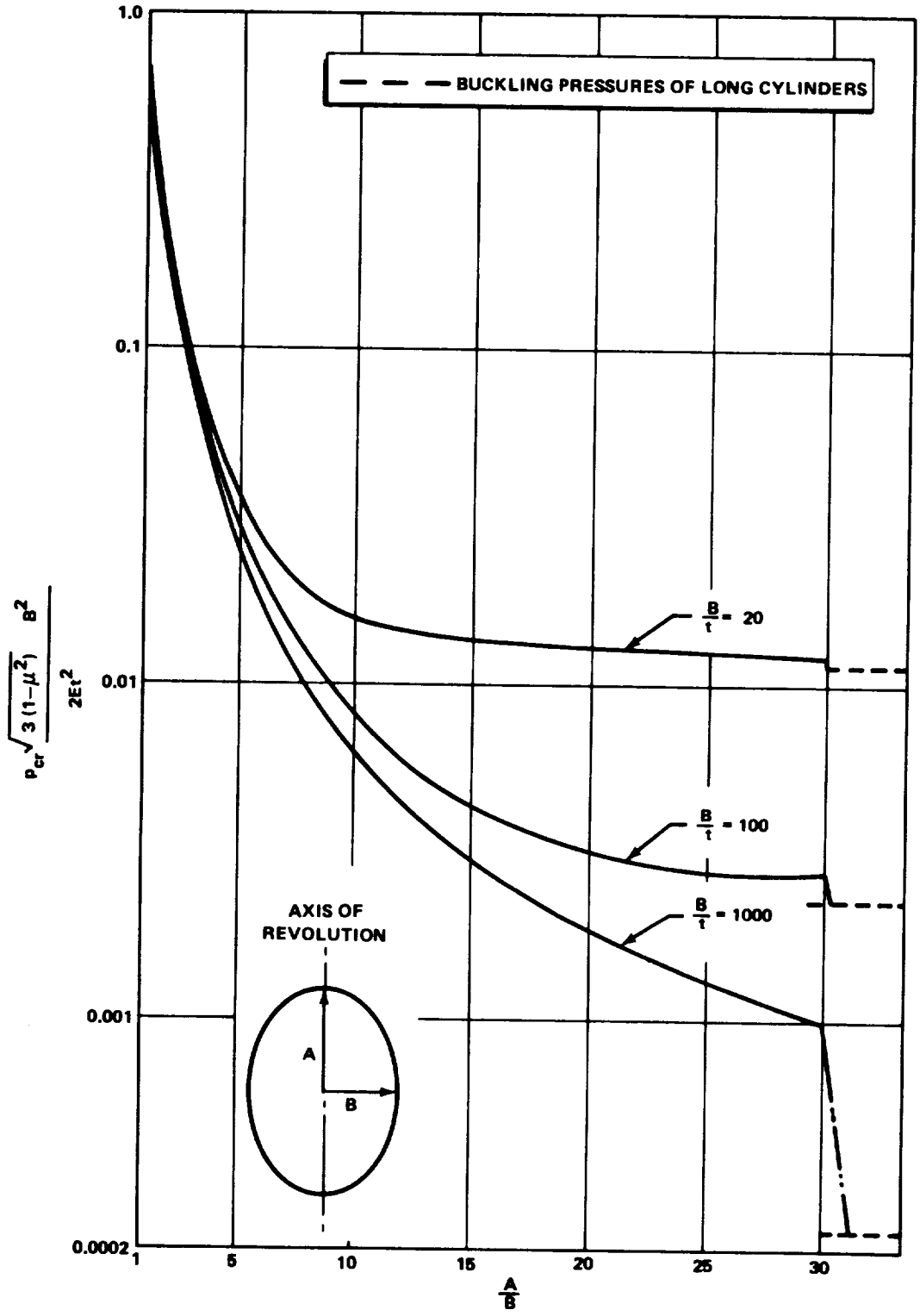

FIGURE 3.3-6a. THEORETICAL EXTERNAL BUCKLING PRESSURES OF PROLATE SPHEROIDS ($\mu = 0.3$)

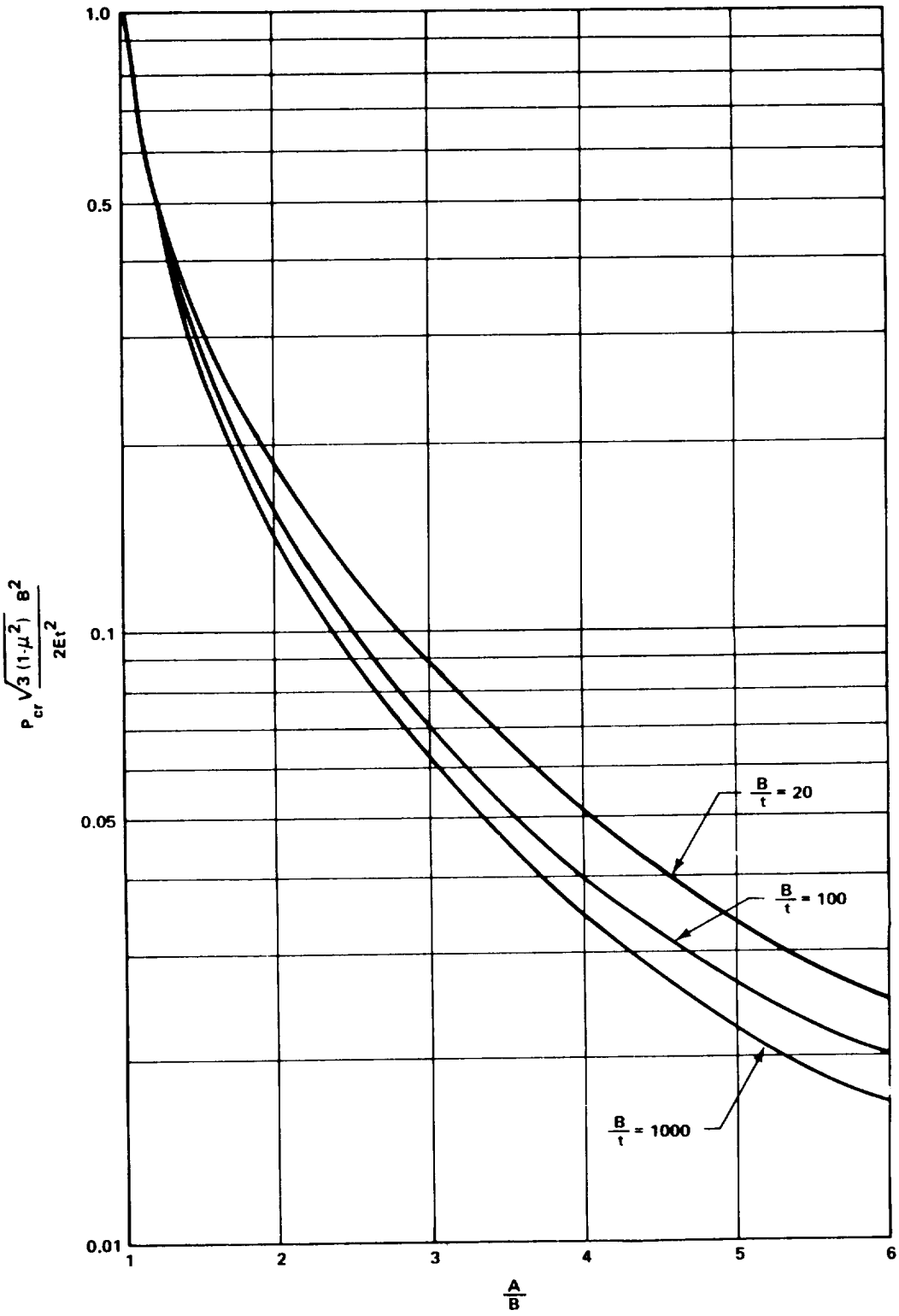

FIGURE 3.3-6b. THEORETICAL EXTERNAL BUCKLING PRESSURES OF PROLATE SPHEROIDS ($\mu = 0.3$) FOR A/B RATIO OF 1:6

The analysis of Reference 21 indicates that theoretical results for thin, oblate spheroidal shells are similar to those for a sphere of radius

$$R_A = \frac{B^2}{A} \quad . \tag{7}$$

The data of Reference 24 show that the experimental results are similar as well. Thus, the external buckling pressure for a thin, oblate spheroid may be approximated by the relationship

$$\frac{\sqrt{3\,(1-\mu^2)}}{2}\left(\frac{R_A}{t}\right)^2 \frac{p}{E} = 0.14 \quad , \tag{8}$$

which is the limit of equation (4) as λ becomes large.

3.3.1.5 Complete Oblate Spheroidal Shells Under Uniform Internal Pressure.

When the ratio A/B of an oblate spheroid is less than $\sqrt{2}/2$, internal pressure produces compressive stresses in the shell, and hence allows instability to occur. The theoretical values of the critical internal pressures given by the analysis of Reference 21 are shown in Figure 3.3-7. No experimental results are available, but the study of the imperfection sensitivity of Reference 21 indicates that there should be good agreement between theory and experiment for shells with $0.5 < A/B < 0.7$.

3.3.1.6 Ellipsoidal and Torispherical Bulkheads Under Internal Pressure.

Clamped oblate spheroidal (ellipsoidal) bulkheads (Fig. 3.3-8) may have the ratio of length of minor and major axes (A/B) less than $\sqrt{2}/2$ without buckling under internal pressure, provided that the thickness exceeds a certain critical value. This problem is investigated in Reference 25.

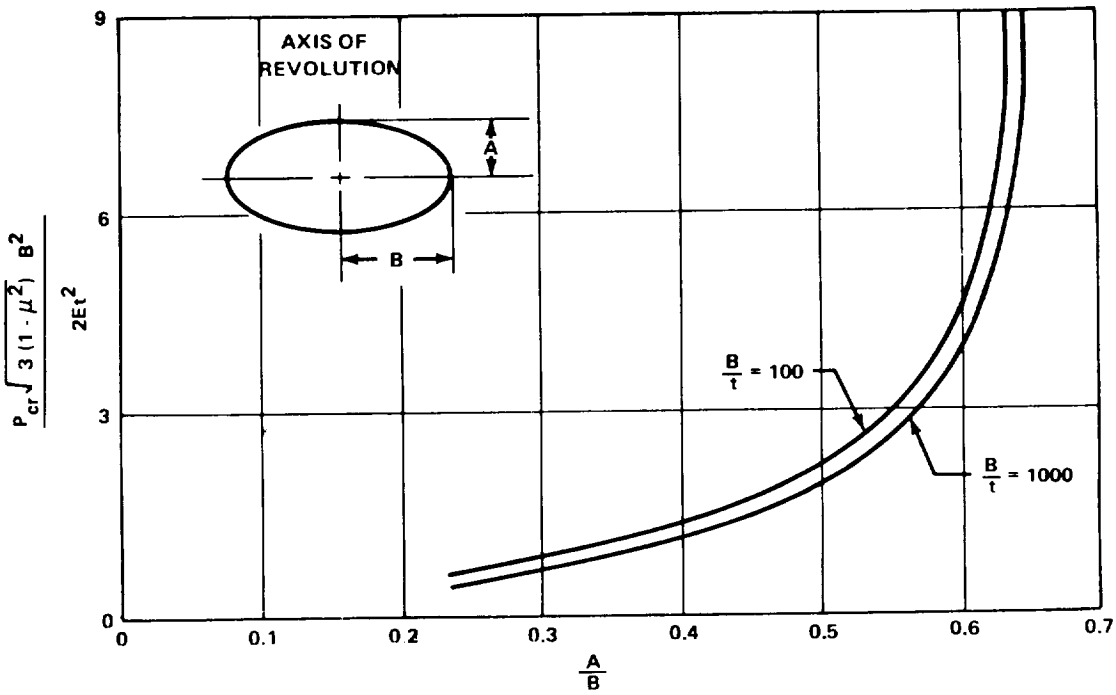

FIGURE 3.3-7. THEORETICAL BUCKLING PRESSURES OF OBLATE SPHEROIDS UNDER INTERNAL PRESSURE ($\mu = 0.3$)

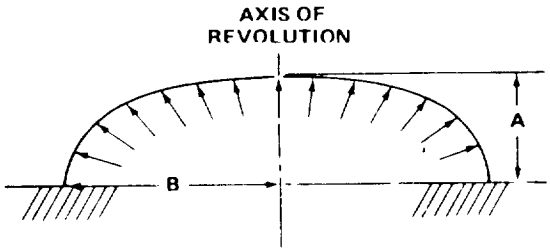

FIGURE 3.3-8. CLAMPED ELLIPSOIDAL BULKHEAD UNDER INTERNAL PRESSURE

A nonlinear bending theory is used to determine the prebuckling stress distribution. The regions of stability are shown in Figure 3.3-9; the calculated variation of buckling pressure with thickness is shown in Figure 3.3-10. The theory has not been verified by experimental results, however, and should be used cautiously.

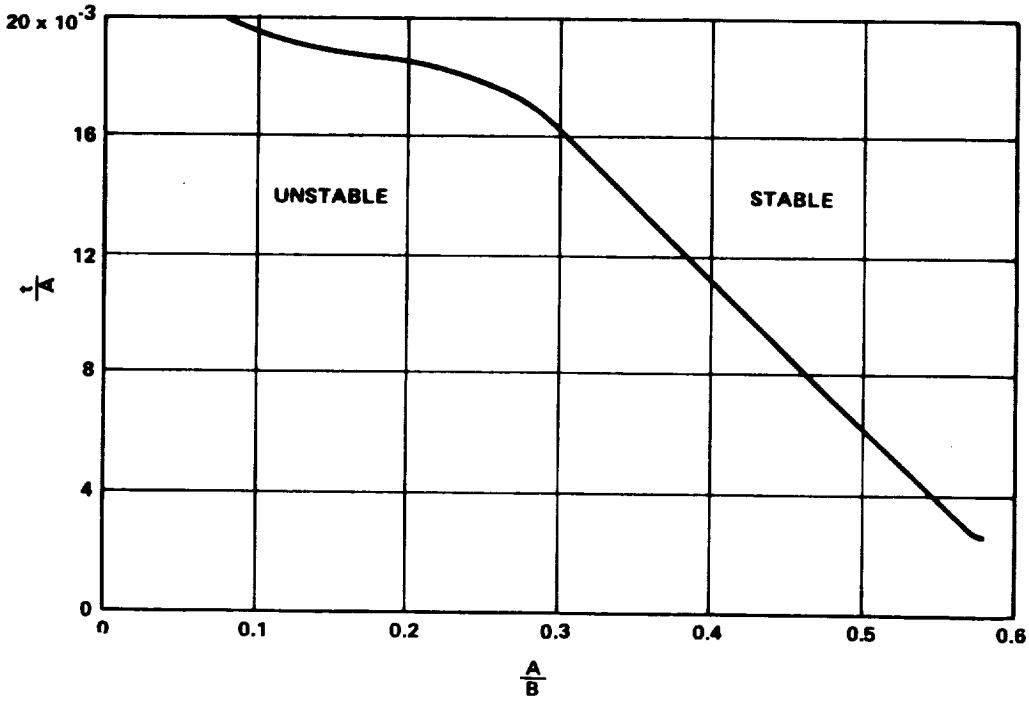

FIGURE 3.3-9. REGION OF STABILITY FOR ELLIPSOIDAL CLOSURES SUBJECTED TO INTERNAL PRESSURE ($\mu = 0.3$)

Torispherical end closures (Fig. 3.3-11) are also investigated in Reference 25. Calculations are made for the prebuckling stress distribution in these bulkheads for ends restrained by cylindrical shells and for buckling pressures for torispherical bulkheads with clamped edge conditions after buckling. The results are shown in Figure 3.3-12. The experimental results of Reference 26 indicate that the theoretically predicted buckling pressures should be multiplied by a correlation factor γ equal to 0.7.

3.3.1.7 Complete Circular Toroidal Shells Under Uniform External Pressure.

The complete circular toroidal shell under uniform external pressure (Fig. 3.3-13) has been investigated and is described in Reference 27; the theoretical results obtained are shown in Figure 3.3-14.

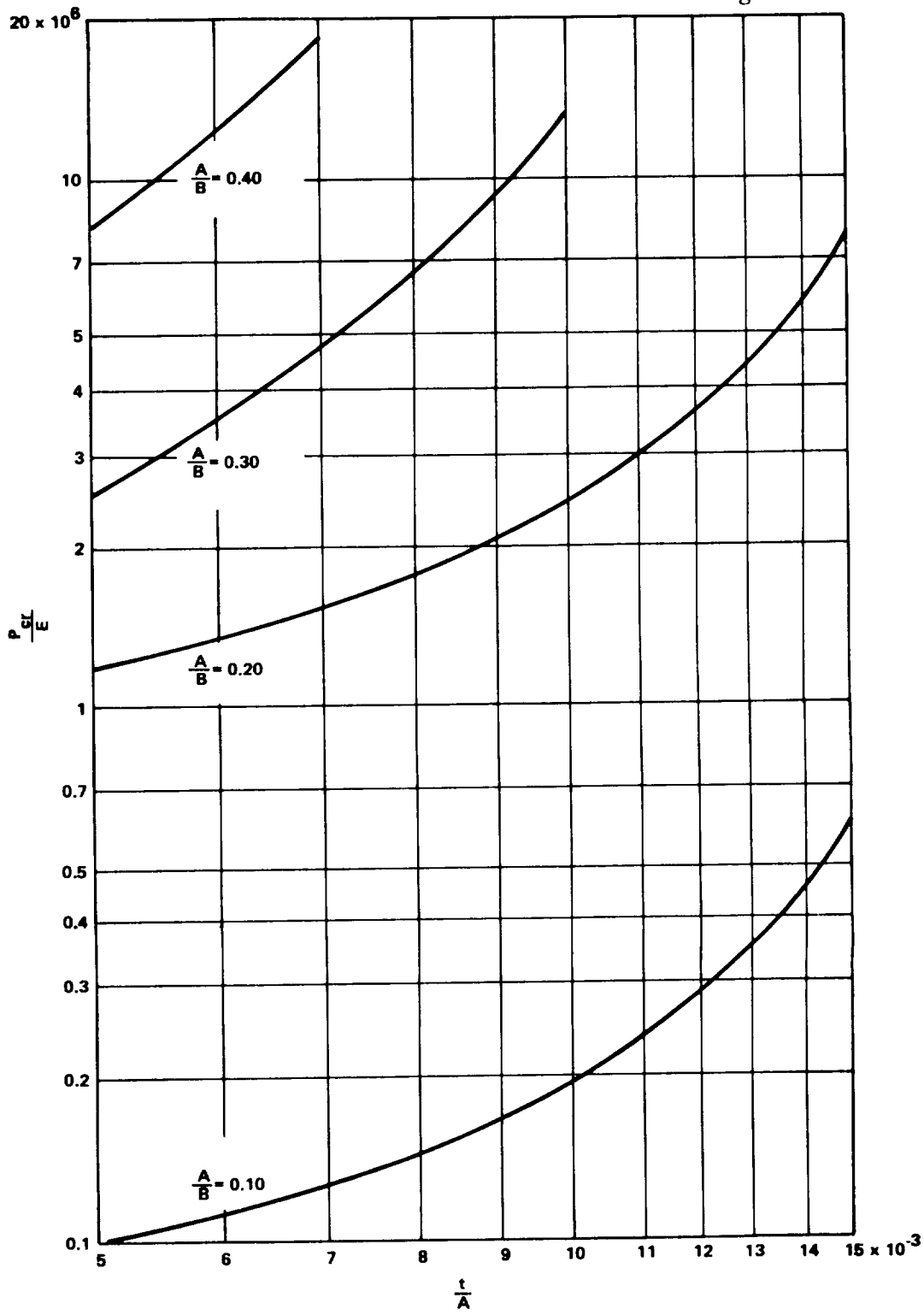

FIGURE 3.3-10. THEORETICAL RESULTS FOR CLAMPED ELLIPSOIDAL BULKHEADS SUBJECTED TO UNIFORM INTERNAL PRESSURE ($\mu = 0.3$)

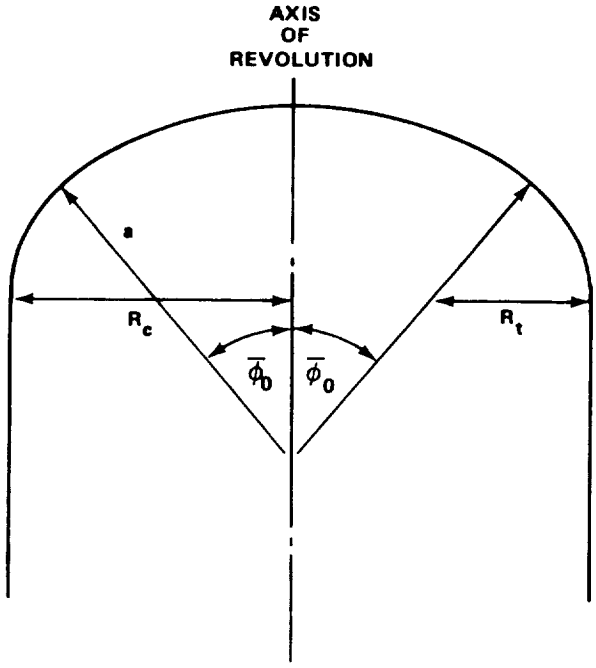

FIGURE 3.3-11. GEOMETRY OF TORISPHERICAL CLOSURE

The experimental results are given in Reference 27 for values of b/a of 6.3 and 8 and indicate good agreement with theory. For values of b/a equal to or greater than 6.3, the theoretical buckling pressure should be multiplied by a factor of 0.9 to yield design values. This correction factor has been recommended in Reference 28 for long cylindrical shells which correspond to a value of b/a of ∞. For values of b/a less than 6.3, the buckling pressure should be verified by test.

3.3.1.8 Shallow Bowed-Out Toroidal Segments Under Axial Loading.

A bowed-out equatorial toroidal segment under axial tension (Fig. 3.3-15) will undergo compressive circumferential stress and will thus be susceptible to buckling. An analysis for simply supported shallow segments is given in Reference 29 and yields the relationship

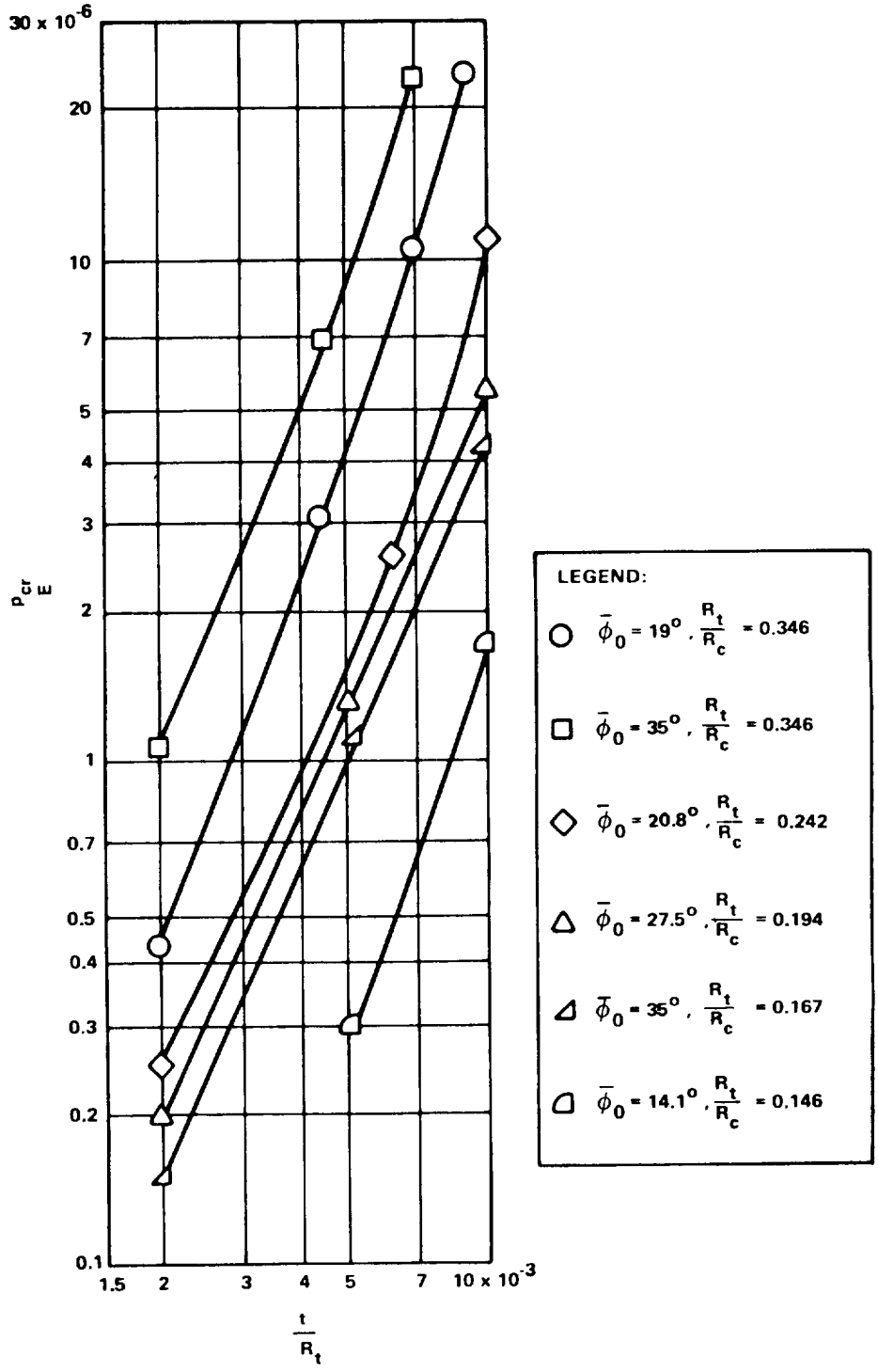

FIGURE 3.3-12. THEORETICAL RESULTS FOR TORISPHERICAL CLOSURES SUBJECTED TO UNIFORM INTERNAL PRESSURE ($\mu = 0.3$)

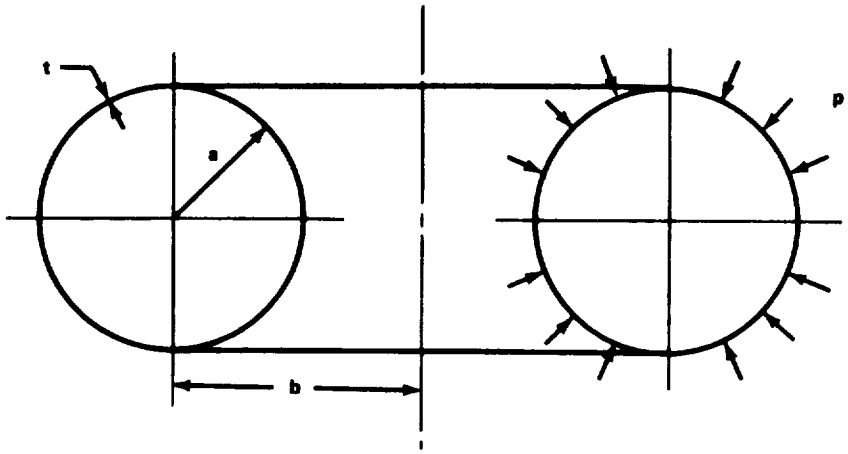

FIGURE 3.3-13. GEOMETRY OF A TOROIDAL SHELL UNDER UNIFORM EXTERNAL PRESSURE

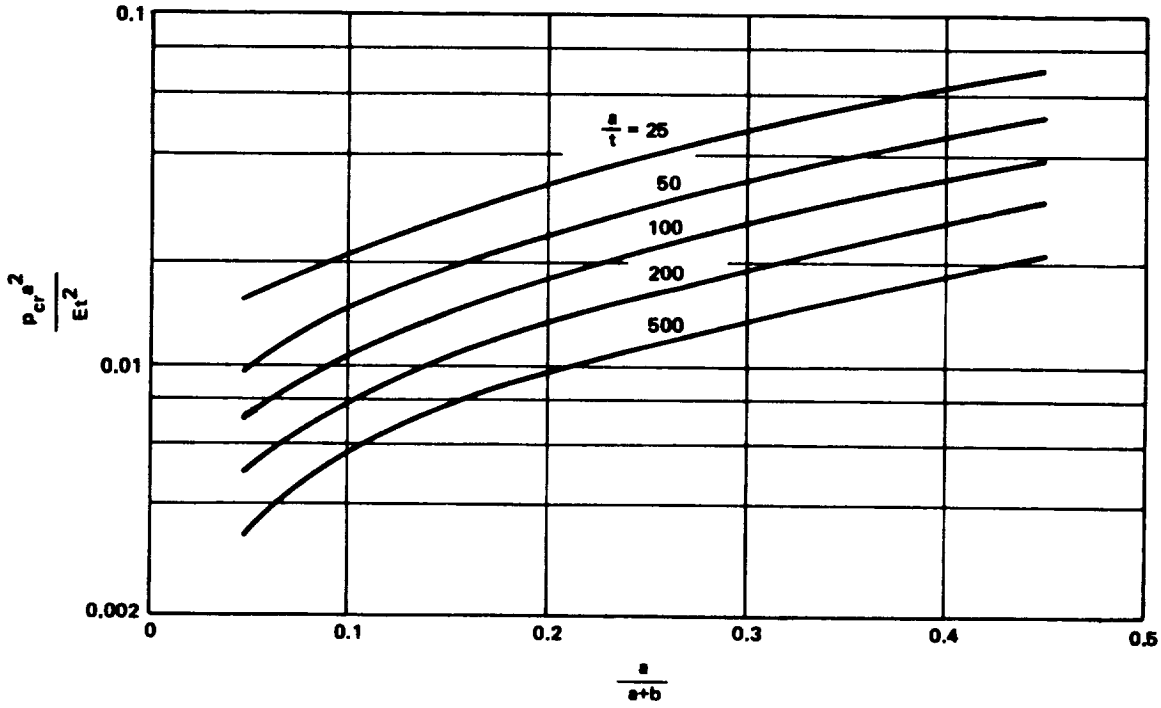

FIGURE 3.3-14. THEORETICAL BUCKLING COEFFICIENTS FOR TOROIDAL SHELLS UNDER UNIFORM EXTERNAL PRESSURE

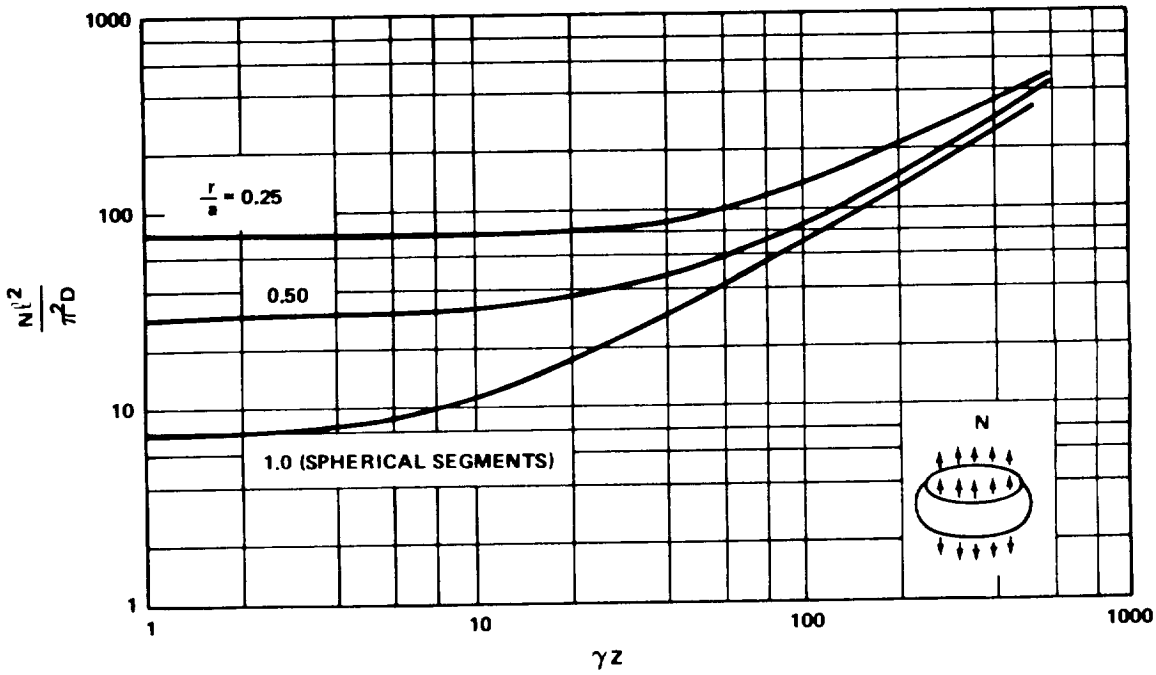

FIGURE 3.3-15. BUCKLING OF BOWED-OUT TOROIDAL SEGMENTS UNDER AXIAL TENSION

$$\frac{N\ell^2}{\pi^2 D} = \frac{1}{\left(\frac{r}{a}\beta^2 - 1\right)} \left[(1+\beta^2)^2 + 12\,\frac{\gamma^2 Z^2}{\pi^4} \left(\frac{1 + \frac{r}{a}\beta^2}{1+\beta^2} \right)^2 \right] \qquad (9)$$

where the correlation coefficient γ has been inserted to account for discrepancies between theory and experiment. The values obtained by minimizing equation (9) with respect to β are shown in Figure 3.3-15. The straight-line portion of the curves is represented by the relationship

$$\frac{N\ell^2}{\pi^2 D} = \frac{4\sqrt{3}}{\pi^2}\,\gamma Z \qquad (10)$$

A similar analytical investigation described in Reference 30 for clamped truncated hemispheres in axial tension yields results in close agreement with those for the curve of Figure 3.3-15 for $r/a = 1$.

The experimental results for the truncated hemisphere given in Reference 30 indicate that the correlation coefficient for the curve for r/a equals 1 is

$$\gamma = 0.35 \quad . \tag{11}$$

The same value of the correlation coefficient may be used for other values of r/a.

Some results for bowed-out equatorial toroidal segments under axial compression are given in Reference 31; the equatorial spherical shell segment loaded by its own weight is treated in Reference 32.

3.3.1.9 Shallow Toroidal Segments Under External Pressure.

The term "lateral pressure" designates an external pressure which acts only on the curved walls of the shell and not on the ends; "hydrostatic pressure" designates an external pressure that acts on both the curved walls and the ends of the shell. Expressions for simply supported shallow equatorial toroidal segments subjected to uniform external lateral or hydrostatic pressure (Figs. 3.3-16 and 3.3-17) are given in Reference 33 as

$$\frac{P_{cr}\, r\ell^2}{\pi^2 D} = \frac{1}{\beta^2}\left[(1+\beta^2)^2 + \frac{12}{\pi^4}\gamma^2 Z^2 \left(\frac{1 \pm \frac{r}{a}\beta^2}{1+\beta^2}\right)^2\right] \tag{12}$$

for lateral pressure, and as

$$\frac{P_{cr}\, r_\ell^2}{\pi^2 D} = \frac{1}{\beta^2\left(1 \mp 1/2\,\frac{r}{a}\right) + 1/2}\left[(1+\beta^2)^2 + \frac{12}{\pi^4}\gamma^2 Z^2 \left(\frac{1 \pm \frac{r}{a}\beta^2}{1+\beta^2}\right)^2\right] \tag{13}$$

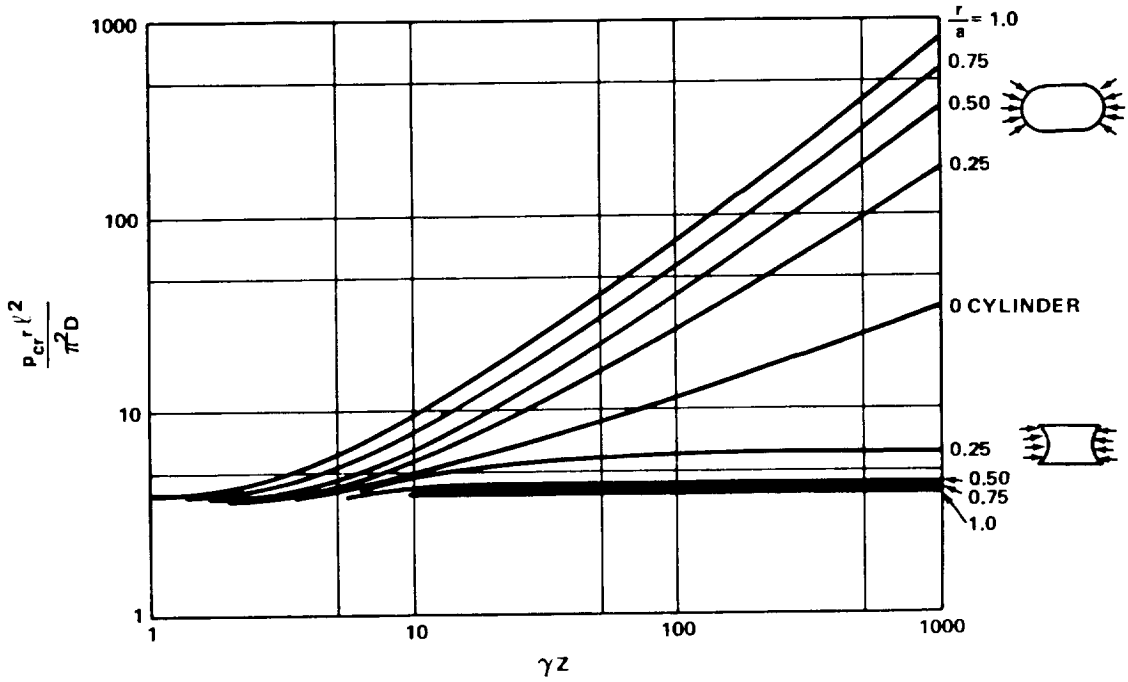

FIGURE 3.3-16. BUCKLING OF TOROIDAL SEGMENTS UNDER UNIFORM LATERAL PRESSURE

for hydrostatic pressure. In equations (12) and (13), the upper sign refers to segments of type (a) of Figure 3.3-18, whereas the lower sign refers to segments of type (b) of Figure 3.3-18. The correlation coefficient γ has been introduced to account for discrepancies between theory and experiment. The results of minimizing the buckling pressure with respect to the circumferential wavelength parameter β are shown in Figures 3.3-16 and 3.3-17. The straight-line portions of the curve for the shells of type (a) of Figure 3.3-18 are represented by the relationships

$$\frac{P_{cr} r_\ell^2}{\pi^2 D} = \frac{4\sqrt{3}}{2} \frac{r}{a} \gamma Z \qquad \text{(lateral pressure)} \quad . \qquad (14a)$$

$$\frac{P_{cr} r_\ell^2}{\pi^2 D} \quad \frac{8\sqrt{3}}{2 - \frac{r}{a}} \frac{r}{a} \gamma Z \qquad \text{(hydrostatic pressure)} \quad . \qquad (14b)$$

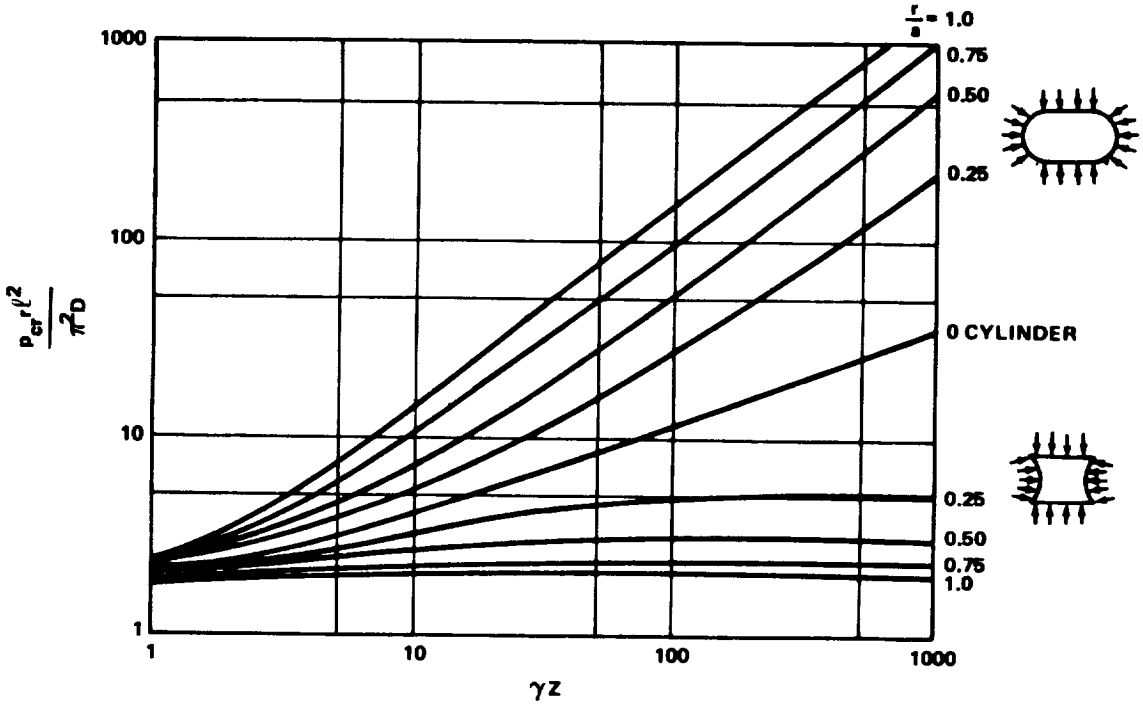

FIGURE 3.3-17. BUCKLING OF TOROIDAL SEGMENTS UNDER UNIFORM EXTERNAL HYDROSTATIC PRESSURE

No experimental data are available except for the cylindrical shell, for which a correlation factor of

$$\gamma = 0.56 \qquad (15)$$

was recommended in Reference 28. The same correlation factor can be used for shells with r/a near zero but should be used with caution for shells of type (b) with values of r/a near unity. For shells of type (a) with values of r/a near unity, the shell can be conservatively treated as a sphere, or the buckling pressure should be verified by test.

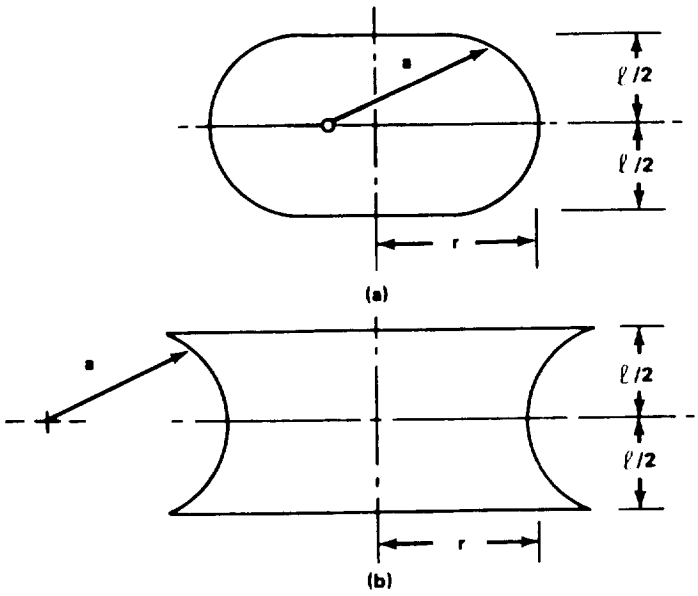

FIGURE 3.3-18. GEOMETRY OF TOROIDAL SEGMENTS NEAR EQUATORS

3.3.2 ORTHOTROPIC DOUBLY CURVED SHELLS.

The term "orthotropic doubly curved shells" covers a wide variety of shells. In its strictest sense, it denotes single- or multiple-layered shells made of orthotropic materials. In this section, the directions of the axes of orthotropy for shells of revolution are assumed to coincide with the meridional and circumferential directions of the shell. The term also denotes types of stiffened shells in which the stiffener spacing is small enough for the shell to be approximated by a fictitious sheet whose orthotropic bending and extensional properties include those of the individual stiffening elements averaged out over representative widths or areas.

The behavior of the various types of orthotropic shells may be described by a single theory, the governing equations of which are equations of equilibrium for the buckled structure, and relationships between force and

moment resultants and extensional and bending strains. The matrix equation relating the inplane forces and bending moments to the inplane strains and curvatures for shells of revolution with axes of orthotropy in the meridional and circumferential directions can be written in the following form:

$$\begin{Bmatrix} N_1 \\ N_2 \\ N_{12} \\ M_1 \\ M_2 \\ M_{12} \end{Bmatrix} = \begin{bmatrix} C_{11} & C_{12} & 0 & C_{14} & C_{15} & 0 \\ C_{12} & C_{22} & 0 & C_{24} & C_{25} & 0 \\ 0 & 0 & C_{33} & 0 & 0 & 0 \\ C_{14} & C_{24} & 0 & C_{44} & C_{45} & 0 \\ C_{15} & C_{25} & 0 & C_{45} & C_{55} & 0 \\ 0 & 0 & 0 & 0 & 0 & C_{66} \end{bmatrix} \begin{Bmatrix} \epsilon_1 \\ \epsilon_2 \\ \epsilon_{12} \\ \kappa_1 \\ \kappa_2 \\ \kappa_{12} \end{Bmatrix} \tag{16}$$

Zero entries in the preceding matrix generally refer to coupling terms for layers whose individual principal axes of stiffnesses are not aligned in meridional and circumferential directions. The values of the various elastic constants used in determining buckling loads of orthotropic shells are different for different types of construction. Some widely used expressions are given in References 1 and 34.

The theory for single-layered shells of orthotropic material is similar to that for isotropic shells since the coupling terms C_{14}, C_{15}, C_{24}, and C_{25} may be set equal to zero. For stiffened doubly curved shells or for shells having multiple orthotropic layers, this is not generally possible, and it is shown in References 35 and 36 that the neglect of coupling terms can lead to serious errors. For example, the inclusion of coupling terms yields a significant difference in theoretical results for stiffened shallow spherical-dome configurations having stiffeners on the inner surface or on the outer surface. The difference vanishes when coupling is neglected.

Very little theoretical or experimental data are available for orthotropic and stiffened doubly curved shells. The general instability loads of pressurized shallow spherical domes with meridional stiffeners are determined in Reference 37, and a semiempirical design formula is given in Reference 38 for stiffened spherical caps. This formula closely approximates the test data given in Reference 38. Buckling loads are given for grid-stiffened spherical domes in Reference 39. References 37 and 39 do not include the effect of stiffener eccentricity.

Stiffener-eccentricity effects are investigated in Reference 35 for grid-stiffened spherical domes. Eccentrically stiffened shallow equatorial toroidal shells under axial load and uniform pressure are investigated in Reference 40. The development of a buckling computer program that includes coupling as well as nonlinear prebuckling bending effects for orthotropic shells of revolution is discussed in References 1 and 34. A further description of this program is given in Subsection 3.4. (The cards and a computer listing for this program are available from COSMIC, University of Georgia, Athens, Ga.) Numerical results obtained from this program [34] were in good agreement with selected experimental results. The computer program can be used to determine the buckling load of the following orthotropic shells:

1. Shells with ring and stringer stiffening.
2. Shells with skew stiffeners.
3. Fiber-reinforced (layered) shells.
4. Layered shells (isotropic or orthotropic).
5. Corrugated ring-stiffened shells.
6. Shells with one corrugated and one smooth skin (with rings).

Boundary conditions may be closed at one or both ends or may be free, fixed, or elastically restrained. Edge rings are permitted on the boundary or as discrete rings in the shell.

This computer program can be used in conjunction with experimentally determined correlation factors to obtain buckling loads for orthotropic shells of revolution. The limitations of the program are given in References 1 and 34 and are also discussed in Subsection 3.4.

The design recommendations that follow are limited to spherical domes; the recommendations should also be verified by test, where feasible. The possibility of local buckling of the shell between stiffening elements should be checked.

The investigation of Reference 39 gives the theoretical buckling pressure of a grid-stiffened spherical dome under uniform external pressure. This analysis assumes that the spherical dome is "deep" and that it contains many buckle wavelengths. In this case, the boundary conditions have little effect on the buckling load. Eccentricity effects are neglected. Experimental results given in Reference 24 tend to support the assumptions of the analysis.

If the analysis of Reference 39 is extended to the materially or geometrically orthotropic shell, the hydrostatic buckling pressure can be expressed as

$$\frac{pr^3}{C_{44}\,\psi_1^{1/2}} = 4\gamma\left(\frac{1 + 2\,\dfrac{C_{45} + C_{66}}{C_{44}} + \dfrac{C_{55}}{C_{44}}}{1 + \dfrac{C_{22}}{C_{11}} + 2\,\dfrac{C_{22}}{\psi_2}}\right)^{1/2} \qquad (17)$$

where

$$\psi_1 = \frac{C_{22}\,r^2}{C_{44}}\left(1 - \frac{C_{22}^2}{C_{11}\,C_{22}}\right) , \qquad (18a)$$

$$\psi_2 = \frac{2\,C_{33}}{1 - \frac{C_{12}^2}{C_{11}\,C_{22}} - 2\,\frac{C_{12}\,C_{33}}{C_{11}\,C_{22}}} \quad . \qquad (18b)$$

The constants C_{11}, C_{12}, C_{22}, C_{33}, C_{44}, C_{45}, C_{55}, and C_{66} are defined in Reference 34 for the various materially and geometrically orthotropic materials. Equation (17) does not include the effect of stiffener eccentricity since the coupling terms C_{14}, C_{15}, C_{24}, and C_{25} in equation (16) have been neglected. Only limited experimental data exist for geometrically or materially orthotropic spherical domes subjected to hydrostatic pressure [24, 38]. In the absence of more extensive test results, it is recommended that the isotropic spherical cap reduction factor shown in equation (4) also be used for the orthotropic spherical shell. The correlation factor is given by

$$\gamma = 0.14 + \frac{3.2}{\lambda^2} \quad . \qquad (19)$$

Refer to Figure 3.3-2 for the plot of this equation. The effective shell thickness to be used in obtaining λ is recommended as

$$t = \sqrt[4]{\frac{C_{44}\,C_{55}}{C_{11}\,C_{22}}}\;\sqrt{12} \quad . \qquad (20)$$

3.3.3 ISOTROPIC SANDWICH DOUBLY CURVED SHELLS.

The term "isotropic sandwich" designates a layered construction formed by bonding two thin isotropic facings to a thick core. Generally, the thin isotropic facings provide nearly all the bending rigidity of the construction. The core separates the facings and transmits shear so that the facings bend about a common neutral axis.

Sandwich construction should be checked for two possible modes of instability failure: (1) general instability failure where the shell fails with core and facings acting together, and (2) local instability failure taking the form of dimpling of the faces or wrinkling of the faces (Fig. 3.1-7).

3.3.3.1 General Failure.

If the sandwich core is resistant to transverse shear so that its shear stiffness can be assumed to be infinite, the sandwich shell can be treated as an equivalent isotropic shell. For unequal thickness facings, the equivalent isotropic material thickness and modulus of elasticity are then given by

$$\bar{t} = \frac{\sqrt{12}\, h}{\sqrt{\frac{E_1 t_1}{E_2 t_2}} + \sqrt{\frac{E_2 t_2}{E_1 t_1}}} \quad , \qquad (21a)$$

$$\bar{E} = \frac{E_1 t_1 + E_2 t_2}{\bar{t}} \qquad (21b)$$

and for equal-thickness facings with the same modulus of elasticity, by

$$\bar{t} = \sqrt{3}\, h \quad , \qquad (22a)$$

$$\bar{E} = \frac{2 E t_f}{\sqrt{3}\, h} \quad . \qquad (22b)$$

These equivalent properties can be used in conjunction with the recommended practices in Paragraph 3.3.1 and with the computer program of Reference 34 to analyze isotropic sandwich doubly curved shells.

Only one theoretical investigation which includes shear flexibility is available. In Reference 41 the buckling of a sandwich sphere comprised of a core layer of low-modulus material and two equal face layers of high-modulus material is discussed. Because there are insufficient theoretical and experimental data, no design recommendations can be given for this case.

3.3.3.2 Local Failure.

Modes of failure other than overall buckling are possible. For honeycomb-core sandwich shells, failure may occur because of core crushing, intracell buckling, and face wrinkling. The use of relatively heavy cores ($\delta > 0.03$) will usually prevent core crushing. Lighter cores may prove to be justified as data become available. Procedures for the determination of intracell buckling and face-wrinkling loads are given in Reference 42.

3.4 COMPUTER PROGRAMS IN SHELL STABILITY ANALYSIS.

The names of various digital computer programs are listed in Table 3.4-1, which indicates their scope for a shell stability analysis. Three classes of problems are specified: cylindrical shells, shells of revolution, and general shells.

Table 3.4-1. Computer Programs for Shell Stability Analysis

Types of Shells	Symmetric System Nonsymmetric Displacements	Nonsymmetric System
Cylindrical Shells	CORCYL[a] DBSTAB[a] SCAR MARK IV	INTACT STAGS
Shells of Revolution	BOSOR[a] BOSOR3 SABOR3-F	
General Shell		BERK3 NASTRAN[a] REXBAT

a. Programs available for use at Marshall Space Flight Center.

Often the stability analysis of cylindrical shells can be solved in closed form. Those concerning shells of revolution can frequently be simplified by separation of variables. Variations in the circumferential direction are assumed to be periodic, and the method of superposition is used for the linear analysis of shells of revolution subjected to nonsymmetric loads. The meridional variation is determined by series expansion, the method of finite

differences, numerical integration, or the method of finite elements. For the analysis of general shells, however, a two-dimensional numerical analysis is required, since the variables cannot be separated. The core storage required and the computer time per case increase very rapidly as the number of mesh points or terms in a double series expansion increases.

Tables 3.4-2, 3.4-3, and 3.4-4 list the programs by name, cite References 1 through 12 in which they are documented, specify the method of numerical analysis used, and briefly describe the major features of the analysis.

In general, CORCYL, DBSTAB, SCAR, MARK IV, INTACT, BOSOR, BOSOR3, and SABOR3-F might be expected to have a higher "confidence index" than the other programs. This is not because of defects in the programs but because of the relative ease of proving that convergence has been obtained. In STAGS, BERK3, NASTRAN, AND REXBAT, core storage is often too small to ascertain conclusively that the stresses obtained are accurate to within a percent or so. In addition, convergence checks are generally very expensive in terms of computer time. Most of the computer programs requiring a two-dimensional numerical analysis are harder to use than those requiring a one-dimensional numerical analysis since more input data must be specified.

A simplified input and output explanation (along with example problems) is given in an MSFC internal document[1] for the programs CORCYL, DBSTAB, BOSOR, and NASTRAN.

1. Structural Analysis Computer Utilization Manual, Astronautics Laboratory, NASA/MSFC (to be published).

Table 3.4-2. Computer Programs for Stability Analysis of Cylindrical Shells

Program Name	Reference No.	Method of Analysis[a]	Comments
CORCYL	1	1	Linear small-deflection theory. Ring-stiffened corrugated cylinder under axial compression. Rings are distributed along the cylinder. Eccentricity of rings with respect to corrugation centerline is considered.
DBSTAB	2	1	Small-deflection theory. Orthogonally stiffened cylindrical shell under axial compression and lateral pressure. Restricted to moderately or heavily stiffened cylinders. Rings and stringers are considered eccentric with respect to the skin's middle surface. Local buckling of the skin between adjacent stringers before general instability is allowed, and the resulting reduction in skin stiffness is determined.
SCAR	3	1	Membrane prebuckled theory and simply supported edges. Various types of wall construction permitted, as well as combined pressure and axial compression. Ring stiffeners and longitudinal stringers permitted.
MARK IV	4	1	SCAR-type analysis for optimization of integrally stiffened cylinders with respect to weight.

Table 3.4-2. (Concluded)

Program Name	Reference No.	Method of Analysis[a]	Comments
INTACT	5	2	Buckling of cylinders under bending, axial compression, and pressure. Interaction curves calculated. Otherwise, same as SCAR.
STAGS	6	4	Nonlinear analysis. Large deflections and elastic-plastic behavior permitted. Discrete rings and stringers included. Maximum number of unknowns is 4300.

a. Method of Analysis:

1 = Closed form
2 = Series expansion
3 = Numerical integration
4 = Finite difference
5 = Finite element

Table 3.4-3. Computer Programs for Stability Analysis of Shells of Revolution

Program Name	Reference No.	Method of Analysis	Comments
BOSOR	7	4	Nonlinear prebuckling effects. General with respect to geometry of meridian, shell wall design, edge conditions, and loading. Axisymmetric loading.
BOSOR3	8	4	Rings can be treated as discrete elastic structures. Option of nonlinear prebuckling effects or linear bending theory for prebuckling analysis. Segmented shells can be analyzed with each segment independent of other segments. Otherwise, same as BOSOR.
SABOR3-F	9[a]	5	Calculation of vibration frequencies of stacked and branched shells.

a. Also, W. A. Loden: SABOR3-F/EIGSYS Instructions, unpublished report, Lockheed Missiles and Space Company, August 1967.

Table 3.4-4. Computer Programs for Stability Analysis of General Shells

Program Name	Reference No.	Method of Analysis	Comments
BERK3	10	5	Flat triangular elements with extensional and bending stiffness are used for the calculation of stresses and vibration frequencies of general shells or shells of revolution with cutouts. Up to 6000 unknowns can be handled. Discrete stiffeners permitted.
NASTRAN	11	5	General-purpose program for elastic structural analysis. Not restricted to shells. Contains library of elements including rods, beams, shear panels, plates, and shells.
REXBAT	12	5	General-purpose program for linear structural analysis with respect to static stresses and vibration frequencies. Up to 6000 unknowns can be handled.

3.5 REFERENCES

REFERENCES FOR CYLINDERS (SUBSECTION 3.1)

1. Baker, E. H., et al.: Shell Analysis Manual. NASA CR-912, April 1968.

2. Almroth, B.; Holmes, A.; and Brush, D.: An Experimental Study of the Buckling of Cylinders under Axial Compression. Paper presented at SESA Spring Meeting, Salt Lake City, Utah, May 6-8, 1964.

3. Koiter, W. T.: The Effect of Axisymmetric Imperfections on the Buckling of Cylindrical Shells under Axial Compression. Rpt. 6-90-6-90-63-86, Lockheed Missiles and Space Company, August 1963.

4. Almroth, B. O.: Influence of Edge Conditions on the Stability of Axially Compressed Cylindrical Shells. AIAA J., vol. 4, no. 1, January 1966.

5. Buckling of Thin-Walled Circular Cylinders. NASA SP-8007, August 1968.

6. Weingarten, V. I.; Morgan, E. J.; and Seide, P.: Elastic Stability of Thin-Walled Cylindrical and Conical Shells Under Axial Compression. AIAA J., vol. 3, no. 3, March 1965, pp. 500-505.

7. Seide, P.; Weingarten, V. I.; and Morgan, E. J.: The Development of Design Criteria for Elastic Stability of Thin Shell Structures. STL/TR-60-0000-19425 (AFBMD/TR-61-7), Space Technology Laboratory, Inc. (now TRW Systems), Dec. 31, 1960.

8. Jones, R. M.: Buckling of Circular Cylindrical Shells with Multiple Orthotropic Layers and Eccentric Stiffeners. AIAA J., vol. 6, no. 12, December 1968, pp. 2301-2305.

REFERENCES (Continued)

9. Dickson, J. N.; and Brolliar, R. H.: The General Instability of Ring-Stiffened Corrugated Cylinders under Axial Compression. NASA TN D-3089, January 1966.

10. Meyer, R. R.: Buckling of Ring-Stiffened Corrugated Cylinders Subjected to Uniform Axial Load and Bending. Report DAC-60698, Douglas Aircraft Company, July 1967.

11. Singer, J.; Baruch, M.; and Harari, O.: On the Stability of Eccentrically Stiffened Cylindrical Shells under Axial Compression. Int. J. Solids Structures, vol. 3, no. 4, July 1967, pp. 445-470.

12. Peterson, J. P.; and Dow, M. B.: Compression Tests on Circular Cylinders Stiffened Longitudinally by Closely Space Z Section Stringers. NASA Memo 2-12-59L, 1959.

13. Peterson, J. P.; Whitley, R. O.; and Deaton, J. W.: Structural Behavior and Compressive Strength of Circular Cylinders with Longitudinal Stiffening. NASA TN D-1251, 1962.

14. Becker, H.; Gerard, G.; and Winter, R.: Experiments on Axial Compressive General Instability of Monolithic Ring-Stiffened Cylinders. AIAA J., vol. 1, no. 7, July 1963, pp. 1614-1618.

15. Card, M. F.; and Jones, R. M.: Experimental and Theoretical Results for Buckling of Eccentrically Stiffened Cylinders. NASA TN D-3639, October 1966.

16. Milligan, R.; Gerard, G.; and Lakshinikantham, C.: General Instability of Orthotropically Stiffened Cylinders under Axial Compression. AIAA J., vol. 4, no. 11, November 1966, pp. 1906-1913.

REFERENCES (Continued)

17. Singer, J.: The Influence of Stiffener Geometry and Spacing on the Buckling of Axially Compressed Cylindrical and Conical Shells. Preliminary Preprint Paper, Second IUTAM Symposium on the Theory of Thin Shells, Copenhagen, September 1967.

18. Kaplan, A.; Morgan, E. J.; and Zophres, W.: Some Typical Shell Stability Problems Encountered in the Design of Ballistic Missiles. Collected Papers on Instability of Shell Structures. NASA TN D-1510, December 1962, pp. 21-33.

19. Card, M. F.; and Peterson, J. P.: On the Stability of Orthotropic Cylinders. Collected Papers on Instability of Shell Structures. NASA TN D-1510, December 1962, pp. 297-308.

20. Hedgepeth, J. M.; and Hall, D. B.: Stability of Stiffened Cylinders. AIAA J., vol. 3, no. 12, December 1965, pp. 2275-2286.

21. Block, D. L.: Buckling of Eccentrically Stiffened Orthotropic Cylinders under Pure Bending. NASA TN D-3351, March 1966.

22. Peterson, J. P.; and Anderson, J. K.: Bending Tests of Large Diameter Ring-Stiffened Corrugated Cylinders. NASA TN D-3336, March 1966.

23. Card, M. F.: Bending Tests of Large Diameter Stiffened Cylinders Susceptible to General Instability. NASA TN D-2200, April 1964.

24. Becker, H.; and Gerard, G.: Elastic Stability of Orthotropic Shells. J. Aeron. Sci., vol. 29, no. 5, May 1962, pp. 505-512, 520.

25. Bodner, S. R.: General Instability of a Ring-Stiffened Circular Cylindrical Shell under Hydrostatic Pressure. J. Appl. Mech., vol. 24, no. 2, June 1957, pp. 269-277.

REFERENCES (Continued)

26. Baruch, M.; and Singer, J.: Effect of Eccentricity of Stiffeners on the General Instability of Stiffened Cylindrical Shells under Hydrostatic Pressure. Journal of Mechanical Engineering Science, vol. 5, no. 1, March 1963, pp. 23-27.

27. Singer, J.; Baruch, M.; and Harari, O.: Further Remarks on the Effect of Eccentricity of Stiffeners on the General Instability of Stiffened Cylindrical Shells. Journal of Mechanical Engineering Science, vol. 8, no. 4, 1966, pp. 363-373.

28. Kendrick, S.: The Buckling under External Pressure of Circular Cylindrical Shells with Evenly Spaced Equal Strength Circular Ring Frames. Part III — Naval Construction Research Establishment. Rpt. R-244, September 1953.

29. Galletly, G. D.; Slankard, R. C.; and Wenk, E., Jr.: General Instability of Ring-Stiffened Cylindrical Shells Subject to External Hydrostatic Pressure — A Comparison of Theory and Experiment. J. Appl. Mech., vol. 25, no. 2, June 1958, pp. 259-266.

30. Simitses, G. J.: Instability of Orthotropic Cylindrical Shells under Combined Torsion and Hydrostatic Pressure. AIAA J., vol. 5, no. 8, August 1967, pp. 1463-1469.

31. Baruch, M.; Singer, J.; and Well, T.: Effect of Eccentricity of Stiffeners on the General Instability of Cylindrical Shells under Torsion. Israel Journal of Technology, vol. 4, no. 1, 1966, pp. 144-154.

32. Milligan, R.; and Gerard, G.: General Instability of Orthotropically Stiffened Cylinders under Torsion. AIAA J., vol. 5, no. 11, November 1967, pp. 2071-2073.

REFERENCES (Continued)

33. Dow, N. F.; Libove, C.; and Hubka, R. E.: Formulas for the Elastic Constants of Plates with Integral Waffle-Like Stiffening. NACA Rpt. 1195, 1954.

34. Crawford, R. F.; and Libove, C.: Shearing Effectiveness of Integral Stiffening. NACA TN 3443, 1955.

35. Meyer, R. R.: Buckling of 45° Eccentric-Stiffened Waffle Cylinders. J. Roy. Aeron. Soc., vol. 71, no. 679, July 1967, pp. 516-520.

36. Peterson, J. P.; and Whitley, R. O.: Local Buckling of Longitudinally Stiffened Curved Plates. NASA TN D-750, April 1961.

37. Anon.: Structural Sandwich Composites. MIL-HBBK-23, Dec. 30, 1968.

38. Libove, C.; and Hubka, R. E.: Elastic Constants for Corrugated Core Sandwich Plates. NACA TN 2289, 1951.

39. Plantema, F. J.: Sandwich Construction, The Bending and Buckling of Sandwich Beams, Plates, and Shells. John Wiley & Sons, Inc., New York, 1966.

40. Stein, M.; and Mayers, J.: Compressive Buckling of Simply Supported Curved Plates and Cylinders of Sandwich Construction. NACA TN 2601, 1952.

41. Zahn, J. J.; and Kuenzi, E. W.: Classical Buckling of Cylinders of Sandwich Construction in Axial Compression — Orthotropic Cores. Rpt. FPL-018, Forest Products Laboratories, 1963.

REFERENCES (Continued)

42. Anon.: Composite Construction for Flight Vehicles. Part I — Fabrication, Inspection, Durability, and Repair. MIL-HDBK-23, Part I, Armed Forces Supply Support Center, October 1959.

43. Anon.: Collected Papers on Instability of Shell Structures, 1962. NASA TN D-1510, 1962.

44. Yusuff, S.: Face Wrinkling and Core Strength in Sandwich Construction. J. Roy. Aeron. Soc., vol. 64, no. 591, March 1960, pp. 164-167.

45. Harris, B.; and Crisman, W.: Face Wrinkling Mode of Buckling of Sandwich Panels. EM3, ASCE Journal of Engineering, Mechanics Division, June 1965.

46. Peterson, J. P.: Weight Strength Studies on Structures Representative of Fuselage Construction. NACA TN 4114, 1957.

47. Kiciman, M. O.; and Konishi, D. Y.: Stability of Honeycomb Sandwich Cylinders. Paper No. 61-AV-36, ASME, 1961.

48. Holston, A., Jr.: Stability of Inhomogeneous Anisotropic Cylindrical Shells Containing Elastic Cores. AIAA J., vol. 5, no. 6, June 1967, pp. 1135-1138.

49. Brush, D. O.; and Pittner, E. V.: Influence of Cushion Stiffness on the Stability of Cushion-Loaded Cylindrical Shells. AIAA J., vol. 3, no. 2, February 1965, pp. 308-316.

50. Seide, P.: The Stability under Axial Compression and Lateral Pressure of a Circular-Cylindrical Shell with an Elastic Core. J. Aeron. Sci., vol. 29, no. 7, July 1962, pp. 851-862.

REFERENCES (Continued)

51. Weingarten, V. I.: Stability under Torsion of Circular Cylinder Shells with an Elastic Core. ARS J., vol. 82, no. 4, April 1962, pp. 637-639.

52. Shanley, F. R.: Weight-Strength Analysis of Aircraft Structures. McGraw-Hill Book Co., Inc., New York, 1952.

53. Block, D. L.: Influence of Ring Stiffeners on Instability of Orthotropic Cylinders in Axial Compression. NASA TN D-2482, 1964.

54. Stein, M.; Sanders, J. L.; and Crate, H.: Critical Stress of Ring-Stiffened Cylinders in Torsion. NACA Rpt. 989, 1950.

55. Batdorf, S. B.: A Simplified Method of Elastic Stability Analysis for Thin Cylindrical Shells. NACA Rpt. 874, 1947.

REFERENCES FOR CONICAL SHELLS (SUBSECTION 3.2)

1. Almroth, B. O.; Bushnell, D.; and Sobel, L. H.: Buckling of Shells of Revolution With Various Wall Constructions, vols. I, II, and III. NASA CR-1049-1051, 1968.

2. Bushnell, D.: Stress, Stability, and Vibration of Complex Shells of Revolution: Analysis and User's Manual for BOSOR3. Lockheed Report SAMSO TR-69-375, September 1969.

3. Seide, P.: Axisymmetric Buckling of Circular Cones Under Axial Compression. J. Appl. Mech., vol. 23, no. 4, December 1956, pp. 625-628.

4. Weingarten, V. I.; Morgan, E. J.; and Seide, P.: Elastic Stability of Thin-Walled Cylindrical and Conical Shells Under Axial Compression. AIAA J., vol. 3, no. 3, March 1965. pp. 500-505.

REFERENCES (Continued)

5. Hausrath, A. H.; and Dittoe, F. A.: Development of Design Strength Levels for the Elastic Stability of Monocoque Cones Under Axial Compression. Collected Papers on Instability of Shell Structures, NASA TN D-1510, 1962, pp. 45-56.

6. Seide, P.; Weingarten, V. I.; and Morgan, E. J.: Final Report on Development of Design Criteria for Elastic Stability of Thin Shell Structures. Rpt. TR-60-0000-19425 (AFBMD-TR-61-7), Space Technology Laboratories, Dec. 31, 1960.

7. Seide, P.: On the Buckling of Truncated Conical Shells Under Uniform Hydrostatic Pressure. Proceedings of the IUTAM Symposium on the Theory of Thin Elastic Shells, Delft, The Netherlands, Aug. 24-28, 1959, North-Holland Publishing Company, The Netherlands, 1960, pp. 363-388.

8. Weingarten, V. I.; and Seide, P.: Elastic Stability of Thin-Walled Cylindrical and Conical Shells Under Combined External Pressure and Axial Compression. AIAA J., vol. 3, no. 5, May 1965, pp. 913-920.

9. Singer, J.; and Eckstein, A.: Recent Experimental Studies of Buckling of Conical Shells Under Torsion and External Pressure. Fifth Israel Conference, Aviation and Astronautics, February 1963, pp. 135-146.

10. Seide, P.: On the Buckling of Truncated Conical Shells in Torsion. J. Appl. Mech., vol. 29, no. 2, June 1962, pp. 321-328.

11. Seide, P.: On the Stability of Internally Pressurized Conical Shells Under Axial Compression. Proceedings of the Fourth U.S. National Congress of Applied Mechanics, University of California Press, Berkeley, Calif., 1962, pp. 761-773.

REFERENCES (Continued)

12. Singer, J.: Donnell-Type Equations for Bending and Buckling of Orthotropic Conical Shells. J. Appl. Mech., vol. 30, no. 2, June 1963, pp. 303-305.

13. Baruch, M.; and Singer, J.: General Instability of Stiffened Circular Conical Shells Under Hydrostatic Pressure. TAE Rpt. 28, Technion-Israel Institute of Technology, June 1963.

14. Singer, J.; and Fersht-Scher, R.: Buckling of Orthotropic Conical Shells Under External Pressure. Aeron. Quart., vol. 15, pt. 2, May 1964, p. 151.

15. Stein, M.; and Mayers, J.: A Small-Deflection Theory for Curved Sandwich Plates. NACA Rpt. 1008, 1951.

16. Becker, H.; and Gerard, G.: Elastic Stability of Orthotropic Shells. J. Aeron. Sci., vol. 29, no. 5, May 1962, pp. 505-512, 520.

17. Singer, J.: On the Buckling of Unstiffened Orthotropic and Stiffened Conical Shells. Seventh International Congress for Aeronautics, Paris, June 14-16, 1965.

18. Baruch, M.; Singer, J.; and Marari, O.: Instability of Conical Shells with Non-Uniformly Spaced Stiffeners Under Hydrostatic Pressure. Seventh Israel Conference, Aviation and Aeronautics, vol. 3, no. 1, Feb. 1965, pp. 62-71.

19. Singer, J.; Fersht-Scher, R.; and Betser, A.: Buckling of Orthotropic Conical Shells Under Combined Torsion and External or Internal Pressure. Sixth Israel Conference, Aviation and Astronautics, Israel Journal of Technology, vol. 2, no. 1, Feb. 1964, pp. 179-189.

REFERENCES (Continued)

20. Plantema, F. J.: Sandwich Construction, The Bending and Buckling of Sandwich Beams, Plates and Shells. John Wiley & Sons, Inc., New York, 1966.

21. Yusuff, S.: Face Wrinkling and Core Strength in Sandwich Construction. J. Roy. Aeron. Soc., vol. 64, no. 591, March 1960, pp. 164-167.

22. Harris, B.; and Crisman, W.: Face-Wrinkling Mode of Buckling of Sandwich Panels. ASCE Journal, Engineering Mechanics Division, EM3, June 1965.

23. Peterson, J. P.: Weight-Strength Studies on Structures Representative of Fuselage Construction. NACA TN 4114, 1957.

REFERENCES FOR DOUBLY CURVED SHELLS (SUBSECTION 3.3)

1. Bushnell, D.: Stress, Stability, and Vibration of Complex Shells of Revolution: Analysis and User's Manual for BOSOR3, Lockheed Report SAMSO TR-69-375, September 1969.

2. Weinitschke, H.: On the Stability Problem for Shallow Spherical Shells. J. Math. and Phys., vol. 38, no. 4, December 1960, pp. 209-231.

3. Budiansky, B.: Buckling of Clamped Shallow Spherical Shells. Proceedings of the IUTAM Symposium on Theory of Thin Elastic Shells, North-Holland Publishing Co., Amsterdam, 1960, pp. 64-94.

4. Huang, N. C.: Unsymmetrical Buckling of Thin Shallow Spherical Shells. J. Appl. Mech., vol. 31, no. 3, September 1964, pp. 447-457.

REFERENCES (Continued)

5. Weinitschke, H.: On Asymmetric Buckling of Shallow Spherical Shells. J. Math. and Phys., vol. 44, no. 2, June 1965, pp. 141-163.

6. Thurston, G. A.; and Penning, F. A.: Effect of Axisymmetric Imperfections on the Buckling of Spherical Caps Under Uniform Pressure. AIAA J., vol. 4, no. 2, February 1966, p. 319.

7. Bushnell, D.: Nonlinear Axisymmetric Behavior of Shells of Revolution. AIAA J., vol. 5, no. 3, March 1967, pp. 432-439.

8. Wang, L. R. L.: Effects of Edge Restraint on the Stability of Spherical Caps. AIAA J., vol. 4, no. 4, April 1966, pp. 718-719.

9. Bushnell, D.: Buckling of Spherical Shells Ring-Supported at the Edges. AIAA J., vol. 5, no. 11, November 1967, pp. 2041-2046.

10. Wang, L. R. L.: Discrepancy of Experimental Buckling Pressures of Spherical Shells. AIAA J., vol. 5, no. 2, February 1967, pp. 357-359.

11. McComb, H. G., Jr.; and Fitcher, W. B.: Buckling of a Sphere of Extremely High Radius-Thickness Ratio. Collected Papers on Instability of Shell Structures, NASA TN D-1510, 1962, pp. 561-570.

12. Mescall, J. F.: Large Deflections of Spherical Shells Under Concentrated Loads. J. Appl. Mech., vol. 32, no. 4, December 1956, pp. 936-938.

13. Fitch, J. R.: The Buckling and Post-Buckling Behavior of Spherical Caps Under Concentrated Load. Int. J. Solids Structures, vol. 4, no. 4, April 1968, pp. 421-446.

REFERENCES (Continued)

14. Bushnell, D.: Bifurcation Phenomena in Spherical Shells Under Concentrated and Ring Loads. AIAA J., vol. 5, no. 11, November 1967, pp. 2034-2040.

15. Ashwell, D. G.: On the Large Deflection of a Spherical Shell With an Inward Point Load. Proceedings of the IUTAM Symposium on the Theory of Thin Elastic Shells, North-Holland Publishing Co., Amsterdam, 1960, pp. 43-63.

16. Evan-Iwanowski, R. M.; Cheng, H. S.; and Loo, T. C.: Experimental Investigations and Deformation and Stability of Spherical Shells Subjected to Concentrated Loads at the Apex. Proceedings of the Fourth U. S. Nat. Engr. Appl. Mech., 1962, pp. 563-575.

17. Penning, F. A.; and Thurston, G. A.: The Stability of Shallow Spherical Shells Under Concentrated Load. NASA CR-265, 1965.

18. Penning, F. A.: Experimental Buckling Modes of Clamped Shallow Shells Under Concentrated Load. J. Appl. Mech., vol. 33, no. 2, June 1966, pp. 297-304.

19. Penning, F. A.: Nonaxisymmetric Behavior of Shallow Shells Loading at the Apex. J. Appl. Mech., vol. 33, no. 3, September 1966, pp. 699-700.

20. Loo, T. C.; and Evan-Iwanowski, R. M.: Interaction of Critical Concentrated Loads Acting on Shallow Spherical Shells. J. Appl. Mech., vol. 33, no. 3, September 1966, pp. 612-616.

21. Danielson, D. A.: Buckling and Initial Postbuckling Behavior of Spheroidal Shells Under Pressure. AIAA J., vol. 7, no. 5, May 1969, pp. 936-944.

REFERENCES (Continued)

22. Hyman, B. I.; and Healey, J. J.: Buckling of Prolate Spheroidal Shells Under Hydrostatic Pressure. AIAA J., vol. 5, no. 8, August 1967, pp. 1469-1477.

23. Nickell, E. H.: Experimental Buckling Tests of Magnesium Monocoque Ellipsoidal Shells Subjected to External Hydrostatic Pressure. Tech. Rpt. 3-42-61-2, vol. IV, Lockheed Missiles and Space Company, June 30, 1961.

24. Meyer, R. R.; and Bellinfante, R. J.: Fabrication and Experimental Evaluation of Common Domes Having Waffle-like Stiffening. Rpt. SM-47742, Douglas Aircraft Company, Inc., 1964.

25. Thurston, G. A.; and Holston, A. E., Jr.: Buckling of Cylindrical Shell End Closures by Internal Pressure. NASA CR-540, 1966.

26. Adachi, J.; and Benicek, M.: Buckling of Torispherical Shells Under Internal Pressure. Exp. Mech., vol. 4, no. 8, August 1964, pp. 217-222.

27. Sobel, L. H.; and Flugge, W.: Stability of Toroidal Shells Under Uniform External Pressure. AIAA J., vol. 5, no. 3, March 1967, pp. 425-431.

28. Anon: Buckling of Thin-Walled Circular Cylinders. NASA Space Vehicle Design Criteria (Structures), NASA SP-8007, revised 1968.

29. Hutchinson, J. W.: Initial Post-Buckling Behavior of Toroidal Shell Segments. Int. J. Solids Structures, vol. 3, no. 1, January 1967, pp. 97-115.

REFERENCES (Continued)

30. Yao, J. C.: Buckling of a Truncated Hemisphere Under Axial Tension. AIAA J., vol. 1, no. 10, October 1963, pp. 2316-2320.

31. Babcock, C. D.; and Sechler, E. E.: The Effect of Initial Imperfections on the Buckling Stress of Cylindrical Shells. Collected Papers on Instability of Shell Structures. NASA TN D-1510, 1962, pp. 135-142.

32. Blum, R. E.; and McComb, H. G., Jr.: Buckling of an Equatorial Segment of a Spherical Shell Loaded by its Own Weight. NASA TN D-4921, 1968.

33. Stein, M.; and McElman, J. A.: Buckling of Segments of Toroidal Shells. AIAA J., vol. 3, no. 9, September 1965, pp. 1704-1709.

34. Almroth, B. O.; Bushnell, D.; and Sobel, L. H.: Buckling of Shells of Revolution with Various Wall Constructions. Vols. I-III, NASA CR-1049 to CR-1051, 1968.

35. Crawford, R. F.: Effects of Asymmetric Stiffening on Buckling of Shells. AIAA Paper No. 65-371, 1965.

36. Bushnell, D.: Symmetric and Nonsymmetric Buckling of Finitely Deformed Eccentrically Stiffened Shells of Revolution. AIAA J., vol. 5, no. 8, August 1967, pp. 1455-1462.

37. Ebner, H.: Angencherte Bestimmung der Tragfahigkeit radial versteifter Kugelschalen unter Druckbelastung. Proceedings of the IUTAM Symposium on the Theory of Thin Elastic Shells. North-Holland Publishing Co., Amsterdam, 1960, pp. 95-121.

REFERENCES (Continued)

38. Kloppel, K.; and Jungbluth, O.: Beitrag zum Durchschlagproblem dunnwandiger Kugelschalen. Der Stahlbau, Vol. VI, 1953, pp. 121-130. (Also available as David Taylor Model Basin Translation 308, May 1966.)

39. Crawford, R. F.; and Schwartz, D. B.: General Instability and Optimum Design of Grid Stiffened Spherical Domes. AIAA J., vol. 3, no. 3, March 1965, pp. 511-515.

40. McElman, J. A.: Eccentrically Stiffened Shallow Shells of Double Curvature. NASA TN D-3826, February 1967.

41. Yao, J. C.: Buckling of Sandwich Sphere Under Normal Pressure. J. Aerospace Sci., vol. 29, no. 3, March 1962, pp. 264-268.

42. Anon: Structural Sandwich Composites. MIL-HDBK 23, December 30, 1968.

REFERENCES FOR COMPUTER PROGRAMS (SUBSECTION 3.4)

1. Dickson, J. N.; and Brolliar, R. H.: The General Instability of Ring-Stiffened Corrugated Cylinders Under Axial Compression, NASA TN D-3089, January 1966.

2. Dickson, J. N.; and Brolliar, R. H.: The General Instability of Eccentrically Stiffened Cylindrical Shells Under Axial Compression and Lateral Pressure, NASA CR-1280, January 1969.

3. Burns, A. B.: Computer Program for the General Instability Analysis of Ring-Stringer Stiffened Cylinders Subjected to Axial Compression and Lateral Pressure. Rpt. 4-11-66-1, Lockheed Missiles and Space Company, March 1966.

REFERENCES (Continued)

4. Burns, A. B.: Optimum Stiffened Cylinders for Combined Axial Compression and Internal or External Pressure. J. Spacecraft Rockets, vol. 5, 1968, pp. 690-699.

5. Mah, G. B.; Almroth, B. O.; and Pittner, E. V.: Buckling of Orthotropic Cylinders. AIAA J., vol. 6, 1968, pp. 598-602.

6. Brogan, F.; and Almroth, B. O.: Buckling of Cylinders with Cutouts. Proceedings of the AIAA Seventh Aerospace Sciences Meeting, New York, January 1969.

7. Almroth, B. O.; Bushnell, D.; and Sobel, L. H.: Buckling of Shells of Revolution with Various Wall Constructions. Vols. I, II, and III, NASA CR 1049-1051, 1968.

8. Bushnell, D.: Stress, Stability, and Vibration of Complex Shells of Revolution. Analysis and User's Manual for BOSOR3, Lockheed Rpt. SAMSO TR-69-375, September 1969.

9. Percy, J. H.; Navaratna, D. R.; and Klein, S.: SABORIII: A FORTRAN Program for the Linear Elastic Analysis of Thin Shells of Revolution Under Asymmetric Loading by Using the Matrix Displacement Method, ASRL TR 121-6, Massachusetts Institute of Technology Aeroelastic and Structures Research Laboratory, May 1965.

10. Loden, W. A.; Morton, F. G.; and Strickland, G. E., Jr.: BERKIII: A Finite Element Program for Linear Static and Dynamic Analysis of Arbitrary Thin Shells with Stiffeners. Rpt. 5-59-69-1, Lockheed Missiles and Space Company, December 1968.

REFERENCES (Concluded)

11. McCormick, C. W., ed.: The NASTRAN User's Manual, NASA SP-222, October 1969.

12. Loden, W. A.: User's Manual in Preparation. Lockheed Missiles and Space Company, January 1969.

SECTION C4

LOCAL INSTABILITY

TABLE OF CONTENTS

* To be supplied

C4.0.0 LOCAL INSTABILITY

C4.1.0 Introduction

This section deals with local instabilities and failures of flat and curved panels. The term "panel" refers to a composite structure consisting of plates and stiffeners. The term "plate" refers to sheet or skin bounded by longitudinal and tranverse members (e.g., stiffeners and frames). Panels in compression are of primary importance in this section. Although panels in shear are discussed, information concerning them is not as extensive as that for panels in compression.

Stability analyses of panels should account for both general and local modes of instability. The general mode of instability for a compression-loaded panel is characterized by deflection of the stiffeners; whereas, for local instability, buckling occurs with modes along (or nearly along) the stiffener-plate juncture (Fig. C4.1.0-1). Some coupling between these modes exists, but this effect is usually small and is generally neglected.

General Instability Local Instability

FIGURE C4.1.0-1. TYPICAL BUCKLE MODES IN LONGITUDINALLY STIFFENED PLATES UNDER LONGITUDINAL LOAD.

Definition of Symbols

Symbol	Definition
a	long-side dimension of a plate, in.
b	short-side dimension of a plate, in.
b'	short-side dimension of a rectangular tube, in.
b_f	width of stiffener flange, in.
b_o	geometric fastener offset, in.
b_s	stiffener spacing, in.
b_T	width of hat top for hat-section stiffeners, in.
b_w	depth of stiffener web, in.
d	fastener diameter, in.
d_f	frame spacing, in.
e	end-fixity coefficient
E	Young's modulus of elasticity, psi
E_s, E_t	secant and tangent moduli, psi
f	actual stress, psi; also effective fastener offset, in.
F	allowable or buckling stress, psi
$F_{0.7}$, $F_{0.85}$	stress at secant modulus, 0.7 E or 0.85 E of skin material
D	flexural stiffness of skin per inch of width, $Et_s^3/12(1-\nu^2)$
g	spacing between staggered columns of fasteners, in.

Definition of Symbols (Continued)

Symbol	Definition
G	elastic shear modulus, psi
h'	long-side dimension of rectangular tube, in.
h	spacing between staggered rows of fasteners, in.
I	bending moment of inertia of stiffener cross section taken about the stiffener centroidal axis, $in.^4$
I_p	polar moment of inertia of section about center of rotation, $in.^4$
J	torsion constant of the stiffener, $in.^4$ (GJ = torque/twist per unit length)
k	rotational spring constant
k_c	compressed skin local buckling coefficient
k_h, k_t, k_w	compressed stiffener local buckling coefficients.
k_s	shear buckling coefficient
k_{wr}	compressed panel wrinkling coefficient
k_{sc}	compressive-local-buckling coefficient for panels with integral stiffeners.
M.S.	margin of safety
N	number of stiffeners
n	shape parameter
r	radius, in.
s	fastener pitch, in.

Definition of Symbols (Continued)

Symbol	Definition
t	thickness, in.
η	plasticity reduction factor
$\bar{\eta}$	cladding reduction factor
ν	Poisson's ratio in elastic range
Γ	torsional-bending constant, $in.^6$
Subscript	
c	compression
e	effective
f	flange
t	tension or top web of hat-section stiffeners
s	skin, shear
w	web
av	average
cir	local compressive inter-fastener buckling
co	cutoff
CRI	local compressive integral stiffener panel buckling
cs	compressive skin buckling
csr	shear skin buckling

Definition of Symbols (Concluded)

Subscripts	Definition
csk	compressive local skin buckling
cst	compressive local stiffener buckling
ct	compressive panel torsional buckling
cw	compressive panel wrinkling
cy	compressive yield
tr	tensile fastener stress
pl	proportional limit

C4.2.0 Conventionally Stiffened Flat Panels in Compression

Buckling resulting from local compression instability in a panel conventionally stiffened (Fig. C4.2.0-1) in the direction of the load may occur in either the stiffener elements or the plate.

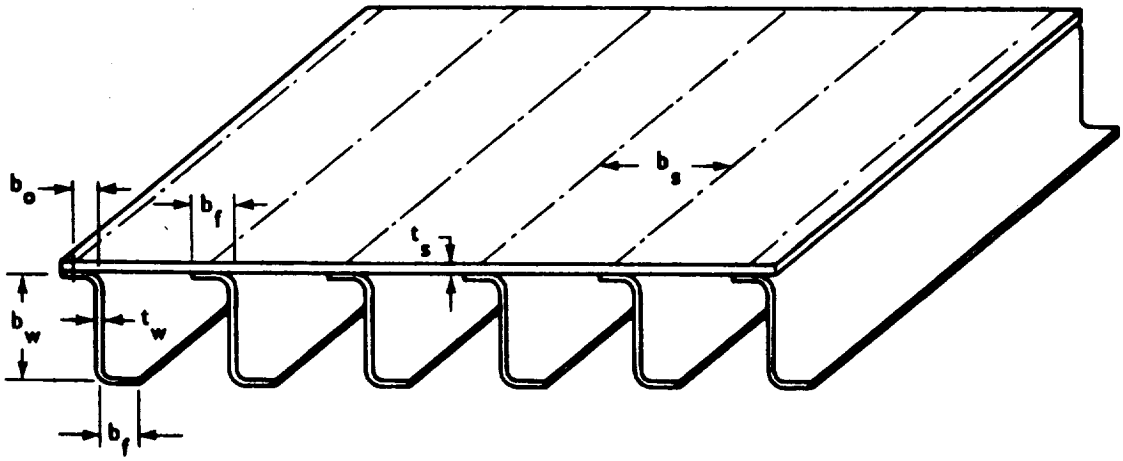

FIGURE C4.2.0-1. TYPICAL CONVENTIONALLY STIFFENED PANEL.

The forms of local instabilities and failures which will be discussed in this section are:

1. Local skin buckling
2. Local stiffener buckling
3. Inter-fastener buckling
4. Panel wrinkling (Forced crippling)
5. Torsional instability

Although these are distinct instability modes, ultimate buckling failure is usually a combination of two or more modes.

Other local modes of failure classified as column post-buckling phenomena are described in the following three paragraphs but are not discussed further in this section of the manual.

1. Stiffener crippling is a local collapse of a composite stiffener section. Crippling is covered in Section C1.3.1 of this manual.

2. Lateral instability consists of a twisting of the stiffener section, accompanied by a distortion of the cross section. The analytical technique presented in "Shell Analysis Manual" [1] is recommended to the reader since this mode is not discussed in this manual at the present time.

3. Monolithic panel failure, an extension of stiffener crippling, is a failure of skin and stiffener so fastened together that they act as a monolithic unit when subjected to crippling stress levels. Analytical methods presented in the documents cited in References 2 and 3 are recommended to the reader since this mode is not discussed in this manual at the present time.
Three of the cited local instability modes are a direct function of the fastener spacing (Fig. C4.2.0-2).

C4.2.1 Local Skin Buckling

A local compression instability mode that is often observed is local skin buckling. This mode can occur in skins between or under stiffeners of a stiffened panel. Although this mode can be a failure in itself, it usually precipitates failure in another mode if the load is appreciably increased.

The normal analytical procedure for this type instability is to treat the skin as a simply supported flat plate of infinite length. The following general equation for skin buckling stress is written in nondimensional form:

$$\frac{F_{csk}}{F_{0.7}} = \eta\,\bar{\eta}\,\frac{k_c\,\pi^2\,E}{12\,(1-\nu^2)\,F_{0.7}}\left(\frac{t_s}{b}\right)^2 \qquad (1)$$

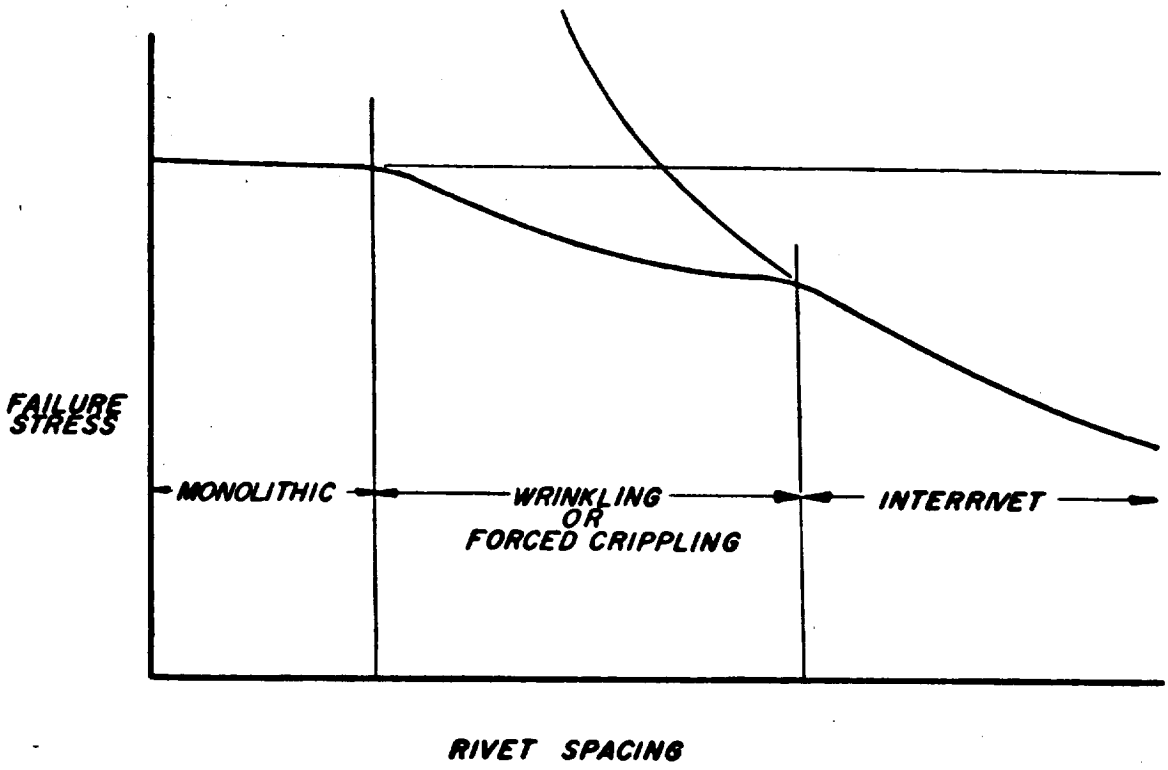

FIGURE C4.2.0-2. FAILURE MODES OF SHORT RIVETED PANELS.

This equation can be solved by the following procedure:

1. Determine $F_{0.7}$ from appropriate stress-strain curve.
2. Determine k_c from Table C2.1.5.5.
3. Determine n from Table C2.1.5.6. If n is not given in the table, it may be obtained from data given in Section C4.2.3.
4. Calculate $$\frac{k_c \pi^2 E}{12 (1-\nu^2) F_{0.7}} \left(\frac{t_s}{b}\right)^2 .$$
5. Enter Figure C2.1.5-4 at value calculated in step four to obtain $F_{csk}/F_{0.7}$, using appropriate n curve.

6. Calculate F_{csk}.

F_{csk} should include plasticity and cladding reduction factors, as given in Tables C2.1.5.1 and C2.1.5.2 respectively, if applicable.

The margin of safety, M.S., can be calculated as follows:

$$M.S. = \frac{F_{csk}}{f_c} - 1 \quad , \tag{2}$$

where f_c is the compressive stress in the skin.

C4.2.2 Local Stiffener Buckling

Local instability or local buckling of a section is to be distinguished from crippling of a section. Crippling is an ultimate type of failure (discussed in Section C1.3.1), while local buckling is an elastic condition which may occur at much lower stresses. Generally, this type of instability will not constitute failure in itself but will usually precipitate failure in another mode.

In stiffeners with flat sides, local instability is defined as that mode of distortion in which the meets of adjoining sides remain stationary. Thus, each side buckles as a plate whose edges parallel to the load rotate through the same angles as those of the adjoining sides and the half-wavelength is of the order of the cross-section dimensions (Fig. C4.2.2-1).

Two of the simplest flange-web shapes are angles and zees. These can be considered as compound plate elements and can be broken up as shown in Figure C4.2.2-2. Information found in Section C2 can be used to determine buckling stresses of the shapes described above.

However, a more direct method for predicting the local buckling stress, taking into account the interaction of the sides, in the elastic range is to use the following equation:

$$F_{cst} = \eta \bar{\eta} \frac{k_i \pi^2 E}{12 (1-\nu^2)} \left(\frac{t}{b}\right)^2 \quad , \qquad (3)$$

where (k_i) is an experimentally determined local buckling coefficient. Figures C4.2.2.-3 through C4.2.2-6 show (k_i) values for various channels, Z-sections, H-sections, rectangular-tube-sections, and hat-sections often used for stiffened-plate construction.

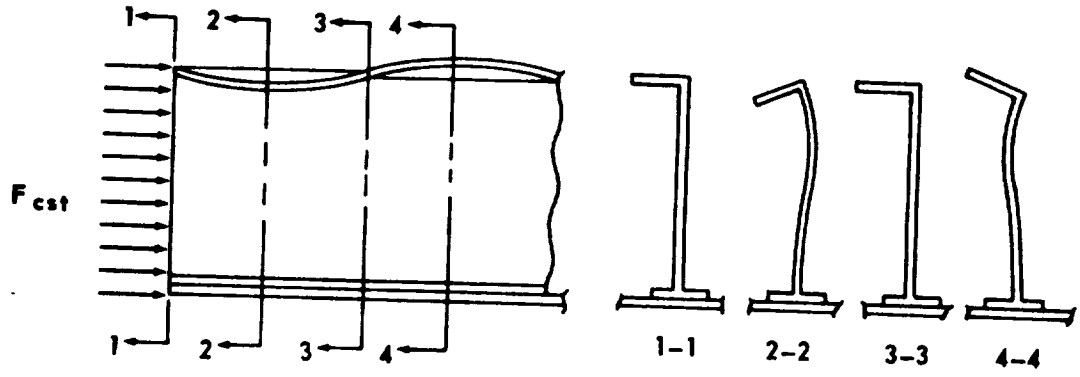

FIGURE C4.2.2-1. TYPICAL STIFFENER LOCAL BUCKLING SHOWING ONLY TWO HALF-WAVES.

A discussion of cladding and plasticity-reduction factors can be found in Section C2.1.1. Figure C4.2.2-7 gives experimentally determined plasticity-reduction factors for stiffener shapes presented in Figures C4.2.2-3 through C4.2.2-6.

The reader should also observe dimensioning differences for formed and extruded stiffeners, as shown in Figure C4.2.2-8, prior to calculating parameters when using the buckling coefficient curves cited above.

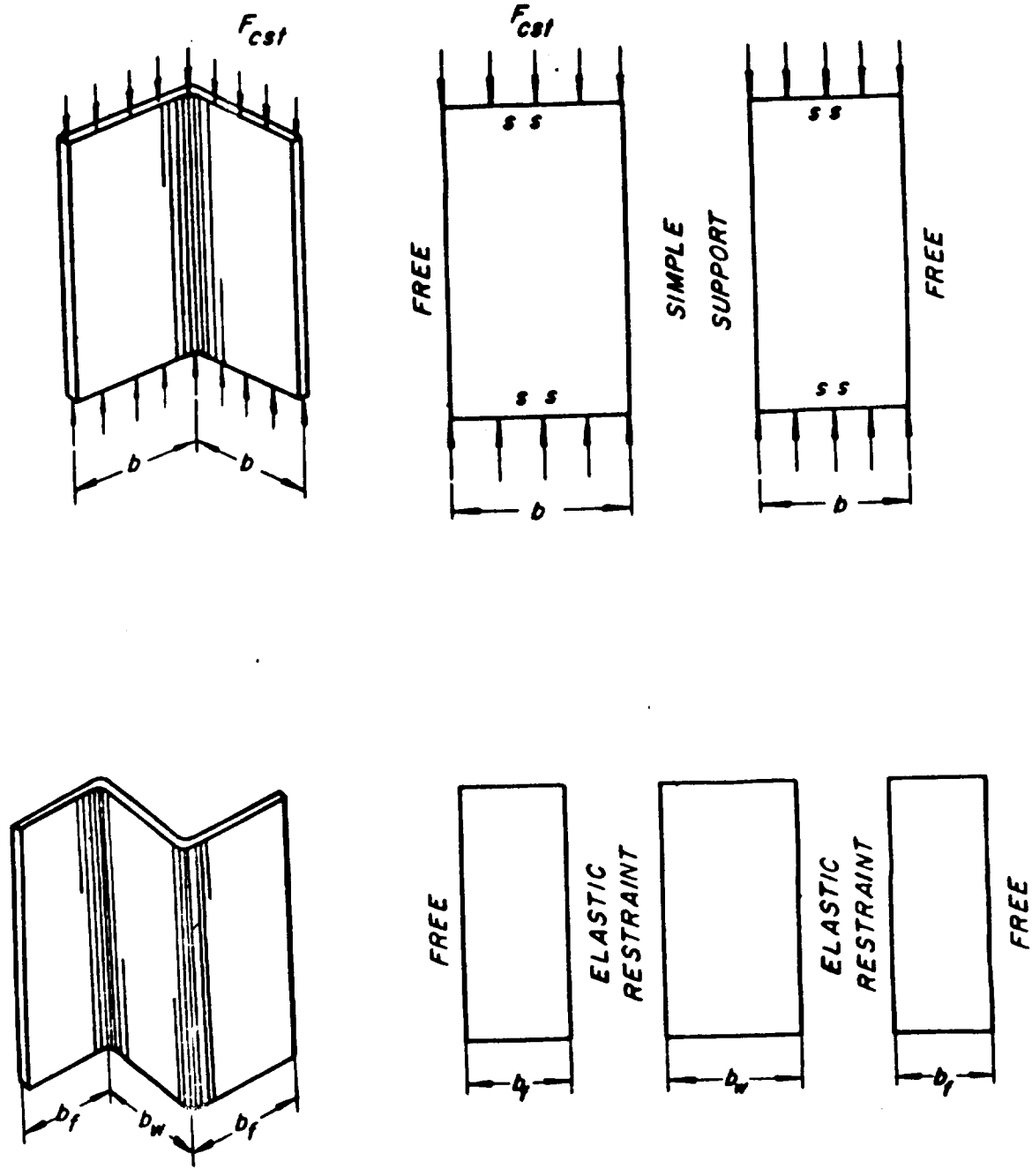

FIGURE C4.2.2-2. BREAKDOWN OF ANGLE AND Z-STIFFENERS INTO COMPONENT PLATE ELEMENTS.

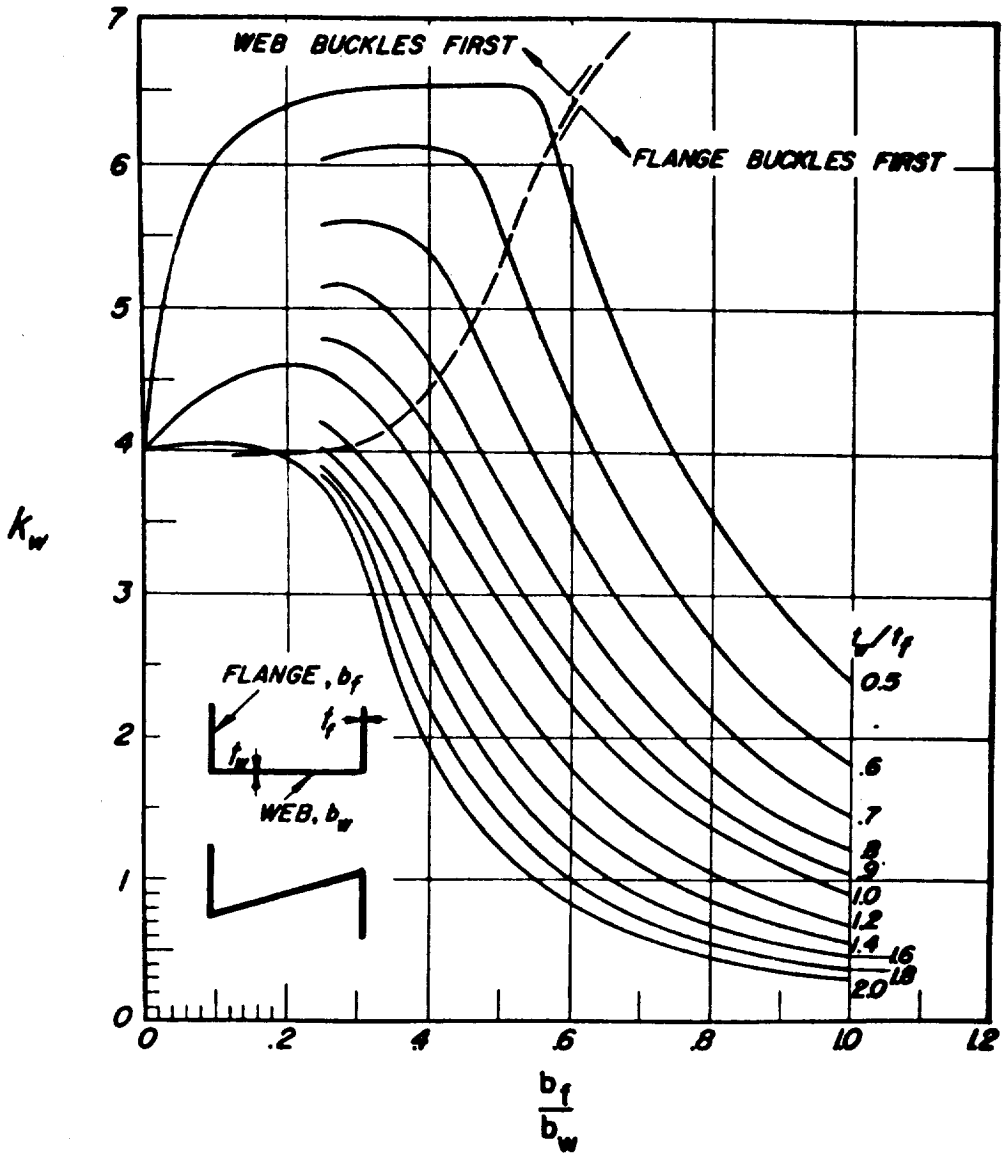

$$F_{cst} = \eta \bar{\eta} \frac{k_w \pi^2 E}{12 (1-\nu^2)} \left(\frac{t_w}{b_w}\right)^2$$

FIGURE C4.2.2-3. COMPRESSION LOCAL BUCKLING COEFFICIENTS FOR CHANNEL AND Z-SECTION STIFFENERS.

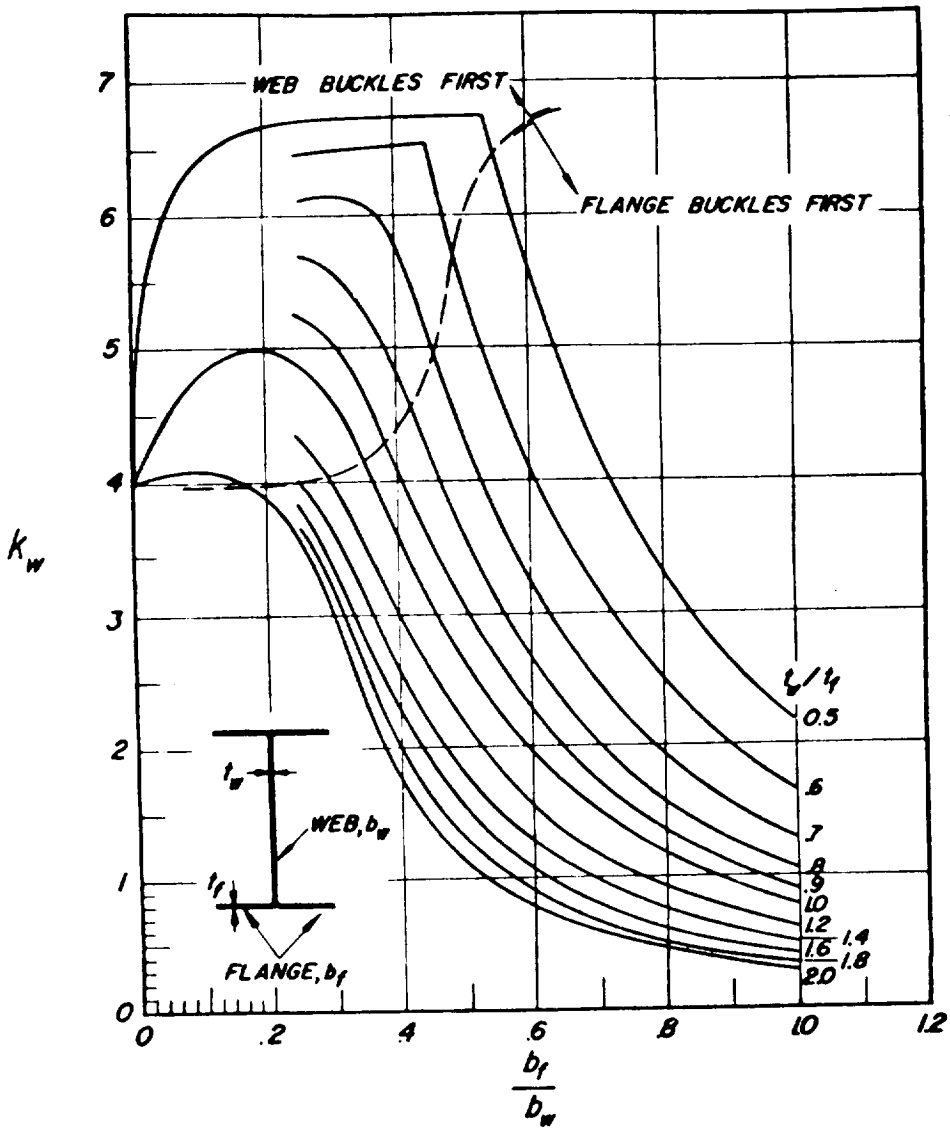

$$F_{cst} = \eta \bar{\eta} \frac{k_w \pi^2 E}{12 (1-\nu^2)} \left(\frac{t_w}{b_w}\right)^2$$

FIGURE C4.2.2-4. COMPRESSION LOCAL BUCKLING COEFFICIENT FOR H-SECTION STIFFENERS.

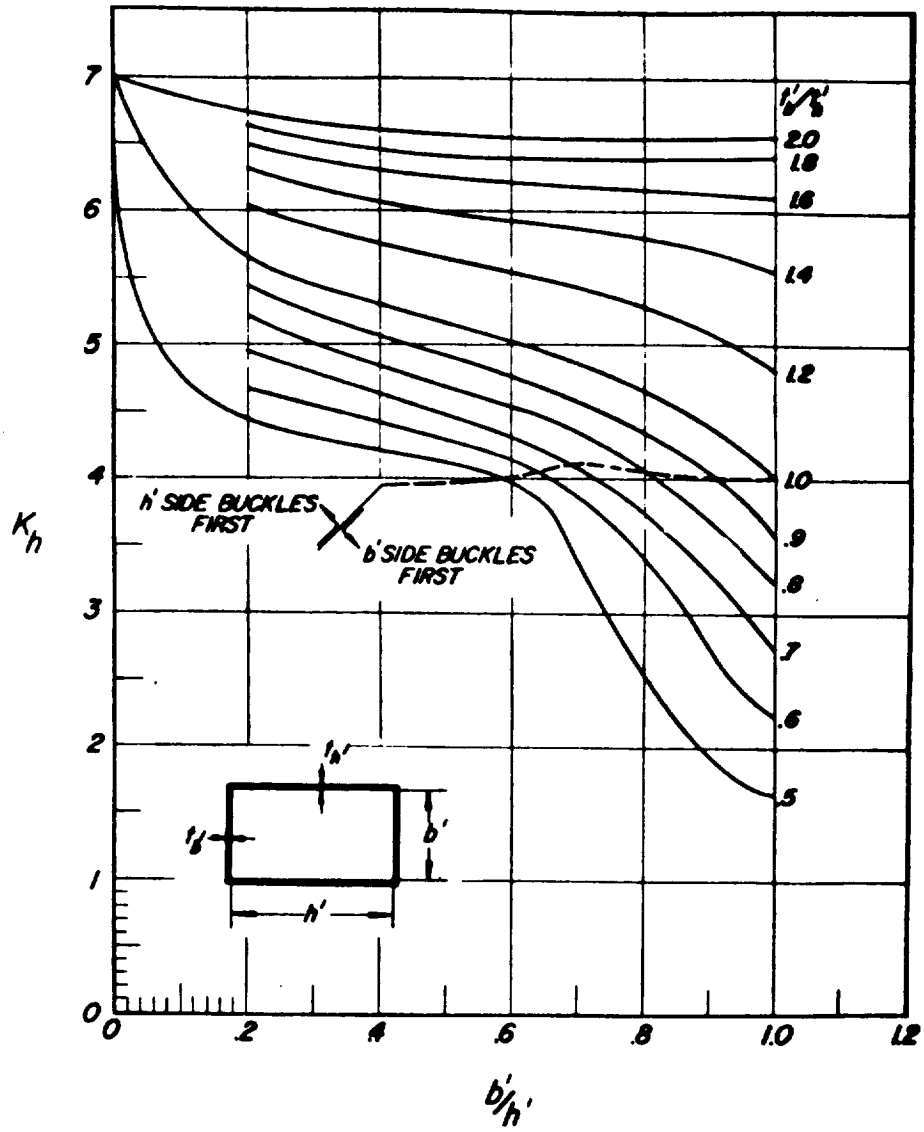

$$F_{cst} = \eta \bar{\eta} \frac{k_h \pi^2 E}{12 (1-\nu^2)} \left(\frac{t_{h'}}{h'}\right)^2$$

FIGURE C4.2.2-5. COMPRESSION LOCAL BUCKLING COEFFICIENT FOR RECTANGULAR-TUBE-SECTION STIFFENERS.

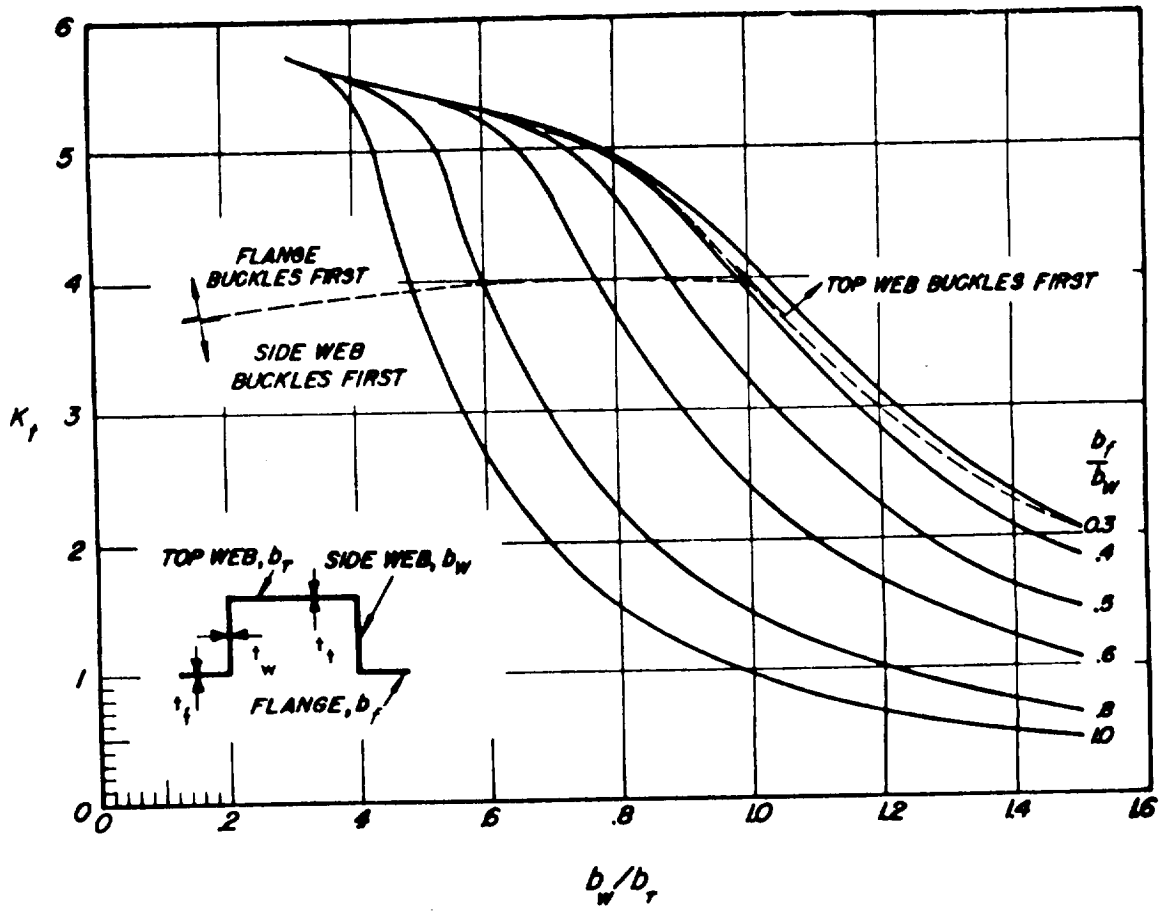

$$F_{cst} = \eta \bar{\eta} \frac{k_t \pi^2 E}{12 (1 - \nu^2)} \left(\frac{t}{b_T} \right)^2$$

FIGURE C4.2.2-6. COMPRESSION LOCAL BUCKLING COEFFICIENT FOR HAT-SECTION STIFFENERS, $t = t_f = t_w = t_t$.

Fig.	Section	Buckling coefficient	Plasticity-reduction factor
C4.2.2-3	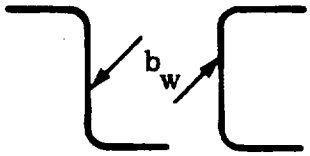	k_w	$(E_s/E)(1-\nu_e^2)/(1-\nu^2)$ is about 5 percent conservative
C4.2.2-4	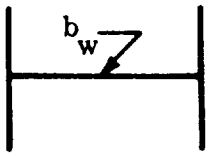	k_w	None reported
C4.2.2-5	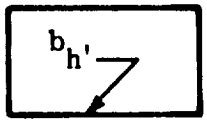	k_h	None reported
C4.2.2-6	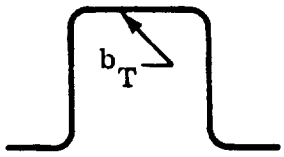	k_t	None reported

FIGURE C4.2.2-7. EXPERIMENTALLY DETERMINED PLASTICITY-REDUCTION FACTORS FOR COMPOSITE SHAPES IN FIGURES C4.2.2-3 THROUGH C4.2.2-6.

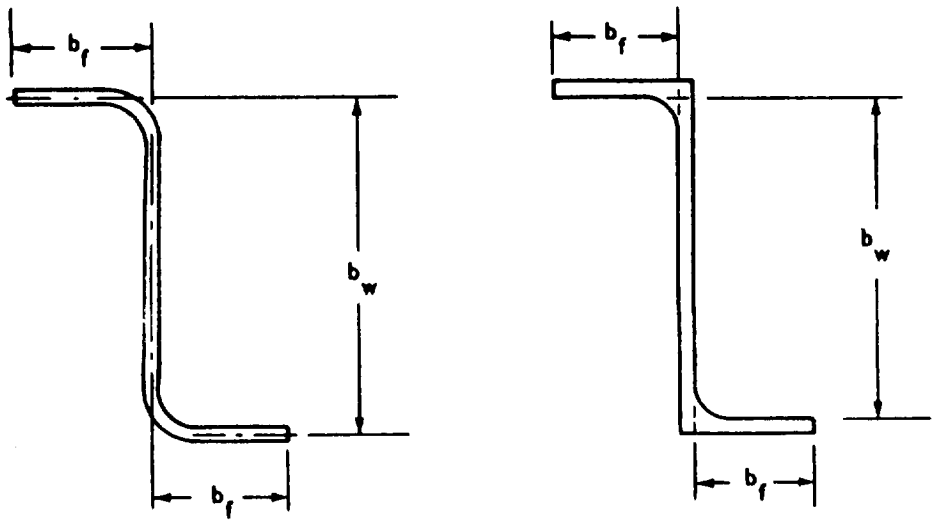

(a) Formed Section (b) Extruded Section

FIGURE C4.2.2-8. TYPICAL DIMENSION FOR FORMED AND EXTRUDED STIFFENERS.

C4.2.3 Inter-Fastener Buckling (Interrivet Buckling)

This mode of local instability, as shown in Figure C4.2.3-1, occurs between fasteners in the skin of longitudinally stiffened panels in compression, causing a separation between the skin and an essentially undistorted stiffener. The action approximates that of a wide column with a width equal to or less than the fastener spacing. Inter-fastener buckling is usually found in stiffened-panel designs where the skin gage is less than the stiffener gage. Any increase in load above the inter-fastener buckling load cannot be supported by the skin; therefore, redistribution of load to the stiffeners and excessive skin deformation occurs.

A criterion for fastener spacing is determined from test data which result from failure in the inter-fastener buckling mode rather from panel

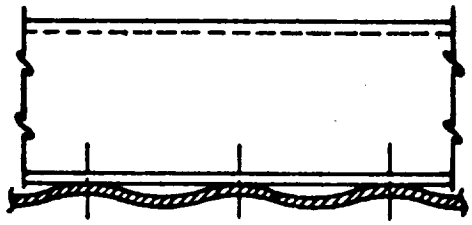

FIGURE C4.2.3-1. TYPICAL INTER-FASTENER BUCKLING.

wrinkling (Section C4.2.4):

$$s/b_s \geq 1.27/(k_{wr})^{1/2} \quad , \qquad (4)$$

where the wrinkling coefficient (k_{wr}) is given in Section C4.2.4. This coefficient is a function of the experimentally determined effective rivet offset (f). Dimensioning rules given in Figure C4.2.2-8 for formed and extruded stiffener sections should be observed.

When inter-fastener buckling is analyzed as a wide column, the following equation applies:

$$F_{cir} = \eta \bar{\eta} \frac{e \pi^2 E_c}{12 (1-\nu^2)} \left(\frac{t_s}{s}\right)^2 \qquad (5)$$

Figure C4.2.3-2 presents a graphical nondimensional form of the equation above. The values needed to enter this chart are: $F_{0.70}$, $F_{0.85}$, E_c, ν, t_s, s, e, and n.

Values of $F_{0.70}$ and $F_{0.85}$ may be obtained from a stress-strain curve as indicated in Figure C4.2.3-3 (a). Values for E_c and ν can be obtained from MIL-HDBK-5A or other well-qualified sources.

If cladding is used on the sheet, the sheet thickness, t_s, will not include the cladding material. The fastener spacing to be used will depend on the pattern of the fasteners. For a single row or double rows the fastener spacing will be the actual distance between fasteners, as shown in Figures C4.2.3-4 (a) and C4.2.3-4 (b). For staggered rows, an effective fastener spacing must be used. This effective spacing, s, may be calculated:

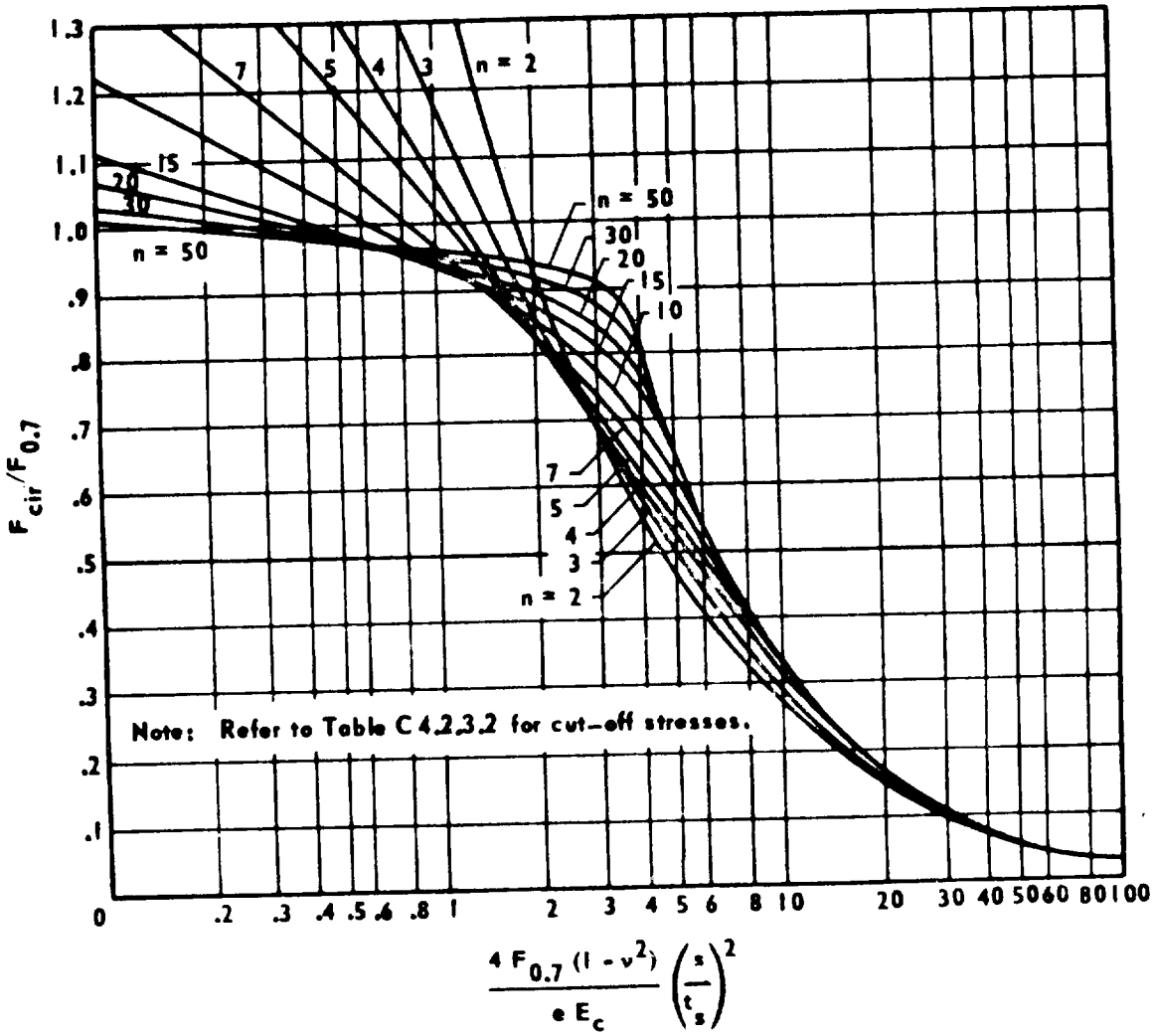

FIGURE C4.2.3-2. CHART OF NONDIMENSIONAL INTERRIVET BUCKLING STRESS.

$$s = \frac{g}{2} + h \qquad (0 \leq g \leq 2s) \qquad , \tag{6}$$

where g and h are shown in Figure C4.2.3-4 (c). If g is greater than 2h, use 2h as the value of s.

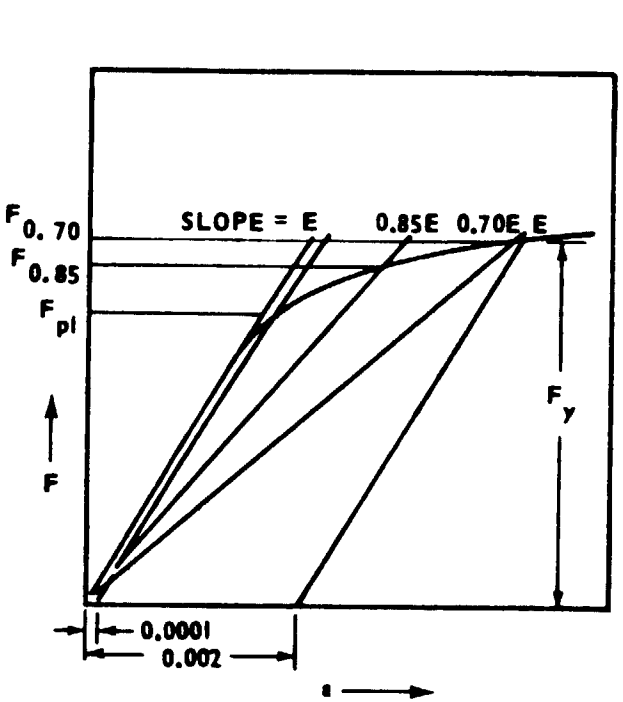

(a) Significant Stress Quantities on a Typical Stress-Strain Curve.

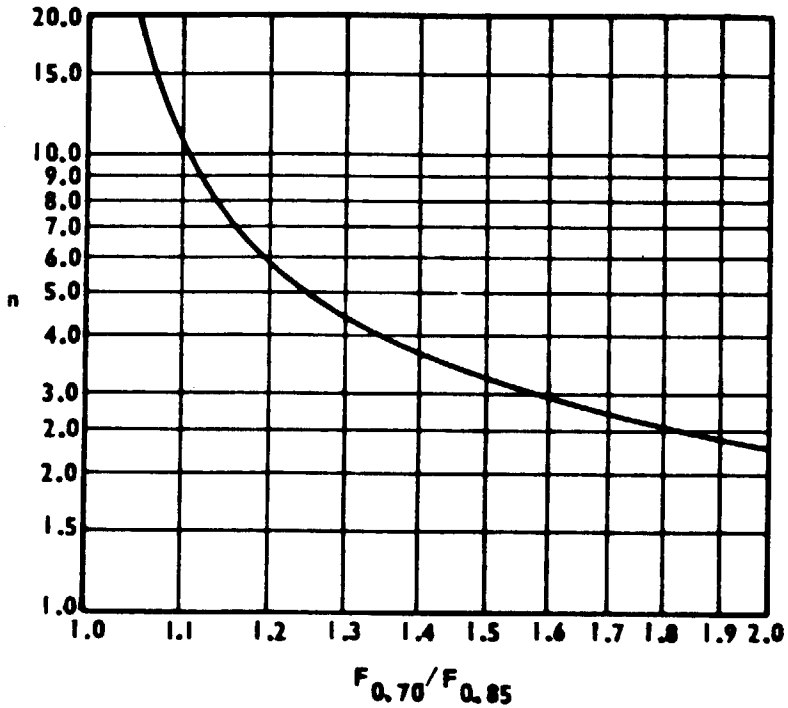

(b) Dependence of Shape Factor on Ratio $F_{0.70}/F_{0.85}$.

$n = 1 + \log_e (17/7)/\log_e (F_{0.70}/F_{0.85})$.

FIGURE C4.2.3-3. CHARACTERISTICS OF STRESS-STRAIN CURVES FOR STRUCTURAL ALLOYS DEPICTING QUANTITIES USED IN THREE-PARAMETER METHOD.

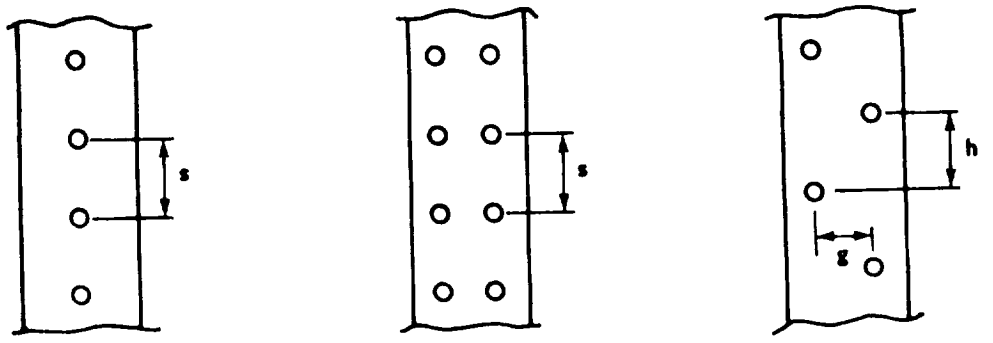

(a) Single row (b) Double rows (c) Staggered rows

FIGURE C4.2.3-4. FASTENER SPACINGS FOR TYPICAL FASTENER PATTERNS.

The value of e is dependent on the type of fastener. Values of e to be used are listed in Table C4.2.3.1 for several types of fasteners.

Table C4.2.3.1. Values of End-Fixity Coefficient "e" for Several Types of Fasteners

Type of Fastener	e
Flathead rivet	4
Spotweld	3.5
Brazierhead rivet	3
Machine csk. rivet	1
Dimpled rivet	1

Values of the shape parameter n for several materials are given in Table C2.1.5.6. For materials not given, the shape parameter may be obtained from Figure C4.2.3-3 (b). If n is out of the range of the curve in that figure, it may be calculated from the following equation:

$$n = 1 + \log_e (17/7)/\log_e (F_{0.70}/F_{0.85}) \quad . \qquad (7)$$

For temperatures other than room temperature, the analysis may be performed using the values of F_{cy}, $F_{0.70}$, $F_{0.85}$ and n for this temperature. These values can be obtained from the appropriate stress-strain curve.

It should be noted that a cutoff stress is used in the interrivet buckling calculations. The values of the cutoff stress recommended for use here are shown in Table C4.2.3.2.

Table C4.2.3.2. Recommended Values for Cutoff Stress

Material	Cutoff Stress (F_{co})
2024-T, 2014-T, 6061-T	$F_{cy}\left[1 + \frac{F_{cy}}{200,000}\right]$
7075-T	$1.075\ F_{cy}$
18-8 (1/2 H)*	$0.835\ F_{cy}$
(3/4 H)	$0.875\ F_{cy}$
(FH)	$0.866\ F_{cy}$
All other materials	F_{cy}

* Cold-rolled, with grain, based on MIL-HDBK-5A properties.

A general procedure for calculating inter-fastener buckling stress and margin of safety is listed below:

1. Determine $F_{0.70}$ and $F_{0.85}$ from appropriate stress-strain curve.
2. Determine n from Table C2.1.5.6. If n is not given in the table,

it may be obtained from Figure C4.2.3-3 (b) or equation (7).

3. Obtain e from Table C4.2.3.1.

4. Calculate $\frac{4 F_{0.7} (1 - \nu^2)}{e E_c} \left(\frac{s}{t_s}\right)^2$.

5. Enter Figure C4.2.3-2 at value calculated in step four to obtain $F_{cir}/F_{0.7}$ using the appropriate n curve.

6. Calculate F_{cir} as

   $F_{cir} = (F_{0.7})$ (Value determined in step five) .

7. Obtain the cutoff stress, F_{co}, from Table C4.2.3.2.

8. Calculate the M.S. as

$$M.S. = \frac{F_{cr}}{f_c} - 1 \quad ,$$

where F_{cr} is the lower of the two values F_{cir} and F_{co}, and f_c is the compressive sheet stress between fasteners.

C.4.2.4 Panel Wrinkling (Forced Crippling)

A mode of local instability failure sometimes encountered when designing stiffened panels is panel wrinkling. This generally occurs in designs where the skin gage is equal to or greater than the stiffener gage.

This mode of failure, shown in Figure C4.2.4-1, results from the existence of a flexible attachment between the skin and stiffener. The skin acts as a column supported at the fastener attachment points on an elastic foundation. The elastic foundation is provided by the stiffener attachment flange to a degree dependent on its geometry: the offset distance of the

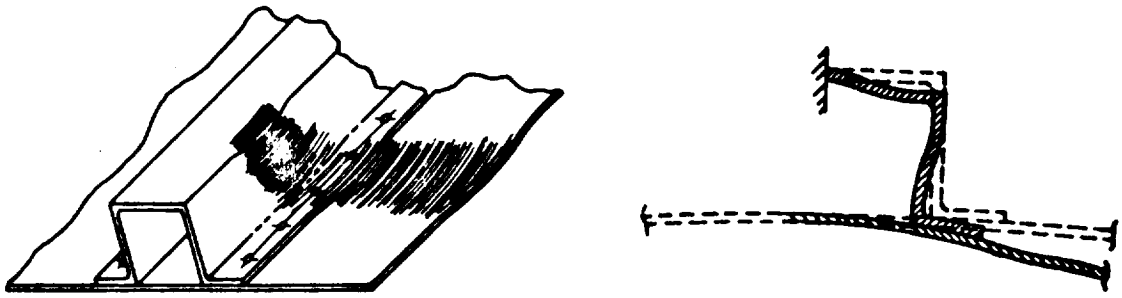

(a) General Appearance of a Wrinkling Failure

(b) A Cross Section at Wrinkle Showing Distortions of Stiffener and Skin

FIGURE C4.2.4-1. TYPICAL PANEL WRINKLING FAILURE.

fastener from the stiffener web, the fastener spacing, diameter, and strength. In the wrinkling mode, the attachment flange of the stiffener follows the skin contour and causes other plate elements of the stiffener to distort, thereby precipitating failure of the panel as a whole.

The most commonly used analytical method for determining wrinkling-buckling stresses is semiempirical in nature. The general equation for wrinkling is

$$F_{cw} = \eta \bar{\eta} \frac{k_{wr} \pi^2 E_c}{12 (1 - \nu^2)} \left(\frac{t_s}{b_s} \right)^2 , \qquad (8)$$

where k_{wr}, the wrinkling coefficient is given in Figure C4.2.4-2. This coefficient is a function of the experimentally determined effective rivet offset (f) which is obtained from Figure C4.2.4-3. Dimensioning rules given in Figure C4.2.2-8 for formed and extruded stiffener sections should be observed. Cladding ($\bar{\eta}$) and plasticity (η) correction factors should be determined in agreement with Section C2.1.1 and should be used accordingly.

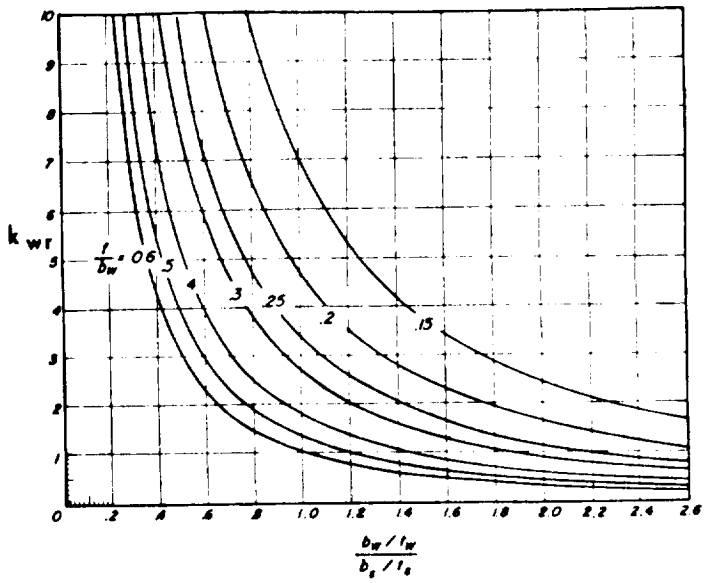

FIGURE C4.2.4-2. EXPERIMENTALLY DETERMINED BUCKLING COEFFICIENT FOR FAILURE IN THE WRINKLING MODE.

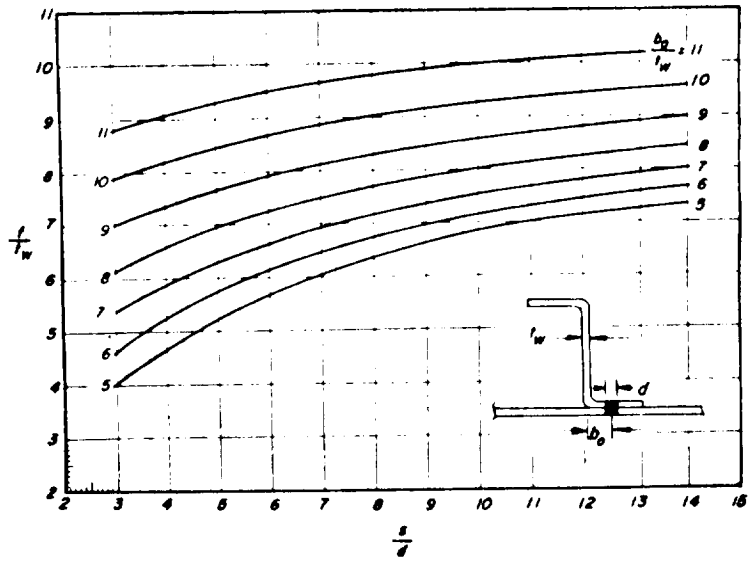

FIGURE C4.2.4-3. EXPERIMENTALLY DETERMINED VALUES OF EFFECTIVE RIVET OFFSET.

A criterion for fastener spacing is determined from test data which result from a wrinkling mode failure:

$$s/b_s < 1.27/(k_{wr})^{1/2} \quad . \tag{9}$$

Wrinkling imposes a high tensile load on the fasteners which are required to make the stiffener attachment flange conform to the wrinkled sheet. An approximate expression for the tensile strength of the fastener is

$$f_{tr} > \frac{0.7}{E_{st}} \frac{b_s}{d} \frac{s}{d} \left(F_{cw}\right)^2 \quad . \tag{10}$$

The tensile strength of the fastener (F_{tr}) is defined in terms of the shank area, and it may be associated with either shank failure or pulling of the countersunk head of the fastener through the sheet.

When the fasteners that are being analyzed are rivets of materials other than 2117-T4 aluminum alloy, the following experimentally proven expressions should be used.

For 2117-T4 rivets whose tensile strength is $F_t = 57$ ksi, the criteria are:

$$F_t = 57 \text{ ksi} \quad , \tag{11}$$

if $d_e/t_{av} \leq 1.67$;

or

$$F_t = \frac{190}{d_e/t_{av}} - \frac{160}{(d_e/t_{av})^2} \quad , \tag{12}$$

if $d_e/t_{av} > 1.67$;

where t_{av} (in inches) is the average of sheet and stiffener thickness. The effective diameter d_e is the diameter for a rivet made from 2117-T4 material.

The effective diameter of a rivet of another material is,

$$d_e/d = (F_{tr}/F_t)^{\frac{1}{2}} \quad , \tag{13}$$

where F_{tr} is the tensile strength of a rivet, defined as maximum tensile load divided by shank area in ksi units.

The following procedure is recommended when analyzing a panel for wrinkling:

1. Calculate s/d.

2. Enter Figure C4.2.4-3 at value calculated in step 1 to obtain f/t_w, using the appropriate b_e/t_w curve.

3. Calculate 1.

4. Calculate $\dfrac{b_w/t_w}{b_s/t_s}$.

5. Enter Figure C4.2.4-2 at value calculated in step 4 to obtain k_{wr} using the appropriate f/b_w curve.

6. Solve equation (9).

   a. If equation is satisfied, continue to step 7.

   b. If equation is not satisfied, wrinkling is not the critical mode; return to Section C4.2.3.

7. Calculate F_{cw} using equation (8).

8. Check fastener tensile stresses using equation (10), and equations (11), (12), and (13) if necessary.

9. Calculate the panel M.S. as

$$M.S. = \frac{F_{cw}}{f_c} - 1 \quad ,$$

where f_c is the compressive stress in the skin, and the fastener M.S. is

$$M.S. = \frac{F_{tr}}{f_{tr}} - 1 \quad ,$$

where F_{tr} is the tensile allowable of the fastener.

C4.2.5 Torsional Instability

Torsional instability of a stiffened panel between frames occurs when the cross section of the stiffener rotates but does not distort or translate in its own plane. Typical antisymmetric and symmetric torsional modes of instability are shown in Figure C4.2.5-1.

The analysis methods of torsional instability of stiffeners attached to sheets, as suggested in Reference 4, will be described. For the case of flat plates or cylinders with typical frame spacing,

$$d_f > \pi \left(E\eta_G I/k\right)^{\frac{1}{4}} \quad , \qquad (14)$$

the allowable torsional instability stress, F_{ct}, for the mode shown in Figure C4.2.5-1 is

$$F_{ct} = G\eta_A \left[\frac{J}{I_p}\right] + 2\left[\frac{\sqrt{\Gamma}}{I_p}\right]\sqrt{E\eta_G k} \quad , \qquad (15)$$

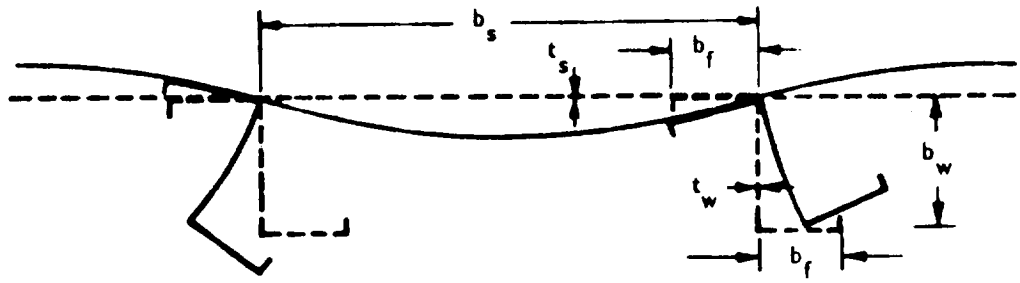

(a) Antisymmetric

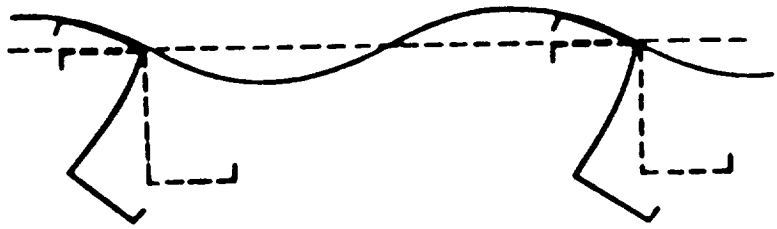

(b) Symmetric

FIGURE C4.2.5-1. MODES OF TORSIONAL INSTABILITY.

where $\frac{J}{I_p}$ and $\frac{\sqrt{\Gamma}}{I_p}$ values for Z and J type stiffeners may be obtained from Figures C4.2.5-2 and C4.2.5-3, respectively.

The plasticity correction factors η_A and η_G may be calculated by an iterative procedure using stress-strain curves (which can be found in MIL-HDBK-5A for most materials) for the given material and by the following expressions:

$$\eta_A = E_s/E \tag{16}$$

$$\eta_G = E_t/E \tag{17}$$

Curves for η_A and η_G for several materials at various temperature levels

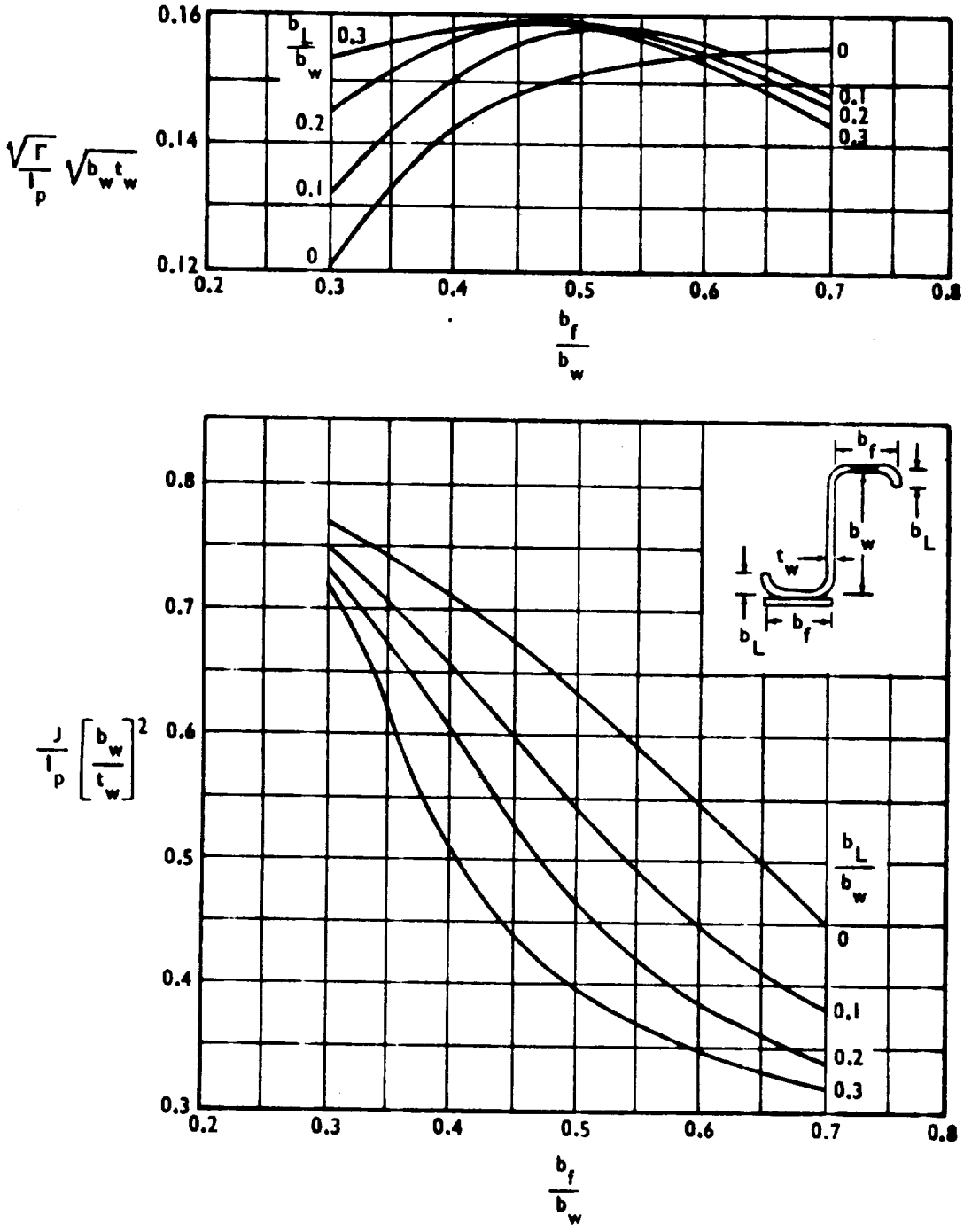

FIGURE C4.2.5-2. TORSIONAL SECTION PROPERTIES FOR LIPPED Z-STIFFENER-SHEET PANELS.

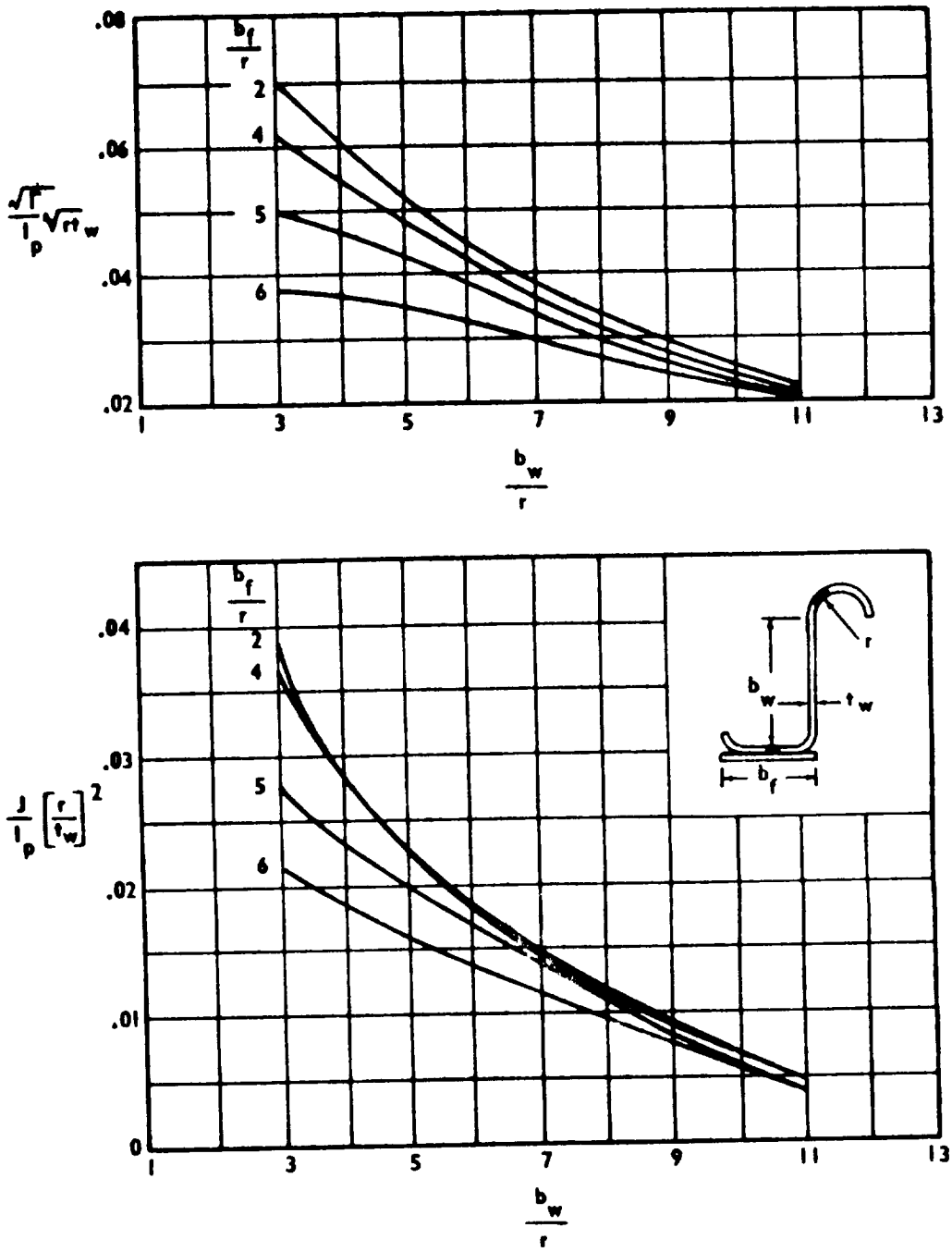

FIGURE C4.2.5-3. TORSIONAL SECTION PROPERTIES FOR J STIFFENER-SHEET PANELS.

may be found in References 1 and 5. Similar curves will be provided in Section C2.1.0 of this manual at a later date.

The rotational spring constant (k) may be found using the following expression:

$$\frac{1}{k} = \frac{1}{k_{web}} + \frac{1}{k_{sheet}} \quad , \tag{18}$$

where

$$k_{web} = \frac{E t_w^3}{4b_w + 6b_f} \tag{19}$$

$$k_{sheet} = \frac{\lambda E t_s^3}{b_s} \tag{20}$$

λ = 1 for the symmetric mode (21)

$$\lambda = \frac{1}{3}\left[1 + 0.6\ \frac{(F_{ct} - F_{crs})}{F_{crs}}\right] \tag{22}$$

for the antisymmetric mode.

If $F_{ct} < 4.33\ F_{crs}$, the antisymmetric mode is critical. If $F_{ct} > 4.33\ F_{crs}$, the symmetric mode of failure is critical. Since λ, η_A, and η_G depend on F_{ct}, the solution for F_{ct} is, in general, a trial-and-error procedure. Starting with the assumption that $\lambda = 1$, $\eta_A = \eta_G = 1$, calculate F_{ct} and correct for plasticity if required. Correct λ if required

and repeat procedure until desired convergence is obtained. Then check to see whether or not $d_f > \pi \left(\frac{E\eta_G\Gamma}{k}\right)^{1/4}$.

If $d_f < \pi \left(\frac{E\eta_G\Gamma}{k}\right)^{1/4}$ the torsional instability stress is

$$F_{ct} = G\eta_A \left(\frac{J}{I_p}\right) + \frac{E\eta_G\Gamma}{I_p}\left(\frac{\pi}{d_f}\right)^2 + \frac{k(d_f/\pi)^2}{I_p} \quad , \qquad (23)$$

where

$$\Gamma = \left(\frac{\sqrt{\Gamma}}{I_p}\right)^2 I_p^2 \quad . \qquad (24)$$

The formulas which have been presented may be used for stiffeners with sections other than those shown in Figures C4.2.5-2 and C4.2.5-3 if the values of I_p, J and Γ are known.

C4.3.0 Integrally Stiffened Flat Panels in Compression

The allowable buckling stress for local compression instability of certain integrally stiffened plates loaded parallel to the integral stiffeners may be found by determining the buckling coefficient k_s from Figures C4.3.0-1 through C4.3.0-5 and solving the equation:

$$F_{CRI} = \eta \bar{\eta} \frac{k_s \pi^2 E_c}{12 (1-\nu^2)} \left(\frac{t_s}{b_s}\right)^2 \quad . \qquad (25)$$

The integral shapes presented include webs, zees, and tees for various t_w/t_f values.

Also, these charts may be used to determine the allowable buckling stress for local compression instability of conventionally stiffened plates which have been idealized into geometries similar to those shown in Figures C4.3.0-1 through C4.3.0-5. When this is done, care should be exercised that the dimensioning rules pertaining to formed and extruded shapes, as shown in Figure C4.2.2-8, are observed.

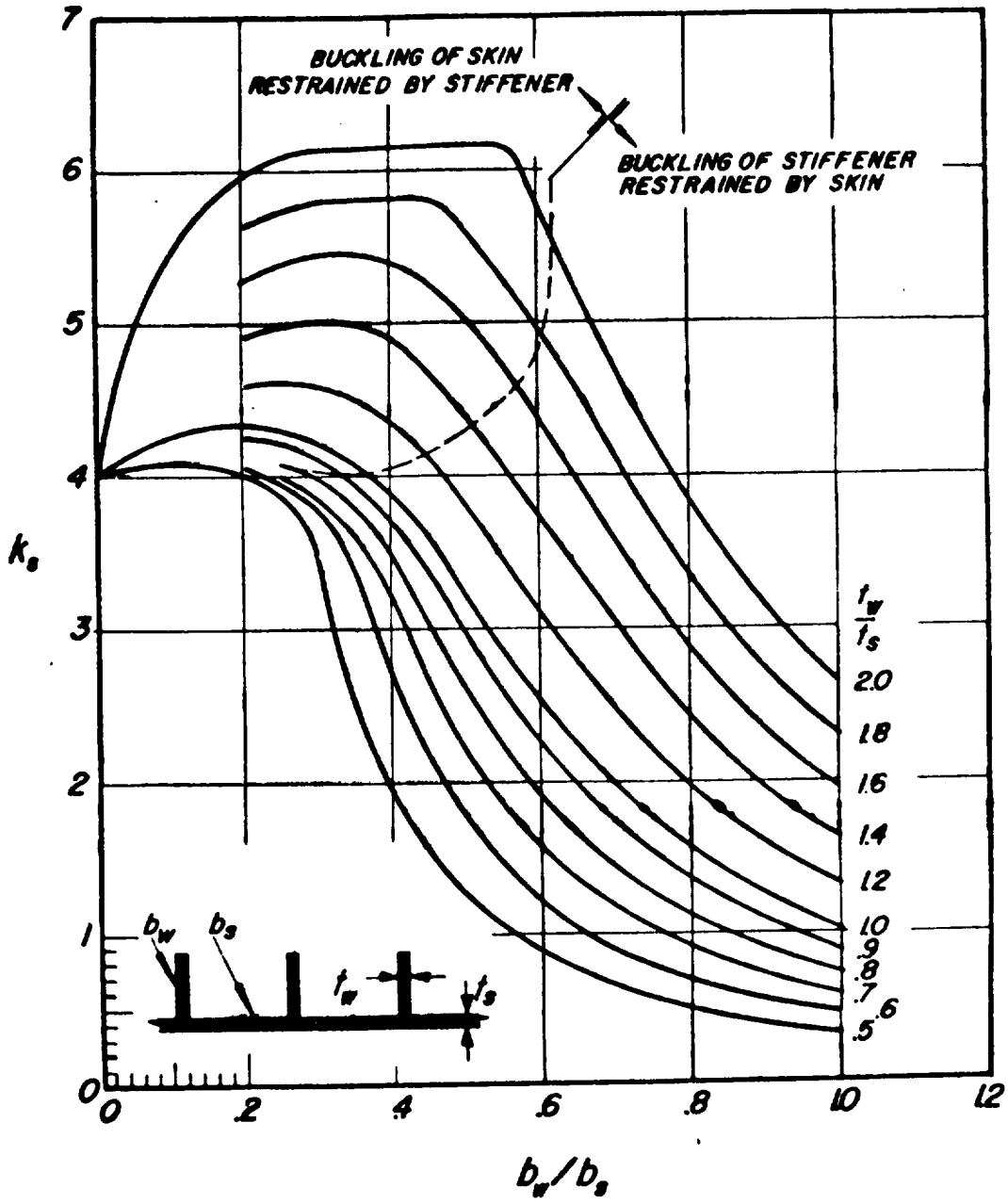

$0.5 < t_w/t_s < 2.0$

FIGURE C4.3.0-1. COMPRESSIVE-LOCAL-BUCKLING COEFFICIENTS FOR INFINITELY WIDE FLAT PLATES HAVING WEB-TYPE INTEGRAL STIFFENERS.

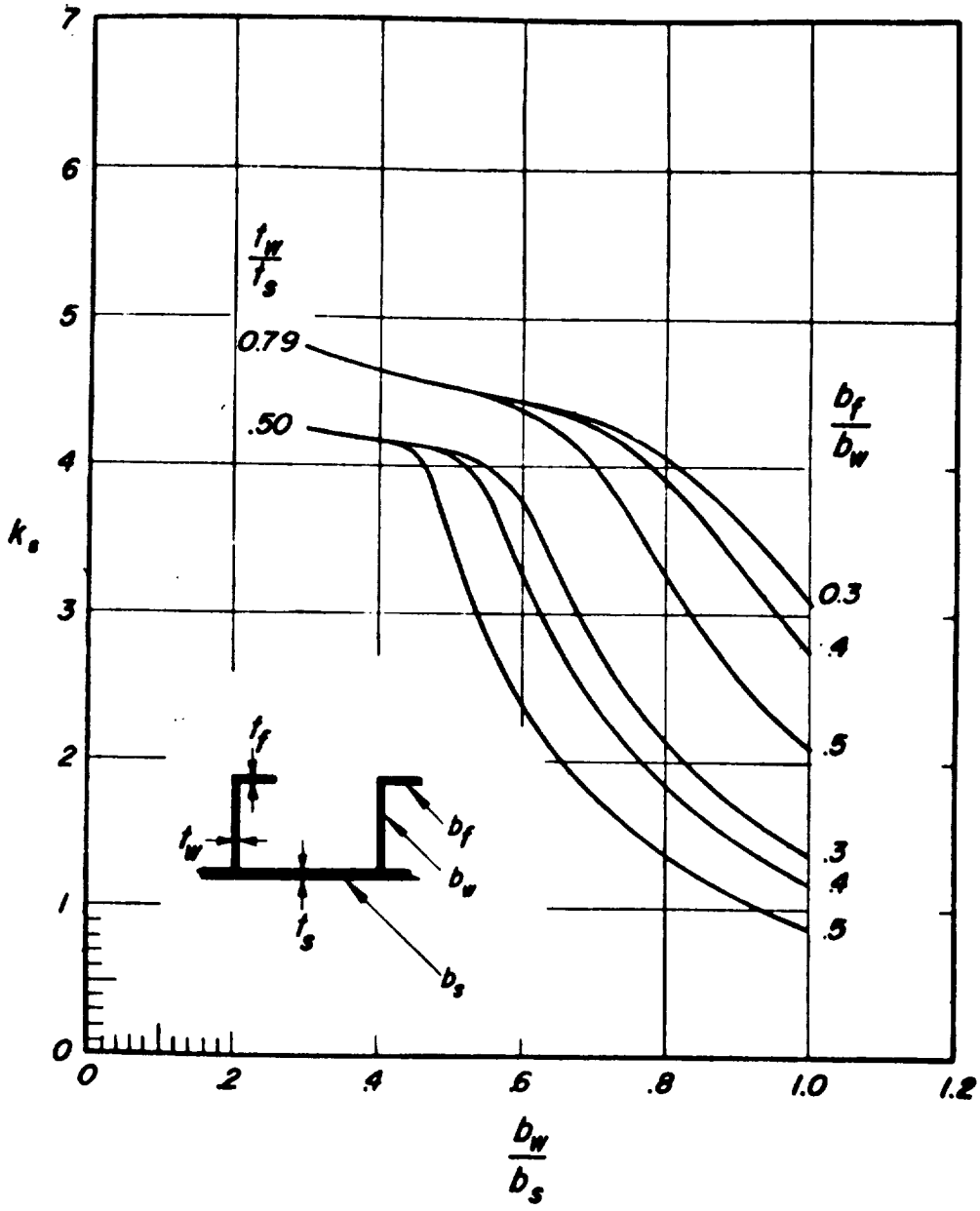

t_w/t_s = 0.50 and 0.79

FIGURE C4.3.0-2. COMPRESSIVE-LOCAL-BUCKLING COEFFICIENTS FOR INFINITELY WIDE FLAT PLATES HAVING Z-SECTION INTEGRAL STIFFENERS.

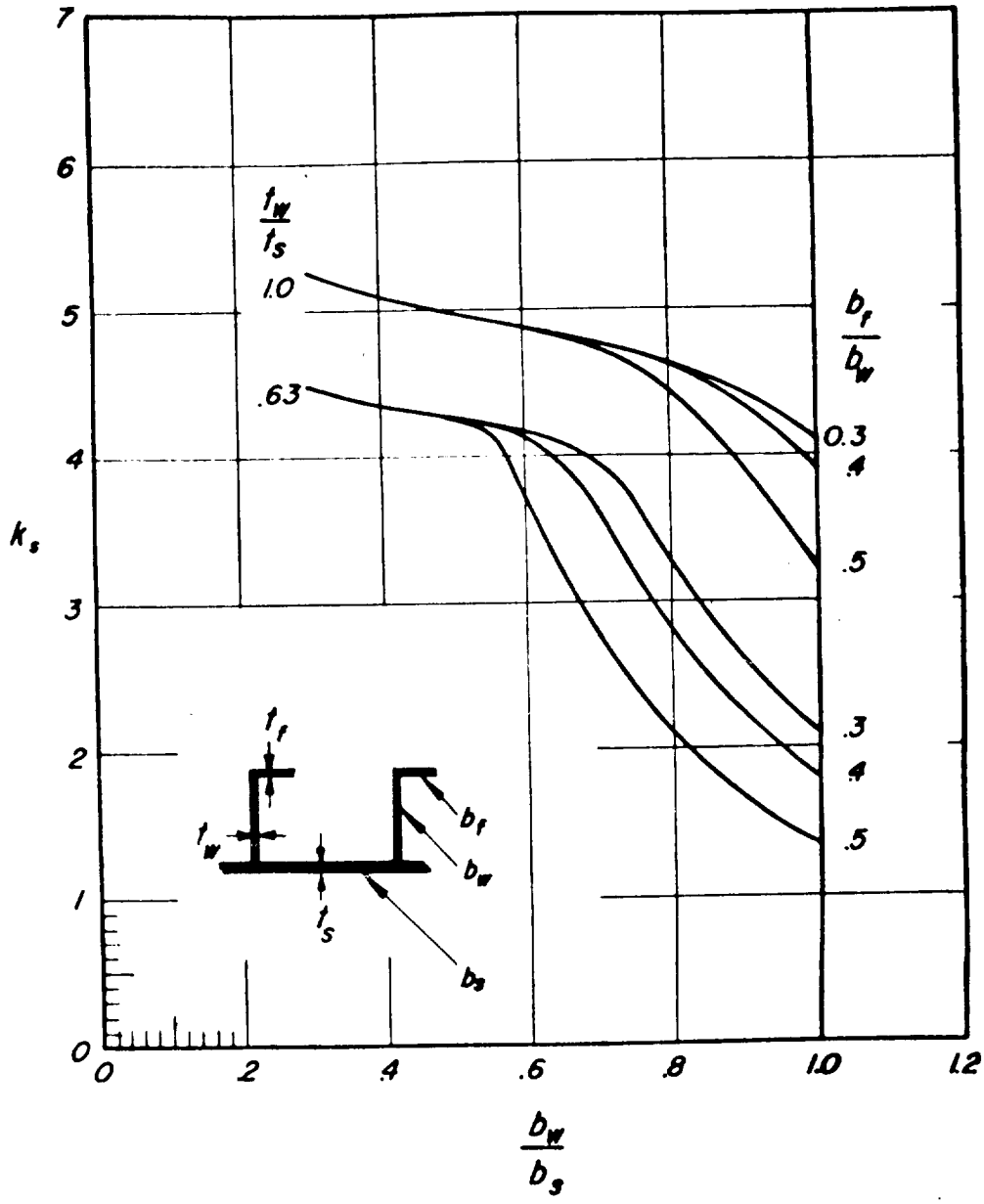

t_w/t_s = 0.63 and 1.0

FIGURE C4.3.0-3. COMPRESSIVE-LOCAL-BUCKLING COEFFICIENT FOR INFINITELY WIDE FLAT PLATES HAVING Z-SECTION INTEGRAL STIFFENERS.

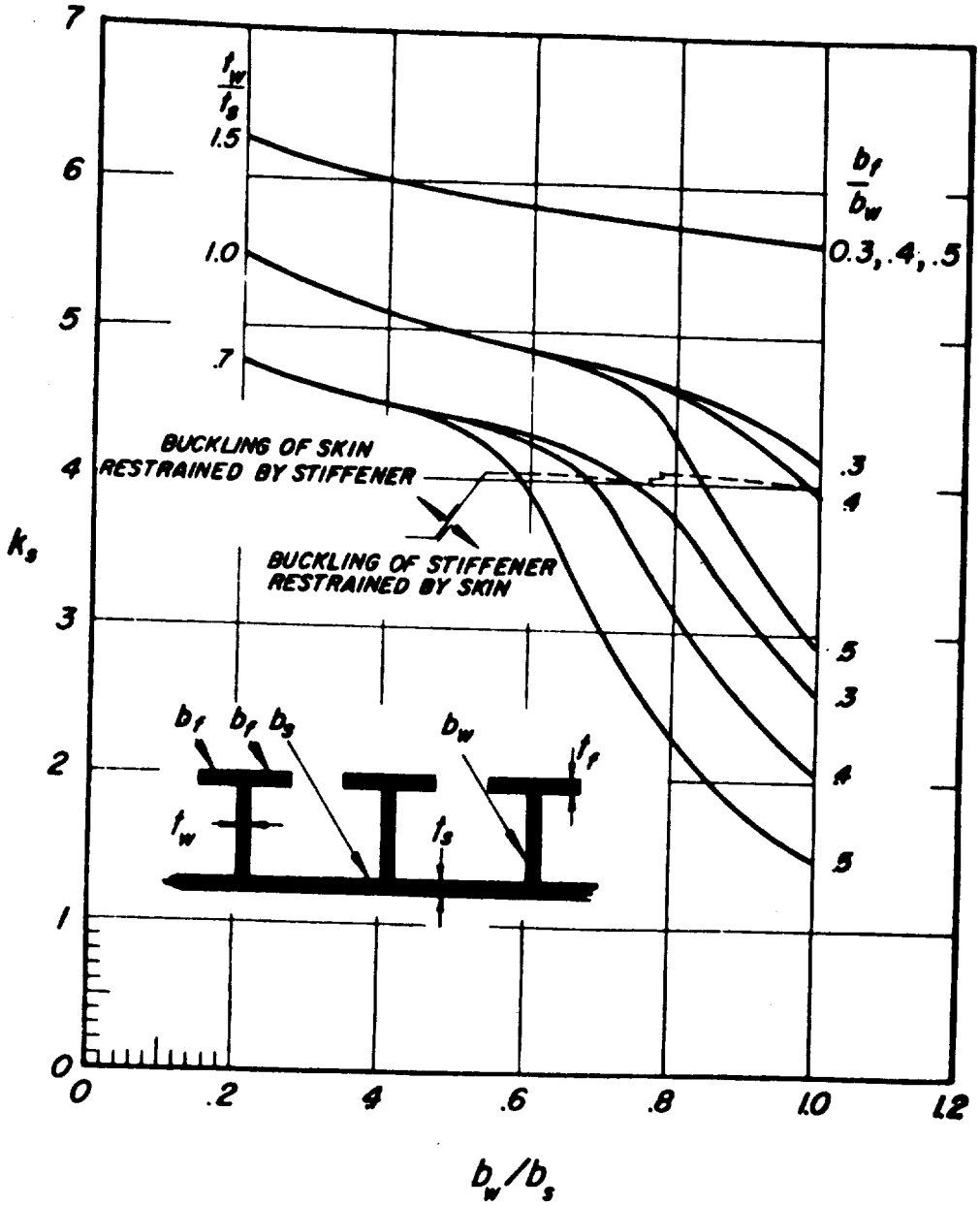

$t_w/t_f = 1.0$; $b_f/t_f > 10$; $b_w/b_s > 0.25$

FIGURE C4.3.0-4. COMPRESSIVE-LOCAL-BUCKLING COEFFICIENT FOR INFINITELY WIDE FLAT PLATES HAVING T-SECTION INTEGRAL STIFFENERS.

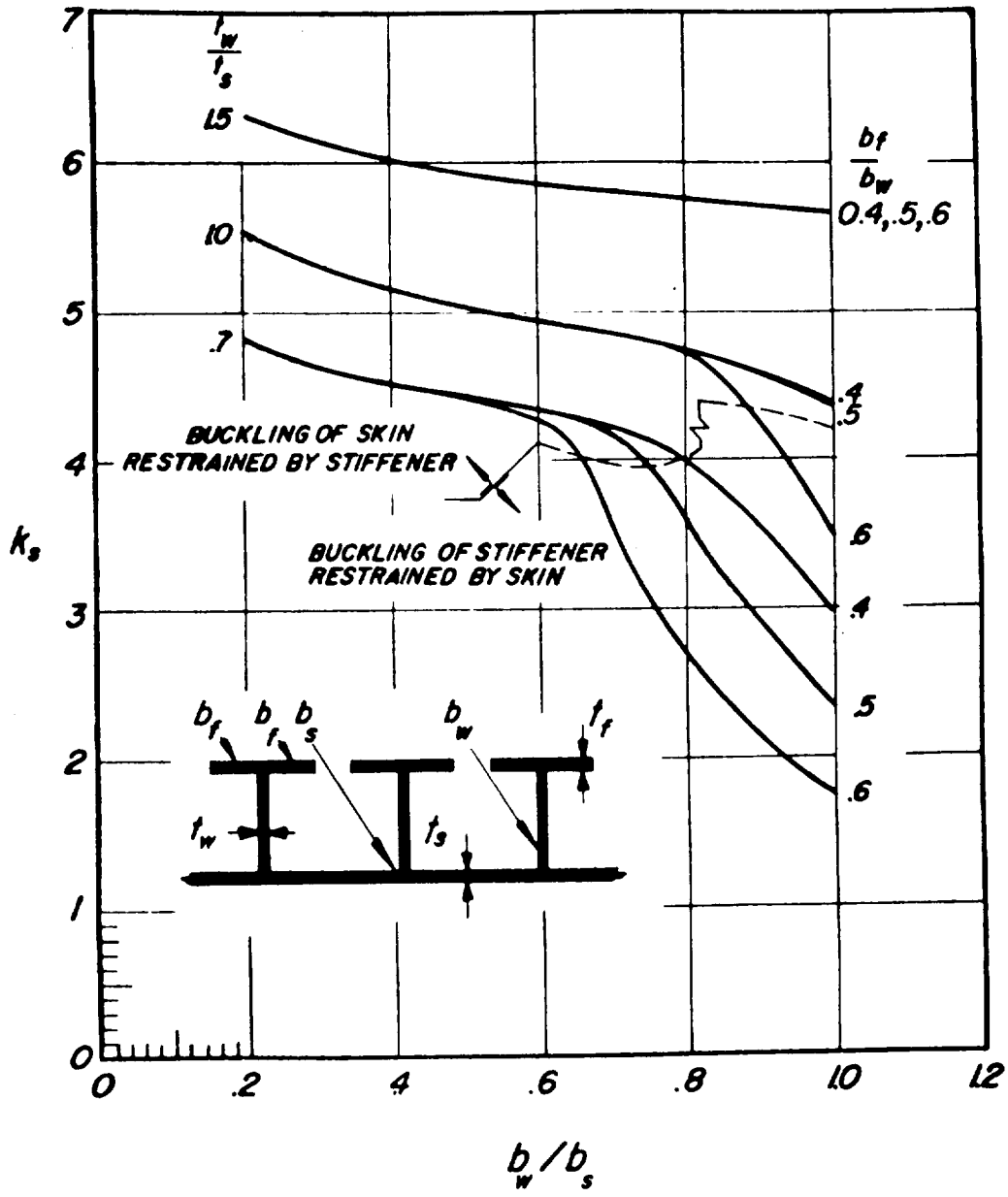

$t_w/t_f = 0.7$; $b_f/t_f > 10$; $b_w/b_s > 0.25$

FIGURE C4.3.0-5. COMPRESSION-LOCAL-BUCKLING COEFFICIENT FOR INFINITELY WIDE FLAT PLATES HAVING T-SECTION INTEGRAL STIFFENERS.

C4.4.0 Stiffened Flat Panels in Shear

Local shear instability methods of analysis for stiffened panels in shear are presented for panels stiffened either longitudinally or transversely. For shear buckling calculations, these two types of stiffened panels may be distinguished by considering panels with stiffeners parallel to the long side of the panel as longitudinally stiffened, and panels with stiffeners parallel to the short side of the panel as transversely stiffened. In instances where stiffened square panels are encountered, use of the analysis for transversely stiffened panels is recommended, to take advantage of the more extensive test data available.

The analysis that follows accounts for the local (no deflection of stiffeners) instability mode of failure only. The parameter EI/b_sD is necessary for determining the criticality of the panel instability mode. At low values of EI/b_sD the general (stiffeners deflect) mode is critical. As EI/b_sD increases, the local mode becomes critical and yields a constant value of the shear buckling coefficient k_s regardless of further increases of EI/b_sD. Thus, in determining the flexural stiffness required in the stiffeners, it is this transition area of EI/b_sD which is important since additional stiffener moment of inertia does nothing to increase allowable local plate buckling stress and less inertia induces general instability.

It is noted at this point that for similar bay geometries for the two different stiffening arrangements, equal local instability stresses will result. Local instability is a function of only the local geometry; whereas, general instability depends upon the orientation of the stiffeners with respect to the panel's long dimension.

The equation for local instability of the skin of a stiffened panel in shear is

$$F_{scr} = \eta \bar{\eta} \frac{k_s \pi^2 E_c}{12 (1-\nu^2)} \left(\frac{t_s}{b_s}\right)^2 , \qquad (26)$$

where k_s, the shear buckling coefficient, can be found by referring to Figure C2.1.5-14.

For longitudinally stiffened panels, using k_s determined above, enter Figure C4.4.0-1 and solve for a stiffener I required to prevent local skin buckling. The ratio between local buckling and general instability is as follows:

$$k_s \text{ (local)} = \frac{k_s \text{ (general)}}{(N+1)^2} , \qquad (27)$$

where N is the number of stiffeners. A stiffener I required to prevent general instability can be calculated in a similar manner using the ratio cited.

For transversely stiffened panels, a similar procedure to that given above can be used to calculate an I for the stiffeners required to resist local buckling; this is done by entering Figure C4.4.0-2 with a known k_s. The relationship between local buckling and general instability is

$$\frac{k_s \text{ (local)}}{b_s^2} = \frac{k_s \text{ (general)}}{a^2} . \qquad (28)$$

Using this relationship and the same figure, a required stiffener I can be calculated to prevent general instability.

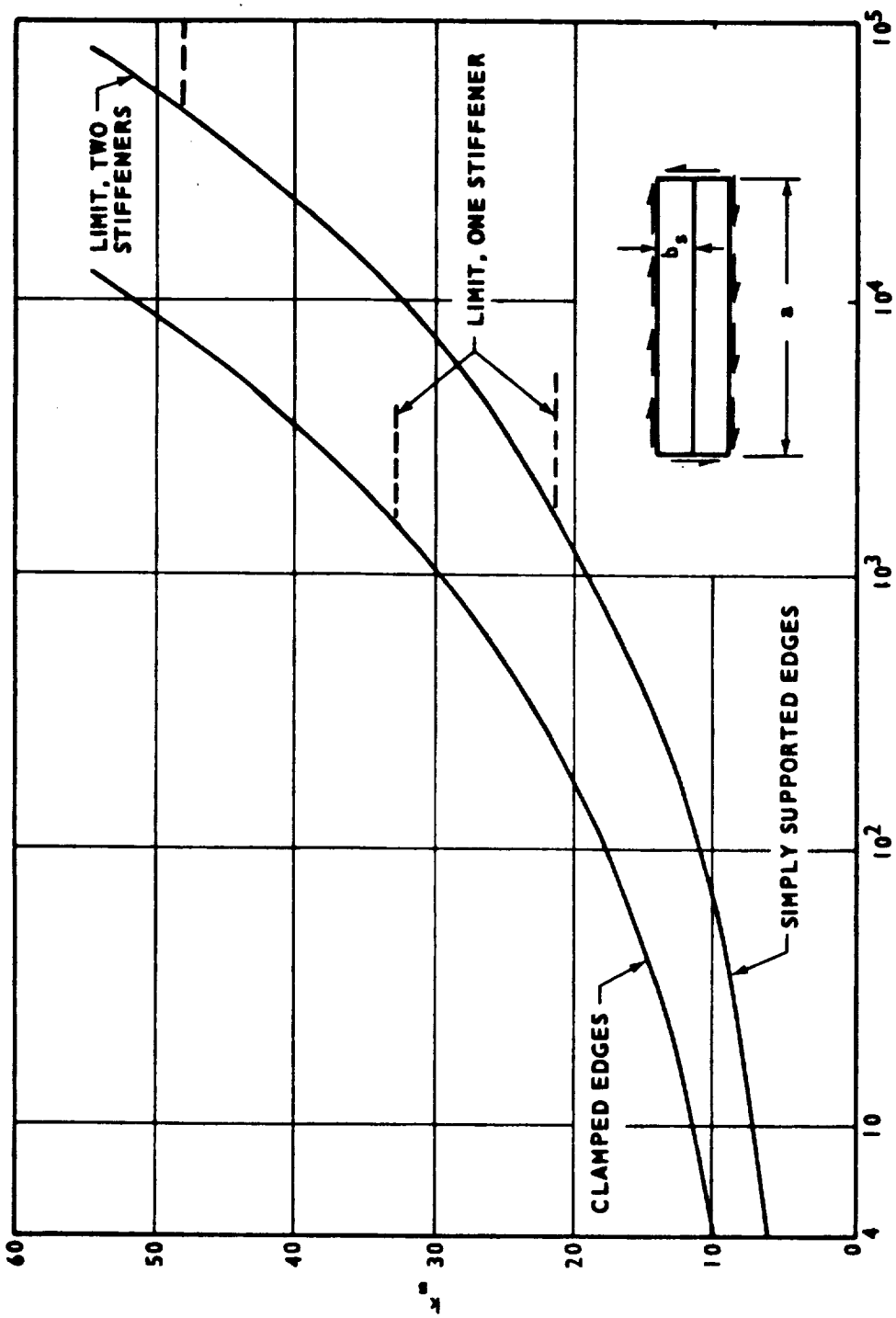

FIGURE C4.4.0-1. SHEAR BUCKLING COEFFICIENTS FOR LONG FLAT PLATES WITH LONGITUDINAL STIFFENERS.

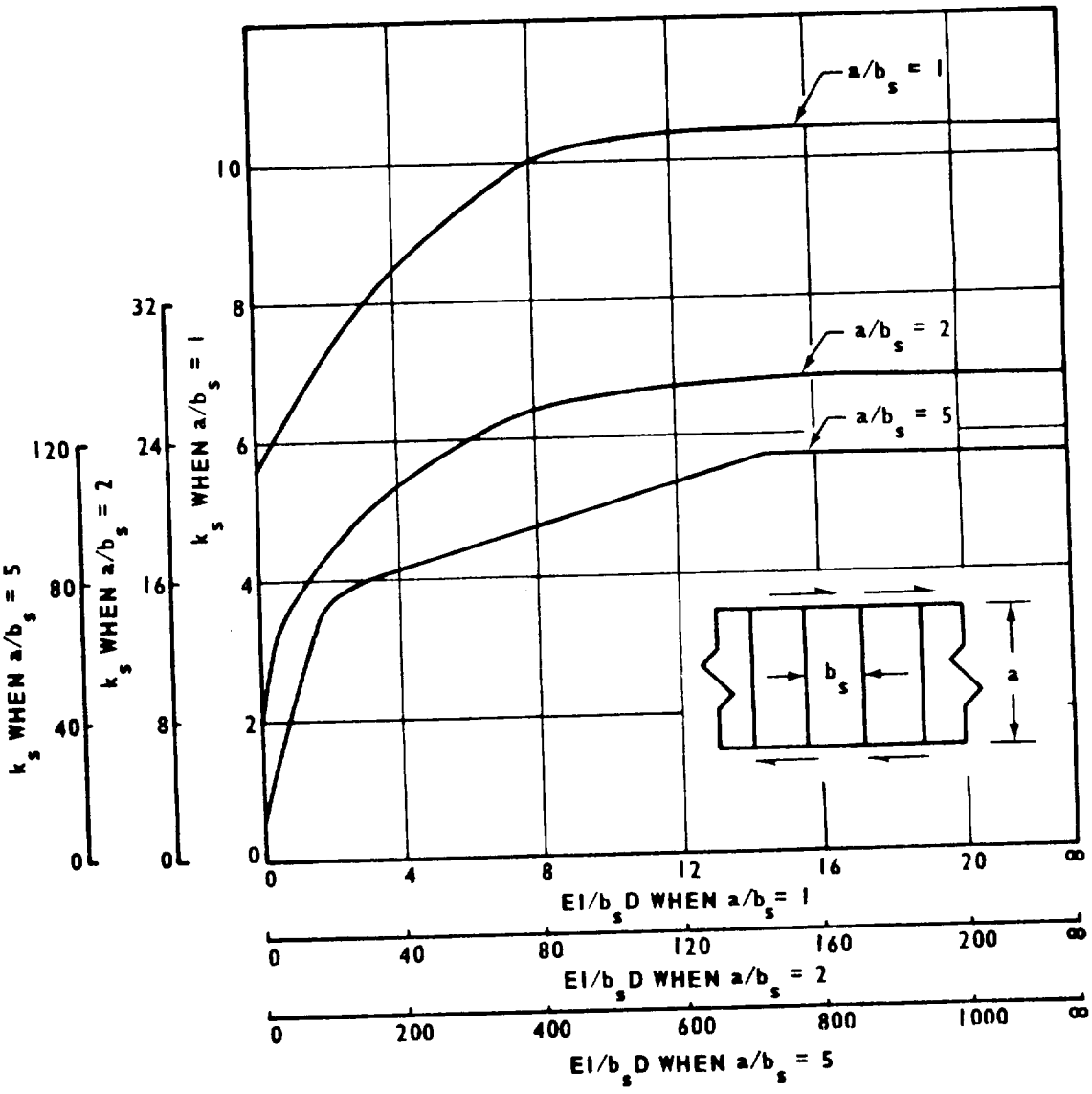

FIGURE C4.4.0-2. SHEAR BUCKLING COEFFICIENTS FOR LONG SIMPLY SUPPORTED FLAT PLATES WITH TRANSVERSE STIFFENERS.

The preceding relationships associate local and general modes of instability. It is then quite simple to discern which mode is critical to the structural integrity of the stiffened panel.

When F_{scr} is calculated, including plasticity and cladding correction factors if necessary, it should not exceed F_{co} given in Table C4.4.0.1, that is,

$$F_{scr} \leq F_{co} \qquad (29)$$

Table C4.4.0.1. Recommended Values for Shear Cutoff Stress

Material	Cutoff Stress (F_{co})
2024-T 2014-T 6061-T 7075-T	0.61 F_{cy}
18-8 (1/2 H)*	0.51 F_{cy}
(3/4 H)	0.53 F_{cy}
(FH)	0.53 F_{cy}
All other materials	0.61 F_{cy}

* Cold-rolled, with grain, based on MIL-HDBK-5A properties.

C4.5.0 Flat Panel Stiffened with Corrugations †

C4.6.0 Stiffened Curved Panels ††

† to be supplied
†† to be supplied

References

1. NASA-Manned Spacecraft Center, Houston, Texas: Shell Analysis Manual.

2. Gerard, G.: Handbook of Structural Stability, Part V — Compressive Strength of Flat Stiffened Panels. NACA TN 3785, 1957.

3. Bruhn, E.: Analysis and Design of Flight Vehicle Structures. Tri-State Offset Company, Cincinnati, Ohio, 1965.

4. Argyris, J.: Flexure-Torsion Failure of Panels. Aircraft Engineering, June - July 1954.

5. North American Aviation, Inc.: Structures Manual.

Bibliography

Argyris, J. and Dunne, P.: Structural Principles and Data, Part 2, Structural Analysis. Handbook of Aero., No. 1, Fourth Edition, Sir Isaac Pitman & Co., Ltd. London, 1952.

Becker, H.: Handbook of Structural Stability, Part II — Buckling of Composite Elements. NACA TN 3782, 1957.

Gerard, G. and Becker, H.: Handbook of Structural Stability, Part I — Buckling of Flat Plates. NACA TN 3781, 1957.

Gerard, G.: Handbook of Structural Stability, Part IV — Failure of Plates and Composite Elements. NACA TN 3784, 1957.

Lockheed — Missiles and Space Division: Structural Methods Handbook.

Semonian, J. and Peterson, J.: An Analysis of the Stability and Ultimate Compressive Strength of Short Sheet-Stringer Panels with Special Reference to the Influence of Riveted Connection Between Sheet and Stringer. NACA TN 3431, 1955.